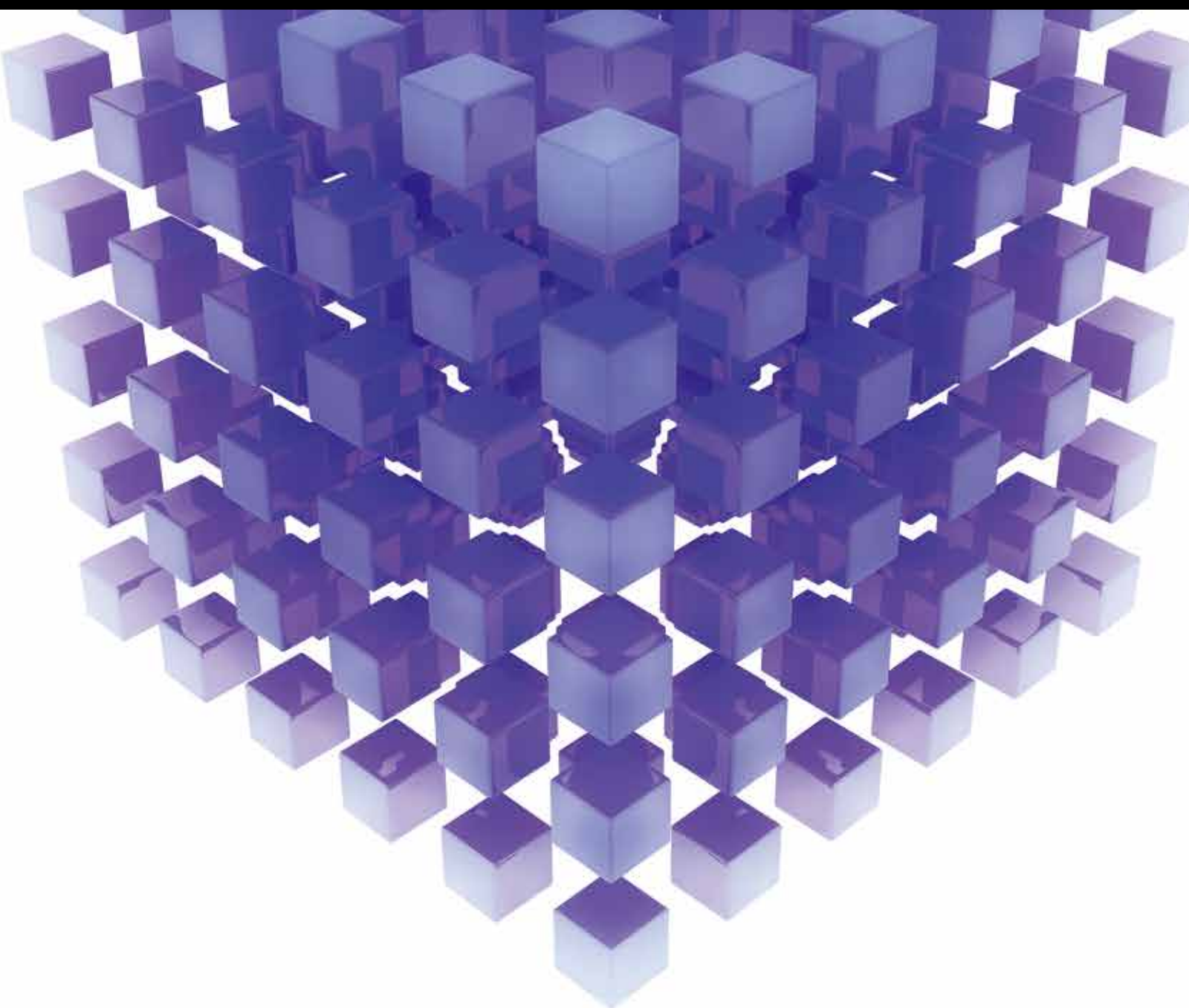


Theory and Applications of Complex Networks 2014

Guest Editors: Tingwen Huang, Qinggang Meng, Zhichun Yang, Chuandong Li, He Huang, and Jianguo Du





Theory and Applications of Complex Networks 2014

Mathematical Problems in Engineering

Theory and Applications of Complex Networks 2014

Guest Editors: Tingwen Huang, Qinggang Meng,
Zhichun Yang, Chuandong Li, He Huang, and Jianguo Du



Copyright © 2015 Hindawi Publishing Corporation. All rights reserved.

This is a special issue published in “Mathematical Problems in Engineering.” All articles are open access articles distributed under the Creative Commons Attribution License, which permits unrestricted use, distribution, and reproduction in any medium, provided the original work is properly cited.

Editorial Board

Mohamed Abd El Aziz, Egypt
Farid Abed-Meraim, France
Silvia Abrahão, Spain
Paolo Addresso, Italy
Claudia Adduce, Italy
Ramesh Agarwal, USA
Juan C. Agüero, Australia
Ricardo Aguilar-López, Mexico
Tarek Ahmed-Ali, France
Hamid Akbarzadeh, Canada
Muhammad N. Akram, Norway
Mohammad-Reza Alam, USA
Salvatore Alfonzetti, Italy
Francisco Alhama, Spain
Juan A. Almendral, Spain
Saiied Aminossadati, Australia
Lionel Amodeo, France
Igor Andrianov, Germany
Sebastian Anita, Romania
Renata Archetti, Italy
Felice Arena, Italy
Sabri Arik, Turkey
Fumihiko Ashida, Japan
Hassan Askari, Canada
Mohsen Asle Zaeem, USA
Francesco Aymerich, Italy
Seungik Baek, USA
Khaled Bahlali, France
Laurent Bako, France
Stefan Balint, Romania
Alfonso Banos, Spain
Roberto Baratti, Italy
Martino Bardi, Italy
Azeddine Beghdadi, France
Abdel-Hakim Bendada, Canada
Ivano Benedetti, Italy
Elena Benvenuti, Italy
Jamal Berakdar, Germany
Enrique Berjano, Spain
Jean-Charles Beugnot, France
Simone Bianco, Italy
David Bigaud, France
Jonathan N. Blakely, USA
Paul Bogdan, USA
Daniela Boso, Italy

Abdel-Ouahab Boudraa, France
Francesco Braghin, Italy
Michael J. Brennan, UK
Gunther Brenner, Germany
Maurizio Brocchini, Italy
Julien Bruchon, France
Javier Buldú, Spain
Tito Busani, USA
Pierfrancesco Cacciola, UK
Salvatore Caddemi, Italy
Jose E. Capilla, Spain
Ana Carpio, Spain
Miguel E. Cerrolaza, Spain
Mohammed Chadli, France
Gregory Chagnon, France
Ching-Ter Chang, Taiwan
Michael J. Chappell, UK
Kacem Chehdi, France
Chunlin Chen, China
Xinkai Chen, Japan
Francisco Chicano, Spain
Hung-Yuan Chung, Taiwan
Joaquim Ciurana, Spain
John D. Clayton, USA
Carlo Cosentino, Italy
Paolo Crippa, Italy
Erik Cuevas, Mexico
Peter Dabnichki, Australia
Luca D'Acerno, Italy
Weizhong Dai, USA
Purushothaman Damodaran, USA
Farhang Daneshmand, Canada
Fabio De Angelis, Italy
Stefano de Miranda, Italy
Filippo de Monte, Italy
Xavier Delorme, France
Luca Deseri, USA
Yannis Dimakopoulos, Greece
Zhengtao Ding, UK
Ralph B. Dinwiddie, USA
Mohamed Djemai, France
Alexandre B. Dolgui, France
George S. Dulikravich, USA
Bogdan Dumitrescu, Finland
Horst Ecker, Austria

Karen Egiazarian, Finland
Ahmed El Hajjaji, France
Fouad Erchiqui, Canada
Anders Eriksson, Sweden
Giovanni Falsone, Italy
Hua Fan, China
Yann Favenec, France
Giuseppe Fedele, Italy
Roberto Fedele, Italy
Jacques Ferland, Canada
Jose R. Fernandez, Spain
Simme Douwe Flapper, The Netherlands
Thierry Floquet, France
Eric Florentin, France
Francesco Franco, Italy
Tomonari Furukawa, USA
Mohamed Gadala, Canada
Matteo Gaeta, Italy
Zoran Gajic, USA
Ciprian G. Gal, USA
Ugo Galvanetto, Italy
Akemi Gálvez, Spain
Rita Gamberini, Italy
Maria Gandarias, Spain
Arman Ganji, Canada
Xin-Lin Gao, USA
Zhong-Ke Gao, China
Giovanni Garcea, Italy
Fernando García, Spain
Laura Gardini, Italy
Alessandro Gasparetto, Italy
Vincenzo Gattulli, Italy
Jürgen Geiser, Germany
Oleg V. Gendelman, Israel
Mergen H. Ghayesh, Australia
Anna M. Gil-Lafuente, Spain
Hector Gómez, Spain
Rama S. R. Gorla, USA
Oded Gottlieb, Israel
Antoine Grall, France
Jason Gu, Canada
Quang Phuc Ha, Australia
Ofer Hadar, Israel
Masoud Hajarian, Iran
Frédéric Hamelin, France

Zhen-Lai Han, China
 Thomas Hanne, Switzerland
 Xiao-Qiao He, China
 María I. Herreros, Spain
 Vincent Hilaire, France
 Eckhard Hitzer, Japan
 Jaromir Horacek, Czech Republic
 Muneo Hori, Japan
 András Horvth, Italy
 Gordon Huang, Canada
 Sajid Hussain, Canada
 Asier Ibeas, Spain
 Giacomo Innocenti, Italy
 Emilio Insfran, Spain
 Nazrul Islam, USA
 Payman Jalali, Finland
 Reza Jazar, Australia
 Khalide Jbilou, France
 Linni Jian, China
 Bin Jiang, China
 Zhongping Jiang, USA
 Ningde Jin, China
 Grand R. Joldes, Australia
 Joaquim Joao Judice, Portugal
 Tadeusz Kaczorek, Poland
 Tamas Kalmar-Nagy, Hungary
 Tomasz Kapitaniak, Poland
 Haranath Kar, India
 Konstantinos Karamanos, Belgium
 C. M. Khalique, South Africa
 Do Wan Kim, Korea
 Nam-Il Kim, Korea
 Oleg Kirillov, Germany
 Manfred Krafczyk, Germany
 Frederic Kratz, France
 Jurgen Kurths, Germany
 Kyandoghere Kyamakya, Austria
 Davide La Torre, Italy
 Risto Lahdelma, Finland
 Hak-Keung Lam, UK
 Antonino Laudani, Italy
 Aime' Lay-Ekuakille, Italy
 Marek Lefik, Poland
 Yaguo Lei, China
 Thibault Lemaire, France
 Stefano Lenci, Italy
 Roman Lewandowski, Poland
 Qing Q. Liang, Australia

Panos Liatsis, UK
 Wanquan Liu, Australia
 Yan-Jun Liu, China
 Peide Liu, China
 Peter Liu, Taiwan
 Jean J. Loiseau, France
 Paolo Lonetti, Italy
 Luis M. López-Ochoa, Spain
 Vassilios C. Loukopoulos, Greece
 Valentin Lychagin, Norway
 F. M. Mahomed, South Africa
 Yassir T. Makkawi, UK
 Nouredine Manamanni, France
 Didier Maquin, France
 Paolo Maria Mariano, Italy
 Benoit Marx, France
 Gefhrard A. Maugin, France
 Driss Mehdi, France
 Roderick Melnik, Canada
 Pasquale Memmolo, Italy
 Xiangyu Meng, Canada
 Jose Merodio, Spain
 Luciano Mescia, Italy
 Laurent Mevel, France
 Yuri Vladimirovich Mikhlin, Ukraine
 Aki Mikkola, Finland
 Hiroyuki Mino, Japan
 Pablo Mira, Spain
 Vito Mocella, Italy
 Roberto Montanini, Italy
 Gisele Mophou, France
 Rafael Morales, Spain
 Aziz Moukrim, France
 Emiliano Mucchi, Italy
 Domenico Mundo, Italy
 Jose J. Muñoz, Spain
 Giuseppe Muscolino, Italy
 Marco Mussetta, Italy
 Hakim Naceur, France
 Hassane Naji, France
 Dong Ngoduy, UK
 Tatsushi Nishi, Japan
 Ben T. Nohara, Japan
 Mohammed Nouari, France
 Mustapha Nourelfath, Canada
 Sotiris K. Ntouyas, Greece
 Roger Ohayon, France
 Mitsuhiro Okayasu, Japan

Eva Onaindia, Spain
 Javier Ortega-Garcia, Spain
 Alejandro Ortega-Moñux, Spain
 Naohisa Otsuka, Japan
 Erika Ottaviano, Italy
 Alkiviadis Paipetis, Greece
 Alessandro Palmeri, UK
 Anna Pandolfi, Italy
 Elena Panteley, France
 Manuel Pastor, Spain
 Pubudu N. Pathirana, Australia
 Francesco Pellicano, Italy
 Mingshu Peng, China
 Haipeng Peng, China
 Zhike Peng, China
 Marzio Pennisi, Italy
 Matjaz Perc, Slovenia
 Francesco Pesavento, Italy
 Maria do Rosário Pinho, Portugal
 Antonina Pirrotta, Italy
 Vicent Pla, Spain
 Javier Plaza, Spain
 Jean-Christophe Ponsart, France
 Mauro Pontani, Italy
 Stanislav Potapenko, Canada
 Sergio Preidikman, USA
 Christopher Pretty, New Zealand
 Carsten Proppe, Germany
 Luca Pugi, Italy
 Yuming Qin, China
 Dane Quinn, USA
 Jose Ragot, France
 Kumbakonam Ramamani Rajagopal, USA
 Gianluca Ranzi, Australia
 Sivaguru Ravindran, USA
 Alessandro Reali, Italy
 Giuseppe Rega, Italy
 Oscar Reinoso, Spain
 Nidhal Rezg, France
 Ricardo Riaza, Spain
 Gerasimos Rigatos, Greece
 José Rodellar, Spain
 Rosana Rodriguez-Lopez, Spain
 Ignacio Rojas, Spain
 Carla Roque, Portugal
 Aline Roumy, France
 Debasish Roy, India
 Rubén Ruiz García, Spain

Antonio Ruiz-Cortes, Spain
Ivan D. Rukhlenko, Australia
Mazen Saad, France
Kishin Sadarangani, Spain
Mehrdad Saif, Canada
Miguel A. Salido, Spain
Roque J. Saltarén, Spain
Francisco J. Salvador, Spain
Alessandro Salvini, Italy
Angel Sánchez, Spain
Maura Sandri, Italy
Miguel A. F. Sanjuan, Spain
Juan F. San-Juan, Spain
Roberta Santoro, Italy
Ilmar Ferreira Santos, Denmark
Jos A. Sanz-Herrera, Spain
Nickolas S. Sapidis, Greece
Evangelos J. Sapountzakis, Greece
Themistoklis P. Sapsis, USA
Andrey V. Savkin, Australia
Valery Sbitnev, Russia
Thomas Schuster, Germany
Mohammed Seaid, UK
Lotfi Senhadji, France
Joan Serra-Sagrasta, Spain
Leonid Shaikhnet, Ukraine
Hassan M. Shanechi, USA
Sanjay K. Sharma, India
Bo Shen, Germany
Babak Shotorban, USA
Zhan Shu, UK
Dan Simon, USA
Luciano Simoni, Italy
Christos H. Skiadas, Greece

Michael Small, Australia
Francesco Soldovieri, Italy
Raffaele Solimene, Italy
Ruben Specogna, Italy
Sri Sridharan, USA
Ivanka Stamova, USA
Yakov Strelniker, Israel
Sergey A. Suslov, Australia
Thomas Svensson, Sweden
Andrzej Swierniak, Poland
Yang Tang, Germany
Sergio Teggi, Italy
Roger Temam, USA
Alexander Timokha, Norway
Rafael Toledo, Spain
Gisella Tomasini, Italy
Francesco Tornabene, Italy
Antonio Tornambe, Italy
Fernando Torres, Spain
Fabio Tramontana, Italy
Sébastien Tremblay, Canada
Irina N. Trendafilova, UK
George Tsiatas, Greece
Antonios Tsoordos, UK
Vladimir Turetsky, Israel
Mustafa Tutar, Spain
Efstratios Tzirtzilakis, Greece
Francesco Ubertini, Italy
Filippo Ubertini, Italy
Hassan Ugail, UK
Giuseppe Vairo, Italy
Kuppalapalle Vajravelu, USA
Robertt A. Valente, Portugal
Raoul van Loon, UK

Pandian Vasant, Malaysia
Miguel E. Vázquez-Méndez, Spain
Josep Vehi, Spain
Kalyana C. Veluvolu, Korea
Fons J. Verbeek, The Netherlands
Franck J. Vernerey, USA
Georgios Veronis, USA
Anna Vila, Spain
Rafael J. Villanueva, Spain
U. E. Vincent, UK
Mirko Viroli, Italy
Michael Vynnycky, Sweden
Yan-Wu Wang, China
Junwu Wang, China
Shuming Wang, Singapore
Yongqi Wang, Germany
Jeroen A. S. Witteveen, The Netherlands
Yuqiang Wu, China
Dash Desheng Wu, Canada
Guangming Xie, China
Xuejun Xie, China
Gen Qi Xu, China
Hang Xu, China
Xinggong Yan, UK
Luis J. Yebra, Spain
Peng-Yeng Yin, Taiwan
Ibrahim Zeid, USA
Huaguang Zhang, China
Qingling Zhang, China
Jian Guo Zhou, UK
Quanxin Zhu, China
Mustapha Zidi, France
Alessandro Zona, Italy

Contents

Theory and Applications of Complex Networks 2014, Tingwen Huang, Qinggang Meng, Zhichun Yang, Chuandong Li, He Huang, Jianguo Du, and Wei Zhang
Volume 2015, Article ID 924967, 2 pages

Identifying Super-Spreader Nodes in Complex Networks, Yu-Hsiang Fu, Chung-Yuan Huang, and Chuen-Tsai Sun
Volume 2015, Article ID 675713, 8 pages

Analysis on Global Asymptotical Stability of Genetic Regulatory Networks with Time-Varying Delays via Convex Combination Method, Yang Liu and Haixia Wu
Volume 2015, Article ID 303918, 5 pages

Distance Constrained Based Adaptive Flocking Control for Multiagent Networks with Time Delay, Qing Zhang, Ping Li, Zhengquan Yang, and Zengqiang Chen
Volume 2015, Article ID 901282, 8 pages

Passivity Analysis of Complex Delayed Dynamical Networks with Output Coupling, Yan-Fang Kang, Lu-Xian Fang, Yue-Hui Zhao, and Shun-Yan Ren
Volume 2015, Article ID 792069, 9 pages

A Knowledge-Based Service Composition Algorithm with Better QoS in Semantic Overlay, Huijun Dai, Hua Qu, and Jihong Zhao
Volume 2015, Article ID 126296, 6 pages

A New Recommendation Algorithm Based on User's Dynamic Information in Complex Social Network, Jiuju Cheng, Yingbo Liu, Huiting Zhang, Xiao Wu, and Fuzhen Chen
Volume 2015, Article ID 281629, 6 pages

A Reliability-Oriented Local-Area Model for Large-Scale Wireless Sensor Networks, Haixia Peng, Hai Zhao, Yuanguo Bi, Shuaizong Si, and Wei Cai
Volume 2015, Article ID 923692, 17 pages

Effective Semisupervised Community Detection Using Negative Information, Dong Liu, Dequan Duan, Shikai Sui, and Guojie Song
Volume 2015, Article ID 109671, 8 pages

Wiretap Channel with Rate-Limited Channel State Information, Xinxing Yin, Liang Pang, and Zhi Xue
Volume 2015, Article ID 643265, 10 pages

A Probabilistic Recommendation Method Inspired by Latent Dirichlet Allocation Model, WenBo Xie, Qiang Dong, and Hui Gao
Volume 2014, Article ID 979147, 10 pages

Node-Dependence-Based Dynamic Incentive Algorithm in Opportunistic Networks, Ruiyun Yu and Pengfei Wang
Volume 2014, Article ID 569129, 14 pages

A Virtual Machine Migration Strategy Based on Time Series Workload Prediction Using Cloud Model,

Yanbing Liu, Bo Gong, Congcong Xing, and Yi Jian

Volume 2014, Article ID 973069, 11 pages

Energy-Efficient Scheduling for Tasks with Deadline in Virtualized Environments, Guangyu Du,

Hong He, and Qinggang Meng

Volume 2014, Article ID 496843, 7 pages

The Regulatory Strategy in Emissions Trading System under Costly Enforcement, Shuai Jin,

Yanlin Zhang, and Zhaohan Sheng

Volume 2014, Article ID 487912, 10 pages

Pinning Synchronization of Linear Complex Coupling Synchronous Generators Network of Hydroelectric Generating Set, Xuefei Wu

Volume 2014, Article ID 476794, 6 pages

Stability and Passivity of Spatially and Temporally Complex Dynamical Networks with Time-Varying Delays, Shun-Yan Ren and Yue-Hui Zhao

Volume 2014, Article ID 412169, 8 pages

Stability of Delayed Hopfield Neural Networks with Variable-Time Impulses, Yangjun Pei, Chao Liu, and Qi Han

Volume 2014, Article ID 154036, 6 pages

Computational Experiment Study on Selection Mechanism of Project Delivery Method Based on Complex Factors, Xiang Ding, Zhaohan Sheng, Jianguo Du, and Qian Li

Volume 2014, Article ID 701652, 8 pages

Existence and Global Uniform Asymptotic Stability of Pseudo Almost Periodic Solutions for Cohen-Grossberg Neural Networks with Discrete and Distributed Delays,

Hongying Zhu and Chunhua Feng

Volume 2014, Article ID 968404, 10 pages

Consensus Analysis of High-Order Multiagent Systems with General Topology and Asymmetric Time-Delays, Fangcui Jiang

Volume 2014, Article ID 136205, 10 pages

Research on Appraisal System of Procurator Performance by Using High-Order CFA Model,

Yong-mao Huang

Volume 2014, Article ID 534304, 9 pages

Consensus of Multiagent Networks with Intermittent Interaction and Directed Topology, Li Xiao

Volume 2014, Article ID 676230, 6 pages

Chaotic Behaviors of Symbolic Dynamics about Rule 58 in Cellular Automata, Yangjun Pei, Qi Han, Chao Liu, Dedong Tang, and Junjian Huang

Volume 2014, Article ID 834268, 9 pages

Research of Innovation Diffusion on Industrial Networks, Yongtai Chen and Shouwei Li
Volume 2014, Article ID 629279, 7 pages

Terminal Sliding Mode Control with Adaptive Feedback Control in a Class of Chaotic Systems,
Degang Yang and Guoying Qiu
Volume 2014, Article ID 267024, 6 pages

CSA: A Credibility Search Algorithm Based on Different Query in Unstructured Peer-to-Peer Networks,
Hongyan Mei, Yujie Zhang, and Xiangwu Meng
Volume 2014, Article ID 197878, 20 pages

Control of the Fractional-Order Chen Chaotic System via Fractional-Order Scalar Controller and Its Circuit Implementation, Qiong Huang, Chunyang Dong, and Qianbin Chen
Volume 2014, Article ID 698507, 9 pages

Analysis on Passivity for Uncertain Neural Networks with Time-Varying Delays, O. M. Kwon, M. J. Park, Ju H. Park, S. M. Lee, and E. J. Cha
Volume 2014, Article ID 602828, 10 pages

A Hybrid Intelligent Algorithm for Optimal Birandom Portfolio Selection Problems, Qi Li, Guo-Hua Cao, and Dan Shan
Volume 2014, Article ID 213518, 6 pages

Energy Efficient Multiresource Allocation of Virtual Machine Based on PSO in Cloud Data Center,
An-ping Xiong and Chun-xiang Xu
Volume 2014, Article ID 816518, 8 pages


Stability and Bifurcation Analysis of a Modified Epidemic Model for Computer Viruses, Chuandong Li, Wenfeng Hu, and Tingwen Huang
Volume 2014, Article ID 784684, 14 pages

The Kirchhoff Index of Toroidal Meshes and Variant Networks, Jia-Bao Liu, Xiang-Feng Pan, Jinde Cao, and Xia Huang
Volume 2014, Article ID 286876, 8 pages

A Study of How the Watts-Strogatz Model Relates to an Economic System's Utility,
Lunhan Luo and Jianan Fang
Volume 2014, Article ID 693743, 7 pages

Combination-Combination Hyperchaos Synchronization of Complex Memristor Oscillator System,
Zhang Jin-E
Volume 2014, Article ID 591089, 13 pages

Study on Evolutionary Path of University Students' Entrepreneurship Training,
Daojian Yang and Xicang Zhao
Volume 2014, Article ID 535137, 11 pages



Sampled-Data Synchronization for Complex Dynamical Networks with Time-Varying Coupling Delay and Random Coupling Strengths, Jian-An Wang and Xin-Yu Wen

Volume 2014, Article ID 457457, 11 pages

Investigating Nonlinear Shoreline Multiperiod Change from Orthophoto Map Information by Using a Neural Network Model, Tienfuan Kerh, Hsienchang Lu, and Rob Saunders

Volume 2014, Article ID 782525, 9 pages

Stability Analysis of Pulse-Width-Modulated Feedback Systems with Time-Varying Delays,

Zhong Zhang, Huahui Han, Qiling Zhao, and Lixia Ye

Volume 2014, Article ID 686389, 7 pages

Modeling and Characteristic Study of Thin Film Based Biosensor Based on COMSOL, Yang Su

Volume 2014, Article ID 581063, 6 pages

Editorial

Theory and Applications of Complex Networks 2014

Tingwen Huang,¹ Qinggang Meng,² Zhichun Yang,³ Chuandong Li,⁴ He Huang,⁵ Jianguo Du,⁶ and Wei Zhang⁷

¹Science Program, Texas A&M University at Qatar, P.O. Box 23874, Doha, Qatar

²Department of Computer Science, Loughborough University, Loughborough, Leicestershire LE11 3TU, UK

³College of Mathematics Sciences, Chongqing Normal University, Chongqing, China

⁴School of Electronics and Information Engineering, Southwest University, Chongqing 400715, China

⁵School of Electronics and Information Engineering, Soochow University, Suzhou 215006, China

⁶School of Management, Jiangsu University, Zhenjiang 212013, China

⁷College of Computer Science, Chongqing University, Chongqing 400044, China

Correspondence should be addressed to Tingwen Huang; tingwen.huang@qatar.tamu.edu

Received 18 December 2014; Accepted 18 December 2014

Copyright © 2015 Tingwen Huang et al. This is an open access article distributed under the Creative Commons Attribution License, which permits unrestricted use, distribution, and reproduction in any medium, provided the original work is properly cited.

The purpose of this special issue is to track the latest process of mathematical and computational analysis, engineering and applications, and others. It is well known that mathematical and computational analysis as a hot topic will promote the development of society in different fields, such as complex networks, neural networks, evolution computation, and researches of optimization and algorithm. Therefore, it is meaningful to investigate the new theory, mythology, and method for the engineering and applications.

We receive many high-quality submissions that have been included in this special issue. These articles cover theoretical contributions and applications in project delivery method and energy-efficient scheduling. A brief summary of these articles is provided below.

Firstly, we are focused on mathematical and computational analysis of nonlinear dynamic networks. In the article “Passivity Analysis of Complex Delayed Dynamical Networks with Output Coupling” by Y.-F. Kang et al., constructing new Lyapunov functional, some sufficient conditions ensuring the input passivity and output passivity are obtained. H. Zhu and C. Feng studied existence and global uniform asymptotic stability of pseudo almost periodic solutions for Cohen-Grossberg neural networks with discrete and distributed delays. J.-E. Zhang investigated combination-combination hyperchaos synchronization of complex memristor oscillator system. T. Kerh et al. investigate nonlinear shoreline

multi-period change from orthophoto map information by using a neural networks model. C. Li et al. extend the three-dimensional SIR model to four-dimensional case and then analyze its dynamical behavior including stability and bifurcation. J.-A. Wang and X.-Y. Wen investigated sampled-data synchronization for complex dynamical networks with time-varying coupling delay and random coupling strengths.

Secondly, we are focused on engineering. The article “Energy-Efficient Scheduling for Tasks with Deadline in Virtualized Environments” by G. Du et al. proposed a novel scheduling algorithm for heterogeneous virtual machines in virtualized environments to effectively reduce energy consumption and finish all tasks before a deadline. They seek to implement an energy-efficient task scheduling algorithm for virtual machines with changeless speed comprising two main steps: assigning as many tasks as possible to virtual machines with lower energy consumption and keeping the makespan of each virtual machine within a deadline. In addition, the new scheduling strategy is simulated using the CloudSim toolkit package. Q. Huang et al. proposed a fractional-order scalar controller and its circuit implementation control for fractional-order Chen chaotic system. X. Wang et al. proposed to fit the multicast need of wireless mesh network based on the MAODV multicast routing protocol of ad hoc network, and a multicast routing protocol DT-MAODV (dynamic topology MAODV) is proposed.

C. Chen et al. proposed the resource allocation problem by the conception of Pareto optimization, a multiobjective optimization approach. C. Ren et al. studied the method of INS auxiliary based on neural network improving the dynamic characteristics of GPS carrier tracking loop. In the article “Computational Experiment Study on Selection Mechanism of Project Delivery Method Based on Complex Factors,” X. Ding et al. propose a new project delivery method by using the project owner (or project manager) for organizing design, construction, and other operations in a construction project.

The third section is focused on applications. D. Yang and X. Zhao aimed at studying the evolution pattern of cultivating the ability of university students’ entrepreneurship; this paper established the payoff matrix between the university and students agents with the evolutionary economics method. N. Shen et al. studied the influence of grinding conditions on resulting surface residual stresses in grinding titanium alloy TC4. In the article “Interactive High Quality Video Streaming via Coequal Support Video Transcoder,” S. Vetrivel and G. Athisha proposed a problem in video transcoding, which is by giving a target bit rate, to determine at spatial resolution. The spatial resolution, chronological resolution, and amplitude classically were proscribed by the quantization step size (QS) to code the video. Y. Li et al. built a model for present earning value of water treatment plants in planning periods, aiming at the influence of water supply radius on present earning value. In consideration of the influence on annual earnings of water treatment plants within planning periods caused by the investment in affiliated pipe network of water treatment plants, this paper adopts the methods of minimal spanning tree and Lagrange’s undetermined multiplier to optimize the pipe network within water supply areas of water treatment plants and then determines the head loss of the optimal pipe section and economical pipe diameter.

In summary, all of these papers presented recent developments, with a focus on mathematical and computational analysis, engineering and applications, information processing, modeling, and control using computational intelligence. These papers presented the latest researches in a coherent way. In this editorial, we artificially categorize them into the above to help readers to understand the organization of this special issue. We hope the reader will share our joy and find this special issue very useful.

*Tingwen Huang
Qinggang Meng
Zhichun Yang
Chuandong Li
He Huang
Jianguo Du
Wei Zhang*

Research Article

Identifying Super-Spreader Nodes in Complex Networks

Yu-Hsiang Fu,¹ Chung-Yuan Huang,² and Chuen-Tsai Sun¹

¹Department of Computer Science, National Chiao Tung University, 1001 Ta Hsueh Road, Hsinchu 300, Taiwan

²Department of Computer Science and Information Engineering, School of Electrical and Computer Engineering, College of Engineering, Chang Gung University, 259 Wen Hwa 1st Road, Taoyuan 333, Taiwan

Correspondence should be addressed to Chung-Yuan Huang; gscott@mail.cgu.edu.tw

Received 26 May 2014; Accepted 25 September 2014

Academic Editor: He Huang

Copyright © 2015 Yu-Hsiang Fu et al. This is an open access article distributed under the Creative Commons Attribution License, which permits unrestricted use, distribution, and reproduction in any medium, provided the original work is properly cited.

Identifying the most influential individuals spreading information or infectious diseases can assist or hinder information dissemination, product exposure, and contagious disease detection. Hub nodes, high betweenness nodes, high closeness nodes, and high k -shell nodes have been identified as good initial spreaders, but efforts to use node diversity within network structures to measure spreading ability are few. Here we describe a two-step framework that combines global diversity and local features to identify the most influential network nodes. Results from susceptible-infected-recovered epidemic simulations indicate that our proposed method performs well and stably in single initial spreader scenarios associated with various complex network datasets.

1. Introduction

Network-spreading studies range from information diffusion via online social media sites, to viral marketing, to epidemic disease identification and control, among many others [1–9]. Key spreader identification strategies are being established and tested to accelerate information dissemination, increase product exposure, detect contagious disease outbreaks, and execute early intervention strategies [10]. Topological structure is a core concept in this identification process [1, 2, 11–15].

Centrality measures for identifying influential social network nodes are broadly categorized as local or global [3, 7, 16]. Degree centrality (the number of nodes that a focal node is connected to) measures node involvement in a network. However, most network node researchers fail to consider global topological structures. Betweenness (which assesses the degree to which a node lies on the shortest path between two other nodes) and closeness (the inverse sum of the shortest distances from a focal node to all other nodes) are the two most widely used measures for overcoming these limitations. Influence is tied to advantageous network positions,

including high degree, high closeness, and high betweenness. In simple network structures, these advantages tend to vary; in complex networks, significant disjunctures can emerge among position characteristics, so that a spreader's location may be simultaneously advantageous and disadvantageous.

Results from k -shell decomposition analyses indicate that network nodes in core layers are capable of spreading throughout much broader areas compared to those in peripheral layers [1, 2]. Although spreading capability differs among nodes, those with similar k -shell values are perceived as having equal importance. To rank spreaders, a method called mixed degree decomposition adds otherwise ignored degree nodes to the decomposition process [3, 6, 8, 17]. Still, researchers have tended to overlook the importance of network topology and node diversity, despite their positive correlations with events such as community economic development [18].

We used the concept of entropy to develop a robust and reliable method for measuring the spreading capability of nodes and identifying super-spreader nodes in complex networks. It can be used to analyze numbers of global network topological layers and local neighborhood nodes

affected by specific individual nodes. Our assumption is that k -shell decomposition [1, 2] can be used for global analysis, with high global diversity/high local centrality nodes capable of penetrating multiple global layers and influencing large numbers of neighbors in local layers of complex networks.

To measure node influence, we propose a two-step framework for acquiring global and local node information within complex networks. Global node information is initially obtained using algorithms (e.g., a community detection algorithm for complex networks [5, 19, 20] or a k -shell decomposition algorithm for core/periphery network layers), after which entropy is used to evaluate network node global diversity. Next, local node information is acquired using various types of local centrality. Last, global diversity and local features are combined to determine node influence. In our experiments, spreading ability equaled the total number of recovered nodes over time. We used a susceptible-infective-recovered (SIR) epidemic simulation with various social network datasets [21–25] to compare the spreading capabilities of our proposed measure and social network local/global centralities [2, 26, 27].

2. Background

To represent a complex network, let an undirected graph $G = (V, E)$, where V is the network node set and E the edge set. $n = |V|$ indicates the number of network nodes and $m = |E|$ the number of edges. Network structure is represented as an adjacency matrix $A = \{a_{ij}\}$ and $a_{ij} \in R^n$, where $a_{ij} = 1$ if a link exists between nodes i and j , otherwise $a_{ij} = 0$.

Degree (or local) centrality is a simple yet effective method for measuring node influence in a complex network. Let $C_d(i)$ denote node i degree centrality. Higher values indicate larger numbers of connections between a node and its neighbors. $NB_h(i)$ denotes the set of node i neighbors at a h -hop distance. Node i degree centrality is therefore defined as

$$C_d(i) = |NB_h(i)| = \sum_{j=1}^n a_{ij}, \quad (1)$$

where $|NB_h(i)|$ is the number of node i neighbors at a h -hop distance; in most cases, $h = 1$ [7].

Betweenness centrality or dependency measures the proportion of shortest paths going through a node in a complex network. $C_b(i)$ denotes node i betweenness centrality. Higher values indicate that a complex network node is located along an important communication path. Accordingly, node i betweenness centrality is defined as

$$C_b(i) = \sum_{s \neq t \neq v \in V} \frac{Q_{st}(i)}{Q_{st}}, \quad (2)$$

where $Q_{st}(i)$ is the number of shortest paths from node s to node t through node i and Q_{st} is the total number of shortest paths from node s to node t [3, 7, 16].

Closeness (or global) centrality measures the average length of the shortest paths from one node to other nodes.

Let $C_l(i)$ denote node i closeness centrality. Higher values indicate node location in the center of a complex network, with a shorter average distance from that node to other nodes. Node i closeness centrality is thus defined as

$$C_l(i) = \frac{1}{l_i}, \quad l_i = \frac{1}{n} \cdot \sum_{j=1}^n d_{ij}, \quad (3)$$

where l_i is the average length of the shortest paths from node i to the other nodes and d_{ij} is the distance from node i to node j [16].

k -shell decomposition [1, 2] iteratively assigns k -shell layer values to all nodes in a complex network. During the first step, let $k = 1$ and remove all nodes where $C_d(n) = k = 1$. Following removal, some remaining network node degrees may be $k = 1$. Nodes are continuously pruned until there are no $k = 1$ nodes. All removed nodes are assigned a k -shell value of 1. The next step is similar: let $k = 2$, prune nodes, and assign a k -shell value of 2 to all removed nodes. Repeat the procedure until all network nodes are removed and assigned k -shell indexes. This method reveals the significant features of a complex network—for example, all Internet nodes can be classified as nuclei, peer-connected components, or isolated components [1].

The SIR epidemic model [2, 26, 27] is used in many fields to study the spreading processes of information, rumors, biological diseases, and other phenomena. The model consists of three states: susceptible (S), infective (I), and recovered (R). S nodes are susceptible to information or diseases, I nodes are capable of infecting neighbors, and R nodes are immune and cannot be reinfected. Initially, almost all network nodes are in the S set, with a small number of infected nodes acting as spreaders. During each time step, I nodes infect their neighbors at a preestablished infection rate, after which they become recovered nodes at a recovery rate of γ . The total number of nodes in an SIR model is $S(t) + I(t) + R(t) = n$, with $S(t)$ denoting the number of susceptible nodes at time t , $I(t)$ the number of infected nodes at time t , $R(t)$ the number of recovered nodes at time t , and $\rho(t) = R(t)/N$ the proportion of immune nodes.

3. The Proposed Measure

Our two-step method for obtaining global and local node information in a complex network is illustrated in the following steps. In step 1, global algorithms (e.g., community detection, graph clustering, and k -shell decomposition) are used to analyze the global features of nodes, and results are used to compute their global diversity. In step 2, degree centrality is used to measure local node features. Global diversity and local features are then combined to determine the influence of complex network nodes.

In step 1, k -shell decomposition was used as an example for obtaining global node information in a complex network, with Shannon's entropy [28] used to calculate node k -shell values and to determine how many network layers are affected by a node. According to (4), maximum entropy indicates a case in which a node is capable of connecting with all layers of a complex network, and minimum entropy

(0) indicates a case in which all node connections are in the same network layer. The k -shell entropy of node i , which ensures that its neighbors' k -shell values are significantly more diverse, is defined as

$$E_i(X_i) = - \sum_{j=1}^{ks_{\max}} p_i(x_j) \cdot \log_2 p_i(x_j), \quad (4)$$

$$p_i(x_j) = \frac{|x_j|}{\sum_{j=1}^{ks_{\max}} x_j}, \quad (5)$$

$$\hat{E}_i(X_i) = \frac{E_i(X_i)}{\log_2 ks_{\max}}, \quad (6)$$

where $X_i = \{1, 2, \dots, ks_{\max}\}$ are the k -shell values of the neighbors of node i , $p_i(x_j)$ the probability of the x_j -core layer of neighbors, $|x_j|$ the number of nodes in the x_j -core layer of the complex network, and $\hat{E}_i(X_i)$ the normalized k -core entropy required for the case under consideration.

In step 2, the node's degree centrality is used to analyze the value of local features in the complex network; the degree centralities of neighbors are also considered. High influence values indicate high degree centralities of a node and its neighbors, meaning that the node is capable of reaching the widest possible local range. The local feature of node i is defined as

$$L_i(i) = \log_2 \left(\sum_{j \in \text{NB}_{h=1}(i)} C_d(j) \right), \quad (7)$$

where $C_d(j)$ is the degree centrality of neighbor j and $\text{NB}_{h=1}(i)$ is the node i neighbor set at a h -hop distance. $L_i(i)$ can be extended to become a "neighbor's neighbor" version, meaning that all node i neighbors with a 2-hop distance are considered.

Finally, E_i and L_i are combined to denote IF_i , the final influence of node i , defined as

$$IF_i = E_i \cdot L_i. \quad (8)$$

4. Results and Discussion

Basic complex network properties and results from a network GCC structure analysis are shown in Table 1. We used three network dataset classifications: scientific collaboration, traditional social, and "other." Measures were degree, betweenness, and closeness centralities; k -shell decomposition; neighbor's core (also known as *coreness*) [29]; PageRank [30]; and our proposed method. Spreading experiment and SIR epidemic model parameters were 1,000 simulations for each dataset, 50 time steps per simulation, and with the top-1 node for each measure serving as the initial spreader. β infection rates are shown in Table 1. According to at least one study, a large infection rate makes no difference in terms of spreading measures [2]. To assign a suitable infection rate for each network dataset, rates were determined by comparing the theoretical epidemic threshold β_{thd} with the number used in referenced studies [29]. Recovery rate was always $\gamma = 1$,

meaning that every node in set I entered set R immediately after infecting its neighbors.

Experimental results and details are shown in Figure 1 and Table 2. We found that the leading group could be defined as the spreading result of measures that are larger than the maximum result minus an inaccuracy factor of 1%:

$$LG = \{m \mid p_m(t) \geq (p_{\max}(t) - \text{err} * p_{\max}(t)), \\ m \in M \text{ and } \text{err} \in [0, 1]\}, \quad (9)$$

where M is the set of measures used in the experiment, $p_{\max}(t)$ is the maximum result at time t , err is the inaccuracy rate (0.01), and time step $t = 50$.

The number of recovered nodes $\rho(t)$ was used to measure and rank the spreading capability of various measures. The leading group can help determine measure stability for identifying the influence of nodes in different networks. Measures inside the leading group had approximately the same spreading capability. The average rank shown in Table 2 was used to interpret the expected rank in different networks: a measure with a lower average rank was viewed as having better discrimination in terms of identifying good spreaders.

According to the inside leading group number (a measure stability indicator), our proposed method performed well in terms of identifying the most influential network nodes and thus is capable of identifying nodes that serve as good spreaders with global diversity in a complex network. In addition to being within the leading group, the method also had a better ranking compared to other measures within that group. The identified influence spreaders were capable of reaching large numbers of network nodes through their diverse global connections, of affecting network layers, and of exerting a maximum spreading effect. Our results also indicate that the degree centrality of a node and its neighbors can be used to maintain the number of contact nodes in the local layer of a complex network. However, important differences were noted among measures. For example, the closeness measure performed well in the top-1 position of the ca-HepTh and Email-Enron networks (Figure 1, Table 2), but not in the ca-GrQc, jazz_musician, or NetScience networks. Since the characteristic the measure wanted to capture may not have been sufficiently strong in those networks, the most influential spreaders could not be identified.

Although our proposed method underscores the robustness and stability of identifying the most influential nodes, we acknowledge two limitations. First, in cases of global node diversity and lower node degree centrality, the spreading capability of nodes is constrained and dependent on the degree centrality of their neighbors. The influence of a node is limited to the local layer of a complex network when the degree centrality of its neighbors is lower. The spreading range is also limited when a node's connected neighbors are located in the network's peripheral layer. However, the spreading range of nodes may be wide when the node's neighbors are located near the hub and within the core network layers and when information and ideas can still be spread to infect a large number of nodes throughout the network.

TABLE 1: Properties of the real-world networks used in this project. We considered only the largest connected network components when the original network was disconnected.

Network type	Network	Description	N	E	$\langle c \rangle$	k_{\max}	$\langle k \rangle$	$k_{S_{\max}}$	$\langle ks \rangle$	H	r	β_{thd}	β
Collaboration	ca-AstroPh	Coauthorship in astro-ph of arxiv.org.	17903	196972	0.63	504	22.00	56	13.11	2.99	0.20	0.02	0.02
	ca-CondMat	Coauthorship in cond-mat category.	21363	91286	0.64	279	8.55	25	5.12	2.63	0.13	0.04	0.05
	ca-GrQc	Coauthorship in gr-qc category.	4158	13422	0.56	81	6.46	43	4.58	2.79	0.64	0.06	0.15
	ca-HepPh	Coauthorship in hep-ph category.	11204	117619	0.62	491	21.00	238	15.93	6.23	0.63	0.01	0.05
	ca-HepTh	Coauthorship in hep-th category.	8638	24806	0.48	65	5.74	31	3.41	2.26	0.24	0.08	0.12
Social	Jazz-Musicians	Collaborations among 1920's jazz musicians.	198	2742	0.62	100	27.70	29	17.27	1.40	0.02	0.03	0.04
	Email-Contacts	Email contacts in the Computer Science Department of the University College, London.	12625	20362	0.11	576	3.23	23	1.65	34.25	-0.39	0.01	0.05
	Email-Enron	Enron email dataset.	33696	180811	0.51	1383	10.73	43	5.73	13.27	-0.12	0.01	0.05
	CelegansNeural	Neural network of the C. Elegans nematode.	297	2148	0.29	134	14.46	10	7.98	1.80	-0.16	0.04	0.06
Other	Dolphins	Frequent associations between 62 Dolphins.	62	159	0.26	12	5.13	4	3.16	1.33	-0.04	0.15	0.15
	LesMis	Les miserables network.	77	254	0.57	36	6.60	9	4.73	1.83	-0.17	0.08	0.08
	NetScience	Network science collaborations.	379	914	0.74	34	4.82	8	3.47	1.66	-0.08	0.12	0.20
	PolBlogs	Political blogs.	1222	16714	0.32	351	27.36	36	14.82	2.97	-0.22	0.01	0.02

 $H = \langle k^2 \rangle / \langle k \rangle^2$, degree heterogeneity [32].

 $\beta_{\text{thd}} = \langle k \rangle / \langle k^2 \rangle$, theoretical epidemic threshold [33].

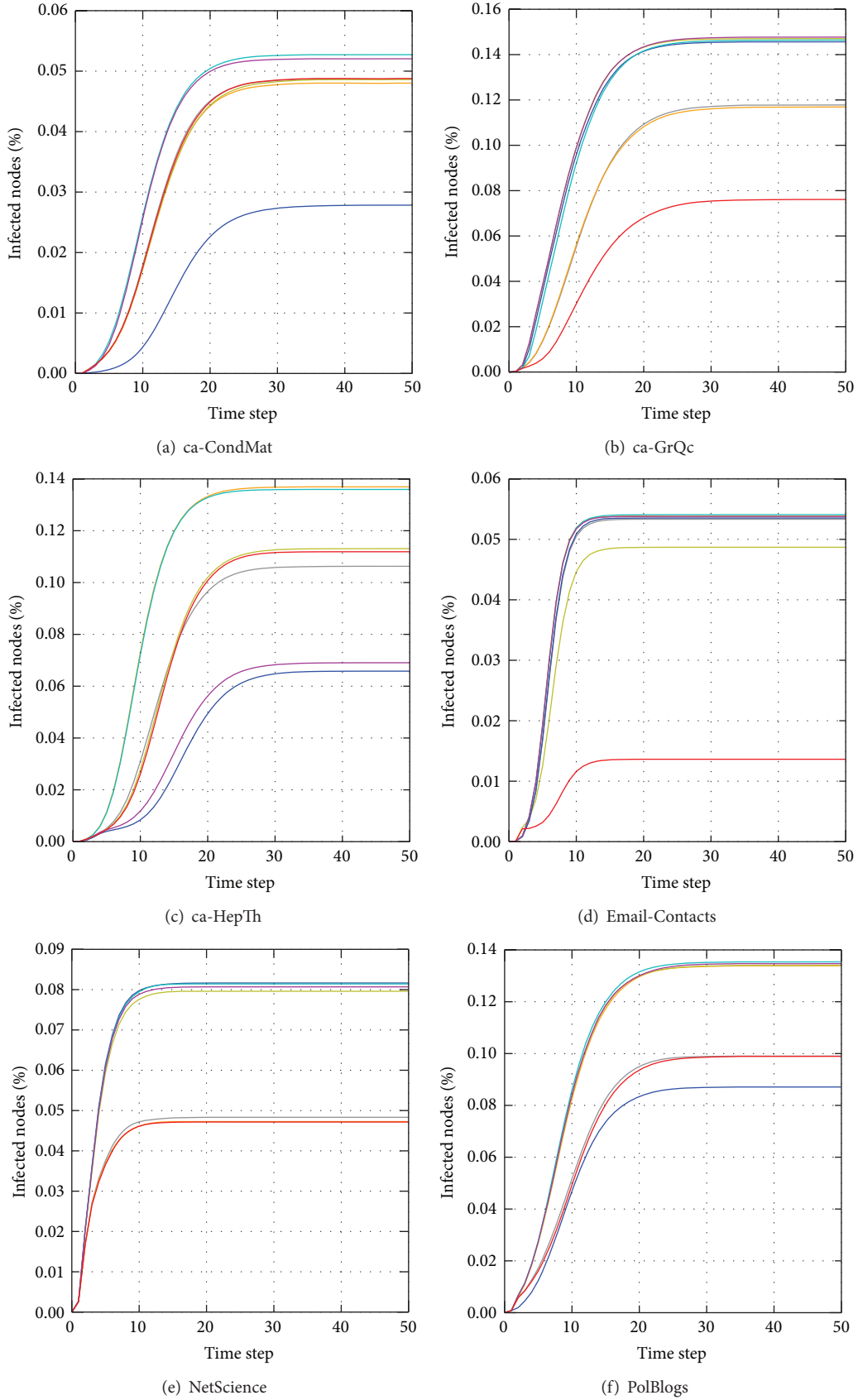


FIGURE 1: Spreading dynamic results for different networks. Measurements shown are betweenness (gray), closeness (orange), degree (yellow), k -core (blue), proposed method (cyan), neighbor-core (magenta) and PageRank (red).

TABLE 2: Comparison of simulation results from different measures (including our proposed method) in experiments using the real-world networks shown in Table 1.

Network name	$\rho(t)$ and $t = 50$					
Giant connected component (GCC)	Degree	Betweenness	Closeness	k-core	Neighbor-core	PageRank
ca-AstroPh	0.1521 ₃	0.1499 ₅	0.1521 ₃	0.1205 ₇	0.1522 ₂	0.1523 ₁
ca-CondMat*	0.0486 ₅	0.0487 ₄	0.0480 ₆	0.0278 ₇	0.0520 ₂	0.0488 ₃
ca-GrQc*	0.1471 ₂	0.1178 ₅	0.1169 ₆	0.1456 ₄	0.1477 ₁	0.0761 ₇
ca-HepPh	0.1953 ₁	0.1940 ₇	0.1952 ₂	0.1951 ₃	0.1950 ₅	0.1951 ₃
ca-HepTh*	0.1131 ₃	0.1063 ₅	0.1369 ₁	0.0658 ₇	0.0690 ₆	0.1119 ₄
Jazz-Musicians	0.3037 ₅	0.3050 ₄	0.3014 ₆	0.2191 ₇	0.3149 ₁	0.3055 ₃
Email-Contacts*	0.0487 ₆	0.0533 ₅	0.0538 ₂	0.0535 ₄	0.0538 ₂	0.0136 ₇
Email-Enron	0.1011 ₅	0.1009 ₆	0.1620 ₁	0.1618 ₄	0.1620 ₁	0.1003 ₇
CelegansNeural	0.1939 ₃	0.1919 ₅	0.1911 ₆	0.0644 ₇	0.1926 ₄	0.2011 ₁
Dolphins	0.1107 ₁	0.0754 ₆	0.0795 ₅	0.0702 ₇	0.1019 ₃	0.1089 ₂
LesMis	0.0885 ₄	0.0890 ₃	0.0893 ₂	0.0792 ₆	0.0753 ₇	0.0878 ₅
NetScience*	0.0796 ₄	0.0483 ₅	0.0473 ₆	0.0816 ₁	0.0807 ₃	0.0472 ₇
PolBlogs*	0.1340 ₃	0.0990 ₅	0.1339 ₄	0.0871 ₇	0.1347 ₂	0.0989 ₆
Inside leading group number:	9	7	9	5	11	7
Average rank:	3.4615	5.0000	3.8461	5.4615	3.0	4.6923
						12
						2.6153

* Network result shown in Figure 1.

Bold: measurement result is inside the leading network group.

Subscript: rank of network in the measurement.

Second, maximum k -shell values are lower and network sizes are considerably smaller in the absence of global diversity in a complex network. As shown in Table 2, nodes with high global diversity in the Dolphins network could not be identified. In that case, the spreading ability of nodes identified by our proposed method decreased to the degree centrality (ignoring the first term), and the influence of nodes was limited to local network layers. In the absence of global diversity, (8) becomes $IF_i \approx L_i$, which favors local network layers (i.e., degree centrality). The spreading ranges of nodes were also limited to local network layers when nodes were located in peripheral layers or inside local and dense clusters. However, broad spreading ranges were observed for nodes located in the network's core layers [2]. In addition, the $\hat{E}_i(X_i)$ normalized global diversity values produced by our proposed method are similar to the participation coefficients reported by Teitelbaum et al. [31], and the high global diversity values of nodes that we observed are similar to those of connector hubs and kinless hubs, both of which have distinct participation coefficients.

5. Conclusion

Our plans are to add considerable detail to our analysis, to introduce a sophisticated method for evaluating spreading ability, and to clarify how the proposed method is affected by network structure. For example, global algorithms such as community detection algorithms can be used to analyze and obtain global information on community network structures and to determine how factors such as position and node role [31] affect the degree to which spreaders distribute information or diseases throughout a complex network. We also plan to study strategies associated with multiple initial spreaders in networks. Since overlapping infected areas for selected spreaders must be minimized [2], a multiple initial spreader scenario may either accelerate or hinder spreading within a complex network.

Conflict of Interests

The authors declare that there is no conflict of interests regarding the publication of this paper.

Acknowledgments

The work was supported in part by a Grant from the Republic of China National Science Council (MOST-103-2221-E-182-052). The work was supported in part by the High Speed Intelligent Communication (HSIC) Research Center, Chang Gung University, Taiwan.

References

- [1] S. Carmi, S. Havlin, S. Kirkpatrick, Y. Shavitt, and E. Shir, "A model of Internet topology using k -shell decomposition," *Proceedings of the National Academy of Sciences of the United States of America*, vol. 104, no. 27, pp. 11150–11154, 2007.
- [2] M. Kitsak, L. K. Gallos, S. Havlin et al., "Identification of influential spreaders in complex networks," *Nature Physics*, vol. 6, no. 11, pp. 888–893, 2010.
- [3] B. Hou, Y. Yao, and D. Liao, "Identifying all-around nodes for spreading dynamics in complex networks," *Physica A: Statistical Mechanics and its Applications*, vol. 391, no. 15, pp. 4012–4017, 2012.
- [4] D. Chen, L. Lü, M.-S. Shang, Y.-C. Zhang, and T. Zhou, "Identifying influential nodes in complex networks," *Physica A: Statistical Mechanics and its Applications*, vol. 391, no. 4, pp. 1777–1787, 2012.
- [5] X. Zhang, J. Zhu, Q. Wang, and H. Zhao, "Identifying influential nodes in complex networks with community structure," *Knowledge-Based Systems*, vol. 42, pp. 74–84, 2013.
- [6] A. Zeng and C.-J. Zhang, "Ranking spreaders by decomposing complex networks," *Physics Letters, Section A: General, Atomic and Solid State Physics*, vol. 377, no. 14, pp. 1031–1035, 2013.
- [7] S. Gao, J. Ma, Z. Chen, G. Wang, and C. Xing, "Ranking the spreading ability of nodes in complex networks based on local structure," *Physica A: Statistical Mechanics and its Applications*, vol. 403, pp. 130–147, 2014.
- [8] J.-G. Liu, Z.-M. Ren, and Q. Guo, "Ranking the spreading influence in complex networks," *Physica A: Statistical Mechanics and Its Applications*, vol. 392, no. 18, pp. 4154–4159, 2013.
- [9] B. Doerr, M. Fouz, and T. Friedrich, "Why rumors spread so quickly in social networks," *Communications of the ACM*, vol. 55, no. 6, pp. 70–75, 2012.
- [10] N. A. Christakis and J. H. Fowler, "Social network sensors for early detection of contagious outbreaks," *PLoS ONE*, vol. 5, no. 9, Article ID e12948, 2010.
- [11] J.-L. Wang and H.-N. Wu, "Local and global exponential output synchronization of complex delayed dynamical networks," *Nonlinear Dynamics*, vol. 67, no. 1, pp. 497–504, 2012.
- [12] J.-L. Wang and H.-N. Wu, "Adaptive output synchronization of complex delayed dynamical networks with output coupling," *Neurocomputing*, vol. 142, pp. 174–181, 2014.
- [13] J.-L. Wang and H.-N. Wu, "Synchronization criteria for impulsive complex dynamical networks with time-varying delay," *Nonlinear Dynamics*, vol. 70, no. 1, pp. 13–24, 2012.
- [14] J. Wang, Z. Yang, T. Huang, and M. Xiao, "Synchronization criteria in complex dynamical networks with nonsymmetric coupling and multiple time-varying delays," *Applicable Analysis*, vol. 91, no. 5, pp. 923–935, 2012.
- [15] J.-L. Wang, Z.-C. Yang, T. W. Huang, and M. Q. Xiao, "Local and global exponential synchronization of complex delayed dynamical networks with general topology," *Discrete and Continuous Dynamical Systems Series B*, vol. 16, no. 1, pp. 393–408, 2011.
- [16] M. E. Newman, *Networks: An Introduction*, Oxford University Press, Oxford, UK, 2010.
- [17] M. G. Kendall, "A new measure of rank correlation," *Biometrika*, vol. 30, no. 1-2, pp. 81–93, 1938.
- [18] N. Eagle, M. Macy, and R. Claxton, "Network diversity and economic development," *Science*, vol. 328, no. 5981, pp. 1029–1031, 2010.
- [19] M. Rosvall and C. T. Bergstrom, "An information-theoretic framework for resolving community structure in complex networks," *Proceedings of the National Academy of Sciences of the United States of America*, vol. 104, no. 18, pp. 7327–7331, 2007.
- [20] M. Girvan and M. E. Newman, "Community structure in social and biological networks," *Proceedings of the National Academy*

of Sciences of the United States of America, vol. 99, no. 12, pp. 7821–7826, 2002.

- [21] Stanford large network dataset collection, <http://snap.stanford.edu/>.
- [22] *Network Datasets Collected by Mark Newman*, <http://www-personal.umich.edu/~mejn/netdata/>.
- [23] Network datasets collected by Hernán Alejandro Makse, http://lisgil.engr.cuny.cuny.edu/~makse/soft_data.html.
- [24] *Jazz Musicians Network Dataset*, http://curtis.ml.cmu.edu/w/courses/index.php/Jazz_musicians_network.
- [25] P. Basaras, D. Katsaros, and L. Tassiulas, “Detecting influential spreaders in complex, dynamic networks,” *Computer*, vol. 46, no. 4, pp. 24–29, 2013.
- [26] R. Pastor-Satorras and A. Vespignani, “Epidemic dynamics and endemic states in complex networks,” *Physical Review E*, vol. 63, no. 6, Article ID 066117, 2001.
- [27] C.-Y. Huang, C.-L. Lee, T.-H. Wen, and C.-T. Sun, “A computer virus spreading model based on resource limitations and interaction costs,” *Journal of Systems and Software*, vol. 86, no. 3, pp. 801–808, 2013.
- [28] C. E. Shannon, “A mathematical theory of communication,” *The Bell System Technical Journal*, vol. 27, no. 3, pp. 379–423, 1948.
- [29] J. Bae and S. Kim, “Identifying and ranking influential spreaders in complex networks by neighborhood coreness,” *Physica A: Statistical Mechanics and its Applications*, vol. 395, pp. 549–559, 2014.
- [30] L. Page, S. Brin, R. Motwani, and T. Winograd, “The PageRank citation ranking: bringing order to the web,” Tech. Rep., Stanford InfoLab, 1999.
- [31] T. Teitelbaum, P. Balenzuela, P. Cano, and J. M. Buldú, “Community structures and role detection in music networks,” *Chaos*, vol. 18, no. 4, Article ID 043105, 2008.
- [32] H.-B. Hu and X.-F. Wang, “Unified index to quantifying heterogeneity of complex networks,” *Physica A: Statistical Mechanics and its Applications*, vol. 387, no. 14, pp. 3769–3780, 2008.
- [33] C. Castellano and R. Pastor-Satorras, “Thresholds for epidemic spreading in networks,” *Physical Review Letters*, vol. 105, no. 21, Article ID 218701, 2010.

Research Article

Analysis on Global Asymptotical Stability of Genetic Regulatory Networks with Time-Varying Delays via Convex Combination Method

Yang Liu¹ and Haixia Wu^{2,3}

¹Department of Computer Engineering, Sichuan Vocational and Technical College of Communications, Chengdu 611130, China

²College of Automation, Chongqing University, Chongqing 400044, China

³Department of Mathematics and Information Engineering, Chongqing University of Education, Chongqing 400065, China

Correspondence should be addressed to Yang Liu; cqliuyang@163.com

Received 7 June 2014; Accepted 22 July 2014

Academic Editor: Chuandong Li

Copyright © 2015 Y. Liu and H. Wu. This is an open access article distributed under the Creative Commons Attribution License, which permits unrestricted use, distribution, and reproduction in any medium, provided the original work is properly cited.

The global asymptotical stability analysis for genetic regulatory networks with time delays is concerned. By using Lyapunov functional theorem, LMIs, and convex combination method, a new delay-dependent stability criterion has been presented in terms of LMIs to guarantee the delayed genetic regulatory networks to be asymptotically stable. The restriction that the derivatives of the time-varying delays are less than one is removed. Our result is applicable to both fast and slow time-varying delays. The stability criterion has less conservative and wider application range. Experimental result has been used to demonstrate the usefulness of the main results and less conservativeness of the proposed method.

1. Introduction

Genetic regulatory networks (GRNs) play a key role in systems biology as they explain the interactions between genes (mRNA) and proteins. In a biological cell, genes may be expressed constantly (i.e., constitutive gene expression) or expressed based on molecular signals (i.e., regulated gene expression) [1–3]. The central dogma of molecular biology states that gene expression consists of two main processes, namely, transcription and translation for prokaryotes, and with the additional step of ribonucleic acid (RNA) splicing for eukaryotes. In the transcriptional process, messenger RNAs (mRNAs) are synthesized from genes by the regulations of transcript factors, which are proteins. In the translational process, the sequence of nucleotides in the mRNA is used in the synthesis of a protein. A genetic regulatory network (GRN) is a nonlinear dynamical system which describes the highly complex interactions between mRNAs and proteins—two main genetic products produced in the transcriptional and translational processes. Nowadays, in systems biology, one of the main challenges is to understand the genetic regulatory networks, for example, how biological activities

are governed by the connectivity of genes and proteins. The study of the nature and functions of GRN has already aroused the interest of many researchers.

Since 1960s, many notable researchers have proposed various kinds of mathematical models to describe GRN. So far, during the past few years, there are two basic models for genetic network models: the Boolean model and the differential equation model [2, 3]. In Boolean models, the expression of each gene in the network is assumed to be either ON or OFF, no “intermediate” activity levels are ever taken into consideration, and the state of a gene is determined by a Boolean function of the states of other related genes. The differential equation model describes the rates of change of the concentrations of gene products, such as mRNAs and proteins, as continuous values. The differential equation model is often preferred over the Boolean model because its accuracy is more secured. In practical biological model, gene expression rates are usually continuous variables rather than ideal ON-OFF switches. Several typical genetic regulatory networks have been modelled and studied experimentally and/or theoretically; see [4–6] for some recent results.

On the other hand, time delays which usually exist in transcription, translation, diffusion, and translocation processes especially in a eukaryotic cell are one of the key factors affecting the dynamics of genetic regulatory network. The delays could be time invariant or time variant. The study of stability is essential for designing or controlling genetic regulatory networks. Up to now, there are already some sufficient conditions that have been proposed to guarantee the asymptotic or robust stability for genetic regulatory networks [7–20].

Motivated by the above discussions, we aim to analyze the stability of genetic regulatory networks with SUM logic in the forms of differential equations. Besides the basic case, we will make contributions on the issues of asymptotical stability for genetic networks with time-varying delays. By choosing an appropriate new Lyapunov functional and employing convex combination method, new delay-derivative-dependent stability criterion is derived based on the consideration of ranges for the time-varying delays. The obtained criterion is given in terms of linear matrix inequalities (LMIs) and is applicable to both fast and slow time-varying delays. Finally, one numerical example is given to demonstrate the effectiveness and the merit of the proposed method.

2. Problem Description and Preliminaries

In [8, 9], the following differential equations have been used to describe GRNs containing n mRNAs and n proteins:

$$\begin{aligned}\dot{m}(t) &= -Am(t) + Wg(p(t - \sigma(t))) + U, \\ \dot{p}(t) &= -Cp(t) + Dm(t - \tau(t)),\end{aligned}\quad (1)$$

where $m(t) = [m_1(t), m_2(t), \dots, m_n(t)]^T$, $p(t) = [p_1(t), p_2(t), \dots, p_n(t)]^T$, and $\dot{p}(t)$ are the concentrations of mRNA and protein of the i th node at time t , respectively; $A = \text{diag}\{a_1, a_2, \dots, a_n\}$ and $C = \text{diag}\{c_1, c_2, \dots, c_n\}$ denote the degradation or dilution rates of mRNAs and proteins; $D = \text{diag}\{d_1, d_2, \dots, d_n\}$ and $W = (w_{ij}) \in \mathbb{R}^{n \times n}$ are the coupling matrices, and W is defined as follows:

$$w_{ij} = \begin{cases} \bar{w}_{ij} & \text{if transcription factor } j \text{ is an activator of gene } i, \\ 0 & \text{if there is no link from node } j \text{ to } i, \\ -\bar{w}_{ij} & \text{if transcription factor } j \text{ is a repressor of gene } i. \end{cases}\quad (2)$$

Furthermore, nonlinear function $g(\cdot) \in \mathbb{R}^n$ represents the feedback regulation of the protein on the transcription, which is the monotonic function in Hill form, $g_j(x) = x^{H_j}/(1+x^{H_j})$, H is the Hill coefficient, and $\tau(t)$ and $\sigma(t)$ are the time-varying delays satisfying $0 \leq \tau(t) \leq \tau$, $0 \leq \sigma(t) \leq \sigma$, respectively; $U = [u_1, u_2, \dots, u_n]^T$, where $u_i = \sum_{j \in u_i} \bar{w}_{ij}$ and u_i is the set of all j nodes which are repressors of gene i .

In the following, we will always shift an intended equilibrium point (m^*, p^*) of the system (1) to the origin by letting

$x(t) = m(t) - m^*$, $y(t) = p(t) - p^*$. Hence, system (1) can be transformed into the following form:

$$\begin{aligned}\dot{x}(t) &= -Ax(t) + Wf(y(t - \sigma(t))), \\ \dot{y}(t) &= -Cy(t) + Dx(t - \tau(t)),\end{aligned}\quad (3)$$

where $f(y(t)) = g(y(t) + p^*) - g(p^*)$. Since g_i is a monotonically increasing function with saturation, it satisfies, for all, $x, y \in \mathbb{R}$ with $x \neq y$ and $0 \leq (g_i(x) - g_i(y))/(x - y) \leq k_i$. From the relationship of $f(\cdot)$ and $g(\cdot)$, we know that $f(\cdot)$ satisfies the sector condition

$$0 \leq \frac{f_i(x)}{x} \leq k_i. \quad (4)$$

Lemma 1 (Schur complement). *Given constant symmetric matrices Σ_1 , Σ_2 , and Σ_3 , where $\Sigma_1 = \Sigma_1^T$ and $0 < \Sigma_2 = \Sigma_2^T$, then $\Sigma_1 + \Sigma_3 \Sigma_2^{-1} \Sigma_3 < 0$ if and only if*

$$\begin{bmatrix} \sum_1 & \sum_3 \\ \sum_3^T & -\sum_2 \end{bmatrix} < 0, \quad \text{or} \quad \begin{bmatrix} -\sum_2 & \sum_3 \\ \sum_3^T & \sum_1 \end{bmatrix} < 0. \quad (5)$$

3. Main Result

Theorem 2. *For given scalars $0 < \tau$, $0 < \sigma$, μ , and d , system (1) is asymptotically stable, if there exist matrices $P_k = P_k^T \geq 0$, $k = 1, 2$, $Q_r = Q_r^T \geq 0$, $r = 1, 2$, $Z_j = Z_j^T > 0$, $j = 1, 2$, $R_i = R_i^T \geq 0$, $i = 1, 2, 3$, $\Lambda = \text{diag}\{\lambda_1, \lambda_2, \dots, \lambda_n\} \geq 0$, $T_j = \text{diag}\{t_{1j}, t_{2j}, \dots, t_{nj}\} \geq 0$, $j = 1, 2$, N_i, M_i, S_i, U_i , $i = 1, 2, \dots, 8$, such that the following LMIs (6) hold:*

$$\begin{aligned}& \begin{bmatrix} Y & \tau M & \sigma S \\ * & -\tau Z_1 & 0 \\ * & * & -\sigma Z_2 \end{bmatrix} < 0, \\ & \begin{bmatrix} Y & \tau M & \sigma U \\ * & -\tau Z_1 & 0 \\ * & * & -\sigma Z_2 \end{bmatrix} < 0, \\ & \begin{bmatrix} Y & \tau N & \sigma S \\ * & -\tau Z_1 & 0 \\ * & * & -\sigma Z_2 \end{bmatrix} < 0, \\ & \begin{bmatrix} Y & \tau N & \sigma U \\ * & -\tau Z_1 & 0 \\ * & * & -\sigma Z_2 \end{bmatrix} < 0,\end{aligned}\quad (6)$$

with

$$Y = \begin{bmatrix} Y_{11} & Y_{12} & Y_{13} & S_1 + M_4 & Y_{15} & -U_1 + M_6 & M_7 & P_1 W + M_8 \\ * & Y_{22} & Y_{23} & Y_{24} & Y_{25} & Y_{26} & Y_{27} & -M_8 + N_8 \\ * & * & Y_{33} & S_3 - N_4 & Y_{35} & -U_3 - N_6 & -N_7 & -N_8 \\ * & * & * & Y_{44} & Y_{45} & -U_4 + S_6 & Y_{47} & S_8 \\ * & * & * & * & Y_{55} & Y_{56} & Y_{57} & Y_{58} \\ * & * & * & * & * & Y_{66} & -U_7 & -U_8 \\ * & * & * & * & * & * & Y_{77} & 0 \\ * & * & * & * & * & * & * & Y_{88} \end{bmatrix} < 0,$$

$$Y_{11} = -P_1 A - A^T P_1 + Q_1 + Q_2 + 2M_1,$$

$$Y_{12} = N_1 - M_1 + M_2, \quad Y_{13} = -N_1 + M_3,$$

$$Y_{15} = U_1 + M_5,$$

$$Y_{22} = -(1 - \mu) Q_2 + N_2 + N_2^T - M_2 - M_2^T,$$

$$Y_{23} = -N_2 + N_3 - M_3, \quad Y_{24} = S_2 + P_2 D - M_4,$$

$$Y_{25} = U_2 - S_2 - M_5 + N_5, \quad Y_{26} = U_2 - M_6 + N_6,$$

$$Y_{27} = -M_7 + \Lambda D + N_7, \quad Y_{35} = U_3 - S_3 - N_5,$$

$$Y_{33} = -Q_1 - M_3 - M_3^T,$$

$$Y_{44} = -P_1 C - C^T P_1 + R_1 + R_2, \quad Y_{45} = U_4 - S_4 + S_5,$$

$$Y_{47} = K T_1 - \Lambda C + S_7,$$

$$Y_{55} = -(1 - d) R_2 + U_5 + U_5^T - S_5 - S_5^T,$$

$$Y_{56} = -U_5 + U_6 - S_6 - N_6,$$

$$Y_{57} = U_7 - S_7 - N_7, \quad Y_{77} = R_3 - 2T_1,$$

$$Y_{58} = K T_2 + U_8 - S_8,$$

$$Y_{66} = R_1 - U_6 - U_6^T, \quad Y_{88} = -(1 - d) R_3 - 2T_2. \quad (7)$$

Proof. The Lyapunov functional of system (1) is defined by

$$V(t) = V_1(t) + V_2(t) + V_3(t) + V_4(t),$$

$$V_1(t) = x^T(t) P_1 x(t) + y^T(t) P_2 y(t) + 2 \sum_{i=1}^n \lambda_i \int_0^{y_i} f_i(s) ds,$$

$$V_2(t) = \int_{t-\tau}^t x^T(s) Q_1 x(s) ds + \int_{t-\sigma}^t y^T(s) R_1 y(s) ds,$$

$$V_3(t) = \int_{t-\tau(t)}^t x^T(s) Q_2 x(s) ds + \int_{t-\sigma(t)}^t [y^T(s) R_2 y(s) + f^T(y(s)) R_3 f(y(s))] ds,$$

$$V_4(t) = \int_{-\tau}^0 \int_{t+\theta}^t \dot{x}^T(s) Z_1 \dot{x}(s) ds d\theta + \int_{-\sigma}^0 \int_{t+\theta}^t \dot{y}^T(s) Z_2 \dot{y}(s) ds d\theta. \quad (8)$$

Calculating the derivative of $V(t)$ along the solutions of system (1), one can get

$$\begin{aligned} \dot{V}_1(t) &= 2x^T(t) P_1 [-Ax(t) + Wf(y(t - \sigma(t)))] \\ &\quad + 2y^T(t) P_2 [-Cy(t) + Dx(t - \tau(t))] \\ &\quad + 2f^T(y(t)) \Lambda [-Cy(t) + Dx(t - \tau(t))], \end{aligned} \quad (9)$$

$$\begin{aligned} \dot{V}_2(t) &= x^T(t) Q_1 x(t) - x^T(t - \tau) Q_1 x(t - \tau) \\ &\quad + y^T(t) R_1 y(t) - y^T(t - \sigma) R_1 y(t - \sigma), \end{aligned} \quad (10)$$

$$\begin{aligned} \dot{V}_3(t) &= x^T(t) Q_2 x(t) - (1 - \mu) x^T(t - \tau(t)) \\ &\quad \times Q_2 x(t - \tau(t)) + y^T(t) R_2 y(t) \\ &\quad - (1 - d) y^T(t - \sigma(t)) R_2 y(t - \sigma(t)) \\ &\quad + f^T(y(t)) R_3 f(y(t)) \\ &\quad - (1 - d) f^T(y(t - \sigma(t))) R_3 f(y(t - \sigma(t))), \end{aligned} \quad (11)$$

$$\begin{aligned} \dot{V}_4(t) &= \dot{x}^T(t) \tau Z_1 \dot{x}(t) - \int_{t-\tau}^t \dot{x}^T(s) Z_1 \dot{x}(s) ds \\ &\quad + \dot{y}^T(t) \sigma Z_2 \dot{y}(t) - \int_{t-\sigma}^t \dot{y}^T(s) Z_2 \dot{y}(s) ds \\ &= \dot{x}^T(t) h_2 Z_1 \dot{x}(t) - \int_{t-\tau}^{t-\tau(t)} \dot{x}^T(s) Z_1 \dot{x}(s) ds \\ &\quad - \int_{t-\tau(t)}^t \dot{x}^T(s) Z_1 \dot{x}(s) ds \\ &\quad + \dot{y}^T(t) \sigma Z_3 \dot{y}(t) - \int_{t-\sigma}^{t-\sigma(t)} \dot{y}^T(s) Z_2 \dot{y}(s) ds \\ &\quad - \int_{t-\sigma(t)}^t \dot{y}^T(s) Z_2 \dot{y}(s) ds. \end{aligned} \quad (12)$$

From the Leibniz-Newton formula, the following equations are true for any matrices $N_i, M_i, U_i, S_i, i = 1, 2, \dots, 8$ with appropriate dimensions:

$$0 = 2\xi(t)^T N \left[x(t - \tau(t)) - x(t - \tau_2) - \int_{t-\tau}^{t-\tau(t)} \dot{x}(s) ds \right], \quad (13)$$

$$0 = 2\xi(t)^T M \left[x(t) - x(t - \tau(t)) - \int_{t-\tau(t)}^t \dot{x}(s) ds \right], \quad (14)$$

$$0 = 2\xi(t)^T U \left[y(t - \sigma(t)) - y(t - \sigma_2) - \int_{t-\sigma}^{t-\sigma(t)} \dot{y}(s) ds \right], \quad (15)$$

$$0 = 2\xi(t)^T S \left[y(t) - y(t - \sigma(t)) - \int_{t-\sigma(t)}^t \dot{y}(s) ds \right], \quad (16)$$

with $\xi(t) = [\xi_1^T(t) \ \xi_2^T(t)]^T$,

$$\begin{aligned} \xi_2^T(t) &= [y^T(t) \ y^T(t-\sigma(t)) \ y^T(t-\sigma) \ f^T(y(t)) \ f^T(y(t-\sigma(t)))]^T. \end{aligned} \quad (17)$$

In addition, from (4), we have $f_i(y_i(t)) \cdot [f_i(y_i(t)) - k_i y_i(t)] \leq 0$, $i = 1, 2, \dots, n$ and $f_i(y_i(t-\sigma(t))) \cdot [f_i(y_i(t-\sigma(t))) - k_i y_i(t-\sigma(t))] \leq 0$, $i = 1, 2, \dots, n$. Thus, for any $T_j = \text{diag}\{t_{1j}, t_{2j}, \dots, t_{nj}\} \geq 0$, $j = 1, 2$, it follows that

$$\begin{aligned} 0 &\leq -2 \sum_{i=1}^n t_{i1} f_i(y_i(t)) [f_i(y_i(t)) - k_i y_i(t)] \\ &\quad - 2 \sum_{i=1}^n t_{i2} f_i(y_i(t-\sigma(t))) \\ &\quad \times [f_i(y_i(t-\sigma(t))) - k_i y_i(t-\sigma(t))] \\ &= -2 f^T(y(t)) T_1 f(y(t)) + 2 y^T(t) K T_1 f(y(t)) \\ &\quad - 2 f^T(y(t-\sigma(t))) T_2 f(y(t-\sigma(t))) \\ &\quad + 2 y^T(t-\sigma(t)) K T_2 f(y(t-\sigma(t))). \end{aligned} \quad (18)$$

Combining (9)–(18), it follows that

$$\begin{aligned} \dot{V}(t) &\leq \xi^T(t) Y \xi(t) - 2 \xi^T(t) N \int_{t-\tau}^{t-\tau(t)} \dot{x}(s) ds \\ &\quad - 2 \xi^T(t) M \int_{t-\tau(t)}^t \dot{x}(s) ds - 2 \xi^T(t) U \int_{t-\sigma}^{t-\sigma(t)} \dot{y}(s) ds \\ &\quad - 2 \xi^T(t) S \int_{t-\sigma(t)}^t \dot{y}(s) ds - \int_{t-\tau}^{t-\tau(t)} \dot{x}^T(s) Z_1 \dot{x}(s) ds \\ &\quad - \int_{t-\tau(t)}^t \dot{x}^T(s) Z_1 \dot{x}(s) ds - \int_{t-\sigma}^{t-\sigma(t)} \dot{y}^T(s) Z_2 \dot{y}(s) ds \\ &\quad - \int_{t-\sigma(t)}^t \dot{y}^T(s) Z_2 \dot{y}(s) ds \\ &= \xi^T(t) Y \xi(t) \\ &\quad + 2 \xi^T(t) [(\tau - \tau(t)) N Z_1^{-1} N^T + \tau(t) M Z_1^{-1} M^T \\ &\quad + (\sigma - \sigma(t)) U Z_2^{-1} U^T + \sigma(t) S Z_2^{-1} S^T] \xi(t) \\ &\quad - \int_{t-\tau}^{t-\tau(t)} [\xi^T(t) N + \dot{x}^T(s) Z_1] Z_1^{-1} [N^T \xi(t) + Z_1 \dot{x}(s)] ds \\ &\quad - \int_{t-\tau(t)}^t [\xi^T(t) M + \dot{x}^T(s) Z_1] Z_1^{-1} [M^T \xi(t) + Z_1 \dot{x}(s)] ds \\ &\quad - \int_{t-\sigma}^{t-\sigma(t)} [\xi^T(t) U + \dot{y}^T(s) Z_2] Z_2^{-1} [U^T \xi(t) + Z_2 \dot{y}(s)] ds \\ &\quad - \int_{t-\sigma(t)}^t [\xi^T(t) S + \dot{y}^T(s) Z_2] Z_2^{-1} [S^T \xi(t) + Z_2 \dot{y}(s)] ds \\ &\leq \xi^T(t) Y(\tau(t), \sigma(t)) \xi(t), \end{aligned} \quad (19)$$

where $Y(\tau(t), \sigma(t)) = Y + Y_1(\tau(t)) + Y_2(\sigma(t))$ and

$$\begin{aligned} Y_1(\tau(t)) &= (\tau - \tau(t)) N Z_1^{-1} N^T + \tau(t) M Z_1^{-1} M^T, \\ Y_2(\sigma(t)) &= (\sigma - \sigma(t)) U Z_2^{-1} U^T + \sigma(t) S Z_2^{-1} S^T. \end{aligned} \quad (20)$$

Thus, when $Y(\tau(t), \delta(t)) < 0$, we have

$$\dot{V}(t) \leq \xi^T(t) Y(\tau(t), \sigma(t)) \xi(t) < 0. \quad (21)$$

It follows from Lyapunov-Krasovskii stability theorem that system (1) with time-varying delays is asymptotically stable.

Notice that $Y_1(\tau(t))$ is a convex combination of matrices $N Z_1^{-1} N^T$ and $M Z_1^{-1} M^T$ on $\tau(t)$ satisfying $0 \leq \tau_1 < \tau(t) < \tau_2$, and $Y_2(\sigma(t))$ is a convex combination of matrices $U Z_2^{-1} U^T$ and $S Z_2^{-1} S^T$ on $\sigma(t)$ satisfying $0 \leq \sigma_1 < \sigma(t) < \sigma_2$. Then $Y(\tau(t), \delta(t)) < 0$ only if

$$\begin{aligned} Y(\tau, \sigma) &= Y + \tau M Z_1^{-1} M^T + \sigma S Z_2^{-1} S^T < 0, \\ Y(\tau, 0) &= Y + \tau M Z_1^{-1} M^T + \sigma U Z_2^{-1} U^T < 0, \\ Y(0, \sigma) &= Y + \tau N Z_1^{-1} N^T + \sigma S Z_2^{-1} S^T < 0, \\ Y(0, 0) &= Y + \tau N Z_1^{-1} N^T + \sigma U Z_2^{-1} U^T < 0. \end{aligned} \quad (22)$$

Applying Lemma 1 (Schur complement) to the four inequalities above, we arrive at LMI (6). \square

Remark 3. In [7, 13], additional information regarding the derivatives of the time-varying delays is needed; that is $\dot{\tau}_1(t) \leq d_1 < 1$, $\dot{\tau}_2(t) \leq d_2 < 1$. From Theorem 2, one can see that the restrictions are removed. In this case, the results in [13] may produce conservative results. Our result is applicable to both fast and slow time-varying delays.

4. Numerical Example

Example 1. Consider the following genetic regulatory networks with time-varying delays, borrowed from [8, 9]:

$$\begin{aligned} \dot{m}(t) &= -A m(t) + W g(p(t - \sigma(t))) + u, \\ \dot{p}(t) &= -C p(t) + D m(t - \tau(t)), \end{aligned} \quad (23)$$

in which

$$\begin{aligned} A &= \text{diag}\{3, 3, 3\}, \quad C = \text{diag}\{2.5, 2.5, 2.5\}, \\ D &= \text{diag}\{0.8, 0.8, 0.8\}, \\ W &= \begin{bmatrix} 0 & 0 & -2.5 \\ -2.5 & 0 & 0 \\ 0 & -2.5 & 0 \end{bmatrix}, \quad \tau = 12.53, \\ \sigma &= 5.61, \quad \mu = 1.1, \quad d = 0.8. \end{aligned} \quad (24)$$

Using LMI Control Toolbox, by our Theorem 2, we can find that system (1) described by Example 1 is asymptotically

stable. Limited to the length of the paper, we only show a part of the feasible solution here:

$$\begin{aligned} P_1 &= \begin{bmatrix} 1.3083 & 0.0011 & 0.0011 \\ 0.0011 & 1.3083 & 0.0011 \\ 0.0011 & 0.0011 & 1.3083 \end{bmatrix}, \\ P_2 &= \begin{bmatrix} 0.7230 & -0.0006 & -0.0006 \\ -0.0006 & 0.7230 & -0.0006 \\ -0.0006 & -0.0006 & 0.7230 \end{bmatrix}. \end{aligned} \quad (25)$$

It should be pointed out that Theorem 1 in [8] and Corollary 3.2 in [9] are not feasible when employing the LMI Toolbox, but using Theorem 2 in this paper, we can find that system (1) is asymptotically stable. Therefore, our method is less conservative than that in [8, 9].

5. Conclusions

This paper presents some new results of stability analysis for genetic regulatory networks with time-varying delays. An appropriate Lyapunov functional is proposed to investigate the delay-derivative-dependent stability problem. The present results improve the existing ones due to a method to estimate the upper bound of the derivative of Lyapunov functional without ignoring some useful terms and the introduction of convex combination method into the proposed Lyapunov functional, which takes into account the relationship between the time-varying delays and their lower and upper bounds. The supplementary requirements that the time derivatives of time-varying delays must be less than one are removed. As a result, the new stability criterion in terms of LMIs is applicable to both fast and slow time-varying delays. One numerical example shows that the proposed criterion is an improvement over some existing results in the literature. In the future, our work will include the problems of filter design and state estimation for genetic networks.

Conflict of Interests

The authors declare that there is no conflict of interests regarding the publication of this paper.

Acknowledgments

This work is supported by National Natural Science Foundation of China (Grant no. 61103211), Postdoctoral Science Foundation of Chongqing (Grant no. XM201310), and Scientific and Technological Research Program of Chongqing Municipal Education Commission (Grant no. KJ1401403).

References

- [1] J. M. Bower and H. Bolouri, *Computational Modelling of Genetic and Biochemical Networks*, MIT Press, Cambridge, Mass, USA, 2001.
- [2] E. Davidson, *Genomic Regulatory Systems*, Academic Press, San Diego, Calif, USA, 2001.
- [3] H. Kitano, *Foundations of Systems Biology*, MIT Press, Cambridge, Mass, USA, 2001.
- [4] P. Smolen, D. A. Baxter, and J. H. Byrne, "Modeling circadian oscillations with interlocking positive and negative feedback loops," *The Journal of Neuroscience*, vol. 21, no. 9, pp. 6644–6656, 2001.
- [5] H. Hirata, S. Yoshiura, T. Ohtsuka et al., "Oscillatory expression of the BHLH factor Hes1 regulated by a negative feedback loop," *Science*, vol. 298, no. 5594, pp. 840–843, 2002.
- [6] J. Lewis, "Autoinhibition with transcriptional delay: a simple mechanism for the zebrafish somitogenesis oscillator," *Current Biology*, vol. 13, no. 16, pp. 1398–1408, 2003.
- [7] C. Li, L. Chen, and K. Aihara, "Stochastic stability of genetic networks with disturbance attenuation," *IEEE Transactions on Circuits and Systems II: Express Briefs*, vol. 54, no. 10, pp. 892–896, 2007.
- [8] F. Ren and J. Cao, "Asymptotic and robust stability of genetic regulatory networks with time-varying delays," *Neurocomputing*, vol. 71, no. 4–6, pp. 834–842, 2008.
- [9] W. Wang and S. Zhong, "Stochastic stability analysis of uncertain genetic regulatory networks with mixed time-varying delays," *Neurocomputing*, vol. 82, no. 1, pp. 143–156, 2012.
- [10] J. Cao and F. Ren, "Exponential stability of discrete-time genetic regulatory networks with delays," *IEEE Transactions on Neural Networks*, vol. 19, no. 3, pp. 520–523, 2008.
- [11] G. Chesi and Y. S. Hung, "Stability analysis of uncertain genetic sum regulatory networks," *Automatica*, vol. 44, no. 9, pp. 2298–2305, 2008.
- [12] W. He and J. Cao, "Robust stability of genetic regulatory networks with distributed delay," *Cognitive Neurodynamics*, vol. 2, no. 4, pp. 355–361, 2008.
- [13] C. Li, L. Chen, and K. Aihara, "Stability of genetic networks with SUM regulatory logic: Lur'e system and LMI approach," *IEEE Transactions on Circuits and Systems I*, vol. 53, no. 11, pp. 2451–2458, 2006.
- [14] F. Wu, "Global and robust stability analysis of genetic regulatory networks with time-varying delays and parameter uncertainties," *IEEE Transactions on Biomedical Circuits and Systems*, vol. 5, no. 4, pp. 391–398, 2011.
- [15] P. Balasubramaniam and L. Jarina Banu, "Robust state estimation for discrete-time genetic regulatory network with random delays," *Neurocomputing*, vol. 122, pp. 349–369, 2013.
- [16] T. Jiao, G. Zong, and W. Zheng, "New stability conditions for GRNs with neutral delay," *Soft Computing*, vol. 17, no. 4, pp. 703–712, 2013.
- [17] X. Zhang, A. Yu, and G. Zhang, "M-matrix-based delay-range-dependent global asymptotical stability criterion for genetic regulatory networks with time-varying delays," *Neurocomputing*, vol. 113, pp. 8–15, 2013.
- [18] Y. Zhu, Q. Zhang, Z. Wei, and L. Zhang, "Robust stability analysis of Markov jump standard genetic regulatory networks with mixed time delays and uncertainties," *Neurocomputing*, vol. 110, pp. 44–50, 2013.
- [19] T. Yu, J. Wang, and X. Zhang, "A less conservative stability criterion for delayed stochastic genetic regulatory networks," *Mathematical Problems in Engineering*, vol. 2014, Article ID 768483, 11 pages, 2014.
- [20] G. He, J.-A. Fang, and X. Wu, "Robust stability of Markovian jumping genetic regulatory networks with mode-dependent delays," *Mathematical Problems in Engineering*, vol. 2012, Article ID 504378, 18 pages, 2012.

Research Article

Distance Constrained Based Adaptive Flocking Control for Multiagent Networks with Time Delay

Qing Zhang,¹ Ping Li,¹ Zhengquan Yang,¹ and Zengqiang Chen^{1,2}

¹ College of Science, Civil Aviation University of China, No. 2898, Jinbei Road, Tianjin 300300, China

² Department of Automation, Nankai University, Tianjin 300071, China

Correspondence should be addressed to Qing Zhang; qz120168@hotmail.com

Received 6 June 2014; Revised 23 September 2014; Accepted 23 September 2014

Academic Editor: He Huang

Copyright © 2015 Qing Zhang et al. This is an open access article distributed under the Creative Commons Attribution License, which permits unrestricted use, distribution, and reproduction in any medium, provided the original work is properly cited.

The flocking control of multiagent system is a new type of decentralized control method, which has aroused great attention. The paper includes a detailed research in terms of distance constrained based adaptive flocking control for multiagent system with time delay. Firstly, the program on the adaptive flocking with time delay of multiagent is proposed. Secondly, a kind of adaptive controllers and updating laws are presented. According to the Lyapunov stability theory, it is proved that the distance between agents can be larger than a constant during the motion evolution. What is more, velocities of each agent come to the same asymptotically. Finally, the analytical results can be verified by a numerical example.

1. Introduction

In recent years, the research on the flocking behavior of multiagent system has attracted great attention. For a series of agents which can apply some simple rules and limited information of neighbors to organize into a coordinated state is called flocking phenomenon. There exist many forms of flocking behavior in nature, for example, flocking of birds, swarming of bacteria, and so on [1, 2]. With the development of technology and the importance of real application, the study of the flocking behaviors of multiagent system has caused attention from a lot of different backgrounds, for example, biology, computer science, physics, and so on [3–8].

There are a plenty of existing works contributing to the flocking problems. Three heuristic rules leading to emergence of the first computer animation of flocking were first reported by Reynolds in 1987 [5]. The essential flocking rules depict how a personal agent maneuvers based on the local flock mates' positions as well as velocities. Vicsek et al. designed a simple flocking model of multiagents which can all move with the same speed but with different directions in the plane. The Vicsek model is a special version of a pattern introduced previously by Reynolds [6]. Jadbabaie et al. put forward the rigorous proof of the convergence for Vicsek model [7]. There

are many generalized species of this model, such as a leader follower strategy which means one agent acts as a group leader and the other agents would just follow the leader and keep the cohesion/separation/alignment rules. Recently, various desired state flocking motions are deduced in most cases [9–13]. Zavlanos et al., especially, proposed connectivity preserving controllers, by designing novel interagent potentials, to realize the flocking of multiagent system under the initial connectivity assumption [12, 13].

The time delays of systems are a very common phenomenon in real life. Many factors, for example, finite signal transmission speeds and memory effects, can cause time delay in spreading and communication. Therefore, it should be considered to design the control scheme for multiagent system with time delay. The effect of exchange delays for consensus problems and formation problems has been discussed [14–19]. According to the matrix theory and the frequency analysis, Su et al. obtained the desired moving model with a delay-dependent formation control algorithm [20]. Yang et al. studied the virtual potential approach for stabilising a group of agents at a desired formation [21]. Adaptive control is a kind of very important method in the control of complex nonlinear systems [22–24]. A good adaptive control can adapt to the changes in a large range of parameters of controlled

system. It can not only maintain stable operation of the system but also keep the optimal in degree. The literatures focus on flocking with collision avoidance. However, the distance between multiagents is required to be larger than a constant r in reality. For example, bird to incite wings must have their own space. Robot teams and UAV (unmanned air vehicles) in the formation movement in order to avoid a collision must consider their size. So, in the flocking control, it is not enough only to require the distance between them to be greater than zero. Motivated by this fact and on the basis of the abovementioned works, distance constrained based adaptive flocking control for multiagent system with time delay is presented in this paper. The innovation of this paper is mainly in the following aspects: the adaptive controller being designed to achieve the adaptive flocking of multiagents with time delays and keeping the distance between multiagents to be larger than a constant r . The stability of the adaptive flocking of the multiagent system with time delays is analyzed theoretically. A sufficient condition is given for the stability of the adaptive control system.

The rest of the paper was structured from the following aspects. In Section 2, the multiagent flocking problem and some preliminaries used throughout this paper are introduced. In Section 3, a controller is designed based on adaptive flocking control laws. In Section 4, the main theory results that velocities of each agent come to the same asymptotically and the distance between agents required to be larger than a constant r are proved. In Section 5, a simulation case is also presented to verify the effectiveness of our theoretical results. In Section 6, the full text content is summarized and the further research in the aspects of adaptive flocking of multiagent networks is investigated.

2. Preliminaries

A set of N ($N \geq 2$) agents moving in an n -dimensional Euclidean space are considered. The dynamics of each agent is characterized by the following dynamic system (see [25]):

$$\begin{aligned}\dot{x}_i(t) &= v_i(t), \\ \dot{v}_i(t) &= f(v_i(t)) + u_i(t), \quad i = 1, 2, \dots, N,\end{aligned}\quad (1)$$

where $x_i(t) \in \mathbb{R}_2^n$ and $v_i(t) \in \mathbb{R}_2^n$ are the position vector and the velocity of agent i , independently, $f(v_i(t))$ is a nonlinear vector-valued continuous function which describes the intrinsic dynamics of agent i , and $u_i(t) \in \mathbb{R}_2^n$ is the control input acting on agent i . Especially, the virtual leader for multiagent system (1) is a special agent described by

$$\dot{x}_l(t) = v_l(t), \quad \dot{v}_l(t) = f(v_l(t)), \quad (2)$$

where $x_l(t) \in \mathbb{R}_2^n$ and $v_l(t) \in \mathbb{R}_2^n$ are the position and velocity vector of the virtual leader, respectively. In this paper, an assumption has been made that all agents can get the information of the virtual leader. The information switching between multiagents with the leader exhibits time delays.

Define error vector

$$e_i = v_i - v_l, \quad i = 1, 2, \dots, N. \quad (3)$$

Based on the definition of e_i , we have the following equations:

$$v_j(t - \tau) - v_l(t - \tau) = e_j(t - \tau) \quad i, j = 1, 2, \dots, N, \quad (4)$$

$$e_i - e_j = (v_i - v_l) - (v_j - v_l) = v_i - v_j \quad i, j = 1, 2, \dots, N. \quad (5)$$

Assumption 1. Assume that there exists a nonnegative constant α satisfying

$$\|f(v_i) - f(v_l)\|_2 \leq \alpha \|e_i\|_2, \quad i = 1, 2, \dots, N. \quad (6)$$

Definition 2. Communication radius R_2 is defined as the biggest distance from which multiagents can get information of other agents. Hysteresis radius R_1 is the distance in which a new edge will not be added to the graph until the distance between any two agents which are not connected decreases to R_1 . Safe radius r is the distance needed by the agent own activities.

Definition 3 (dynamic graphs [10]). We call $G(t) = (V, E(t))$ a dynamic graph which consists of a set of vertices $V = \{1, 2, \dots, N\}$ indexed by the set of agents and a time varying set of links $E(t) = \{(i, j) \mid i, j \in V\}$, such that, for any $0 < r < R_1 < R_2$,

- (1) if $r < \|x_i(t) - x_j(t)\| \leq R_1$, then $(i, j) \in E(t)$,
- (2) if $R_2 \leq \|x_i(t) - x_j(t)\|$, then $(i, j) \notin E(t)$.

Dynamic graphs $G(t)$ meet the conditions that $(i, j) \in E(t)$ if and only if $(j, i) \in E(t)$ are called undirected, which constitute the key point of the paper. If any vertices i and j in an undirected graph $G(t)$ are joined by a link $(i, j) \in E(t)$, we can call them adjacent or neighbors at time t and denote them by $i \sim j$. Let $L(t) = A(t) - \Delta(t)$ be equivalently represented by a dynamic negative Laplacian matrix, where $A(t) = (a_{ij}(t))$ is a weighted adjacency matrix of the graph $G(t)$, which satisfies that $a_{ij}(t) > 0$ if $i \sim j$, $a_{ii} = -\sum_{j=1, j \neq i}^N a_{ij}$, and $a_{ij}(t) = 0$, otherwise. A topological invariance of graphs, that is, graph connectivity, is of great interest for this paper. The switching process of dynamic graphs can be shown in Figure 1.

Definition 4 (graph connectivity). We say that a dynamic graph $G(t)$ is connected at time t if there exists a path, that is, a sequence of distinct vertices such as the fact that consecutive vertices are adjacent, between any two vertices in $G(t)$.

Hence, the problem which is mentioned can be formally stated as follows.

Definition 5 (flocking). Consider the set of connected graphs C_N on N vertices determining the distribution of control laws $u_i(t)$ for all agents i . If the initial network $G(t_0) \in C_N$ and the initial distance of each agent is bigger than r , $G(t) \in C_N$ for all time $t \geq t_0$, and the distance of multiagents satisfies $\|x_{ij}\| > r$. Moreover, the velocity of each agent asymptotically approaches the same.

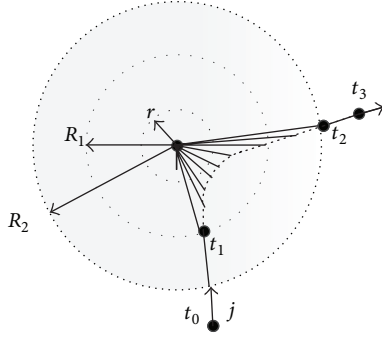


FIGURE 1: The switching process of dynamic graphs according to Definition 3.

3. The Design for Virtual Leader Based Adaptive Flocking Control Laws

In view of any dynamic graph $G(t) = (V, E(t))$, we can define the set of control laws,

$$u_i = -2 \sum_{j=1}^N a_{ij} \nabla_{x_i} V_{ij} - 2 \sum_{j=1, j \neq i}^N a_{ij} (v_i(t-\tau) - v_j(t-\tau)) - d_i e_i, \quad i = 1, 2, \dots, N, \quad (7)$$

$$\dot{d}_i = k_i e_i^T e_i,$$

where d_i is the updating parameters, $\{k_i, i = 1, 2, \dots, N\}$ are positive constants, τ is the coupling time delay, and $\nabla_{x_i} V_{ij}$ is a direction vector of the negative gradient of an artificial potential function defined by the following equation:

$$V_{ij}(x_{ij}) = \frac{1}{R_2^2 - \|x_{ij}\|^2} + \frac{1}{\|x_{ij}\|^2 - r^2}, \quad \|x_{ij}\| \in (r, R_2) \quad (8)$$

with $x_{ij} = x_i - x_j$, where V_{ij} grows unbound when $\|x_{ij}\| \rightarrow R_2^-$, or $\|x_{ij}\| \rightarrow r^+$.

Based on the definition of V_{ij} , we have the following equation:

$$\nabla_{x_{ij}} V_{ij}(x_{ij}) = \nabla_{x_i} V_{ij}(x_{ij}) = -\nabla_{x_j} V_{ij}(x_{ij}) \quad i, j = 1, 2, \dots, N. \quad (9)$$

From equations of (4), (7) and $a_{ii} = -\sum_{j=1, j \neq i}^N a_{ij}$, it was concluded that

$$\begin{aligned} u_i &= -2 \sum_{j=1}^N a_{ij} \nabla_{x_i} V_{ij} - 2 \sum_{j=1, j \neq i}^N a_{ij} (v_i(t-\tau) - v_j(t-\tau)) - d_i e_i \\ &= -2 \sum_{j=1}^N a_{ij} \nabla_{x_i} V_{ij} - 2 \sum_{j=1, j \neq i}^N a_{ij} v_i(t-\tau) \\ &\quad + 2 \sum_{j=1, j \neq i}^N a_{ij} v_j(t-\tau) - d_i e_i \end{aligned}$$

$$\begin{aligned} &= -2 \sum_{j=1}^N a_{ij} \nabla_{x_i} V_{ij} + 2 a_{ii} v_i(t-\tau) + 2 \sum_{j=1, j \neq i}^N a_{ij} v_j(t-\tau) - d_i e_i \\ &= -2 \sum_{j=1}^N a_{ij} \nabla_{x_i} V_{ij} + 2 \sum_{j=1}^N a_{ij} v_j(t-\tau) - d_i e_i \\ &= -2 \sum_{j=1}^N a_{ij} \nabla_{x_i} V_{ij} + 2 \sum_{j=1}^N a_{ij} v_j(t-\tau) - 2 \sum_{j=1}^N a_{ij} v_l(t-\tau) - d_i e_i \\ &= -2 \sum_{j=1}^N a_{ij} \nabla_{x_i} V_{ij} + 2 \sum_{j=1}^N a_{ij} e_j(t-\tau) - d_i e_i \end{aligned} \quad i = 1, 2, \dots, N. \quad (10)$$

From (1), (2), and (10), we can get the error equation

$$\begin{aligned} \dot{e}_i &= f(v_i) - f(v_l) - 2 \sum_{j=1}^N a_{ij} \nabla_{x_i} V_{ij} + 2 \sum_{j=1}^N a_{ij} e_j(t-\tau) - d_i e_i \\ &\quad i = 1, 2, \dots, N. \end{aligned} \quad (11)$$

We will give some main results for our proposed scheme in next chapter.

4. The Main Theory Results

For the considered multiagent system, we can assume that $G(t)$ switches at time t_p for $p = 1, 2, \dots$. That is to say, $G(t)$ is a fixed graph in each time interval $[t_{p-1}, t_p)$. At the same time, we can define a switching signal $g(t) : [t_0, \infty) \rightarrow C_N$ associated with connected graphs, and we can have the following conclusion.

Theorem 6. For the multiagent systems (1) and (2), the switching signal $g(t)$ satisfies $E(t_p) \subseteq E(t_q)$ for any pair of switching times $t_p \leq t_q$ under the control laws (10).

Proof. Consider the following semipositive definite function:

$$V_G = \frac{1}{2} \sum_{i=1}^N e_i^T e_i + \frac{1}{2} \sum_{i=1}^N \frac{(d_i - \hat{d}_i)^2}{k_i} + \sum_{i=1}^N \sum_{j=1}^N a_{ij} V_{ij} \quad (12)$$

$$+ \sum_{i=1}^N \int_{-\tau}^0 e_i^T(t+\eta) e_i(t+\eta) d\eta,$$

where \hat{d}_i is a sufficiently large positive constant.

The generalized time derivative of V_G is

$$\begin{aligned} \dot{V}_G &= \sum_{i=1}^N e_i^T \dot{e}_i + \sum_{i=1}^N \frac{(d_i - \hat{d}_i)}{k_i} \dot{d}_i + \sum_{i=1}^N \sum_{j=1}^N a_{ij} \dot{V}_{ij} \\ &\quad + \sum_{i=1}^N [e_i^T e_i - e_i^T(t-\tau) e_i(t-\tau)]. \end{aligned} \quad (13)$$

Due to (9), we have

$$\begin{aligned}
 \sum_{i=1}^N \sum_{j=1}^N a_{ij} \dot{V}_{ij} &= \sum_{i=1}^N \sum_{j=1}^N a_{ij} \dot{x}_{ij}^T \nabla_{x_{ij}} V_{ij} \\
 &= \sum_{i=1}^N \sum_{j=1}^N a_{ij} \left(\dot{x}_i^T \nabla_{x_{ij}} V_{ij} - \dot{x}_j^T \nabla_{x_{ij}} V_{ij} \right) \\
 &= \sum_{i=1}^N \sum_{j=1}^N a_{ij} \left(\dot{x}_i^T \nabla_{x_i} V_{ij} + \dot{x}_j^T \nabla_{x_j} V_{ij} \right) \quad (14) \\
 &= \sum_{i=1}^N \sum_{j=1}^N a_{ij} \left(v_i^T \nabla_{x_i} V_{ij} + v_j^T \nabla_{x_j} V_{ij} \right) \\
 &= \sum_{i=1}^N \sum_{j=1}^N a_{ij} \left(v_i^T - v_j^T \right) \nabla_{x_i} V_{ij}.
 \end{aligned}$$

Then, from (5), we have

$$\begin{aligned}
 \sum_{i=1}^N \sum_{j=1}^N a_{ij} \left(v_i^T - v_j^T \right) \nabla_{x_i} V_{ij} \\
 &= \sum_{i=1}^N \sum_{j=1}^N a_{ij} \left(e_i^T - e_j^T \right) \nabla_{x_i} V_{ij} \\
 &= \sum_{i=1}^N \sum_{j=1}^N \left(a_{ij} e_i^T \nabla_{x_i} V_{ij} + a_{ij} e_j^T \nabla_{x_j} V_{ij} \right) \quad (15) \\
 &= 2 \sum_{i=1}^N \sum_{j=1}^N a_{ij} e_i^T \nabla_{x_i} V_{ij}.
 \end{aligned}$$

The first two parts of (13) can be rewritten as the following forms:

$$\begin{aligned}
 \sum_{i=1}^N e_i^T \dot{e}_i + \sum_{i=1}^N \frac{(d_i - \hat{d}_i)}{k_i} \dot{d}_i \\
 &= \sum_{i=1}^N e_i^T \left(f(v_i) - f(v_l) - 2 \sum_{j=1}^N a_{ij} \nabla_{x_i} V_{ij} \right. \\
 &\quad \left. + 2 \sum_{j=1}^N a_{ij} e_j(t - \tau) - d_i e_i \right) + \sum_{i=1}^N (d_i - \hat{d}_i) e_i^T e_i \\
 &= \sum_{i=1}^N e_i^T (f(v_i) - f(v_l)) - 2 \sum_{i=1}^N \sum_{j=1}^N a_{ij} e_i^T \nabla_{x_i} V_{ij} \\
 &\quad + 2 \sum_{i=1}^N \sum_{j=1}^N a_{ij} e_i^T e_j(t - \tau) - \sum_{i=1}^N d_i e_i^T e_i + \sum_{i=1}^N (d_i - \hat{d}_i) e_i^T e_i \\
 &= \sum_{i=1}^N e_i^T (f(v_i) - f(v_l)) - 2 \sum_{i=1}^N \sum_{j=1}^N a_{ij} e_i^T \nabla_{x_i} V_{ij} \\
 &\quad + 2 \sum_{i=1}^N \sum_{j=1}^N a_{ij} e_i^T e_j(t - \tau) - \sum_{i=1}^N e_i^T \hat{d}_i e_i
 \end{aligned}$$

$$\begin{aligned}
 &= -2 \sum_{i=1}^N \sum_{j=1}^N a_{ij} e_i^T \nabla_{x_i} V_{ij} + 2 \sum_{i=1}^N \sum_{j=1}^N a_{ij} e_i^T e_j(t - \tau) \\
 &\quad + \sum_{i=1}^N e_i^T (f(v_i) - f(v_l) - \hat{d}_i e_i) \\
 &\leq -2 \sum_{i=1}^N \sum_{j=1}^N a_{ij} e_i^T \nabla_{x_i} V_{ij} + 2 \sum_{i=1}^N \sum_{j=1}^N a_{ij} e_i^T e_j(t - \tau) \\
 &\quad + \sum_{i=1}^N (\alpha - \hat{d}_i) e_i^T e_i. \quad (16)
 \end{aligned}$$

Thus, we can obtain

$$\begin{aligned}
 \dot{V}_G &\leq -2 \sum_{i=1}^N \sum_{j=1}^N a_{ij} e_i^T \nabla_{x_i} V_{ij} + 2 \sum_{i=1}^N \sum_{j=1}^N a_{ij} e_i^T e_j(t - \tau) \\
 &\quad + \sum_{i=1}^N (\alpha - \hat{d}_i) e_i^T e_i + 2 \sum_{i=1}^N \sum_{j=1}^N a_{ij} e_i^T \nabla_{x_i} V_{ij} \\
 &\quad + \sum_{i=1}^N [e_i^T e_i - e_i^T(t - \tau) e_i(t - \tau)] = 2 \sum_{i=1}^N \sum_{j=1}^N a_{ij} e_i^T e_j(t - \tau) \\
 &\quad + \sum_{i=1}^N [e_i^T e_i - e_i^T(t - \tau) e_i(t - \tau)] + \sum_{i=1}^N (\alpha - \hat{d}_i) e_i^T e_i \\
 &\leq 2 \sum_{i=1}^N \sum_{j=1}^N |a_{ij}| \|e_i\| \|e_j(t - \tau)\| - \sum_{i=1}^N e_i^T(t - \tau) e_i(t - \tau) \\
 &\quad + \sum_{i=1}^N e_i^T e_i + \sum_{i=1}^N (\alpha - \hat{d}_i) e_i^T e_i \\
 &= 2 \mathbf{e}^T \Gamma \mathbf{e}(t - \tau) - \mathbf{e}(t - \tau)^T \mathbf{e}(t - \tau) + \mathbf{e}^T \Lambda \mathbf{e} \\
 &\leq \mathbf{e}^T \Gamma^T \Gamma \mathbf{e} + \mathbf{e}^T \Lambda \mathbf{e} = \mathbf{e}^T (\Gamma^T \Gamma + \Lambda) \mathbf{e}, \quad (17)
 \end{aligned}$$

where

$$\begin{aligned}
 \mathbf{e} &= (\|e_1\|_2, \|e_2\|_2, \dots, \|e_N\|_2)^T, \\
 \mathbf{e}(t - \tau) &= (\|e_1(t - \tau)\|_2, \|e_2(t - \tau)\|_2, \dots, \|e_N(t - \tau)\|_2)^T, \\
 \Gamma &= (|a_{ij}|)_{N \times N}, \\
 \Lambda &= \begin{pmatrix} \alpha - \hat{d}_1 + 1 & & 0 \\ & \ddots & \\ 0 & & \alpha - \hat{d}_N + 1 \end{pmatrix}. \quad (18)
 \end{aligned}$$

As α and $|a_{ij}|$ are nonnegative, one can select suitable positive constants \hat{d}_i ($1 \leq i \leq N$) to make

$$(\Lambda + \Gamma^T \Gamma) \leq 0. \quad (19)$$

So, it follows that $\dot{V}_G \leq 0$. Hence, \dot{V}_G is negative semidefinite for any signal $g(t)$.

Because \dot{V}_G is negative semidefinite, V_G cannot increase for all time. In addition, the V_G is bounded. In other words, it means that, for any $(i, j) \in E(t)$, V_{ij} is bounded. On the one hand, if for some $(i, j) \in E(t)$, $\|x_{ij}\| \rightarrow R_2$, $V_{ij}(x_{ij}) \rightarrow \infty$. Thus, by continuity of V_G , it follows that $\|x_{ij}\| < R_2$, for all $(i, j) \in E(t)$ and $t \in [t_p, t_{p+1}]$. In other words, all links in V_G are preserved between switching times, which implies that $E(t_p) \subseteq E(t_q)$. Apply this recursive argument to complete the proof. A similar argument for the case where $x_{ij} \rightarrow r^+$ can be used to establish that the distance of multiagents satisfies $\|x_{ij}\| > r$ for all time $t \geq t_0$. \square

Clearly, Theorem 6 explains that the switching signal will satisfy $G(t) \in C_N$ for all time $t > t_0$, if $G(t_0) \in C_N$. We, specially, have the following corollary.

Corollary 7. *Under control law (7), the total number of switching times of system (1) is finite.*

Proof. The size of the set of links $E(t_0)$ forms an increasing sequence and

$$\sup_{t \geq t_0} |E(t)| - |E(t_0)| = \frac{n(n-1)}{2} - (n-1), \quad (20)$$

where $n-1$ is the number of links in $G(t_0)$ if it is minimally connected, that is, if it is a tree, and $n(n-1)/2$ corresponds to the number of links in a complete graph. \square

Theorem 8. *Take a group of N agents with dynamics (1), (2), each steered by protocol (10) into account. Suppose that initial network $G(t)$ is connected and the initial distance of each agent is bigger than r . Then, $G(t)$ is connected for all $t \geq 0$, the velocity of each agent asymptotically approaches the same, and the distance of each agent is bigger than r for all $t \geq 0$.*

Proof. The number of switching times of the closed loop system is finite by Corollary 7. And by Theorem 6 if $G(t_0)$ is connected, we can draw the conclusion that $G(t)$ is connected for all time $t > t_0$ and so eventually $G(t) \rightarrow G \in C_N$.

Referring to the analysis method of [22–24], we will give the proof of the conclusions that the velocity of each agent asymptotically approaches the same and the distance of each agent is bigger than r for all $t \geq 0$.

From (17) and (19), we know that V_G is monotonically decreasing and having a lower bound. So, it concludes that V_G asymptotically converges to a finite nonnegative value. And, from (17), we have $\dot{V}_G \leq \mathbf{e}^T(\Lambda + \Gamma^T \Gamma)\mathbf{e}$. When \hat{d}_i , $i = 1, 2, \dots, N$ are sufficiently large positive constants, we can see that there exists a nonnegative constant λ satisfying

$$\dot{V}_G \leq -\lambda \mathbf{e}^T \mathbf{e}. \quad (21)$$

Thus, we have

$$\|\mathbf{e}\|^2 \leq -\frac{\dot{V}_G}{\lambda}. \quad (22)$$

Because $\lim_{t \rightarrow +\infty} \int_0^t -(\dot{V}_G/\lambda) d\eta$ exists, we can derive from (22) that $\lim_{t \rightarrow +\infty} \int_0^t \|\mathbf{e}\|^2 d\eta$ exists by the generalized integral principle.

We can define

$$\begin{aligned} V_{G1} &= \frac{1}{2} \sum_{i=1}^N \frac{(d_i - \hat{d}_i)^2}{k_i}, \\ V_{G2} &= \sum_{i=1}^N \sum_{j=1}^N a_{ij} V_{ij}, \\ V_{G3} &= \sum_{i=1}^N \int_{-\tau}^0 \mathbf{e}_i^T(t + \eta) \mathbf{e}_i(t + \eta) d\eta. \end{aligned} \quad (23)$$

Then, we can get the following equation:

$$V_G = \frac{1}{2} \sum_{i=1}^N \mathbf{e}_i^T \mathbf{e}_i + V_{G1} + V_{G2} + V_{G3}. \quad (24)$$

The generalized time derivative of V_{G1} is $\dot{V}_{G1} = \sum_{i=1}^N (d_i - \hat{d}_i) \mathbf{e}_i^T \mathbf{e}_i$. It is negative when $\{\hat{d}_i, i = 1, 2, \dots, N\}$ are sufficiently large positive constants. We can conclude that V_{G1} asymptotically converges to a finite nonnegative value. On the other hand, V_{G2} asymptotically converges to a finite nonnegative value based on the definition of V_{ij} (refer to (8)). At the same time, the generalized time derivative of V_{G3} is $\dot{V}_{G3} = \sum_{i=1}^N [\mathbf{e}_i^T \mathbf{e}_i - \mathbf{e}_i^T(t - \tau) \mathbf{e}_i(t - \tau)]$ which asymptotically converges to zero. Therefore, we can derive that V_{G3} asymptotically converges nonnegative value. By the boundedness of V_G and (24), therefore, we can derive that $\lim_{t \rightarrow +\infty} \sum_{i=1}^N \mathbf{e}_i^T \mathbf{e}_i$ exists and is a nonnegative real number. In what follows, we will prove that

$$\lim_{t \rightarrow +\infty} \sum_{i=1}^N \mathbf{e}_i^T \mathbf{e}_i = 0. \quad (25)$$

If this is not true, we have

$$\lim_{t \rightarrow +\infty} \sum_{i=1}^N \mathbf{e}_i^T \mathbf{e}_i = \mu_1 > 0. \quad (26)$$

Then, there obviously exists a real number $M > 0$ and $0 < \mu < \mu_1$, such that $\sum_{i=1}^N \mathbf{e}_i^T \mathbf{e}_i > \mu > 0$ for $t \geq M$. From (21), we can get

$$\dot{V}_G \leq -\lambda \sum_{i=1}^N \mathbf{e}_i^T \mathbf{e}_i < -\lambda \mu, \quad t \geq M. \quad (27)$$

By integrating (25) with respect to t over the time period M to $+\infty$, we can obtain

$$\begin{aligned} -V_G(M) &\leq V_G(+\infty) - V_G(M) \\ &= \int_M^{+\infty} \dot{V}_G(t) dt < -\int_M^{+\infty} \lambda \mu dt = -\infty. \end{aligned} \quad (28)$$

This yields a contradiction, and so

$$\lim_{t \rightarrow +\infty} \sum_{i=1}^N e_i^T e_i = 0 \quad (29)$$

which implies that $\lim_{t \rightarrow +\infty} e_i = 0$. Moreover, it is natural to see $\lim_{t \rightarrow +\infty} v_i = v_l$. Thus, in the steady state, all agent velocities asymptotically become the same. Furthermore, in the steady state, since $e_i = 0$ for $i = 1, 2, \dots, N$, we can get

$$\frac{d}{dt} \|x_i - x_j\|^2 = 2(x_i - x_j)^T (v_i - v_j) = 0, \quad (30)$$

and so the distances between agents are invariant. \square

Finally, we prove that the distance of each agent is bigger than r for all $t \geq 0$. From above proof, we have that V_G is bounded for all $t \geq t_0$. Also from the definite of potential function, if $x_{ij} \rightarrow r$, we can get that V_G is unbounded. Therefore, the distance of each agent is bigger than r for all $t \geq 0$.

5. Simulation Results

In this section, an example was presented to show the effectiveness of our proposed algorithm. The potential function V_{ij} is defined in (8) with $R_2 = 5$, $r = 1$, and with hysteresis $R_1 = 4.5$. The simulation is performed with 20 agents in R_2^2 . Each agent's initial velocities, labeled with dots, are randomly selected in the unit square. The initial positions distributed on the perimeter of a circle of radius $d = 1.5$ on average (Figure 2). In particular, we assume the velocity is $v_0(t) = [\sin(t), \cos(t)]^T$ and send a signal to one agent which is selected randomly in this simulation. Solid curves connecting every agent indicate the vicinal traveled paths, while arrows indicate the agents velocities. The networks connectivity is guaranteed for all time and the groups asymptotic flocking is achieved, where $\tau = 0.5$. Figure 2 is the initial state. Figure 3 indicates the final steady state configuration. Figure 4 is the velocity error plot which is used for describing the errors between agent actual velocities, where the velocity error curves were indicated by the solid lines, and it demonstrates that all agent velocities asymptotically tend to the same. Figure 5 is changing curve of control laws. Figure 6 is the distance $\|x_{ij}\|$ between agent i and agent j and agent $i, j \in N(t)$. From which one can see that the distance between all agents is larger than $r = 1$ for all $t \geq 0$. This simulation results have well verified the theory results.

6. Conclusions

In this paper, the adaptive flocking of multiagents with time delay is studied. A novel adaptive flocking control method for multiagents is proposed, and the control law is designed depending on functions of the state information and the external signal. By the control law, all agents can follow the virtual leader and can ensure freedom from collisions between neighboring agents. Some theoretical results are

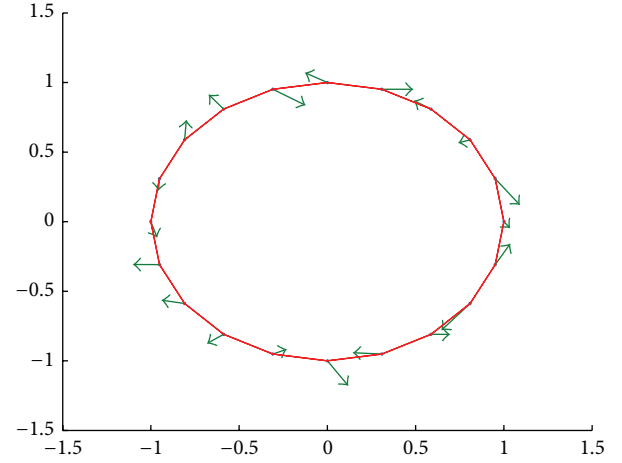


FIGURE 2: Initial configuration.

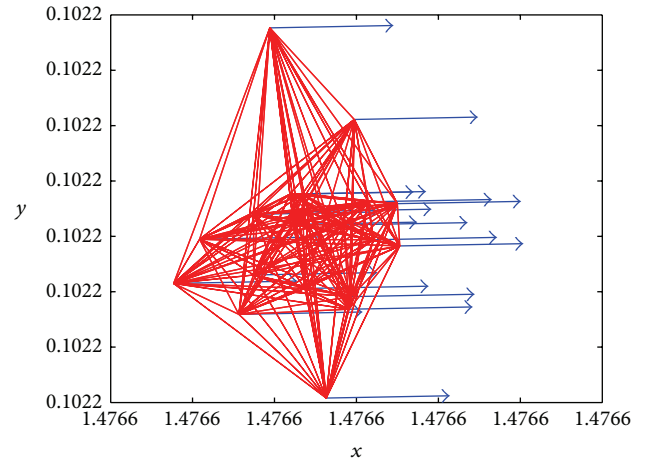


FIGURE 3: End configuration.

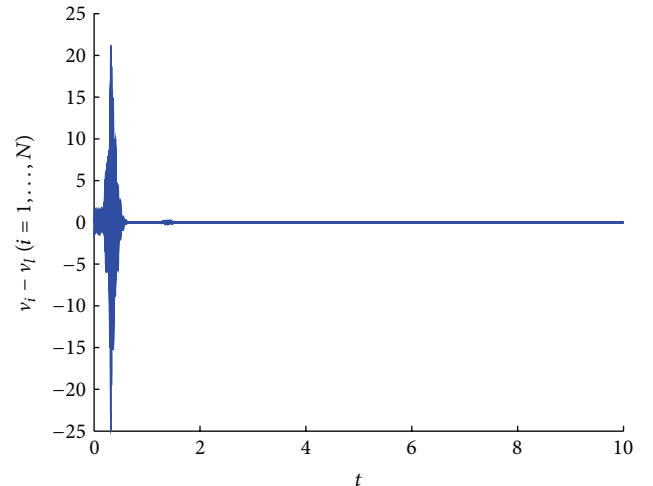


FIGURE 4: Velocity errors.

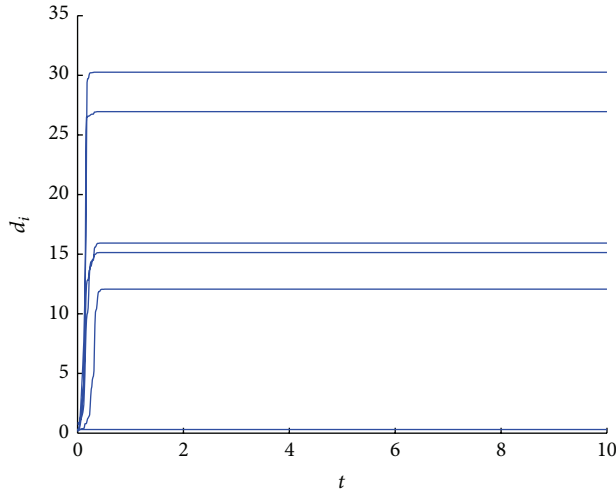


FIGURE 5: Changing curve of control laws.

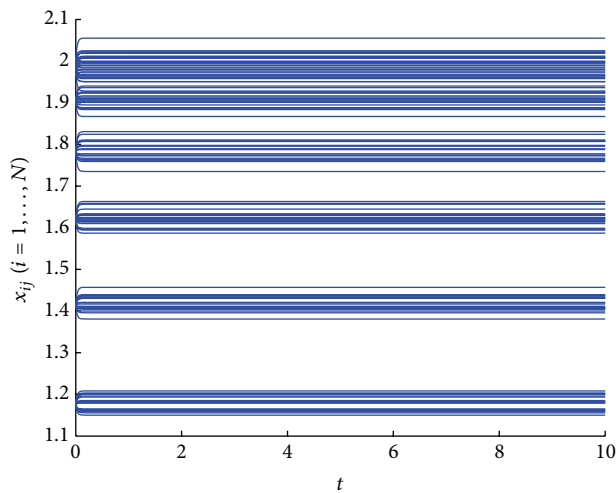


FIGURE 6: Distance of multiagents.

attained, and a numerical example is given to show the practicability of the proposed method. The distance constrained based adaptive flocking control for multiagent system with time delay is proposed in this paper, which has received the expected results. But there are still some problems to be resolved in future research. Firstly, the research of the distance constrained based adaptive flocking control for multiagent system with time delay is achieved on the basics of the strongly connected network. We can study the adaptive flocking control for multiagent system based on the networks which contains a directed spanning tree. Secondly, we can apply the algorithm proposed in this paper to the concrete platform of multiple mobile robots or wireless sensor network, which can combine theory with practice better.

Conflict of Interests

The authors declare that there is no conflict of interests regarding the publication of this paper.

Acknowledgments

This work is supported by National Natural Science Foundation of China (61174094, 61039001), National Natural Science Foundation of Tianjin (14JCYBJC18700), Technology and Innovation Fund Project of Civil Aviation University Of China (SY-1415), and Basic Research Projects of High Education (ZXH2010D011, ZXH2012 K002).

References

- [1] E. Shaw, "Fish in schools," *Nature History*, vol. 84, no. 8, pp. 40–45, 1975.
- [2] M. S. Tang, X. J. Mao, and Z. Guessoum, "Research on an infectious disease transmission by flocking birds," *The Scientific World Journal*, vol. 2013, Article ID 196823, 7 pages, 2013.
- [3] K. D. Do, "Flocking for multiple elliptical agents with limited communication ranges," *IEEE Transactions on Robotics*, vol. 27, no. 5, pp. 931–942, 2011.
- [4] A. Ferrara and C. Vecchio, "Collision avoidance strategies and coordinated control of passenger vehicles," *Nonlinear Dynamics*, vol. 49, no. 4, pp. 475–492, 2007.
- [5] C. W. Reynolds, "Flocks, herds, and schools: a distributed behavioral model," in *Proceedings of the 14th Annual Conference on Computer Graphics and Interactive Techniques*, (SIGGRAPH '87), vol. 21, pp. 25–34, ACM, 1987.
- [6] T. Vicsek, A. Czirók, E. Ben-Jacob, I. Cohen, and O. Shochet, "Novel type of phase transition in a system of self-driven particles," *Physical Review Letters*, vol. 75, no. 6, pp. 1226–1229, 1995.
- [7] A. Jadbabaie, J. Lin, and A. S. Morse, "Coordination of groups of mobile autonomous agents using nearest neighbor rules," *IEEE Transactions on Automatic Control*, vol. 48, no. 6, pp. 988–1001, 2003.
- [8] J. Toner, Y. Tu, and S. Ramaswamy, "Hydrodynamics and phases of flocks," *Annals of Physics*, vol. 318, no. 1, pp. 170–244, 2005.
- [9] R. Olfati-Saber, "Flocking for multi-agent dynamic systems: algorithms and theory," *IEEE Transactions on Automatic Control*, vol. 51, no. 3, pp. 401–420, 2006.
- [10] H. G. Tanner, A. Jadbabaie, and G. J. Pappas, "Stable flocking of mobile agents, part I: fixed topology," in *Proceedings of the 42nd IEEE Conference on Decision and Control*, pp. 2010–2015, Maui, Hawaii, USA, December 2003.
- [11] H. G. Tanner, A. Jadbabaie, and G. J. Pappas, "Stable flocking of mobile agents, part II: dynamic topology," in *Proceedings of the IEEE Conference on Decision and Control*, pp. 2016–2021, Maui, Hawaii, USA, 2003.
- [12] M. M. Zavlanos, A. Jadbabaie, and G. J. Pappas, "Flocking while preserving network connectivity," in *Proceedings of the 46th IEEE Conference on Decision and Control (CDC '07)*, pp. 2919–2924, New Orleans, La, USA, December 2007.
- [13] H. G. Tanner, A. Jadbabaie, and G. J. Pappas, "Flocking in fixed and switching networks," *IEEE Transactions on Automatic Control*, vol. 52, no. 5, pp. 863–868, 2007.
- [14] L. Moreau, "Stability of continuous-time distributed consensus algorithms," Tech. Rep., School of Electronics and Computer Science, University of Southampton, 2004, <http://arxiv.org/pdf/math/0306426.pdf>.
- [15] R. Olfati-Saber and R. M. Murray, "Consensus problems in networks of agents with switching topology and time-delays," *IEEE Transactions on Automatic Control*, vol. 49, no. 9, pp. 1520–1533, 2004.

- [16] J. P. Hu and Y. G. Hong, "Leader-following coordination of multi-agent systems with coupling time delays," *Physica A*, vol. 374, no. 2, pp. 853–863, 2007.
- [17] F. Xiao and L. Wang, "State consensus for multi-agent systems with switching topologies and time-varying delays," *International Journal of Control*, vol. 79, no. 10, pp. 1277–1284, 2006.
- [18] C.-L. Liu and Y.-P. Tian, "Formation control of multi-agent systems with heterogeneous communication delays," *International Journal of Systems Science*, vol. 40, no. 6, pp. 627–636, 2009.
- [19] S. Ristian and F. Cesare, "Formation control over delayed communication networks," in *Proceedings of the IEEE International Conference on Robotics and Automation*, pp. 536–538, Pasadena, Calif, USA, May 2008.
- [20] H. Su, N. Zhang, M. Z. Chen, H. Wang, and X. Wang, "Adaptive flocking with a virtual leader of multiple agents governed by locally Lipschitz nonlinearity," *Nonlinear Analysis: Real World Applications*, vol. 14, no. 1, pp. 798–806, 2013.
- [21] Z. Yang, Q. Zhang, Z. Jiang, and Z. Chen, "Flocking of multi-agents with time delay," *International Journal of Systems Science*, vol. 43, no. 11, pp. 2125–2134, 2012.
- [22] J.-L. Wang, H.-N. Wu, and L. Guo, "Novel adaptive strategies for synchronization of linearly coupled neural networks with reaction-diffusion terms," *IEEE Transactions on Neural Networks and Learning Systems*, vol. 25, no. 2, pp. 429–440, 2014.
- [23] J. L. Wang and H. N. Wu, "Synchronization and adaptive control of an array of linearly coupled reaction-diffusion neural networks with hybrid coupling," *IEEE Transactions on Cybernetics*, vol. 44, no. 8, pp. 1350–1361, 2014.
- [24] J.-L. Wang and H.-N. Wu, "Adaptive output synchronization of complex delayed dynamical networks with output coupling," *Neurocomputing*, vol. 142, pp. 174–181, 2014.
- [25] J.-L. Wang and H.-N. Wu, "Leader-following formation control of multi-agent systems under fixed and switching topologies," *International Journal of Control*, vol. 85, no. 6, pp. 695–705, 2012.

Research Article

Passivity Analysis of Complex Delayed Dynamical Networks with Output Coupling

Yan-Fang Kang,¹ Lu-Xian Fang,² Yue-Hui Zhao,² and Shun-Yan Ren³

¹*School of Economics, Wuhan University of Technology, Wuhan 430070, China*

²*The College of Post and Telecommunication, Wuhan Institute of Technology, Wuhan 430070, China*

³*School of Computer Science and Software Engineering, Tianjin Polytechnic University, Tianjin 300387, China*

Correspondence should be addressed to Yue-Hui Zhao; zhyh83@tom.com

Received 12 May 2014; Revised 29 August 2014; Accepted 30 August 2014

Academic Editor: Zhichun Yang

Copyright © 2015 Yan-Fang Kang et al. This is an open access article distributed under the Creative Commons Attribution License, which permits unrestricted use, distribution, and reproduction in any medium, provided the original work is properly cited.

A new complex dynamical network model with output coupling is proposed. This paper is concerned with input passivity and output passivity of the proposed network model. By constructing new Lyapunov functionals, some sufficient conditions ensuring the input passivity and output passivity are obtained. Finally, two numerical examples are provided to demonstrate the effectiveness of the proposed results.

1. Introduction

Recently, there has been increasing interest in the study of complex dynamical networks. The main reason is that many practical systems can be characterized by various models of complex networks. It is well known that one of the most significant and interesting dynamical phenomena of complex networks is the synchronization of systems. Many interesting results on synchronization have been derived for various complex networks [1–10]. But, it should be noticed that the complex networks with state coupling were considered in these papers.

To our knowledge, Jiang et al. [11] first introduced a complex network model with output coupling without time delays. Some conditions for synchronization were established based on the Lyapunov stability theory. However, time delays always exist in complex networks due to the finite speeds of transmission and/or the traffic congestion, and most of delays are notable. So it is crucial for us to take the delay into the consideration when we study complex networks. Practically, many phenomena in nature can be modeled as complex networks with output coupling. The cooperative control problem of multiple agents has received much attention recently since it has challenging features and many applications, for example, large object moving, formation control, rescue

mission, and satellite clustering. It is well known that the state of agent is difficult to be observed or measured because of technology limitations and environmental disturbances. For instance, the measuring of velocity is more difficult than that of position. In some circumstances, the information of velocity is unavailable for agents [12]. Therefore, it is quite necessary to design protocols based on the output variables. In this case, the closed-loop systems can be described by the complex networks with output coupling. Hence, study of complex networks with output coupling is very interesting and important in both theory and application. A complex delayed dynamical network model with output coupling was proposed in [13, 14]. Wang and Wu [13] investigated the output synchronization of the proposed network model, and some criteria on local and global exponential output synchronization were derived.

Passivity [15–33] is an important concept of system theory and provides a nice tool for analyzing the stability of systems and has found applications in diverse areas such as stability, complexity, signal processing, chaos control and synchronization, and fuzzy control. Many researchers have studied the passivity of fuzzy systems [19–22] and neural networks [23–28]. Liang et al. [20] discussed the passivity and passification problems for a class of uncertain stochastic fuzzy systems with time-varying delays. In [26] Song et al.

investigated the passivity for a class of discrete-time stochastic neural networks with time-varying delays, and a delay-dependent passivity condition was obtained by constructing proper Lyapunov-Krasovskii functional. However, there are few work on the passivity of complex networks [29, 30, 32, 33]. In [29, 30], Yao et al. obtained some sufficient conditions on passivity properties for linear (or linearized) complex networks with and without coupling delays (constant delay). However, in practical evolutionary processes of the networks, absolute constant delay may be scarce and delays are frequently varied with time. Therefore, it is important to further study the passivity of complex networks with time-varying delays. Wang et al. [32] considered input passivity and output passivity for a generalized complex network with nonlinear, time-varying, nonsymmetric, and delayed coupling. By constructing some suitable Lyapunov functionals, several sufficient conditions ensuring input passivity and output passivity were derived. To the best of our knowledge, the input passivity and output passivity of complex delayed dynamical network model with output coupling have not yet been established. Therefore, it is interesting to study the input passivity and output passivity of complex delayed dynamical network model with output coupling.

Motivated by the above discussions, we propose a new complex delayed dynamical network model with output coupling. The objective of this paper is to study the input and output passivity of the proposed network model. Some sufficient conditions ensuring input passivity and output passivity are obtained by Lyapunov functional method.

The rest of this paper is organized as follows. A new complex network model is introduced and some useful preliminaries are given in Section 2. Several input and output passivity criteria are established in Section 3. In Section 4, two numerical examples are given to illustrate the effectiveness of the proposed results. Conclusions are finally given in Section 5.

2. Network Model and Preliminaries

Let R^n be the n -dimensional Euclidean space, and let $R^{n \times m}$ be the space of $n \times m$ real matrices. $P \geq 0$ ($P \leq 0$) means that matrix P is real symmetric and semipositive (seminegative) definite. $P > 0$ ($P < 0$) means that matrix P is real symmetric and positive (negative) definite. I_n denotes the $n \times n$ identity matrix. B^T denotes the transpose of a square matrix B . $C([- \tau, 0], R^n)$ is a Banach space of continuous functions mapping the interval $[- \tau, 0]$ into R^n with the norm $\|\phi\|_\tau = \sup_{-\tau \leq \theta \leq 0} \|\phi(\theta)\|$, where $\|\cdot\|$ is the Euclidean norm.

In this paper, we consider a complex delayed dynamical network consisting of N identical nodes with diffusive and output coupling. The mathematical model of the coupled network can be described as follows:

$$\begin{aligned} \dot{x}_i(t) &= f(x_i(t)) + \frac{a}{k_i^{\beta_\omega}} \sum_{j=1}^N L_{ij} \Gamma y_j(t - \tau(t)) + B_i u_i(t), \\ y_i(t) &= C_i x_i(t) + D_i u_i(t), \end{aligned} \quad (1)$$

where $i = 1, 2, \dots, N$. $\tau(t)$ is the time-varying delay with $0 \leq \tau(t) \leq \tau$.

The function $f(\cdot)$, describing the local dynamics of the nodes, is continuously differentiable and capable of producing various rich dynamical behaviors, $x_i(t) = (x_{i1}(t), x_{i2}(t), \dots, x_{in}(t))^T \in R^n$ is the state variable of node i , $y_i(t) \in R^n$ is the output of node i , $u_i(t) \in R^n$ is the input vector of node i , B_i , C_i , and D_i are known matrices with appropriate dimensions, $\Gamma \in R^{n \times n}$ is inner-coupling matrix, which describes the individual coupling between two connected nodes of the network, $a > 0$ represents the overall coupling strength, k_i is the degree of node i , β_ω is a tunable weight parameter, and the real matrix $L = (L_{ij})_{N \times N}$ is a symmetric matrix with diagonal entries $L_{ii} = -k_i$ and off-diagonal entries $L_{ij} = 1$ if node i and node j are connected by a link, and $L_{ij} = 0$ otherwise.

In this paper, we always assume that complex network (1) is connected. Let $x(t) = (x_1^T(t), x_2^T(t), \dots, x_N^T(t))^T$, $y(t) = (y_1^T(t), y_2^T(t), \dots, y_N^T(t))^T$, and $u(t) = (u_1^T(t), u_2^T(t), \dots, u_N^T(t))^T$. The initial condition associated with the complex network (1) is given in the form

$$\begin{aligned} x(0) &= x_0, \quad x_0 = (x_{10}^T, x_{20}^T, \dots, x_{N0}^T)^T, \quad x_{i0} \in R^n, \\ y(s) &= \Phi(s), \quad s \in [-\tau, 0], \quad \phi_i \in C([- \tau, 0], R^n), \quad (2) \\ \Phi(s) &= (\phi_1^T(s), \phi_2^T(s), \dots, \phi_N^T(s))^T, \quad i = 1, 2, \dots, N. \end{aligned}$$

Next, we give several useful definitions.

Definition 1 (see [32]). Complex network (1) is called input passive if there exist two constants $\gamma > 0$ and $\beta \in R$ such that

$$2 \int_0^{t_p} y^T(s) u(s) ds \geq -\beta^2 + \gamma \int_0^{t_p} u^T(s) u(s) ds, \quad (3)$$

for all $t_p \geq 0$.

Definition 2 (see [32]). Complex network (1) is called output passive if there exist two constants $\gamma > 0$ and $\beta \in R$ such that

$$2 \int_0^{t_p} y^T(s) u(s) ds \geq -\beta^2 + \gamma \int_0^{t_p} y^T(s) y(s) ds, \quad (4)$$

for all $t_p \geq 0$.

Definition 3 (see [34]). Let $A = (a_{ij})_{m \times n} \in R^{m \times n}$, and let $B = (b_{ij})_{p \times q} \in R^{p \times q}$. Then the Kronecker product (or tensor product) of A and B is defined as the matrix

$$A \otimes B = \begin{bmatrix} a_{11}B & a_{12}B & \cdots & a_{1n}B \\ a_{21}B & a_{22}B & \cdots & a_{2n}B \\ \vdots & \vdots & \ddots & \vdots \\ a_{m1}B & a_{m2}B & \cdots & a_{mn}B \end{bmatrix} \in R^{mp \times nq}. \quad (5)$$

The Kronecker product has the following properties:

$$\begin{aligned}
 (1) \quad & (A \otimes B)^T = A^T \otimes B^T; \\
 (2) \quad & (\alpha A) \otimes B = A \otimes (\alpha B); \\
 (3) \quad & (A + B) \otimes C = A \otimes C + B \otimes C; \\
 (4) \quad & (A \otimes B)(C \otimes D) = (AC) \otimes (BD),
 \end{aligned} \tag{6}$$

where $\alpha \in R, C$, and D are matrices with suitable dimensions.

3. Main Results

In this section, we shall investigate the input passivity and output passivity of the complex delayed dynamical networks with output coupling.

In [32, 35], authors make the assumption that the function $f(\cdot)$ is in the QUAD function class. In this paper, we make similar assumptions.

(A1) There exist a positive definite diagonal matrix $P = \text{diag}(p_1, p_2, \dots, p_n)$ and a diagonal matrix $\Delta = \text{diag}(\delta_1, \delta_2, \dots, \delta_n)$ such that f satisfies the following inequality:

$$x^T P (f(x) - \Delta x) \leq -\eta x^T x, \tag{7}$$

for some $\eta > 0$ and all $x \in R^n$.

For the convenience, we denote

$$\begin{aligned}
 \hat{P} &= \text{diag}(P, P, \dots, P), \quad \hat{\Delta} = \text{diag}(\Delta, \Delta, \dots, \Delta), \\
 B &= \text{diag}(B_1, B_2, \dots, B_N), \quad C = \text{diag}(C_1, C_2, \dots, C_N), \\
 D &= \text{diag}(D_1, D_2, \dots, D_N).
 \end{aligned} \tag{8}$$

In the following, we first give two input passivity criteria.

Theorem 4. Let (A1) hold, and let $\dot{\tau}(t) \leq \sigma < 1$. The complex network (1) is input passive if there exist matrix $Q \geq 0$ and a scalar $\gamma > 0$ such that

$$\begin{pmatrix} W_1 & a\hat{P}(G \otimes \Gamma) & W_2 \\ a(G \otimes \Gamma)^T \hat{P} & -(1-\sigma)Q & 0 \\ W_2^T & 0 & W_3 \end{pmatrix} \leq 0, \tag{9}$$

where

$$\begin{aligned}
 W_1 &= -2\eta I_{nN} + 2\hat{P}\hat{\Delta} + C^T Q C, \\
 W_2 &= \hat{P}B + C^T Q D - C^T, \\
 W_3 &= -(D + D^T - \gamma I_{nN} - D^T Q D).
 \end{aligned} \tag{10}$$

Proof. For convenient analysis, we let

$$G_{ij} = \frac{L_{ij}}{k_i^{\beta_\omega}}. \tag{11}$$

Then, complex network (1) can be rewritten as follows:

$$\begin{aligned}
 \dot{x}_i(t) &= f(x_i(t)) + a \sum_{j=1}^N G_{ij} \Gamma y_j(t - \tau(t)) + B_i u_i(t), \\
 y_i(t) &= C_i x_i(t) + D_i u_i(t),
 \end{aligned} \tag{12}$$

where $i = 1, 2, \dots, N$. $G = (G_{ij})_{N \times N}$ is a coupling matrix, accounting for the topology of complex dynamical network. We can rewrite system (12) in a compact form as follows:

$$\begin{aligned}
 \dot{x}(t) &= F(x(t)) + a(G \otimes \Gamma)y(t - \tau(t)) + Bu(t), \\
 y(t) &= Cx(t) + Du(t),
 \end{aligned} \tag{13}$$

where

$$\begin{aligned}
 x(t) &= (x_1^T(t), x_2^T(t), \dots, x_N^T(t))^T, \\
 u(t) &= (u_1^T(t), u_2^T(t), \dots, u_N^T(t))^T, \\
 y(t) &= (y_1^T(t), y_2^T(t), \dots, y_N^T(t))^T, \\
 F(x(t)) &= (f^T(x_1(t)), f^T(x_2(t)), \dots, f^T(x_N(t)))^T, \\
 y(t - \tau(t)) &= (y_1^T(t - \tau(t)), y_2^T(t - \tau(t)), \dots, y_N^T(t - \tau(t)))^T.
 \end{aligned} \tag{14}$$

Construct Lyapunov functional for system (13) as follows:

$$V(t) = x^T(t) \hat{P} x(t) + \int_{t-\tau(t)}^t y^T(\alpha) Q y(\alpha) d\alpha. \tag{15}$$

The derivative of $V(t)$ satisfies

$$\begin{aligned}
 \dot{V}(t) &= 2x^T(t) \hat{P} \dot{x}(t) + y^T(t) Q y(t) \\
 &\quad - (1 - \dot{\tau}(t)) y^T(t - \tau(t)) Q y(t - \tau(t)) \\
 &\leq 2x^T(t) \hat{P} \dot{x}(t) + y^T(t) Q y(t) \\
 &\quad - (1 - \sigma) y^T(t - \tau(t)) Q y(t - \tau(t)) \\
 &= 2x^T(t) \hat{P} F(x(t)) + 2ax^T(t) \hat{P} (G \otimes \Gamma) y(t - \tau(t)) \\
 &\quad + 2x^T(t) \hat{P} B u(t) + y^T(t) Q y(t) \\
 &\quad - (1 - \sigma) y^T(t - \tau(t)) Q y(t - \tau(t)).
 \end{aligned} \tag{16}$$

Then, we can get

$$\begin{aligned}
 \dot{V}(t) &- 2y^T(t) u(t) + \gamma u^T(t) u(t) \\
 &\leq 2x^T(t) \hat{P} F(x(t)) + 2ax^T(t) \hat{P} (G \otimes \Gamma) y(t - \tau(t))
 \end{aligned}$$

$$\begin{aligned}
& + 2x^T(t) \hat{P}Bu(t) + y^T(t) Qy(t) \\
& - (1 - \sigma) y^T(t - \tau(t)) Qy(t - \tau(t)) \\
& - 2x^T(t) C^T u(t) - u^T(t) (D + D^T - \gamma I_{nN}) u(t).
\end{aligned} \tag{17}$$

According to (A1), we can obtain

$$\begin{aligned}
x^T(t) \hat{P}F(x(t)) &= \sum_{i=1}^N x_i^T(t) Pf(x_i(t)) \\
&\leq \sum_{i=1}^N [-\eta x_i^T(t) x_i(t) + x_i^T(t) P \Delta x_i(t)] \\
&= x^T(t) (-\eta I_{nN} + \hat{P}\hat{\Delta}) x(t).
\end{aligned} \tag{18}$$

It follows from (9) and (18) that

$$\begin{aligned}
\dot{V}(t) - 2y^T(t) u(t) + \gamma u^T(t) u(t) \\
\leq x^T(t) (-2\eta I_{nN} + 2\hat{P}\hat{\Delta} + C^T QC) x(t) \\
+ 2ax^T(t) \hat{P}(G \otimes \Gamma) y(t - \tau(t)) \\
+ 2x^T(t) (\hat{P}B + C^T QD - C^T) u(t) \\
- (1 - \sigma) y^T(t - \tau(t)) Qy(t - \tau(t)) \\
- u^T(t) (D + D^T - \gamma I_{nN} - D^T QD) u(t) \\
= \xi^T(t) \begin{pmatrix} W_1 & a\hat{P}(G \otimes \Gamma) & W_2 \\ a(G \otimes \Gamma)^T \hat{P} & -(1 - \sigma) Q & 0 \\ W_2^T & 0 & W_3 \end{pmatrix} \xi(t) \\
\leq 0,
\end{aligned} \tag{19}$$

where $\xi(t) = (x^T(t), y^T(t - \tau(t)), u^T(t))^T$.

By integrating (19) with respect to t over the time period 0 to t_p , we get

$$\begin{aligned}
2 \int_0^{t_p} y^T(s) u(s) ds \\
\geq V(t_p) - V(0) + \gamma \int_0^{t_p} u^T(s) u(s) ds.
\end{aligned} \tag{20}$$

From the definition of $V(t)$, we have $V(t_p) \geq 0$ and $V(0) \geq 0$. Thus,

$$2 \int_0^{t_p} y^T(s) u(s) ds \geq -\beta^2 + \gamma \int_0^{t_p} u^T(s) u(s) ds, \tag{21}$$

for all $t_p \geq 0$, $\beta = \sqrt{V(0)}$. The proof is completed. \square

Theorem 5. Let (A1) hold, and let $\dot{\tau}(t) \leq \sigma < 1$. The complex network (1) is input passive if there exist two matrices $Z \geq 0$ and $Q \geq 0$ and a scalar $\gamma > 0$ such that

$$\begin{pmatrix} S_1 & a\hat{P}(G \otimes \Gamma) & S_2 \\ a(G \otimes \Gamma)^T \hat{P} & -(1 - \sigma) Q & 0 \\ S_2^T & 0 & S_3 \end{pmatrix} \leq 0, \tag{22}$$

where

$$\begin{aligned}
S_1 &= -2\eta I_{nN} + 2\hat{P}\hat{\Delta} + C^T (Q + \tau Z) C, \\
S_2 &= \hat{P}B - C^T + C^T (Q + \tau Z) D, \\
S_3 &= -[D + D^T - \gamma I_{nN} - D^T (Q + \tau Z) D].
\end{aligned} \tag{23}$$

Proof. Define the following Lyapunov functional for system (13):

$$\begin{aligned}
V(t) &= x^T(t) \hat{P}x(t) + \int_{-\tau(t)}^0 \int_{t+\beta}^t y^T(\alpha) Zy(\alpha) d\alpha d\beta \\
&+ \int_{t-\tau(t)}^t y^T(\alpha) Qy(\alpha) d\alpha.
\end{aligned} \tag{24}$$

The derivative of $V(t)$ satisfies

$$\begin{aligned}
\dot{V}(t) &= 2x^T(t) \hat{P}\dot{x}(t) + y^T(t) Qy(t) \\
&- \int_{t-\tau(t)}^t y^T(\alpha) Zy(\alpha) d\alpha + \tau(t) y^T(t) Zy(t) \\
&+ \dot{\tau}(t) \int_{t-\tau(t)}^t y^T(\alpha) Zy(\alpha) d\alpha \\
&- (1 - \dot{\tau}(t)) y^T(t - \tau(t)) Qy(t - \tau(t)) \\
&\leq 2x^T(t) \hat{P}\dot{x}(t) + y^T(t) (Q + \tau Z) y(t) \\
&- (1 - \sigma) y^T(t - \tau(t)) Qy(t - \tau(t)) \\
&= 2x^T(t) \hat{P}F(x(t)) + 2ax^T(t) \hat{P}(G \otimes \Gamma) y(t - \tau(t)) \\
&+ 2x^T(t) \hat{P}Bu(t) + y^T(t) (Q + \tau Z) y(t) \\
&- (1 - \sigma) y^T(t - \tau(t)) Qy(t - \tau(t)).
\end{aligned} \tag{25}$$

Then, we can get

$$\begin{aligned}
\dot{V}(t) - 2y^T(t) u(t) + \gamma u^T(t) u(t) \\
\leq 2x^T(t) \hat{P}F(x(t)) + 2ax^T(t) \hat{P}(G \otimes \Gamma) y(t - \tau(t)) \\
+ 2x^T(t) (\hat{P}B - C^T) u(t) + y^T(t) (Q + \tau Z) y(t) \\
- (1 - \sigma) y^T(t - \tau(t)) Qy(t - \tau(t)) \\
- u^T(t) (D + D^T - \gamma I_{nN}) u(t).
\end{aligned} \tag{26}$$

It follows from (18) and (22) that

$$\begin{aligned}
\dot{V}(t) - 2y^T(t) u(t) + \gamma u^T(t) u(t) \\
\leq x^T(t) [-2\eta I_{nN} + 2\hat{P}\hat{\Delta} + C^T (Q + \tau Z) C] x(t) \\
+ 2ax^T(t) \hat{P}(G \otimes \Gamma) y(t - \tau(t)) \\
+ 2x^T(t) [\hat{P}B - C^T + C^T (Q + \tau Z) D] u(t)
\end{aligned}$$

$$\begin{aligned}
& -u^T(t) [D + D^T - \gamma I_{nN} - D^T(Q + \tau Z)D] u(t) \\
& - (1 - \sigma) y^T(t - \tau(t)) Q y(t - \tau(t)) \\
& = \xi^T(t) \begin{pmatrix} S_1 & a\hat{P}(G \otimes \Gamma) & S_2 \\ a(G \otimes \Gamma)^T \hat{P} & -(1 - \sigma)Q & 0 \\ S_2^T & 0 & S_3 \end{pmatrix} \xi(t) \quad (27) \\
& \leq 0,
\end{aligned}$$

where $\xi(t) = (x^T(t), y^T(t - \tau(t)), u^T(t))^T$.

By integrating (27) with respect to t over the time period 0 to t_p , we can get

$$\begin{aligned}
& 2 \int_0^{t_p} y^T(s) u(s) ds \\
& \geq V(t_p) - V(0) + \gamma \int_0^{t_p} u^T(s) u(s) ds. \quad (28)
\end{aligned}$$

From the definition of $V(t)$, we have $V(t_p) \geq 0$ and $V(0) \geq 0$. Thus,

$$2 \int_0^{t_p} y^T(s) u(s) ds \geq -\beta^2 + \gamma \int_0^{t_p} u^T(s) u(s) ds, \quad (29)$$

for all $t_p \geq 0$, $\beta = \sqrt{V(0)}$. The proof is completed. \square

In the above, two sufficient conditions are given to ensure the input passivity of complex network (1). In the following, we shall discuss the output passivity of complex network (1).

Theorem 6. Let (A1) hold, and let $\dot{\tau}(t) \leq \sigma < 1$. The complex network (1) is output passive if there exist matrix $Q \geq 0$ and scalar $\gamma > 0$ such that

$$\begin{pmatrix} M_1 & a\hat{P}(G \otimes \Gamma) & M_2 \\ a(G \otimes \Gamma)^T \hat{P} & -(1 - \sigma)Q & 0 \\ M_2^T & 0 & M_3 \end{pmatrix} \leq 0, \quad (30)$$

where

$$\begin{aligned}
M_1 &= -2\eta I_{nN} + 2\hat{P}\hat{\Delta} + C^T(Q + \gamma I_{nN})C, \\
M_2 &= \hat{P}B + C^T(Q + \gamma I_{nN})D - C^T, \\
M_3 &= -[D + D^T - D^T(Q + \gamma I_{nN})D]. \quad (31)
\end{aligned}$$

Proof. Construct the same Lyapunov functional as (15) for system (13). Then, we can get

$$\begin{aligned}
\dot{V}(t) & \leq 2x^T(t) \hat{P}F(x(t)) + 2ax^T(t) \hat{P}(G \otimes \Gamma) y(t - \tau(t)) \\
& + 2x^T(t) \hat{P}Bu(t) + y^T(t) Q y(t) \\
& - (1 - \sigma) y^T(t - \tau(t)) Q y(t - \tau(t)). \quad (32)
\end{aligned}$$

Therefore, we have

$$\begin{aligned}
& \dot{V}(t) - 2y^T(t) u(t) + \gamma y^T(t) y(t) \\
& \leq 2x^T(t) \hat{P}F(x(t)) + 2ax^T(t) \hat{P}(G \otimes \Gamma) y(t - \tau(t)) \\
& + 2x^T(t) (\hat{P}B - C^T) u(t) + y^T(t) (Q + \gamma I_{nN}) y(t) \\
& - (1 - \sigma) y^T(t - \tau(t)) Q y(t - \tau(t)) \\
& - u^T(t) (D + D^T) u(t). \quad (33)
\end{aligned}$$

It follows from (18) and (30) that

$$\begin{aligned}
& \dot{V}(t) - 2y^T(t) u(t) + \gamma y^T(t) y(t) \\
& \leq x^T(t) [-2\eta I_{nN} + 2\hat{P}\hat{\Delta} + C^T(Q + \gamma I_{nN})C] x(t) \\
& + 2ax^T(t) \hat{P}(G \otimes \Gamma) y(t - \tau(t)) \\
& + 2x^T(t) [\hat{P}B + C^T(Q + \gamma I_{nN})D - C^T] u(t) \\
& - (1 - \sigma) y^T(t - \tau(t)) Q y(t - \tau(t)) \\
& - u^T(t) [D + D^T - D^T(Q + \gamma I_{nN})D] u(t) \\
& = \xi^T(t) \begin{pmatrix} M_1 & a\hat{P}(G \otimes \Gamma) & M_2 \\ a(G \otimes \Gamma)^T \hat{P} & -(1 - \sigma)Q & 0 \\ M_2^T & 0 & M_3 \end{pmatrix} \xi(t) \\
& \leq 0, \quad (34)
\end{aligned}$$

where $\xi(t) = (x^T(t), y^T(t - \tau(t)), u^T(t))^T$.

By integrating (34) with respect to t over the time period 0 to t_p , we get

$$\begin{aligned}
& 2 \int_0^{t_p} y^T(s) u(s) ds \\
& \geq V(t_p) - V(0) + \gamma \int_0^{t_p} y^T(s) y(s) ds. \quad (35)
\end{aligned}$$

From the definition of $V(t)$, we have $V(t_p) \geq 0$ and $V(0) \geq 0$. Thus,

$$2 \int_0^{t_p} y^T(s) u(s) ds \geq -\beta^2 + \gamma \int_0^{t_p} y^T(s) y(s) ds, \quad (36)$$

for all $t_p \geq 0$, $\beta = \sqrt{V(0)}$. The proof is completed. \square

Theorem 7. Let (A1) hold, and let $\dot{\tau}(t) \leq \sigma < 1$. The complex network (1) is output passive if there exist two matrices $Z \geq 0$ and $Q \geq 0$ and a scalar $\gamma > 0$ such that

$$\begin{pmatrix} H_1 & a\hat{P}(G \otimes \Gamma) & H_2 \\ a(G \otimes \Gamma)^T \hat{P} & -(1 - \sigma)Q & 0 \\ H_2^T & 0 & H_3 \end{pmatrix} \leq 0, \quad (37)$$

where

$$\begin{aligned} H_1 &= -2\eta I_{nN} + 2\hat{P}\hat{\Delta} + C^T (Q + \tau Z + \gamma I_{nN}) C, \\ H_2 &= \hat{P}B - C^T + C^T (Q + \tau Z + \gamma I_{nN}) D, \\ H_3 &= -[D + D^T - D^T (Q + \tau Z + \gamma I_{nN}) D]. \end{aligned} \quad (38)$$

Proof. Construct the same Lyapunov functional as (24) for system (13). Then, we can obtain

$$\begin{aligned} \dot{V}(t) &\leq 2x^T(t) \hat{P}F(x(t)) + 2ax^T(t) \hat{P}(G \otimes \Gamma) y(t - \tau(t)) \\ &\quad + 2x^T(t) \hat{P}Bu(t) + y^T(t) (Q + \tau Z) y(t) \\ &\quad - (1 - \sigma) y^T(t - \tau(t)) Q y(t - \tau(t)). \end{aligned} \quad (39)$$

Therefore, we have

$$\begin{aligned} \dot{V}(t) &- 2y^T(t) u(t) + \gamma y^T(t) y(t) \\ &\leq 2x^T(t) \hat{P}F(x(t)) + 2ax^T(t) \hat{P}(G \otimes \Gamma) y(t - \tau(t)) \\ &\quad + 2x^T(t) (\hat{P}B - C^T) u(t) + y^T(t) (Q + \tau Z + \gamma I_{nN}) y(t) \\ &\quad - (1 - \sigma) y^T(t - \tau(t)) Q y(t - \tau(t)) \\ &\quad - u^T(t) (D + D^T) u(t). \end{aligned} \quad (40)$$

It follows from (18) and (37) that

$$\begin{aligned} \dot{V}(t) &- 2y^T(t) u(t) + \gamma y^T(t) y(t) \\ &\leq x^T(t) [-2\eta I_{nN} + 2\hat{P}\hat{\Delta} + C^T (Q + \tau Z + \gamma I_{nN}) C] x(t) \\ &\quad + 2ax^T(t) \hat{P}(G \otimes \Gamma) y(t - \tau(t)) \\ &\quad + 2x^T(t) [\hat{P}B - C^T + C^T (Q + \tau Z + \gamma I_{nN}) D] u(t) \\ &\quad - (1 - \sigma) y^T(t - \tau(t)) Q y(t - \tau(t)) \\ &\quad - u^T(t) [D + D^T - D^T (Q + \tau Z + \gamma I_{nN}) D] u(t) \\ &= \xi^T(t) \begin{pmatrix} H_1 & a\hat{P}(G \otimes \Gamma) & H_2 \\ a(G \otimes \Gamma)^T \hat{P} & -(1 - \sigma)Q & 0 \\ H_2^T & 0 & H_3 \end{pmatrix} \xi(t) \\ &\leq 0, \end{aligned} \quad (41)$$

where $\xi(t) = (x^T(t), y^T(t - \tau(t)), u^T(t))^T$.

By integrating (41) with respect to t over the time period 0 to t_p , we get

$$\begin{aligned} 2 \int_0^{t_p} y^T(s) u(s) ds \\ \geq V(t_p) - V(0) + \gamma \int_0^{t_p} y^T(s) y(s) ds. \end{aligned} \quad (42)$$

From the definition of $V(t)$, we have $V(t_p) \geq 0$ and $V(0) \geq 0$. Thus,

$$2 \int_0^{t_p} y^T(s) u(s) ds \geq -\beta^2 + \gamma \int_0^{t_p} y^T(s) y(s) ds, \quad (43)$$

for all $t_p \geq 0$, $\beta = \sqrt{V(0)}$. The proof is completed. \square

Remark 8. In recent years, some researchers have studied the input passivity and output passivity of the complex networks with state coupling, and many interesting results have been derived. To the best of our knowledge, this is the first paper to investigate the input passivity and output passivity of complex delayed dynamical networks with output coupling. By constructing new Lyapunov functionals, some sufficient conditions ensuring the input passivity and output passivity are established in this paper.

4. Examples

In this section, two illustrative examples are provided to verify the effectiveness of the proposed theoretical results.

Example 1. Consider a three-order dynamical system as the dynamical node of the complex network (1) which is described by

$$\begin{pmatrix} \dot{x}_1 \\ \dot{x}_2 \\ \dot{x}_3 \end{pmatrix} = \begin{pmatrix} -10x_1 + 2x_2 \\ 2x_1 - 10x_2 - x_1x_3 \\ x_1x_2 - 6x_3 \end{pmatrix}. \quad (44)$$

Clearly, we can take $\eta = 6$, $P = \text{diag}(1, 1, 1)$, and $\Delta = \text{diag}(0, 0, 0)$. Take

$$\begin{aligned} \Gamma &= \begin{pmatrix} 0.4 & 0.2 & 0.2 \\ 0.3 & 0.2 & 0.3 \\ 0.3 & 0.1 & 0.2 \end{pmatrix}, & C_i &= \begin{pmatrix} 0.3 & 0.2 & 0.1 \\ 0.4 & 0.1 & 0.5 \\ 0.4 & 0.3 & 0.2 \end{pmatrix}, \\ B_i &= \begin{pmatrix} 0.3 & 0.1 & 0.1 \\ 0.4 & 0.1 & 0.3 \\ 0.7 & 0 & 0.2 \end{pmatrix}, & D_i &= \begin{pmatrix} 2.5 & 0 & 0 \\ 0 & 3.6 & 0 \\ 0 & 0 & 2.6 \end{pmatrix}, \end{aligned} \quad (45)$$

$a = 0.2$, $\beta_\omega = 1$, and $i = 1, 2, \dots, 10$. The matrix L is chosen as follows:

$$\begin{pmatrix} -3 & 1 & 1 & 0 & 0 & 0 & 0 & 0 & 0 & 1 \\ 1 & -4 & 1 & 0 & 1 & 0 & 1 & 0 & 0 & 0 \\ 1 & 1 & -5 & 1 & 0 & 1 & 0 & 0 & 0 & 1 \\ 0 & 0 & 1 & -3 & 1 & 0 & 0 & 0 & 1 & 0 \\ 0 & 1 & 0 & 1 & -3 & 1 & 0 & 0 & 0 & 0 \\ 0 & 0 & 1 & 0 & 1 & -3 & 1 & 0 & 0 & 0 \\ 0 & 1 & 0 & 0 & 0 & 1 & -4 & 1 & 0 & 1 \\ 0 & 0 & 0 & 0 & 0 & 0 & 1 & -2 & 1 & 0 \\ 0 & 0 & 0 & 1 & 0 & 0 & 0 & 1 & -2 & 0 \\ 1 & 0 & 1 & 0 & 0 & 0 & 1 & 0 & 0 & -3 \end{pmatrix}. \quad (46)$$

Obviously, network (1) is connected, and matrix G is

$$\begin{pmatrix} -1 & \frac{1}{3} & \frac{1}{3} & 0 & 0 & 0 & 0 & 0 & 0 & \frac{1}{3} \\ \frac{1}{4} & -1 & \frac{1}{4} & 0 & \frac{1}{4} & 0 & \frac{1}{4} & 0 & 0 & 0 \\ \frac{1}{5} & \frac{1}{5} & -1 & \frac{1}{5} & 0 & \frac{1}{5} & 0 & 0 & 0 & \frac{1}{5} \\ 0 & 0 & \frac{1}{3} & -1 & \frac{1}{3} & 0 & 0 & 0 & \frac{1}{3} & 0 \\ 0 & \frac{1}{3} & 0 & \frac{1}{3} & -1 & \frac{1}{3} & 0 & 0 & 0 & 0 \\ 0 & 0 & \frac{1}{3} & 0 & \frac{1}{3} & -1 & \frac{1}{3} & 0 & 0 & 0 \\ 0 & \frac{1}{4} & 0 & 0 & 0 & \frac{1}{4} & -1 & \frac{1}{4} & 0 & \frac{1}{4} \\ 0 & 0 & 0 & 0 & 0 & 0 & \frac{1}{2} & -1 & \frac{1}{2} & 0 \\ 0 & 0 & 0 & \frac{1}{2} & 0 & 0 & 0 & \frac{1}{2} & -1 & 0 \\ \frac{1}{3} & 0 & \frac{1}{3} & 0 & 0 & 0 & \frac{1}{3} & 0 & 0 & -1 \end{pmatrix}. \quad (47)$$

Next, we analyze the input passivity of complex network (1).

Setting $\tau(t) = 0.5 - 0.5e^{-t}$, then $0 \leq \tau(t) \leq \tau = 0.5$ and $\dot{\tau}(t) = 0.5e^{-t} \leq 0.5$, for $t \geq 0$.

We can find the following matrix Q satisfying (9) with $\gamma = 0.2$. Consider the following:

$$\begin{aligned} Q = & \text{diag}(0.5341, 0.4135, 0.3429, 0.5341, 0.4135, 0.3429, \\ & 0.5341, 0.4135, 0.3429, 0.5341, 0.4135, 0.3429, \\ & 0.5341, 0.4135, 0.3429, 0.5341, 0.4135, 0.3429, \\ & 0.5341, 0.4135, 0.3429, 0.5341, 0.4135, 0.3429, \\ & 0.5341, 0.4135, 0.3429, 0.5341, 0.4135, 0.3429). \end{aligned} \quad (48)$$

Hence, it follows from Theorem 4 that complex network (1) with above given parameters is input passive.

Example 2. Consider a three-order dynamical system as the dynamical node of the complex network (1) which is described by

$$\begin{pmatrix} \dot{x}_1 \\ \dot{x}_2 \\ \dot{x}_3 \end{pmatrix} = \begin{pmatrix} -9x_1 + 2x_2 \\ x_1 - 9x_2 - x_1x_3 \\ x_1x_2 - 7x_3 \end{pmatrix}. \quad (49)$$

Clearly, we can take $\eta = 7$, $P = \text{diag}(1, 1, 1)$, and $\Delta = \text{diag}(0, 0, 0)$. Take

$$\Gamma = \begin{pmatrix} 0.1 & 0.4 & 0.6 \\ 0.3 & 0.4 & 0.1 \\ 0.3 & 0.5 & 0.2 \end{pmatrix}, \quad C_i = \begin{pmatrix} 0.6 & 0.3 & 0.4 \\ 0.2 & 0.1 & 0.3 \\ 0.1 & 0.3 & 0.7 \end{pmatrix},$$

$$B_i = \begin{pmatrix} 0.1 & 0.5 & 0.3 \\ 0.5 & 0.3 & 0.1 \\ 0.2 & 0.7 & 0.2 \end{pmatrix}, \quad D_i = \begin{pmatrix} 2.9 & 0 & 0 \\ 0 & 3.3 & 0 \\ 0 & 0 & 2.8 \end{pmatrix}, \quad (50)$$

$a = 0.3$, $\beta_\omega = 1$, and $i = 1, 2, \dots, 10$. The matrix L is chosen as follows:

$$\begin{pmatrix} -2 & 0 & 0 & 0 & 0 & 0 & 0 & 0 & 1 & 1 \\ 0 & -1 & 1 & 0 & 0 & 0 & 0 & 0 & 0 & 0 \\ 0 & 1 & -2 & 0 & 0 & 0 & 0 & 0 & 0 & 1 \\ 0 & 0 & 0 & -1 & 0 & 0 & 0 & 0 & 0 & 1 \\ 0 & 0 & 0 & 0 & -1 & 0 & 0 & 0 & 0 & 1 \\ 0 & 0 & 0 & 0 & 0 & -1 & 0 & 0 & 1 & 0 \\ 0 & 0 & 0 & 0 & 0 & 0 & -1 & 1 & 0 & 0 \\ 0 & 0 & 0 & 0 & 0 & 0 & 1 & -2 & 1 & 0 \\ 1 & 0 & 0 & 0 & 0 & 1 & 0 & 1 & -4 & 1 \\ 1 & 0 & 1 & 1 & 1 & 0 & 0 & 0 & 1 & -5 \end{pmatrix}. \quad (51)$$

Obviously, network (1) is connected, and matrix G is

$$\begin{pmatrix} -1 & 0 & 0 & 0 & 0 & 0 & 0 & 0 & \frac{1}{2} & \frac{1}{2} \\ 0 & -1 & 1 & 0 & 0 & 0 & 0 & 0 & 0 & 0 \\ 0 & \frac{1}{2} & -1 & 0 & 0 & 0 & 0 & 0 & 0 & \frac{1}{2} \\ 0 & 0 & 0 & -1 & 0 & 0 & 0 & 0 & 0 & 1 \\ 0 & 0 & 0 & 0 & -1 & 0 & 0 & 0 & 0 & 1 \\ 0 & 0 & 0 & 0 & 0 & -1 & 0 & 0 & 1 & 0 \\ 0 & 0 & 0 & 0 & 0 & 0 & -1 & 1 & 0 & 0 \\ 0 & 0 & 0 & 0 & 0 & 0 & \frac{1}{2} & -1 & \frac{1}{2} & 0 \\ \frac{1}{4} & 0 & 0 & 0 & 0 & \frac{1}{4} & 0 & \frac{1}{4} & -1 & \frac{1}{4} \\ \frac{1}{5} & 0 & \frac{1}{5} & \frac{1}{5} & \frac{1}{5} & 0 & 0 & 0 & \frac{1}{5} & -1 \end{pmatrix}. \quad (52)$$

In the following, we analyze the output passivity of complex network (1).

Setting $\tau(t) = 0.5 - 0.5e^{-t}$, then $0 \leq \tau(t) \leq \tau = 0.5$ and $\dot{\tau}(t) = 0.5e^{-t} \leq 0.5$, for $t \geq 0$.

We can find the following matrix Q satisfying (30) with $\gamma = 0.1$. Consider the following:

$$\begin{aligned} Q = & \text{diag}(0.3548, 0.3893, 0.1592, 0.3548, 0.3893, 0.1592, \\ & 0.3548, 0.3893, 0.1592, 0.3548, 0.3893, 0.1592, \\ & 0.3548, 0.3893, 0.1592, 0.3548, 0.3893, 0.1592, \\ & 0.3548, 0.3893, 0.1592, 0.3548, 0.3893, 0.1592). \end{aligned} \quad (53)$$

By Theorem 6, we know that complex network (1) with above given parameters is output passive.

5. Conclusion

A new complex delayed dynamical network model with output coupling has been introduced. We have considered

the input passivity and output passivity of the proposed network model. Some input passivity and output passivity criteria have been established by constructing new Lyapunov functionals. Moreover, two illustrative examples have been provided to verify the correctness and effectiveness of the obtained results. In future work, we shall study the input passivity and output passivity of impulsive complex delayed dynamical networks with output coupling.

Conflict of Interests

The authors declare that there is no conflict of interests regarding the publication of this paper.

Acknowledgments

The authors would like to thank the Associate Editor and anonymous reviewers for their valuable comments and suggestions. This work was supported in part by the Fundamental Research Funds for the Central University (2013-YB-017).

References

- [1] J. Wang and H. Wu, "Synchronization criteria for impulsive complex dynamical networks with time-varying delay," *Nonlinear Dynamics*, vol. 70, no. 1, pp. 13–24, 2012.
- [2] J.-L. Wang and H.-N. Wu, "Stability analysis of impulsive parabolic complex networks," *Chaos, Solitons and Fractals*, vol. 44, no. 11, pp. 1020–1034, 2011.
- [3] J.-L. Wang, Z.-C. Yang, T.-W. Huang, and M.-Q. Xiao, "Local and global exponential synchronization of complex delayed dynamical networks with general topology," *Discrete and Continuous Dynamical Systems B*, vol. 16, no. 1, pp. 393–408, 2011.
- [4] J. Wang, Z. Yang, T. Huang, and M. Xiao, "Synchronization criteria in complex dynamical networks with nonsymmetric coupling and multiple time-varying delays," *Applicable Analysis*, vol. 91, no. 5, pp. 923–935, 2012.
- [5] T. Huang, G. Chen, and J. Kurths, "Synchronization of chaotic systems with time-varying coupling delays," *Discrete and Continuous Dynamical Systems B: A Journal Bridging Mathematics and Sciences*, vol. 16, no. 4, pp. 1071–1082, 2011.
- [6] W. Yu, G. Chen, and M. Cao, "Consensus in directed networks of agents with nonlinear dynamics," *IEEE Transactions on Automatic Control*, vol. 56, no. 6, pp. 1436–1441, 2011.
- [7] W. W. Yu, J. D. Cao, and J. H. Lü, "Global synchronization of linearly hybrid coupled networks with time-varying delay," *SIAM Journal on Applied Dynamical Systems*, vol. 7, no. 1, pp. 108–133, 2008.
- [8] X. Yang, J. Cao, and J. Lu, "Stochastic synchronization of complex networks with nonidentical nodes via hybrid adaptive and impulsive control," *IEEE Transactions on Circuits and Systems. I. Regular Papers*, vol. 59, no. 2, pp. 371–384, 2012.
- [9] G. Wang, J. Cao, and J. Lu, "Outer synchronization between two nonidentical networks with circumstance noise," *Physica A*, vol. 389, no. 7, pp. 1480–1488, 2010.
- [10] L. Y. Xiang and J. J. H. Zhu, "On pinning synchronization of general coupled networks," *Nonlinear Dynamics*, vol. 64, no. 4, pp. 339–348, 2011.
- [11] G. P. Jiang, W. K. S. Tang, and G. R. Chen, "A state-observer-based approach for synchronization in complex dynamical networks," *IEEE Transactions on Circuits and Systems I: Regular Papers*, vol. 53, no. 12, pp. 2739–2745, 2006.
- [12] Y. Gao and L. Wang, "Consensus of multiple dynamic agents with sampled information," *IET Control Theory & Applications*, vol. 4, no. 6, pp. 945–956, 2010.
- [13] J. L. Wang and H. N. Wu, "Local and global exponential output synchronization of complex delayed dynamical networks," *Nonlinear Dynamics*, vol. 67, no. 1, pp. 497–504, 2012.
- [14] J. L. Wang and H. N. Wu, "Adaptive output synchronization of complex delayed dynamical networks with output coupling," *Neurocomputing*, vol. 142, pp. 174–181, 2014.
- [15] J. L. Wang and H. N. Wu, "Passivity of delayed reaction-diffusion networks with application to a food web model," *Applied Mathematics and Computation*, vol. 219, no. 24, pp. 11311–11326, 2013.
- [16] R. Lozano, B. Brogliato, O. Eegland, and B. Maschke, *Dissipative Systems Analysis and Control: Theory and Applications*, Communications and Control Engineering Series, Springer, London, UK, 2000.
- [17] H. Gao, T. Chen, and T. Chai, "Passivity and passification for networked control systems," *SIAM Journal on Control and Optimization*, vol. 46, no. 4, pp. 1299–1322, 2007.
- [18] J. L. Chen and L. Lee, "Passivity approach to feedback connection stability for discrete-time descriptor systems," in *Proceeding of the 40th IEEE Conference on Decision and Control (CDC '01)*, vol. 3, pp. 2865–2866, Orlando, Fla, USA, December 2001.
- [19] X. W. Liu, "Passivity analysis of uncertain fuzzy delayed systems," *Chaos, Solitons and Fractals*, vol. 34, no. 3, pp. 833–838, 2007.
- [20] J. Liang, Z. Wang, and X. Liu, "Robust passivity and passification of stochastic fuzzy time-delay systems," *Information Sciences*, vol. 180, no. 9, pp. 1725–1737, 2010.
- [21] W. J. Chang, C. C. Ku, and P. H. Huang, "Fuzzy controller design for passive continuous-time affine T-S fuzzy models with relaxed stability conditions," *ISA Transactions*, vol. 48, no. 3, pp. 295–303, 2009.
- [22] C. Li, H. Zhang, and X. Liao, "Passivity and passification of fuzzy systems with time delays," *Computers & Mathematics with Applications*, vol. 52, no. 6–7, pp. 1067–1078, 2006.
- [23] X. Y. Lou and B. T. Cui, "Passivity analysis of integro-differential neural networks with time-varying delays," *Neurocomputing*, vol. 70, no. 4–6, pp. 1071–1078, 2007.
- [24] J. H. Park, "Further results on passivity analysis of delayed cellular neural networks," *Chaos, Solitons and Fractals*, vol. 34, no. 5, pp. 1546–1551, 2007.
- [25] B. Chen, H. Li, C. Lin, and Q. Zhou, "Passivity analysis for uncertain neural networks with discrete and distributed time-varying delays," *Physics Letters A*, vol. 373, no. 14, pp. 1242–1248, 2009.
- [26] Q. Song, J. Liang, and Z. Wang, "Passivity analysis of discrete-time stochastic neural networks with time-varying delays," *Neurocomputing*, vol. 72, no. 7–9, pp. 1782–1788, 2009.
- [27] Q. Song and Z. Wang, "New results on passivity analysis of uncertain neural networks with time-varying delays," *International Journal of Computer Mathematics*, vol. 87, no. 1–3, pp. 668–678, 2010.
- [28] C. G. Li and X. F. Liao, "Passivity analysis of neural networks with time delay," *IEEE Transactions on Circuits and Systems II: Express Briefs*, vol. 52, no. 8, pp. 471–475, 2005.
- [29] J. Yao, H. O. Wang, Z. H. Guan, and W. S. Xu, "Passive stability and synchronization of complex spatio-temporal switching

- networks with time delays,” *Automatica*, vol. 45, no. 7, pp. 1721–1728, 2009.
- [30] J. Yao, Z. H. Guan, and D. J. Hill, “Passivity-based control and synchronization of general complex dynamical networks,” *Automatica*, vol. 45, no. 9, pp. 2107–2113, 2009.
- [31] J. L. Wang, H. N. Wu, and L. Guo, “Passivity and stability analysis of reaction-diffusion neural networks with dirichlet boundary conditions,” *IEEE Transactions on Neural Networks*, vol. 22, no. 12, pp. 2105–2116, 2011.
- [32] J.-L. Wang, Z.-C. Yang, and H.-N. Wu, “Passivity analysis of complex dynamical networks with multiple time-varying delays,” *Journal of Engineering Mathematics*, vol. 74, pp. 175–188, 2012.
- [33] J.-L. Wang and H.-N. Wu, “Robust stability and robust passivity of parabolic complex networks with parametric uncertainties and time-varying delays,” *Neurocomputing*, vol. 87, pp. 26–32, 2012.
- [34] A. J. Laub, *Matrix Analysis for Scientists and Engineers*, Society for Industrial and Applied Mathematics, Philadelphia, PA, USA, 2005.
- [35] W. L. Guo, F. Austin, and S. H. Chen, “Global synchronization of nonlinearly coupled complex networks with non-delayed and delayed coupling,” *Communications in Nonlinear Science and Numerical Simulation*, vol. 15, no. 6, pp. 1631–1639, 2010.

Research Article

A Knowledge-Based Service Composition Algorithm with Better QoS in Semantic Overlay

Huijun Dai,¹ Hua Qu,¹ and Jihong Zhao^{1,2}

¹*School of Electronic Information, Xi'an Jiaotong University, Xi'an, Shaanxi 710049, China*

²*Department of Communication Engineering, Xi'an University of Posts and Telecommunications, Xi'an, Shaanxi 710061, China*

Correspondence should be addressed to Huijun Dai; ddahjun@gmail.com

Received 1 May 2014; Revised 21 August 2014; Accepted 22 August 2014

Academic Editor: Chuandong Li

Copyright © 2015 Huijun Dai et al. This is an open access article distributed under the Creative Commons Attribution License, which permits unrestricted use, distribution, and reproduction in any medium, provided the original work is properly cited.

A semantic overlay network (SON) is a visual framework clustered under similar metaknowledge units such as ontologies, algorithms, and rule engines. Knowledge-based service composition (KC) has become a prominent aspect of building new and creative composed service through a combination of semantically similar information at the knowledge level. In this study, a promising approach to construct a standard knowledge model is developed to utilize the progress of KC. To evaluate and optimize the composition, we define the quantity of service (QoS) regarding user requirements in the KC instance, and a KC instance path with better QoS is found in the model using the KC algorithm. Simulation results prove that our approach has a tradeoff between efficiency and equality.

1. Introduction

Knowledge-based applications are organized according to semantic relevance and context in semantic overlay network (SON) with the purpose of retrieving the service in a large-scale intelligent information system [1]. In a SON, many groups of nodes with similar content or documents compose reusable software service into an integrated heterogeneous virtual platform for sharing information [2]. Content-addressable network (CAN) is also essentially a type of SON via content cached at nodes based on content routing for locating content [3, 4]. With the accumulation of massive amounts of service or application from many different domains (e.g., scientific research and personal and corporate communications or interactions [5]) for specific service supplying, the SON aims to thoroughly bind such individual and distributed services into workflow systems that support different kinds of knowledge sharing [6]. The approach of composition must support the evaluation of quality of service (QoS) to optimize the composition effect of reusable software. Therefore, the purpose of knowledge-based composition

(KC) is not different from that of traditional service composition because the former can reuse the more units (e.g., databases, algorithms, and tools from different fields which could also be regarded as individual service [7]) in semantic level. While, knowledge-based service composition makes information sharing more dynamic, flexible, and scalable.

Therefore, KC is intended to share a wider range of information or services scattered across numerous distributed nodes. There are multiple QoS attributes that users pay attention to including price, reputation, reliability, and delay [8]. Although previous studies related to better QoS have contributed significantly to service composition in semantic web, most of them are still limited to traditional semantic web service and do not extend to overlay based on knowledge. This study aims to find a novel way to compose service based on knowledge sharing with better QoS in an SON.

The rest of this paper is organized as follows. The approach is formally modeled and related studies are reviewed in Section 2. Section 3 presents the adopted KC model in a SON. The exhaustive algorithm process is detailed and implemented in Section 4. In Section 5, the algorithm

is examined and evaluated by simulation. The conclusion is provided in Section 6.

2. Related Works

The massive amounts of distributed service or units such as those available from digital libraries and web-accessible text databases motivate researchers to work toward efficient service management in highly distributed environments [9]. By correlating these isolated islands of information, individuals can gain new insights, discover new relationships, and produce more knowledge [10]. A large body of work on knowledge-based service composition in SONs has been generated [6, 9, 11–13]. Certain approaches use algebra in composing ontologies that represent the terminologies from distinct, typically autonomous domains to compose knowledge [14, 15]. Usually, the links of ontology among the domains are called intersections [16].

Knowledge-based service composition is different from knowledge discovery [17] or knowledge creation [18] because that the former enable users to collectively create, share, browse, and query their own individual knowledge [13, 19, 20]. Some recommendations or recommender systems compose a set of services into data processing logic which combine the service according to user preferences or its execution environment [15].

Significant research has focused on optimizing the QoS of service composition [21, 22]. Existing approaches often show a tradeoff in every aspect to gain balanced performance [23, 24]. In fact, KC can be implemented and utilized in e-ScienceNet [25], e-Flow with customized services [26]. Cross-enterprise collaboration has emerged using automatic business composition in the global market [27]. In the scientific research, medical information, and collaborative manufacturing, the creative approach of the KC for a SON is also presented [28] for searching service-oriented knowledge utilities [29]. The process of KC should include information retrieval, knowledge representation, and databases, as well as exploiting pieces of knowledge from the multitude of heterogeneous sources available. In [30], the candidates with the same functionality are organized as a class and ACO4WS is used to test the feasibility and soundness of the approach.

Based on the aforementioned study, such a conclusion can be reached. Firstly, SONs have received growing attention as a scalable and distributed platform for knowledge-sharing applications. Then, KC dynamically combines two or more basic services (called units) into potentially complex value-added knowledge-based workflow to fulfill the functional requirements of the user. Finally, the key to KC is to choose a scheme with better QoS under the QoS constraints.

3. Problem Formulation

In knowledge repository, a unit (subservice) can be expressed as $K = \{I, O, Q\}$, I is the input set, O represents the output set, and Q is the QoS. The QoS of a KC consists of the following parameters: $\{Q_1, Q_2, \dots, Q_n\}$.

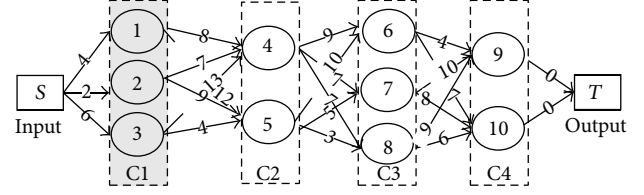


FIGURE 1: Units in SON.

The QoS attributes Q_i are availability, cost, time overhead, and so on. The model can be classified into subservice and compositional service. The subservice is a single unit cached in SON just like the one shown in Figure 1. The model enables the incorporation of various composition approaches by starting from the input of the first unit, traversing through the chosen unit, and ending at the output of the final unit in different knowledge repositories.

N different but semantically related subservice constructs a body of compositional service from M SONs, and KC involves mapping from the composite template to instantiated knowledge. The previous subservice output should be consistent with the next subservice input at the knowledge level. Each subservice in an SON has a few candidates called units, which are those that have the same or similar meaning or function. In Figure 1, points 1, 2, and 3 are candidates in SON1. The points and links between them can form an indirect graph from source to target. A weighted link between points represents the QoS of discovering or retrieving the next node. The QoS labeled in links merges the different QoS attributes of nodes using a cost function. The KC with different QoS indicates different paths in the knowledge graph. So, we can get the following.

The QoS of KC indicates the overall QoS of the instantiated knowledge path, which can be calculated as follows: $Q_{com} = \sum_{i=1}^n Q_i$, where Q_i represents the merged QoS of nodes and links. For example, the availability and time of the overall QoS of composition can be expressed as

$$\ln \frac{1}{A_{com}} = \sum_{i=1}^n \ln \frac{1}{A_{node(i)}} + \sum_{j=1}^{n-1} \ln \frac{1}{A_{link(j)}}, \quad (1)$$

$$Time_{com} = \sum_{i=1}^n RTT_i + \sum_{j=1}^{n-1} Delay_j.$$

$A_{node(i)}$ refers to the availability of node i , $A_{link(j)}$ stands for the availability of the conjoint link j , and RTT_i and $Delay_j$ represent the round trip time of node and links' delay. Given the semantic similarity of the nodes, their QoS in the same SONs can be considered as equal, and the QoS of the links are not equal because of the different locations. Because the QoS of KC path can translate into the additive metrics, the best QoS of KC also indicates the smallest QoS of links in the knowledge graph.

The KC progress can be formulated based on the knowledge graph model shown in Figure 2 which is converted from Figure 1. In Figure 2, the QoS has been marked in links.

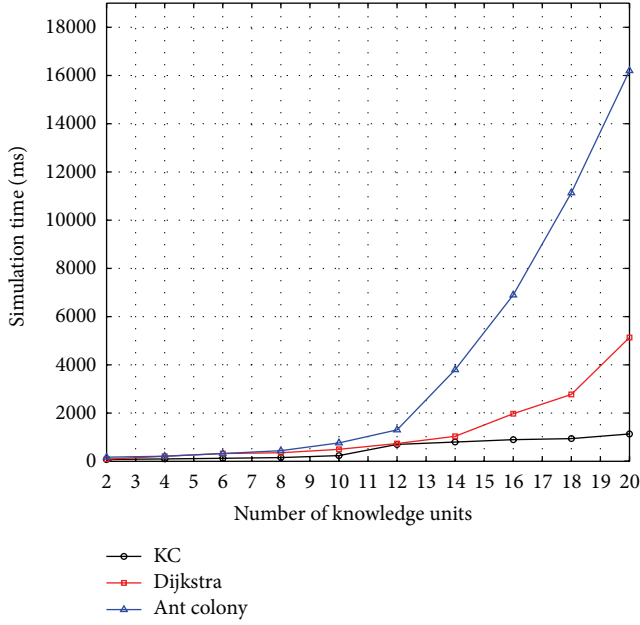


FIGURE 2: Time curves with metaknowledge.

TABLE 1: Adjacent matrix 1.

	S	1	2	3
S	0	4	2	6
1		0	0	0
2			0	0
3				0

4. KC Approach with Better QoS

The target of KC is to find an optimal path in the graph by comparing the total QoS as the cost function. Instead of searching the entire SON, the KC algorithm involves three basic steps: probing and collecting the information; path; backwording.

4.1. An Instance. There is an instance to show how this approach works. In probing, matrices of different nodes in neighbor SONs are constructed filling with the QoS values of the links. Because the knowledge model graph is indirect, the constructing matrix is symmetrical.

During the probing, the constructing matrixes are as in Tables 1, 2, 3, and 4.

The searching results are saved with link-table.

During probing and constructing, we can find an initial path. In this example, from the node of S, the next node of 2 should be chosen. Then from the node 2, the node of 4 should be chosen. Thus, the node sequence is $S \rightarrow 2 \rightarrow 4 \rightarrow 7 \rightarrow 10 \rightarrow T$, in which the QoS of the total path is the sum of each link's QoS indicated as Cal_sum . Now, the Cal_sum is "24" in this example.

During the path, the minimum is found and chosen from the second matrix of Table 2. The nodes with minimum link are located, then search the shortest link starting from the

TABLE 2: Adjacent matrix 2.

	1	2	3	4	5
1	0	0	0	8	12
2		0	0	7	9
3			0	13	4
4				0	0
5					0

TABLE 3: Adjacent matrix 3.

	4	5	6	7	8
4	0	0	9	7	7
5		0	10	5	3
6			0	0	0
7				0	0
8					0

TABLE 4: Adjacent matrix 4.

	6	7	8	9	10
6	0	0	0	4	7
7		0	0	10	8
8			0	9	6
9				0	0
10					0

nodes. The searching include forward and backward until a path was been chosen.

The backwording progress will traverse all the matrixes and give out different paths with better QoS in their SON. Then, there are M (the number of SON) paths with their nodes and QoS are saved and compared. The final Cal_sum of smallest QoS is 19, and the node sequence is $S \rightarrow 3 \rightarrow 5 \rightarrow 8 \rightarrow 10 \rightarrow T$.

In this example, the KC instance is found in which the path with smaller QoS is obtained through a simple linear search algorithm. The time complexity does not depend on the number of SONs (matrixes). This approach may not find a path with best QoS because of the local optimization. But it will get a tradeoff between efficiency and equality. Although the nodes in knowledge model graph continually grow with the number of metaknowledge units, the time complexity of this approach will not soar but increase linearly.

5. Simulation and Analysis

5.1. Simulation Environment. To evaluate the performance of proposed KC algorithms with better QoS, we use them in the specified application. We suppose that the application has certain user requirements as input and the expected results as the output. The number of metaknowledge units spreading across different specific P2P systems is less than 20 (including source and target), and each metaknowledge has a few candidates with the same meaning, input, and output. Then, the workflow graph of this application can be formulated as shown in Figure 2, where N , ($N < 20$)

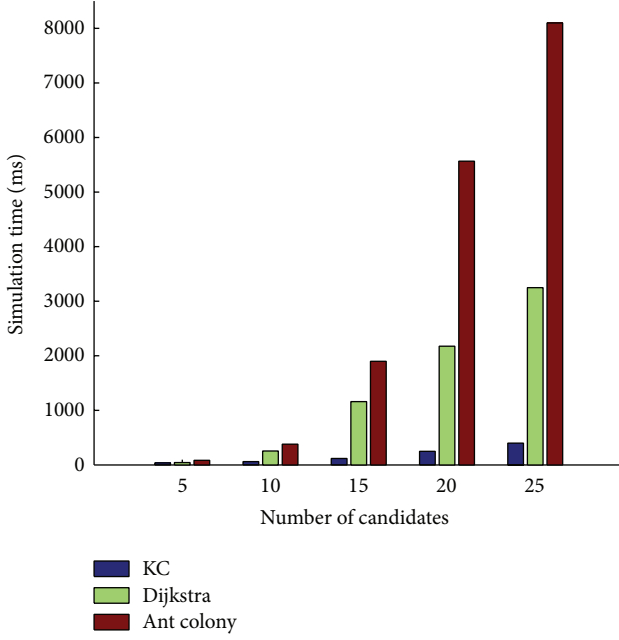


FIGURE 3: Time curves with candidates.

groups of nodes are shown. The underlying physical topology is generated by GT-ITM using n -node transit-stub models. To simulate the performance variation in the real world and the initial availability of each node, we distribute the QoS of each link uniformly in a certain range.

To verify the effectiveness of the proposed approach (KC), we compare it with two types of algorithms: one is the shortest path algorithm with optimal results and the other is the heuristic algorithm (ant colony) with local optimal results in service composition. We have attempted to provide the same conditions (e.g., interface and input data) for three kinds of algorithms.

5.2. Simulation Results. With regard to the optimal algorithm, Dijkstra and ant colony algorithms require more time and calculation to obtain the solution. Therefore, from the perspective of theoretical analysis, the time complexity of the Dijkstra $\Theta(N^2)$ and the time complexity of traditional ant colony algorithms were greater than that of our approach. These two solutions employ the global optimization approach but do not show promising running speed. The time complexity of the KC algorithm increases linearly.

For the sake of a number of candidates in many SONs, which continuously increase along with the growth of the SON, by taking more storage space in computing service (numerous matrices with the QoS of links), the approach obviously has quick convergence speed. However, the KC algorithm is not optimal. In the worst case, the iterations would reach $\Theta(N)$. Three simulation time curves of those algorithms which would vary with the numbers of meta-knowledge units or the candidates are shown in Figures 2 and 3. The number of meta-knowledge units influences our approach, whereas the number of the candidates influences the two other approaches.

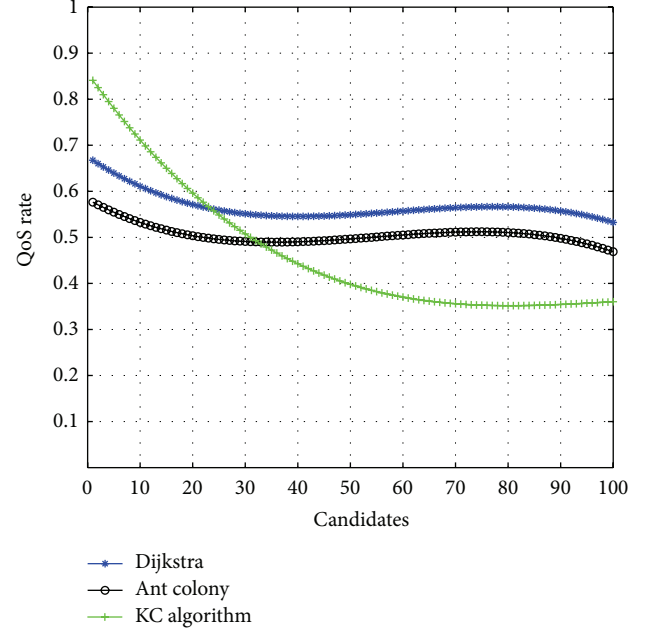


FIGURE 4: QoS rate of three algorithms.

The metric for evaluating the KC approach performance is the QoS rate. This rate is defined as

$$\text{QoS rate} = \frac{\text{numbers of satisfied instances}}{\text{numbers of required}}. \quad (2)$$

For this target, our approach has a lower QoS rate just like what is shown in Figure 4. This figure shows that our QoS rate is less than that of the other algorithms, particularly when a number of candidates exist. Comparing with other algorithms, our approach simplified the composition progress at the cost of QoS rate.

We also implement another two common heuristic algorithms used in service composition for comparison. One is ACO4WS [30], which is based on a general knowledge model, and the other is mixed integer linear programming, an algorithm for semiautomatic merging and alignment ontologies. Both algorithms are applicable to a wide range of knowledge representation and ontology development systems. Three algorithms are based on a different model, but the similarity is that all of them map the function modules into node graphs, and all focus on the matrix of QoS. Three simulation time curves of those algorithms varied with the candidates, as shown in Figure 5.

The experimental results indicate that the QoS rate of each algorithm decreases slightly with the increase of function modules because finding a path in a more complex graph is difficult. However, the QoS rate of KC has a higher value than that of the two other algorithms because KC uses a simple principle to measure QoS (smaller is better), which can fulfill most of the QoS attributes.

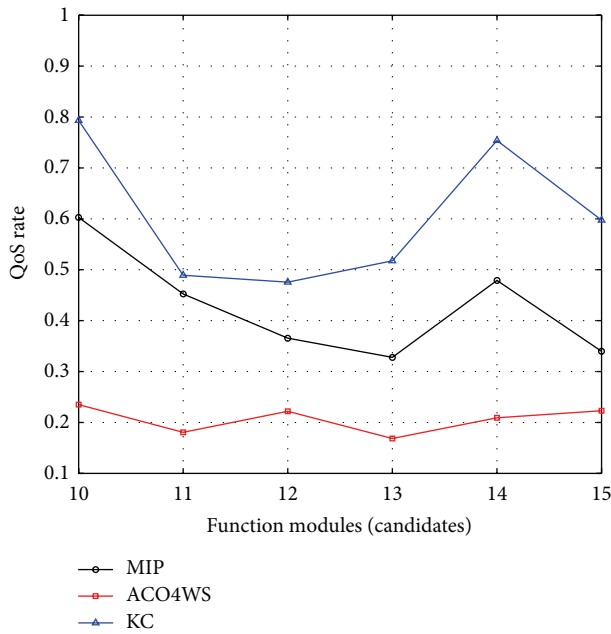


FIGURE 5: QoS rate with three local optimization methods.

6. Conclusions

In this study, we investigated the KC algorithm in the SON based on distributed knowledge systems. Unlike various existing studies, our work converts the problem into two sections for analysis. First, the knowledge-based service composition is transformed into the instance path in the graph with a sequence work flow with interface between the previous output and successor input. Second, the KC algorithm with better QoS is transformed into the shortest path problem, which has a local optimization result related to the KC model. Regarding the performance shown in Section 5, we believe that the proposed approach can open a wide range of new studies intended to improve the performance of knowledge-based information sharing or create new combined service across various disciplines (e.g., digital biomedical and aerospace material industries). We intend to study another algorithm to address such problems in the future. Such an algorithm with better QoS can be solved by adapting other optimization algorithms as part of our future work.

Conflict of Interests

The authors declare that there is no conflict of interests regarding the publication of this paper.

References

- [1] A. Crespo and H. Garcia-Molina, "Semantic overlay networks for P₂P systems," in *Agents and Peer-to-Peer Computing*, vol. 3601 of *Lecture Notes in Computer Science*, pp. 1–13, Springer, Berlin, Germany, 2005.
- [2] R. Yin, "Study of composing web service based on SOA," in *Proceedings of the 2nd International Conference on Green Communications and Networks 2012 (GCN 2012): Volume 2*, vol. 224 of *Lecture Notes in Electrical Engineering*, pp. 209–214, Springer, Berlin, Germany, 2013.
- [3] Z. Zhengdong, H. Yahong, W. Weiguo, W. Yong, and L. Zengzhi, "CAN-based P2P semantic web services composite architecture," *Journal of Xi'an Jiaotong University*, no. 2, pp. 6–10, 2010.
- [4] A. Fiat and J. Saia, "Censorship resistant peer-to-peer content addressable networks," in *Proceedings of the 13th ACM-SIAM Symposium on Discrete Algorithms (SODA '02)*, pp. 94–103, SIAM, Philadelphia, Pa, USA, 2002.
- [5] C. Tang, Z. Xu, and S. Dwarkadas, "Peer-to-peer information retrieval using self-organizing semantic overlay networks," in *Proceedings of the ACM Conference on Computer Communications (SIGCOMM '03)*, pp. 175–186, New York, NY, USA, August 2003.
- [6] A.-L. Lamprecht, T. Margaria, and B. Steffen, "Bio-jETI: a framework for semantics-based service composition," *BMC Bioinformatics*, vol. 10, supplement 10, article S8, 19 pages, 2009.
- [7] A.-L. Lamprecht, T. Margaria, and B. Steffen, "Bio-jETI: a framework for semantics-based service composition," *BMC Bioinformatics*, vol. 10, supplement 10, article S8, 19 pages, 2009.
- [8] A.-L. Lamprecht, T. Margaria, and B. Steffen, "Bio-jETI: a framework for semantics-based service composition," *BMC Bioinformatics*, vol. 10, supplement 10, article S8, 2009.
- [9] B. Aleman-Meza, C. Halaschek, and I. B. Arpinar, *Collective Knowledge, Composition in a Peer-to-Peer Network: A survey for Peer-to-Peer applications*, Idea-Group, 2005.
- [10] G. Deconinck and K. Vanthournout, "Agora: a semantic overlay network," *International Journal of Critical Infrastructures*, vol. 5, no. 1-2, pp. 175–195, 2009.
- [11] Y. Mao, B. T. Loo, Z. Ives, and J. M. Smith, "MOSAIC: declarative platform for dynamic overlay composition," *Computer Networks*, vol. 56, no. 1, pp. 64–84, 2012.
- [12] P. Küngas and M. Matskin, "Semantic web service composition through a P₂P-based multi-agent environment," in *Agents and Peer-to-Peer Computing*, Z. Despotovic, S. Joseph, and C. Sartori, Eds., vol. 4118 of *Lecture Notes in Computer Science*, pp. 106–119, Springer, Berlin, Germany, 2006.
- [13] C. Radeck, A. Lorz, G. Blichmann, and K. Meißner, "Hybrid recommendation of composition knowledge for end user development of mashups," in *Proceedings of the 7th International Conference on Internet and Web Applications and Services (ICIW '12)*, 2012.
- [14] S. R. Chowdhury, F. Daniel, and F. Casati, "Efficient, interactive recommendation of mashup composition knowledge," in *Service-Oriented Computing*, vol. 7084 of *Lecture Notes in Computer Science*, pp. 374–388, Springer, Berlin, Germany, 2011.
- [15] M. Bajaj, "Knowledge composition methodology for effective analysis problem formulation in simulation-based design," ProQuest, 2008.
- [16] J. Gama, *Knowledge Discovery from Data Streams*, Chapman & Hall/CRC Data Mining and Knowledge Discovery Series, Chapman & Hall/CRC, Boca Raton, Fla, USA, 2010.
- [17] J. Gama, *Knowledge Discovery from Data Streams*, Chapman & Hall, CRC Press, Boca Raton, Fla, USA, 2010.
- [18] S. Kalasapur, M. Kumar, and B. A. Shirazi, "Dynamic service composition in pervasive computing," *IEEE Transactions on Parallel and Distributed Systems*, vol. 18, no. 7, pp. 907–918, 2007.

- [19] K. Nahrstedt and W. Balke, "A taxonomy for multimedia service composition," in *proceedings of the 12th ACM International Conference on Multimedia*, pp. 88–95, New York, NY, USA, October 2004.
- [20] X. Gu, K. Nahrstedt, R. N. Chang, and C. Ward, "QoS-assured service composition in managed service overlay networks," in *Proceedings of the 23rd International Conference on Distributed Computing Systems*, pp. 194–201, 2003.
- [21] F. Mardukhi, N. NematBakhsh, K. Zamanifar, and A. Barati, "QoS decomposition for service composition using genetic algorithm," *Applied Soft Computing Journal*, vol. 13, no. 7, pp. 3409–3421, 2013.
- [22] J. Liao, Y. Liu, X. Zhu, T. Xu, and J. Wang, "Niching particle swarm optimization algorithm for service composition," in *Proceedings of the IEEE Global Telecommunications Conference (GLOBECOM '11)*, pp. 1–6, Houston, Tex, USA, December 2011.
- [23] C. Bussler and A. Haller, *Towards P2P-Based Semantic Web Service Discovery with QoS Support*, Springer, Berlin, Germany, 2006.
- [24] T. Classe, R. Braga, F. Campos, and J. M. N. David, "A semantic peer-to-peer network for service composition in scientific domains," in *Proceedings of the International Conference on Project MANagement/ (HCIST '13), International Conference on Health and Social Care Information Systems and Technologies, Procedia Technology*, vol. 9, 2013, pp. 215–225.
- [25] F. Casati, S. Ilnicki, L. J. Jin, V. Krishnamoorthy, and M.-C. Shan, "Adaptive and dynamic service composition in eFlow," in *Advanced Information Systems Engineering*, vol. 1789 of *Lecture Notes in Computer Science*, pp. 13–31, 2000.
- [26] F. Skopik, D. Schall, and S. Dustdar, "Managing social overlay networks in semantic open enterprise systems," in *Proceedings of the International Conference on Web Intelligence, Mining and Semantics (WIMS '11)*, May 2011.
- [27] M. Gharzouli and M. Boufaida, "PM4SWS: a P2P model for semantic web services discovery and composition," *Journal of Advances in Information Technology*, vol. 2, no. 1, pp. 15–26, 2011.
- [28] C.-H. Wu, K. Chiang, R.-J. Yu, and S.-D. Wang, "Locality and resource aware peer-to-peer overlay networks," *Journal of the Chinese Institute of Engineers*, vol. 31, no. 7, pp. 1207–1217, 2008.
- [29] P. Świątek, P. Stelmach, A. Prusiewicz, and K. Juszczyszyn, "Service composition in knowledge-based SOA systems," *New Generation Computing*, vol. 30, no. 2-3, pp. 165–188, 2012.
- [30] D. Ardagna and B. Pernici, "Adaptive service composition in flexible processes," *IEEE Transactions on Software Engineering*, vol. 33, no. 6, pp. 369–384, 2007.

Research Article

A New Recommendation Algorithm Based on User's Dynamic Information in Complex Social Network

Jiujun Cheng,¹ Yingbo Liu,² Huiting Zhang,³ Xiao Wu,² and Fuzhen Chen²

¹Department of Computer Science and Technology, Tongji University, Shanghai 201804, China

²Key Laboratory of Embedded System and Service Computing of Ministry of Education, Tongji University, Shanghai 201804, China

³Shanghai Modern Circulation School, No. 4800 Caoan Road, Shanghai 201804, China

Correspondence should be addressed to Yingbo Liu; yingbooryu@gmail.com

Received 25 May 2014; Revised 14 October 2014; Accepted 14 October 2014

Academic Editor: He Huang

Copyright © 2015 Jiujun Cheng et al. This is an open access article distributed under the Creative Commons Attribution License, which permits unrestricted use, distribution, and reproduction in any medium, provided the original work is properly cited.

The development of recommendation system comes with the research of data sparsity, cold start, scalability, and privacy protection problems. Even though many papers proposed different improved recommendation algorithms to solve those problems, there is still plenty of room for improvement. In the complex social network, we can take full advantage of dynamic information such as user's hobby, social relationship, and historical log to improve the performance of recommendation system. In this paper, we proposed a new recommendation algorithm which is based on social user's dynamic information to solve the cold start problem of traditional collaborative filtering algorithm and also considered the dynamic factors. The algorithm takes user's response information, dynamic interest, and the classic similar measurement of collaborative filtering algorithm into account. Then, we compared the new proposed recommendation algorithm with the traditional user based collaborative filtering algorithm and also presented some of the findings from experiment. The results of experiment demonstrate that the new proposed algorithm has a better recommended performance than the collaborative filtering algorithm in cold start scenario.

1. Introduction

A social network site, such as Facebook, Twitter, and Sina Weibo, has become an indispensable part of Internet users online life. It is also an important way of user information sharing and obtaining. However, with the number of social network users going into explosive growth, the information generated by the user also increases numerously. Therefore, when the user's ability to process information cannot keep up with the speed of the network information explosion, the user will have the problem of information overload [1]. It will increase the cost of obtaining useful information. Recommendation system [2, 3] as a kind of technology can effectively alleviate the information overload problem and provides users with excellent personalized service.

In the traditional personalized recommendation algorithm, collaborative filtering algorithm [4, 5] is undoubtedly the most successful one. The collaborative filtering recommendation algorithm is based on the similarity preference

between users of some certain items. More generally speaking, if they have similar interests in some items, it is most possible that they are interested in some other items. The defect of collaborative filtering algorithm is that it does not reflect that the user's preferences are not immutable but has the feature of the dynamic changes [6–8]. It also did not take the user's contextual factors into consideration. Therefore, the traditional collaborative filtering algorithm has some defects compared with other algorithms. Recently some published papers show that the improved algorithm will result in better recommendation performance by considering the user dynamic context factors in social network scenario [9, 10].

In this paper, we proposed the recommendation algorithm based on user's dynamic information in complex social network to address the above problems. By considering the dynamic information of user's response information and time factor to reflect the user's dynamic preference feature, we proposed an improved recommendation algorithm, combined with a new similarity measurement. Then the

experiments show that the new proposed algorithm has better recommendation performance than the traditional collaborative filtering recommendation algorithm.

2. Related Work

The collaborative filtering recommendation algorithm is one of the most successful recommendation algorithms. The core idea of it can be divided into three parts: first, to calculate the similarity between users from the user's historical interest information; then, to select the K nearest neighbors according to the similarity of users to predict the user's preference for particular items; finally, to select several items whose prediction score is enough high as a result of recommendation system recommended to the user.

2.1. The Traditional Similarity Measurement Method. The key point of the collaborative filtering recommendation is the measurement of similarity between different users. The widely adopted method is based on the similarity calculation of users' common historical ratings data. Among the similarity calculation methods, although each one has its own advantages and disadvantages, the most common method [2, 5, 11–14] is the Pearson similarity [2, 11] and the Cosine similarity [5, 10].

(1) Pearson similarity method: in the process of Pearson similarity calculation, we can get the similarity between different users based on the common items preference ratings. We give formalized representation here. Let user x, y 's rated common item set be $I_{x,y}$; $r_{x,i}$ and $r_{y,i}$ represent the user's historical rating score of the item; furthermore, in order to eliminate the influence of the user rating score scale problem, we will subtract the user's average score in the process of calculating user similarity; let \bar{r}_x and \bar{r}_y represent the average rating score of the item of user x and user y , respectively, which comes from the equation $\bar{r}_x = (1/|I_{x,y}|) \sum_{i \in I_{x,y}} r_{x,i}$ of user x and the equation $\bar{r}_y = (1/|I_{x,y}|) \sum_{i \in I_{x,y}} r_{y,i}$ of user y . So the Pearson similarity between user x and user y can be defined as

$$\text{Sim}(x, y) = \frac{\sum_{i \in I_{x,y}} (r_{x,i} - \bar{r}_x)(r_{y,i} - \bar{r}_y)}{\sqrt{\sum_{i \in I_{x,y}} (r_{x,i} - \bar{r}_x)^2} \sqrt{\sum_{i \in I_{x,y}} (r_{y,i} - \bar{r}_y)^2}}. \quad (1)$$

(2) Cosine similarity method: in the process of Cosine similarity calculation, we treat user's historical rating score as an m -dimensional vector. The similarity between two users x and y is defined as the cosine of these two vectors. Let user x and user y 's historical rating vectors be \vec{x} and \vec{y} , and the rated item set is I_x, I_y . So the cosine similarity of users is given by

$$\begin{aligned} \text{Sim}(x, y) &= \cos(\vec{x}, \vec{y}) = \frac{\vec{x} \cdot \vec{y}}{\|\vec{x}\| \times \|\vec{y}\|} \\ &= \frac{\sum_{i \in I_{x,y}} r_{x,i} r_{y,i}}{\sqrt{\sum_{i \in I_x} r_{x,i}^2} \sqrt{\sum_{i \in I_y} r_{y,i}^2}}. \end{aligned} \quad (2)$$

Once we get the set of nearest neighbor users [15] based on the similarity measures, we named the set N_u . Then the

prediction rating score on an item i for target user u by using this formula is as follows:

$$R_{u,i} = \bar{r}_u + \frac{\sum_{u' \in N_u} \text{Sim}(u, u') \times (r_{u',i} - \bar{r}_{u'})}{\sum_{u' \in N_u} (|\text{Sim}(u, u')|)}, \quad (3)$$

where $\text{Sim}(u, u')$ is the similarity between target user u and one of the nearest neighbor users u' , $r_{u',i}$ is the interest rating score of user u' to item i , and \bar{r}_u and $\bar{r}_{u'}$, respectively, represent the average interest rating score of users u and u' to item set. N_u is the nearest neighbors set of target user. The recommendation system can predict target user u for its possible interest degree in the item which he or she has not known and then select several high predicted interest degree items as the recommendation result to the target user.

2.2. The Traditional Dynamic User Interest Model. For the context of social user and user's dynamic interest pattern, the traditional collaborative filtering recommendation algorithm did not take them into account. And the already proposed method defined the time weight function $f_{\text{time_weight}}(t)$ to represent user's dynamic interest pattern and then combined this function with recommendation algorithm [6, 13, 16]. One of the simple ways is to assume that the user's interest is a monotonic decreasing function with time [16] and combine it with the user interest prediction function, or divide the user's dynamic interest in more details by different time segments and construct the corresponding time weight function [6]. All these methods improved the recommendation algorithm's recommended result.

3. The New Method

3.1. The Similarity Based on Social User's Dynamic Information. In the social network, the most common way to construct the relationship of users is the graph construction $G = (V, E)$. The V represents the set of vertices corresponding to users or items. Using the edge e to connect the different vertices, E is the set of edges which means the friendship of different users or user's social behavior historical relationship between user and item. In this paper, the exact means of set E is the relationship of user's interest response information to item. We take into account of user's the different types of response information and the time factor to propose a new recommendation algorithm.

In social network, we can regard the behavior of information forwarding, collection, and other actions as the positive response type. So when the user u is at timestamp t , the number of positive responses can be defined as

$$R^+(u, t) = \{i_k \mid t_{u,i_k} < t, (u, i_k) \in G\}, \quad (4)$$

where G represents the relationship graph of user u ; U represents the set of social users $U = \{u_1, u_2, \dots, u_n\}$, where $u \in U$; I is the set of items $I = \{i_1, i_2, \dots, i_n\}$ and $i_k \in I$; the k means the number of items and $k = \{1, 2, \dots, n\}$; $t_{u,i}$ is the timestamp when user u gives the response information to item i .

Similarly, if user did not show any interest in the item or even take actions such as shielding, cancelling the attention, and so on we can regard those actions as the negative response information. So when user u is at timestamp t , the amount of negative response information can be defined as

$$R^-(u, t) = \{i_k \mid t_{u,i_k} < t, (u, i_k) \in G\}. \quad (5)$$

Based on the above response type definition, at the same time, considering the time effect of user interest preferences and the drawback of traditional collaborative filtering algorithm to this aspect, this paper put forward the new type of user similarity measurement.

We defined the user similarity by considering the user response information and the benefits of only considering the user's response information without paying too much attention to the content of the response information are that it can ensure the diversity of the recommendation results compared with the traditional collaborative filtering recommendation algorithm [6]. Due to the time of different user response to the same item is different, it means the interest degree in this item of different user is also not the same, so after being considered to give the response of time weight, it can more accurately reflect the dynamic feature of user's interest pattern. The user similarity measurement based on users' positive response can be defined as

$$\text{Sim}^+(u, u') = \frac{|R^+(u, t) \cap R^+(u', t)|}{|R^+(u, t)| |R^+(u', t)|} \cdot \sum_{k=1}^n f_{\text{time}}(t), \quad (6)$$

where $|R^+(u, t)|$ and $|R^+(u', t)|$, respectively, represent the set of items which users u and u' gave their positive response to and $|R^+(u, t) \cap R^+(u', t)|$ is the common set of items the users u and u' responded to. The value of n is the common item set size. The $f_{\text{time}}(t)$ is used to reflect the dynamic interest of use and detailed information of it will be discussed later.

Similarly, we can get the user similarity measurement based on user negative response from this formula:

$$\text{Sim}^-(u, u') = \frac{|R^-(u, t') \cap R^-(u', t')|}{|R^-(u, t')| |R^-(u', t')|} \cdot \sum_{k=1}^m f_{\text{time}}(t'). \quad (7)$$

The meanings of sets are similar with the situation of positive response; m is the size of the common item set which users u and u' responded to with their negative feedback or ignored.

To take the dynamic interest and response information of social user into consideration, we design a decreasing time function to model the user's dynamic interest feature in social network sites and then combine it with the new proposed similarity measurement. The $f_{\text{time}}(t)$ function shows in the part of formulas (6) and (7). The definition of this time weight function is given by

$$f_{\text{time}}(t) = \frac{R(u, t)}{|\Delta t|^\lambda}, \quad (8)$$

where $|\Delta t| = |t_{u,i_k} - t_{u',i_k}|$ means the interval time of two users that give the same type response information. We can tune

the parameter λ to determine the decay rate of user's dynamic interest. The default value of λ is 1.8, but you can also change the value to make the recommendation system have the best performance according to your application environment. The $R(u, t)$ represents the number of common items users gave their positive response to, which equals the number of the common sets $|R^+(u, t) \cap R^+(u', t)|$.

Then, we will use the regulatory factor α to combine with these two types of different similarity measurements, so the combination similarity calculation method can be defined as

$$\text{Sim}'(u, u') = \alpha \text{Sim}^+(u, u') + (1 - \alpha) \text{Sim}^-(u, u'), \quad (9)$$

where the value of regulatory factor $\alpha \in [0, 1]$ and α and $(1 - \alpha)$, respectively, represent the weight of positive response and negative response in the equation. We can adopt the optimal weight value to optimize the recommendation result.

Finally, we try to combine the similarity measurement based on social user response with the similarity calculation process of traditional collaborative filtering recommendation algorithm. On the one hand, in the early stage of the new register user, the traditional recommendation system cannot give a good recommendation result, due to the fact that no available user historical data can be used. But once the recommendation got enough user preference historical data, the performance of it will be much better. But it takes time to collect user useful time.

By combination with the user's response information, we can alleviate the cold start problem of recommendation system. It collects the response information more quickly by just some user clicks and gives the preliminary recommendation to user. On the other hand, it can also guarantee a certain diversity of the recommendation result by only focusing on the amount of response information not the content. The formalized user Pearson similarity method can be defined as

$$\text{Sim}(u, u') = \frac{\sum_{i \in I_{x,y}} (r_{x,i} - \bar{r}_x)(r_{y,i} - \bar{r}_y)}{\sqrt{\sum_{i \in I_{x,y}} (r_{x,i} - \bar{r}_x)^2} \sqrt{\sum_{i \in I_{x,y}} (r_{y,i} - \bar{r}_y)^2}} \cdot \text{Sim}'(u, u'). \quad (10)$$

And the Cosine similarity method is

$$\text{Sim}(u, u') = \frac{\sum_{i \in I_{x,y}} r_{x,i} r_{y,i}}{\sqrt{\sum_{i \in I_x} r_{x,i}^2} \sqrt{\sum_{i \in I_y} r_{y,i}^2}} \cdot \text{Sim}'(u, u'). \quad (11)$$

3.2. The Predication Score Based on Social User's Dynamic Information. After calculating the user similarity, the highest K nearest neighbor to target user will be selected as the base set, in order to ensure the recommendation system recommend effect. Let the target user u rated item set be I_u ; the prediction score of any item i ($i \notin I_u$), which user u may give, can be obtained by calculation of the user u' one of the K nearest neighbor's historical rating scores of the item i . The calculation method shows below:

$$R(u, i) = \bar{r}_u + \frac{\sum_{i=1}^n [\text{Sim}(u, u') (r_{u',i} - \bar{r}_{u'})]}{\sum_{i=1}^n \text{Sim}(u, u')}, \quad (12)$$

Input: User set U , Item set I , Rating Matrix $R_{U \times I}$
Output: Users Similarity $\text{Sim}(u, u')$
Step 1. let $k_u = 0$;
Step 2. when $k_u < |U|$, go to Step 3; otherwise, end;
Step 3. let $k_i = k_u + 1$; when $k_i < |I|$, compute to get the users similarity according to formula (1) or (2); otherwise, $++k_u$, go back to Step 2.

ALGORITHM 1: The traditional user similarity measurement.

where $\text{Sim}(u, u')$ is the similarity between the target user u and the nearest neighbor user u' ; $r_{u',i}$ represents the historical rating score of user u' to the item i ; the sign of \bar{r}_u and $\bar{r}_{u'}$, respectively, means the average rating score value of users u and u' . We can obtain the target user's prediction rating of the item and then generate the recommended list to target user by using certain strategies to deal with.

3.3. The Time Complexity Analysis of Algorithm. In the process of recommendation algorithm, the algorithm involves a big part of user similarity computation. In particular when faced with the large data level of processing historical data, the performance of recommendation algorithm becomes extremely important. Here, we will analyze the time complexity of new proposed recommendation algorithm. The user similarity computation mainly involves two parts: one is the traditional similarity measure like Pearson similarity or Cosine similarity and other one is the similarity measure based on social user's dynamic response information. The collaborative filtering algorithm mainly includes user similarity calculation and forecasts the target user's rating scores.

According to Algorithms 1 and 2 process, we can know that the main factors which impact the time complexity of algorithm are the size of social user set U and item set I , while calculating the similarity. Let the size of user set be $|U|$ and the size of item set $|I|$. According to the traditional user similarity measurement formulas (1) and (2), the time complexity of computing one pair of users' similarity is $O(|I|)$; then, the time complexity of computing any two different users' similarity is $(|U| \times (|U| - 1)/2) \times O(|I|) = O(|U|^2 \cdot |I|)$. Considering the time complexity of traditional similarity calculation, we proposed selecting the K nearest neighbor user set and then computing those $|K|$ users' similarity. Let the time complexity of similarity measurement based on user's positive response be $O(R^+)$ and the time complexity of similarity measurement based on user's negative response $O(R^-)$; then we can simplify the formula and get the time complexity of the integrated similarity measurement as $O(|I|) \cdot O(\alpha|R^+| + (1 - \alpha)|R^-|) = O(|I| \cdot |R|)$. Then the time complexity of new proposed user similarity of any two users is $(|K| \times (|K| - 1)/2) \times O(|I| \cdot |R|) = O(|K|^2 \cdot |I| \cdot |R|)$. In the part of user prediction score computation, the main factors influencing the time complexity of algorithm are the size of nearest neighbor set $|K|$ and the size of item set $|I|$.

Input: Target User u , Target Item i , Nearest Neighbor Set K , Item Set I , Timestamp t , Decay Rate Parameter λ , Regulatory Factor α ;
Output: the prediction score $R(u, i)$ of target user u for the item i ;
Step 1. let $k_u = 0$;
Step 2. when $k_u < |K|$, go to Step 3; otherwise, go to Step 4;
Step 3. when $k_i < |I|$, get the number of user positive and negative response $R^+(u, t)$ and $R^-(u, t)$ according to formula (4) and (5); otherwise, $++k_u$, go back to Step 2;
Step 4. when $u, u' \in U$, compute the $\text{Sim}^+(u, u')$, $\text{Sim}^-(u, u')$ of user u and u' according to (6), (7);
Step 5. get the user similarity according to formula (9);
Step 6. get the integrated user similarity by (10) or (11);
Step 7. finally, get the predication score $R(u, i)$ of user u to item i according to (12).

ALGORITHM 2: The user similarity measurement based on social user dynamic information and prediction score calculation.

4. Experimental Evaluation

In order to validate the fact that the new proposed recommendation algorithm has better performance than the traditional user based collaborative filtering recommendation algorithm, we have collected the data of domestic mainstream social network site called Sina Weibo to complete the relevant experiments.

Since the grabbed data from the original Sina Weibo site has a lot of redundant information, therefore, it needs to extract and transform the raw data, commonly known as the process of ETL, eliminate the irrelevant information, and get the exact information we need. The data has about 6040 Sina users with about 3682 pieces of Weibo information, and 100 thousand response information logs. Considering the scenario in Sina Weibo, the negative response information of user is very difficult to define. The situation of without the user's browsing, no forwarding, no comments, and so forth often denotes the user has no interest in this information. So consider that the new similarity measurement regulatory factor α is set as $\alpha = 1$, which means only social user's positive response information be considered. We regard this situation of user collection, forwarding, and comment microblog information as positive response type.

For the existing data set, the data set is equally divided into 10 subsets by way of random selection, of which nine were randomly selected as the training set and the remaining one was selected as the test set. Due to the presence of the decreasing function parameter λ , which characterizes the dynamic of user interest, to get the optimization value of parameter λ will have a great influence on the final recommendation results. So we will get the optimal parameter before we do the further experiments. We use the average absolute deviation MAE [6, 11, 17, 18] as the evaluation metric to evaluate the performance of recommendation algorithm. The lower the MAE is, the more accurately recommended

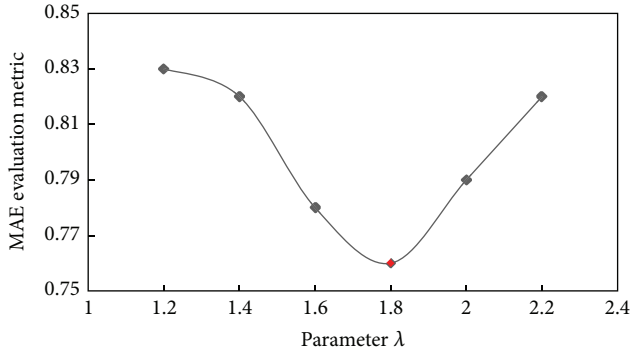


FIGURE 1: The impact of the user interest decay rate λ to recommendation algorithm results.

result the recommendation can give. We can obtain the evaluation metric MAE data of the improved recommendation algorithm by changing the parameter λ as 1.0, 1.5, 1.8, and 2.1. Then, we can also get Figure 1.

We can draw a conclusion that the improved algorithm has the best performance from Figure 1, when the decay rate parameter λ is 1.8. But the optimal value of parameter λ may be different from this value; it should be tuned according to your specific environmental factors. One of the main factors influencing recommendation algorithm performances is the feature of data set.

Once we determined the parameter λ , we designed the comparative experiment between the new recommendation algorithm based on social user's dynamic information and the user based collaborative filtering recommendation algorithm. The collaborative filtering algorithm is one of the classic and most successful recommendation algorithms; so as a comparison basis, it will have some convincing. Under the same experiment conditions, the data set is also equally divided into 10 equal subsets by way of random selection, of which nine were randomly selected as the training set and the remaining one was selected as the test set; then the average MAE value of 10 experiments was the MAE evaluation metric result of the recommendation algorithm. We can get the following figure by changing the number of nearest neighbors to 5, 10, 15, 20, and 25. The experiment result shows in Figure 2.

From Figure 2, the improved algorithm outperforms better recommendation result than the traditional user based collaborative filtering algorithm at the same number of nearest neighbors. Further, from the same type of algorithm, but with different number of nearest neighbors, we can see that as the number of nearest neighbor users increases, the recommendation algorithm gets better results; namely, the value of MAE presents a descending trend, but not infinite decline. It will become one kind of steady state. Therefore, the contrast experiment gives us a lesson that how to select the optimal set of parameters will have a great effect on the recommended result of recommendation algorithm in the specific personalized recommendation system application environment. It also can involve some optimization and method to get the best recommendation performance.

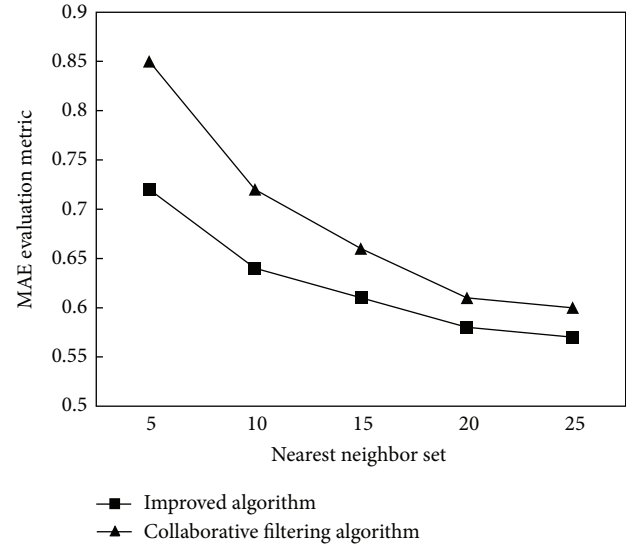


FIGURE 2: Comparative experiment results of two algorithms.

5. Conclusion

In this paper, the theory of collaborative filtering recommendation algorithm is briefly introduced. The collaborative filtering recommendation algorithm is a kind of widely used and more mature algorithms and has a good recommended effect of recommendation algorithm. However, the collaborative filtering recommendation algorithm is a flawed one, in some aspects. For example, the traditional collaborative filtering algorithm did not take into account the temporal characteristics of user's interest while computing the similarity, so it will lose a part of the recommendation accuracy and diversity. Meanwhile, with the rise of social network, the social network user surged, so the users are faced with the problem of information overload on social network sites. But the social user contains rich contextual information; therefore, this paper takes the dynamic information of social user into account to propose the improved algorithm to alleviate the problem and validates the fact that the new improved algorithm has the improvement of recommended effect by contrast experiment. However, the social network user's dynamic information not just only the response information and time factor; there are also geographical information, social relationship information, and other context information. We will continually optimize the current deficiency of the proposed algorithm and also try to do the work of how to better model social user's dynamic information, dig deeper into the user's behavior patterns, and combine them into recommendation algorithm to improve the recommendation algorithm performance in our next step of research.

Conflict of Interests

The authors declare that there is no conflict of interests regarding the publication of this paper.

Acknowledgments

This work was supported in part by NSFC Grant nos. 61472284, 61472004, and 61202384, by National 863 Programs Grant no. 2012AA062800, by Natural Science Foundation Programs of Shanghai Grant no. 13ZR1443100, and by ISTCP Grant no. 2013FM10100.

References

- [1] A. Edmunds and A. Morris, "The problem of information overload in business organizations: a review of the literature," *International Journal of Information Management*, vol. 20, no. 1, pp. 17–28, 2000.
- [2] P. Resnick, N. Iakovou, M. Sushak, P. Bergstrom, and J. Riedl, "GroupLens: an open architecture for collaborative filtering of netnews," in *Proceedings of the ACM Conference on Computer Supported Cooperative Work*, pp. 175–186, Chapel Hill, NC, USA, 1994.
- [3] W. Hill, L. Stead, M. Rosenstein, and G. Furnas, "Recommending and evaluating choices in a virtual community of use," in *Proceedings of the Conference on Human Factors in Computing Systems*, pp. 194–201, Denver, Colo, USA, May 1995.
- [4] G. Linden, B. Smith, and J. York, "Amazon.com recommendations: item-to-item collaborative filtering," *IEEE Internet Computing*, vol. 7, no. 1, pp. 76–80, 2003.
- [5] B. Sarwar, G. Karypis, J. Konstan et al., "Item-based collaborative filtering recommendation algorithms," in *Proceedings of the 10th International World Wide Web Conference*, pp. 285–295, New York, NY, USA, 2001.
- [6] D. Li, Q. Lv, X. Xie et al., "Interest-based real-time content recommendation in online social communities," *Knowledge-Based Systems*, vol. 28, pp. 1–12, 2012.
- [7] Z. Chen, Y. Jiang, and Y. Zhao, "A collaborative filtering recommendation algorithm based on user interest change and trust evaluation," *International Journal of Digital Content Technology and its Applications*, vol. 4, no. 9, pp. 106–113, 2010.
- [8] L. Xiang, Q. Yuan, S. Zhao et al., "Temporal recommendation on graphs via long- and short-term preference fusion," in *Proceedings of the 16th ACM SIGKDD International Conference on Knowledge Discovery and Data Mining (KDD '10)*, pp. 723–731, ACM Press, New York, NY, USA, July 2010.
- [9] J. Chen, W. Geyer, C. Dugan, M. Muller, and I. Guy, "Make new friends, but keep the old—recommending people on social networking sites," in *Proceedings of the 27th International Conference Extended Abstracts on Human Factors in Computing Systems (CHI '09)*, pp. 201–210, Boston, Mass, USA, April 2009.
- [10] J. Hannon, M. Bennett, and B. Smyth, "Recommending twitter users to follow using content and collaborative filtering approaches," in *Proceedings of the 4th ACM Recommender Systems Conference (RecSys '10)*, pp. 199–206, ACM, Barcelona, Spain, September 2010.
- [11] U. Shardanand and P. Maes, "Social information filtering: algorithms for automating 'word of mouth,'" in *Proceedings of the Conference on Human Factors in Computing Systems*, pp. 210–217, May 1995.
- [12] J. S. Breese, D. Heckerman, and C. Kadie, "Empirical analysis of predictive algorithms for collaborative filtering," in *Proceedings of the 14th Conference on Uncertainty in Artificial Intelligence*, pp. 43–52, Madison, Wis, USA, 1998.
- [13] T. Q. Lee, Y. Park, and Y.-T. Park, "A time-based approach to effective recommender systems using implicit feedback," *Expert Systems with Applications*, vol. 34, no. 4, pp. 3055–3062, 2008.
- [14] M. H. Yang and Z. M. Gu, "Personalized recommendation based on partial similarity of interests," in *Advanced Data Mining and Applications*, vol. 4093 of *Lecture Notes in Computer Science*, pp. 509–516, Springer, Berlin, Germany.
- [15] M. Deshpande and G. Karypis, "Item-based top-n recommendation algorithms," *ACM Transactions on Information Systems*, vol. 22, no. 1, pp. 143–177, 2004.
- [16] L. Wang and J. Zhai Z, "Collaborative filtering algorithm based on time weight," *Journal of Computer Applications*, vol. 27, no. 9, pp. 2302–2303, 2007.
- [17] T. Zhoua, Z. Kuscsik, J.-G. Liu, M. Medo, J. R. Wakeling, and Y.-C. Zhang, "Solving the apparent diversity-accuracy dilemma of recommender systems," *Proceedings of the National Academy of Sciences of the United States of America*, vol. 107, no. 10, pp. 4511–4515, 2010.
- [18] J. S. Breese, D. Heckerman, and C. Kadie, "Empirical analysis of predictive algorithms for collaborative filtering," in *Proceedings of the 14th Conference on Uncertainty in Artificial Intelligence (UAI '98)*, pp. 43–52, Madison, Wis, USA, 1998.

Research Article

A Reliability-Oriented Local-Area Model for Large-Scale Wireless Sensor Networks

Haixia Peng,^{1,2} Hai Zhao,¹ Yuanguo Bi,¹ Shuaizong Si,¹ and Wei Cai¹

¹Northeastern University, Shenyang, Liaoning 110819, China

²University of Waterloo, Waterloo, ON, Canada N2L 3G1

Correspondence should be addressed to Haixia Peng; penghaixia@neuera.com

Received 19 May 2014; Revised 29 September 2014; Accepted 13 October 2014

Academic Editor: Qinggang Meng

Copyright © 2015 Haixia Peng et al. This is an open access article distributed under the Creative Commons Attribution License, which permits unrestricted use, distribution, and reproduction in any medium, provided the original work is properly cited.

Large-scale wireless sensor networks (WSNs) have demonstrated some complex features which are similar to those of other types of complex networks, such as social networks. Based on these complex features, evolution process and characteristic of WSNs, we represent a WSN topologically by building a suitable model, which is named as the reliability-oriented local-area model (ROLM) and aimed at improving the performance of WSNs. For analyzing the performance of the ROLM, we define the reliability as the probability of that the relative error between the measurement and the true value is equal to or less than ε ($\varepsilon \geq 0$) and proposed a parameter η to measure the reliability of the network. Based on them, we use η to analyze the influence of network structure on the reliability, and compared the reliabilities of the ROLM and the existing WSNs. Experiment results prove that the large-scale WSN follows a power-law distribution, and it has scale-free characteristic and small world characteristic. And it also shows that, comparing with existing model, ROLM not only balances energy consumption by limiting the connectivity of each node to prolong the lifetime of the network, but also improves the reliability substantially. And the ROLM can be used to express the topology of reliability-oriented WSNs and analyze the structure preferably.

1. Introduction

Complex networks are currently being studied in many scientific fields [1] and many systems actually can be described through complex networks such as biological networks [2], metabolic networks [3], social networks [4], software network [5], scientific collaboration networks [6], and World Wide Web [7, 8]. Wireless sensor networks (WSNs), as a particular type of complex networks, are different from other types of complex networks. A large-scale WSN consists of a large number of distributed sensor nodes, and therefore a large-scale WSN has some complex features of complex networks [9]. Due to short communication range and energy constraints, these sensor nodes autonomously establish connections through wireless communications with the other nodes that are within their local-area. Here the concept of local-area can be seen as a domain surrounding these nodes where their signals can be reached. In fact, there is also local-area in other networks, for example, a community structure in social networks, a regional cooperative group in economic

networks, and a domain in the internet, all of which are local-areas.

In order to model a WSN, most researches consider that the WSN consists of the same types of nodes and links. Reference [10] shows that it is possible to model a WSN as a small world network by using multiple cluster nodes that can emulate the long edge required in small world networks. In [11], a novel evolving network model is based on random walk to study the fault tolerance of the WSN due to node failure and discuss the spreading dynamic behavior of viruses in the evolution model. Considering the diversities of nodes and links in a real WSN, [9] proposes a local-world heterogeneous model for the WSN. In [9], nodes are divided into two classes: sensor nodes (SNs) and cluster-head nodes (CHs), and there are two kinds of links: the bidirectional edge between CHs ($CH \leftrightarrow CH$) and the directional link pointing to CHs from SNs ($SN \rightarrow CH$). The model in [9] is different from the aforementioned models with homogeneous nodes and links, and it balances energy consumption by limiting the connectivity of CHs to prolong the lifetime of the network.

However, recent advancements in wireless communications and sensor technologies have enabled most SNs to relay data packets [12]; that is, there are always $SN \leftrightarrow SN$ in many practical applications. Reference [9] only considers two kinds of links and neglects the links among SNs, which makes the model in [9] be not suitable for most current practical applications.

On the other hand, in practical WSN applications, SNs are usually deployed in some inaccessible and dangerous environments to gather information from the physical world to a sink node (base station); for example, WSNs can be used to monitor environmental changes (such as weather, gas in coal mine) [13, 14], monitor habitats [15, 16], track objects [17], manage disasters [18], and so on. Most recent researches about WSNs try to improve energy efficiency and prolong the lifetime of the network. Several international research projects dedicated to energy-efficient (EE) wireless communications have been carried out. In [19], a link-adaptive transmission scheme for MIMO-OFDM systems is proposed, which maximizes EE in terms of bits-per-Joule using dynamic power allocation based on the channel state as well as the circuit power consumption. Based on the complex network theory, a new topological evolving model is proposed in. In the evolution of the topology of sensor networks, the energy-aware mechanism is taken into account, and the phenomenon of change of the link and node in the network is discussed. Although they are energy-efficient and have long lifetime, they are not suitable for some applications with the requirement of high reliability (this is critically important in some study of the WSN [20], and the concept of reliability will be given in the next section). Reference [21] shows that, in WSNs, due to environment noise, reliable data communications cannot be definitely achieved. Even under ideal conditions, the packet loss rate of a WSN may be above 1% or close to 1% due to packet collisions. When the communication environment becomes hostile, the packet loss rate will definitely go up, and a successful data transmission over links in the WSN can be guaranteed with a certain probability (less than 100%). As most applications of WSNs need to aggregate sensed data from environment [20], and if we want to aggregate the sensed data in the network, just a part of sensed data from SNs will be sent to the sink node, the aggregation result provided by the WSN cannot be ensured to be accurate, and there is a need to study this issue for WSN's some aggregation operators. As we define the reliability to describe this issue in our research, we call this issue as the reliability of WSN. Even though some researches such as [9] can prolong the lifetime of WSNs through balancing energy consumption, the reliability of the WSN should also be taken into account for reliable data communications.

For the above reasons, a reliability-oriented network model which is consistent with the actual network is very important to the WSN application development. In this paper, we propose a reliability-oriented local-area model for the WSN with the help of growth and preferential attachment mechanism. The influence of the local-area scale C , the scale of WSNs, the strategy of evolution on the reliability of WSNs, and topological properties are investigated. Firstly, to

measure the reliability of the WSN, we present the concept of reliability and verify its mathematical rationality and find that the reliability η of a large-scale WSN can be represented as a function of the maximum value ω of cluster layer of SNs. Secondly, we show that this model has intrinsic characteristics, the assortative connectivity correlation, and characteristic of power law. The energy efficiency of this model is better than that of [9], and the lifetime is identical and it has higher reliability compared with the model in [9]. Moreover, from the perspective of the reliability of the WSN, we reveal that the reliability of the WSN evolving from ROLM is much better than that of [9], and when the network scale is larger than 1000, the reliability of the WSN evolving from [9] is far less than that of the ROLM.

2. Model of WSNs

There are two kinds of nodes (SNs and CHs, which will be identified by IEEE address [22]) in the WSN: the SNs will connect with a CH or other SNs, and the CHs can connect with the sink node or other CHs. These two kinds of nodes perform different functions in the WSN evolving from ROLM, such that SN is responsible for sensing information from geographical environment and sending its sensed data to a CH which it belongs to, while a CH collects sensed data from its cluster members. After processing the whole data it will retransmit the aggregation result to the next hop CH. Considering the complex futures of WSNs, ROLM is designed based on the existing complex system modeling method. Take BA model, for example, [23]. There is one new-incoming node entering a preexisting network at every step and choosing one or some nodes from the preexisting network to connect with a certain probability. After a node connects to the network, there will be another new-incoming node entering the network in the next step until the number of nodes in this network reaches the preset network scale.

As a special kind of complex networks, WSNs have some specific characteristics. Therefore, we should consider some factors such as the node transmission range, the hop-constraints between nodes, the reliability of network, and transmission delay. In WSNs, because of the constraint of node transmission range, each node in the network can only communicate with those nodes located within its coverage, which is named as local-area connections. On the other hand, when the monitoring area has the similar condition, every wireless link (the link between two nodes which has one hop between them) in the network has the same packet loss probability, which means that the sensed data will be sent successfully over one link with a probability q ($q \leq 1$) [24]. And apparently, if the sensed data has to be delivered to a node two hops away, then it will be over two links and the successful transmission probability of this data is q^2 . As the probability q is equal to or less than 1, the more hops the sensed data needs to be delivered, the lower the probability that the sensed data will be sent successfully to the sink node. Therefore, just a part of sensed data will be sent to the sink node when the WSN performing an aggregation operator and the reliability of the WSN for this aggregation

operator will decrease consequently. ROLM tries to reduce the number of links between two connected nodes to improve the reliability. Based on the local-area and fitness models in complex networks theory, this paper studies the evolution model while considering the constraints of transmission range and the reliability of the WSN in a novel approach.

2.1. Problem Definition. To facilitate researching on ROLM and the reliability of the WSN evolving from ROLM in this paper, we will briefly introduce some related definitions as follows in this part. It includes sink layer, cluster layer, round, ε -estimate, reliability, η , unbiased estimate, and round.

Definition 1 (sink layer). For node i (CH or SN), if its father node is the sink node, then we define that its sink layer is 1 and express it as $\omega_i = 1$; if its father node j 's $\omega_j = 1$, then its $\omega_i = 2$, and so on.

Definition 2 (cluster layer). For a SN_i , if its father node is a CH, then we define that its cluster layer is 1 and express it as $\omega_s^i = 1$; if its father node j 's $\omega_s^j = 1$, then its $\omega_s^i = 2$, and so on.

The concepts of ω_i and ω_s^i show that CH_i has only value of ω_i ; and SN_j has both ω_j and ω_s^j , and the values of ω_j and ω_s^j for SN_j are different.

Definition 3 (degree). The total number of links pointing to node i from other nodes is called the degree of node i , expressed in k^i . If node i can connect with the other k_{\max}^i nodes, then define its saturated degree as k_{\max}^i .

There are many types of aggregation result (Sum, Average, Max, and so on) which we can get from the WSNs [25]. In order to specifically study the reliability of the WSN evolving from ROLM, we take the SUM aggregation operator as an example and propose the concept of reliability and η parameter to measure the reliability of the WSN. For the other aggregation operator, their processing methods are the same as that of SUM aggregation operator, such that we can get the Average result from the process of calculating the Sum result (the sum value in every cluster divided by the number of members of this cluster, and then the CH will transfer their quotient values to the sink node).

At time t , if the WSN can only aggregate a part of sensed data from its nodes, it will provide an approximated SUM, expressed in $\text{Sum}(S_t)'$. If it aggregates all sensed data in the WSN, it will get an accurate SUM, called $\text{Sum}(S_t)$.

Definition 4 (ε -estimate). $\text{Sum}(S_t)'$ is called an ε -estimate of $\text{Sum}(S_t)$ if $|\text{Sum}(S_t)' - \text{Sum}(S_t)| / \text{Sum}(S_t) \leq \varepsilon$ for any ε ($\varepsilon \geq 0$).

Definition 5 (reliability). For a given network and ε ($\varepsilon \geq 0$), reliability is the probability of that $\text{Sum}(S_t)'$ is the ε -estimate of $\text{Sum}(S_t)$ [20].

Definition 6 (η). For a given network and ε ($\varepsilon \geq 0$), η ($0 \leq \eta \leq 1$) is the lower bound of probability of that $\text{Sum}(S_t)'$

is the ε -estimate of $\text{Sum}(S_t)$; that is, $\eta \leq P(|\text{Sum}(S_t)' - \text{Sum}(S_t)| / \text{Sum}(S_t) \leq \varepsilon)$.

Definition 7 (unbiased estimate). $\text{Sum}(S_t)'$ is an unbiased estimate of $\text{Sum}(S_t)$ if the mathematical expectation of $\text{Sum}(S_t)'$ is equal to $\text{Sum}(S_t)$; that is, $E(\text{Sum}(S_t)') = \text{Sum}(S_t)$; otherwise $\text{Sum}(S_t)'$ is a biased estimator of $\text{Sum}(S_t)$.

Definition 8 (round). The amount of time from the sink node initiates a data collection command to all sensed data from SNs being sent to the sink node, no matter how long it will last. This amount of time is called one round.

2.2. Reliability-Oriented Local-Area Model. In this section, we model a WSN as a network with growth and preferential attachment and propose an evolution model ROLM with high reliability. Different from [9], the WSN evolving from ROLM includes three kinds of links. They are the bidirectional link between CHs ($CH \leftrightarrow CH$), the directional link from SN to CH ($SN \rightarrow CH$), and the bidirectional link between SNs ($SN \leftrightarrow SN$). For CH_i , let k_c^i be the current degree that is the total number of links pointing to CH_i from other nodes, and let E_c^i be its initial energy value. And for a SN_i , provide that k_s^i is the degree that is the total number of links pointing to SN_i from other SNs and E_s^i represents the initial energy value of SN_i . Define that E_c^i is a random variable following the uniform distribution $\rho(E_c)$ in the interval $[E_{\min c}, E_{\max c}]$ and E_s^i is a random variable following the uniform distribution $\rho(E_s)$ in the interval $[E_{\min s}, E_{\max s}]$. Set E_c^i as much larger than E_s^i . Here, $E_{\max c} \geq E_{\min c} \geq E_{\max s} \geq E_{\min s}$, $E_{\max c}$ is the maximum initial energy of CHs, and a CH with $E_{\max c}$ could connect with less than $k_{\max c}$ nodes. Similarly, $E_{\max s}$ is the maximum initial energy of SNs, and the SN with $E_{\max s}$ could connect with less than $k_{\max s}$ SNs. Let $k_{\max c}^i$ and $k_{\max s}^i$ be the saturated degree of CH_i and SN_i respectively; then we define

$$\begin{aligned} k_{\max c}^i &= k_{\max c} \frac{E_c^i}{E_{\max c}}, \\ k_{\max s}^i &= k_{\max s} \frac{E_s^i}{E_{\max s}}. \end{aligned} \quad (1)$$

The basic settings for ROLM can be described as shown in Algorithm 1.

The growth in the WSN evolving from ROLM is starting with an existing network with a small number of c_0 nodes (all of these c_0 nodes are connected with each other. As SNs connect to the sink node by CHs, there must be at least one CH among these c_0 nodes). Referring to the BA modeling method in complex networks, ROLM can be described as follows.

- (a) At every step, a new-incoming node (CH or SN) connects to one node in an existing network. If the new-incoming node is a CH with energy value E_c^i , it may connect to the other CHs within its local-area, while if the new-incoming node is a SN with energy value E_s^i , it may connect to a CH or a SN


```

//defining the variables
CHi:
    Var  $k_c^i, E_c^i$ 
SNi:
    Var  $k_s^i, E_s^i$ 
Begin
    //////////////////////////////////////
    //the types of node in ROLM
    For  $i = 1$  to NumberOfNetworks do
    {
        probability  $P$ :
            nodeKind == CH;
        probability  $1 - P$ :
            nodeKind == SN;
    }
    //initializing node energy
    For  $i = 1$  to NumberOfNetworks do
    {
        If nodeKind == CH
             $E_c^i = \rho(E_c)$ ; //the initial energy value of CHi
        Else if nodeKind == SN
             $E_s^i = \rho(E_s)$ ; //the initial energy value of SNi, and  $E_{\max c} \geq E_{\min c} \geq E_{\max s} \geq E_{\min s}$ 
    }
    //calculating the saturated degree of CHi and SNi
    For  $i = 1$  to NumberOfNetworks do
    {
         $k_{\max c}^i = k_{\max c} \frac{E_c^i}{E_{\max c}}$ ; //the saturated degree of CHi, and set the value of  $k_{\max c}$  to be 20
         $k_{\max s}^i = k_{\max s} \frac{E_s^i}{E_{\max s}}$ ; //the saturated degree of SNi, and set the value of  $k_{\max s}$  to be 7
    }

```

ALGORITHM 1

within its local-area. For a new-incoming CH, it enters the preexisting network with probability p (the probability p is the proportion of CHs in the WSN evolving from ROLM), as new-incoming nodes include CHs and SNs; thus the proportion of SNs in the WSN evolving from ROLM is $(1 - p)$, and the probability for a new-incoming SN entering the preexisting network is $(1 - p)$.

- (b) Preferential attachment: the new-incoming CH connects to a selected CH in the preexisting network, and the new-incoming SN connects to a selected CH or a SN from the preexisting network. In this case, as the node in WSNs has the constraints of energy and connectivity, it only communicates with one CH or SN in the local-area to avoid data redundancy. Firstly, we mark C nodes randomly from the preexisting network as the local-area Φ . As the scale of local-area Φ is based on the new-incoming node's communication range, and the directly connected nodes of each node are chosen from these C nodes, we set $C \geq \max\{k_{\max s}, k_{\max c}\}$. Considering that nodes have constraints of energy and connectivity, and ROLM is trying to improve the reliability of the WSN for some aggregation operators, in the WSN evolving

from ROLM, the new-incoming nodes (CHs or SNs) will connect to CH_i in the local-area Φ according to the probability \prod_c^i , and SN_i in the local-area Φ will be connected by new-incoming SNs according to the probability \prod_s^i :

$$\prod_c^i = \frac{E_{rc}^i k_c^i / \omega_i}{\sum_{j \in \Phi} E_{rc}^j k_c^j / \omega_j} \quad (2)$$

$$\prod_s^i = \frac{E_{rs}^i k_s^i / \omega_i}{\sum_{j \in \Phi} E_{rs}^j k_s^j / \omega_j}, \quad (3)$$

where E_{rc}^i and E_{rs}^i are the residual energy of CH_i and SN_i.

Considering the fact that every link connected to node i will consume some energy of node i , we simply define

$$E_{rc}^i = E_c^i - b k_c^i, \quad (4)$$

$$E_{rs}^i = E_s^i - b k_s^i, \quad (5)$$

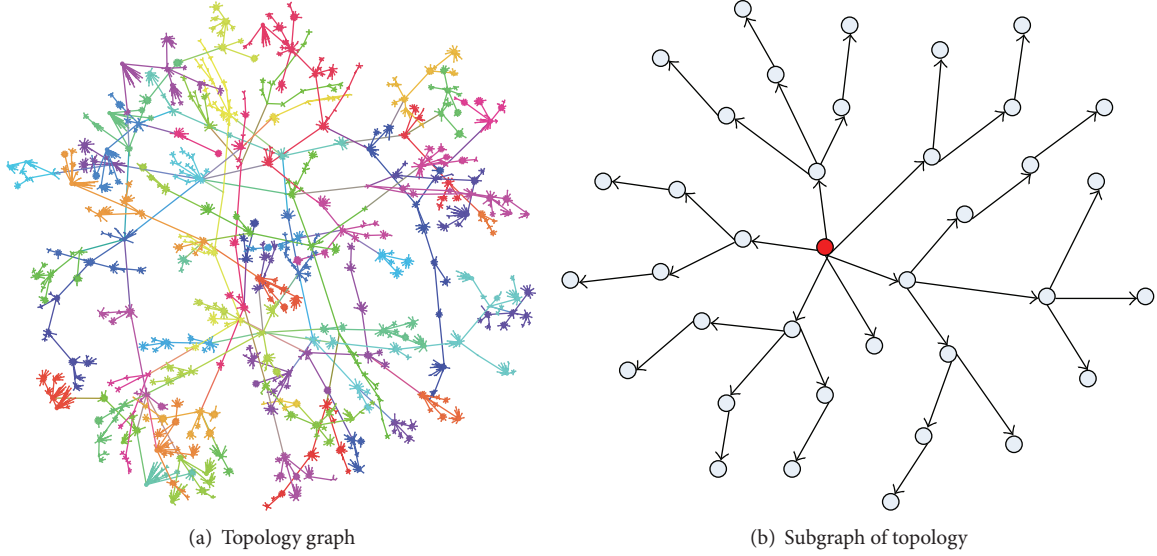


FIGURE 1: The topology graph and subgraph of topology of the WSN, where nodes' sizes represent their current degree, the nodes' color reflects their community structure, nodes with the same color means that they have the same modularity, and the communication among them will be more frequent.

where b is a constant and can be regarded as the energy consumed by every link. Formulas (4) and (5) mean that the closer the degree of node i is to $k_{\max c}^i$ or $k_{\max s}^i$, the less the residual energy of the node i will be left. Replacing E_{rc}^i and E_{rs}^i with (4) and (5) in formulas (2) and (3), respectively, we can get

$$\prod_c^i = \frac{(E_c^i - bk_c^i) / \omega_i}{\sum_{j \in \Phi} (E_c^j - bk_c^j) / \omega_j}, \quad (6)$$

$$\prod_s^i = \frac{(E_s^i - bk_s^i) / \omega_i}{\sum_{j \in \Phi} (E_s^j - bk_s^j) / \omega_j}.$$

- (c) After step (b), when a new-incoming SN enters into the preexisting network, and if the degree of an existing SN_i is $k_s^i < k_{\max s}^i$, return to step (b); otherwise remove SN_i from the local-area Φ ; that is to say, a new node cannot connect to this SN_i even though SN_i is within the local-area Φ . When a new-incoming node (CH or SN) enters into the pre-existing network, if the degree of CH_i is $k_c^i < (k_{\max c}^i - 1)$ (it could avoid all these $k_{\max c}^i$ nodes connected to one CH_i are SNs, and the new-incoming CH cannot joint into the pre-existing network as all CHs within the local-area Φ have reached their saturated degrees), and the new-incoming node is a SN, then return to step (b), otherwise remove CH_i from the local-area Φ ; if the degree of CH_i is $k_c^i < k_{\max c}^i$, and the new-incoming node is a CH, then return to step (b), otherwise remove CH_i from the local-area Φ .

The description of ROLM with pseudocode is shown as in Pseudocode 1.

For a WSN with a certain number of nodes, through the above three steps, the nodes in the WSN can be connected with each other. When the number of nodes is 5000, $k_{\max s} = 7$, $k_{\max c} = 20$, the topology graph is shown in Figure 1(a), and Figure 1(b) is an example for detailed topology of one cluster in Figure 1(a). The three steps of ROLM show that the probability of a new-incoming node connecting to a preexisting CH_i or SN_i not only depends on its current state: k_c^i (or k_s^i) and ω_c^i (or ω_s^i) but also has the constraint of $k_c^i < k_{\max c}^i \leq k_{\max c}$ (or $k_s^i < k_{\max s}^i \leq k_{\max s}$), and k_c^i (k_s^i) depends on the node i 's initial energy. ROLM has considered the diversities of nodes and links and balanced the energy consumption globally by limiting the links to a CH and the links to a father SN. Furthermore, it also improves the reliability of WSNs for an aggregation operator (the smaller the ω_s^i is, the higher the reliability of WSNs will be, and it will be proved in the next section for SUM aggregation operator) without shortening the lifetime of the network. As high-reliability and energy efficiency are both critically important for most WSNs applications [26, 27], the WSN evolving from ROLM can perform more efficiently under such environment.

3. Mathematic Principle of η

Since this paper is dedicated to present an evolution model ROLM to improve the reliability of WSNs, in the following sections we analytically calculate the reliability of the WSN evolving from ROLM for SUM aggregation operator. Section 2.2 shows that, when the number of network nodes is given, through the three steps in Section 2.2, we can connect these nodes to form a complete WSN. Here, we provide that


```

//starting with an existing network with a small number of  $c_0$  nodes and at least one CH node among them
//using the Function_ROLM_Model to construct the WSN
Function_ROLM_Model
Begin
For  $m = 1$  to NumberOfNetworks do
{
//Firstly, we mark  $C$  nodes randomly from the pre-existing network as the local-area  $\Phi$ 
local-area  $\Phi$ :  $C$  nodes,  $C \geq \max\{k_{\max s}, k_{\max c}\}$ 
If nodeKind == SN
{
For  $i = 1$  to  $C$  do
{
If  $k_s^i \leq k_{\max s}^i$ 
{

$$\prod_s^i = \frac{E_{rs}^i k_s^i / \omega_i}{\sum_{j \in \Phi} E_{rs}^j k_s^j / \omega_j}$$
;  $E_{rs}^i$  is the residual energy of  $SN_i$ ,  $\omega_i$  and  $\omega_j$  are
the sink layer values of node  $i$  and node  $j$ 
}
}
}
node( $i$ ) =  $\max(\prod_s^i)$ ; //select the node with max probability  $\prod_s^i$  from the local-area  $\Phi$ 
CONNECT(node( $m$ ), node( $i$ )); //connect node( $m$ ) & node( $i$ ), link( $m, i$ )
 $E_{rs}^i = E_s^i - bk_s^i$ ; //b is regarded as the energy consumed by every link
 $k_s^i + 1$ ;
}
}
Else if nodeKind == CH
{
For  $i = 1$  to  $C$  do
{
If  $k_c^i < (k_{\max c}^i - 1)$  && nodeKind == CH
{

$$\prod_c^i = \frac{E_{rc}^i k_c^i / \omega_i}{\sum_{j \in \Phi} E_{rc}^j k_c^j / \omega_j}$$
;  $E_{rc}^i$  is the residual energy of  $CH_i$ ,  $\omega_i$  and  $\omega_j$  are
the sink layer values of node  $i$  and node  $j$ 
}
}
}
Node( $i$ ) =  $\max(\prod_c^i)$ ; //select the node with max probability  $\prod_c^i$  from the local-area  $\Phi$ 
CONNECT(node( $m$ ), node( $i$ )); //connect node( $m$ ) & node( $i$ ), link( $m, i$ )
 $E_{rc}^i = E_c^i - bk_c^i$ ; //b is regarded as the energy consumed by every link
 $k_c^i + 1$ ;
}
}
}
End_ROLM

```

PSEUDOCODE 1

the two kinds of nodes in the WSN are uniformly distributed in the monitoring environment and p is the proportion of CHs.

Let N_t be the number of SNs in the WSN at time t . Let s_i ($1 \leq i \leq N_t$) be the sensed data of SN_i at time t , and let $S_t = \{s_1, s_2, \dots, s_{N_t}\}$ be the set of all sensed data in the WSN at time t . Since the value of sensed data is bounded, we use $\sup(S_t)$ to denote the upper bound of all sensed data, and the metric of data depends on the category of sensors.

From the analysis in Section 2.2, except the sink node and the links between CHs and sink node, we can construct a WSN consisting of two kinds of nodes (CHs and SNs) and

three kinds of links ($CH \leftrightarrow CH$, $SN \rightarrow CH$, and $SN \leftrightarrow SN$). The WSN is divided into a number of clusters which are disjointed with each other, and a cluster consists of one CH and many SNs. Here, we define that the WSN is divided into n clusters. Let $\omega = \max\{\omega_s^i, 1 \leq i \leq (1-p)N_t\}$ be the maximum value of cluster layer of SNs at time t , and let $m_1, m_2, m_3, \dots, m_\omega$ be the numbers of SNs whose $\omega_s^i = 1, \omega_s^i = 2, \omega_s^i = 3, \dots$, and $\omega_s^i = \omega$ at time t , respectively. Let $S_{t,1} = \{s_{t,1}^1, s_{t,1}^2, s_{t,1}^3, \dots, s_{t,1}^{m_1}\}$ be the set of sensed data from SNs with $\omega_s^i = 1$ at time t , and let $S_{t,2}, S_{t,3}, \dots, S_{t,\omega}$ be the sets of sensed data from SNs with $\omega_s^i = 2$, SNs with $\omega_s^i = 3, \dots$, and SNs with $\omega_s^i = \omega$ at time t , respectively. Then the relationship among

$S_t, S_{t,1}, S_{t,2}, S_{t,3}, \dots, S_{t,\omega}$ can be described as $S_{t,1} \subseteq S_t, S_{t,2} \subseteq S_t, S_{t,3} \subseteq S_t, \dots, S_{t,\omega} \subseteq S_t, S_t = \{S_{t,1}, S_{t,2}, S_{t,3}, \dots, S_{t,\omega}\}$.

As the WSN for practical applications is not ideal deterministic network model, a data transmission over the wireless link of the real WSN is successfully conducted with a certain probability [28]. Here, when the sink node initiating one time of data collecting at time t , we provide that a link $SN \rightarrow CH$ or $SN \leftrightarrow SN$ is connected successfully with probability q . In our model, CHs' initial energy is larger; we define that the timeout retransmission mechanism is used among CHs and sink node, and therefore data communications over $CH \leftrightarrow CH$ links can be successfully conducted with probability 1.

According to the above analysis, at time t , the sensed data of SNs with $\omega_s^i = 1$ will be sent successfully to the sink node with a certain probability q . Similarly, the sensed data from SNs with $\omega_s^i = 2$, SNs with $\omega_s^i = 3, \dots$, and SNs with $\omega_s^i = \omega$ will be sent successfully to the sink node with the probabilities $q^2, q^3, \dots, q^\omega$, respectively. To facilitate our research on data analysis, let $B_{(q)}, B_{(q^2)}, B_{(q^3)}, \dots, B_{(q^\omega)}$ be the set of sensed data that are sent successfully to the sink node from the SNs with $\omega_s^i = 1$, SNs with $\omega_s^i = 2$, SNs with $\omega_s^i = 3, \dots$, and SNs with $\omega_s^i = \omega$ at time t respectively. In order to deliver the sensed data successfully to the sink node, the medium access schedule of our network model is similar to that in [29].

In order to specifically study the reliability of the WSN, we take the SUM aggregation operator as an example (the other operator also can be got with the same processing method) and propose the concept of reliability and η parameter to measure the reliability of the WSN. Here, the accurate SUM of the WSN at time t is defined as $\text{Sum}(S_t) = \sum_{i=1}^{m_1} s_{t,1}^i + \sum_{i=1}^{m_2} s_{t,2}^i + \sum_{i=1}^{m_3} s_{t,3}^i + \dots + \sum_{i=1}^{m_\omega} s_{t,\omega}^i$. In the next section, we will analyze the mathematic principle of η and study whether the approximated SUM can replace the accurate SUM, which is one of the basic requirements of researching on the reliability of the WSN. It also determines whether we need to measure the reliability of the WSN. After that, we will research on how to calculate the value of η and use it to measure the reliability of the WSN.

3.1. Estimator of Sum. As the definitions show above, $S_{t,1}, S_{t,2}, S_{t,3}, \dots, S_{t,\omega}$ are the sets of sensed data from SNs with $\omega_s^i = 1$, SNs with $\omega_s^i = 2$, SNs with $\omega_s^i = 3, \dots$, and SNs with $\omega_s^i = \omega$ at time t , respectively, and $B_{(q)}, B_{(q^2)}, B_{(q^3)}, \dots, B_{(q^\omega)}$ are the sets of sensed data which are sent successfully to the sink node from SNs with $\omega_s^i = 1$, SNs with $\omega_s^i = 2$, SNs with $\omega_s^i = 3, \dots$, and SNs with $\omega_s^i = \omega$ at time t , respectively. The approximated SUM is denoted by $\text{Sum}(S_t)'$, and $\text{Sum}(S_t)'$ can be computed by

$$\begin{aligned} \text{Sum}(S_t)' &= \frac{1}{q} \sum_{s_{t,1}^i \in B_{(q)}} s_{t,1}^i + \frac{1}{q^2} \sum_{s_{t,2}^i \in B_{(q^2)}} s_{t,2}^i \\ &+ \dots + \frac{1}{q^\omega} \sum_{s_{t,\omega}^i \in B_{(q^\omega)}} s_{t,\omega}^i. \end{aligned} \quad (7)$$

According to the definition of unbiased estimate in Section 2.1, the following Theorem 9 will show that $\text{Sum}(S_t)'$ is the unbiased estimator of $\text{Sum}(S_t)$.

Theorem 9. Let $E(\text{Sum}(S_t)')$ be the expectation of $\text{Sum}(S_t)'$, and let $\text{Var}(\text{Sum}(S_t)')$ be the variance. Then,

$$\begin{aligned} E(\text{Sum}(S_t)') &= \text{Sum}(S_t) \\ \text{Var}(\text{Sum}(S_t)') &\leq \sup(S_t) \text{Sum}(S_t) \frac{1 - q^\omega}{q^\omega}. \end{aligned} \quad (8)$$

Theorem 9 will be proved in Appendix A. It shows that the mathematic estimator of $\text{Sum}(S_t)'$ is the unbiased estimator of $\text{Sum}(S_t)$ and the upper bound of $\text{Var}(\text{Sum}(S_t)')$ is inversely proportional to q . That is to say, with the increase of q , the upper bound of $\text{Var}(\text{Sum}(S_t)')$ can be arbitrarily small. Reference [30] shows that, with q increasing, the relative error between $\text{Sum}(S_t)'$ and $\text{Sum}(S_t)$ gradually decreases, and if q is sufficiently large, this relative error can be arbitrarily small.

3.2. Calculation of η . The steps of calculating the value of η are

- proving that $\text{Sum}(S_t)'$ follows normal distribution;
- transforming the normal distribution into standard normal distribution;
- utilizing characteristics of standard normal distribution to calculate the value of η .

For any i , let the variable Y_{vi} ($1 \leq v \leq \omega$) denote the following equations:

$$\begin{aligned} Y_{1i} &= \begin{cases} s_{t,1}^i & \text{if } s_{t,1}^i \in B_{(q)} \\ 0 & \text{if } s_{t,1}^i \notin B_{(q)} \end{cases} \\ &\vdots \\ Y_{\omega i} &= \begin{cases} s_{t,\omega}^i & \text{if } s_{t,\omega}^i \in B_{(q^\omega)} \\ 0 & \text{if } s_{t,\omega}^i \notin B_{(q^\omega)}. \end{cases} \end{aligned} \quad (9)$$

There is $\text{Sum}(S_t)' = (1/q) \sum_{s_{t,1}^i \in B_{(q)}} s_{t,1}^i + (1/q^2) \sum_{s_{t,2}^i \in B_{(q^2)}} s_{t,2}^i + \dots + (1/q^\omega) \sum_{s_{t,\omega}^i \in B_{(q^\omega)}} s_{t,\omega}^i$. Firstly, we need to prove that $\text{Sum}(S_t)'$ follows normal distribution. In view of the linear combination of n independent normal distribution variables still follow normal distribution, through proving that the sum of sensed data of SNs with $\omega_s^i = 1$, the sum of sensed data of SNs with $\omega_s^i = 2, \dots$, and the sum of sensed data of SNs with $\omega_s^i = \omega$ all follow normal distribution to prove that $\text{Sum}(S_t)'$ follows normal distribution. Reference [31] shows that, if sensed data from SNs with $\omega_s^i = v$ ($1 \leq v \leq \omega$) is conformed to Lyapunov condition, the sum of sensed data from SNs with $\omega_s^i = v$ will meet the application conditions of central limit theorem; that is, the sum of sensed data from SNs with $\omega_s^i = v$ will follow normal distribution. And Theorem 10 proves that

sensed data from SNs with $\omega_s^i = 1$, SNs with $\omega_s^i = 2, \dots$, and SNs with $\omega_s^i = \omega$ are all conformed to Lyapunov condition, respectively.

Theorem 10. *These ω groups of sequence of random variables Y_{vi} ($1 \leq v \leq \omega$) satisfy Lyapunov condition; that is, $\exists \xi_v > 0$ satisfies the following:*

$$\lim_{m_v \rightarrow \infty} \frac{1}{s_{m_v}^{2+\xi_v}} \sum_{i=1}^{m_v} E(|Y_{vi} - \mu_{vi}|^{2+\xi_v}) = 0, \quad (10)$$

where $1 \leq v \leq \omega$, m_v is the number of sensed data from SNs with cluster layer v at time t , and $s_{m_v}^2 = \sum_{i=1}^{m_v} \sigma_{vi}^2$, and for all i ($1 \leq i \leq m_v$) there are $\mu_{vi} = E(Y_{vi})$ and $\sigma_{vi} = \text{Var}(Y_{vi})$.

The proof for Theorem 10 will be given in Appendix B [31]. Theorem 10 shows that these ω groups of random variable sequences Y_{vi} ($1 \leq v \leq \omega$) satisfy Lyapunov conditions. That is, the sum of sensed data from SNs with $\omega_s^i = v$ ($1 \leq v \leq \omega$) $\text{Sum}(S_{t,v})' = \sum_{i=1}^{m_v} Y_{vi}$ follows normal distribution. As the successful transmissions of the sensed data from SNs with $\omega_s^i = v$ to the sink node are independent of other SNs with ω_s^i , $\text{Sum}(S_t)'$ is the sum of these ω independent variable normal distributions $\text{Sum}(S_{t,v})'$. Thus $\text{Sum}(S_t)'$ follows normal distribution. For a given relative error limit ε , the following Theorem 11 describes how to calculate the η of the WSN.

Theorem 11. *Define $\delta = 1 - \eta$, and $\phi_{\delta/2}$ is the $\delta/2$ quantile of standardized normal distribution, if $\phi_{\delta/2}$ satisfies*

$$\phi_{\delta/2}^2 \leq \frac{q^\omega \inf(N_t) \inf(S_t) \varepsilon^2}{(1 - q^\omega) \sup(S_t)}. \quad (11)$$

Then, the probability that the relative error between $\text{Sum}(S_t)'$ and $\text{Sum}(S_t)$ satisfies the given error limit ε will be equal to or greater than η ; that is,

$$\Pr\left(\left|\frac{\text{Sum}(S_t)' - \text{Sum}(S_t)}{\text{Sum}(S_t)}\right| \leq \varepsilon\right) \geq \eta. \quad (12)$$

We will prove Theorem 11 in Appendix C [32]. In Theorem 11, η is an important parameter which could measure the reliability of the WSN in our research. Combining with the above analysis, we can conclude that the problem of the calculation of η can be described as follows.

- Input.** (1) $S_{t,1} = \{s_{t,1}^1, s_{t,1}^2, s_{t,1}^3, \dots, s_{t,1}^{m_1}\}, S_{t,2}, S_{t,3}, \dots, S_{t,\omega}$;
 (2) ε ($\varepsilon \geq 0$), ω and q ;
 (3) SUM aggregation operator.

Output. The value of η .

4. The Degree Distribution of Nodes

To achieve a better understanding of the considered model, in this section, ROLM will be analyzed in comparison with the model in [9]. When we apply the preferential attachment strategy of [9] to the network evolution, the new-incoming node (CH or SN) will connect to CH_i in the local-area Φ

according to the probability $\prod_c^{ii'}$, and SN_i in the local-area Φ will be connected by a new-incoming SN according to the probability $\prod_s^{ii'}$:

$$\begin{aligned} \prod_c^{ii'} &= \frac{(E_c^i - bk_c^i) \cdot k_c^i}{\sum_{j \in \Phi} (E_c^j - bk_c^j) \cdot k_c^j}, \\ \prod_s^{ii'} &= \frac{(E_s^i - bk_s^i) \cdot k_s^i}{\sum_{j \in \Phi} (E_s^j - bk_s^j) \cdot k_s^j}. \end{aligned} \quad (13)$$

Here b is a constant and can be regarded as the energy consumed by every link. Considering that a small number of CHs would make lots of SNs connected to them and large number of CHs will waste the network resource, this paper will control the number of CHs in a low proportion. In order to compare these two evolution models fairly, in our experiment, all parameters are set in the same way in [9], and set the number of WSN nodes to be 5000, $k_{\max s} = 7$, $k_{\max c} = 20$, $p = 0.1$, $\rho(E_c) \sim U[0.7, 1]$, $\rho(E_s) \sim U[0.3, 0.7]$. Then we will use the evolution strategy of ROLM and the evolution strategy of [9] to connect the nodes and define that there are two kinds of nodes and three kinds of links in this WSN. Next, we will focus on the cumulative degree distribution $\log_{10}(P(k))$ of nodes in WSNs evolving from ROLM and [9]. To find the cumulative degree distribution $\log_{10}(P(k))$, we first need to do degree statistics (i.e., get the probability of a node with k links). The statistical result is shown as in Figure 2.

Figure 2 shows the statistical results of $C = 25$, $C = 35$, and $C = 45$ for WSNs evolving from ROLM and [9], respectively. The left and right three figures in Figure 2 indicate that the change of local-area scale C does not cause the cumulative degree distribution to change greatly. For the WSN evolving from ROLM, the slopes of fitting curves for these three C are within $[-2.5, -2]$. And for [9], the slopes of fitting curves are within $[-3.6, -3.2]$. That is, in these two evolution models, the scale of local-area C has a weak effect on the cumulative degree distribution.

On the other hand, the six constant variables of the above six fitting curves exhibit that the power-law fitting of the WSN evolving from ROLM is better than that of [9], the WSN evolving from ROLM follows a power-law distribution that can be found generally in the so-called scale-free networks, and the power-law features of the WSN evolving from ROLM are more obvious than that of [9]. The six figures in Figure 2 could also reveal the proportion of the nodes (SNs who are father nodes and CHs) with high degree and low degree. There are a low proportion of nodes with high degree and the proportion of nodes with low degree is large. And the degree of most of the nodes k_c^i (or k_s^i) is far smaller than their maximum degree $k_{\max c}$ (or $k_{\max s}$), which could prevent the CHs and father SNs from consuming energy too quickly; then the lifetime of the WSN would be prolonged.

5. The Discussion of Network Performances

In this section, we will discuss the performance of WSNs evolving from ROLM and [9]. As our purpose is to give an

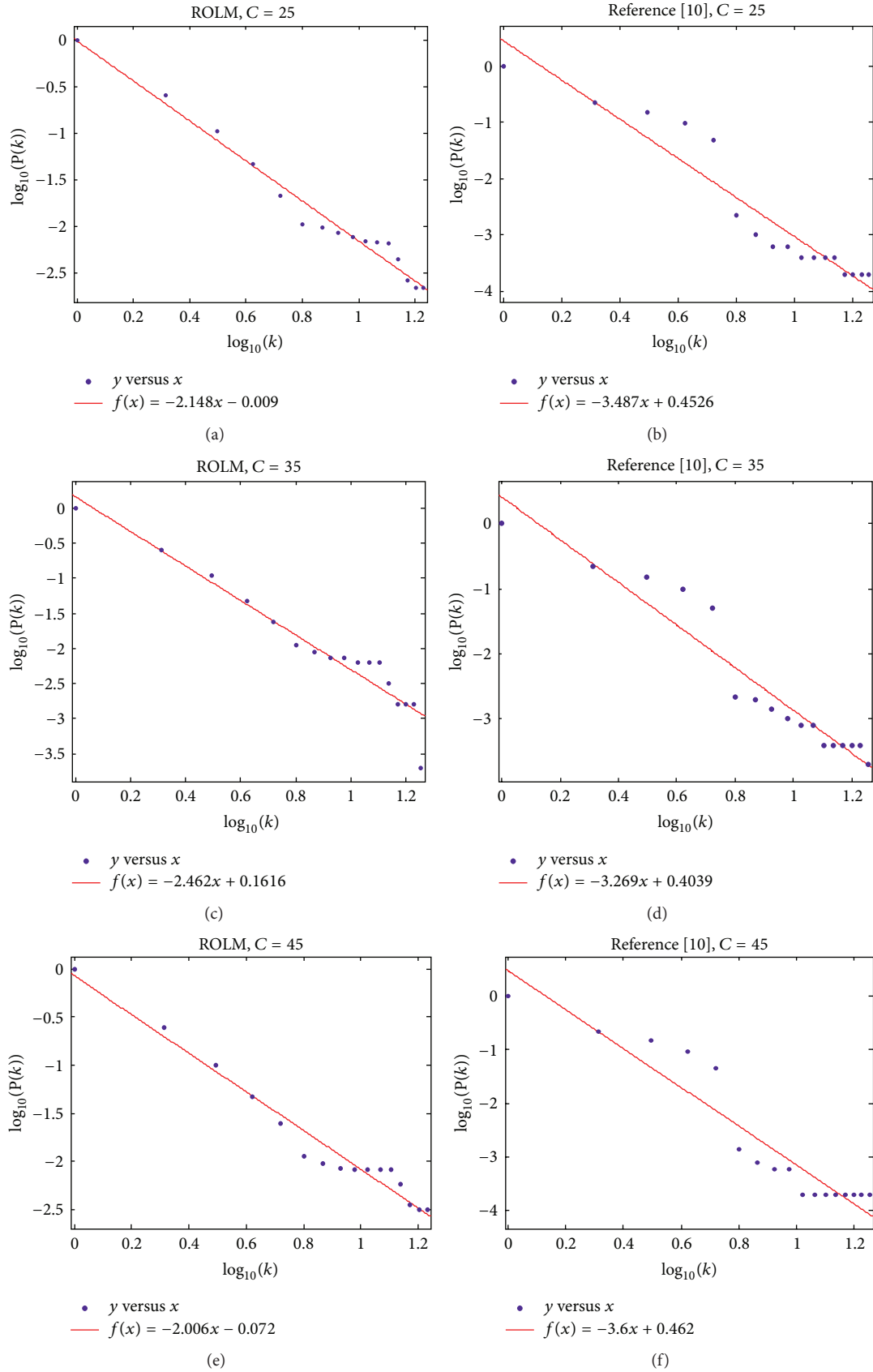


FIGURE 2: The cumulative degree distribution $\log_{10}(P(k))$ of nodes in WSNs evolving from ROLM and [9].

evolution model which is reliability-oriented, we will first analyze the reliability of WSNs evolving from ROLM and [9]. Considering that the advantage of [9] is prolonging the lifetime of WSN, we also analyze the lifetime of WSNs evolving from ROLM and [9] in this section. Finally, we study the average length of shortest path of these two WSNs.

5.1. The Analysis of Reliability. In this set of experiments, all parameters are set as follows: the scale of network is to be [0, 6000], the probability q locates within the interval [0.85, 0.9] [33], $C = 25$, $k_{\max s} = 7$, $k_{\max c} = 20$, $p = 0.1$, $\rho(E_c) \sim U[0.7, 1]$, $\rho(E_s) \sim U[0.3, 0.7]$. As the other parameters of formula (11) are decided by the actual use of the WSN, and when we compare the reliability of the WSN evolving from ROLM with that of [9], these parameters have no effects on the comparative results if we set them in the same way. Therefore, we just choose an example setting for these experiments in this part. And for different network scales and q , we can get corresponding WSNs evolving from ROLM and [9] and the maximum value of cluster layer of SNs for these networks. Then, in combination with Section 3, we can calculate the reliability of the corresponding networks with different network scale and q . The results are shown in Figure 3 (for $q = 0.85$) and Figure 4 (for $q = 0.9$).

Firstly, the four figures in Figures 3 and 4 show that, with the increasing of network scale, the reliability of network presents a downward trend (not monotonously decreasing). As the CHs enter into the preexisting network in probability p and the new-incoming nodes will link to CH_i or SN_i in the local-area Φ in accordance with the probability \prod_c^i or \prod_s^i in the WSN evolving from ROLM and \prod_c^{ii} or \prod_s^{ii} in the WSN evolving from [9], WSNs evolving from ROLM or [9] are not unique. That is, every evolution may end with a different network, and this leads to the fluctuating in Figures 3 and 4. Secondly, for the same q and network scale, the WSN evolving from ROLM will get a higher reliability than that of [9], such that the reliability of the WSN evolving from ROLM is 0.857 when $N_t = 1000$, $q = 0.85$, while the reliability of [9] is only 0.0011. This is due to the difference between the preferential attachment principles of ROLM and [9]. Reference [9] only considers balancing energy consumption globally to prolong the lifetime of the WSN, while ROLM not only considers balancing energy consumption globally but also tries to improve the reliability of data aggregation. The experiment results shown in Figures 3 and 4 indicate that ROLM can improve the reliability of WSN significantly. Lastly, experiment results in Figures 3(a) and 4(a) show that ROLM can guarantee the WSN a higher reliability for small-scale WSN and large-scale WSN. Even under the conditions where $N_t = 20000$, $q = 0.85$, the reliability of the WSN evolving from ROLM can maintain about 0.6399.

5.2. Network Lifetime of ROLM. After discussing the reliability of the WSN evolving from ROLM, we will analyze the network lifetime of the WSN evolving from ROLM in this part. Same as Section 5.1, here we will compare the lifetime of the WSN evolving from ROLM with that of [9]. According to the definition of round in Section 2.1, in

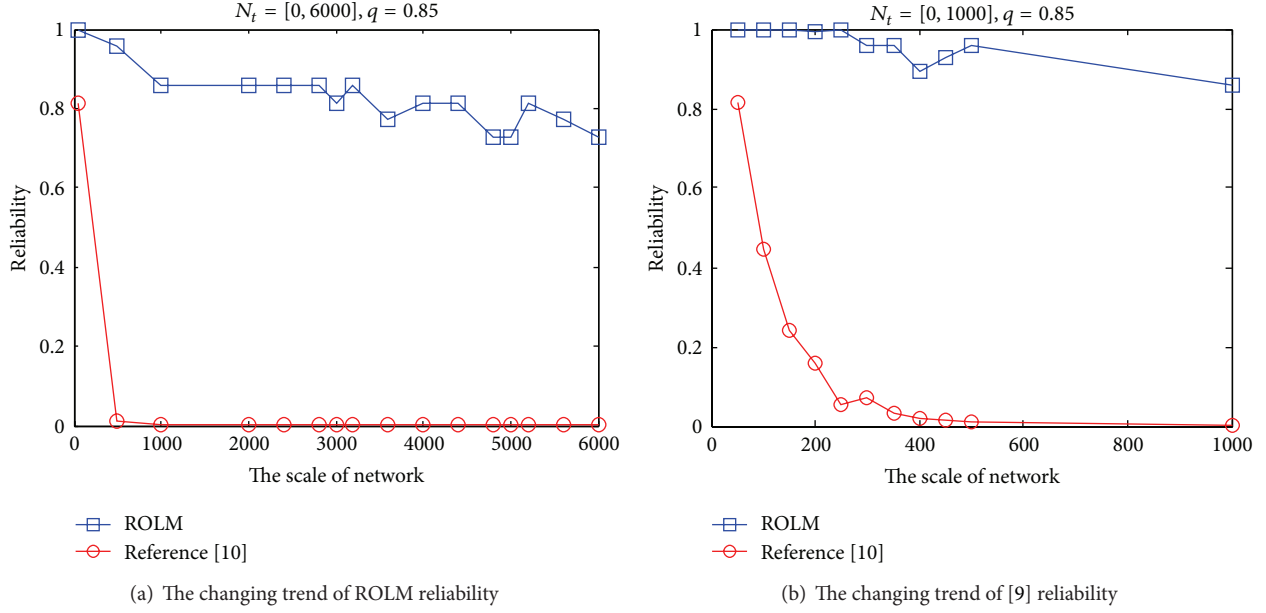
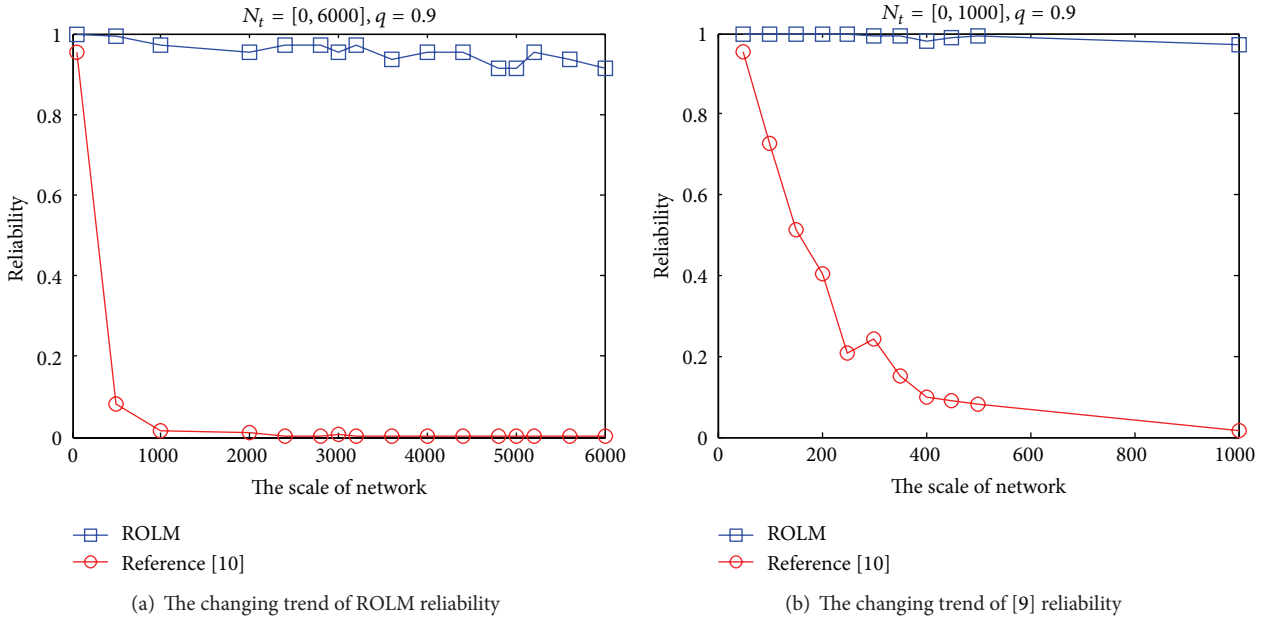
order to facilitate the statistics of round, we define that all nodes will aggregate its own sensed data and the sensed data from other nodes with fixed-length l bits and then send it to its father node. According to [34], for one SN, the energy expenditure of sending 1-bit data is equal to that of executing 1000 commands. Therefore, here we just calculate the communication energy expenditure and ignore that of executing overhead. In this group's experiments, assuming a node expends b energy to send a l bits packet, we set $b = E_{\max c}/500$. That is, the energy of each node decreases by b in every round. If a node has less than b energy, then we consider that the node and all its son nodes are dead (the sensed data of its son nodes need it to relay their sensed data). Except from the $N_t = 5000$, the rest of other variables are set as in Section 5.1. Under the above assumptions, the number of nodes alive will decrease with the increase of network running rounds, and the comparing results of lifetimes of WSNs evolving from ROLM and [9] are shown in Figure 5.

There are three groups of number in Figure 5; they are network lifetimes in different network scale of 1000, 3000, and 5000. From Figures 5(a), 5(c), and 5(e), we find that, under the same assumptions, WSNs evolving from ROLM and [9] have the same lifetime, the network lifetime of both WSNs evolving from ROLM and [9] is 438, and their initial time of attenuation is 125. That is, some nodes begin to die from the 125th round, and all nodes are dead in the 438th round. Both of them have set the same $k_{\max c}$ and $k_{\max s}$ to prolong the lifetime of network.

Figures 5(b), 5(d), and 5(f) are detailed graphs of one part from Figures 5(a), 5(c), and 5(e), respectively. These three figures reveal that the number of nodes alive in the WSN evolving from [9] decreased quickly and the number of death nodes in the 125th round is much larger than that of ROLM. For the network with scale of 1000, the number of alive nodes in the WSN evolving from ROLM is larger than or equal to that of [9] among the rounds within [1, 175]. And for the network with scale of 5000, the number of alive nodes in the WSN evolving from ROLM is larger than or equal to that of [9] among the rounds within [1, 200]. That is, the WSN evolving from ROLM is more energy-efficient than that of [9]. This is because [9] only considers the energy consumption of nodes and did not control the maximum value of nodes' cluster layer, which leads to the result that the new-incoming nodes have a tendency to link to the SNs that are far away from the sink node which can increase the hops among any two nodes and energy consumption for processing data and finally decrease the energy efficient.

The above two groups of experiments about the network reliability and the network lifetime prove that ROLM can ensure a higher reliability which is much larger than that of [9], ROLM can be used in larger-scale network where [9] could not, and the energy efficiency of the WSN evolving from ROLM among some rounds is better than that of [9].

5.3. $\langle L \rangle$ -The Average Length of Shortest Path. In the WSN, SNs collect and send data to their father nodes (SNs or CHs) and then forward them to the sink node via multihops, so all SNs or CHs who act as a father node play an important role in data

FIGURE 3: The changing trend of reliability with the increase of network scale ($q = 0.85$).FIGURE 4: The changing trend of reliability with the increase of network scale ($q = 0.9$).

collecting and transmitting. We use $\langle L \rangle$ -the average length of shortest path to measure the average hops among SNs and CHs for data processing; its calculation can be written as [23]

$$\langle L \rangle = \frac{1}{N(N-1)} \cdot \sum_{i \neq j} d_{ij}, \quad (14)$$

where d_{ij} is the length of shortest path between any two nodes (SNs or CHs) i and j , N is the number of nodes in the network, and $d_{ij} = +\infty$ if there is no path between nodes

i and j . Different from [9], considering that every path in the network can reflect the efficiency of the network, we use the d_{ij} between every two nodes in the network to calculate the value of $\langle L \rangle$. The smaller $\langle L \rangle$ means fewer hops and less energy consumption for data processing.

On the other hand, [9] just analyzed the relationships among p , C , and $\langle L \rangle$, and these can reflect the influences of p and C on $\langle L \rangle$ but cannot reflect the efficiency of the evolution models. Therefore, in this part, we study the relationship among the scale of network N , $\langle L \rangle$, and C ($C = 25$ and

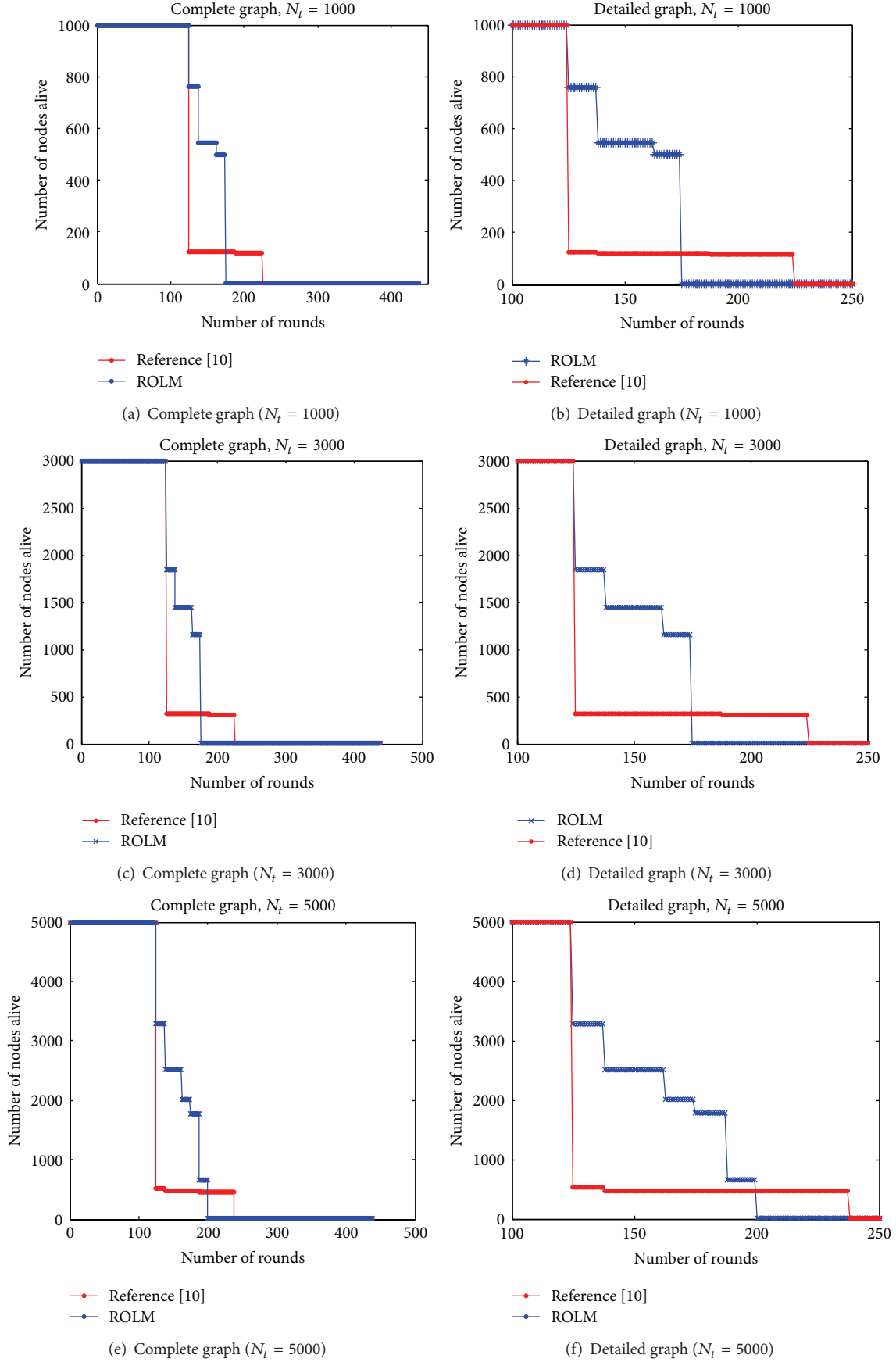


FIGURE 5: WSNs lifetimes in different network scale of 1000, 3000, and 5000.

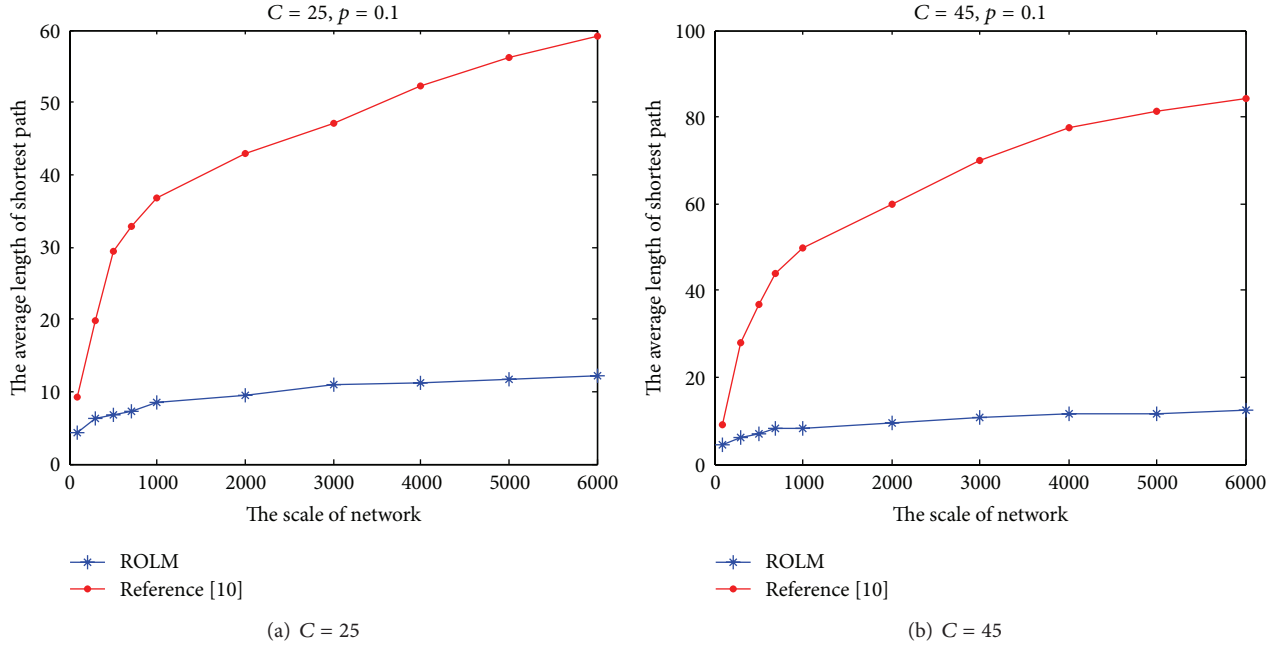


FIGURE 6: The plot of $\langle L \rangle$ -network scale with $\rho(E) \sim U$, $C = 25$ and 45 for WSNs evolving from ROLM and [9].

$C = 35$) for WSNs evolving from ROLM and [9] and fix $\rho(E_c) \sim U[0.7, 1]$, $\rho(E_s) \sim U[0.3, 0.7]$, $k_{\max s} = 7$, $k_{\max c} = 20$, $p = 0.1$ (shown as in Figure 6).

From Figure 6, we can find that, for each N , $\langle L \rangle$ of the WSN evolving from ROLM is smaller than that of [9] no matter whether $C = 25$ (shown as in Figure 6(a)) or $C = 45$ (shown as in Figure 6(b)), such that when $N = 2000$ and $C = 25$, there are $\langle L \rangle = 9.587719786$ for the WSN evolving from ROLM and $\langle L \rangle = 42.89694797$ for the WSN evolving from [9]. When $N = 2000$ and $C = 45$, there are $\langle L \rangle = 9.441435432$ for the WSN evolving from ROLM and $\langle L \rangle = 59.72642678$ for the WSN evolving from [9]. That means the number of hops among two nodes in the WSN evolving from ROLM is less than that in [9] which can ensure a better synchronization, and the energy consumption for data processing in the WSN evolving from ROLM is less than that of [9]. It also explains the results shown in Figure 5 in which the WSN evolving from ROLM has better energy efficiency than that of [9]. That is because we try to reduce the cluster layer in the WSN evolving from ROLM while [9] does not consider it.

The two blue lines in Figure 6 indicate that the slopes of blue lines decrease with the increase of N (when $N > 1000$), and the red lines do not have this phenomenon. That is, the WSN evolving from ROLM has more obvious small world characteristic than that of [9]. For different values of C , the change extent of $\langle L \rangle$ in the WSN evolving from ROLM is weaker than that in the WSN evolving from [9], which means that C has a weak effect on the WSN evolving from ROLM. Because [9] only considers the energy of nodes to evolve the WSN, for big C , the new-incoming node will tend to connect to the preexisting node whose residual energy is larger

(no matter how many its cluster layers), and the change of C affects the $\langle L \rangle$ of the WSN evolving from [9].

The above analysis and Section 4 show that the WSN evolving from ROLM has steadier complex network features than that of [9].

6. Conclusions

Consider large-scale WSNs have showed many complex features and an appropriate evolution model is very necessary for improving the performances of WSNs. In this paper, we are trying to build an evolution model which could evolve a WSN with high reliability and find out a way to measure the reliability of network. Describing the WSN as a model with two kinds of nodes and three kinds of links, we proposed a reliability-oriented large-scale model (ROLM) to improve the reliability of the WSN for some aggregation operators and presented the reliability parameter η to measure the reliability of network for SUM aggregation operator. After proving the mathematical rationality of parameter η theoretically and deriving the calculating method of η , we use η as one of performance metrics of WSNs.

The analysis of degree distribution of nodes shows that both of WSNs evolving from ROLM and [9] follow a power-law distribution and ROLM has a more obvious scale-free characteristic. From the experiments, we can find that, for a specific network scale, the reliability of the WSN evolving from ROLM is higher than that of [9]; for example, when $q = 0.85$, the evolution model in [9] is unusable when the network scale is larger than 1000 nodes, while ROLM can ensure the reliability of the WSN to be 0.6399 even with 20000 nodes in the network. On the other hand, the experiment

results also show that ROLM balanced energy consumption by limiting the connectivity of nodes to prolong the life of the network, and the WSN evolving from ROLM achieves the same long lifetime with that of [9]. Within many rounds, the energy efficiency of the WSN evolving from ROLM is better than that of [9]. Lastly, we also give experiments to analyze the average length of shortest path of WSNs evolving from ROLM and [9]. The results indicate that the hops among two nodes in the WSN evolving from ROLM are fewer than those in [9] which can ensure a better synchronization, and the energy consumption for data processing in the WSN evolving from ROLM is less than that of [9]. The experiments about the degree distribution and the average length of shortest path show that the WSN evolving from ROLM has steadier complex network features than that of [9]. And the experiments about the network reliabilities and lifetimes prove that the energy efficiency of the WSN evolving from ROLM within some rounds is better than that of [9], ROLM can ensure a higher reliability which is much larger than that of [9], and ROLM can be used in larger-scale network where [9] could not be.

Appendices

A. The Proof for Theorem 9

For any i ($1 \leq i \leq m_v, 1 \leq v \leq \omega$), let random variables $X_{1i}, X_{2i}, X_{3i}, \dots, X_{\omega i}$ satisfy the following equations, respectively:

$$\begin{aligned} X_{1i} &= \begin{cases} 1 & \text{if } s_{t,1}^i \in B_{(q)} \\ 0 & \text{if } s_{t,1}^i \notin B_{(q)} \end{cases} \\ &\vdots \\ X_{\omega i} &= \begin{cases} 1 & \text{if } s_{t,\omega}^i \in B_{(q^\omega)} \\ 0 & \text{if } s_{t,\omega}^i \notin B_{(q^\omega)} \end{cases} \end{aligned} \quad (\text{A.1})$$

Clearly, there are $P(X_{1i} = 1) = q, P(X_{1i} = 0) = 1 - q, P(X_{2i} = 1) = q^2, P(X_{2i} = 0) = 1 - q^2, \dots, P(X_{\omega i} = 1) = q^\omega, P(X_{\omega i} = 0) = 1 - q^\omega$. Meanwhile, according to the lognormal shadowing model, for $1 \leq i \neq j \leq m_v$, there are random variables X_{vi} and X_{vj} which are independent of each other ($1 \leq v \leq \omega$). Furthermore, the distribution of X_{vi} ($1 \leq v \leq \omega$) shows there are $E(X_{1i}) = q, E(X_{2i}) = q^2, \dots, E(X_{\omega i}) = q^\omega, \text{Var}(X_{1i}) = q(1 - q), \text{Var}(X_{2i}) = q^2(1 - q^2), \dots, \text{Var}(X_{\omega i}) = q^\omega(1 - q^\omega)$.

Combining with $\text{Sum}(S_t)' = (1/q) \sum_{s_{t,1}^i \in B_{(q)}} s_{t,1}^i + (1/q^2) \sum_{s_{t,1}^i \in B_{(q^2)}} s_{t,2}^i + \dots + (1/q^\omega) \sum_{s_{t,\omega}^i \in B_{(q^\omega)}} s_{t,\omega}^i$ (equation (7) in the main body), we can get

$$\begin{aligned} \text{Sum}(S_t)' &= \frac{1}{q} \sum_{i=1}^{m_1} s_{t,1}^i X_{1i} + \frac{1}{q^2} \sum_{i=1}^{m_2} s_{t,2}^i X_{2i} \\ &+ \dots + \frac{1}{q^\omega} \sum_{i=1}^{m_\omega} s_{t,\omega}^i X_{\omega i}. \end{aligned} \quad (\text{A.2})$$

As $E(X_{1i}) = q, E(X_{2i}) = q^2, \dots, E(X_{\omega i}) = q^\omega$, there is

$$E(\text{Sum}(S_t)') = \sum_{i=1}^{m_1} s_{t,1}^i + \sum_{i=1}^{m_2} s_{t,2}^i + \dots + \sum_{i=1}^{m_\omega} s_{t,\omega}^i = \text{Sum}(S_t). \quad (\text{A.3})$$

For two independent events X and Y , let $D(X)$ and $D(Y)$ be the variances of X and Y , respectively; then $D(X + Y) = D(X) + D(Y)$. And combining with $\text{Var}(X_{1i}) = q(1 - q), \dots, \text{Var}(X_{\omega i}) = q^\omega(1 - q^\omega)$, we can get

$$\begin{aligned} \text{Var}(\text{Sum}(S_t)') &= \frac{(1 - q)}{q} \sum_{i=1}^{m_1} (s_{t,1}^i)^2 + \frac{(1 - q^2)}{q^2} \sum_{i=1}^{m_2} (s_{t,2}^i)^2 \\ &+ \dots + \frac{(1 - q^\omega)}{q^\omega} \sum_{i=1}^{m_\omega} (s_{t,\omega}^i)^2 \\ &\leq \frac{(1 - q)}{q} \text{Sup}(S_t) \sum_{i=1}^{m_1} s_{t,1}^i + \frac{(1 - q^2)}{q^2} \text{Sup}(S_t) \sum_{i=1}^{m_2} s_{t,2}^i \\ &+ \dots + \frac{(1 - q^\omega)}{q^\omega} \text{Sup}(S_t) \sum_{i=1}^{m_\omega} s_{t,\omega}^i \\ &= \frac{(1 - q^\omega)}{q^\omega} \text{Sup}(S_t) \times \left[\frac{q^{\omega-1}}{(1 + q + q^2 + \dots + q^{\omega-1})} \sum_{i=1}^{m_1} s_{t,1}^i \right. \\ &\quad + \frac{q^{\omega-2}}{(1 + q^2 + q^4 + \dots + q^{\omega-2})} \sum_{i=1}^{m_2} s_{t,2}^i \\ &\quad + \frac{q^{\omega-3}}{(1 + q^3 + q^6 + \dots + q^{\omega-3})} \sum_{i=1}^{m_3} s_{t,3}^i \\ &\quad \left. + \dots + \sum_{i=1}^{m_\omega} s_{t,\omega}^i \right]. \end{aligned} \quad (\text{A.4})$$

According to formula (A.4), as $q^{\omega-1}/(1 + q + q^2 + \dots + q^{\omega-1}) \leq 1, q^{\omega-2}/(1 + q^2 + q^4 + \dots + q^{\omega-2}) \leq 1, q^{\omega-3}/(1 + q^3 + q^6 + \dots + q^{\omega-3}) \leq 1, \dots$, we can get

$$\begin{aligned} \text{Var}(\text{Sum}(S_t)') &\leq \frac{(1 - q^\omega)}{q^\omega} \text{Sup}(S_t) \\ &\times \left[\sum_{i=1}^{m_1} s_{t,1}^i + \sum_{i=1}^{m_2} s_{t,2}^i + \sum_{i=1}^{m_3} s_{t,3}^i + \dots + \sum_{i=1}^{m_\omega} s_{t,\omega}^i \right] \\ &= \frac{(1 - q^\omega)}{q^\omega} \text{Sup}(S_t) \times \text{Sum}(S_t). \end{aligned} \quad (\text{A.5})$$

B. The Proof for Theorem 10

Combining with the above analysis, sensed data from SNs with $\omega_s^i = 1$, SNs with $\omega_s^i = 2, \dots$, and SNs with $\omega_s^i = \omega$ will be

sent successfully to the sink node with certain probabilities $q, q^2, q^3, \dots, q^\omega$, respectively. $S_{t,1}, S_{t,2}, S_{t,3}, \dots, S_{t,\omega}$ are the sets of sensed data from SNs with $\omega_s^i = 1$, SNs with $\omega_s^i = 2, \dots$, and SNs with $\omega_s^i = \omega$ at time t , respectively, and $B_{(q)}, B_{(q^2)}, B_{(q^3)}, \dots, B_{(q^\omega)}$ are the sets of sensed data which are sent successfully to the sink node from SNs with $\omega_s^i = 1$, SNs with $\omega_s^i = 2, \dots$, and SNs with $\omega_s^i = \omega$ at time t , respectively.

For SNs with $\omega_s^i = 1$ ($v = 1$). There are $\mu_{1i} = E(Y_{1i}) = qs_{t,1}^i$ and $\sigma_{1i} = \text{Var}(Y_{1i}) = (s_{t,1}^i)^2 q(1-q)$.

Let $\xi_1 = 1$, and according to the above analysis, for all i ($1 \leq i \leq m_1$), there is

$$\begin{aligned} E(|Y_{1i} - \mu_{1i}|^{2+\xi_1}) &= E(|Y_{1i} - \mu_{1i}|^3) \\ &= q(s_{t,1}^i - qs_{t,1}^i)^3 + (1-q)(qs_{t,1}^i)^3 \quad (\text{B.1}) \\ &= (s_{t,1}^i)^3 q(1-q)(1-2q+2q^2). \end{aligned}$$

Meanwhile we have

$$s_{m_1}^{2+\xi} = s_{m_1}^3 = \sum_{i=1}^{m_1} (s_{t,1}^i)^2 q(1-q) \sqrt{\sum_{i=1}^{m_1} (s_{t,1}^i)^2 q(1-q)}. \quad (\text{B.2})$$

Combining with formula (B.1) and formula (B.2), there is

$$\begin{aligned} \lim_{m_1 \rightarrow \infty} \frac{1}{s_{m_1}^3} \sum_{i=1}^{m_1} E(|Y_{1i} - \mu_{1i}|^3) \\ &= \frac{1-2q+2q^2}{\sqrt{(q(1-q))}} \lim_{m_1 \rightarrow \infty} \frac{\sum_{i=1}^{m_1} (s_{t,1}^i)^3}{\sum_{i=1}^{m_1} (s_{t,1}^i)^2 \sqrt{\sum_{i=1}^{m_1} (s_{t,1}^i)^2}} \quad (\text{B.3}) \\ &\leq \frac{1-2q+2q^2}{\sqrt{(q(1-q))}} \frac{\sup(S_{t,1})^3}{\inf(S_{t,1})^3} \lim_{m_1 \rightarrow \infty} \frac{1}{\sqrt{m_1}}. \end{aligned}$$

Among them, $\inf(S_t, 1)$ and $\sup(S_t, 1)$ present the lower bound and upper bound of sensed data from SNs with $\omega_s^i = 1$, respectively. $|\inf(S_{t,1})|, |\sup(S_{t,1})| \ll +\infty$, hence $\lim_{m_1 \rightarrow \infty} (1/s_{m_1}^3) \sum_{i=1}^{m_1} E(|Y_{1i} - \mu_{1i}|^3) \leq 0$; meanwhile, $s_{m_1}^3 \geq 0$ and $E(|Y_{1i} - \mu_{1i}|^3) \geq 0$; therefore $\lim_{m_1 \rightarrow \infty} (1/s_{m_1}^3) \sum_{i=1}^{m_1} E(|Y_{1i} - \mu_{1i}|^3) \geq 0$. In conclusion, $\lim_{m_1 \rightarrow \infty} (1/s_{m_1}^3) \sum_{i=1}^{m_1} E(|Y_{1i} - \mu_{1i}|^3) = 0$; that is, when $v = 1$, there is ξ_1 ($\xi_1 = 1$) satisfying formula (10) in Theorem 10, and Y_{1i} satisfies Lyapunov condition. According to [31], $\text{Sum}(S_{t,1})' = \sum_{i=1}^{m_1} Y_{1i}$ meets application conditions of central limit theorem; that is, $\text{Sum}(S_{t,1})'$ follows normal distribution.

Without considering the analysis of other ω_s^i (their researching methods are the same as $v = 1$), we next describe the analysis of SNs with $\omega_s^i = \omega$; that is, $v = \omega$.

For SNs with $\omega_s^i = \omega$ ($v = \omega$). Same as $v = 1$, for $\omega_s^i = \omega$, there are $u_{\omega i} = E(Y_{\omega i}) = q^\omega s_{t,\omega}^i$ and $\sigma_{\omega i} = \text{Var}(Y_{\omega i}) =$

$q^\omega(1-q^\omega)(s_{t,\omega}^i)^\omega$. for all i ($1 \leq i \leq m_\omega$), if we let $\xi_\omega = 1$, then there will be

$$\begin{aligned} E(|Y_{\omega i} - u_{\omega i}|^{2+\xi}) &= E(|Y_{\omega i} - u_{\omega i}|^3) \\ &= q^\omega (s_{t,\omega}^i - q^\omega s_{t,\omega}^i)^3 \\ &\quad + (1-q^\omega) |0 - q^\omega s_{t,\omega}^i|^3 \\ &= q^\omega (s_{t,\omega}^i)^3 (1-q^\omega) (1-2q^\omega+2q^{2\omega}), \end{aligned} \quad (\text{B.4})$$

$$s_{m_\omega}^{2+\xi} = s_{m_\omega}^3 = \sum_{i=1}^{m_\omega} (s_{t,\omega}^i)^2 q^\omega (1-q^\omega) \sqrt{\sum_{i=1}^{m_\omega} (s_{t,\omega}^i)^2 q^\omega (1-q^\omega)}. \quad (\text{B.5})$$

Combining with formula (B.4) and formula (B.5), there is

$$\begin{aligned} \lim_{m_\omega \rightarrow \infty} \frac{1}{s_{m_\omega}^3} \sum_{i=1}^{m_\omega} E(|Y_{\omega i} - u_{\omega i}|^3) \\ &= \frac{(1-2q^\omega+2q^{2\omega})}{q^\omega(1-q^\omega)} \lim_{m_\omega \rightarrow \infty} \frac{\sum_{i=1}^{m_\omega} (s_{t,\omega}^i)^3}{\sum_{i=1}^{m_\omega} (s_{t,\omega}^i)^2 \sqrt{\sum_{i=1}^{m_\omega} (s_{t,\omega}^i)^2}} \\ &\leq \frac{(1-2q^\omega+2q^{2\omega})}{q^\omega(1-q^\omega)} \frac{\sup(S_{t,\omega})^3}{\inf(S_{t,\omega})^3} \lim_{m_\omega \rightarrow \infty} \frac{1}{\sqrt{m_\omega}}. \end{aligned} \quad (\text{B.6})$$

That is to say, for cluster layer ω , ξ_ω ($\xi_\omega = 1$) satisfies formula (10) in Theorem 10, and $Y_{\omega i}$ also satisfies Lyapunov condition. Referring to [31], $\text{Sum}(S_{t,\omega})' = \sum_{i=1}^{m_\omega} Y_{\omega i}$ meets the application conditions of central limit theorem; that is, $\text{Sum}(S_{t,\omega})'$ follows normal distribution.

C. The Proof for Theorem 11

From formula (11), there is $\inf(N_t) \inf(S_t) \varepsilon^2 \geq \phi_{\delta/2}^2 \sup(S_t) ((1-q^\omega)/q^\omega)$. As $\inf(N_t)$ and $\inf(S_t)$ are the lower bound of N_t and the lower bound of the value of sensed data, respectively, there is $\text{Sum}(S_t) = \sum_{i=1}^{N_t} s_i \geq \inf(N_t) \inf(S_t)$. Hence,

$$\varepsilon^2 \text{Sum}(S_t) \geq \phi_{\delta/2}^2 \sup(S_t) \frac{(1-q^\omega)}{q^\omega}. \quad (\text{C.1})$$

Theorem 9 shows that $\text{Var}(\text{Sum}(S_t)') \leq ((1-q^\omega)/q^\omega) \sup(S_t) \text{Sum}(S_t)$, $E(\text{Sum}(S_t)') = \text{Sum}(S_t)$ and as $\text{Sum}(S_t)'$ follows normal distribution, from formula (12), there is

$$\Pr \left\{ \frac{|\text{Sum}(S_t)' - \text{Sum}(S_t)|}{\phi_{\delta/2} \sqrt{\text{Var}(\text{Sum}(S_t)')}} \geq 1 \right\} = \delta. \quad (\text{C.2})$$

Combining with the knowledge of standard normal distribution quantile [32], (C.1), (C.2), and $\delta = 1 - \eta$, we can get

$$\Pr\left(\left|\frac{\text{Sum}(S_t)' - \text{Sum}(S_t)}{\text{Sum}(S_t)}\right| \leq \varepsilon\right) \geq \eta. \quad (\text{C.3})$$

Conflict of Interests

The authors declare that there is no conflict of interests regarding the publication of this paper.

Acknowledgments

This work is supported by the China Scholarship Council, the National Key Technology Research and Development Program of the Ministry of Science and Technology of China (Grant no. 2012BAH82F04), the National Natural Science Foundation of China (Grant no. 61101121), and the National High Technology Research and Development Program of China (Grant no. 2013AA102505).

References

- [1] X. F. Wang and G. Chen, "Complex networks: small-world, scale-free and beyond," *IEEE Circuits and Systems Magazine*, vol. 3, no. 1, pp. 6–20, 2003.
- [2] H. Jeong, S. P. Mason, A.-L. Barabási, and Z. N. Oltvai, "Lethality and centrality in protein networks," *Nature*, vol. 411, no. 6833, pp. 41–42, 2001.
- [3] H. Jeong, B. Tombor, R. Albert, Z. N. Oltvai, and A.-L. Barabási, "The large-scale organization of metabolic networks," *Nature*, vol. 407, no. 6804, pp. 651–654, 2000.
- [4] C. Wu and B. Zhou, "Complex network analysis of tag as a social network," *Journal of Zhejiang University*, vol. 44, no. 11, pp. 2194–2197, 2010.
- [5] W.-K. Jia and L.-C. Wang, "A unified unicast and multicast routing and forwarding algorithm for software-defined datacenter networks," *IEEE Journal on Selected Areas in Communications*, vol. 31, no. 12, pp. 2646–2657, 2013.
- [6] R. Lara-Cabrera, C. Cotta, and A. J. Fernández-Leiva, "An analysis of the structure and evolution of the scientific collaboration network of computer intelligence in games," *Physica A: Statistical Mechanics and Its Applications*, vol. 395, pp. 523–536, 2014.
- [7] S. H. Yeganeh, J. Habibi, H. Rostami, and H. Abolhassani, "Semantic web service composition testbed," *Computers and Electrical Engineering*, vol. 36, no. 5, pp. 805–817, 2010.
- [8] G. D. Paparo, M. Müller, F. Comellas, and M. A. Martín-Delgado, "Quantum google in a complex network," *Scientific Reports*, vol. 3, article 2773, 2013.
- [9] S. Li, L. Li, and Y. Yang, "A local-world heterogeneous model of wireless sensor networks with node and link diversity," *Physica A: Statistical Mechanics and Its Applications*, vol. 390, no. 6, pp. 1182–1191, 2011.
- [10] S. Chinnappen-Rimer and G. P. Hancke, "Modelling a wireless sensor network as a small world network," in *Proceedings of the International Conference on Wireless Networks and Information Systems (WNIS '09)*, pp. 7–10, Shanghai, China, December 2009.
- [11] Y. Q. Wang and X. Y. Yang, "A random walk evolution model of wireless sensor networks and virus spreading," *Chinese Physics B*, vol. 22, no. 1, Article ID 010509, 2013.
- [12] A. M. Shamsan Saleh, B. M. Ali, H. Mohamad, M. F. A. Rasid, and A. Ismail, "RRSEB: a reliable routing scheme for energy-balancing using a self-adaptive method in wireless sensor networks," *KSII Transactions on Internet and Information Systems*, vol. 7, no. 7, pp. 1585–1609, 2013.
- [13] N. Sabri, S. A. Aljunid, B. Ahmad, A. Yahya, R. Kamaruddin, and M. S. Salim, "Wireless sensor actor network based on fuzzy inference system for greenhouse climate control," *Journal of Applied Sciences*, vol. 11, no. 17, pp. 3104–3116, 2011.
- [14] D. Kumar, "Monitoring forest cover changes using remote sensing and GIS: a global prospective," *Research Journal of Environmental Sciences*, vol. 5, pp. 105–123, 2011.
- [15] A. Rozyyev, H. Hasbullah, and F. Subhan, "Indoor child tracking in wireless sensor network using fuzzy logic technique," *Research Journal of Information Technology*, vol. 3, no. 2, pp. 81–92, 2011.
- [16] E. Stattner, N. Vidot, P. Hunel, and M. Collard, "Wireless sensor network for habitat monitoring: a counting heuristic," in *Proceedings of the IEEE 37th Conference on Local Computer Networks Workshops (LCN Workshops '12)*, pp. 753–760, Clearwater, Fla, USA, 2012.
- [17] J. X. Chen, L. Zhou, Y. Zhang, and D. F. Ferreira, "Human motion tracking with wireless wearable sensor network: experience and lessons," *KSII Transactions on Internet and Information Systems*, vol. 7, no. 5, pp. 998–1013, 2013.
- [18] Y.-C. Tseng, M.-S. Pan, and Y.-Y. Tsai, "Wireless sensor networks for emergency navigation," *Computer*, vol. 39, no. 7, pp. 55–62, 2006.
- [19] G. Miao, N. Himayat, and G. Y. Li, "Energy-efficient link adaptation in frequency-selective channels," *IEEE Transactions on Communications*, vol. 58, no. 2, pp. 545–554, 2010.
- [20] J. Z. Li and S. Y. Cheng, "(ϵ, δ)-Approximate aggregation algorithms in dynamic sensor networks," *IEEE Transactions on Parallel and Distributed Systems*, vol. 23, no. 3, pp. 385–396, 2012.
- [21] M. Zuniga and B. Krishnamachari, "Analyzing the transitional region in low power wireless links," in *Proceedings of the 1st Annual IEEE Communications Society Conference on Sensor and Ad Hoc Communications and Networks (IEEE SECON '04)*, pp. 517–526, October 2004.
- [22] IEEE Standards Association, "Wireless medium access control (MAC) and physical layer (PHY) specifications for low-rate wireless personal area networks (LR-WPANs)," IEEE Standards 802.15.4-2006, IEEE, New York, NY, USA, 2006.
- [23] S. Z. Guo and Z. M. Lu, *The Basic Theories of Complex Network*, Science Press, Beijing, China, 2012.
- [24] S. Nithyakalyani and S. S. Kumar, "Data aggregation in wireless sensor network using node clustering algorithms—a comparative study," in *Proceedings of the IEEE Conference on Information and Communication Technologies (ICT '13)*, pp. 508–513, Jeju Island, Republic of Korea, April 2013.
- [25] X.-Y. Li, X. Xu, S. Wang et al., "Efficient data aggregation in multi-hop wireless sensor networks under physical interference model," in *Proceedings of the IEEE 6th International Conference on Mobile Adhoc and Sensor Systems (MASS '09)*, pp. 353–362, Macau, China, October 2009.
- [26] P. Wang, Y. He, and L. Huang, "Near optimal scheduling of data aggregation in wireless sensor networks," *Ad Hoc Networks*, vol. 11, no. 4, pp. 1287–1296, 2013.

- [27] G. Anastasi, M. Conti, M. Di Francesco, and A. Passarella, "Energy conservation in wireless sensor networks: a survey," *Ad Hoc Networks*, vol. 7, no. 3, pp. 537–568, 2009.
- [28] Y. Liu, Q. Zhang, and L. Ni, "Opportunity-based topology control in wireless sensor networks," *IEEE Transactions on Parallel and Distributed Systems*, vol. 21, no. 3, pp. 405–416, 2010.
- [29] H. Guanyan, L. Xiaowei, and H. Jing, "Dynamic minimal spanning tree routing protocol for large wireless sensor networks," in *Proceedings of the IEEE Conference on Industrial Electronics and Applications*, pp. 1–5, Singapore, May 2006.
- [30] S. Bernstein and R. Bernstein, *Elements of Statistics Ii: Inferential Statistics*, McGraw-Hill, Columbus, Ohio, USA, 1st edition, 2004.
- [31] H. Fischer, *A History of the Central Limit Theorem: From Classical to Modern Probability Theorem*, Springer, New York, NY, USA, 1st edition, 2011.
- [32] Z. Shen, S. Q. Xie, and C. Y. Pan, *Probability Theory Mathematical Statistics*, Higher Education Press, Beijing, China, 2005.
- [33] F.-M. Li, P. Han, and T. Luo, "Adaptive area location algorithm combining with packet lost rate and RSSI in wireless sensor networks," *Journal on Communications*, vol. 30, no. 9, pp. 15–23, 2009.
- [34] J. Kabara and M. Calle, "MAC protocols used by wireless sensor networks and a general method of performance evaluation," *International Journal of Distributed Sensor Networks*, vol. 2012, Article ID 834784, 11 pages, 2012.

Research Article

Effective Semisupervised Community Detection Using Negative Information

Dong Liu,¹ Dequan Duan,¹ Shikai Sui,¹ and Guojie Song²

¹*School of Computer and Information Engineering, Henan Normal University, Xinxiang 453007, China*

²*School of Electronics Engineering and Computer Science, Peking University, Beijing 100871, China*

Correspondence should be addressed to Dong Liu; liudonghtu@gmail.com

Received 5 June 2014; Accepted 13 October 2014

Academic Editor: Qinggang Meng

Copyright © 2015 Dong Liu et al. This is an open access article distributed under the Creative Commons Attribution License, which permits unrestricted use, distribution, and reproduction in any medium, provided the original work is properly cited.

The semisupervised community detection method, which can utilize prior information to guide the discovery process of community structure, has aroused considerable research interests in the past few years. Most of the former works assume that the exact labels of some nodes are known in advance and presented in the forms of individual labels and pairwise constraints. In this paper, we propose a novel type of prior information called negative information, which indicates whether a node does not belong to a specific community. Then the semisupervised community detection algorithm is presented based on negative information to efficiently make use of this type of information to assist the process of community detection. The proposed algorithm is evaluated on several artificial and real-world networks and shows high effectiveness in recovering communities.

1. Introduction

Many networked systems, including social and biological networks, are found to divide natural communities, that is, groups of vertices which are densely connected to each other while less connected to the vertices outside [1]. The community structure in real networks always has a specific function such as cycles or pathways in metabolic networks or collections of pages on the same or related topics on the web community [2]. To comprehensively understand the function of different networks, much research effort has been devoted to develop methods that can extract community structure from networks.

A lot of models and algorithms have been proposed for community detection, such as betweenness-based algorithms [1, 3], modularity-based methods [2, 4–6], spin model [7], and stochastic blockmodels [8]; see [9, 10] for a more comprehensive review. However, almost all existing approaches for community detection only make use of the network topology information, which completely ignore the background information of the network. However, in many real-world

applications, we may know some prior information that could be useful in detecting the community structures. For instance, a few proteins have been known to belong to certain functional classes in protein-protein interaction networks [11]. Therefore, how to utilize prior information to guide the discovery process of community structure is an interesting question that is worthy of working on.

In recent years, a variety of semisupervised community detection algorithms have been proposed. Ma et al. [12] proposed a semisupervised method based on symmetric nonnegative matrix factorization, which incorporates pairwise constraints (via must-links and cannot-link) on the cluster assignments of nodes for identifying community structure in network. Eaton and Mansbach [13] presented a semisupervised algorithm based on spin-glass model, which can incorporate prior knowledge in the forms of individual labels (via known cluster assignments for a fraction of nodes) and pairwise constraints into the process of extracting community structure. Zhang et al. [14, 15] developed the methods that implicitly encode the pairwise constraints by modifying the adjacency matrix of the network, which can also be

regarded as the denoising process of the consensus matrix of the community structures. Liu et al. [16, 17] put forward two semisupervised algorithms based on discrete potential and label propagation, respectively. Both algorithms are especially suitable for the network with obscure community structure and exhibit almost linear complexity in time.

Although these approaches can improve accuracy and degree of noise resistant to community detection, they mostly focus on one kind of prior information; that is, the exact labels of a small portion of nodes are given. In some real application, it may not be easy to identify the exact community of a node, whereas we can easily point out the community that one node does not belong to. For a simplified example, assume that the web network can be grouped into some communities which represent pages on related topics. Further, supposing that the web page describes a female soccer game, it is hard to determine whether the web page belongs to sport community or feminism community. However, it does not belong to automobile community.

In machine learning, the negative information was first proposed by Hou et al. [18]. In their work, the negative information indicates whether a point does not belong to a specific category. They utilized the negative information to guide the process of semisupervised learning and made some experiments on image, digit, spoken letter, and text classification tasks. The experimental results showed the effectiveness of negative information. As far as we know, there is no community detection method concerning the negative information, although this information arises naturally in some applications.

In this paper, we propose a novel semisupervised community detection approach based on negative information. It has near-linear complexity in time and can incorporate the negative information into community detection. The algorithm has been evaluated on synthetic LFR benchmark networks [19] and on various real-world networks with community structure. The results show that negative information is helpful to improve the accuracy of identifying communities. Specifically, the algorithm exhibits almost linear complexity in time.

The rest of the paper is structured as follows. Section 2 includes reviews of the basic formulation and notations used in our approach. In Section 3, we describe our new semisupervised community detection algorithm in detail. Experimental results on artificial and real-world networks are given in Section 4. Finally, a conclusion is presented in Section 5.

2. Problem Formulation and Notations

We first give the notations of network representation which will be used throughout this paper. Let $G = \{V, E\}$ denote an unweighted and undirected network, where $V = \{v_1, v_2, \dots, v_n\}$ is the set of nodes and $E \subseteq V \times V$ is the set of edges. Multiple edges and self-connections are not allowed. The network structure is determined by $n \times n$ adjacency matrix A . Each element A_{ij} of A is equal to 1 if there is an

edge connecting nodes i to j , and it is 0 otherwise. If there are k communities, a community-number (label) set $K = \{1, 2, \dots, k\}$ is defined.

Assume that there are three kinds of nodes, that is, traditional label (TL) nodes V^{TL} , negative label (NL) nodes V^{NL} , and unlabeled (UL) nodes V^{UL} . Define the set of TL nodes $V^{\text{TL}} = \{v_1, v_2, \dots, v_t\}$ with cardinality $|V^{\text{TL}}| = t$, the set of NL nodes $V^{\text{NL}} = \{v_{t+1}, v_{t+2}, \dots, v_{t+l}\}$ with cardinality $|V^{\text{NL}}| = l$, and the set of UL nodes $V^{\text{UL}} = \{v_{t+l+1}, v_{t+l+2}, \dots, v_{t+l+u}\}$ with $|V^{\text{NL}}| = u$, where typically $t \ll u, l \ll u$, and $t+l+u = n$. Further, suppose that we are given a set of nodes $V = V^{\text{TL}} \cup V^{\text{NL}} \cup V^{\text{UL}}$. The label indicator matrix of V^{TL} is defined as follows: $L_{ij}^{\text{TL}} = 1$ if and only if v_i belongs to the j th community; otherwise $L_{ij}^{\text{TL}} = 0$. We define the label indicator matrix of V^{NL} as $L_{ij}^{\text{NL}} = 1$ if and only if v_i does not belong to the j th community; otherwise $L_{ij}^{\text{NL}} = 0$. Note that, different from L^{TL} , the row vectors of L^{NL} may have more than one element which is equal to 1. The goal of our approach is to infer the exact labels for nodes in $V^{\text{NL}} \cup V^{\text{UL}}$.

In this paper, label propagation task is to propagate the TL under the guidance of NL information to all of the nodes in $V^{\text{NL}} \cup V^{\text{UL}}$, accomplishing label prediction of nodes without TL. The result of label propagation for community detection depends on the weights of the edges of network, so how to construct the weight matrix W plays a decisive role. In this work, the simple weight matrix can be defined as

$$W_{ij} = \frac{A_{ij}}{\deg(i)}, \quad (1)$$

where $\deg(i)$ represents the degree of node i . Obviously, in label propagation process, the labeled nodes propagate seed labels to their neighbours with uniform probability.

3. The Proposed Algorithm

In this section, the details of our proposed algorithm based on negative information are presented, and then the time complexity and the convergence property of the algorithm are analyzed. There are mainly two steps of the algorithm. The first is to determine the particular parameter matrices, and the second is to propagate labels via an iterative process.

3.1. Parameter Matrices Construction. Using the idea of the work by Hou et al. [18], we introduce two matrices, that is, the initial label matrix $L \in R^{(t+l+u) \times K}$ and the parameter matrix $P \in R^{(t+l+u) \times K}$, where K is number of communities. L_{ij} represents the probability that v_i belongs to the j th community, and P is a matrix that shows the role of each node and indicates when an NL node can be regarded as a TL node and when it is considered as an unlabeled node. We also define two parameters $0 < \alpha_l < 1$ and $0 < \alpha_u < 1$, which take different values for labeled nodes (including TL and NL) and unlabeled nodes.

For any node v_i , the L_i and P_i are defined as follows.

(1) If v_i Has the TL. Based on the indicator matrix L^{TL} , if v_i belongs to the j th community, then

$$L_{ix} = \begin{cases} 1, & x = j; \\ 0, & x \neq j, \end{cases} \quad (2)$$

$$P_{ix} = \alpha_l \quad \text{for } x = 1, 2, \dots, k. \quad (3)$$

(2) If v_i Has the NLs. According to the L^{NL} , we can define an index set $I_i = (i_1, i_2, \dots, i_p)$, which contains the sets that v_i does not belong to; then

$$L_{ix} = 0 \quad \text{for } x = 1, 2, \dots, k. \quad (4)$$

$$P_{ix} = \begin{cases} \alpha_l, & x \in I_i; \\ \alpha_u, & x \notin I_i. \end{cases} \quad (5)$$

(3) If v_i Is an Unlabeled Node. Consider

$$L_{ix} = 0 \quad \text{for } x = 1, 2, \dots, k, \quad (6)$$

$$P_{ix} = \alpha_u \quad \text{for } x = 1, 2, \dots, k. \quad (7)$$

How to make use of these two matrices in the proposed algorithm will be explained in the next subsection. Note that α_l is close to 0 and α_u is close to 1.

3.2. Description of the Algorithm. The algorithm is motivated by the fact that the nodes having the same traditional label are grouped together as one community through labels propagation process. We initialize a small number of nodes with user-defined labels based on prior information (including TLs and NLs) and let the TLs propagate through the network. As the labels propagate, the exact labels of the NL and unlabeled nodes can be achieved. Then we will show how to iteratively propagate the TL under the guidance of NL information and unlabeled nodes.

This process is iteratively performed, where, at every step, each node absorbs some label information from its neighbors and retains some label information of its initial state. Let \mathcal{F} denote a set of computed label matrices, for all $F \in \mathcal{F} \subset R^{(t+l+u) \times K}$; its row vector corresponds to the possibilities of a specific node belonging to all the communities. The exact label of one node can be determined by the index of the largest element of the corresponding row vector of F . The iterative formula is defined as follows:

$$F_{ij}^{h+1} = P_{ij} \sum_{x=1}^n W_{ix} F_{xj}^h + (1 - P_{ij}) L_{ij}, \quad (8)$$

where h denotes the times of iterations. The first term shows the label information that v_i absorbs from its neighbors and the second term represents the label information retained from its initial label.

Specifically, if v_i has a TL which indicates it belongs to the j th community, then $L_{ij} = 1$ and $L_{ix} = 0$ ($x \neq j$). In this case $L_{ix} = \alpha_l$ for $x \in K$ and α_l is close to 0. Thus, the second term in (8) plays a major role in each iteration; that is, the predicted label is consistent with the given TL. If v_i has an NL indicating that v_i belongs to the j th community, that is, $j \in I_i$, then $P_{ij} = \alpha_l$ and $F_{ij}^{h+1} \approx (1 - P_{ij})L_{ij} \approx L_{ij} \approx 0$. On the contrary, if $j \notin I_i$, no much prior information can help to determine whether v_i belongs to the j th community or not. Therefore, we regard it as an unlabeled node and $P_{ix} = \alpha_u$, $L_{ix} = 0$. In this case, the first term in (8) plays a major role in each iteration. If v_i is unlabeled, there is no prior information about its label and $P_{ix} = \alpha_u$, $L_{ix} = 0$. Thus (8) is dominated by its second term. In summary, the iteration equation can be rewritten as

$$F^{h+1} = PWF^h + (I - P)L, \quad (9)$$

where I denotes an $n \times n$ identity matrix.

To summarize, the main procedure of the method is presented in Algorithm 1.

3.3. Analysis of the Algorithm. In this subsection we will analyze our method theoretically. First we will discuss the time complexity of the algorithm. Second we will analyze the convergence property of the iteration of the algorithm.

The algorithm mainly contains three computational parts: constructing the weight matrix W , constructing the label and parameter matrices L , P , and iterating (9) until convergence. In the first part, $O(m)$ time is required to construct the weight matrices, where m denotes the number of edges. In the second part, the label and parameter matrices can be derived with computational complexity $O(n)$, where n denotes the number of nodes. In the last part, the time complexity of each iteration is $O(m)$. Assuming (9) is converged at h iterations, the last part of the algorithm requires $O(hm)$ time. Since the time complexity of the algorithm depends on the highest complexity of the three parts involved in it, the overall time complexity is $O(hm)$ for the proposed algorithm.

The convergence of the algorithm is analyzed as follows. According to the initial condition that $F^0 = L$, (9) can be rewritten as

$$F^h = (PW)^h L + (I - P) \sum_{i=1}^{h-1} (PW)^i L. \quad (10)$$

Since $w_{ij} \geq 0$ and $\sum_i w_{ij} = 1$, from the theorem of Perron-Frobenius [20], the spectral radius of W satisfies $\rho(W) \leq 1$. Recall that the elements of P are either α_l or α_u , where $0 < \alpha_l < 1$ and $0 < \alpha_u < 1$; thus

$$\lim_{t \rightarrow \infty} (PW)^t = 0 \quad (11)$$

$$\lim_{t \rightarrow \infty} \sum_{i=0}^{t-1} (PW)^i = (I - PW)^{-1}.$$

input: adjacency matrix A , the initial label matrix L^{TL}, L^{NL} , the constants α_l and α_u

output: The TL of all the nodes

- (1) construct the weight matrix W by (1).
- (2) for $i = 1 : n$
- (3) If v_i has the TL
- (4) construct L and P by (2) and (3), respectively.
- (5) If v_i has the NLs
- (6) construct L and P by (4) and (5), respectively.
- (7) If v_i is unlabeled node
- (8) construct L and P by (6) and (7), respectively.
- (9) iterate (9) until convergence.
- (10) output the labels of each node v_i by $f_i = \operatorname{argmax}_{i \ll k} F_{ij}$.

ALGORITHM 1: Semisupervised community detection using negative information.

Obviously, (9) will converge to

$$\lim_{t \rightarrow \infty} F^t = (I - P)(I - PW)^{-1}L. \quad (12)$$

4. Experiments and Discussion

In this section, we give a set of experiments to show the effectiveness of the proposed algorithm. The relevant data sets involving the experiments are LFR artificial networks [19] and real-world networks including the Zachary's network of karate club [21] and the Lusseau's network of bottlenose dolphins [22]. In all the experiments of this section, α_l and α_u are set to 0.05 and 0.95, respectively.

4.1. Artificial Networks. In this subsection, the ability of the algorithm to identify communities is tested in LFR benchmark networks. Our experiments include evaluating the performance of the algorithm with various amounts of NL nodes, measuring the ability of the algorithm to recover communities with different parameter μ in benchmark networks, comparing the accuracy of our algorithm with label propagation algorithm (LPA) [23] and Infomap algorithm [24] and analyzing the relationship between the percentage of NL nodes and the percentage of TL nodes in the proposed algorithm. In the following experiments, the choice of NL and TL nodes is random, and the number of NLs of each NL node is set to 20 percent of the number of communities. Note that the NLs of each NL node are selected randomly.

The LFR benchmark network is an artificial network for community detection, which is claimed to possess some basic statistical properties found in real networks, such as heterogeneous distributions of degree and community size. Many parameters are involved to specify properties of generated networks in this benchmark: N (number of nodes), $\langle k \rangle$ (average degree), k_{\max} (maximum degree), c_{\min} and c_{\max} (minimum and maximum community size), τ_1 (exponent of power-law distribution of nodes degree), τ_2 (exponent of power-law distribution of community sizes), and μ (mixing parameter).

To evaluate the performance of our algorithm on discovering community structures, the normalized mutual information (NMI) measure [25] is used to quantitatively

compare the known partition with the partition found by the algorithm:

$$\text{NMI}(A, B) = \frac{-2 \sum_{i=1}^{c_A} \sum_{j=1}^{c_B} N_{ij} \log(N_{ij}N / N_i N_j)}{\sum_{i=1}^{c_A} N_i \log(N_i / N) + \sum_{j=1}^{c_B} N_j \log(N_j / N)}, \quad (13)$$

where c_A is the real number of community and c_B denotes the number of found community. The matrix N presents the confusion matrix, where N_{ij} is simply the number of nodes in the real community i that appears in the found community j . N_i and N_j are the sum over row i and column j of confusion matrix, respectively. N is obviously the number of nodes. If the found partition is identical to the real communities, then NMI takes its maximum value, 1. However, if the found partition is entirely independent of the real partition, NMI = 0 corresponds to the situation that the entire network is found to be one community. The closer to 1 of the NMI, the better partition of the network will be.

The number of NL nodes in each community is an important factor that affects the ability of the algorithm to identify communities. In order to quantify the relationship between the accuracy of the algorithm and the number of NL nodes in each community, the experiment is performed on the LFR benchmark networks (see Figure 1). The following parameters were employed: $N = 1000$, $\langle k \rangle = 15$, $\mu = \{0.7, 0.8\}$, $\tau_1 = 2$, $\tau_2 = 1$, $c_{\min} = 20$, and $c_{\max} = 50$. We fix the percentage of TL nodes 20% in each community. The result of the experiment suggests that the partition accuracy of the algorithm increases with increase of the percentage of NL nodes in each community.

In the LFR networks, the mixing parameter μ represents the ratio between the external degree of each vertex with respect to its community and the total degree of the node. The larger the value μ of the network is, the harder its community structure is detected. Then the experiment is designed for testing the accuracy of our algorithm with the various parameter μ (see Figure 2). In the experiment, we randomly select 4 and 8 labeled nodes in each community, respectively. The following parameters about the LFR benchmark networks were employed: $N = 1000$, $\langle k \rangle = 15$, $\mu = \{0.1, 0.2, \dots, 0.9\}$, $\tau_1 = 2$, $\tau_2 = 1$, $c_{\min} = 20$, and $c_{\max} = 50$. We fix the percentage

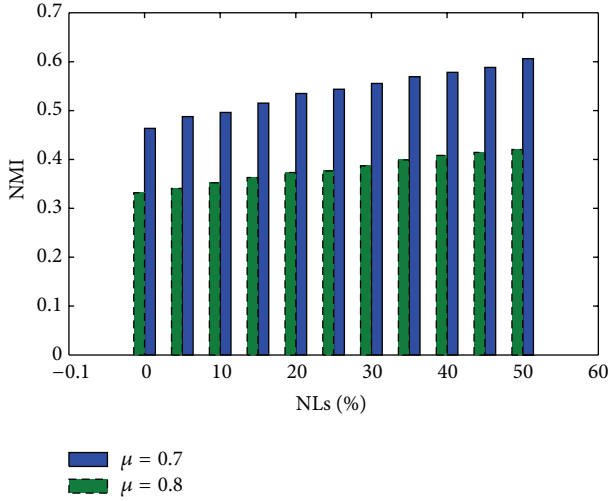


FIGURE 1: The relationship between the accuracy of the algorithm and the number of NL nodes in each community. In the LFR benchmark, $\mu = \{0.7, 0.8\}$, the partition accuracy of the algorithm increases with the increase of the percentage of NL nodes in each community. Each point in the figure represents the average over 100 runs on randomly generated LFR benchmark networks with the given parameters.

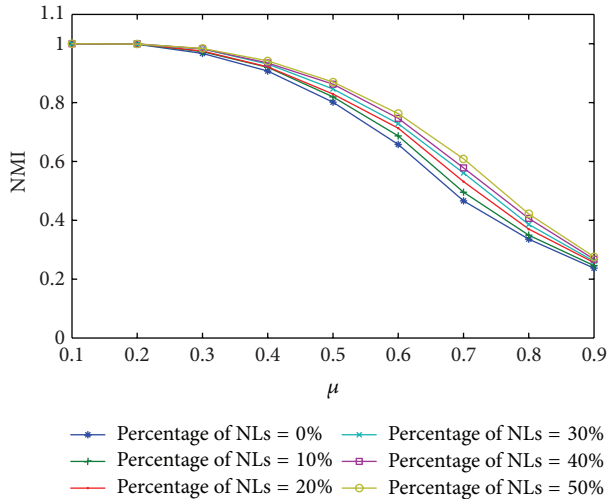


FIGURE 2: Testing the accuracy of our algorithm with the various parameter μ . Each point in the graph represents the average over 100 runs on randomly generated LFR benchmark networks with the given parameters.

of TL nodes 20% in each community and determine the percentage of NL nodes in each community by searching the grid $\{0\%, 10\%, \dots, 50\%\}$.

To evaluate the effectiveness of our algorithm, we compare it to label propagation algorithm (LPA) and Infomap algorithm. Both algorithms can discover community structure without prior knowledge. We generate benchmark networks with the following parameters: $N = 1000$, $\langle k \rangle = 15$, $\mu = \{0.1, 0.2, \dots, 0.9\}$, $\tau_1 = 2$, $\tau_2 = 1$, $c_{\min} = 20$, and

$c_{\max} = 50$. Then, we randomly select 20% TL nodes and, respectively, select 0% and 20% NL nodes in each community (see Figure 3).

Figure 3 presents the advantages of our algorithm under a certain situation. Compared with the two comparative algorithms, our proposed algorithm gives almost the same results as the LPA and Infomap when the mix parameter ranges from 0.1 to 0.3. Our algorithm also presents better quality than LPA. Although our algorithm is no better than the Infomap algorithm during the mix parameter covers from 0.4 to 0.7, it outperforms under the condition that the mix parameter is high. In particular the mix parameter arrives at 0.8; the NMI value of the Infomap algorithm is almost 0, while it is more than 0.3 for our algorithm, as depicted in Figure 3. It means that our algorithm is particularly suitable for the community detection of high parameter μ . In other words, our algorithm is more favorable with obscure community structure in networks. On the other hand, the result of the experiment shows that the NL nodes can help increase the accuracy of community partition.

In the proposed algorithm, the percentage of NL nodes and the percentage of TL nodes are important factors that influence the accuracy of community partition. To analyze the relationship between NL and TL, we, respectively, set the percentage of TL nodes to $\{5\%, 10\%, \dots, 50\%\}$ and the percentage of NL nodes to $\{0\%, 10\%, \dots, 50\%\}$ (see Figure 4). We generate benchmark networks with the following parameters: $N = 1000$, $\langle k \rangle = 15$, $\mu = 0.5$, $\tau_1 = 2$, $\tau_2 = 1$, $c_{\min} = 20$, and $c_{\max} = 50$.

As can be seen from Figure 4, the proposed algorithm performs better with the increase of TL nodes. It is consistent with intuition, since there is more exact label information available. Moreover, with the increase of NL nodes, the algorithm can achieve higher accuracies. This means that NL is actually helpful to community detection and the algorithm can use this information effectively. In particular, NL is more beneficial when TL nodes are rare, since the increase of accuracy brought by NL will become smaller with the increase of TL nodes.

4.2. Real-World Networks. In this subsection, we verify our algorithm from empirical networks, the karate club network and the dolphins social network, which have been applied as benchmarks to evaluate many community detection algorithms since the true community structures are known in the two networks. In general, the karate club network can be split into two disjointed groups due to the disagreement between the administrator and the instructor of the club, and the dolphins social network can be separated into two groups due to the temporary disappearance of a dolphin. However, the NL node is equivalent to TL node provided that the networks are divided into two communities. In the following experiments, we assume that Donetti's result [26] is the true partition of the karate club network and Pan's conclusion [27] is the true community of dolphin social network.

The karate club network is constructed by Zachary over a period of two years and is composed of 34 nodes corresponding to members of the club and 78 edges representing

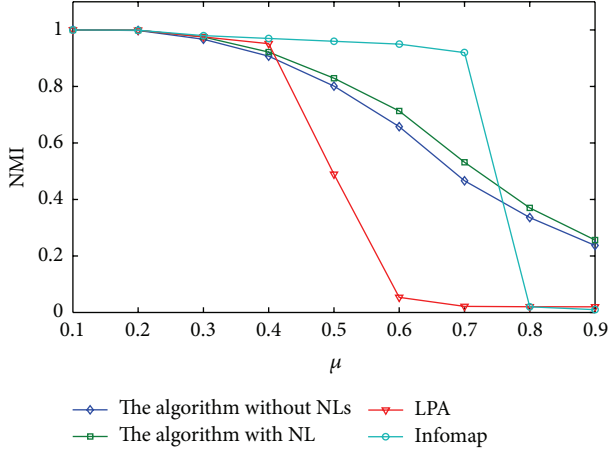


FIGURE 3: Results (NMI) of community detection algorithms in the LFR benchmark networks. The algorithms include LPA, Infomap, and the proposed algorithm with different parameters. Each point in the graph represents the average over 100 runs on randomly generated LFR benchmark networks with the given parameters.

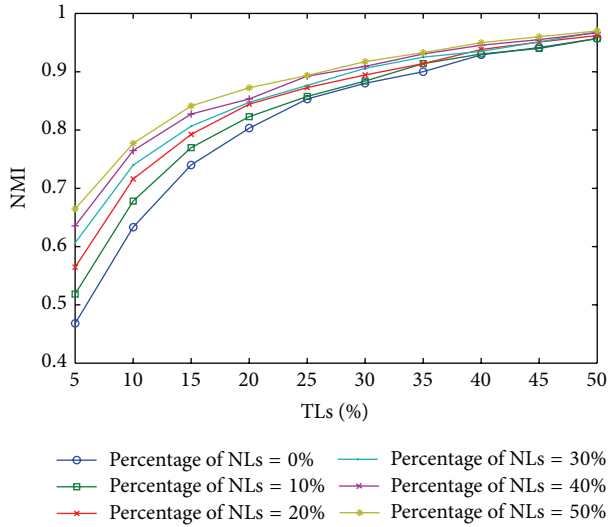


FIGURE 4: Results (NMI) of the proposed algorithm with different selections of NL and TL in the LFR benchmark networks. Each point in the graph represents the average over 100 runs on randomly generated LFR benchmark networks with the given parameters.

the connections of the individuals outside the activities of the club. In Donetti's result, the network is split into four communities. We select the nodes {25, 33, 17, 1} as TL nodes and the nodes {28, 4, 3, 11} as NL nodes for four different communities, respectively. Each NL node has one NL. The parameters a_u and a_l are set to 0.95 and 0.05, respectively. Applying the proposed algorithm, the results of community detection for karate club network are shown in Figure 5. It is clear that the result of our proposed method is in agreement with the partition of Donetti's method.

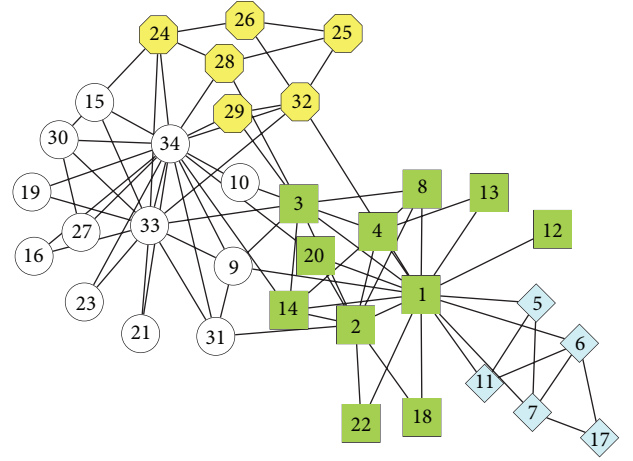


FIGURE 5: Detecting community structure in the karate club network via the proposed algorithm. Four communities are detected, which are denoted by the different shapes.

The dolphin social network, consisting of 62 nodes indicating bottlenose dolphins and 159 edges representing the associations between dolphin pairs occurring more often than expected by chance, is constructed by Lusseau over a period of seven years from 1994 to 2001. In Pan's conclusion, the network is divided into four communities. We select the nodes {SN63, Trigger, SN90, Oscar} as TL nodes and the nodes {TSN103, MN105, SN89, Bumper} as NL nodes for four different communities, respectively. Each NL node has one NL. The parameters a_u and a_l are 0.95 and 0.05, respectively. Applying the proposed algorithm, the results of community detection for dolphin social network are shown in Figure 6. It is obvious that the result of our proposed method is approximately consistent with the result of Pan's methods.

5. Conclusions

In this paper, a semisupervised community detection algorithm is proposed based on negative information, which indicates whether a node does not belong to a specific community. It has near-linear complexity in time and can incorporate the NL and TL into community detection. As seen from our experimental results on both real and artificial networks, incorporating NL into community detection procedure can significantly improve performance, especially in the situation where the traditional labels are rare. Moreover, the more TLs and NLs applied in our algorithm, the better the community partition result.

Unfortunately, it is an implicit restriction that the number of communities must be known in advance, since the selection of the TL nodes should cover all the communities. Our future work will concentrate on the issue of detecting communities without preknowing the community number. In other words, we will devote part of our energy on the research

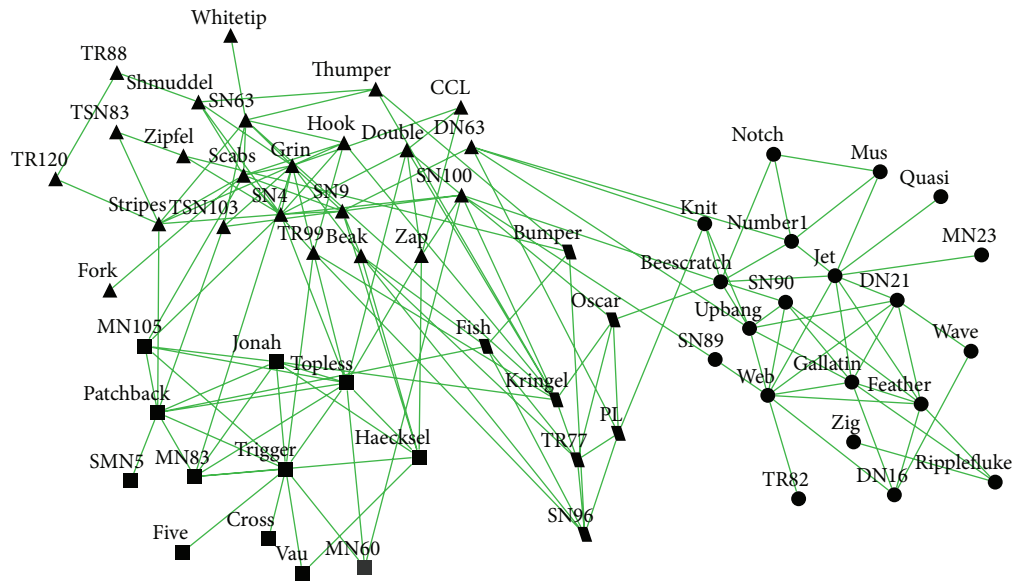


FIGURE 6: Detecting community structure in the dolphin social network via the proposed algorithm. Four communities are detected, which are denoted by the different shapes.

of an improved semisupervised community detection algorithm which is capable of identifying communities accurately without labeled nodes of any community in the future.

Conflict of Interests

The authors declare that there is no conflict of interests regarding the publication of this paper.

Acknowledgments

This work was supported by the National High-Tech Research and Development Program (863 Program) (no. 2014A A015103), the Joint Funds of the National Natural Science Foundation of China (no. U1404604), the Natural Science Plan Project of the Education Department of Henan Province (nos. 2010B520014 and 2010A520024), and the Soft Science Research Program of Science and Technology Department of Henan Province (no. 112400450405).

References

- [1] M. Girvan and M. E. Newman, "Community structure in social and biological networks," *Proceedings of the National Academy of Sciences of the United States of America*, vol. 99, no. 12, pp. 7821–7826, 2002.
- [2] M. E. J. Newman, "Modularity and community structure in networks," *Proceedings of the National Academy of Sciences of the United States of America*, vol. 103, no. 23, pp. 8577–8582, 2006.
- [3] M. E. J. Newman, "Fast algorithm for detecting community structure in networks," *Physical Review E*, vol. 69, no. 6, Article ID 066133, 2004.
- [4] M. E. J. Newman and M. Girvan, "Finding and evaluating community structure in networks," *Physical Review E: Statistical, Nonlinear, and Soft Matter Physics*, vol. 69, no. 2, Article ID 026113, 2004.
- [5] J. Duch and A. Arenas, "Community detection in complex networks using extremal optimization," *Physical Review E*, vol. 72, no. 2, Article ID 027104, 2005.
- [6] V. D. Blondel, J.-L. Guillaume, R. Lambiotte, and E. Lefebvre, "Fast unfolding of communities in large networks," *Journal of Statistical Mechanics: Theory and Experiment*, vol. 2008, no. 10, Article ID P10008, 2008.
- [7] S.-W. Son, H. Jeong, and J. D. Noh, "Random field Ising model and community structure in complex networks," *European Physical Journal B*, vol. 50, no. 3, pp. 431–437, 2006.
- [8] B. Karrer and M. E. J. Newman, "Stochastic blockmodels and community structure in networks," *Physical Review E*, vol. 83, no. 1, Article ID 016107, 2011.
- [9] S. Fortunato, "Community detection in graphs," *Physics Reports: A Review Section of Physics Letters*, vol. 486, no. 3–5, pp. 75–174, 2010.
- [10] M. E. J. Newman, "Communities, modules and large-scale structure in networks," *Nature Physics*, vol. 8, no. 1, pp. 25–31, 2012.
- [11] J. Weston, C. Leslie, E. Ie, D. Y. Zhou, A. Elisseeff, and W. S. Noble, "Semi-supervised protein classification using cluster kernels," *Bioinformatics*, vol. 21, no. 15, pp. 3241–3247, 2005.
- [12] X. Ma, L. Gao, X. Yong, and L. Fu, "Semi-supervised clustering algorithm for community structure detection in complex networks," *Physica A: Statistical Mechanics and Its Applications*, vol. 389, no. 1, pp. 187–197, 2010.
- [13] E. Eaton and R. Mansbach, "A spin-glass model for semi-supervised community detection," in *Proceedings of the 26th AAAI Conference on Artificial Intelligence and the 24th Innovative Applications of Artificial Intelligence Conference (AAAI '12)*, pp. 900–906, July 2012.
- [14] Z.-Y. Zhang, "Community structure detection in complex networks with partial background information," *Europhysics Letters*, vol. 101, no. 4, Article ID 48005, 2013.

- [15] Z. Y. Zhang, K.-D. Sun, and S. Q. Wang, "Enhanced community structure detection in complex networks with partial background information," *Scientific Reports*, vol. 3, article 3241, 2013.
- [16] D. Liu, X. Liu, W. Wang, and H. Bai, "Semi-supervised community detection based on discrete potential theory," *Physica A: Statistical Mechanics and its Applications*, vol. 416, pp. 173–182, 2014.
- [17] D. Liu, H.-Y. Bai, H.-J. Li, and W.-J. Wang, "Semi-supervised community detection using label propagation," *International Journal of Modern Physics B*, vol. 28, Article ID 1450208, 2014.
- [18] C. Hou, F. Nie, F. Wang, C. Zhang, and Y. Wu, "Semisupervised learning using negative labels," *IEEE Transactions on Neural Networks*, vol. 22, no. 3, pp. 420–432, 2011.
- [19] A. Lancichinetti, S. Fortunato, and F. Radicchi, "Benchmark graphs for testing community detection algorithms," *Physical Review E*, vol. 78, no. 4, Article ID 046110, 2008.
- [20] G. H. Golub and C. F. van Loan, *Matrix Computations*, vol. 3, JHU Press, 2012.
- [21] W. Zachary, "An information flow model for conflict and fission in small groups1," *Journal of Anthropological Research*, vol. 33, no. 4, pp. 452–473, 1977.
- [22] D. Lusseau, K. Schneider, O. J. Boisseau, P. Haase, E. Slooten, and S. M. Dawson, "The bottlenose dolphin community of doubtful sound features a large proportion of long-lasting associations: can geographic isolation explain this unique trait?" *Behavioral Ecology and Sociobiology*, vol. 54, no. 4, pp. 396–405, 2003.
- [23] U. N. Raghavan, R. Albert, and S. Kumara, "Near linear time algorithm to detect community structures in large-scale networks," *Physical Review E—Statistical, Nonlinear, and Soft Matter Physics*, vol. 76, no. 3, Article ID 036106, 2007.
- [24] M. Rosvall and C. T. Bergstrom, "Maps of random walks on complex networks reveal community structure," *Proceedings of the National Academy of Sciences of the United States of America*, vol. 105, no. 4, pp. 1118–1123, 2008.
- [25] L. Danon, A. Diaz-Guilera, J. Duch, and A. Arenas, "Comparing community structure identification," *Journal of Statistical Mechanics: Theory and Experiment*, no. 9, Article ID P09008, pp. 219–228, 2005.
- [26] L. Donetti and M. A. Muñoz, "Detecting network communities: a new systematic and efficient algorithm," *Journal of Statistical Mechanics: Theory and Experiment*, vol. 2004, Article ID P10012, 2004.
- [27] Y. Pan, D.-H. Li, J.-G. Liu, and J.-Z. Liang, "Detecting community structure in complex networks via node similarity," *Physica A: Statistical Mechanics and Its Applications*, vol. 389, no. 14, pp. 2849–2857, 2010.

Research Article

Wiretap Channel with Rate-Limited Channel State Information

Xinxing Yin, Liang Pang, and Zhi Xue

Department of Electrical Engineering, Shanghai Jiao Tong University, Shanghai 200240, China

Correspondence should be addressed to Xinxing Yin; yinxinxing@sjtu.edu.cn

Received 21 March 2014; Revised 12 July 2014; Accepted 21 July 2014

Academic Editor: Qinggang Meng

Copyright © 2015 Xinxing Yin et al. This is an open access article distributed under the Creative Commons Attribution License, which permits unrestricted use, distribution, and reproduction in any medium, provided the original work is properly cited.

We revisit a channel coding problem where the channel state information (CSI) is rate-limited (or coded) and available to the channel encoder. A wiretapper is added into this model, and the confidential message is intended only for the legal receiver and should be kept from being eavesdropped by the wiretapper. Equivocation analysis is provided to evaluate the level of information leakage to the wiretapper. We characterize an achievable rate-equivocation region as well as an outer bound for this security model. To achieve the rate-equivocation triples, we propose an efficient coding scheme, in which the coded CSI serves as the CSI for the channel encoder, based on *Gel'fand and Pinsker's coding* and *Wyner's random coding*. Furthermore, an example of Gaussian wiretap channel with rate-limited CSI is presented, of which a lower bound on the secrecy capacity is obtained. By simulation, we find there exists an optimal rate of the coded CSI at which the biggest secrecy transmission rate of the Gaussian case is achieved.

1. Introduction

The problem of coding for channels with CSI has been studied actively. In these models, CSI is generated by nature and provided to the transmitter and/or to the receiver in a causal or noncausal manner. Shannon first studied the discrete memoryless channel (DMC) with causal CSI only at the encoder and got its capacity [1]. It was found that the capacity was the same as the capacity of the DMC without CSI. The problem where CSI was only noncausally known to the channel encoder was solved by Gel'fand and Pinsker [2]. They showed a different capacity expression from [1] and provided a different coding strategy which was now known as *Gel'fand and Pinsker's coding*. The key idea of *Gel'fand and Pinsker's coding* is that the codeword chosen for the transmitted message is jointly typical with the state sequence. Actually, the capacity for the causal case in [1] can be got from [2] by letting the auxiliary random variable be independent of CSI. Some other extended channel models with CSI at both the encoder and the decoder were studied in [3–7]. Among them, Heegard and El Gamal first investigated a more practical channel with the unique feature that CSI at encoder and decoder was subject to a rate constraint [3]. The motivation of this unique feature, that is, rate-limited CSI, was that

CSI was transmitted over way-side channels for which only limited resources (bandwidth, operation time, memory, etc.) of the system were allocated. They only gave inner bounds on the capacity region for this model. Rosenzweig et al. then revisited this model and gave the capacity region of the model with rate-limited CSI at encoder and full CSI at the decoder [4]. For the model where CSI was fully known at the encoder and rate-limited at the decoder, capacity region was obtained in [5].

It is known that secure information transmission is an essential communication requirement. The above state-dependent channel models [1–7] considered no secrecy constraint. Recently, the works [8–15] have introduced the wiretapper in channels with CSI to model a safe communication model. Chen and Vinck explored the discrete memoryless wiretap channel with noncausal CSI and presented an achievable rate-equivocation region [8]. The region was established using a combination of *Gel'fand and Pinsker's coding* and *Wyner's random coding*. They showed that CSI helped to get a larger secrecy capacity for the Gaussian wiretap channel. In [9], an achievable rate-equivocation region for the Gaussian wiretap with side information was given. The authors proposed a perfect-secrecy-achieving coding strategy for the model based on code-partition technique.

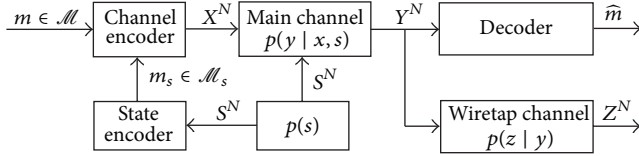


FIGURE 1: Wiretap channel with rate-limited channel state information at the encoder.

The code-partition technique divided a random code into bins so that high rates could be achieved with asymptotic perfect secrecy. Dai and Luo improved the results of [8] by providing upper bounds on the secrecy capacity [10]. Liu and Chen got a lower bound on the secrecy capacity of the model where CSI was available noncausally at both the encoder and the decoder [11], and an upper bound was established by [12]. Action-dependent channel models involving secrecy were studied in [13–15]. Dai et al. provided the inner and outer bounds on the capacity-equivocation region for the wiretap channel with action-dependent states [13]. Then, they extended the model by adding a noiseless feedback link between the transmitter and receiver [14], in which the feedback served as a secret key. We restricted the rate of the feedback by introducing a rate-limited feedback link and obtained the corresponding capacity-equivocation region. Then, we explored information embedding on the actions in wiretap channel where part of the message was embedded on the actions [15] and characterized the tradeoff between the sum secrecy rate and the information embedding rate.

We are motivated to revisit a state-dependent channel model by adding a wiretapper (shown in Figure 1), that is, discrete memoryless wiretap channel with rate-limited channel state information. The CSI is known to the encoder and not known to the decoder. In our setup, the CSI at the encoder is subject to a rate constraint R_s , as in the work [3]. Note that the CSI in previous works considered that secrecy constraint [8, 10] was rate-unlimited, which is different from our rate-limited setup. However, we will later see that the model in [8, 10] is actually a special case of our model. In addition, the confidential message is intended only for the receiver and should be kept secret from the wiretapper as much as possible.

To the best of our knowledge, the model in Figure 1 involving secure information transmission has not been explored. Our goal is to characterize the inner and outer bounds on the capacity-equivocation region of the model. Particularly, we are interested in getting the corresponding bounds on the secrecy capacity for which perfect secrecy is realized. The perfect secrecy means that no information is leaked to the wiretapper. We also provide efficient coding schemes to achieve the rate-equivocation triple by means of *Gel'fand and Pinsker's coding* and *Wyner's random coding*. Moreover, an example of Gaussian wiretap channel with rate-limited CSI is given and its lower bound on the secrecy capacity is also calculated. The simulation results show that there exists an optimal rate of the coded CSI at which the

biggest secrecy transmission rate of the Gaussian example is achieved.

The remainder of the paper is organized as follows. Section 2 describes the wiretap channel with rate-limited CSI and outlines the inner and outer bounds on the capacity-equivocation region. Section 3 calculates the corresponding bounds on the secrecy capacity and presents an example. Section 4 proposes a coding scheme to achieve the rate-equivocation triples and gives the outer bound proof. We conclude in Section 5 with a summary of the whole work and some future directions.

2. Channel Model and Main Results

In this section, the model of wiretap channel with rate-limited CSI is described. Then, we present the inner and outer bounds on the capacity-equivocation region.

2.1. Channel Model. In this paper, calligraphic letters, for example, \mathcal{X} , are used to denote the finite sets. We use $\|\mathcal{X}\|$ to denote the cardinality of the set \mathcal{X} . We use Z_i^j to denote the $(j - i + 1)$ vectors $(Z_i, Z_{i+1}, \dots, Z_j)$ of random variables for $1 \leq i \leq j$ and will always drop the subscript when $i = 1$. Besides, for $X \sim p(x)$ and $0 \leq \epsilon \leq 1$, the set of the typical N -sequences x^N is defined as $\mathcal{T}_X^N(\epsilon) = \{x^N : |\pi(x | x^N) - p(x)| \leq \epsilon p(x) \text{ for all } x \in \mathcal{X}\}$, where $\pi(x | x^N)$ denotes the frequency of occurrences of letter x in the sequence x^N . The set of the jointly typical sequences, for example, $\mathcal{T}_{XY}^N(\epsilon)$, follows similarly. The base of the log function in this paper is 2.

The channel model is described as follows. We consider the rate-limited CSI setup where a rate-limited description of the channel states is provided to the channel encoder. This setup is motivated by the limited capacity of the channel over which the channel states are transmitted. The input of the state encoder is the channel state S^N which is independently and identically distributed (i.i.d.) $\sim p(s)$, and the output is $M_s \in \{1, 2, \dots, 2^{NR_s}\}$. The channel encoder encodes the messages M and M_s into X^N . The main channel is a DMC with discrete input alphabet $\mathcal{X} \times \mathcal{S}$ and output alphabet \mathcal{Y} . The channel is memoryless in the sense that $p(y^N | x^N, s^N) = \prod_{i=1}^N p(y_i | x_i, s_i)$, where $y^N \in \mathcal{Y}^N$, $x^N \in \mathcal{X}^N$, and $s^N \in \mathcal{S}^N$. The receiver decodes the message with the observation Y^N . The output of the decoder is \hat{M} . The probability of error for the decoder is defined as $P_e = \Pr\{\hat{M} \neq M\}$. The wiretap channel is also a DMC with input Y^N and output Z^N . The wiretap channel is memoryless in the sense that $p(z^N | y^N) = \prod_{i=1}^N p(z_i | y_i)$, where $z^N \in \mathcal{Z}^N$. The uncertainty of the message for the wiretapper is measured by $\lim_{N \rightarrow \infty} \Delta = \lim_{N \rightarrow \infty} (H(M | Z^N)/N)$.

A $(2^{NR}, 2^{NR_s}, N)$ code for the model in Figure 1 includes a state encoder, channel encoder, and decoder. The state encoder $g_1 : \mathcal{S}^N \rightarrow \mathcal{M}_s$ maps the state sequence s^N into m_s , where $m_s \in \mathcal{M}_s = \{1, 2, \dots, 2^{NR_s}\}$. The stochastic channel encoder g_2 is specified by a matrix of conditional probability

distributions $g_2(x^N | m, m_s)$, where $m \in \mathcal{M} = \{1, 2, \dots, 2^{NR}\}$. Note that $\sum_{x^N} g_2(x^N | m, m_s) = 1$ and $g_2(x^N | m, m_s)$ is the probability that the messages m and m_s are encoded as the channel input x^N . The decoder $g_3 : \mathcal{Y}^N \rightarrow \mathcal{M}$ maps the output sequence y^N into decoded message \widehat{m} . Before stating the main results, we give the definitions of “achievable” and “secrecy capacity” as follows.

Definition 1. A rate-equivocation triple (R, R_s, R_e) is said to be *achievable* for the model in Figure 1 if there exists a $(2^{NR}, 2^{NR_s}, N)$ code such that

$$\lim_{N \rightarrow \infty} \frac{\log \|\mathcal{M}\|}{N} = R, \quad (1)$$

$$\lim_{N \rightarrow \infty} \frac{\log \|\mathcal{M}_s\|}{N} = R_s,$$

$$\lim_{N \rightarrow \infty} \frac{H(M | Z^N)}{N} \geq R_e, \quad (2)$$

$$P_e \leq \epsilon, \quad (3)$$

where ϵ is an arbitrary small positive real number, R is the rate of the message M , R_s is the rate of the coded message M_s , and R_e is the rate of equivocation. The capacity-equivocation region is defined as the convex closure of all achievable rate-equivocation triples (R, R_s, R_e) .

Definition 2. The *secrecy capacity* is the maximum rate at which the confidential message can be sent to the receiver in perfect secrecy with the constraint on R_s . The secrecy capacity is

$$C_s = \max_{(R, R_s, R_e=R) \in \mathcal{R}, R_s \geq \Gamma} R, \quad (4)$$

where \mathcal{R} is the capacity-equivocation region and Γ is the constraint condition of rate R_s .

2.2. Main Results. We first give an achievable rate-equivocation region for the wiretap channel with rate-limited CSI and then present an outer bound. Some comments on the theorems are given subsequently. Further discussion about the results and comparison with other existing models are shown in Section 3.

Theorem 3. An inner bound on the capacity-equivocation region of the wiretap channel with rate-limited CSI is the set

$$\begin{aligned} \mathcal{R}_i = \{ & (R, R_s, R_e) : \\ & R \leq I(V; Y) - I(V; U), \\ & R_s \geq I(U; S), \\ & R_e \leq R, \\ & R_e \leq I(V; Y) - \max\{I(V; Z), I(V; U)\} \}, \end{aligned} \quad (5)$$

where $V \rightarrow (X, U) \rightarrow Y \rightarrow Z$ form a Markov chain.

Theorem 4. An outer bound on the capacity-equivocation region of the wiretap channel with rate-limited CSI is the set

$$\begin{aligned} \mathcal{R}_o = \{ & (R, R_s, R_e) : \\ & R \leq I(V; Y) - I(V; S | U), \\ & R_s \geq I(U; S), \\ & R_e \leq R, \\ & R_e \leq I(V; Y) - I(V; S | K_2) - I(K_2; Z | K_1) \}, \end{aligned} \quad (6)$$

where $U \rightarrow V \rightarrow S, U \rightarrow K_2 \rightarrow K_1$, and $(V, K_1, K_2) \rightarrow (X, U) \rightarrow Y \rightarrow Z$ form Markov chains.

We have the following comments:

- (1) The sets \mathcal{R}_i and \mathcal{R}_o are convex; the proof is similar to the proof of Proposition 1 in [5].
- (2) Theorem 3 tells that any rate-equivocation triple belonging to \mathcal{R}_i is achievable. Theorem 4 tells that all achievable rate-equivocation triples are contained in \mathcal{R}_o . The capacity-equivocation region of the model in Figure 1 is between \mathcal{R}_i and \mathcal{R}_o .
- (3) Equivocation was introduced by Wyner [16] to measure the amount of information leaked to the wiretapper. It is always wished that as large as possible equivocation for the wiretapper can be achieved at any acceptable rate of reliable transmission to the legitimate receiver. From the formulas of \mathcal{R}_i , it is obvious that if $(R, R_s, R_e = I(V; Y) - \max\{I(V; Z), I(V; U)\})$ is achievable, the rate-equivocation triples (R, R_s, R'_e) are also achievable for every $R'_e \leq I(V; Y) - \max\{I(V; Z), I(V; U)\}$. This reminds us that it is sufficient to show that $(R, R_s, R_e = I(V; Y) - \max\{I(V; Z), I(V; U)\})$ is achievable.
- (4) We are considerably interested in finding the maximum secrecy rate when $R_e = R$ which implies perfect secrecy. It is explained as follows. Since $\lim_{N \rightarrow \infty} (H(M | Z^N)/N) \geq R_e$ and $\lim_{N \rightarrow \infty} (H(M)/N) = R$, we can get $\lim_{N \rightarrow \infty} (H(M | Z^N)/N) \geq \lim_{N \rightarrow \infty} (H(M)/N)$ when $R_e = R$. Since conditioning does not increase entropy, we have $\lim_{N \rightarrow \infty} (H(M | Z^N)/N) = \lim_{N \rightarrow \infty} (H(M)/N)$, which indicates that no information was leaked to the wiretapper.
- (5) The proof of the two theorems is given in Section 4, in which we construct a coding scheme to achieve the rate-equivocation triple in \mathcal{R}_i based on *Gelfand and Pinsker's coding* and *Wyner's random coding*. We also give the identification of the auxiliary random variables in the outer bound proof.

Further discussion about the theorems and the comparison with other existing results are given in Section 3.

3. Discussion and Gaussian Example

In this section, we first calculate the lower and upper bounds on the secrecy capacity of the model in Figure 1. Subsequently, we compare our results with other existing state-dependent channel models. Then, we provide a (physically) degraded example of Gaussian wiretap channel with rate-limited CSI and calculate a lower bound on the secrecy capacity subject to a rate constraint on R_s . By simulation, we find that there exists an optimal rate of the coded CSI at which the biggest secrecy transmission rate of the Gaussian example is achieved.

3.1. Discussion and Comparison. The lower and upper bounds on the secrecy capacity are presented in Corollary 5.

Corollary 5. *The lower and upper bounds on the secrecy capacity of wiretap channel with rate-limited CSI are*

$$C_l = \max_{p(u,v,x,s), R_s \geq I(U;S)} \{I(V; Y) - \max\{I(V; Z), I(V; U)\}\}, \quad (7)$$

$$C_u = \max_{p(u,v,k_1,k_2,x,s), R_s \geq I(U;S)} \min\{I(V; Y) - I(V; S | U), \\ I(V; Y) - I(V; S | K_2) - I(K_2; Z | K_1)\}, \quad (8)$$

respectively.

Proof. We first prove (8). According to the definition of formula (4), we let $R_e = R$ in \mathcal{R}_o and then get the upper bounds on R subject to $R_s \geq I(U; S)$ as follows. Consider

$$R \leq I(V; Y) - I(V; S | U), \quad (9)$$

$$R \leq I(V; Y) - I(V; S | K_2) - I(K_2; Z | K_1).$$

Based on the definition of secrecy capacity, (9), we prove (8). Similarly, substituting $R_e = R$ into \mathcal{R}_i , we get the upper bounds on R subject to $R_s \geq I(U; S)$ as

$$R \leq I(V; Y) - I(V; U), \quad (10)$$

$$R \leq I(V; Y) - \max\{I(V; Z), I(V; U)\}. \quad (11)$$

Formula (10) can be obtained from (11). Hence, according to the definition of secrecy capacity and (11), formula (7) is proved. \square

The comparison of the secrecy capacity between [10] and our results is given as follows. We first present Dai's main results in [10].

Dai and Luo [10] characterized the lower and upper bounds on the secrecy capacity of wiretap channel with full and noncausal CSI at the encoder, depicted in Figure 2, as

$$C_{l\text{dai}} = \max_{p(v,x,s)} \{I(V; Y) - \max\{I(V; Z), I(V; S)\}\}, \quad (12)$$

$$C_{u\text{dai}} = \max_{p(v,k_1,k_2,x,s)} \min\{I(V; Y) - I(V; S), \\ I(V; Y) - I(K_2; Z | K_1)\}, \quad (13)$$

respectively.

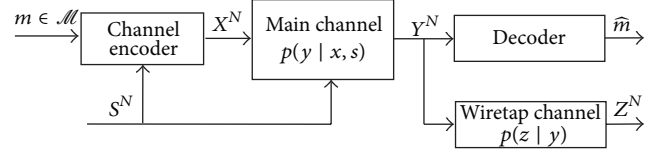


FIGURE 2: Wiretap channel with full CSI at the encoder.

The comparison is listed below.

- (1) The lower bounds (7) and (12) share the same expression. We note that, in the rate-limited CSI setup, CSI is not directly known to the channel encoder. The CSI is encoded by the state encoder, and it is the coded version that serves as the channel states to the channel encoder. In the coding scheme (presented in Section 4), the coded CSI U serves as the CSI S in the jointly typical encoding. Based on this observation, it is easy to see that (7) and (12) share the same expression (without considering the constraint on rate of the coded CSI).
- (2) For deriving the upper bounds (8) and (13), the auxiliary random variables are different. In [10], there are three auxiliary random variables K_2 , K_1 , and V , while there are four auxiliary random variables K_2 , K_1 , U , and V in our derivations. The detailed expression of these random variables is given in Section 4.
- (3) Besides, in Theorem 4, we have the Markov chain $U \rightarrow V \rightarrow S$. Then,

$$\begin{aligned} I(V; S | U) &= I(V, U; S) - I(U; S) \\ &= I(V; S) + I(U; S | V) - I(U; S) \\ &= I(V; S) - I(U; S), \end{aligned} \quad (14)$$

where (14) is from the Markov chain $U \rightarrow V \rightarrow S$. If we let U be independent of S , the conditional mutual information $I(V; S | U) = I(V; S)$. In this case, it is easy to see $C_u \leq C_{u\text{dai}}$.

3.2. Gaussian Example. In this subsection, we look at the (physically) degraded Gaussian wiretap channel with rate-limited CSI shown in Figure 3. We treat $\eta_1 \sim \mathcal{N}(0, N_1)$ and $\eta_2 \sim \mathcal{N}(0, N_2)$ in Figure 3 as noise. Let $S \sim \mathcal{N}(0, Q)$ and $U = S$. Similarly to [8, 9], consider $V = X + \alpha U$, where X and U are independent from each other and X is distributed as $X \sim \mathcal{N}(0, P)$. The parameter α is to be determined. We assume that the correlation coefficient of X and S is ρ_{XS} . Then, using similar derivations in [8, 9], we have

$$\begin{aligned} I(V; Y) &= \log(f(N_1)), \\ I(V; Z) &= \log(f(N_1 + N_2)), \\ I(V; U) &= I(V; S) = \Lambda_1, \\ I(U; S) &= H(S) = \Lambda_2, \end{aligned} \quad (15)$$

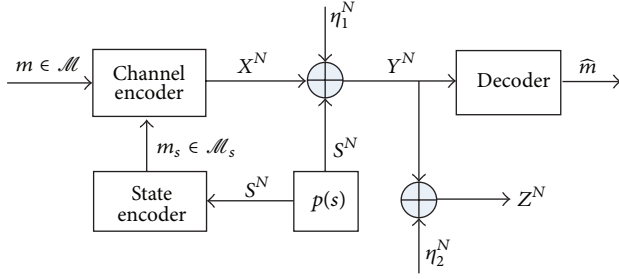


FIGURE 3: Gaussian wiretap channel with rate-limited channel state information at the encoder.

where

$$f(N) = \left[(P + \alpha^2 Q + 2\alpha(PQ)^{1/2} \rho_{XS}) \times (P + Q + N + 2(PQ)^{1/2} \rho_{XS}) \times ((1 - \alpha)^2 PQ (1 - \rho_{XS}^2)) + N (P + \alpha^2 Q + 2\alpha(PQ)^{1/2} \rho_{XS})^{-1} \right]^{1/2}, \quad (16)$$

$$\Lambda_1 = \log \left[\frac{P + \alpha^2 Q + 2\alpha(PQ)^{1/2} \rho_{XS}}{P(1 - \rho_{XS}^2)} \right]^{1/2},$$

$$\Lambda_2 = \log(2\pi e Q)^{1/2}.$$

Note that the expressions of $I(V; Y)$, $I(V; Z)$, $I(V; U)$ are the same as those in [8, 9], and the difference is that here we have the rate constraint on R_s ; that is, $R_s \geq \Lambda_2$.

Applying Corollary 5, we get the lower bound on the secrecy capacity of the Gaussian case as

$$C_{IG}(\alpha) = \min \{ \log f(N_1) - \log f(N_1 + N_2), \log f(N_1) - \Lambda_1 \}, \quad (17)$$

which is subject to the constraint $R_s \geq \Lambda_2$. The graph of $C_{IG}(\alpha)$ as a function of α for fixed P, Q, N_1, N_2 , and ρ_{XS} is presented in Figure 4. It can be seen that, for the six cases in Figure 4, the lower bound on the secrecy capacity achieves the maximum value at different values of α . By setting a proper value to the parameter α , we can achieve the maximum value of $C_{IG}(\alpha)$. Besides, we see that when the noise power of the wiretap channel decreases (or the noise power of the main channel increases), $C_{IG}(\alpha)$ is reduced. This is straightforward.

Moreover, if we let $R_s = I(U; S)$, the lower bound C_{IG} can be expressed as a function of R_s when P, N_1, N_2, ρ_{XS} , and α are fixed. When P, N_1, N_2, ρ_{XS} , and α are fixed at certain values, the graph of $C_{IG}(R_s)$ as a function of R_s is depicted in Figure 5. Five different cases are considered:

- (1) $P = N_1 = N_2 = 1, \rho_{XS} = 0, \alpha = 1$. The noise power of the main channel and wiretap is big, and variable X is independent of S ; that is, $\rho_{XS} = 0$;
- (2) $P = N_1 = N_2 = 1, \rho_{XS} = 0.5, \alpha = 0.35$. The noise power of the main channel and wiretap is big, and variable X is not independent of S ;

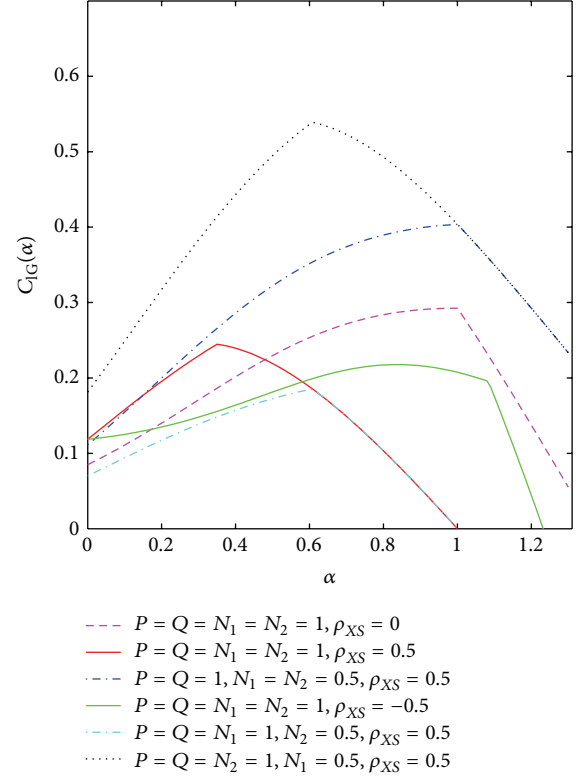


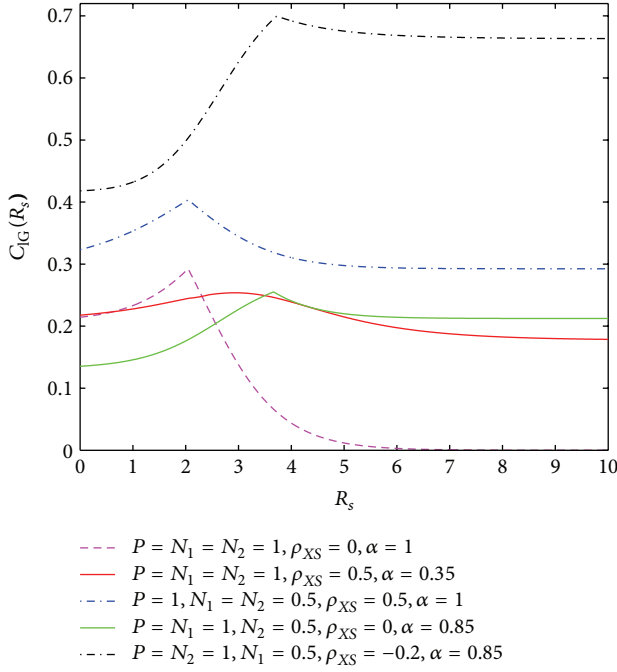
FIGURE 4: $C_{IG}(\alpha)$ as a function of α .

- (3) $P = 1, N_1 = N_2 = 0.5, \rho_{XS} = 0.5, \alpha = 1$. The noise power of the main channel and wiretap is small, and variable X is not independent of S ;
- (4) $P = N_1 = 1, N_2 = 0.5, \rho_{XS} = 0.5, \alpha = 0.85$. Wiretap channel is less noisy than main channel, and variable X is not independent of S ;
- (5) $P = N_2 = 1, N_1 = 0.5, \rho_{XS} = 0.5, \alpha = 0.85$. Main channel is less noisy than wiretap channel, and variable X is not independent of S .

It can be seen that, in general, when R_s is small, $C_{IG}(R_s)$ increases with R_s . However, there exists an optimal value of R_s at which $C_{IG}(R_s)$ is the biggest. When R_s is bigger than the optimal value, $C_{IG}(R_s)$ decreases. On the one hand, we see that, for case 1 where variable X is independent of S , secrecy rate $C_{IG}(R_s)$ decreases sharply with the CSI rate R_s (when R_s passes the optimal value). On the other hand, when variable X is not independent of S (case 2–5), $C_{IG}(R_s)$ decreases slowly with R_s .

Besides, comparing cases 2 and 3, we find that the smaller the noise power is, the higher the secrecy rate $C_{IG}(R_s)$ is. This means if information transmission happens in good channels, we can achieve higher secrecy transmission rate.

Furthermore, comparing cases 4 and 5, it can be seen that when the main channel is less noisy than the wiretap channel, higher secrecy rate $C_{IG}(R_s)$ is achieved. This result is straightforward since the main channel is better than the wiretap channel.

FIGURE 5: $C_{IG}(R_s)$ as a function of R_s .

4. Proof of Theorems 3 and 4

In this section, two theorems in Section 2 are proved. To show Theorem 3, we construct a coding scheme to achieve the rate-equivocation triple in \mathcal{R}_i based on *Gelfand and Pinsker's coding* and *Wyner's random coding* and give the equivocation analysis in Section 4.1. Then, we prove Theorem 4 and give the identification of the auxiliary random variables in Section 4.2.

4.1. Proof of Theorem 3. We show that all triples $(R, R_s, R_e) \in \mathcal{R}_i$ are achievable. Concretely, we need to prove that any rate-equivocation triple $(R, R_s, R_e) \in \mathcal{R}_i$ and decoding error probability P_e satisfy

$$\begin{aligned}
 R &= \lim_{N \rightarrow \infty} \frac{\log \|\mathcal{M}\|}{N}, \\
 R_s &= \lim_{N \rightarrow \infty} \frac{\log \|\mathcal{M}_s\|}{N}, \\
 R_e &\leq \lim_{N \rightarrow \infty} \frac{H(M | Z^N)}{N}, \\
 P_e &\leq \epsilon.
 \end{aligned} \tag{18}$$

It is obvious that if $(R, R_s, R_e = I(V; Y) - \max(I(V; Z), I(V; U)))$ is achievable, the rate-equivocation triples (R, R_s, R'_e) are also achievable for every $R'_e \leq I(V; Y) - \max(I(V; Z), I(V; U))$. Therefore, we try to prove $(R, R_s, R_e = I(V; Y) - \max(I(V; Z), I(V; U)))$ is achievable.

Let $R = I(V; Y) - I(V; U) - \lambda$, where λ is a fixed positive number. Since $R_e \leq R$, we can get $\lambda \leq \max(I(V; Z), I(V; U)) - I(V; U)$. For each $m_s \in \{1, 2, \dots, 2^{NR_s}\}$, an i.i.d sequence

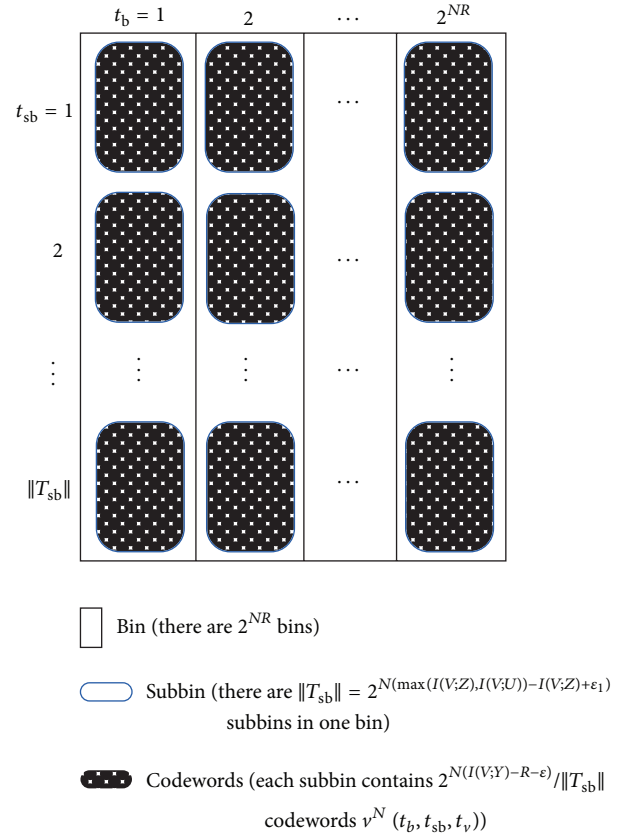


FIGURE 6: Codebook structure.

$u^N(m_s)$ is generated according to $p(u^N) = \prod_{i=1}^N p(u_i)$. We find a $u^N(m_s)$ such that $(u^N(m_s), s^N) \in \mathcal{T}_{US}^N$. Let the message M be uniformly distributed over \mathcal{M} . Then, we generate $2^{N(I(V; Y) - \epsilon)}$ i.i.d codewords v^N according to $p(v^N) = \prod_{i=1}^N p(v_i)$. These codewords are put into 2^{NR} bins such that each bin contains $2^{N(I(V; Y) - R - \epsilon)}$ codewords. The index of the bin is denoted by $t_b \in \{1, 2, \dots, 2^{NR}\}$. The codewords in each bin are put into $\|T_{sb}\| = 2^{N(\max(I(V; Z), I(V; U)) - I(V; Z) + \epsilon_1)}$ subbins which are indexed by $t_{sb} \in \{1, 2, \dots, 2^{N(\max(I(V; Z), I(V; U)) - I(V; Z) + \epsilon_1)}\}$. The number of the codewords in each subbin is $2^{N(I(V; Y) - R - \epsilon)} / \|T_{sb}\|$. We use t_v to index the codeword in the subbin. The codebook structure is presented in Figure 6.

To send m , the transmitter tries to find a $v^N(t_b, t_{sb}, t_v)$ such that $(v^N(t_b, t_{sb}, t_v), u^N(m_s)) \in \mathcal{T}_{VU}^N$ in the bin indexed by $t_b = m$. Then, the input sequence of the main channel is generated by $p(x^N | v^N, s^N) = \prod_{i=1}^N p(x_i | v_i, s_i)$.

To decode the message, the decoder finds a unique codeword $v^N(\hat{t}_b, \hat{t}_{sb}, \hat{t}_v)$ such that $(v^N(\hat{t}_b, \hat{t}_{sb}, \hat{t}_v), y^N) \in \mathcal{T}_{VY}^N$ and outputs $\hat{m} = \hat{t}_b$. Since the number of the codewords v^N is $2^{N(I(V; Y) - \epsilon)}$, this decoding step succeeds with high probability. Moreover, the number of $u^N(m_s)$ is $2^{NR_s} \geq 2^{NI(U; S)}$, so we can find a $u^N(m_s)$ such that $(u^N(m_s), s^N) \in \mathcal{T}_{US}^N$ with high probability. Similarly, since each bin contains $2^{N(I(V; Y) - R - \epsilon)} = 2^{N(I(V; U) + \lambda - \epsilon)}$ codewords v^N , the error probability of finding

a $v^N(t_b, t_{sb}, t_v)$ such that $(v^N(t_b, t_{sb}, t_v), u^N(m_s)) \in \mathcal{T}_{VU}^N$ in a given bin indexed by t_b approaches zero.

We focus on analyzing the uncertainty of M given the wiretapper's observation Z^N . Consider

$$\begin{aligned}
H(M | Z^N) &= H(M, Z^N) - H(Z^N) \\
&= H(M, Z^N, V^N) - H(V^N | M, Z^N) \\
&\quad - H(Z^N) \\
&= H(M, V^N) + H(Z^N | M, V^N) \\
&\quad - H(V^N | M, Z^N) - H(Z^N) \\
&\geq H(V^N) + H(Z^N | V^N) \\
&\quad - H(V^N | M, Z^N) - H(Z^N) \\
&\geq H(V^N) - I(V^N; Z^N) \\
&\quad - H(T_{sb}, V^N | M, Z^N) \\
&= H(V^N) - I(V^N; Z^N) - H(T_{sb} | M, Z^N) \\
&\quad - H(V^N | M, Z^N, T_{sb}) \\
&\geq I(V^N; Y^N) - I(V^N; Z^N) \\
&\quad - H(T_{sb}) - H(V^N | M, Z^N, T_{sb}) \\
&\geq NI(V; Y) - NI(V; Z) \\
&\quad - H(T_{sb}) - H(V^N | M, Z^N, T_{sb}),
\end{aligned} \tag{19}$$

(20)

where (19) is from the Markov chain $M \rightarrow V^N \rightarrow Z^N$ and (20) is from the fact that the codewords v^N are i.i.d and the channels are discrete memoryless.

Next, we bound $H(T_{sb})$ and $H(V^N | M, Z^N, T_{sb})$ in (20). Since $\|\mathcal{T}_{sb}\| = 2^{N(\max\{I(V;U), I(V;Z)\} - I(V;Z) + \epsilon_1)}$, we have $H(T_{sb}) \leq \log \|\mathcal{T}_{sb}\| = N(\max\{I(V;U), I(V;Z)\} - I(V;Z) + \epsilon_1)$.

The explanation for bounding $(1/N)H(V^N | M, Z^N, T_{sb})$ is presented as follows. We first show that, given M and T_{sb} , the probability of error for Z^N to decode V^N satisfies $P'_e \leq \nu$. Here, ν is small for sufficiently large N . Given the knowledge of M and T_{sb} , the total number of possible codewords of V^N is

$$\begin{aligned}
\frac{2^{N(I(V;Y) - R - \epsilon)}}{\|\mathcal{T}_{sb}\|} &= \frac{2^{N(I(V;Y) - R - \epsilon)}}{2^{N(\max\{I(V;Z), I(V;U)\} - I(V;Z) + \epsilon_1)}} \\
&= 2^{N(I(V;U) + \lambda - \epsilon - \max\{I(V;Z), I(V;U)\} + I(V;Z) - \epsilon_1)} \\
&\leq 2^{N(I(V;Z) - \epsilon - \epsilon_1)} \\
&\leq 2^{NI(V;Z)},
\end{aligned} \tag{21}$$

(22)

where (21) is from $\lambda \leq \max\{I(V;Z), I(V;U)\} - I(V;U)$. Based on (22), we can easily show that a unique codeword $v^N(t_b, t_{sb}, t_v)$ exists such that $(v^N(t_b, t_{sb}, t_v), z^N) \in T_{VZ}^N$ with high probability. This indicates that the probability of error for Z^N to decode V^N satisfies $P'_e \leq \nu$. Therefore, by Fano's inequality, we obtain

$$\begin{aligned}
\frac{1}{N}H(V^N | M, Z^N, T_{sb}) \\
\leq \frac{1}{N} \left(1 + P'_e \log \left(\frac{2^{N(I(V;Y) - R - \epsilon)}}{\|\mathcal{T}_{sb}\|} \right) \right) \leq \nu',
\end{aligned} \tag{23}$$

where ν' is small for sufficiently large N .

Substituting these two results into (20) and utilizing (2), we finish the proof of $\lim_{N \rightarrow \infty} \Delta \geq R_e$ for the model in Figure 1 with rate-limited CSI. The proof of Theorem 3 is completed.

4.2. Proof of Theorem 4. We need to prove that all achievable rate-equivocation triples (R, R_s, R_e) are contained in \mathcal{R}_o . Precisely, for any triple (R, R_s, R_e) satisfying (1), (2), and (3), we need to show

$$R \leq I(V; Y) - I(V; S | U), \tag{24}$$

$$R_s \geq I(U; S), \tag{25}$$

$$R_e \leq R, \tag{26}$$

$$R_e \leq I(V; Y) - I(V; S | K_2) - I(K_2; Z | K_1). \tag{27}$$

Condition (24) is proved as follows. Consider

$$R = \lim_{N \rightarrow \infty} \frac{\log \|\mathcal{M}\|}{N} \tag{28}$$

$$\begin{aligned}
&= \lim_{N \rightarrow \infty} \frac{H(M)}{N} \\
&= \lim_{N \rightarrow \infty} \frac{1}{N} [I(M; Y^N) + H(M | Y^N)] \\
&\leq \lim_{N \rightarrow \infty} \frac{1}{N} [I(M; Y^N) + \delta(P_e)],
\end{aligned} \tag{29}$$

where (28) is from the fact that M is uniformly distributed over \mathcal{M} and (29) is from Fano's inequality. The term $I(M; Y^N)$ is calculated as follows. Consider

$$I(M; Y^N) = I(M; Y^N) - I(M; S^N) \tag{30}$$

$$= I(M; Y^N) - I(M; S^N | M_s) \tag{31}$$

$$\begin{aligned}
&= \sum_{i=1}^N I(M; Y_i | Y_{i+1}^N) - \sum_{i=1}^N I(M; S_i | S^{i-1}, M_s) \\
&= \sum_{i=1}^N [I(M, S^{i-1}, M_s; Y_i | Y_{i+1}^N) \\
&\quad - I(S^{i-1}, M_s; Y_i | M, Y_{i+1}^N)] \\
&\quad - \sum_{i=1}^N [I(M, Y_{i+1}^N; S_i | S^{i-1}, M_s) \\
&\quad - I(Y_{i+1}^N; S_i | M, S^{i-1}, M_s)] \\
&= \sum_{i=1}^N [I(M, S^{i-1}, M_s; Y_i | Y_{i+1}^N) \\
&\quad - I(M, Y_{i+1}^N; S_i | S^{i-1}, M_s)] \\
&\leq \sum_{i=1}^N [I(M, S^{i-1}, M_s, Y_{i+1}^N; Y_i) \\
&\quad - I(M, Y_{i+1}^N, S^{i-1}, M_s; S_i | S^{i-1}, M_s)] \\
&\leq \sum_{i=1}^N [I(V_i; Y_i) - I(V_i; S_i | U_i)].
\end{aligned} \tag{32}$$

$$\tag{33}$$

In the above derivation, formula (30) is from the fact that the message is independent of the state sequence. Therefore, we have $I(M; S^N) = 0$. Formula (31) is from the fact that $I(M; S^N | M_s) = 0$ which is proved in (35). Consider

$$I(M; S^N | M_s) = H(M | M_s) - H(M | S^N, M_s) \tag{34}$$

$$\begin{aligned}
&\leq H(M) - H(M | S^N) \\
&= I(M; S^N) \\
&= 0,
\end{aligned} \tag{35}$$

where (34) is from the fact that M_s is a function of S^N and the fact that conditioning does not increase entropy. Formula (32) is from the sum equality in (36). One has

$$\sum_{i=1}^N I(S^{i-1}, M_s; Y_i | M, Y_{i+1}^N) = \sum_{i=1}^N I(Y_{i+1}^N; S_i | M, S^{i-1}, M_s). \tag{36}$$

The sum equality (36) can be proved using similar methods in [13, 17]. Formula (33) is from defining $V_i = (M, S^{i-1}, M_s, Y_{i+1}^N)$ and $U_i = (S^{i-1}, M_s)$.

Condition (25) is proved as follows. Consider

$$\begin{aligned}
R_s &= \frac{\log \|\mathcal{M}_s\|}{N} \\
&\geq \frac{H(M_s)}{N} \\
&= \frac{1}{N} I(M_s; S^N)
\end{aligned} \tag{37}$$

$$\begin{aligned}
&= \frac{1}{N} \sum_{i=1}^N I(M_s; S_i | S^{i-1}) \\
&= \frac{1}{N} \sum_{i=1}^N I(M_s, S^{i-1}; S_i) \\
&= \frac{1}{N} \sum_{i=1}^N I(U_i; S_i),
\end{aligned} \tag{38}$$

where (37) is from the fact that S_i is independent of S^{i-1} .

Condition (26) is proved as follows. Consider

$$R_e \leq \lim_{N \rightarrow \infty} \frac{H(M | Z^N)}{N} \tag{39}$$

$$\begin{aligned}
&\leq \lim_{N \rightarrow \infty} \frac{H(M)}{N} \\
&= R,
\end{aligned} \tag{40}$$

where (39) is from (2).

To prove condition (27), we consider

$$\begin{aligned}
H(M | Z^N) &= H(M | Z^N) - H(M | Y^N) + H(M | Y^N) \\
&= H(M | Z^N) - H(M) + H(M) \\
&\quad - H(M | Y^N) + H(M | Y^N) \\
&= I(M; Y^N) - I(M; Z^N) + H(M | Y^N) \\
&\leq I(M; Y^N) - I(M; Z^N) + \delta(P_e).
\end{aligned} \tag{41}$$

The first two terms in (41) are calculated as follows.

From (32), one has

$$\begin{aligned}
I(M; Y^N) &= \sum_{i=1}^N [I(M, S^{i-1}, M_s; Y_i | Y_{i+1}^N) \\
&\quad - I(M, Y_{i+1}^N; S_i | S^{i-1}, M_s)].
\end{aligned} \tag{42}$$

Similarly, we can get

$$\begin{aligned}
I(M; Z^N) &= \sum_{i=1}^N [I(M, S^{i-1}, M_s; Z_i | Z_{i+1}^N) \\
&\quad - I(M, Z_{i+1}^N; S_i | S^{i-1}, M_s)].
\end{aligned} \tag{43}$$

Then, we substitute (42) and (43) into (41) and get

$$\begin{aligned}
& H(M | Z^N) \\
& \leq I(M; Y^N) - I(M; Z^N) + \delta(P_e) \\
& = \sum_{i=1}^N \left[I(M, S^{i-1}, M_s; Y_i | Y_{i+1}^N) \right. \\
& \quad \left. - I(M, Y_{i+1}^N; S_i | S^{i-1}, M_s) \right] \\
& \quad - \sum_{i=1}^N \left[I(M, S^{i-1}, M_s; Z_i | Z_{i+1}^N) \right. \\
& \quad \left. - I(M, Z_{i+1}^N; S_i | S^{i-1}, M_s) \right] + \delta(P_e) \\
& = \sum_{i=1}^N \left[I(M, S^{i-1}, M_s; Y_i | Y_{i+1}^N) \right. \\
& \quad \left. - I(M, Z_{i+1}^N, Y_{i+1}^N; S_i | S^{i-1}, M_s) \right] \\
& \quad - \sum_{i=1}^N \left[I(M, S^{i-1}, M_s; Z_i | Z_{i+1}^N) \right. \\
& \quad \left. - I(M, Z_{i+1}^N; S_i | S^{i-1}, M_s) \right] + \delta(P_e) \\
& = \sum_{i=1}^N \left[I(M, S^{i-1}, M_s; Y_i | Y_{i+1}^N) \right. \\
& \quad \left. - I(Y_{i+1}^N; S_i | M, Z_{i+1}^N, S^{i-1}, M_s) \right] \\
& \quad - \sum_{i=1}^N I(M, S^{i-1}, M_s; Z_i | Z_{i+1}^N) + \delta(P_e) \\
& \leq \sum_{i=1}^N \left[I(M, S^{i-1}, M_s; Y_{i+1}^N) \right. \\
& \quad \left. - I(Y_{i+1}^N, M, S^{i-1}, M_s; S_i | M, Z_{i+1}^N, S^{i-1}, M_s) \right] \\
& \quad - \sum_{i=1}^N I(M, S^{i-1}, M_s, Z_{i+1}^N; Z_i | Z_{i+1}^N) + \delta(P_e) \\
& = \sum_{i=1}^N \left[I(V_i; Y_i) - I(V_i; S_i | K_{2i}) \right] \\
& \quad - \sum_{i=1}^N I(K_{2i}; Z_i | K_{1i}) + \delta(P_e),
\end{aligned} \tag{44}$$

where (44) is from the Markov chain $S_i \rightarrow (S^{i-1}, M_s, M, Y_{i+1}^N) \rightarrow Z_{i+1}^N$ and (45) from defining $K_{2i} = (M, Z_{i+1}^N, S^{i-1}, M_s)$ and $K_{1i} = Z_{i+1}^N$.

To serve the single-letter characterization, let us introduce a time-sharing random variable J independent of

all other random variables and uniformly distributed over $\{1, 2, \dots, N\}$. Set

$$\begin{aligned}
U &= (U_J, J), & V &= (V_J, J), \\
K_2 &= (K_{2J}, J), & K_1 &= (K_{1J}, J) \\
S &= S_J, & X &= X_J, & Y &= Y_J, & Z &= Z_J.
\end{aligned} \tag{46}$$

Then, substituting the above new random variables into (33), (38), and (45), conditions (24), (25), and (27) are verified by standard time-sharing argument. From the definition of the auxiliary random variables, the Markov chains $U \rightarrow V \rightarrow S, U \rightarrow K_2 \rightarrow K_1$, and $(V, K_1, K_2) \rightarrow (X, U) \rightarrow Y \rightarrow Z$ are easily verified. We complete the proof of Theorem 4.

5. Conclusion

This paper has investigated the problem of rate-limited CSI in state-dependent channels under secrecy constraint. It is an extension of the rate-limited CSI setup without secrecy. This model is more general than the existing wiretap channel with full CSI at the transmitter. We proposed an achievable rate-equivocation region and an outer bound on the capacity-equivocation region. To achieve the rates, a proper coding scheme is constructed based on *Gel'fand and Pinsker's coding* and *Wyner's random coding*.

Our setup can be probably extended in the following directions.

- (i) In this current model as well as [1–7], the CSI is generated by nature. However, in some practical communication systems, the transmitter can take actions to affect the formation of the CSI. This idea called action-dependent states is from [18]. We can further explore the impact of the action-dependent states in the wiretap channel with rate-limited CSI.
- (ii) Only inner and outer bounds on the capacity-equivocation region are obtained at present. We can try to find some special cases where the two bounds match.
- (iii) In our model, the CSI is rate-limited and known to the encoder. We can study the model where the CSI is rate-limited and known to the decoder (or both the decoder and the encoder) under the secrecy constraint.

Conflict of Interests

The authors declare that there is no conflict of interests regarding the publication of this paper.

Acknowledgment

This work was supported in part by the National Natural Science Foundation of China under Grant nos. 61332010, 61171173, and 60932003.

References

- [1] C. E. Shannon, "Channels with side information at the transmitter," *Journal of Research and Development*, vol. 2, pp. 289–293, 1958.
- [2] S. I. Gel'fand and M. S. Pinsker, "Coding for channel with random parameters," *Problems of Control and Information Theory*, vol. 9, no. 1, pp. 19–31, 1980.
- [3] C. Heegard and A. El Gamal, "On the capacity of computer memory with defects," *IEEE Transactions on Information Theory*, vol. 43, no. 6, pp. 1986–1992, 1997.
- [4] A. Rosenzweig, Y. Steinberg, and S. Shamai, "On channels with partial channel state information at the transmitter," *Institute of Electrical and Electronics Engineers. Transactions on Information Theory*, vol. 51, no. 5, pp. 1817–1830, 2005.
- [5] Y. Steinberg, "Coding for channels with rate-limited side information at the decoder, with applications," *IEEE Transactions on Information Theory*, vol. 54, no. 9, pp. 4283–4295, 2008.
- [6] Y. Steinberg, "Coding for the degraded broadcast channel with random parameters, with causal and noncausal side information," *IEEE Transactions on Information Theory*, vol. 51, no. 8, pp. 2867–2877, 2005.
- [7] M. H. M. Costa, "Writing on dirty paper," *IEEE Transactions on Information Theory*, vol. 29, no. 3, pp. 439–441, 1983.
- [8] Y. Chen and A. J. H. Vinck, "Wiretap channel with side information," *IEEE Transactions on Information Theory*, vol. 54, no. 1, pp. 395–402, 2008.
- [9] C. Mitropant, A. J. Han Vinck, and Y. Luo, "An achievable region for the Gaussian wiretap channel with side information," *IEEE Transactions on Information Theory*, vol. 52, no. 5, pp. 2181–2190, 2006.
- [10] B. Dai and Y. Luo, "Some new results on the wiretap channel with side information," *Entropy*, vol. 14, no. 9, pp. 1671–1702, 2012.
- [11] W. Liu and B. Chen, "Wiretap channel with two-sided channel state information," in *Proceedings of the Conference Record of the 41st Asilomar Conference on Signals, Systems and Computers (ACSSC '07)*, pp. 893–897, Pacific Grove, Calif, USA, November 2007.
- [12] Y. Chia and A. El Gamal, "Wiretap channel with causal state information," *IEEE Transactions on Information Theory*, vol. 58, no. 5, pp. 2838–2849, 2012.
- [13] B. Dai, A. J. H. Vinck, Y. Luo, and X. Tang, "Wiretap channel with action-dependent channel state information," *Entropy*, vol. 15, no. 2, pp. 445–473, 2013.
- [14] B. Dai, A. J. Han Vinck, and Y. Luo, "Wiretap channel in the presence of action-dependent states and noiseless feedback," *Journal of Applied Mathematics*, vol. 2013, Article ID 423619, 17 pages, 2013.
- [15] X. Yin and Z. Xue, "Wiretap channel with information embedding on actions," *Entropy*, vol. 16, no. 4, pp. 2105–2130, 2014.
- [16] A. D. Wyner, "The wire-tap channel," *The Bell System Technical Journal*, vol. 54, no. 8, pp. 1355–1387, 1975.
- [17] I. Csisz and J. Köner, "Broadcast channels with confidential messages," *Institute of Electrical and Electronics Engineers. Transactions on Information Theory*, vol. 24, no. 3, pp. 339–348, 1978.
- [18] T. Weissman, "Capacity of channels with action-dependent states," *IEEE Transactions on Information Theory*, vol. 56, no. 11, pp. 5396–5411, 2010.

Research Article

A Probabilistic Recommendation Method Inspired by Latent Dirichlet Allocation Model

WenBo Xie,¹ Qiang Dong,^{1,2} and Hui Gao^{1,2}

¹ Web Sciences Center, School of Computer Science and Engineering, University of Electronic Science and Technology of China, Chengdu 611731, China

² Big Data Research Center, University of Electronic Science and Technology of China, Chengdu 611731, China

Correspondence should be addressed to Qiang Dong; dongq@uestc.edu.cn

Received 27 May 2014; Accepted 15 August 2014; Published 29 September 2014

Academic Editor: Qinggang Meng

Copyright © 2014 WenBo Xie et al. This is an open access article distributed under the Creative Commons Attribution License, which permits unrestricted use, distribution, and reproduction in any medium, provided the original work is properly cited.

The recent decade has witnessed an increasing popularity of recommendation systems, which help users acquire relevant knowledge, commodities, and services from an overwhelming information ocean on the Internet. Latent Dirichlet Allocation (LDA), originally presented as a graphical model for text topic discovery, now has found its application in many other disciplines. In this paper, we propose an LDA-inspired probabilistic recommendation method by taking the user-item collecting behavior as a two-step process: every user first becomes a member of one latent user-group at a certain probability and each user-group will then collect various items with different probabilities. Gibbs sampling is employed to approximate all the probabilities in the two-step process. The experiment results on three real-world data sets MovieLens, Netflix, and Last.fm show that our method exhibits a competitive performance on precision, coverage, and diversity in comparison with the other four typical recommendation methods. Moreover, we present an approximate strategy to reduce the computing complexity of our method with a slight degradation of the performance.

1. Introduction

The advent of Internet has confronted us with an exploding information era. We find that it is very difficult to select the relevant ones from countless candidates on the e-commerce websites. As an automatic way to help people make right decisions under the information overload, the recommendation system has become a significant issue for both academic and industrial communities.

During the last decade, lots of recommendation methods have been proposed, including collaborative filtering methods [1, 2], content-based methods [3], spectral methods [4, 5], and iterative refinement methods [6, 7]. These methods are all based on the computation of either user similarity or item similarity or both. Recently, some network-based recommendation methods have been proposed to mine the latent relevance of users and items, such as the methods based on mass diffusion or association rules [8, 9].

Latent Dirichlet Allocation (LDA) was first presented as a graphical model for text topic discovery by Blei et al.

in 2003 [10], which can be used to find the inherent relation of words and generate document set through the model. LDA has been widely used in document analysis [11–13], document classification, and document clustering [14–16]. LDA was first introduced into recommender systems for analyzing the context in content-based methods [17]. Now in tag-based recommendation systems, LDA is widely used to find the latent relation between keywords of item description and item tags created by users, such that the items can be recommended based on the tags [18–20]. For instance, Kang et al. [21] proposed an LA-LDA model which considers not only the tags created by the target user but also the tags created by his/her friends in the social network to extend the scope of candidate tags created by the target user.

In this paper, we propose a new content-unaware probabilistic recommendation method inspired by LDA model. Users' collecting behaviors are probabilistic events, in which one user belongs to multiple user-groups and users in each user-group have different collecting preferences. In our method, the collecting process is regarded as two joined

probabilistic processes intermediated by the user-group; that is, every user is a member of one latent user-group at a certain probability, while each user-group will collect various items with different probabilities.

Calculating the probabilities on the entire data set is time-consuming and space-consuming. In order to reduce the computing complexity of our method, we introduce an approximate strategy with a slight degradation of the performance, which samples a part of the data set to build a rough probabilistic recommendation model.

Many products on an e-commerce website are not popular; that is, the sale of every single product lies in the tail of sale curve, but the sales of all these unpopular products constitute a big portion of the whole income. That is the so-called long tail phenomenon. Therefore, a good recommender system must focus on both the accuracy and the diversity. The experiment results on three real-world data sets, MovieLens, Netflix, and Last.fm, show that our method exhibits a competitive performance not only on the precision and the coverage but also on the diversity.

2. Materials and Methods

2.1. Recommendation Model. People have different and multiple inner attributes, including physiological characteristics, preferences, taboos, and religious beliefs. These attributes can be clustered into lots of user-groups which can represent users with similar attributes. Actually, a user does not belong to only one user-group. For example, user A is a male and he is a high school student, minor, Chinese, and a Christian as well. One user belongs to multiple user-groups while users in different user-groups have different habits. For instance, users in the user-groups which contain the attribute of “elder” are more likely to buy health care products and presbyopia glasses than those who belong to the user-groups containing the attribute of “younger.” In our recommendation model, we put forward two assumptions:

- (1) the users’ collecting behaviors are probabilistic events;
- (2) one user belongs to multiple user-groups and users in the same user-group have similar collecting preference.

The collecting action of users on items is therefore considered as a two-step probabilistic process; that is, users are observed as members of several latent user-groups and users in user-groups will collect items based on the group-item probability distributions. Here we assume that z is a user-group which a user belongs to; θ is the probability vector between users and user-groups. Each column of the vector represents the probability that a user belongs to this user-group. The probability that a user d belongs to user-group z can be expressed as $p(z | d) = \theta_z^d$; φ is the commodity probability vector and each column of vector represents the probability that the users of current user-group will collect this item, while the probability that a user who belongs to user-group z will buy item w can be expressed as $p(w | z, \varphi^z) = \varphi_w^z$. In fact, θ reflects the degree of association between users and user-groups and φ shows which item the

users who belong to this user-group are more likely to buy. For example, a user who loves both basketball and music belongs to two user-groups, but he prefers to play basketball rather than listening to music. The association intensity between user and user-group could be demonstrated by the probability that the user belongs to each user-group. For a student, he may not care about household items but usually buy books for study. Based on the assumption above, if there are T groups, the probability for user d to buy item w can be expressed as

$$p(w | d) = \sum_z p(w | z) p(z | d) = \sum_z \varphi_w^z \cdot \theta_z^d. \quad (1)$$

As long as θ and φ are calculated, the collecting probability vector of the users can be computed. We can get a list ranked in order of the probabilities. Deducing from the list, a proper recommendation can be given to the users. In fact, it is not easy to calculate θ and φ directly.

Considering that, the Latent Dirichlet Allocation (LDA) is a probabilistic model that uses a latent topic to bridge documents and words. Using the latent topic, LDA constructs the documents via two probabilistic processes that chooses a topic after the first probability prediction and then collects words from the attributes of the topic-word according to the topic. Inspired by the LDA, the structure of our recommendation model is designed as a three-layer structure of Bayesian, that is, the user layer, followed by the user-group layer and the item layer. To construct it, parameters are used in pairs. The recommendation model is determined by the hyper parameters α and β , in which α describes the relative intensity between user-groups, $\theta \sim \text{Dirichlet}(\alpha)$, and β reflecting the probability distribution of each user-group, $\varphi \sim \text{Dirichlet}(\beta)$. The complete graphical model representation of LDA for probabilistic recommendation model is as shown in Figure 1. Indeed, we can construct the model without the items or user descriptions. So it is a content-unaware probabilistic recommendation model.

In our method, the probability that a user d has an attribute z is expressed as $p(z | d, \alpha) = \theta_z^d$; the probability that users who have attribute z purchased items w is expressed as $p(w | z, d, \beta) = \varphi_w^z$; and the probability that user d purchases item w is expressed as

$$p(w | d, \alpha, \beta) = \sum_z p(w | z, d, \beta) \cdot p(z | d, \alpha) = \sum_z \varphi_w^z \cdot \theta_z^d. \quad (2)$$

2.2. Parameters Estimation. There are many approximate inference strategies to estimate parameters θ and φ in LDA, such as Laplace approximate, variational inference, Gibbs sampling, and expectation propagation. Griffiths and Steyvers put forward that the perplexity and speed of Gibbs sampling method is better than those of other methods [11]. Since the structure of our method is similar to that of LDA, we chose Gibbs sampling algorithm to estimate parameters θ and φ as well. Gibbs sampling is a simple MCMC (Markov chain Monte Carlo) method. It constructs a Markov chain which converges to the target distribution and samples. Each

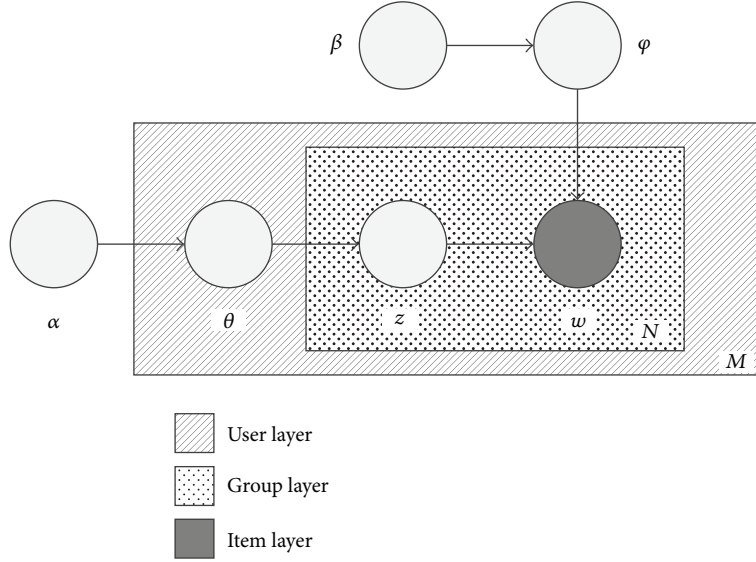


FIGURE 1: Graphical model representation of our method.

state of the Markov chain represents the value of the user-group, and the sampling variable is an implicit variable, which is assigned to items collected by users. The transition between states follows a simple rule. By sampling on the current values of all variables and data set of users' purchases, the chain can translate to the next state.

Here, we use the posterior distribution $p(z_j | z, d, w_i, \alpha, \beta)$, which is calculated by counting the user-groups assigned to items, as the transition probability of user-group shifts from z to z_j for item w which is purchased by user d , as shown in

$$p(z_j | z, d, w_i, \alpha, \beta) \propto \frac{n_{-i,j}^{(w_i)} + \beta}{n_{-i,j}^{(*)} + W\beta} \times \frac{n_{-i,j}^{(d)} + \alpha}{n_{-i,*}^{(d)} + T\alpha}. \quad (3)$$

Here, $n_{-i}^{(*)}$ is a count that does not include the assignment of item w ; $n_{-i,j}^{(w_i)}$ is the number of times that item w has been assigned to user-group j ; $n_{-i,j}^{(*)}$ represents the number of times that all items have been assigned to user-group j ; $n_{-i,j}^{(d)}$ is the number of times that items purchased by user d have been assigned to user-group j ; $n_{-i,*}^{(d)}$ represents the quantity of items that user d had purchased.

When the Markov chain is near the target distribution after adequate iterations, we recorded its current values of the implicit variable z and used it to estimate θ and φ as shown in (4) and (5):

$$\hat{\varphi}_j^{(w)} = \frac{n_j^{(w)} + \beta}{n_j^{(*)} + W\beta}, \quad (4)$$

$$\hat{\theta}_j^{(d)} = \frac{n_j^{(d)} + \alpha}{n_{*,*}^{(d)} + T\alpha}. \quad (5)$$

Here $n_j^{(w)}$ is the number of times item w has been assigned to user-group j ; $n_j^{(*)}$ represents the number of times that all items have been assigned to user-group j ; $n_j^{(d)}$ is the number of times that items purchased by user d have been assigned to user-group j ; and $n_{*,*}^{(d)}$ represents the quantity of items that user d has purchased.

2.3. Approximate Model. Actually, the data set is updated every day. It is not only time-consuming but also space-consuming to use the entire data set to structure the recommendation model. To save time and space, we prefer to model with less data and the recommended items are only listed when required instead of preparing them in advance. In this paper, we present an approximation method to structure the approximate model of the probabilistic recommendation.

In the approximation method, we sample part of the users' collection data from the data set to structure an imprecise probabilistic recommendation model. The imprecise model will serve as a guide to create a recommendation list from two sides. On one hand, the latent user-group vector z will be initiated by using the parameter φ of imprecise model. On the other hand, the transition probability $p(z_j | z, d, w_i, \alpha, \beta)$ is defined as the product of constant φ calculated in the imprecise model and iteration parameter θ , as shown in

$$p(z_j | z, d, w_i, \alpha, \beta) \propto \varphi_j^{(w_i)} \times \frac{n_{-i,j}^{(d)} + \alpha}{n_{-i,*}^{(d)} + T\alpha}. \quad (6)$$

The processes of the approximate method are described as follows.

- (1) Choose part of users from the data set for constructing the approximate model, called approximating data.

TABLE 1: The basic statistical features of the three data sets.

Data set	Users	Items	Links	Sparsity
MovieLens	6,040	3,952	1,000,209	4.19×10^{-2}
Netflix	10,000	6,000	701,947	1.17×10^{-2}
Last.fm	1,882	17,632	186,480	5.62×10^{-3}

- (2) Use the approximating data to initiate the Markov chain: random user-group z from 1 to T is assigned to each item i collected by user d .
- (3) Use (3) to iterate the Markov chain until it is converged. Equation (4) will be used to work out the φ and then used to construct the approximate model.
- (4) When user d needs a recommendation list, user-group z is assigned to each item i collected by user d . The parameter φ , collecting probability of the user-group, which was consequently worked out in Step (3), will be used to initialize z from 1 to T probabilistically. This is the initial state of the Markov chain for user d .
- (5) Use (6) to iterate for appreciable number of times, and we denote the result as b , also called burn-in space. It is thought that the Markov chain is near the target distribution. Then, we record the current values of z .
- (6) Sample once in a certain number of times c which is called thinning space [22]. According to (5), we can estimate θ , the purchasing probability of user d in each user-group.
- (7) By ranking the product of φ and θ , the recommendation list can be provided.

The time consumption of the approximate model depends on the size of approximating data. Indeed, the performance of the approximate model depends on the size as well. In the experiment, we use different percentages of data as approximation data to find the optimal size. Approximate model is, however, imprecise owing to the use of data locality. Meanwhile, the performance oscillates when different data is chosen to do approximate modeling. Different strategies (random: randomly choose users within the entire data; item degree: according to each user's average degree of items sampled proportionally; user degree: according to the average degree of user sampled proportionally; quick classification: use a quick classification method to classify the users and then sample proportionally) are compared to find out the user distribution offered by which strategy is most similar to that of the entire data and has the same tendency of performance. In the experiment, we use the average value and the upper bound value to represent the performance of the approximate model.

3. Experiments and Results

3.1. Data Description. Three benchmark data sets (Table 1) are used to evaluate the performance of the proposed LDA-based recommender method. The first data set *MovieLens* is

provided by GroupLens Project at the University of Minnesota. The second data set *Netflix* is a randomly selected subset of the huge data set released by the DVD rental company Netflix for its Netflix Prize. The third data set *Last.fm* was released in the framework of the 2nd International Workshop on Information Heterogeneity and Fusion in Recommender Systems (HetRec 2011). According to the chronological order of the data in MovieLens, we chose the early 80 percent of the data as the training set and the later 20 percent as the probe set. For the Netflix and Last.fm data sets, the data is randomly selected into two parts: the training set contains 90% of the data and the remaining 10% of the data constitutes the probe set in the experiment.

3.2. Evaluation Metrics and Comparison Methods. Three evaluation metrics were used to assess the recommendation's effect in the experiment: precision, coverage, and diversity. Precision is a basic evaluating metric. It is defined as the proportion of users that accept the recommended items:

$$P = \frac{R \cap U}{U}. \quad (7)$$

Here, R represents the list of items recommend to users; U represents the set of items that the user has bought.

Different algorithm will provide different recommendation list to users. The union set of recommendation lists R_i can be used to work out the proportion of recommended items in the entire item set. We use coverage to define this proportion, as shown in

$$\text{Cov} = \frac{\bigcup R_i}{A}. \quad (8)$$

Here, R_i represents the list of items recommended to user i and A represents the quantity of all items. Diversity is an important metric for personalized recommender systems. It is used to evaluate the difference between users' recommendation lists, and we use the average hamming distance of recommendation list to define diversity as follows:

$$H_{ij}(L) = 1 - \frac{R_i(L) \cap R_j(L)}{L}, \quad (9a)$$

$$\text{Div} = \frac{2 \sum_{i \neq j} H_{ij}}{I(I-1)}. \quad (9b)$$

$H_{ij}(L)$ is the hamming distance of recommendation list between user i and user j ; L is the length of the recommendation list; and I represents the quantity of users.

For comparison, we present the results of the four recommendation methods which are the probabilistic spreading (ProbS), heat spreading (HeatS), user-based collaborative filtering (UserCF), and the association rule algorithm (ARule). User-based collaborative filtering algorithm is one of the most classic collaborative filtering methods. Based on the similarity of purchased items between users, it recommends the items that similar users have bought but not yet bought by the user himself. The association rule method is also widely used in recommender systems. This method concentrates on

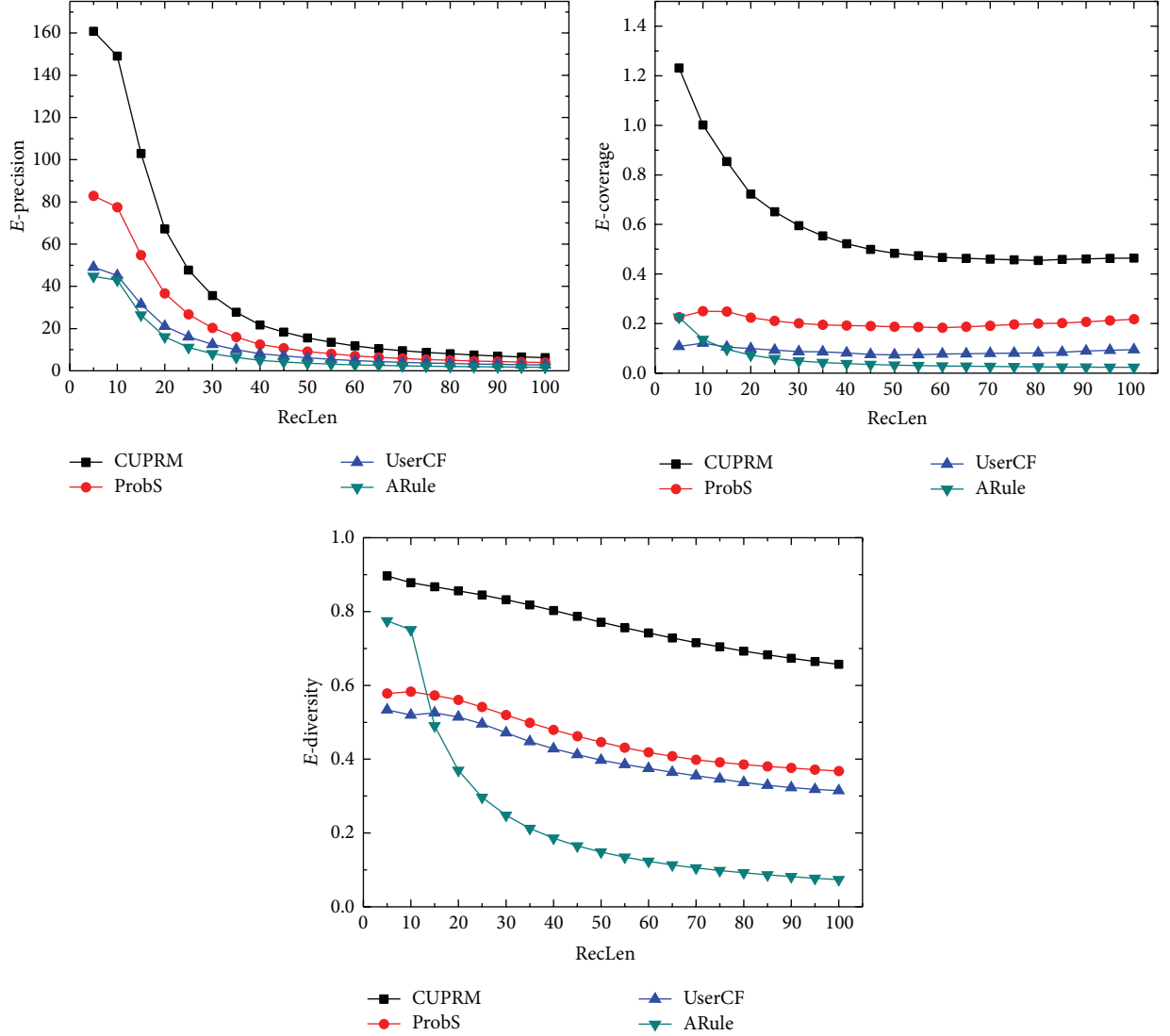


FIGURE 2: The recommendation performances on MovieLens; our method uses exponential constant parameters: $t = 100$, $\alpha = 0.5$, and $\beta = 0.1$.

the latent relationship between items. To find these relationships, every user's item list is analyzed to create a list of the most related items called association rule. Heat spreading method, a variant of probabilistic spreading method, has the highest rate of coverage and diversity in current recommendation algorithms, but it ignores accuracy. In the experiment, we use accuracy of recommendation as the lower bound of precision and use its coverage and diversity rate as the upper bound. Therefore, we use the enhance metrics to evaluate the performance, as shown in (10a)–(10c). Heat spreading and probabilistic spreading are integrated methods which do well on precision but are not so good on coverage and diversity:

$$E\text{-Precision} = \frac{P}{P_{\text{HeatS}}}, \quad (10a)$$

$$E\text{-Coverage} = \frac{\text{Cov}}{\text{Cov}_{\text{HeatS}}}, \quad (10b)$$

$$E\text{-Diversity} = \frac{\text{Div}}{\text{Div}_{\text{HeatS}}}. \quad (10c)$$

To evaluate the performance of the approximate model, missing rate M and comprehensive Comp are defined in the metric, as shown in (11). Here, M_* presents the missing rate of performance such as precision, coverage, and diversity; PN_* presents the performances of normal model and PA_* is the approximate performance of the model; per denotes the percentage of approximate data in the entire data set; Δ is the controlling parameter that accommodates the floating of M ; a , b , and c are the weight of metrics (precision, coverage, and diversity) for comprehensive rate:

$$M_* = \frac{PN_* - PA_*}{PN_*},$$

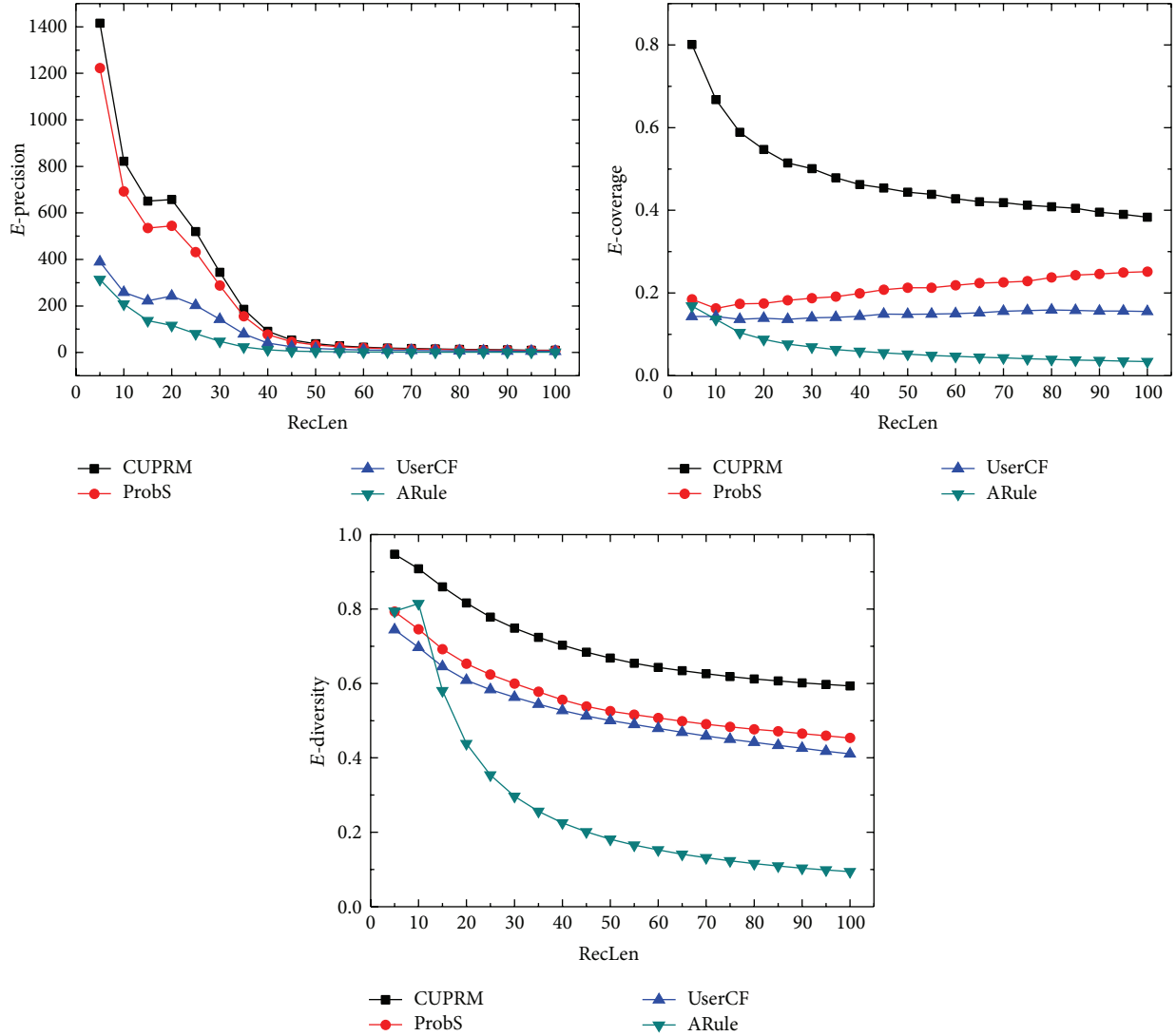


FIGURE 3: The recommendation performances on Netflix; our method uses experiential constant parameters: $t = 100$, $\alpha = 0.5$, and $\beta = 0.1$.

$$\text{Comp} = \frac{(a \times M_p + b \times M_{\text{Cov}} + c \times M_{\text{Div}}) \times (\text{per} + \Delta)}{\Delta}. \quad (11)$$

3.3. Results. The recommendation performances of different methods on the MovieLens, Netflix, and Last.fm data sets are shown in Figures 2, 3, and 4, respectively. The parameters in our method will affect the result. Here we use experiential constant parameters: $T = 100$, $\alpha = 0.5$, and $\beta = 0.1$.

The performances of our method are far better than those of the other methods on MovieLens data set which has the most links in the experiment, with ProbS running a close second, while both UserCF and ARule performed significantly worse. When the length of recommendation is lower than 20, the performance of our method is at least twice as well as the other two methods. On the Netflix data set, our

method consistently performs very well in terms of precision, coverage, and diversity. The precision of ProbS goes near to that of our method while its other performances are much worse. In addition, our method gets good comprehensive performance on Last.fm which is the sparsest data set in the experiment. When the recommendation list length is over 50, the precision of our method is lower than that of ARule, and coverage runs a close second. Furthermore, the consistency of its diversity could be rated as the best. The performances of the approximate model are shown in Figures 5 and 6.

Different metrics are drawn on different maps to show their tendency of coverage, as shown in Figure 5. For precision, with the increasing of data size, the missing rate declines more slowly and is leveled out in the end. The missing rate is controlled between 0 and 20%. The tendency of coverage is different from that of precision. The missing rate will increase,

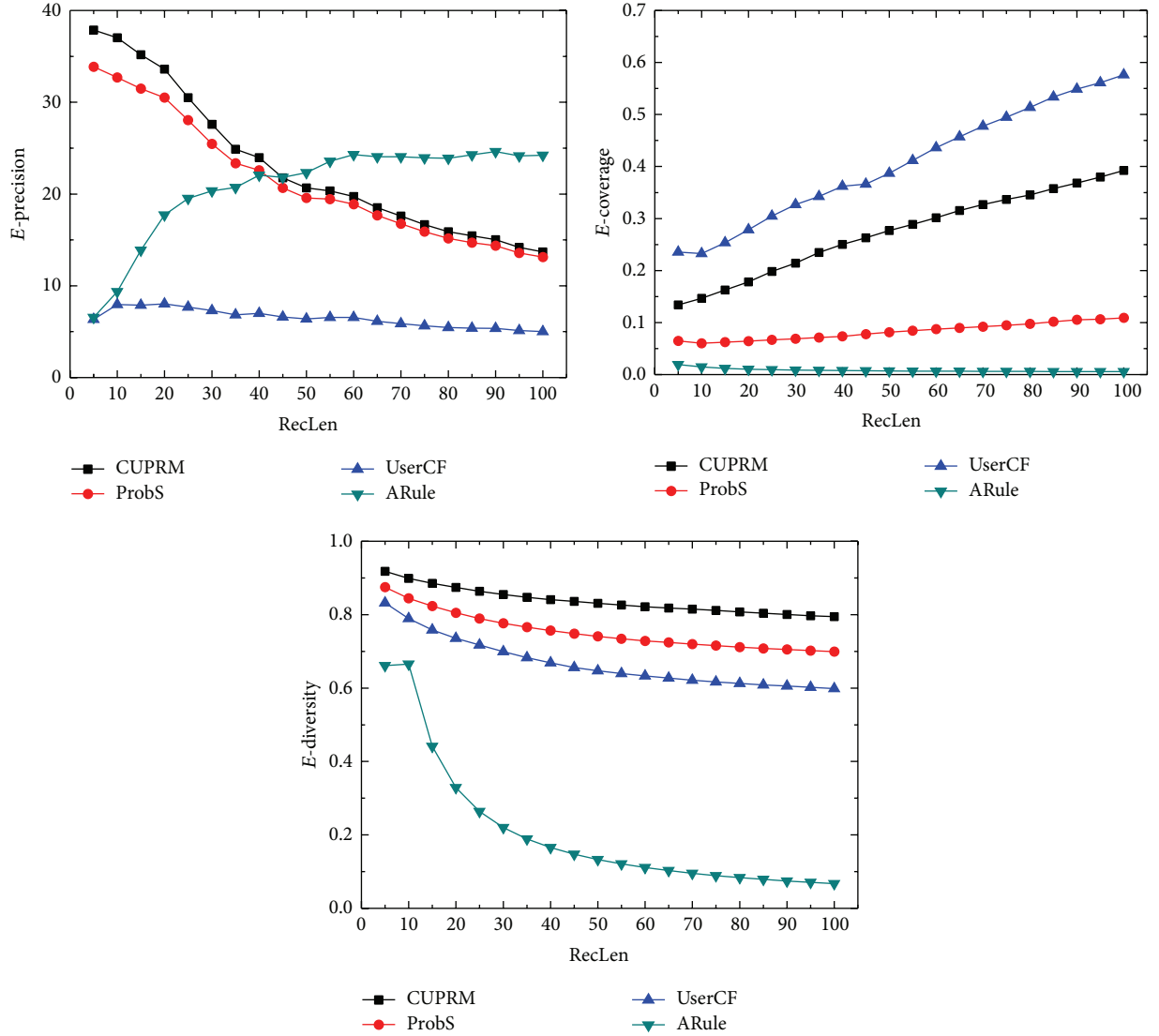


FIGURE 4: The recommendation performances on Last.fm; our method uses experiential constant parameters: $t = 100$, $\alpha = 0.5$, and $\beta = 0.1$.

at first, while the transition occurs in the range of 5 to 10 (percentage). On the contrary, the missing rate of diversity is very high in the heat of the line. The lowest point is located in the range of 5 to 10 as well, and the missing rate is leveled out at the tail.

Figure 6 shows the comprehensive performances of approximate model. Different comprehensive curve will be drawn depending on the parameters, and we kept the parameters fixed as $\Delta = 10$, $a = 0.50$, $b = 0.15$, and $c = 0.35$ in the experiment. There are some differences between the two data sets on their comprehensive curve. The comprehensive curve of MovieLens data set is flat, and less lower values lay on the heat of the curve while slight oscillation comes on the tail. In contrast, the comprehensive curve of Netflix data set is like a hook. Considering the above-mentioned factors, the optimal value occurs near 10 (percentage).

4. Conclusions

In this paper, we proposed a method which makes use of users' behaviors to give recommendation. Instead of modeling with tags or contexts, our method takes the collecting lists to construct a recommendation model without the contents of items. As shown in the experiment, our method exhibits an all-round competitive performance on precision, coverage, and diversity, in comparison with four typical classes of recommendation algorithms. To reduce the computing complexity of our method, approximate model is also proposed in this paper, where the adjusting parameters are the determinant of performance curve of approximate model. As shown in the experiment, the approximate method is feasible since the optimal value is under 20%. When precision is considered to be the most important metric, it is

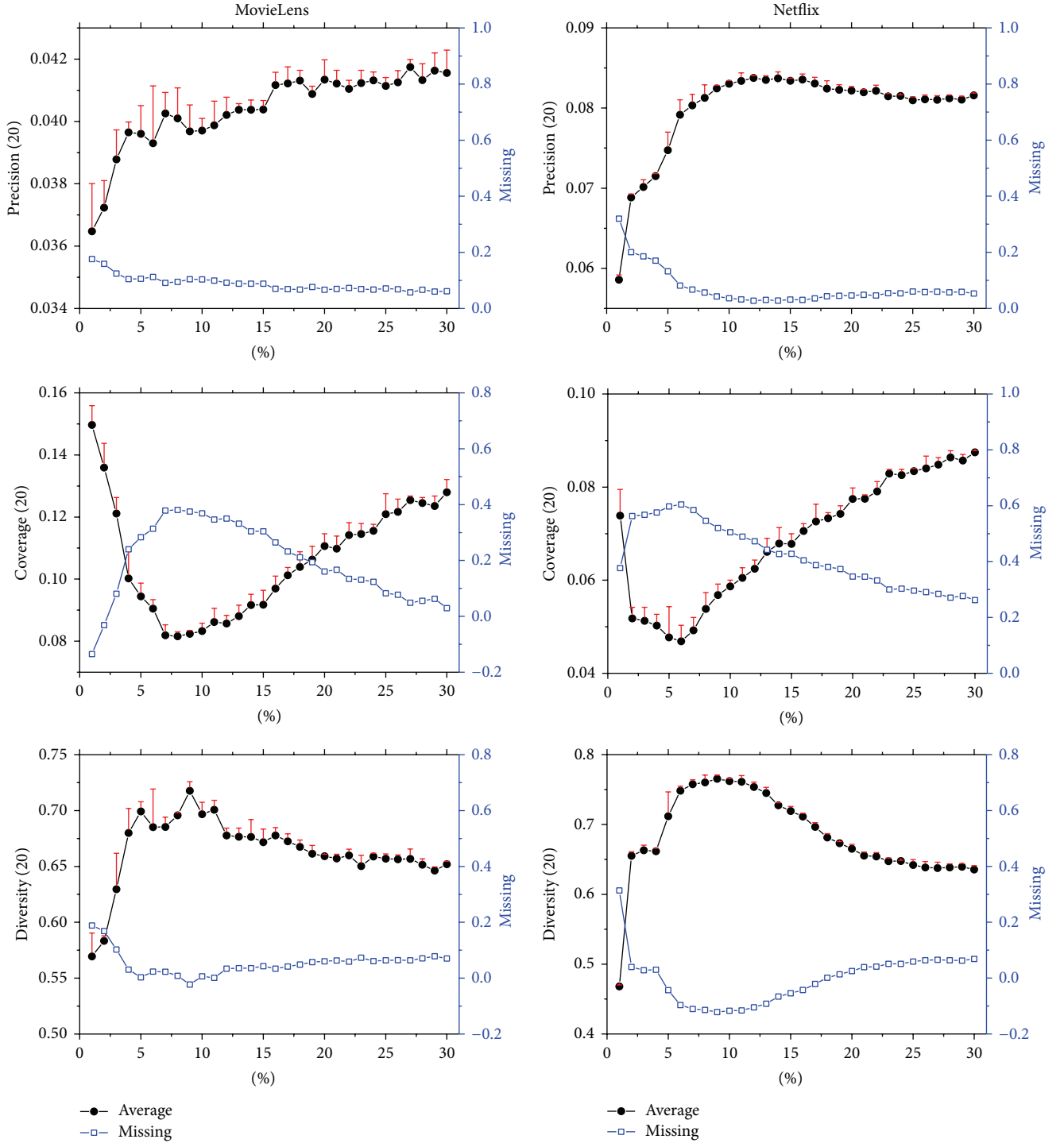


FIGURE 5: The performances of approximate model.

more appropriate to use less than 10% of the data to construct the approximate model.

Conflict of Interests

The authors declare that there is no conflict of interests regarding the publication of this paper.

Acknowledgments

This work was supported by the National Natural Science Foundation of China (nos. 61300018 and 61103109), Research Fund for the Doctoral Program of Higher Education of China (no. 20120185120017), China Postdoctoral Science Foundation (nos. 2013M531951 and 2014T70860),

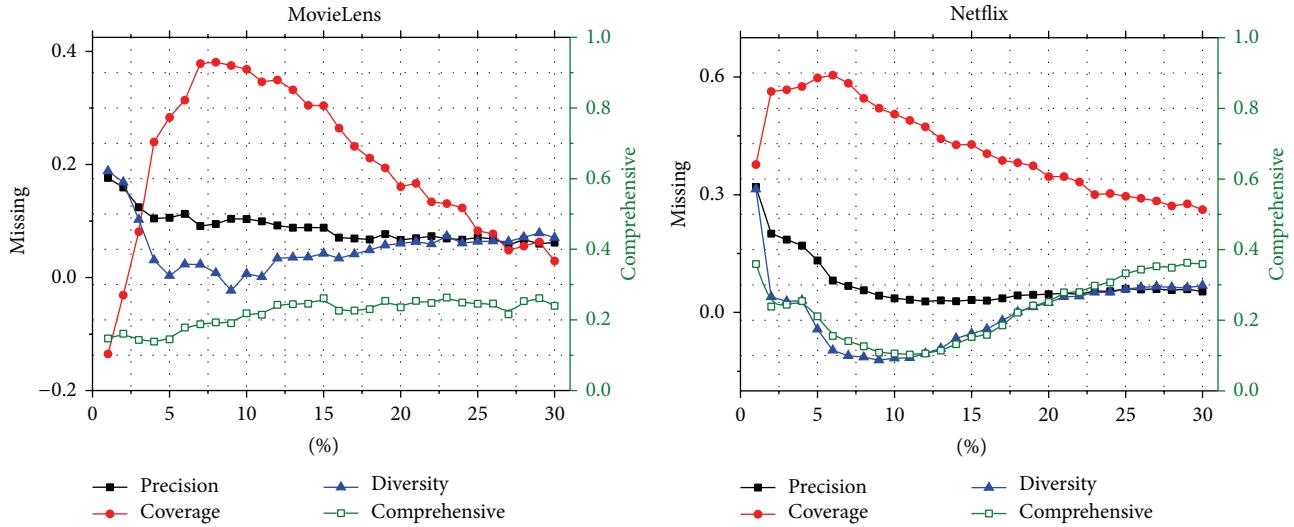


FIGURE 6: The missing rates and comprehensive rates on MovieLens and Netflix in which $\Delta = 10$, $a = 0.50$, $b = 0.15$, and $c = 0.35$.

Fundamental Research Funds for the Central Universities (no. ZYGX2012J071), and Special Project of Sichuan Youth Science and Technology Innovation Research Team (no. 2013TD0006).

References

- [1] J. B. Schafer, D. Frankowski, J. Herlocker, and S. Sen, "Collaborative filtering recommender systems," *Lecture Notes in Computer Science*, vol. 4321, pp. 291–324, 2007.
- [2] B. Sarwar, G. Karypis, and J. Konstan, "Item-based collaborative filtering recommendation algorithms," in *Proceedings of the 10th international conference on World Wide Web (WWW '01)*, 2001, Item-Based Collaborative Filtering Recommendation Algorithms.
- [3] M. J. Pazzani and D. Billsus, "Content-based recommendation systems," in *The Adaptive Web*, vol. 4321 of *Lecture Notes in Computer Science*, pp. 325–341, Springer, 2007.
- [4] K. Goldberg, T. Roeder, D. Gupta, and C. Perkins, "Eigentaste: a constant time collaborative filtering algorithm," *Information Retrieval*, vol. 4, no. 2, pp. 133–151, 2001.
- [5] S. Maslov and Y.-C. Zhang, "Extracting hidden information from knowledge networks," *Physical Review Letters*, vol. 87, no. 24, Article ID 248701, 2001.
- [6] P. Laureti, L. Moret, Y. Zhang, and Y. Yu, "Information filtering via iterative refinement," *Europhysics Letters*, vol. 75, no. 6, pp. 1006–1012, 2006.
- [7] J. Ren, T. Zhou, and Y.-C. Zhang, "Information filtering via self-consistent refinement," *Europhysics Letters*, vol. 82, Article ID 58007, 2008.
- [8] R. Agrawal, T. Imielinski, and A. Swami, "Mining association rules between sets of items in large databases," in *Proceedings of the 1993 ACM SIGMOD international conference on Management of data (SIGMOD '93)*, vol. 22, no. 2, pp. 207–216.
- [9] W. Lin, S. A. Alvarez, and C. Ruiz, "Efficient adaptive-support association rule mining for recommender systems," *Data Mining and Knowledge Discovery*, vol. 6, no. 1, pp. 83–105, 2002.
- [10] D. M. Blei, A. Y. Ng, and M. I. Jordan, "Latent Dirichlet allocation," *Journal of Machine Learning Research*, vol. 3, no. 4-5, pp. 993–1022, 2003.
- [11] T. L. Griffiths and M. Steyvers, "Finding scientific topic," *Proceedings of the National Academy of Sciences of the United States of America*, vol. 101, no. 1, 2004.
- [12] D. M. Blei and J. D. Lafferty, "Correlated topicmodels," in *Advances in Neural Information Processing Systems*, vol. 18, 2005.
- [13] F.-F. Li and P. Perona, "A bayesian hierarchical model for learning natural scene categories," in *Proceedings of the IEEE Computer Society Conference on Computer Vision and Pattern Recognition (CVPR '05)*, vol. 2, pp. 524–531, June 2005.
- [14] X. Wei and W. B. Croft, "LDA-based document models for ad-hoc retrieval," in *Proceedings of the 29th Annual International ACM SIGIR Conference on Research and Development in Information Retrieval (SIGIR '06)*, pp. 178–185, August 2006.
- [15] Z. Wang and X. Qian, "Text categorization based on LDA and SVM," in *Proceedings of the International Conference on Computer Science and Software Engineering (CSSE '08)*, vol. 1, pp. 674–677, December 2008.
- [16] D. Ramage, P. Heymann, C. D. Manning, and H. Garcia-Molina, "Clustering the tagged web," in *Proceeding of the 2nd ACM International Conference on Web Search and Data Mining (WSDM '09)*, pp. 54–63, New York, NY, USA, February 2009.
- [17] K. Yu, B. Zhang, H. Zhu, H. Cao, and J. Tian, "Towards personalized context-aware recommendation by mining context logs through topic models," *Lecture Notes in Computer Science*, vol. 7301, no. 1, pp. 431–443, 2012.
- [18] R. Krestel, P. Fankhauser, and W. Nejdl, "Latent Dirichlet allocation for tag recommendation," in *Proceedings of the 3rd ACM Conference on Recommender Systems*, pp. 61–68, October 2009.
- [19] Y. Song, L. Zhang, and C. L. Giles, "Automatic tag recommendation algorithms for social recommender systems," *ACM Transactions on the Web*, vol. 5, article 4, no. 1, 2011.
- [20] X. Si and M. Sun, "Tag-LDA for scalable real-time tag recommendation," *Journal of Computational Information Systems*, vol. 6, no. 1, pp. 23–31, 2009.

- [21] J.-H. Kang, K. Lerman, and L. Getoor, “LA-LDA: a limited attention topic model for social recommendation,” in *Social Computing, Behavioral-Cultural Modeling and Prediction*, vol. 7812 of *Lecture Notes in Computer Science*, pp. 211–220, Springer, Berlin, Germany, 2013.
- [22] T. Hofmann, “Unsupervised learning by probabilistic Latent Semantic Analysis,” *Machine Learning*, vol. 42, no. 1-2, pp. 177–196, 2001.

Research Article

Node-Dependence-Based Dynamic Incentive Algorithm in Opportunistic Networks

Ruiyun Yu and Pengfei Wang

Software College, Northeastern University, Shenyang 110819, China

Correspondence should be addressed to Ruiyun Yu; yury@mail.neu.edu.cn

Received 8 June 2014; Accepted 7 September 2014; Published 28 September 2014

Academic Editor: Qinggang Meng

Copyright © 2014 R. Yu and P. Wang. This is an open access article distributed under the Creative Commons Attribution License, which permits unrestricted use, distribution, and reproduction in any medium, provided the original work is properly cited.

Opportunistic networks lack end-to-end paths between source nodes and destination nodes, so the communications are mainly carried out by the “store-carry-forward” strategy. Selfish behaviors of rejecting packet relay requests will severely worsen the network performance. Incentive is an efficient way to reduce selfish behaviors and hence improves the reliability and robustness of the networks. In this paper, we propose the node-dependence-based dynamic gaming incentive (NDI) algorithm, which exploits the dynamic repeated gaming to motivate nodes relaying packets for other nodes. The NDI algorithm presents a mechanism of tolerating selfish behaviors of nodes. Reward and punishment methods are also designed based on the node dependence degree. Simulation results show that the NDI algorithm is effective in increasing the delivery ratio and decreasing average latency when there are a lot of selfish nodes in the opportunistic networks.

1. Introduction

The occurrence of plenty of mobile smart devices equipped with short-range wireless communications boosts the fast rise of opportunistic networks. One of the main features of the opportunistic network is that it does not require a complete path existing from a source node to a destination node. The opportunistic network is a kind of delay tolerant networks (DTNs), and it utilizes communication opportunities obtained from node movement to relay packets.

Opportunistic networks have been widely used in the wildlife tracking [1], pocket switched network [2], automobile network [3], and so forth. The basic routing strategy of opportunistic networks is “store-carry-forward.” Data transmission is mainly dependent on intermediate nodes’ relay, so node cooperation is a critical factor that deeply affects performance of opportunistic networks. However, researchers have proved that a large amount of nodes would like to gain more and pay less [4], which makes it important to stimulate nodes to cooperate.

There are usually three kinds of nodes in opportunistic networks, including ordinary nodes, malicious nodes, and selfish nodes [5].

A selfish node usually propagates its packets with the help of other nodes, while it refuses to relay other nodes’ packets. Such behavior does reduce nodes’ own resource consumption, but it decreases the network’s delivery ratio and causes longer delivery delay.

A great number of selfish nodes will damage the reliability of networks, and the experiment shows that when the number of selfish nodes increases to 10%–40%, the delivery ratio of the network will decrease by 16%–32% [4].

In order to decrease the number of selfish nodes in a network, a lot of work has been done. The main incentive methods to stimulate selfish nodes are divided into three kinds, which are based on reputation, virtual currency, and gaming, respectively.

1.1. Reputation Based Incentive Algorithms. Marti et al. [4] propose a routing protocol which can detect behaviors of neighbor nodes to improve performance of ad hoc networks. The protocol contains Watchdog and Pathrater. The Watchdog stores node reputation and finds misbehavior nodes, and the Pathrater is used to choose a routing path which does not include misbehavior nodes.

Buchegger and Le Boudec [6, 7] propose the CONFIDANT protocol which evolves from [4] and adds the mechanism that can obtain node's indirect neighborhoods' reputations. The CONFIDANT protocol achieves the goal of isolating and punishing selfish nodes very well.

We also propose a kind of an Accumulated Reputation Model [8] to stimulate the nodes to provide more accurate and truthful data in a Participatory Sensing System.

1.2. Virtual Currency Based Incentive Algorithms. In virtual currency based incentive algorithms each node usually owns equal virtual currency when initializing the network. In order to enhance mutual cooperation, a node will obtain some virtual currency after it helps others to relay packets. Accordingly, when a node asks for assistance from other nodes, it also should pay some virtual currency to them. Buttyan and Hubaux [9] propose a virtual currency based incentive algorithm to promote the cooperation in the network, and this kind of virtual currency is called "Nuglet."

In the domain of electronic commerce involving resource allocation, the well-known Vickrey-Clarke-Groves (VCG) mechanism [10–12] is efficient. A number of incentive mechanisms are proposed by exploiting VCG strategy, such as Ad Hoc-VCG [13], Corsac [14], Team [15], and RPP [16].

1.3. Gaming Based Incentive Algorithms. Gaming based approaches are good ways on modeling incentive processes using classical game theory [17].

The Ad Hoc-VCG algorithm is also a gaming based incentive algorithm. It is a reactive and cost-efficient routing protocol. The nodes are motivated to reveal their true costs for forwarding data. The protocol also guarantees that routing is done along the most cost-efficient path by paying to the intermediate nodes a premium over their actual costs for forwarding data packets.

Srinivasan et al. [18] propose a GTFT model which uses the tit for tat (TFT) strategy to balance profits among nodes. Zhang et al. [19] propose a game based incentive algorithm using four important context parameters and Kalman filtering for prediction.

Dynamic repeated game theory is appropriate to be used in stimulating nodes in opportunistic networks. In dynamic gaming, a node decides to cooperate or not by considering its opponent's last choice. Generally, a node prefers to refuse its opponent when noncooperation has been chosen by the opponent in current gaming phase. However, meeting opportunity is precious in opportunistic networks, so nodes should tolerate a certain level of noncooperation for maintaining good network performance.

In our previous work [20], we designed the original model of node-dependence-based dynamic gaming incentive (NDI) algorithm. We improved the NDI algorithm by using entropy weight method to calculate weights, providing a new reward method and doing more meaningful simulation in this paper.

The NDI algorithm provides a tolerance mechanism in which several times of refusal to relay packets are tolerable, while reward and punishment are also provided based on the node dependence degree.

The remainder of this paper is organized as follows. The system model is illustrated in Section 2; Section 3 specifies the NDI algorithm; extensive simulations have been done for performance evaluation in Section 4; Section 5 concludes the paper.

2. System Model

2.1. Basic Hypothesis

- (i) The opportunistic network is modeled as a graph $G = (V, E)$, where $V = (v_1, v_2, \dots, v_n)$ is the vertex set and E is the edge set. In addition, there exists a communication link if and only if two nodes are within the transmission range.
- (ii) The sizes of data packets over the opportunistic network are about the same, and it costs the same in sending and relaying packets.
- (iii) The network running time is divided into a series of time slices t_1, t_2, \dots, t_n , and each time slice guarantees that a packet can reach to another relay node or the destination node.
- (iv) All nodes can be trusted, with using existing trust models [21, 22]. Other reliability problems are not considered in this paper.

2.2. Node Data Structure. Each node i stores information of every other node j and updates it upon receiving a response to its relay request. The items of the data structure of node i is shown Table 1.

Description of each column of the data structure is detailed in the table. N_{ij} is not the total times that node j rejects node i , whereas it is just a relative value. When it is bigger than T_{ij} , node j will be punished by node i (see Section 3).

3. Algorithm Design

In this section, the node active coefficient (NAC) and the node isolation coefficient (NIC) are defined firstly, and then the node dependence degree is calculated on the basis of NAC, NIC, and T_{ij} . The node-dependence-based dynamic gaming incentive (NDI) algorithm is finally elaborated.

3.1. Node Dependence Degree

3.1.1. Node Active Coefficient. The node active coefficient (NAC) is the probability of a node to meet other nodes. The bigger the NAC is, the more the nodes it probably meets, and hence it has more opportunities to request others for relaying packets. The fuzzy set is exploited to define NAC, and its membership function is shown as formula (1). Consider

$$\alpha = \left[\alpha' + (1 - \alpha') \frac{x}{m} \right] \gamma, \quad (1)$$

where α is the NAC value and α' is the previous NAC value before updating. The number of nodes in the network is set to

TABLE 1: Data structure for node i .

Columns	Description
j	Identification of j
N_{ij}	Relative times that i has been rejected by j
T_{ij}	Tolerance times that i is rejected by j
F_{ij}	Flag for whether i is punishing j or not, Boolean type; flag = 1 means punishing
N_{ji}	Relative times that j has been rejected by i
T_{ji}	Tolerance times that j is rejected by i
F_{ji}	Flag for whether j is punishing i or not, Boolean type; flag = 1 means punishing.

m , x is the number of nodes that the node met during the last time period, and γ is an aging factor which falls in the range $[0, 1]$. Each node updates its NAC after a period of time by formula (1). When a node initializes, α and α' will be set to 0.5 which means the node is in a fuzzy state. The NAC value α will tend to be active or inactive through adjusting those parameters.

3.1.2. Node Isolation Coefficient. The node isolation coefficient (NIC) is the level of isolation in the network. If a node performs selfishly to another node for a number of times, it will be isolated by the node. The NIC value σ is calculated as follows:

$$\sigma = \frac{f + 1}{g + 1}, \quad (2)$$

where g is the total number that a node meets and f is the number of the nodes which are isolating the node.

If a node accumulated a high NIC value, the nodes which are isolating it will refuse to relay its packets even though it has a high NAC value.

3.1.3. Node Dependence Degree. The node dependence degree (NDD) is the degree to which a node relies on another node.

It is widely acknowledged that the communications are usually fulfilled through multiple hops in opportunistic networks. The source node might never meet the destination node, so the source node also cannot know exactly which intermediate nodes relay the packets to the destination node. It is hard to calculate NDD by the records of successful relay and hit on destination, because it has no idea which node helped it. Here, we approximately calculate NDD through NAC, NIC, and T_{ji} . High NAC and T_{ji} will lead to low NDD, and similarly high NIC results in high NDD.

An entropy weighted method is proposed to calculate NDD with different weights. NDD is computed through current and historical values of NAC, NIC, and T_{ji} . The entropy weighted method is a method determining weights objectively.

Firstly, a 3×3 evaluation matrix is used to record NAC, NIC, and T_{ji} in recent three times. The evaluation matrix is shown as (3). The first row stands for values that the node possesses currently.

Consider

$$R = \begin{pmatrix} r_{11} & r_{12} & r_{13} \\ r_{21} & r_{22} & r_{23} \\ r_{31} & r_{32} & r_{33} \end{pmatrix}. \quad (3)$$

And each row is valued through (4), where w ranges from 1 to 3.

Consider

$$\begin{aligned} r_{w1} &= (1 - \alpha)_w, \\ r_{w2} &= \sigma_w, \\ r_{w3} &= \left(\frac{1}{\sqrt{T_{ji}}} \right)_w. \end{aligned} \quad (4)$$

The entropy method is used to obtain the weight of each column in matrix R .

Consider

$$z_{wv} = \frac{r_{wv}}{\sum_{w=1}^3 r_{wv}}. \quad (5)$$

Firstly, z_{wv} is defined using (5), where v varies from 1 to 3. Then, entropy for each column can be calculated as shown in (6), where $c = 1/\ln 3$.

Consider

$$e_v = -c \sum_{w=1}^3 z_{wv} \ln z_{wv}. \quad (6)$$

Define $W = (w_1 \ w_2 \ w_3)$ as the weight vector; each element is calculated by

$$w_v = \frac{(1 - e_v)}{\sum_{v=1}^3 (1 - e_v)}. \quad (7)$$

The current NDD value Ψ can be obtained through

$$\text{NDD} = W \circ R_1^T = (w_1 \ w_2 \ w_3) \circ (r_{11} \ r_{12} \ r_{13})^T. \quad (8)$$

Because the weight should be calculated through three-time contact of two nodes, the weights are initialized to 1/3 in the first two contacts.

3.2. Dynamic Gaming. The process of requesting to relay packets between two nodes can be regarded as a gaming process.

Each node has a strategy space $S = \{C, D\}$, where C represents "accept relay request of its opponent," and D stands for "refuse to relay." During every stage of the gaming process, a node will choose a strategy from its strategy space. For a one-stage gaming, the two counterparts only care about one-time profit, and the payoff matrix is shown in Table 2.

If two nodes do not cooperate with each other, they have no benefit or consumption. In such case, both parts acquire 0 profits.

Apparently, when two nodes only care about one-time profit they will reach to $\{D, D\}$, which is not expected to

TABLE 2: Payoff matrix for one-stage gaming.

Strategy	j : C	j : D
i : C	$i = v - c, j = v - c$	$i = -c, j = v$
i : D	$i = v, j = -c$	$i = 0, j = 0$

c is the cost for helping a node to relay a packet, including resources consumptions and so forth; the benefit one node obtains because of opponent's cooperation is represented by v .

see in an opportunistic network. All nodes choosing not to cooperate will ruin the network.

Fortunately a repeated gaming is a good choice to reach a subgame perfect Nash equilibrium and achieve mutual cooperation [21].

In this paper, the node-dependence-based dynamic gaming incentive (NDI) algorithm is proposed which stimulates nodes to cooperate on data forwarding by elaborate design of a subgame perfect Nash equilibrium.

Node j chooses to accept or refuse upon receiving a packet relay request from node i while node i will consider whether to reward or punish node j according to its response based on the node dependence degree (NDD).

In NDI, node i rewards or punishes node j by increasing or decreasing tolerance times T_{ij} . If the punishment tends to high, a selfish node will be likely to suspend its selfish behavior in time. When a node is highly dependent on another one, it will reward the node properly.

If a node is a common node, it will unconditionally help others to relay packets, unless it has objective reasons to refuse, such as node j is transmitting data, buffer is full, and so forth. If a node is a selfish node, when it wants to reject other nodes' request, it should consider its condition and whether other nodes will punish it or not.

Let $U(\infty, \delta)$ stand for an infinite repeated gaming process between node i and node j , where δ is a weight coefficient to indicate the extent of addressing future profit. The bigger the δ is, the more the node pays attention to future profit. Table 3 shows the profit sequence for node j when both counterparts choose to cooperate [23].

The profit that a common node j obtains is calculated as formula (9). Consider

$$(v - c) + \delta(v - c) + \delta^2(v - c) + \dots = \frac{v - c}{1 - \delta}. \quad (9)$$

Similarly, the profit that a common node i obtains is also $(v - c)/(1 - \delta)$. If the profit of a node is over $(v - c)/(1 - \delta)$, it means that the node has chosen to be selfish during previous gaming. If node i tolerated node j 's noncooperation for T_{ij} times in an infinite repeated gaming, the maximum total profit of node j would reach to $((v - c)/(1 - \delta)) + c(\delta^{q_1} + \delta^{q_2} + \dots + \delta^{q_x})$ (q_1, q_2, \dots, q_x are the superscripts of T_{ij} profit items when node j rejects node i). Based on the profit of node j , we can adjust the maximum total profit of node j by changing T_{ij} . The NDI algorithm is detailed in Algorithm 1.

Where $f(T_{ij})$ is the punishment function and $g(T_{ij})$ is the reward function. The intensity of punishment method is $T_{ij} - f(T_{ij})$, and the intensity of reward method is $g(T_{ij}) - T_{ij}$.

The punishment function should rely on NDD. If NDD is big, it means "I rely on you a lot"; the punishment strength should be lower. On the contrary, if NDD is small, it means "I rely on you little"; the punishment strength can be higher than with bigger NDD. The reward function actually should be steadier than punishment method. In practice, the cooperation should be continuous and steady. A node also should consider the NDD value. The bigger the NDD is, the more heavily it should be rewarded by the other one.

Based on the above analysis, the punishment function and the reward function should meet the following conditions.

- (1) The punishment is designed to be heavier than the rewarding which helps to keep the balance of cooperation, so the condition $(T_{ij} - f(T_{ij})) > (g(T_{ij}) - T_{ij})$ should be met.
- (2) In order to stimulate nodes to help other relay packets, approaches for rewarding nodes are proposed. T_{ij} should increase steadily, when counterparts cooperate with each other for a long time. In other words, $g(T_{ij})$ should be a linear function to ensure the increase of T_{ij} .
- (3) Accordingly, to punish nodes which would not like to cooperate with each other, the function $f(T_{ij})$ should lower others' T_{ij} . The punishment method follows the principle that the more I "trust" you, the more the intensity of punishment is if you betray me. The intensity of punishment will be heavier with the increase of T_{ij} .

Based on the above analysis, the punishment method is designed as formula (10), and the reward function is designed as formula (11).

Because NDD varies from 0 to 1, the level of reward and punishment can be adjusted according to the NDD value. Consider

$$f(T_{ij}) = \lfloor (1 + \Psi) \sqrt{T_{ij}} \rfloor, \quad (10)$$

$$g(T_{ij}) = \lfloor 2\Psi + T_{ij} \rfloor. \quad (11)$$

Figure 1(a) depicts formula (10) with different Ψ . It is clear to conclude that T_{ij} will be decreased after being recalculated by $f(T_{ij})$, which satisfies the abovementioned conditions.

The initial value of T_{ij} should be set by considering different conditions of opportunistic networks. And T_{ij} is usually set as 4, and the value of $1/\sqrt{T_{ji}}$ equals 0.5.

The punishment intensity with different Ψ is shown in Figure 1(b). With the increase of T_{ij} , the intensity of punishment is also improved faster. It meets the principle that the more I "trust" you, the more the intensity of punishment will be if you betray me.

From Figure 1(b), it is verified that the smaller the node dependence degree (NDD) is, the heavier the punishment intensity is. The punishment intensity is higher with the increasing of T_{ij} and Ψ .

Formula (11) with different Ψ is depicted in Figure 1(c), which also satisfies the conditions proposed above.

TABLE 3: Profit sequence for node j .

Stage	1	2	...	T	...
Choice set	{C, C}	{C, C}	...	{C, C}	{C, C}
Profit for node j	$v - c$	$v - c$...	$v - c$	$v - c$

```

(1) Initialize the parameters in Table 1 and the weight coefficient  $\delta$  when nodes encounter
    at the first time, and Calculate NAC, NIC, and NDD.
(2) Node  $i$  asks node  $j$  for relaying a packet, and waits for  $j$ 's response.
(3) if  $j$  rejects  $i$ 
(4)   if  $F_{ij} == \text{false}$ 
(5)      $N_{ij} \leftarrow N_{ij} + 1$ 
(6)   end if
(7)   if  $F_{ij} == \text{false}$  and  $N_{ij} \geq T_{ij}$ 
(8)      $F_{ij} \leftarrow \text{true}$ 
(9)      $T_{ij} \leftarrow f(T_{ij})$ 
(10)  end if
(11) else
(12)   if  $F_{ij} == \text{true}$ 
(13)      $N_{ij} \leftarrow N_{ij} - 1$ 
(14)     if  $N_{ij} \leq T_{ij}$ 
(15)        $F_{ij} \leftarrow \text{false}$ 
(16)     end if
(17)   end if
(18)   if  $j$  is not punished for a time period  $T$ 
(19)      $T_{ij} \leftarrow g(T_{ij})$ 
(20)   end if
(21) end if

```

ALGORITHM 1: The Node-dependence-based dynamic gaming incentive algorithm.

$g(T_{ij})$ is a linear function, the reward of each time is 2Ψ , and $g(T_{ij})$ satisfies the fact that T_{ij} should be increase steadily.

In addition, the reward and punishment history may also be leveraged when calculating the $f(\Psi)$ and $g(\Psi)$. This is left to future study.

When a selfish node j is “smart” enough, it will not reject i after rejecting it for T_{ij} times; otherwise, it will be punished by node i and has to return back much profit if it wants to be forgiven by node i . So a “smart” node will choose to cooperate after rejecting another one for T_{ij} times. So a “smart” selfish node will always perform rationally to obtain high profit.

The profit sequence of a “smart” selfish node is shown in Table 4. It shows that T_{ij} decides the maximum m profit that node j could obtain and the maximum loss that node i would suffer.

The maximum loss for node i and the maximum profit for node j can be calculated by formulas (12) and (13), respectively. Consider

$$c + \delta c + \dots + \delta^{T_{ij}-1} c = \frac{c(1 - \delta^{T_{ij}})}{1 - \delta}, \quad (12)$$

$$v + \delta v + \dots + \delta^{T_{ij}-1} v = \frac{v(1 - \delta^{T_{ij}})}{1 - \delta}. \quad (13)$$

When the profit of node j obtained because of selfish behaviors exceeds $v(1 - \delta^{T_{ij}})/(1 - \delta)$, node i will severely punish node j . Whereas a selfish node j has to cooperate when N_{ij} approaches T_{ij} in case it will be punished.

If two nodes encountered for several times and if the condition of Line 6 in Algorithm 1 holds in these rounds, T_{ij} will finally be set to 1. This is a kind of classical gaming method, known as “tit for tat (TFT)” [16]. This method advocates “Deal with a man as he,” and it is an alternative to promote long-term cooperation. We simulate NDI and this method for performance comparison in Section 4.3.

Except for punishment, the NDI algorithm also provides a reward mechanism. When node j always chooses to cooperate upon receiving packet relay requests of i for a time period T , node i will reward node j as shown in formula (11). This will encourage nodes to relay packets and hence promote efficiency of the network.

The following will analyze the profits when a node is “smart,” “stupid,” or “ordinary.”

Ignoring the node’s attention to the further profits δ , a node’s profit mainly relies on the T_{ij} . As said above, maintaining a high T_{ij} is a good strategy to obtain a high profit. However, NDI is an incentive algorithm to stimulate nodes by changing T_{ij} . N_{ij} can stand for the profit that a node obtains.

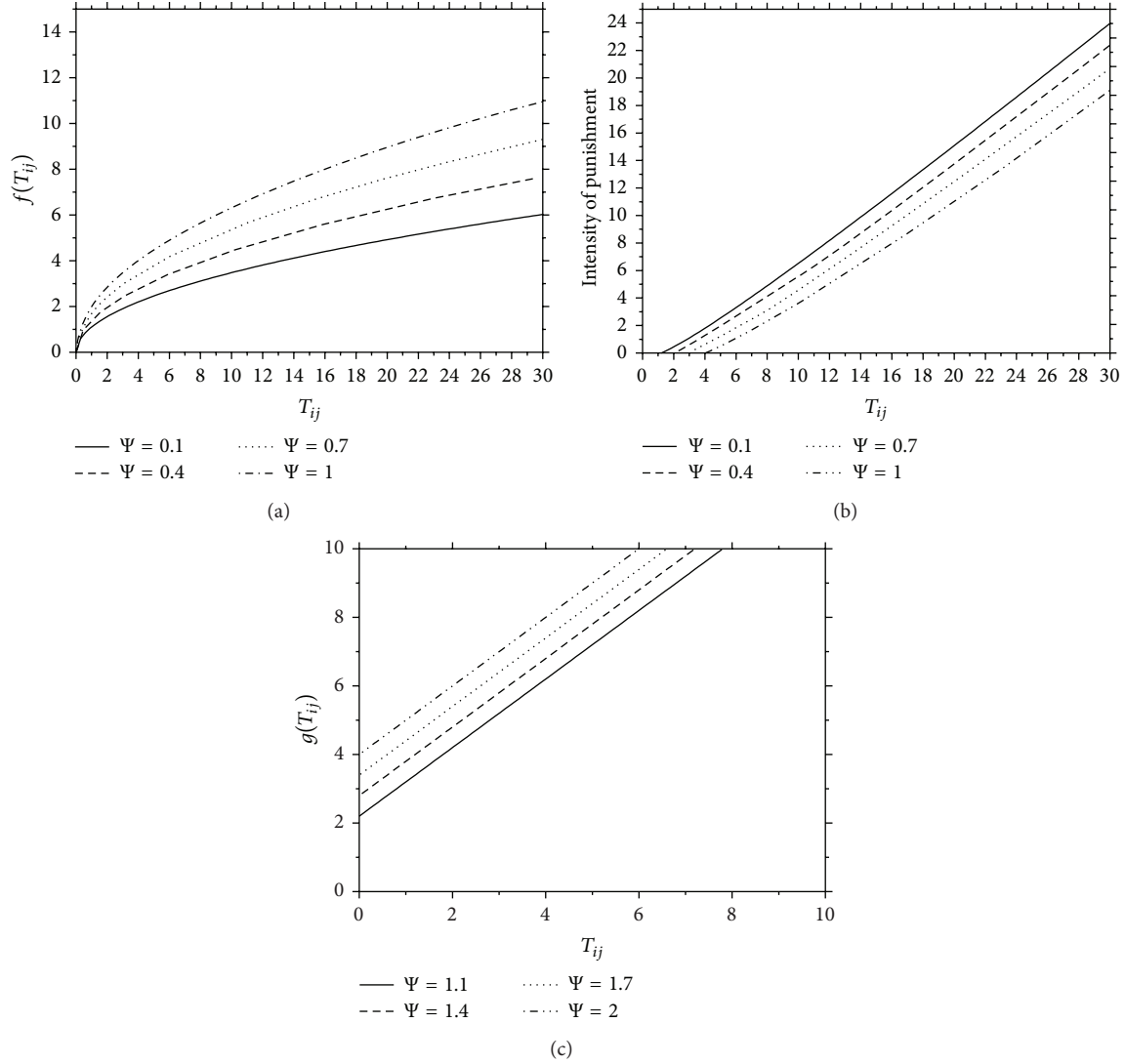


FIGURE 1: (a) $f(T_{ij})$ with different Ψ . (b) Punishment intensity with different Ψ . (c) $g(T_{ij})$ with different Ψ .

TABLE 4: Profit sequence when node j is a “smart” selfish node.

Stage	1	...	T	...	$T + T_{ij}$
Choice	{C, C}	{C, C}	{C, D}	{C, D}	{C, D}
Profit sequence for node i	$v - c$	$v - c$	$-c$	$-c$	$-c$
Profit sequence for node j	$v - c$	$v - c$	v	v	v

A “smart” selfish node would like to reject other nodes’ request $T_{ij} - 1$ times, where it can obtain the highest profit and will not be punished at the same time. With the time passing, the profits can be described as in Figure 2(a). The initial T_{ij} is set as 8 in Figure 2(a), and the NDI algorithm is added in it.

A “smart” selfish node will not be punished because it always rejects others $T_{ij} - 1$ times. However, the T_{ij} will be increased because of the rewarding of long time cooperation.

A “stupid” selfish node will not cooperate with others at any time, and the profit of a “stupid” selfish node is shown in Figure 2(b).

As shown in Figure 2(b), this kind of selfish node hardly obtains profit from others. So it must choose cooperation to improve its T_{ij} which can improve its profit.

An “ordinary” selfish node is a kind of node that acts more in reality; it will firstly choose noncooperation. After finding the high decreasing of profit, it will try its best to improve its

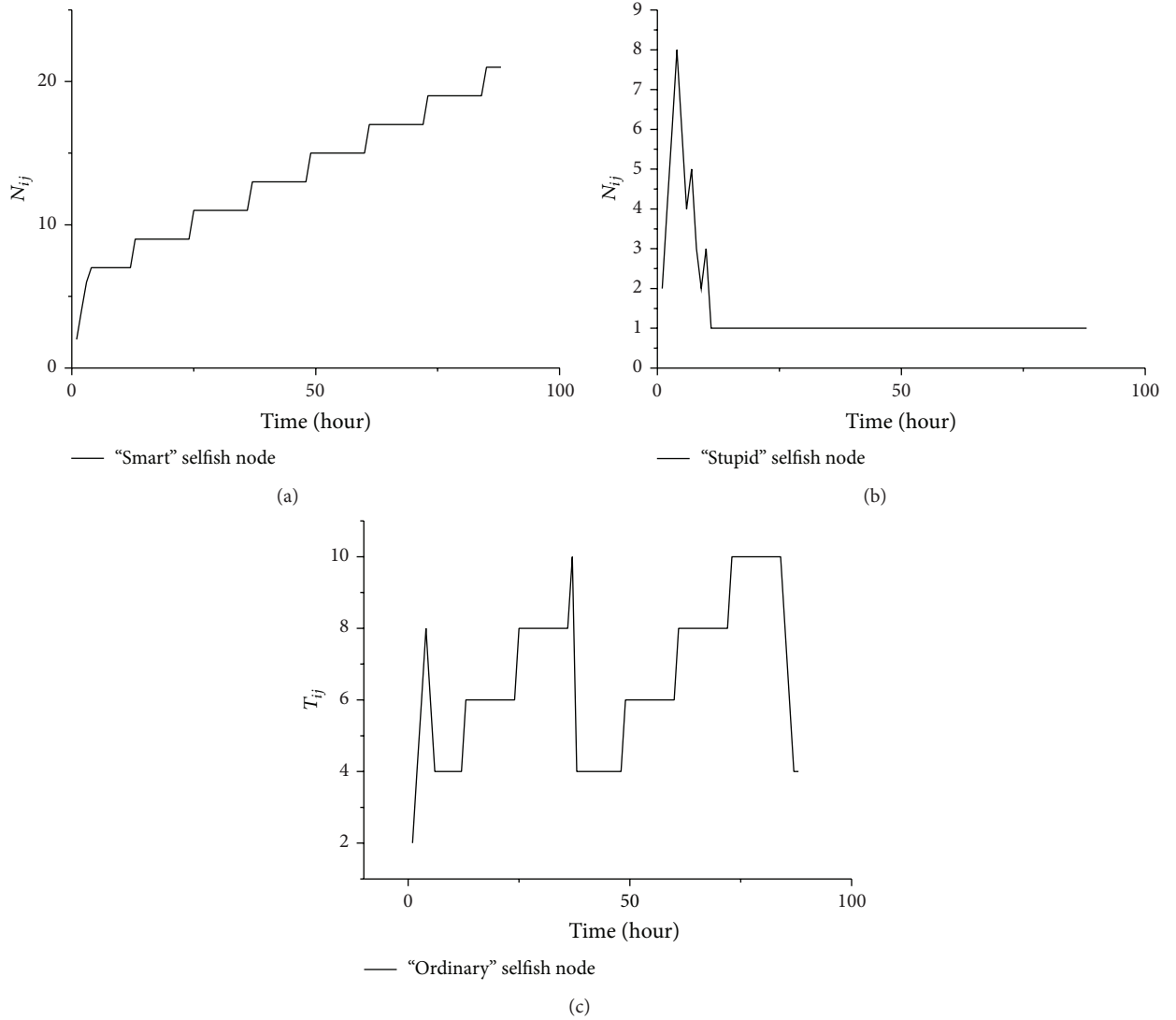


FIGURE 2: (a) The profit of "smart" selfish node with time increasing. (b) The profit of "stupid" selfish node with time increasing. (c) The profit of "ordinary" selfish node with time increasing.

profit and maintain it. The profit of an ordinary selfish node can be described as in Figure 2(c).

The profit of an "ordinary" node firstly increases quickly, and then the node will be punished. After that, the "ordinary" node notices that it must cooperate to improve its profit, so it will choose to help others to relay packets.

In conclusion, if a node chooses to cooperate, it will obtain a higher profit than these which chose not to cooperate.

4. Simulation Analysis

Simulations are run on the opportunistic networking environment (ONE) [24, 25] which is developed by Helsingin Yliopisto. ONE simulator is a simulator designed especially for opportunistic networks.

4.1. Evaluation Criteria. In order to verify the effectiveness of the NDI algorithm, delivery ratio (*delivery_ratio*), delivery delay (*delivery_delay*), and average hop count (*hopcount_avg*) are chosen for evaluation criteria.

The delivery ratio is the ratio between the number of packets which are delivered to the destination nodes successfully and the number of all packets that are created in networks. This is a critical criterion to value the performance of a routing algorithm [26]. The delivery ratio (*delivery_ratio*) is calculated by formula

$$delivered_prob = \frac{delivered}{created}, \quad (14)$$

where *delivered* is the number of packets that have been delivered successfully and *created* is the number of packets that has been created in the network.

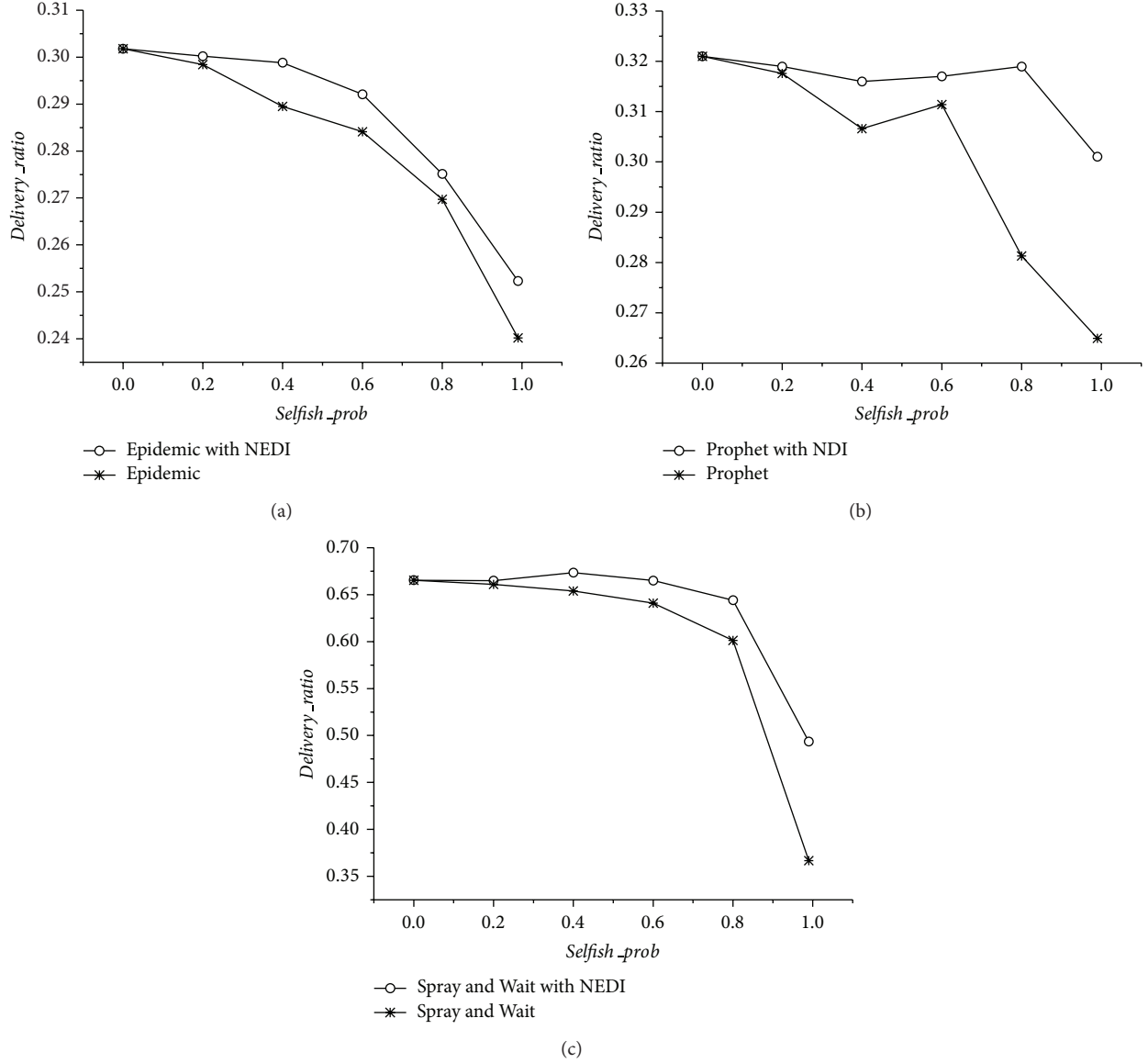


FIGURE 3: (a) The delivery ratio of Epidemic with and without NDI. (b) The delivery ratio of Prophet with and without NDI. (c) The delivery ratio of Spray and Wait with and without NDI.

Delivery delay is the time period from when a packet is created to when it is delivered successfully. Because environments of networks are different and delivery delays of all packets are not the same, the average delivery latency (*latency_avg*) is used to evaluate the algorithm performance. The smaller the average delivery latency is, the better the performance the algorithms have.

Hop count is the number of relay nodes on the path from the source to the destination. Average hop count (*hopcount_avg*) is used to value performance of networks, and the smaller the better.

To simulate the impact of nodes' selfish behaviors on evaluation criteria (delivery ratio, delivery delay, and average hop count), the concept of selfish probability (*selfish_prob*) is put forward. The selfish probability is the probability of nodes choosing to reject packet relay requests.

4.2. Simulation I

4.2.1. Simulation Setup. Three routing algorithms including Epidemic [27], Prophet [28], and Spray and Wait [29] are used in simulation I to simulate the NDI algorithm.

The Helsinki city is chosen as the scene, where there are 160 mobile nodes divided into two groups. Each node is equipped with a Bluetooth device, and the communication radius of nodes is set to 10 meters. The time period T for rewarding a node is 6 hours. More settings can be found in Table 5.

4.2.2. Delivery Ratio. Simulations are carried out at different selfish probabilities using Epidemic, Prophet, and Spray and Wait with or without NDI algorithm, respectively.

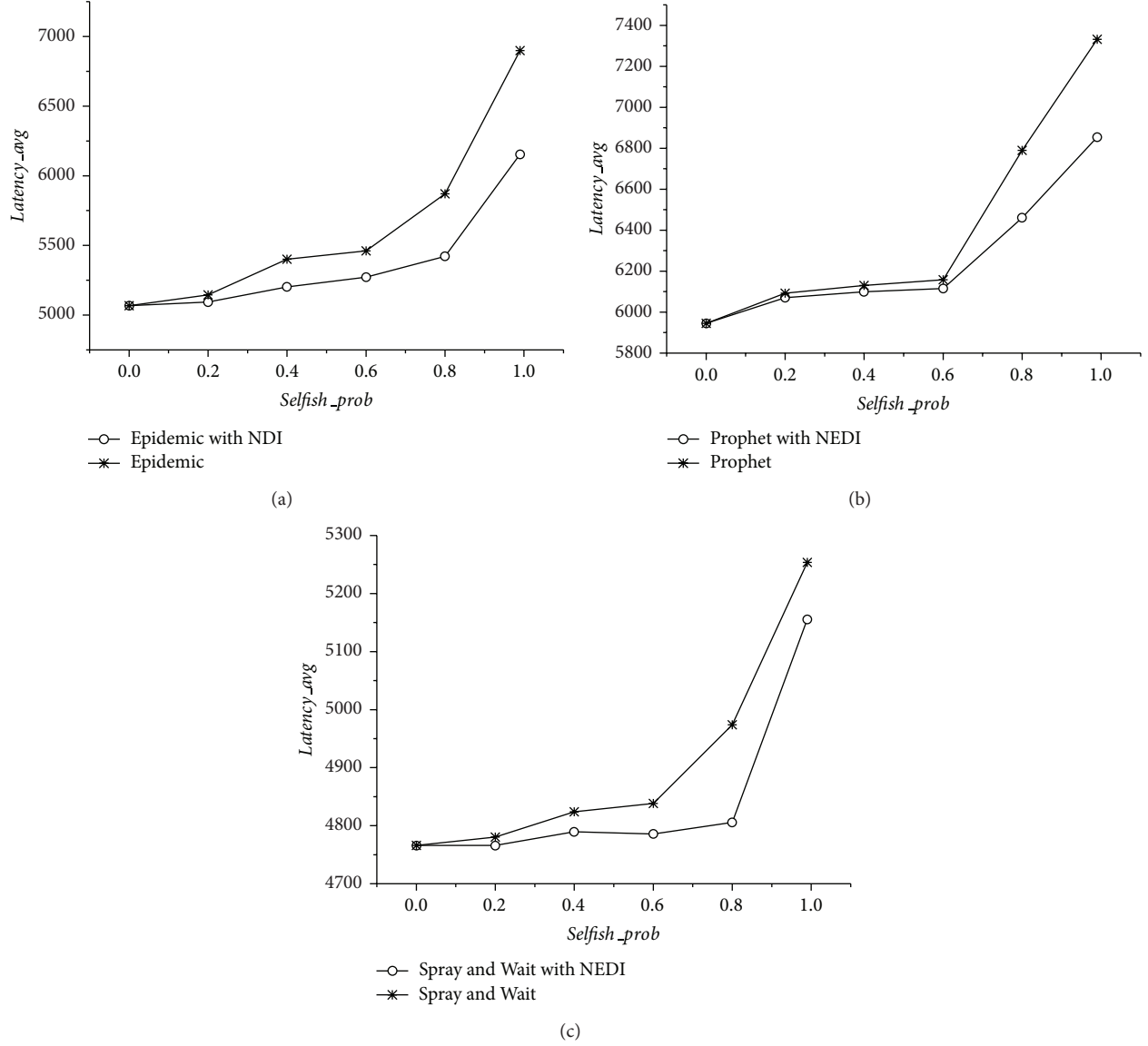


FIGURE 4: (a) The average latency of Epidemic with and without NDI. (b) The average latency of Prophet with and without NDI. (c) The average latency of Spray and Wait with and without NDI.

TABLE 5: Parameter settings for simulation I.

Type	Parameter	Value
Scene features	Simulation time	24 h
	Field area	4500 m * 3400 m
	Scene	Helsinki
Node features	Mobility model	SPMBM
	Movement speed	0.5–1.5 m/s
	Transmission rate	250 KB/s
	Maximum transmission range	10 m
	Transmission mode	Broadcast
	Cache size	10 MB
Message features	Packet size	500 KB–1 MB at random
	TTL	5 h
	Frequency of creating packets	From 25 s to 35 s at random

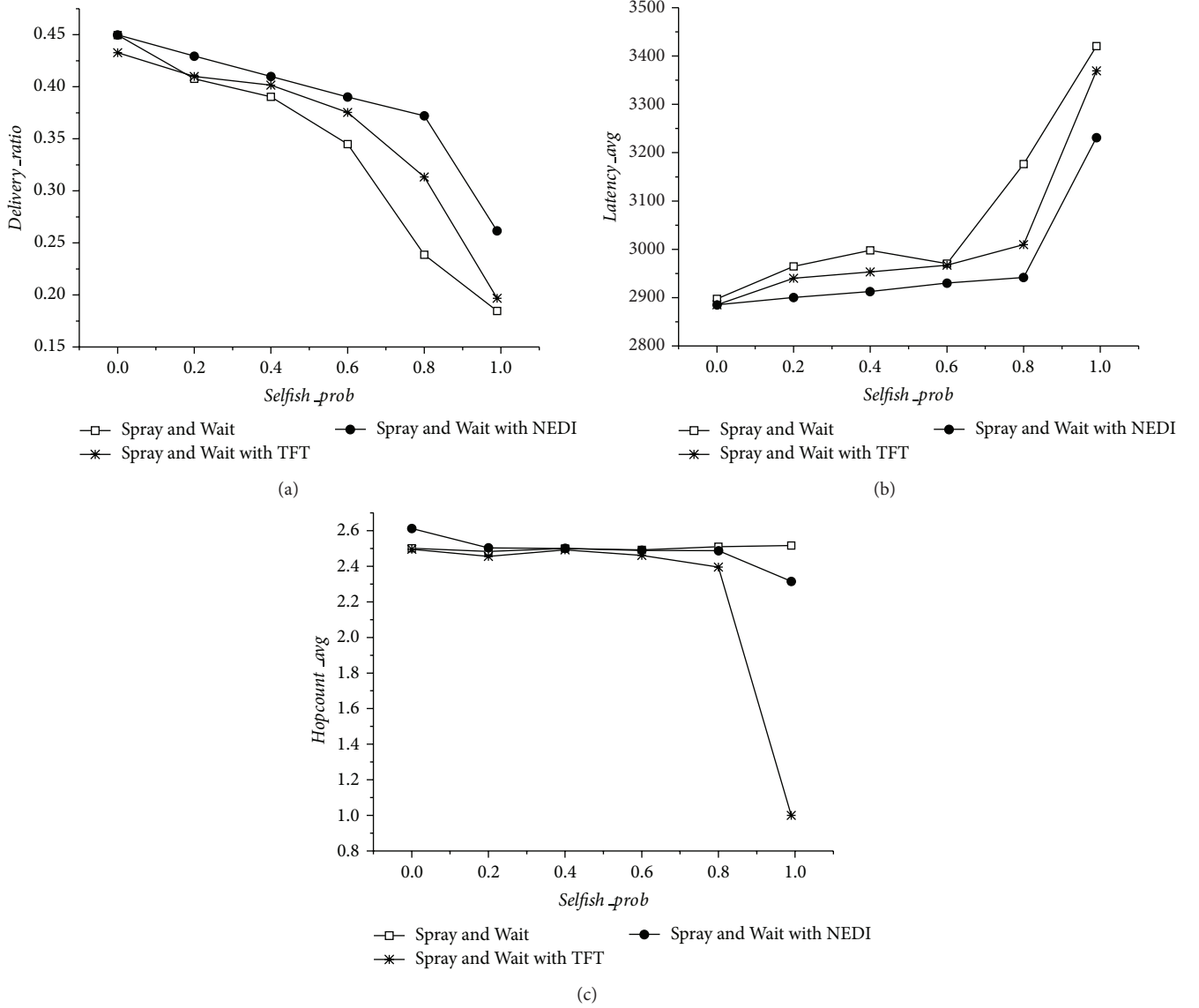


FIGURE 5: (a) The delivery ratio of three algorithms. (b) The average latency of three algorithms. (c) The average hop count of three algorithms.

The delivery ratio at different selfish probabilities is shown in Figure 3.

The simulations show that the NDI algorithm increases the packet delivery ratio in all three routing algorithms at almost every selfish probability, especially in the Spray and Wait scheme. While the selfish probability increases, the improvement tends to be higher.

The Spray and Wait routing algorithm limits the packet copies, so the NDI algorithm does not have so much effect on it; however, it still can get remarkable improvement on the delivery ratio when the selfish probability is over 60%.

4.2.3. Delivery Delay. The delivery delay of three routing algorithms with and without the NDI algorithm at different selfish probabilities is shown in Figure 4.

As mentioned above, the average latency averages the delay of all successful routing. When the selfish probability increases, the average latency increases accordingly. In all three routing schemes, the NDI algorithm makes them more efficient on delivering packets to the destinations. It is obvious that the NDI algorithm presents better performance along with the selfish probability increasing.

The curves of routing schemes with NDI are much flatter than the original ones, which show that the NDI algorithm has positive effect on lowering transmission latency of packet no matter how selfish the nodes are.

4.3. Simulation II. From simulation I, the Spray and Wait routing algorithm exhibits better performance than the other

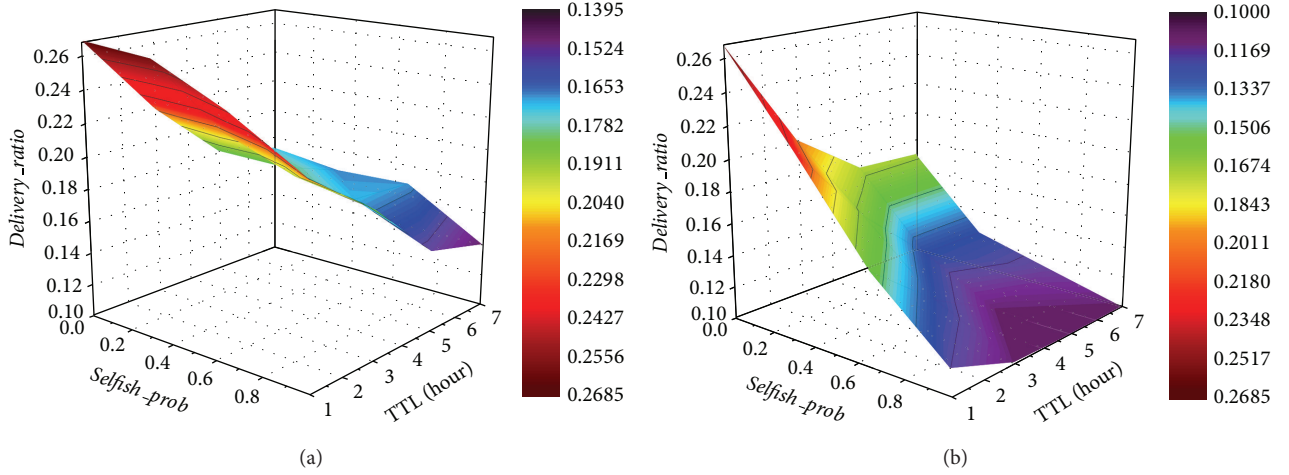


FIGURE 6: (a) The relationship among selfish probability, TTL, and delivery ratio with NDI. (b) The relationship among selfish probability, TTL, and delivery ratio without NDI.

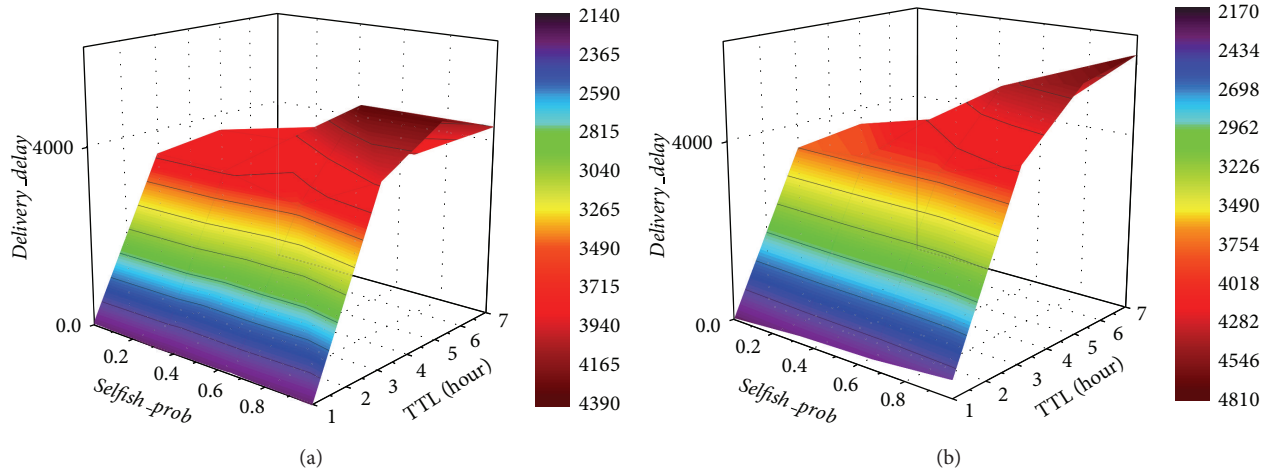


FIGURE 7: (a) The relationship among selfish probability, TTL, and delivery delay with NDI. (b) The relationship among selfish probability, TTL, and delivery delay without NDI.

two ones, so we use simulate the Spray and Wait routing algorithm in simulation II. The TFT method [16] is introduced for performance comparison.

4.3.1. Simulation Setup. The Helsinki city is also chosen as the scene, where there are 160 mobile nodes divided into four groups, including 3 pedestrian groups and a car group. Each node is equipped with a Bluetooth device, and the time period T for rewarding a node is 6 hours. More settings are detailed in Table 6.

4.3.2. Delivery Ratio. Simulations are run under different selfish probabilities which are 0, 0.2, 0.4, 0.6, 0.8, and 0.99, respectively. The delivery ratios of the Spray and Wait algorithm and the other two variations (with NDI and TFT) are shown in Figure 5(a).

The Spray and Wait with NDI algorithm is much better than the original one and the TFT variation on packet

delivery probability. The Spray and Wait with TFT algorithm lowers down the delivery ratio when the selfish probability is zero. TFT algorithm will result in a worse performance than the NDI algorithm when selfish probability gets higher.

The reason lies in the “Deal with a man as he” mechanism of TFT algorithm. If a node is rejected by its opponent, it will immediately punish the opponent by rejecting any relay request. The NDI algorithm overcomes this drawback and hence performs much better than the TFT scheme.

4.3.3. Delivery Delay. The average latency at different selfish probabilities for each algorithm is shown in Figure 5(b). The Spray and Wait with NDI algorithm has an optimization compared with TFT algorithm on average latency, while the Spray and Wait with TFT algorithm incurs a little higher latency than that with NDI algorithm when the selfish probability increases. This is also an effect of the “tit for tat.” Higher

TABLE 6: Parameter settings for simulation II.

Type	Parameter	Value
Scene features	Simulation time	12 h
	Field area	4500 m * 3400 m
	Scene	Helsinki
Node features	Mobility model	SPMBM
	Movement speed for cars	2.7–13.9 m/s
	Movement speed for pedestrian	0.5–1.5 m/s
	Transmission rate	250 KB/s
	Maximum transmission range	10 m
	Transmission mode	Broadcast
	Cache size	5 MB
Message features	Packet size	500 KB–1 MB at random
	TTL	5 h
	Frequency of creating packets	From 25 s to 35 s at random

TABLE 7: Parameter settings for simulation III.

Type	Parameter	Value
Scene features	Simulation time	12 h
	Field area	4500 m * 3400 m
	Scene	Helsinki
Node features	Mobility model	SPMBM
	Movement speed for cars	2.7–13.9 m/s
	Movement speed for pedestrian	0.5–1.5 m/s
	Transmission rate	250 KB/s
	Maximum transmission range	10 m
	Transmission mode	Broadcast
	Cache size	100 MB
Message features	Packet size	500 KB–1 MB at random
	Frequency of creating packets	From 25 s to 35 s at random

chance of nodes' rejection on packet relay inevitably leads to higher latency when delivering packet to its destination.

4.3.4. Average Hop Count. The average hop count for each algorithm is shown in Figure 5(c). When the selfish probabilities increase, the average hop count of packed delivery is slightly smaller in the NDI and TFT variations of the Spray and Wait algorithm.

The most attractive point is when selfish probability is 0.99; the average hop count of the Spray and Wait with TFT algorithm is approximated to 1. The reason is that when the selfish probability is big enough, nodes would not like to relay packets for other nodes and most nodes will deliver their packets directly to the destinations. However, the Spray and Wait with NDI algorithm has adequate tolerance to the rejection of relay requests, so it performs well in this scenario.

4.4. Simulation III. The Epidemic routing algorithm [23] is simulated for performance measure in simulation III, because it does not limit the number of message copies.

4.4.1. Simulation Setup. There are 160 mobile nodes which are divided into four groups, including 3 pedestrian groups and a car group. Each node is equipped with a Bluetooth chip, and the time period T for rewarding a node is 3 hours. More settings are detailed in Table 7.

4.4.2. Delivery Ratio. The relationship among selfish probability, TTL, and delivery ratio is investigated, and the result is shown in Figure 6. Due to the fixed size of cache, the delivery ratio decreases even though the TTL is increasing. However, the approach with NDI performs better than the one without NDI on the descending rate. Simulation results also show that higher selfish probability leads to less delivery ratio.

4.4.3. Delivery Delay. Figure 7 shows the relationship among selfish probability, TTL, and delivery delay. As depicted in Figures 7(a) and 7(b), TTL affects the delivery delay very much. Larger TTL causes higher delay. When the selfish probability increases, the approach with NDI can suppress the delay increase compared to the one without NDI.

5. Conclusion

To stimulate nodes to cooperate on data forwarding in opportunistic networks, the node-dependence-based dynamic gaming incentive (NDI) algorithm is proposed by elaborate design of a subgame perfect Nash equilibrium in a dynamic repeated gaming process. The NDI algorithm provides a mechanism where several times of refusal to relay packets are tolerant, and reward and punishment methods are also designed based on the node dependence degree.

Extensive simulations are implemented for performance evaluation. The results show that the NDI algorithm is effective in increasing the delivery ratio and decreasing average latency when there are a lot of selfish nodes in the opportunistic networks.

Conflict of Interests

The authors declare that there is no conflict of interests regarding the publication of this paper.

Acknowledgments

This work is supported by the National Natural Science Foundation of China under Grant no. 61272529 and the Fundamental Research Funds for the Central Universities under Grants no. N120417002 and no. N130817003.

References

- [1] P. Juang, H. Oki, Y. Wang, M. Martonosi, L.-S. Peh, and D. Rubenstein, "Energy-efficient computing for wildlife tracking: design tradeoffs and early experiences with ZebraNet," in *Proceedings of the 10th International Conference on Architectural Support for Programming Languages and Operating Systems*, pp. 96–107, New York, NY, USA, October 2002.
- [2] P. Hui, A. Chaintreau, J. Scott, R. Gass, J. Crowcroft, and C. Diot, "Pocket switched networks and human mobility in conference environments," in *Proceedings of the ACM SIGCOMM Workshop on Delay-Tolerant Networking (WDTN '05)*, pp. 244–251, Philadelphia, Pa, USA, August 2005.
- [3] B. Hull, V. Bychkovsky, Y. Zhang et al., "CarTel: a distributed mobile sensor computing system," in *Proceedings of the 4th International Conference on Embedded Networked Sensor Systems*, pp. 125–138, 2006.
- [4] S. Marti, T. J. Giuli, K. Lai, and M. Baker, "Mitigating routing misbehavior in mobile ad hoc networks," in *Proceedings of the 6th Annual International Conference on Mobile Computing and Networking (MOBICOM '00)*, pp. 255–265, Boston, Mass, USA, August 2000.
- [5] C.-L. Chiou and L.-J. Chen, "An evaluation study of routing reliability in opportunistic networks," in *Proceedings of the 9th ACM International Symposium on Mobile Ad Hoc Networking and Computing (MobiHoc '08)*, pp. 455–456, Hong Kong, May 2008.
- [6] S. Buchegger and J. Y. Le Boudec, "Performance analysis of the CONFIDANT protocol (Co-operation of nodes: fairness in dynamic Ad Hoc networks)," in *Proceedings of the IEEE/ACM Workshop on Mobile Ad Hoc Networking and Computing*, pp. 226–236, Lausanne, Switzerland, 2002.
- [7] S. Buchegger and J.-Y. Le Boudec, "Self-policing mobile ad hoc networks by reputation systems," *IEEE Communications Magazine*, vol. 43, no. 7, pp. 101–107, 2005.
- [8] R. Yu, R. Liu, X. Wang, and J. Cao, "Improving data quality with an accumulated reputation model in participatory sensing systems," *Sensors*, vol. 14, no. 3, pp. 5573–5594, 2014.
- [9] L. Buttyan and J. P. Hubaux, "Nuglets: a virtual currency to stimulate cooperation in self-organized mobile Ad Hoc networks," Tech. Rep. DSC/2001/001, Swiss Federal Institute of Technology (EPFL), 2001.
- [10] W. Vickrey, "Counterspeculation, auctions, and competitive sealed tenders," *Journal of Finance*, vol. 16, no. 1, pp. 8–39, 1961.
- [11] E. H. Clarke, "Multipart pricing of public goods," *Public Choice*, vol. 11, no. 1, pp. 17–33, 1971.
- [12] T. Groves, "Incentives in teams," *Econometrica*, vol. 41, pp. 617–631, 1973.
- [13] L. Anderegg and S. Eidenbenz, "Ad hoc-VCG: a truthful and cost-efficient routing protocol for mobile ad hoc networks with selfish agents," in *Proceedings of the 9th Annual International Conference on Mobile Computing and Networking (MobiCom '03)*, pp. 245–259, ACM Press, New York, NY, USA, September 2003.
- [14] S. Zhong, L. E. Li, Y. G. Liu, and Y. R. Yang, "On designing incentive-compatible routing and forwarding protocols in wireless ad-hoc networks : an integrated approach using game theoretic and cryptographic techniques," *Wireless Networks*, vol. 13, no. 6, pp. 799–816, 2007.
- [15] J. Cai and U. Pooch, "Play alone or together—truthful and efficient routing in wireless ad hoc networks with selfish nodes," in *Proceedings of the IEEE International Conference on Mobile Ad-Hoc and Sensor Systems (MASS '04)*, pp. 457–465, Washington, DC, USA, October 2004.
- [16] M.-Y. Wu and W. Shu, "RPF: a distributed routing mechanism for strategic wireless ad hoc networks," in *Proceedings of the IEEE Global Telecommunications Conference (GLOBECOM '04)*, pp. 2885–2889, Washington, DC, USA, December 2004.
- [17] D. Fudenberg and J. Tirole, *Game Theory*, MIT Press, Boston, Mass, USA, 1991.
- [18] V. Srinivasan, P. Nuggehalli, C. F. Chiasserini, and R. R. Rao, "Cooperation in wireless ad hoc networks," in *Proceedings of the 22nd Annual Joint Conference on the IEEE Computer and Communications Societies*, pp. 808–817, April 2003.
- [19] C. Zhang, Q.-S. Zhu, and Z.-Y. Chen, "Game-based data-forward decision mechanism for opportunistic networks," *Journal of Computers*, vol. 5, no. 2, pp. 298–305, 2010.
- [20] R. Yu, P. Wang, and Z. Zhao, "NDI: node dependence-based dynamic gaming incentive algorithm in opportunistic networks," in *Proceedings of the 23rd International Conference on Computer Communications and Networks (ICCCN '14)*, pp. 581–588, Shanghai, China, 2014.
- [21] J. Jiang, G. Han, F. Wang, L. Shu, and M. Guizani, "An efficient distributed trust model for wireless sensor networks," *IEEE Transactions on Parallel and Distributed Systems*, 2014.
- [22] G. Han, J. Jiang, L. Shu, J. Niu, and H.-C. Chao, "Management and applications of trust in Wireless Sensor Networks: a survey," *Journal of Computer and System Sciences*, vol. 80, no. 3, pp. 602–617, 2014.
- [23] C. M. Gui, Q. Jian, H. M. Wang, and Q. Y. Wu, "Repeated game theory based penalty-incentive mechanism in internet-based virtual computing environment," *Journal of Software*, vol. 21, no. 12, pp. 3042–3055, 2010.

- [24] TKK/COMNET, 2014, <http://www.netlab.tkk.fi/tutkimus/dtn/theone/>.
- [25] A. Keränen, J. Ott, and T. Kärkkäinen, "The ONE simulator for DTN protocol evaluation," in *Proceedings of the 2nd International Conference on Simulation Tools and Techniques*, p. 55, ICST (Institute for Computer Sciences, Social-Informatics and Telecommunications Engineering), 2009.
- [26] S. Ganeriwa, R. Kumar, and M. B. Srivastava, "Timing-synch protocol for sensor networks," in *Proceedings of the 1st Conference of Embedded Network Sensor Systems*, pp. 138–149, New York, NY, USA, 2003.
- [27] V. D. Becker, "Epidemic routing for partially connected ad hoc networks," *Proceedings of Technique Report*, Department of Computer Science, Duke University, Durham, UK, 2000.
- [28] A. Lindgren, A. Doria, and O. Schelén, "Probabilistic routing in intermittently connected networks," *ACM SIGMOBILE Mobile Computing and Communications Review*, vol. 7, no. 3, pp. 19–20, 2003.
- [29] T. Spyropoulos, K. Psounis, and C. S. Raghavendra, "Spray and wait: An efficient routing scheme for intermittently connected mobile networks," in *Proceedings of the ACM SIGCOMM Workshop on Delay-Tolerant Networking*, pp. 252–259, ACM, Philadelphia, Pa, USA, August 2005.

Research Article

A Virtual Machine Migration Strategy Based on Time Series Workload Prediction Using Cloud Model

Yanbing Liu,¹ Bo Gong,¹ Congcong Xing,² and Yi Jian¹

¹ *Engineering Laboratory of Network and Information Security, Chongqing University of Posts and Telecommunications, Chongqing 400065, China*

² *Department of Mathematics and Computer Science, Nicholls State University, Thibodaux, LA 70310, USA*

Correspondence should be addressed to Yanbing Liu; liuyb@cqupt.edu.cn

Received 6 June 2014; Accepted 19 August 2014; Published 28 September 2014

Academic Editor: Chuandong Li

Copyright © 2014 Yanbing Liu et al. This is an open access article distributed under the Creative Commons Attribution License, which permits unrestricted use, distribution, and reproduction in any medium, provided the original work is properly cited.

Aimed at resolving the issues of the imbalance of resources and workloads at data centers and the overhead together with the high cost of virtual machine (VM) migrations, this paper proposes a new VM migration strategy which is based on the cloud model time series workload prediction algorithm. By setting the upper and lower workload bounds for host machines, forecasting the tendency of their subsequent workloads by creating a workload time series using the cloud model, and stipulating a general VM migration criterion workload-aware migration (WAM), the proposed strategy selects a source host machine, a destination host machine, and a VM on the source host machine carrying out the task of the VM migration. Experimental results and analyses show, through comparison with other peer research works, that the proposed method can effectively avoid VM migrations caused by momentary peak workload values, significantly lower the number of VM migrations, and dynamically reach and maintain a resource and workload balance for virtual machines promoting an improved utilization of resources in the entire data center.

1. Introduction

With the rapid and continuous growth of cloud computing on a global scale, typical cloud computing techniques such as virtualization, parallel computation, and distributed database and storage have gained substantial development and been applied extensively in different areas. In particular, as one of the foundational components of cloud computing architecture, virtualization technique plays a critical role in delivering guaranteed cloud computing services [1]. By creating multiple simulating virtual machines (VMs) on the cluster of high performance network servers and providing on-demand services to users via these virtual machines, virtualization is a fundamental technique that can be used to realize the rapid deployment, dynamic allocation, and cross-domain management of IT resources [2–4]. Note however that driven by the constantly changing users' demands, both the number and the workloads of virtual machines vary frequently, which, incidentally, presents a new challenge for resources scheduling and migrations of virtual machines. It has been recognized, by virtue of virtual machine migration

process, that the selections of the source host machine and destination host machine are the most significant steps for virtual machine migrations.

Toward making decisions as to the selections of source and destination host machines, and also avoiding unnecessary virtual machine migrations caused by momentary peak workload values, the so-called live migration strategy for virtual machines is proposed by some researchers [5–8]. Currently, there are two types of virtual machine migration approaches existing in the literature: one is to combine the upper threshold and lower threshold of the host machine to manage the use of resources [9, 10]; the other is to use the workload threshold of the host machine to predict the trend of its subsequent workloads [11–14]. While the former approach is able to resolve the issue of resource waste inflicted by the static workload balancing strategy, it cannot resolve the issue of aggregation conflict which exists in traditional workload balancing strategies. On the other hand, the latter approach is able to resolve the issue of “false alarm” virtual machine migrations caused by some transient peak workload values but fails to put into consideration the uncertainty and

the stochastic nature of the workload values, as well as the combination of both, on host machines.

As such, toward bringing the uncertainty and randomness issue of workload values into the decision process of virtual machine migrations, and thus resulting in a more robust migration strategy, we in this paper propose a new virtual machine migration strategy which is based on the time series predication in cloud theory. This strategy basically works as follows: it first sets up the upper and lower workload thresholds for host machines, then forecasts the future workload tendency of the host machine using cloud theory, and finally stipulates a migration selection criterion and uses this criterion to select the source host machine, destination host machine, and the virtual machine to perform the desired migration. We argue that our proposed virtual machine migration strategy offers a comprehensive treatment for the uncertainty, fuzziness, and randomness of the workload values, converts qualitative notions to quantitative ones and vice versa, eliminates the aggregation conflict problem induced by virtual machine migrations due to some transient and momentary peak workload values, and contributes to obtaining a dynamic balancing of virtual machine resources.

The rest of the paper is structured as follows: Section 2 overviews related work in the literature as to the virtual machine migrations. Section 3 reviews the background knowledge of cloud model and introduces the computation of time series workload prediction. Our proposed virtual machine migration algorithm is presented in Section 4. Section 5 demonstrates the experimental results and analyses of the proposed migration strategy in comparison with other peer works, and Section 6 concludes the paper.

2. Related Work

The subject of virtual machine migration has been extensively studied [15–19]. The primary reason for this is that there is a constant increase in the number of virtual machines at cloud computing data centers, which presents new challenges in terms of the virtual machine resource scheduling and deployment. Due to the fact that the workload of a host machine for virtual machines changes dynamically in accordance with the ever-changing users' service demands, simple and static virtual machine migration strategies are no longer adequate in delivering quality services for users.

Conventional virtual machine migration strategies can be classified into single-threshold method and dual-threshold method [20, 21]. While the single-threshold method only places an upper bound on the workloads of host machines and initiates the virtual machine migration if the workload value is over this upper bound, dual-threshold method places both an upper bound and a lower bound on the workloads of host machines and initiates the migration when the workload is over the upper bound or below the lower bound. Beloglazov et al. [22–25] suggested an adaptive energy-efficient and threshold-based heuristic algorithm which controls the virtual machine migration by monitoring the resource utilization rate. Unfortunately, threshold-based migration strategies lack the ability to foresee the possible

future workload trend of host machines, and consequently may trigger unnecessary and wasteful virtual machine migrations if the workload of the host machine peaks just for a moment (for arbitrary reasons).

Various workload prediction techniques are also used in the context of virtual machine migrations [26–29]. In [28], Khan et al. proposed a hidden Markov model based prediction method with the restriction that the applicability of this method depends on the correlation of time and domain of the workload. Gmach et al. [26] presented a resource pool management strategy on the basis of workload analysis and demand predication but did not address the issue of the actual virtual machine migrations. Zhao and Shen [30] used the autoregressive (AR) model in time series prediction techniques, which predicts future values on the basis of a sequence of n past values ordered in time, to forecast the future workload values. Generally speaking, much of the current research work on prediction techniques fails to relate the workload predication analysis of host machines with the resource management of virtual machines to obtain a more desirable migration strategy.

The main purpose of our work is to improve the existing virtual machine migration strategies by applying the cloud model time series workload prediction technique to the decision procedure and process in virtual machine migrations.

3. Time Series Workload Predication Based on Cloud Model

Cloud model was proposed by Li et al. [14] in 2000, which deals with the conversion between qualitative concepts and quantitative descriptions subject to the notion of uncertainty. There exists a certain kind of mapping between the generally ambiguous describing ability of any natural languages and what objectively exists in the world and is intended to be described by the natural languages. It is interesting to note that this mapping is matched, in a primitive manner, by the essence of the cloud model.

3.1. Cloud Model Basics. Let U be a quantitative domain of precise values and C be a qualitative concept over U . For any $x \in U$, there exists a random number $\mu(x)$ with a stable tendency, which represents the relevance of x with respect to the concept C . The distribution of x over the domain U is called a cloud. Each x corresponds to a cloud droplet $\text{drop}(x_i, y_i)$. A cloud can be quantitatively characterized by 3 numerical values: expectation E_x , entropy E_n , and hyper entropy H_e (see Figure 1), where

- (i) E_x denotes the most typical quantitative expectation for the qualitative concept,
- (ii) E_n indicates the uncertainty of the concept. The value of E_n shows the range of U over which the concept can be accepted (with distinct uncertainty),
- (iii) H_e is the uncertainty measure of E_n and is affected by both the randomness and the fuzziness of E_n . The value of E_n indirectly indicates the cohesion degree of cloud droplet $\text{drop}(x_i, y_i)$.

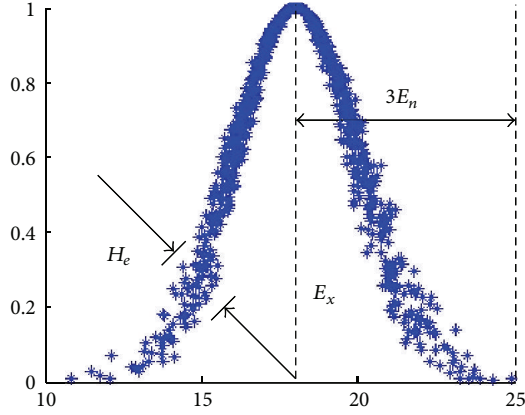


FIGURE 1: The numerical characteristics of cloud model.

A massive amount of cloud droplets gives rise to a cloud. Each droplet represents the phenomenon that the qualitative concept can be quantified to a point in U . According to the cloud generating mechanism in cloud model, there are forward cloud generators and backward cloud generators [31].

As shown in Figure 2(a), cloud droplets (a quantitative notion) are produced by the forward cloud generator using the 3 numerical values E_x , E_n , and H_e which are the characterization of a cloud (a qualitative notion). Every produced droplet is a concrete realization of the qualitative cloud. Conversely, as shown in Figure 2(b), backward cloud generator reverses the process of forward cloud generator by converting cloud droplets $\text{drop}(x_i, y_i)$ into the 3 numerical values E_x , E_n , and H_e (which are an abstract representation of a qualitative cloud).

3.2. The Computation for Time Series Workload Prediction. The procedure to obtain a time series workload prediction is depicted in Figure 3. There are four core modules in this procedure: parameter setting/optimization, data preprocessing, prediction modeling by cloud model, and model evaluation, with data preprocessing and prediction modeling by cloud model being the primary ones. The setting of parameters is extremely important as it may affect the accuracy of the prediction results. Collected sample data will be first processed into standardized form via zero-mean operation, difference operation, and center compression operation and then fed into the prediction module to get the preliminary result. Final prediction result will be obtained by performing reversed difference operations on the preliminary prediction result.

Specific steps for computing the workload prediction are given as follows.

Step 1. Let $\{y_t\}$ ($t = 1, 2, \dots, n$) be a known workload sequence indexed by time. Process $\{y_t\}$ by performing zero-mean operation on $\{y_t\}$ to obtain the sequence $\{y'_t\}$. Then

calculate the first-order difference $\Delta y'_t$ of y'_t and the second-order difference $\Delta^2 y'_t$ of y'_t as follows:

$$\begin{aligned}\Delta y'_t &= y'_{t+1} - y'_t, \\ \Delta^2 y'_t &= \Delta y'_{t+1} - \Delta y'_t.\end{aligned}\quad (1)$$

We use $\{D_t\}$ ($t = 1, 2, \dots, n-2$) to denote $\{\Delta^2 y'_t\}$ in subsequent steps.

Step 2. Suppose we need to predict k subsequent workload values. Using the deviation technique in nonlinear data standardizations, standardize $\{D_t\}$ obtained in Step 1 as follows:

$$F_t = \frac{D_t - \overline{D_t}}{\delta}, \quad (2)$$

where $\overline{D_t}$ is the average of $\{D_t\}$ and δ is the standard deviation of $\{D_t\}$.

Step 3. Let F_{\max} be the maximum value of $\{F_t\}$ calculated in Step 2, and μ_t be the ratio of F_t with F_{\max} . Process $\{F_t\}$ by eliminating all F_t 's in $\{F_t\}$ whose $\mu_t > 0.9999$; call the result $\{X_t\}$ ($t = 1, 2, \dots, m$). By the relevant formulas in backward cloud generator, calculate expectation E_x , entropy E_n , and hyper entropy H_e as follows:

$$\begin{aligned}E_x &= \text{mean}(x_t), \\ E_n &= \sqrt{\frac{\pi}{2}} * \frac{1}{n} \sum_{t=1}^m |x_t - E_x|, \\ S^2 &= \frac{\sum_{t=1}^m (x_t - E_x)^2}{m-1}, \\ H_e &= \sqrt{S^2 - E_n^2}.\end{aligned}\quad (3)$$

Step 4. Feed E_x , E_n , and H_e obtained in Step 3 into a forward cloud generator. Generate a normal random number E'_{n_t} with E_n being expectation and H_e^2 being variance by $E'_{n_t} = \text{NORM}(E_n, H_e^2)$, and a following normal random number x_t with E_x being expectation and $E'_{n_t}^2$ being variance by $x_t = \text{NORM}(E_x, E'_{n_t}^2)$. Then calculate the certainty degree d_t as follows:

$$d_t = \exp \left[-\frac{(x_t - E_x)^2}{2(E'_{n_t})^2} \right]. \quad (4)$$

Repeating these calculations k times will produce the set of cloud droplets $\{x_t, d_t\}$ ($t = 1, 2, \dots, k$), which is denoted by $\{P_t\}$ (the preliminary predication result). Then process $\{P_t\}$ by reversed difference operation twice in combination with $\{\Delta y'_t\}$ and $\{y'_t\}$, and that will yield the final result.

4. The Virtual Machine Migration Strategy

Virtual machine migrations in cloud computing environment are generally composed of the following steps: (1) determine

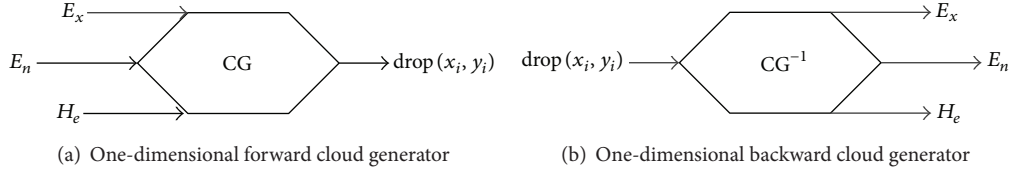


FIGURE 2: The cloud generators.

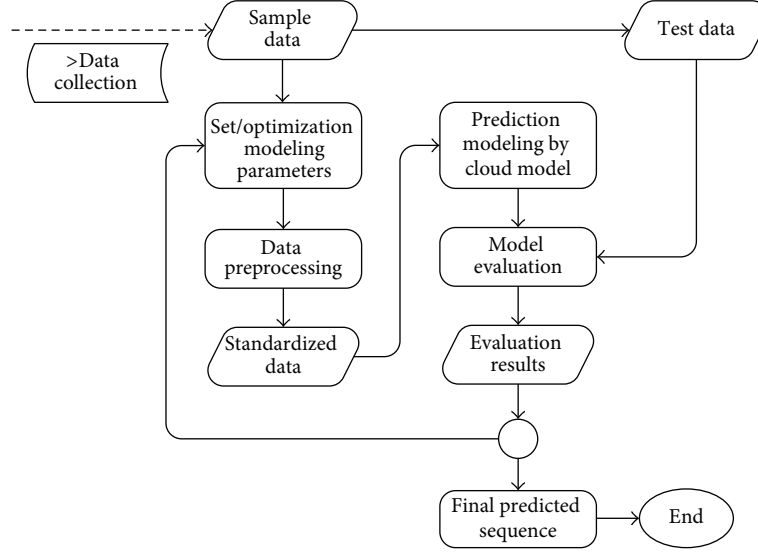


FIGURE 3: The flow chart of the time series workload prediction via cloud model.

the source host machine from which some virtual machine is to be removed; (2) determine the destination host machine to which some virtual machine will be moved; (3) choose an appropriate migration scheme (such as static migration, dynamic migration, or mixed migration); (4) carry out the virtual machine migration; and (5) delete the mirror image files associated with the removed virtual machine on the source host machine.

The novelty of our work is to apply the cloud model based time series prediction technique to the migration of virtual machines, namely, to the selections of source host machine, destination host machine, and the virtual machine to be migrated.

4.1. The Strategy Outline. The controlling idea of our virtual machine migration strategy may be characterized as workload-aware migration (WAM). We use the cloud model based time series prediction technique introduced in Section 3 to forecast the future workloads for each host machine. If there exists a host machine whose workload keeps going beyond the upper workload threshold, then this machine will be labeled as a potential source host machine. In a similar manner, if this machine's workload keeps staying between the upper threshold and the lower threshold, then it will be labeled as a potential destination host machine. The flow chart of the proposed virtual machine migration strategy is shown in Figure 4.

Since the workload of each host machine at a data center changes frequently in accordance with the users'

ever-changing service demands, we need to monitor in real time the changes of the workload for all host machines. This constitutes the data source phase in Figure 4. Collected workload data will then be standardized into desired format as the input to the cloud model based prediction engine. The next step is to forecast the future workloads for host machines by the cloud model based prediction engine, and based on the prediction result, to carry out the migration by appropriately selecting the source and destination host machines as well as the virtual machine to be migrated. Finally, the virtual machine mirror image files on the source host machine will be deleted, and the virtual machine on the destination host machine will be started to continue the user services.

4.2. Workload Prediction. The history of the workload of a host machine is formed by its actual past workload values which are collected by the data collection module at data centers. A machine's CPU workload is used as the indicator for the entire workload of that machine since a higher CPU utilization rate suggests a higher consumption of resource of the machine. In the simulation test for our virtual machine migration strategy, data collected from the PlanetLab [32] platform which can be accessed from within the cloud computing simulation software CloudSim [33] are used as the CPU workload simulation. The set of workload history of host machines is denoted by C_h (For the sake of convenience, we list notations and their meanings used in our workload prediction algorithm in Notation and Their Meanings Section).

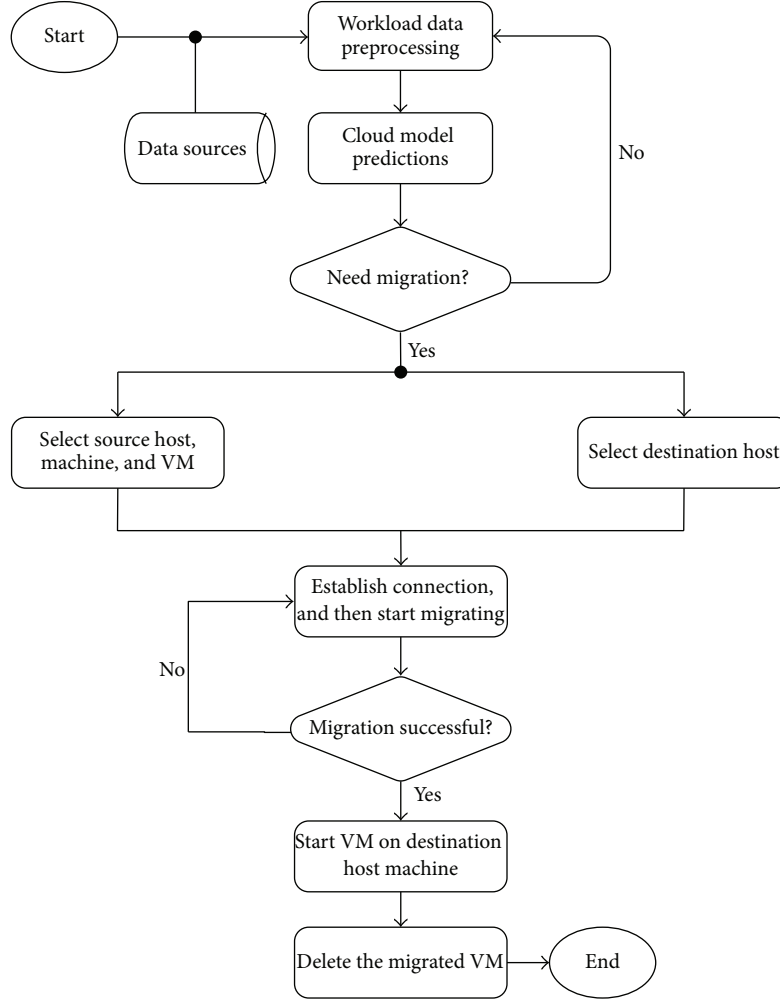


FIGURE 4: The flow chart of virtual machine migration.

In order to eliminate the virtual machine migrations which are caused by momentary peak workload values, we analyze in advance the possibility of overload or underload of host machines by forecasting the future workload trend for host machines via the cloud model based workload time series prediction technique. The workload upper threshold and lower threshold are denoted by L_u and L_d , respectively. Both L_u and L_d are heuristic values. The three characteristic values E_x , E_n , and H_e of a cloud are produced by a one-dimensional backward cloud generator, which are then fed into a one-dimensional forward cloud generator to produce the prediction of host machine workloads. The set of predicted future workloads for host machine n (index number of host machine) is denoted by C_f .

4.3. The Selections of Source Host Machine, Destination Host Machine, and Virtual Machine

4.3.1. The List of Source Host Machines. For each set C_f of the predicted workload values, compute its average and denote the result as $L_a(n)$. If

$$L_a(n) > L_u \quad (5)$$

holds, then host machine n will be added to the list Q_s of source host machines. Here, note that the chance of the virtual machine migration triggered by a single momentary peak workload value is eliminated by (5).

Also, if the predicted workload value is below the lower threshold, there would be a need to migrate the virtual machines as well. Specifically, if

$$L_a(n) < L_d \quad (6)$$

holds, then host machine n will be added to the list Q_l of underload host machines, which indicates that all virtual machines on this host machine n need to be migrated.

4.3.2. The List of Virtual Machines. There are two cases to be dealt with for the virtual machine selection depending on whether the host machine is overloaded or underloaded. For the case of underloaded host machines, every virtual machine on every host machine in the list Q_l is to be migrated. Hence all virtual machines will be added to the list S_l which records the index number of the host machine on which a virtual machine resides as well as the average running workload value of the virtual machine. The virtual machine

```

Input:  $C_h, L_u, L_d$ .
Output:  $Q_a$ .
Procedure begin
(1)  for each  $n$  in  $C_h$  do
(2)    Use cloud model to predict  $k$  future workloads for host  $n$ , and push results into list
(3)     $C_f$ . Calculate the average of the predicted workloads and push result into list  $L_a$ ;
(4)    if  $(L_a(n) > L_u)$  then
(5)      Add host ID  $n$  into the list  $Q_s$ , select the VM with the largest average history
(6)      workload value on the host  $n$ , and add the VM into queue  $S_o$ ;
(7)    end if
(8)    if  $(L_a(n) < L_d)$  then
(9)      Add host ID  $n$  into list  $Q_l$ , and add all the virtual machines on the host into  $S_l$ ;
(10)   end if
(11)   if  $((L_a(n) < L_u) \&\& (L_a(n) > L_d))$  then
(12)     Add host ID  $n$  into list  $Q_d$ ;
(13)   end if
(14)   end for
(15)   for each  $L_m(i)$  in  $(S_o \cup S_l)$  do
(16)     for each  $L_a(j)$  in  $Q_d$  do
(17)       if  $(L_m(i) + L_a(j) < L_u)$  then
(18)         Migrate virtual machine  $i$  to host  $j$ , add VM information into list  $Q_a$ ;
(19)       end if
(20)     end for
(21)   end for
(22)   return  $Q_a$ ;
end Procedure

```

ALGORITHM 1: The virtual machine migration algorithm.

workload values in this list are sorted from large to small. For the case of overloaded host machines, the list Q_s needs to be traversed to select, on each host machine, the virtual machine with the largest average running workload value and to add the selected virtual machine to the list S_o , which, like the list S_l , records the index number of the host machine on which a virtual machine resides as well as the average running workload value of the virtual machine. Again, as for the previous case, the virtual machine workload values in this list are sorted from large to small. Note that in consideration of the migration efficiency, the available virtual machine with the largest workload value should be chosen to be migrated so that the maximum migration benefit tends to be acquired by the minimum number of migrations.

4.3.3. The List of Destination Host Machines. A host machine will be chosen as a candidate for virtual machine migrations if its predicted workload value is between the upper threshold and the lower threshold. That is, if

$$L_d < L_a(n) < L_u \quad (7)$$

holds, then the host machine n will be added to the list Q_d .

4.4. The Migration of Virtual Machines. The actual migration of a virtual machine can be decided by using the previously obtained lists of host machines and virtual machines. If

$$L_m(i) + L_a(j) < L_u \quad (8)$$

holds, where $L_a(j)$ is taken from the list Q_d and $L_m(i)$ is a virtual machine workload value taken from the list S_o ; then the corresponding virtual machine will be migrated to the host machine indexed by j ; subsequently, $L_m(i)$ and $L_a(j)$ will be removed from the lists S_o and Q_d , respectively. The index numbers of the source host machine and destination host machine will be released back to C_h .

For underloaded host machines, all virtual machines will be migrated to the destination host machines by (8), if the list Q_l is not empty. All information about a virtual machine will be saved into the list Q_a after the virtual machine is migrated. The detailed algorithm for virtual machine migration is shown in Algorithm 1.

5. Simulation Results

Simulation experiments are performed to test the effectiveness of our cloud model based time series workload predication algorithm in comparison with the autoregressive (AR) time series workload prediction model [30]. Data collected via the popular cloud computing simulation software CloudSim [33] in conjunction with global network platform PlanetLab [32] are used as input to predict the future workload trend for host machines.

5.1. Raw Data. Table 1 contains the workload data of a physical node over 96 successive and 5-minute-spaced time points collected on the PlanetLab on April 20, 2011. The first 90 entries in Table 1 are used as sample input to the two workload prediction algorithms, and the remaining 6

TABLE 1: Collected raw workload data.

Original workloads collected (Time: T ($i = 1, 2, \dots, 96$), $T_{i+1} - T_i = 5$ min)									
16.0000	12.0000	15.0000	26.0000	41.0000	27.0000	22.0000	16.0000	14.0000	22.0000
28.0000	60.0000	18.0000	32.0000	23.0000	26.0000	19.0000	6.0000	22.0000	43.0000
30.0000	31.0000	21.0000	27.0000	40.0000	61.0000	32.0000	25.0000	27.0000	26.0000
29.0000	18.0000	16.0000	23.0000	24.0000	17.0000	16.0000	50.0000	17.0000	74.0000
51.0000	22.0000	36.0000	23.0000	20.0000	14.0000	70.0000	22.0000	12.0000	20.0000
19.0000	22.0000	36.0000	23.0000	31.0000	24.0000	77.0000	16.0000	22.0000	19.0000
6.0000	20.0000	22.0000	31.0000	24.0000	18.0000	22.0000	10.0000	18.0000	16.0000
16.0000	20.0000	15.0000	18.0000	20.0000	28.0000	10.0000	28.0000	20.0000	16.0000
80.0000	50.0000	23.0000	24.0000	20.0000	27.0000	15.0000	20.0000	28.0000	24.0000
29.0000	22.0000	18.0000	67.0000	16.0000	42.0000				

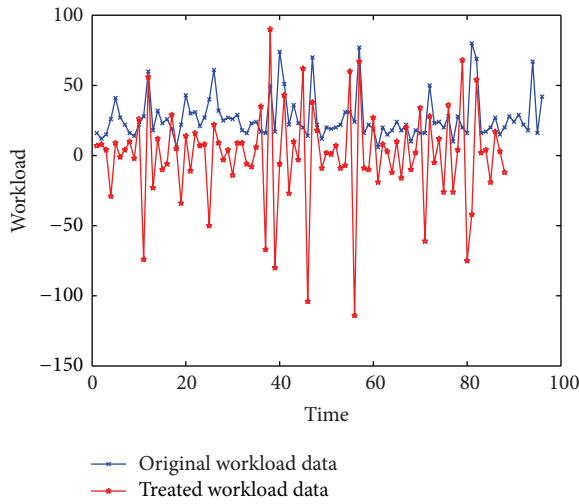


FIGURE 5: The original workloads and workloads after being treated twice with difference operations.

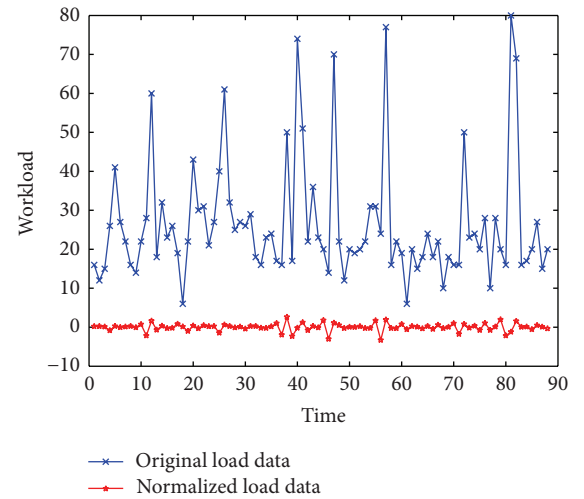


FIGURE 6: The original workloads and workloads after being normalized.

entries are used to check the correctness and accuracy of the prediction results of the algorithms.

5.2. Experiment Metrics. Standard error measurement tools in statistics mean absolute error (MAE) and root mean squared error (RMSE) are used to evaluate the accuracy of the algorithms. If the predicated workload sequence is $\{p_1, p_2, \dots, p_k\}$ and the actual workload sequence is $\{q_1, q_2, \dots, q_k\}$, then MAE and RMSE are given by

$$\begin{aligned} \text{MAE} &= \frac{\sum_{i=1}^k |p_i - q_i|}{k}, \\ \text{RMSE} &= \sqrt{\frac{\sum_{i=1}^k (p_i - q_i)^2}{k}}. \end{aligned} \quad (9)$$

Although formulated differently and having separate usability and appropriateness, both MAE and RMSE provide an indication as to how well the predication results match the actual data. A smaller MAE value or RMSE value means that the prediction results fit the actual data more closely and thus are superior.

5.3. Experiment Results. Due to their unstable and discrete nature, the originally collected workload data are processed by the difference operation and the normalization operation before they are used to generate the predictions. The results of applying these operations to the original data are depicted in Figures 5 and 6, respectively.

The prediction results of our cloud model based algorithm are compared with that of the AR model; details of the comparison are recorded in Table 2 and are contrasted in Figures 7 and 8. We can see that our cloud model based algorithm has lower values than that of AR in terms of both absolute error and error rate. The MAE value and RMSE value of our algorithm and the AR model are, respectively, 2.9310, 3.0334 and 6.5187, 7.3504, which are shown in Table 3 and graphed in Figures 9 and 10. Again, it can be seen that our cloud model based algorithm yields much more accurate prediction results than the AR model, and thus it can select more appropriate host machines and virtual machines in the process of virtual machine migrations.

Finally, the prediction results of our algorithm and the AR model together with the actual workload data are charted in Figure 11 to present a simultaneous visual comparison

TABLE 2: The comparison of cloud model based algorithm with AR model.

Original load value	Predicted load value		Absolute error		Error rate	
	Cloud model	AR model	Cloud model	AR model	Cloud model	AR model
29.0000	25.1528	26.1580	3.8472	2.8420	13.27%	9.80%
22.0000	24.6020	19.1136	2.6020	2.8864	11.83%	13.12%
18.0000	20.3683	24.6645	2.3683	6.6645	13.16%	37.03%
67.0000	64.5862	58.3297	2.4138	8.6703	3.60%	12.94%
16.0000	20.1804	21.4680	4.1804	5.4680	26.13%	34.18%
42.0000	39.8258	29.4192	2.1742	12.5808	5.18%	29.95%

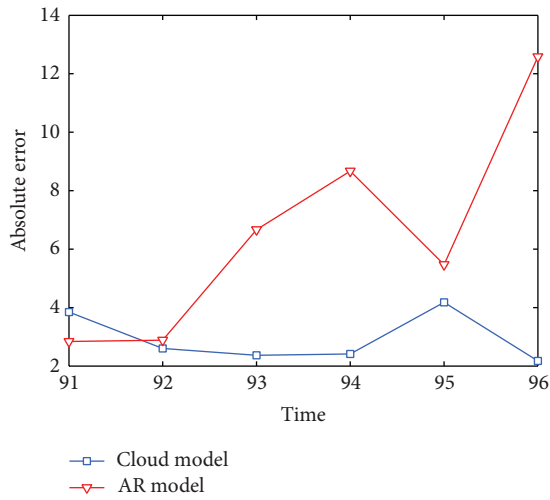


FIGURE 7: Absolute error comparison between cloud model and AR model.

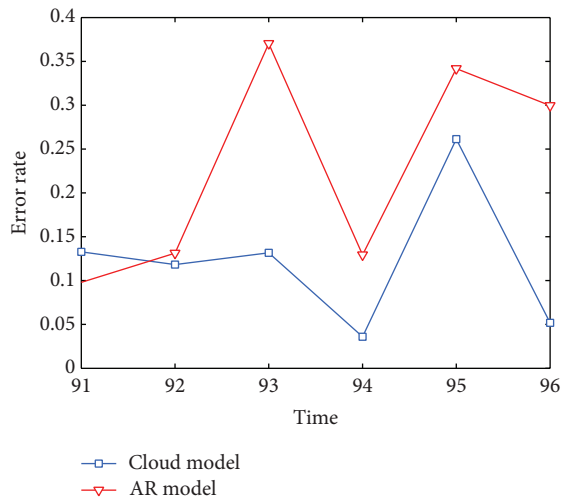


FIGURE 8: Error rate comparison between cloud model and AR model.

of the effectiveness of the algorithms, and the fact that the prediction results of our algorithm approximate the actual data curve well following the sample data curve is shown in Figure 12. Both of these figures are further evidence

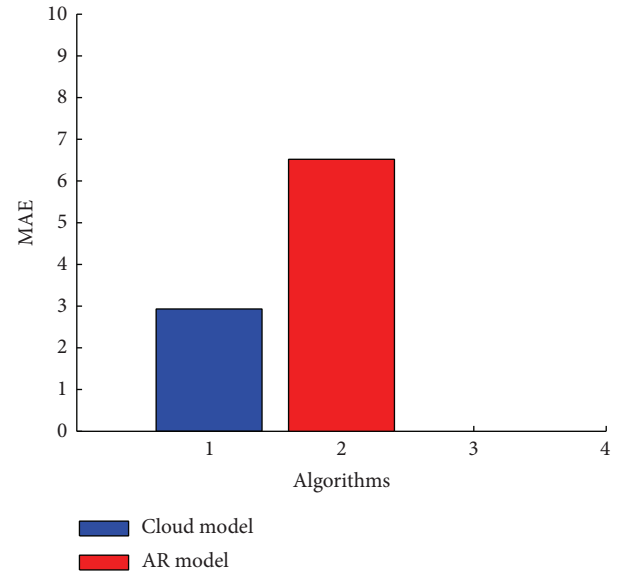


FIGURE 9: MAE comparison between cloud model and AR model.

TABLE 3: MAE and RMSE values of cloud model and AR model.

Metrics	Cloud model	AR model
MAE	2.9310	6.5187
RMSE	3.0334	7.3504

supporting the claim that our cloud model based algorithm is more desirable than the AR model.

6. Conclusion

We proposed in this paper a new virtual machine migration strategy which predicts future workloads of host machines by using the forward and backward cloud generators in cloud model, determines source and destination host machines on the basis of the prediction result and by the WAM criterion, and selects the most resource-demanding virtual machine on source host machines to perform the migration. Through the comparison with the peer AR model time series workload prediction technique, we found that our algorithm clearly delivers a more precise workload prediction result than the AR model, and thus it provides more effective support for the selection of host machines in virtual machine migration

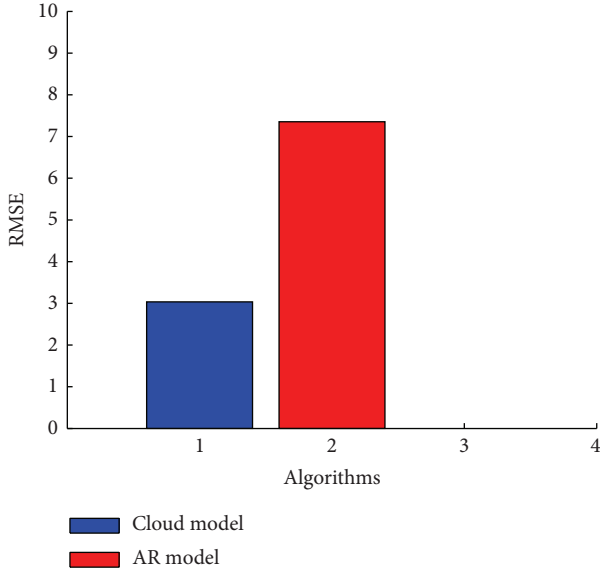


FIGURE 10: RMSE comparison between cloud model and AR model.

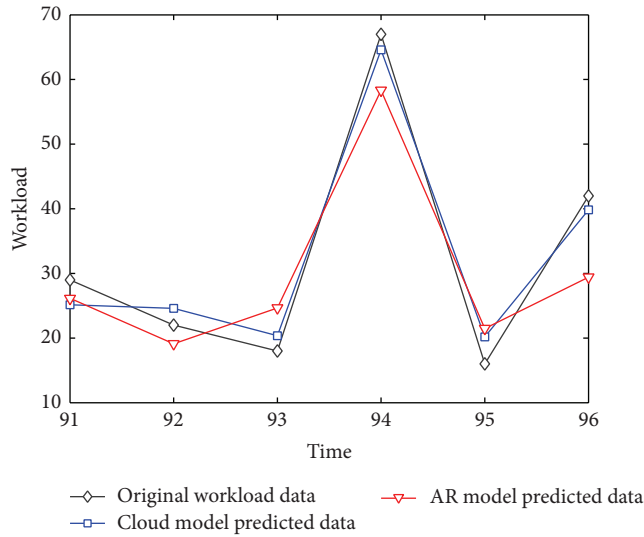


FIGURE 11: Comparison of predicted data with the original data.

process, reduces the number of virtual machine migrations, and eventually promotes the system to reach a dynamic resource balance improving the resource utilization rate and the virtual service quality.

Notation and Their Meanings

- C_h : The set of workload history of host machines
- L_u : The workload upper threshold
- L_d : The workload lower threshold
- C_f : The set of predicted future workloads for host machines

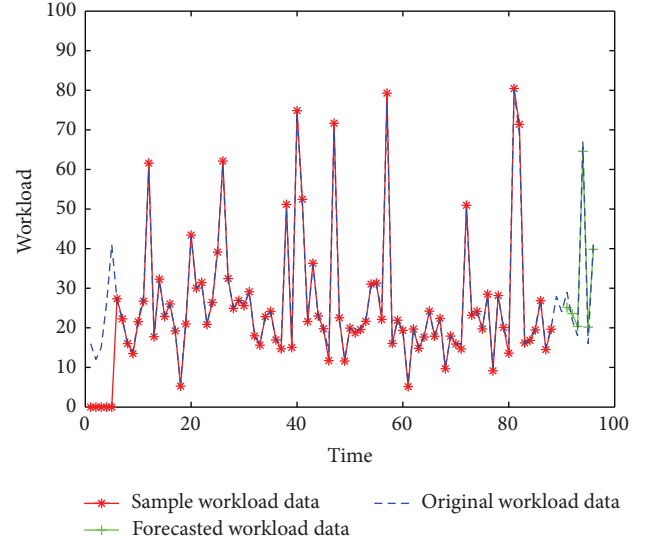


FIGURE 12: Cloud model prediction results with respect to original data and sample input.

- $L_a(n)$: The average value of predicted future workloads for host machine (indexed by n)
- Q_s : The list of source host machines
- Q_l : The list of low workload host machines
- S_l : The list of to-be-migrated virtual machines on low workload host machines
- S_o : The list of to-be-migrated virtual machines on high workload (overloaded) host machines
- Q_d : The list of destination host machines
- $L_a(j)$: The average value of predicted future workloads for host machine (indexed by j)
- $L_m(i)$: The average value of predicted future workloads for virtual machine (indexed by i)
- Q_a : The list of migrated virtual machines
- L_a : The average value set of predicted future workloads for host machines.

Conflict of Interests

The authors declare that there is no conflict of interests regarding the publication of this paper.

Acknowledgments

This work is supported in part by the following Grants: National Science Foundation of China (Grant no. 61272400), Chongqing Innovative Team Fund for College Development Project (Grant no. KJTD201310), Chongqing Youth Innovative Talent Project (Grant no. cstc2013kjrc-qnrc40004), Ministry of Education of China and China Mobile Research Fund (Grant no. MCM20130351), and Science and Technology on Information Transmission and Dissemination in Communication Networks Laboratory Open Project (Grant no. ITD-U13002/KX132600009).

References

- [1] A. J. Younge, R. Henschel, J. T. Brown, G. von Laszewski, J. Qiu, and G. C. Fox, "Analysis of virtualization technologies for high performance computing environments," in *Proceedings of the IEEE International Conference on Cloud Computing (CLOUD '11)*, pp. 9–16, Washington, DC, USA, July 2011.
- [2] Q. Li, Q.-F. Hao, L.-M. Xiao, and Z.-J. Li, "Adaptive management and multi-objective optimization for virtual machine placement in cloud computing," *Chinese Journal of Computers*, vol. 34, no. 12, pp. 2253–2264, 2011.
- [3] H. B. Mi, H. M. Wang, G. Yin, D. X. Shi, Y. F. Zhou, and L. Yuan, "Resource on-demand reconfiguration method for virtualized data centers," *Journal of Software*, vol. 22, no. 9, pp. 2193–2205, 2011.
- [4] Y. Wen, D. Meng, and J.-F. Zhan, "Adaptive virtualized resource management for application's SLO guarantees," *Journal of Software*, vol. 24, no. 2, pp. 358–377, 2013.
- [5] C. Clark, K. Fraser, S. Hand et al., "Live migration of virtual machines," in *Proceedings of the 2nd Symposium on Networked Systems Design and Implementation*, vol. 2, pp. 273–286, 2005.
- [6] Y. Wu and M. Zhao, "Performance modeling of virtual machine live migration," in *Proceedings of the IEEE 4th International Conference on Cloud Computing (CLOUD '11)*, pp. 492–499, IEEE, Washington, DC, USA, July 2011.
- [7] J. Hu, J. Gu, G. Sun, and T. Zhao, "A scheduling strategy on load balancing of virtual machine resources in cloud computing environment," in *Proceeding of the 3rd International Symposium on Parallel Architectures, Algorithms and Programming (PAAP '10)*, pp. 89–96, Dalian, China, December 2010.
- [8] C. Weng, Q. Liu, L. Yu, and M. Li, "Dynamic adaptive scheduling for virtual machines," in *Proceeding of the 20th ACM International Symposium on High-Performance Parallel and Distributed Computing (HPDC '11)*, pp. 239–250, New York, NY, USA, June 2011.
- [9] M. Mishra, A. Das, P. Kulkarni, and A. Sahoo, "Dynamic resource management using virtual machine migrations," *IEEE Communications Magazine*, vol. 50, no. 9, pp. 34–40, 2012.
- [10] W. Zhao, Z. Wang, and Y. Luo, "Dynamic memory balancing for virtual machines," *ACM SIGOPS Operating Systems Review*, vol. 43, no. 3, pp. 37–47, 2009.
- [11] Y. Shi, X. Jiang, and K. Ye, "An energy-efficient scheme for cloud resource provisioning based on CloudSim," in *Proceedings of the IEEE International Conference on Cluster Computing (CLUSTER '11)*, pp. 595–599, September 2011.
- [12] K. Ye, X. Jiang, D. Huang, J. Chen, and B. Wang, "Live migration of multiple virtual machines with resource reservation in cloud computing environments," in *Proceedings of the IEEE 4th International Conference on Cloud Computing (CLOUD '11)*, pp. 267–274, July 2011.
- [13] X. Chen and J. Zhang, "Virtual machines scheduling algorithm oriented load forecast," in *Proceedings of the International Conference on Network Computing and Information Security (NCIS '11)*, pp. 113–117, May 2011.
- [14] D. Y. Li, K. Di, D. Li, and X. Shi, "Mining association rules with linguistic cloud models," *Journal of Software*, vol. 11, no. 2, pp. 143–158, 2000.
- [15] M. Andreolini, S. Casolari, M. Colajanni, and M. Messori, "Dynamic load management of virtual machines in cloud architectures," in *Cloud Computing*, vol. 34 of *Lecture Notes of the Institute for Computer Sciences, Social-Informatics and Telecommunications Engineering*, pp. 201–214, 2010.
- [16] R. N. Calheiros, R. Ranjan, A. Beloglazov, C. A. F. de Rose, and R. Buyya, "CloudSim: a toolkit for modeling and simulation of cloud computing environments and evaluation of resource provisioning algorithms," *Software: Practice and Experience*, vol. 41, no. 1, pp. 23–50, 2011.
- [17] S. Akoush, R. Sohan, A. Rice, A. W. Moore, and A. Hopper, "Predicting the performance of virtual machine migration," in *Proceeding of the 18th Annual IEEE/ACM International Symposium on Modeling, Analysis and Simulation of Computer and Telecommunication Systems (MASCOTS '10)*, pp. 37–46, Miami Beach, Fla, USA, August 2010.
- [18] W. Hu, A. Hicks, L. Zhang et al., "A quantitative study of virtual machine live migration," in *Proceedings of the ACM Cloud and Autonomic Computing Conference*, pp. 1–11, 2013.
- [19] V. Medina and J. M. García, "A survey of migration mechanisms of virtual machines," *ACM Computing Surveys*, vol. 46, no. 3, p. 30, 2014.
- [20] Y. C. Chang, R. S. Chang, and F. W. Chuang, "A predictive method for workload forecasting in the cloud environment," in *Advanced Technologies, Embedded and Multimedia for Human-Centric Computing*, vol. 260 of *Lecture Notes in Electrical Engineering*, pp. 577–585, Springer, 2014.
- [21] H. Ren, Y. Lan, and C. Yin, "The load balancing algorithm in cloud computing environment," in *Proceedings of the 2nd International Conference on Computer Science and Network Technology (ICCSNT '12)*, pp. 925–928, Changchun, China, December 2012.
- [22] A. Beloglazov, J. Abawajy, and R. Buyya, "Energy-aware resource allocation heuristics for efficient management of data centers for Cloud computing," *Future Generation Computer Systems*, vol. 28, no. 5, pp. 755–768, 2012.
- [23] A. Beloglazov and R. Buyya, "Energy efficient resource management in virtualized cloud data centers," in *Proceedings of the 10th IEEE/ACM International Symposium on Cluster, Cloud, and Grid Computing (CCGrid '10)*, pp. 826–831, Melbourne, Australia, May 2010.
- [24] A. Beloglazov and R. Buyya, "Adaptive threshold-based approach for energy-efficient consolidation of virtual machines in cloud data centers," in *Proceedings of the 8th International Workshop on Middleware for Grids, Clouds and e-Science*, p. 4, 2010.
- [25] A. Beloglazov and R. Buyya, "Optimal online deterministic algorithms and adaptive heuristics for energy and performance efficient dynamic consolidation of virtual machines in Cloud data centers," *Concurrency Computation Practice and Experience*, vol. 24, no. 13, pp. 1397–1420, 2012.
- [26] D. Gmach, J. Rolia, L. Cherkasova, and A. Kemper, "Workload analysis and demand prediction of enterprise data center applications," in *Proceedings of the 10th IEEE International Symposium on Workload Characterization (IISWC '07)*, pp. 171–180, September 2007.
- [27] N. Roy, A. Dubey, and A. Gokhale, "Efficient autoscaling in the cloud using predictive models for workload forecasting," in *Proceedings of the IEEE International Conference on Cloud Computing (CLOUD '11)*, pp. 500–507, Washington, DC, USA, July 2011.
- [28] A. Khan, X. Yan, S. Tao, and N. Anerousis, "Workload characterization and prediction in the cloud: a multiple time series approach," in *Proceedings of the IEEE Network Operations and Management Symposium (NOMS '12)*, pp. 1287–1294, Maui, Hawaii, USA, April 2012.

- [29] Y. Wu, K. Hwang, Y. Yuan, and W. Zheng, "Adaptive workload prediction of grid performance in confidence windows," *IEEE Transactions on Parallel and Distributed Systems*, vol. 21, no. 7, pp. 925–938, 2010.
- [30] Y. Zhao and L. Shen, "Application of time series auto regressive model in price forecast," in *Proceedings of the International Conference on Business Management and Electronic Information (BMEI '11)*, pp. 768–771, May 2011.
- [31] D. Y. Li, "Uncertainty in knowledge representation," *China Engineering Science*, vol. 2, no. 10, pp. 73–79, 2000.
- [32] Princeton University, "PlanetLab: an open platform for developing, deploying, and accessing planetary-scale services," 2014, <https://www.planet-lab.org>.
- [33] Melbourne Clouds Lab, "CloudSim : A Framework For Modeling and Simulation of Cloud Computing Infrastructures and Services," 2014, <http://www.cloudbus.org/cloudsim/>.

Research Article

Energy-Efficient Scheduling for Tasks with Deadline in Virtualized Environments

Guangyu Du,¹ Hong He,¹ and Qinggang Meng²

¹ School of Mechanical, Electrical & Information Engineering, Shandong University, Weihai, Shandong 264209, China

² Department of Computer Science, Loughborough University, Loughborough, Leicestershire LE11 3TU, UK

Correspondence should be addressed to Hong He; hehong@sdu.edu.cn

Received 22 May 2014; Accepted 10 July 2014; Published 25 September 2014

Academic Editor: Chuandong Li

Copyright © 2014 Guangyu Du et al. This is an open access article distributed under the Creative Commons Attribution License, which permits unrestricted use, distribution, and reproduction in any medium, provided the original work is properly cited.

Data centers, as resource providers, take advantage of virtualization technology to achieve excellent resource utilization, scalability, and high availability. However, large numbers of computing servers containing virtual machines of data centers consume a tremendous amount of energy. Thus, it is necessary to significantly improve resource utilization. Among the many issues associated with energy, scheduling plays a very important role in successful task execution and energy consumption in virtualized environments. This paper seeks to implement an energy-efficient task scheduling algorithm for virtual machines with changeless speed comprised of two main steps: assigning as many tasks as possible to virtual machines with lower energy consumption and keeping the makespan of each virtual machine within a deadline. We propose a novel scheduling algorithm for heterogeneous virtual machines in virtualized environments to effectively reduce energy consumption and finish all tasks before a deadline. The new scheduling strategy is simulated using the CloudSim toolkit package. Experimental results show that our approach outperforms previous scheduling methods by a significant margin in terms of energy consumption.

1. Introduction

Nowadays, large-scale data centers take advantage of virtualization technology [1–3] to achieve excellent resource utilization, scalability, and high availability, such as cloud computing. Cloud computing has achieved tremendous success in offering infrastructure/platform/software as a service based on virtualization technology. Virtualized environments provide computing resource to the clients in the form of a virtual machine (VM) which is a software machine implemented on physical machines. VM behaves like a physical machine, such that it could run different operating systems and applications. Due to poor task assignment optimization, current data centers having huge numbers of heterogeneous servers consume and simultaneously waste massive power to execute numerous assigned tasks. Out of the various energy issues, scheduling plays a very important role in successful execution of tasks in virtualized environments. Scheduling seeks maximum utilization of resources by appropriate assignment of tasks to the resources available like

CPU, memory, and storage [4–6]. It is necessary for service providers and requesters to devise efficient scheduling.

In virtualized environments such as cloud computing, end-users simply use the available services and pay for the used services without owning any part of the infrastructure. Several criteria determine the quality of the provided service and the duration of this service (makespan), and the consumed energy is among these criteria. As shown in Section 4, energy consumption and execution time are always two opposite variables. That is to say, in general, there exists no solution which is close to the optimal value on both objectives (makespan and energy consumption) at the same time. For this kind of conflicting problems, these compromise solutions are often used to get trade-offs. Therefore, we will tackle the problem in a compromise way which means that we mainly optimize one objective with the second objective maintained at a reasonable value. For the problem in this paper, it can be represented as minimizing the energy consumption under the premise that the makespan is within a threshold value. However, since

finding the optimal makespan is usually NP-hard, we aim to develop an energy-efficient task scheduling algorithm to complete tasks on heterogeneous virtual machines (VMs) in virtualized environments within a certain deadline, and the total energy consumption is minimized at the same time. Numbers of real applications can be modeled as this kind of problem such as parallel picture transmission and real-time iteration procedure of algorithm in real-time multiprocessing systems and environments.

Most of the current energy-efficient scheduling strategies are based on the dynamic voltage scaling (DVS) [7] or dynamic voltage frequency scaling (DVFS) [8, 9] with the changeable voltage and power supply. However, the current processors with available variable voltage/speed have only several discrete voltage/speed settings [10], which mean that the DVS is still in the development stage. In this paper, we mainly focus on the energy issue in task scheduling, particularly on the condition that the processors or VMs have changeless voltage supply. We prove that assigning as many tasks as possible to the VM with small speed is the key strategy of energy-efficient task scheduling and propose a new task scheduling algorithm that takes into account the makespan and energy consumption at the same time. Our new approach investigates the problem of minimizing energy consumption with schedule length constraint on VMs in virtualized environments.

The rest of the paper is organized as follows. Section 2 discusses the related works. Section 3 defines the task scheduling problem of minimizing energy consumption with schedule length constraint. A new strategy for minimizing energy of task assignment is proposed and the task scheduling algorithm based on the strategy is described mathematically in Section 4. Section 5 presents and discusses the simulations and performance analysis. We conclude our work in Section 6.

2. Related Work

Currently, green computing is applied more and more extensively in data centers. A number of new green scheduling algorithms for saving energy and resource have been proposed, such as [11, 12]. In [13], researchers developed energy-efficient algorithms by incorporating DVS and frequency scaling technology to minimize energy consumption. For the tasks with or without precedence, scheduling algorithms proposed in [14] adopted shared slack reclamation on variable voltage/speed processors to minimize energy consumption. Researchers proved in [7] that only when all tasks were executed with the same power (or at the same speed), the total energy consumption for a computer with multiple identical processors is minimal. Some studies also investigated different ways of minimizing the energy consumption of cloud computing [15].

Numbers of studies focused on parallel applications with precedence constraint and algorithms to minimize the makespan [16–21]. The QoS-based workflow scheduling algorithm proposed in [16] tried to minimize the cost of workflow execution under user-defined deadline constraint based on a novel concept called partial critical paths (PCP).

The HEFT (heterogeneous earliest finish time) algorithm [17] is a kind of heuristic method based on list scheduling consisting of two phrases: calculating task prioritization and processor selection. Many previous studies [18–20] proved that HEFT could get competitive result with low complexity.

Genetic algorithm (GA) [22] and the other 10 heuristics are implemented and compared in [23] and the results show that genetic algorithm (GA) behaves best in all the tested algorithms for task scheduling problems. Hybrid particle swarm optimization algorithm (HPSO) [24] belongs to the modified particle swarm optimization algorithms and researchers in [25] showed that the HPSO algorithm for task scheduling problem performs competitively in comparison with the GA based algorithm.

Most previous studies on energy consumption of task scheduling are based on homogeneous computing systems [14, 26–28] or single-processor systems [29]. Researchers in [30] extend the work in [14] with AND/OR model applications which focus on shared-memory multiprocessor systems without consideration of communication. In [28], the researchers adopted DVS (i.e., slack reclamation) to develop a system based on linear programming which exploits slack using. Two scheduling algorithms for bag-of-tasks applications on clusters are proposed in [26]. Researchers of [31] proposed an energy-aware scheduling algorithm with a detailed discussion of slack time computation. The problem of energy-aware task allocation for a computational grid with DVS was studied in [32]. Energy-conscious scheduling heuristic (ECS) that takes into account both makespan and energy consumption is devised in [33].

3. Problem Definition

In the world of virtualized environments (such as cloud computing), successful task scheduling is dependent on the effectiveness of techniques used to execute the task. In our definition, the environment is assumed to be hosted in a data center composed of heterogeneous servers which provide resource by VMs. The servers and VMs may have different memory sizes, processing capacities, and failure rates. Similarly, the communication links may have different bandwidths. It is also assumed that computation can be overlapped with communication. The communications among processors are assumed to perform at the same speed on all links without contentions. Let d be the data center comprised of servers s_1, s_2, \dots, s_s . Let $s_j = \{vm_{j1}, vm_{j2}, \dots, vm_{jm}\}$, where $vm_{j1}, vm_{j2}, \dots, vm_{jm}$ are VMs in the server s_j . Each VM has its own computing capability or speed represented by the number of instructions per second (MIPS).

A parallel application consisting of tasks can be generally represented by a directed acyclic graph (DAG). The vertices of DAG represent the partitioned tasks of the application and the edges of DAG represent precedence constraints among the tasks (if any), as shown in Figure 1. In this paper, we only focus on independent tasks that all the solutions do not contain idle time. Many real world problems can be modeled as a DAG, such as iterative solution of systems of equations, power system simulations, and VLSI simulation programs. A DAG, $G = (N, E)$, consists of a set N of n nodes and a

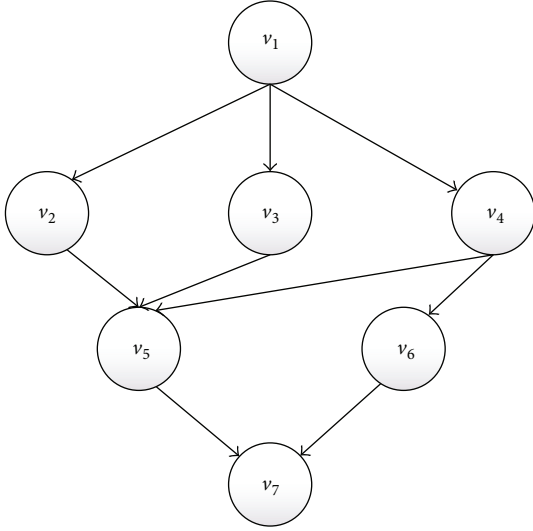


FIGURE 1: A simple task group.

set E of e edges. Let $V = \{v_1, v_2 \dots v_n\}$, where v_1, v_2, \dots, v_n are the sets of tasks to be executed in the data center. Let $r = \{r_1, r_2, \dots, r_n\}$, where r_1, r_2, \dots, r_n are the sizes of the tasks (execution requirement or the number of instructions).

Because of the dissimilar natures of tasks and VMs, the execution times and energy consumption of a task running on different VMs are different. When a task runs on different VMs, the execution time of it may be different. Similarly, when the communication among two tasks is transmitted through different communication paths, the communication time may be different. Notice that when tasks are assigned to the same VM, the communication cost is zero and thus can be ignored. For ease of discussion, we only consider the independent tasks with no communication.

The scheduling optimization problem of makespan and energy consumption is defined as follows: m VMs in a data center are used to finish n tasks by the deadline time T . Assume that n_i is the number of tasks which are assigned to VM i , for $i = 1, 2, \dots, m$; then $n = \sum_{i=1}^m n_i$. A changeless speed for each VM is denoted as s_i . The speed is defined as MIPS. The number of instructions of task v_k is denoted as r_k . The execution time for task v_k on VM i is r_k/s_i . The total execution time for n_i tasks on VM i is defined as $T_i = \sum_{k=1}^{n_i} r_k/s_i$. According to [7], the energy consumption for task v_k on VM i is $E_k = r_k s_i^{\alpha-1}$, where $\alpha = 1 + 2/\gamma \geq 3$ for $0 < \gamma \leq 1$, $i = 1, 2, \dots, m$ and $k = 1, 2, \dots, n_i$. The total energy is $E = \sum_{i=1}^m \sum_{k=1}^{n_i} r_k s_i^{\alpha-1}$. The optimization problem is given below.

Minimize $E = \sum_{i=1}^m \sum_{k=1}^{n_i} r_k s_i^{\alpha-1}$ with constraints $1 \leq n_i \leq n - m + 1$, $n = \sum_{i=1}^m n_i$, $n > m$, $\sum_{k=1}^{n_i} r_k/s_i \leq T$, for $i = 1, 2, \dots, m$, and $k = 1, 2, \dots, n_i$.

Taking into account energy consumption in task scheduling adds another complexity layer to an already complicated problem. Applications in our study are real-time application which means the applications are deadline-constrained. To evaluate the quality of schedules, both makespan and energy consumption should be measured explicitly. Therefore, we

consider both makespan and energy consumption as the performance criteria and try to minimize the energy consumption with the makespan constraint. In Section 4, we propose a new energy-efficient task scheduling algorithm that can find an optimal or near optimal schedule to complete all n tasks on m VMs with minimum or near minimum energy E by the deadline T .

4. Energy-Efficient Scheduling with Makespan Constraint

4.1. Energy-Efficient Analysis. As discussed before, the makespan objective is a given hard constraint and we aim at determining the least possible energy consumption. We mainly focus on the biobjective problem to minimize makespan and minimize energy consumption. Unfortunately, these objectives are conflicting. Inspired by [34], we propose Proposition 1 presenting that the minimum energy consumption is obtained only when all the tasks are mapped to the VM which has the minimum speed. However, mapping all the tasks to the VM which has the minimum speed would lead to a schedule that is arbitrarily far from the optimal makespan.

Proposition 1. *Let Sch be a schedule assigning all tasks to VM j_0 (s_{j_0} is minimal) in topological order. Let enc be the energy consumption of the successful execution of schedule Sch . Then, any schedule $Sch' \neq Sch$, with energy consumption enc' , is such that $enc \leq enc'$.*

Proof. Suppose that $j_0 = 0$ (i.e., $\forall j : s_0 \leq s_j$). Let C_0 be the completion time of all the tasks mapped to VM 0; then, $enc = \sum_{i=0}^{n_0} r_i s_0^{\alpha-1} = s_0^\alpha \sum_{i=0}^{n_0} (r_i/s_0) = C_0 s_0^\alpha$. Let C'_j be the completion time of the last task on VM j with schedule Sch' . Therefore, $enc' = \sum_{j=0}^m C'_j s_j^\alpha$. Let N be the task set and L the task sets that are not executed on VM 0 by schedule Sch' . Then, $C'_0 = C_0 - (\sum_{i \in L} r_i)/s_0$ (there are still some tasks of $N - L$ to be executed on VM 0). Let $L = L_1 \cup L_2 \cup \dots \cup L_m$, where L_j is task set executed on VM j by schedule Sch' ($\forall j_1 \neq j_2, L_{j_1} \cap L_{j_2} = \emptyset$). Then, $\forall j, 1 \leq j \leq m, C'_j = (\sum_{i \in L_j} r_i)/s_j$. Let us compute the difference $enc' - enc$:

$$enc' - enc$$

$$= \sum_{j=0}^m C'_j s_j^\alpha - C_0 s_0^\alpha$$

$$= C'_0 s_0^\alpha + \sum_{j=1}^m C'_j s_j^\alpha - C_0 s_0^\alpha$$

$$= s_0^\alpha \left(C_0 - s_0^{-1} \sum_{i \in L} r_i \right) + \sum_{j=1}^m \left(s_j^{\alpha-1} \sum_{i \in L_j} r_i \right) - C_0 s_0^\alpha$$

$$= \sum_{j=1}^m \left(s_j^{\alpha-1} \sum_{i \in L_j} r_i \right) - s_0^{\alpha-1} \sum_{i \in L} r_i$$


```

{
  Sort all the tasks in the decreasing order of  $r_i$  in a waiting list
  Let  $i = 1$ 
  while the waiting list is not null
    Compute  $M(i)$  for task  $i$ 
    if  $M(i)$  is not null then
      Choose the VM  $j$  that has the minimum  $s_j$  from  $M(i)$ 
      Assign task  $i$  to VM  $j$ 
      Update the completion date of VM  $j$ 
      if the completion date of VM  $j$  is bigger than the given threshold then
        Mark VM  $j$  as non reusable
      end if
    else
      return no solution
    end while
  return the generated schedule
}

```

ALGORITHM 1: The proposed algorithm for task scheduling problem.

$$\begin{aligned}
&= \sum_{j=1}^m \left(s_j^{\alpha-1} \sum_{i \in L_j} r_i \right) - s_0^{\alpha-1} \sum_{j=1}^m \left(\sum_{i \in L_j} r_i \right) \\
&= \sum_{j=1}^m \left((s_j^{\alpha-1} - s_0^{\alpha-1}) \sum_{i \in L_j} r_i \right) \\
&\geq 0 \quad (\text{because } \forall j: s_0^{\alpha-1} \leq s_j^{\alpha-1}).
\end{aligned} \tag{1}$$

Proposition 1 presents that assigning all tasks to the VM that has minimal speed could achieve the goal of minimizing energy consumption. On the basis of Proposition 1, we present below an approximation algorithm based on list scheduling which has a lower complexity and is easy to implement.

Let ω be the given makespan (deadline of tasks). Let $M(i) = \{j \mid C_j + r_i/s_j \leq \omega\}$, where C_j is the completion time of the formal last task on VM j . It is obvious that if task i is executed on $j \notin M(i)$, then the makespan will be greater than ω , and $\forall i, i' \in N$ such that $r_i \leq r_{i'}$, $M(i') \subseteq M(i)$. It can be seen from the definition of $M(i)$ that if task i has less operations than task i' , then all the machines able to schedule i' with makespan less than ω can also be able to schedule i with makespan less than ω . Notice that if ω is very large, $M(i)$ would contain all VMs and hence all the tasks will be scheduled on the VM with the minimal s_i leading to the most energy-efficient schedule. The proposed approach is illustrated in the proposed algorithm. \square

4.2. Algorithm Analysis. The time complexity of the proposed algorithm is in $O(n \log n + m \log m)$. The proposed algorithm could be carried out around a heap. The cost of sorting tasks is in $O(n \log n)$ and sorting VMs costs $O(m \log m)$. The cost of heap operations is in $O(m \log m)$ and scheduling operations costs $O(n)$. The schedule returned by the proposed algorithm

could ensure that the makespan is lower than ω or no such schedule exists.

Researchers in [34] proposed a task scheduling algorithm named CMLT which is also a kind of list scheduling. Different from our algorithm, CMLT tackles the reliability of task scheduling problems and it guarantees the makespan is lower than 2ω (not ω) or returns no solution (Algorithm 1).

5. Experiments and Result Analysis

5.1. Experimental Scenarios. In the verification experiments of our algorithm, the comparison experiments were conducted on a PC with a 2.6 GHz Pentium Dual Core Processor, Windows XP platform. Besides, the experiments used CloudSim 3 simulator [35] to simulate virtualized environments. The toolkit of CloudSim 3 simulator supports modeling of virtualized environments like cloud system components such as data centers, host, VMs, and policies of scheduling. Lots of previous studies conducted evaluation experiments based on CloudSim platform.

In our experiments, a set of VMs are created with different speeds (MIPS) using VM components of CloudSim and the RAM size for all the VMs is set to 512 MB. The number of the VM set is fixed at 12. The speed of each VM (MIPS) is chosen uniformly in $[10^2, 10^3]$. The VM set is used for running the task sets to get the makespan and energy consumption results.

To evaluate the performance of the proposed task scheduling algorithm in virtualized environments, randomly generated problem instances are used. We have randomly generated 10 sets of tasks using Cloudlet component where the length of each task (the computation requirement) is chosen uniformly in $[10^5, 10^7]$ and the number of each task set is set from 100 to 1000 with an increment of 100. These numbers may not be very realistic but provide comprehensive results of the tasks that are easy to read. The task sets are scheduled by the proposed algorithm and comparison algorithms when running in the VM set.

The experiment consists of two steps: firstly, the proposed algorithm and comparison algorithms schedule task sets to the VM set to get the makespan and energy consumption; secondly, the makespan and energy consumption of different algorithms are handled and evaluated. The performance of each phase of the proposed algorithm is presented in comparison with the HEFT, GA, and HPSO algorithms, which are three of the best existing scheduling algorithms. As mentioned earlier, the HEFT heuristic algorithm proposed in [17] which is a kind of list scheduling heuristic method could achieve excellent schedule in terms of makespan for independent-constraint tasks. Eleven heuristics are implemented and compared in [23] and the results show that genetic algorithm (GA) behaves best in all the tested algorithms for task scheduling problems. Researchers in [25] showed that the HPSO algorithm for task assignment problem performs competitively in comparison with the GA based algorithm. To evaluate the performance of the proposed algorithm, we implement HEFT, GA, and HPSO as well as the proposed algorithm to compare their performance. Some changes have to be made to the formal HEFT, GA, and HPSO for convenient implementation and comparison. Besides the primary properties of HEFT, GA, and HPSO, we add the constraint of deadlines: given $\forall j \in Q, L_j$ is the task set consisting of tasks assigned to VM j , and then $\sum_{i \in L_j} r_i/s_j \leq \omega$.

The energy consumption of a schedule has been defined earlier: $E = \sum_{i=1}^n \sum_{k=1}^{m_i} r_k s_i^{\alpha-1}$, where $\alpha = 1 + 2/\gamma \geq 3$ for $0 < \gamma \leq 1$. The makespan is computed as follows: $M = \max\{\sum_{i \in L_j} r_i/s_j\}$. Moreover, some algorithms such as GA which are stochastic approaches may yield different result with each independent running process; we thus run each algorithm 8 times for every problem instance and report the average results. The average percentage improvement (API) is chosen to conduct the performance analysis of the algorithms. The API in the energy consumption for the proposed algorithm over the HEFT, GA, and HPSO, respectively, is computed as (take HEFT for instance)

$$\left(1 - \frac{\text{Enc}_{\text{the proposed algorithm}}}{\text{Enc}_{\text{HEFT}}}\right) \times 100\%. \quad (2)$$

5.2. Results Analysis. Experiments conducted with different numbers of tasks lead to similar results as shown in Figures 2, 3, and 4. These figures plot the makespan, the energy consumption, and the execution time, respectively, with tasks from 100 to 1000. Figure 2 shows that the proposed algorithm is more efficient than HEFT, GA, and HPSO in terms of energy consumption. In these experiments, we consider schedule length and energy consumption as the main metric. The schedule length of the proposed algorithm for different numbers of tasks is bigger than the other algorithms. This is because the selection of VM order in the proposed algorithm is conducted by giving priority to the VMs with low speed under the threshold makespan constraint, which leads to a greater makespan compared with the results of HEFT, GA, and HPSO algorithms. Notice that the HPSO is slightly better than GA in terms of makespan.

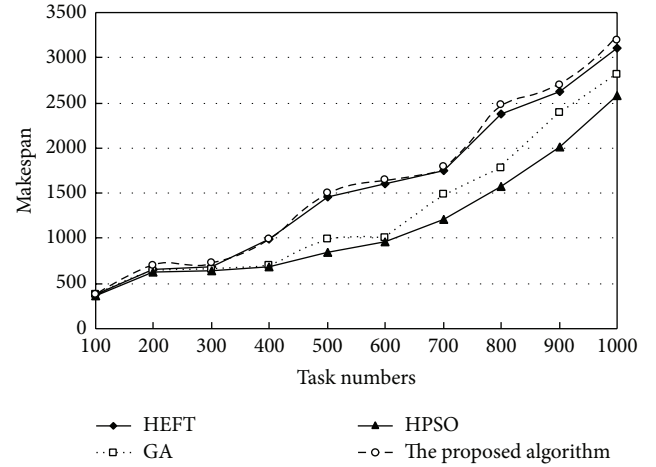


FIGURE 2: Makespan of HEFT, GA, HPSO, and the proposed algorithm with different numbers of tasks.

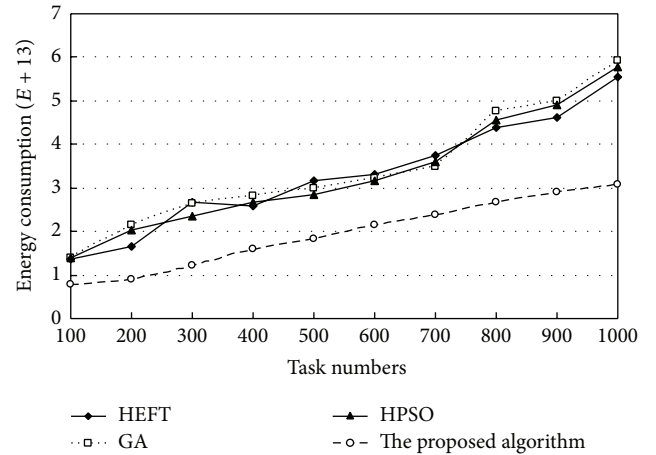


FIGURE 3: Energy consumption of HEFT, GA, HPSO, and the proposed algorithm with different numbers of tasks.

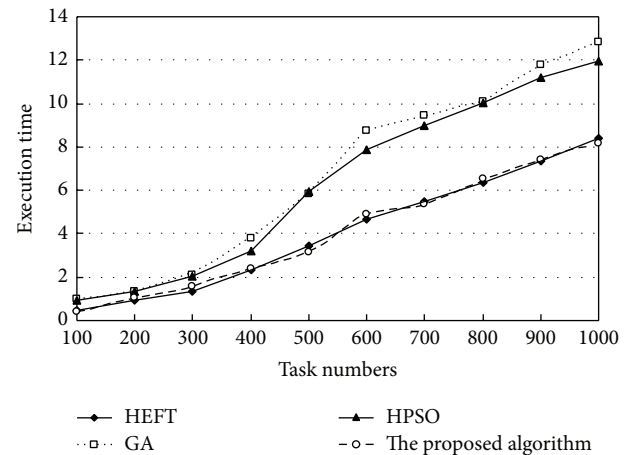


FIGURE 4: Execution time of HEFT, GA, HPSO, and the proposed algorithm with different numbers of tasks.

TABLE 1: Computational results for HEFT, GA, HPSO, and the proposed algorithm (denoted as Alg).

N	Enc($E + 13$)			API (%)			
	HEFT	GA	HPSO	Alg	/HEFT	/GA	/HPSO
10	1.3778	1.3818	1.3983	0.7786	43.49	43.65	44.32
20	1.6587	2.1356	2.0215	0.9023	45.54	57.75	55.36
30	2.6818	2.6512	2.3426	1.2194	54.53	54.01	47.95
40	2.5874	2.8063	2.6862	1.5984	38.22	43.04	40.51
50	3.1639	2.9899	2.8415	1.8165	42.59	39.25	36.07
60	3.3024	3.2114	3.1632	2.1437	35.09	33.25	33.23
70	3.7576	3.4919	3.6034	2.3796	36.67	31.85	33.96
80	4.3788	4.7745	4.5689	2.6832	38.82	43.80	41.27
90	4.6321	4.9899	4.9128	2.8987	37.42	41.91	40.99
100	5.5504	5.9123	5.7867	3.0896	44.34	47.74	46.61

As Figure 3 shows, the proposed algorithm performs best according to energy consumption indicator. The energy consumption results with different task numbers of the proposed algorithm are much better than those of HEFT, GA, and HPSO. The more detailed results and API are presented in Table 1. As we can see from Table 1, our algorithm is better than metaheuristics (GA and HPSO) and HEFT in terms of energy consumption (e.g., its API with HPSO is from 33.23% to 55.36%). It can be also found from Figure 3 that, for the energy consumption indicator, GA is slightly better than HPSO.

Figure 4 shows the average execution times for HEFT, GA, HPSO, and the proposed algorithm. As the number of tasks increases, the running times of algorithms become longer. As Figure 4 shows, the running times of GA and the HPSO are higher than our algorithm. The running time of HEFT is nearly similar to ours. Moreover, list scheduling heuristics (the proposed algorithm and HEFT) performs better than metaheuristics (GA and HPSO) in terms of running time. The reason for this result is that heuristics based on list scheduling tends to get competitive solutions with low time complexity.

6. Conclusions

This paper has focused on energy-efficient task scheduling on VMs in virtualized environments with changeless variable speed, keeping the makespan of each VM within a deadline. We define the problem of minimizing energy consumption with the constraint of schedule length on VMs in virtualized environments. It has been proved in this paper that the speed of the VMs plays a key role in optimal solutions for energy consumption. Based on the analysis, an energy-efficient task scheduling algorithm has been proposed by combining the list scheduling and the key property of VM speed. Task scheduling on VMs has been implemented in simulation and the results demonstrated the better performance of our algorithm in comparison with three other excellent algorithms (HEFT, GA, and HPSO).

Conflict of Interests

The authors declare that there is no conflict of interests regarding the publication of this paper.

Acknowledgment

This work is supported by Shandong Province Natural Science Foundation.

References

- [1] P. Barham, B. Dragovic, K. Fraser et al., "Xen and the art of virtualization," *ACM SIGOPS Operating Systems Review*, vol. 37, no. 5, pp. 164–177, 2003.
- [2] VMware: Virtual Infrastructure Software, <http://www.vmware.com/>.
- [3] A. Kivity, Y. Kamay, D. Laor, U. Lublin, and A. Liguori, "KVM: the linux virtual machine monitor," in *Proceedings of the Ottawa Linux Symposium (OLS '07)*, pp. 225–230, 2007.
- [4] L. M. Zhang, K. Li, and Y. Zhang, "Green task scheduling algorithms with speeds optimization on heterogeneous cloud servers," in *Proceedings of the IEEE/ACM International Conference on Green Computing and Communications (GreenCom '10)*, pp. 76–80, Hangzhou, China, December 2010.
- [5] S. Albers, "Energy-efficient algorithms," *Communications of the ACM*, vol. 53, no. 5, pp. 86–96, 2010.
- [6] A. Beloglazov and R. Buyya, "Energy efficient allocation of virtual machines in cloud data centers," in *Proceedings of the 10th IEEE/ACM International Symposium on Cluster, Cloud, and Grid Computing (CCGrid '10)*, pp. 577–578, Melbourne, Australia, May 2010.
- [7] K. Li, "Performance analysis of power-aware task scheduling algorithms on multiprocessor computers with dynamic voltage and speed," *IEEE Transactions on Parallel and Distributed Systems*, vol. 19, no. 11, pp. 1484–1497, 2008.
- [8] M. Maurer, V. C. Emeakaro, I. Brandic, and J. Altmann, "Cost-benefit analysis of an SLA mapping approach for defining standardized Cloud computing goods," *Future Generation Computer Systems*, vol. 28, no. 1, pp. 39–47, 2012.

- [9] D. Borgetto, H. Casanova, G. da Costa, and J. M. Pierson, "Energy-aware service allocation," *Future Generation Computer Systems*, vol. 28, no. 5, pp. 769–779, 2012.
- [10] G. Qu, "What is the limit of energy saving by dynamic voltage scaling," in *Proceedings of the International Conference on Computer-Aided Design (ICCAD '01)*, pp. 560–563, 2001.
- [11] V. T. D. Truong, Y. Sato, and Y. Inoguchi, "Performance evaluation of a green scheduling algorithm for energy savings in cloud computing," in *Proceedings of the IEEE International Symposium on Parallel & Distributed Processing, Workshops and PhD Forum (IPDPSW '10)*, pp. 1–8, 2010.
- [12] A. Kamthe and S. Lee, "Stochastic approach to scheduling multiple divisible tasks on a heterogeneous distributed computing system," in *Proceeding of the 21st International Parallel and Distributed Processing Symposium (IPDPS '07)*, pp. 1–11, Long Beach, Calif, USA, March 2007.
- [13] Y. C. Lee and A. Y. Zomaya, "On effective slack reclamation in task scheduling for energy reduction," *Journal of Information Processing Systems*, vol. 5, no. 4, pp. 175–186, 2009.
- [14] D. Zhu, R. Melhem, and B. R. Childers, "Scheduling with dynamic voltage/speed adjustment using slack reclamation in multiprocessor real-time systems," *IEEE Transactions on Parallel and Distributed Systems*, vol. 14, no. 7, pp. 686–700, 2003.
- [15] M. Mezma, N. Melab, Y. Kessaci et al., "A parallel bi-objective hybrid metaheuristic for energy-aware scheduling for cloud computing systems," *Journal of Parallel and Distributed Computing*, vol. 71, no. 11, pp. 1497–1508, 2011.
- [16] S. Abrishami and M. Naghibzadeh, "Deadline-constrained workflow scheduling in software as a service Cloud," *Scientia Iranica*, vol. 19, no. 3, pp. 680–689, 2012.
- [17] H. Topcuoglu, S. Hariri, and M. Y. Wu, "Performance-effective and low-complexity task scheduling for heterogeneous computing," *IEEE Transactions on Parallel and Distributed Systems*, vol. 13, no. 3, pp. 260–274, 2002.
- [18] S. C. Kim, S. Lee, and J. Hahm, "Push-pull: deterministic search-based DAG scheduling for heterogeneous cluster systems," *IEEE Transactions on Parallel and Distributed Systems*, vol. 18, no. 11, pp. 1489–1502, 2007.
- [19] Y. C. Lee and A. Y. Zomaya, "A productive duplication-based scheduling algorithm for heterogeneous computing systems," in *Proceedings of International Conference on High Performance Computing and Communications (HPCC '05)*, pp. 203–212, 2005.
- [20] D. Bozdog, U. Catalyurek, and F. Ozguner, "A task duplication based bottom-up scheduling algorithm for heterogeneous environments," in *Proceedings of the IEEE International Parallel and Distributed Processing Symposium (IPDPS '06)*, pp. 1–12, 2006.
- [21] E. Angel, E. Bampis, and V. Chau, "Low complexity scheduling algorithms minimizing the energy for tasks with agreeable deadlines," *Discrete Applied Mathematics*, vol. 175, pp. 1–10, 2014.
- [22] Y. Xu, K. Li, and J. Hu, "A genetic algorithm for task scheduling on heterogeneous computing systems using multiple priority queues," *Information Sciences*, vol. 270, pp. 255–287, 2014.
- [23] T. D. Braun, H. J. Siegel, N. Beck et al., "A comparison of eleven static heuristics for mapping a class of independent tasks onto heterogeneous distributed computing systems," *Journal of Parallel and Distributed Computing*, vol. 61, no. 6, pp. 810–837, 2001.
- [24] S. Jiang, Z. Ji, and Y. She, "A novel particle swarm and gravitational search solving economic emission load dispatch problems with various practical constraints," *International Journal of Electrical Power & Energy Systems*, vol. 55, pp. 628–644, 2014.
- [25] P. Yin, S. Yu, P. Wang, and Y. Wang, "A hybrid particle swarm optimization algorithm for optimal task assignment in distributed systems," *Computer Standards and Interfaces*, vol. 28, no. 4, pp. 441–450, 2006.
- [26] K. H. Kim, R. Buyya, and J. Kim, "Power aware scheduling of bag-of-tasks applications with deadline constraints on DVS-enabled clusters," in *Proceeding of the 7th IEEE International Symposium on Cluster Computing and the Grid (CCGrid '07)*, pp. 541–548, Rio de Janeiro, Brazil, May 2007.
- [27] R. Ge, X. Feng, and K. W. Cameron, "Performance-constrained distributed DVS scheduling for scientific applications on power-aware clusters," in *Proceedings of the ACM/IEEE Super computing Conference (SC '05)*, pp. 34–44, Seattle, Wash, USA, November 2005.
- [28] B. Rountree, D. K. Lowenthal, S. Funk, V. W. Freeh, B. R. de Supinski, and M. Schulz, "Bounding energy consumption in large-scale MPI programs," in *Proceedings of the ACM/IEEE Conference on Super computing (SC '07)*, pp. 1–9, November 2007.
- [29] X. Zhong and C. Xu, "Energy-aware modeling and scheduling for dynamic voltage scaling with statistical real-time guarantee," *IEEE Transactions on Computers*, vol. 56, no. 3, pp. 358–372, 2007.
- [30] D. Zhu, D. Mossé, and R. Melhem, "Power-aware scheduling for AND/OR graphs in real-time systems," *IEEE Transactions on Parallel and Distributed Systems*, vol. 15, no. 9, pp. 849–864, 2004.
- [31] L. Wang, G. von Laszewski, J. Dayal, and F. Wang, "Towards energy aware scheduling for precedence constrained parallel tasks in a cluster with DVFS," in *Proceeding of the 10th IEEE/ACM International Symposium on Cluster, Cloud, and Grid Computing (CCGrid '10)*, pp. 368–377, Melbourne, Australia, May 2010.
- [32] S. U. Khan and I. Ahmad, "A cooperative game theoretical technique for joint optimization of energy consumption and response time in computational grids," *IEEE Transactions on Parallel and Distributed Systems*, vol. 20, no. 3, pp. 346–360, 2009.
- [33] Y. C. Lee and A. Y. Zomaya, "Minimizing energy consumption for precedence-constrained applications using dynamic voltage scaling," in *Proceedings of the 9th IEEE/ACM International Symposium on Cluster Computing and the Grid (CCGRID '09)*, pp. 92–99, May 2009.
- [34] E. Jeannot, E. Saule, and D. Trystram, "Optimizing performance and reliability on heterogeneous parallel systems: approximation algorithms and heuristics," *Journal of Parallel and Distributed Computing*, vol. 72, no. 2, pp. 268–280, 2012.
- [35] N. Rodrigo, R. Rajiv, B. Anton, A. Csar, and R. Buyya, "CloudSim: a toolkit for modeling and simulation of cloud computing environments and evaluation of resource provisioning algorithms," *Software: Practice and Experience*, vol. 41, no. 1, pp. 23–50, 2011.

Research Article

The Regulatory Strategy in Emissions Trading System under Costly Enforcement

Shuai Jin,^{1,2} Yanlin Zhang,¹ and Zhaohan Sheng²

¹ School of Management, Jiangsu University, Zhenjiang 212013, China

² Computational Experiment Center for Social Science, Nanjing University, Nanjing 210093, China

Correspondence should be addressed to Shuai Jin; sjin@ujs.edu.cn

Received 6 June 2014; Accepted 27 July 2014; Published 25 September 2014

Academic Editor: Jianguo Du

Copyright © 2014 Shuai Jin et al. This is an open access article distributed under the Creative Commons Attribution License, which permits unrestricted use, distribution, and reproduction in any medium, provided the original work is properly cited.

In a two-stage dynamic game of regulator and polluting firms, the optimal regulatory strategy to achieve a fixed aggregate emissions target cost-effectively in emissions trading system was studied under the context of costly monitoring and sanctioning, including the monitoring level, the aggregate supply of permits, and the penalty shape for noncompliance. Based on gaming analysis, a heterogeneous agent-based experiment platform for regional emissions trading system was established using computational experiment. Then further analyses were done from perspectives of dynamic and bounded rationality. The results show that the optimal strategy to achieve target is to induce full compliance. This is not simply setting severe punishment, but seeking tradeoff between the level of monitoring and punishment. Finally, integrating the permit price directly into the penalty shape allows the policy objective to be achieved more cost-effective.

1. Introduction

For nowadays, more and more environmental problems are regulated through economic instruments. As an important instrument, emissions trading has been practiced and evolved into an important approach to reduce pollution cost-effectively over the world. In order to mitigate the sharply growing contradictions between economic development and environmental protection, China has put it on important agenda as early as late 1980's. In particular, since the "11th five-year plan," along with the strategic changing of economic growth and environmental management, and the promoting of total quantity control, energy conservation, and emissions reduction strategies, the emissions trading program has received high attentions from each level of Chinese government and has been launched in many areas and industries, such as Taihu Basin and Pearl River Delta. At the same time, lots of environmental property rights exchanges have set up subsequently in Beijing, Tianjin, Shanghai, and so on. However, the pilot programs have failed to bring remarkable success in emissions control for the moment and the development of emissions trading program in China has

been seriously hindered by costly enforcement and significant noncompliance, which could be directly derived from the constraints of budget and capability making the regulators do not have sufficient resources to achieve full compliance [1]. Therefore, it is most anxious to set up the regulatory strategy adapting to the Chinese national conditions to guarantee effective enforcement.

In the environmental regulation research, Downing and Watson Jr. (1974) first proposed the theoretical model of the enforcement of environmental policy [2]. Harford (1978) mainly analyzed the firms' behavior under imperfectly enforceable emission standards and taxes [3]. With emissions trading gradually popularized, many scholars started to devote themselves to the research of the firms' behavior and optimal enforcement under this policy. However, lots of theoretical literatures focus on the outcome of emissions trading system under full compliance [4, 5]; several literatures mainly assume that full compliance cannot be achieved [6–9]. Regarding the fact that the insufficient enforcement resources became an important limitation in practice, some scholars examine the optimal enforcement strategy of a budget-constrained regulator who does not have sufficient

resources to induce full compliance [10]. Stranlund (2007) further addresses whether emissions trading systems should be designed and implemented to achieve full compliance in order to achieve a fixed aggregate emissions target cost-effectively [11]. However, the existing theoretical literature on optimal enforcement and regulatory of emissions trading system often makes particular assumptions on the penalty function, while the empirical studies confirm the use of both gravity and nongravity components in the structure of penalty [12]. Meanwhile, the pollution level is usually treated as an exogenous variable. Actually, once the permit is endowed with negotiability, it will be bound to the property and production factors of firms along with labor and raw materials, and many links of firms operation will be obviously affected. So it is necessary to consider firms production, abatement, and permits trading together from the individual level. In addition, simply analyzing from individual level is not enough, the chronicity of ecosystem restoration has ordained the emissions trading programs which usually requires a long process of implementation; thus, it is also very necessary to reexamine the effectiveness and efficiency of regulatory strategy from the long-time dynamical evolution perspective.

According to above analysis and literature review, a two-stage dynamic game of regulator and polluting firms is built to research on the optimal regulatory strategy to achieve the fixed aggregate emissions target cost-effectively in emissions trading system from three aspects: the aggregate supply of permits for initial allocation, monitoring level, and penalty shape. Then, an agent-based experiment platform is established using computational experiment method for a further discussion on the feasibility and efficiency of the regulatory strategy from the dynamic evolution perspective.

2. The Model and the Game Analysis

This work moves from the paper by Stranlund (2007) [11] and makes some adjustments, involving a regulatory model in which the regulator chooses the optimal strategy to which the firms react. Throughout consider a regulator and a fixed set of N heterogeneous risk-neutral firms emitting the same uniformly mixed pollutant in an emissions trading system without any forms of banking and borrowing.

Under the current environmental monitoring system, the regulator cannot get complete information of firms' actual emissions, and therefore, the profit-driven nature and the environmental externalities make firms' operation decision-making is based on the cost-benefit analysis of various schemes. The firm i generates pollution as the result of its production activity. The pollution level emitted in the absence of any regulation is denoted by e_i . Further assume $e_i = k_i q_i$, where q_i and k_i , respectively, denote the firm's output and pollution generation coefficient. More formally, define the revenue function to be the following: $b_i(e_i) = \theta_i q_i - d_i(q_i)$, where θ_i denotes the market price of the product, $d_i(q_i)$ denotes the production cost, $b_i'(e_i) > 0$, $b_i''(e_i) < 0$. The pollution can be abated at a cost $c_i(a_i)$, where a_i is the firm's abatement, with the usual assumptions $c_i'(a_i) > 0$, $c_i''(a_i) > 0$, $a_i \geq 0$. Each

permit confers the legal right to release one unit of emissions. Let l_i^0 be the number of permits that are initially allocated to firm i and let l_i be the number of permits that it chooses to hold after trade. In permit market equilibrium, all trades take place at a single market price p . If the firm is compliant, in order to achieve total quantity control objectives, $e_i \leq a_i + l_i$ and the violation $v_i = 0$; otherwise, its pollution emitted would exceed the number of permits holding and the violation $v_i = e_i - a_i - l_i > 0$. Assume that permits cannot be banked or borrowed, thus the firm's rational action is $e_i = l_i + v_i + a_i$. When $l_i^0 > l_i$, the firm will sell the surplus permits; conversely, it will buy from the market. Moreover, let E , A , and V denote the aggregate pollutions generated, abatements, and violations of all firms, respectively.

The regulator can readily observe l_i^0 and l_i for each firm i , but cannot observe the firm's actual emissions emitted without a costly and perfectly accurate monitoring activity. Assume the firm is inspected with probability $\pi_i \in [0, 1]$, namely, the monitoring level on firm i . Suppose the monitoring cost per inspection is $\mu > 0$. Without loss of generality, assume the violation is penalized according to a penalty function $F(v_i) = F_0 + f(v_i)$ once the firm is inspected, where F_0 is fixed penalties, $f(v_i)$ is variable penalties, $f' \geq 0$, $F(0) = 0$, $f(0) = 0$. However, the sanctioning is costly too. Let $\beta > 0$ be the per-unit cost of collecting penalties from noncompliant firms. Hence, the total expected enforcement costs are: $TE(\pi, \mathbf{v}) = \sum_{i=1}^N \pi_i [\beta F(v_i) + \mu]$, where $\pi = (\pi_1, \pi_2, \dots, \pi_N)$, $\mathbf{v} = (v_1, v_2, \dots, v_N)$. In order to holding aggregate emissions to a pre-specified target \bar{E} , the regulator has various strategic choices. If there exists noncompliance in region, the regulator can adjust the aggregate supply of permits $L \leq \bar{E} - V$, or induce the noncompliant firms to decrease their violations by increasing π_i or $F(v_i)$. However, the regulation will inevitably affect the region's economic output, social abatement costs, enforcement costs, and so forth. Let $C(\mathbf{a}, L)$ and $B(\mathbf{e}, L)$ represent the aggregate abatement costs and the social economic output, respectively, when the aggregate supply of permits is L , where $C(\mathbf{a}, L) = \sum_{i=1}^N c_i(a_i)$, $B(\mathbf{e}, L) = \sum_{i=1}^N b_i(e_i)$, $\mathbf{a} = (a_1, a_2, \dots, a_N)$, $\mathbf{e} = (e_1, e_2, \dots, e_N)$. Throughout assume the regulator's objective is to maximize the social welfare.

As shown above, the relationship between regulator and polluting firms is a dynamic gaming process. Firstly, the regulator selects the regulatory strategy including L , π , and $F(v)$ to achieve the fixed aggregate emissions target cost-effectively; then firms make optimal decisions to maximize net profit under given π_i and $F(v)$. The regulatory choice could be modelled as a two-stage game with complete information as the following:

$$\max_{\{L, \pi, F(\cdot), \mathbf{v}\}} SW = B(\mathbf{e}, L) - C(\mathbf{a}, L) - TE(\pi, \mathbf{v}) \quad (1)$$

$$\begin{aligned} \text{s.t. } \max_{\{e_i, a_i, v_i\}} \Pi_i &= b_i(e_i) - c_i(a_i) - p(e_i - a_i - v_i - l_i^0) \\ &\quad - \pi_i F(v_i) \quad i = 1, 2, \dots, N, \end{aligned} \quad (2)$$

where $\mathbf{e} \geq 0$, $\mathbf{a} \geq 0$, $\mathbf{v} \geq 0$, $\mathbf{e} - \mathbf{a} - \mathbf{v} \geq 0$, $L + V \leq \bar{E}$.

The problem above is solved by backward induction.

2.1. The Behavior of the Firm. Given π_i and $F(v_i)$, the firm makes decision in two steps: firstly determines whether compliance is cost-effective or not and then makes the optimal operation decision.

Lemma 1. *Given π_i , $F(v)$, the firm's optimal decision is $c'_i(a_i) = p$, $b'_i(e_i) = p$, no matter the firm is compliant or not. But if the firm is noncompliant, the necessary condition that its violations is cost-effective is $\pi_i f'(v) = p$, the firm's optimal violation is the following:*

$$\begin{aligned} \text{If } F_0 = 0, \quad \text{then } v_i^* &= \begin{cases} 0, & \pi_i f'(0) \geq p \\ v, & \pi_i f'(v) = p; \end{cases} \\ \text{if } F_0 > 0, \quad \text{then } v_i^* &= \begin{cases} 0, & \pi_i F(v) \geq pv \\ v, & \pi_i F(v) < pv. \end{cases} \end{aligned} \quad (3)$$

Proof. If the firm chooses to reach the standard, then $a_i + l_i = e_i$, $v_i = 0$, put into formula (2), from its first-order conditions, the firm's optimal decision meets $b'_i(e_i) = p$, $c'_i(a_i) = p$; If the firm chooses to be noncompliant, then $a_i + l_i + v_i = e_i$, $v_i > 0$, so the first-order conditions of formula (2) are as following:

$$c'_i(a_i) - \pi_i f'(v_i) = 0, \quad (4)$$

$$p - \pi_i f'(v_i) = 0, \quad (5)$$

$$p - b'_i(e_i) = 0. \quad (6)$$

Combining formula (4) and formula (5) yields $c'_i(a_i) = p$. Furthermore, when $F_0 = 0$, $\pi_i = p/f'(v)$ implies the firm's violations is v , then the equilibrium condition for encouraging the firm to be compliant is $\pi_i = p/f'(0)$, such that if $\pi_i \geq p/f'(0)$, compliance will be the optimal decision of the firm; otherwise, the optimal violation will be $v_i^* = \varphi^{-1}(p/\pi_i) > 0$, where $\varphi(x) = f'(x)$. When $F_0 > 0$, the objective function of the firm is discontinuous at $v = 0$, then if $\pi_i = p/f'(v)$, the firms still have to compare the expected costs of complying and noncomplying. In this case, if $pv \leq \pi_i F(v)$, then $v_i^* = 0$; otherwise, $v_i^* = v$. This completes the proof. \square

From Lemma 1, (a) the firms' optimal decision of production and abatement only depends on permit price, independent of π_i and $f(v)$; (b) F_0 does not affect the firm's marginal behavior and just increases its expected costs in the event of noncompliance. So the threshold of monitoring level inducing the firms to comply with regulation is $p/f'(0)$ when $F_0 = 0$, and it would be less than $p/f'(0)$ while $F_0 > 0$; (c) no matter what F_0 is, as long as the firm chooses to be noncompliant, the firm's violation choice depends only on the permit price and enforcement variables, not on its own parametric characteristics, such as production and abatement costs. In particular, since the permit price and enforcement variables do not vary across firms, some academics such as Stranlund have already pointed out that even a budget-constrained regulator should not use parametric differences among regulated firms to guide its decisions about distributing monitoring and enforcement efforts [10, 11].

Consequently, there is a main feature of firm's behavior under emissions trading system differing from that under command-and-control means. Under the latter, the firms facing high abatement costs or stringent emission standards have greater motivation to be noncompliant, therefore, the exogenous characteristics of firm is the key factor to the design of the optimal monitoring and enforcement of emissions standards [13]. In emissions trading system, the permit price tightly links firms' decision-making of the production, abatement, and violation together and turns into the important indicator to measure the cost-effectiveness of firms' operation decisions. Thorough permits trading, permits flow directly from the firms of lower abatement costs to the higher, and the social abatement costs will be reduced; meanwhile, the resources flow to the firms have higher productivity indirectly, and then the resource utilization and social capital will be improved, among which the market price of permits fulfills two important functions in the system: rationing function and allocative function [14].

2.2. The Optimal Regulatory Strategy Analysis. From above analysis regulator can infer the optimal decision of the firms under given π and $F(v)$ and then can select the optimal strategy to achieve the fixed aggregate emissions target cost-effectively.

Lemma 2. *If $L^* = \bar{E} - Nv^*$, $\pi^* = p/f'(v^*)$, $v^* < \bar{E}/N$, then p^* , E^* , and A^* are constants, and $A^* = E^* - \bar{E}$.*

Proof. Using contradiction, assume there exists two equilibrium permit price p^1 and p^2 with $p^1 > p^2$. Under given p^1 and p^2 , the pollution, abatement, permits holding, and violation of firm i are e_i^1 , a_i^1 , l_i^1 , v_i^1 , and e_i^2 , a_i^2 , l_i^2 , v_i^2 , then $e_i^1 = a_i^1 + l_i^1 + v_i^1$, $e_i^2 = a_i^2 + l_i^2 + v_i^2$. From Lemma 1, it is obvious that $b'_i(e_i^1) = c'_i(a_i^1) = p^1$, $b'_i(e_i^2) = c'_i(a_i^2) = p^2$. Because of $b''_i(e_i) < 0$, $c''_i(a_i) > 0$, $e_i^1 < e_i^2$, $a_i^1 > a_i^2$, so $l_i^1 + v_i^1 < l_i^2 + v_i^2$, then $\sum_{i=1}^N (l_i^1 + v_i^1) < \sum_{i=1}^N (l_i^2 + v_i^2)$. The total amount of permits will not get changed after market redistribution, hence $L^* + \sum_{i=1}^N v_i^1 < L^* + \sum_{i=1}^N v_i^2$. From Lemma 1, under given π^* , $v_i^1 = v_i^2 = v^*$, $L^* + Nv^* < L^* + Nv^*$ can be obtained, thus the assumption is false. Therefore, when the condition of Lemma 2 is satiated, the only equilibrium price p^* exists. From Lemma 1, the optimal decision a_i^* and e_i^* both are constants, so A^* and E^* both are defined, and $A^* = \sum_{i=1}^N a_i^* = E^* - \sum_{i=1}^N l_i - \sum_{i=1}^N v_i = E^* - \bar{E}$. This completes the proof. \square

It can be seen that the regional abatement costs and economic benefits are only related to the environmental capacity and not affected by any alternative regulatory strategies if only the regulator allocates the permits in strict accordance with the aggregate emissions target. Then, the design of socially optimal regulatory strategy is to ensure the enforcement cost-effective. From Lemma 1, although noncompliance is the reaction of the regulatory scheme, the regulator still can regulate it by changing the monitoring level or penalty scheme, and so forth; thus, the violations of firms can be treated as regulators decision variables. Therefore under a

given punishment scheme, the optimal regulatory strategy can be translated into

$$\begin{aligned} \min_{\{\pi, \nu\}} \quad & \beta\pi F(\nu) + \mu\pi \\ \text{s.t.} \quad & \pi f'(\nu) - p = 0, \quad \nu \geq 0. \end{aligned} \quad (7)$$

Formula (7) shows regulator's dilemma most adequately. The monitoring costs have positive correlation to π , lower π makes lower monitoring costs, but ν will get increased, and then expected sanction costs would increase. So, the regulator has to make tradeoffs between the monitoring costs and the sanction cost. Then, if the cost-effective strategy does not allow any violation, the regulator should keep $L^* = \bar{E}$; otherwise, induce firms to be noncompliance, $L^* = \bar{E} - N\nu^*$, but with the condition $\nu^* \leq \bar{E}/N$, or the emissions trading would be gradually reduced to the pollution discharge fee system.

Proposition 3. *The sufficient condition of the optimal strategy inducing compliance is: $(\mu + \beta F_0)f''(0) \leq \beta f'^2(0)$, $\pi^* = p/f'(0)$; the necessary condition of the optimal strategy inducing noncompliance is $(\mu + \beta F_0)f''(0) > \beta f'^2(0)$ and meets $\pi^* = p/f'(\nu^*)$, $\beta f'^2(\nu^*) = (\mu + \beta F_0)f''(\nu^*)$, $L^* = \bar{E} - N\nu^*$.*

Proof. The Lagrange function of formula (7) is $L = \pi[\mu + \beta F(\nu)] + \lambda[\pi f'(\nu) - p] - \lambda_2 \nu$, then the necessary and sufficient condition of its optimality should meet

$$L'_\nu = \pi\beta f'(\nu) + \lambda\pi f''(\nu) - \lambda_2 = 0, \quad (8)$$

$$L'_\pi = \mu + \beta F(\nu) + \lambda f'(\nu) = 0, \quad (9)$$

$$\pi f'(\nu) - p = 0, \quad (10)$$

$$\lambda_2 \nu = 0, \quad \lambda_2 \geq 0. \quad (11)$$

First of all, consider the situation that the optimal regulatory strategy inducing compliance, that is, $\nu = 0$. From formula (11), $\lambda_2 \geq 0$. Putting it into formula (8), we get

$$\beta f'(0) + \lambda f''(0) \geq 0. \quad (12)$$

From formula (9) we get

$$\mu + \beta F_0 + \lambda f'(0) = 0. \quad (13)$$

Put formulae (12) and (13) together, it is obvious that the necessary and sufficient condition of the optimal regulatory strategy that encourage firms to follow the rules is

$$\beta f'^2(0) \geq (\mu + \beta F_0) f''(0). \quad (14)$$

However, when $F_0 > 0$, the enforcement costs are discontinuous at $\nu = 0$. Even if the conditions above cannot be met, if F_0 is large enough, it still can make a deterrence on firms; thus, formula (14) is not the necessary condition that induces compliance. When $\beta f'^2(0) < (\mu + \beta F_0)f''(0)$, inducing noncompliance is the optimal strategy, but a large enough F_0 still can drive firms to be compliant,

thus, $\beta f'^2(0) < (\mu + \beta F_0)f''(0)$ is just a necessary condition that induces noncompliance. Only if $F_0 = 0$, the conditions above are necessary and sufficient.

When the optimal strategy need regulator induce noncompliance, that is, $\nu > 0$, from formula (11), $\lambda_2 = 0$. Put it into formula (8), it is obvious that $\beta f'(\nu) + \lambda f''(\nu) = 0$. Thus, if the regulator needs to induce noncompliance, the optimal strategy should meet $\beta f'^2(\nu) = (\mu + \beta F_0)f''(\nu)$ and $\pi f'(\nu) - p = 0$. This completes the proof. \square

Proposition 4. *If the optimal regulatory strategy is encouraging compliance, then $f''(0) = 0$, $f'(0)$ the bigger the better; otherwise, $f'(0) = 0$, $f''(0)$ the bigger the better. But in any case, $F_0 = 0$.*

Proof. If the optimal regulatory is encouraging compliance, then the sanctions costs will be 0. Thus, the pursuing of social welfare maximization turns into minimizing the monitoring costs. From Lemma 1, when $F_0 = 0$, the optimal regulatory level π is in inverse proportion to $f'(0)$, so that the greater $f'(0)$ the greater social welfare; when $F_0 > 0$, the increasing F_0 will lead to the threshold of firms violation increased, the optimal regulatory level $\pi < p/f'(0)$. At this time, seem like the bigger F_0 the better, but the precondition is to ensure F_0 is able to drive the firms to be compliant, otherwise, the optimal violations is only related to the marginal penalty; thus, the intervention of F_0 will bring greater risk of violations. Proposition 3 still shows that, the bigger $f'(0)$, the smaller F_0 and $f''(0)$, the sufficient condition of the optimal strategy encouraging compliance is easier to meet.

If inducing noncompliance is the optimal strategy, there will be costs of sanctions. From the proof of Proposition 3, F_0 does not affect the optimal condition, but it will increase the sanctions costs, thus social welfare will be better when $F_0 = 0$. Use Taylor Series Expansion to approximately $f(\nu)$, then $F(\nu) = f'(0)\nu + f''(0)\nu^2/2$. It is obvious that, when $2df'(0) + \nu df''(0) = 0$, the fines collected are the same under all penalty schemes that optimal violations induced equals to ν . Differentiating the lagrange function in Proposition 3, we obtain

$$\begin{aligned} \frac{dL}{df'(0)} &= \frac{\partial L}{\partial f'(0)} - \frac{\partial L}{\partial f''(0)} \frac{df''(0)}{df'(0)} \\ &= \pi [(\beta\nu + \lambda) df'(0) - (\beta\nu + 2\lambda) df'(0)] \\ &= -\lambda\pi df'(0). \end{aligned} \quad (15)$$

From formula (9), $\lambda < 0$, $dL/df'(0) > 0$. Thus, when the fines are given, the rising of $f'(0)$ will increase enforcement costs, and reduce social welfare. Due to $df''(0)/df'(0) = -2/\nu$, the smaller $f'(0)$ makes the bigger $f''(0)$. Thus, if the optimal strategy is inducing firms to break the rules, than the social welfare will be superior when $f'(0) = 0$. This completes the proof. \square

However, aggregate supply of permits and optimal monitoring level depend on whether the regulator chooses to induce compliance or noncompliance. Thus, the regulator still has to make a choice between the two strategies.

Proposition 5. *The social optimal regulatory strategy to achieve the fixed aggregate emissions target is encouraging the firms to be compliant, and meets: $L = \bar{E}$, $\pi^* = p/f'(0)$, $F(v) = f'(0)v$, and $f'(0) > p$.*

Proof. Assume that the strategy of encouraging compliance and the strategy of inducing noncompliance are implemented in the same region with the same $\hat{\pi}$. Using subscript 0 and v to distinguish the two strategies, then the monitoring costs under the two strategies is $N\mu\hat{\pi}$. When the regulator encouraging compliance, $f'_0(0) = p/\hat{\pi}$, expected fine is zero, $TE_0 = N\mu\hat{\pi}$; when inducing noncompliance, $f'_v(0) + f''_v(0)v = p/\hat{\pi}$, $v > 0$, the expected fine is higher than zero, $TE_v > N\mu\hat{\pi}$. So, it is obvious that $TE_0 \leq TE_v$. Moreover, the optimal design of regulatory strategy encouraging compliance is independent of the regulator's costs function, and only related to the permit price. In addition, put Proposition 4 into Proposition 3, we can conclude that the necessary condition to encourage compliance is $\beta f'^2(0) \geq 0$, it means this strategy will play a role only if $\beta \geq 0$; and the optimal strategy design to induce noncompliance is $\beta v^{*2} f''(0) = \mu$, because $v^* \leq \bar{E}/N$, $\beta \bar{E}^2 f''(0) \geq \mu N^2$, so under this case need $\beta \geq \mu N^2 / [\bar{E}^2 f''(0)] > 0$. Therefore, in contrast, the strategy encouraging compliance has a wider range of application space than that inducing noncompliance. This completes the proof. \square

It is worthwhile to note that the proposition above holds only if $\beta > 0$; that is, sanctioning is likely to be costly, including the administrative costs of collecting evidences, imposing penalties, and so on. But if the regulator can gain benefits from the administrative sanctions, the seeking for the cost-effectiveness of the regulator will lead to the absence of regulation. This is worth considering in China's environmental regulation.

3. Further Analyses Based on Computational Experiment

Using a game analysis, the optimal regulatory strategy in emissions trading system is analyzed from the static equilibrium perspective. However, there implies an important assumption implied; that is, the regulator and the firms have rational expectation of permit price. In reality, the emissions trading system is a complex system that is composed of numerous autonomic and adaptive agents. The incompleteness of information, the nonlinear correlation between elements, and the framing effect driven by experience and the behavioral bias make the evolution of the system unstable and have polymorphic equilibrium. The regulator cannot predict the system state effectively and choose the optimal strategy consequently. Meanwhile, the regulation and other external disturbance would aggravate the uncertainty of system evolution. Thus, based on the game analysis, an experimental model for emissions trading system is established using computational experiment method to further analyze the regulatory strategy closer to the reality from the perspective of dynamic and bounded rationality and give the argument of

the feasibility and economic rationality of different regulatory choices.

3.1. Computational Experiment Modeling. The summary of computational experiment model in this study is shown in Figure 1. Use multi-agent technology to realize the modeling of the heterogeneity of agents, according to the game analysis, set the corresponding process and decision rules, and entrust the abilities of independent decision-making, memory, and self-learning to the agents as follows.

(a) *Sample Structure.* For firm i , $d'_i(q) = d_i^F + d_i^V q$, $d'_i(q) = d_i^F + d_i^V q$, and let d_i^V , c_i^V be variable cost, effected mainly by the price of raw material, fuel and power. Then the firm's net income under given q_i can be calculated by $\Pi_i = \theta_i k_i q_i - k_i(d_i^F q_i - c_i^F a_i) - k_i^2(d_i^V q_i^2 - c_i^V a_i^2) + \xi$, where ξ denotes fixed-income. As ξ does not affect the marginal behavior of firms, set $\xi = 0$. In consideration of there has visible difference between k_i , θ_i , d_i^V , and c_i^V in the real, use multiagent technology to generate heterogeneous samples and assume the same specific attribute among firms approximately follow a lognormal distribution.

(b) *Initial Allocation.* From the Coase Theorem, it can be known that if transaction costs are zero, the optimal distribution of permits can be achieved by permits trading among firms, no matter how the permits are initial allocated. Therefore, assume that the government adopts uniform proportion reduction method to allocate permits. The reduction rate is $R = 1 - \bar{E}/E$. Then permits that firm i is allocated can be calculated by $l_i^0 = R \cdot e_i$.

(c) *Firm's Behavior.* When each trading period begins, the firms predict the permit price p_i^t based on specific decision-making mechanism and then make its operation decisions; see Lemma 1. If the permits are more than needed, the surplus will be sold at the price not less than p_i^t ; otherwise, buy from the market, but the purchasing price of permits should no higher than $c_i^t(e_i - l_i^0)$. That is, the demander who has a lower p_i^t also can buy t_i permits at market price to lower the marginal abatement cost in current period $c_i^t(e_i - l_i^0 - t_i) = p^t > p_i^t$, in order to make up for the loss from predicting falloff as much as possible. After each period, the demanders who have not purchased enough permits would keep on abating emissions in order to fulfill responsibility of emissions control. Meanwhile, the suppliers who have not sold out surplus permits would adjust its abatement plan to fit the permits holding; and then the firms get in to the learning process to improve the accuracy of future predictions.

(d) *Permits Trading Market.* After suppliers and demanders anonymously submit the quantity of supply and demand and reserve prices, the model will run into permits price formation process. The model does not describe the market trading mechanisms commonly practiced detailedly, such as sealed auction, but adopts a trading mechanism as a Walrasian auction of permits simulating the dynamic process of market trading [15]. The government similar to the Walrasina

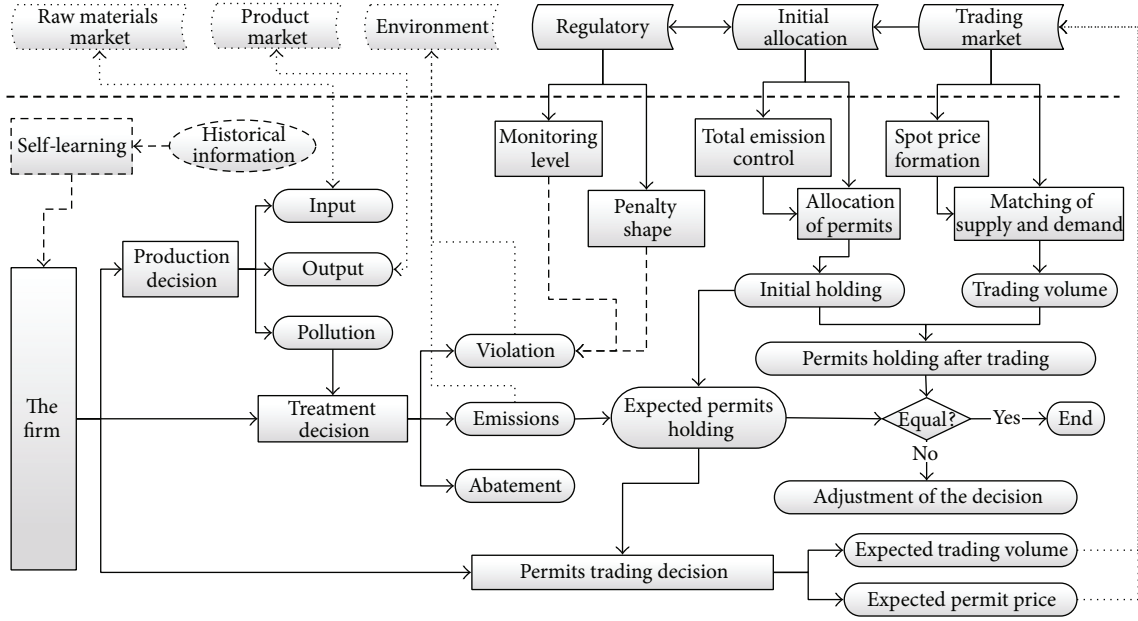


FIGURE 1: Sequence of events in a typical period.

auctioneer, who has information on supply and demand of permits as well as the reserve prices of firms, takes use of the computer to match the suppliers and the demanders so that the permit in the market would realize the optimal allocation, and further obtains the spot price at every trading period. In other words, the auction consists of two stages: a search stage, in which the auctioneer searches for the equilibrium price that meets to be no less than the reserve price of seller and no higher than the maximum purchasing price of demanders; and a second stage, in which transactions are effectuated at market equilibrium prices.

3.2. Experiment Design and Result Analysis. From the game analysis, it is found that the optimal strategy to achieve the fixed emissions target is $L = \bar{E}$, $f'(0) = p/\pi$, encouraging compliance. However, there exists deviation between the equilibrium and the prediction of permit price value in reality. Thus, introduce the notion of the level of punishment to describe the rate of the actual marginal penalty and theoretical marginal penalty. Then, we can fix the level of monitoring and specifically examine the regulatory strategy under incomplete information conditions from the level of punishment. The experimental procedure is as follows: first of all, generate the experimental sample, simulate the evolution of the system under given punishment level. Each simulation runs 80 periods. Besides, regarding the fact that the firms' decision-making is not irreversible and pate dependent, and affected by other random factors, each experiment result only is a path of system evolution. Therefore, for the analysis, the above experiment runs for 500 times to eliminate these interference factors. Above is a group of experiments. Set the level of punishment from 0.025 to 1.5, respectively, and 60 groups of experiments are taken. In each group

of experiments, in order to ensure the homogeneity of the experimental samples, the model adopts the pseudo-random number generator to initialize the same set of firm agents for each simulation.

Initial parameters setting: $N = 100$, $\pi = 0.5$, $\beta = 0$, $\mu = 0$, $E(k_i) = 1$, $D(k_i) = 0.2$, $\bar{E} = L = 50000$ ton, $D(d_i^V) = D(c_i^V) = 0.5$ RMB/kg, $E(d_i^V) = E(c_i^V) = 2$ RMB/kg, $E(\theta_i) = 6$ RMB/kg, $D(\theta_i) = 2$ RMB/kg.

Through the data processing of the final state of system evolution under different scenarios, the influence of punishment level on system evolution is obtained, as shown in Figure 2. From Figure 2, when the punishment level is higher than the theoretical value, that is, 1, the system can evolve close to equilibrium state eventually, and higher punishment level bring any change. However, the permit price declines rapidly with the punishment level bring down from 1; when the punishment level is lower than 0.45, the permits are almost worthless. Meanwhile, the standard deviation of the permit price increase than decrease, it indicate that when the punishment level is lower than 1, the market price would gradually lose the functions of rationing and allocative, particularly when the punishment level is lower than 0.6, the price variance is even higher than the mean value, the system almost runs in chaos. Furthermore, the aggregate abatements and permits trading volume decrease with the decline of punishment level; although the social economic output is growing, the situation of sharp cutoff of social welfare becomes blindingly obvious. Thus, the inharmony between the level of punishment and monitoring will have negative effects on the permit price, which would react on the decision-making of firms, and result in the lower efficiency. Moreover, the decrease of punishment level would make the aggregate abatement costs decreasing, but the costs seemingly disappear has passed to the firms in the form of penalties,

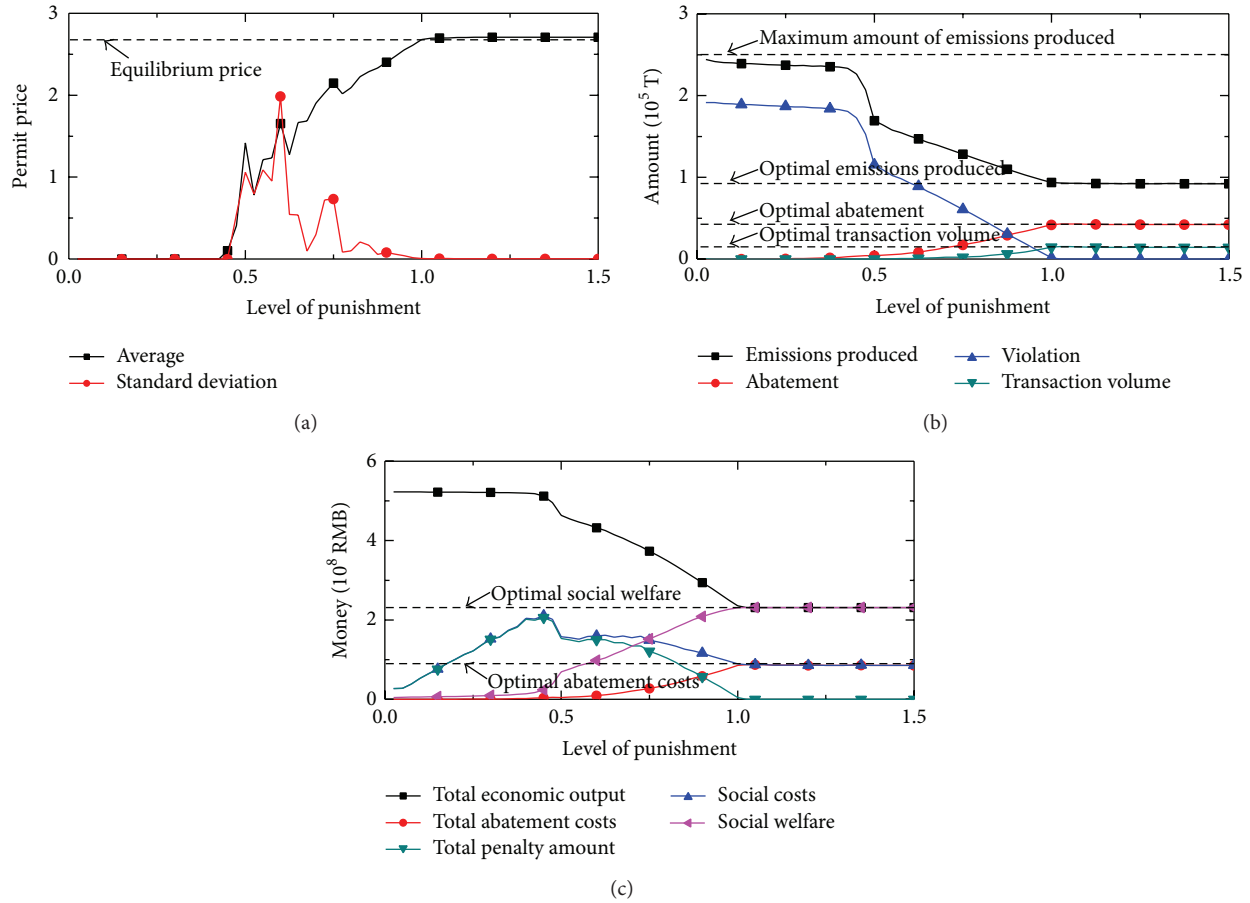


FIGURE 2: Evolution results under difference punishment.

and make the pressure of firms not decrease but increase; Besides, if $\beta > 0$, the regulator would bear the greater pressure of enforcement costs. Thus, it can be seen that reasonable matching between the level of punishment and monitoring is the key factor to the efficiency of the system and a hard nut to crack in reality.

To deeply understand how the punishment level affects the system evolution, through the data processing of the evolution process, the tendency of permit price, aggregate violations, and social welfare in the first 30 cycle under different scenarios are sorted out, as shown in Figure 3. It is easy to find that a reasonable punishment level also has an important impact on the effective running of system. The higher punishment level makes the more stable order of permit price, tending to equilibrium. When punishment level is improper, the market price will be in fluctuating, and the amplitude decrease with the increasing of punishment level; meanwhile, violations and social welfare both are stay in nonoptimal levels. The deeply analysis of Figure 3(b) makes us maintain vigilance of pursuing the reasonable regulatory strategy. On one hand, a little inappropriate punishment level may serious damage the environment, for example, when punishment level is 0.75, the violations are already exceed the environment capacity, even if the regulator do not allocate permits, the environmental quality will still

deteriorate. On the other hand, at any punishment level, the effect of the regulatory is obviously hysteretic. The regulator cannot judge from the price that whether the level setting is proper. Moreover, the noncompliance cannot be completely eradicated at initial stage. Even if the punishment level is 1, there exist high violations, although the violations would gradually disappear with the system running. Furthermore, the openness of emissions trading system has ordained that it would be inevitably influenced by external environmental. Based on the previous experimental setting for the base year, adopt the Producer Price Index (PPI) from 1985 to 2008 to reflect the fluctuant trend of the products prices, and use the Purchasing Price Index of raw material, fuel, and power in the same period to reflect the fluctuant trend of the costs of firms' production and abatement. By experiment, we get the fluctuant trend of the equilibrium price of permits under dynamic economy, showed in Figure 4. Figure 4 indicates that the permit price changes from 2.6 RMB/kg in the base year to 11 RMB/kg as time goes on, nearing a fourfold increase. Thus, the variability of permit price under dynamic economy must be a big obstacle to the effective enforcement.

It can be seen that, the hysteretic of regulatory effect and the variability of permit price make the static regulatory strategy under which the regulator decide the punishment

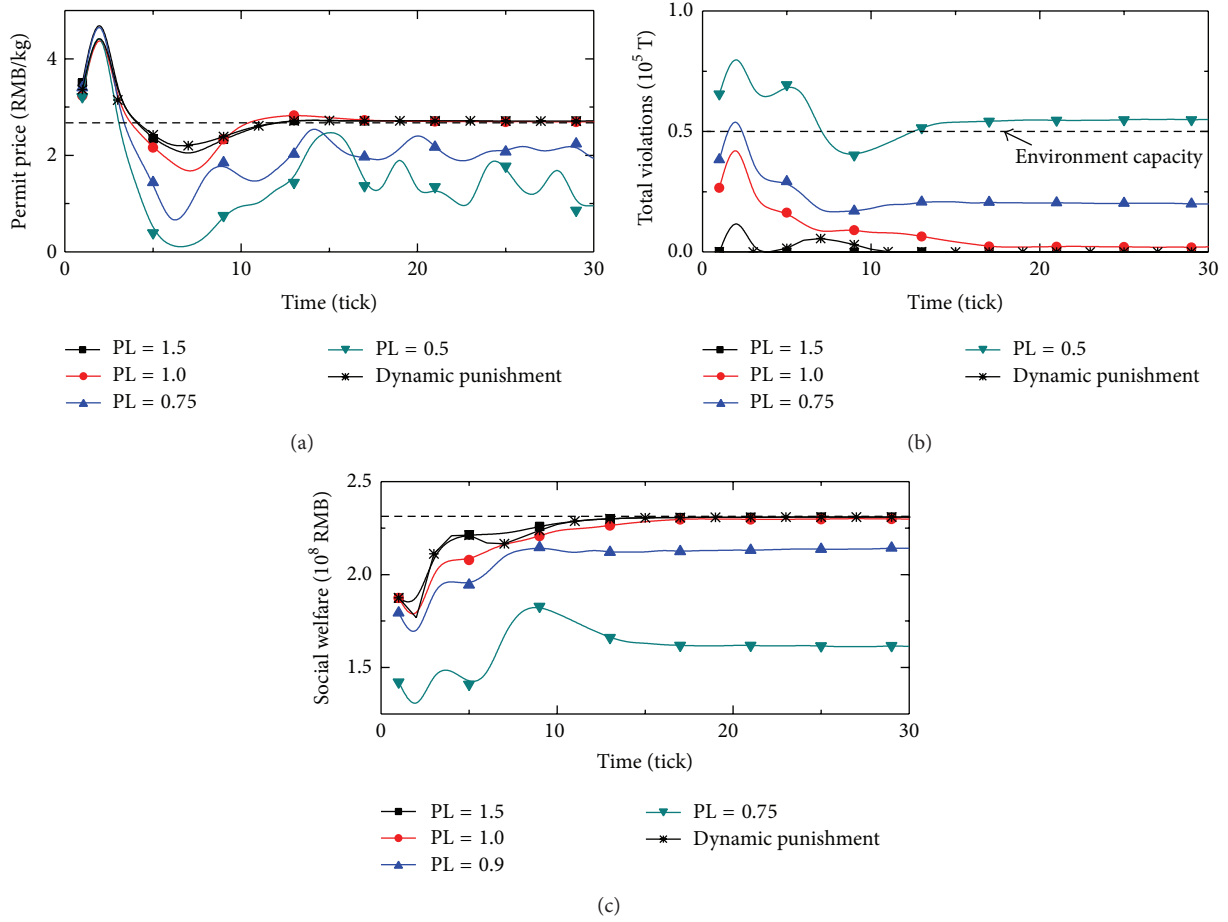


FIGURE 3: Evolution processes under different punishment.

schemas prior to the firm cannot ensure the cost-effectiveness of enforcement. Although checking and ratifying the permit price need the complete information of firms' abatement costs, under incomplete information condition, only if the market price of permits can fully reflect its scarcity, then the optimal design of regulatory strategy will only related to the price, this is another obvious characteristic that emissions trading different from the traditional regulation. In view of this, a dynamic regulatory strategy integrating the market price of permits is introduced by Stranlund (2007) [11]: the regulator preannounces to the firms that the marginal penalty for violations would be T times of market price of permits p , that is $f'(0) = Tp$, $T > 1$. From Proposition 5, full compliance can be realized when $\pi^* = 1/T$. Since firms make decision before the trading and punishment, this strategy actually endows the regulator with the initiative in the game and internalizes compliance into the decision-making of firms. Based on the previous experiment setting, another group of experiments are carried out under this strategy; for comparing with the static regulatory strategy, the results are shown in Figure 3. Experimental results show that dynamic regulatory strategy is superior to the static strategy. Under dynamic strategy, the noncompliance could be more effectively controlled than that under static regulation with

punishment level is 1, and the maximum violations is even lower than the violations when punishment level is 1.5. Furthermore, the implement of dynamic regulatory strategy will lead to a better tendency of permit price. Although the social welfare shows a little lower than that under high punishment level, but brings a significant increase than that under theoretical punishment level. Thus, the dynamic regulatory strategy can be a better choice to achieve the aggregate emissions target cost effectively.

4. Conclusions

It can be included that the regulatory strategy would influence on the cost-effectiveness of emissions trading system significantly. The inharmony between the level of punishment and monitoring has negative effects on the price formation of permits, which would react on the firms' decision-making and result in the suboptimal emissions control efficiency and social welfare at the macro level. It has certain enlightenment on understanding that the existing pilot programs in China in general are lack of effect. Besides the restrictions of resources, legislation, and so on, the existing regulatory strategies are ill-adapted with reality. In particular, the penalty for noncompliance has been imposed many restrictions including the

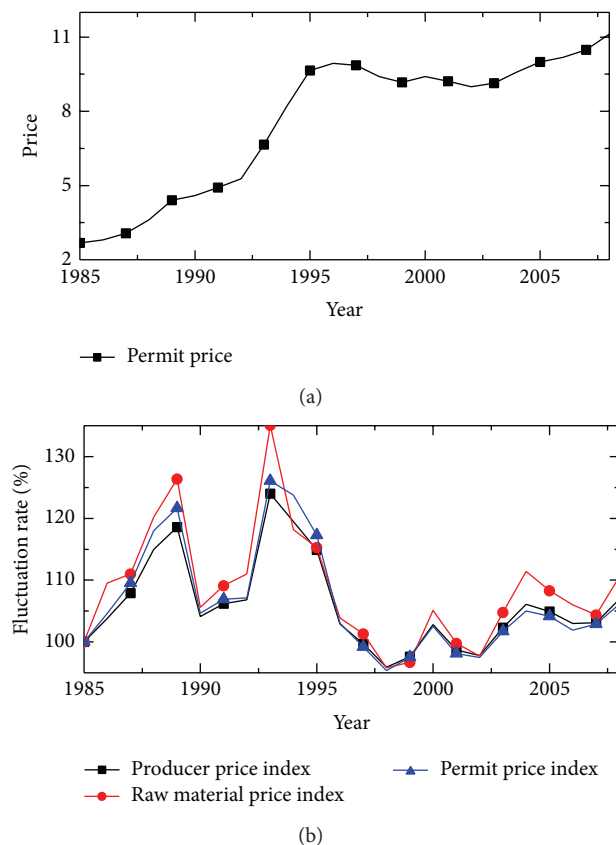


FIGURE 4: Permit price trend under dynamic economy.

marginal and the maximum amount, in many administrative documents such as Atmospheric Pollution Prevention Law and Water Pollution Prevention Law and lead the regulators also lack of the enforcement measures facing high costs of monitoring, sanctioning and administration. In many pilot programs, the penalty schemes for noncompliance are made according to pollution discharge fees, which simply cannot fully reflect the social abatement costs and environment values. What is more, some other reasons exist, such as total quantity control does not reach the designated goal and the regulatory mechanisms are too rigid. In a word, the firm behavior and the institutional selection in China are still inertially affected and stimulated by traditional regulations such as pollution discharge fees.

One of the keys to forge the reasonable regulatory strategy is to identify and grasp the features the emissions trading regulation distinguishes from traditional regulations. The superiority of emissions trading is rooted in the marketization of resource environmental capacity. The results indicate that the strategy of integrating the market prices of permits is the better choice to achieve the aggregate emissions target cost effectively. International experiences also could confirm the necessity of the strategy. Throughout practices related to emissions trading on CO_2 , SO_2 , and NO_x , it is easy to find that the permit price is uncertain because of the dynamic effect from socio-economic system. Taking Acid Rain Program for an example, the lowest price of SO_2 allowance reached 60

dollars, but the highest price reached 900 dollars during the years from 1990 to 2008. However, Acid Rain Program has apparently achieved a perfect compliance record. It can surely attribute to the continuous emission monitoring system which can achieve the real time monitoring of firms and severe punishment for noncompliance; the penalty scheme dynamically adjusting with the consumer price index equally plays an important role, which well eliminates the impact of price uncertainty. However, the RECLAM program has experienced noncompliant firms from its inception, especially in 2000, the prices for NO_x and SO_2 rose dramatically.

What is more, dynamic regulatory strategy stimulated by market to organic bond with administrative regulatory, so that it show better effectiveness and flexibility under the dynamic economy. Dynamic regulation makes compliance internalized into the decision of firms, firms' expectations and preference of market dynamics can be fully reflected in the market price of permits through spontaneous market transactions between firms. Consequently, the limitation of regulatory capacity is no longer the important obstacle of effective enforcement. As this strategy only depends on the regulatory ability, it not only saves costs of regional environmental value accounting and others, but also helps regulators setting from multifarious affairs, so that regulators can focus on the improvement of market mechanism and regulation of market behavior. We hold the view that the dynamic regulation is a valid try in China. However, existing practices pay too more attention to the construction of the initial allocation market, a reasonable price formation mechanism has not yet established. On the other hand, too many administrative measures restrain the market functions, and make the administrative institutions overburdened.

Conflict of Interests

The authors declare that there is no conflict of interests regarding the publication of this paper.

Acknowledgments

This work was supported by the National Natural Science Foundation of China under Grants 71201071, 71171099, and 71373105; Humanities and Social Science Research Foundation of Education Ministry of China under Grant 12YJCZH090; Postdoctoral Science Foundation of China under Grant 2013M531293; Jiangsu Planned Projects for Postdoctoral Research Funds under Grant 1102127C.

References

- [1] J. Wang, Z. Dong, J. Yang, Y. Li, and G. Yan, "Practices and prospects of emission trading programs in China," *Ecological Economy*, no. 10, pp. 31–45, 2008.
- [2] P. B. Downing and W. D. Watson Jr., "The economics of enforcing air pollution controls," *Journal of Environmental Economics and Management*, vol. 1, no. 3, pp. 219–236, 1974.
- [3] J. D. Harford, "Firm behavior under imperfectly enforceable pollution standards and taxes," *Journal of Environmental Economics and Management*, vol. 5, no. 1, pp. 26–43, 1978.

- [4] C. A. Chavez and J. K. Stranlund, "Enforcing transferable permit systems in the presence of market power," *Environmental and Resource Economics*, vol. 25, no. 1, pp. 65–78, 2003.
- [5] Z. Bing, Y. Qinqin, and B. Jun, "Policy design and performance of emissions trading markets: an adaptive agent-based analysis," *Environmental Science and Technology*, vol. 44, no. 15, pp. 5693–5699, 2010.
- [6] A. S. Malik, "Markets for pollution control when firms are noncompliant," *Journal of Environmental Economics and Management*, vol. 18, no. 2, pp. 97–106, 1990.
- [7] J. R. Mrozek and A. G. Keeler, "Pooling of uncertainty: enforcing tradable permits regulation when emissions are stochastic," *Environmental and Resource Economics*, vol. 29, no. 4, pp. 459–481, 2004.
- [8] H. Konishi, "Intergovernmental versus intersource emissions trading when firms are noncompliant," *Journal of Environmental Economics and Management*, vol. 49, no. 2, pp. 235–261, 2005.
- [9] T. N. Cason and L. Gangadharan, "Emissions variability in tradable permit markets with imperfect enforcement and banking," *Journal of Economic Behavior and Organization*, vol. 61, no. 2, pp. 199–216, 2006.
- [10] J. K. Stranlund and K. K. Dhanda, "Endogenous monitoring and enforcement of a transferable emissions permit system," *Journal of Environmental Economics and Management*, vol. 38, no. 3, pp. 267–282, 1999.
- [11] J. K. Stranlund, "The regulatory choice of noncompliance in emissions trading programs," *Environmental and Resource Economics*, vol. 38, no. 1, pp. 99–117, 2007.
- [12] C. Arguedas, "To comply or not to comply? Pollution standard setting under costly monitoring and sanctioning," *Environmental and Resource Economics*, vol. 41, no. 2, pp. 155–168, 2008.
- [13] D. Garvie and A. Keeler, "Incomplete enforcement with endogenous regulatory choice," *Journal of Public Economics*, vol. 55, no. 1, pp. 141–162, 1994.
- [14] S. Weishaar, "CO₂ emission allowance allocation mechanisms, allocative efficiency and the environment: a static and dynamic perspective," *European Journal of Law and Economics*, vol. 24, no. 1, pp. 29–70, 2007.
- [15] Y. Ermoliev, M. Michalevich, and A. Nentjes, "Markets for tradeable emission and ambient permits: a dynamic approach," *Environmental and Resource Economics*, vol. 15, no. 1, pp. 39–56, 2000.

Research Article

Pinning Synchronization of Linear Complex Coupling Synchronous Generators Network of Hydroelectric Generating Set

Xuefei Wu

School of Computer Engineering, Shenzhen Polytechnic, Shenzhen 518055, China

Correspondence should be addressed to Xuefei Wu; wuxuefei@szpt.edu.cn

Received 28 May 2014; Accepted 21 August 2014; Published 25 September 2014

Academic Editor: Chuandong Li

Copyright © 2014 Xuefei Wu. This is an open access article distributed under the Creative Commons Attribution License, which permits unrestricted use, distribution, and reproduction in any medium, provided the original work is properly cited.

A novel linear complex system for hydroturbine-generator sets in multimachine power systems is suggested in this paper and synchronization of the power-grid networks is studied. The advanced graph theory and stability theory are combined to solve the problem. Here we derive a sufficient condition under which the synchronous state of power-grid networks is stable in disturbance attenuation. Finally, numerical simulations are provided to illustrate the effectiveness of the results by the IEEE 39 bus system.

1. Introduction

Types of grid electricity generation have thermal power generation types, hydropower, wind power, and solar photovoltaic power generation, and there are mainly thermal power generation and hydropower in our country. Combined power generation is the problem the power plants are most concerned with in the power generation process. That is to say, power plants generating electricity need to be incorporated into the power grid to run. As most regional power supply and power generation are separately controlled by power plants and substations, power plants need to obey the scheduling, power supply bureau allowed the electricity are fed into the power grid, power plants can generate electricity. After that, excess electricity can be used by other users and if electricity generated by plant power is insufficient, the large power in the power grid can be used as a supplement. It would not be that off-grid power and self-financing. So how to make each generator successful to incorporate into the power grid is vital to the stability of the power system in entire region. In general, combined power generation must meet several requirements: voltage equal; frequency stability; and same phase. Missing any of these conditions is likely to lead to loss of synchronization of the entire generator set and then spread to the relevant local grid. Accordingly, this chapter focuses

on that when synchronous generators are subject to random noise, how to quickly return to a new equilibrium and to synchronize again.

In the aspect of ensuring stability of the power system, power systems engineering experts and scholars have done a lot of research work, such as the authors of [1] discuss the self-synchronization of the power system and enhanced synchronization capability approach; a novel nonequilibrium complete synchronization condition of dynamical smart grid was proposed, whose results have improved synchronization conditions in [2]. The authors of [3] studied synchronization of the natural frequency bimodal distribution of complex power networks, and derived synchronization coupling critical condition. At the same time, the research results are applied to the European interconnected high-voltage power systems; literature [4] uses a coarse-grained scale model to study the self-organizing network synchronization power system model; they found that the more decentralized network of its dynamical behavior of nodes was, the more sensitive the random disturbance was, the more robust its topology was; literature [5] uses orthogonal decomposition method and Galerkin method to explore New Zealand's electricity network global instability, which can help to predict the real global power network instability. Ph. D. thesis [6, 7] studied the conditions of the electricity network synchronization.

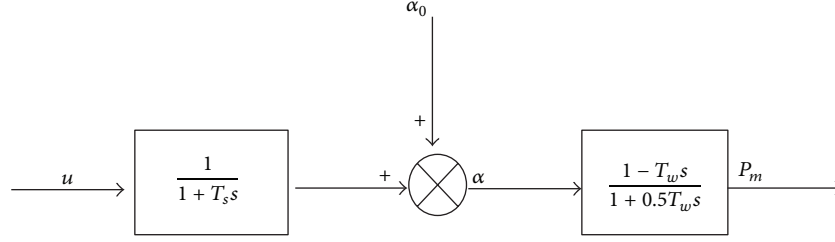


FIGURE 1: Hydroturbine speed control system block diagram.

Based on the above, we put the hydroelectric power system as the research object and discussed in detail the incorporate into the power grid of hydroelectric synchronous generators. The basic principles of hydroelectric system (hydroelectric power) are taking advantage of water flow of those rivers and lakes in high and with potential energy flow to the lower, the potential energy is converted into kinetic energy contained there in the turbine, and the turbine is regarded as the driving force to promote the generator to produce electricity. Here, we focus on the hydrogrid synchronization, namely, the voltage, frequency, and phase of all the generators connecting with each other realizing synchronization and incorporating into the power grid. In the network comprising n alternators, the synchronization status can be described as follows:

$$\dot{\delta}_1 = \dot{\delta}_2 = \dots = \dot{\delta}_n, \quad (1)$$

where $\delta_i = \delta_i(t)$ denotes the rotation phase of the i generator and $\dot{\cdot}$ denotes time derivative.

We take the hydrogroup in some power plant as a small network which is composed by several synchronous generator (node) and the power transmission line (edge) connected to each other, referred to as hydrogroup synchronous generator network. Our purpose is to verify that the conditions of synchronous generators remain stable.

We will start with the following equation of motion:

$$\frac{2H_i}{\omega_R} \frac{d^2 \delta_i}{dt^2} = P_{mi} - P_{ei}, \quad (2)$$

namely, swing equation. This swing equation describes the dynamic characteristics of the generator i based on the current equation. The parameters H_i are the inertia constant of the generator, ω_R is the rated angular speed of the system, $2H_i/\omega_R$ means that all rotational inertia of rotating mass attached on the rotor shaft, the unit is $\text{kg}\cdot\text{m}^2$; δ_i is the mechanical torque angle (subscript) with respect to synchronous rotation reference axis, the unit is rad; P_{mi} is mechanical power provided by the generator, P_{ei} is the generator load power in the network. In balance point, $P_{mi} = P_{ei}$ and the frequency $\omega_i \equiv \dot{\delta}_i$, for all i , and frequencies will maintain equality with a constant; in (1), for frequency synchronization, this is a valid condition.

When the system is running at steady load conditions, due to the failure or fluctuation changes P_{ei} will change. According to (2), once the system changes, the difference

between the load power and mechanical power is to be compensated by the increase or decrease of the rotor angular momentum which is generated by the generator rotor. The changes in angular momentum will not remove the difference between P_{mi} and P_{ei} and only compensated for the difference until synchronization. Although when entering the transient period, the synchronization will be lost, but in the total process, the generator will realize synchronization by again adjusting its voltage phase angle; Each generator in power network is how to realize synchronization? Below, we will take the actual hydropower model as an example for research.

2. Preparation and Model Description

Hydroelectric work with the aid of hydroturbines which connect directly to the synchronous generator, when considering the impact of nonplastic water hammer, hydroturbine speed control system block diagram and description is in Figure 1 [9].

$1 + T_s s$ is water-gate and the servo system, T_s is time constant of a hydroturbine opening control servo motor, $(1 - T_w s)/(1 + 0.5 T_w s)$ is hydroturbine model, T_w is the diversion system inertia time constant, u is the amount of input control, α_0 is the reference value of the hydroturbine vanes, α is the guide vane opening, and P_m is hydroturbine output mechanical power. We assume that an excellent excitation controller has been adopted, so as to maintain a constant potential in q axis in the whole dynamic process. The hydroelectric system mainly consists of two parts, hydroturbine and its speed control system model and the generator model. According to Figure 1, we can derive single dynamic model of hydroturbine and its speed control system model:

$$\begin{aligned} \dot{P}_m &= \frac{2}{T_w} [-P_m + \alpha - T_w \dot{\alpha}], \\ \dot{\alpha} &= \frac{1}{T_s} (-\alpha + \alpha_0 + u). \end{aligned} \quad (3)$$

And single synchronous generator rotor dynamic model is

$$\begin{aligned} \dot{\delta} &= \omega \\ \dot{\omega} &= \frac{\omega_R}{2H} [P_m - P_e - D\omega], \end{aligned} \quad (4)$$

where δ is the rotation phase of the generator, ω is the rotor speed, and $\omega_R = 2\pi f_0$, $f_0 = 60$ Hz. D is mechanical damping

coefficient, H is the inertia time constant of the rotor. P_e is the load power (the electric power of generator output), whereby we can get four-order hydroelectric system dynamic model [5, 9]:

$$\begin{aligned} \frac{d\delta_i}{dt} &= \omega_i, \\ \frac{d\omega_i}{dt} &= \frac{\pi f_0}{H_i} \left\{ -D_i \omega_i + P_{mi} - G_{ii} E_i^2 \right. \\ &\quad \left. - \sum_{j=1, j \neq i}^n [E_i E_j G_{ij} \cos(\delta_i - \delta_j) \right. \\ &\quad \left. + S_{ij} \sin(\delta_i - \delta_j)] \right\}, \\ \frac{dP_{mi}}{dt} &= \frac{2}{T_{wi}} [-P_{mi} + \alpha_i - T_w \dot{\alpha}_i], \\ \frac{d\alpha_i}{dt} &= \frac{1}{T_{si}} (-\alpha_i + \alpha_{0i} + u_i). \end{aligned} \quad (5)$$

$x_i = [\delta_i, \omega_i, P_{mi}, \alpha_i] \in \mathbb{R}^4$ is the state variable of the i generator and $f(x_i, t) = [f_1(x_i), f_2(x_i), f_3(x_i), f_4(x_i)] : \mathbb{R}^4 \times [0, +\infty) \rightarrow \mathbb{R}^4$ is a continuous mapping as follows:

$$f(x_i, t) = \begin{cases} \omega_i \\ \frac{\pi f_0}{H_i} [-D_i \omega_i + P_{mi} - G_{ii} E_i^2] \\ \frac{2}{T_{wi}} [-P_{mi} + \alpha_i - T_w \dot{\alpha}_i] \\ \frac{1}{T_{si}} (-\alpha_i + \alpha_{0i} + u_i). \end{cases} \quad (6)$$

It is the dynamic equation of isolated nodes, denoting $Y_{ij} = G_{ij} + iB_{ij}$ as transmission circuit admittance, G_{ij} denotes the transmit circuitry conductance, S_{ij} denotes the susceptance, and E_i denotes the node voltage of the generator; based on the above, hydroelectric generating set synchronous generator network (5) can be rewritten as a more simple form as follows:

$$\begin{aligned} \dot{x}_i(t) &= f(x_i(t), t) + \sum_{j=1}^n a_{ij} \Gamma x_j(t) \\ &\quad + \sum_{j=1}^n b_{ij} \Gamma x_j(t), \quad i = 1, \dots, n, \end{aligned} \quad (7)$$

where $A = [a_{ij}] \in \mathbb{R}^{n \times n}$, when $i \neq j$, then $a_{ij} = (\pi f_0 / H_i) E_i E_j G_{ij} \cos \delta_{ij}^*$, $a_{ij} = -\sum_{j=1, j \neq i}^n a_{ij}$, $i, j = 1, 2, \dots, n$, $B = [b_{ij}] \in \mathbb{R}^{n \times n}$, $b_{ij} = (\pi f_0 / H_i) E_i E_j S_{ij} \sin \delta_{ij}^*$, $b_{ij} = -\sum_{j=1, j \neq i}^n b_{ij}$, $i, j = 1, 2, \dots, n$ denote the network topology, respectively. δ_{ij}^* denotes the phase difference while the system is stable. Next, we will discuss the synchronization of hydroelectric generating set synchronous generator network (7). To achieve synchronization, we add a node controller in the first

generator. So, hydroelectric generating set synchronous generator network pinned control can be described as follows:

$$\begin{aligned} \dot{x}_1(t) &= f(x_1(t), t) + c \sum_{j=1}^n a_{1j} \Gamma x_j(t) \\ &\quad + c \sum_{j=1}^n b_{1j} \Gamma x_j(t) - c \varepsilon \Gamma (x_1(t) - \bar{x}(t)), \\ \dot{x}_i(t) &= f(x_i(t), t) + c \sum_{j=1}^n a_{ij} \Gamma x_j(t) \\ &\quad + c \sum_{j=1}^n b_{ij} \Gamma x_j(t), \quad i = 2, \dots, n, \end{aligned} \quad (8)$$

where c is the control strength and $\bar{x}(t) = (1/n) \sum_{i=1}^n x_i(t)$.

3. Synchronization Analysis of Hydroelectric Generating Set

In this section, we discuss pinning a hydroelectric generating set synchronous generator network with linear delay irreducible symmetric coupling matrix.

Theorem 1. *If hydroelectric generating set synchronous generator network satisfied the condition as follows:*

$$I \otimes K + \bar{A}^S \otimes \Gamma + B^S \otimes \Gamma < 0, \quad (9)$$

where $A^S = (A + A^T)/2$, then the controlled hydroelectric generating set synchronous generator network (8) can be globally synchronized to \bar{x} , where

$$K = \begin{bmatrix} 0 & 1 & 0 & 0 \\ 0 & -\frac{\pi f_0 D_i}{H} & \frac{\pi f_0}{H} & 0 \\ 0 & 0 & -\frac{2}{T_w} & \frac{2}{T_w} + \frac{2}{T_s} \\ 0 & 0 & 0 & -\frac{1}{T_s} \end{bmatrix}, \quad (10)$$

$$\bar{A} = (\bar{a}_{ij})_{n \times n} = A - \text{diag} \left\{ \left(1 - \frac{1}{n}\right) \varepsilon, 0, \dots, 0 \right\}.$$

Proof. Define $\Delta x_i(t) = x_i(t) - \bar{x}(t)$. Because $\sum_{j=1}^n a_{ij} \bar{x}(t) = 0$, we can easily get

$$\sum_{j=1}^m a_{ij} x_j(t) = \sum_{j=1}^m a_{ij} \Delta x_j(t), \quad (11)$$

so the error system of hydroelectric generating set synchronous generator network (8) of can be rewritten as

$$\begin{aligned} \frac{d\Delta x_1(t)}{dt} &= f(x_1(t), t) - f(\bar{x}(t), t) + \sum_{j=1}^n a_{1j} \Gamma \Delta x_j(t) \\ &\quad + \sum_{j=1}^n b_{1j} \Gamma \Delta x_j(t) - \left(1 - \frac{1}{n}\right) \varepsilon \Gamma \Delta x_1(t) + J, \\ \frac{d\Delta x_i(t)}{dt} &= f(x_i(t), t) - f(\bar{x}(t), t) + \sum_{j=1}^n a_{ij} \Gamma \Delta x_j(t) \\ &\quad + \sum_{j=1}^n b_{ij} \Gamma \Delta x_j(t) + J, \quad i = 2, \dots, n, \end{aligned} \quad (12)$$

where, $J = f(\bar{x}(t), t) - (1/n) \sum_{i=1}^n f(x_i(t), t)$.

Take Lyapunov function

$$V(t) = \frac{1}{2} \sum_{i=1}^n \Delta x_i^T(t) \Delta x_i(t) \quad (13)$$

and define $\Delta x(t) = (\Delta x_1^T(t), \dots, \Delta x_n^T(t))^T, i = 1, \dots, n$. Now we calculate

$$\begin{aligned} \dot{V}(t) &|_{(12)} \\ &= \sum_{i=1}^n \Delta x_i^T(t) \\ &\quad \times \left[f(x_i(t), t) - f(\bar{x}(t), t) \right. \\ &\quad \left. + \sum_{j=1}^n \bar{a}_{ij} \Gamma \Delta x_j(t) + \sum_{j=1}^n b_{ij} \Gamma \Delta x_j(t) + J \right] \\ &= \sum_{i=1}^n \Delta x_i^T(t) K \Delta x_i(t) \\ &\quad + \sum_{i=1}^n \Delta x_i^T(t) \sum_{j=1}^n \bar{a}_{ij} \Gamma \Delta x_j(t) \\ &\quad + \sum_{i=1}^n \Delta x_i^T(t) \sum_{j=1}^n b_{ij} \Gamma \Delta x_j(t) \\ &= \Delta x^T(t) (I \otimes K) \Delta x(t) + \Delta x^T(t) (\bar{A} \otimes \Gamma) \Delta x(t) \\ &\quad + \Delta x^T(t) (B \otimes \Gamma) \Delta x(t) \\ &= \Delta x^T(t) (I \otimes K + \bar{A} \otimes \Gamma + B \otimes \Gamma) \Delta x(t). \end{aligned} \quad (14)$$

We know, based on Theorem 1, that \bar{A} is negative definite matrix; obviously, the condition (9) can be satisfied easily; therefore, we can get $\dot{V}(t) < 0$. Theorem 1 is proved. \square

Remark 2. If the hydroelectric generating set synchronous generator network meet the condition $I \otimes K + \bar{A} \otimes \Gamma + B \otimes \Gamma < 0$,

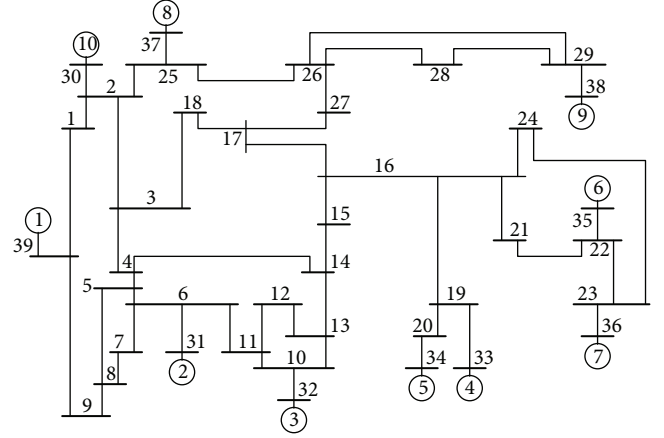


FIGURE 2: Grid network structure (which is generator nodes connected with circle, a total of 10, and the remaining nodes are nongenerator nodes. [2, 8]).

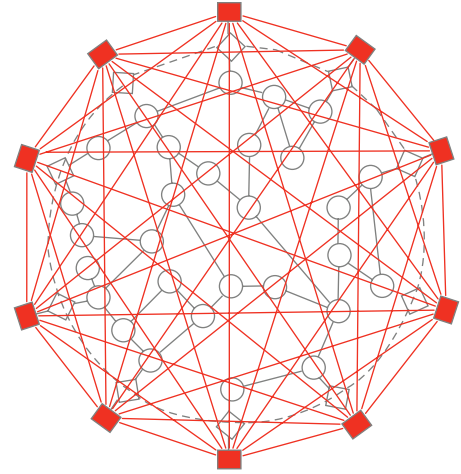


FIGURE 3: Network topology after simplifying Figure 2 by using Kron method (the 10 red nodes in the figure are the generator nodes, all links between the generator nodes. [2]).

then the controlled hydroelectric generating set synchronous generator network (8) can be globally synchronized. Here, the synchronization of network is decided by electric system itself and the network structure.

4. Numerical Simulation

Numerical simulation of this section, we mainly consider IEEE 39 test grid (data using 100 MVA, 60 Hz) [8], as shown in Figure 2 and Table 1. Figure 3 shows network topology after simplifying Figure 2 by using Kron method.

In the numerical experiments, let the nominal angular velocity $\omega_0 = 60$ Hz, the reference value of hydroturbine guide vane $\alpha_0 = 1$, the mechanical damping coefficient $D = 0.5$, rotor inertia time constant $H = 4$, inertia time constant of diversion system $T_w = 4$, and hydroturbine opening control servo motor time constant $T_s = 4$. In this paper, we let u be 0, we can verify it satisfies theorem. Each of the generator

TABLE 1: P.S. IEEE39 power network node admittance.

i	j	Y_{ij}
1	2	$0.0035 + 0.0411i$
1	39	$0.0020 + 0.050i$
2	3	$0.0013 + 0.0151i$
2	25	$0.0070 + 0.0086i$
3	4	$0.0013 + 0.0213i$
3	18	$0.0011 + 0.0133i$
4	5	$0.00080 + 0.0128i$
4	14	$0.00080 + 0.0129i$
5	6	$0.00020 + 0.0026i$
5	8	$0.00080 + 0.0112i$
6	7	$0.00060 + 0.0092i$
6	11	$0.00070 + 0.0082i$
7	8	$0.00040 + 0.0046i$
8	9	$0.0023 + 0.0363i$
9	39	$0.0010 + 0.025i$
10	11	$0.00040 + 0.0043i$
10	13	$0.00040 + 0.0043i$
13	14	$0.00090 + 0.0101i$
14	15	$0.0018 + 0.0217i$
15	16	$0.00090 + 0.0094i$
16	17	$0.00070 + 0.0089i$
16	19	$0.0016 + 0.0195i$
16	21	$0.00080 + 0.0135i$
16	24	$0.00030 + 0.0059i$
17	18	$0.00070 + 0.0082i$
17	27	$0.0013 + 0.0173i$
21	22	$0.00080 + 0.014i$
22	23	$0.00060 + 0.0096i$
23	24	$0.0022 + 0.035i$
25	26	$0.0032 + 0.0323i$
26	27	$0.0014 + 0.0147i$
26	28	$0.0043 + 0.0474i$
26	29	$0.0057 + 0.0625i$
28	29	$0.0014 + 0.0151i$
2	30	$0.0181i$
6	31	$0.050i$
6	31	$0.0 + 0.050i$
10	32	$0.0 + 0.020i$
12	11	$0.0016 + 0.0435i$
12	13	$0.0016 + 0.0435i$
19	20	$0.00070 + 0.0138i$
19	33	$0.00070 + 0.0142i$
20	34	$0.00090 + 0.018i$
22	35	$0.0 + 0.0143i$
23	36	$0.00050 + 0.0272i$
25	37	$0.00060 + 0.0232i$
29	38	$0.00080 + 0.0156i$

initial speed is randomly generated by the computer (attached generator admittance between nodes); using the function

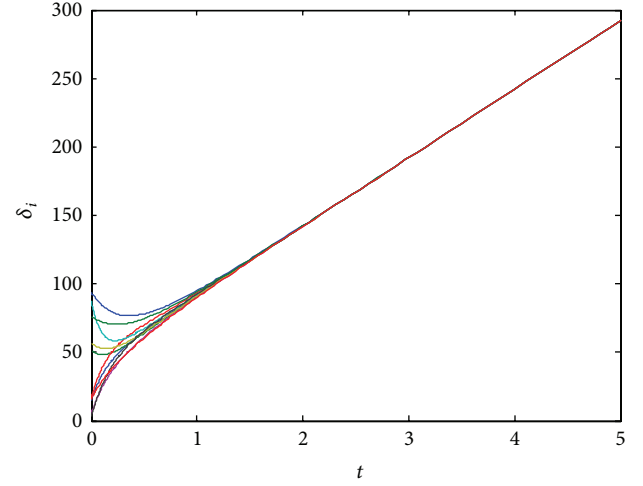


FIGURE 4: The evolution process of pinning the rotor phase of 10 generator nodes.

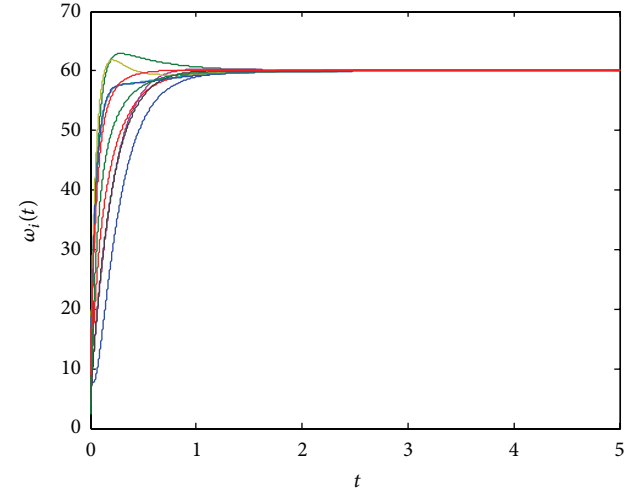


FIGURE 5: The evolution process of pinning the rotor frequency of 10 generator nodes.

ode45 in MATLAB solve (7), we can obtain the numerical results of the individual states for each node.

Figures 4 and 5 are evolution schematic diagrams with hydroelectric generating set synchronous generator network of 10 generator nodes, generator rotor phase, and the rotor frequency. Figures 6 and 7 are mechanical power for the generator and the guide vane opening states. From the figures, we can obviously find that all the generators are synchronized which indicate that the algorithm described in this chapter is valid to achieve synchronization of hydroelectric generating set synchronous generator network.

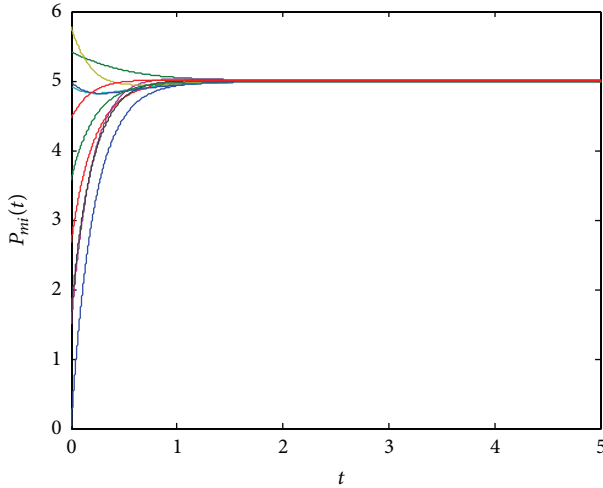


FIGURE 6: The trajectory with mechanical power of 10 generator nodes.

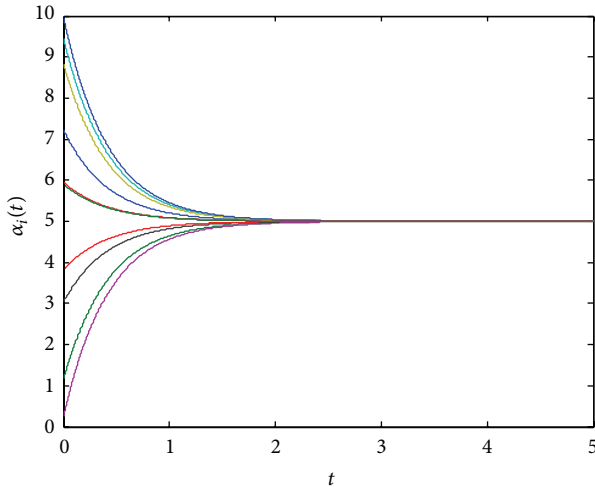


FIGURE 7: The trajectory with guide vane opening of 10 generator nodes.

5. Conclusion

Synchronization is a very important research field in the application of science and engineering; particularly in complex power network generator synchronizing has more application prospects. How to simplify the system pinning process is of vital significance to improve the efficiency of the system. So, based on existing work, the synchronization of hydroelectric generating set synchronous generator network is discussed. The parameters will be dimension, and the corresponding complex network model is established; we also design a linear feedback controller adding the first generator to realize the phase and frequency synchronization of hydroelectric generating set synchronous generator by using the stability theory for hydrogenerator units to realize synchronous conditions in theory. In the end, we provided some numerical simulation to verify the validity of the theorem.

Conflict of Interests

The author declares that there is no conflict of interests regarding the publication of this paper.

Acknowledgments

The author thanks the referees and the editor for their valuable comments on this paper. This work was supported by Shenzhen Basic Research Project (JCYJ20130331152625792).

References

- [1] A. E. Motter, S. A. Myers, M. Anghel, and T. Nishikawa, "Spontaneous synchrony in power-grid networks," *Nature Physics*, vol. 9, no. 3, pp. 191–197, 2013.
- [2] F. A. Dörfler, *Dynamics and Control in Power Grids and Complex Oscillator Networks*, University of California, 2013.
- [3] S. Lozano, L. Buzna, and A. Díaz-Guilera, "Role of network topology in the synchronization of power systems," *The European Physical Journal B*, vol. 85, no. 7, article 231, 2012.
- [4] M. Rohden, A. Sorge, M. Timme, and D. Witthaut, "Self-organized synchronization in decentralized power grids," *Physical Review Letters*, vol. 109, no. 6, Article ID 064101, 2012.
- [5] Y. Susuki, I. Mezic, and T. Hikiyara, "Global swing instability in the New England power grid model," in *Proceedings of the American Control Conference (ACC '09)*, pp. 3446–3451, June 2009.
- [6] F. Dörfler, M. Chertkov, and F. Bullo, "Synchronization in complex oscillator networks and smart grids," *Proceedings of the National Academy of Sciences of the United States of America*, vol. 110, no. 6, pp. 2005–2010, 2013.
- [7] F. Dörfler and F. Bullo, "Synchronization in complex networks of phase oscillators: a survey," *Automatica*, vol. 50, no. 6, pp. 1539–1564, 2014.
- [8] M. A. Pai, *Energy Function Analysis for Power System Stability*, Springer, New York, NY, USA, 1989.
- [9] Q. Lu, Y. Sun, Y. Sun et al., "Nonlinear decentralized robust governor control for hydroturbine-generator sets in multi-machine power systems," *International Journal of Electrical Power and Energy System*, vol. 26, no. 5, pp. 333–339, 2004.

Research Article

Stability and Passivity of Spatially and Temporally Complex Dynamical Networks with Time-Varying Delays

Shun-Yan Ren¹ and Yue-Hui Zhao²

¹ School of Computer Science & Software Engineering, Tianjin Polytechnic University, Tianjin 300387, China

² College of Post and Telecommunication of WIT, Wuhan 430070, China

Correspondence should be addressed to Shun-Yan Ren; renshunyan@163.com

Received 7 May 2014; Accepted 16 August 2014; Published 3 September 2014

Academic Editor: Zhichun Yang

Copyright © 2014 S.-Y. Ren and Y.-H. Zhao. This is an open access article distributed under the Creative Commons Attribution License, which permits unrestricted use, distribution, and reproduction in any medium, provided the original work is properly cited.

This paper proposes a new complex dynamical network model, in which the state, input, and output variables are varied with the time and space variables. By utilizing the Lyapunov functional method combined with the inequality techniques, several criteria for passivity and global exponential stability are established. Finally, numerical simulations are given to illustrate the effectiveness of the obtained results.

1. Introduction

Complex networks can be seen everywhere, which have become an important part of our daily life. Recently, the topology and dynamical behavior of complex dynamical networks have been extensively studied by the researchers. In particular, special attention has been focused on synchronization in complex dynamical networks, and many interesting results on synchronization were derived for various complex networks [1–10].

To our knowledge, in most existing works on the complex networks, they always assume that the node state is only dependent on the time. However, such simplification does not match the peculiarities of some real networks. Food webs are among the most well-known examples of complex networks and hold a central place in ecology to study the dynamics of animal populations. A food web can be characterized by a model of complex network, in which a node represents a species. To our knowledge, species are usually inhomogeneously distributed in a bounded habitat and the different population densities of predators and preys may cause different population movements; thus it is important and interesting to investigate their spatial density in order to better protect and control their population. In such a case,

the state variable of node will represent the spatial density of the species. Moreover, the input and output variables are also dependent on the time and space in many practical situations. Therefore, it is essential to study the complex networks, in which the state, input, and output variables are varied with the time and space variables.

Recently, food web [11–24] has become a focal research topic and attracted increasing attention from many fields of scientific research. In [17], Pao discussed the asymptotic behavior of time-dependent solutions of a three-species reaction-diffusion system in a bounded domain under a Neumann boundary condition. Kim and Lin [21] considered the blowup properties of solutions for a parabolic system with homogeneous Dirichlet boundary conditions, which describes dynamic properties of three interacting species in a spatial habitat. As a natural extension of the existing network models, we propose a complex dynamical network with time-varying delays, which is described by a system of parabolic partial differential equations. In addition, we investigate the global exponential stability of the proposed network model.

Stability problems are often linked to the theory of dissipative systems, which postulate that the energy dissipated inside a dynamic system is less than that supplied from external source. Passivity is part of a broader and a general

theory of dissipativeness. The main point of passivity theory is that the passive properties of systems can keep the systems internally stable. The passivity theory has found successful applications in diverse areas such as complexity [25], signal processing [26], stability [27, 28], chaos control and synchronization [29, 30], and fuzzy control [31]. Although research on passivity has attracted so much attention, little of that had been devoted to the passivity properties of spatially and temporally complex dynamical networks until Wang et al. [32] obtained some sufficient conditions on passivity properties for a class of reaction-diffusion neural networks with Dirichlet boundary conditions. To the best of our knowledge, very few researchers have investigated the passivity of complex dynamical networks with spatially and temporally varying state variables. Therefore, we also study the passivity of the proposed network model, and some sufficient conditions ensuring input strict passivity and output strict passivity are obtained by constructing appropriate Lyapunov functionals and using inequality techniques.

2. Network Model and Preliminaries

In this paper, we consider a parabolic complex network consisting of N nonidentical nodes with diffusive and delay coupling. The entire network is described by

$$\begin{aligned} \frac{\partial w_i(x, t)}{\partial t} &= d_i \Delta w_i(x, t) + p_i w_i(x, t) + u_i(x, t) \\ &\quad + \sum_{j=1}^N G_{ij} w_j(x, t - \tau_j(t)), \\ y_i(x, t) &= g_i w_i(x, t) + h_i u_i(x, t), \end{aligned} \quad (1)$$

where $i = 1, 2, \dots, N$, $\Omega = \{x = (x_1, x_2, \dots, x_m)^T \mid |x_k| < l_k, k = 1, 2, \dots, m\}$ is the bounded domain with smooth boundary $\partial\Omega$, $d_i \in \mathbb{R} > 0$, $p_i, g_i, h_i \in \mathbb{R}$, $(x, t) \in \Omega \times \mathbb{R}^+$, $\tau_j(t)$ is the time-varying delay with $0 \leq \tau_j(t) \leq \tau$, $w_i(x, t) \in \mathbb{R}$ is the state of node i , $u_i(x, t)$, $y_i(x, t)$ are the input and output of node i at time t and in space x , respectively, $\Delta = \sum_{k=1}^m (\partial^2 / \partial x_k^2)$ is the Laplace diffusion operator on Ω , and $G = (G_{ij})_{N \times N}$ represents the topological structure of network and coupling strength between nodes, where G_{ij} is defined as follows: if there is a connection from node i to node j ($i \neq j$), then $G_{ij} > 0$; otherwise, $G_{ij} = 0$ ($i \neq j$), and $G_{ii} = -\sum_{j=1, j \neq i}^N G_{ij}$.

Let $w(x, t) = (w_1(x, t), w_2(x, t), \dots, w_N(x, t))^T$. The initial value and boundary value conditions associated with the network (1) are given in the form

$$\begin{aligned} w(x, t) &= \Phi(x, t), \quad (x, t) \in \Omega \times [-\tau, 0], \\ \Phi(x, t) &= (\phi_1(x, t), \phi_2(x, t), \dots, \phi_N(x, t))^T, \\ w(x, t) &= 0, \quad (x, t) \in \partial\Omega \times [-\tau, +\infty), \end{aligned} \quad (2)$$

where $\phi_i(x, t)$ ($i = 1, 2, \dots, N$) is bounded and continuous on $\Omega \times [-\tau, 0]$. Let $w(x, t, \Phi)$ be the state trajectory of network (1) from the above initial value and boundary value conditions.

Next, we introduce some notations and definitions.

For any $e(x, t) = (e_1(x, t), e_2(x, t), \dots, e_N(x, t))^T \in \mathbb{R}^N$, $\|e(x, t)\|_2$ denotes

$$\|e(x, t)\|_2 = \left(\int_{\Omega} \sum_{i=1}^N e_i^2(x, t) dx \right)^{1/2}; \quad (3)$$

for any $\Theta(x, t) = (\theta_1(x, t), \theta_2(x, t), \dots, \theta_N(x, t))^T \in \mathbb{R}^N$, $(x, t) \in \Omega \times [-\tau, 0]$, we define

$$\|\Theta\|_{\tau} = \sup_{-\tau \leq t \leq 0} \|\Theta(x, t)\|_2. \quad (4)$$

Definition 1. The complex network (1) is said to be globally exponentially stable if there exist constants $\epsilon > 0$ and $M \geq 1$ such that for any two solutions $w(x, t, \Phi)$, $w(x, t, \Psi)$ of network (1) with initial functions Φ, Ψ , respectively, it holds that

$$\|w(x, t, \Psi) - w(x, t, \Phi)\|_2 \leq M \|\Psi - \Phi\|_{\tau} e^{-\epsilon t} \quad (5)$$

for all $t \geq 0$. If such $w(x, t, \Phi)$ is an equilibrium solution (or periodic solution), then this equilibrium solution (or periodic solution) is said to be globally exponentially stable.

Definition 2 (see [32]). A system with input $u(x, t)$ and output $y(x, t)$ where $u(x, t)$, $y(x, t) \in \mathbb{R}^p$ is said to be passive if there is a constant $\beta \in \mathbb{R}$ such that

$$\int_0^{t_p} \int_{\Omega} y^T(x, s) u(x, s) dx ds \geq -\beta^2 \quad (6)$$

for all $t_p \geq 0$, where Ω is a bounded compact set. If in addition, there are constants $\gamma_1 \geq 0$ and $\gamma_2 \geq 0$ such that

$$\begin{aligned} &\int_0^{t_p} \int_{\Omega} y^T(x, s) u(x, s) dx ds \\ &\geq -\beta^2 + \gamma_1 \int_0^{t_p} \int_{\Omega} u^T(x, s) u(x, s) dx ds \\ &\quad + \gamma_2 \int_0^{t_p} \int_{\Omega} y^T(x, s) y(x, s) dx ds \end{aligned} \quad (7)$$

for all $t_p \geq 0$, then the system is input-strictly passive if $\gamma_1 > 0$ and output-strictly passive if $\gamma_2 > 0$.

Remark 3. In [23], Wang and Wu discussed the global exponential stability and passivity of a parabolic complex network. In network model (1), the coupling matrix G is diffusive. Namely, $G_{ii} = -\sum_{j=1, j \neq i}^N G_{ij}$, $i = 1, 2, \dots, N$. Compared with the network model considered in [23], the network

model considered in this paper may be more reasonable. On the other hand, we investigate the input strict passivity and output strict passivity of the complex network (1), which are totally different from the work in [23].

Lemma 4 (see [33]). Let Ω be a cube $|x_k| < l_k$ ($k = 1, 2, \dots, m$) and let $h(x)$ be a real-valued function belonging to $C^1(\Omega)$ which vanishes on the boundary $\partial\Omega$ of Ω , that is, $h(x)|_{\partial\Omega} = 0$. Then,

$$\int_{\Omega} h^2(x) dx \leq l_k^2 \int_{\Omega} \left(\frac{\partial h}{\partial x_k} \right)^2 dx, \quad (8)$$

where $x = (x_1, x_2, \dots, x_m)^T$.

3. Stability and Passivity of Parabolic Complex Network

3.1. Stability Analysis

Theorem 5. Let $\dot{\tau}_j(t) \leq \sigma < 1$. The complex network (1) is globally exponentially stable if there exist constants $\lambda_i > 0$ and $\epsilon > 0$ such that

$$2\lambda_i\epsilon + 2\lambda_i p_i - 2\lambda_i \sum_{k=1}^m \frac{d_i}{l_k^2} + \sum_{j=1}^N \frac{\lambda_j |G_{ji}| e^{2\epsilon\tau}}{1-\sigma} + \lambda_i \sum_{j=1}^N |G_{ij}| \leq 0, \quad (9)$$

where $i, j = 1, 2, \dots, N$.

Proof. Firstly, we can get from (1) that

$$\begin{aligned} \frac{\partial w_i(x, t)}{\partial t} &= d_i \Delta w_i(x, t) + p_i w_i(x, t) \\ &+ u_i(x, t) + \sum_{j=1}^N G_{ij} w_j(x, t - \tau_j(t)), \end{aligned} \quad (10)$$

where $i = 1, 2, \dots, N$.

Define $z(x, t) = w(x, t, \Psi) - w(x, t, \Phi)$, $\Psi_z(x, t) = \Psi(x, t) - \Phi(x, t)$, and then the dynamics of the difference vector $z(x, t) = (z_1(x, t), z_2(x, t), \dots, z_N(x, t))^T$ is governed by the following equation:

$$\begin{aligned} \frac{\partial z_i(x, t)}{\partial t} &= d_i \Delta z_i(x, t) \\ &+ \sum_{j=1}^N G_{ij} z_j(x, t - \tau_j(t)) + p_i z_i(x, t), \end{aligned} \quad (11)$$

where $i = 1, 2, \dots, N$. Define the following Lyapunov functional for the system (11):

$$\begin{aligned} V(t) &= \sum_{i=1}^N \lambda_i \left\{ e^{2\epsilon t} \int_{\Omega} z_i^2(x, t) dx + \frac{e^{2\epsilon\tau}}{1-\sigma} \sum_{j=1}^N |G_{ij}| \right. \\ &\quad \times \left. \int_{t-\tau_j(t)}^t \int_{\Omega} z_j^2(x, s) e^{2\epsilon s} dx ds \right\}. \end{aligned} \quad (12)$$

Calculating the time derivative of $V(t)$ along the trajectory of system (11), we can get

$$\begin{aligned} \dot{V}(t) &= \sum_{i=1}^N \lambda_i e^{2\epsilon t} \left\{ 2\epsilon \int_{\Omega} z_i^2(x, t) dx + \int_{\Omega} 2z_i(x, t) \frac{\partial z_i(x, t)}{\partial t} dx \right. \\ &\quad + \frac{e^{2\epsilon\tau}}{1-\sigma} \sum_{j=1}^N |G_{ij}| \int_{\Omega} z_j^2(x, t) dx \\ &\quad - \frac{e^{2\epsilon\tau}}{1-\sigma} \sum_{j=1}^N (1 - \dot{\tau}_j(t)) |G_{ij}| e^{-2\epsilon\tau_j(t)} \\ &\quad \times \left. \int_{\Omega} z_j^2(x, t - \tau_j(t)) dx \right\} \\ &\leq \sum_{i=1}^N \lambda_i e^{2\epsilon t} \left\{ (2\epsilon + 2p_i) \int_{\Omega} z_i^2(x, t) dx \right. \\ &\quad + 2d_i \int_{\Omega} z_i(x, t) \Delta z_i(x, t) dx \\ &\quad + 2 \int_{\Omega} z_i(x, t) \sum_{j=1}^N G_{ij} z_j(x, t - \tau_j(t)) dx \\ &\quad + \frac{e^{2\epsilon\tau}}{1-\sigma} \sum_{j=1}^N |G_{ij}| \int_{\Omega} z_j^2(x, t) dx \\ &\quad \left. - \sum_{j=1}^N |G_{ij}| \int_{\Omega} z_j^2(x, t - \tau_j(t)) dx \right\}. \end{aligned} \quad (13)$$

From Green's theorem and the boundary condition, we have

$$\int_{\Omega} z_i(x, t) \Delta z_i(x, t) dx = - \sum_{k=1}^m \int_{\Omega} \left(\frac{\partial z_i(x, t)}{\partial x_k} \right)^2 dx. \quad (14)$$

According to Lemma 4, we can obtain

$$\sum_{k=1}^m \int_{\Omega} \left(\frac{\partial z_i(x, t)}{\partial x_k} \right)^2 dx \geq \sum_{k=1}^m \int_{\Omega} \frac{z_i^2(x, t)}{l_k^2} dx. \quad (15)$$

Therefore,

$$\begin{aligned}
\dot{V}(t) &\leq \sum_{i=1}^N \left\{ \lambda_i \left(2\epsilon + 2p_i - 2 \sum_{k=1}^m \frac{d_i}{l_k^2} \right) \int_{\Omega} z_i^2(x, t) dx \right. \\
&\quad + \frac{\lambda_i e^{2\epsilon\tau}}{1-\sigma} \sum_{j=1}^N |G_{ij}| \int_{\Omega} z_j^2(x, t) dx \\
&\quad + 2\lambda_i \int_{\Omega} z_i(x, t) \sum_{j=1}^N G_{ij} z_j(x, t - \tau_j(t)) dx \\
&\quad \left. - \lambda_i \sum_{j=1}^N |G_{ij}| \int_{\Omega} z_j^2(x, t - \tau_j(t)) dx \right\} e^{2\epsilon t} \\
&\leq \sum_{i=1}^N \left\{ \lambda_i \left(2\epsilon + 2p_i - 2 \sum_{k=1}^m \frac{d_i}{l_k^2} \right) \int_{\Omega} z_i^2(x, t) dx \right. \\
&\quad + 2\lambda_i \sum_{j=1}^N |G_{ij}| \sqrt{\int_{\Omega} z_i^2(x, t) dx} \\
&\quad \times \sqrt{\int_{\Omega} z_j^2(x, t - \tau_j(t)) dx} \\
&\quad + \frac{\lambda_i e^{2\epsilon\tau}}{1-\sigma} \sum_{j=1}^N |G_{ij}| \int_{\Omega} z_j^2(x, t) dx \\
&\quad \left. - \lambda_i \sum_{j=1}^N |G_{ij}| \int_{\Omega} z_j^2(x, t - \tau_j(t)) dx \right\} e^{2\epsilon t} \\
&\leq e^{2\epsilon t} \sum_{i=1}^N \left\{ \left(2\lambda_i \epsilon + 2\lambda_i p_i - 2\lambda_i \sum_{k=1}^m \frac{d_i}{l_k^2} + \lambda_i \sum_{j=1}^N |G_{ij}| \right) \right. \\
&\quad \times \int_{\Omega} z_i^2(x, t) dx + \frac{\lambda_i e^{2\epsilon\tau}}{1-\sigma} \sum_{j=1}^N |G_{ij}| \\
&\quad \times \int_{\Omega} z_j^2(x, t) dx \Big\} \\
&= e^{2\epsilon t} \sum_{i=1}^N \left\{ \left(2\lambda_i \epsilon + 2\lambda_i p_i - 2\lambda_i \sum_{k=1}^m \frac{d_i}{l_k^2} + \lambda_i \sum_{j=1}^N |G_{ij}| \right) \right. \\
&\quad \left. + \sum_{j=1}^N \frac{\lambda_j |G_{ji}| e^{2\epsilon\tau}}{1-\sigma} \right\} \times \int_{\Omega} z_i^2(x, t) dx \Big\}. \tag{16}
\end{aligned}$$

From (9), we can get

$$\dot{V}(t) \leq 0. \tag{17}$$

So $V(t) \leq V(0)$, $t \geq 0$. Since

$$\begin{aligned}
V(0) &= \sum_{i=1}^N \lambda_i \left\{ \int_{\Omega} z_i^2(x, 0) dx \right. \\
&\quad \left. + \frac{e^{2\epsilon\tau}}{1-\sigma} \sum_{j=1}^N |G_{ij}| \int_{-\tau_j(0)}^0 \int_{\Omega} z_j^2(x, s) e^{2\epsilon s} dx ds \right\} \\
&\leq \left[\max_{i=1,2,\dots,N} \{\lambda_i\} + \max_{i=1,2,\dots,N} \left\{ \frac{\tau e^{2\epsilon\tau}}{1-\sigma} \sum_{j=1}^N \lambda_j |G_{ji}| \right\} \right] \|\Psi_z\|_{\tau}^2, \\
V(t) &\geq \min_{i=1,2,\dots,N} \{\lambda_i\} e^{2\epsilon t} \|z(x, t)\|_2^2. \tag{18}
\end{aligned}$$

Let $\lambda_- = \min_{i=1,2,\dots,N} \{\lambda_i\}$, $\lambda^+ = \max_{i=1,2,\dots,N} \{\lambda_i\}$, and

$$M = \sqrt{\frac{\lambda^+ + \max_{i=1,2,\dots,N} \{(\tau e^{2\epsilon\tau} / (1-\sigma)) \sum_{j=1}^N \lambda_j |G_{ji}|\}}{\lambda_-}}. \tag{19}$$

Then $M \geq 1$, and we can obtain

$$\|z(x, t)\|_2 \leq M e^{-\epsilon t} \|\Psi_z\|_{\tau}. \tag{20}$$

Namely,

$$\|w(x, t, \Psi) - w(x, t, \Phi)\|_2 \leq M \|\Psi - \Phi\|_{\tau} e^{-\epsilon t}. \tag{21}$$

This completes the proof of Theorem 5. \square

Practically, Theorem 5 not only can judge the global exponential stability of complex network (1), but also can guarantee the existence and uniqueness of the periodic solution in some circumstances.

Assume that $u_i(x, t)$ and $\tau_i(t)$ ($i = 1, 2, \dots, N$) are periodic continuous functions with period ω . Then we can get from (1) that

$$\begin{aligned}
\frac{\partial w_i(x, t)}{\partial t} &= d_i \Delta w_i(x, t) + p_i w_i(x, t) + u_i(x, t) \\
&\quad + \sum_{j=1}^N G_{ij} w_j(x, t - \tau_j(t)), \tag{22}
\end{aligned}$$

where $u_i(x, t + \omega) = u_i(x, t)$, $\tau_i(t + \omega) = \tau_i(t)$, $i = 1, 2, \dots, N$.

Theorem 6. Let $\dot{\tau}_j(t) \leq \sigma < 1$. The system (22) has a unique ω -periodic solution if there exist constants $\lambda_i > 0$ and $\epsilon > 0$ such that

$$\begin{aligned}
2\lambda_i \epsilon + 2\lambda_i p_i - 2\lambda_i \sum_{k=1}^m \frac{d_i}{l_k^2} \\
+ \sum_{j=1}^N \frac{\lambda_j |G_{ji}| e^{2\epsilon\tau}}{1-\sigma} + \lambda_i \sum_{j=1}^N |G_{ij}| \leq 0, \tag{23}
\end{aligned}$$

where $i, j = 1, 2, \dots, N$.

Proof. Define

$$\begin{aligned} w_t(\Psi) &= w(x, t + s, \Psi), \quad s \in [-\tau, 0], \quad t \geq 0, \\ w_t(\Phi) &= w(x, t + s, \Phi), \quad s \in [-\tau, 0], \quad t \geq 0. \end{aligned} \quad (24)$$

Obviously, from Theorem 5, we can derive

$$\|w(x, t, \Psi) - w(x, t, \Phi)\|_2 \leq Me^{-\epsilon t} \|\Psi - \Phi\|_\tau \quad (25)$$

for $t \geq 0$, where $M \geq 1$. We can choose a positive integer N such that

$$Me^{-\epsilon(N\omega - \tau)} \leq \frac{1}{3}. \quad (26)$$

Now define a Poincaré mapping $P : C(\Omega \times [-\tau, 0], \mathbb{R}^N) \rightarrow C(\Omega \times [-\tau, 0], \mathbb{R}^N)$ by

$$\Psi \longrightarrow P(\Psi) = w_\omega(\Psi). \quad (27)$$

Since the periodicity of system (22), one has $P^N(\Psi) = w_{N\omega}(\Psi)$. From (25) and (26), one obtains

$$\|P^N(\Psi) - P^N(\Phi)\|_\tau \leq \frac{1}{3} \|\Psi - \Phi\|_\tau. \quad (28)$$

This implies that P^N is a contraction mapping, so there exists one unique fixed point $\Psi^* \in C(\Omega \times [-\tau, 0], \mathbb{R}^N)$ such that

$$P^N(\Psi^*) = \Psi^*. \quad (29)$$

Since $P^N(P(\Psi^*)) = P(P^N(\Psi^*)) = P(\Psi^*)$, so $P(\Psi^*)$ is also a fixed point of P^N , then

$$P(\Psi^*) = \Psi^*. \quad (30)$$

Let $w(x, t, \Psi^*)$ be the solution of system (22) with initial conditions Ψ^* , then $w(x, t + \omega, \Psi^*)$ is also a solution of system (22). Obviously,

$$w(x, t + \omega, \Psi^*) = w(x, t, w_\omega(x, \Psi^*)) = w(x, t, \Psi^*) \quad \forall t \geq 0. \quad (31)$$

This means that $w(x, t, \Psi^*)$ is exactly one ω -periodic solution of system (22). This completes the proof of Theorem 6. \square

3.2. Passivity Analysis

Theorem 7. Let $\dot{\tau}_j(t) \leq \sigma < 1$. The complex network (1) is input-strictly passive if there exist constants $\lambda_i > 0$ and $\gamma > 0$ such that

$$\begin{pmatrix} M_i & \lambda_i - g_i \\ \lambda_i - g_i & \gamma - 2h_i \end{pmatrix} \leq 0, \quad (32)$$

where $M_i = -\sum_{k=1}^m (2\lambda_i d_i / l_k^2) + 2p_i \lambda_i + \lambda_i \sum_{j=1}^N |G_{ij}| + \sum_{j=1}^N (\lambda_j |G_{ji}| / (1 - \sigma))$, $i, j = 1, 2, \dots, N$.

Proof. Firstly, construct a Lyapunov functional for the network (1) as follows:

$$\begin{aligned} V(t) &= \sum_{i=1}^N \lambda_i \left\{ \int_{\Omega} w_i^2(x, t) dx \right. \\ &\quad \left. + \frac{1}{1 - \sigma} \sum_{j=1}^N |G_{ij}| \int_{t-\tau_j(t)}^t \int_{\Omega} w_j^2(x, s) dx ds \right\}. \end{aligned} \quad (33)$$

Calculating the time derivative of $V(t)$ along the trajectory of system (1), we can get

$$\begin{aligned} \dot{V}(t) &= \sum_{i=1}^N \lambda_i \left\{ 2 \int_{\Omega} w_i(x, t) \frac{\partial w_i(x, t)}{\partial t} dx \right. \\ &\quad + \frac{1}{1 - \sigma} \sum_{j=1}^N |G_{ij}| \int_{\Omega} w_j^2(x, t) dx \\ &\quad - \frac{1}{1 - \sigma} \sum_{j=1}^N |G_{ij}| (1 - \dot{\tau}_j(t)) \\ &\quad \times \left. \int_{\Omega} w_j^2(x, t - \tau_j(t)) dx \right\} \\ &\leq \sum_{i=1}^N \lambda_i \left\{ 2d_i \int_{\Omega} w_i(x, t) \Delta w_i(x, t) dx \right. \\ &\quad + 2p_i \int_{\Omega} w_i^2(x, t) dx + 2 \int_{\Omega} w_i(x, t) u_i(x, t) dx \\ &\quad + 2 \int_{\Omega} w_i(x, t) \sum_{j=1}^N G_{ij} w_j(x, t - \tau_j(t)) dx \\ &\quad + \frac{1}{1 - \sigma} \sum_{j=1}^N |G_{ij}| \int_{\Omega} w_j^2(x, t) dx \\ &\quad - \left. \sum_{j=1}^N |G_{ij}| \int_{\Omega} w_j^2(x, t - \tau_j(t)) dx \right\} \\ &\leq \sum_{i=1}^N \lambda_i \left\{ 2d_i \int_{\Omega} w_i(x, t) \Delta w_i(x, t) dx \right. \\ &\quad + 2p_i \int_{\Omega} w_i^2(x, t) dx + 2 \int_{\Omega} w_i(x, t) u_i(x, t) dx \\ &\quad + \frac{1}{1 - \sigma} \sum_{j=1}^N |G_{ij}| \int_{\Omega} w_j^2(x, t) dx \\ &\quad + 2 \sum_{j=1}^N |G_{ij}| \sqrt{\int_{\Omega} w_i^2(x, t) dx} \\ &\quad \times \sqrt{\int_{\Omega} w_j^2(x, t - \tau_j(t)) dx} \\ &\quad - \left. \sum_{j=1}^N |G_{ij}| \int_{\Omega} w_j^2(x, t - \tau_j(t)) dx \right\} \end{aligned}$$

$$\begin{aligned}
&\leq \sum_{i=1}^N \lambda_i \left\{ 2d_i \int_{\Omega} w_i(x,t) \Delta w_i(x,t) dx \right. \\
&\quad + 2p_i \int_{\Omega} w_i^2(x,t) dx + 2 \int_{\Omega} w_i(x,t) u_i(x,t) dx \\
&\quad + \frac{1}{1-\sigma} \sum_{j=1}^N |G_{ij}| \int_{\Omega} w_j^2(x,t) dx \\
&\quad \left. + \sum_{j=1}^N |G_{ij}| \int_{\Omega} w_i^2(x,t) dx \right\}. \quad (34)
\end{aligned}$$

From Green's theorem and the boundary condition, we have

$$\int_{\Omega} w_i(x,t) \Delta w_i(x,t) dx = - \sum_{k=1}^m \int_{\Omega} \left(\frac{\partial w_i(x,t)}{\partial x_k} \right)^2 dx. \quad (35)$$

According to Lemma 4, we can obtain

$$\sum_{k=1}^m \int_{\Omega} \left(\frac{\partial w_i(x,t)}{\partial x_k} \right)^2 dx \geq \sum_{k=1}^m \int_{\Omega} \frac{w_i^2(x,t)}{l_k^2} dx. \quad (36)$$

Therefore,

$$\begin{aligned}
&\dot{V}(t) - 2 \sum_{i=1}^N \int_{\Omega} y_i(x,t) u_i(x,t) dx + \gamma \sum_{i=1}^N \int_{\Omega} u_i^2(x,t) dx \\
&\leq \sum_{i=1}^N \left\{ \left(-2\lambda_i \sum_{k=1}^m \frac{d_i}{l_k^2} + \lambda_i \sum_{j=1}^N |G_{ij}| + 2p_i \lambda_i \right) \right. \\
&\quad \times \int_{\Omega} w_i^2(x,t) dx + (\gamma - 2h_i) \int_{\Omega} u_i^2(x,t) dx \\
&\quad + 2(\lambda_i - g_i) \int_{\Omega} w_i(x,t) u_i(x,t) dx \\
&\quad \left. + \frac{\lambda_i}{1-\sigma} \sum_{j=1}^N |G_{ij}| \int_{\Omega} w_j^2(x,t) dx \right\} \\
&= \sum_{i=1}^N \left\{ \left(-2\lambda_i \sum_{k=1}^m \frac{d_i}{l_k^2} + 2p_i \lambda_i \right. \right. \\
&\quad \left. \left. + \lambda_i \sum_{j=1}^N |G_{ij}| + \sum_{j=1}^N \frac{\lambda_j |G_{ji}|}{1-\sigma} \right) \int_{\Omega} w_i^2(x,t) dx \right. \\
&\quad + 2(\lambda_i - g_i) \int_{\Omega} w_i(x,t) u_i(x,t) dx \\
&\quad \left. + (\gamma - 2h_i) \int_{\Omega} u_i^2(x,t) dx \right\} \\
&= \sum_{i=1}^N \int_{\Omega} \begin{pmatrix} w_i(x,t) \\ u_i(x,t) \end{pmatrix}^T \begin{pmatrix} M_i & \lambda_i - g_i \\ \lambda_i - g_i & \gamma - 2h_i \end{pmatrix} \begin{pmatrix} w_i(x,t) \\ u_i(x,t) \end{pmatrix} dx. \quad (37)
\end{aligned}$$

It follows from (32) that

$$\begin{aligned}
&\dot{V}(t) - 2 \sum_{i=1}^N \int_{\Omega} y_i(x,t) u_i(x,t) dx \\
&\quad + \gamma \sum_{i=1}^N \int_{\Omega} u_i^2(x,t) dx \leq 0. \quad (38)
\end{aligned}$$

By integrating (38) with respect to t over the time period 0 to t_p , we can get

$$2 \sum_{i=1}^N \int_0^{t_p} \int_{\Omega} y_i(x,t) u_i(x,t) dx dt \quad (39)$$

$$\geq V(t_p) - V(0) + \gamma \sum_{i=1}^N \int_0^{t_p} \int_{\Omega} u_i^2(x,t) dx dt.$$

From the definition of $V(t)$, we have $V(t_p) \geq 0$ and $V(0) \geq 0$. Thus,

$$\sum_{i=1}^N \int_0^{t_p} \int_{\Omega} y_i(x,t) u_i(x,t) dx dt \quad (40)$$

$$\geq -\beta^2 + \frac{\gamma}{2} \sum_{i=1}^N \int_0^{t_p} \int_{\Omega} u_i^2(x,t) dx dt$$

for all $t_p \geq 0$, where $\beta = \sqrt{V(0)/2}$. The proof is completed. \square

By a minor modification of the proof of Theorem 7, we can easily get the following.

Theorem 8. Let $\dot{t}_j(t) \leq \sigma < 1$. The complex network (1) is output-strictly passive if there exist constants $\lambda_i > 0$ and $\gamma > 0$ such that

$$\begin{pmatrix} \widehat{M}_i & \lambda_i - g_i + \gamma g_i h_i \\ \lambda_i - g_i + \gamma g_i h_i & \gamma h_i^2 - 2h_i \end{pmatrix} \leq 0, \quad (41)$$

where $i, j = 1, 2, \dots, N$, $\widehat{M}_i = -2\lambda_i \sum_{k=1}^m (d_i/l_k^2) + 2p_i \lambda_i + \lambda_i \sum_{j=1}^N |G_{ij}| + \gamma g_i^2 + \sum_{j=1}^N (\lambda_j |G_{ji}|/(1-\sigma))$.

Remark 9. In [22], two kinds of impulsive parabolic complex networks were considered, in which the node states are dependent on the time and space variables. Several global exponential stability and robust global exponential stability criteria were derived for the impulsive parabolic complex networks. Both global exponential stability and passivity are taken into consideration in this paper, and some sufficient conditions are established.

4. Example

In this section, an illustrative example is provided to verify the effectiveness of the proposed theoretical results.

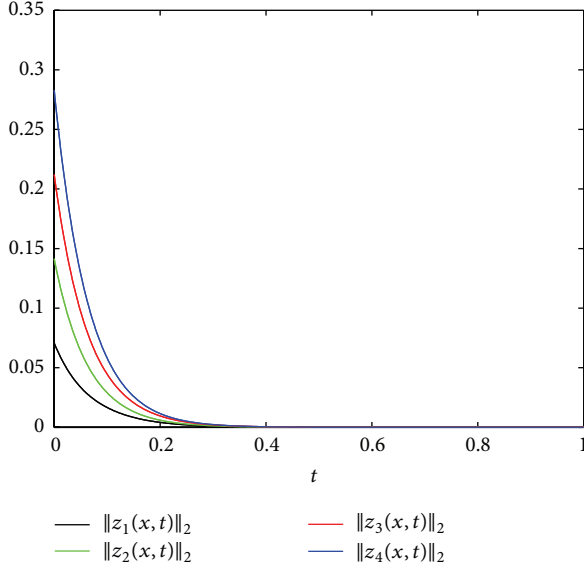


FIGURE 1: The change processes of $\|z_i(x, t)\|_2$, $i = 1, 2, 3, 4$.

Consider a complex network model, in which each node is a 1-dimensional dynamical system described by

$$\begin{aligned} \frac{\partial w_i(x, t)}{\partial t} \\ = d_i \frac{\partial^2 w_i(x, t)}{\partial x^2} + p_i w_i(x, t), \quad i = 1, 2, 3, 4. \end{aligned} \quad (42)$$

Take $d_i = 0.4$, $p_i = 0.1i$, $g_i = 1$, $h_i = 2$, $\tau_j(t) = 0.2 - (e^{-t}/(4 + j))$, $\tau = 0.2$, $\sigma = 0.2$, $x \in (-0.5, 0.5)$. The matrix G is chosen as

$$\begin{pmatrix} -0.3 & 0.1 & 0.15 & 0.05 \\ 0.2 & -0.3 & 0.1 & 0 \\ 0.05 & 0.05 & -0.3 & 0.2 \\ 0.1 & 0 & 0.1 & -0.2 \end{pmatrix}. \quad (43)$$

It is easy to verify that (9) is satisfied if $\lambda_1 = \lambda_2 = \lambda_3 = \lambda_4 = 1$ and $\epsilon = 0.25$. From Theorem 5, complex network (1) with above given parameters is globally exponentially stable. Moreover, if we take $\lambda_1 = \lambda_2 = \lambda_3 = \lambda_4 = 1$ and $\gamma = 1.5$, then (32) is satisfied. According to Theorem 7, complex network (1) with above given parameters is also input-strictly passive. The simulation results are shown in Figures 1 and 2.

5. Conclusion

A parabolic complex network model has been introduced, in which the state, input, and output variables are dependent on the time and space variables. The input strict passivity, output strict passivity, and global exponential stability of the proposed network model have been discussed in this paper, and several sufficient conditions have been established. Illustrative simulations have been provided to verify the correctness and effectiveness of the obtained results. In future work, we shall study the passivity and robust passivity of parabolic complex networks with impulsive effects.

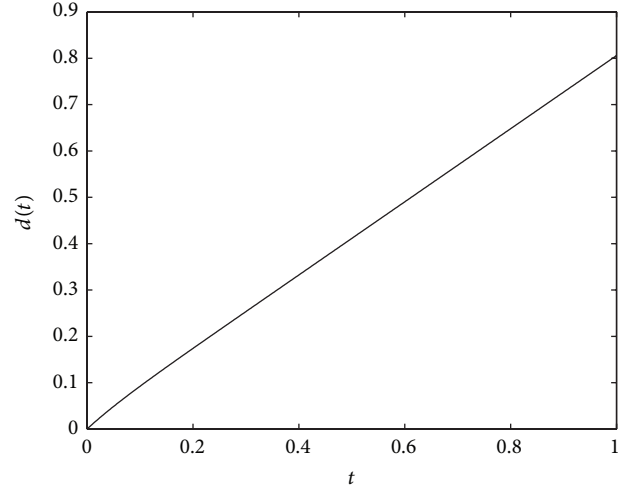


FIGURE 2: The change process of $d(t) = \sum_{i=1}^4 \int_0^t \int_{\Omega} y_i(x, s) u_i(x, s) dx ds - 0.75 \sum_{i=1}^4 \int_0^t \int_{\Omega} u_i^2(x, s) dx ds$, in which $u_i(x, t) = 0.2i \sin(2\pi x)$, $i = 1, 2, 3, 4$.

Conflict of Interests

The authors declare that there is no conflict of interests regarding the publication of this paper.

Acknowledgment

The authors would like to thank Professor J.-L. Wang (Tianjin Polytechnic University, Tianjin, China) for his kind help.

References

- [1] J. Lu and G. Chen, "A time-varying complex dynamical network model and its controlled synchronization criteria," *IEEE Transactions on Automatic Control*, vol. 50, no. 6, pp. 841–846, 2005.
- [2] W. Yu, G. Chen, and J. Lü, "On pinning synchronization of complex dynamical networks," *Automatica*, vol. 45, no. 2, pp. 429–435, 2009.
- [3] W. Yu, J. Cao, and J. Lu, "Global synchronization of linearly hybrid coupled networks with time-varying delay," *SIAM Journal on Applied Dynamical Systems*, vol. 7, no. 1, pp. 108–133, 2008.
- [4] J. L. Wang, H. N. Wu, and L. Guo, "Novel adaptive strategies for synchronization of linearly coupled neural networks with reaction-diffusion terms," *IEEE Transactions on Neural Networks and Learning Systems*, vol. 25, pp. 429–440, 2014.
- [5] J. L. Wang and H. N. Wu, "Synchronization and adaptive control of an array of linearly coupled reaction-diffusion neural networks with hybrid coupling," *IEEE Transactions on Cybernetics*, vol. 44, no. 8, pp. 1350–1361, 2014.
- [6] J. L. Wang, Z. C. Yang, T. W. Huang, and M. Q. Xiao, "Synchronization criteria in complex dynamical networks with nonsymmetric coupling and multiple time-varying delays," *Applicable Analysis*, vol. 91, no. 5, pp. 923–935, 2012.
- [7] J. L. Wang, Z. C. Yang, and T. W. Huang, "Local and global exponential synchronization of complex delayed dynamical networks with general topology," *Discrete and Continuous Dynamical Systems B*, vol. 16, no. 1, pp. 393–408, 2011.

- [8] J.-L. Wang and H.-N. Wu, "Local and global exponential output synchronization of complex delayed dynamical networks," *Nonlinear Dynamics*, vol. 67, no. 1, pp. 497–504, 2012.
- [9] J. Wang and H. Wu, "Synchronization criteria for impulsive complex dynamical networks with time-varying delay," *Nonlinear Dynamics*, vol. 70, no. 1, pp. 13–24, 2012.
- [10] J. L. Wang and H. N. Wu, "Adaptive output synchronization of complex delayed dynamical networks with output coupling," *Neurocomputing*, vol. 142, pp. 174–181, 2014.
- [11] M. D. Holland and A. Hastings, "Strong effect of dispersal network structure on ecological dynamics," *Nature*, vol. 456, no. 7223, pp. 792–795, 2008.
- [12] J. M. Montoya, S. L. Pimm, and R. V. Solé, "Ecological networks and their fragility," *Nature*, vol. 442, no. 7100, pp. 259–264, 2006.
- [13] W. Ko and I. Ahn, "Dynamics of a simple food chain model with a ratio-dependent functional response," *Nonlinear Analysis: Real World Applications*, vol. 12, no. 3, pp. 1670–1680, 2011.
- [14] Y.-M. Wang, "Asymptotic behavior of solutions for a Lotka-Volterra mutualism reaction-diffusion system with time delays," *Computers & Mathematics with Applications*, vol. 58, no. 3, pp. 597–604, 2009.
- [15] Y. M. Wang, "Asymptotic behavior of solutions for a class of predator-prey reaction-diffusion systems with time delays," *Journal of Mathematical Analysis and Applications*, vol. 328, no. 1, pp. 137–150, 2007.
- [16] C. Wang, S. Wang, F. Yang, and L. Li, "Global asymptotic stability of positive equilibrium of three-species Lotka-Volterra mutualism models with diffusion and delay effects," *Applied Mathematical Modelling*, vol. 34, no. 12, pp. 4278–4288, 2010.
- [17] C. V. Pao, "The global attractor of a competitor-competitor-mutualist reaction-diffusion system with time delays," *Nonlinear Analysis: Theory, Methods and Applications*, vol. 67, no. 9, pp. 2623–2631, 2007.
- [18] C. V. Pao, "Global attractor of a coupled finite difference reaction diffusion system with delays," *Journal of Mathematical Analysis and Applications*, vol. 288, no. 1, pp. 251–273, 2003.
- [19] C. V. Pao, "Convergence of solutions of reaction-diffusion systems with time delays," *Nonlinear Analysis. Theory, Methods & Applications*, vol. 48, pp. 349–362, 2002.
- [20] M. R. Garvie, "Finite-difference schemes for reaction-diffusion equations modeling predator-prey interactions in MATLAB," *Bulletin of Mathematical Biology*, vol. 69, no. 3, pp. 931–956, 2007.
- [21] K. I. Kim and Z. Lin, "Blowup in a three-species cooperating model," *Applied Mathematics Letters*, vol. 17, no. 1, pp. 89–94, 2004.
- [22] J. Wang and H. Wu, "Stability analysis of impulsive parabolic complex networks," *Chaos, Solitons and Fractals*, vol. 44, no. 11, pp. 1020–1034, 2011.
- [23] J. L. Wang and H. N. Wu, "Robust stability and robust passivity of parabolic complex networks with parametric uncertainties and time-varying delays," *Neurocomputing*, vol. 87, pp. 26–32, 2012.
- [24] J.-L. Wang, H.-N. Wu, and L. Guo, "Pinning control of spatially and temporally complex dynamical networks with time-varying delays," *Nonlinear Dynamics*, vol. 70, no. 2, pp. 1657–1674, 2012.
- [25] L. O. Chua, "Passivity and complexity," *IEEE Transactions on Circuits and Systems. I. Fundamental Theory and Applications*, vol. 46, no. 1, pp. 71–82, 1999.
- [26] L. Xie, M. Fu, and H. Li, "Passivity analysis and passification for uncertain signal processing systems," *IEEE Transactions on Signal Processing*, vol. 46, no. 9, pp. 2394–2403, 1998.
- [27] D. J. Hill and P. J. Moylan, "Stability results for nonlinear feedback systems," *Automatica*, vol. 13, no. 4, pp. 377–382, 1977.
- [28] G. L. Santosuosso, "Passivity of nonlinear systems with input-output feedthrough," *Automatica*, vol. 33, no. 4, pp. 693–697, 1997.
- [29] W. Yu, "Passive equivalence of chaos in Lorenz system," *IEEE Transactions on Circuits and Systems I: Fundamental Theory and Applications*, vol. 46, no. 7, pp. 876–878, 1999.
- [30] C. W. Wu, "Synchronization in arrays of coupled nonlinear systems: passivity, circle criterion, and observer design," *IEEE Transactions on Circuits and Systems. I. Fundamental Theory and Applications*, vol. 48, no. 10, pp. 1257–1261, 2001.
- [31] G. Calcev, R. Gorez, and M. De Neyer, "Passivity approach to fuzzy control systems," *Automatica*, vol. 34, no. 3, pp. 339–344, 1998.
- [32] J. Wang, H. Wu, and L. Guo, "Passivity and stability analysis of reaction-diffusion neural networks with dirichlet boundary conditions," *IEEE Transactions on Neural Networks*, vol. 22, no. 12, pp. 2105–2116, 2011.
- [33] J. G. Lu, "Global exponential stability and periodicity of reaction-diffusion delayed recurrent neural networks with Dirichlet boundary conditions," *Chaos, Solitons and Fractals*, vol. 35, no. 1, pp. 116–125, 2008.

Research Article

Stability of Delayed Hopfield Neural Networks with Variable-Time Impulses

Yangjun Pei,¹ Chao Liu,² and Qi Han¹

¹ School of Electrical and Information Engineering, Chongqing University of Science and Technology, Chongqing 401331, China

² College of Computer Science and Engineering, Chongqing University of Technology, Chongqing 400050, China

Correspondence should be addressed to Chao Liu; xiuwenzheng2000@163.com

Received 3 April 2014; Accepted 22 July 2014; Published 1 September 2014

Academic Editor: Chuandong Li

Copyright © 2014 Yangjun Pei et al. This is an open access article distributed under the Creative Commons Attribution License, which permits unrestricted use, distribution, and reproduction in any medium, provided the original work is properly cited.

In this paper the globally exponential stability criteria of delayed Hopfield neural networks with variable-time impulses are established. The proposed criteria can also be applied in Hopfield neural networks with fixed-time impulses. A numerical example is presented to illustrate the effectiveness of our theoretical results.

1. Introduction

Hopfield neural networks [1], which were referred by Hopfield in 1984, have attracted many attentions of researchers and have been applied in many fields such as pattern recognition, associative memory, and combinatorial optimization. Stability, a crucial dynamic feature of Hopfield neural networks, has been intensively investigated over the past decades. Some significant sufficient results can be referred in [2–6].

It is well known that time delay is unavoidable due to finite switching speeds of the amplifiers and it may cause oscillations or instability of dynamic systems. The effects of time delay on the dynamical behavior of neural networks are nonnegligible. Some stability criteria for delayed Hopfield neural networks have been proposed in [7–10]. Meanwhile, impulsive phenomena exist in a wide variety of evolutionary processes, such as financial systems and nanoscale electronic circuits in which many state variables change instantaneously, in the form of impulses. On the other hand, impulsive control is also applied widely in many fields of information science, electronics, automated control systems, computer networking, artificial intelligence, robotics and telecommunications, and so forth. Neural networks may jump instantaneously because of environmental changes (such as external noise and disturbance). We may also introduce impulses deliberately to stabilize the oscillating and chaotic neural networks. Many

researchers have investigated impulsive Hopfield neural networks and have obtained many interesting stability results [11–19].

However, up to now, the vast majority of stability results for impulsive Hopfield neural networks are focused on the case of fixed-time impulses. As we know, variable-time impulses arise naturally in biological and physiological systems. The primary difference between neural network with fixed-time impulses and neural network with variable-time impulses is the impulsive instant. In the neural network with fixed-time impulses, the impulsive instant is completely fixed and not about the state of system. But in neural network with variable-time impulses, the impulsive instant is not fixed and determined by state of system. In [20], we have focused on BAM neural networks with variable-time impulses and have obtained some crucial theoretical results. In [21], we have investigated the stabilizing effects of impulses for Hopfield neural networks and have shown that Hopfield neural networks with unstable continuous component may be still stable because of the stabilizing effects of impulses. In this paper, we focus on the destabilizing effects of Hopfield neural networks with variable-time impulses. It is shown that the impulsive Hopfield neural networks may preserve the global exponential stability of the impulse-free Hopfield neural networks even if the impulses have enlarging effects on the states of neurons. For this purpose, it is always assumed that the states of neurons enlarge at impulsive time.

This paper is organized as follows. In the coming section we introduce some notations, definition, and lemmas. In Section 3 we consider the stability of Hopfield neural networks with time delays and variable-time impulses and establish stability criteria. In Section 4, one example is given to illustrate the effectiveness of our theoretical results.

2. Preliminaries

In this paper, we consider the following Hopfield neural networks with variable-time impulses:

$$\begin{aligned}\dot{\tilde{x}}(t) &= -A\tilde{x}(t) + B\tilde{f}(\tilde{x}(t - \tau)) + \tilde{I}, \quad t \neq \tilde{t}_k(x), \\ \Delta\tilde{x}(t) &= \tilde{J}_k(\tilde{x}(t^-)), \quad t = \tilde{t}_k(x),\end{aligned}\quad (1)$$

$$\tilde{x}(t_0 + s) = \tilde{\phi}(s), \quad s \in [-\tau, 0],$$

where $\tilde{x} = (\tilde{x}_1, \dots, \tilde{x}_n)^T$ is the neuron state vector, $\tau > 0$ is the transmission delay, $A = \text{diag}(a_1, \dots, a_n)$ with $a_i > 0$, $i = 1, \dots, n$, $B = [b_{ij}]_{n \times n}$ is the delayed connection weight matrix, and $\tilde{f}(\cdot) = (\tilde{f}_1(\cdot), \dots, \tilde{f}_n(\cdot))^T$ is neuron activation function. \tilde{I} is the external input, $0 \leq t_0 < \tilde{t}_1(\tilde{x}) < \dots < \tilde{t}_k(\tilde{x}) < \dots$, $\tilde{t}_k(\tilde{x}) \rightarrow \infty$ as $k \rightarrow \infty$, $\tilde{x}(t^+) = \lim_{s \rightarrow t^+} \tilde{x}(s)$, and $\tilde{x}(t^-) = \lim_{s \rightarrow t^-} \tilde{x}(s)$. In this paper we always assume that $\tilde{x}(t) = \tilde{x}(t^+)$ as $t = \tilde{t}_k(\tilde{x})$. We further assume that

$$(A1) \text{ there is } l_i > 0, i = 1, \dots, n, \text{ such that } |\tilde{f}_i(\alpha) - \tilde{f}_i(\beta)| \leq l_i |\alpha - \beta|, \text{ for any } \alpha, \beta \in R.$$

Throughout this paper, it is always assumed that there is at least one equilibrium point of (1). As usual, we shift an equilibrium point $x^* = (x_1^*, \dots, x_n^*)^T$ to the origin by transformation $x = \tilde{x} - x^*$. Then system (1) can be rewritten as follows:

$$\begin{aligned}\dot{x}(t) &= -Ax(t) + Bf(x(t - \tau)), \quad t \neq t_k(x), \\ \Delta x(t) &= J_k(x(t^-)), \quad t = t_k(x), \\ x(t_0 + s) &= \phi(s), \quad s \in [-\tau, 0],\end{aligned}\quad (2)$$

where $f(x(t)) = \tilde{f}(x(t) + x^*) - \tilde{f}(x^*)$, $J_k(x(t^-)) = \tilde{J}_k(x(t^-) + x^*)$, $t_k(x) = \tilde{t}_k(x + x^*)$, and $\phi(s) = \tilde{\phi}(s) - x^*$.

In the sequel, we introduce some notations, basic definition, and lemmas:

$$R_+ = [0, +\infty); \quad S_k = \{(t, x) \in R_+ \times R^n : t = t_k(x)\};$$

$$N_k = \{t \in R_+ : \text{there is } x \in R^n \text{ such that } (t, x) \in S_k\};$$

$$d_k = d(N_{k-1}, N_k) = \inf_{\substack{\tilde{t} \in N_k \\ t \in N_{k-1}}} |\tilde{t} - t|;$$

$$d_k^* = d^*(N_{k-1}, N_k) = \sup_{\substack{\tilde{t} \in N_k \\ t \in N_{k-1}}} |\tilde{t} - t|;$$

$$L = \text{diag}(l_1, \dots, l_n);$$

$\lambda_{\max}(\cdot)$, $\lambda_{\min}(\cdot)$ denote the maximum and the minimum eigenvalues of the corresponding matrix, respectively.

$\|\cdot\|$ denotes the Euclidean norm of a vector or a square matrix.

$A > 0$ denotes that A is positive definite matrix.

$PC = PC(I, R^n) = \{\psi : I \rightarrow R^n \mid \psi(t^+) = \psi(t) \text{ for } t \in I, \psi(t^-) \text{ exists for } t \in I, \psi(t^-) = \psi(t) \text{ for all } t \in I \text{ but at most finite points}\}$, where I is an interval:

$$\|y\|_\tau = \sup_{\tau \leq s \leq 0} \|y(s)\| \quad \text{for } y \in PC([- \tau, 0], R^n). \quad (4)$$

Definition 1. The equilibrium point $x^* = (x_1^*, x_2^*, \dots, x_n^*)^T$ of (1) is said to be globally exponentially stable if, for any solution $\tilde{x}(t, t_0, \tilde{\phi})$ with the initial condition $\tilde{\phi} \in PC$, there are constant $\varepsilon > 0$ and $M > 1$ such that $\|\tilde{x}(t, t_0, \tilde{\phi}) - x^*\| \leq M \|\tilde{\phi} - x^*\|_\tau e^{-\varepsilon(t-t_0)}$.

Lemma 2 (Berman and Plemmons [22]). Let $A \in R^{n \times n}$; then

$$\lambda_{\min}(A) x^T x \leq x^T A x \leq \lambda_{\max}(A) x^T x, \quad (5)$$

for any $x \in R^n$, if A is a symmetric matrix.

Lemma 3. Consider the following differential inequality:

$$\begin{aligned}D^+V(t) &\leq -\alpha V(t) + \beta V(t - \tau), \quad t \neq t_k, \\ V(t) &\leq c_k V(t^-), \quad t = t_k,\end{aligned}\quad (6)$$

where $V(t) \geq 0$, $\alpha > \beta > 0$, and $c_k > 1$, $k = 1, 2, \dots$. Denote $\delta^* = \sup_k \{t_{k+1} - t_k\}$, $\delta = \inf_k \{t_{k+1} - t_k\}$. For $d^* \geq \delta^*$, $0 < d \leq \delta$, and $\theta > 0$ such that $-\alpha + \beta e^{-\theta\tau} = -\theta$, where $U = \max_k \{c_k^{-1} \dots c_{k+N}^{-1}\}$ for $N = \lfloor \tau/d^* \rfloor > 0$ and $U = 1$ for $N = 0$, one has

$$V(t) \leq M \prod_{i=0}^{k-1} c_i \bar{V}(t_0) e^{-\theta(t-t_0)}, \quad t \in [t_{k-1}, t_k], \quad (7)$$

where $c_0 = 1$, $\bar{V}(t_0) = \sup_{s \in [-\tau, 0]} V(t_0 + s)$, and $M \geq 1$ is a constant.

Proof. See the Appendix section. \square

Remark 4. In Lemma 3, if $\tau < d^*$, we have $U = 1$. Based on the proof, we know that $\theta = \varepsilon$ (please see the Appendix section for meaning of ε). If $\tau \geq d^*$, we obtain $U < 1$. It is obvious to know that $\theta > \varepsilon$. Generally speaking, (7) is more valuable because the convergence rate in (7) is larger than that in (A.1) when $\tau \geq d^*$. Because $c_k > 1$, we can use Lemma 3 to investigate the stability of impulsive differential systems in which the impulses are with destabilizing effects.

The solutions of system (1) may hit the same switching surface S_k finite or infinite times causing “beating phenomenon” or “pulse phenomenon.” In a similar way in [17], we can get the following lemma easily which guarantees that beating phenomenon does not exist.

Lemma 5. Suppose that

- (i) for any $k = 1, 2, \dots, \tilde{t}_k(x)$ is bounded;
- (ii) for any $(t_0, \tilde{\phi})$ there is a solution of continuous subsystem of system (1) in $[t_0, +\infty)$;
- (iii) $(\partial \tilde{t}_k(\tilde{x}) / \partial \tilde{x})(-A\tilde{x} + B\tilde{f}(\tilde{x}(t - \tau)) + I) < 1$;
- (iv) $\tilde{t}_k(\tilde{x}) \geq \tilde{t}_k(\tilde{x} + \tilde{J}_k(\tilde{x}))$, and $\tilde{t}_{k+1}(\tilde{x} + \tilde{J}_k(\tilde{x})) > \tilde{t}_k(\tilde{x})$.

Then there is solution of system (1) in $[t_0, +\infty)$, and it hits each switching surface $S_k : t = \tilde{t}_k(\tilde{x})$ exactly once in turn.

From Theorem 1.1.4 in [23], we know that there exists a unique solution of system (1) without impulses in our paper on $[t_0, +\infty)$, if $\|f(x) - f(y)\| \leq K\|x - y\|$, which yields that there exists a unique solution for any $\sum_k = \{(t, x) : t_{k-1}(x) \leq t < t_k(x)\}$ and any initial condition. Therefore, by mathematical induction, we know the global uniqueness and existence of solution. From now on we always assume that there exists a unique solution of system (1) $\tilde{x}(t) = \tilde{x}(t, t_0, \tilde{\phi})$ satisfying the conditions of Lemma 5; namely, it hits each switching surface $S_i, i \geq k$, only once [11]. In addition, we also always assume that $\{t_i\}_{i=1}^{\infty}$ are the moments that integral curve $(t, \tilde{x}(t, t_0, \tilde{\phi}))$ hits each switching surface $\{S_{k_i}\}_{i=1}^{\infty}$ in turn; namely, $t_i = \tilde{t}_{k_i}(x(t_i))$ and $t_i < t_{i+1}$.

3. Main Results

In this section, we establish some sufficient criteria for the exponential stability of system (1).

Theorem 6. Assume that, in addition to condition (A1), the following conditions are satisfied:

- (A2) $\tilde{J}_k(\tilde{x}(t)) = S_k(\tilde{x}(t) - x^*)$ with $S_k = \text{diag}(s_{1k}, s_{2k}, \dots, s_{nk})$;
- (A3) $d = \inf_k \{d_k\} > 0, d^* = \sup_k \{d_k^*\} < \infty$;
- (A4) there are a symmetric positive definite matrix P , constants $\mu > 0, q > 0, c_k > 0, \varepsilon > 0$, and $\alpha > \beta$ such that

$$\begin{aligned} -A^T P - PA + \mu^{-1} P B B^T P &\leq -\alpha P, \\ \mu L^T L &\leq \beta P, \end{aligned} \quad (8)$$

$$P + S_k^T P + P S_k + S_k^T P S_k \leq c_k P,$$

$c_k < e^{\varepsilon d}$, and $-\alpha + \beta e^{\varepsilon \tau} U = -\varepsilon$, where $U = \max_k \{c_k^{-1} \dots c_{k+N}^{-1}\}$ for $N = \lfloor \tau/d^* \rfloor > 0$ and $U = 1$ for $N = 0$.

Then the equilibrium point x^* of system (1) is globally exponentially stable.

Proof. Based on (A2), we know that $J_k(x(t^-)) = S_k x(t^-)$. We choose the Lyapunov function of system (2) as follows:

$$V(t, x(t)) = x^T(t) P x(t). \quad (9)$$

Let $V(t) = V(t, x(t))$ briefly. When $t \neq t_i$, we have

$$\begin{aligned} D^+ V(t) &= \dot{x}^T(t) P x(t) + x^T(t) P \dot{x}(t) \\ &= (-Ax(t) + Bf(x(t - \tau)))^T P x(t) \\ &\quad + x^T(t) P (-Ax(t) + Bf(x(t - \tau))) \\ &\leq x^T(t) (-A^T P - PA) x(t) \\ &\quad + \mu^{-1} x^T(t) P B B^T P x(t) + \mu f^T(x(t)) f(x(t)) \\ &\leq x^T(t) (-A^T P - PA + \mu^{-1} P B B^T) x(t) \\ &\quad + \mu^{-1} x^T(t - \tau) L^T L x(t - \tau) \\ &\leq -\alpha V(t) + \beta V(t - \tau). \end{aligned} \quad (10)$$

When $t = t_i$, we have

$$\begin{aligned} V(t_i) &= x^T(t_i) P x(t_i) \\ &= (x(t_i^-) + S_{k_i} x(t_i^-))^T P (x(t_i^-) + S_{k_i} x(t_i^-)) \\ &= x^T(t_i^-) (P + S_{k_i}^T P + P S_{k_i} + S_{k_i}^T P S_{k_i}) x(t_i^-) \\ &\leq c_{k_i} V(t_i^-). \end{aligned} \quad (11)$$

Therefore, we have

$$\begin{aligned} D^+ V(t) &\leq -\alpha V(t) + \beta V(t - \tau), \quad t \neq t_i, \\ V(t_i) &\leq c_{k_i} V(t_i^-), \quad i = 1, 2, \dots \end{aligned} \quad (12)$$

On the basis of (7) and Lemma 3, we have

$$V(t) \leq M \prod_{l=1}^i c_{k_l} \bar{V}(t_0) e^{-\varepsilon(t-t_0)}, \quad t \in [t_i, t_{i+1}). \quad (13)$$

From condition (A4), we know that there is $0 < \zeta < \varepsilon$ such that $c_l \leq e^{(\varepsilon-\zeta)d} \leq e^{(\varepsilon-\zeta)(t_{i+1}-t_l)}$, $l = 1, 2, \dots$. Therefore, we have

$$\begin{aligned} V(t) &\leq M \prod_{l=1}^i e^{(\varepsilon-\zeta)(t_{i+1}-t_l)} e^{-\varepsilon(t-t_0)} \\ &= M e^{-\zeta(t-t_0)} e^{(\varepsilon-\zeta)(t_{i+1}-t-t_0-t_1)} \\ &\leq M e^{-\zeta(t-t_0)} e^{(\varepsilon-\zeta)d^*}. \end{aligned} \quad (14)$$

Denote $\bar{M} = e^{(\varepsilon+\zeta)d^*}$; then we have

$$V(t) \leq \bar{M} \bar{M} \bar{V}(t_0) e^{-\zeta(t-t_0)}. \quad (15)$$

Based on (9) and Lemma 2, we obtain that

$$\|x(t)\| \leq \sqrt{\frac{\bar{M} \bar{M} \lambda_{\max}(P)}{\lambda_{\min}(P)}} \|\tilde{\phi}\|_r e^{-(\zeta/2)(t-t_0)}. \quad (16)$$

By virtue of $x(t) = \tilde{x}(t) - x^*$, we have

$$\|\tilde{x}(t) - x^*\| \leq \sqrt{\frac{M\bar{M}\lambda_{\max}(P)}{\lambda_{\min}(P)}} \|\tilde{\phi} - x^*\|_{\tau} e^{-(\zeta/2)(t-t_0)}, \quad (17)$$

which yields that the equilibrium point x^* of system (1) is globally exponentially stable. \square

Remark 7. Because $\alpha > \beta$, we know that impulse-free neural network is stable. The impulses may be of destabilizing effects due to $c_k > 1$. It is shown that impulsive Hopfield neural networks will preserve the global exponential stability of the impulse-free Hopfield neural networks even if the impulses have enlarging effects on the states of neurons.

As mentioned in [17], the impulsive differential systems in which impulses occur in fixed time can be viewed as particular impulsive differential systems with variable-time impulses. Therefore, based on Theorem 6, we can obtain the stability criterion for the following format of Hopfield neural networks:

$$\begin{aligned} \dot{\tilde{x}}(t) &= -A\tilde{x}(t) + B\tilde{f}(\tilde{x}(t - \tau)) + \tilde{I}, \quad t \neq \tilde{t}_k, \\ \Delta\tilde{x}(t) &= \tilde{J}_k(\tilde{x}(t^-)), \quad t = \tilde{t}_k, \\ \tilde{x}(t_0 + s) &= \tilde{\phi}(s), \quad s \in [-\tau, 0]. \end{aligned} \quad (18)$$

Theorem 8. Assume that (A1), (A2) hold, and

$$(A5) \quad \delta = \inf_k \{\delta_k\} > 0, \delta^* = \sup_k \{\delta_k^*\} < \infty;$$

(A6) there are a symmetric positive definite matrix P , constants $\mu > 0$, $q > 0$, $c_k > 0$, $\varepsilon > 0$, and $\alpha > \beta$ such that

$$\begin{aligned} -A^T P - PA + \mu^{-1} P B B^T P &\leq -\alpha P, \\ \mu L^T L &\leq \beta P, \\ P + S_k^T P + P S_k + S_k^T P S_k &\leq c_k P, \end{aligned} \quad (19)$$

$c_k < e^{\varepsilon d}$, and $-\alpha + \beta e^{\varepsilon \tau} U = -\varepsilon$, where $U = \max_k \{c_k^{-1} \cdots c_{k+N}^{-1}\}$ for $\underline{N} = \lfloor \tau/\delta^* \rfloor > 0$ and $U = 1$ for $\underline{N} = 0$.

Then the equilibrium point x^* of system (18) is globally exponentially stable.

4. Numeric Example

In this section, we consider one example to illustrate the effectiveness of theoretical results.

Example 1. Consider the following system:

$$\begin{aligned} \dot{\tilde{x}}_1(t) &= -\tilde{x}_1(t) + 0.1 \sin(\tilde{x}_1(t - 0.8)) \\ &\quad + 0.4 \sin(\tilde{x}_2(t - 0.8)) + \pi, \\ \dot{\tilde{x}}_2(t) &= -\tilde{x}_2(t) + 0.4 \sin(\tilde{x}_1(t - 0.8)) \\ &\quad + 0.1 \sin(\tilde{x}_2(t - 0.8)) + \pi, \quad t \neq \tilde{t}_k(\tilde{x}), \\ \Delta\tilde{x}_1(t) &= -2.2(\tilde{x}_1(t) - \pi), \\ \Delta\tilde{x}_2(t) &= -2.2(\tilde{x}_2(t) - \pi), \quad t = \tilde{t}_k(\tilde{x}), \end{aligned} \quad (20)$$

where $\tilde{t}_k(\tilde{x}) = -(2/5\pi^2) \arctan^2(\tilde{x}_1 + \tilde{x}_2 - 2\pi) + 0.7k$. It is easy to obtain that $A = \text{diag}(1, 1)$, $B = \begin{bmatrix} 0.1 & 0.4 \\ 0.4 & 0.1 \end{bmatrix}$, $S_k = \text{diag}(-2.2, -2.2)$, $\tau = 0.8$, $d = 0.6$, $d^* = 0.8$, $L = E$, and $x^* = (\pi, \pi)^T$.

Now we verify that there is no beating phenomenon in system (20).

- (1) It is obvious that, for $k = 1, 2, \dots$, $\tilde{t}_k(x) = -(2/5\pi^2) \arctan^2(\tilde{x}_1 + \tilde{x}_2 - 2\pi) + 0.7k$ is bounded.
- (2) Based on [24], it is easy to predicate the existence of solutions for system (20).
- (3) Let $y = \tilde{x}_1 + \tilde{x}_2 - 2\pi$, $F_1 = \sin(\tilde{x}_1(t - 0.8))$, and $F_2 = \sin(\tilde{x}_2(t - 0.8))$. We have

$$\begin{aligned} &\frac{\partial \tilde{t}_k(\tilde{x})}{\partial \tilde{x}} (-A\tilde{x} + B\tilde{f}(\tilde{x}(t - \tau)) + I) \\ &= -\frac{4}{5\pi^2} \frac{\arctan(y)}{1 + y^2} (-y + 0.5F_1 + 0.5F_2) \\ &\leq \frac{4}{5\pi^2} \frac{|y|}{1 + y^2} (|y| + 0.5|F_1| + 0.5|F_2|) \\ &\leq \frac{4}{5\pi^2} \left(\frac{y^2}{1 + y^2} + 0.5 \left(\frac{|F_1| + |F_2|}{1 + y^2} \right) \right) \leq \frac{8}{5\pi^2} < 1. \end{aligned} \quad (21)$$

- (4) It is easy to see that $\tilde{t}_k(\tilde{x}) \geq t_k(\tilde{x} + \tilde{J}_k(\tilde{x}))$ and $\tilde{t}_{k+1}(\tilde{x} + \tilde{J}_k(\tilde{x})) > \tilde{t}_k(\tilde{x})$.

Therefore, all the conditions of Lemma 5 are satisfied; that is to say, there is no beating phenomenon in system (20).

For convenience, choose $P = E$, $\mu = 1$, $\alpha = 1.7$, $\beta = 1$, and $c_k = 1.44$. It is easy to verify that $\varepsilon = 0.792$ and all the conditions of Theorem 6 are satisfied. Therefore, system (20) is globally exponentially stable, although the impulses are of destabilizing effects, as shown in Figure 1.

Appendix

Proof of Lemma 3

Let ε be the largest positive solution satisfying the inequality $-\alpha + \beta e^{\varepsilon \zeta} \leq -\varepsilon$. We claim that

$$V(t) \leq \prod_{i=0}^{k-1} \bar{c}_i \bar{V}(t_0) e^{-\varepsilon(t-t_0)}, \quad (A.1)$$

where $t \in [t_{k-1}, t_k)$, $k = 1, 2, \dots$

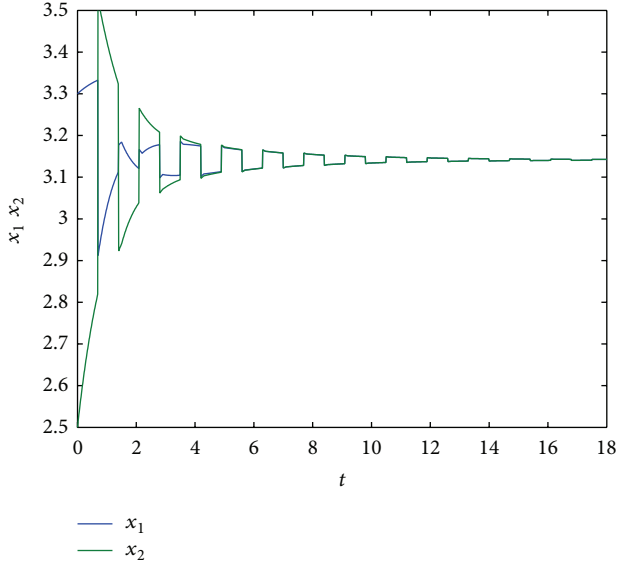


FIGURE 1: The time response curves of system (20).

First, for $t \in [t_0 - \tau, t_0]$, we have $V(t) \leq \bar{V}(t_0) \leq \bar{V}(t_0)e^{-\varepsilon(t-t_0)}$. Particularly, $V(t_0) \leq \bar{V}(t_0)e^{-\varepsilon(t_0-t_0)} = c_0 \bar{V}(t_0)e^{-\varepsilon(t_0-t_0)}$. Now we show that (A.1) holds for $k = 1$; namely,

$$V(t) \leq c_0 \bar{V}(t_0) e^{-\varepsilon(t-t_0)}, \quad t \in [t_0, t_1]. \quad (\text{A.2})$$

If (A.2) does not hold, there is $t^* \in [t_0, t_1]$ such that

$$\begin{aligned} V(t^*) &= c_0 \bar{V}(t_0) e^{-\varepsilon(t^*-t_0)}, \\ D^+ V(t^*) &> -\varepsilon c_0 \bar{V}(t_0) e^{-\varepsilon(t^*-t_0)}. \end{aligned} \quad (\text{A.3})$$

However, based on (6), we have

$$\begin{aligned} D^+ V(t^*) &\leq -\alpha V(t^*) + \beta V(t^* - \tau) \\ &\leq -\alpha c_0 \bar{V}(t_0) e^{-\varepsilon(t^*-t_0)} + \beta c_0 \bar{V}(t_0) e^{-\varepsilon(t^*-\tau-t_0)} \\ &= (-\alpha + \beta e^{\varepsilon\tau}) c_0 \bar{V}(t_0) e^{-\varepsilon(t^*-t_0)} \\ &\leq -\varepsilon c_0 \bar{V}(t_0) e^{-\varepsilon(t^*-t_0)}, \end{aligned} \quad (\text{A.4})$$

which contradicts (A.3).

Now suppose that, for $k = \bar{k}$, $\bar{k} \geq 1$, (A.1) holds. Namely, $V(t) \leq \prod_{i=0}^{\bar{k}-1} c_i \bar{V}(t_0) e^{-\varepsilon(t-t_0)}$, $t \in [t_{\bar{k}-1}, t_{\bar{k}}]$. We prove that (A.1) is also satisfied for $k = \bar{k} + 1$. From (6) we can obtain $V(t_{\bar{k}}) = \prod_{i=0}^{\bar{k}} c_i \bar{V}(t_0) e^{-\varepsilon(t_{\bar{k}}-t_0)}$. If this claim is not true, there is $t^{**} \in [t_{\bar{k}}, t_{\bar{k}+1})$ such that

$$\begin{aligned} V(t^{**}) &= \prod_{i=0}^{\bar{k}} c_i \bar{V}(t_0) e^{-\varepsilon(t^{**}-t_0)}, \\ D^+ V(t^{**}) &> -\varepsilon \prod_{i=0}^{\bar{k}} c_i \bar{V}(t_0) e^{-\varepsilon(t^{**}-t_0)}. \end{aligned} \quad (\text{A.5})$$

There is a nonnegative integer h ($0 \leq h \leq \bar{k} + 1$) such that $t^{**} - \tau \in [t_{h-1}, t_h]$ (if $h = 0$, $t_{h-1} = t_0 - \tau$). Then we have

$$V(t^{**} - \tau) \leq \prod_{i=0}^{h-1} c_i \bar{V}(t_0) e^{-\varepsilon(t^{**}-\tau-t_0)}. \quad (\text{A.6})$$

By virtue of (6), we obtain

$$\begin{aligned} D^+ V(t^{**}) &\leq -\alpha V(t^{**}) + \beta V(t^{**} - \tau) \\ &\leq -\alpha \prod_{i=0}^{\bar{k}} c_i \bar{V}(t_0) e^{-\varepsilon(t^{**}-t_0)} \\ &\quad + \beta \prod_{i=0}^{h-1} c_i \bar{V}(t_0) e^{-\varepsilon(t^{**}-\tau-t_0)} \\ &= \prod_{i=0}^{\bar{k}} c_i \bar{V}(t_0) e^{-\varepsilon(t^{**}-t_0)} \left(-\alpha + \beta \prod_{i=h}^{\bar{k}} c_i^{-1} e^{\varepsilon\tau} \right) \\ &\leq \prod_{i=0}^{\bar{k}} c_i \bar{V}(t_0) e^{-\varepsilon(t^{**}-t_0)} (-\alpha + \beta e^{\varepsilon\tau}) \\ &\leq -\varepsilon \prod_{i=0}^{\bar{k}} c_i \bar{V}(t_0) e^{-\varepsilon(t^{**}-t_0)}, \end{aligned} \quad (\text{A.7})$$

which contradicts (A.5), which yields that (A.1) holds for $k = \bar{k} + 1$.

We can find $k^* \geq 1$ such that $t_{k^*} - \tau \geq t_0$. For any $t \in [t_{k-1}, t_k]$, $k \leq k^*$, from (A.1) we have

$$\begin{aligned} V(t) &\leq \prod_{i=0}^{k-1} c_i \bar{V}(t_0) e^{-\varepsilon(t-t_0)} \\ &\leq \prod_{i=0}^{k-1} c_i \bar{V}(t_0) e^{-\varepsilon(t-t_0)} e^{(\theta-\varepsilon)(t-t_0)} \\ &\leq \prod_{i=0}^{k-1} c_i \bar{V}(t_0) e^{-\theta(t-t_0)} e^{(\theta-\varepsilon)(k^* d^* + t_1 - t_0)} \\ &= M \prod_{i=0}^{k-1} c_i \bar{V}(t_0) e^{-\theta(t-t_0)}, \end{aligned} \quad (\text{A.8})$$

where $M = e^{(\theta-\varepsilon)(k^* d^* + t_1 - t_0)}$. That is to say, (7) holds for any $k \leq k^*$.

Now we show that (7) holds for $k > k^*$. For $k = k^* + 1$, if (7) does not hold, there is $t^{***} \in [t_{k^*}, t_{k^*+1})$ such that

$$\begin{aligned} V(t^{***}) &= M \prod_{i=0}^{k^*} c_i \bar{V}(t_0) e^{-\theta(t^{***}-t_0)}, \\ D^+ V(t^{***}) &> -\theta M \prod_{i=0}^{k^*} c_i \bar{V}(t_0) e^{-\theta(t^{***}-t_0)}. \end{aligned} \quad (\text{A.9})$$

Note that there is a positive integer h^* ($1 \leq h^* \leq k^* + 1$) such that $t^{***} - \tau \in [t_{h^*-1}, t_{h^*})$. Then we have

$$\begin{aligned}
 D^+V(t^{***}) &\leq -\alpha V(t^{***}) + \beta V(t^{***} - \tau) \\
 &\leq -\alpha M \prod_{i=0}^{k^*} c_i \bar{V}(t_0) e^{-\theta(t^{***}-t_0)} \\
 &\quad + \beta M \prod_{i=0}^{h^*-1} c_i \bar{V}(t_0) e^{-\theta(t^{***}-\tau-t_0)} \\
 &\leq M \prod_{i=0}^{k^*} c_i \bar{V}(t_0) e^{-\theta(t^{***}-t_0)} \left(-\alpha + \beta \prod_{i=h^*}^{k^*} c_i^{-1} e^{\theta\tau} \right) \\
 &\leq M \prod_{i=0}^{k^*} c_i \bar{V}(t_0) e^{-\theta(t^{***}-t_0)} (-\alpha + \beta e^{\theta\tau} U) \\
 &\leq -\theta M \prod_{i=0}^{k^*} c_i \bar{V}(t_0) e^{-\theta(t^{***}-t_0)},
 \end{aligned} \tag{A.10}$$

which contradicts (A.9). Therefore (7) holds for $k = k^* + 1$.

By mathematical induction, it is easy to illustrate that (7) holds for $k > k^* + 1$. The proof is complete.

Conflict of Interests

The authors declare that there is no conflict of interests regarding the publication of this paper.

Acknowledgments

This research is funded by the Research Foundation of The Natural Foundation of Chongqing City (cstc2014jcyjA40024, cstc2012jjA1459), Teaching & Research Program of Chongqing Education Committee (KJ1401307, KJ131401), and Research Project of Chongqing University of Science and Technology (CK2013B15).

References

- [1] J. J. Hopfield, "Neurons with graded response have collective computational properties like those of two-state neurons," *Proceedings of the National Academy of Sciences of the United States of America*, vol. 81, no. 10, pp. 3088–3092, 1984.
- [2] Z. H. Guan, G. R. Chen, and Y. Qin, "On equilibria, stability, and instability of Hopfield neural networks," *IEEE Transactions on Neural Networks*, vol. 11, no. 2, pp. 534–540, 2000.
- [3] J. C. Juang, "Stability analysis of Hopfield-type neural networks," *IEEE Transactions on Neural Networks*, vol. 10, no. 6, pp. 1366–1374, 1999.
- [4] D. Lee, "New stability conditions for Hopfield networks in partial simultaneous update mode," *IEEE Transactions on Neural Networks*, vol. 10, no. 4, pp. 975–978, 1999.
- [5] X. B. Liang, "Equivalence between local exponential stability of the unique equilibrium point and global stability for Hopfield-type neural networks with two neurons," *IEEE Transactions on Neural Networks*, vol. 11, no. 5, pp. 1194–1196, 2000.
- [6] H. Yang and T. S. Dillon, "Exponential stability and oscillation of Hopfield graded response neural network," *IEEE Transactions on Neural Networks*, vol. 5, no. 5, pp. 719–729, 1994.
- [7] T. Chen, "Global exponential stability of delayed Hopfield neural networks," *Neural Networks*, vol. 14, no. 8, pp. 977–980, 2001.
- [8] K. Gopalsamy and X. Z. He, "Stability in asymmetric Hopfield nets with transmission delays," *Physica D: Nonlinear Phenomena*, vol. 76, no. 4, pp. 344–358, 1994.
- [9] P. van den Driessche and X. F. Zou, "Global attractivity in delayed Hopfield neural network models," *SIAM Journal on Applied Mathematics*, vol. 58, no. 6, pp. 1878–1890, 1998.
- [10] D. Xu, H. Zhao, and H. Zhu, "Global dynamics of Hopfield neural networks involving variable delays," *Computers & Mathematics with Applications*, vol. 42, no. 1-2, pp. 39–45, 2001.
- [11] H. Akça, R. Alassar, V. Covachev, Z. Covacheva, and E. Al-Zahrani, "Continuous-time additive Hopfield-type neural networks with impulses," *Journal of Mathematical Analysis and Applications*, vol. 290, no. 2, pp. 436–451, 2004.
- [12] Z. H. Guan and G. Chen, "On delayed impulsive Hopfield neural networks," *Neural Networks*, vol. 12, no. 2, pp. 273–280, 1999.
- [13] Z. T. Huang, Q. G. Yang, and X. S. Luo, "Exponential stability of impulsive neural networks with time-varying delays," *Chaos, Solitons and Fractals*, vol. 35, no. 4, pp. 770–780, 2008.
- [14] S. Long and D. Xu, "Delay-dependent stability analysis for impulsive neural networks with time varying delays," *Neurocomputing*, vol. 71, no. 7-9, pp. 1705–1713, 2008.
- [15] X. F. Yang, X. Liao, D. J. Evans, and Y. Tang, "Existence and stability of periodic solution in impulsive Hopfield neural networks with finite distributed delays," *Physics Letters A*, vol. 343, no. 1-3, pp. 108–116, 2005.
- [16] C. J. Li, C. D. Li, and T. W. Huang, "Exponential stability of impulsive high-order Hopfield-type neural networks with delays and reaction-diffusion," *International Journal of Computer Mathematics*, vol. 88, no. 15, pp. 3150–3162, 2011.
- [17] C. Li, C. Li, X. Liao, and T. Huang, "Impulsive effects on stability of high-order BAM neural networks with time delays," *Neurocomputing*, vol. 74, no. 10, pp. 1541–1550, 2011.
- [18] C. J. Li, W. W. Yu, and T. W. Huang, "Impulsive synchronization schemes of stochastic complex networks with switching topology: average time approach," *Neural Networks*, vol. 54, pp. 85–94, 2014.
- [19] Q. Han, X. Liao, and C. Li, "Analysis of associative memories based on stability of cellular neural networks with time delay," *Neural Computing and Applications*, vol. 23, no. 1, pp. 237–244, 2013.
- [20] C. Liu, C. Li, and X. Liao, "Variable-time impulses in BAM neural networks with delays," *Neurocomputing*, vol. 74, no. 17, pp. 3286–3295, 2011.
- [21] C. Liu, C. D. Li, T. W. Huang, and C. J. Li, "Stability of Hopfield neural networks with time delays and variable-time impulses," *Neural Computing & Applications*, vol. 22, no. 1, pp. 195–202, 2013.
- [22] A. Berman and R. J. Plemmons, *Nonnegative Matrices in Mathematical Sciences*, Academic Press, New York, NY, USA, 1979.
- [23] X. L. Fu, B. Q. Wang, and Y. S. Liu, *Nonlinear Impulsive Differential Systems*, Science Press, 2008.
- [24] X. Liu and G. Ballinger, "Existence and continuability of solutions for differential equations with delays and state-dependent impulses," *Nonlinear Analysis*, vol. 51, no. 4, pp. 633–647, 2002.

Research Article

Computational Experiment Study on Selection Mechanism of Project Delivery Method Based on Complex Factors

Xiang Ding,^{1,2} Zhaohan Sheng,¹ Jianguo Du,^{1,3} and Qian Li¹

¹ School of Management and Engineering, Nanjing University, Nanjing 210093, China

² School of Civil Engineering, The University of Sydney, Sydney, NSW 2006, Australia

³ School of Management, Jiangsu University, Zhenjiang 212013, China

Correspondence should be addressed to Qian Li; qianli@nju.edu.cn

Received 30 May 2014; Accepted 14 July 2014; Published 31 August 2014

Academic Editor: Zhichun Yang

Copyright © 2014 Xiang Ding et al. This is an open access article distributed under the Creative Commons Attribution License, which permits unrestricted use, distribution, and reproduction in any medium, provided the original work is properly cited.

Project delivery planning is a key stage used by the project owner (or project investor) for organizing design, construction, and other operations in a construction project. The main task in this stage is to select an appropriate project delivery method. In order to analyze different factors affecting the PDM selection, this paper establishes a multiagent model mainly to show how project complexity, governance strength, and market environment affect the project owner's decision on PDM. Experiment results show that project owner usually choose Design-Build method when the project is very complex within a certain range. Besides, this paper points out that Design-Build method will be the prior choice when the potential contractors develop quickly. This paper provides the owners with methods and suggestions in terms of showing how the factors affect PDM selection, and it may improve the project performance.

1. Introduction

In the construction industry, project delivery method not only distributes the rights and responsibilities but also organizes the coordination between project owner and contractors [1]. PDM has a very important impact on the project strategic objectives, including project cost control, time planning, quality, and construction operations. Due to different modes relying on different situation, the project owners or project managers have to consider the experience and bias when they estimate PDM. More importantly, they need to seriously analyze many complex factors, such as construction environment, project features, ability of project owner, and ability of potential contractors.

There are some literatures mainly researching the relationship between PDM and project performance. Based on the comparative study on 351 cases in American construction industry, Konchar and Snvido [2] indicated the performance differences among cost control, quality, and time planning under different PDMs. Ling et al. [3] built a prediction model for project performance in Design-Build (DB) project and

Design-Bid-Build project by using multivariable method. In addition, there are some other researches on the decision-making methods to the selection of PDM based on different ways. The research of Mahdi [4] pointed out the indicators affecting the selection of PDM and the index weights with the help of analytic hierarchy process (AHP). Similarly, Mafkheri et al. [5] applied the improved AHP to establish selection model of PDM with multistandards and multilevels, as a result, the negative influence caused by the uncertainty from experts can be decreased. Luu et al. [6, 7] showed the mechanism of how project owner's demand, project features, and project environment affected the PDM selection based on the empirical conclusion. By using artificial neural network (ANN), Ling and Liu [8] measured and calculated the project performance in the DB projects. Chen et al. [9] also used ANN to find the cardinal rules on PDM selection. Unlike [8], [9] verified the validity of the model by using cases from China.

As mentioned above, PDM selection is very important to the project owner. Recent researches mainly focused on the foundation of index system. However, to establish

a reasonable index system was usually affected by the rationality of indicators, the objective evaluation from experts, the validation of the large scale data, and so forth. Apart from this, recent researches did not describe the mechanism how these factors affect PDM selection. Therefore, this paper focused on two methods which are widely applied in construction industry, DBB and DB. In this paper, project owner and project contractor are regarded as agents. Based on the analysis of behavior and decision-making rules of project owner agent and contractor agent, we established a computational experiment model and discussed how these factors, including project complexity, governance strength, and market environment, affect the PDM selection.

2. Complex Factors Affecting PDM Selection

Project delivery method defines the stakeholders involved in the implementing sequence of project design, procurement, and construction, and it also defines the benefits and risks of various stakeholders by the types of contract and design of system. As a result, we can use three dimensions to redefine the project delivery mode: (1) logical dimensions, including tasks in three stages: design, procurement, and construction, (2) dimensions of management subject, including project owner, design units, construction units, and the general contractor, and (3) contract dimensions, including general contract of design and construction and separate contract of design and construction. These elements can be combined into different PDMs according to different dimensions. For example, Design-Build contains two tasks: design and build; the general contractor is the subject manager, who signs a single contract with project owner on both design and build. In addition, there are some methods which are frequently used in the construction industry, including Design-Bid-Build, Engineering Procurement Construction (EPC), Turnkey, and Fast Track. In the early years, the traditional DBB mode occupies the majority share of the construction market in China. Currently, with the development of both engineering technology and management science, DB is gradually applied to a number of large-scale infrastructure constructions, such as Hong Kong-Zhuhai-Macao Bridge, which applied the DB to its most complex subproject, Island-Tunnel project. Therefore, this paper mainly focused on DBB and DB mode, and we assumed that project owner had to make a choice only between DBB and DB.

There are several advantages and disadvantages by using DB, compared with traditional DBB mode. The advantages include more close coordination relationship between design units and construction units, more specific boundary of rights and responsibilities, and better ability to cope with risks. The disadvantages include harder measurement of contributions of construction and design and harder maintenance of the individuality of design. In summary, any method has specific application conditions. Before project owners decide to choose PDM, they have to analyze the specific construction environments (not only the natural environment but also the political environment and the economic environment) and construction demands seriously in order to find the balance among environment, feature, and method.

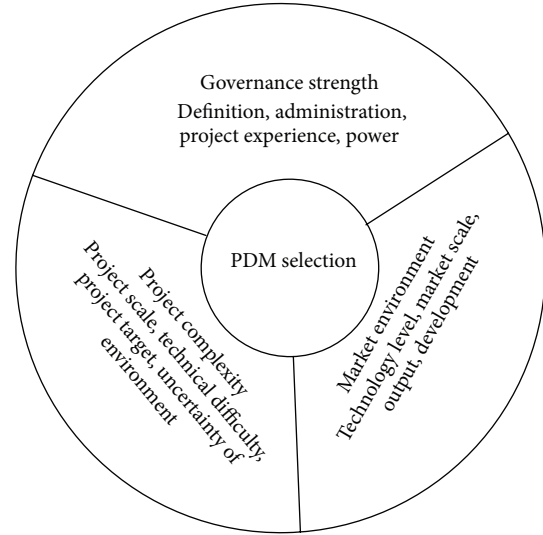


FIGURE 1: Complex factors affecting PDM selection.

Ibrahim suggested that the project owner needs to consider 7 aspects, including owner's feature, project's feature, design feature, legal system for contract, the ability and bias of potential contractors, project risk, and compensation [4]. Similarly, Chen inclined to project target (time planning, cost control, and project risk), project feature (type, scale, and complexity), owner's feature, contractor's ability, and project environment (construction industry, technology environment, and legal system) affecting the project delivery planning [9].

Here, we mainly discuss factors from inside and outside of the project. We establish a computational experiment model to revise how project complexity, governance strength, and market environment affect project owner in selecting project delivery method, Design-Build, or Design-Bid-Build, as seen in Figure 1. Specifically, we use 4 items, including project scale, technical complexity, construction environment, and construction targets, to describe the project complexity. As for governance ability, project owners have different abilities to govern. For DBB mode, the project owner does have the ability not only to revise the plans of both contractor and designer, but also to perform a delicate balancing act between the different sides in the conflict. For DB mode, the project owner should definitely have demands and the ability to choose appropriate contractors; besides, the project owner has to give the general contractors enough rights while transferring project risks to them. Finally, how to refine the market environment: there are many different angles to define market environment, such as the angle of economy and technology. In this paper, we mainly discuss the market consisting of different levels of construction company, and we focused on whether the growth of market can affect the PDM selection. Accordingly, technology level, market scale, output, and development are indispensable to describe market environment. In addition, we use resource integration, internal coordination, and technical innovation to describe contractor's ability.

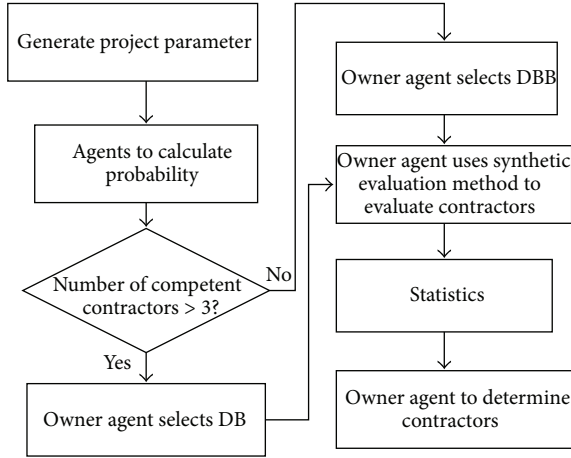


FIGURE 2: Flowchart of owner's interactive process.

3. Multiagent Design

3.1. Owner Agent. We consider a model which includes one project owner and 50 potential contractors (both designers and constructors). Owner has three activities in the experiment.

The decision-making process for project owner is set in this experiment as Figure 2.

(1) *Market Investigation.* The project owner has to estimate the potential contractors before bidding. In this model, we considered potential contractors as competent contractors depending on whether contractors' properties are equal to the project complexity index χ or not. When the amount of competent contractors is up to 3, the DB mode will be; available in the owner agent's optional list.

(2) *Choosing Bidding Mode.* At the scene when DB mode can be applied, the probability for owner to select DB mode is calculated as follows:

$$P_{\text{bidding}} = \varepsilon\chi + \delta(1 - \psi). \quad (1)$$

We use ε as the weight of project complexity and δ as the weight of governance strength. ψ stands for the governance strength. If the project owner selects DBB mode, the project owner will require the potential bidders to join design and construction bidding, respectively.

(3) *Evaluating and Determining.* In this model, we use synthetic evaluation method to calculate the weighted average value of each bidder and project owner on the design and construction task. Contractor i got the initial value to describe their ability randomly at the beginning of each experiment, and synthetic score of market environment can be calculated by weighted average value between project targets and contractor's abilities.

3.2. Contractor Agent. Contractors have two activities in this model.

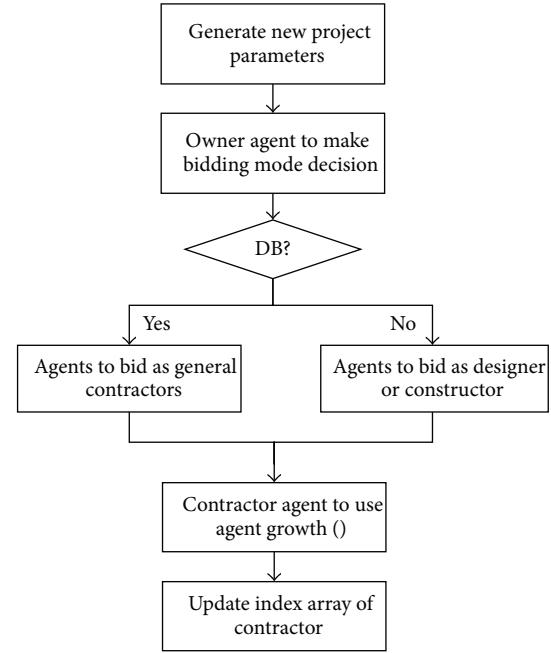


FIGURE 3: Flowchart of contractor's interactive process.

The decision-making process of contractor agent can be described in Figure 3.

(1) *Bidding.* According to the selected bidding mode by the project owner, the contractor agent chooses different strategies. If the project owner selects the DB mode, the contractor agents submit entire design and build values as general contractor. Otherwise, as to DBB mode, the contractor will choose design bidding or construction bidding relying on the higher value.

(2) *Growing Up.* The contractors have the ability to grow up after each experiment, and the value of contractor's ability will increase. In this paper, we build a growth model to make contractor agents increase their value of ability after each experiment tick. In the model, self-growth of agent's ability can be described as formula

$$\frac{dX_i(t+1)}{dt} = r_{\text{growth}}(t) X_i(t) \left(1 - \frac{X_i(t)}{k_i}\right). \quad (2)$$

$X_i(t)$ stands for index array of contractor i 's ability at the t tick. In the construction industry, there will be a development bottleneck for each enterprise based on enterprise theory. Therefore, we use k_i to describe the maximum ability once a contractor can reach. k_i will be set up at the beginning and will stay unchangeable until the end of experiment. The market will get growth and the growth rate is r_{growth} .

4. Experiment Scenarios and Initial Settings

In order to make the model get to work, we adopt Netlogo to implement the agent-based modeling and simulation. The initial parameters are shown in Table 1. The initial value of contractors' ability follows the Gaussian distributions.

TABLE 1: Initializations of experiment parameters.

Parameters	Standing for	Scale
ε	The weight of project complexity	0.5
δ	The weight of project governance strength	0.5
T_{growth}	Growth times of contractor	50
r_{growth}	Growth rate of contractor	Random float number between 0 and 0.1
α_{des}	The design ability value of designer	Random float number between 0.5 and 1
β_{des}	The construction ability value of designer	Random float number between 0 and 0.1
α_{cons}	The design ability value of constructor	Random float number between 0 and 0.1
β_{cons}	The construction ability value of contractor	Random float number between 0.5 and 1
U	The weight of design	[0.15, 0.075, 0.075, 0.075, 0.15]
V	The weight of construction	[0.175, 0.105, 0.105, 0.105, 0.055]

We focus on the impacts of different complex factors on the PDM selection. First, we research on the impact of the project complexity. The method is that we change the parameter of project complexity in each experiment and keep other parameters, such as market environment, constant during all experiments. We change the values of project complexity from 0.1 to 0.9 to revise the selection probability. Then, we run the experiments to revise the relationship between governance strength and PDM selection by using the same method as the first one.

Finally, we build two comparative experiment scenarios to study the relationship between the market environment and PDM selection. The contractor's growth is ignored in one experiment whilst the contractor's growth is considered in another experiment.

In order to acquire reliable data and to decrease the deviation of the experiment results, each experiment will be repeated ten times and we will use the average level [10, 11].

5. Experiment Results and Discussions

5.1. The Impact of Project Complexity. Project complexity affects the project delivery method mainly through two aspects. For one thing, the complexity of the particular project directly determines whether to select Design-build mode, due to risk transfer from project owner to general contractors, and it also can be considered as a risk reduction. For another thing, project complexity affects project owner's power of administering, including construction contracts, time planning, construction operations, estimating process, and construction labor [12].

In this experiment, the abilities of both owner and contractor remain unchanged, and the parameter of project governance strength is set as 0.5 during the whole experiment. Moreover, both designers and constructors not grow up.

For the given values, the average ability of construction contractor agents is 0.751 and of designers is 0.749, we make the experiment run 100 times and each experiment repeats 10 times to acquire the average data for statistical analysis, and Figure 4 shows the results.

Analysed from Figure 4, the following conclusions and discussions can be drawn.

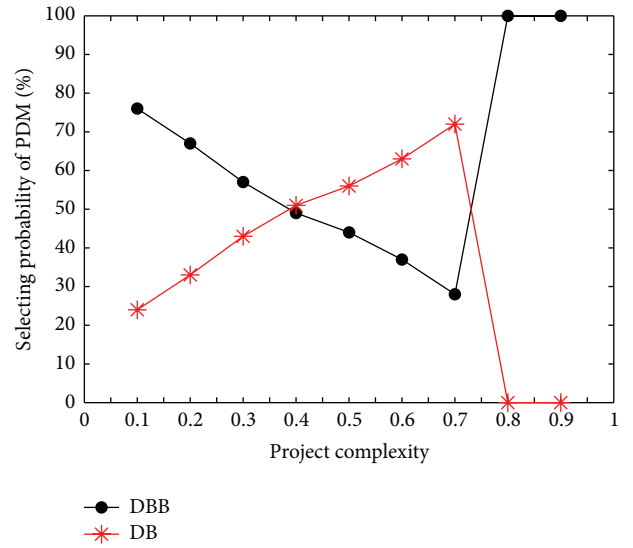


FIGURE 4: PDM selection under different project complexities.

- (1) Project owner inclines to Design-Bid-Build mode in simple or not complex project. When the complexity degree of a project is less than 0.5, the project is easy to be designed and built relying on the existing engineering technology and management. Besides, the project owner has enough experience and ability to administrate the building process. In the low-risk and regular project, case study in China has shown that the project owner/manager is more likely to choose DBB mode to enforce their administration on the whole construction period and the entire process and, in this way, the project can be implemented within high quality and low cost [13].
- (2) With the increase of project complexity degree, project owner is more likely to choose Design-Build mode. When the complexity degree of a project is between 0.5 and 0.8, project owner needs high ability to control the building process and to coordinate the multirelationship (such as designer, different contractors, consultant, and even the local government)

due to the increase of the project scale, the difficulty of construction technology, and environment uncertainty. Particularly, in many countries, the contractors are usually more professional than the project owners. As a result, project owner inclines to allocate more tasks of project management to experienced and competent contractors in order to control the budget and risk so well to reduce the project changes and claims [14].

- (3) Project owner prefers to select DBB mode in complex megaprojects. To be specific, when the complexity degree is up to 0.8, this project only can be realized by general contractors with extraordinary qualified credential in both design and build. It is very hard to find a construction company or a joint venture consisted of several companies including designer, constructor, and consultant, to deal with the technical and management difficulty. Therefore, project owner has to decompose the project into different modules and subprojects and, then, project owner finds the qualified contractors to fulfill the decomposed project under DBB mode.

5.2. The Impact of Governance Strength. How to evaluate a good project owner: first of all, a good owner has to define the project target clearly in order to organize the implementation effectively. Moreover, the capacity to estimate the quality of design and to coordinate the conflicts during the whole construction period is inevitable [15]. Finally, a good owner can deal with emergency and risk properly and efficiently.

During the experiment, we keep project complexity and market environment unchanged; the average ability of constructor and designer remains 0.742 and 0.756 respectively. The parameter of project complexity is set as 0.5 and both designers and constructors do not grow up after each experiment.

Figure 5 shows the probability for owners to decide which project delivery mode to choose.

As shown in Figure 5, project owners rely on DB mode to a great extent when they do not have enough ability to handle the project management. All of the involved contractors including designer, constructor, supervisor, and consultant take responsibility directly to project owner according to the contract, and project owner needs to coordinate different sections and to administrate the whole construction procedure [16].

However, general contractors are in charge of the design and build process under DB mode, and project owner has to revise the job of just one general contractor.

In summary, with the impact of enhancement of governance strength, project owner will have a strong desire to participate in every procedure, and this makes DBB mode more and more popular to project owners.

5.3. The Impact of Market Environment. The former two experiments are based on the ignoring the market growing. As a matter of fact, contractors not only achieve the growth in construction technology and project management, acquiring

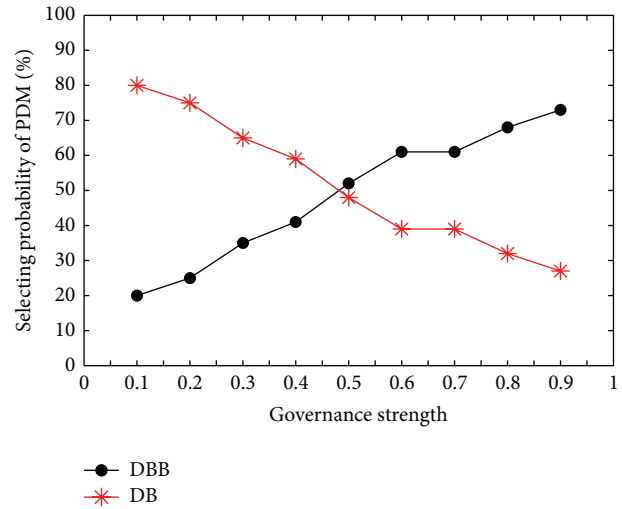


FIGURE 5: PDM selection under different governance strength.

abundant experience, but also cultivate talents in different construction field. Even contractors fail in project bidding, yet they will recognize their inadequacy better, and then they will also grow up. Indeed, it is very useful to revise how the average level of construction industry affects PDM selection. For this purpose, we repeat the former two groups of experiments on the basis of adding self-growth model, and then we compare the new results with the former experiments.

5.3.1. The Impact of Project Complexity under Market Growing. We let each index degree of contractor's ability increase every 50 experiment ticks and repeat the experiment process as in Section 5.1. Besides, in order to estimate the relationship between growth rate and PDM selection, we set different values and run three groups of experiments. To be more precise, all of the three groups share the same parameters except r_{growth} which stands for contractor's growth rate. The growth rate changes from 0, 0.05 to 0.1, meaning *remain-stagnant*, *slow-growth*, and *fast-growth*, respectively.

We can see from Figures 6(a), 6(b), and 6(c) that, when remain-stagnant agents compared with growth agents, DB mode has the chance to be chosen by the project owner while it is never considered in the highly complex projects within the complexity degree up to 0.8. With the help of practices, contractor's ability improved constantly. In this way, a number of experienced contractors with high reputation and excellent performance emerged in construction industry [17]. These enterprises have the ability to become DB general contractors, and they can reduce the risk and cost if project owner decides to use DB. In consideration of potential benefits from project time control and quality, project owner takes DB mode as alternative solutions.

Comparing slow-growth agents with fast-growth agents, as seen in Figures 6(b) and 6(c), project owner will incline to select DB mode even in the most complex project. Actually, project owner usually does not have enough confidence to handle rather complex project, especially in so-called

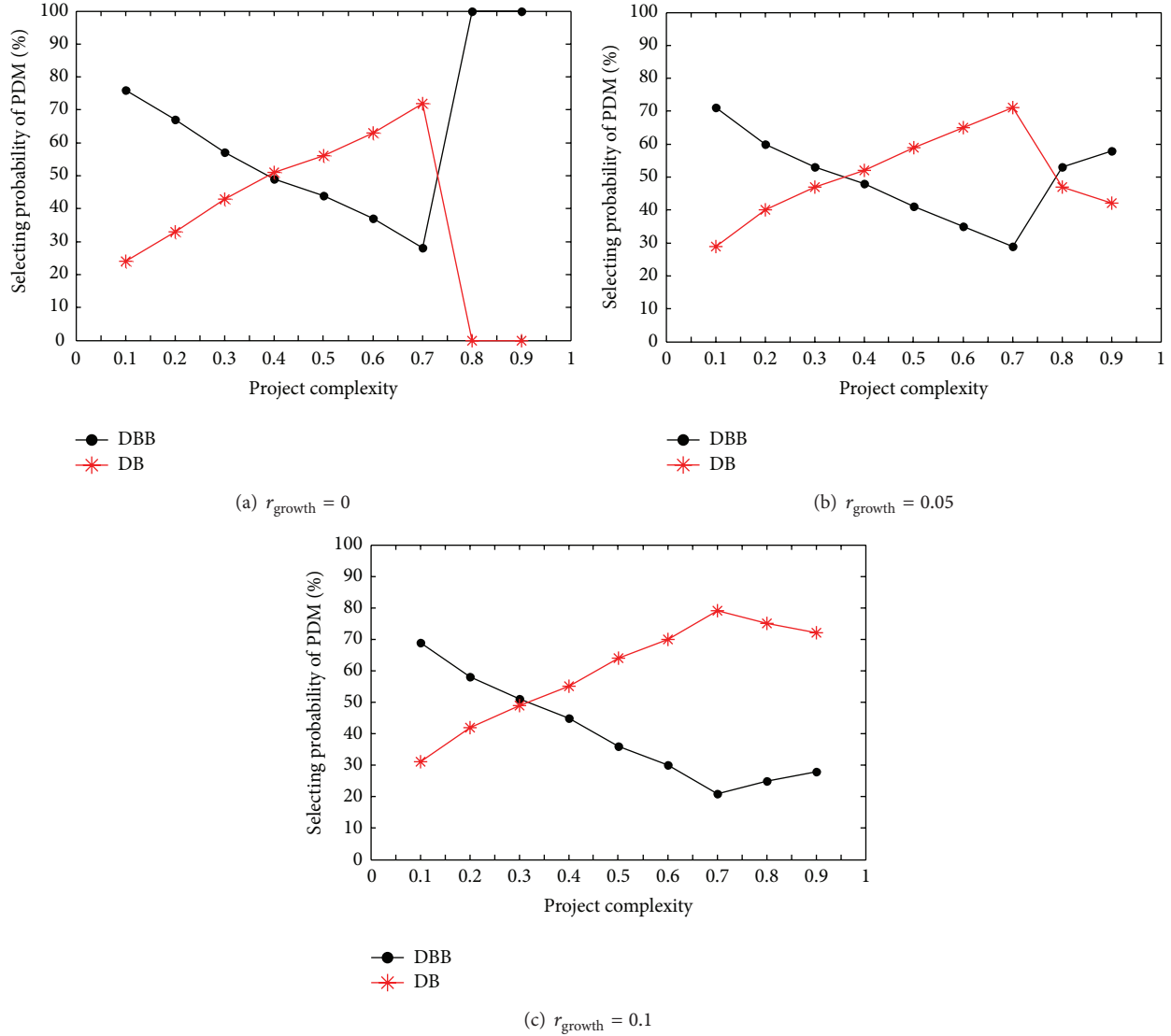


FIGURE 6: PDM selection under different project complexities considering market growing.

unparalleled megaprojects, and the project owner will hope to transfer management risk to contractors in order to reduce project risk. The faster the contractor grows up, the more likely the ability of contractor administrates the complex project. As a result, project owner will be apt to use DB mode while there are fast-growth contractors in construction industry.

5.3.2. The Impact of Governance Strength under Contractor's Self-Growth. Similar to experiment procedure in Section 5.3.1, we also repeat experiments in Section 5.2 and get three groups of experiment results.

Figure 7 shows probability of project owner whether to choose DB or DBB as project delivery mode under different growth rate of contractor agents. It is undoubtedly that project owners used to choose DB for managing the building process when their ability level under about 0.5, or we can define these project owners as weak owners, from

Figures 7(a), 7(b), and 7(c). For weak owners, they do not have enough experience and knowledge to administrate the whole building procedure. As mentioned earlier in this paper, weak owners need contractors who can undertake much of the risk of project management.

When contract agents grow up, the value describing their ability will increase continuously. Therefore, there will be many contractors who can successfully act as designers, builders, and even general contractors. For strong owners (with the ability level up to 0.5) who can easily administrate the project delivery, it is difficult for them to determine which method is the best choice, as we can see from the comparison between Figures 7(a) and 7(b). Project owner will make the decision of PDM according to their preference and experience.

When the value of governance strength rises at a certain level, the probability of selecting DB method and DBB mode are not far from each other. What is the key factor affecting

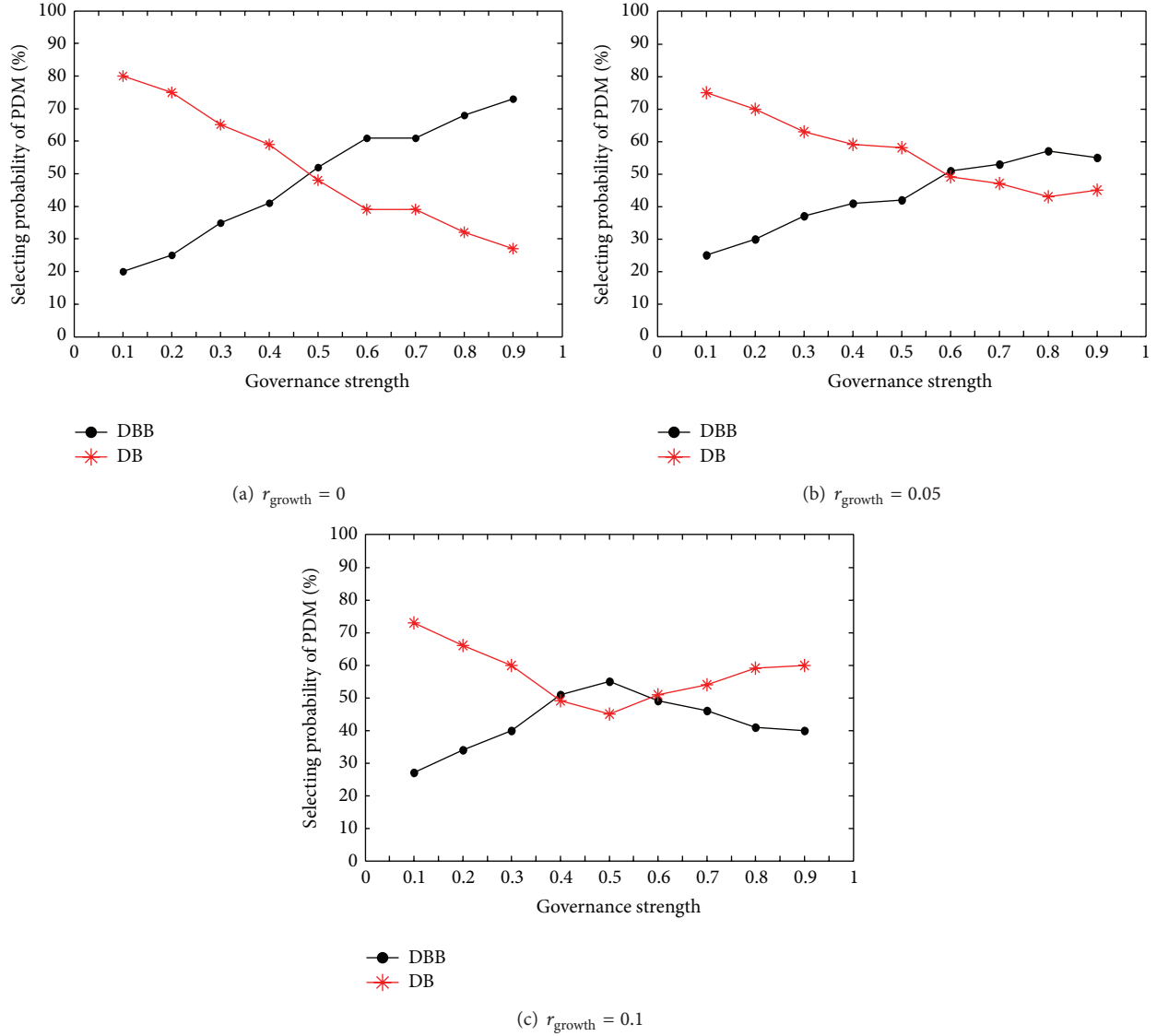


FIGURE 7: PDM selection under different governance strength considering market growing.

decision of the project owner? From Figures 7(b) and 7(c), it is obvious that the project owner is more likely to select DB mode when the contractor agents in this experiment have higher growth rate. Compared with slow-growth contractors, fast-growth contractors have many advantages at planning, monitoring, coordinating, controlling, communication, and decision-making [18]. All of these advantages greatly help project owner reduce the project risk and ease their burden. Therefore, in order to achieve the success of project efficiently, DB mode become project owner's first choice when the potential companies develop quickly in the construction industry.

Based on the former experiments, we may find that market environment is a crucial factor affecting PDM selection. Above all, in order to promote Design-Build project delivery method, it is very important for companies to develop their ability by self-growth.

6. Conclusions

The scientific and reasonable selection of project delivery method is crucial for project owners to deal with project complexity and to achieve project success. This paper assumes that project owner focus on many factors that may affect the PDM selection, and these factors and their interrelationships contribute to a complex factor system. We establish an agent-based simulation model in order to analyze the selection mechanism of project delivery method based on computational experiment. And we revise the relationship between given factors and selection probabilities by statistical analysis of different groups of experiment results. This paper mainly discusses three factors, including project complexity, governance strength, and market environment.

Experimental results show that project complexity, governance strength, and market environment have significant

influences on PDM selection. Project owners are more likely to use Design-Build to deliver the project at the condition that their abilities are weak and the projects are complex. Otherwise, when project owners have the ability to administer project procedure, they are willing to be in charge of every process of design and building, so they prefer to choose DBB method. In addition, the increasing ability of contractor reduces the risk for project owners to deliver the project by DB; thus they have greater preference to choose DB general contractors. Under different type of construction market, project owner prefer Design-Build method to Design-Bid-Build method when the potential contractors develop quickly.

In summary, there are some other factors that should be revised, although we have obtained some useful results about PDM selection. In the near future, we will study more micro factors that affect project owner selecting project delivery modes.

Conflict of Interests

The authors declare that there is no conflict of interests regarding the publication of this paper.

Acknowledgments

The authors are indebted to editors and the anonymous reviewers for their insightful comments and beneficial suggestions, which help ameliorate the quality of this paper. This work is supported by the National Natural Science Foundation of China (Grant no. 71390521, no. 71301062, no. 71301070, no. 71390521, no. 71101069, no. 71171099, and no. 71001049) and the National Eleventh-Five Year Research Program of China (Grant no. 2011BAG07B05).

References

- [1] American Society of Civil Engineers, *Quality in the Constructed Project: A Guide for Owners, Designers and Constructors*, ASCE Publication, Reston, Va, USA, 2000.
- [2] M. Konchar and V. Sanvido, "Comparison of U.S. project delivery systems," *Journal of Construction Engineering and Management*, vol. 124, no. 6, pp. 435–444, 1998.
- [3] F. Y. Y. Ling, S. L. Chan, E. Chong, and L. P. Ee, "Predicting performance of design-build and design-bid-build projects," *Journal of Construction Engineering and Management*, vol. 130, no. 1, pp. 75–83, 2004.
- [4] I. M. Mahdi and K. Alreshaid, "Decision support system for selecting the proper project delivery method using analytical hierarchy process (AHP)," *International Journal of Project Management*, vol. 23, no. 7, pp. 564–572, 2005.
- [5] F. Mafakheri, L. Dai, D. Slezak, and F. Nasiri, "Project delivery system selection under uncertainty: multicriteria multilevel decision aid model," *Journal of Management in Engineering*, vol. 23, no. 4, pp. 200–206, 2007.
- [6] D. T. Luu, S. Thomas Ng, and S. E. Chen, "A case-based procurement advisory system for construction," *Advances in Engineering Software*, vol. 34, no. 7, pp. 429–438, 2003.
- [7] D. T. Luu, S. T. Ng, and S. E. Chen, "Formulating procurement selection criteria through case-based reasoning approach," *Journal of Computing in Civil Engineering*, vol. 19, no. 3, pp. 269–276, 2005.
- [8] F. Y. Y. Ling and M. Liu, "Using neural network to predict performance of design-build projects in Singapore," *Building and Environment*, vol. 39, no. 10, pp. 1263–1274, 2004.
- [9] Y. Q. Chen, J. Y. Liu, B. Li, and B. Lin, "Project delivery system selection of construction projects in China," *Expert Systems with Applications*, vol. 38, no. 5, pp. 5456–5462, 2011.
- [10] S. M. R. Loghmanian, H. Jamaluddin, R. Ahmad, R. Yusof, and M. Khalid, "Structure optimization of neural network for dynamic system modeling using multi-objective genetic algorithm," *Neural Computing and Applications*, vol. 21, no. 6, pp. 1281–1295, 2012.
- [11] M. Qingfeng, D. Jianguo, L. Zhen, and C. Jingxian, "Evolutionary dynamics of sales agents promotional effort on small-world networks," *Neural Computing and Application*, vol. 24, no. 1, pp. 3–12, 2014.
- [12] W. H. Daniel and W. W. Ronald, *Construction Management*, John Wiley & Sons, New York, NY, USA, 4th edition, 2010.
- [13] F. Y. Y. Ling, S. P. Low, S. Q. Wang, and H. H. Lim, "Key project management practices affecting Singaporean firms' project performance in China," *International Journal of Project Management*, vol. 27, no. 1, pp. 59–71, 2009.
- [14] S. M. Levy, *Design-Build Project Delivery: Managing the Building Process from Proposal through Construction*, The McGraw-Hill, New York, NY, USA, 2006.
- [15] F. Y. Y. Ling and B. H. M. Poh, "Problems encountered by owners of design-build projects in Singapore," *International Journal of Project Management*, vol. 26, no. 2, pp. 164–173, 2008.
- [16] S. Lu and G. Hao, "The influence of owner power in fostering contractor cooperation: evidence from China," *International Journal of Project Management*, vol. 31, no. 4, pp. 522–531, 2013.
- [17] J. Huang, "Study on the problem of slowness in pushing the project general contracting mode in Chinese construction industry: the perspective of institutional change," *East China Economic Management*, vol. 25, no. 7, pp. 65–68, 2011.
- [18] A. Hamimah, B. Fauziah, S. Azizan, and A. Mohd, "Success factors of design and build projects in public universities," *Procedia—Social and Behavioral Sciences*, vol. 35, pp. 170–179, 2012.

Research Article

Existence and Global Uniform Asymptotic Stability of Pseudo Almost Periodic Solutions for Cohen-Grossberg Neural Networks with Discrete and Distributed Delays

Hongying Zhu¹ and Chunhua Feng²

¹ School of Information and Statistics, Guangxi University of Finance and Economics, Nanning 530003, China

² School of Mathematics Science, Guangxi Normal University, Guilin 541004, China

Correspondence should be addressed to Hongying Zhu; zhy71118@163.com

Received 11 March 2014; Accepted 28 July 2014; Published 18 August 2014

Academic Editor: Zhichun Yang

Copyright © 2014 H. Zhu and C. Feng. This is an open access article distributed under the Creative Commons Attribution License, which permits unrestricted use, distribution, and reproduction in any medium, provided the original work is properly cited.

This paper studies the existence and uniform asymptotic stability of pseudo almost periodic solutions to Cohen-Grossberg neural networks (CGNNs) with discrete and distributed delays by applying Schauder fixed point theorem and constructing a suitable Lyapunov functional. An example is given to show the effectiveness of the main results.

1. Introduction

Since the model of Cohen-Grossberg neural networks (CGNNs) was first proposed and studied by Cohen and Grossberg [1], it has been widely investigated because of the theoretical interest as well as the application considerations such as optimization, pattern recognition, automatic control, image processing, and associative memories. In recent years, there are many important results on dynamic behaviors of CGNNs. For instance, many sufficient conditions have been successively obtained to ensure the existence and stability of equilibrium point of CGNNs [1–10]. Some attractivity and asymptotic stability results have also been published [3, 11–14]. Many authors specially devote themselves to study the existence and global exponential stability of periodic or almost periodic solution to CGNNs [15–30]; for the other dynamic properties, see also the literatures [31, 32]. However, to the best of our knowledge, few authors have discussed the existence and the global uniform asymptotic stability of pseudo almost periodic solutions to CGNNs.

In this paper, we discuss the existence and the global uniform asymptotic stability of pseudo almost periodic solutions to the following CGNNs:

$$\begin{aligned} x_i'(t) = & -a_i(x_i(t)) \\ & \times \left[b_i(x_i(t)) - \sum_{j=1}^m c_{ij}(t) f_j(x_j(t)) \right. \\ & \left. - \sum_{j=1}^m d_{ij}(t) g_j(x_j(t - \tau_{ij}(t))) \right. \\ & \left. - \sum_{j=1}^m p_{ij}(t) \int_{-\infty}^t G_{ij}(t-s) h_j(x_j(s)) ds - I_i(t) \right], \\ & t \geq 0, \\ x_i(t) = & \Phi_i(t), \quad t < 0, \end{aligned} \quad (1)$$

where $c_{ij}(t)$, $d_{ij}(t)$, $p_{ij}(t)$, $I_i(t)$, $\Phi_i(t) \in C(R, R)$, $\tau_{ij}(t) \in C(R, R^+)$ are pseudo almost periodic functions.

The organization of this paper is as follows. In Section 2, some basic definitions, marks, and lemmas are given. In Section 3, some results are given to ascertain the existence of pseudo almost periodic solution to the system (1) by

applying Schauder fixed point theorem. In Section 4, the global uniform asymptotic stability of pseudo almost periodic solutions to the system (1) is obtained. In Section 5, an example is provided to demonstrate the effectiveness of the main results. In Section 6, the final conclusions are drawn.

2. Preliminaries

In this section, some basic definitions, lemmas, and assumptions are introduced.

Definition 1 (see [33]). $f(t) \in BC(R, R)$ is said to be Bohr almost periodic if, for all $\epsilon > 0$, set

$$T(f, \epsilon) = \{t \in \mathbb{R} : |f(t + \tau) - f(t)| < \epsilon, \forall t \in \mathbb{R}\} \quad (2)$$

is relatively dense. Namely, for any $\epsilon > 0$ there exists a number $l = l(\epsilon) > 0$ such that every interval $[a, a + l]$ contains at least one point of $\tau = \tau(\epsilon)$ such that $|f(t + \tau) - f(t)| < \epsilon$ for every $t \in \mathbb{R}$. The collection of those functions is denoted by $AP(R, R^m)$. Define the class of functions $PAP_0(R, R^m)$ as follows:

$$PAP_0(R, R^m) = \left\{ f \in BC(R, R^m) \mid \lim_{T \rightarrow +\infty} \frac{1}{2T} \int_{-T}^T \|f(t)\| dt = 0 \right\}. \quad (3)$$

Definition 2 (see [34]). A function $f \in BC(R, R^m)$ is called pseudo almost periodic if it can be expressed as

$$f = f_1 + f_0, \quad (4)$$

where $f_1 \in AP(R, R^m)$ and $f_0 \in PAP_0(R, R^m)$. The collection of such functions will be denoted by $PAP(R, R^m)$.

Remark 3. From the definitions above, we have $AP(R, R^m) \subset PAP(R, R^m)$.

Lemma 4 (see [3]). $PAP(R, R^m)$ is a Banach space with the norm $|\phi| = \sup_{t \in \mathbb{R}} |\phi(t)|$.

Lemma 5 (see [19]). If $f(t, u) \in C(R \times D, R^m)$, where D is an open set in R^m or $D = R^m$, $C(R \times D, R^m)$ denote continuous function class. Suppose $f \in PAP(R \times D)$ satisfies the Lipschitz condition

$$|f(t, u) - f(t, v)| \leq L|u - v|, \quad \forall t \in \mathbb{R}, u, v \in D; \quad (5)$$

if $\phi(t) \in PAP(R)$, then the composite function $f(t, \phi(t)) \in PAP(R)$. Suppose $f : R \times C \rightarrow R^m$; then the equation

$$x'(t) = f(t, x_t) \quad (6)$$

is called lagging-type almost periodic differential equation. The following system (7) is defined as the product systems of (6):

$$x'(t) = f(t, x_t(t)), \quad y'(t) = f(t, y_t(t)). \quad (7)$$

Lemma 6. Suppose $\phi(t) \in PAP(R, R^m)$; then $\phi(t - \tau) \in PAP(R, R^m)$ for all $\tau \in \mathbb{R}$.

Proof. From Definition 2 of the PAP, we have $\phi = \phi_1 + \phi_0$, where $\phi_1 \in AP(R, R^m)$ and $\phi_0 \in PAP_0(R, R^m)$. Clearly $\phi(t - \tau) = \phi_1(t - \tau) + \phi_0(t - \tau)$; it is easy to know $\phi_1(t - \tau) \in AP(R, R^m)$ and

$$\begin{aligned} 0 &\leq \frac{1}{2T} \int_{-T}^T |\phi_0(t - \tau)| dt = \frac{1}{2T} \int_{-(T+\tau)}^{T-\tau} |\phi_0(t)| dt \\ &\leq \frac{T + \tau}{T} \cdot \frac{1}{2(T + \tau)} \int_{-(T+\tau)}^{T+\tau} |\phi_0(t)| dt. \end{aligned} \quad (8)$$

This indicates that $\phi_0(t - \tau) \in PAP_0(R, R^m)$. So $\phi(t - \tau) \in PAP(R, R^m)$. \square

Definition 7. Assume that $x^*(t)$ is a pseudo almost periodic solution of system (1). By a translation transformation $y(t) = x(t) - x^*(t)$, system (1) is transformed into a new system. If the zero solution of new system is globally uniformly asymptotically stable, then the pseudo almost periodic solution of system (1) is said to be globally uniformly asymptotically stable. As for the uniform asymptotical stability, see [35].

Lemma 8 (see [33]). There is a continuous functional $V(t, \varphi, \psi)$ for $t \geq 0$, $\varphi, \psi \in C_H$, $C_H = \{\varphi : \varphi \in C, |\varphi| < H\}$, $|\varphi| = \sup_{\theta \in [-r, 0]} |\varphi(\theta)|$ such that

$$(H'2.1) \quad u(|\varphi - \psi|) \leq V(t, \varphi, \psi) \leq v(|\varphi - \psi|);$$

$$(H'2.2) \quad |V(t, \varphi_1, \psi_1) - V(t, \varphi_2, \psi_2)| \leq k(|\varphi_1 - \varphi_2| + |\psi_1 - \psi_2|);$$

$$(H'2.3) \quad V'_{(7)}(t, \varphi, \psi) \leq -aV(t, \varphi, \psi),$$

where a is a positive constant and $u(s)$ and $v(s)$ are continuous nondecreasing functions; when $s \rightarrow 0$, $u(s) \rightarrow 0$, k is a positive constant. At this time, if (7) has a bounded solution $x(t, \sigma, \varphi)$ such that $|x(t, \sigma, \varphi)| \leq H_1$, where $t \geq \sigma \geq 0$, $H > H_1 > 0$, then (6) in C_H has a unique almost periodic solution which is uniformly asymptotically stable.

Throughout this paper, we make the following assumptions.

(H2.1): Functions $a_i(u)$ are continuous bounded and there are positive constants a_i^+, a_i^- such that

$$0 < a_i^- \leq a_i(u) \leq a_i^+, \quad \forall u \in \mathbb{R}, i = 1, 2, \dots, m. \quad (9)$$

(H2.2): Functions $b_i(u) \in C(R, R)$ and there exist positive constants b_i^-, b_i^+ such that

$$\begin{aligned} b_i^- &\leq \frac{b_i(u) - b_i(v)}{u - v} \leq b_i^+, \quad u \neq v, \\ \forall u, v \in \mathbb{R}, b_i(0) &= 0. \end{aligned} \quad (10)$$

(H2.3): $c_{ij}(t), d_{ij}(t), p_{ij}(t), I_i(t) \in C(R, R)$, $\tau_{ij}(t) \in C(R, R^+)$ are pseudo almost periodic functions:

$$\begin{aligned} \sup_{t \in \mathbb{R}} c_{ij}(t) &= c_{ij}^+ > 0, & \sup_{t \in \mathbb{R}} d_{ij}(t) &= d_{ij}^+ > 0, \\ \sup_{t \in \mathbb{R}} p_{ij}(t) &= p_{ij}^+ > 0, & \sup_{t \in \mathbb{R}} I_i(t) &= I_i^+ > 0, \end{aligned} \quad (11)$$

where $R^+ = [0, \infty)$, $i, j = 1, 2, \dots, m$.

(H2.4): Delay kernel functions $G_{ij} : [0, +\infty) \rightarrow [0, +\infty)$ are piecewise continuous and integrable

$$\begin{aligned} \int_0^{+\infty} G_{ij}(u) du &= 1, \\ \int_0^{\infty} u G_{ij}(u) du &< +\infty, \\ i, j &= 1, 2, \dots, m. \end{aligned} \quad (12)$$

(H2.5): Functions $f_j(u), g_j(u), h_j(u) \in C(R, R)$ satisfy the Lipschitz condition; namely, there exist nonnegative constants L_j^f, L_j^g , and L_j^h such that

$$\begin{aligned} |f_j(u) - f_j(v)| &\leq L_j^f |u - v|, \quad \forall u, v \in R, \quad j = 1, 2, \dots, m, \\ |g_j(u) - g_j(v)| &\leq L_j^g |u - v|, \quad \forall u, v \in R, \quad j = 1, 2, \dots, m, \\ |h_j(u) - h_j(v)| &\leq L_j^h |u - v|, \quad \forall u, v \in R, \quad j = 1, 2, \dots, m. \end{aligned} \quad (13)$$

3. The Existence of Pseudo Almost Periodic Solution

In this section, we study the existence of pseudo almost periodic solution to system (1).

It follows from (H2.1) that the antiderivative of $1/a_i(x_i)$ exists. Then we choose an antiderivative $F_i(x_i)$ of $1/a_i(x_i)$ that satisfies $F_i(0) = 0$. Clearly, $F_i'(x_i) = 1/a_i(x_i)$. Because $a_i(x_i) > 0$, $F_i(x_i)$ is increasing about x_i and the inverse function $F_i^{-1}(x_i)$ of $F_i(x_i)$ is existential, continuous, and differential. Then $(F_i^{-1}(x_i))' = a_i(x_i)$. Denote $F_i'(x_i)x_i'(t) = x_i'(t)/a_i(x_i(t)) \doteq u_i'(t)$; we get $x_i(t) = F_i^{-1}(u_i(t))$. Substituting these equations into system (1), we get the following equivalent equation:

$$\begin{aligned} u_i'(t) &= -b_i(F_i^{-1}(u_i(t))) \\ &+ \sum_{j=1}^m c_{ij}(t) f_j(F_j^{-1}(u_j(t))) \\ &+ \sum_{j=1}^m d_{ij}(t) g_j(F_j^{-1}(u_j(t - \tau_{ij}(t)))) \\ &+ \sum_{j=1}^m p_{ij}(t) \int_{-\infty}^t G_{ij}(t-s) h_j(F_j^{-1}(u_j(s))) ds \\ &+ I_i(t), \quad t \geq 0, \\ u_i(t) &= F_i^{-1}(\Phi_i(t)) = \varphi_i(t), \quad t < 0. \end{aligned} \quad (14)$$

From (14), we get $b_i(F_i^{-1}(u_i(t))) = [b_i(F_i^{-1}(\theta_i u_i(t)))]' u_i(t) \doteq b_i^-(u_i(t)) u_i(t)$, where $0 \leq \theta_i \leq 1$. Putting it into (14), we obtain

$$\begin{aligned} u_i'(t) &= -b_i^-(u_i(t)) u_i(t) \\ &+ \sum_{j=1}^m c_{ij}(t) f_j(F_j^{-1}(u_j(t))) \\ &+ \sum_{j=1}^m d_{ij}(t) g_j(F_j^{-1}(u_j(t - \tau_{ij}(t)))) \\ &+ \sum_{j=1}^m p_{ij}(t) \int_{-\infty}^t G_{ij}(t-s) h_j(F_j^{-1}(u_j(s))) ds \\ &+ I_i(t), \quad t \geq 0, \\ u_i(t) &= F_i^{-1}(\Phi_i(t)) = \varphi_i(t), \quad t < 0. \end{aligned} \quad (15)$$

Thus, system (1) has at least one pseudo almost periodic solution if and only if the system (15) has at least one pseudo almost periodic solution. So we only consider the pseudo almost periodic solution of system (15). By Lagrange theorem, we have

$$\begin{aligned} |F_i^{-1}(u) - F_i^{-1}(v)| &= |[F_i^{-1}(v + \theta_i(u - v))]'(u - v)| \\ &= |a_i(v + \theta_i(u - v))| |u - v|. \end{aligned} \quad (16)$$

Again by (H2.1), we get

$$a_i^- |u - v| \leq |F_i^{-1}(u) - F_i^{-1}(v)| \leq a_i^+ |u - v|. \quad (17)$$

Combined with (H2.2), we have

$$(H3.6): b_i^- a_i^- \leq b_i'(F_i^{-1}(\cdot)) \leq b_i^+ a_i^+.$$

In order to prove the main results, we give the following lemma.

Lemma 9. Suppose that assumptions (H2.2)–(H2.5) hold and if $\phi(t) \in PAP(R, R^m)$, then

$$\begin{aligned} C_{ij} &= \int_{-\infty}^t G_{ij}(t-s) \phi_j(s) ds \in PAP(R, R), \\ i &= 1, 2, \dots, m. \end{aligned} \quad (18)$$

Proof. From Definition 2, we have $\phi_j = \phi_{j1} + \phi_{j0}$; then

$$\begin{aligned} C_{ij} &= \int_{-\infty}^t G_{ij}(t-s) \phi_{j1}(s) ds + \int_{-\infty}^t G_{ij}(t-s) \phi_{j0}(s) ds \\ &= C_{ij1} + C_{ij0}. \end{aligned} \quad (19)$$

Firstly, we prove $C_{ij1} \in AP(R, R)$. For any $\epsilon > 0$, there exists a number $l = l(\epsilon) > 0$ such that every interval $[a, a + l]$

contains at least one point of $\tau = \tau(\epsilon)$ such that $|\phi_{j1}(t + \tau) - \phi_{j1}(t)| \leq \epsilon$ for every $t \in R$. Therefore, from (H2.2)–(H2.4), we obtain

$$\begin{aligned}
 & |C_{ij1}(t + \tau) - C_{ij1}(t)| \\
 &= \left| \int_{-\phi}^{t+\tau} G_{ij}(t + \tau - s) \phi_{j1}(s) ds \right. \\
 &\quad \left. - \int_{-\infty}^t G_{ij}(t - s) \phi_{j1}(s) ds \right| \\
 &\leq \int_{-\infty}^t |G_{ij}(t - s)| |\phi_{j1}(s + \tau) - \phi_{j1}(s)| ds \\
 &\leq \epsilon \int_{-\infty}^t |G_{ij}(t - s)| ds \\
 &\leq \epsilon
 \end{aligned} \tag{20}$$

so that $C_{ij1} \in AP(R, R)$.

And then we show that $C_{ij0} \in PAP_0(R, R)$ because

$$\begin{aligned}
 & \lim_{T \rightarrow +\infty} \frac{1}{2T} \int_{-T}^T |C_{ij0}| dt \\
 &= \sup_{t \in R} \lim_{T \rightarrow +\infty} \frac{1}{2T} \int_{-T}^T \left| \int_{-\infty}^t G_{ij}(t - s) \phi_{j0}(s) ds \right| dt \\
 &\leq \sup_{t \in R} \lim_{T \rightarrow +\infty} \frac{1}{2T} \int_0^{+\infty} |G_{ij}(u)| \left| \int_{-(T+u)}^{T+u} \phi_{j0}(v) dv \right| du \\
 &= 0.
 \end{aligned} \tag{21}$$

Thus $C_{ij0} \in PAP_0(R, R)$. So $C_{ij} \in PAP(R, R)$. \square

Theorem 10. Suppose that (H2.1)–(H2.5) and (H3.6) hold; if

$$\delta = \max_{1 \leq i \leq m} \left\{ \frac{a_i^+}{b_i^- a_i^-} \sum_{j=1}^m (L_j^f c_{ij}^+ + L_j^g d_{ij}^+ + L_j^h p_{ij}^+) \right\} < 1, \tag{22}$$

then the system (1) has at least one pseudo almost periodic solution.

Proof. For all $z(t) = \phi(t)^T = (\phi_1(t), \dots, \phi_m(t))^T \in PAP(R, R^m)$, we define the nonlinear operator $T : z(t) \rightarrow T(z)(t) = z_{(\phi)}(t) = (x_{\phi}(t))^T$, where

$$\begin{aligned}
 x_{\phi_i}(t) &= \int_{-\infty}^t e^{-\int_s^t b_i^-(\phi_i(\tau)) d\tau} \\
 &\times \left[\sum_{j=1}^m c_{ij}(s) f_j(F_j^{-1}(\phi_j(s))) \right.
 \end{aligned}$$

$$\begin{aligned}
 &+ \sum_{j=1}^m d_{ij}(s) g_j(F_j^{-1}(\phi_j(s - \tau_{ij}(s)))) \\
 &+ \sum_{j=1}^m p_{ij}(s) \int_{-\infty}^t G_{ij}(s - v) h_j(F_j^{-1}(\phi_j(v))) dv \\
 &\left. + I_i(s) \right] ds.
 \end{aligned} \tag{23}$$

Now, we prove that

$$T : PAP(R, R^m) \longrightarrow PAP(R, R^m). \tag{24}$$

Let

$$\begin{aligned}
 E_{ij} &= \sum_{j=1}^m c_{ij}(s) f_j(F_j^{-1}(\phi_j(s))) \\
 &+ \sum_{j=1}^m d_{ij}(s) g_j(F_j^{-1}(\phi_j(s - \tau_{ij}(s)))) \\
 &+ \sum_{j=1}^m p_{ij}(s) \int_{-\infty}^t G_{ij}(s - v) h_j(F_j^{-1}(\phi_j(v))) dv + I_i(s).
 \end{aligned} \tag{25}$$

For $z(t) \in PAP(R, R^m)$, conditions (H2.2)–(H2.4), Lemmas 5, 6, and 9, and the composition theorem in [16], we will get $E_{ij} \in PAP(R, R)$, $\forall i, j = 1, 2, \dots, m$.

From Definition 2, we have $E_{ij} = E_{ij1} + E_{ij0}$, $\forall i, j = 1, 2, \dots, m$. Where $E_{ij1} \in AP(R, R)$ and $E_{ij0} \in PAP_0(R, R)$. Then

$$\begin{aligned}
 x_{\phi_i}(t) &= \int_{-\infty}^t e^{-\int_s^t b_i^-(\phi_i(\tau)) d\tau} E_{ij1}(s) ds \\
 &+ \int_{-\infty}^t e^{-\int_s^t b_i^-(\phi_i(\tau)) d\tau} E_{ij0}(s) ds \\
 &= T_{ij1} + T_{ij0},
 \end{aligned} \tag{26}$$

where $T_{ij1} = \int_{-\infty}^t e^{-\int_s^t b_i^-(\phi_i(\tau)) d\tau} E_{ij1}(s) ds$ and $T_{ij0} = \int_{-\infty}^t e^{-\int_s^t b_i^-(\phi_i(\tau)) d\tau} E_{ij0}(s) ds$.

Because $E_{ij1} \in AP(R, R)$, for any $\epsilon > 0$, there exists a number $l = l(\epsilon) > 0$ such that every interval $[a, a + l]$ contains at least one point of $\delta = \delta(\epsilon)$ such that $\sup_{t \in R} |E_{ij1}(t + \delta) - E_{ij1}(t)| \leq \epsilon$ for every $t \in R$ and $\forall i, j = 1, 2, \dots, m$. Hence, we obtain

$$\begin{aligned}
 & |T_{ij1}(t + \delta) - T_{ij1}(t)| \\
 &= \left| \int_{-\infty}^{t+\delta} e^{-\int_s^t b_i^-(\phi_i(\tau)) d\tau} E_{ij1}(s) ds \right.
 \end{aligned}$$

$$\begin{aligned}
& \left| - \int_{-\infty}^t e^{-\int_s^t b_i^-(\phi_i(\tau))d\tau} E_{ij1}(s) ds \right| \\
& \leq \int_{-\infty}^{t+\tau} \left| e^{-b_i^- a_i^-(t-s)} |E_{ij1}(s+\delta) - E_{ij1}(s)| ds \right| \\
& \leq \frac{\epsilon}{b_i^- a_i^-}
\end{aligned} \tag{27}$$

so that $T_{ij1} \in AP(R, R)$.

And because

$$\begin{aligned}
& \lim_{T \rightarrow +\infty} \frac{1}{2T} \int_{-T}^T \left| \int_{-\infty}^t e^{-\int_s^t b_i^-(\phi_i(\tau))d\tau} E_{ij0}(s) ds \right| dt \\
& \leq \lim_{T \rightarrow +\infty} \frac{1}{2T} \int_{-T}^T \left| \int_{-T}^t e^{-\int_s^t b_i^-(\phi_i(\tau))d\tau} E_{ij0}(s) ds \right| dt \\
& \quad + \lim_{T \rightarrow +\infty} \frac{1}{2T} \int_{-T}^T \left| \int_{-\infty}^{-T} e^{-\int_s^t b_i^-(\phi_i(\tau))d\tau} E_{ij0}(s) ds \right| dt \\
& \leq \lim_{T \rightarrow +\infty} \frac{1}{2T} \int_{-T}^T \|E_{ij0}(t)\| dt \int_{-T}^t e^{-b_i^- a_i^-(t-s)} ds \\
& \quad + \lim_{T \rightarrow +\infty} \frac{\sup_{t \in R} |E_{ij0}(t)|}{2T} \int_{-T}^T dt \left(\int_{-\infty}^{-T} |e^{-b_i^- a_i^-(t-s)}| ds \right) \\
& \leq \lim_{T \rightarrow +\infty} \frac{1}{2T b_i^- a_i^-} \int_{-T}^T \|E_{ij0}(t)\| dt \\
& \quad + \lim_{T \rightarrow +\infty} \frac{\sup_{t \in R} |E_{ij0}(t)|}{2T (b_i^- a_i^-)^2} (1 - e^{-b_i^- a_i^-(2T)}) \\
& = 0 + \lim_{T \rightarrow +\infty} \frac{\sup_{t \in R} |E_{ij0}(t)|}{2T (b_i^- a_i^-)^2} (1 - e^{-b_i^- a_i^-(2T)}) \\
& = 0,
\end{aligned} \tag{28}$$

thus $T_{ij0} \in PAP_0(R, R)$. So $\forall i, j = 1, 2, \dots, m, x_{\phi_i}(t) \in PAP(R, R)$. Therefore $z_{(\phi)^T}(t) \in PAP(R, R^m)$.

From Lemma 9, $X = PAP(R, R^m)$ is a Banach space. If

$$\delta < 1, \tag{29}$$

then there exists a sufficiently large $\beta \geq 1$ such that

$$\delta \leq 1 - \beta^{-1} I, \tag{30}$$

where

$$I = \max_{1 \leq i \leq m} \left\{ \frac{I_i^+}{b_i^- a_i^-} \right\}. \tag{31}$$

We choose a closed subset

$$B = \{z(t) = \phi(t)^T = (\phi_1(t), \dots, \phi_m(t))^T \in X : \|z\| \leq \beta\}. \tag{32}$$

Firstly, we prove that $T : B \rightarrow B$; that is, $TB \subset B$.

From (29)–(32) and for $\forall z \in B$, we get

$$\begin{aligned}
|x_{\phi_i}(t)| & \leq \max_{1 \leq i \leq m} \left\{ \frac{a_i^+}{b_i^- a_i^-} \sum_{j=1}^n (L_j^f c_{ij}^+ + L_j^g d_{ij}^+ + L_j^h p_{ij}^+) \right\} \\
& \quad \times \|z\| + \max_{1 \leq i \leq m} \left\{ \frac{I_i^+}{b_i^- a_i^-} \right\} \leq \beta \delta + I \leq \beta.
\end{aligned} \tag{33}$$

Secondly, we prove that the mapping T is completely continuous.

By the continuity of the function f_j, g_j, h_j , for any $\epsilon > 0$, there is $\gamma = \gamma(\epsilon, \beta)$ such that

$$\begin{aligned}
|f_j(u) - f_j(v)| & \leq \frac{L_j^f \epsilon}{\delta}, \quad |u - v| \leq \gamma, \\
& \quad \forall u, v \in B, \quad j = 1, 2, \dots, m, \\
|g_j(u) - g_j(v)| & \leq \frac{L_j^g \epsilon}{\delta}, \quad |u - v| \leq \gamma, \\
& \quad \forall u, v \in B, \quad j = 1, 2, \dots, m, \\
|h_j(u) - h_j(v)| & \leq \frac{L_j^h \epsilon}{\delta}, \quad |u - v| \leq \gamma, \\
& \quad \forall u, v \in B, \quad j = 1, 2, \dots, m.
\end{aligned} \tag{34}$$

Let $w(t) = (\psi_1(t), \dots, \psi_m(t))$, $z, w \in B$, and $\|z - w\| \leq \gamma$; then $\|z\| \leq \gamma$, $\|w\| \leq \gamma$ and $\phi_j(t), \psi_j(t) \in C(R, B)$; then, for any $s \in R$, we get $|\phi_j(s) - \psi_j(s)| \leq \gamma$. So, we have

$$\begin{aligned}
|f_j(F_j^{-1}(\phi_j(s))) - f_j(F_j^{-1}(\psi_j(s)))| & \leq \frac{L_j^f \epsilon}{\delta}, \quad |u - v| \leq \gamma, \\
|g_j(F_j^{-1}(\phi_j(s))) - g_j(F_j^{-1}(\psi_j(s)))| & \leq \frac{L_j^g \epsilon}{\delta}, \quad |u - v| \leq \gamma, \\
|h_j(F_j^{-1}(\phi_j(s))) - h_j(F_j^{-1}(\psi_j(s)))| & \leq \frac{L_j^h \epsilon}{\delta}, \quad |u - v| \leq \gamma.
\end{aligned} \tag{35}$$

Thus

$$\begin{aligned}
& \|T(z)(t) - T(w)(t)\| \\
& \leq \max_{1 \leq i \leq m} \left\{ \frac{1}{b_i^- a_i^-} \sum_{j=1}^m a_i^+ (L_j^f c_{ij}^+ + L_j^g d_{ij}^+ + L_j^h p_{ij}^+) \right\} \frac{\epsilon}{\delta} \\
& \leq \delta \frac{\epsilon}{\delta} \leq \epsilon.
\end{aligned} \tag{36}$$

Therefore, T is continuous.

Thirdly, we show that T is compact.

Let $S = \{z(t) \in X : \|z\| \leq K\}$, where $K > 0$ to be any constant. We denote $\rho = \max_{1 \leq i \leq m} \{(a_i^+ / b_i^- a_i^-) \sum_{j=1}^m K(L_j^f c_{ij}^+ + L_j^g d_{ij}^+ + L_j^h p_{ij}^+) + I_i^+\}$. Then we have

$$\|T(z)(t)\| = \sup_{t \in R} \max_{1 \leq i \leq m} |x_{\phi_i}(t)| \leq \rho, \quad \forall z \in S. \tag{37}$$

Hence, T is uniformly bounded. Then, from (23), we get

$$\begin{aligned}
 \left[|x_{\phi_i}(t)| \right]' &= -b_i^-(x_{\phi_i}(t)) x_{\phi_i}(t) \\
 &+ \sum_{j=1}^m c_{ij}(t) f_j(F_j^{-1}(\phi_j(t))) \\
 &+ \sum_{j=1}^m d_{ij}(t) g_j(F_j^{-1}(\phi_j(t - \tau_{ij}(t)))) \\
 &+ \sum_{j=1}^m p_{ij}(t) \int_{-\infty}^t G_{ij}(t-s) h_j(F_j^{-1}(\phi_j(s))) ds \\
 &+ I_i(t) \\
 &\leq b_i^+ \rho + \sum_{j=1}^m a_j^+ K (L_j^f c_{ij}^+ + L_j^g d_{ij}^+ + L_j^h p_{ij}^+) + I_i^+ \leq L,
 \end{aligned} \tag{38}$$

where

$$L = \max_{1 \leq i \leq m} \left\{ b_i^+ \rho + \sum_{j=1}^m a_j^+ K (L_j^f c_{ij}^+ + L_j^g d_{ij}^+ + L_j^h p_{ij}^+) + I_i^+ \right\}. \tag{39}$$

Therefore, T is equicontinuous. By the Ascoli-Arzelà theorem, the operator T is compact; then it is completely continuous. By the Schauder fixed point theorem, the system (1) has at least one pseudo almost periodic solution. \square

4. The Global Uniform Asymptotic Stability of Pseudo Almost Periodic Solution

In order to discuss the global uniform asymptotic stability of pseudo almost periodic solution to system (1), we give the following assumptions:

(H4.1): delay functions $\tau_{ij}(t) \in C^1(\mathbb{R}, \mathbb{R}^+)$ satisfy that $\dot{\tau}_{ij}(t) \leq \tau_{ij}^* < 1$, $i, j = 1, 2, \dots, m$;

(H4.2): $N = \min_{1 \leq i \leq m} \{N_i\} > 0$, where $N_i = b_i^- - \sum_{j=1}^m c_{ij}^+ L_j^f - \sum_{j=1}^m (d_{ij}^+ L_j^g / (1 - \tau_{ij}^*)) - \sum_{j=1}^m p_{ij}^+ L_j^h$.

Theorem 11. Assume that (H2.1)–(H2.5) and (H4.1)–(H4.2) hold; then the pseudo almost periodic solution of system (1) is globally uniformly asymptotically stable.

Proof. The product system of the system (1) is

$$\begin{aligned}
 x_i'(t) &= -a_i(x_i(t)) \\
 &\times \left[b_i(x_i(t)) - \sum_{j=1}^m c_{ij}(t) f_j(x_j(t)) \right.
 \end{aligned}$$

$$\begin{aligned}
 &- \sum_{j=1}^m d_{ij}(t) g_j(x_j(t - \tau_{ij}(t))) \\
 &- \sum_{j=1}^m p_{ij}(t) \int_{-\infty}^t G_{ij}(t-s) h_j(x_j(s)) ds - I_i(t) \Big], \\
 y_i'(t) &= -a_i(y_i(t)) \\
 &\times \left[b_i(y_i(t)) - \sum_{j=1}^m c_{ij}(t) f_j(y_j(t)) \right. \\
 &- \sum_{j=1}^m d_{ij}(t) g_j(y_j(t - \tau_{ij}(t))) \\
 &- \sum_{j=1}^m p_{ij}(t) \int_{-\infty}^t G_{ij}(t-s) h_j(y_j(s)) ds - I_i(t) \Big].
 \end{aligned} \tag{40}$$

In order to apply the conclusion of Lemma 8, we construct a Lyapunov functional about product system (40)

$$V(t) = V_1(t) + V_2(t) + V_3(t), \tag{41}$$

where

$$\begin{aligned}
 V_1(t) &= \sum_{i=1}^m \left| \int_{y_i(t)}^{x_i(t)} \frac{1}{a_i(s)} ds \right|; \\
 V_2(t) &= \sum_{i=1}^m \sum_{j=1}^m \frac{d_{ij}^+ L_j^g}{1 - \tau_{ij}^*} \int_{t-\tau_{ij}(t)}^t |x_i(s) - y_i(s)| ds; \\
 V_3(t) &= \sum_{i=1}^m \sum_{j=1}^m p_{ij}^+ L_j^h \int_0^{+\infty} G_{ij}(s) \int_{t-s}^t |x_i(u) - y_i(u)| du ds.
 \end{aligned} \tag{42}$$

Let $X(t) = x(t)^T = (x_1(t), \dots, x_m(t))^T$ and $Y(t) = y(t)^T = (y_1(t), \dots, y_m(t))^T$. For product system (X, Y) , we receive

$$\begin{aligned}
 |X - Y| &\leq V(t, X(t), Y(t)) \\
 &\leq \sum_{i=1}^m \left\{ \frac{1}{a_i^-} + \sum_{j=1}^m \frac{d_{ij}^+ L_j^g \tau_{ij}^+}{1 - \tau_{ij}^*} + \sum_{j=1}^n p_{ij}^+ L_i^h \int_0^{+\infty} G_{ij}(s) ds \right\} \\
 &\quad \times |x_i(t) - y_i(t)| \\
 &\leq M_i \sum_{i=1}^m |x_i(t) - y_i(t)| \\
 &\leq M |X - Y|,
 \end{aligned} \tag{43}$$

where $M_i = (1/a_i^-) + \sum_{j=1}^m (d_{ij}^+ L_j^g \tau_{ij}^+ / (1 - \tau_{ij}^*)) + \sum_{j=1}^n p_{ij}^+ L_i^h \int_0^{+\infty} G_{ij}(s) ds$ and $M = \max_{1 \leq i \leq m} \{M_i\}$. Let

$u(s) = s$ and $v(s) = Ms$; we easily know it satisfies condition $(H'2.1)$ of Lemma 8. Then we obtain

$$\begin{aligned}
& |V(t, X, Y) - V(t, X^*, Y^*)| \\
&= \left| \sum_{i=1}^m \left| \int_{y_i(t)}^{x_i(t)} \frac{1}{a_i(s)} ds \right| - \sum_{i=1}^m \left| \int_{y_i^*(t)}^{x_i^*(t)} \frac{1}{a_i(s)} ds \right| \right. \\
&\quad + \sum_{i=1}^m \sum_{j=1}^m \frac{d_{ij}^+ L_j^g}{1 - \tau_{ij}^*} \int_{t-\tau_{ij}(t)}^t |x_i(s) - y_i(s)| ds \\
&\quad - \sum_{i=1}^m \sum_{j=1}^m \frac{d_{ij}^+ L_j^g}{1 - \tau_{ij}^*} \int_{t-\tau_{ij}(t)}^t |x_i^*(s) - y_i^*(s)| ds \\
&\quad - \sum_{i=1}^m \sum_{j=1}^m p_{ij}^+ L_j^h \int_0^{+\infty} G_{ij}(s) \int_{t-s}^t |x_i(u) - y_i(u)| du ds \\
&\quad \left. - \sum_{i=1}^m \sum_{j=1}^m p_{ij}^+ L_j^h \int_0^{+\infty} G_{ij}(s) \int_{t-s}^t |x_i^*(u) - y_i^*(u)| du ds \right| \\
&\leq \sum_{i=1}^m \frac{1}{a_i^-} |x_i(t) - x_i^*(t)| + \sum_{i=1}^m \frac{1}{a_i^-} |y_i(t) - y_i^*(t)| \\
&\quad + \sum_{i=1}^m \sum_{j=1}^m \frac{d_{ij}^+ L_j^g}{1 - \tau_{ij}^*} \\
&\quad \times \int_{t-\tau_{ij}(t)}^t (|x_i(s) - x_i^*(s)| + |y_i(s) - y_i^*(s)|) ds \\
&\quad + \sum_{i=1}^m \sum_{j=1}^m p_{ij}^+ L_j^h \int_0^{+\infty} G_{ij}(s) \\
&\quad \times \int_{t-s}^t ds (|x_i(t) - x_i^*(t)| + |y_i(t) - y_i^*(t)|) \\
&\leq M(|X - X^*| + |Y - Y^*|). \tag{44}
\end{aligned}$$

We also know that it satisfies condition $(H'2.2)$ of Lemma 8.

Calculating the upright derivative of $V_1(t)$, $V_2(t)$, and $V_3(t)$ along the system (40), respectively, and noting that $((1 - \dot{\tau}_{ij}(t))/(1 - \tau_{ij}^*)) > 1$, we have

$$\begin{aligned}
& D^+ V_1(t) \Big|_{(40)} \\
&= \sum_{i=1}^m \text{Sgn}(x_i(t) - y_i(t)) \left[\frac{x_i'(t)}{a_i(x_i(t))} - \frac{y_i'(t)}{a_i(y_i(t))} \right] \\
&\leq \sum_{i=1}^m \left\{ -\frac{b_i(x_i(t)) - b_i(y_i(t))}{x_i(t) - y_i(t)} |x_i(t) - y_i(t)| \right. \\
&\quad \left. + \sum_{j=1}^m c_{ij}^+ L_j^f |x_j(t) - y_j(t)| \right\}
\end{aligned}$$

$$\begin{aligned}
& + \sum_{j=1}^m d_{ij}^+ L_j^g |x_j(t - \tau_{ij}(t)) - y_j(t - \tau_{ij}(t))| \\
& + \sum_{j=1}^n p_{ij}^+ L_j^h \int_0^{+\infty} G_{ij}(s) |x_j(t - s) - y_j(t - s)| ds \Big\} \\
&\leq \sum_{i=1}^m \left\{ -b_i^- |x_i(t) - y_i(t)| + \sum_{j=1}^m c_{ij}^+ L_j^f |x_j(t) - y_j(t)| \right. \\
&\quad + \sum_{j=1}^m d_{ij}^+ L_j^g |x_j(t - \tau_{ij}(t)) - y_j(t - \tau_{ij}(t))| \\
&\quad \left. + \sum_{j=1}^n p_{ij}^+ L_j^h \int_0^{+\infty} G_{ij}(s) |x_j(t - s) - y_j(t - s)| ds \right\};
\end{aligned}$$

$$\begin{aligned}
& D^+ V_2(t) \Big|_{(40)} \\
&= \sum_{i=1}^m \sum_{j=1}^m \frac{d_{ij}^+ L_j^g}{1 - \tau_{ij}^*} |x_i(t) - y_i(t)| \\
&\quad - \sum_{i=1}^m \sum_{j=1}^m \frac{d_{ij}^+ L_j^g}{1 - \tau_{ij}^*} |x_i(t - \tau_{ij}(t)) - y_i(t - \tau_{ij}(t))|; \\
& D^+ V_3(t) \Big|_{(40)} \\
&= \sum_{i=1}^m \sum_{j=1}^m p_{ij}^+ L_j^h \int_0^{+\infty} G_{ij}(s) |x_i(t) - y_i(t)| ds \\
&\quad - \sum_{i=1}^m \sum_{j=1}^m p_{ij}^+ L_j^f \int_0^{+\infty} G_{ij}(s) |x_i(t - s) - y_i(t - s)| ds. \tag{45}
\end{aligned}$$

Combining (45) and assumptions $(H4.1)$ and $(H4.2)$, we get

$$\begin{aligned}
& D^+ V(t) \Big|_{(40)} \\
&\leq \sum_{i=1}^m \left\{ -b_i^- + \sum_{j=1}^m c_{ij}^+ L_j^f + \sum_{j=1}^m \frac{d_{ij}^+ L_j^g}{1 - \tau_{ij}^*} + \sum_{j=1}^m p_{ij}^+ L_j^h \right\} \\
&\quad \times |x_i(t) - y_i(t)| \\
&\leq -N \sum_{j=1}^m |x_j(t) - y_j(t)| \\
&\leq -aV(t).
\end{aligned} \tag{46}$$

From assumption $(H4.2)$, we have $a = N/M > 0$.

By Lemma 8, the pseudo almost periodic solutions of system (1) are globally uniformly asymptotically stable. This completes the proof. \square

Corollary 12. Consider the following periodic CGNNs systems:

$$\begin{aligned}
 x_i'(t) = & -a_i(x_i(t)) \\
 & \times \left[b_i(x_i(t)) - \sum_{j=1}^m c_{ij}(t) f_j(x_j(t)) \right. \\
 & \quad \left. - \sum_{j=1}^m d_{ij}(t) f_j(x_j(t - \tau_{ij}(t))) \right. \\
 & \quad \left. - \sum_{j=1}^m p_{ij}(t) \int_{-\infty}^t G_{ij}(t-s) f_j(x_j(s)) ds - I_i(t) \right], \\
 & t \geq 0, \\
 x_i(t) = & \Phi_i(t), \quad t < 0,
 \end{aligned} \tag{47}$$

where $i = 1, 2, \dots, m$, and the following assumptions hold.

(G4.1): Functions $a_i(u)$ are continuous bounded and there are positive constants a_i^+, a_i^- such that

$$0 < a_i^- \leq a_i(u) \leq a_i^+, \quad \forall u \in R, \quad i = 1, 2, \dots, m. \tag{48}$$

(G4.2): Functions $b_i(u) \in C(R, R)$ and there exist positive constants b_i^-, b_i^+ such that

$$\begin{aligned}
 b_i^- \leq \frac{b_i(u) - b_i(v)}{u - v} \leq b_i^+, \quad u \neq v, \\
 \forall u, v \in R, \quad b_i(0) = 0.
 \end{aligned} \tag{49}$$

(G4.3): $c_{ij}(t), d_{ij}(t)$ and $p_{ij}(t), I_i(t) \in C(R, R), \tau_{ij}(t) \in C(R, R^+)$ are all periodic functions, and

$$\begin{aligned}
 \sup_{t \in R} c_{ij}(t) = c_{ij}^+ > 0, \quad \sup_{t \in R} d_{ij}(t) = d_{ij}^+ > 0, \\
 \sup_{t \in R} p_{ij}(t) = p_{ij}^+ > 0, \quad \sup_{t \in R} I_i(t) = I_i^+ > 0,
 \end{aligned} \tag{50}$$

where $R^+ = [0, \infty)$, $i, j = 1, 2, \dots, m$.

(G4.4): Delay kernel functions $G_{ij} : [0, +\infty) \rightarrow [0, +\infty)$ are piecewise continuous and integrable

$$\begin{aligned}
 \int_0^{+\infty} G_{ij}(u) du = 1, \quad \int_0^{+\infty} u G_{ij}(u) du < +\infty, \\
 i, j = 1, 2, \dots, m.
 \end{aligned} \tag{51}$$

(G4.5): Functions $f_j(u) \in C(R, R)$ satisfy the Lipschitz condition; namely, there exist nonnegative constants L_j such that

$$\begin{aligned}
 |f_j(u) - f_j(v)| \leq L_j |u - v|, \\
 \forall u, v \in R, \quad j = 1, 2, \dots, m.
 \end{aligned} \tag{52}$$

$$(G4.6): \text{If } \delta = \max_{1 \leq i \leq m} \{(a_i^+ / b_i^- a_i^-) \sum_{j=1}^m L_j (c_{ij}^+ + d_{ij}^+ + p_{ij}^+)\} < 1,$$

then the system (47) has at least one periodic solution.

Corollary 13. Assume that (G4.1)–(G4.6) hold and suppose further that

(G4.7): delay functions $\tau_{ij}(t) \in C^1(R, R^+)$ satisfy that $\dot{\tau}_{ij}(t) \leq \tau_{ij}^* < 1, i, j = 1, 2, \dots, m$.

(G4.8): $N = \min_{1 \leq i \leq m} \{N_i\} > 0$, where $N_i = b_i^- - \sum_{j=1}^m c_{ij}^+ L_j - \sum_{j=1}^m (d_{ij}^+ L_j / (1 - \tau_{ij}^*)) - \sum_{j=1}^m p_{ij}^+ L_j$; then the periodic solution of system (47) is globally uniformly asymptotically stable.

Remark 14. Recently, the global exponential stability of periodic or almost periodic solution to CGNNs is studied by many scholars (see [15–30]). However, few authors pay attention to the global uniform asymptotic stability. Corollaries 12 and 13 provide some new results.

5. An Example

An example is given to illustrate the feasibility of main results in this paper. Consider the following simple neural networks:

$$\begin{aligned}
 x_i'(t) = & -a_i(x_i(t)) \\
 & \times \left[b_i(x_i(t)) - \sum_{j=1}^2 c_{ij}(t) f_j(x_j(t)) \right. \\
 & \quad \left. - \sum_{j=1}^2 d_{ij}(t) g_j(x_j(t - \tau_{ij}(t))) \right. \\
 & \quad \left. - \sum_{j=1}^2 p_{ij}(t) \int_{-\infty}^t G_{ij}(t-s) h_j(x_j(s)) ds - I_i(t) \right], \\
 & t \geq 0, \quad i = 1, 2,
 \end{aligned} \tag{53}$$

where the initial functions $x_1(t) = 4 + \cos(\pi t), t < 0, x_2(t) = 5 + \sin(2t), t < 0, a_i(x_i(t)) = 4 + \cos \pi t - e^{-|x_i(t)|}, b_i(x_i(t)) = 5 + \sin 2t - e^{-|x_i(t)|}$. Let

$$\begin{aligned}
 & \begin{pmatrix} c_{11}(t) & c_{12}(t) \\ c_{21}(t) & c_{22}(t) \end{pmatrix} \\
 & = \frac{1}{14} \begin{pmatrix} \cos t + e^{-t^4 \cos^4 t} & \cos(\sqrt{2}t) + e^{-t^4 \sin^4 t} \\ \cos(\sqrt{5}t) + e^{-t^4 \cos^4 t} & \sin(2t) + e^{-t^2 \cos^4 t} \end{pmatrix},
 \end{aligned}$$

$$\begin{aligned}
& \begin{pmatrix} d_{11}(t) & d_{12}(t) \\ d_{21}(t) & d_{22}(t) \end{pmatrix} \\
&= \frac{1}{14} \begin{pmatrix} \sin t + e^{-t^2 \cos^2 t} & \cos(\sqrt{4}t) + e^{-t^2 \cos^4 t} \\ \sin(\sqrt{3}t) + e^{-t^4 \cos^4 t} & \sin(2t) + e^{-t^4 \cos^4 t} \end{pmatrix}, \\
& \begin{pmatrix} p_{11}(t) & p_{12}(t) \\ p_{21}(t) & p_{22}(t) \end{pmatrix} \\
&= \frac{1}{14} \begin{pmatrix} \cos(\sqrt{5}t) + e^{-t^2 \cos^2 t} & \sin(\sqrt{3}t) + e^{-t^4 \cos^4 t} \\ \cos(\sqrt{3}t) + e^{-t^2 \cos^2 t} & \sin(2t) + e^{-t^4 \cos^4 t} \end{pmatrix}. \quad (54)
\end{aligned}$$

$I_1(t) = I_2(t) = 2(\sin(\sqrt{3}t) + e^{-t^2 \cos^4 t})$, $f_j(x_j) = g_j(x_j) = h_j(x_j) = (|x+1| - |x-1|)/2$, $G_{ij}(u) = e^{-u}$, $\tau_{ij}^* = 4/5$. Then, we have $a_i^+ = 5$, $a_i^- = 2$, $b_i^- = 3$, $c_{ij}^+ = d_{ij}^+ = p_{ij}^+ = 1/7$, $L_j^f = L_j^g = L_j^h = 1$, where $i, j = 1, 2$. Moreover

$$\begin{aligned}
\delta &= \max_{1 \leq i \leq 2} \left\{ \frac{a_i^+}{b_i^- a_i^-} \sum_{j=1}^2 (L_j^f c_{ij}^+ + L_j^g d_{ij}^+ + L_j^h p_{ij}^+) \right\} = \frac{5}{7} < 1, \\
N_i &= b_i^- - \sum_{j=1}^2 c_{ij}^+ L_j^f - \sum_{j=1}^2 \frac{d_{ij}^+ L_j^g}{1 - \tau_{ij}^*} - \sum_{j=1}^2 p_{ij}^+ L_j^h = 1 > 0, \\
& i = 1, 2. \quad (55)
\end{aligned}$$

Thus, by Theorem 10, we know that system (53) has at least one pseudo almost periodic solution. It follows from Theorem 11 that the unique pseudo almost periodic solution of system (53) is globally uniformly asymptotically stable (Figure 1).

6. Conclusions

In this paper, the existence and uniform asymptotic stability of pseudo almost periodic solutions of system (1) is discussed. By applying Schauder fixed point theorem and constructing a suitable Lyapunov functional, some sufficient conditions are obtained to ensure the existence and uniform asymptotic stability of pseudo almost periodic solutions of system (1). The results have important leading significance in the design and applications of CGNNs. In addition, an example is given to demonstrate the effectiveness of main results.

Conflict of Interests

The authors declare that there is no conflict of interests regarding the publication of this paper.

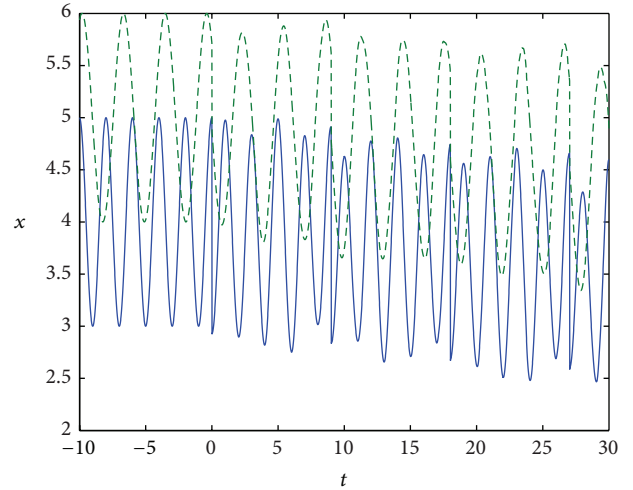


FIGURE 1: Simulated results of the solutions.

Acknowledgments

This work was supported by the National Natural Science Foundation of China (11361010) and Scientific Research Project in Guangxi of China Department of Education (201106LX613).

References

- [1] M. A. Cohen and S. Grossberg, "Absolute stability of global pattern formation and parallel memory storage by competitive neural networks," *IEEE Transactions on Systems, Man, and Cybernetics*, vol. 13, no. 5, pp. 815–826, 1983.
- [2] X. Fu and X. Li, "LMI conditions for stability of impulsive stochastic Cohen-Grossberg neural networks with mixed delays," *Communications in Nonlinear Science and Numerical Simulation*, vol. 16, no. 1, pp. 435–454, 2011.
- [3] X. Huang, J. Cao, and D. W. C. Ho, "Existence and attractivity of almost periodic solution for recurrent neural networks with unbounded delays and variable coefficients," *Nonlinear Dynamics*, vol. 45, no. 3-4, pp. 337–351, 2006.
- [4] K. Li, "Stability analysis for impulsive Cohen-Grossberg neural networks with time-varying delays and distributed delays," *Nonlinear Analysis: Real World Applications*, vol. 10, no. 5, pp. 2784–2798, 2009.
- [5] J. J. Oliveira, "Global stability of a Cohen-Grossberg neural network with both time-varying and continuous distributed delays," *Nonlinear Analysis: Real World Applications*, vol. 12, no. 5, pp. 2861–2870, 2011.
- [6] J.-L. Wang, H.-N. Wu, and L. Guo, "Stability analysis of reaction-diffusion Cohen-Grossberg neural networks under impulsive control," *Neurocomputing*, vol. 106, no. 15, pp. 21–30, 2013.
- [7] J.-L. Wang, H.-N. Wu, and L. Guo, "Passivity and stability analysis of reaction-diffusion neural networks with dirichlet boundary conditions," *IEEE Transactions on Neural Networks*, vol. 22, no. 12, pp. 2105–2116, 2011.
- [8] L. Wang, "Stability of Cohen-Grossberg neural networks with distributed delays," *Applied Mathematics and Computation*, vol. 160, no. 1, pp. 93–110, 2005.

- [9] H. Zhao, L. Chen, and Z. Mao, "Existence and stability of almost periodic solution for Cohen-Grossberg neural networks with variable coefficients," *Nonlinear Analysis: Real World Applications*, vol. 9, no. 2, pp. 663–673, 2008.
- [10] Q. Zhu and J. Cao, "Exponential stability analysis of stochastic reaction-diffusion Cohen-Grossberg neural networks with mixed delays," *Neurocomputing*, vol. 74, no. 17, pp. 3084–3091, 2011.
- [11] L. V. Hien, T. T. Loan, B. T. H. Trang, and H. Trinh, "Existence and global asymptotic stability of positive periodic solution of delayed Cohen-Grossberg neural networks," *Applied Mathematics and Computation*, vol. 240, pp. 200–212, 2014.
- [12] C.-H. Li and S.-Y. Yang, "Existence and attractivity of periodic solutions to non-autonomous Cohen-Grossberg neural networks with time delays," *Chaos, Solitons & Fractals*, vol. 41, no. 3, pp. 1235–1244, 2009.
- [13] X. Liao and C. Li, "Global attractivity of Cohen-Grossberg model with finite and infinite delays," *Journal of Mathematical Analysis and Applications*, vol. 315, no. 1, pp. 244–262, 2006.
- [14] L. Wan and Q. Zhou, "Asymptotic behaviors of stochastic Cohen-Grossberg neural networks with mixed time-delays," *Applied Mathematics and Computation*, vol. 225, pp. 541–549, 2013.
- [15] C. Bai, "Global exponential stability and existence of periodic solution of Cohen-Grossberg type neural networks with delays and impulses," *Nonlinear Analysis: Real World Applications*, vol. 9, no. 3, pp. 747–761, 2008.
- [16] F. Chérif, "Existence and global exponential stability of pseudo almost periodic solution for SICNNs with mixed delays," *Journal of Applied Mathematics and Computing*, vol. 39, no. 1–2, pp. 235–251, 2012.
- [17] X. Chen and Q. Song, "Global exponential stability of the periodic solution of delayed Cohen-Grossberg neural networks with discontinuous activations," *Neurocomputing*, vol. 73, no. 16–18, pp. 3097–3104, 2010.
- [18] T. Liang, Y. Yang, Y. Liu, and L. Li, "Existence and global exponential stability of almost periodic solutions to Cohen-Grossberg neural networks with distributed delays on time scales," *Neurocomputing*, vol. 123, no. 10, pp. 207–215, 2014.
- [19] Y. Li and X. Fan, "Existence and global exponential stability of almost periodic solution for Cohen-Grossberg BAM neural networks with variable coefficients," *Applied Mathematical Modelling*, vol. 33, no. 4, pp. 2114–2120, 2009.
- [20] B. Li and D. Xu, "Existence and exponential stability of periodic solution for impulsive Cohen-Grossberg neural networks with time-varying delays," *Applied Mathematics and Computation*, vol. 219, no. 5, pp. 2506–2520, 2012.
- [21] F. Long, Y. Wang, and S. Zhou, "Existence and exponential stability of periodic solutions for a class of Cohen-Grossberg neural networks with bounded and unbounded delays," *Nonlinear Analysis: Real World Applications*, vol. 8, no. 3, pp. 797–810, 2007.
- [22] S. Mandal and N. C. Majee, "Existence of periodic solutions for a class of Cohen-Grossberg type neural networks with neutral delays," *Neurocomputing*, vol. 74, no. 6, pp. 1000–1007, 2011.
- [23] F. Ren and J. Cao, "Periodic solutions for a class of higher-order Cohen-Grossberg type neural networks with delays," *Computers and Mathematics with Applications*, vol. 54, no. 6, pp. 826–839, 2007.
- [24] D. Wang and L. Huang, "Almost periodic dynamical behaviors for generalized Cohen-Grossberg neural networks with discontinuous activations via differential inclusions," *Communications in Nonlinear Science and Numerical Simulation*, vol. 19, no. 10, pp. 3857–3879, 2014.
- [25] D. Wang and L. Huang, "Periodicity and global exponential stability of generalized Cohen-Grossberg neural networks with discontinuous activations and mixed delays," *Neural Networks*, vol. 51, no. 3, pp. 80–95, 2014.
- [26] J.-L. Wang, H. Jiang, and C. Hu, "Existence and stability of periodic solutions of discrete-time Cohen-Grossberg neural networks with delays and impulses," *Neurocomputing*, vol. 142, no. 22, pp. 542–550, 2014.
- [27] J. Wang and L. Huang, "Almost periodicity for a class of delayed Cohen-Grossberg neural networks with discontinuous activations," *Chaos, Solitons and Fractals*, vol. 45, no. 9–10, pp. 1157–1170, 2012.
- [28] H. Xiang and J. Cao, "Almost periodic solution of Cohen-Grossberg neural networks with bounded and unbounded delays," *Nonlinear Analysis: Real World Applications*, vol. 10, no. 4, pp. 2407–2419, 2009.
- [29] Z. Yuan, D. Hu, L. Huang, and G. Dong, "Existence and global exponential stability of periodic solution for Cohen-Grossberg neural networks with delays," *Nonlinear Analysis: Real World Applications*, vol. 7, no. 4, pp. 572–590, 2006.
- [30] F. Zhang, B. Liu, and L. Huang, "Existence and exponential stability of periodic solutions for a class of Cohen-Grossberg neural networks with bounded and unbounded delays," *Computers and Mathematics with Applications*, vol. 53, no. 9, pp. 1325–1338, 2007.
- [31] J.-L. Wang, H.-N. Wu, and L. Guo, "Novel adaptive strategies for synchronization of linearly coupled neural networks with reaction-diffusion terms," *IEEE Transactions on Neural Networks and Learning Systems*, vol. 25, no. 2, pp. 429–440, 2013.
- [32] J.-L. Wang and H.-N. Wu, "Synchronization and adaptive control of an array of linearly coupled reaction-diffusion neural networks with hybrid coupling," *IEEE Transactions on Cybernetics*, vol. 44, no. 8, pp. 1350–1361, 2014.
- [33] Z. Zheng, *Theory of Functional Differential Equation*, Anhui Education Publishing Press, 1994.
- [34] C. Y. Zhang, *Pseudo almost periodic functions and their applications [Ph.D. thesis]*, University of Western Ontario, 1992.
- [35] J. Hale, *Theory of Functional Differential Equations*, Springer, New York, NY, USA, 1977.

Research Article

Consensus Analysis of High-Order Multiagent Systems with General Topology and Asymmetric Time-Delays

Fangcui Jiang

School of Mathematics and Statistics, Shandong University, Weihai 264209, China

Correspondence should be addressed to Fangcui Jiang; jiangfcsdu@sdu.edu.cn

Received 4 June 2014; Accepted 22 July 2014; Published 13 August 2014

Academic Editor: Zhichun Yang

Copyright © 2014 Fangcui Jiang. This is an open access article distributed under the Creative Commons Attribution License, which permits unrestricted use, distribution, and reproduction in any medium, provided the original work is properly cited.

This paper focuses on the consensus problem for high-order multiagent systems (MAS) with directed network and asymmetric time-varying time-delays. It is proved that the high-order multiagent system can reach consensus when the network topology contains a spanning tree and time-delay is bounded. The main contribution of this paper is that a Lyapunov-like design framework for the explicit selection of protocol parameters is provided. The Lyapunov-like design guarantees the robust consensus of the high-order multiagent system with respect to asymmetric time-delays and is independent of the exact knowledge of the topology when the communication linkages among agents are undirected and connected.

1. Introduction

In the last few years, substantial research effort from a number of researchers has been poured on the study of consensus problems for multiagent systems (MAS) due to its powerful engineering applications, such as formation control of autonomous vehicles, collective behavior of flocks, and distributed decision making in sensor networks, to name a few. The pioneering contributions in systems and control community have been made by [1, 2]. Until now, it has been proved that the consensus problem for single-integrator MAS can always be solved under certain mild conditions on the network topology [3–5].

Due to the complexity of real systems, the study on single-integrator MAS can not meet the needs of practical applications. Thus, recently, widespread interest in MAS with agents modeled by general dynamics has been excited among researchers, such as double-integrator model [6, 7] and high-order-integrator model. Specifically, high-order-integrator (or high-order) MAS have been studied in [8], where the proposed consensus protocol involves the relative information of all-order derivatives of agents's state. Reference [9] has further extended the partial results of [8] and derived a linear-matrix-inequality-based protocol design. Reference [10] has

provided a scheme to choose the coupling strength for fixed and connected topology.

In most practical networks, communication time-delays caused by limited transmission speed and distance cannot be neglected. Within the literature on consensus for MAS with time-delays, recent years have witnessed the introduction of numerous distributed protocols. According to the inducements of time-delays, these protocols can be categorized into the ones in which delays only affect the state information of the agents' neighbors [11], the ones in which delays affect both the agents' own state information and their neighbors' state information [4, 7, 12–16], the ones containing distributed delays [17], and so forth. In particular, [4] has shown that the consensus of single-integrator MAS might be destabilized by large delays. By using Laplace transform technique, [7] has proved that second-order multiagent systems with bounded and constant time-delays can reach consensus. Based on nonexpansiveness of constant delay operator and Gershgorin's circle theorem, [11] has derived a local controller for high-order MAS with diverse constant time-delays. However, time-varying communication delays are very common in MAS due to the mobility of agents and the disturbance from environment. Hence, it is necessary to study the consensus for

high-order MAS with time-varying communication delays by exploring other method of protocol design.

In this paper, we investigate the consensus problem for high-order MAS with directed interactions and asymmetric time-varying communication delays. By asymmetric communication delays, we mean that the delay in communication channel from the agent to its neighbor differs from the one in the reversed channel if there are bidirectional communication linkages between them. We assume that the agent can only observe the information of the first state variable of its neighbors, and we propose a distributed protocol by applying both the instantaneous information of the agent's own and the time-delayed relative information with respect to its neighbors. Based on a reduced-order time delay system, we derive some sufficient conditions characterized by linear matrix inequalities (LMIs), according to Lyapunov-Krasovskii functional approach. The main contribution of this paper is that we establish a Lyapunov-like design framework for the explicit selection of protocol parameters. The protocol design framework can not only guarantee the solvability of the LMIs aforementioned but also is independent of the exact knowledge of the topology when the communication linkages among agents are undirected and connected. This implies that the Lyapunov-like protocol design guarantees the robust consensus of high-order MAS with respect to asymmetric time-varying communication delays. Compared with the protocol design in [9], our design is not based on LMI but only needs to solve a simple Lyapunov equation and a simple algebraic inequality. In contrast to the literature on single-/double-integrator MAS, the results here are not simple extensions of the results therein since the protocol parameters have important effect on the consensus convergence of high-order MAS.

The remainder of this paper is organized as follows. Section 2 states the problem formulation and Section 3 presents the main results. Section 4 carries out some numerical examples and the last section provides some concluding remarks.

Notations. We let \mathbb{R} be the set of real numbers. \mathbb{R}^n is the n -dimensional real vector space. \mathbb{R}_n is the set of n -by- n matrices with elements in \mathbb{R} . $I_n \in \mathbb{R}_n$ is an identity matrix. Given a matrix $X \in \mathbb{R}_n$, $\sigma(X)$ denotes its spectrum (set of eigenvalues); $X < 0$ means that X is negative definite. $\text{diag}\{a_1, \dots, a_n\}$ defines a diagonal matrix with diagonal elements being a_1, \dots, a_n . Sometimes $0_{m-1} \in \mathbb{R}_{m-1}$ is used to denote zero matrix. Consider $\mathbf{1}_N = [1 \ \dots \ 1]^T \in \mathbb{R}^N$. $\underline{N} = \{1, \dots, N\}$ and $\underline{m-1} = \{1, \dots, m-1\}$ are two index sets. \otimes denotes the Kronecker product.

2. Problem Formulation

Consider a dynamical system of N autonomous agents, which are labelled 1 through N . Each agent is modelled as the following m th order integrator:

$$\begin{aligned} \xi_i^{(m)} &= u_i, \quad t \geq 0, \quad i \in \underline{N}, \\ \xi_i(0) &= \xi_{i0}, \dots, \xi_i^{(m-1)}(0) = \xi_{i0}^{(m-1)}, \end{aligned} \quad (1)$$

where $m \geq 1$ is a positive integer and denotes the order of the differential equations; $\xi_i \in \mathbb{R}$, and $\xi_i^{(k)}$, $k = 1, \dots, m$, is the k th order derivative of ξ_i ; $u_i \in \mathbb{R}$ is the control input; $x_i(0) := [\xi_{i0} \ \dots \ \xi_{i0}^{(m-1)}]^T$ is the initial state of agent i .

The interaction/communication topology among agents can be conveniently modeled by weighted directed graph $\mathcal{G}(\mathcal{A}) = \{\mathcal{V}, \mathcal{E}, \mathcal{A}\}$, where $\mathcal{V} = \{v_1, \dots, v_N\}$ is the vertex set, $\mathcal{E} \subset \mathcal{V} \times \mathcal{V}$ is the arc set, and $\mathcal{A} = [a_{ij}] \in \mathbb{R}_N$ is the adjacency matrix with $a_{ij} \geq 0$. An arc of \mathcal{E} , denoted by (v_i, v_j) , is an ordered pair of distinct vertices of \mathcal{V} ; v_i and v_j are called the tail and the head of the arc, respectively. An arc $(v_i, v_j) \in \mathcal{E}$ if and only if $a_{ji} > 0$. If $(v_i, v_j) \in \mathcal{E}$, then we say that v_i is a neighbor of v_j . Denote the collection of neighbors of v_i by $\mathcal{N}_i = \{v_j : (v_j, v_i) \in \mathcal{E}\}$. In this paper, we assume that $(v_i, v_i) \notin \mathcal{E}$ and each element of \mathcal{E} is unique. Each vertex in $\mathcal{G}(\mathcal{A})$ represents an agent of the dynamical system (1); $(v_i, v_j) \in \mathcal{E}$ indicates that there is a communication linkage from agent i to agent j ; the element a_{ji} in \mathcal{A} is the weight of the linkage.

A path from v_i to v_j means that there is a sequence of distinct arcs in \mathcal{E} , $(v_i, v_1), (v_1, v_2), \dots, (v_k, v_j)$. A directed tree is a directed graph, where every vertex has exactly one tail except for one special vertex without any tail. We say a graph contains a spanning tree if there exists a subset of arcs $\mathcal{E}' \subset \mathcal{E}$ such that the graph $\mathcal{G}' = (\mathcal{V}, \mathcal{E}')$ is a directed tree. A graph is said to be balanced if for each vertex v_i the weights of its linkages satisfy $\sum_{j=1}^N a_{ij} = \sum_{j=1}^N a_{ji}$, $i \in \underline{N}$. A graph is said to be undirected if the associated adjacency matrix \mathcal{A} is symmetric. Then it is easy to see that any undirected graph is balanced. A directed graph is called strongly connected if there exists a path between any two distinct vertices of the graph; for undirected graph it is called connected. An undirected graph is called complete if for any $i \neq j$, $(v_i, v_j) \in \mathcal{E}$. The Laplacian matrix $\mathcal{L} = [l_{ij}] \in \mathbb{R}_N$ of $\mathcal{G}(\mathcal{A})$ is defined as

$$l_{ij} = \begin{cases} -a_{ij}, & i \neq j \\ \sum_{v_j \in \mathcal{N}_i} a_{ij}, & i = j. \end{cases} \quad (2)$$

Let $\mathcal{D} = \text{diag}\{d_1, \dots, d_N\}$ with $d_i = \sum_{v_j \in \mathcal{N}_i} a_{ij}$, $i \in \underline{N}$. Then \mathcal{D} and d_i are called the in-degree matrix of $\mathcal{G}(\mathcal{A})$ and the in-degree of vertex v_i , respectively. From the definition, it is not hard to obtain that $\mathcal{L} = \mathcal{D} - \mathcal{A}$ and $\mathcal{L}\mathbf{1}_N = 0$. Spectral properties of the Laplacian matrix can be found in [5, 18]. Hence the details are omitted.

For the system (1), the consensus protocol is described by

$$\begin{aligned} u_i(t) &= - \sum_{k=1}^{m-1} c_k \xi_i^{(k)}(t) \\ &\quad - \sum_{j \in \mathcal{N}_i} \kappa_0 a_{ij} [\xi_i(t - \tau_{ij}(t)) - \xi_j(t - \tau_{ij}(t))], \end{aligned} \quad (3)$$

where $c_k > 0$, $k \in \underline{m-1}$ and $\kappa_0 > 0$ are, respectively, the feedback gains of absolute and relative information (for convenience, we refer to the gains c_k , $k \in \underline{m-1}$, and κ_0 , as the protocol parameters); piecewise continuous function $\tau_{ij}(t)$ is the time-varying delay affecting the communication

linkage from agent j to agent i at time t . Notice that, different from [4, 14, 19, 20], the delays in transmissions from agent i to agent j and from agent j to agent i (if there are bidirectional communication linkages between them) can be asymmetric; that is, $\tau_{ij}(\cdot) \neq \tau_{ji}(\cdot)$.

Remark 1. In protocol (3), the agent i is able to measure its own instantaneous state information and equipped with memories to store the signals $\xi_i(\cdot)$ which can be used at some future time and needs only to receive the time-delayed signals $\xi_j(t - \tau_{ij}(t))$ of its neighbors. The control input $u_i(t)$ can be implemented by computing the instantaneous information of all-order derivatives of $\xi_i(t)$ and the time-delayed relative information $\xi_i(t - \tau_{ij}(t)) - \xi_j(t - \tau_{ij}(t))$. The determination of $\tau_{ij}(t)$ can be carried out by assuming that the stored signals $\xi_i(\cdot)$ of each agent are time-stamped and neighbor j transmits not only the time-delayed signal $\xi_j(t - \tau_{ij}(t))$ but also the time stamp. The above situation can be found in [13, 15] and also satisfied easily in practice.

Let $x_i(t) = [\xi_i(t) \cdots \xi_i^{(m-1)}(t)]^T$ and $x(0) = [x_1(0)^T \cdots x_N(0)^T]^T$ be the state of agent i and the stacked vector of the agents' initial states, respectively. In this paper, we are devoted to solving the following consensus problem for the MAS (1).

Definition 2. Consider the MAS (1) with some given protocol $u_i(t)$. If, for any initial state $x(0)$, the states of agents satisfy $x_i(t) - x_j(t) \rightarrow 0$ as $t \rightarrow \infty$ for all $i, j \in \underline{N}$, then we say that the system solves a consensus problem asymptotically. In addition, if there exists $\xi^* \in \mathbb{R}^m$ such that, for any initial state $x(0)$, $x_i(t) \rightarrow \xi^*$ as $t \rightarrow \infty$, for all $i \in \underline{N}$, then we say ξ^* is the consensus state of the system.

In order to develop the main results, some helpful lemmas are introduced as follows.

Suppose that \mathcal{G}_c is a complete undirected graph of N vertices and \mathcal{L}_c is the associated Laplacian matrix. From the definition, we have $\mathcal{L}_c \mathbf{1}_N = 0$, $\mathbf{1}_N^T \mathcal{L}_c = 0$, and the rank of \mathcal{L}_c is $N - 1$. Let U_c be an orthogonal matrix such that $U_c^T \mathcal{L}_c U_c = \text{diag}\{0, J'\}$, where $J' \in \mathbb{R}_{N-1}$ is a diagonal matrix. Define $U_c = [\nu_1 \ \nu_2 \ \cdots \ \nu_N]$ with $\nu_i \in \mathbb{R}^N$, $i \in \underline{N}$. It follows that $\nu_1 = (1/\sqrt{N})\mathbf{1}_N$. For convenience, we let $\widehat{U} = [\nu_2 \ \cdots \ \nu_N]$. Then $\widehat{U}^T \widehat{U} = I_{N-1}$ and $\widehat{U}^T \nu_1 = 0$. Based on this observation and the property of Laplacian matrix, we can obtain the result below.

Lemma 3. Suppose that \mathcal{G} is a graph with the associated Laplacian matrix \mathcal{L} . Then $U_c^T \mathcal{L} U_c$ is in the form of $\begin{bmatrix} 0 & l^T \\ 0 & \widehat{L} \end{bmatrix}$, where $\widehat{L} \in \mathbb{R}_{N-1}$ and $l \in \mathbb{R}^{N-1}$; $\sigma(\widehat{L}) \subset \sigma(\mathcal{L})$. In addition, if \mathcal{G} is balanced, then $l = 0$; if \mathcal{G} is strongly connected and balanced, then $\widehat{L}^T + \widehat{L}$ is positive definite.

Proof. See the Appendix: Proofs of Lemmas. \square

The following result can be considered as a special case of Jensen's integral inequality given in [21].

Lemma 4 (see [21]). For any differentiable vector function $y(t) \in \mathbb{R}^n$ and any positive definite matrix $P \in \mathbb{R}_n$, the following inequality holds:

$$\begin{aligned} & \tau^{-1} [y(t) - y(t - \tau(t))]^T P [y(t) - y(t - \tau(t))] \\ & \leq \int_{t-\tau(t)}^t \dot{y}^T(s) P \dot{y}(s) ds, \quad t \geq 0, \end{aligned} \quad (4)$$

where $\tau > 0$ and $0 \leq \tau(t) \leq \tau$.

Lemma 5 (Schur complement, see [22]). Let X, Y, Z be some given matrices with appropriate dimensions and let X, Z be symmetric; then $\begin{bmatrix} X & Y \\ Y^T & Z \end{bmatrix} < 0$ if and only if $X < 0$, $Z - Y^T X^{-1} Y < 0$, or $Z < 0$, $X - Y Z^{-1} Y^T < 0$.

3. Main Results

In this section, we first provide an equivalent condition for the consensus convergence of the systems (1) and (3) based on an orthogonal state transformation and a reduced-order time delay system. Then we give a Lyapunov-like parameter design for the protocol and prove that the maximum allowable upper bounds of time-varying delays can be determined by solving some optimization problems.

Suppose that the interaction topology of the system (1) is modelled by $\mathcal{G}(\mathcal{A})$; the associated Laplacian matrix is \mathcal{L} . Then the dynamics of agent i can be written as

$$\begin{aligned} \dot{x}_i(t) &= E_m x_i(t) - \sum_{j \in \mathcal{N}_i} \kappa_{0ij} \\ & \times F_m [x_i(t - \tau_{ij}(t)) - x_j(t - \tau_{ij}(t))], \end{aligned} \quad (5)$$

where

$$\begin{aligned} E_m &= \begin{bmatrix} 0 & I_{m-1} \\ 0 & \theta^T \end{bmatrix}, \quad F_m = \begin{bmatrix} 0 & 0_{m-1} \\ 1 & 0 \end{bmatrix}, \\ \theta &= [-c_1 \ -c_2 \ \cdots \ -c_{m-1}]^T. \end{aligned} \quad (6)$$

Denote $x(t) = [x_1^T(t) \cdots x_N^T(t)]^T$ by the stacked vector of the agents' states. The closed-loop dynamics of the systems (1) and (3) are in the form of

$$\dot{x}(t) = (I_N \otimes E_m) x(t) - \sum_{k=1}^M (\kappa_0 \mathcal{L}_k \otimes F_m) x(t - \tau_k(t)), \quad (7)$$

where M denotes the number of different time-delays over the communication channels of the system (it is easy to get that $M \leq N(N - 1)$); $\tau_k(t) \in \{\tau_{ij}(t) : i, j \in \underline{N}, i \neq j\}$ for $k = 1, \dots, M$; $\mathcal{L}_k = [l_{ij}^k] \in \mathbb{R}_N$ is defined as

$$l_{ij}^k = \begin{cases} -a_{ij}, & j \neq i, \ \tau_{ij}(\cdot) = \tau_k(\cdot), \\ 0, & j \neq i, \ \tau_{ij}(\cdot) \neq \tau_k(\cdot), \\ -\sum_{n=1}^N l_{in}^k, & j = i. \end{cases} \quad (8)$$

Next, we assume that the time-delays in (7) satisfy

$$0 \leq \tau_k(t) \leq \tau_k, \quad t \geq 0, \quad k = 1, \dots, M, \quad (9)$$

where $\tau_k > 0$. Define $\tau_0 = \max\{\tau_k : k = 1, \dots, M\}$. The initial state of the system (7) is assumed to be $\phi(t) = x(0)$, $t \in [-\tau_0, 0]$.

Remark 6. The matrix \mathcal{L}_k in (7) amounts to consider a Laplacian matrix that is associated with a subgraph of $\mathcal{G}(\mathcal{A})$ with all linkages affected by the same time-delay. Hence, $\mathcal{L}_k \mathbf{1}_N = 0$ and $\sum_{k=1}^M \mathcal{L}_k = \mathcal{L}$. According to Lemma 3, we can let $U_c^T \mathcal{L}_k U_c = \begin{bmatrix} 0 & l_k^T \\ 0 & \hat{L}_k \end{bmatrix}$, $U_c^T \mathcal{L} U_c = \begin{bmatrix} 0 & l^T \\ 0 & \hat{L} \end{bmatrix}$, where U_c is given as therein. Then $\sum_{k=1}^M \hat{L}_k = \hat{L}$. Furthermore, it is important to point out that even when the topology $\mathcal{G}(\mathcal{A})$ is undirected, \mathcal{L}_k is unnecessarily symmetric due to $\tau_{ij}(\cdot) \neq \tau_{ji}(\cdot)$. Consequently, the results of [4, 14, 19, 20] are invalid to deal with the consensus problem for MAS with asymmetric communication delays.

Applying the orthogonal linear transformation $x(t) = (U_c \otimes I_m)y(t)$ to the system (7) and denoting $y(t) = [y_1^T(t) \ y_2^T(t)]^T$ with $y_1(t) \in \mathbb{R}^m$ and $y_2(t) \in \mathbb{R}^{(N-1)m}$, we have

$$\dot{y}_1(t) = E_m y_1(t) - \sum_{k=1}^M (\kappa_0 l_k^T \otimes F_m) y_2(t - \tau_k(t)), \quad (10)$$

$$\dot{y}_2(t) = (I_{N-1} \otimes E_m) y_2(t) - \sum_{k=1}^M (\kappa_0 \hat{L}_k \otimes F_m) y_2(t - \tau_k(t)), \quad (11)$$

where l_k and \hat{L}_k are defined as in Remark 6. It can be seen that the system (11) is independent of the dynamics of $y_1(t)$ and has the order $(N-1)m$; the system (10) can be regarded as a forced system with the forced motion caused by the delayed state of $y_2(t)$. From $U_c = [(1/\sqrt{N})\mathbf{1}_N \ \hat{U}]$ and some direct computation, it follows that

$$x(t) = (U_c \otimes I_m) y(t) = \frac{1}{\sqrt{N}} \mathbf{1}_N \otimes y_1(t) + (\hat{U} \otimes I_m) y_2(t). \quad (12)$$

In addition, Proposition 7 will indicate that $y_2(t)$ can be considered as the disagreement state of the system (7). Note that, for the time delay system in (10) and (11), we assume that the initial state is $\phi(t) = (U_c^T \otimes I_m)x(0) \triangleq [y_{10}^T \ y_{20}^T]^T$, $t \in [-\tau_0, 0]$, where $y_{10} \in \mathbb{R}^m$, $y_{20} \in \mathbb{R}^{(N-1)m}$, and τ_0 is given in (7).

We are now in a position to present an equivalent condition for the consensus convergence of the system (7).

Proposition 7. *Consider the system (7) with topology $\mathcal{G}(\mathcal{A})$. The system solves a consensus problem asymptotically if and only if each solution of the reduced-order system (11) converges to zero.*

Proof. Necessity. Suppose that $y_2(t)$ is any solution of the system (11) with initial state $\phi_2(t) = y_{20} \in \mathbb{R}^{(N-1)m}$,

$t \in [-\tau_0, 0]$. Let $y_1(t) \in \mathbb{R}^m$ be continuously differentiable and satisfy the dynamics (10) with initial state y_{10} . From (12), it follows that $x(t) = (1/\sqrt{N})\mathbf{1}_N \otimes y_1(t) + (\hat{U} \otimes I_m)y_2(t)$ is a solution of the system (7) with initial state $\phi(t) = (U_c \otimes I_m)[y_{10}^T \ y_{20}^T]^T$, $t \in [-\tau_0, 0]$. Denote $(\hat{U} \otimes I_m)y_2(t) = [z_1^T(t) \ \dots \ z_N^T(t)]^T$ with $z_i(t) \in \mathbb{R}^m$, $i \in \underline{N}$. Then (12) implies that $z_j(t) - z_1(t) = x_j(t) - x_1(t)$, $j = 2, \dots, N$, where $x_j(t)$ is the state of agent j . If the system (7) solves a consensus problem asymptotically, then $x_j(t) - x_1(t) \rightarrow 0$ as $t \rightarrow \infty$, $j = 2, \dots, N$. Hence $z_j(t) - z_1(t) \rightarrow 0$ as $t \rightarrow \infty$, $j = 2, \dots, N$, which is equivalent to $(\hat{U} \otimes I_m)y_2(t) = [z_1^T(t) \ \dots \ z_N^T(t)]^T \rightarrow \mathbf{1}_N \otimes z_1(t)$. Due to $\hat{U}^T \hat{U} = I_{N-1}$ and $\hat{U}^T \mathbf{1}_N = 0$, $y_2(t) = (\hat{U}^T \otimes I_m)(\hat{U} \otimes I_m)y_2(t) \rightarrow (\hat{U}^T \otimes I_m)(\mathbf{1}_N \otimes z_1(t)) = 0$. Hence each solution of the system (11) converges to zero.

Sufficiency. Suppose that each solution of the system (11) converges to zero, and $x(t)$ is the solution of the system (7) with any initial state $\phi(t) = x(0)$, $t \in [-\tau_0, 0]$. Let $y(t) = (U_c^T \otimes I_m)x(t) \triangleq [y_1^T(t) \ y_2^T(t)]^T$, where $y_1(t) \in \mathbb{R}^m$, $y_2(t) \in \mathbb{R}^{(N-1)m}$. Then $y(t)$ is a solution of the systems (10) and (11) with initial state $\phi(t) = (U_c^T \otimes I_m)x(0)$, $t \in [-\tau_0, 0]$. The assumption implies that $y_2(t) \rightarrow 0$ as $t \rightarrow \infty$. Due to (12), $\lim_{t \rightarrow \infty} x_i(t) = (1/\sqrt{N})\lim_{t \rightarrow \infty} y_1(t)$, $i \in \underline{N}$ in which $y_1(t)$ evolves according to (10). This indicates that the system (7) solves a consensus problem asymptotically with the consensus state $(1/\sqrt{N})\lim_{t \rightarrow \infty} y_1(t)$. \square

Remark 8. It should be pointed out that the orthogonal linear transformation $x(t) = (U_c \otimes I_m)y(t)$ is not uniquely defined by U_c . Actually, any orthogonal matrix with the first column being $(1/\sqrt{N})\mathbf{1}_N$ also can derive the result of Proposition 7. In addition, the above orthogonal linear transformation can be seen as an improvement of the transformation on disagreement space which was displayed in Lemma 5.2 of [20].

Remark 9. In contrast to the transformation (7) of [15] and the tree-type transformation of [16], the order of the reduced-order system (11) induced by the orthogonal linear transformation $x(t) = (U_c \otimes I_m)y(t)$ is lower than those of the reduced-order systems induced by them (in the context that all of the three transformations are applied to the system (7)). It is easy to see that the order of the reduced-order system (11) is $Nm - m$, whereas the order of the reduced-order system which is derived from the transformation (7) of [15] (or the tree-type transformation of [16]) is $Nm - 1$. Seen from the linear-matrix-inequality-based sufficient conditions which will be given in Theorem 12, our orthogonal linear transformation can derive lower-order linear matrix inequalities. This will reduce the computation cost to some extent when estimating the maximum allowable upper bound τ_0 of time-varying delays.

Before presenting the main result, the following lemmas are introduced to give the parameter design of protocol (3).

Lemma 10. Consider E_m and F_m in (5). Suppose that E_m has only one zero eigenvalue and other nonzero eigenvalues have negative real parts, and $\kappa_0 > 0$ is a constant. Let $\widehat{Q}_1 = \text{diag}\{0, q_2, \dots, q_m\}$ with $q_i > 0$, $i = 2, \dots, m$; $P_m = [p_{ij}] \in \mathbb{R}_m$ is a positive definite solution of the Lyapunov equation $E_m^T P_m + P_m E_m = -\widehat{Q}_1$; $z = \alpha + \sqrt{-1}\beta$ is a complex number with $\alpha > 0$; $D_z = \begin{bmatrix} \alpha & \beta \\ -\beta & \alpha \end{bmatrix}$. Then $(I_2 \otimes E_m - \kappa_0 D_z \otimes F_m)^T (I_2 \otimes P_m) + (I_2 \otimes P_m)(I_2 \otimes E_m - \kappa_0 D_z \otimes F_m) < 0$ if and only if

$$\kappa_0 < \frac{2\alpha p_{1m}}{(\alpha^2 + \beta^2) \sum_{i=2}^m (p_{im}^2/q_i)}. \quad (13)$$

In particular, when $\beta = 0$, $(E_m - \kappa_0 \alpha F_m)^T P_m + P_m (E_m - \kappa_0 \alpha F_m) < 0$ if and only if $\kappa_0 < 2p_{1m}/\alpha \sum_{i=2}^m (p_{im}^2/q_i)$.

Proof. See the Appendix: Proofs of Lemmas. \square

Lemma 11. Suppose that $\mathcal{G}(\mathcal{A})$ contains a spanning tree; the associated Laplacian matrix is \mathcal{L} , $U_c^T \mathcal{L} U_c = \begin{bmatrix} 0 & I^T \\ 0 & \widehat{L} \end{bmatrix}$; the parameters c_i , $i \in \underline{m-1}$ are chosen such that E_m has only one zero eigenvalue and other nonzero eigenvalues have negative real parts; $\widehat{Q}_1 = \text{diag}\{0, q_2, \dots, q_m\}$ with $q_i > 0$, $i = 2, \dots, m$, and $P_m = [p_{ij}] \in \mathbb{R}_m$ is a positive definite solution of the Lyapunov equation $E_m^T P_m + P_m E_m = -\widehat{Q}_1$. If

$$0 < \kappa_0 < \min \left\{ \frac{2rp_{1m}}{(r^2 + d^2) \sum_{i=2}^m (p_{im}^2/q_i)}, \frac{4p_{1m}}{5d \sum_{i=2}^m (p_{im}^2/q_i)} \right\}, \quad (14)$$

then $I_{N-1} \otimes E_m - \kappa_0 \widehat{L} \otimes F_m$ is Huiwitz stable, where $r = \min\{\text{Re}(\lambda) : \lambda \in \sigma(\mathcal{L}) \setminus \{0\}\}$ and $d = \max_{i \in \underline{N}} \{d_i\}$ is the maximum vertex in-degree over $\mathcal{G}(\mathcal{A})$.

Proof. See the Appendix: Proofs of Lemmas. \square

By choosing the parameters c_i , $i \in \underline{m-1}$ and κ_0 as in Lemma 11 and making use of Proposition 7, we can obtain the following theorem.

Theorem 12. Consider the system (7) with fixed topology $\mathcal{G}(\mathcal{A})$. Suppose that $\mathcal{G}(\mathcal{A})$ contains a spanning tree; the associated Laplacian matrix \mathcal{L} has the form of $U_c^T \mathcal{L} U_c = \begin{bmatrix} 0 & I^T \\ 0 & \widehat{L} \end{bmatrix}$, where U_c is given as in Lemma 3; the parameters c_i , $i \in \underline{m-1}$ and κ_0 are chosen as in Lemma 11. Then the system solves a consensus problem asymptotically if the time-varying delays satisfy $\tau_{ij}(t) \leq \tau_0$, where τ_0 is obtained from the following optimization problem:

$$\begin{aligned} & \text{maximize} \quad \tau_0 \\ & \text{subject to} \quad \begin{bmatrix} G^T P + PG & PH & \Phi_{13} \\ * & 0 & \Phi_{23} \\ * & * & 0 \end{bmatrix} \\ & \quad < \tau_0^{-1} \text{diag}\{0, \Phi_0, \Phi_0\}, \\ & \quad P > 0, \quad Q_k > 0, \quad k = 1, \dots, M, \end{aligned} \quad (15)$$

where

$$\begin{aligned} G &= I_{N-1} \otimes E_m - \kappa_0 \widehat{L} \otimes F_m, \\ H &= [\kappa_0 \widehat{L}_1 \otimes F_m \cdots \kappa_0 \widehat{L}_M \otimes F_m], \\ \Phi_{13} &= [G^T Q_1 \cdots G^T Q_M], \\ \Phi_{23} &= [H^T Q_1 \cdots H^T Q_M], \\ \Phi_0 &= \text{diag}\{Q_1, \dots, Q_M\}, \end{aligned} \quad (16)$$

and “*” represents the elements below the main diagonal of a symmetric matrix.

Proof. We first show that there must exist some positive definite matrices P and Q_k such that the first LMI in (15) is solvable. From the selection of protocol parameters and Lemma 11, we know that G is Hurwitz stable. Hence there is a positive definite matrix \tilde{P} such that $G^T \tilde{P} + \tilde{P} G < 0$. By Lemma 5, the first LMI in (15) is equivalent to

$$\underbrace{\begin{bmatrix} G^T P + PG & PH \\ * & -\tau_0^{-1} \Phi_0 \end{bmatrix}}_{\triangleq \Sigma_1} + \left(\mathbf{1}_M^T \otimes \begin{bmatrix} G^T \\ H^T \end{bmatrix} \right) \tau_0 \Phi_0 \times (\mathbf{1}_M \otimes [G \ H]) < 0, \quad (17)$$

and $\Sigma_1 < 0$ is equivalent to $G^T P + PG + \tau_0 PH \Phi_0^{-1} H^T P < 0$. Consequently, if we choose $P = \tilde{P}$, $Q_k = I_{(N-1)m}$, $k = 1, \dots, M$, then for some sufficiently small τ_0 , $G^T \tilde{P} + \tilde{P} G + \tau_0 \tilde{P} H H^T \tilde{P} < 0$ holds. This means that $P = \tilde{P}$ and $Q_k = I_{(N-1)m}$ satisfy the LMIs in (15).

According to Proposition 7, it suffices to prove that the zero solution of the reduced-order system (11) is asymptotically stable under the condition (15). To do this, consider the following Lyapunov-Krasovskii functional candidate:

$$\begin{aligned} V(y_2(t)) &= y_2^T(t) P y_2(t) \\ &+ \sum_{k=1}^M \int_{-\tau_k}^0 \int_{t+\theta}^t \dot{y}_2^T(s) Q_k \dot{y}_2(s) ds d\theta. \end{aligned} \quad (18)$$

Note that Remark 6 implies that $\sum_{k=1}^M \hat{L}_k = \hat{L}$. Then the time derivative of $V(y_2(t))$ along the trajectory of (11) is

$$\begin{aligned}
\dot{V}(y_2(t)) &= 2y_2^T(t) P \dot{y}_2(t) \\
&\quad + \sum_{k=1}^M \left[\tau_k \dot{y}_2^T(t) Q_k \dot{y}_2(t) \right. \\
&\quad \quad \left. - \int_{-\tau_k}^0 \dot{y}_2^T(t+\theta) Q_k \dot{y}_2(t+\theta) d\theta \right] \\
&= 2y_2^T(t) P G y_2(t) \\
&\quad + 2y_2^T(t) P \left[\sum_{k=1}^M \kappa_0 (\hat{L}_k \otimes F_m) \right. \\
&\quad \quad \left. \times (y_2(t) - y_2(t - \tau_k(t))) \right] \\
&\quad + \sum_{k=1}^M \left[\tau_k \dot{y}_2^T(t) Q_k \dot{y}_2(t) \right. \\
&\quad \quad \left. - \int_{-\tau_k}^0 \dot{y}_2^T(t+\theta) Q_k \dot{y}_2(t+\theta) d\theta \right] \\
&\leq 2y_2^T(t) P G y_2(t) \\
&\quad + 2y_2^T(t) P \left[\sum_{k=1}^M \kappa_0 (\hat{L}_k \otimes F_m) \right. \\
&\quad \quad \left. \times (y_2(t) - y_2(t - \tau_k(t))) \right] \\
&\quad + \sum_{k=1}^M \left[\tau_k \dot{y}_2^T(t) Q_k \dot{y}_2(t) \right. \\
&\quad \quad \left. - \int_{t-\tau_k(t)}^t \dot{y}_2^T(s) Q_k \dot{y}_2(s) ds \right] \\
&\leq 2y_2^T(t) P G y_2(t) \\
&\quad + 2y_2^T(t) P \left[\sum_{k=1}^M \kappa_0 (\hat{L}_k \otimes F_m) \right. \\
&\quad \quad \left. \times (y_2(t) - y_2(t - \tau_k(t))) \right] \\
&\quad + \sum_{k=1}^M \left\{ \tau_k \dot{y}_2^T(t) Q_k \dot{y}_2(t) \right. \\
&\quad \quad \left. - \tau_k^{-1} [y_2(t) - y_2(t - \tau_k(t))]^T \right. \\
&\quad \quad \left. \times Q_k [y_2(t) - y_2(t - \tau_k(t))] \right\}, \tag{19}
\end{aligned}$$

where G is given as in (15). Let $z_k(t) = y_2(t) - y_2(t - \tau_k(t))$ and replace $\dot{y}_2(t)$ with the right-hand term of (11). It follows that

$$\begin{aligned}
\dot{V}(y_2(t)) &\leq 2y_2^T(t) P G y_2(t) \\
&\quad + 2y_2^T(t) P \left[\sum_{k=1}^M \kappa_0 (\hat{L}_k \otimes F_m) z_k(t) \right] \\
&\quad - \sum_{k=1}^M \tau_0^{-1} z_k^T(t) Q_k z_k(t) \\
&\quad + \sum_{k=1}^M \left\{ \tau_0 \left[G y_2(t) \right. \right. \\
&\quad \quad \left. \left. + \sum_{k=1}^M \kappa_0 (\hat{L}_k \otimes F_m) z_k(t) \right]^T \right. \\
&\quad \quad \left. \times Q_k \left[G y_2(t) \right. \right. \\
&\quad \quad \left. \left. + \sum_{k=1}^M \kappa_0 (\hat{L}_k \otimes F_m) z_k(t) \right] \right\} \\
&= [y_2^T(t) Z^T(t)] \\
&\quad \times \left\{ \begin{bmatrix} G^T P + PG & PH \\ * & -\tau_0^{-1} \Phi_0 \end{bmatrix} \right. \\
&\quad \quad \left. + \begin{bmatrix} G^T & \cdots & G^T \\ H^T & \cdots & H^T \end{bmatrix} \tau_0 \Phi_0 \begin{bmatrix} G & H \\ \vdots & \vdots \\ G & H \end{bmatrix} \right\} \begin{bmatrix} y_2(t) \\ Z(t) \end{bmatrix} \\
&= [y_2^T(t) Z^T(t)] \\
&\quad \times \left\{ \begin{bmatrix} G^T P + PG & PH \\ * & -\tau_0^{-1} \Phi_0 \end{bmatrix} \right. \\
&\quad \quad \left. - \begin{bmatrix} \Phi_{13} \\ \Phi_{23} \end{bmatrix} (-\tau_0^{-1} \Phi_0)^{-1} [\Phi_{13}^T \Phi_{23}^T] \right\} \begin{bmatrix} y_2(t) \\ Z(t) \end{bmatrix}, \tag{20}
\end{aligned}$$

where $Z(t) = [z_1^T(t) \cdots z_M^T(t)]^T$; H , Φ_0 , Φ_{13} , and Φ_{23} are given as in (15). From Lemma 5 and (15), we have $\dot{V}(y_2(t)) < 0$. Hence there exists a positive real number a_0 such that

$$\begin{aligned}
\dot{V}(y_2(t)) &< -a_0 [y_2^T(t) y_2(t) + Z^T(t) Z(t)] \\
&< -a_0 y_2^T(t) y_2(t). \tag{21}
\end{aligned}$$

This proves that the zero solution of the reduced-order system (11) is asymptotically stable. Thus the conclusion holds. \square

Remark 13. From the proof of Theorem 12, it can be seen that the parameter design of protocol (3) in the theorem (i.e., the selection of c_i , $i \in \underline{m-1}$, and κ_0) guarantees the solvability of the LMIs in (15). According to the nature of the parameter design (see Lemma 11), we refer to it as a *Lyapunov-like parameter design*.

In Lemma 11, when $\mathcal{G}(\mathcal{A})$ is undirected and connected, \hat{L} is positive definite. Hence $\lambda_i \in \sigma(\mathcal{L}) \setminus \{0\}$, $i = 2, \dots, N$, are positive real numbers, $r = \min\{\lambda_2, \dots, \lambda_N\}$ and $r \leq \lambda_i \leq 2d$. In this case, for any $\kappa_0 : 0 < \kappa_0 < \min\{2p_{1m}/r \sum_{i=2}^m (p_{im}^2/q_i), p_{1m}/d \sum_{i=2}^m (p_{im}^2/q_i)\} = p_{1m}/d \sum_{i=2}^m (p_{im}^2/q_i)$, $G = I_{N-1} \otimes E_m - \kappa_0 \hat{L} \otimes F_m$ is Hurwitz stable. From Lemma 10, it follows that when $0 < \kappa_0 < p_{1m}/d \sum_{i=2}^m (p_{im}^2/q_i)$, $(E_m - \kappa_0 \lambda_i F_m)^T P_m + P_m (E_m - \kappa_0 \lambda_i F_m) < 0$ for any $\lambda_i \in \sigma(\mathcal{L}) \setminus \{0\}$. Since \hat{L} is positive definite, there is an orthogonal matrix S such that $S^T \hat{L} S = \text{diag}\{\lambda_2, \dots, \lambda_N\}$. Thus when $0 < \kappa_0 < p_{1m}/d \sum_{i=2}^m (p_{im}^2/q_i)$, $G^T(I_{N-1} \otimes P_m) + (I_{N-1} \otimes P_m)G = (S \otimes I_m)[(I_{N-1} \otimes E_m - \kappa_0 \text{diag}\{\lambda_2, \dots, \lambda_N\} \otimes F_m)^T(I_{N-1} \otimes P_m) + (I_{N-1} \otimes P_m)(I_{N-1} \otimes E_m - \kappa_0 \text{diag}\{\lambda_2, \dots, \lambda_N\} \otimes F_m)](S^T \otimes I_m) < 0$. In the light of the proof of Theorem 12, the inequalities in (15) hold by taking $P = I_{N-1} \otimes P_m$, $Q_k = I_{(N-1)m}$, and sufficiently small τ_0 . This result can be summarized as the following corollary.

Corollary 14. Consider the system (7) with fixed topology $\mathcal{G}(\mathcal{A})$. Suppose that $\mathcal{G}(\mathcal{A})$ is undirected and connected; the parameters c_i , $i \in \underline{m-1}$, are chosen such that E_m has only one zero eigenvalue and other nonzero eigenvalues have negative real parts; $\hat{Q}_1 = \text{diag}\{0, q_2, \dots, q_m\}$ with $q_i > 0$, $i = 2, \dots, m$, and $P_m = [p_{ij}] \in \mathbb{R}_m$ is a positive definite solution of the Lyapunov equation $E_m^T P_m + P_m E_m = -\hat{Q}_1$; κ_0 satisfies

$$0 < \kappa_0 < \frac{p_{1m}}{d \sum_{i=2}^m (p_{im}^2/q_i)}, \quad (22)$$

where $d = \max_{i \in N} \{d_i\}$ is the maximum vertex in-degree over $\mathcal{G}(\mathcal{A})$. Then the system solves a consensus problem asymptotically if the time-varying delays satisfy $\tau_{ij}(t) \leq \tau_0$, where τ_0 is obtained from (15) with $P = I_{N-1} \otimes P_m$ and $Q_k = I_{(N-1)m}$.

Remark 15. Corollary 14 indicates that the selection of parameters c_i , $i \in \underline{m-1}$, and κ_0 is independent of the eigenvalues of Laplacian matrix but only depends on the maximum vertex in-degree of the graph. It will reduce greatly the computation and storage costs for the protocol design of practical MAS. Therefore, we can say that the parameter design in Theorem 12 is independent of the precise interaction topology when the underlying graph is connected and guarantees the robust consensus with respect to asymmetric time-varying delays for the high-order MAS (7).

Remark 16. It is worth pointing out that the results of [19] can not be applied to the high-order MAS straightforwardly, since the parameters c_j , $j \in \underline{m-1}$, and κ_0 have important effect on the consensus of the system. Whereas the Lyapunov-like parameter design given in Theorem 12 can solve the consensus problem for the high-order MAS (7) very well.

Remark 17. Compared with the existing results, the main contribution of this paper is giving the Lyapunov-like parameter design which is easy to implement, independent of the precise interaction topology for the case of connected graphs, and robust with respect to asymmetric time-varying delays. Moreover, the parameter design can guarantee the existence of solution of the linear matrix inequalities given in Theorem 12, although it seems that the estimations of τ_0 are conservative. More excellent estimation on the maximum allowable upper bound of time-varying delays is a commonly unsolved problem. This requires us to explore other analysis techniques which could reduce the dependence of that estimation on the knowledge of network topology.

4. Numerical Examples

Consider the system (7) of six agents with dynamics described by a triple-order integrator. The interaction topology among agents is depicted by a cycle with the arcs (v_1, v_2) , (v_2, v_3) , (v_3, v_4) , (v_4, v_5) , (v_5, v_6) , (v_6, v_1) . Assume that the weights of the arcs are $a_{21} = a_{32} = a_{43} = a_{54} = a_{65} = a_{16} = 1$ and the communication delays affecting on the linkages are different from each other. Then the maximum vertex in-degree of the graph is $d = 1$, and the minimum real part of nonzero eigenvalues of the associated Laplacian matrix is $r = 1/2$.

In what follows, we design the protocol parameters c_1 , c_2 , and κ_0 according to Theorem 12 (or Lemma 11).

It is not hard to obtain that the characteristic polynomial of E_3 in the system (7) is $s(s^2 + c_2 s + c_1)$. Then any positive numbers c_1 and c_2 make E_3 satisfy the assumption in Lemma 11. Let $P_3 = [p_{ij}] \in \mathbb{R}_3$ and $\hat{Q}_1 = \text{diag}\{0, q_2, q_3\}$ with $q_2 > 0$, $q_3 > 0$. By solving $E_3^T P_3 + P_3 E_3 = -\hat{Q}_1$, we have $p_{11} = c_1 p_{13}$, $p_{12} = c_2 p_{13}$, $p_{22} = (c_2^2/c_1) p_{13} + (c_2/2c_1 + 1/2c_2) q_2 + (c_1/2c_2) q_3$, $p_{23} = (c_2/c_1) p_{13} + (1/2c_1) q_2$, and $p_{33} = (1/c_1) p_{13} + (1/2c_1 c_2) q_2 + (1/2c_2) q_3$. As a result, the 1-by-1, 2-by-2, and 3-by-3 leading principle minors of P_3 are, respectively, $c_1 p_{13}$, $c_1 p_{13}(((c_2 + 1)/2c_1) q_2 + (c_1/2c_2) q_3)$, and $(1/4) p_{13} [q_2 q_3 + (1/c_2^2)(q_2 + c_1 q_3)^2]$. Hence P_3 is positive definite for any $p_{13} > 0$. If we take $q_2 = 2c_2 p_{13}$, $q_3 = (4c_2/c_1) p_{13}$ with $p_{13} > 0$, then the condition (14) becomes $0 < \kappa_0 < \min\{rc_1^2 c_2/(r^2 + d^2)(2c_1 + c_2^2), 2c_1^2 c_2/5d(2c_1 + c_2^2)\}$. Thus when $c_1 = 24$ and $c_2 = 8$, the constraint on κ_0 can be calculated as $0 < \kappa_0 < 576/35 \approx 16.4571$. We choose $c_1 = 24$, $c_2 = 8$, and $\kappa_0 = 5$ for the simulation.

With the parameters chosen as above and by solving the optimization problem in (15), we can obtain that the maximum allowable upper bound of time-delays is $\tau_0 = 1.2305$. Assume that $\tau_{21}(t) \leq 0.4$, $\tau_{32}(t) \leq 0.6$, $\tau_{43}(t) \leq 0.9$, $\tau_{54}(t) \leq 0.7$, $\tau_{65}(t) \leq 0.5$, and $\tau_{16}(t) \leq 0.8$, all of which are piecewise constant functions of time t . The states of agents in the system (7) asymptotically reach consensus as shown in Figure 1.

5. Conclusions

This paper has studied the consensus problem for high-order MAS with directed network and asymmetric time-varying

communication delays. An equivalent condition for the consensus convergence has been established based on an orthogonal linear transformation. A Lyapunov-like protocol design has been given, which is robust with respect to asymmetric time-varying communication delays and directed interactions. The maximum allowable upper bounds of delays have been determined by solving some optimization problems. Finally, numerical examples have been worked out to demonstrate the effectiveness of the theoretical results.

Appendix

Proofs of Lemmas

Proof of Lemma 3. From the property of U_c , let $U_c = [(1/\sqrt{N})\mathbf{1}_N \ v_2 \ \cdots \ v_N]$ and $\widehat{U} = [v_2 \ \cdots \ v_N]$. Then $\mathcal{L}\mathbf{1}_N = 0$ implies that

$$\begin{aligned} U_c^T \mathcal{L} U_c &= \begin{bmatrix} \frac{1}{\sqrt{N}} \mathbf{1}_N^T \\ v_2^T \\ \vdots \\ v_N^T \end{bmatrix} [0 \ \mathcal{L} v_2 \ \cdots \ \mathcal{L} v_N] \\ &= \begin{bmatrix} 0 & \frac{1}{\sqrt{N}} \mathbf{1}_N^T \mathcal{L} v_2 & \cdots & \frac{1}{\sqrt{N}} \mathbf{1}_N^T \mathcal{L} v_N \\ 0 & v_2^T \mathcal{L} v_2 & \cdots & v_2^T \mathcal{L} v_N \\ \vdots & \vdots & \ddots & \vdots \\ 0 & v_N^T \mathcal{L} v_2 & \cdots & v_N^T \mathcal{L} v_N \end{bmatrix}. \end{aligned} \quad (\text{A.1})$$

Denote that $l = [(1/\sqrt{N})\mathbf{1}_N^T \mathcal{L} v_2 \ \cdots \ (1/\sqrt{N})\mathbf{1}_N^T \mathcal{L} v_N]^T$ and $\widehat{L} = \widehat{U}^T \mathcal{L} \widehat{U}$. Then $U_c^T \mathcal{L} U_c$ is in the form of $\begin{bmatrix} 0 & l^T \\ 0 & \widehat{L} \end{bmatrix}$. Due to the fact that $U_c^T = U_c^{-1}$ and similarity transformation does not change the eigenvalues of matrix, $\sigma(\mathcal{L}) = \{0\} \cup \sigma(\widehat{L})$. It follows that $\sigma(\widehat{L}) \subset \sigma(\mathcal{L})$. If \mathcal{G} is balanced, then $\mathbf{1}_N^T \mathcal{L} = 0$. Thus $l = [(1/\sqrt{N})\mathbf{1}_N^T \mathcal{L} v_2 \ \cdots \ (1/\sqrt{N})\mathbf{1}_N^T \mathcal{L} v_N]^T = 0$. If \mathcal{G} is strongly connected and balanced, according to Theorem 7 in [4], we obtain that $(\mathcal{L}^T + \mathcal{L})/2$ is a valid Laplacian matrix of an undirected graph. Then the strong connectivity of \mathcal{G} implies that the corresponding graph of $(\mathcal{L}^T + \mathcal{L})/2$ is connected. Hence $(\mathcal{L}^T + \mathcal{L})/2$ is positive semidefinite and its rank is $N - 1$. This proves that $\widehat{L}^T + \widehat{L}$ is positive definite. \square

Proof of Lemma 10. Denote $x = [x_1 \ \cdots \ x_m]^T \in \mathbb{R}^m$. Since $x^T P_m E_m x$ is a scalar, we can write $-x^T \widehat{Q}_1 x = -(q_2 x_2^2 + \cdots + q_m x_m^2) = x^T (E_m^T P_m + P_m E_m) x = 2x^T P_m E_m x = 2[x_2(p_{11}x_1 + \cdots + p_{m1}x_m) + \cdots + x_m(p_{1(m-1)}x_1 + \cdots + p_{m(m-1)}x_m) + (-c_1x_2 - c_2x_3 - \cdots - c_{m-1}x_m)(p_{1m}x_1 + \cdots + p_{mm}x_m)]$. The coefficient of the term x_1x_2 in $2x^T P_m E_m x$ is $2(p_{11} - c_1p_{1m})$. From the equality of the left-hand and right-hand coefficients in $-x^T \widehat{Q}_1 x = x^T (E_m^T P_m + P_m E_m) x$, we have $p_{11} = c_1p_{1m}$. Notice that $p_{11} > 0$ due to P_m being positive definite. Then $c_1 > 0$ implies that $p_{1m} > 0$.

Let $\widehat{Q}_2 = -(I_2 \otimes E_m - \kappa_0 D_z \otimes F_m)^T (I_2 \otimes P_m) - (I_2 \otimes P_m) (I_2 \otimes E_m - \kappa_0 D_z \otimes F_m)$. In what follows, we only need to prove that \widehat{Q}_2 is positive definite when κ_0 satisfies (13). By directly computing, we obtain

$$\widehat{Q}_2 = \begin{bmatrix} 2\kappa_0\alpha p_{1m} & \kappa_0\alpha p_{2m} & \cdots & \kappa_0\alpha p_{mm} & \vdots & 0 & -\kappa_0\beta p_{2m} & \cdots & -\kappa_0\beta p_{mm} \\ \kappa_0\alpha p_{2m} & q_2 & \cdots & 0 & \vdots & \kappa_0\beta p_{2m} & 0 & \cdots & 0 \\ & & \ddots & & \vdots & & & \ddots & \\ \kappa_0\alpha p_{mm} & 0 & \cdots & q_m & \vdots & \kappa_0\beta p_{mm} & 0 & \cdots & 0 \\ \cdots & \cdots & \cdots & \cdots & \cdots & \cdots & \cdots & \cdots & \cdots \\ 0 & \kappa_0\beta p_{2m} & \cdots & \kappa_0\beta p_{mm} & \vdots & 2\kappa_0\alpha p_{1m} & \kappa_0\alpha p_{2m} & \cdots & \kappa_0\alpha p_{mm} \\ -\kappa_0\beta p_{2m} & 0 & \cdots & 0 & \vdots & \kappa_0\alpha p_{2m} & q_2 & \cdots & 0 \\ & & \ddots & & \vdots & & & \ddots & \\ -\kappa_0\beta p_{mm} & 0 & \cdots & 0 & \vdots & \kappa_0\alpha p_{mm} & 0 & \cdots & q_m \end{bmatrix}. \quad (\text{A.2})$$

Denote the k -by- k leading principle minor of \widehat{Q}_2 by $\widehat{Q}_2(k)$. For $\widehat{Q}_2(1), \dots, \widehat{Q}_2(m)$, it follows by expanding them with respect to their last rows, respectively, that

$$\widehat{Q}_2(k) = \kappa_0\alpha \left(\prod_{i=2}^k q_i \right) \left[2p_{1m} - \kappa_0\alpha \left(\sum_{i=2}^k \frac{p_{im}^2}{q_i} \right) \right],$$

$$k = 2, \dots, m.$$

$$\widehat{Q}_2(1) = \kappa_0\alpha(2p_{1m}), \quad (\text{A.3})$$

For $\widehat{Q}_2(m+k)$, $k = 1, \dots, m$, we first multiply the first row and the first column by $-\beta/\alpha$ and add to the $(m+1)$ th row and the $(m+1)$ th column, respectively. Then multiply, respectively, the second, third, \dots , m th, and $(m+1)$ th column by $-\kappa_0\alpha p_{2m}/q_2, -\kappa_0\alpha p_{3m}/q_3, \dots, -\kappa_0\alpha p_{mm}/q_m$, and $\alpha\beta/(\alpha^2 + \beta^2)$; add all of them to the first column. At last, expanding the resultant determinant with respect to the first column and making use of the results of $\widehat{Q}_2(k)$, $k = 1, \dots, m$, we have

$$\begin{aligned} \widehat{Q}_2(m+1) &= 2\kappa_0^2\alpha p_{1m} \prod_{i=2}^m q_i \left[2\alpha p_{1m} - \kappa_0(\alpha^2 + \beta^2) \left(\sum_{i=2}^m \frac{p_{im}^2}{q_i} \right) \right], \\ \widehat{Q}_2(m+k) &= \kappa_0^2 \prod_{i=2}^m q_i \left[2\alpha p_{1m} - \kappa_0(\alpha^2 + \beta^2) \left(\sum_{i=2}^m \frac{p_{im}^2}{q_i} \right) \right] \\ &\quad \times \prod_{i=2}^k q_i \left[2\alpha p_{1m} - \kappa_0(\alpha^2 + \beta^2) \left(\sum_{i=2}^k \frac{p_{im}^2}{q_i} \right) \right], \\ &\quad k = 2, \dots, m. \end{aligned} \quad (\text{A.4})$$

Hence \widehat{Q}_2 is positive definite if and only if $\widehat{Q}_2(k) > 0$ for all $k = 1, \dots, 2m$. From the assumption, it is easy to see that $\widehat{Q}_2(1) > 0$. Since P_m is positive definite, $p_{mm} > 0$. As a result, $\sum_{i=2}^m (p_{im}^2/q_i) > 0$. In addition, it is not hard to get $\sum_{i=2}^k (p_{im}^2/q_i) = 0$ if and only if $p_{2m} = \dots = p_{km} = 0$. Consider $\widehat{Q}_2(2), \dots, \widehat{Q}_2(m)$. Suppose that $k' \in \{2, \dots, m-1\}$ which satisfies $p_{2m} = \dots = p_{k'm} = 0$ and $p_{(k'+1)m} \neq 0$. Then we have $\sum_{i=2}^k (p_{im}^2/q_i) = 0$ for $k = 2, \dots, k'$ and $\sum_{i=2}^k (p_{im}^2/q_i) > 0$ for $k = k' + 1, \dots, m$. Consequently, $\widehat{Q}_2(2) > 0, \dots, \widehat{Q}_2(k') > 0$ for any $\kappa_0 > 0$, and $\widehat{Q}_2(k' + 1) > 0, \dots, \widehat{Q}_2(m) > 0$ if and only if $\kappa_0 < 2p_{1m}/\alpha \sum_{i=2}^m (p_{im}^2/q_i)$. Next, consider $\widehat{Q}_2(m+1), \dots, \widehat{Q}_2(2m)$. It is evident that $\widehat{Q}_2(m+1) > 0$ if and only if κ_0 satisfies (13). Following the similar guidelines of the proof of $\widehat{Q}_2(2), \dots, \widehat{Q}_2(m)$, we have $\widehat{Q}_2(m+2) > 0, \dots, \widehat{Q}_2(2m) > 0$ if and only if κ_0 satisfies (13). By summing up the discussion above and making use of the fact that $\alpha/(\alpha^2 + \beta^2) \leq 1/\alpha$, we obtain the first conclusion. The second conclusion follows directly from the first one. \square

To prove Lemma 11, we introduce the following result.

Lemma A.1 (see Theorem 4.6 in [20]). Consider E_m and F_m in (5). Suppose graph $\mathcal{G}(\mathcal{A})$ contains a spanning tree; the associated Laplacian matrix is \mathcal{L} , $U_c^T \mathcal{L} U_c = \begin{bmatrix} 0 & 1 \\ 0 & \widehat{\mathcal{L}} \end{bmatrix}$ (U_c is given as in Lemma 3); the parameters c_i , $i \in m-1$, are chosen such that E_m has only one zero eigenvalue and other nonzero

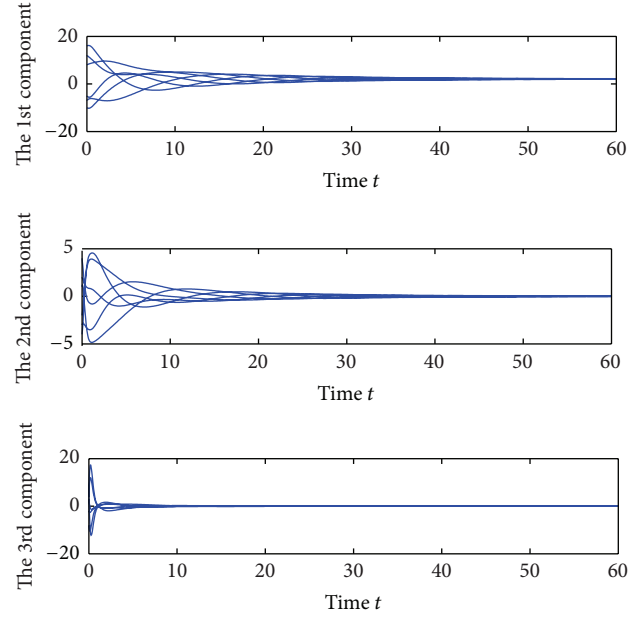


FIGURE 1: Trajectories of the first, the second, and the third state components of six agents with a directed circle and asymmetric time-varying delays.

eigenvalues have negative real parts. If there exist some positive definite matrices P , Q and a positive real number κ_0 such that

$$\begin{aligned} &[I_2 \otimes E_m - \kappa_0(D_1 \otimes F_m)]^T P \\ &\quad + P[I_2 \otimes E_m - \kappa_0(D_1 \otimes F_m)] < 0, \\ &[I_2 \otimes E_m - \kappa_0(D_2 \otimes F_m)]^T Q \\ &\quad + Q[I_2 \otimes E_m - \kappa_0(D_2 \otimes F_m)] < 0, \end{aligned} \quad (\text{A.5})$$

then $I_{N-1} \otimes E_m - \kappa_0 \widehat{\mathcal{L}} \otimes F_m$ is Hurwitz stable, where $D_1 = \begin{bmatrix} r & d \\ -d & r \end{bmatrix}$, $D_2 = \begin{bmatrix} 2d & d \\ -d & 2d \end{bmatrix}$, $r = \min\{\text{Re}(\lambda) : 0 \neq \lambda \in \sigma(\mathcal{L})\}$, $d = \max_{i \in \underline{N}} \{d_i\}$ is the maximum vertex in-degree over $\mathcal{G}(\mathcal{A})$.

Proof of Lemma 11. We only need to prove that the inequalities in (A.5) hold. Take $P = Q = I_2 \otimes P_m$. From Lemma 10, (14) implies (A.5). The proof is completed. \square

Conflict of Interests

The author declares that there is no conflict of interests regarding the publication of this paper.

Acknowledgments

This work was supported by the National Natural Science Foundation of China under Grant no. 61304163, the Natural Science Foundation of Shandong Province (no. ZR2013FQ008), and the Independent Innovation Foundation of Shandong University (no. 2013ZRQP006).

References

- [1] V. Borkar and P. P. Varaiya, "Asymptotic agreement in distributed estimation," *IEEE Transactions on Automatic Control*, vol. 27, no. 3, pp. 650–655, 1982.
- [2] J. N. Tsitsiklis and M. Athans, "Convergence and asymptotic agreement in distributed decision problems," *IEEE Transactions on Automatic Control*, vol. 29, no. 1, pp. 42–50, 1984.
- [3] A. Jadbabaie, J. Lin, and A. S. Morse, "Coordination of groups of mobile autonomous agents using nearest neighbor rules," *IEEE Transactions on Automatic Control*, vol. 48, no. 6, pp. 988–1001, 2003.
- [4] R. Olfati-Saber and R. M. Murray, "Consensus problems in networks of agents with switching topology and time-delays," *IEEE Transactions on Automatic Control*, vol. 49, no. 9, pp. 1520–1533, 2004.
- [5] W. Ren and R. W. Beard, "Consensus seeking in multiagent systems under dynamically changing interaction topologies," *IEEE Transactions on Automatic Control*, vol. 50, no. 5, pp. 655–661, 2005.
- [6] G. Xie and L. Wang, "Consensus control for a class of networks of dynamic agents," *International Journal of Robust and Nonlinear Control*, vol. 17, no. 10–11, pp. 941–959, 2007.
- [7] B. Liu, G. Xie, Y. Gao, J. Wu, J. Zhang, and W. Luo, "Consensus analysis of second-order multiagent systems with general topology and time delay," *Journal of Applied Mathematics*, vol. 2013, Article ID 359750, 8 pages, 2013.
- [8] W. Ren, K. Moore, and Y. Chen, "High-order and model reference Luo, Wenguangconsensus algorithms in cooperative control of multi-vehicle systems," *Journal of Dynamic Systems, Measurement, and Control*, vol. 129, no. 5, pp. 678–688, 2007.
- [9] P. Wieland, J. Kim, H. Scheu, and F. Allgower, "On consensus in multi-agent systems with linear high-order agents," in *Proceedings of the 17th World Congress, International Federation of Automatic Control (IFAC '08)*, pp. 1541–1546, Seoul, Korea, July 2008.
- [10] W. Yu, G. Chen, W. Ren, J. Kurths, and W. X. Zheng, "Distributed higher order consensus protocols in multiagent dynamical systems," *IEEE Transactions on Circuits and Systems I: Regular Papers*, vol. 58, no. 8, pp. 1924–1932, 2011.
- [11] D. Lee and M. W. Spong, "Agreement with non-uniform information delays," in *Proceedings of the American Control Conference*, pp. 756–761, Minneapolis, Minn, USA, June 2006.
- [12] J. Qin, H. Gao, and W. X. Zheng, "A new result on average consensus for multiple agents with switching topology and communication delay," in *Proceedings of the 48th IEEE Conference on Decision and Control held jointly with 28th Chinese Control Conference (CDC/CCC '09)*, pp. 3703–3708, Shanghai, China, December 2009.
- [13] P. Lin and Y. Jia, "Consensus of a class of second-order multi-agent systems with time-delay and jointly-connected topologies," *IEEE Transactions on Automatic Control*, vol. 55, no. 3, pp. 778–784, 2010.
- [14] P. Bliman and G. Ferrari-Trecate, "Average consensus problems in networks of agents with delayed communications," *Automatica*, vol. 44, no. 8, pp. 1985–1995, 2008.
- [15] Y. G. Sun and L. Wang, "Consensus problems in networks of agents with double-integrator dynamics and time-varying delays," *International Journal of Control*, vol. 82, no. 10, pp. 1937–1945, 2009.
- [16] Y. G. Sun and L. Wang, "Consensus of multi-agent systems in directed networks with uniform time-varying delays," *IEEE Transactions on Automatic Control*, vol. 54, no. 7, pp. 1607–1613, 2009.
- [17] U. Münz, A. Papachristodoulou, and F. Allgöwer, "Consensus reaching in multi-agent packet-switched networks with non-linear coupling," *International Journal of Control*, vol. 82, no. 5, pp. 953–969, 2009.
- [18] C. Godsil and G. Royle, *Algebraic Graph Theory*, vol. 207 of *Graduate Texts in Mathematics*, Springer, New York, NY, USA, 2001.
- [19] Y. G. Sun, L. Wang, and G. Xie, "Average consensus in networks of dynamic agents with switching topologies and multiple time-varying delays," *Systems & Control Letters*, vol. 57, no. 2, pp. 175–183, 2008.
- [20] F. Jiang and L. Wang, "Consensus seeking of high-order dynamic multi-agent systems with fixed and switching topologies," *International Journal of Control*, vol. 83, no. 2, pp. 404–420, 2010.
- [21] K. Gu, V. L. Kharitonov, and J. Chen, *Stability of Time-Delay Systems*, Birkhäuser, Boston, Mass, USA, 2003.
- [22] B. Boyd, L. El Ghaoui, E. Feron, and V. Balakrishnan, *Linear Matrix Inequalities in System and Control Theory*, SIAM, Philadelphia, Pa, USA, 1994.

Research Article

Research on Appraisal System of Procurator Performance by Using High-Order CFA Model

Yong-mao Huang^{1,2}

¹ School of Management, Jiangsu University, Zhenjiang 212013, China

² People's Procuratorate of Jingdezhen, JiangXi, Jingdezhen 333000, China

Correspondence should be addressed to Yong-mao Huang; huangyongmao12@163.com

Received 9 June 2014; Accepted 15 July 2014; Published 13 August 2014

Academic Editor: Jianguo Du

Copyright © 2014 Yong-mao Huang. This is an open access article distributed under the Creative Commons Attribution License, which permits unrestricted use, distribution, and reproduction in any medium, provided the original work is properly cited.

The prosecutor is the main body of procuratorial organs. The performance appraisal system plays an important role in promoting the work efficiency of procurator. In this paper, we establish the performance appraisal system of procurators by high-order confirmatory factor analysis method and evaluate procurators' performance by fuzzy comprehensive evaluation method based on the 360 degrees. The results have some help to performance management of procuratorial organs.

1. Introduction

Procurator is the principal and dominant part for procuratorial organs to conduct procuratorial business and perform its functions. The establishment of a scientific and rational appraisal system will mobilize their enthusiasm, raise their work efficiency, and increase the whole procuratorial organ's work level. The existing documents, law rules, and regulations serve as basis for the establishment of the evaluation system of procurators. However, from current practical evaluation of procuratorial organs, there are prominent problems in setting targets, selecting evaluation indicators, and applying evaluation results and further improvements are needed. Many existing papers have discussed this topic such as Bouskila-Yam and Kluger (2011) [1], Jin (2010) [2], and Samuel et al. (2014) [3]. However, most of them are qualitative researches and quantitative researches are less. Given this, this paper deploys the cross validation of EFA and CFA to establish structure of the performance evaluation system to make the system more reasonable on the basis of related performance evaluation theory. This is not frequently used in other papers about the same topic and we will use fuzzy comprehensive evaluation to make instance analysis based on full circle appraisal.

2. Acquire Appraisal Index

The Article 26 of Law of Procurator stipulates that procurator appraisal includes their job performance, ideology and morality, professional skill and theoretical level of law, working attitude, and working style. And the focus lies in their job performance. Guided by this requirement, the research group has invited seven procurators in leadership position from a procuratorial organ in JiangXi in depth interview. At first, the compere introduces the purpose and requirements about this interview and invites them to analyze and discuss their work selectively. Based on related theories of performance appraisal system [4–8], we can explain performance from conduct, result, and capability. According to the three dimensionalities, we can acquire thirty-two initial evaluation factors, presented by $a_1 \sim a_{32}$ [9, 10].

2.1. Initial Evaluation Elements Based on Conduct. These include (1) Job responsibility (a_1); (2) observance of procedural law (a_2); (3) work initiative and enthusiasm (a_3); (4) observance of business specification (a_4); (5) observance of "Responsibilities Certificate for Ethnical Members of CPC" (a_5); (6) team spirit (a_6); (7) observance of related prohibitions (a_7); (8) refusal of gifts and bribery (a_8); (9) political thoughts (a_9); (10) political theory level (a_{10}); (11) outlook

of right and wrong and outlook of values (a_{11}); (12) work organization (a_{12}); and (13) deployment of effective methods (a_{13}).

2.2. Initial Evaluation Elements Based on Results. These include (1) completing required work load (a_{14}); (2) fulfilling duties and responsibilities as required (a_{15}); (3) mistaken rate (a_{16}); (4) the satisfaction degree of the social public (a_{17}); (5) saving litigation costs (a_{18}); (6) meeting targets and requirements of job performance (a_{19}); and (7) saving economic costs for the country (a_{20}).

2.3. Initial Evaluation Elements Based on Capability. These include (1) awareness and capability to accept professional training (a_{21}); (2) professional techniques and capability (a_{22}); (3) capability to deal with accidents (a_{23}); (4) capability to cooperate (a_{24}); (5) professional knowledge level (a_{25}); (6) capability to comprehend and analyze (a_{26}); (7) proficiency of professional works (a_{27}); (8) ability to apply new knowledge and accommodate new fields (a_{28}); (9) mastering foreign language and computer (a_{29}); (10) capability to manage (a_{30}); (11) capability to make observance and discovery (a_{31}); and (12) oral expression and writing (a_{32}).

3. Design Appraisal Index System

3.1. Determine the Structure of Appraisal Index System. We use EFA to further refine initial appraisal factors and work out the structure of appraisal index system. Based on initial appraisal factors, we designed the initial questionnaire on the basis of Likert scale and surveyed 100 procurators. We have recycled 88 valid samples and the valid return rate is 88%.

After reliability test, we figure out that Cronbach's α is 0.951, larger than the fundamental reliability requirements 0.7. So the overall reliability result is satisfactory. The outcome of KMO analysis is 0.860, larger than the fundamental requirement 0.7. χ^2 in Bartlett test of sphericity is 2087 and the significance level is 0.000, smaller than 0.01. These show that the questionnaire is appropriate for component analysis.

Through the principal component analysis and Varimax orthogonal rotation, we figure out the factor loading of different components whose six eigenvalues are all larger than 1. The results are shown in Table 1.

In component one, the evaluation elements whose factor loadings are larger than 0.6 are a_{12} , a_{13} , a_{14} , a_{16} , a_{17} , a_{19} , and a_{20} . Because these indexes primarily reflect the job performance, so we name component one job performance component. In component two, the evaluation elements whose factor loadings are larger than 0.6 are a_{21} , a_{23} , a_{24} , a_{28} , and a_{30} ; we name component two job capability component. In component three, the evaluation elements whose factor loadings are larger than 0.6 are a_1 , a_3 , and a_6 and we name component three working attitude component. In component four, the evaluation elements whose factor loadings are larger than 0.6 are a_2 , a_4 , a_5 , a_7 , and a_8 and we name component four professional quality component. In component five, the evaluation elements whose factor loadings are larger than 0.6 are a_9 , a_{10} , and a_{11} and we name

component five ethnic component. In component six, only two components' factor loadings are larger than 0.6, that are, a_{22} and a_{29} . Because evaluative elements are too little and the job capability has been reflected by component two, so we delete component six. Besides, all factor loadings of a_{15} , a_{18} , a_{25} , a_{26} , a_{27} , a_{31} , and a_{32} are smaller than 0.6. This means their convergent validities are far from satisfaction, so they should be deleted.

3.2. Determine Index Weight. There are many methods to determine the index weight. In this paper, we use CFA. Reasons are shown as follows. (1) The results of structural equation model are based on many questionnaires whose objectivity can be fully guaranteed compared with other methods which are more subjective. (2) CFA could make further verification of EFA result and make much contribution to ensure the rationality of the performance evaluation structure. (3) The structural equation model could amend the initial model with its dedicated tools to reach the ideal requirements. (4) The structural equation model has been widely used in many performance appraisal systems which are difficult to qualify and performance evaluation index of procurators in this paper is also one difficult to be qualified. So it is reasonable to use this model. (5) Now most researches are using path coefficient obtained through structural equation model to figure out the interaction intensity between components. However, this paper uses the path coefficient obtained through higher CFA model to acquire weight factor. This method has not been frequently used in researches of procuratorial organs' performance appraisal. This has broadened the application of the structural equation model and is fairly innovative.

To conduct CFA, the research group has given out 300 questionnaires to staff in procuratorial organs in JiangXi and teachers in universities and colleges. We finally collect 273 questionnaires and the return rate is 91%. To make the CFA model more rational, this paper will start with oblique factor model and achieve the expecting results through consistent examination and correction.

3.2.1. Oblique Multifactor Model. Supposing there exists correlation between job performance, job capability, working attitude, professional quality, and ethnic, the results of the maximum likelihood method are as follows.

(1) *Model Identification.* The number of data point is 276 and the amount of estimated parameters is 56. Data point is larger than parameter and DOF is 220. This shows this model is an excessive identification one. So it has met the requirements of SEM model.

(2) *Parameter Estimation.* The results of standardized estimation of oblique multifactor model are shown in Figure 1. The correlation coefficient between the standardized regression coefficient and latent variable is verified through significance test.

(3) *Verification of Incremental Fit Measures.* ① The chi-square value (χ^2) is 590.811 and the number of χ^2/df is

TABLE 1: Rotated component matrix after Varimax orthogonal rotation.

Initial evaluation elements	Component					
	1	2	3	4	5	6
a_1	0.142	0.091	0.654	0.33	-0.173	-0.237
a_2	-0.017	0.123	0.174	0.784	0.026	0.256
a_3	0.142	0.369	0.716	0.064	0.088	0.218
a_4	0.115	0.058	0.223	0.783	0.157	-0.13
a_5	0.188	0.087	0.213	0.767	-0.047	0.077
a_6	0.122	0.328	0.754	0.023	0.009	0.281
a_7	0.104	0.116	0.151	0.692	0.072	-0.02
a_8	0.054	0.21	-0.309	0.71	0.199	0.021
a_9	0.247	0.22	0.013	0.182	0.818	-0.043
a_{10}	0.176	0.197	0.013	0.099	0.829	0.101
a_{11}	0.013	0.008	0.424	-0.024	0.623	0.375
a_{12}	0.701	0.342	0.081	0.16	0.119	0.138
a_{13}	0.678	0.196	0.03	0.347	0.119	0.27
a_{14}	0.619	0.196	0.172	-0.084	0.026	0.507
a_{15}	0.402	0.183	0.569	0.319	0.285	-0.075
a_{16}	0.768	0.341	0.257	0.06	0.108	-0.006
a_{17}	0.861	0.162	0.12	0.1	0.081	0.052
a_{18}	0.446	0.146	0.394	0.362	0.333	0.099
a_{19}	0.765	0.107	0.105	-0.032	0.102	0.215
a_{20}	0.699	0.27	0.178	0.174	0.154	0.131
a_{21}	0.335	0.773	0.079	0.091	0.155	0.224
a_{22}	0.448	0.247	0.011	-0.076	0.024	0.712
a_{23}	0.384	0.642	0.206	0.109	0.187	0.151
a_{24}	0.23	0.705	0.276	0.132	0.089	0.167
a_{25}	0.456	0.4	0.212	0.234	0.25	-0.001
a_{26}	0.321	0.419	0.447	0.172	0.326	0.273
a_{27}	0.096	0.401	0.534	0.295	0.231	0.292
a_{28}	0.362	0.687	0.336	0.226	0.208	0.046
a_{29}	0.229	0.161	0.197	0.221	0.173	0.666
a_{30}	0.25	0.654	0.368	0.256	0.036	0.094
a_{31}	0.262	0.231	0.508	0.191	0.29	0.366
a_{32}	0.268	0.489	0.507	0.125	0.201	-0.044

2.68 (590.811/220). This number is between one and three, meaning that the overall fit measure can meet requirements. ② The RMR of residual mean square and square root is 0.056, larger than 0.05 but close to 0.05. This means that the fit measure is up to requirements. ③ GFI is 0.823 and AGFI is 0.778. They both fail to meet the ideal requirements. ④ PRATIO (0.87), PNFI (0.669), and PCFI (0.73) are all larger than 0.50 so they can meet the requirements. ⑤ RMSEA is 0.82 and it means that the fit measure is general.

(4) *Internal Quality Evaluation of the Model.* ① Validity reflects the degree of actual measurement of underlying characteristics that target variable that it wants to measure. For SEM model, if the load capacity has reached significance level which means P is smaller than 0.05 and $|t|$ is larger than 1.96, then target variable can effectively reflect the latent variable that it measures and the measurement has high

validity. Because all load capacities are smaller than 0, so this model is of good validity.

② Individual observation variable reflects the consistency of measurement and observed variables' multivariate square reflects the reliability of latent variable. It is larger than 0.50 and that means the individual item is reliable. After calculation, among twenty-three measured variables, there are eight individual items whose separation reliability is larger than 0.50, so this model is qualified.

③ Composite reliability is also called construct reliability which is used to evaluate the unity of potential construction indicators. Higher composite reliability means higher unity between measurement index and vice versa. The calculation formula is $\rho_c = (\sum \lambda)^2 / [(\sum \lambda)^2 + \sum \theta]$. ρ_c is composite reliability, λ is standardized parameter of observed variable compared with latent variable, and θ is error variance of target variable. If ρ_c is larger than 0.60, the composite reliability is

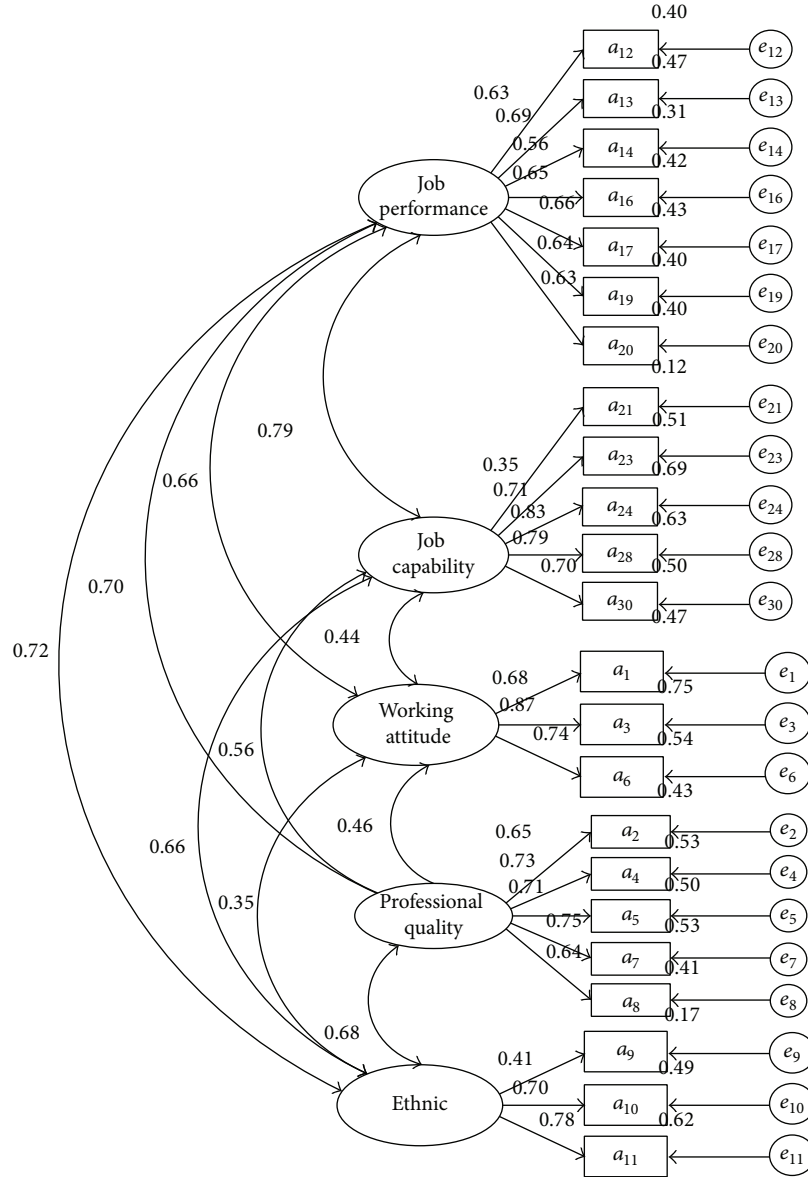


FIGURE 1: Standardized parameter estimates of oblique multifactor model.

qualified. After calculation, we figure out that $\rho_{c1} = 0.827$, $\rho_{c2} = 0.818$, $\rho_{c3} = 0.808$, $\rho_{c4} = 0.822$, and $\rho_{c5} = 0.676$. And they, respectively, reflect composite reliability of job performance, job capability, working attitude, professional quality, and ethnic. They are all larger than 0.60, so this model is of high composite reliability.

④ Average variance extracted (AVE) indicates variation of target variable which latent variable can explain when compared with the error variance. The calculation formula $\rho_v = \sum \lambda^2 / [\sum \lambda^2 + \sum \theta]$ is extracted variance of mean, ρ_v is standardized parameter of observed variable on latent variable, and θ is the error variance of target variable. If ρ_v is larger than 0.50, the observed variable can reflect the latent variable and the latent variable is of high reliability and validity. If ρ_v is smaller than 0.50, the variation of target variable that measuring error can explain is larger

than variation that basic latent variable explains. And it means the latent variable has low reliability and validity. After calculation, we figure out that $\rho_{v1} = 0.406$, $\rho_{v2} = 0.489$, $\rho_{v3} = 0.586$, $\rho_{v4} = 0.481$, and $\rho_{v5} = 0.426$. And they, respectively, reflect composite reliability of job performance, job capability, working attitude, professional quality, and ethnic. They are all smaller than 0.50, except ρ_{v3} , and it shows that this model is of low internal quality.

From the external quality inspection (incremental fit measures) and internal quality inspection (reliability and validity test) of oblique multifactor model, we can see that partial incremental fit measures indicator and reliability and validity test indicator are unsatisfactory and needs further improvements. At the same time, correlation coefficient between latent variables shows that the five latent variables have high degree of correlation and there may exist another

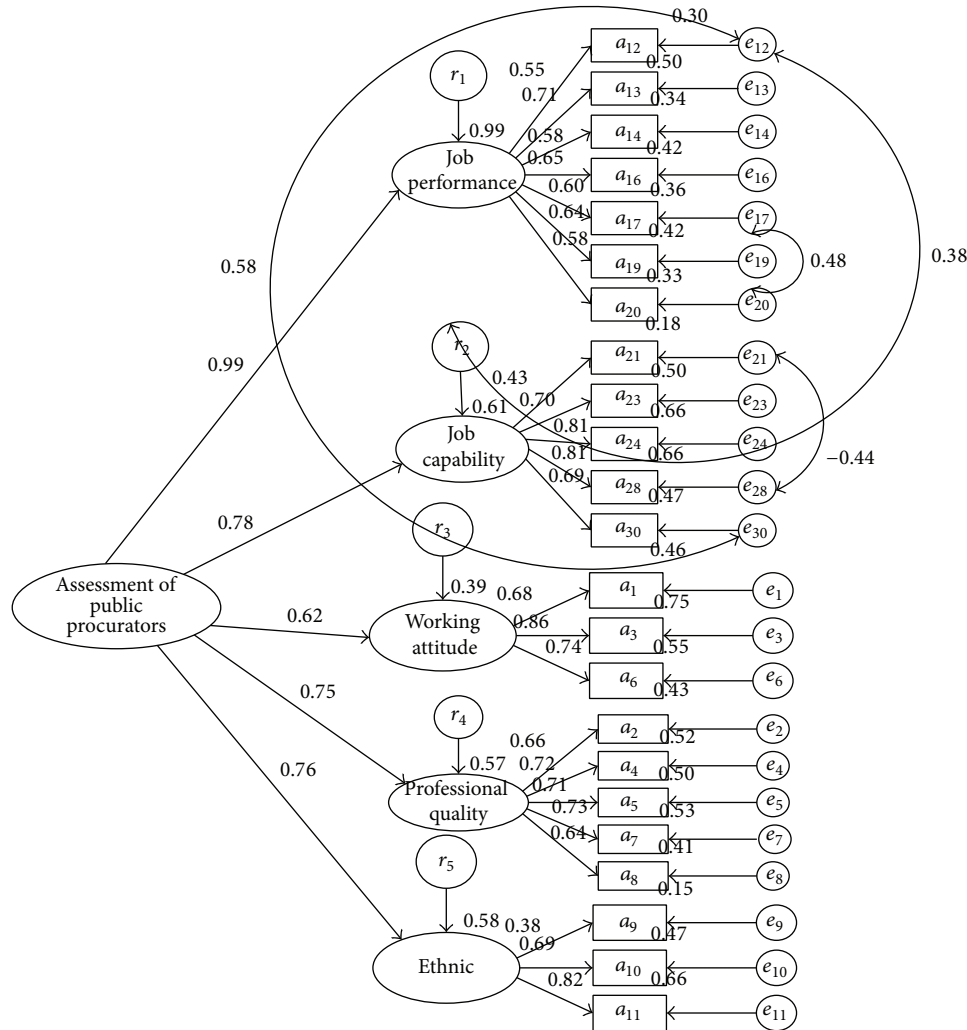


FIGURE 2: Standardized parameter estimates of revised second order CFA models.

high-order common factor. It serves as basis for second order CFA model. So on the basis of oblique multifactor model and needs of appraisal system of procurators, we set up a second order CFA model, make amendments to it, and finally establish the appraisal system of procurators.

3.2.2. Second Order CFA Model. Supposing that job performance, job capability, working attitude, professional quality, and ethnic are all influenced by a high-order component, the five latent variables have transformed into internal latent variables and a new item-estimated residual is added. And we also suppose that there is no error covariation and cross-load and each latent variable is only influenced by one first-stage component. Then we set up a second order CFA model, modify covariance of the model, release modification indices which are larger than 15, filter four groups of variables whose critical ratio of error variance is smaller than 0.1, and restrict a same parameter for them. The results are as follows.

(1) Pattern Recognition. The data points of the model are 276, while parameter estimates in total are 51. So the data points

of the model exceed parameter estimates and the degree of freedom is 225, indicating that this model is the necessary condition of the SEM Model.

(2) Simulation Model Parameter Estimation. Figure 2 presents the standardized parameter estimates of revised second order CFA models. In the diagram, standardized regression coefficient and coefficient of association among the latent variables pass the significance test.

(3) Inspection of Model Adaptation Degree. ① The chi-square value (χ^2) is 399.625 and the number of χ^2/df is 1.776 (399.625/225), which means revised model chi-square significantly decreases, and Chi-square degrees of freedom is between 1 and 3, indicating that fitting degree of the model gets optimized, meeting the requirement. ② Residual mean square and square RMR are 0.048, below 0.05, indicating that fitting degree of the model meets the requirement. ③ Goodness-of-fit index GFI equals 0.870, fixed adaptation degree index AGFI equals 0.840, although not reaching the level of 0.9, close enough, still meeting the requirement.

TABLE 2: Appraisal system of prosecutors' performance.

Numbers	Level-1 indicators (weight)	Level-2 indicator (weight)
1	A ₁ : Work performance (0.254)	<i>a</i> ₁₂ : organization in work (0.127)
		<i>a</i> ₁₃ : ability to make effective solutions (0.165)
		<i>a</i> ₁₄ : work completed (0.134)
		<i>a</i> ₁₆ : mistaken case rate (0.150)
		<i>a</i> ₁₇ : social public satisfaction (0.139)
		<i>a</i> ₁₉ : ability to successfully meet work expectations (0.150)
		<i>a</i> ₂₀ : national economic loss redeemed (0.134)
2	A ₂ : Work ability (0.200)	<i>a</i> ₂₁ : willingness and capacity of accepting work training (0.124)
		<i>a</i> ₂₃ : ability to handle emergencies (0.205)
		<i>a</i> ₂₄ : ability to contact and to cooperate (0.236)
		<i>a</i> ₂₈ : ability to employ new knowledge and to adapt to new fields (0.236)
		<i>a</i> ₃₀ : management ability (0.200)
3	A ₃ : Work attitude (0.159)	<i>a</i> ₁ : responsibility in work (0.297)
		<i>a</i> ₃ : positive initiative in work (0.379)
		<i>a</i> ₆ : team spirit (0.325)
4	A ₄ : Professional quality (0.192)	<i>a</i> ₂ : abidance by law (0.189)
		<i>a</i> ₄ : abidance by work rules and regulations (0.209)
		<i>a</i> ₅ : abidance by <i>the responsibility of party members</i> (0.205)
		<i>a</i> ₇ : violations of the probations (0.211)
		<i>a</i> ₈ : refusal of the bribe (0.186)
5	A ₅ : Ideology and morality (0.195)	<i>a</i> ₉ : political thoughts (0.204)
		<i>a</i> ₁₀ : level of political theory (0.364)
		<i>a</i> ₁₁ : outlook of right and wrong and value (0.432)

④ Simple adjustment measure PRATIO equals 0.889, PNFI equals 0.751, along with PCFI, all above 0.50, meeting the requirement. ⑤ Gradual residual and square root RMSEA is 0.058, below uncorrected ones, or between 0.05 and 0.08, indicating fitting degree of the model fair.

According to the data above, most of goodness-of-fit index of second order CFA models meet the requirement, indicating the external quality of second order CFA Models favorable.

(4) *Internal Quality Evaluation of the Model.* ① *Validity.* All factor loadings in this model are far from 0, indicating the validity of the model favorable. ② *Individual Item Reliability.* Among 28 variables, 13 kinds of individual item reliability are above 0.50, showing that the internal quality of the model fair. ③ *Composite Reliability.* The composite reliability result of higher order factor "Assessment of Public Procurators" $\rho_c = 0.891$. Because ρ_c is larger than 0.6, the overall composite reliability is very ideal. ④ Extracted value of variance of mean of latent variables is AVE. Variance of mean extracted of the higher order factor "Assessment of Public Prosecutors" is 0.627. The result indicates that this latent variance has favorable reliability and validity.

It is easy to find that most of goodness-of-fit index of revised second order CFA Models meet the requirement, indicating that this model has sound reliability and validity in terms of internal quality assessment. As a result, this model can be set as the final model in the construction of index system.

Final system of assessment of prosecutors' performance can be gained by normalization of path coefficient of revised second order CFA Model, which is shown in Table 2.

4. Appraisal Instances

According to the appraisal system of prosecutors' performance above, assessment of prosecutors' performances can be implemented. This research group assesses one prosecutor's performance of a certain procuratorate in Jiangxi Province by taking the fuzzy comprehensive evaluation method based on 360 degrees of main-body evaluation [11–13].

(1) *Determine Appraisal Factor Aggregation.* The appraisal factor aggregation stems from 5 level-1 indicators and 23 level-2 indicators in the performance appraisal system.

(2) *Determine Aggregation of Factor Rankings.* According to the general principle set by level appraisal aggregation, degree of each kind of indicator can be classified into 5 grades, which are excellent, favorable, medium, pass, and Poor, thus determining the fuzzy judging set $V = \{\text{Excellent, Favorable, Medium, Pass, Poor}\}$, according to which, membership sets are, respectively, classified into 95, 85, 75, 65, and 55, and the grade evaluation matrix is $V = [95, 85, 75, 65, 55]$.

TABLE 3: Summary table of primitive matrix of fuzzy comprehensive appraisal for each indicator.

Indicators	Superior					Vis-a-vis					Self				
	A	B	C	D	E	A	B	C	D	E	A	B	C	D	E
a_{12}	1/5	4/5	0	0	0	1/5	3/5	1/5	0	0	0	1	0	0	0
a_{13}	1/5	3/5	1/5	0	0	1/5	4/5	0	0	0	0	1	0	0	0
a_{14}	2/5	3/5	0	0	0	2/5	1/5	2/5	0	0	1	0	0	0	0
a_{16}	2/5	2/5	1/5	0	0	3/5	2/5	0	0	0	0	1	0	0	0
a_{17}	0	4/5	1/5	0	0	1/5	4/5	0	0	0	0	1	0	0	0
a_{19}	1/5	3/5	1/5	0	0	2/5	3/5	0	0	0	1	0	0	0	0
a_{20}	2/5	3/5	0	0	0	3/5	1/5	1/5	0	0	0	1	0	0	0
a_{21}	3/5	2/5	0	0	0	2/5	3/5	0	0	0	1	0	0	0	0
a_{23}	2/5	2/5	1/5	0	0	3/5	2/5	0	0	0	0	1	0	0	0
a_{24}	0	3/5	2/5	0	0	1/5	4/5	0	0	0	0	1	0	0	0
a_{28}	0	4/5	1/5	0	0	2/5	3/5	0	0	0	0	1	0	0	0
a_{30}	3/5	2/5	0	0	0	3/5	2/5	0	0	0	1	0	0	0	0
a_1	2/5	2/5	1/5	0	0	0	3/5	2/5	0	0	0	1	0	0	0
a_3	3/5	2/5	0	0	0	2/5	3/5	0	0	0	0	1	0	0	0
a_6	1/5	3/5	1/5	0	0	2/5	2/5	1/5	0	0	0	1	0	0	0
a_2	2/5	2/5	1/5	0	0	1/5	2/5	2/5	0	0	0	1	0	0	0
a_4	0	2/5	3/5	0	0	0	3/5	2/5	0	0	0	1	0	0	0
a_5	3/5	1/5	1/5	0	0	2/5	3/5	0	0	0	0	1	0	0	0
a_7	1/5	3/5	1/5	0	0	2/5	2/5	1/5	0	0	1	0	0	0	0
a_8	3/5	2/5	0	0	0	2/5	3/5	0	0	0	1	0	0	0	0
a_9	2/5	3/5	0	0	0	3/5	1/5	1/5	0	0	0	1	0	0	0
a_{10}	1/5	2/5	2/5	0	0	2/5	2/5	1/5	0	0	0	1	0	0	0
a_{11}	2/5	2/5	1/5	0	0	3/5	2/5	0	0	0	0	1	0	0	0

A, B, C, D, and E, respectively, represent “excellent,” “favorable,” “medium,” “pass,” and “poor.”

(3) *Determine the Appraisal Subject.* The thinking of 360-degree assessment method being used for reference and in order to make the appraisal result disinteresting, 5 superior prosecutors, vis-a-vis 5, and the prosecutor itself 1, making it the total of 11 participants of the fuzzy comprehensive appraisal. Respective weights are determined through discussion among the experts, making the superior 0.6, vis-a-vis 0.2 and the self 0.2.

(4) *Determine Fuzzy Relation Matrix.* Primitive matrix of fuzzy comprehensive appraisal is gained by fuzzy comprehensive appraisal of each main part. See Table 3.

According to the method of fuzzy comprehensive appraisal, the prosecutor's level-1 indicator grades can be computed to be 86.821, 86.7725, 87.0010, 86.5850, and 86.8560, making it final grade 86.821, 86.7725, 87.0010, 86.5850, and 86.8560 and work performance ranking number 2 in the 5 indicators, showing that the most important work performance of the prosecutor is sound in the 4 indicators. Generally speaking, all indicator grades are close. According to the maximum membership principle, the appraisal result of the prosecutor is “favorable.” The comprehensive grades of other prosecutors can be gained by employing the same method. The ranking can be important factors for promotion and reward through sorting different prosecutors' grades based on the final grades. In the actual operations, the

computation process can be completed by computer software, simplifying the operation process.

5. Conclusion

This study combined uses exploratory factor analysis and high-order confirmatory factor analysis to establish the prosecutor performance appraisal system. The study also conducts instance analysis based on 360-degree fuzzy comprehensive appraisal of the main target. Adopting this method is a beneficial trial of using high-order CFA Model, perfecting, and enriching the existing appraisal system of prosecutors' performance and then making the appraisal and evaluation more scientific and reasonable. Meanwhile, such a system built through this thinking not only helps to compare different working indicator result of prosecutors, but also can enlighten what should be corrected and improved. Besides, such a system can make the ranking of various appraisal grades, through which promotion, rewards, and punishments can find their grounds. In practice, it is very operative-oriented because all computations can be accurately done by computers. In the future studies, this system will constitute an important role in further segmenting the appraisal indicators in order to enhance the operability of the indicator system.

TABLE 4

Number	Evaluation factors	Importance				
		1	2	3	4	5
(1) Importance based on behaviors						
1	Responsibility in work					
2	Abidance by law in dealing with cases					
3	Positive initiative in work					
4	Abidance by work rules and regulations					
5	Abidance by the responsibility of party members					
6	Team spirit in work					
7	Nonviolations of the probations					
8	Refusal of the bribe					
9	Political thoughts					
10	Level of political theory					
11	Outlook of right and wrong and value					
12	Organization in work					
13	Ability to make effective solutions					
(2) Importance based on results						
14	Work completed					
15	Ability to finish the duties as required					
16	Mistaken case rate					
17	Social public satisfaction					
18	Ability to cut litigation cost					
19	Ability to successfully meet work expectations					
20	National economic loss redeemed					
(3) Importance based on abilities						
21	Innovation ability					
22	Skills of handling cases					
23	Ability to handle emergencies					
24	Professional proficiency					
25	Professional knowledge					
26	Ability to understand and analyze					
27	Ability to contact and to cooperate					
28	Ability to employ new knowledge and to adapt to new fields					
29	English and computer proficiency and operability					
30	Ability to manage and control					
31	Acute observation					
32	Oral expression and writing ability					

Appendix

A. Questionnaire of Prosecutors' Performance Assessment

Dear Sir or Madam,

Thank you very much for taking the time out of your busy schedule to fill in this questionnaire! The questionnaire aims to gather information, based on which related factors and incidence influencing a prosecutor's performance can be understood and evaluated in order to provide evidences for the design of assessment system. This questionnaire employs the method of anonymous survey to acquire data

which is used only for the study. Therefore, we promise you the confidentiality of all of your provided information. To guarantee the reliability and the validity, please answer the questions according to your actual situation without being affected by other people's opinion. Thanks very much for your cooperation!

There are two parts in the questionnaire. The first part is your personal information and the second is the main part.

A.1. Personal Information. Please mark the "√" in the brackets.

(1) Gender: male (); female ()

- (2) Politics status:
Member of communist party of China (); general public (); democracy parties ()
- (3) Age: under 25 (); 26–35 (); 36–45 (); 46–55 (); older than 55 ()
- (4) Education background: senior high school graduates (); junior college graduates (); undergraduate graduates; postgraduate or above ()
- (5) Ranks or positions: section member (); vice section (); section chief (); deputy director (); directing officer ()

A.2. Main Part of the Questionnaire. Indicator factors involving behaviors, results, and abilities which possibly influence prosecutors' performances are listed above. Please give your opinion on the importance of each factor by marking "√." Note that "1," "2," and "3," respectively, represent "Dispensable," "Unimportant," "Important," "Necessary," and "Imperative." See Table 4.

Conflict of Interests

The author declares that there is no conflict of interests regarding the publication of this paper.

References

- [1] O. Bouskila-Yam and A. N. Kluger, "Strength-based performance appraisal and goal setting," *Human Resource Management Review*, vol. 21, no. 2, pp. 137–147, 2011.
- [2] B. Jin, "On the difficult problems of several procuratorial organs performance evaluation," *Chinese Prosecutor*, no. 11, pp. 3–4, 2010.
- [3] O. W. Samuel, M. O. Omisore, and E. J. Atajeromavwo, "Online fuzzy based decision support system for human resource appraisal," *Measurement*, vol. 55, no. 2, pp. 452–461, 2014.
- [4] H. J. Bernardin, J. S. Kane, S. Ross, J. D. Spina, and D. L. Johnson, "Performance appraisal design, development, and implementation," in *Handbook of Human Resource Management*, Blackwell, Cambridge, Mass, USA, 1995.
- [5] D. E. Mathews, "Developing a perioperative peer performance appraisal system," *AORN Journal*, vol. 72, no. 6, pp. 1039–1042, 1044, 1046, 2000.
- [6] K. Geukes, C. Mesagno, S. J. Hanrahan, and M. Kellmann, "Testing an interactionist perspective on the relationship between personality traits and performance under public pressure," *Psychology of Sport and Exercise*, vol. 13, no. 3, pp. 243–250, 2012.
- [7] E. Fichera, S. Nikolova, and M. Sutton, "Comparative performance evaluation: quality," in *Encyclopedia of Health Economics*, pp. III–116, 2014.
- [8] L. K. Choon and M. A. Embi, "Subjectivity, organizational justice and performance appraisal: understanding the concept of subjectivity in leading towards employees' perception of fairness in the performance appraisal," *Procedia—Social and Behavioral Sciences*, vol. 62, pp. 189–193, 2012.
- [9] D. Lilley and S. Hinduja, "Police officer performance appraisal and overall satisfaction," *Journal of Criminal Justice*, vol. 35, no. 2, pp. 137–150, 2007.
- [10] J. R. Chang, C. H. Cheng, and L. S. Chen, "A fuzzy-based military officer performance appraisal system," *Applied Soft Computing*, vol. 7, no. 3, pp. 936–945, 2007.
- [11] M. Espinilla, R. de Andrés, F. J. Martínez, and L. Martínez, "A 360-degree performance appraisal model dealing with heterogeneous information and dependent criteria," *Information Sciences*, vol. 222, pp. 459–471, 2013.
- [12] S. Thammasitboon, K. Breetz, J. Phillips, and R. Moore, "An innovative 360-degree assessment instrument: using a relative ranking model to enhance the appraisal performance," *Academic Pediatrics*, vol. 9, no. 4, p. e9, 2009.
- [13] R. Sepehrirad, A. Azar, and A. Sadeghi, "Developing a hybrid mathematical model for 360-degree appraisal: a case study," *Procedia*, vol. 62, no. 12, pp. 844–848, 2012.

Research Article

Consensus of Multiagent Networks with Intermittent Interaction and Directed Topology

Li Xiao

Department of Mathematics and Information Engineering, Chongqing University of Education, Chongqing 400067, China

Correspondence should be addressed to Li Xiao; xsxiaoli@163.com

Received 24 May 2014; Revised 22 July 2014; Accepted 22 July 2014; Published 12 August 2014

Academic Editor: Chuandong Li

Copyright © 2014 Li Xiao. This is an open access article distributed under the Creative Commons Attribution License, which permits unrestricted use, distribution, and reproduction in any medium, provided the original work is properly cited.

Intermittent interaction control is introduced to solve the consensus problem for second-order multiagent networks due to the limited sensing abilities and environmental changes periodically. And, we get some sufficient conditions for the agents to reach consensus with linear protocol from the theoretical findings by using the Lyapunov control approach. Finally, the validity of the theoretical results is validated through the numerical example.

1. Introduction

The problem of coordinating the motion of multiagent networks has attracted increasing attention. Research on multiagent coordinated control problems not only helps in better understanding the general mechanisms and interconnection rules of natural collective phenomena but also carries out benefits in many practical applications of networked cyber-physical systems, such as tracking [1], flocking [2, 3], and formation [4]. Consensus, along with stability [5] and bifurcation [6], is a fundamental phenomenon in nature [7]. Roughly speaking, consensus means that all agents in network will converge to some common state by negotiating with their neighbors. A consensus algorithm is an interaction rule on how agents update their states.

To realize consensus, many effective approaches were proposed [8–10]. Since the network can be regarded as a graph, the issues can be depicted by the graph theory. The recent approaches concentrate on matrix analysis [11], convex analysis [12, 13], and graph theory [14]. The concept of spanning tree especially is widely used to describe the communicability between agents in networks that can guarantee the consensus [15]. For more consensus problems, the reader may refer to [16–21] and the references therein.

As we know, sometimes only the intermittent states of its neighbors can be obtained by the agents to the transmission capacity, communication cost, sensing abilities, and

the environmental changes. To decrease the control cost, only the intermittent states of its neighbors are obtained [22]. This is mainly because such networks are constrained by the following operational characteristics: (i) they may not have a centralized entity for facilitating computation, communication, and timesynchronization, (ii) the network topology may not be completely known to the nodes of the network, and (iii) in the case of sensor networks, the computational power and energy resources may be very limited. Inspired by the above consideration, the goal in this setting is to design algorithms by exploiting partial state sampling at each node; it is possible to reduce the amount of data which needs to be transmitted in networks, thereby saving bandwidth and energy, extending the network lifetime, and reducing latency. Also, the linear local interaction protocol can guarantee the linear nature of distributed multiagent networks in real world and linear algorithm is simple and easy to implement so as to be widely used in practical engineering especially in the limited transmission environment. Using the Lyapunov control approach, some sententious conditions are obtained in this paper for reaching consensus in multiagent networks.

The rest of this paper is organized as follows. In Section 2, some preliminaries on the graph theory and the model formulation are given. The main results are established in Section 3. In Section 4, a numerical example is simulated to verify the theoretical analysis. Concise conclusions are finally drawn in Section 5.

2. Preliminaries and Model

2.1. Graph Theory. In this subsection, some basic concepts and result of algebraic graph theory are introduced. Suppose that information exchange among agents in multiagent networks can be modeled by an interaction digraph.

Let $g = (V, \varepsilon, A)$ denote a directed graph with the set of nodes $V = \{1, 2, \dots, N\}$, where $\varepsilon \subseteq V \times V$ represents the edge set and $A = (a_{ij})_{N \times N}$ is the adjacency matrix with nonnegative elements a_{ij} . A directed edge ε_{ij} in the network g is denoted by the ordered pair of nodes (i, j) , where i is the receiver and j is the sender, which means that node i can receive information from node j . We always assume that there is no self-loop in network g . An adjacency matrix A of a directed graph can be defined such that a_{ij} is a nonnegative element if $\varepsilon_{ij} \in \varepsilon$, while $a_{ij} = 0$ if $\varepsilon_{ij} \notin \varepsilon$. The set of neighbors of node i is denoted by $N_i = \{j \in V : (i, j) \in \varepsilon\}$. A sequence of edges of the form $(i, j_1), (j_1, j_2), \dots, (j_m, j) \in \varepsilon$ composes a directed path beginning with i and ending with j in the directed graph g with distinct nodes $j_k, k = 1, 2, \dots, m$, which means the node j is reachable from node i . A directed graph is strongly connected if for any distinct nodes i and j , there exists a directed path from node i to node j . A directed graph has a directed spanning tree if there exists at least one node called root which has a directed path to all the other nodes [16]. Let (generally nonsymmetrical) Laplacian matrix $L = (l_{ij})_{N \times N}$ associated with directed network g be defined by

$$l_{ij} = \begin{cases} \sum_{k=1, k \neq i}^N a_{ik}, & i = j, \\ -a_{ij}, & i \neq j, \end{cases} \quad (1)$$

which ensure the diffusion property $\sum_{j=1}^N l_{ij} = 0$. Suppose L is irreducible. Then, $L \mathbf{1}_N = \mathbf{0}_N$ and there is a positive vector $\xi = (\xi_1, \xi_2, \dots, \xi_N)^T$ satisfying $\xi^T L = \mathbf{0}_N^T$ and $\xi^T \mathbf{1}_N = 1$. In addition, there exists a positive definite diagonal matrix $\Xi = \text{diag}(\xi_1, \xi_2, \dots, \xi_N)$ such that $\bar{L} = (\Xi L + L^T \Xi)/2$ is symmetric and $\sum_{j=1}^N \bar{L}_{ij} = \sum_{j=1}^N \bar{L}_{ji} = 0$ for all $i = 1, 2, \dots, N$ [18].

For simplicity, some mathematical notations are used throughout this paper. $I_n(\mathbf{0}_n)$ denotes the identity (zero) matrix with n dimensions. Let $\mathbf{1}_n(\mathbf{0}_n)$ be the vector with all n elements being 1(0). R^n is the n -dimensional real vector space. The notation \otimes denotes the Kronecker product.

2.2. Model Description. The discretization process of a continuous-time system cannot entirely preserve the dynamics of the continuous-time part even small sampling period is adopted. So, we consider the following second-order multiagent networks of N agents in [19] with intermittent measurements. The i th agent in the directed network g is governed by double-integrator dynamics

$$\begin{aligned} \dot{x}_i(t) &= v_i(t), \\ \dot{v}_i(t) &= d(t) \left(\sum_{j=1, j \neq i}^N a_{ij} (x_j(t) - x_i(t)) \right. \\ &\quad \left. + \kappa \sum_{j=1, j \neq i}^N a_{ij} (v_j(t) - v_i(t)) \right), \\ i &= 1, 2, \dots, N, \end{aligned} \quad (2)$$

where $x_i(t) \in R^n$ and $v_i(t) \in R^n$ are the position and velocity states of the i th agent, respectively. κ denotes the coupling strengths. $d(t)$ denotes the intermittent control as follows:

$$d(t) = \begin{cases} 1, & t_0 + k\omega < t \leq t_0 + k\omega + \delta, \\ 0, & t_0 + k\omega + \delta < t \leq t_0 + (k+1)\omega, \end{cases} \quad (3)$$

where $\omega > 0$ is the control period and $\delta > 0$ is called the control width.

Equivalently, model (2) can be rewritten as follows:

$$\begin{aligned} \dot{x}_i(t) &= v_i(t), \\ \dot{v}_i(t) &= -d(t) \left(\sum_{j=1}^N l_{ij} x_j(t) + \kappa \sum_{j=1}^N l_{ij} v_j(t) \right), \\ i &= 1, 2, \dots, N. \end{aligned} \quad (4)$$

In this paper, our goal is to design suitable ω, δ such that the network reaches consensus. In the following we present the following lemma and definitions.

Lemma 1 (see [23]). Suppose that $M \in R^{n \times n}$ is positive definite and $N \in R^{n \times n}$ is symmetric. Then $\forall x \in R^n$, and the following inequality holds:

$$\lambda_{\max}(M^{-1}N) x^T M x \geq x^T N x \geq \lambda_{\min}(M^{-1}N) x^T M x. \quad (5)$$

Definition 2 (see [18]). Let ξ, Ξ , and \bar{L} be defined as in Section 2.1. For a strongly connected network with Laplacian matrix L , let

$$a(L) = \min_{x^T \xi = 0, x \neq 0} \frac{x^T \bar{L} x}{x^T \Xi x}, \quad b(L) = \max_{x^T \xi = 0, x \neq 0} \frac{x^T \bar{L} x}{x^T \Xi x}. \quad (6)$$

Definition 3. Periodic intermittent consensus in the second-order multiagent networks (2) is said to be achieved if, for any initial conditions,

$$\begin{aligned} \lim_{t \rightarrow \infty} \|x_i(t) - x_j(t)\| &= 0, \\ \lim_{t \rightarrow \infty} \|v_i(t) - v_j(t)\| &= 0, \quad \forall i, j = 1, 2, \dots, N. \end{aligned} \quad (7)$$

3. Main Results

In this section, we will focus on consensus analysis of second-order multiagent networks via intermittent control in the strongly connected networks, simply for that a matrix G is irreducible if and only if its corresponding system G is strongly connected [24].

Let $\bar{x} = \sum_{k=1}^N \xi_k x_k(t)$, $\bar{v} = \sum_{k=1}^N \xi_k v_k(t)$ represent the average position and velocity of agent. Naturally, $\hat{x}_i(t) = x_i(t) - \bar{x}$ and $\hat{v}_i(t) = v_i(t) - \bar{v}$ represent the position and velocity vectors relative to the average position and velocity of the agents in network. Then the error dynamical system can be rewritten in a compact matrix form as

$$\dot{y}(t) = (\hat{L} \otimes I_n) y(t), \quad (8)$$

where $\hat{L} = \begin{pmatrix} 0_N & I_N \\ -\alpha d(t)L & -\beta d(t)L \end{pmatrix}$.

Theorem 4. Suppose that the agent network is strongly connected; then the linear consensus in the multiagent networks (2) via periodic intermittent interaction is achieved if the following conditions are satisfied:

- (1) $a(L) > 1/\kappa^2$,
- (2) $\gamma(\omega - \delta) + \eta\delta < 0$, $\gamma > 0$, $\eta < 0$,

where

$$\begin{aligned} \gamma &= 2\lambda_{\max}(B^{-1}E) > 0, & \eta &= 2\lambda_{\max}(C)/\lambda_{\max}(D) < 0, \\ B &= \begin{pmatrix} 2\kappa a(L)\Xi & \Xi \\ \Xi & \kappa\Xi \end{pmatrix}, & C &= \begin{pmatrix} -a(L)\Xi & O_N \\ O_N & \Xi - \kappa^2 a(L)\Xi \end{pmatrix}, \\ D &= \begin{pmatrix} 2\kappa b(L)\Xi & \Xi \\ \Xi & \kappa\Xi \end{pmatrix}, \\ E &= \begin{pmatrix} O_N & (\kappa/2)(\Xi L + L^T \Xi) \\ (\kappa/2)(\Xi L + L^T \Xi) & \Xi \end{pmatrix}. \end{aligned} \quad (9)$$

Proof. The potential Lyapunov function is defined to be

$$V(t) = \frac{1}{2} y^T(t) (\Omega \otimes I_n) y(t), \quad (10)$$

where $\Omega = \begin{pmatrix} 2\kappa\bar{L} & \Xi \\ \Xi & \kappa\Xi \end{pmatrix}$. Computing by the Definition 2, one obtains

$$\begin{aligned} V(t) &= \frac{1}{2} \hat{x}^T(t) ((2\kappa\bar{L}) \otimes I_n) \hat{x}(t) + \frac{1}{2} \hat{x}^T(t) ((\Xi) \otimes I_n) \hat{v}(t) \\ &\quad + \frac{1}{2} \hat{v}^T(t) ((\Xi) \otimes I_n) \hat{x}(t) + \frac{1}{2} \hat{v}^T(t) ((\kappa\Xi) \otimes I_n) \hat{v}(t) \\ &\geq \frac{1}{2} y^T(t) (B \otimes I_n) y(t), \\ V(t) &\leq \frac{1}{2} y^T(t) (D \otimes I_n) y(t), \end{aligned} \quad (11)$$

where $B = \begin{pmatrix} 2\kappa a(L)\Xi & \Xi \\ \Xi & \kappa\Xi \end{pmatrix}$, $D = \begin{pmatrix} 2\kappa b(L)\Xi & \Xi \\ \Xi & \kappa\Xi \end{pmatrix}$.

$B > 0$ is equivalent to $\Xi > 0$ and $2\kappa a(L)\Xi - (1/\kappa)\Xi > 0$ by Schur Complement Lemma. And it is clear that $a(L) > 1/2\kappa^2$; thus $B > 0$. So $V(t) \geq 0$ and $V(t) = 0$ if and only if $y = 0$.

Because the control gain $d(t)$ works intermittently by the control period and the control width, the consensus is discussed in the two different intervals, respectively.

Firstly, for $t_0 + k\omega < t \leq t_0 + k\omega + \delta$ and $\hat{L} = \begin{pmatrix} O_N & I_N \\ -L & -\kappa L \end{pmatrix}$, taking the derivative of $V(t)$ along the trajectories of (8), it can be obtained that

$$\dot{V}(t) = \frac{1}{2} y^T(t) [(\Omega\hat{L} + \hat{L}^T\Omega) \otimes I_n] y(t). \quad (12)$$

In addition,

$$\begin{aligned} \Omega\hat{L} &= \begin{pmatrix} 2\kappa\bar{L} & \Xi \\ \Xi & \kappa\Xi \end{pmatrix} \begin{pmatrix} O_N & I_N \\ -d(t)L & -\kappa d(t)L \end{pmatrix} \\ &= \begin{pmatrix} -\Xi L & 2\kappa\bar{L} - \kappa\Xi L \\ -\kappa\Xi L & \Xi - \kappa^2\Xi L \end{pmatrix}, \\ \hat{L}^T\Omega &= \begin{pmatrix} -L^T\Xi & -\kappa L^T\Xi \\ 2\kappa\bar{L} - \kappa L^T\Xi & \Xi - \kappa^2 L^T\Xi \end{pmatrix}. \end{aligned} \quad (13)$$

Thus, one obtains that

$$\frac{\Omega\hat{L} + \hat{L}^T\Omega}{2} = \begin{pmatrix} -\bar{L} & O_N \\ O_N & \Xi - \kappa^2\bar{L} \end{pmatrix}. \quad (14)$$

Therefore, from (12) to (14), one obtains

$$\dot{V}(t) \leq \|y\|^T C \|y\|, \quad (15)$$

where $C = \begin{pmatrix} -a(L)\Xi & O_N \\ O_N & \Xi - \kappa^2 a(L)\Xi \end{pmatrix}$.

Using $a(L) > 1/\kappa^2$ in condition (2), C is a negative-definite matrix.

Thus,

$$\dot{V}(t) \leq \lambda_{\max}(C) y^T(t) y(t), \quad (\lambda_{\max}(C) < 0). \quad (16)$$

And, on the other hand,

$$\begin{aligned} V(t) &= \frac{1}{2} y^T(t) (\Omega \otimes I_n) y(t) \leq \frac{1}{2} y^T(t) (D \otimes I_n) y(t) \\ &\leq \frac{1}{2} \lambda_{\max}(D) y^T(t) y(t). \end{aligned} \quad (17)$$

Consequently,

$$\dot{V}(t) \leq \eta V(t), \quad \eta = \frac{2\lambda_{\max}(C)}{\lambda_{\max}(D)} < 0, \quad (18)$$

$$t_0 + k\omega < t \leq t_0 + k\omega + \delta.$$

Thus, we can obtain

$$V(t) \leq V(t_0 + k\omega) e^{\eta(t-t_0-k\omega)}, \quad t_0 + k\omega < t \leq t_0 + k\omega + \delta. \quad (19)$$

Then let us consider the period $t_0 + k\omega + \delta < t \leq t_0 + (k+1)\omega$. For $\hat{L} = \begin{pmatrix} O_N & I_N \\ O_N & O_N \end{pmatrix}$, we can derive

$$\begin{aligned} \dot{V}(t) &= y^T(t) (\Omega \otimes I_n) [(\hat{L} \otimes I_n) y(t)] \\ &= \frac{1}{2} y^T(t) [(\Omega\hat{L} + \hat{L}^T\Omega) \otimes I_n] y(t), \end{aligned} \quad (20)$$

where

$$\begin{aligned} \Omega\hat{L} &= \begin{pmatrix} 2\kappa\bar{L} & \Xi \\ \Xi & \kappa\Xi \end{pmatrix} \begin{pmatrix} O_N & I_N \\ O_N & O_N \end{pmatrix} = \begin{pmatrix} O_N & 2\kappa\bar{L} - \kappa\Xi L \\ O_N & \Xi \end{pmatrix}, \\ \hat{L}^T\Omega &= \begin{pmatrix} O_N & O_N \\ 2\kappa\bar{L} & \alpha\Xi \end{pmatrix}. \end{aligned} \quad (21)$$

Then,

$$\frac{\Omega \hat{L} + \hat{L}^T \Omega}{2} = \begin{pmatrix} O_N & \kappa \bar{L} \\ \kappa \bar{L}^T & \Xi \end{pmatrix}. \quad (22)$$

Based on the above, one obtains

$$\dot{V}(t) \leq y^T(t) E y(t), \quad (23)$$

where $E = \begin{pmatrix} O_N & (\kappa/2)(\Xi L + L^T \Xi) \\ (\kappa/2)(\Xi L + L^T \Xi) & \Xi \end{pmatrix}$.

From Lemma 1, we obtain

$$\begin{aligned} \dot{V}(t) &\leq y^T(t) E y(t) \leq \lambda_{\max}(B^{-1}E) y^T(t) B y(t) \\ &\leq 2\lambda_{\max}(B^{-1}E) V(t). \end{aligned} \quad (24)$$

We set $\gamma = 2\lambda_{\max}(B^{-1}E) > 0$, so as to obtain

$$\begin{aligned} V(t) &\leq V(t_0 + k\bar{\omega} + \delta) e^{\gamma(t-t_0-k\bar{\omega}-\delta)}, \\ t_0 + k\bar{\omega} + \delta &< t \leq t_0 + (k+1)\bar{\omega}. \end{aligned} \quad (25)$$

Now, we can obtain from (19) and (25) that

$$\begin{aligned} V(t_0 + (k+1)\bar{\omega}) &\leq V(t_0 + k\bar{\omega} + \delta) e^{\gamma(\bar{\omega}-\delta)} \\ &\leq V(t_0 + k\bar{\omega}) e^{\gamma(\bar{\omega}-\delta)+\eta\delta} \\ &\leq \dots \leq V(t_0) e^{[\gamma(\bar{\omega}-\delta)+\eta\delta](n+1)}. \end{aligned} \quad (26)$$

It is clear that there is a constant $n_0 \geq 0$ satisfying $t_0 + n_0\bar{\omega} < t \leq t_0 + (n_0+1)\bar{\omega}$ for any $t > t_0$. Thus we get that for $t_0 + n_0\bar{\omega} < t \leq t_0 + n_0\bar{\omega} + \delta$,

$$\begin{aligned} V(t) &\leq V(t_0) e^{\eta(t-t_0-n_0\bar{\omega})} e^{[\gamma(\bar{\omega}-\delta)+\eta\delta]n_0} \\ &\leq V(t_0) e^{[\gamma(\bar{\omega}-\delta)+\eta\delta]n_0} \\ &= V(t_0) e^{-[\gamma(\bar{\omega}-\delta)+\eta\delta]} e^{[\gamma(\bar{\omega}-\delta)+\eta\delta](n_0+1)} \\ &\leq V(t_0) e^{-[\gamma(\bar{\omega}-\delta)+\eta\delta]} e^{-(\gamma(\bar{\omega}-\delta)+\eta\delta)/\bar{\omega}t_0} e^{((\gamma(\bar{\omega}-\delta)+\eta\delta)/\bar{\omega})t} \end{aligned} \quad (27)$$

and for $t_0 + n_0\bar{\omega} + \delta < t \leq t_0 + (n_0+1)\bar{\omega}$,

$$\begin{aligned} V(t) &\leq V(t_0) e^{\gamma(t-t_0-n_0\bar{\omega}-\delta)} e^{[\gamma(\bar{\omega}-\delta)+\eta\delta]n_0} \\ &\leq V(t_0) e^{((\gamma(\bar{\omega}-\delta)+\eta\delta)/\bar{\omega})[\bar{\omega}(n_0+1)+t_0-t_0]} \\ &\leq V(t_0) e^{-((\gamma(\bar{\omega}-\delta)+\eta\delta)/\bar{\omega})t_0} e^{((\gamma(\bar{\omega}-\delta)+\eta\delta)/\bar{\omega})t}. \end{aligned} \quad (28)$$

Hence, let $K = V(t_0) e^{-[\gamma(\bar{\omega}-\delta)+\eta\delta]} e^{-((\gamma(\bar{\omega}-\delta)+\eta\delta)/\bar{\omega})t_0}$, and we can conclude the following from the above analysis:

$$V(t) \leq K e^{((\gamma(\bar{\omega}-\delta)+\eta\delta)/\bar{\omega})t}, \quad t > t_0, \quad (29)$$

which means that the states of agents can achieve consensus. The proof is complete. \square

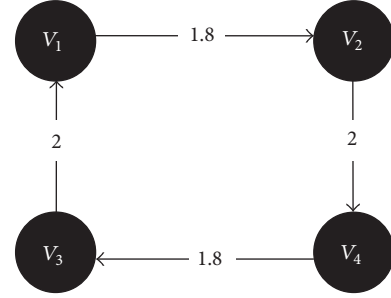


FIGURE 1: The directed interaction topology of multiagent networks.

4. Numerical Simulations

A multiagent network of four agents is considered as the simulation example. The multiagent network topology is described by a directed network \mathcal{g} shown in Figure 1. It can be seen that the network is strongly connected.

Let $\kappa = 2$ and $n = 3$. With simple calculations, we obtain the $a(L) = 1.8 > 1/\kappa^2$, $\eta = -2.1204$, and $\gamma = 3.5980$. From condition (3), we obtain $\delta/\bar{\omega} > 0.6292$. So if we set $\delta = 0.07$ and $\bar{\omega} = 0.1$, second-order consensus can be achieved in system (2). The initial position and velocity values of agents are $x_1 = (3, 1, -3)^T$, $x_2 = (6, 2, -6)^T$, $x_3 = (-5, 3, -9)^T$, $x_4 = (9, 4, -12)^T$, $v_1 = (2, 3, -2)^T$, $v_2 = (-5, 6, 3)^T$, $v_3 = (1, -4, 2)^T$, and $v_4 = (3, 4, -5)^T$, respectively. Figure 2 shows the linear consensus of position and velocity states of four agents with intermittent control.

5. Conclusions

In this paper, we have considered the linear consensus of multiagent networks with periodic intermittent interaction and directed topology. We choose to show the consensus with linear local interaction protocols, partly for simplifying the problem. On the other hand, it is simple and easy to implement so as to be widely used in practical engineering. The tools from algebraic graph theory, matrix theory, and Lyapunov control approach have been adopted. It is shown that the consensus is determined commonly by the general algebraic connectivity, control period, and control width. And the states of agents converge exponentially.

Conflict of Interests

The author declares that there is no conflict of interests regarding the publication of this paper.

Acknowledgments

The author sincerely thanks Junjie Bao (Department of Mathematics and Information Engineering, Chongqing University of Education) for his helpful work that led to the present version. And the work was supported by the Foundation

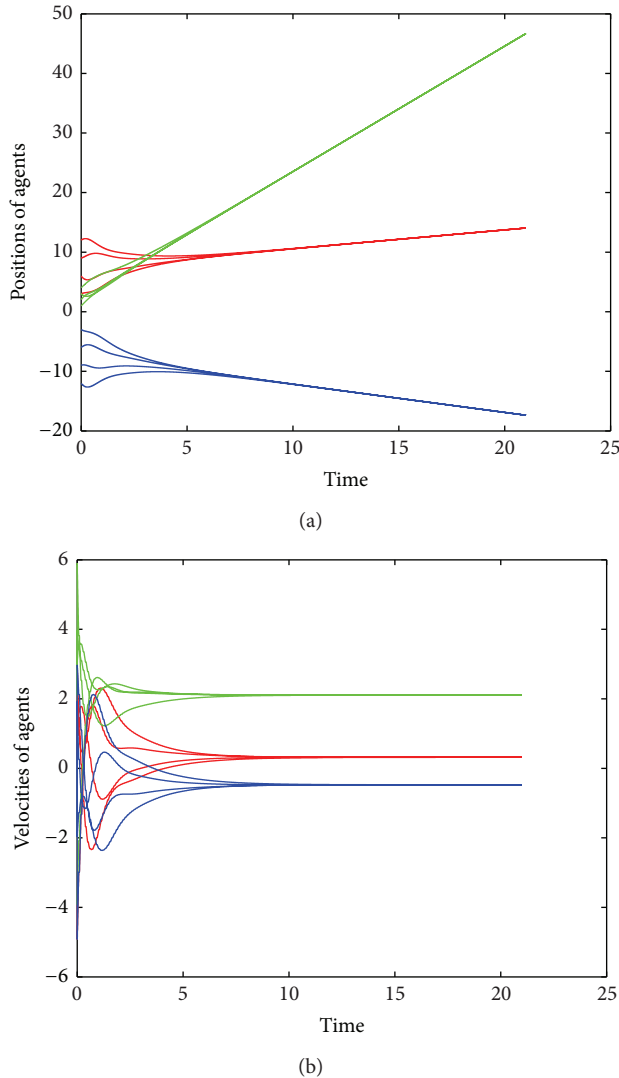


FIGURE 2: Position and velocity states of four agents in the network.

Project of CQCSTC (no. cstc2014jcyjA40041), the National Natural Science Foundation of China (no. 60973114), and the Foundation of Chongqing University of Education (no. KY201318B).

References

- [1] G. Hu, "Robust consensus tracking of a class of second-order multi-agent dynamic systems," *Systems and Control Letters*, vol. 61, no. 1, pp. 134–142, 2012.
- [2] H. G. Tanner, A. Jadbabaie, and G. J. Pappas, "Flocking in fixed and switching networks," *IEEE Transactions on Automatic Control*, vol. 52, no. 5, pp. 863–868, 2007.
- [3] H. Zhang, C. Zhai, and Z. Chen, "A general alignment repulsion algorithm for flocking of multi-agent systems," *IEEE Transactions on Automatic Control*, vol. 56, no. 2, pp. 430–435, 2011.
- [4] P. Lin and Y. Jia, "Distributed rotating formation control of multi-agent systems," *Systems & Control Letters*, vol. 59, no. 10, pp. 587–595, 2010.
- [5] C. Li, C. Li, X. Liao, and T. Huang, "Impulsive effects on stability of high-order BAM neural networks with time delays," *Neurocomputing*, vol. 74, no. 10, pp. 1541–1550, 2011.
- [6] X. He, C. Li, and Y. Shu, "Bogdanov-Takens bifurcation in a single inertial neuron model with delay," *Neurocomputing*, vol. 89, pp. 193–201, 2012.
- [7] C. W. Wu and L. O. Chua, "Synchronization in an array of linearly coupled dynamical systems," *IEEE Transactions on Circuits and Systems*, vol. 42, no. 8, pp. 430–447, 1995.
- [8] J. Hu and Y. Hong, "Leader-following coordination of multi-agent systems with coupling time delays," *Physica A: Statistical Mechanics and its Applications*, vol. 374, no. 2, pp. 853–863, 2007.
- [9] W. Yu, G. Chen, Z. Wang, and W. Yang, "Distributed consensus filtering in sensor networks," *IEEE Transactions on Systems, Man, and Cybernetics B*, vol. 39, no. 6, pp. 1568–1577, 2009.
- [10] A. K. Das, R. Fierro, V. Kumar, J. P. Ostrowski, J. Spletzer, and C. J. Taylor, "A vision-based formation control framework," *IEEE Transactions on Robotics and Automation*, vol. 18, no. 5, pp. 813–825, 2002.
- [11] Y. Chen, J. Lü, F. Han, and X. Yu, "On the cluster consensus of discrete-time multi-agent systems," *Systems and Control Letters*, vol. 60, no. 7, pp. 517–523, 2011.
- [12] H. Wang, X. Liao, T. Huang, and C. Li, "Cooperative distributed optimization in multi-agent networks with delays," *IEEE Transactions on Systems, Man, and Cybernetics: Systems*, no. 99, p. 1, 2014.
- [13] L. Moreau, "Stability of multiagent systems with time-dependent communication links," *IEEE Transactions on Automatic Control*, vol. 50, no. 2, pp. 169–182, 2005.
- [14] H. Wang, X. Liao, T. Huang, and C. Li, "Improved weighted average prediction for multi-agent networks," *Circuits, Systems and Signal Processing*, vol. 33, no. 6, pp. 1721–1736, 2014.
- [15] B. Liu, W. Lu, and T. Chen, "Consensus in networks of multiagents with switching topologies modeled as adapted stochastic processes," *SIAM Journal on Control and Optimization*, vol. 49, no. 1, pp. 227–253, 2011.
- [16] H. Li, X. Liao, T. Dong, and L. Xiao, "Second-order consensus seeking in directed networks of multi-agent dynamical systems via generalized linear local interaction protocols," *Nonlinear Dynamics*, vol. 70, no. 3, pp. 2213–2226, 2012.
- [17] L. Xiao and X. Liao, "Periodic intermittent consensus of second-order agents networks with nonlinear dynamics," *International Journal of Control, Automation and Systems*, vol. 12, no. 1, pp. 23–28, 2014.
- [18] W. Yu, G. Chen, M. Cao, and J. Kurths, "Second-Order consensus for multiagent systems with directed topologies and nonlinear dynamics," *IEEE Transactions on Systems, Man, and Cybernetics, Part B: Cybernetics*, vol. 40, no. 3, pp. 881–891, 2010.
- [19] S. Wang and D. Xie, "Consensus of second-order multi-agent systems via sampled control: undirected fixed topology case," *IET Control Theory & Applications*, vol. 6, no. 7, pp. 893–899, 2012.
- [20] F. Xiao and L. Wang, "Asynchronous consensus in continuous-time multi-agent systems with switching topology and time-varying delays," *IEEE Transactions on Automatic Control*, vol. 53, no. 8, pp. 1804–1816, 2008.
- [21] Y. Zhang and Y. P. Tian, "Consentability and protocol design of multi-agent systems with stochastic switching topology," *Automatica*, vol. 45, no. 5, pp. 1195–1201, 2009.

- [22] J. Huang, C. Li, and X. He, "Stabilization of a memristor-based chaotic system by intermittent control and fuzzy processing," *International Journal of Control, Automation and Systems*, vol. 11, no. 3, pp. 643–647, 2013.
- [23] S. Boyd, L. El Ghaoui, E. Feron, and V. Balakrishnan, *Linear Matrix Inequalities in System and Control Theory*, vol. 15, Society for Industrial Mathematics, 1994.
- [24] R. A. Horn and C. R. Johnson, *Matrix Analysis*, Cambridge University Press, 1985.

Research Article

Chaotic Behaviors of Symbolic Dynamics about Rule 58 in Cellular Automata

Yangjun Pei,¹ Qi Han,¹ Chao Liu,¹ Dedong Tang,¹ and Junjian Huang²

¹ School of Electrical and Information Engineering, Chongqing University of Science and Technology, Chongqing 401331, China

² Department of Mathematics and Information Engineering, Chongqing University of Education College, Chongqing 400065, China

Correspondence should be addressed to Qi Han; hanqicq@163.com

Received 14 April 2014; Accepted 25 June 2014; Published 22 July 2014

Academic Editor: Chuandong Li

Copyright © 2014 Yangjun Pei et al. This is an open access article distributed under the Creative Commons Attribution License, which permits unrestricted use, distribution, and reproduction in any medium, provided the original work is properly cited.

The complex dynamical behaviors of rule 58 in cellular automata are investigated from the viewpoint of symbolic dynamics. The rule is Bernoulli σ_r -shift rule, which is members of Wolfram's class II, and it was said to be simple as periodic before. It is worthwhile to study dynamical behaviors of rule 58 and whether it possesses chaotic attractors or not. It is shown that there exist two Bernoulli-measure attractors of rule 58. The dynamical properties of topological entropy and topological mixing of rule 58 are exploited on these two subsystems. According to corresponding strongly connected graph of transition matrices of determinative block systems, we divide determinative block systems into two subsets. In addition, it is shown that rule 58 possesses rich and complicated dynamical behaviors in the space of bi-infinite sequences. Furthermore, we prove that four rules of global equivalence class ε_4^3 of CA are topologically conjugate. We use diagrams to explain the attractors of rule 58, where characteristic function is used to describe that some points fall into Bernoulli-shift map after several times iterations, and we find that these attractors are not global attractors. The Lameray diagram is used to show clearly the iterative process of an attractor.

1. Introduction

Cellular automaton (CA) was first introduced in 1951 [1]. CA is a mathematical model consisting of large numbers of simple identical components with local interactions [2]. The simple components act together to produce complex global behavior. CA performs complex computation with high degree of efficiency and robustness. Three major factors have resulted in the revival of interest in the behavior of cellular systems [3]. First, the development of powerful computers and microprocessors has made the rapid simulation of CA possible. Second, the use of CA to simulate physical systems has attracted much interest in the scientific community. Third, the advent of VLSI as an implementation medium has focused attention on the communication requirements of successful hardware algorithms. In recent years, many applications of CA have been reported, especially in cryptography [4–9], image processing [10, 11], and associative memory [12, 13].

In recent years, many researches were devoted to find properties of rules of CA, especially binary one-dimensional

CA. Because the rules of binary one-dimensional CA are simple to study, the evolutions of these rules can be reflected directly by image. In 1980s, Wolfram proposed CA as models for physical systems which exhibit complex or even chaotic behaviors based on empirical observations, and he divided the 256 ECA (binary one-dimensional CA with radius 1) rules informally into four classes using dynamical concepts like periodicity, stability, and chaos [14–16]. Recently, [17–22] focused on ECA in detail. In [17], Chua et al. listed 256 Boolean function “cubes” defining all Boolean functions of three binary variables, and they elucidated that every binary cellular automata of any spatial dimension was a special case of a cellular automaton with the same neighborhood size. In [18], Chua et al. partitioned the entire set of 256 local rules into 16 different gene families. Chua et al. [19] mentioned that each rule has three globally equivalent local rules determined by three corresponding global transformations, namely, left-right transformation T^+ , global complementation \bar{T} , and left-right complementation T^* . Each equivalence class is identified by ε_m^κ , where κ is complexity index and m is index of κ th class. In [20], the authors presented that 112 rules of

256 local rules were Bernoulli σ_τ -shift rules. Each of the 112 Bernoulli σ_τ -shift rules has an ID code $B_N[\alpha, \beta, \tau]$, where α denotes the number of attractors of rule N , β denotes the slope of the Bernoulli σ_τ -shift map, and τ denotes the relevant forward time- τ . Hence, the space-time evolution of any one of the 112 rules on their attractors can be uniquely predicted by two parameters: $\beta = \pm 2^\sigma$ and τ . For example, rule 58 has two attractors ($\beta = 2$, $\sigma = 1$, $\tau = 1$) and ($\beta = 1/2$, $\sigma = -1$, $\tau = 2$). Wolfram considered that Bernoulli σ_τ -shift rules were simple as periodic, but he did not find other complex dynamical behaviors. Recently, some authors [23–28] found that some rules of Bernoulli σ_τ -shift rules are chaotic in the sense of both Li-York and Devaney. However, they did not involve and studied the dynamical behavior of rule 58. For 256 rules, every rule has its properties which are different from other rules. So, we need to study these special properties for every rule for practical application.

In this paper, the complex dynamical behavior of rule 58 in cellular automata is studied in detail. It will be shown that rule 58 with bi-infinite bit strings possesses rich and complicated dynamical behaviors. The rest of the paper is organized as follows. In Section 2, the basic concepts of one-dimension CA (1DCA) and symbolic dynamics are introduced. The Boolean functions of rule 58 are also presented, and expressions of two attractors are given. In Section 3, two subsystems of rule 58 are characterized. We prove that rule 58 is topologically mixing and chaotic in the sense of Li-York and Devaney on the Λ_1^{58} and Λ_2^{58} , respectively. We also prove that four rules of global equivalence class ε_4^3 of CA are topologically conjugate. In Section 4, characteristic function is used to describe that all points of rule 58 fall into Bernoulli-shift map after several times iterations, and the Lameray diagram is used to show clearly the iterative process of an attractor. We mention that rule 58 can be used in associative memory. Section 5 presents some conclusions.

2. Preliminaries

For simplicity, for some notations about symbolic dynamics, one can refer to [27–29].

It follows from [30] that the Boolean function of rule 58 is

$$[f_{58}(x)]_i = x_{i-1} \cdot \bar{x}_i \oplus \bar{x}_{i-1} \cdot x_{i+1} \quad (1)$$

$\forall x \in S^Z$, $i \in Z$, where “ \cdot ,” “ $-$,” and “ \oplus ” stand for “AND,” “NOT,” and “XOR” logical operation, respectively. Sometimes, “ \cdot ” is omitted for simplicity. The truth table of Boolean functions of rule 58 is shown in Table 1. The subsets, denoted by Λ_1^{58} and Λ_2^{58} , are derived from the parameters of rules 58: $\beta = 2$, $\sigma = 1$, and $\tau = 1$ and $\beta = 1/2$, $\sigma = -1$, and $\tau = 2$, respectively; that is,

$$\begin{aligned} \Lambda_1^{58} &= \{x \in S^Z \mid [f_{58}(x)]_i = x_{i+1}, \forall i \in Z\}, \\ \Lambda_2^{58} &= \{x \in S^Z \mid [f_{58}^2(x)]_i = x_{i-1}, \forall i \in Z\}, \end{aligned} \quad (2)$$

where $f^2(\cdot)$ denotes two iterations for a bit.

The subsets Λ_1^{58} and Λ_2^{58} will be rigorously characterized from the viewpoint of symbolic dynamics.

TABLE 1: The truth table of Boolean function of rules 58.

$x_{i-1}x_ix_{i+1}$	$x_{i-1}\bar{x}_i \oplus \bar{x}_{i-1}x_{i+1}$
000	0
001	1
010	0
011	1
100	1
101	1
110	0
111	0

3. Dynamical Behaviors of f_{58} on Two Subsystems

In this section, dynamical behaviors of f_{58} will be researched. We find that rule 58 is chaotic in the sense of Li-York and Devaney on its two subsystems.

Proposition 1. *For rule 58, there exists a subset $\Lambda_1^{58} \subset S^Z$ which satisfies $f_{58}|_{\Lambda_1^{58}} = v|_{\Lambda_1^{58}}$ if and only if $\forall x = (\dots, x_{-1}, x_0, x_1, \dots) \in \Lambda_1^{58}$, x_{i-1} , x_i and x_{i+1} have the following relations:*

- (i) if $x_i = 1$, then $x_{i-2} = 1$, $x_{i-1} = 0$, $x_{i+1} = 0$, and $x_{i+2} = 1$; $x_{i-2} = 0$, $x_{i-1} = 0$, $x_{i+1} = 1$, and $x_{i+2} = 0$; $x_{i-2} = 0$, $x_{i-1} = 1$, $x_{i+1} = 0$, and $x_{i+2} = 1$;
- (ii) if $x_i = 0$, then $x_{i-2} = 0$, $x_{i-1} = 0$, $x_{i+1} = 0$, $x_{i+2} = 0$, $x_{i-1} = 1$, and $x_{i+1} = 1$.

The explicit proof of this proposition is presented in the Appendix.

Remark 2. From the definition of subsystem, we know that (Λ_1^{58}, f_{58}) is subsystems of (S^Z, f_{58}) .

The dynamical behaviors of $f_{58}(x)$ on the set Λ_1^{58} are shown as follows.

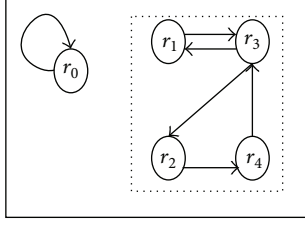
Let $P_1^{58} = \{r_0, r_1, r_2, r_3, r_4\}$ be a new state set, where $r_0 = (000)$, $r_1 = (010)$, $r_2 = (011)$, $r_3 = (101)$, $r_4 = (110)$, and $\omega_1^{58} = \{(rr') \mid r = (b_0b_1b_2), r' = (b'_0b'_1b'_2) \in P_1^{58}, \forall 1 \leq j \leq 2 \text{ such that } b_j = b'_{j-1}\}$. Furthermore, subshift $\Lambda_{\omega_1^{58}}$ of v is defined as $\Lambda_{\omega_1^{58}} = \{r = (\dots r_{-1}, r_0, r_1 \dots) \in P_1^{58Z} \mid r_i \in P_1^{58}, r_i r_{i+1} \in \omega_1^{58}, \forall i \in Z\}$. The transition matrix B_1^{58} of the $v|_{\Lambda_{\omega_1^{58}}}$ is

$$B_1^{58} = \begin{bmatrix} 1 & 0 & 0 & 0 & 0 \\ 0 & 0 & 0 & 1 & 0 \\ 0 & 0 & 0 & 0 & 1 \\ 0 & 1 & 1 & 0 & 0 \\ 0 & 0 & 0 & 1 & 0 \end{bmatrix}. \quad (3)$$

In order to give our results, in the following, some definitions need be introduced.

Definition 3 (see [31]). A square $\{0, 1\}$ matrix A is irreducible, if for every pair of indices i and j there is an n such that $A_{ij}^n > 0$.

Definition 4 (see [31]). A square $\{0, 1\}$ matrix A is aperiodic, if there exists N , such that $A_{ij}^n > 0$ and $n > N$, $\forall i, j$.

FIGURE 1: The corresponding graph G_{58}^1 of the matrix B_1^{58} .

Definition 5 (see [31]). Suppose that $g : X \rightarrow Y$ is a continuous mapping, where X is a compact topological space. g is said to be topologically mixing if, for any two open sets $U, V \subset X$, $\exists N > 0$, such that $g^n(U) \cap V \neq \emptyset$, $\forall n \geq N$.

Definition 6 (see [24]). Let (X, f) and (Y, g) be compact spaces, one says that f and g are topologically conjugate if there is homeomorphism $h : X \rightarrow Y$, such that $h \circ f = g \circ h$.

A square $\{0, 1\}$ matrix corresponds to a directed graph. The vertices of the graph are the indices for the rows and columns of A . There is an edge from vertex i to vertex j if $A_{ij} = 1$. A square $\{0, 1\}$ matrix is irreducible if and only if the corresponding graph is strongly connected. If Λ_A is a two-order subshift of finite type, then it is topologically mixing if and only if A is irreducible and aperiodic [31].

We give corresponding graph G_{58}^1 of the matrix B_1^{58} in Figure 1. We find that G_{58}^1 is not a strongly connected graph. Therefore, $f_{58}|_{\Lambda_1^{58}}$ is not topologically mixing. But the subgraphs r_0 and r_1, r_2, r_3 , and r_4 are strongly connected graph, respectively. So, we can divide P_1^{58} into two subsets: $\mathcal{H}_1^{58} = \{r_0\}$ and $\mathcal{X}_1^{58} = \{r_1, r_2, r_3, r_4\}$.

Let $\mathcal{H}_1^{58} = \{(rr') \mid r = (b_0 b_1 b_2), r' = (b'_0 b'_1 b'_2) \in P_1^{58}, \forall 1 \leq j \leq 2, \text{ such that } b_j = b'_{j-1}\}$ corresponding to \mathcal{H}_1^{58} and $\mathcal{X}_1^{58} = \{(rr') \mid r = (b_0 b_1 b_2), r' = (b'_0 b'_1 b'_2) \in P_1^{58}, \forall 1 \leq j \leq 2, \text{ such that } b_j = b'_{j-1}\}$ corresponding to \mathcal{X}_1^{58} . We can obtain the transition matrix C_1^{58} corresponding to $v|_{\Lambda_{\mathcal{H}_1^{58}}}$ and transition matrix D_1^{58} corresponding to $v|_{\Lambda_{\mathcal{X}_1^{58}}}$, where

$$C_1^{58} = [1], \quad D_1^{58} = \begin{bmatrix} 0 & 0 & 1 & 0 \\ 0 & 0 & 0 & 1 \\ 1 & 1 & 0 & 0 \\ 0 & 0 & 1 & 0 \end{bmatrix}. \quad (4)$$

Based on the above definition and analysis, we give the following results.

Proposition 7. Consider the following:

- (a) $\Lambda_{\mathcal{H}_1^{58}} \cup \Lambda_{\mathcal{X}_1^{58}} = \Lambda_1^{58}$, where $\mathcal{H}_1^{58} \cup \mathcal{X}_1^{58} = P_1^{58}$ and $\mathcal{H}_1^{58} \cap \mathcal{X}_1^{58} = \emptyset$.
- (b) $v : \Lambda_{\mathcal{H}_1^{58}} \rightarrow \Lambda_{\mathcal{H}_1^{58}}$ and $v : \Lambda_{\mathcal{X}_1^{58}} \rightarrow \Lambda_{\mathcal{X}_1^{58}}$ are topologically conjugate.
- (c) $v : \Lambda_{\mathcal{X}_1^{58}} \rightarrow \Lambda_{\mathcal{X}_1^{58}}$ is topologically mixing.
- (d) $f_{58} : \Lambda_{\mathcal{X}_1^{58}} \rightarrow \Lambda_{\mathcal{X}_1^{58}}$ is topologically mixing.

- (e) The topological entropy $\text{ent}(f_{58}|_{\Lambda_{\mathcal{X}_1^{58}}}) = \text{ent}(v|_{\Lambda_{\mathcal{X}_1^{58}}}) = 0.2812$.

Proof. (a) Let $x = \{\dots, x_{-1}, x_0, x_1\}$. It is obvious that if $w' < x$, $w' \in \mathcal{H}_1^{58}$, then $\forall w'' \in \mathcal{X}_1^{58}$, $w'' \not< x$, thus $x \in \Lambda_{\mathcal{H}_1^{58}}$; conversely, if $w' < x$, $w' \in \mathcal{X}_1^{58}$, then $\forall w'' \in \mathcal{H}_1^{58}$, $w'' \not< x$, thus $x \in \Lambda_{\mathcal{X}_1^{58}}$; namely, $\forall x \in \Lambda_1^{58}$, $x \in \Lambda_{\mathcal{H}_1^{58}}$, or $x \in \Lambda_{\mathcal{X}_1^{58}}$. Hence, $\Lambda_{\mathcal{H}_1^{58}} \cup \Lambda_{\mathcal{X}_1^{58}} = \Lambda_1^{58}$.

The proofs of (b), (c), (d), and (e) can be referred to in Proposition 2 in [28]. \square

Theorem 8. f_{58} is chaotic in the sense of both Li-Yorke and Devaney on $\Lambda_{\mathcal{X}_1^{58}}$.

Proof. It follows from [32] that the positive topological entropy implies chaos in the sense of Li-Yorke, and topological mixing implies chaos in the sense of Li-Yorke and Devaney, since rule $N = 58$ possesses very rich and complicated dynamical properties on $\Lambda_{\mathcal{X}_1^{58}}$. \square

Remark 9. Though, $\forall n > 0$, $(C_1^{58})^n > 0$, we cannot believe that $f_{58}|_{\Lambda_1^{58}}$ is topologically mixing. Because C_1^{58} is not a square $\{0, 1\}$ matrix. The topological entropy $\text{ent}(f_{58}|_{\Lambda_{\mathcal{H}_1^{58}}}) = 0$. So, f_{58} is not chaotic in the sense of both Li-Yorke and Devaney on $\Lambda_{\mathcal{H}_1^{58}}$.

Remark 10. Carefully observing Figure 1, we find that there are several strongly connected subgraphs: $r_2 \rightarrow r_3 \rightarrow r_4 \rightarrow r_2$, $r_1 \rightarrow r_3 \rightarrow r_1$, $r_1 \rightarrow r_3 \rightarrow r_2 \rightarrow r_4 \rightarrow r_3 \rightarrow r_1$, and $r_0 \rightarrow r_0$. The elements of Λ_1^{58} are composed by all vertices of those strongly connected subgraphs, respectively. For example, $x \in \Lambda_1^{58}$ and x is composed of vertices of subgraph $r_2 \rightarrow r_3 \rightarrow r_4 \rightarrow r_2$; then we have $r_0 \not< x$ and $r_1 \not< x$, and all vertices of the subgraph will appear in x , if $|x| = 3k, k = 1, 2, \dots$

Proposition 11. For rule 58, there exists a subset $\Lambda_2^{58} \subset S^Z$ which satisfies $f_{58}^2|_{\Lambda_2^{58}} = c|_{\Lambda_2^{58}}$ if and only if, $\forall x = (\dots, x_{-1}, x_0, x_1, \dots) \in \Lambda_2^{58}$, $x_{i-1}x_i x_{i+1}$ cannot equal to 010, $\forall i \in \mathbb{Z}$.

Proof. The global map of rule 58 is $[f_{58}(x)]_i = x_{i-1}\bar{x}_i \oplus \bar{x}_{i-1}x_{i+1}$, so

$$\begin{aligned} [f_{58}^2(x)]_i &= [f_{58}(x)]_{i-1} \cdot \overline{[f_{58}(x)]_i} \oplus \overline{[f_{58}(x)]_{i-1}} \cdot [f_{58}(x)]_{i+1} \\ &= [(x_{i-2}\bar{x}_{i-1} \oplus \bar{x}_{i-2}x_i) \cdot \overline{x_{i-1}\bar{x}_i \oplus \bar{x}_{i-1}x_{i+1}}] \\ &\quad \oplus [\overline{x_{i-2}\bar{x}_{i-1} \oplus \bar{x}_{i-2}x_i} \cdot (x_i\bar{x}_{i+1} \oplus \bar{x}_i x_{i+2})]. \end{aligned} \quad (5)$$

Then, the proof is similar to proof of necessity and sufficiency in Proposition 1, so the details are omitted. \square

Let $P_2^{58} = \{r_0, r_1, r_2, r_3, r_4, r_5, r_6\}$, where $r_0 = (000)$, $r_1 = (001)$, $r_2 = (011)$, $r_3 = (100)$, $r_4 = (101)$, $r_5 = (110)$, and $r_6 = (111)$.

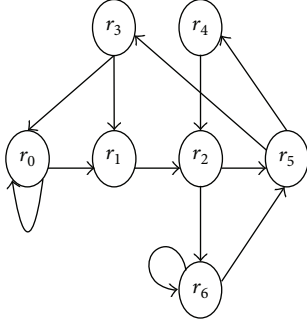


FIGURE 2: The corresponding graph G_{58}^2 of the matrix B_2^{58} .

Remark 12. The transition matrix of subshift $(\Lambda_2^{58}, \varsigma)$ is

$$B_2^{58} = \begin{bmatrix} 1 & 1 & 0 & 0 & 0 & 0 & 0 \\ 0 & 0 & 1 & 0 & 0 & 0 & 0 \\ 0 & 0 & 0 & 0 & 0 & 1 & 1 \\ 1 & 1 & 0 & 0 & 0 & 0 & 0 \\ 0 & 0 & 1 & 0 & 0 & 0 & 0 \\ 0 & 0 & 0 & 1 & 1 & 0 & 0 \\ 0 & 0 & 0 & 0 & 0 & 1 & 1 \end{bmatrix}. \quad (6)$$

We give corresponding graph G_{58}^2 of the matrix B_2^{58} in Figure 2. It is obvious that G_{58}^2 is a strongly connected graph. So, B_2^{58} is irreducible.

Based on the above analysis, we have the following results.

Proposition 13. Consider the following:

- (a) $\varsigma|_{\Lambda_2^{58}}$ is topologically mixing.
- (b) $f_{58}^2|_{\Lambda_2^{58}}$ is topologically mixing.
- (c) The topological entropy $\text{ent}(f_{58}^2|_{\Lambda_2^{58}}) = \text{ent}(\varsigma|_{\Lambda_2^{58}}) = 0.5624$.

Proof. (a) Because $(B_2^{58})^n > 0, \forall n \geq 4$, the transition matrix B_2^{58} of subshift of finite type ς is irreducible and aperiodic. By [32, 33], $\varsigma|_{\Lambda_2^{58}}$ is topologically mixing. \square

Theorem 14. f_{58}^2 is chaotic in the sense of both Li-Yorke and Devaney on Λ_2^{58} .

Proof. It follows from [32] that topological mixing implies chaos in the sense of Li-Yorke and Devaney. \square

Proposition 15. Consider $f(x) \in \Lambda_2^{58}, \forall x \in \Lambda_2^{58}$.

Proof. We check that $x_1, x_2 \in \Lambda_2^{58}$, where $x_1 = \{\dots, a_{-2}, a_{-1}, a_0, a_1, a_2, \dots\}$. Let $f_{58}^2(x_1) = x_2$. Suppose that $f_{58}(x_1) = y_1$ and $f_{58}(x_2) = y_2$, where $y_1 = \{\dots, b_{-2}, b_{-1}, b_0, b_1, b_2, \dots\}$ and $y_2 = \{\dots, c_{-3}, c_{-2}, c_{-1}, c_0, c_1, \dots\}$. Table 2 shows the iterative process of bit string x_1 . Observing Table 2, we have $f_{58}(a_{-1}a_0a_1) = b_0 = c_0, \dots, f_{58}(a_{i-1}a_i a_{i+1}) = b_i = c_i, \dots$. So, we get $f_{58}^2(y_1) = y_2$. Therefore, $y_1, y_2 \in \Lambda_2^{58}$. Hence, $f(x) \in \Lambda_2^{58}, \forall x \in \Lambda_2^{58}$. \square

TABLE 2: The iterative process of bit string x_1 .

x_1	\dots	a_{-2}	a_{-1}	a_0	a_1	a_2	\dots
y_1	\dots	b_{-2}	b_{-1}	b_0	b_1	b_2	\dots
x_2	\dots	a_{-3}	a_{-2}	a_{-1}	a_0	a_1	\dots
y_2	\dots	c_{-3}	c_{-2}	c_{-1}	c_0	c_1	\dots

Corollary 16. Consider $f_{58}^2|_{\Lambda_2^{58}} = (f_{58}|_{\Lambda_2^{58}})^2$.

Proposition 17. Consider the following:

- (a) $f_{58}|_{\Lambda_2^{58}}$ is topologically mixing.
- (b) The topological entropy $\text{ent}(f_{58}|_{\Lambda_2^{58}}) = 0.2812$.

The explicit proof of this proposition is presented in the Appendix.

Theorem 18. f_{58} is chaotic in the sense of both Li-Yorke and Devaney on Λ_2^{58} .

Remark 19. It is obviously that (Λ_2^{58}, f_{58}) are subsystems of (S^Z, f_{58}) . Hence, there are two subsystems for (S^Z, f_{58}) .

Next, we will discuss the relationship on four rules of global equivalence class ϵ_4^3 .

Remark 20. From [20, 28–30], the following results can be obtained:

- (1) $f_{58} : S^Z \rightarrow S^Z$ and $f_{114} : S^Z \rightarrow S^Z$ are topologically conjugate;
- (2) $f_{58} : S^Z \rightarrow S^Z$ and $f_{163} : S^Z \rightarrow S^Z$ are topologically conjugate;
- (3) $f_{58} : S^Z \rightarrow S^Z$ and $f_{177} : S^Z \rightarrow S^Z$ are topologically conjugate.

Remark 21. f_{58}, f_{114}, f_{163} , and f_{177} are topologically conjugate, respectively. Therefore, if we know that one of four rules is chaotic in the sense of both Li-Yorke and Devaney in its attractors, we can deem that others of four rules are chaotic in the sense of both Li-Yorke and Devaney in their attractors, respectively. The phenomenon also presents that the global equivalence class introduced by Chua et al. [22] is useful and important for research of rule of cellular automata.

4. Using Diagrams to Explain Attractors of Four Rules

From a definition on global characteristic function in [20], the Boolean string x can be associated with a real number $0.x_0x_1\dots x_{I-1}x_I$ on the unit interval $[0, 1]$:

$$x = [x_0x_1\dots x_{I-1}x_I] \mapsto \phi \triangleq 0.x_0x_1\dots x_{I-1}x_I, \quad (7)$$

$$x_i \in \{0, 1\},$$

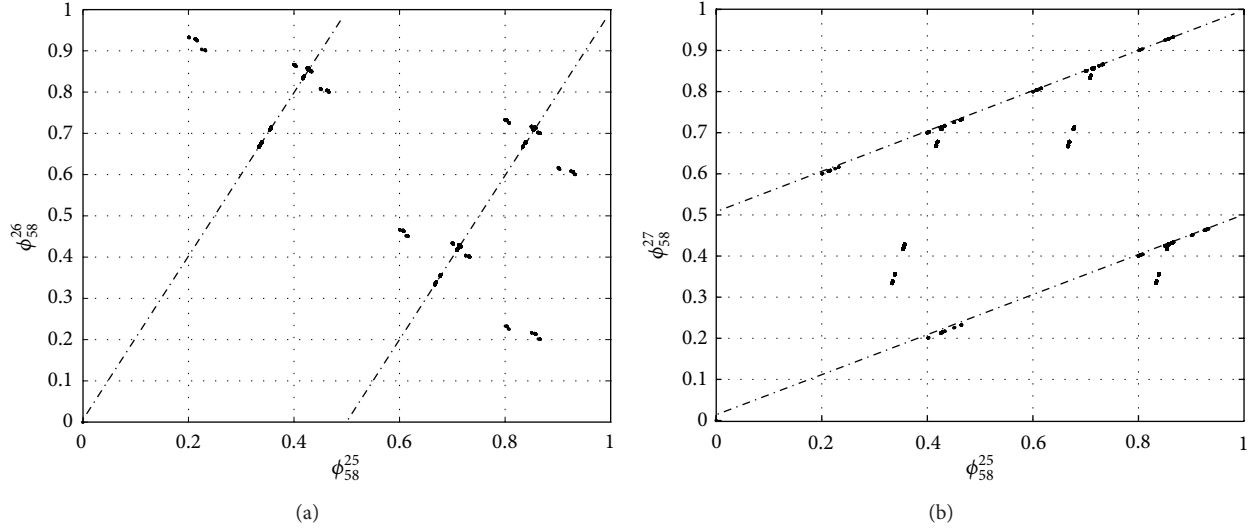


FIGURE 3: All points fall into Bernoulli-shift map after several iterations under rule 58, where $I = 13$.

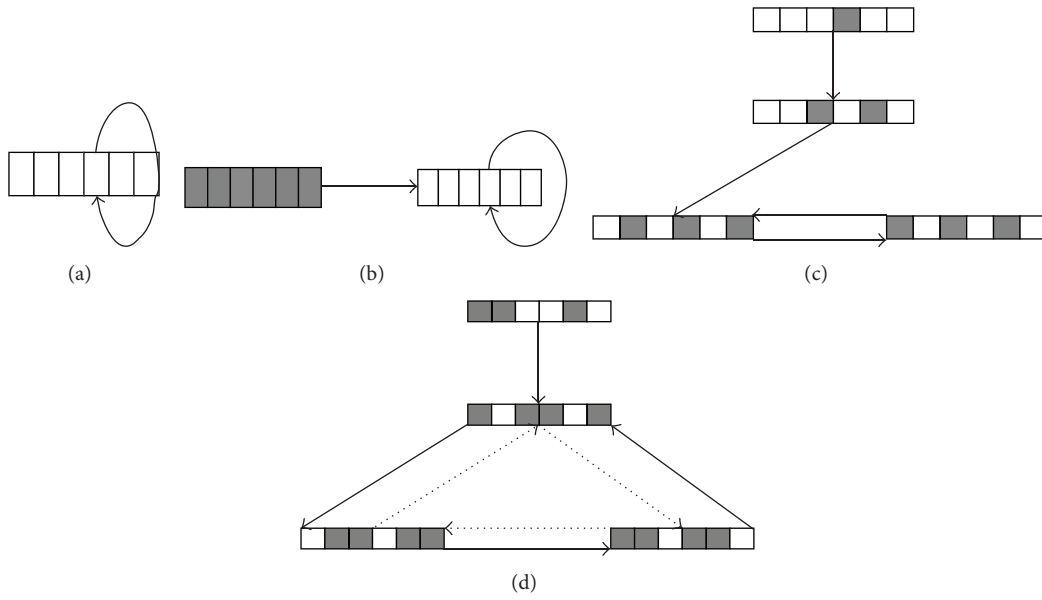


FIGURE 4: Some attractors of rule 58, where $I = 5$, and the white lattice stands for 0 and black for 1.

where $\phi = \sum_{i=0}^I 2^{-(i+1)} x_i$ is the decimal form of Boolean string $x = [x_0 x_1 \dots x_{I-1} x_I]$. The CAs' characteristic function χ_N of rule N is defined as

$$\chi_N : Q[0, 1] \longrightarrow Q[0, 1], \quad (8)$$

$$\text{that is, } \phi_n = \chi_N^1(\phi_{n-1}), \quad \phi_n = \chi_N^2(\phi_{n-2}),$$

where Q denotes rational numbers.

Let $I = 13$. Figure 3 shows characteristic functions of rule 58. Figure 3(a) describes that some points of rule 58 fall into Bernoulli-shift map after twenty-six iterations, respectively, where $\tau = 1$. Figure 3(b) describe that some points of four rules fall into Bernoulli-shift map after twenty-seven iterations, respectively, where $\tau = 2$.

If we choose different values of I for the four rules, we can get different initial binary configuration for the evolution of four rules. The different initial binary configuration may lead to different attractor periods. If the value of I is fixed, we find that the attractor period may be different. Let $I = 5$; then we can obtain Figure 4, which shows some attractors of rule 58. Figures 4(a) and 4(b) show that the period of attractor is 1, and the attractor belongs to $\Lambda_{h_1^{58}}$ and Λ_2^{58} ; Figure 4(c) shows that the period of attractor is 2, and the attractor belongs to $\Lambda_{\lambda_1^{58}}$; Figure 4(d) shows that the attractor belongs to both $\Lambda_{\lambda_1^{58}}$ and Λ_2^{58} , where the solid lines represent that the attractor belongs to $\Lambda_{\lambda_1^{58}}$ and the dotted lines represent that the attractor belongs to Λ_2^{58} . Let $I = 4$; then we can obtain

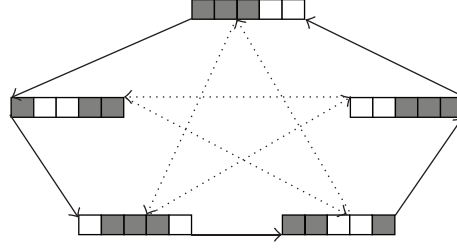


FIGURE 5: Period-5 isle of Eden is shown, where $I = 4$, and the white lattice stands for 0 and black for 1.

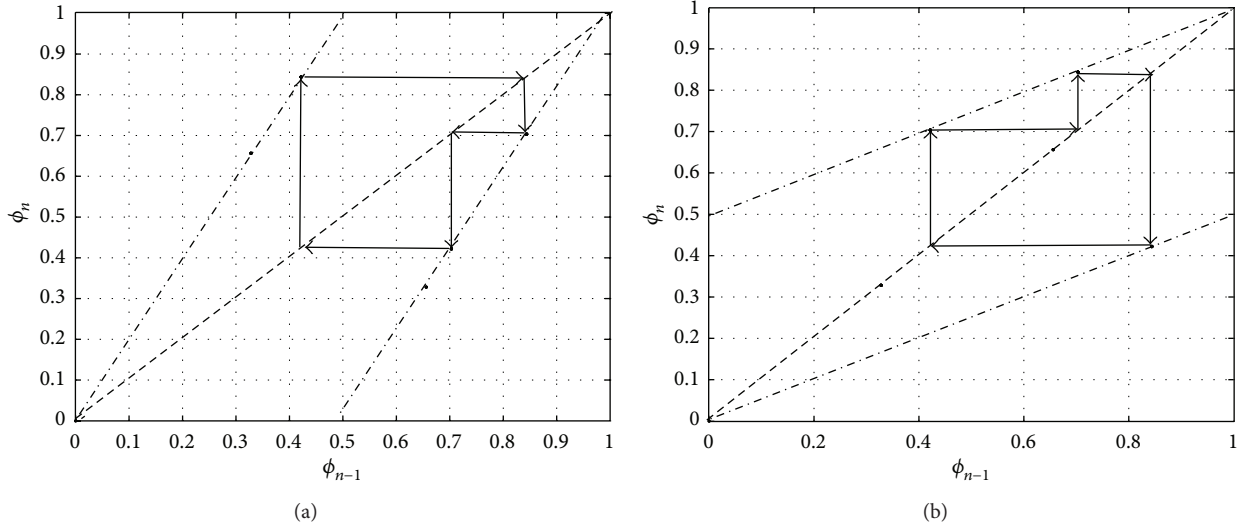


FIGURE 6: The evolution of characteristic function of the period-3 attractor, where the values of characteristic function of the attractor are 0.7031, 0.4219, and 0.8438, respectively. (a) shows the iterative process of an attractor, where $\tau = 1$, and (b) shows the iterative process of an attractor, where $\tau = 2$.

Figure 5, where the solid lines stand for the real evolution of binary configuration 11100, and the dotted lines stand for the attractor belonging to Λ_2^{58} .

Next, we use the Lameray diagram [33] to present our attractors. The diagrams show clearly the iterative process of attractors. In terms of the attractor of Figure 4(d), we get that the values of characteristic function of the attractor are 0.7031, 0.4219, and 0.8438, respectively. Figure 6(a) shows the iterative process of an attractor, where $\tau = 1$, and Figure 6(b) shows the iterative process of an attractor, where $\tau = 2$. Then, we can associate the period-3 attractor of rule 58 in Figure 6(a) as a period-3 point of a continuous map $f : [0, 1] \rightarrow [0, 1]$ which we know that it is chaotic because “period-3 implies chaos” [34]. We can also consider Figure 6(b) by the above method. Chaos implies that rules 58 have infinite period orbits on its subsystems.

In recent years, associative memory was researched in many papers [12, 13]. It is obvious that rule 58 can be used in associative memory. By strongly connected graph of rule 58, we can know the elements on its attractors. Then, we can choose a bit string which belongs to an attractor as memory pattern. Since there are infinite orbits, the storage capability is very large. For example, we can choose 010101 as a memory pattern in Figure 4(c). The associative memory model

provides a solution to problem where time to recognize a pattern is independent of the number of patterns stored.

5. Conclusions

In this paper, the dynamical behaviors of rule 58 in cellular automata, which is Bernoulli σ_τ -shift rule, are carefully investigated from viewpoint of symbolic dynamics. We derive the conditions according to Bernoulli σ_τ -shift evolution for rule 58. Then, in terms of the transition matrices of determinative block systems of subsystems of rule 58, we obtain the values of topological entropy of subsystems. According to corresponding strongly connected graph of transition matrices of determinative block systems of subsystems Λ_1^{58} , we divide determinative block systems into two subsets. Then, we find that rule 58 is topologically mixing on Λ_1^{58} . Furthermore, we find that $f_{58}|_{\Lambda_2^{58}}$ is topologically mixing. So, rule 58 is chaotic in the sense of both Li-Yorke and Devaney. Then, we prove that four rules belonging to global equivalence class \mathcal{E}_4^3 of CA are topologically conjugate. We use diagrams to explain the attractors of rule 58, where characteristic function and the Lameray diagram are used to describe that some points fall into Bernoulli-shift map after several times iterations and to show clearly the iterative process of an attractor, respectively.

Appendix

Proof of Proposition 1.

Necessity. Suppose that there exists a subset $\Lambda_1^{58} \in S^Z$ such that $f_{58}|_{\Lambda_1^{58}} = \nu|_{\Lambda_1^{58}}$. Then, $\forall x = (\dots, x_{-1}, x_0, x_1, \dots) \in \Lambda_1^{58}$, we have $[f_{58}(x)]_i = x_{i+1}, \forall x \in Z$.

- (1) If $x_i = 1$, then $x_{i-1}\bar{x}_i \oplus \bar{x}_{i-1}x_{i+1} = 0 \oplus \bar{x}_{i-1}x_{i+1}$; according to Table 1, we get $x_{i-1} = 0, x_{i+1} = 0, x_{i+2} = 1; x_{i-1} = 0, x_{i+1} = 1$, and $x_{i+2} = 0; x_{i-2} = 0, x_{i-1} = 1, x_{i+1} = 0, x_{i+2} = 1$.
- (2) If $x_i = 0$, then $x_{i-1}\bar{x}_i \oplus \bar{x}_{i-1}x_{i+1} = x_{i-1} \oplus \bar{x}_{i-1}x_{i+1}$; according to Table 1, we get $x_{i-2} = 0, x_{i-1} = 0, x_{i+1} = 0; x_{i-2} = 0, x_{i-1} = 0$, and $x_{i+1} = 1; x_{i-1} = 1$, and $x_{i+1} = 1$.
- (3) Now, we prove that $(001) \not\prec x, x \in \Lambda_1^{58}$. The proof is by contradiction. Suppose that $(001) \prec x, x \in \Lambda_1^{58}$. We can check that $y \in \Lambda_1^{58}$, where $f(y) = x$ and $x = (\dots, x_{-3}, x_{-2}, 0, 0, 1, x_2, x_3, \dots)$. The following is considered in Table 1.

① Let $y = (y_{-k}, \dots, y_{-3}, 0, 0, 0, 1, y_3, \dots, y_k)$. Firstly, $y_{-3} = 0, y_{-4} = 0, \dots, y_{-n} = 0, \dots$; otherwise, there exists $(100) \prec y$ which does not belong to Λ_1^{58} . Secondly, there certainly exists $(y_i y_{i+1} y_{i+2}) = (100) \prec y$, where $3 \leq i \leq k$.

② Let $y = (y_{-k}, \dots, y_{-3}, y_{-2}, 0, 1, 0, y_2, y_3, \dots, y_k)$. We cannot get $f(y_{-2}01) = 0$ in Λ_1^{58} .

③ Let $y = (y_{-k}, \dots, y_{-3}, y_{-2}, 1, 1, 0, y_2, y_3, \dots, y_k)$. We cannot get $f(y_{-2}11) = 0$ in Λ_1^{58} .

Based on the above analysis, these arrive at contradictions.

Therefore, we get that x_{i-1}, x_i , and x_{i+1} have the following relations:

- (i) if $x_i = 1$, then $x_{i-2} = 1, x_{i-1} = 0, x_{i+1} = 0, x_{i+2} = 1; x_{i-2} = 0, x_{i-1} = 0, x_{i+1} = 1$, and $x_{i+2} = 0; x_{i-2} = 0, x_{i-1} = 1, x_{i+1} = 0$, and $x_{i+2} = 1$.
- (ii) If $x_i = 0$, then $x_{i-2} = 0, x_{i-1} = 0, x_{i+1} = 0$, and $x_{i+2} = 0; x_{i-1} = 1$ and $x_{i+1} = 1$.

Sufficiency. Suppose that there exists a subset $\Lambda_1^{58} \subset S^Z$, and, $\forall x \in \Lambda_1^{58}$, the relations between x_{i-1}, x_i , and x_{i+1} satisfy the conditions (i) and (ii) in Proposition 1, $\forall i \in Z$.

- (i) If $x_i = 1$, we have $[f_{58}(x)]_i = x_{i-1}\bar{x}_i \oplus \bar{x}_{i-1}x_{i+1} = 0 \oplus \bar{x}_{i-1}x_{i+1}$.

Therefore,

$$[f_{58}(x)]_i = \begin{cases} 0, & x_{i-1} = 0, & x_{i+1} = 0, \\ 1, & x_{i-1} = 0, & x_{i+1} = 1, \\ 0, & x_{i-1} = 1, & x_{i+1} = 0. \end{cases} \quad (A.1)$$

- (ii) If $x_i = 0$, we have $[f_{58}(x)]_i = x_{i-1}\bar{x}_i \oplus \bar{x}_{i-1}x_{i+1} = x_{i-1} \oplus \bar{x}_{i-1}x_{i+1}$.

Therefore,

$$[f_{58}(x)]_i = \begin{cases} 0, & x_{i-1} = 0, & x_{i+1} = 0, \\ 1, & x_{i-1} = 1, & x_{i+1} = 1. \end{cases} \quad (A.2)$$

Hence, $[f_{58}(x)]_i = x_{i+1}$. \square

Proof of Proposition 17. (a) Let any two open sets $U, V \subset \Lambda_2^{58}$. By Proposition 13 (b), we know that $f_{58}^2|_{\Lambda_2^{58}}$ is topologically mixing; then there exists $N_1 > 0$, such that $(f_{58}^2|_{\Lambda_2^{58}})^n(U) \cap V \neq \emptyset, \forall n \geq N_1$. Then we consider the following two cases.

Case 1. Consider $n = 2k, k \in Z^+$; then

$$\begin{aligned} & (f_{58}|_{\Lambda_2^{58}})^n(U) \cap V \\ &= (f_{58}|_{\Lambda_2^{58}})^{2k}(U) \cap V \\ &= (f_{58}^2|_{\Lambda_2^{58}})^k(U) \cap V \neq \emptyset, \quad \forall n \geq 2N_1. \end{aligned} \quad (A.3)$$

Case 2. Consider $n = 2k + 1, k \in Z^+$. It is obvious that Λ_2^{58} is surjective. Suppose that there exist $y, y_1 \in \Lambda_2^{58}$ such that $f_{58}(y) = f_{58}(y_1)$. Thus, $f_{58}^2(y) = f_{58}^2(y_1)$ holds, which implies $y = y_1$. Therefore, $f_{58}|_{\Lambda_2^{58}}$ is injective. Since Λ_2^{58} is a compact Hausdorff space and $f_{58}|_{\Lambda_2^{58}}$ is one-to-one onto, and continuous, $f_{58}^{-1}|_{\Lambda_2^{58}}$ exists and is continuous. Therefore, $f_{58}|_{\Lambda_2^{58}}$ is a homeomorphism, which implies that $f_{58}(U)$ is an open set. Thus,

$$\begin{aligned} & (f_{58}|_{\Lambda_2^{58}})^n(U) \cap V \\ &= (f_{58}|_{\Lambda_2^{58}})^{2k} \circ f_{58}(U) \cap V \neq \emptyset, \quad \forall n \geq 2N_1 + 1. \end{aligned} \quad (A.4)$$

Hence, for any two open sets $U, V, \exists N = 2N_1 + 1$, such that $(f_{58}|_{\Lambda_2^{58}})^n(U) \cap V \neq \emptyset, \forall n \geq N$; namely, $f_{58}|_{\Lambda_2^{58}}$ is topologically mixing.

- (b) Consider $\text{ent}(f_{58}|_{\Lambda_2^{58}}) = (1/2)\text{ent}(f_{58}^2|_{\Lambda_2^{58}}) = 0.2812$. \square

Conflict of Interests

The authors declare that there is no conflict of interests regarding the publication of this paper.

Acknowledgments

This work was supported in part by Research Project of Chongqing University of Science and Technology

(CK2013B15), in part by Scientific and Technological Research Program of Chongqing Municipal Education Commission (Grants nos. KJ131401 and KJ131416), in part by Natural Science Foundation Project of CQ CSTC (Grants nos. cstc2012jjB0095 and cstc2012jjA1459), in part by the National Natural Science Foundation of China (51275547), in part by Achievement Transfer Program of Institutions of Higher Education in Chongqing (KJ121413), and in part by Teaching & Research Program of Chongqing University of Science and Technology (X2012-29-S).

References

- [1] J. Neumann, *The General and Logical Theory of Automata*, Pergamon Press, London, UK, 1951.
- [2] H. Beigy and M. R. Meybodi, "Cellular learning automata with multiple learning automata in each cell and its applications," *IEEE Transactions on Systems, Man, and Cybernetics B: Cybernetics*, vol. 40, no. 1, pp. 54–65, 2010.
- [3] W. Pries, A. Thanailakis, and H. C. Card, "Group properties of cellular automata and VLSI applications," *IEEE Transactions on Computers C*, vol. 35, no. 12, pp. 1013–1024, 1986.
- [4] K. M. Faraoun, "Design of fast one-pass authenticated and randomized encryption schema using reversible cellular automata," *Communications in Nonlinear Science and Numerical Simulation*, vol. 19, no. 9, pp. 3136–3148, 2014.
- [5] P. Ping, F. Xu, and Z. Wang, "Color image encryption based on two-dimensional cellular automata," *International Journal of Modern Physics C*, vol. 24, no. 10, Article ID 1350071, 14 pages, 2013.
- [6] S. Nandi, B. K. Kar, and P. Pal Chaudhuri, "Theory and applications of cellular automata in cryptography," *IEEE Transactions on Computers*, vol. 43, no. 12, pp. 1346–1357, 1994.
- [7] M. Tomassini and M. Perrenoud, "Cryptography with cellular automata," *Applied Soft Computing*, vol. 1, no. 2, pp. 151–160, 2001.
- [8] J.-C. Jeon and K.-Y. Yoo, "Elliptic curve based hardware architecture using cellular automata," *Mathematics and Computers in Simulation*, vol. 79, no. 4, pp. 1197–1203, 2008.
- [9] J. Machicao, A. G. Marco, and O. M. Bruno, "Chaotic encryption method based on life-like cellular automata," *Expert Systems with Applications*, vol. 39, no. 16, pp. 12626–12635, 2012.
- [10] Z. Eslami, S. H. Razzaghi, and J. Z. Ahmadabadi, "Secret image sharing based on cellular automata and steganography," *Pattern Recognition*, vol. 43, no. 1, pp. 397–404, 2010.
- [11] R. J. Chen and S. J. Horng, "Novel SCAN-CA-based image security system using SCAN and 2-D von Neumann cellular automata," *Signal Processing: Image Communication*, vol. 25, no. 6, pp. 413–426, 2010.
- [12] P. Maji and P. Pal Chaudhuri, "Non-uniform cellular automata based associative memory: evolutionary design and basins of attraction," *Information Sciences*, vol. 178, no. 10, pp. 2315–2336, 2008.
- [13] N. Ganguly, P. Maji, B. K. Sikdar, and P. P. Chaudhuri, "Design and characterization of cellular automata based associative memory for pattern recognition," *IEEE Transactions on Systems, Man, and Cybernetics B*, vol. 34, no. 1, pp. 672–679, 2004.
- [14] S. Wolfram, "Universality and complexity in cellular automata," *Physica D: Nonlinear Phenomena*, vol. 10, no. 1-2, pp. 1–35, 1984.
- [15] S. Wolfram, *Theory and Application of Cellular Automata*, World Scientific, Singapore, 1986.
- [16] S. Wolfram, *A New Kind of Science*, Wolfram Media, Champaign, Ill, USA, 2002.
- [17] L. O. Chua, S. Yoon, and R. Dogaru, "A nonlinear dynamics perspective of Wolfram's new kind of science. I. Threshold of complexity," *International Journal of Bifurcation and Chaos in Applied Sciences and Engineering*, vol. 12, no. 12, pp. 2655–2766, 2002.
- [18] L. O. Chua, V. I. Sbitnev, and S. Yoon, "A nonlinear dynamics perspective of Wolfram's new kind of science, part II: universal neuron," *International Journal of Bifurcation and Chaos in Applied Sciences and Engineering*, vol. 13, no. 9, pp. 2377–2491, 2003.
- [19] L. O. Chua, V. I. Sbitnev, and S. Yoon, "A nonlinear dynamics perspective of Wolfram's new kind of science. III. Predicting the unpredictable," *International Journal of Bifurcation and Chaos in Applied Sciences and Engineering*, vol. 14, no. 11, pp. 3689–3820, 2004.
- [20] L. O. Chua, V. I. Sbitnev, and S. Yoon, "A nonlinear dynamics perspective of Wolfram's new kind of science, part IV: from Bernoulli shift to $1/f$ spectrum," *International Journal of Bifurcation and Chaos in Applied Sciences and Engineering*, vol. 15, no. 4, pp. 1045–1183, 2005.
- [21] L. O. Chua, V. I. Sbitnev, and S. Yoon, "A nonlinear dynamics perspective of Wolfram's new kind of science. V. Fractals everywhere," *International Journal of Bifurcation and Chaos in Applied Sciences and Engineering*, vol. 15, no. 12, pp. 3701–3849, 2005.
- [22] L. O. Chua, V. I. Sbitnev, and S. Yoon, "A nonlinear dynamics perspective of Wolfram's new kind of science, part VI: from time-reversible attractors to the arrow of time," *International Journal of Bifurcation and Chaos*, vol. 16, no. 5, pp. 1097–1373, 2006.
- [23] F. Y. Chen, W. F. Jin, G. R. Chen, F. F. Chen, and L. Chen, "Chaos of elementary cellular automata rule 42 of Wolfram's class II," *Chaos*, vol. 19, no. 1, Article ID 013140, 2009.
- [24] F. F. Chen and F. Y. Chen, "Complex dynamics of cellular automata rule 119," *Physica A: Statistical Mechanics and its Applications*, vol. 388, no. 6, pp. 984–990, 2009.
- [25] L. Chen, F. Y. Chen, and W. Jin, "Complex symbolic dynamics of bernoulli shift cellular automata rule," in *Proceedings of the 9th International Conference for Young Computer Scientists (ICYCS '08)*, pp. 2868–2873, Hunan, China, November 2008.
- [26] W. Jin, F. Chen, G. Chen, L. Chen, and F. Chen, "Extending the symbolic dynamics of Chua's Bernoulli-shift rule 56," *Journal of Cellular Automata*, vol. 5, no. 1-2, pp. 121–138, 2010.
- [27] L. Chen, F. Chen, W. Jin, and G. Chen, "Some nonrobust Bernoulli-shift rules," *International Journal of Bifurcation and Chaos*, vol. 19, no. 10, pp. 3407–3415, 2009.
- [28] Q. Han, X. F. Liao, C. D. Li, and L. P. Feng, "Complex dynamics behaviors in cellular automata rule 35," *Journal of Cellular Automata*, vol. 6, no. 6, pp. 487–504, 2011.
- [29] Q. Han, X. F. Liao, and C. D. Li, "Complex dynamic behaviors in cellular automata rule 14," *Discrete Dynamics in Nature and Society*, vol. 2012, Article ID 258309, 12 pages, 2012.
- [30] J. Guan, S. Shen, C. Tang, and F. Chen, "Extending Chua's global equivalence theorem on Wolfram's new kind of science," *International Journal of Bifurcation and Chaos*, vol. 17, no. 12, pp. 4245–4259, 2007.
- [31] B. Kitchens, *Symbolic Dynamics: One-sided, Two-sided and Countable State Markov Shifts*, Springer, Berlin, Germany, 1990.

- [32] Z. Zhou, *Symbolic Dynamics*, Shanghai Scientific and Technological Education Publishing House, Shanghai, China, 1997, (Chinese).
- [33] L. P. Shilnikov, A. L. Shilnikov, D. V. Turaev, and L. O. Chua, *Methods of Qualitative Theory in Nonlinear Dynamics*, World Scientific, Singapore, 1998.
- [34] T. Y. Li and J. A. Yorke, "Period three implies chaos," *The American Mathematical Monthly*, vol. 82, no. 10, pp. 985–992, 1975.

Research Article

Research of Innovation Diffusion on Industrial Networks

Yongtai Chen¹ and Shouwei Li²

¹ School of Management and Engineering, Nanjing University, Nanjing 210008, China

² School of Management, Jiangsu University, Zhenjiang 212013, China

Correspondence should be addressed to Shouwei Li; shouweili1996@163.com

Received 10 January 2014; Revised 22 June 2014; Accepted 25 June 2014; Published 14 July 2014

Academic Editor: Chuandong Li

Copyright © 2014 Y. Chen and S. Li. This is an open access article distributed under the Creative Commons Attribution License, which permits unrestricted use, distribution, and reproduction in any medium, provided the original work is properly cited.

The real value of innovation consists in its diffusion on industrial network. The factors which affect the diffusion of innovation on industrial network are the topology of industrial network and rules of diffusion. Industrial network is a complex network which has scale-free and small-world characters; its structure has some affection on threshold, length of path, enterprise's status, and information share of innovation diffusion. Based on the cost and attitude to risk of technical innovation, we present the "avalanche" diffusing model of technical innovation on industrial network.

1. Introduction

Innovation is often expressed as a single event. The appearance of innovation would activate the diffusion of it necessarily, but the diffusion always displays a continuous and slow process. The diffusion of innovation decides the steps of economic development and the rate of productivity finally. The innovation could contribute to society when it is adopted by many adopters. It is obvious that the real value of innovation is not itself but the diffusion of it [1]. So, there is a very important significance to research the diffusion process of innovation.

Under the environment of market economy, all kinds of relationships between enterprises would be generated through the process of their manufacture and management, such as codevelopment, share hold, and transfer of technique. The relationship among some enterprises in industry can form a network which covers the whole industry. Industrial network is constructed by many enterprises and relationships between them. These enterprises consist of many forms, researching institute and government department, which hold their special resource. These nodes in industry network depend on each other because of holding different resources. Some formal or informal reciprocal relationships come into being through their interaction of manufacture and cooperation. Industrial network is a configuring mode of resources between enterprises [2]. Industrial network can play an

important role in the development of area economy. It does not only present the platform of interaction for every node in industrial network, but also saves the cost of trade between enterprises, quickens the speed of circulation and studying of information, and then strengthens the competition of enterprises and industry. The structure of industry network would affect the diffusion process of technical innovation.

The new theory of industry area which is represented by Potter strengthens the forming and exterior effect of industrial networks. The essence that industrial networks can enhance the advantage of competition is the alliance of stratagem between enterprises by their cooperation. It is important that the relationship exist between leaguers in industrial networks. The relationships in industrial networks are all kinds of contact which are generated in the process of resources exchanging and transferring between enterprises. These relationships do not only include the "real" relationship, such as industrial chain, service chain, financial chain, and technical chain, but also include the "virtual" relationship, such as knowledge chain and information chain. These "real" and "virtual" relationships do not always overlap each other. The innovative power of industrial networks is represented by the complex character of inner associating mode and interaction between enterprises extremely.

How would the structure of industry network be like? How does it affect the diffusion process of technical innovation? If there is a technical innovation which takes place in

a node (enterprise), how fast does the technical innovation diffuse in the industry network? What scale does it diffuse? These problems are very interesting and should be focused on by researchers and enterprisers. If we know some laws of innovation diffusion, the power of technical innovation should be amplified to generate more competitive ability. So, the diffusion of innovation on industrial networks will be researched in the paper. A whole diffusing process on network should at least include two aspects: establishment of diffusing rules and choice of network topology structure. The network topology decides the path and mode of innovation diffusion; the rules of diffusion are always determined by the cost and tendency of enterprise's innovation. In Section 2, we analyze the structure of industry network and its affection on innovation diffusion. In Section 3, we present the avalanche model of innovation diffusion on industry network and give more detailed analysis about the distribution after the diffusion process. At last, some conclusions are summarized in the paper.

2. Affection of Industrial Networks on Innovation Diffusion

2.1. Diffusing Mode of Innovation. The system of region innovation always includes four kinds of innovation: institutional innovation, innovation of management, innovation of service, and technical innovation. Because the institution, management, and service cannot be copied directly, the studier must understand and grasp the idea behind them profoundly. The things that are diffused by the former three innovations are no-coded knowledge mostly, so the institutional, administrant, and service innovations are called by a joint name, knowledge innovation. Because the technical innovations are always adhering to product, the technical innovation can be divided into product innovation and craft innovation.

Industrial network has two characters: one is the technical character which is based on industrial chain; another is social character which is based on value chain at the same time; interaction between enterprises is frequent; the industrial network is propitious to the diffusion of innovation specially, but the mode of diffusion is different between knowledge innovation and technical innovation. Technical innovation diffuses through the "real" relationship of industrial network, but knowledge innovation diffuses through the "virtual" relationship of industrial network. Because the "real" relationship can be investigated and analyzed easily, the affection of industrial network topology on innovation diffusion would be analyzed in the following by the "real" relationship between enterprises. So, the structure of industry network is analyzed in the following part.

2.2. Complex Topology of Industrial Network. If we analyze the affection of industrial network topology on innovation diffusion, the topology of industrial network should be cognized firstly. The industrial network also is a kind of network. The research of network could be divided into three phases approximately: regular network, random network, and complex network.

Complex networks are the massive networks which have complex topology structure and dynamic behavior [3]; complex networks are the graphs which are constructed by many interlinks among a mass of nodes. The main characters [4, 5] of complex network include three aspects: distribution of node degree, average shortest length, and clustering coefficient. If the probability distribution $p(k)$ of node degree k in a network follows power-law distribution, $p(k) \sim k^{-r}$, $2 < r \leq 3$, the network would be called scale-free network. The networks which have smaller average shortest length and larger clustering coefficient are called small-world network. The scale-free network and small-world network are called by a joint name, complex network. Complex network is a kind of network which is between regular and random network; it is researched widely in recent years because of the veracity depicting real world.

We investigate the relationships between integrate circuit (IC) enterprises in the Yangtze River delta area in china. The relationships include cooperation, strategy alliance, investment, and technical trading. Based on the "real" relationship between enterprises, the industrial network of IC industry in Yangtze River delta area is presented as follows (Figure 1 is drawn by using Ucinet software). There are almost 500 institutes and more than 1200 ties in the industry network.

Applying the statistical analysis method of complex network [4, 5], we compute the distribution of node degree and clustering coefficient of the IC industrial network by using Ucinet software. Then the results are showed as follows (Figures 2 and 3).

In order to judge the small-world character of it, we also compute some parameters of the IC industrial network (Table 1). It is noticeable that the ER random network is generated according to the size and density of IC industrial network.

From Figure 1, we can make out that the distribution of node's degree in the IC industrial network follows power-law distribution, $p(k) \sim k^{-r}$, $r = 2.81$; from Figure 2 and Table 1, we can make out that the IC industrial network has larger clustering coefficient and smaller average shortest length.

Following the above analysis, we can conclude that industrial network is not only a scale-free network, but also a small-world network. It has the three complex characters: small-world, scale-free, and clustering, which has the affection of different degree and mode on innovation diffusion in industrial network.

2.3. Affections of Industrial Network Complex Topology on Innovation Diffusion. The researches of diffusing threshold on network are mainly based on the famous epidemic models SIS and SIR, but these conclusions are also the same with innovation diffusion on industrial network. The diffusing threshold is not small value in regular network; the diffusing threshold of small-world network is smaller than that of regular network clearly. Under the same intension of diffusion, the spreading size of diffusion in small-world network is larger than that in regular network distinctly [6]. The diffusing behavior is only different on quantity from regular network to small-world network, but the diffusing behavior on scale-free network puts up some characters far from the former two

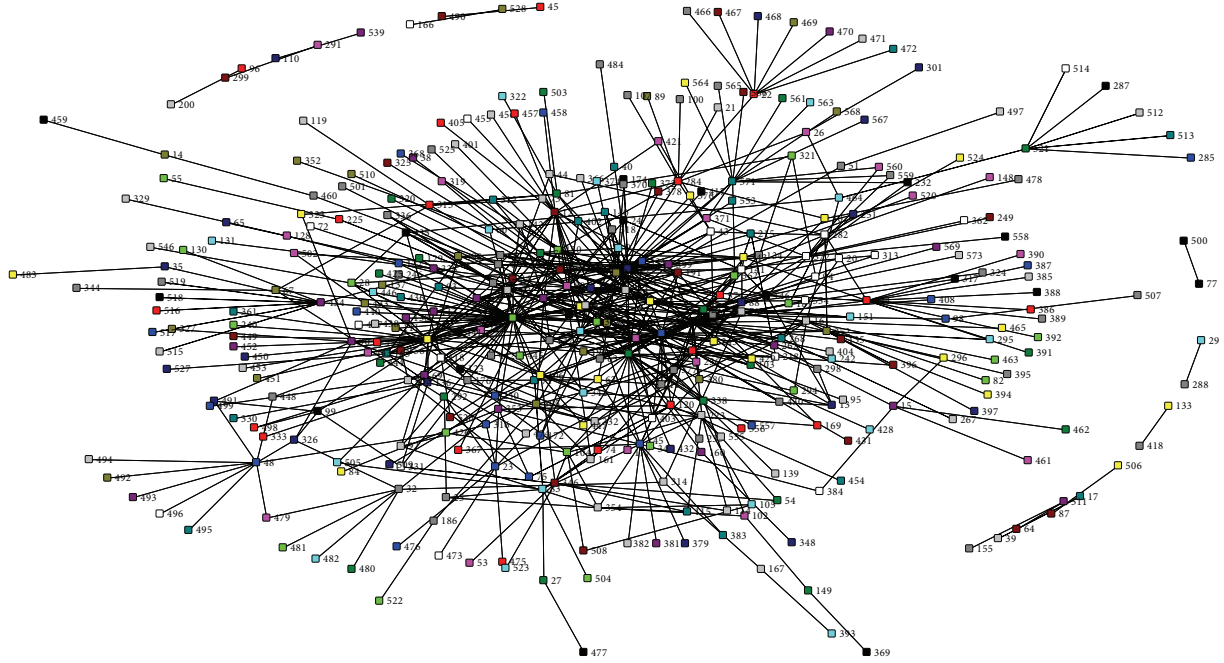


FIGURE 1: The industrial network of IC industry in Yangtze River delta area.

TABLE 1: Comparison between IC industrial network and random ER network.

Type of network	Average degree of network	Max degree of node	Average shortest length of network	Average clustering coefficient
IC industrial network	3.503	53	3.554	0.046
ER random network	3.472	10	4.261	0.016

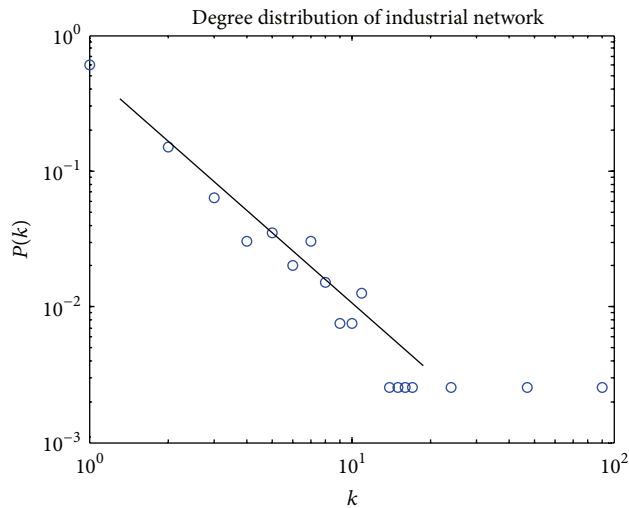


FIGURE 2: The distribution of node's degree of the industry network (double logarithmic coordinate).

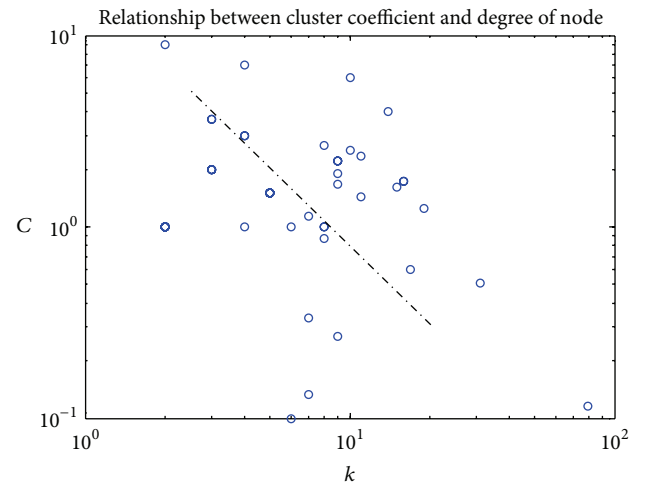


FIGURE 3: The relationship between clustering coefficient and node's degree (double logarithmic coordinate).

networks. The diffusing threshold is negative or close to zero on scale-free network [7]. From these above analyses, we can know that innovation always exists and constantly diffuses and the diffusion would spread to the whole industry.

From Figures 1 and 2, we can see that the distribution of relationship links in industry network is asymmetry very much. There are a few "Hub" enterprises which have larger links and many enterprises which have a few links. The

TABLE 2: Affections of industrial network topology on innovation diffusion.

Type	Content
Diffusing mode	Technical innovation spreads on “real” relationship Knowledge innovation spreads on “virtual” relationship
Diffusing threshold	Industrial network is a scale-free network; innovation can diffuse easily on it, and the diffusing threshold is zero
Diffusing path	Industrial network is a small-world network; the path of innovation diffusion is shorter
Sharing innovation	The clustering coefficient of industrial network is very larger; the shared degree of innovation is higher
Innovation affection	The distribution of node’s degree in industrial network; the affection of enterprise innovation on industrial network is different extremely

innovation of those “Hub” enterprises will bring greater affection to industrial network than others.

From Figure 3, we can see that the clustering coefficient of each enterprise is different, and the local clustering coefficient $C(k)$ depends on the degree k of enterprise strongly. The degrees of innovation shared between some associated enterprises are different very much. We can know that some enterprises have different status and role in innovation share through the clustering coefficient of them in industrial network.

The new knowledge and new technique are not monopolized by other enterprises immediately. They always diffuse through network, so the average shortest path of industrial network may measure the average shortest length of innovation passing during diffusion. In the IC industrial network of Yangtze River delta area, diffusion of innovation would spread to the whole industry through 2~3 enterprises. The small-world character of IC industrial network shows that the diffusion of innovation on industrial network is a quick diffusing process.

Based on the former analyses, we give some conclusions showed by Table 2.

3. Rules of Innovation Diffusion and the “Avalanche” Model of Technical Innovation

Because the variability and chanciness of “virtual” relationships between enterprises is larger, the measurement of knowledge innovation diffusion is very difficult. Knowledge innovations are almost noncoded information, which always diffuse through overflow of knowledge [8]. The “real” relationships between enterprises are stable comparatively, which bring convenience for measurement of technical innovation diffusion. We mainly consider the diffusion of technical innovation on industrial network in the following part.

The enterprise decides whether it upgrades its technical level according to local information generally; that is, the enterprise makes the decision of upgrading technique level based on the technical level of some enterprises which link to it [9].

In order to understand the complex dynamic of technical upgrade in the diffusion process of technical innovation, we should consider how to simulate some local interaction affecting diffusion through industrial network. Most of the times, these “waves” of diffusion come in terms of intermittent bursts separating relatively long periods of quiescence;

in other words, the system exhibits “punctuated equilibrium” behavior. Certainly some technologies, like cellular phones or VCRs, seem to lurk in the background for years and then suddenly explode into mass use [10].

There are two main mechanisms involved in the diffusion of innovations in industrial network that any mathematical model should take into account. On the one hand, there is a pressure for adopting a new product or technology coming from marketing campaigns and mass media. These external processes are essentially independent of the industrial network structure and one can view their effects as a random independent process on the enterprises. On the other hand, there is the influence of the surrounding enterprises which link to it in industrial network. Once an enterprise decides to adopt a new technology, those who are in contact with it can evaluate the new payoff and risk the enterprise has got from acquiring the new technology and compare it with their current benefits. By balancing the payoff increment with the associated upgrading cost, they may decide to adopt, or not, the new technology. In this way, the local flux of information plays a key role in diffusing new techniques. It is important to notice that we are not considering any compatibility constraint among the enterprises.

In this article we propose a simple model of diffusion of technological innovations with costs and attitude (related to risk). At the same time, we will give the theoretic analyses of distribution of innovation diffusion.

3.1. Model of Technical Diffusion on Industrial Network. Each enterprise i is characterized by the real variable a_i . This variable stands for their technological level; that is, the higher the a_i is, the more advanced (technologically speaking) it is. We will assume that the payoff that an enterprise receives from possessing a certain technological level is simply proportional to it. The model is then simulated as follows.

(i) At each time step, a randomly selected enterprise a_i updates its technological level

$$a_i \longrightarrow a_i + \Delta_i, \quad (1)$$

where Δ_i is a random variable exponentially distributed with mean $1/\beta$; that is, $p(\Delta) = \beta e^{-\beta\Delta}$. This driving process accounts for the external pressure that may lead to a spontaneous new technology adoption by any of the population enterprises.

This step means that the technical innovation takes place on node i at some time in industry network; then the technical

level becomes higher than in the past. The difference Δ_i follows exponential distribution with parameter $1/\beta$, which indicates the time interval of independent technical innovation. Here, Beta denotes the press of technical innovation from actual situation. The larger the Beta is, the larger the press is and the shorter the time interval of independent technical innovation is.

(ii) All enterprises $j \in \Gamma(i)$ ($\Gamma(i)$ being the set of neighbors of enterprise i) decide whether they also want to upgrade or not, according to the following rule:

$$a_i - a_j \geq \frac{C}{p} \implies a_j \longrightarrow a_i, \quad (2)$$

where C (cost) is a constant parameter that stands for the price an enterprise must pay in order to upgrade his technology as well as its personal “resistance” to change. p is a random variable which is defined on $[0, 1]$, and p is used to denote the attitude of enterprise to upgrade its technology level. So p is called enterprise attitude of technical innovation. $p = 0$ denotes that the enterprise would not like to upgrade its technical level. $p = 1$ denotes that the enterprise can upgrade its technical level instantly. $0 < p < 1$ denotes the degree of attitude to upgrade.

This step means that the technical innovation diffuses from node i to node j under the condition of cost and probability. If the diffusion happened, the technical level of node j should become large. The larger the cost is, the more difficult the diffusion is. The larger the probability is, the less difficult the diffusion is.

(iii) If any a_j has decided to also upgrade its level, we let their neighbors also choose whether to upgrade or not. This procedure is repeated until no one else wants to upgrade, concluding a technological avalanche. Whenever an enterprise a_i decides to upgrade, their neighbors become aware of the new technology and balance the profit they may obtain in case of also adopting it ($a_i - a_j$) with its cost C/p . It may well happen that if the technological innovation spontaneously adopted by the seed of the avalanche is high enough compared with the cost, the avalanche may end up spanning a large portion of the population.

This step means that the technical innovation diffuses from node j to its neighbors. Then, the process is repeated on industry network, which is just same as an avalanche ensued in the whole network.

3.2. Distribution of Technical Diffusion. Assume that there are n nodes and $N(n)$ links in industrial network. From the former demonstration, we can see that industrial network has scale-free and small-world characters. After the enterprise has a technical innovation, its technical level is upgraded. Because there are many links (relationships) between enterprises in industrial network, the technical innovations should spread to its neighbor enterprises.

3.2.1. Probability of Technical Upgrading for Enterprise. Neighbor enterprises would choose whether to upgrade or not according to the affection of innovation diffusion. From formula (1), if $a_i - a_j = \Delta a \geq C/p$, the enterprise would adopt

the new technology and upgrade its technical level. So the probability p_1 of technical upgrading for an enterprise is as follows:

$$p_1 = P\left(\Delta a \geq \frac{C}{p}\right) = 1 - P\left(\Delta a < \frac{C}{p}\right). \quad (3)$$

Because Δa follows exponential distribution $e(\beta)$ with parameter β , that is, $f(x) = \beta e^{-\beta x}$, then $P(x) = 1 - e^{-\beta x}$. Therefore we have

$$p_1 = 1 - P\left(\Delta a < \frac{C}{p}\right) = e^{-\beta C/p}. \quad (4)$$

The technical upgrading of enterprise could improve the diffusion of innovation in industry network. The higher the probability of technical upgrading is, the larger and faster the diffusion of innovation is. We can find that the probability of technical upgrading follows exponential distribution with negative index from formula (4). If the cost C increases, the probability of technical upgrading would decrease, so the size and speed of innovation diffusion are smaller and slower, respectively.

3.2.2. Diffusing Tree of Technical Innovation

Definition 1. A graph is called a *tree* of order (size) k if it has k vertices and is connected and if none of its subgraphs is a cycle.

A tree of order k has evidently $k - 1$ edges.

From formula (1), we can see that after technical innovation diffuses, all the enterprises which upgrade their technical level from innovation diffusion reach the same technical level lastly. There is no diffusion between the enterprises which have upgraded their technical level, sequentially a tree should be formed during the diffusion of technical innovation, called *diffusing tree*.

Apparently, a tree of order k is a diffusing tree if and only if the k nodes all upgrade their technical level. So the probability of a tree being a diffusing tree which has k nodes is as follows:

$$p_2 = (p_1)^k = \exp\left(-\frac{\beta C k}{p}\right). \quad (5)$$

From formula (5) of p_2 , we can find that the probability of diffusing tree follows exponential distribution with negative index. The probability of diffusing tree decreases if the size of diffusing tree (k) increases.

After the new technology has diffused, we should consider the diffusion size of technical innovation; that is, how many nodes (enterprises) upgrade their technical level during innovation diffusion. In the other words, we should consider the probability of emergence of diffusing tree of k order during innovation diffusion in industrial network.

In industrial network, we have the following.

Theorem 2. The distribution of diffusing tree of k order in industrial network follows Poisson Distribution $P(\lambda)$ with parameter λ , where

$$\begin{aligned}\lambda &= \lambda_1 p_1, \\ p_1 &= \exp\left(-\frac{\beta C}{p}\right), \\ \lambda_1 &= \frac{(2\sigma)^{k-1} k^{k-2}}{k!}, \\ \lim_{n \rightarrow +\infty} \frac{N(n)}{n^{(k-2)/(k-1)}} &= \sigma.\end{aligned}\quad (6)$$

In order to prove the theorem, we need the lemma as follows.

Lemma 3. If $\lim_{n \rightarrow +\infty} (N(n)/n^{(k-2)/(k-1)}) = \sigma > 0$ and τ_k denotes the number of isolated trees of order k in network $\Gamma_{n,N}$, then

$$\lim_{n \rightarrow +\infty} P_{n,N}(\tau_k = j) = \frac{\lambda_1^j e^{-\lambda_1}}{j!}, \quad j = 0, 1, 2, \dots, \quad (7)$$

where

$$\lambda_1 = \frac{(2\sigma)^{k-1} k^{k-2}}{k!}. \quad (8)$$

The Proof of Lemma 3 can be found in literature [11].

Proof of Theorem 2. From the topology structure of industrial network, it can be obtained that industrial network satisfies the condition $\lim_{n \rightarrow +\infty} (N(n)/n^{(k-2)/(k-1)}) = \sigma > 0$. \square

Assume that random variable X denotes the number of diffusing trees. According to Lemma 3, the probability $P(X = m)$ of emergence of m trees of k order satisfies $P(X = m) = (\lambda_1^m / m!) e^{-\lambda_1}$ in industrial network. The diffusing tree of k order must be generated from all trees of k order in industrial network. That is, the m diffusing trees of k order can be generated for $m, m+1, \dots, m+n, \dots$ trees of k order. Then we can obtain the following:

$$\begin{aligned}P(X = m) &= \sum_{n=0}^{\infty} P(X = m+n) C_{m+n}^m p_1^m (1-p_1)^n \\ &= \sum_{n=0}^{\infty} \frac{\lambda_1^{m+n} e^{-\lambda_1}}{(m+n)!} \frac{(m+n)!}{m!n!} p_1^m (1-p_1)^n \\ &= \frac{\lambda_1^m}{m!} e^{-\lambda_1} p_1^m \sum_{n=0}^{\infty} \frac{((1-p_1)\lambda_1)^n}{n!} \\ &= \frac{\lambda_1^m}{m!} e^{-\lambda_1} p_1^m \cdot e^{(1-p_1)\lambda_1} \\ &= \frac{(\lambda_1 p_1)^m}{m!} e^{-\lambda_1 p_1}.\end{aligned}\quad (9)$$

From Theorem 2, we can judge the size of innovation diffusion when the process of innovation diffusion is completed in industry network. The number of diffusing tree with k -nodes follows Poisson distribution, which its mean

value and variance equal the parameter λ . If λ is very large, the distribution of diffusing tree of k -nodes would approach normal distribution, which consists with the actual situation approximately.

4. Conclusions

Industrial network can be formed by some interacting relationship between enterprises in area industry. It has an important affection on the diffusion of innovation.

From the empirical data of IC industry, we construct the industry network. And then we find that the industry network has three characters: scale-free, small-world, and clustering, which have an important affection on the diffusion of technical innovation on industry network.

Because industrial network is a scale-free network, it makes the diffusion of innovation on industrial network very easily, and each enterprise has different affection on the whole industry. Because industrial network is a small-world network, the average path length of innovation diffusion is shorter when it spreads to whole industry. Because the clustering coefficient of industrial network is larger, the sharing degree of innovation is higher.

Knowledge innovations are always noncoded information, which spread by overflow of knowledge, so knowledge innovations diffuse mainly on the “virtual” relationship of industrial network. Technical innovations always adhere to product, which spread by the value chain of product, so technical innovations diffuse mainly on the “real” relationship of industrial network.

A technical innovation of an enterprise can upgrade itself and diffuse to some neighbor enterprises. The neighbor enterprises decide whether to upgrade their technical level or not by analyzing local information (the cost and risk of technical innovation). The process is repeated constantly on industrial network, so an “avalanche” of technical innovation is formed. In order to trigger the “avalanche” of technical innovation, we should reduce the cost of technical innovation and recognize the risk of technical innovation accurately.

The avalanche model of technical innovation diffusion on industry network could extend our ability to management innovation and its diffusion in an industry. One the one hand, we can forecast the size and speed of a technical innovation diffusion after it happens at some time. On the other hand, from the situation of diffusing tree, we can judge the cost and probability of technical innovation diffusion. So, we can decrease the cost and increase the probability to speed up the rate of diffusion and enlarge the size of technical innovation affection.

Conflict of Interests

The authors declare that there is no conflict of interests regarding the publication of this paper.

Acknowledgments

This research was supported by the Major project of National Natural Science Foundation of China under Grant no.

71390521, the National Natural Science Foundation of China under Grant nos. 71171099, 71301070, the National Social Foundation of China under Grant no. 11BJL074, the Humanity and Social Science Foundation of Ministry of Education of China under Grant no. 12YJCZH020, and the Colleges and Universities in Jiangsu Province Plans to Graduate Research and Innovation Projects under Grant no. CXLX13_057.

References

- [1] Y. Q. Mo, T. Z. Wu, and C. J. Wu, "An innovation diffusion study based on social networks," *Soft Science*, vol. 18, no. 3, pp. 4–6, 2004 (Chinese).
- [2] Y. Z. Gai and G. J. Sui, "A model of industrial network formation based on contraction theory: the viewpoint of overall cost," *Modern Economic Science*, vol. 26, no. 5, pp. 56–59, 2004 (Chinese).
- [3] J. Ma, F. C. Tang, J. Guo, and Y. M. Xi, "The application of complex networks theory in organization networks study," *Studies in Science of Science*, vol. 23, no. 2, pp. 173–178, 2005.
- [4] M. E. J. Newman, "The structure and function of complex networks," *SIAM Review*, vol. 45, no. 2, pp. 167–256, 2003.
- [5] R. Albert and A. Barabási, "Statistical mechanics of complex networks," *Reviews of Modern Physics*, vol. 74, no. 1, pp. 47–97, 2002.
- [6] C. Moore and M. E. J. Newman, "Epidemics and percolation in small-world networks," *Physical Review E—Statistical Physics, Plasmas, Fluids, and Related Interdisciplinary Topics*, vol. 61, no. 5B, pp. 5678–5682, 2000.
- [7] R. Pastor-Satorras and A. Vespignani, "Epidemic spreading in scale-free networks," *Physical Review Letters*, vol. 86, no. 14, pp. 3200–3203, 2001.
- [8] J. Wei, "SMEs. Cluster innovation: network effects and knowledge spillovers," *Science Research Management*, vol. 24, no. 4, pp. 54–60, 2003 (Chinese).
- [9] X. Guardiola, A. Díaz-Guilera, C. J. Pérez, A. Arenas, and M. Llas, "Modeling diffusion of innovations in a social network," *Physical Review E*, vol. 66, no. 2, Article ID 026121, 2002.
- [10] P. R. Krugman, *The Self-Organizing Economy*, Blackwell, Malden, Mass, USA, 1996.
- [11] P. Erdős and A. Rényi, "On the evolution of random graphs," *Publications of the Mathematical Institute of the Hungarian Academy of Sciences*, vol. 5, pp. 17–61, 1960.

Research Article

Terminal Sliding Mode Control with Adaptive Feedback Control in a Class of Chaotic Systems

Degang Yang and Guoying Qiu

College of Computer and Information Science, Chongqing Normal University, Chongqing 401331, China

Correspondence should be addressed to Degang Yang; 460494731@qq.com

Received 1 May 2014; Accepted 22 June 2014; Published 13 July 2014

Academic Editor: Chuandong Li

Copyright © 2014 D. Yang and G. Qiu. This is an open access article distributed under the Creative Commons Attribution License, which permits unrestricted use, distribution, and reproduction in any medium, provided the original work is properly cited.

This paper analyzes semifinite time stability for a general chaotic system. By cooperating methods terminal sliding mode (TSM) with adaptive feedback control (AFC), a controller based on the two methods is derived to achieve semifinite time stability. The theoretical analysis employs the theories of linear matrix inequalities and Lyapunov functional method. Finally, numerical simulation is given to illustrate the derived theoretical results.

1. Introduction

Chaos phenomenon can be found in many physics and engineering systems in practice. However, to improve the system's performance, it is often desirable to avoid chaos, and various methods are proposed. Due to different emphases, controllers have different merits and drawbacks. For example, TSM establishes terminal sliding mode surface to couple system variables and control them to reach equilibrium points. Its control is effective, but it can only control system states coupled in the sliding mode surface; readers are referred to [1–7] for more detailed information. As for impulse control [8–16], they add impulse effects to continuous differential equation and, by constructing comparison system, establish relationships between parameters of system and impulse. Their controllers are effective, but design processes of their controllers are too much complex. For adaptive feedback control as in [17–21], similar to TSM, they have unified the format with different parameters. AFC has a wide range of applications in various fields, but its dynamic is not as good as the first two.

For the system's structure constructed in this paper, we design controllers from methods TSM and AFC, both of which have unified formats. If TSM is used only, we should design several TSM surfaces. If AFC is used only,

its controller is very simple and flexible, but it can only achieve asymptotical stability. Combining their merits and drawbacks, a cooperative controller is proposed in the paper. TSM method finite-timely controls system states, which are coupled in TSM surface, as in [4–7]. Simple AFC is introduced as a supplementary control into the remaining states of the system, controlling system states which are outside TSM surface and making them asymptotically stable [18, 20], and, finally, the overall system tends to be semifinite-time stable [5].

This design scheme can control main elements of system finite-time stability, firstly, then use AFC method to ensure that other dimensions are asymptotically stable, and finally realize the overall system's semifinite time stability. Compared with TSM only, this design can greatly reduce the control input and simplify the design process of controller; compared with AFC only, it has obvious advantages in time sequence.

The rest of the paper is organized as follows. In Section 2, a general chaotic system model and some preliminaries are presented. In Section 3, we will show theoretical analysis, establish several sufficient conditions for SFTS, and formulate controller. In Section 4, numerical simulation is presented to verify the validity of theoretical results. Finally, the conclusions are drawn in Section 5.

2. Problem Statement and Preliminaries

We use the following differential equation to describe general dynamic chaos system:

$$\dot{y} = f(y). \quad (1)$$

In this paper, we are committed to solve the stability analysis of chaotic systems which can be organized into the following form:

$$\begin{aligned} \dot{x}_1 &= A_{11}x_1 + A_{12}x_2 \\ \dot{x}_2 &= A_{21}x_1 + A_{22}x_2 + f_2(x_1, x_2, x_3) \end{aligned} \quad (2)$$

$$\dot{x}_3 = f_3(x_1, x_2, x_3),$$

where $x_1 = (y_1, \dots, y_r)^T$, $x_2 = (y_{r+1}, \dots, y_s)^T$, $x_3 = (y_{s+1}, \dots, y_t)^T$, f_2, f_3 , are nonlinear part.

Definition 1 (finite-time stability [22, 23]). Consider that $x(t) \in R^n$ are system states. If there exists constant $T > 0$, such that $\lim_{t \rightarrow T} \|x\| = 0$ and if $t \geq T$, $\|x(t)\| = 0$, then the system realizes finite-time stability.

Definition 2 (semifinite-time stability [5]). Take dynamic system (2), for example; after adding controllers, if the states x_1 and x_2 are finite-time stable and the states x_3 are asymptotically stable, then we call the system semifinite-time stable.

Lemma 3 (see [23]). Assume that a continuous, positive-definite function $V(t)$ satisfies the following differential inequality:

$$\dot{V}(t) \leq -cV^\tau(t), \quad \forall t \geq t_0, \quad V(t_0) \geq 0, \quad (3)$$

where $c > 0$, $0 < \tau \leq 1$ are two constants. Then, for any given t_0 , $V(t)$ satisfies the following results. $V(t) \equiv 0$, $\forall t \geq t_1$ with t_1 being given by

$$t_1 = t_0 + \frac{V^{1-\tau}(t_0)}{c(1-\tau)}. \quad (4)$$

Assumption 4. Assume that there exist positive constants l_k ($k = 1, \dots, m$), f_2, f_3 satisfying

$$\|f(x)\| \leq \sum_{k=1}^m l_k \|x\|^k, \quad \|x\| = \max |y_i|, \quad (i = s+1, \dots, t). \quad (5)$$

3. Main Results

In this section, controller is designed from TSM and AFC separately with detailed theoretical analysis. TSM portion is used to derive x_1, x_2 finite-time stability, and AFC is for asymptotical stability of x_3 . Finally, system (2) tends to semifinite time stability.

3.1. Terminal Sliding Mode Portion Design. Take the system's first two parts of the states and add controlling part:

$$\begin{aligned} \dot{x}_1 &= A_{11}x_1 + A_{12}x_2 \\ \dot{x}_2 &= A_{21}x_1 + A_{22}x_2 + f_2(x_1, x_2, x_3) + u_1. \end{aligned} \quad (6)$$

Generally speaking, the process of terminal sliding mode control can be divided into two stages: the first stage is to establish the nonsingular terminal sliding model surface; the second is to design TSM controller, which can make the system variables reach and maintain the TSM surface within finite time.

So in this paper, a nonsingular TSM surface is introduced as follows:

$$s = C_1x_1 + C_2x_2 + C_3x_1^{q/p}, \quad (7)$$

where parameters $C_1, C_2, C_3, 0 < q < p$ are odd matrices determined by the designer.

Theorem 5. In the system (6), we add the following controller:

$$\begin{aligned} u_1 &= -\frac{1}{C_2} \left[\left(C_1 + C_3 \frac{q}{p} x_1^{(q-p)/p} \right) (A_{11}x_1 + A_{12}x_2) \right] \\ &\quad - (A_{21}x_1 + A_{22}x_2 + f_2(x_1, x_2, x_3)) - \frac{\psi s}{C_2} \end{aligned} \quad (8)$$

$$\psi = \mu + \eta \|s\|^{\xi-1},$$

where $\mu > 0$, $\eta > 0$, and $0 < \xi < 1$. Then the system states slide on the switch surface $s = 0$.

Proof. Introduce the following Lyapunov function:

$$V_1 = \frac{1}{2} s^T s. \quad (9)$$

Differentiating the function along the trajectories of s , we will obtain

$$\begin{aligned} \dot{V}_1 &= s^T \dot{s} \\ &= s^T \left(C_1 + C_3 \frac{q}{p} x_1^{(q-p)/p} \right) (A_{11}x_1 + A_{12}x_2) \\ &\quad + s^T C_2 (A_{21}x_1 + A_{22}x_2 + f_2(x_1, x_2, x_3)) + s^T u_1 \\ &= -s^T \psi s \\ &= -\mu s^T s - \eta \|s\|^{\xi+1} \\ &\leq -\eta \|s\|^{\xi+1} \\ &\leq -2^{(\xi+1)/2} \eta V_1^{(\xi+1)/2}. \end{aligned} \quad (10)$$

From Lemma 3 and Definition 1, TSM surface could reach the equilibrium point within finite time.

When the system states slide on the switch surface $s = 0$, they satisfy the following equations:

$$\begin{aligned} s &= 0, \\ \dot{s} &= 0. \end{aligned} \quad (11)$$

Then

$$x_2 = -C_2^{-1} (C_1x_1 + C_3x_1^{q/p}). \quad (12)$$

Thus, we can get the following sliding mode dynamics:

$$\dot{x}_1 = (A_{11} - A_{12}C_1C_2^{-1})x_1 - A_{12}C_3C_2^{-1}x_1^{q/p}. \quad (13)$$

□

Theorem 6. For differential equation (13), if there exist a positive symmetric matrix P and matrices C_1C_2 , introduced in (7), satisfying the following conditions:

$$\begin{aligned} P(A_{11} - A_{12}C_1C_2^{-1}) + (A_{11} - A_{12}C_1C_2^{-1})^T P &< 0 \\ PA_{12}C_3C_2^{-1} &= \text{diag}\{b_i\}, \quad b_i > 0, \quad i = 1, \dots, r, \\ b &= \min\{b_i\}, \end{aligned} \quad (14)$$

then the system (6) is finite-time stable.

Proof. Introduce the following Lyapunov function:

$$V_2 = x_1^T P x_1, \quad (15)$$

where P is a symmetric positive definite matrix satisfying the conditions in (14).

It can be proved easily that

$$\|x_1\| \geq \sqrt{\frac{V(x_1)}{\lambda}}, \quad \lambda = \lambda_{\max}(P), \quad (16)$$

where $\lambda_{\max}(P)$ is the maximum eigenvalue of P .

Calculate its derivative along the solution of system (13) and we can obtain

$$\begin{aligned} \dot{V}_2 &= 2x_1^T P \dot{x}_1 \\ &= 2x_1^T P [(A_{11} - A_{12}C_1C_2^{-1})x_1 - A_{12}C_3C_2^{-1}x_1^{q/p}] \\ &= x_1^T [P(A_{11} - A_{12}C_1C_2^{-1}) + (A_{11} - A_{12}C_1C_2^{-1})^T P] x_1 \\ &\quad - 2x_1^T PA_{12}C_3C_2^{-1}x_1^{q/p} \\ &\leq -2 \sum_{i=1}^r b_i (x_{1i}^2)^{(q+p)/2p} \\ &\leq -2b \|x_1\|^{(p+q)/p} \\ &\leq -\frac{2b}{\lambda^{(q+p)/2p}} V(x_1)^{(q+p)/2p}. \end{aligned} \quad (17)$$

Then differential equation (13) is exponentially finite-time stable; state x_1 tends to zero within finite time. By (12), x_2 also tends to zero; then, the desired objective, finite-time stability of system (6), is achieved. □

3.2. Adaptive Feedback Control Portion Design. After the finite-time convergence of system (6), system (4) transforms into

$$\dot{x}_3 = f(x_3). \quad (18)$$

Show each state of x_3 as the following form:

$$\dot{x} = f(x). \quad (19)$$

Theorem 7. AFC controller u_2 is designed as follows and added to the system (19) on the right side:

$$u_2 = \sum_{k=1}^m \beta_k x^{2k-1}, \quad (20)$$

where β_k ($k = 1, \dots, m$) are adaptive parameters whose adaptive laws are

$$\dot{\beta}_k = - \sum_{j=1}^n \gamma_{kj} x^{2(j+k)-2}. \quad (21)$$

Then, the controlled system changes into the following form:

$$\dot{x} = f(x) + u_2 \quad (22)$$

and it is asymptotically stable.

Proof. We introduce the following Lyapunov function:

$$V_3 = \frac{1}{2} \sum_{j=1}^n \frac{1}{j} x^{2j} + \frac{1}{2} \sum_{k=1}^m \frac{1}{\gamma_k} (\beta_k + L)^2, \quad (23)$$

where L is a constant bigger than the maximum of

$$\begin{aligned} \left[\frac{m}{2} \right] + l_{2k-1} \quad & \left(k = 1, 2, \dots, \left[\frac{m+1}{2} \right] \right), \\ \left[\frac{m}{2} \right] + \frac{nl_{2k}^2}{4} \quad & \left(k = 1, 2, \dots, \left[\frac{m}{2} \right] \right), \end{aligned} \quad (24)$$

where $[m/2]$ denotes the largest integer, no more than $m/2$.

The derivative of V_3 along trajectories of (23) is

$$\begin{aligned} \dot{V}_3 &= \sum_{j=1}^n x^{2j-1} \dot{x} + \sum_{k=1}^m \frac{1}{\gamma_k} (\beta_k + L) \dot{\beta}_k \\ &\leq \sum_{j=1}^n |x|^{2j-1} \sum_{k=1}^m l_k \|x\|^k - L \sum_{k=1}^m \sum_{j=1}^n |x|^{2(j+k)-2} \\ &= \sum_{j=1}^n \sum_{k=1}^{[(m+1)/2]} |x|^{2j-1} l_{2k-1} \|x\|^{2k-1} + \sum_{j=1}^n \sum_{k=1}^{[m/2]} |x|^{2j-1} l_{2k} \|x\|^{2k} \\ &\quad - L \sum_{j=1}^n \sum_{k=1}^m |x|^{2(j+k)-2} \\ &\leq \sum_{j=1}^n \sum_{k=1}^{[(m+1)/2]} l_{2k-1} |x|^{2(j+k)-2} + \sum_{j=1}^n \sum_{k=1}^{[m/2]} |x|^{4j-2} \\ &\quad + \sum_{j=1}^n \sum_{k=1}^{[m/2]} \frac{l_{2k}^2}{4} |x|^{4k} - L \sum_{j=1}^n \sum_{k=1}^m |x|^{2(j+k)-2} \end{aligned}$$

$$\begin{aligned}
&\leq \sum_{j=1}^n \sum_{k=1}^{[(m+1)/2]} l_{2k-1} |x|^{2(j+k)-2} + \left[\frac{m}{2}\right] \sum_{j=1}^n \sum_{k=1}^m |x|^{2(j+k)-2} \\
&\quad + \frac{nl_{2k}^2}{4} \sum_{j=1}^n \sum_{k=1}^{[m/2]} |x|^{2(j+k)-2} - L \sum_{j=1}^n \sum_{k=1}^m |x|^{2(j+k)-2} \\
&\leq - \sum_{k=1}^{[(m+1)/2]} \left(L - \left[\frac{m}{2}\right] - l_{2k-1} \right) \sum_{j=1}^m |x|^{2(j+k)-2} \\
&\quad - \sum_{k=1}^{[m/2]} \left(L - \left[\frac{m}{2}\right] - \frac{nl_{2k}^2}{4} \right) \sum_{j=1}^m |x|^{2(j+k)-2} \\
&\leq 0.
\end{aligned} \tag{25}$$

So if and only if $x = 0$, $\dot{V}_3 = 0$, then asymptotical stability of (22) is proved. \square

Remark 8. Add related terms of i to prove course; introduce Lyapunov function:

$$\begin{aligned}
V &= \frac{1}{2} \sum_{i=s+1}^t \sum_{j=1}^n \frac{1}{j} y_i^{2j} \\
&\quad + \frac{1}{2\gamma_{ki}} \sum_{i=s+1}^t \sum_{k=1}^m (\beta_{ki} + L)^2
\end{aligned} \tag{26}$$

by the same method and almost the same process; we can prove the globally asymptotical stability of system state (18) with AFC controller. So AFC acts as a single-state control and also can be designed globally.

4. Simulation Results

After the theoretical analyses are investigated, we discuss the following numerical example to illustrate the derived theoretical results. From [13], we can obtain the system model of Chua's Oscillator:

$$\begin{aligned}
\dot{x}_1 &= \alpha(-x_1 + x_2 - f(x_1)), \\
\dot{x}_2 &= x_1 - x_2 + x_3, \\
\dot{x}_3 &= -\beta x_2 - \gamma x_3,
\end{aligned} \tag{27}$$

where $f(x_1) = bx_1 + ((a-b)/2)(|x_1+1| - |x_1-1|)$.

The Chua oscillator is illustrated in Figures 1 and 2. For simulation, the system parameters are used as $\alpha = 8.72$, $\beta = 14.29$, $\gamma = 0.01$, $a = -8/7$, $b = -5/7$, with initial conditions $(x_1(t_0), x_2(t_0), x_3(t_0))^T = (-2.1213, -0.0662, 2.8811)^T$.

With constraint condition (14), we get $C_1 = 2$, $C_2 = C_3 = 1$, introduced from (7); we take $\mu = \eta = 10$, $\xi = 1/2$, in (9); via (8), obtain u_1 , added to system (6). Its effectiveness is shown in Figure 3. After the convergence of x_1 , x_2 , there is only $\dot{x}_3 = -0.01x_3$ in (18). So we let $m = 1$, $n = 2$, and $\gamma_{kj} = 1$; in (20) and (21), get u_2 , added to system (22). Its effectiveness is shown in Figure 4.

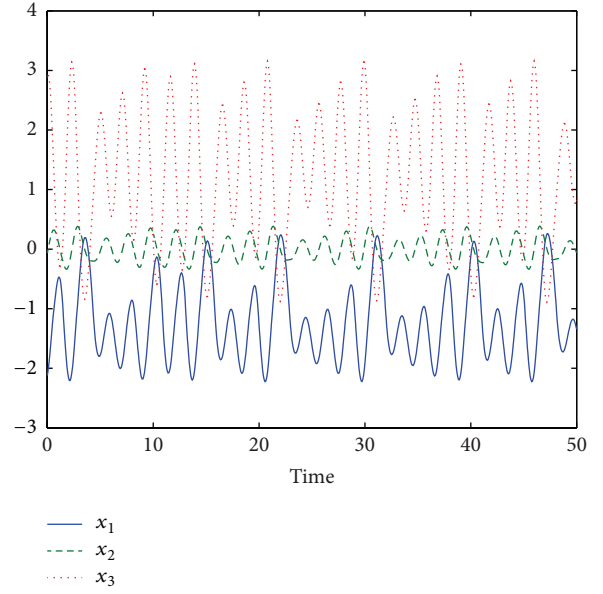


FIGURE 1: The time series of uncontrolled Chua oscillator.

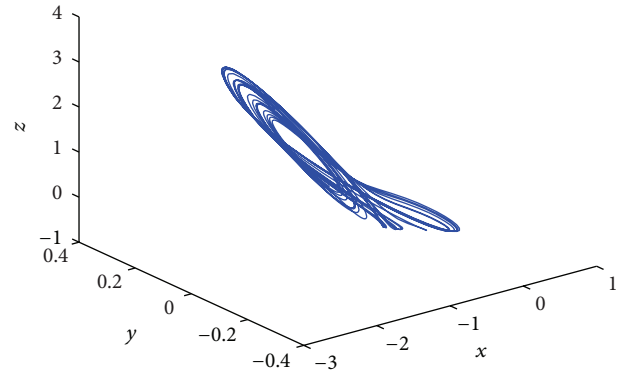


FIGURE 2: Chaotic attractor of uncontrolled Chua oscillator.

According to simulation results, it is easy to find that, the TSM method can effectively control the first two of system states and realize their finite-time stability. Comparing Figures 3 and 4, we can find that AFC controller effectively controls the remaining one of system state and makes it asymptotically stable. Finally, system states globally tend to semifinite time stable and we complete the expected objectives.

5. Conclusions

A controller, cooperating TSM with AFC, is proposed to control a class of chaotic system as described above in this paper. Two methods are complementary in the procedure and finally achieve good effectiveness. Complex TSM method controls main elements of chaotic system to finite-time stability; then, simple AFC method controls dimension elements of chaotic system to asymptotic stability and finally the overall system goes to semifinite time stability. This design scheme can not only guarantee the system's convergence but also

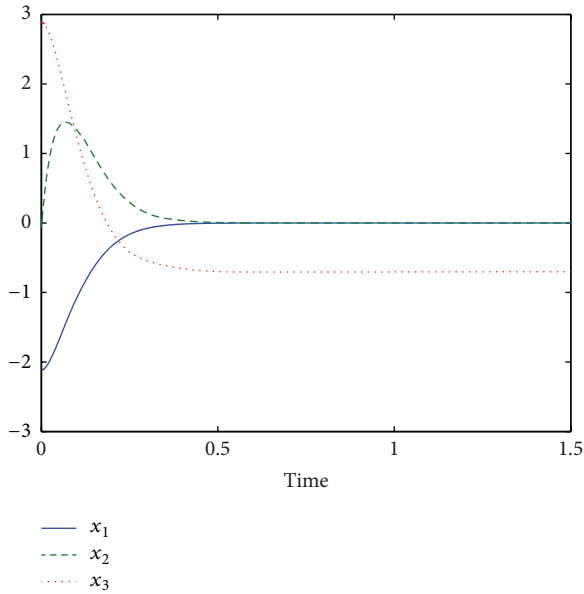


FIGURE 3: Time series of Chua oscillator with TSM only.

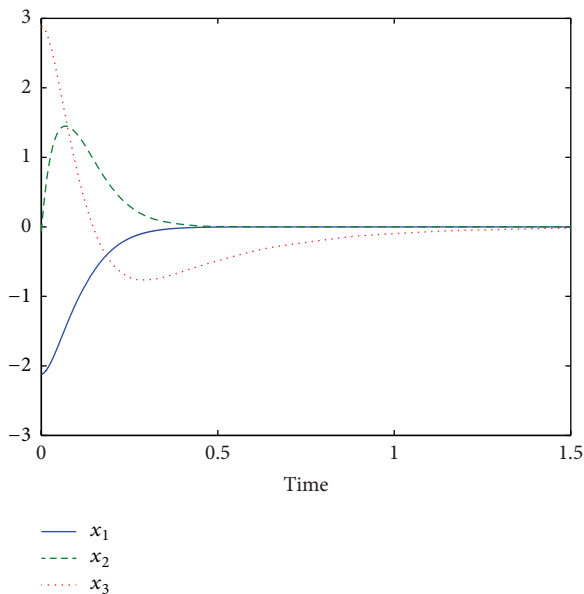


FIGURE 4: Time series of Chua oscillator with both TSM and AFC.

reduce the system's control-input spending and also further improve their applications in chaos control.

In this paper, effective performance of the simulation results proves the feasibility of this design scheme. The proposed method can be applied in many famous chaotic systems such as Lorenz, Liu chaotic system, and Chua's circuit.

Conflict of Interests

The authors declare that there is no conflict of interests regarding the publication of this paper.

Acknowledgments

The authors are greatly indebted to the anonymous referees for their constructive comments. The work described in this paper was partially supported by the National Natural Science Foundation of China (no. 10971240), the Natural Science Foundation Project of CQ CSTC (nos. cstc2012jjA40052, cstc2013jcyjA0973, and cstc2013jcyjA80013), Applying Basic Research Program of Chongqing Education Committee (nos. KJ120615, KJ120630, KJ130611, and KJ1400505), the Foundation Project of Chongqing Normal University (no. 13XLZ01), and the Program of Chongqing Innovation Team Project in University under Grant no. KJTD201308.

References

- [1] Y. Feng, X. Yu, and Z. Man, "Non-singular terminal sliding mode control of rigid manipulators," *Automatica*, vol. 38, no. 12, pp. 2159–2167, 2002.
- [2] Z. Man and X. Yu, "Terminal sliding mode control of MIMO linear systems," in *Proceedings of the 35th IEEE Conference on Decision and Control*, vol. 4, IEEE, 1996.
- [3] X. Yu and M. Zhihong, "Fast terminal sliding-mode control design for nonlinear dynamical systems," *IEEE Transactions on Circuits and Systems I: Fundamental Theory and Applications*, vol. 49, no. 2, pp. 261–264, 2002.
- [4] H. Wang, X. Zhang, X. Wang, and X. Zhu, "Finite time chaos control for a class of chaotic systems with input nonlinearities via TSM scheme," *Nonlinear Dynamics*, vol. 69, no. 4, pp. 1941–1947, 2012.
- [5] Z. Yang and D. Xu, "Stability analysis and design of impulsive control systems with time delay," *IEEE Transactions on Automatic Control*, vol. 52, no. 8, pp. 1448–1454, 2007.
- [6] Z. Yang and D. Xu, "Stability analysis of delay neural networks with impulsive effects," *Dynamics of Continuous, Discrete & Impulsive Systems A*, vol. 13, no. 5, pp. 563–573, 2006.
- [7] Y. Zhao and J. Wang, "Exponential synchronization of impulsive complex networks with output coupling," *International Journal of Automation and Computation*, vol. 10, no. 4, pp. 350–359, 2013.
- [8] X. Lou, Q. Ye, and B. Cui, "Impulsive stabilization of fuzzy neural networks with time-varying delays," *Arabian Journal of Mathematics*, vol. 2, no. 1, pp. 65–79, 2013.
- [9] H. Wang and C. Ding, "A new nonlinear impulsive delay differential inequality and its applications," *Journal of Inequalities and Applications*, vol. 2011, article 11, 2011.
- [10] D. Wang and Y. Zheng, "Stabilizing a class of chaotic systems by using adaptive feedback control," *Physics Procedia*, vol. 24, pp. 1922–1927, 2012.
- [11] V. I. Utkin, "Sliding mode control design principles and applications to electric drives," *IEEE Transactions on Industrial Electronics*, vol. 40, no. 1, pp. 23–36, 1993.
- [12] Y. Hong, G. Yang, L. Bushnell, and H. O. Wang, "Global finite-time stabilization: from state feedback to output feedback," in *Proceedings of the 39th IEEE Conference on Decision and Control*, pp. 2908–2913, Sydney, Australia, December 2000.
- [13] Y. Yu and J. Yu, *Impulsive modeling and stability study on nonlinear circuits and systems*, [Ph.D. thesis], Electronic Science and Technology University, 2008.
- [14] R. Palm, "Sliding mode fuzzy control," in *Proceedings of the IEEE Conference on Fuzzy Systems*, pp. 519–526, San Diego, Calif, USA, 1992.

- [15] Y. Wang, X. Shi, Z. Zuo, M. Z. Q. Chen, and Y. Shao, "On finite-time stability for nonlinear impulsive switched systems," *Nonlinear Analysis: Real World Applications*, vol. 14, no. 1, pp. 807–814, 2013.
- [16] Y. Wang, G. Wang, X. Shi, and Z. Zuo, "Finite-time stability analysis of impulsive switched discrete-time linear systems: the average dwell time approach," *Circuits, Systems, and Signal Processing*, vol. 31, no. 5, pp. 1877–1886, 2012.
- [17] M. M. El-Dessoky and M. T. Yassen, "Adaptive feedback control for chaos control and synchronization for new chaotic dynamical system," *Mathematical Problems in Engineering*, vol. 2012, Article ID 347210, p. 12, 2012.
- [18] W. Guo and D. Liu, "Adaptive control of chaos in Chua's circuit," *Mathematical Problems in Engineering*, vol. 2011, Article ID 620946, 14 pages, 2011.
- [19] R. Zhang and S. Yang, "Stabilization of fractional-order chaotic system via a single state adaptive-feedback controller," *Nonlinear Dynamics*, vol. 68, no. 1-2, pp. 45–51, 2012.
- [20] M. Feki, "An adaptive feedback control of linearizable chaotic systems," *Chaos, Solitons & Fractals*, vol. 15, no. 5, pp. 883–890, 2003.
- [21] Q. Zhong and S. Xu, "Exponential stabilization for takagi-sugeno fuzzy systems with time delay via impulsive control," in *Advanced Intelligent Computing*, D.-S. Huang, Y. Gan, V. Bevilacqua, and J. C. Figueroa, Eds., vol. 6838 of *Lecture Notes in Computer Science*, pp. 619–625, Springer, Berlin, Germany, 2011.
- [22] D. Xin and Y. Liu, *Finite-time stability analysis and control design research [M.S. thesis]*, Shandong University, 2008.
- [23] Y. Feng, L. Sun, and X. Yu, "Finite time synchronization of chaotic systems with unmatched uncertainties," in *Proceedings of the 30th Annual Conference of the IEEE Industrial Electronics Society (IECON '04)*, pp. 2911–2916, Busan, Republic of Korea, November 2004.

Research Article

CSA: A Credibility Search Algorithm Based on Different Query in Unstructured Peer-to-Peer Networks

Hongyan Mei,^{1,2} Yujie Zhang,^{1,2} and Xiangwu Meng^{1,2}

¹ Beijing Key Laboratory of Intelligent Telecommunications Software and Multimedia,
Beijing University of Posts and Telecommunications, Beijing 100876, China

² School of Computer Science, Beijing University of Posts and Telecommunications, Beijing 100876, China

Correspondence should be addressed to Hongyan Mei; liaoning_mhy@126.com

Received 27 February 2014; Revised 12 June 2014; Accepted 13 June 2014; Published 10 July 2014

Academic Editor: He Huang

Copyright © 2014 Hongyan Mei et al. This is an open access article distributed under the Creative Commons Attribution License, which permits unrestricted use, distribution, and reproduction in any medium, provided the original work is properly cited.

Efficient searching for resources has become a challenging task with less network bandwidth consumption in unstructured peer-to-peer (P2P) networks. Heuristic search mechanism is an effective method which depends on the previous searches to guide future ones. In the proposed methods, searching for high-repetition resources is more effective. However, the performances of the searches for nonrepetition or low-repetition or rare resources need to be improved. As for this problem, considering the similarity between social networks and unstructured P2P networks, we present a credibility search algorithm based on different queries according to the trust production principle in sociology and psychology. In this method, queries are divided into familiar queries and unfamiliar queries. For different queries, we adopt different ways to get the credibility of node to its each neighbor. And then queries should be forwarded by the neighbor nodes with higher credibility. Experimental results show that our method can improve query hit rate and reduce search delay with low bandwidth consumption in three different network topologies under static and dynamic network environments.

1. Introduction

In the past ten years, peer-to-peer (P2P) networks have gained full development and become an important part of the Internet. P2P networks are divided into structured P2P networks and unstructured P2P networks. Unstructured P2P networks are characterized with self-organization, distributed resource sharing, semantic queries, and so forth, which have been widely applied on the Internet, such as Gnutella [1], FastTrack [2] and KaZaA [3]. However, because of the dynamic characteristics of unstructured P2P networks, it is difficult to capture correctly global behavior [4, 5]. Each node in unstructured peer-to-peer networks does not have global information about the whole network topology and the location of queried resources. Thus, designing an efficient search algorithm has been a hot research issue in unstructured P2P networks.

There are mainly two kinds of search methods in unstructured P2P networks: blind search methods and informed

search methods. In the former, such as flooding [1], peers possess no knowledge to guide the search process, resulting in great blindness. When the size of network increases, the search time will be extended, a large number of redundant messages will be created, and large amounts of network bandwidth will be consumed. In order to reduce the bandwidth consumption, many improved methods [6–15] have been proposed on the basis of the blind search algorithms. And literatures [8–10] have improved flooding algorithm in network bandwidth consumption while preserving large coverage, response time, and flexibility of flooding in dynamic environment. The effective and optimizing search algorithms have been presented in literatures [11, 12], which achieve higher performance than random walks in terms of number of hits, network overhead, and response time by adopting stochastic process knowledge and estimating of the popularity of a resource, respectively. A hybrid search scheme [13] and light flood [14] are proposed by combining flooding and random walks and make full use of the both merits so as to minimize

redundant messages. In literature [15], RFSA limits effectively that the message be received and forwarded repeatedly in blind search methods by using the real-time search path information and the local messages index caching mechanism, thus reducing the production of a great number of redundant messages.

In contrast to the blind search methods, many informed search algorithms have been more extensively studied and proposed, such as intelligent search [16], APS [17], PQR [18] and SPUN [19]. In literature [16], an intelligent search is proposed where a query is forwarded to neighbors that have answered the most queries similar to the current query. APS [17] is a popular adaptive probability k random walks search algorithm and is also bandwidth efficient and easy to implement unstructured P2P search algorithm. APS utilizes the feedback information from previous searches to guide the future ones probabilistically. In APS, each node maintains an index table to record success rate of each neighbor for each requested resource in previous searches. APS probabilistically selects those neighbor nodes which get higher success rate for the requested resource from previous searches. Thus, the search will be successfully guided to the requested resource. At the same time, the success rate is updated dynamically based on whether a peer returns a hit or miss for a given query. PQR [18] is a novel query routing mechanism for improving query performance in unstructured P2P networks. In PQR, a data structure called traceable gain matrix (TGM) is designed and used to record gain value of every query at each peer along the query hit path. By TGM, PQR can optimize query routing decision effectively and achieve high query hit rate with low bandwidth consumption. TGM is an important component of PQR with a compound data structure and maintains query routing information. In these methods [16–18], peers update index values only based on the return type of the query message, success, or failure. And in APS and PQR, peers also have a tendency to use the first discovered neighbor node which reduces search performance in dynamic environments. As for these problems, SPUN is proposed in [19]. SPUN is an informed search algorithm that improves upon state-of-the-art APS. Each peer in SPUN maintains a vector of relative success rates (RSRV) along a query path for a given neighbor for a requested resource resulting in a more informed decision in SPUN. SPUN uses best path gradient (BPG) as neighbor node selection mechanism, which firstly calculates PG values of different paths through neighbor nodes and then discovers more successful query paths through the neighbors according to PG values. The purpose of SPUN is to select neighbor node with the most successful query path to forward query message. However, the most successful query path is often “traffic arteries” for the requested resources, which can cause search bottleneck problem. On the other hand, it only considers the success of a path with no consideration to the distance information of the path. The most successful path may be the longest and the most congested, thereby increasing the search time and network overhead.

The common characteristic of these methods above is to guide future searches through search information recorded previously. Therefore, in the search process, these algorithms

are effective for the repeated queries for the same objects (resources) or similar objects (resources). Because these algorithms can gain heuristic information from the relevant indexes such as TGM (in PQR) or RSRV (in SPUN). But for those nonrepetitive queries such as queries for rare resources, there is no heuristic information in the relevant indexes, so the queries will be forwarded to a random neighbor node (peer). At this moment, the search is inefficient in these methods and their overall search performance will be reduced.

The main motivation of our research is to solve the inefficient problem for nonrepetition or low-repetition or rare resources queries. So, a credible search algorithm (CSA) based on different query is proposed in this paper. The main purpose is to improve the search performance of the searching for nonrepetition or low-repetition or rare resources and repeated queries through the effective guidance and then achieve the higher overall search performance. The contributions of this paper are shown as follows. (1) It is the first in which queries are divided into familiar queries and unfamiliar queries and for different query adopting different calculation method to obtain credibility information and then selecting neighbor nodes with higher credibility as passers. (2) We give a credibility calculation method to calculate neighbor's credibility according to familiarity and similarity among queries and nodes based on the trust production principle in sociology and psychology. (3) Design a new data structure: query credible matrix (QCM), recording the credibility of each neighbor node for each specific object. (4) The proposed methods can achieve high query hit rate with low search delay and low bandwidth consumption and improve the search performance for nonrepetitive queries, such as rare resource queries.

2. Credibility Calculation Method

The studies of literature [20] show that trust among humans consists of two parts: the one generated by the familiarity and the other one by similarity. In social networks, the more familiar among humans, the more trust produced will be. The more similar people are in their interests and hobbies, the easier they will trust each other. So, through familiarity and similarity to calculate trust among humans can reflect the generating process of trust in social networks. Considering the similarity between unstructured P2P networks and social networks, the principle of trust generated among humans in social network can be used to the credibility calculation of node to its neighbors in unstructured P2P networks. The credibility of node to its neighbors is also divided into the trust generated by the familiarity and the trust generated by the similarity.

Suppose p_t stands for an arbitrary peer in unstructured P2P networks and p_j is an arbitrary neighbor peer of the peer p_t . The credibility of p_t to p_j is calculated as

$$\text{Cre}(p_t, p_j) = \text{fam}(p_t, p_j) + \text{sim}(p_t, p_j), \quad (1)$$

where $\text{Cre}(p_t, p_j)$ represents the credibility of the peer p_t to its neighbor peer p_j . $\text{fam}(p_t, p_j)$ refers to the trust generated

by the familiarity between p_t and p_j . In familiarity study, people often gain the familiarity through the number of contacts among humans. In our study, $\text{fam}(p_t, p_j)$ is defined as the success rate of the communications between p_t and p_j . The more the number of success communications is, the higher the success communication rate is and then the more familiar is between p_t and p_j . And the credibility of p_t to p_j is higher. $\text{sim}(p_t, p_j)$ denotes the trust generated by the similarity between p_t and p_j . In unstructured P2P networks, contents stored on a peer reflect the interests and hobbies of this peer and then $\text{sim}(p_t, p_j)$ will be obtained according to the similarity of contents stored on p_t and p_j .

2.1. Credibility Calculation Based on Familiarity. In social networks, familiarity among humans mainly derives from the mutual help and constant contacts, and so forth. Similar to social networks, in unstructured P2P networks, whether peer and its neighbor are familiar will be decided through the behavior of communications between the peer and its neighbor.

In general, the more the numbers of communications are between p_t and p_j , the more familiar they are. At the same time, this communication is bidirectional. If only p_t sends query messages to p_j and p_j cannot return successful messages to p_t , then, although the number of communications between them becomes more, the neighbor peer p_j is still not credible for the future search. So the number of communications between p_t and p_j cannot reflect better the familiarity of p_t to p_j . We can not only use the number of communications as the credibility of p_t to p_j generated by the familiarity.

Because query tends to be passed to the first peers found [17] or the peers with higher degree [21] in the informed methods, then these peers have more opportunities to be selected as passers. And thus, these peers can get higher number of success return messages than those peers that have less opportunity to be selected as passers, even though most query messages forwarded through the peers can be successfully returned. Meanwhile the first peers or peers with higher degrees will be selected repeatedly to forward messages. And thus search bottleneck problem on these peers will be produced and the broadness of search will be reduced.

For example, suppose the number of messages of p_t sending to p_1 is 7 and the number of messages of success return is also 7. The number of messages of p_t sending to p_2 is 20, and the number of messages of success return is 10. If we adopt the number of success communications as the credibility of p_t to p_j generated by the familiarity, then $\text{fam}(p_t, p_1) = 7$, $\text{fam}(p_t, p_2) = 10$. Although all messages of p_t sending to p_1 have been all returned successfully, because the number of query messages forwarded by p_1 is less, the number of messages of success return of p_1 is still less than that of p_2 . Thus p_2 gains more confidence than p_1 and will be more selected, which will cause bottleneck problem of the peer p_2 and ignores the selection for p_1 . So, we calculate the trust of p_t to p_j generated by the familiarity according to communication success rate in this paper. And

thus, $\text{fam}(p_t, p_1) = 1$ and $\text{fam}(p_t, p_2) = 0.5$; the peer p_1 can gain more trust and it will be more selected than p_2 , which reduces bottleneck problem of p_2 and improves performance of search in future search.

Therefore, the credibility of p_t to p_j generated by familiarity is calculated as

$$\text{fam}(p_t, p_j) = \frac{|SR_{p_t \leftarrow p_j}|}{|F_{p_t \rightarrow p_j}|}. \quad (2)$$

In formula (2), $F_{p_t \rightarrow p_j}$ is a set of messages from p_t forwarded to p_j . $SR_{p_t \leftarrow p_j}$ is also a set of messages from p_j success return to p_t . Where $\text{fam}(p_t, p_j) \in [0, 1]$, when $\text{fam}(p_t, p_j) = 0$, no success message is returned to p_t through p_j . When $\text{fam}(p_t, p_j) = 1$, the query messages forwarded to p_j are all returned successfully to p_t . Thereby the greater $\text{fam}(p_t, p_j)$ is, the more credible p_j is and selecting p_j to forward the query will get the higher probability of success hit.

2.2. Credibility Calculation Based on Similarity. In social networks, trust can be built on among humans who have similar family background, race, values, interests, hobbies, and so forth. Similar to social networks, in unstructured P2P networks, the different contents stored on peers contain preferences information of these peers. At the same time, studies [22, 23] show that a better search performance can be get though clustering similar peers into the same group based on the similarity of preferences of the peers, such as interests or hobbies, and then searching in these groups. This suggests peer can get more success hit from neighbor peers similar with the peer. So the more similar peer and its neighbor are, the more they will trust each other. In this section, we obtain the preferences information of peers from contents stored on the peers and then according to the similarity of the preferences information of peers to calculate the credibility between peer and its neighbor generated by similarity.

Given an object set of peer p_t : $O_t = \{o_1, o_2, \dots, o_j, \dots, o_m\}$ with m elements, because of advances in metadata retrieval technology [24–26], it is easier to obtain keywords information of every object. Let $K_{o_j} = \{k_{j1}, k_{j2}, \dots, k_{jn}, \dots\}$ be a set of keywords used to describe an object o_j . We denote the keywords set of all objects peer p_t held by $K_{p_t} = \bigcup_{j=1}^m K_{o_j}$ and the characteristics (preferences information) of peer p_t are defined as a vector of weights $\vec{p}_t = (\omega_{t,k1}, \omega_{t,k2}, \dots, \omega_{t,kn}, \dots)$, where the weight $\omega_{t,kn}$ denotes the preference of peer p_t for objects described by the keyword k_n as follows:

$$\omega_{t,kn} = \frac{|O_{t,kn}|}{|O_t|}, \quad (3)$$

where O_t is the set of objects held by peer p_t and $O_{t,kn}$ is a subset of O_t containing objects tagged by keyword k_n .

The similarity $\text{sim}(p_t, p_j)$ between p_t and p_j can be measured by comparing their preferences. There are several methods such as the correlation coefficient, the cosine similarity measure [27], and the Euclidean distance that can be used to compute the distance between two description vectors and return a quantitative value to represent the similarity between peers. In this context, we use the cosine similarity measure to quantify the similarity $\text{sim}(p_t, p_j)$ as follows:

$$\begin{aligned} \text{sim}(p_t, p_j) &= \cos(\vec{p}_t, \vec{p}_j) \\ &= \frac{\vec{p}_t \cdot \vec{p}_j}{\|\vec{p}_t\|_2 \times \|\vec{p}_j\|_2} \\ &= \frac{\sum_{k=1}^m \omega_{t,k} \omega_{j,k}}{\sqrt{\sum_{k=1}^m \omega_{t,k}^2 \sum_{k=1}^m \omega_{j,k}^2}}, \end{aligned} \quad (4)$$

where m is the total number of keywords. If p_t and p_j have similar interests in the contents they hold, then a bigger value $\text{sim}(p_t, p_j)$ will be obtained.

2.3. Credibility Calculation Based on Query. In a real world, when a person is asked to do a task, who tends to choose his (her) credible and capable friends to complete this matter? For example, in six degrees of segmentation principle, everyone who receives the letter usually passes the letter to his friends who have similar information with the letter.

In unstructured P2P networks, for a specific query q_h , we use $\text{sim}(q_h, p_t, p_j)$ to denote the credibility between p_t and its neighbor p_j based on the specific query q_h . The value of $\text{sim}(q_h, p_t, p_j)$ is calculated as

$$\text{sim}(q_h, p_t, p_j) = \frac{|K_{q_h} \cap K_{p_j}|}{|K_{q_h}|}, \quad (5)$$

where K_{q_h} is a set of keywords included in the query q_h , K_{p_j} denotes the keywords set of all objects peer p_j hold, and $\text{sim}(q_h, p_t, p_j) \in [0, 1]$. There are no similar keywords with the specific query q_h in peer p_j , if $\text{sim}(q_h, p_t, p_j) = 0$. All keywords of the specific q_h are contained in the keywords set of objects peer p_j hold, if $\text{sim}(q_h, p_t, p_j) = 1$. So, the more the number of similar keywords is between q_h and p_j , the bigger the value of $\text{sim}(q_h, p_t, p_j)$ is; then the neighbor peer p_j is more credible for the specific query q_h .

According to calculation method of the credibility $\text{fam}(p_t, p_j)$ generated by familiarity in Section 2.1, we denote the credibility $\text{fam}(q_h, p_t, p_j)$ generated by familiarity based on the specific query q_h as follows:

$$\text{fam}(q_h, p_t, p_j) = \frac{\left| \text{SR}_{p_t \xleftarrow{K_{q_h}} p_j} \right|}{\left| F_{p_t \xrightarrow{K_{q_h}} p_j} \right|}, \quad (6)$$

where $F_{p_t \xrightarrow{K_{q_h}} p_j}$ is a set of all messages that contain keywords K_{q_h} from p_t forwarded to p_j . $\text{SR}_{p_t \xleftarrow{K_{q_h}} p_j}$ is a set of all messages that contain K_{q_h} from p_j success return to p_t and $\text{fam}(q_h, p_t, p_j) \in [0, 1]$. If $\text{fam}(q_h, p_t, p_j) = 0$, no message containing keywords K_{q_h} is returned successfully to p_t from p_j ; then the credibility of p_t to p_j generated by familiarity for the specific query q_h is 0. If $\text{fam}(q_h, p_t, p_j) = 1$, all messages containing keywords K_{q_h} are returned successfully to p_t from p_j ; then the credibility of p_t to p_j generated by familiarity for the specific query q_h is 1. So, the bigger the value of $\text{fam}(q_h, p_t, p_j)$ is, the more credible the neighbor peer p_j is for the query q_h .

Above, we introduce the calculation method of credibility between peer and its neighbor and also describe the calculation method of credibility based on specific query between peers. In this method, we choose different credibility calculation methods to obtain trust for its neighbor peers according to different query types and then select neighbor peers with higher credibility to pass messages. Our algorithm will be described in detail in Section 4.

3. Data Structure and Update Mechanism in CSA

3.1. Message Structure in CSA

Query Message. We describe a query message *meg* initiated at peer p_s using a tuple of seven elements $\text{meg}(id, p_s, p_f, \text{state}, \text{hops}, K_{q_h}, \text{path})$. Where *id* denotes the unique identifier of a message in the unstructured P2P networks. p_s is the source peer that initiates the query message *meg*. p_f stands for the sender of the query message. *state* is type of the *meg* and contains three types: *Forward*, *Success_Return*, and *Failure_Return*. We define *hops* as the current hop value of the query message. K_{q_h} is a set of keywords included in the queried object. *path* describes search path of the query message and consists of peers that have traveled by the query, including the source peer p_s .

3.2. Index Structure in CSA. In CSA, credible neighbor list (short for CNL) and credible query matrix (short for CQM) are two main index structures that maintain peer local information. In CNL, each item describes the credibility of peer to each neighbor generated by similarity. The query information of each neighbor peer for each requested object is recorded in each item of CQM. We need two auxiliary data structures: query object list (short for QOL) and query peer list (short for QPL) before CQM is produced. The QOL of a peer is a set of objects that records all objects requested and forwarded from this peer. The QPL of a peer is a subset of its neighbors that records neighbors that one or more requested objects forwarded through the neighbors and returned successfully. In CQM, each row stands for each object in QOL and each column stands for each peer in QPL. Given O is a set of all objects in QOL with m elements, an arbitrary $o_i \in O$, $i \in [1, m]$. P is a set of all peers in QPL with

n elements, an arbitrary $p_j \in P$, $j \in [1, n]$. CQM is an $m \times n$ matrix like this:

$$\begin{matrix} & p_1 & p_2 & \cdots & p_j & \cdots & p_n \\ \begin{matrix} o_1 \\ \vdots \\ o_i \\ \vdots \\ o_m \end{matrix} & \begin{pmatrix} \text{Cre}_{11} & \text{Cre}_{12} & \cdots & \text{Cre}_{1j} & \cdots & \text{Cre}_{1n} \\ \vdots & \vdots & \cdots & \vdots & \cdots & \vdots \\ \text{Cre}_{i1} & \text{Cre}_{i2} & \cdots & \text{Cre}_{ij} & \cdots & \text{Cre}_{in} \\ \vdots & \vdots & \cdots & \vdots & \cdots & \vdots \\ \text{Cre}_{m1} & \text{Cre}_{m2} & \cdots & \text{Cre}_{mj} & \cdots & \text{Cre}_{mn} \end{pmatrix} \end{matrix}, \quad (7)$$

where each item Cre_{ij} has a compound data structure and is represented by a tuple of three elements: $\text{Cre}_{ij} = \langle F_{\text{num}_{ij}}, H_{\text{num}_{ij}}, \text{fam}_{\text{value}_{ij}} \rangle$. $F_{\text{num}_{ij}}$ is the number of query messages containing object o_i and forwarded by neighbor peer p_j . $H_{\text{num}_{ij}}$ is the number of query hit messages containing object o_i and forwarded by neighbor peer p_j . $\text{fam}_{\text{value}_{ij}}$ is calculated by formula (6) and denotes the credibility for neighbor p_j generated by familiarity for the query containing object o_i . $F_{\text{num}_{ij}}$ will be updated, if p_j is selected to forward the query containing object o_i . When the query is returned with hit by p_j , the value of $H_{\text{num}_{ij}}$ will be updated. At the same time, the value of $\text{fam}_{\text{value}_{ij}}$ will be updated according to formula (6). The dynamic update way in the search process adapts for dynamic characteristics of the unstructured P2P networks and avoids the bottleneck problem of the peer with higher credible. For example, when the value of $\text{fam}_{\text{value}_{ij}}$ is higher and there are multiple queries containing object o_i in peer, p_j will be multiselected. If the message is only to be forwarded, but not returned, then $F_{\text{num}_{ij}}$ will be increased and $H_{\text{num}_{ij}}$ not and thus the value of $\text{fam}_{\text{value}_{ij}}$ will be decreased. And then neighbor peers except p_j in CQM will have chances to forward the queries containing object o_i , thus reducing the burden of p_j and expanding the scope of the search. For the new query q_h containing object o_i , the credibility rate $\text{fam}(q_h, p_t, p_j)$ of p_t to its neighbor p_j by CQM is calculated as

$$\text{fam}(q_h, p_t, p_j) = \frac{|\text{Cre}_{ij}|}{\sum_{j=1}^n |\text{Cre}_{ij}|} = \frac{\text{fam}_{\text{value}_{ij}}}{\sum_{j=1}^n \text{fam}_{\text{value}_{ij}}}. \quad (8)$$

According to formula (2), on the basis of CQM, the credibility of p_t to its neighbor p_j generated by familiarity is shown as

$$\text{fam}(p_t, p_j) = \frac{\sum_{i=1}^m H_{\text{num}_{ij}}}{\sum_{i=1}^m F_{\text{num}_{ij}}}. \quad (9)$$

3.3. Update Mechanism. At the beginning of the search, both QOL and QPL are empty at each peer, as well as the corresponding CQM. Because there is no communication information between node and each of its neighbor nodes, the credibility of the familiarity to its each neighbor is 0 and the credibility of the similarity to its each neighbor is computed according to the formula (4). When a new query arrives,

peer firstly checks whether the requested object information is included in QOL; if not, the requested object information (keywords) will be joined in the QOL. When a neighbor node is selected to pass the query and the neighbor node is not in QPL, then it will be added in the QPL. At the same time, in CQM, the corresponding object row and node column information will be established and set the corresponding element $\text{Cre}_{ij} \cdot F_{\text{num}_{ij}} = 1$; if the requested object has been included in the QOL and the QPL contains the selected node, then the requested object position information $\text{position}(o_i)$ and the selected node position information $\text{position}(p_j)$ will be got from QOL and QPL, respectively, and then set the corresponding $\text{Cre}_{ij} \cdot F_{\text{num}_{ij}} = \text{Cre}_{ij} \cdot F_{\text{num}_{ij}} + 1$ in CQM. If the requested object has been included in QOL and the selected node is not in QPL, then the selected node will be added to QPL and the corresponding objects row and node column information will be established in CQM. After the query hit return happens, set $\text{Cre}_{ij} \cdot F_{\text{num}_{ij}} = 1$ and $\text{Cre}_{ij} \cdot H_{\text{num}_{ij}} = \text{Cre}_{ij} \cdot H_{\text{num}_{ij}} + 1$ in CQM and update $\text{Cre}_{ij} \cdot \text{fam}_{\text{value}_{ij}}$ according to formula (6). If the query returns failure, the corresponding information in QPL, QOL, and CQM will be deleted.

4. Search Algorithm CSA

4.1. Problem Analysis. In the existing heuristic search algorithm, such as APS, PQR, and SPUN, search mechanisms show that, when a node receives a query message, it firstly tests whether there is relevant information with the query in its index table. If there is, the query will be guided to forward according to the previous record information. And if there is no information, it will be forwarded based on random walks way. Thus, these methods are valid for the queries with high repetition rate. But for some queries with low repetition rate, such as a new query or query for rare resources, there is no or little heuristic guide information in these methods. At this moment, these methods are low efficient and their performances are equivalent to that of random walks. We simulate the three methods APS, PQR, and SPUN in experiments (experimental configuration given in Section 5.1); the simulation results are shown in Figure 1. In Figure 1, “total number” represents all number of selected neighbor nodes. “Random selection” means the number of neighbor nodes chosen randomly. “APS selection,” “PQR selection,” and “SPUN selection,” respectively, denote the number of neighbor nodes selected by the heuristic information given in the three algorithms. From Figure 1, we find that only about a third of neighbor nodes are selected according to the heuristic strategies given in the search processing and two-thirds of the neighbor node is still selected randomly in the three algorithms. Therefore, our motivation is to improve the search performance with high repetition rate as well as low repetition rate. In our method, queries firstly can be divided into familiar queries and strange (unfamiliar) ones and then using different neighbor node selection strategy to select neighbor peer forwarding different queries, respectively.

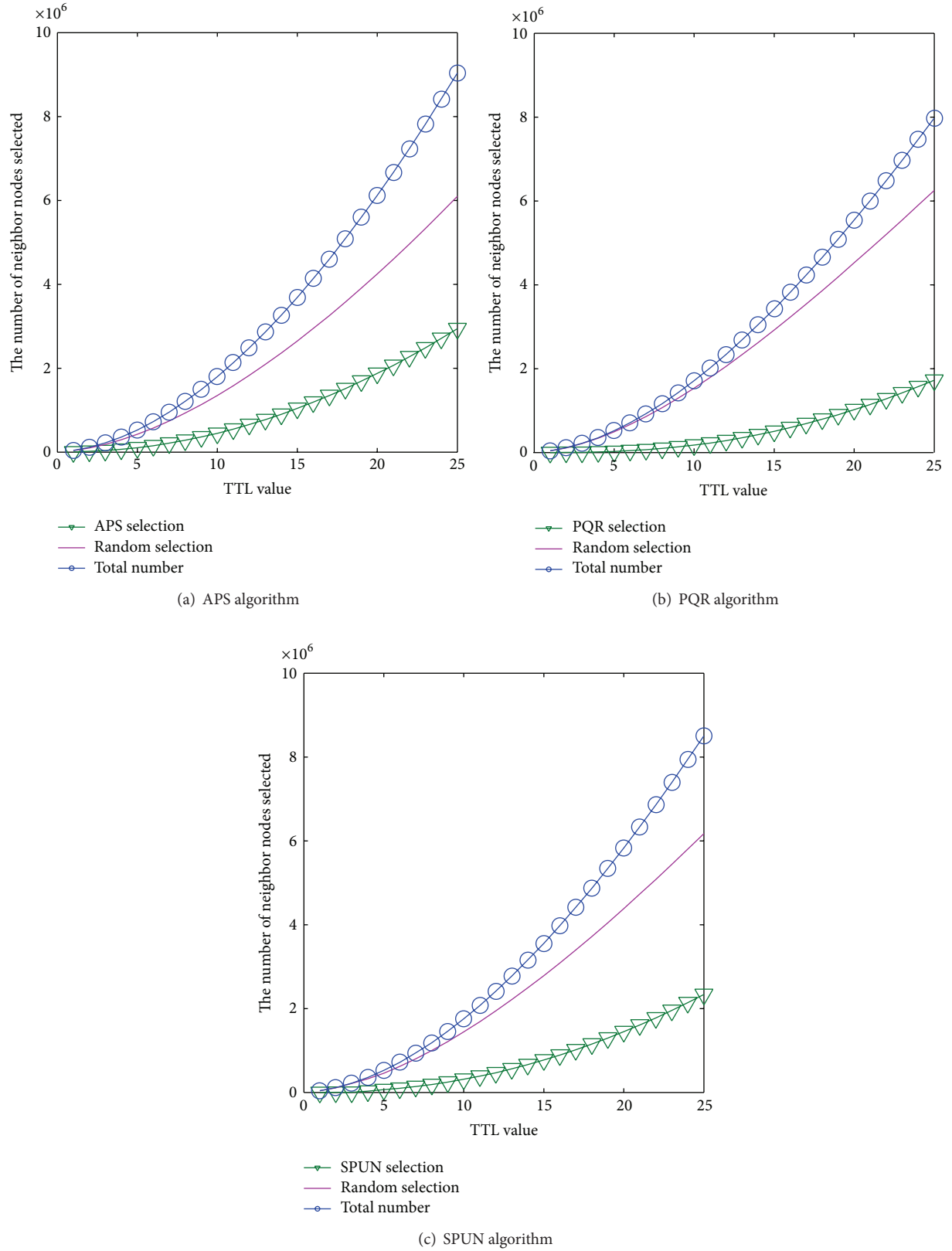


FIGURE 1: The comparison of the number of neighbor nodes selected.

4.2. Peer Selection Criteria. When a node receives a query message, if there is relevant information with the query in index table of this node, then the query is defined as familiar query. The familiar query will be processed according to previous search information. And if no, then the query is defined as strange query. Different from familiar query, there is no heuristic information for strange query in this node. Therefore, for strange query, our method firstly gets the credibility of the node to each neighbor node based on all the previous queries and the similarity between the requested object information and the contents stored on each neighbor node and then chooses the neighbor nodes with higher credibility to transfer the strange query. According to different query, familiar query, or strange query, the different credibility is described below. According to Sections 2 and 3, for a familiar query, the credibility of the node p_t to its neighbor node p_j is calculated as follows:

$$\begin{aligned} \text{Cre}(q_h, p_t, p_j) &= \text{fam}(q_h, p_t, p_j) \cdot r + \text{sim}(q_h, p_t, p_j) \\ &= \frac{\left| \text{SR}_{p_t \leftarrow p_j}^{K_{q_h}} \right|}{\left| F_{p_t \rightarrow p_j}^{K_{q_h}} \right|} + \frac{\left| K_{q_h} \cap K_{p_j} \right|}{\left| K_{q_h} \right|} \\ &= \frac{\text{fam}_{\text{value}_{ij}}}{\sum_{j=1}^n \text{fam}_{\text{value}_{ij}}} + \frac{\left| K_{q_h} \cap K_{p_j} \right|}{\left| K_{q_h} \right|}. \end{aligned} \quad (10)$$

For a strange query, the credibility of the node p_t to its neighbor node p_j is calculated as follows:

$$\begin{aligned} \text{Cre}(q_h, p_t, p_j) &= \text{fam}(p_t, p_j) + \text{sim}(q_h, p_t, p_j) \\ &= \frac{\left| \text{SR}_{p_t \leftarrow p_j} \right|}{\left| F_{p_t \rightarrow p_j} \right|} + \frac{\left| K_{q_h} \cap K_{p_j} \right|}{\left| K_{q_h} \right|} \\ &= \frac{\sum_{i=1}^m H_{\text{num}_{ij}}}{\sum_{i=1}^m F_{\text{num}_{ij}}} + \frac{\left| K_{q_h} \cap K_{p_j} \right|}{\left| K_{q_h} \right|}. \end{aligned} \quad (11)$$

In the search process, our method firstly determines a query whether it is a familiar query or a strange query. If it is a familiar query, we calculate the credibility of node to its neighbor nodes according to the formula (10). If it is a strange query, we compute the credibility of node to its neighbor nodes according to the formula (11) and then select the neighbor nodes with high credibility as passers. The proposed algorithm is described in Section 4.3.

4.3. Algorithm Description. The credibility search algorithm includes the process of the neighbor node selection and updating process, which is described in detail in Algorithm 1.

5. Experiments and Performance Evaluation

P2P networks are large-scale networks with millions of nodes, which join and leave frequently. The dynamic characteristics

TABLE 1: Simulation parameters.

Parameters	Value
Network size	10000
Kind of file (object)	100
Total number of files (object)	10000
Total number of queries	10000
Object distribution	Zipf (alpha = 0.8)
Beta in small-word network	0.5
walkers (k)	4

of P2P networks are challenging to deal with. It is not feasible to evaluate a new protocol in a real environment. To save time and improve efficiency, we use Peersim [28] as a simulation platform, which is a Java-based, open-source, large-scale P2P simulation platform and suitable for P2P dynamic characteristics. In this paper, we expand Peersim code for simulation and deploy four search strategies APS, PQR, SPUN, and CSA in the three most representative network topologies including random graph network structure (random graph), small world model network structure (small world), and scale-free network structure (scale-free). We evaluate the performance of the four search strategies in terms of network overhead, query hit rate, search delay, and the query hit rate for rare resources under static and dynamic network conditions.

5.1. Experimental Setting. Studies have shown that Gnutella, Napster, and Web users request tend to follow Zipf-like distributions [29]. In order to reveal the real network environment, the object popularity follows Zipf-like distribution in our experiments and is given by the formula [30]:

$$P_{\text{Zipf-like}}(x) = \frac{x^{-\alpha}}{\sum_{j=1}^C j^{-\alpha}}, \quad (12)$$

where C is the number of objects (resources) and α denotes the exponent characterizing of the distribution. Research [31] shows that α is usually between 0.6 and 0.8. x is the relative position of a resource or object. In experiments, we provide a total of 10,000 objects that are divided into 100 classes. Each class object is set up corresponding popularity based on the formula (12). We set the appropriate number of each type of object on the basis of its popularity and make objects or resources with high popularity to obtain a higher replication rate. Each object or resource is duplicated to a random node. As for queries, each node obtains query objects from 100 classes based on the popularity of objects. The objects with high popularity are more likely to be selected as the query objects. So the queries in our method can be more close to real networks. Table 1 shows the experimental parameters and their default values. And three kinds of network topologies, respectively, constructed, and node degree and its distribution are analyzed in our experiments. The results of the analysis are shown in Table 2.

Input: The relevant parameters, such as: query message number, network topology model, network size, TTL (Time-to-Live)

Output: Result (success or fail), the hops number of the first success return message, message information

Peer p_t gets a query message $meg \langle id, p_s, p_f, state, hops, K_{qh}, path \rangle$

If ($meg \cdot state = Forward$) {

If (K_{qh} hits at p_t) then { // the requested objects are included in p_t

$meg \cdot state = Success_Return$;

Peer p_t sends successful meg to p_s along with the reverse $meg \cdot path$. }

Else if ($meg \cdot hops = TTL$) then { // the requested objects are not included in p_t

$meg \cdot state = Failure_Return$;

Peer p_t sends failure meg to p_s along with the reverse $meg \cdot path$. }

Else if ($meg \cdot K_{qh} \in p_t \cdot QOL$) { // the query is familiar query

return $K_{qh} \cdot position i$ in $p_t \cdot QOL$;

calculates the value $fam(q_h, p_t, p_j)$ of each corresponding neighbor node of the i th row in $p_t \cdot CQM$ according to formula (6) and then gets the value $fam(q_h, p_t, p_j) \cdot r$ according to formula (10); selects the neighbor node p_j with higher credibility value and forwards meg to p_j ; updates

$Cre_{ij} \cdot F_{num_{ij}} = Cre_{ij} \cdot F_{num_{ij}} + 1$. }

Else { // $meg \cdot K_{qh} \notin p_t \cdot QOL$, the query is strange query

calculates the credibility value of each neighbor node according to formula (11) and selects the neighbor node p_j with higher credibility value and forwards meg to p_j ; adds the requested object and p_j to $p_t \cdot QOL$ and $p_t \cdot QPL$, respectively. }

End if }

Else if ($meg \cdot state = Success_Return$) { // Updates the corresponding information in $p_t \cdot QPL$, $p_t \cdot QOL$ and $p_t \cdot CQM$

If ($p_t \cdot QOL \neq \phi$ and $K_{qh} \in p_t \cdot QOL$) then { returns $K_{qh} \cdot position i$ in $p_t \cdot QOL$. }

Else { $p_t \cdot QOL \cdot add(K_{qh})$; returns $K_{qh} \cdot position i$ in $p_t \cdot QOL$. }

End if

Peer $p_j \leftarrow meg \cdot p_f$

If ($p_t \cdot QPL \neq \phi$ and $p_j \in p_t \cdot QPL$) then { returns $p_j \cdot position j$ in $p_t \cdot QPL$. }

Else { $p_t \cdot QPL \cdot add(p_j)$; returns $p_j \cdot position j$ in $p_t \cdot QPL$. }

End if

If ($p_t \cdot CQM \cdot Cre_{ij} = \phi$) then { $p_t \cdot CQM \cdot add(Cre_{ij})$; $Cre_{ij} \cdot F_{num_{ij}} = Cre_{ij} \cdot H_{num_{ij}} = Cre_{ij} \cdot fim_{value_{ij}} = 1$. }

Else { $Cre_{ij} \cdot H_{num_{ij}} = Cre_{ij} \cdot H_{num_{ij}} + 1$; updates $Cre_{ij} \cdot fim_{value_{ij}}$ according to formula (9). }

End if

Peer p_t sends meg to p_s along with the reverse $meg \cdot path$. }

Else { // $meg \cdot state = Failure_Return$, deletes the corresponding information in $p_t \cdot QPL$, $p_t \cdot QOL$ and $p_t \cdot CQM$

Peer $p_j \leftarrow meg \cdot p_f$

If ($p_j \in p_t \cdot QPL$ and $K_{qh} \in p_t \cdot QOL$) {

returns $K_{qh} \cdot position i$ in $p_t \cdot QOL$ and $p_j \cdot position j$ in $p_t \cdot QPL$;

updates $p_t \cdot CQM \cdot Cre_{ij} \cdot H_{num_{ij}} = p_t \cdot CQM \cdot Cre_{ij} \cdot H_{num_{ij}} - 1$;

If ($p_t \cdot CQM \cdot Cre_{ij} \cdot H_{num_{ij}} \leq 0$) then {

$p_t \cdot CQM \cdot remove(Cre_{ij})$ in CQM ;

For ($j = 1$ to n) do $p_t \cdot CQM \cdot sum(Cre_{ij} \cdot H_{num_{ij}})$ End for

If ($p_t \cdot CQM \cdot sum(Cre_{ij} \cdot H_{num_{ij}}) \leq 0$) then $p_t \cdot QOL \cdot remove(K_{qh})$ End if

For ($i = 1$ to m) do $p_t \cdot CQM \cdot sum(Cre_{ij} \cdot H_{num_{ij}})$ End for

If ($p_t \cdot CQM \cdot sum(Cre_{ij} \cdot H_{num_{ij}}) \leq 0$) then $p_t \cdot QPL \cdot remove(p_j)$ End if }

End if }

End if }

End if }

End if.

ALGORITHM 1: Credibility search algorithm (CSA).

5.2. Performance Evaluation

5.2.1. Performance Analysis in Static Network Environments.

In this section, we try to analyze the performance of four search strategies CSA, PQR, SPUN, and APS in static network environments where no peer or object departure or remove happens from the following several aspects.

(1) *Comparative Analysis of Query Hit Rate.* Figure 2 shows the query hit rates of the four methods: APS, PQR, SPUN, and CSA for different TTL value in three different network topologies. The four curves in Figure 2 show that the query hit rates are increasing with the increase of TTL value. The curve of PQR is similar to that of SPUN and slightly higher than SPUN. And the curves of PQR and SPUN are located in

TABLE 2: Analysis of node degree.

Topology	Min (degree)	Max (degree)	Avg. (degree)	Count min	Count max
Scale-free network	2	220	4	4993	1
Small world network	6	19	10	84	3
Random graph	6	26	12	19	1

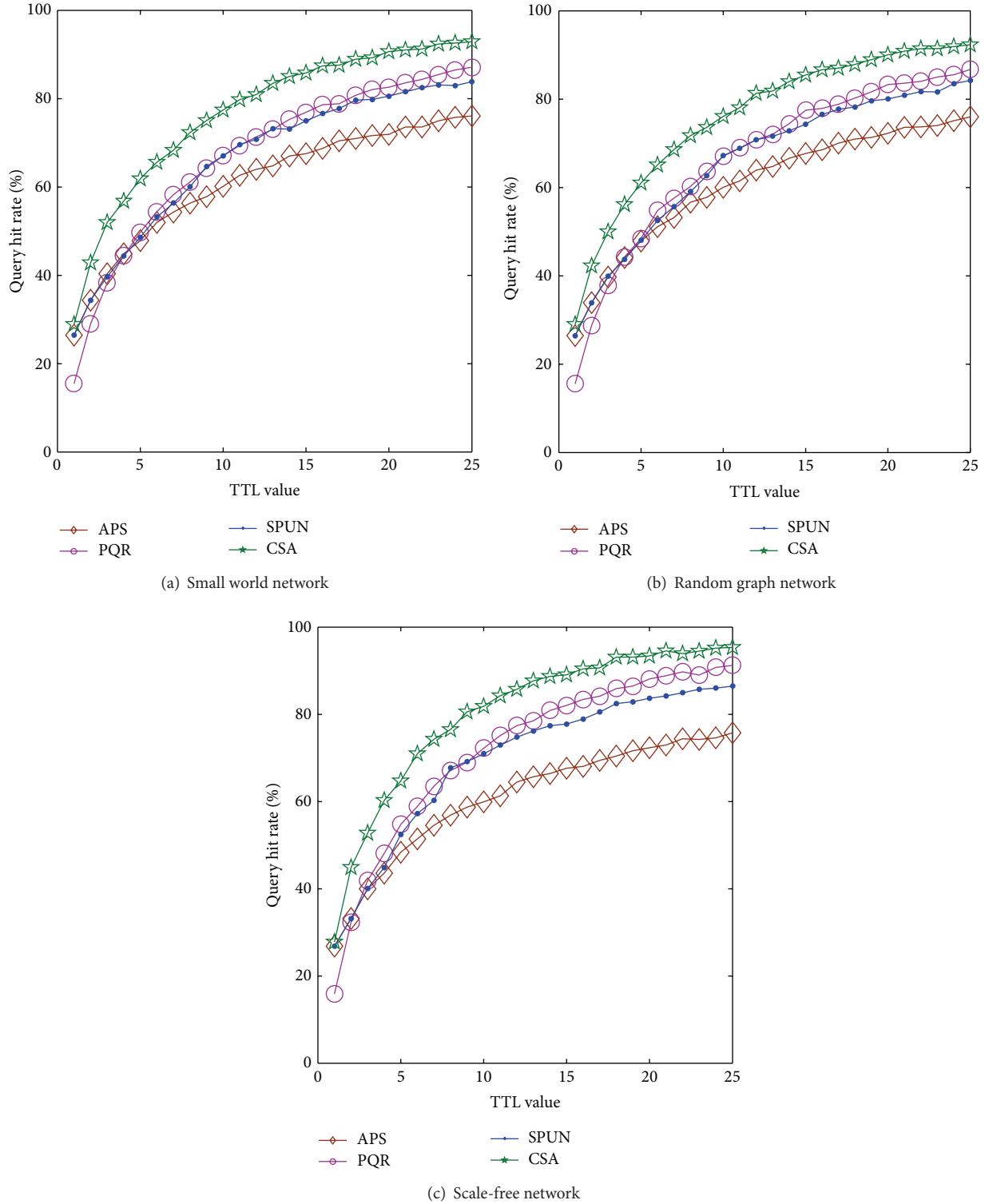


FIGURE 2: Query hit rate versus TTL value in static network environments.

the middle of the curves of APS and CSA. The query hit rate of APS is the lowest in the four algorithms and that of CSA is highest. The query hit rate of CSA exceeds that of APS by about 22% and those of PQR and SPUN by about 9% and 10% when TTL value is greater than 5.

The rare resource query hit rates of the four algorithms are shown in Figure 3. The query hit rate of CSA for rare resources is significantly improved and better than those of the other three methods. Even compared to the PQR algorithm with better performance, the query hit rate for rare resources in CSA is still increased by about 20%. The main reason is that searches for rare resources are nonrepetitive search or less repetitive search; there is little or no historical experience used in the other three methods. So the other three methods can only adopt a random manner to forward query messages. However, in this paper, for nonrepetitive search or less repetitive search, we give full consideration for the overall success rate of the previous search experience and the similarity between the query itself and the contents stored in the neighbor node and obtain effective heuristic information to avoid blind random search, thus resulting in better performance in method CSA.

(2) *Comparative Analysis of Search Delay.* In our experiments, searching is based on the deployment of k walkers and k is set to 4. So each request may receive multiple query hits. In this paper, the search delay is defined as the *hops* value of hit message returned the first time successfully. Figure 4 displays the search delays of the four methods: APS, PQR, SPUN, and CSA for different TTL value in three different network topologies. The search delay of CSA is basically stable at 4 hops when TTL value is greater than 16. And those of the other three methods stepwise grow with the increase of TTL value. Meanwhile, Figure 4 shows the search delay of CSA is lower about 1 hop than those of the other three methods in the same range of TTL value when TTL value is less than 23. When TTL value is greater than 23, the advantage of CSA is more obvious.

(3) *Comparative Analysis of Average Number of Messages.* Figure 5 shows the average number of messages generated per query in different networks. The performance of CSA is also the best one in the four methods: PQR, SPUN, APS, and CSA. At the same time, the reduction rate of the average number of messages generated per query in CSA is indicated in Figure 5, in contrast to the best performance one in the other three methods PQR, SPUN, and APS. From Figure 5, we can see that the average number of messages per query of CSA is reduced 12.8%, 13.4%, and 12.9% in three different network topologies, respectively, when TTL value comes up to 25.

(4) *Comparative Analysis of Network Overhead.* In the search processing, network overhead is constituted by the number of messages generated per query and network bandwidth consumed by these messages. In this paper, we use the actual number of bytes of IP packets generated per message as network overhead.

By Section 3.1, the message structure in CSA is $meg(id, p_s, p_f, state, hops, K_{q_h}, path)$. In our experiments, id is made

up of 10 bytes. The information of node p_s and p_f is composed of "IP + port number," 6 bytes, a total of 48 bits. *hops* and *state* possess 2 bytes, respectively. 4 bytes are assigned to K_{q_h} . The number of bytes of *path* is dynamic change in the search progress.

On the other hand, since the total number of bytes generated per message is small, it cannot produce fragmentation. And then message packet is a UDP packet. And thus, the total number of bytes generated by per message will contain a total of 28 bytes of the IP header and UDP header.

Figure 6 illustrates the comparison of network overhead among the four search strategies. Similar to Figure 5, we mark the reduction rate of the network overhead in CSA in contrast to the best performance one in the other three methods PQR, SPUN, and APS in Figure 6. Figure 6 shows that, when TTL value is 5, the network overhead of CSA is slightly higher than the best performance one of the other three methods PQR, SPUN, and APS by 0.2% and 1.0% in small world model network and scale-free network, respectively. But in the initial stage of the search, the entire bandwidth consumption is very low, so the small increase will not bring burden to the network. With the increase of TTL value, the network overhead of CSA is reduced continuously. When TTL value is 15 and 25, the reduction rate of the network overhead is up to the highest 10.3% and 17.0%, in scale-free network and random graph network, respectively. At this time, the performance of CSA is the best in the four algorithms.

5.2.2. *Performance Analysis in Dynamic Network Environments.* Here, we conduct a series of experiments similar to Section 5.2.1 to evaluate the performance of CSA under dynamic network environments. The total experimental runtime is divided into 100 time slices. At the end of each time slice, we add 10 new nodes and allocate 100 resources to these nodes according to the Zipf distribution. At the same time, 100 nodes from the network are selected randomly and each node deletes one resource from its resource list randomly. In this dynamic environment, we deploy four query strategies CSA, PQR, SPUN, and APS in three different network topologies; results shown in Figures 7, 8, and 9 and Tables 3 and 4.

Figure 7 shows the comparison of query hit rates of the four algorithms CSA, PQR, SPUN, and APS under dynamic network environments. From Figure 7, the query hit rate of CSA is the highest one in the four search strategies in three different network topologies. In the small world network, especially, the query hit rate of CSA exceeds PQR, SPUN, and APS by about 14%, 18%, and 26%, respectively.

Figure 8 illustrates the comparison of query hit rates of the four algorithms CSA, PQR, SPUN, and APS for rare resources. We can see the query hit rate of CSA algorithm is still the highest and it surpasses those of the other three methods by about 20% under dynamic network environments.

Figure 9 presents the comparison of the search delays of the four methods under dynamic network environments. The search delay of CSA is lower than the other three algorithms by about 1 hop in Figure 9. When TTL value is greater than 20, the search delay of CSA is stable at 6 hops while the other

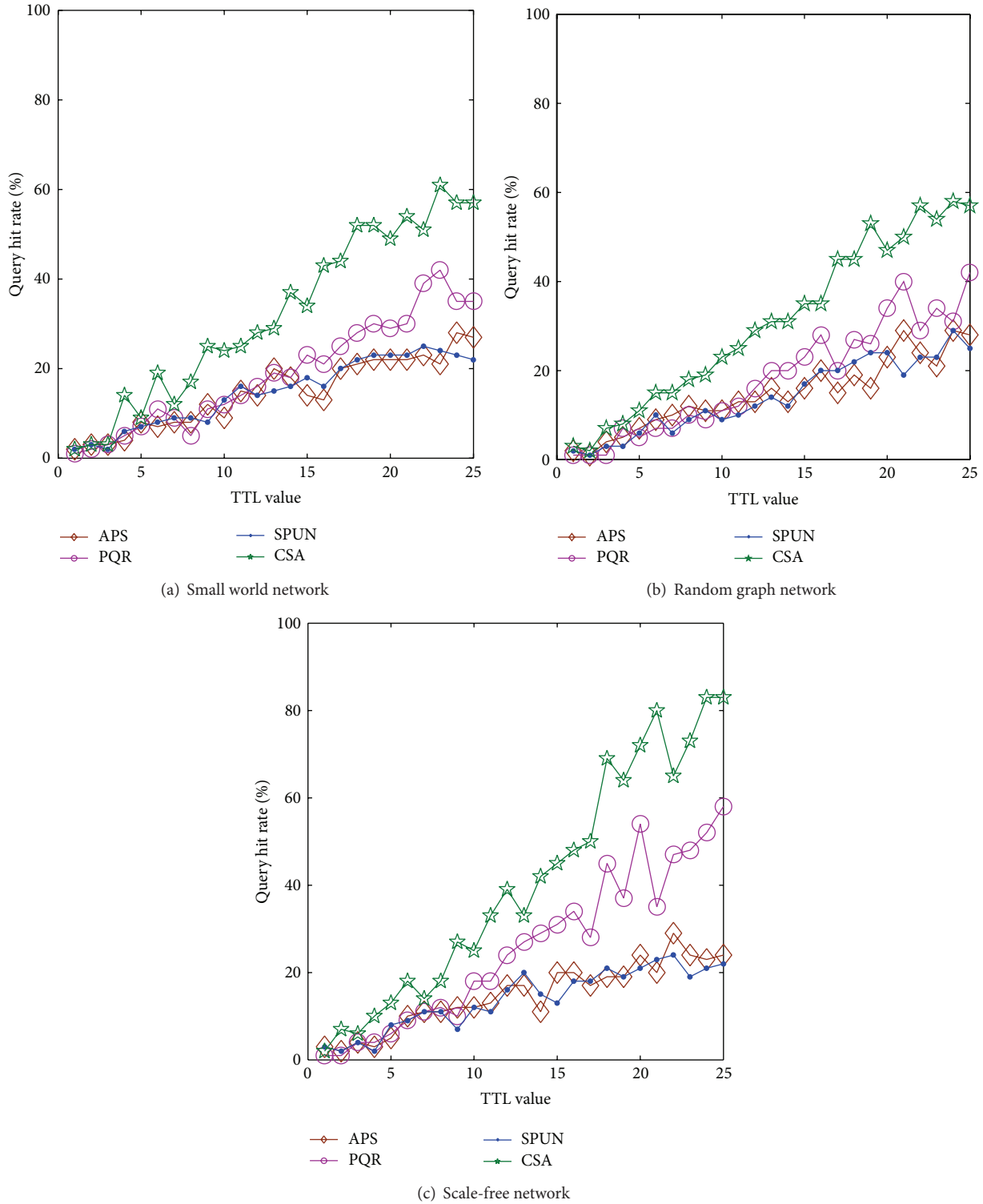


FIGURE 3: Query hit rate of rare resources versus TTL value in static network environments.

three algorithms reflect continued stepwise growth trend with the increase of TTL value.

Table 3 shows the average number of messages generated per query in the three different kinds of network topologies. It consists of data of two-hop interval in the TTL value from

1 to 25. So the TTL value is a sequence of 1, 4, 7, ..., 25 in Table 3. As can be seen from Table 3, in the four methods, the average number of messages generated per query is basically the same, when the TTL value is less than or equal to 7. However, when the TTL value is greater than or equal to 10,

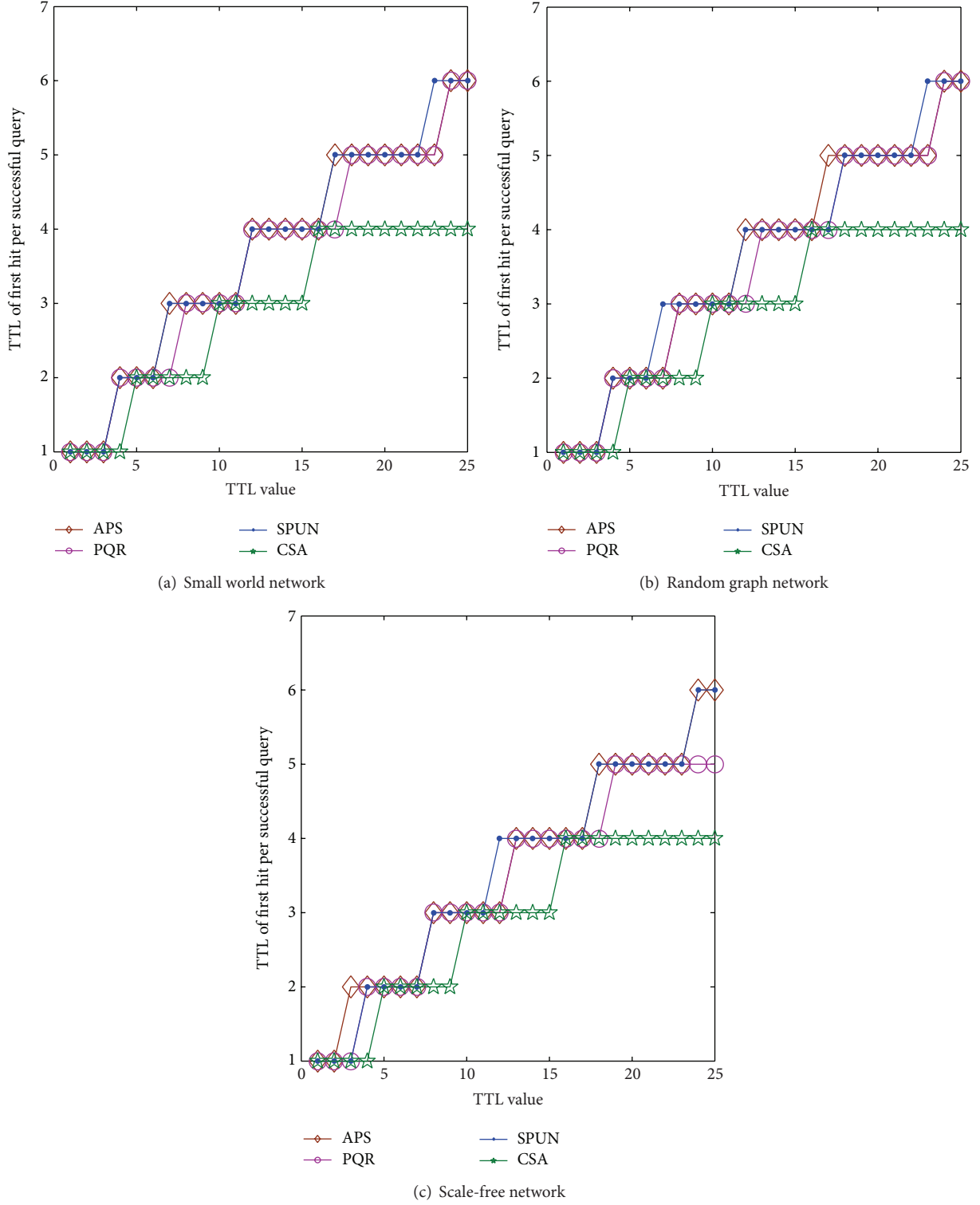


FIGURE 4: Search delay versus TTL value in static network environments.

the average number of messages generated per query in CSA is lower than the other three methods at most by about 9.6%.

Table 4 illustrates the network overhead generated by the four search strategies. Similar to Table 3, we also extract experimental data of two-hop interval among 1 to 25 hops

to form Table 4. From Table 4, we can see that the network overhead of CSA is less than or equal to those of the other three methods with the increase of TTL value and those of the other three methods are basically the same. At the same time, after the 10th hops, the network overhead of CSA is reduced

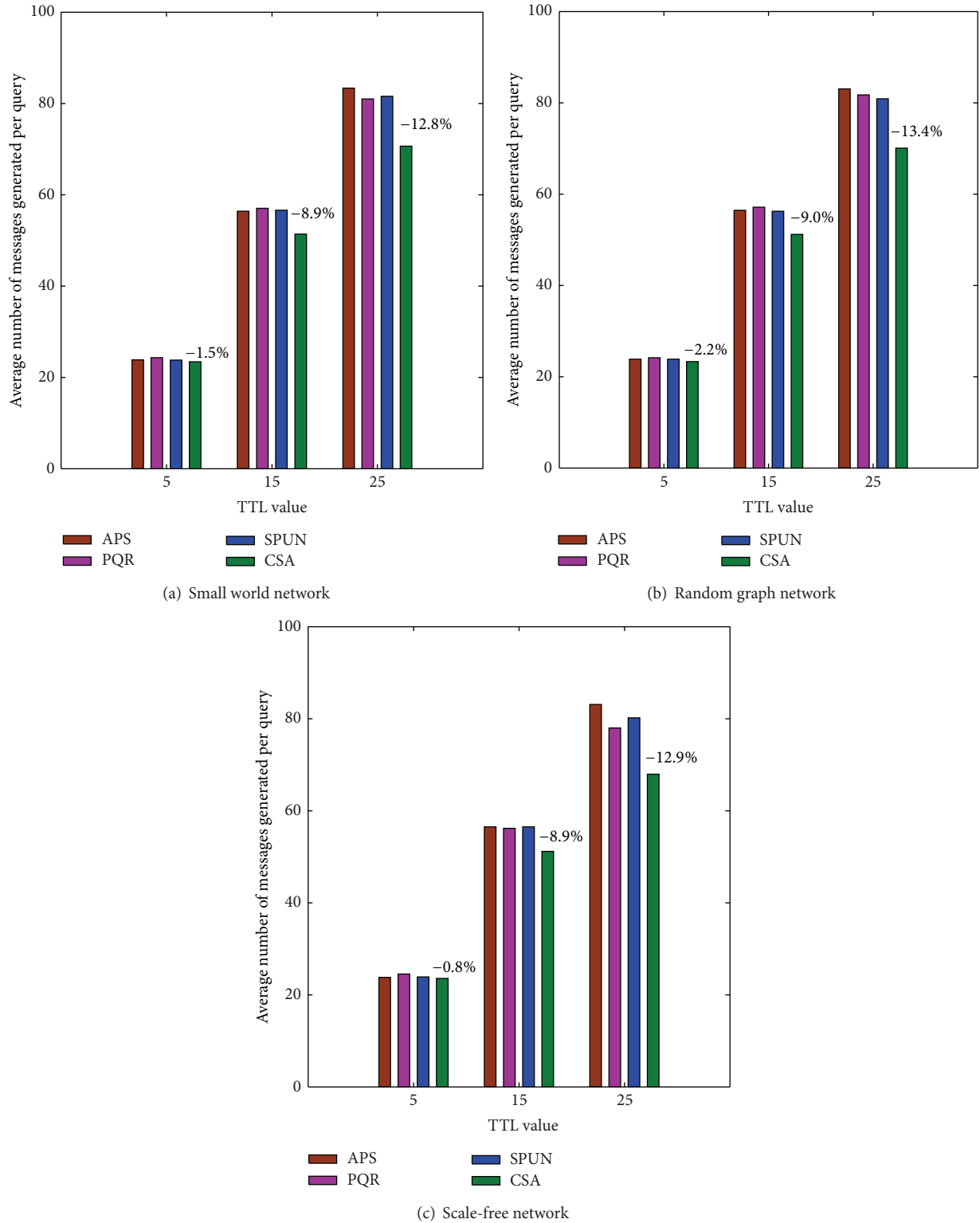


FIGURE 5: Average number of messages generated per query versus TTL value in static network environments.

by about 11.2% at most compared to the others in the three different network topologies.

In summary, we can see that the performances of the four algorithms are reduced to some extent in the dynamic

network environments. For example, in the dynamic environments, the query hit rates of the four search strategies CSA, PQR, SPUN, and APS for scarce resources are reduced on average by about 20%, compared with the static network

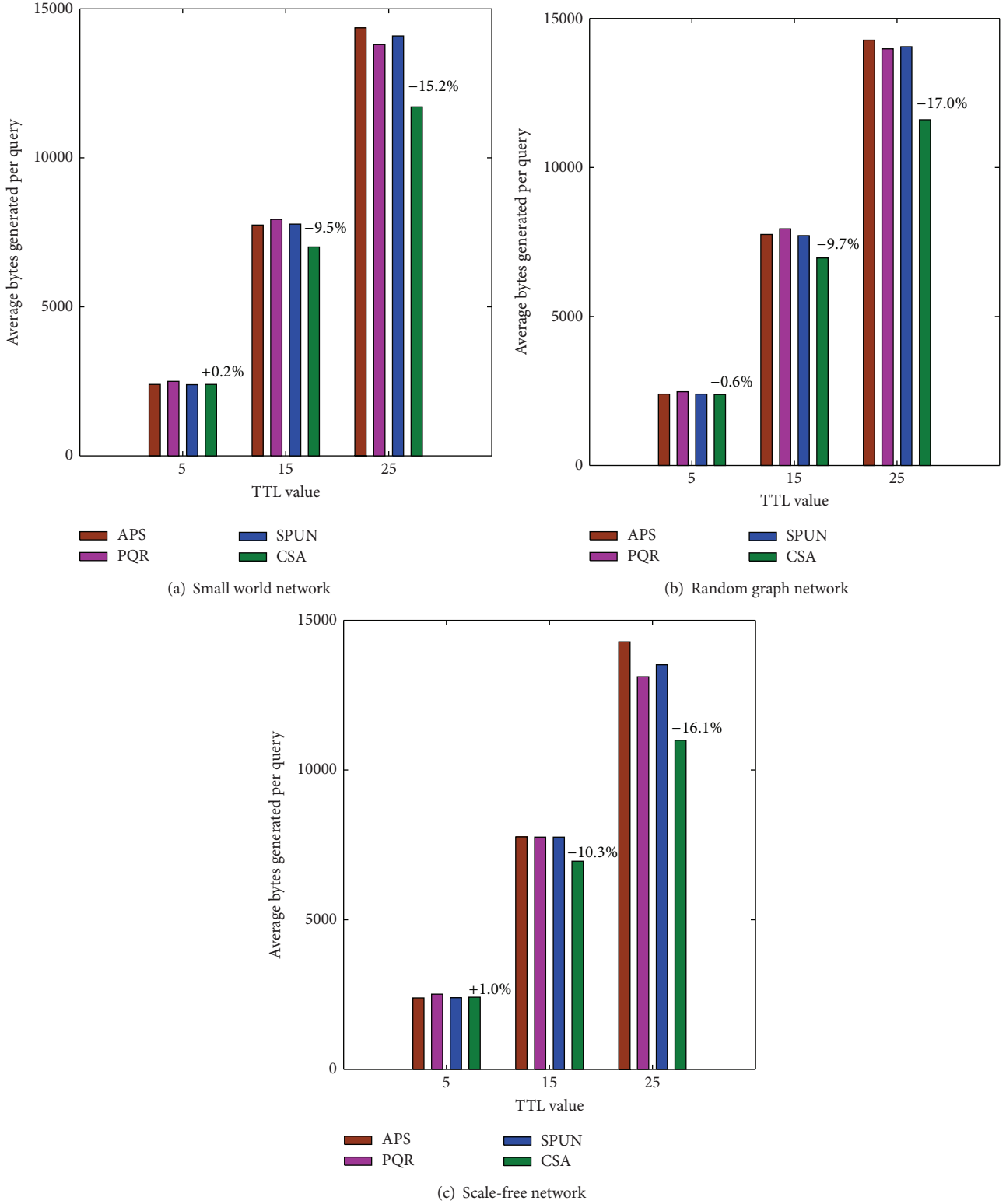


FIGURE 6: Network overhead versus TTL values in static network environments.

environments as shown in Figures 3 and 8. And, although the search delays of the four strategies are also stepwise growth similar to the static network environments, but its gradient is larger as shown in Figures 4 and 9. The main reason is that

the churn of network influences the performances of searches, but which has less effect on the CSA algorithm compared with the other three ones. For example, the query hit rate of CSA drops slightly in Figure 7 and less than 7%

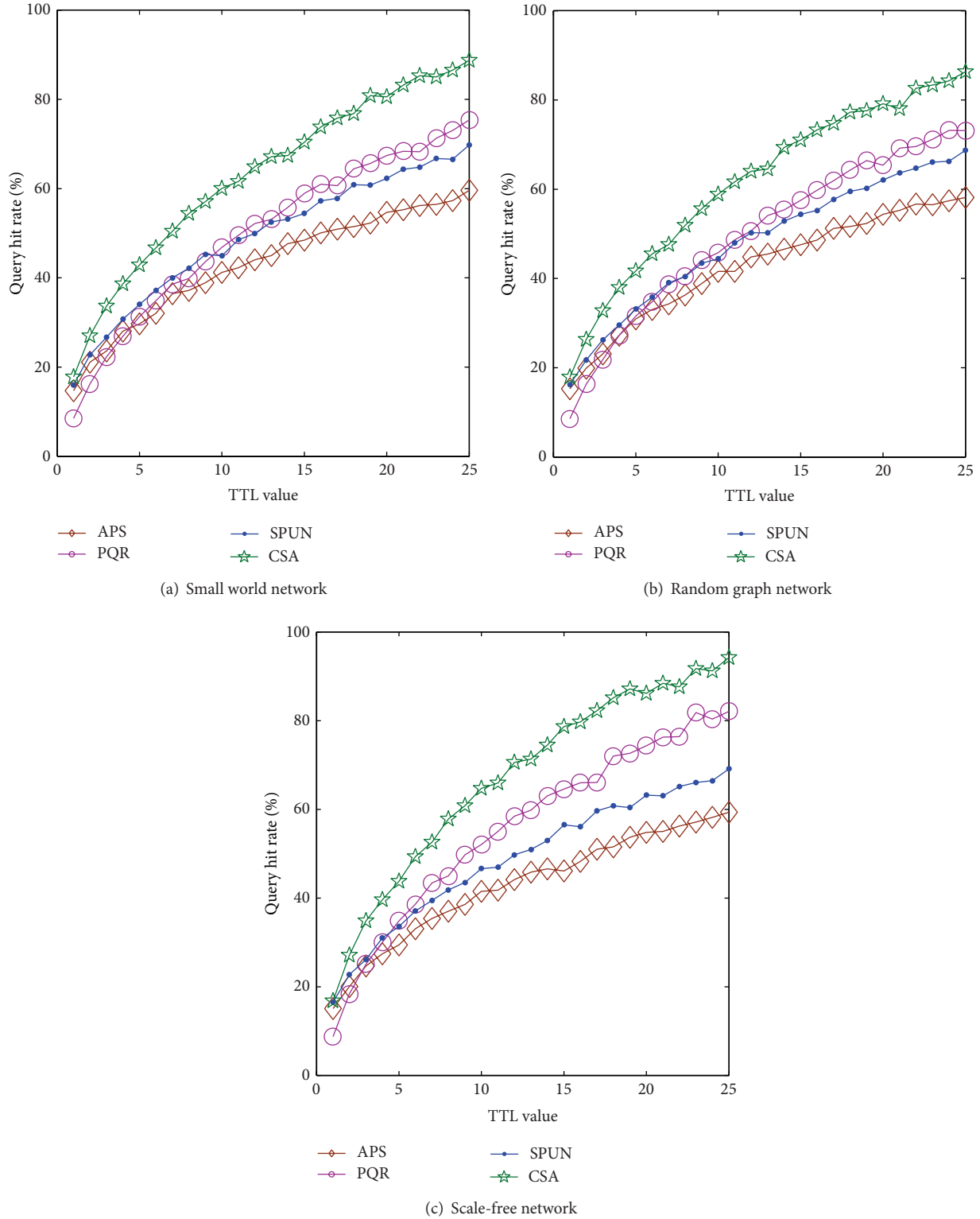


FIGURE 7: Query hit rate versus TTL value in dynamic network environments.

compared to that in Figure 2. Moreover the query hit rates of the other three methods are reduced by more than 10%. At the same time, in the dynamic network environments, CSA method shows better performance than the other three

algorithms, compared with static environments. For example, in the static network environments, the query hit rate of CSA is improved by about 9%, 10%, and 22% compared to the algorithm PQR, SPUN, and APS in Figure 2 and in the dynamic

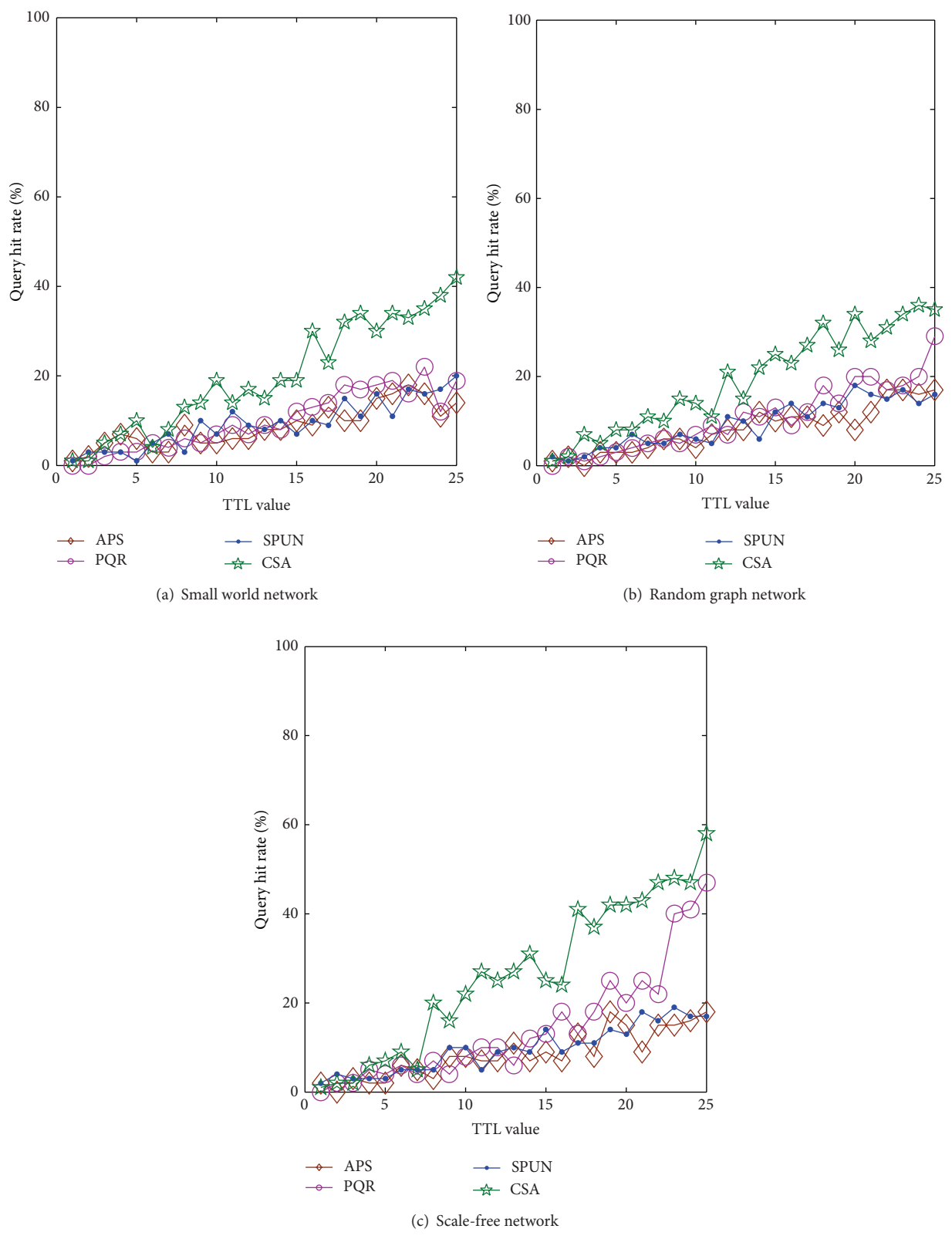


FIGURE 8: Query hit rate of rare resources versus TTL value in dynamic network environments.

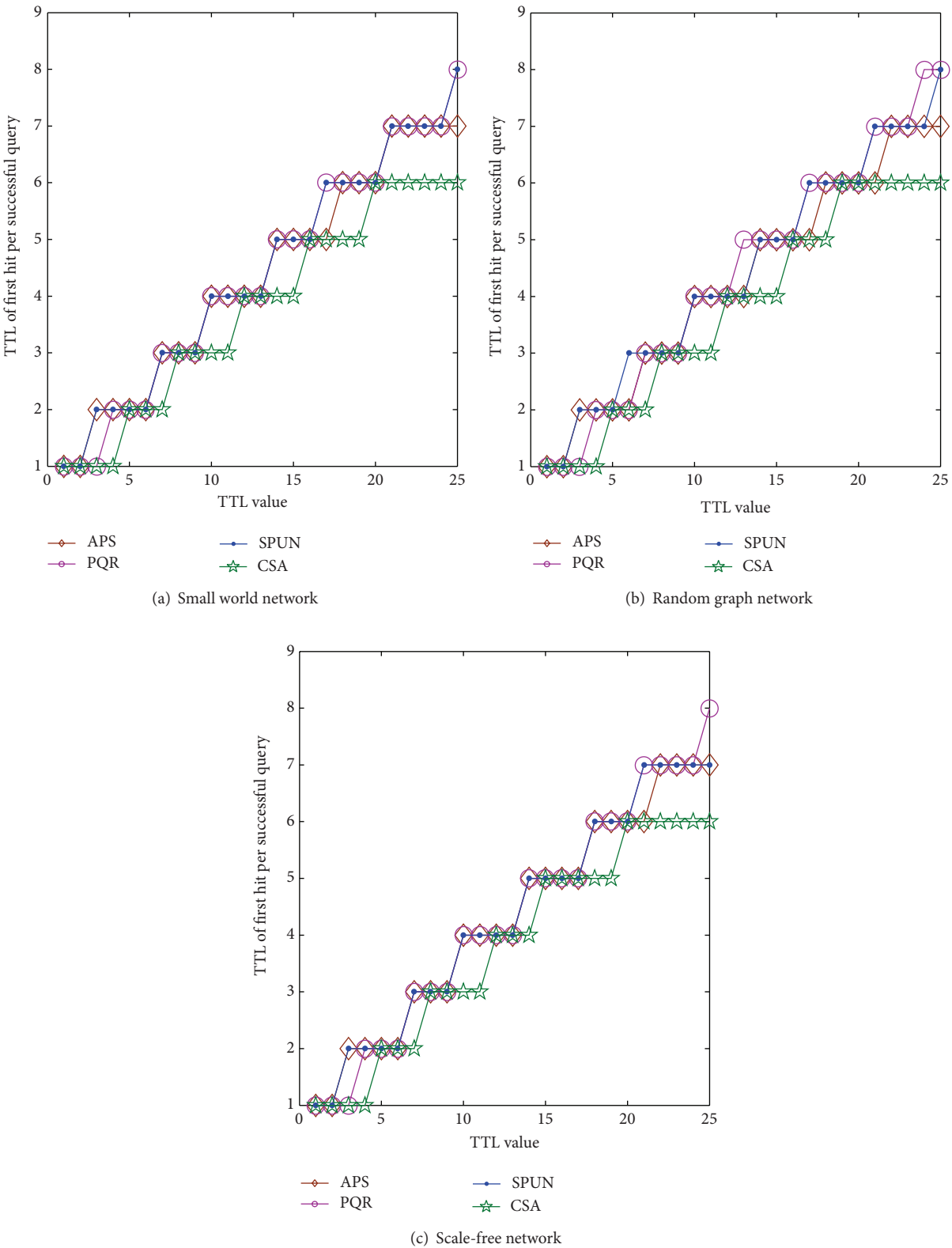


FIGURE 9: Search delay versus TTL value in dynamic network environments.

TABLE 3: Average number of messages generated per query versus TTL value in dynamic network environments.

TTL	Small world				Random graph				Scale-free			
	CSA	PQR	SPUN	APS	CSA	PQR	SPUN	APS	CSA	PQR	SPUN	APS
1	8	8	8	8	8	8	8	8	8	8	8	8
4	20	20	20	20	20	20	20	20	20	20	20	20
7	31	32	31	31	30	32	31	31	31	32	31	31
10	41	43	42	42	40	43	42	42	41	43	42	42
13	50	53	52	53	49	53	52	53	50	52	53	53
16	58	63	62	63	58	63	62	63	58	62	62	63
19	66	72	71	72	67	72	72	72	65	71	72	72
22	73	81	80	82	74	80	81	82	72	79	80	82
25	80	88	89	90	80	88	89	91	78	86	88	90

TABLE 4: Network overhead versus TTL value in dynamic network environments (M).

TTL	Small world				Random graph				Scale-free			
	CSA	PQR	SPUN	APS	CSA	PQR	SPUN	APS	CSA	PQR	SPUN	APS
1	0.7	0.7	0.7	0.7	0.7	0.7	0.7	0.7	0.7	0.7	0.7	0.7
4	1.9	1.9	1.9	1.9	1.9	1.9	1.9	1.9	1.9	2.0	1.9	1.9
7	3.3	3.4	3.3	3.3	3.3	3.4	3.3	3.3	3.3	3.4	3.3	3.3
10	4.8	5.1	4.9	4.9	4.8	5.1	4.9	4.9	4.8	5.0	4.9	4.9
13	6.4	6.8	6.7	6.7	6.3	6.9	6.7	6.8	6.4	6.8	6.7	6.7
16	8.0	8.8	8.6	8.7	8.1	8.8	8.7	8.7	8.0	8.6	8.6	8.7
19	9.8	10.9	10.6	10.8	9.9	10.8	10.7	10.8	9.5	10.6	10.7	10.8
22	11.5	13.0	12.8	13.1	11.7	12.9	12.9	13.1	11.3	12.6	12.8	13.1
25	13.4	15.1	15.1	15.3	13.4	15.0	15.1	15.5	12.9	14.6	15.0	15.4

environment increased by about 14%, 18%, and 26% in Figure 7. Therefore, whether it is under the dynamic or static environments, CSA can achieve high query hit rate with less network overhead and lower search delay. So, CSA can get the better performance than the other three algorithms PQR, SPUN, and APS.

5.3. Discussion. In CSA, the space cost is mainly composed of four indexes CNL, CQM, QPL, and QOL in each node. CNL, QPL, and QOL are linear lists. The number of elements in CNL is equal to the number of all neighbors of a node. The length of QPL does not exceed the length of CNL. At the same time, the length of QOL is also not large because it records only different query objects. CQM is a two-dimensional matrix. If the length of the QOL is m and the length of the QPL is n then the length of CQM is $m \times n$. So, the space cost of CNL, QPL, and QOL is negligibly small compared with that of CQM in each node because of their linear length. Thus the space complexity of each node in CSA is $o(m \times n)$ which is the same with the PQR and APS method, less SPUN ($o(m \times n \times \text{TTL})$) algorithm. Meanwhile, such space cost is not a burden for computing device in current P2P networks. However, if the storage capacity of node is very low, the node can choose a small size of CQM and update it according to first in first out (FIFO) policy or least recent used (LRU) policy.

In the search process, the worst case is that all the k walkers travel TTL hops and then return a hit or miss message along query path. Therefore the number of messages generated per query is $2 \times k \times \text{TTL}$ in the worst case and which is the same as the other three methods: PQR, SPUN, and APS. But simulation experiments in this paper have shown that CSA produced less number of messages and lower network consumption compared with the other methods, whether it is in a dynamic P2P environment or in a static P2P environment. The main reasons lie in two aspects. On the one hand, the credibility generated on the basis of familiarity and similarity as the heuristic information is very effective to guide the future searches, which improves the query hit rate, reduces the search delay, and shortens the length of the search path, resulting in reducing the number of messages generated and the network consumption. On the other hand, it is reasonable that queries are classified. At the same time, the credibility information provided in CSA is trustworthy, which guides effectively the strange queries to the requested objects, and superior to the random walks way in the other three methods. The improvement of scarce resources query hit rates in CSA may succeed to verify it in our experiments.

CSA can make full use of the advantages of the previous informed algorithms such as APS, PQR, and SPUN, using the previous search information to guide the future searches.

Thus, CSA is similar to these methods on the handling of the queries with high repetition rate. The difference is that, in the acquisition process of heuristic information, APS, PQR, and SPUN methods only consider hit information of successful path, while in CSA the similar information between the queried contents and contents stored on node is also considered as the heuristic information to guide the future searches. So, the query message is forwarded to nodes that are more likely to provide the necessary resources node in CSA.

The main difference between CSA and APS, PQR, and SPUN is that queries are classified as familiar queries and strange (unfamiliar) ones according to the similarity between the requested resources and those have been received in the query node in CSA. For the strange queries, there is no or little heuristic guide information in APS, PQR, and SPUN methods and the queries will be forwarded based on random walks way. However, in CSA, based on the trust production principle in sociology and psychology, CSA method firstly gets the credibility of the node to each neighbor node according to all the previous queries and the similarity between the requested object information and the contents stored on each neighbor node and then selects the nodes with higher credibility to forward the strange queries. In contrast to random manner in APS, PQR, and SPUN methods, the one in CSA greatly reduce the search blindness.

The main feature of CSA method is that it makes full use of the query information and resources information nodes themselves hold. Based on node local information, the searches are effectively forwarded. This method does not require too complicated structure and does not need to track search path information, so it has a good adaptability for dynamic characteristics of unstructured P2P networks.

6. Conclusion

In this paper, a credibility search algorithm (CSA) has been presented. The main feature of this method is that it can improve query performance in unstructured P2P networks. CSA can gain the effective heuristic information and credibility of node to its neighbor by combining with the trust production principle in sociology and psychology, so that the familiar query and the strange query can be guided successfully. Experimental results show that the proposed algorithm outperforms the other three methods: PQR, SPUN, and APS furthermore can achieve high query hit rate with less search delay and lower bandwidth consumption in three different types of network topologies under static and dynamic network conditions. At the same time, CSA is also very effective for the search of rare resources. In the scale-free network especially, the query hit of CSA for rare resources can reach up to about 85% when TTL value comes up to 24. Compared to PQR and APS, the query hit of CSA for rare resources is increased by about 20% and 40%, respectively, with the increase of TTL value in three different network topologies.

Conflict of Interests

The authors declare that there is no conflict of interests regarding the publication of this paper.

Acknowledgments

This study is supported by the National Natural Science Foundation of China (Grant no. 60872051) and the Program of the Co-Construction with Beijing Municipal Commission of Education of China.

References

- [1] Open Source Community, "Gnutella," 2001, <http://eg.wego.com/>.
- [2] FastTrack Peer-to-Peer Technology Company, "Fast track," 2001, <http://fasttrack.nu/>.
- [3] KaZaA lesharing network, "KaZaA," 2002, <http://www.kazaa.com/>.
- [4] D. Stutzbach, R. Rejaie, N. Duffield, S. Sen, and W. Willinger, "Sampling techniques for large, dynamic graphs," in *Proceedings of the 25th IEEE International Conference on Computer Communications (INFOCOM '06)*, pp. 1–6, April 2006.
- [5] A. H. Rasti, D. Stutzbach, and R. Rejaie, "On the long-term evolution of the two-tier Gnutella overlay," in *Proceedings of the 25th IEEE International Conference on Computer Communications (INFOCOM '06)*, pp. 1–6, April 2006.
- [6] B. Yang and H. Garcia-Molina, "Improving search in peer-to-peer networks," in *Proceedings of the 22nd IEEE International Conference on Distributed Computing (ICDCS '02)*, pp. 5–14, IEEE, July 2002.
- [7] Q. Lv, P. Cao, E. Cohen, K. Li, and S. Shenker, "Search and replication in unstructured peer-to-peer networks," in *Proceedings of the International Conference on Supercomputing*, pp. 84–95, June 2002.
- [8] Y. Chawathe, S. Ratnasamy, L. Breslau, N. Lanham, and S. Shenker, "Making gnutell-like p2p systems scalable," in *Proceeding of the Conference on Applications, Technologies, Architectures, and Protocols for Computer Communications (SIGCOMM '03)*, pp. 407–418, August 2003.
- [9] M. Andreolini and R. Lancellotti, "A flexible and robust lookup algorithm for P2P systems," in *Proceedings of the 23rd IEEE International Parallel and Distributed Processing Symposium (IPDPS '09)*, pp. 1–8, May 2009.
- [10] R. Gaeta and M. Sereno, "Generalized probabilistic flooding in unstructured peer-to-peer networks," *IEEE Transactions on Parallel and Distributed Systems*, vol. 22, no. 12, pp. 2055–2062, 2011.
- [11] C. Gkantsidis, M. Mihail, and A. Saberi, "Random walks in peer-to-peer networks," in *Proceedings of the 23rd Annual Joint Conference of the IEEE Computer and Communications Societies (INFOCOM '04)*, vol. 1, pp. 7–11, March 2004.
- [12] N. Bisnik and A. A. Abouzeid, "Optimizing random walk search algorithms in P2P networks," *Computer Networks*, vol. 51, no. 6, pp. 1499–1514, 2007.
- [13] C. Gkantsidis, M. Mihail, and A. Saberi, "Hybrid search schemes for unstructured peer-to-peer networks," in *Proceedings of 24th Annual Joint Conference of the IEEE Computer and*

- Communications Societies (INFOCOM '05)*, vol. 3, pp. 1526–1537, Miami, Fla, USA, March 2005.
- [14] S. Jiang, L. Guo, X. Zhang, and H. Wang, “LightFlood: minimizing redundant messages and maximizing scope of peer-to-peer search,” *IEEE Transactions on Parallel and Distributed Systems*, vol. 19, no. 5, pp. 601–614, 2008.
 - [15] H. Y. Mei, Y. J. Zhang, X. W. Meng, and W. M. Ma, “Limited search mechanism for unstructured peer-to-peer network,” *Journal of Software*, vol. 24, no. 9, pp. 2132–2150, 2013.
 - [16] V. Kalogeraki, D. Gunopulos, and D. Zeinalipour-Yazti, “A local search mechanism for peer-to-peer networks,” in *Proceedings of the 11th International Conference on Information and Knowledge Management (CIKM '02)*, pp. 300–307, McLean, Va, USA, November 2002.
 - [17] D. Tsoumakos and N. Roussopoulos, “Adaptive probabilistic search in peer-to-peer networks,” in *Proceedings of the 3rd International Conference on Peer-to-Peer Computing (P2P '03)*, pp. 102–109, September 2003.
 - [18] M. Xu, S. Zhou, J. Guan, and X. Hu, “A path-traceable query routing mechanism for search in unstructured peer-to-peer networks,” *Journal of Network and Computer Applications*, vol. 33, no. 2, pp. 115–127, 2010.
 - [19] D. M. R. Himali and S. K. Prasad, “SPUN: a P2P probabilistic search algorithm based on successful paths in unstructured networks,” in *Proceedings of the 25th IEEE International Symposium on Parallel and Distributed Processing Workshops and Phd Forum (IPDPSW '11)*, pp. 1610–1617, May 2011.
 - [20] B. Zuo and Q. Gao, “The effects of familiarity and similarity on the interpersonal attraction,” *Chinese Journal of Clinical Psychology*, vol. 16, no. 6, pp. 634–636, 2008.
 - [21] W. Ma, X. Meng, and Y. Zhang, “Bidirectional random walk search mechanism for unstructured P2P network,” *Journal of Software*, vol. 23, no. 4, pp. 894–911, 2012.
 - [22] G. Chen, C. P. Low, and Z. Yang, “Enhancing search performance in unstructured P2P networks based on users’ common interest,” *IEEE Transactions on Parallel and Distributed Systems*, vol. 19, no. 6, pp. 821–836, 2008.
 - [23] K. C. Lin, C. Wang, C. Chou, and L. Golubchik, “SocioNet: A social-based multimedia access system for unstructured P2P networks,” *IEEE Transactions on Parallel and Distributed Systems*, vol. 21, no. 7, pp. 1027–1041, 2010.
 - [24] C. G. M. Snoek, M. Worring, J. C. van Gemert, J.-M. Geusebroek, and A. W. M. Smeulders, “The challenge problem for automated detection of 101 semantic concepts in multimedia,” in *Proceedings of the 14th Annual ACM International Conference on Multimedia (MULTIMEDIA '06)*, pp. 421–430, October 2006.
 - [25] M. S. Lew, N. Sebe, C. Djeraba, and R. Jain, “Content-based multimedia information retrieval: State of the art and challenges,” *ACM Transactions on Multimedia Computing, Communications and Applications*, vol. 2, no. 1, pp. 1–19, 2006.
 - [26] C. J. Lin, S. C. Tsai, Y. T. Chang, and C. F. Chou, “Enabling keyword search and similarity search in small-world-based P2P systems,” in *Proceedings of the 16th International Conference on Computer Communications and Networks (ICCCN '07)*, pp. 115–120, August 2007.
 - [27] G. Salton, *Automatic Text Processing: The Transformation, Analysis, and Retrieval of Information by Computer*, Addison-Wesley, 1988.
 - [28] “The peersim simulator,” 2007, <http://peersim.sourceforge.net/>.
 - [29] K. Sripanidkulchai, “The popularity of Gnutella queries and its implications on scalability,” 2001, <http://www.cs.cmu.edu/~kunwadee/research/p2p/paper.html>.
 - [30] L. Breslau, P. Cao, L. Fan, G. Phillips, and S. Shenker, “Web caching and Zipf-like distributions: evidence and implications,” in *Proceedings of the 18th Annual Joint Conference of the IEEE Computer and Communications Societies (INFOCOM '99)*, pp. 126–134, March 1999.
 - [31] P. Backx, “A comparison of peer-to-peer architectures,” in *Proceedings of the Eurescom 2002 Powerful Networks for Profitable Services*, pp. 1–8, 2002.

Research Article

Control of the Fractional-Order Chen Chaotic System via Fractional-Order Scalar Controller and Its Circuit Implementation

Qiong Huang, Chunyang Dong, and Qianbin Chen

Key Lab of Mobile Communication Technology, Chongqing University of Posts and Telecommunications, Chongqing 400065, China

Correspondence should be addressed to Qianbin Chen; 18502321237@163.com

Received 20 March 2014; Revised 26 May 2014; Accepted 4 June 2014; Published 22 June 2014

Academic Editor: Chuandong Li

Copyright © 2014 Qiong Huang et al. This is an open access article distributed under the Creative Commons Attribution License, which permits unrestricted use, distribution, and reproduction in any medium, provided the original work is properly cited.

A fractional-order scalar controller which involves only one state variable is proposed. By this fractional-order scalar controller, the unstable equilibrium points in the fractional-order Chen chaotic system can be asymptotically stable. The present control strategy is theoretically rigorous. Some circuits are designed to realize these control schemes. The outputs of circuit agree with the results of theoretical results.

1. Introduction

In the last few decades, chaotic behaviors have been discovered in many areas of science and engineering such as mathematics, physics, chemistry, electronics, medicine, economy, biological science, and social science. In 1990, Ott et al. presented the OGY method of chaotic control [1]. After that, chaos control has attracted increasing attention among scientists in various fields. Many control schemes [1, 2] have been presented, such as feedback control, parametric perturbation control, adaptive control, and fuzzy control. On the other hand, the chaotic or hyperchaos behaviors have been found in many fractional-order dynamical systems. Many fractional-order chaotic systems have been presented, the fractional-order Chua's chaotic circuit [3], the fractional-order Duffing chaotic system [4], the fractional-order memristor-based chaotic system [5], the fractional-order Lorenz chaotic system [6], the fractional-order Chen chaotic system [7], and so forth [8, 9]. Moreover, control and synchronization of fractional-order chaotic systems have attracted much attention in the recent years [10–16].

Compared to the traditional controller (integer-order controller), the fractional-order controller has many advantages, such as less sensitivity to parameter variations and better disturbance rejection ratios [17]. It is possible that traditional controller (integer-order controller) will be replaced

by fractional-order controller in the future. Recently, a fractional-order vector controller is addressed to stabilize the unstable equilibrium points for integer-order chaotic systems by Tavazoei and Haeri [17]. Zhou and Kuang have presented another fractional-order vector controller to stabilize the nonequilibrium points for integer-order chaotic systems [18]. However, only integer-order chaotic systems are discussed in [17, 18], and only fractional-order vector controller is investigated.

Up to now, to the best of our knowledge, very few results on chaotic control are reported by fractional-order scalar controller. Motivated by the above-mentioned discussions, some fractional-order scalar controllers are presented to control the fractional-order Chen chaotic systems in this paper. Only one system state variable is used in the fractional-order scalar controller. The control scheme is simple and theoretical. Moreover, some circuits are designed to realize these control schemes, and the circuit results agree with the theoretical results.

The outline of this paper is as follows. In Section 2, some mathematical preliminaries are addressed for the fractional-order system. In Section 3, some fractional-order scalar controller are proposed to stabilize the unstable equilibrium points in the fractional-order Chen chaotic system. In Section 4, some circuits are designed to realize the control schemes. The conclusion is finally drawn in Section 5.

2. Mathematical Preliminaries

In this paper, we use the Caputo definition of fractional derivative, which is

$$D^q h(t) = \frac{1}{\Gamma(l-q)} \int_0^t h^{(l)}(\tau) (t-\tau)^{l-q-1} d\tau, \quad l-1 < q < l, \quad (1)$$

where D^q denoted the Caputo operator, l is the first integer which is not less than q , and $h^{(l)}(t)$ is the l -order derivative for $h(t)$; that is, $h^{(l)}(t) = d^l h(t)/dt^l$.

Consider the following nonlinear fractional-order system:

$$D^q x = F(x), \quad (2)$$

where $F: R^n \rightarrow R^n$ are continuous function, $0 < q < 1$ are fractional order, and $x \in R^n$ are state vectors.

First, we recall the stability results of nonlinear fractional-order systems [19–24]. Let the equilibrium point of system (2) be x_0 and let the Jacobian matrix be $\partial F/\partial x|_{x=x_0}$. λ_i ($i = 1, 2, \dots, n$) are the eigenvalues of the Jacobian matrix $\partial F/\partial x|_{x=x_0}$. If $|\arg \lambda_i| > 0.5\pi q$ ($i = 1, 2, \dots, n$) are satisfied, then the equilibrium point x_0 is asymptotically stable [19–24].

Second, we recall the improved version of Adams-Bashforth-Moulton algorithm [14] for the fractional-order systems. Consider the following two-dimensional nonlinear fractional-order system:

$$\begin{aligned} D^{q_1} x_1 &= h_1(x_1, x_2), \\ D^{q_2} x_2 &= h_2(x_1, x_2), \end{aligned} \quad (3)$$

with initial condition $(h_1(0), h_2(0))$. Let $\tau = T/N$ and let $t_n = n\tau$ ($n = 0, 1, 2, \dots, N$). Then, the two-dimensional fractional-order system can be discretized as follows

$$\begin{aligned} x_1(n+1) &= h_1(0) + \frac{\tau^{q_1}}{\Gamma(q_1+2)} \left[h_1(x_1^m(n+1), x_2^m(n+1)) \right. \\ &\quad \left. + \sum_{j=0}^n \kappa_{1,j,n+1} h_1(x_1(j), x_2(j)) \right], \\ x_2(n+1) &= h_2(0) + \frac{\tau^{q_2}}{\Gamma(q_2+2)} \left[h_2(x_1^m(n+1), x_2^m(n+1)) \right. \\ &\quad \left. + \sum_{j=0}^n \kappa_{2,j,n+1} h_2(x_1(j), x_2(j)) \right], \end{aligned} \quad (4)$$

where

$$\begin{aligned} x_1^m(n+1) &= x_1(0) + \frac{1}{\Gamma(q_1)} \sum_{j=0}^n \sigma_{1,j,n+1} h_1(x_1(j), x_2(j)), \\ x_2^m(n+1) &= x_2(0) + \frac{1}{\Gamma(q_2)} \sum_{j=0}^n \sigma_{2,j,n+1} h_2(x_1(j), x_2(j)), \\ \kappa_{i,j,n+1} &= \begin{cases} n^{q_i+1} - (n-q_i)(n+1)^{q_i}, & j=0, \\ (n-j+2)^{q_i+1} + (n-j)^{q_i+1} \\ \quad - 2(n-j+1)^{q_i+1}, & 1 \leq j \leq n, \quad (i=1,2), \\ 1, & j=n+1, \end{cases} \\ \sigma_{i,j,n+1} &= \frac{\tau^{q_i}}{q_i} \left[(n-j+1)^{q_i} - (n-j)^{q_i} \right], \\ &\quad 0 \leq j \leq n, \quad (i=1,2). \end{aligned} \quad (5)$$

The error of this algorithm is

$$\begin{aligned} |x_i(t_n) - x_i(n)| &= o(\tau^{\alpha_i}), \\ \alpha_i &= \min(2, 1+q_i), \quad (i=1,2). \end{aligned} \quad (6)$$

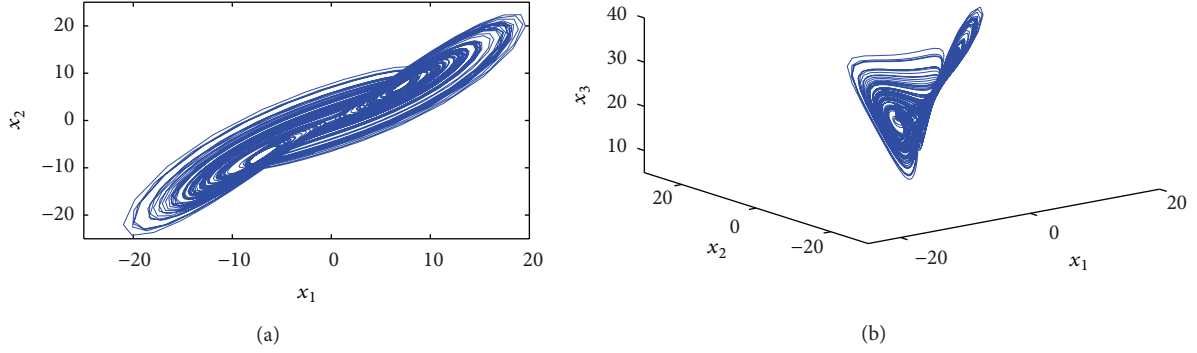
3. Control of the Unstable Equilibrium Points for the Fractional-Order Chen Chaotic System via a Fractional-Order Scalar Controller

In this section, some fractional-order scalar controllers which involve only one state variable are addressed. The unstable equilibrium points of the fractional-order Chen chaotic system can be asymptotically stable by these fractional-order scalar controllers.

In 1963, E. N. Lorenz reported the first chaotic model that revealed the complex and fundamental behaviors of the nonlinear dynamical systems. In 1999, Chen found another chaotic model in a simple three-dimensional autonomous system, which nevertheless is not topologically equivalent to the Lorenz chaotic model. The fractional-order Chen chaotic model is described as

$$\begin{aligned} D^q x_1 &= 35(x_2 - x_1), \\ D^q x_2 &= -7x_1 + 28x_2 - x_1 x_3, \\ D^q x_3 &= x_1 x_2 - 3x_3, \end{aligned} \quad (7)$$

where $0 < q < 1$ is the fractional order. The fractional-order Chen chaotic system has chaotic attractor for $q \geq 0.83$ [19]. The fractional-order Chen chaotic attractor with $q = 0.9$ is shown as in Figure 1.

FIGURE 1: The fractional-order Chen chaotic attractor with $q = 0.9$.

There are three unstable equilibrium points in the above fractional-order Chen chaotic system. The unstable equilibrium points are $S_0 = (0, 0, 0)$ and $S_{\pm} = (\pm\sqrt{63}, \pm\sqrt{63}, 21)$, respectively. Our goal is how to control the unstable equilibrium points via a fractional-order scalar controller.

3.1. Case 1: Control of the Unstable Equilibrium Point $S_0 = (0, 0, 0)$

Theorem 1. Let the controlled system be

$$\begin{aligned} D^q x_1 &= 35(x_2 - x_1) + l_1 D^q x_2 + l_2 x_2, \\ D^q x_2 &= -7x_1 + 28x_2 - x_1 x_3, \\ D^q x_3 &= x_1 x_2 - 3x_3, \end{aligned} \quad (8)$$

where $l_1 D^q x_2 + l_2 x_2$ is the scalar fractional-order controller and l_1 and l_2 are feedback coefficients. If $l_1 > -1$ and $l_2 > 105$, then the controlled system (8) will be asymptotically converged to the equilibrium point $S_0 = (0, 0, 0)$.

Proof. The unstable equilibrium point $S_0 = (0, 0, 0)$ in the fractional-order Chen chaotic system is also the equilibrium point in the controlled system (8). The Jacobi matrix of the controlled system at equilibrium point $S_0 = (0, 0, 0)$ is

$$J_{(0,0,0)} = \begin{vmatrix} -35 - 7l_1 & 35 + 28l_1 + l_2 & 0 \\ -7 & 28 & 0 \\ 0 & 0 & -3 \end{vmatrix}. \quad (9)$$

The eigenvalues are

$$\begin{aligned} \lambda_{\pm} &= -0.5(7 + 7l_1) \\ &\quad \pm 0.5\sqrt{(7 + 7l_1)^2 - 4(7l_2 - 21 \times 35)}, \quad \lambda_3 = -3, \end{aligned} \quad (10)$$

because

$$l_1 > -1, \quad l_2 > 105. \quad (11)$$

So

$$\operatorname{Re}(\lambda_{\pm}) < 0. \quad (12)$$

Therefore, all eigenvalues of the Jacobi matrix at equilibrium point $S_0 = (0, 0, 0)$ in the controlled system (8) have negative real part. This result implies that the controlled system will be asymptotically converged to the equilibrium point $S_0 = (0, 0, 0)$. The proof is completed. \square

Theorem 2. Consider the controlled system is as follows:

$$\begin{aligned} D^q x_1 &= 35(x_2 - x_1), \\ D^q x_2 &= -7x_1 + 28x_2 - x_1 x_3 + l_3 D^q x_1 + l_4 x_1, \\ D^q x_3 &= x_1 x_2 - 3x_3, \end{aligned} \quad (13)$$

where $l_3 D^q x_2 + l_4 x_2$ is a fractional-order scalar controller and l_3 and l_4 are feedback coefficients. If $l_3 < 0.2$ and $-(35l_3 - 7)^2/140 \leq l_4 + 21 < 0$, then the controlled system (13) will be asymptotically converged to the equilibrium point $S_0 = (0, 0, 0)$.

Proof. It is easily to obtain that the unstable equilibrium point $S_0 = (0, 0, 0)$ in the fractional-order Chen chaotic system is also the equilibrium point in the controlled system (13). The Jacobi matrix of the controlled system (13) at equilibrium point $S_0 = (0, 0, 0)$ is

$$J_{(0,0,0)} = \begin{vmatrix} -35 & 35 & 0 \\ -7 - 35l_3 + l_4 & 28 + 35l_3 & 0 \\ 0 & 0 & -3 \end{vmatrix}. \quad (14)$$

The eigenvalues are

$$\begin{aligned} \lambda_{\pm} &= 0.5(35l_3 - 7) \\ &\quad \pm 0.5\sqrt{(35l_3 - 7)^2 + 140(21 + l_4)}, \quad \lambda_3 = -3, \end{aligned} \quad (15)$$

because

$$l_3 < 0.2, \quad -\frac{(35l_3 - 7)^2}{140} \leq l_4 + 21 < 0. \quad (16)$$

So

$$\operatorname{Re}(\lambda_{\pm}) < 0. \quad (17)$$

Therefore, all eigenvalues of the Jacobi matrix at equilibrium point $S_0 = (0, 0, 0)$ in the controlled system (13) have negative real part. This result indicates that the controlled system (13) will be asymptotically converged to the equilibrium point $S_0 = (0, 0, 0)$. The proof is completed. \square

3.2. Case 2: Control of the Unstable Equilibrium Points $S_{\pm} = (\pm\sqrt{63}, \pm\sqrt{63}, 21)$

Theorem 3. Consider the controlled system is

$$\begin{aligned} D^q x_1 &= 35(x_2 - x_1), \\ D^q x_2 &= -7x_1 + 28x_2 - x_1x_3 + l_5 D^q x_1, \\ D^q x_3 &= x_1x_2 - 3x_3, \end{aligned} \quad (18)$$

where $l_5 D^q x_1$ is the scalar fractional-order controller and l_5 is feedback coefficient. If $35l_5 < 19 - \sqrt{1551}$, then the controlled system (18) will be asymptotically converged to the equilibrium point $S_+ = (\sqrt{63}, \sqrt{63}, 21)$.

Proof. The Jacobian matrix at the equilibrium point $S_+ = (\sqrt{63}, \sqrt{63}, 21)$ in the controlled system (18) is

$$J = \begin{vmatrix} -35 & 35 & 0 \\ -28 - 35l_5 & 28 + 35l_5 & -\sqrt{63} \\ \sqrt{63} & \sqrt{63} & -3 \end{vmatrix}. \quad (19)$$

Its characteristic equation is

$$\lambda^3 + c_1 \lambda^2 + c_2 \lambda + c_3 = 0, \quad (20)$$

where $c_1 = 10 - 35l_5$, $c_2 = 3(28 - 35l_5)$, and $c_3 = 4410$.

Because $35l_5 < 19 - \sqrt{1551}$, the following yields

$$c_1 > 0, \quad c_2 > 0, \quad c_1 c_2 - c_3 > 0. \quad (21)$$

This result indicates that all eigenvalues of the Jacobi matrix at equilibrium point $S_+ = (\sqrt{63}, \sqrt{63}, 21)$ in the controlled system (18) have negative real part. So, the controlled system (18) will be asymptotically converged to the equilibrium point $S_+ = (\sqrt{63}, \sqrt{63}, 21)$. The proof is completed. \square

Similarly, we can easily control the fractional-order Chen chaotic system that will be asymptotically converged to the unstable equilibrium point $S_- = (-\sqrt{63}, -\sqrt{63}, 21)$.

Remark 4. In this section, we only discuss that all eigenvalues of the Jacobi matrix at equilibrium point in the controlled system have negative real part. Recently, Li and Ma [25] reported the more rigorous result on the local asymptotical stability of the nonlinear fractional differential system. Their result also can be applied to control the unstable equilibrium point in the fractional-order Chen chaotic system.

Remark 5. Only one system state variable and its fractional-order derivative are used in our fractional-order scalar controller. This is the main contribution in our work.

4. Circuit Implementation of the Control Scheme for the Fractional-Order Chen Chaotic System

In this subsection, some circuits are designed to realize these control schemes for the fractional-order Chen chaotic system, and the circuit results fit the theoretical results mentioned in Section 3.

Now, many references on the guidelines to design circuits for the fractional-order chaotic systems are reported. By the circuit design methods [9, 26–29], the circuits are designed as mentioned below to realize the fractional-order chaotic system (8), (13), and (18), and the circuit experiments are obtained.

4.1. Case 1: Realize Physically the Controlled Fractional-Order Chen Chaotic System (8). Now, let $l_1 = 1$ and $l_2 = 200$ in the controlled system (8). According to Theorem 1, the controlled system (8) will be asymptotically converged to the unstable equilibrium point $S_0 = (0, 0, 0)$. By the circuit design method [9, 27, 28], the circuit diagram designed to realize the controlled system (8) is presented as shown in Figures 2 and 3.

The first equation, the second equation, and the third equation in controlled system (8) are realized by Figures 2(a), 2(b), and 2(c), respectively. The operator d^q/dt^q is realized by Figure 3.

According to the circuit design methods, the resistors in Figure 2 are chosen as $R_1 = 100 \text{ k}\Omega$, $R_2 = 2.86 \text{ k}\Omega$, $R_3 = 3.57 \text{ k}\Omega$, $R_4 = 14.3 \text{ k}\Omega$, $R_5 = 33.3 \text{ k}\Omega$, $R_6 = 100 \text{ k}\Omega$, and $R_7 = 0.5 \text{ k}\Omega$, respectively. Here and later, the capacitors and resistors in Figure 3 are chosen as $R_{11} = 62.84 \text{ M}\Omega$, $R_{22} = 0.25 \text{ M}\Omega$, $R_{33} = 0.0025 \text{ M}\Omega$, $C_{11} = 1.232 \text{ }\mu\text{F}$, $C_{22} = 1.84 \text{ }\mu\text{F}$, and $C_{33} = 1.1 \text{ }\mu\text{F}$. The operational amplifiers are of the type of LF353N, the multipliers are of the type of AD633, and the power is supplied by $\pm 15 \text{ V}$.

By choosing the circuit output x_1 in Figure 2(a) as the vertical axis input, Figure 4(a) shows the circuit experiment displayed on the oscilloscope. Similarly, Figure 4(b) shows the circuit experiment displayed on the oscilloscope with the circuit outputs x_2 in Figure 2(b) and Figure 4(c) shows the circuit experiment displayed on the oscilloscope with the circuit outputs x_3 in Figure 2(c). In this paper, the vertical coordinate unit is V (volt) and the horizontal coordinate unit is second (s).

According to Figure 4, the circuit results fit the theoretical results mentioned in Theorem 1.

4.2. Case 2: Realize Physically the Controlled Fractional-Order Chen Chaotic System (13). Now, let $l_3 = -1$ and $l_4 = -30$ in the controlled system (13). According to Theorem 2, the controlled system (8) will be asymptotically converged to the unstable equilibrium point $S_0 = (0, 0, 0)$. Similarly, the circuit diagram designed to realize the controlled system (13) is shown in Figure 5.

Here, the first equation, the second equation, and the third equation in controlled system (13) are realized by Figures 5(a), 5(b), and 5(c), respectively. The operator d^q/dt^q is realized by Figure 3.

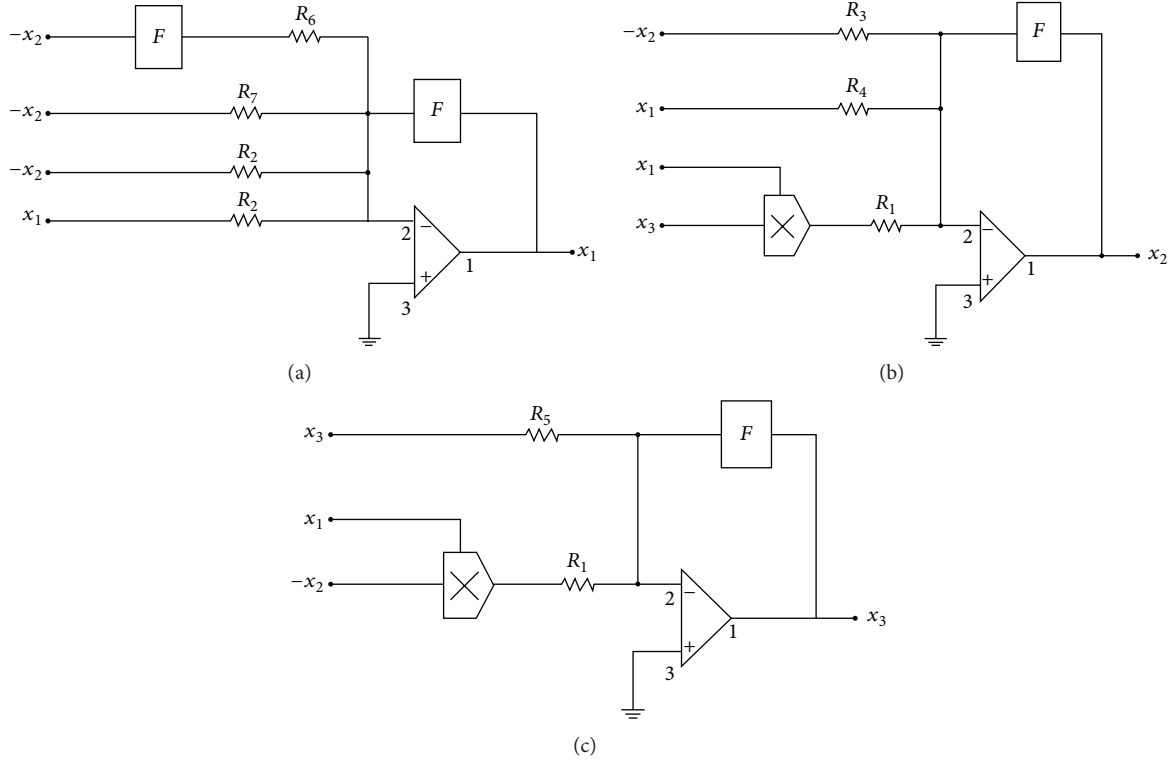


FIGURE 2: The circuit diagram designed to realize the fractional-order controlled system (8) for $q = 0.9$.

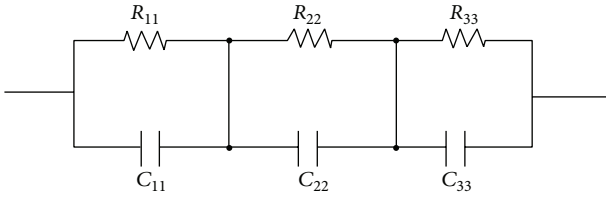


FIGURE 3: Circuit diagram for box F .

According to the circuit design methods, the resistors in Figure 5 are chosen as $R_8 = 100 \text{ k}\Omega$, and $R_9 = 3.33 \text{ k}\Omega$, respectively. The resistors R_i ($i = 1, 2, \dots, 7$) are the same as in Figure 2.

Similarly, by choosing the circuit output x_1 in Figure 5(a) as the vertical axis input, Figure 6(a) shows the circuit experiment displayed on the oscilloscope. Similarly, Figure 6(b) shows the circuit experiment displayed on the oscilloscope with the circuit outputs x_2 in Figure 5(b) and Figure 6(c) shows the circuit experiment displayed on the oscilloscope with the circuit outputs x_3 in Figure 5(c).

According to Figure 6, the circuit results agree with the theoretical results mentioned in Theorem 2.

4.3. Case 3: Realize Physically the Controlled Fractional-Order Chen Chaotic System (18). Now, let $l_5 = -1$ in the controlled system (18). According to Theorem 3, the controlled system (18) will be asymptotically converged to the unstable equilibrium point $S_+ = (\sqrt{63}, \sqrt{63}, 21)$. Similarly, the circuit

diagram designed to realize the controlled system (18) is displayed as shown in Figure 7.

Similarly, the first equation, the second equation, and the third equation in controlled system (18) are realized by Figures 7(a), 7(b), and 7(c), respectively. The operator d^q/dt^q is realized by Figure 3. The resistors and capacitors in Figure 7 are chosen as Case 1 and Case 2.

By choosing the circuit output x_1 in Figure 7(a) as the vertical axis input, Figure 8(a) shows the circuit experiment displayed on the oscilloscope. Similarly, Figure 8(b) shows the circuit experiment displayed on the oscilloscope with the circuit outputs x_2 in Figure 7(b) and Figure 8(c) shows the circuit experiment displayed on the oscilloscope with the circuit outputs x_3 in Figure 7(c).

According to Figure 8, the circuit results agree with the theoretical results mentioned in Theorem 3.

5. Conclusions

In order to control of the unstable equilibrium points for the fractional-order Chen chaotic system, some fractional-order scalar controllers are proposed, and only one state variable is used in the fractional-order scalar controller. The control scheme is theoretically rigorous. Moreover, three fractional-order chaotic circuits are designed to realize the control strategy, and the circuit experiments are obtained. The experiment results agree with the theoretical results. Furthermore, some results [30–33] on the effect of noises or disturbances in control or synchronization problems of chaotic systems have been proposed. The anticontrol or

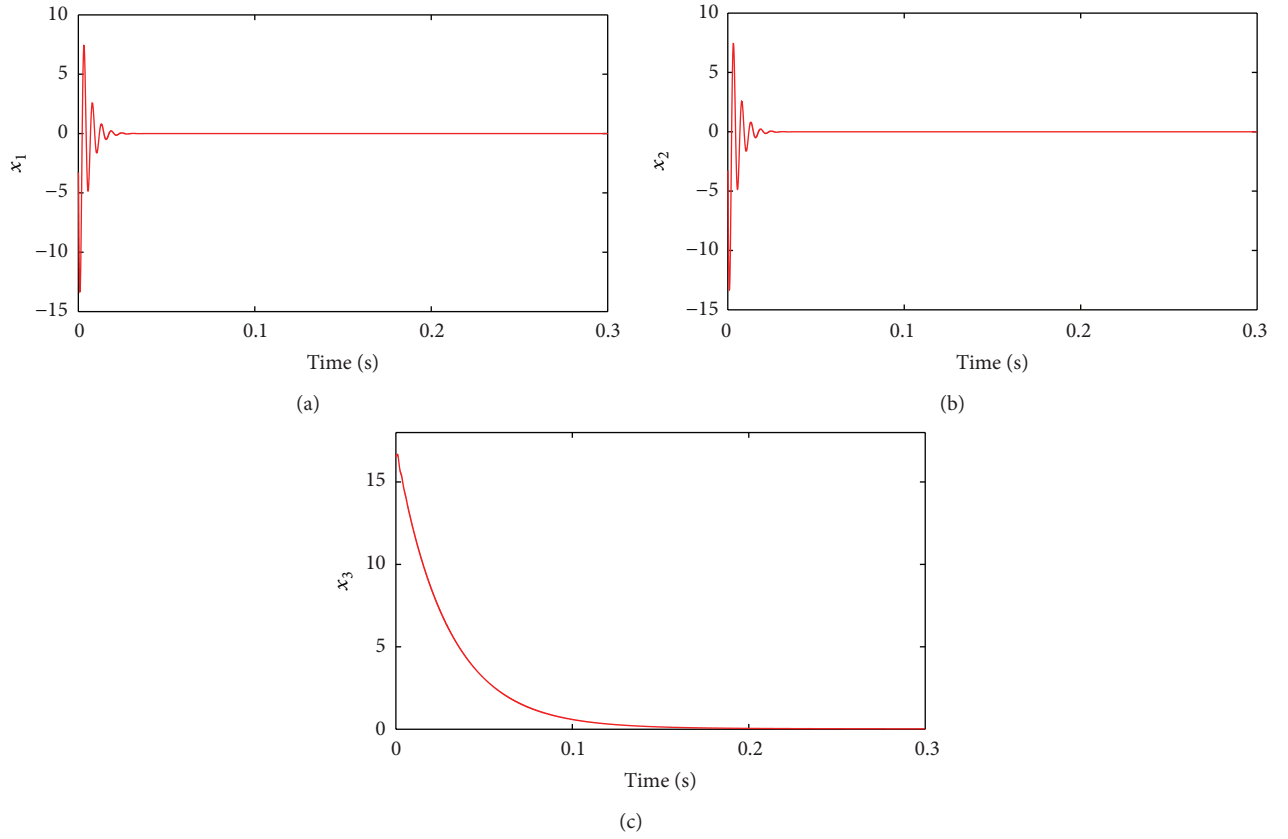
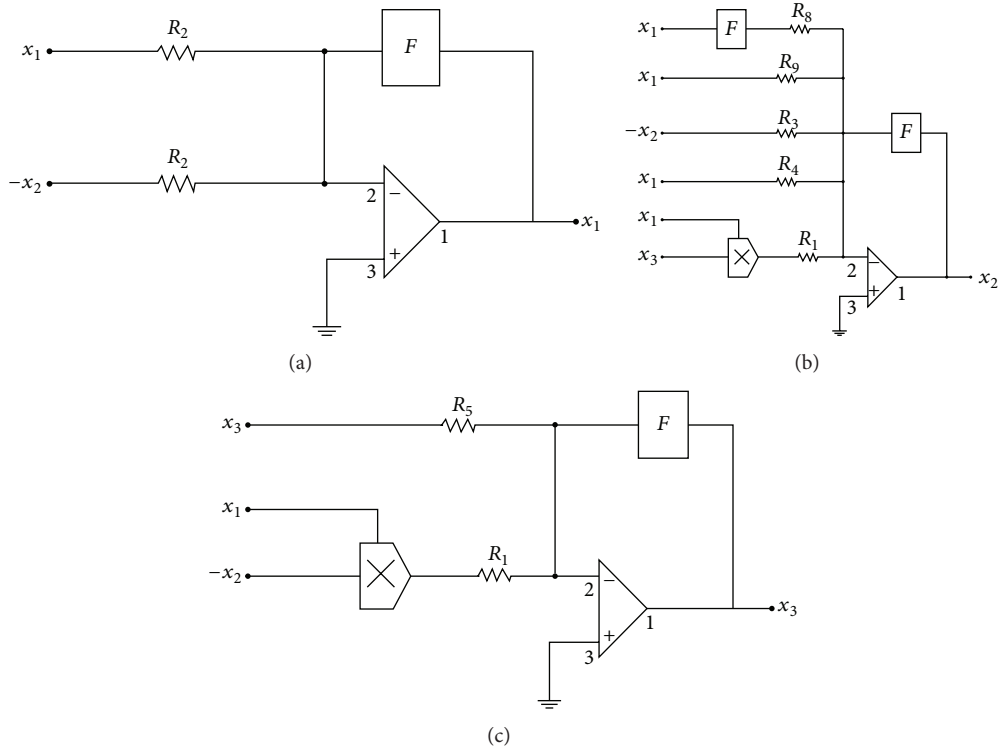


FIGURE 4: The circuit experiment displayed on the oscilloscope.

FIGURE 5: The circuit diagram designed to realize the fractional-order controlled system (13) for $q = 0.9$.

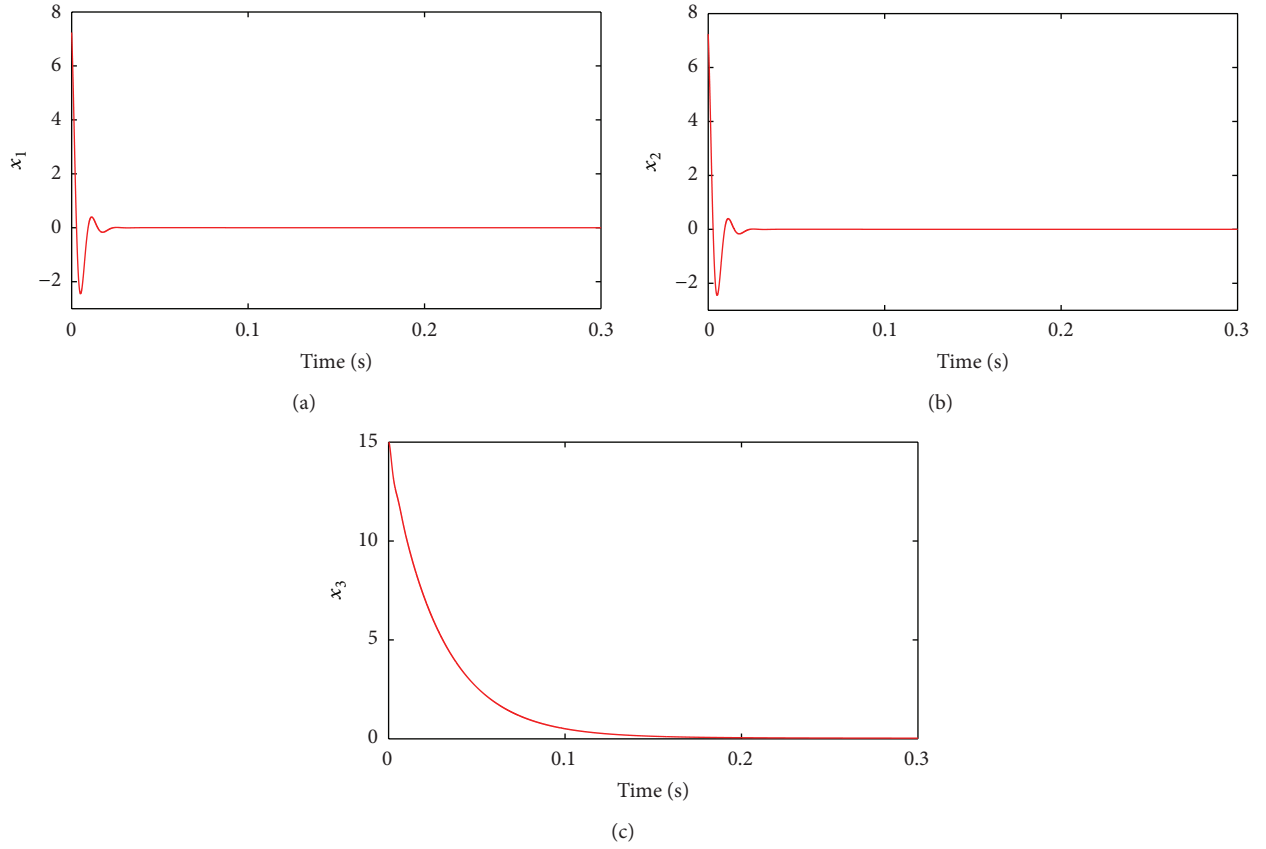
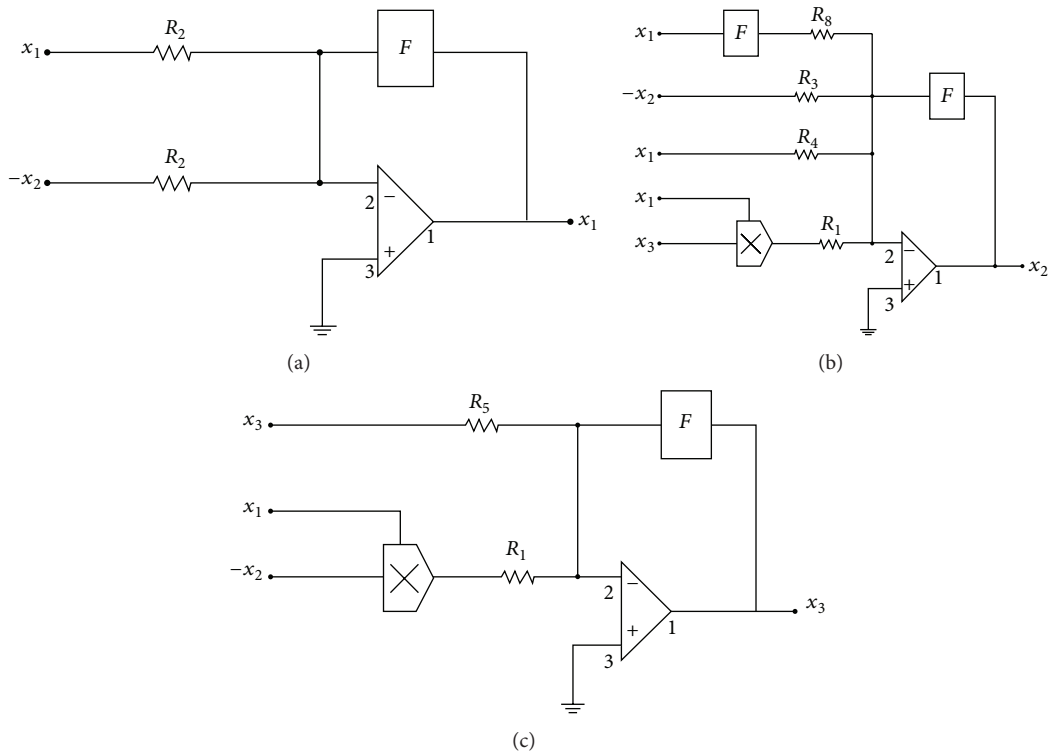


FIGURE 6: The circuit experiment displayed on the oscilloscope.

FIGURE 7: The circuit diagram designed to realize the fractional-order controlled system (18) for $q = 0.9$.

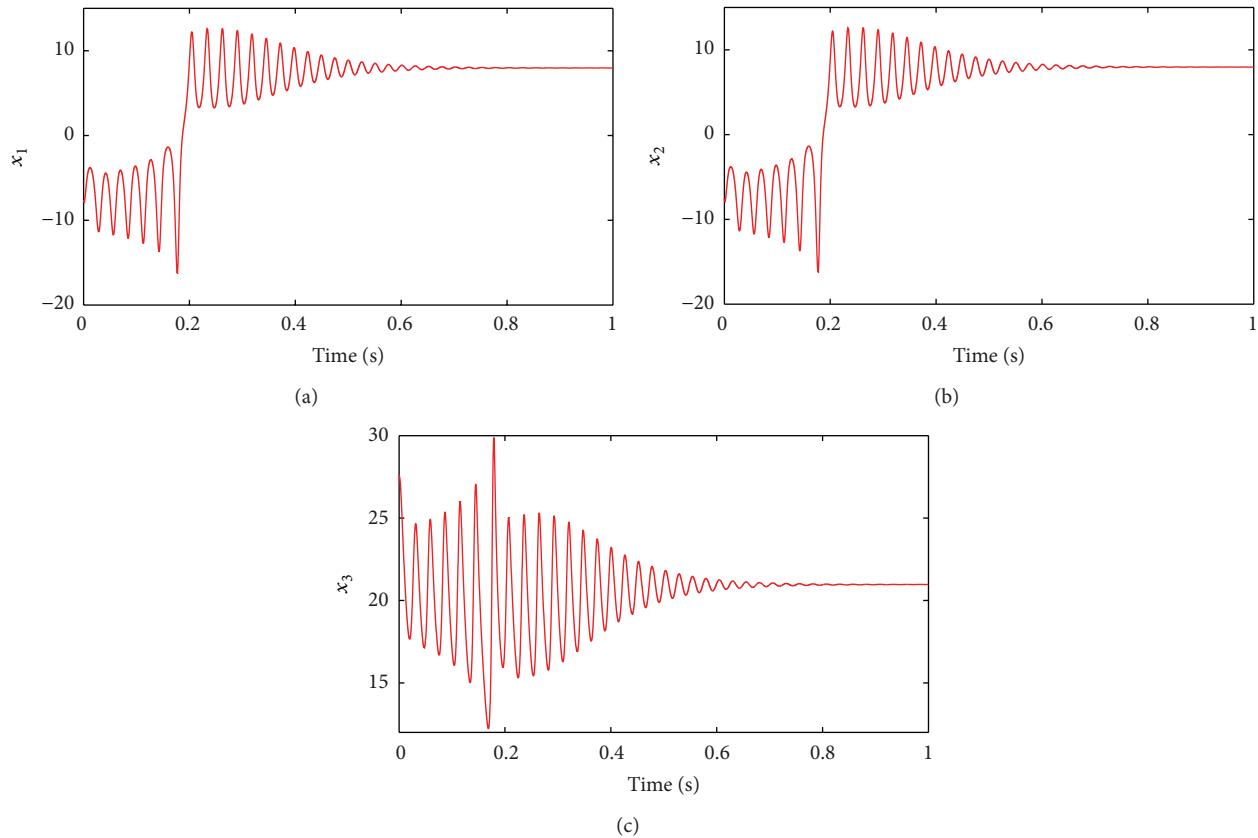


FIGURE 8: The circuit experiment displayed on the oscilloscope.

antisynchronization problems for fractional chaotic systems with disturbances or noises have been also discussed in [34]. So, the effect of noises or disturbances for our control scheme is our further work.

Conflict of Interests

The authors declare that there is no conflict of interests regarding the publication of this paper.

Acknowledgments

This work is supported by the National Science and Technology Specific Project of China (2012YQ20022404), National Natural Science Foundation of China (no. 60972070), Program for Changjiang Scholars and Innovative Research Team in University (IRT1299), and the special fund of Chongqing key laboratory (CSTC).

References

- [1] E. Ott, C. Grebogi, and J. A. Yorke, "Controlling chaos," *Physical Review Letters*, vol. 64, no. 11, pp. 1196–1199, 1990.
- [2] G. Chen and X. Yu, *Chaos Control: Theory and Applications*, Springer, Berlin, Germany, 2003.
- [3] T. T. Hartley, C. F. Lorenzo, and H. K. Qammer, "Chaos in a fractional order Chua's system," *IEEE Transactions on Circuits and Systems I: Fundamental Theory and Applications*, vol. 42, no. 8, pp. 485–490, 1995.
- [4] Z. M. Ge and C. Y. Ou, "Chaos in a fractional order modified Duffing system," *Chaos, Solitons and Fractals*, vol. 34, no. 2, pp. 262–291, 2007.
- [5] D. Cafagna and G. Grassi, "On the simplest fractional-order memristor-based chaotic system," *Nonlinear Dynamics*, vol. 70, no. 2, pp. 1185–1197, 2012.
- [6] I. Grigorenko and E. Grigorenko, "Chaotic dynamics of the fractional Lorenz system," *Physical Review Letters*, vol. 91, no. 3, pp. 034101–034104, 2003.
- [7] C. Li and G. Peng, "Chaos in Chen's system with a fractional order," *Chaos, Solitons and Fractals*, vol. 22, no. 2, pp. 443–450, 2004.
- [8] P. Zhou and F. Y. Yang, "Hyperchaos, chaos, and horseshoe in a 4D nonlinear system with an infinite number of equilibrium points," *Nonlinear Dynamics*, vol. 76, no. 1, pp. 473–480, 2014.
- [9] P. Zhou and K. Huang, "A new 4-D non-equilibrium fractional-order chaotic system and its circuit implementation," *Communications in Nonlinear Science and Numerical Simulation*, vol. 19, no. 6, pp. 2005–2011, 2014.
- [10] P. Zhou, R. Ding, and Y. Cao, "Multi drive-one response synchronization for fractional-order hyperchaotic systems," *Nonlinear Dynamics*, vol. 70, no. 2, pp. 1263–1271, 2012.
- [11] L. Pan, W. Zhou, L. Zhou, and K. Sun, "Chaos synchronization between two different fractional-order hyperchaotic systems," *Communications in Nonlinear Science and Numerical Simulation*, vol. 16, no. 6, pp. 2628–2640, 2011.

- [12] S. S. Delshad, M. M. Asheghan, and M. H. Beheshti, "Synchronization of N -coupled incommensurate fractional-order chaotic systems with ring connection," *Communications in Nonlinear Science and Numerical Simulation*, vol. 16, no. 9, pp. 3815–3824, 2011.
- [13] H. Taghvafard and G. H. Erjaee, "Phase and anti-phase synchronization of fractional order chaotic systems via active control," *Communications in Nonlinear Science and Numerical Simulation*, vol. 16, no. 10, pp. 4079–4088, 2011.
- [14] R. X. Zhang and S. P. Yang, "Adaptive synchronization of fractional-order chaotic systems via a single driving variable," *Nonlinear Dynamics*, vol. 66, no. 4, pp. 831–837, 2011.
- [15] D. Cafagna and G. Grassi, "Observer-based projective synchronization of fractional systems via a scalar signal: application to hyperchaotic Rössler systems," *Nonlinear Dynamics*, vol. 68, no. 1-2, pp. 117–128, 2012.
- [16] R. Zhang and S. Yang, "Stabilization of fractional-order chaotic system via a single state adaptive-feedback controller," *Nonlinear Dynamics*, vol. 68, no. 1-2, pp. 45–51, 2012.
- [17] M. S. Tavazoei and M. Haeri, "Chaos control via a simple fractional-order controller," *Physics Letters A*, vol. 372, no. 6, pp. 798–807, 2008.
- [18] P. Zhou and F. Kuang, "A novel control method for integer orders chaos systems via fractional-order derivative," *Discrete Dynamics in Nature and Society*, vol. 2011, Article ID 217843, 8 pages, 2011.
- [19] P. Zhou and W. Zhu, "Function projective synchronization for fractional-order chaotic systems," *Nonlinear Analysis: Real World Applications*, vol. 12, no. 2, pp. 811–816, 2011.
- [20] D. Matignon, "Stability results for fractional differential equations with application to control processing," in *Proceedings of the International IMACS IEEE-SMC Multiconference on Computational Engineering in Systems Applications*, pp. 963–1031, Lille, France, July 1996.
- [21] E. Ahmed, A. M. A. El-Sayed, and H. A. A. El-Saka, "Equilibrium points, stability and numerical solutions of fractional-order predator-prey and rabies models," *Journal of Mathematical Analysis and Applications*, vol. 325, no. 1, pp. 542–553, 2007.
- [22] Z. M. Odibat, "Adaptive feedback control and synchronization of non-identical chaotic fractional order systems," *Nonlinear Dynamics*, vol. 60, no. 4, pp. 479–487, 2010.
- [23] Z. Odibat, "A note on phase synchronization in coupled chaotic fractional order systems," *Nonlinear Analysis: Real World Applications*, vol. 13, no. 2, pp. 779–789, 2012.
- [24] X. Wang, Y. He, and M. Wang, "Chaos control of a fractional order modified coupled dynamos system," *Nonlinear Analysis: Theory, Methods and Applications*, vol. 71, no. 12, pp. 6126–6134, 2009.
- [25] C. P. Li and Y. T. Ma, "Fractional dynamical system and its linearization theorem," *Nonlinear Dynamics*, vol. 71, pp. 621–633, 2013.
- [26] F. Q. Wang and C. X. Liu, "Study on the critical chaotic system with fractional order and circuit experiment," *Acta Physica Sinica*, vol. 55, pp. 3922–3927, 2006.
- [27] P. Zhou, X. Cheng, and M. Zhang, "One new fractional-order chaos system and its circuit simulation by electronic workbench," *Chinese Physics B*, vol. 17, no. 9, pp. 3252–3257, 2008.
- [28] H. Q. Li, X. F. Liao, and M. W. Luo, "A novel non-equilibrium fractional-order chaotic system and its complete synchronization by circuit implementation," *Nonlinear Dynamics*, vol. 68, no. 1-2, pp. 137–149, 2012.
- [29] Z. Ruo-Xun and Y. Shi-Ping, "Chaos in fractional-order generalized lorenz system and its synchronization circuit simulation," *Chinese Physics B*, vol. 18, no. 8, pp. 3295–3302, 2009.
- [30] C. K. Ahn, S. Jung, S. Kang, and S. Joo, "Adaptive H_∞ synchronization for uncertain chaotic systems with external disturbance," *Communications in Nonlinear Science and Numerical Simulation*, vol. 15, no. 8, pp. 2168–2177, 2010.
- [31] C. K. Ahn, "Adaptive H_∞ anti-synchronization for time-delayed chaotic neural networks," *Progress of Theoretical Physics*, vol. 122, no. 6, pp. 1391–1403, 2009.
- [32] C. K. Ahn, "T-S fuzzy H_∞ synchronization for chaotic systems via delayed output feedback control," *Nonlinear Dynamics*, vol. 59, no. 4, pp. 535–543, 2010.
- [33] C. K. Ahn, "Output feedback H_∞ synchronization for delayed chaotic neural networks," *Nonlinear Dynamics*, vol. 59, no. 1-2, pp. 319–327, 2010.
- [34] C. K. Ahn, "An H_∞ approach to anti-synchronization for chaotic systems," *Physics Letters A: General, Atomic and Solid State Physics*, vol. 373, no. 20, pp. 1729–1733, 2009.

Research Article

Analysis on Passivity for Uncertain Neural Networks with Time-Varying Delays

O. M. Kwon,¹ M. J. Park,¹ Ju H. Park,² S. M. Lee,³ and E. J. Cha⁴

¹ School of Electrical Engineering, Chungbuk National University, 52 Naesudong-Ro, Cheongju 361-763, Republic of Korea

² Nonlinear Dynamics Group, Department of Electrical Engineering, Yeungnam University, 280 Daehak-Ro, Kyongsan 712-749, Republic of Korea

³ School of Electronics Engineering, Daegu University, Gyungsan 712-714, Republic of Korea

⁴ Department of Biomedical Engineering, School of Medicine, Chungbuk National University, 52 Naesudong-Ro, Cheongju 361-763, Republic of Korea

Correspondence should be addressed to Ju H. Park; jessie@ynu.ac.kr

Received 14 April 2014; Accepted 29 May 2014; Published 17 June 2014

Academic Editor: He Huang

Copyright © 2014 O. M. Kwon et al. This is an open access article distributed under the Creative Commons Attribution License, which permits unrestricted use, distribution, and reproduction in any medium, provided the original work is properly cited.

The problem of passivity analysis for neural networks with time-varying delays and parameter uncertainties is considered. By the consideration of newly constructed Lyapunov-Krasovskii functionals, improved sufficient conditions to guarantee the passivity of the concerned networks are proposed with the framework of linear matrix inequalities (LMIs), which can be solved easily by various efficient convex optimization algorithms. The enhancement of the feasible region of the proposed criteria is shown via two numerical examples by the comparison of maximum allowable delay bounds.

1. Introduction

Neural networks are the networks of mutual elements that behave like biological neurons, which can be mathematically described by difference or differential equations. For this reason, during a few decades, neural networks have been extensively applied in many areas such as reconstruction of moving image, signal processing, the tasks of pattern recognition, associative memories, and fixed-point computations [1–10]. Also, the stability analysis of the concerned neural networks is a very important and prerequisite job because the application of neural networks heavily depends on the dynamic behavior of equilibrium points.

On the other hand, we need to pay keen attention to a delay in the time and passivity. It is well known that time-delay is a natural concomitant of the finite speed of information processing in the implementation of the networks and often causes undesirable dynamic behaviors such as oscillation and instability of the networks. In various scientific and engineering problems, stability issues are often linked to the theory of dissipative systems. It postulates that the energy

dissipated inside a dynamic system is less than the energy supplied from the external source [11]. Based on the concept of energy, the passivity is the property of dynamical systems and describes the energy flow through the system. It is also an input/output characterization and related to Lyapunov method. In the field of nonlinear control, the concept of dissipativeness was firstly introduced by Willems [12] in the form of inequality including supply rate and the storage function. The main idea of passivity theory is that passive properties of a system can keep the system internally. Therefore, the study on passivity analysis for uncertain neural networks with time-delay has been widely investigated in [13–19] since parametric uncertainties, which sometimes affect the stability of systems, are also undesirable dynamics in the hardware implementation of neural networks due to the fact that the connection weights of the neurons are dependent on the values of certain resistances and capacitances including variations of fluctuations [20]. In [16], two types of time-varying delays were considered in passivity analysis of uncertain neural networks. Recently, in [17], by considering some useful terms which were ignored in previous literatures and

utilizing free-weighting matrix techniques, the enhancement of feasible region of passivity criteria was shown. In [18], by proposing a complete delay-decomposing approach and utilizing a segmentation technique, improved conditions for passivity of neural networks were presented. In the authors' previous work [19], some less conservative conditions for passivity of neural networks were derived by taking more information of states. All the works [13–19] show their advantages of the proposed methods via comparison of maximum delay bounds with the previous works since delay bounds for guaranteeing the passivity of the concerned networks are recognized as one of the most important index for checking the conservatism of criteria. Very recently, up to now, one of the most remarkable methods in reducing the conservatism of stability criteria is Wirtinger-based integral inequality [21] which reduced Jensen's gap effectively. Therefore, there are rooms for further improvements in passivity analysis of the neural networks with both time-delay and parameter uncertainties.

With this motivation mentioned above, in this paper, the problem on passivity for uncertain neural networks with time-varying delays is addressed. In Theorem 6, by utilizing Wirtinger-based integral inequality [21], a passivity condition for neural networks with time-varying delays and parameter uncertainties is introduced with the framework of LMIs. Based on the results of Theorem 6, a newly constructed Lyapunov-Krasovskii functional is introduced and further improved results will be derived in Theorem 7. Inspired by the work of [22, 23], the reciprocally convex approach and some zero equality will be utilized in Theorems 6 and 7. Finally, through two numerical examples, it will be shown that Theorems 6 and 7 obtain the less conservative results.

Notation. Throughout this paper, the used notations are standard. \mathbb{R}^n is the n -dimensional Euclidean vector space and $\mathbb{R}^{m \times n}$ denotes the set of all $m \times n$ real matrices. For symmetric matrices X and Y , $X > Y$ means that the matrix $X - Y$ is positive definite, whereas $X \geq Y$ means that the matrix $X - Y$ is nonnegative. I_n , 0_n , and $0_{m \times n}$ denote $n \times n$ identity matrix and $n \times n$ and $m \times n$ denote zero matrices, respectively. $\text{diag}\{\dots\}$ denotes the block diagonal matrix. For square matrix X , $\text{sym}\{X\}$ means the sum of X and its symmetric matrix X^T ; that is, $\text{sym}\{X\} = X + X^T$. $X_{[f(t)]} \in \mathbb{R}^{m \times n}$ means that the elements of matrix $X_{[f(t)]}$ include the scalar value of $f(t)$; that is, $X_{[f_0]} = X_{[f(t)=f_0]}$.

2. Preliminaries and Problem Statement

Consider the following uncertain neural networks with time-varying delays:

$$\begin{aligned} \dot{x}(t) = & -(A + \Delta A(t))x(t) + (W_0 + \Delta W_0(t))f(x(t)) \\ & + (W_1 + \Delta W_1(t))f(x(t-h(t))) + u(t), \\ y(t) = & C_1 f(x(t)) + C_2 f(x(t-h(t))), \end{aligned} \quad (1)$$

where n denotes the number of neurons in a neural network, $x(t) = [x_1(t), x_2(t), \dots, x_n(t)]^T \in \mathbb{R}^n$ is the neuron state vector, $f(x(t)) = [f(x_1(t)), f(x_2(t)), \dots, f(x_n(t))]^T \in \mathbb{R}^n$

denotes the neuron activation function vector, $y(t) \in \mathbb{R}^n$ is the output vector, $u(t) \in \mathbb{R}^n$ is the input vector, $A = \text{diag}\{a_1, \dots, a_n\} \in \mathbb{R}^{n \times n}$ is a positive diagonal matrix, $W_i \in \mathbb{R}^{n \times n}$ ($i = 0, 1$) are the interconnection weight matrices, $C_i \in \mathbb{R}^{n \times n}$ ($i = 1, 2$) are known constant matrices, and $\Delta A(t)$ and $\Delta W_i(t)$ ($i = 0, 1$) are the parameter uncertainties of the form

$$[\Delta A(t), \Delta W_0(t), \Delta W_1(t)] = DF(t)[E_a, E_0, E_1], \quad (2)$$

where $D \in \mathbb{R}^{n \times l}$, $E_a \in \mathbb{R}^{l \times n}$, $E_0 \in \mathbb{R}^{l \times n}$, and $E_1 \in \mathbb{R}^{l \times n}$ are the constant matrices and $F(t) \in \mathbb{R}^{l \times l}$ is the time-varying nonlinear function satisfying

$$F^T(t)F(t) \leq I_l, \quad \forall t \geq 0. \quad (3)$$

The delay $h(t)$ is time-varying function satisfying

$$0 \leq h(t) \leq h_M, \quad \dot{h}(t) \leq h_D, \quad (4)$$

where h_M and h_D are known positive scalars.

It is assumed that the neuron activation functions satisfy the following condition.

Assumption 1. The neuron activation functions $f_i(\cdot)$ ($i = 1, \dots, n$) are continuous, bounded and satisfy

$$k_i^- \leq \frac{f_i(u) - f_i(v)}{u - v} \leq k_i^+, \quad (5)$$

$$\forall u, v \in \mathbb{R}, \quad u \neq v, \quad f_i(0) = 0,$$

where k_i^+ and k_i^- are constants.

From (5), if $v = 0$, then we have

$$k_i^- \leq \frac{f_i(u)}{u} \leq k_i^+, \quad \forall u \neq 0. \quad (6)$$

Also, the conditions (5) and (6) are, respectively, equivalent to

$$[f_i(u) - f_i(v) - k_i^-(u - v)][f_i(u) - f_i(v) - k_i^+(u - v)] \leq 0, \quad (7)$$

$$[f_i(u) - k_i^-u][f_i(u) - k_i^+u] \leq 0. \quad (8)$$

The systems (1) can be rewritten as

$$\begin{aligned} \dot{x}(t) = & -Ax(t) + W_0 f(x(t)) \\ & + W_1 f(x(t-h(t))) + u(t) + Dp(t), \\ p(t) = & F(t)q(t), \\ q(t) = & -E_a x(t) + E_0 f(x(t)) + E_1 f(x(t-h(t))), \\ y(t) = & C_1 f(x(t)) + C_2 f(x(t-h(t))). \end{aligned} \quad (9)$$

The objective of this paper is to investigate delay-dependent passivity conditions for system (9). Before deriving our main results, the following definition and lemmas are introduced.

Definition 2. The system (1) is called passive if there exists a scalar $\gamma \geq 0$ such that

$$-\gamma \int_0^{t_p} u^T(s) u(s) ds \leq 2 \int_0^{t_p} y^T(s) u(s) ds, \quad (10)$$

for all $t_p \geq 0$ and for all solution of (1) with $x(0) = 0$.

Lemma 3 (see [21]). For a given matrix $M > 0$, the following inequality holds for all continuously differentiable function x in $[a, b] \rightarrow \mathbb{R}^n$:

$$\begin{aligned} & \int_a^b \dot{x}^T(s) M \dot{x}(s) ds \\ & \geq \frac{1}{b-a} \xi_1^T(t) M \xi_1(t) + \frac{3}{b-a} \xi_2^T(t) M \xi_2(t), \end{aligned} \quad (11)$$

where $\xi_1(t) = x(b) - x(a)$ and $\xi_2(t) = x(b) + x(a) - (2/(b-a)) \int_a^b x(s) ds$.

Lemma 4 (see [22]). For any vectors x_1, x_2 , constant matrices M, S , and real scalars $0 \leq \alpha \leq 1$ satisfying that $\begin{bmatrix} M & S \\ S^T & M \end{bmatrix} \geq 0$, the following inequality holds:

$$\begin{aligned} & -\frac{1}{\alpha} x_1^T M x_1 - \frac{1}{1-\alpha} x_2^T M x_2 \\ & \leq -\begin{bmatrix} x_1 \\ x_2 \end{bmatrix}^T \begin{bmatrix} M & S \\ S^T & M \end{bmatrix} \begin{bmatrix} x_1 \\ x_2 \end{bmatrix}. \end{aligned} \quad (12)$$

Lemma 5 (see [24]). Let $\zeta \in \mathbb{R}^n$, $\Phi = \Phi^T \in \mathbb{R}^{n \times n}$, and $B \in \mathbb{R}^{m \times n}$ such that $\text{rank}(B) < n$. Then, the following statements are equivalent:

- (i) $\zeta^T \Phi \zeta < 0$, $B\zeta = 0$, $\zeta \neq 0$,
- (ii) $(B^\perp)^T \Phi B^\perp < 0$, where B^\perp is a right orthogonal complement of B ,
- (iii) $\exists X \in \mathbb{R}^{n \times m}$: $\Phi + XB + (XB)^T < 0$.

3. Main Results

In this section, new passivity criteria for the system (9) will be proposed in Theorems 6 and 7.

For the sake of simplicity on matrix representation, $e_i \in \mathbb{R}^{(13n+l) \times n}$ ($i = 1, 2, \dots, 13$) and $e_{14} \in \mathbb{R}^{(13n+l) \times l}$ are defined as block entry matrices. For example, $e_5 = [0_{n \times 4n}, I_n, 0_{n \times 8n}, 0_{n \times l}]^T$

and $e_{14} = [0_{l \times 13n}, I_l]^T$. And the notations of several matrices are defined as

$$\begin{aligned} \zeta(t) = \text{col} \left\{ & x(t), x(t-h(t)), x(t-h_M), \right. \\ & \dot{x}(t), \dot{x}(t-h_M), \frac{1}{h(t)} \int_{t-h(t)}^t x(s) ds, \\ & \frac{1}{h_M-h(t)} \int_{t-h_M}^{t-h(t)} x(s) ds, \\ & f(x(t)), f(x(t-h(t))), \\ & f(x(t-h_M)), \int_{t-h(t)}^t f(x(s)) ds, \\ & \left. \int_{t-h_M}^{t-h(t)} f(x(s)) ds, u(t), p(t) \right\}, \end{aligned}$$

$$Y = [-A, 0_{n \times 2n}, -I_n, 0_{n \times 3n}, W_0, W_1, 0_{n \times 3n}, I_n, D],$$

$$\Psi_{1[h(t)]} = \begin{bmatrix} I_n & 0_n & 0_n & 0_n \\ 0_n & I_n & 0_n & 0_n \\ 0_n & 0_n & h(t) I_n & 0_n \\ 0_n & 0_n & (h_M-h(t)) I_n & 0_n \\ 0_n & 0_n & 0_n & I_n \\ 0_n & 0_n & 0_n & I_n \end{bmatrix},$$

$$\Psi_2 = \left[\begin{array}{c|c} \text{diag}\{R_1, 3R_1\} & S_1 \\ \hline S_1^T & \text{diag}\{R_1, 3R_1\} \end{array} \right],$$

$$\Psi_3 = \begin{bmatrix} R_2 & S_2 \\ S_2^T & R_2 \end{bmatrix},$$

$$\Psi_4 = \mathcal{R}_4 + \begin{bmatrix} 0_n & Z_1 \\ Z_1^T & 0_n \end{bmatrix},$$

$$\Psi_5 = \mathcal{R}_4 + \begin{bmatrix} 0_n & Z_2 \\ Z_2^T & 0_n \end{bmatrix},$$

$$\begin{aligned} \Xi_{1[h(t)]} = \text{sym} \{ & [e_1, e_3, e_6, e_7, e_{11}, e_{12}] \Psi_{1[h(t)]} \\ & \times \mathcal{P}[e_4, e_5, e_1 - e_3, e_8 - e_{10}]^T \}, \end{aligned}$$

$$\begin{aligned} \Xi_2 = & [e_1, e_4, e_8] \mathcal{Q}_1 [e_1, e_4, e_8]^T \\ & - [e_3, e_5, e_{10}] \mathcal{Q}_1 [e_3, e_5, e_{10}]^T \\ & + \text{sym} \{ [e_8 - e_1 K^-] \Lambda e_4^T + [e_1 K^+ - e_8] \Delta e_4^T \}, \end{aligned}$$

$$\Xi_3 = [e_1, e_8] \mathcal{Q}_2 [e_1, e_8]^T - (1 - h_D) [e_2, e_9] \mathcal{Q}_2 [e_2, e_9]^T,$$

$$\Xi_4 = h_M^2 e_4 R_1 e_4^T$$

$$- \left[\begin{array}{c} e_1^T - e_2^T \\ e_1^T + e_2^T - 2e_6^T \\ e_2^T - e_3^T \\ e_2^T + e_3^T - 2e_7^T \end{array} \right]^T \Psi_2 \left[\begin{array}{c} e_1^T - e_2^T \\ e_1^T + e_2^T - 2e_6^T \\ e_2^T - e_3^T \\ e_2^T + e_3^T - 2e_7^T \end{array} \right],$$

$$\begin{aligned}
\Xi_5 &= h_M^2 e_8 R_2 e_8^T - [e_{11}, e_{12}] \Psi_3 [e_{11}, e_{12}]^T, \\
\Xi_{6[h(t)]} &= h_M^2 e_1 R_3 e_1^T - h_M e_6 (h(t) R_3) e_6^T \\
&\quad - h_M e_7 ((h_M - h(t)) R_3) e_7^T, \\
\Xi_7 &= h_M [e_1, e_4] \mathcal{R}_4 [e_1, e_4]^T + e_1 Z_1 e_1^T \\
&\quad - e_2 (Z_1 - Z_2) e_2^T - e_3 Z_2 e_3^T, \\
\Omega_1 &= -\text{sym} \{ [e_8 - e_9 - (e_1 - e_2) K^-] \\
&\quad \times H_1 [e_8 - e_9 - (e_1 - e_2) K^+]^T \\
&\quad + [e_9 - e_{10} - (e_2 - e_3) K^-] \\
&\quad \times H_2 [e_9 - e_{10} - (e_2 - e_3) K^+]^T \}, \\
\Omega_2 &= -\text{sym} \{ [e_8 - e_1 K^-] H_3 [e_8 - e_1 K^+]^T \\
&\quad + [e_9 - e_2 K^-] H_4 [e_9 - e_2 K^+]^T \\
&\quad + [e_{10} - e_3 K^-] H_5 [e_{10} - e_3 K^+]^T \}, \\
\Gamma &= -\text{sym} \{ e_8 C_1^T e_{13}^T + e_9 C_2^T e_{13}^T \} - \gamma e_{13} e_{13}^T, \\
\Xi_{[h(t)]} &= \Xi_{1[h(t)]} + \Xi_2 + \Xi_3 + \Xi_4 + \Xi_5 + \Xi_{6[h(t)]} + \Xi_7, \\
\Theta &= \epsilon \{ (-E_1 e_1^T + E_2 e_8^T + E_3 e_9^T)^T \\
&\quad \times (-E_1 e_1^T + E_2 e_8^T + E_3 e_9^T) - e_{14} e_{14}^T \}. \tag{13}
\end{aligned}$$

Then, the following theorem is given as the first main result.

Theorem 6. For given positive scalars h_M , h_D and diagonal matrices $K^- = \text{diag}\{k_1^-, \dots, k_n^-\}$ and $K^+ = \text{diag}\{k_1^+, \dots, k_n^+\}$, the system (9) is passive for $0 \leq h(t) \leq h_M$ and $\dot{h}(t) \leq h_D$, if there exist positive scalars ϵ and γ , positive diagonal matrices $\Lambda = \text{diag}\{\lambda_1, \dots, \lambda_n\} \in \mathbb{R}^{n \times n}$, $\Delta = \text{diag}\{\delta_1, \dots, \delta_n\} \in \mathbb{R}^{n \times n}$, $H_i = \text{diag}\{h_{1i}, \dots, h_{ni}\}$ ($i = 1, 2, \dots, 5$), positive definite matrices $\mathcal{P} \in \mathbb{R}^{4n \times 4n}$, $\mathcal{Q}_1 \in \mathbb{R}^{3n \times 3n}$, $\mathcal{Q}_2 \in \mathbb{R}^{2n \times 2n}$, $R_i \in \mathbb{R}^{n \times n}$ ($i = 1, 2, 3$), $\mathcal{R}_4 \in \mathbb{R}^{2n \times 2n}$, any symmetric matrices $Z_i \in \mathbb{R}^{n \times n}$ ($i = 1, 2$), and any matrices $\mathcal{S}_1 \in \mathbb{R}^{2n \times 2n}$, $\mathcal{S}_2 \in \mathbb{R}^{n \times n}$ satisfying the following LMIs:

$$(\Upsilon^\perp)^T (\Xi_{[0]} + \Omega_1 + \Omega_2 + \Gamma + \Theta) \Upsilon^\perp < 0, \tag{14}$$

$$(\Upsilon^\perp)^T (\Xi_{[h_M]} + \Omega_1 + \Omega_2 + \Gamma + \Theta) \Upsilon^\perp < 0, \tag{15}$$

$$\Psi_i > 0 \quad (i = 2, 3, 4, 5), \tag{16}$$

where the notation 0 in (14)–(16) means a zero matrix with an appropriate dimension.

Proof. Let us consider the following Lyapunov-Krasovskii functional candidate as

$$V = \sum_{i=1}^7 V_i, \tag{17}$$

where

$$\begin{aligned}
V_1 &= \begin{bmatrix} x(t) \\ x(t-h_M) \\ \int_{t-h_M}^t x(s) ds \\ \int_{t-h_M}^t f(x(s)) ds \end{bmatrix}^T \mathcal{P} \begin{bmatrix} x(t) \\ x(t-h_M) \\ \int_{t-h_M}^t x(s) ds \\ \int_{t-h_M}^t f(x(s)) ds \end{bmatrix}, \\
V_2 &= \int_{t-h_M}^t \begin{bmatrix} x(s) \\ \dot{x}(s) \\ f(x(s)) \end{bmatrix}^T \mathcal{Q}_1 \begin{bmatrix} x(s) \\ \dot{x}(s) \\ f(x(s)) \end{bmatrix} ds \\
&\quad + 2 \sum_{i=1}^n \left(\lambda_i \int_0^{x_i(t)} (f_i(s) - k_i^- s) ds \right. \\
&\quad \left. + \delta_i \int_0^{x_i(t)} (k_i^+ s - f_i(s)) ds \right), \tag{18} \\
V_3 &= \int_{t-h(t)}^t \begin{bmatrix} x(s) \\ f(x(s)) \end{bmatrix}^T \mathcal{Q}_2 \begin{bmatrix} x(s) \\ f(x(s)) \end{bmatrix} ds, \\
V_4 &= h_M \int_{t-h_M}^t \int_s^t \dot{x}^T(u) R_1 \dot{x}(u) du ds, \\
V_5 &= h_M \int_{t-h_M}^t \int_s^t f^T(x(u)) R_2 f(x(u)) du ds, \\
V_6 &= h_M \int_{t-h_M}^t \int_s^t x^T(u) R_3 x(u) du ds, \\
V_7 &= \int_{t-h_M}^t \int_s^t \begin{bmatrix} x(u) \\ \dot{x}(u) \end{bmatrix}^T \mathcal{R}_4 \begin{bmatrix} x(u) \\ \dot{x}(u) \end{bmatrix} du ds.
\end{aligned}$$

The time-derivatives of V_1 , V_2 , and V_3 can be calculated as

$$\begin{aligned}
\dot{V}_1 &= 2 \begin{bmatrix} x(t) \\ x(t-h_M) \\ \left(\frac{h(t)}{h(t)} \int_{t-h(t)}^t x(s) ds + \frac{h_M - h(t)}{h_M - h(t)} \int_{t-h_M}^{t-h(t)} x(s) ds \right) \\ \int_{t-h(t)}^t f(x(s)) ds + \int_{t-h_M}^{t-h(t)} f(x(s)) ds \end{bmatrix}^T \\
&\quad \times \mathcal{P} \begin{bmatrix} \dot{x}(t) \\ \dot{x}(t-h_M) \\ x(t) - x(t-h_M) \\ f(x(t)) - f(x(t-h_M)) \end{bmatrix} \\
&= \zeta^T(t) \Xi_{1[h(t)]} \zeta(t),
\end{aligned} \tag{19}$$

$$\begin{aligned}
\dot{V}_2 &= \begin{bmatrix} x(t) \\ \dot{x}(t) \\ f(x(t)) \end{bmatrix}^T \mathcal{Q}_1 \begin{bmatrix} x(t) \\ \dot{x}(t) \\ f(x(t)) \end{bmatrix} - \begin{bmatrix} x(t-h_M) \\ \dot{x}(t-h_M) \\ f(x(t-h_M)) \end{bmatrix}^T \\
&\quad \times \mathcal{Q}_1 \begin{bmatrix} x(t-h_M) \\ \dot{x}(t-h_M) \\ f(x(t-h_M)) \end{bmatrix} \\
&\quad + 2[f(x(t)) - K_m x(t)]^T \Lambda \dot{x}(t) \\
&\quad + 2[K_p x(t) - f(x(t))]^T \Delta \dot{x}(t) \\
&= \zeta^T(t) \Xi_2 \zeta(t),
\end{aligned} \tag{20}$$

$$\begin{aligned}
\dot{V}_3 &\leq \begin{bmatrix} x(t) \\ f(x(t)) \end{bmatrix}^T \mathcal{Q}_2 \begin{bmatrix} x(t) \\ f(x(t)) \end{bmatrix} \\
&\quad - (1-h_D) \begin{bmatrix} x(t-h(t)) \\ f(x(t-h(t))) \end{bmatrix}^T \mathcal{Q}_2 \begin{bmatrix} x(t-h(t)) \\ f(x(t-h(t))) \end{bmatrix} \\
&= \zeta^T(t) \Xi_3 \zeta(t).
\end{aligned} \tag{21}$$

By the use of Lemma 3, \dot{V}_4 is bounded as

$$\begin{aligned}
\dot{V}_4 &= h_M^2 \dot{x}^T(t) R_1 \dot{x}(t) - h_M \int_{t-h(t)}^t \dot{x}^T(s) R_1 \dot{x}(s) ds \\
&\quad - h_M \int_{t-h_M}^{t-h(t)} \dot{x}^T(s) R_1 \dot{x}(s) ds \\
&\leq h_M^2 \dot{x}^T(t) R_1 \dot{x}(t) - \frac{h_M}{h(t)} (\xi_{1,1}^T R_1 \xi_{1,1} + 3\xi_{1,2}^T R_1 \xi_{1,2}) \\
&\quad - \frac{h_M}{h_M - h(t)} (\xi_{2,1}^T R_1 \xi_{2,1} + 3\xi_{2,2}^T R_1 \xi_{2,2}),
\end{aligned} \tag{22}$$

where

$$\begin{aligned}
\xi_{1,1} &= x(t) - x(t-h(t)), \\
\xi_{1,2} &= x(t) + x(t-h(t)) - \frac{2}{h(t)} \int_{t-h(t)}^t x(s) ds, \\
\xi_{2,1} &= x(t-h(t)) - x(t-h_M), \\
\xi_{2,2} &= x(t-h(t)) + x(t-h_M) - \frac{2}{h_M - h(t)} \int_{t-h_M}^{t-h(t)} x(s) ds.
\end{aligned} \tag{23}$$

Furthermore, if $\Psi_2 > 0$, then applying Lemma 4 to (22) leads to

$$\begin{aligned}
\dot{V}_4 &\leq h_M^2 \dot{x}^T(t) R_1 \dot{x}(t) - \frac{1}{\alpha(t)} (\xi_{1,1}^T R_1 \xi_{1,1} + 3\xi_{1,2}^T R_1 \xi_{1,2}) \\
&\quad - \frac{1}{1-\alpha(t)} (\xi_{2,1}^T R_1 \xi_{2,1} + 3\xi_{2,2}^T R_1 \xi_{2,2}) \\
&\leq h_M^2 \dot{x}^T(t) R_1 \dot{x}(t)
\end{aligned}$$

$$\begin{aligned}
&\quad - \begin{bmatrix} \xi_{1,1} \\ \xi_{1,2} \end{bmatrix}^T \text{diag}\{R_1, 3R_1\} \begin{bmatrix} \xi_{1,1} \\ \xi_{1,2} \end{bmatrix} - \begin{bmatrix} \xi_{1,1} \\ \xi_{1,1} \end{bmatrix}^T \mathcal{S}_1 \begin{bmatrix} \xi_{2,1} \\ \xi_{2,2} \end{bmatrix} \\
&\quad - \begin{bmatrix} \xi_{1,1} \\ \xi_{1,2} \end{bmatrix}^T \mathcal{S}_1^T \begin{bmatrix} \xi_{2,1} \\ \xi_{2,2} \end{bmatrix} - \begin{bmatrix} \xi_{2,1} \\ \xi_{2,2} \end{bmatrix}^T \text{diag}\{R_1, 3R_1\} \begin{bmatrix} \xi_{2,1} \\ \xi_{2,2} \end{bmatrix} \\
&= \zeta^T(t) \Xi_4 \zeta(t),
\end{aligned} \tag{24}$$

where $1/\alpha(t) = h_M/h(t)$ and \mathcal{S}_1 is any $2n \times 2n$ matrix.

By the use of Lemma 3 and Jensen's inequality [25], if $\Psi_3 > 0$, then \dot{V}_5 can be bounded as

$$\begin{aligned}
\dot{V}_5 &\leq h_M^2 f^T(x(t)) R_2 f(x(t)) \\
&\quad - \begin{bmatrix} \int_{t-h(t)}^t f(x(s)) ds \\ \int_{t-h_M}^{t-h(t)} f(x(s)) ds \end{bmatrix}^T \begin{bmatrix} R_2 & S_2 \\ S_2^T & R_2 \end{bmatrix} \begin{bmatrix} \int_{t-h(t)}^t f(x(s)) ds \\ \int_{t-h_M}^{t-h(t)} f(x(s)) ds \end{bmatrix} \\
&= \zeta^T(t) \Xi_5 \zeta(t),
\end{aligned} \tag{25}$$

where S_2 is any $n \times n$ matrix.

And an upper bound of \dot{V}_6 with Jensen's inequality [25] can be obtained as

$$\begin{aligned}
\dot{V}_6 &= h_M^2 x^T(t) R_3 x(t) - h_M \int_{t-h(t)}^t x^T(s) R_3 x(s) ds \\
&\quad - h_M \int_{t-h_M}^{t-h(t)} x^T(s) R_3 x(s) ds \\
&\leq h_M^2 x^T(t) R_3 x(t) \\
&\quad - h_M \left(\frac{1}{h(t)} \int_{t-h(t)}^t x(s) ds \right)^T \\
&\quad \times h(t) R_3 \left(\frac{1}{h(t)} \int_{t-h(t)}^t x(s) ds \right) \\
&\quad - h_M \left(\frac{1}{h_M - h(t)} \int_{t-h_M}^{t-h(t)} x(s) ds \right)^T \\
&\quad \times (h_M - h(t)) R_3 \left(\frac{1}{h_M - h(t)} \int_{t-h_M}^{t-h(t)} x(s) ds \right) \\
&= \zeta^T(t) \Xi_6 \zeta(t).
\end{aligned} \tag{26}$$

Before calculating the estimation of \dot{V}_7 , inspired by the work of [23], the following zero equalities with any symmetric matrices Z_1 and Z_2 are considered as a tool of reducing the conservatism of criterion

$$\begin{aligned} \Xi_{ZE} = & \underbrace{x^T(t)Z_1x(t) - x^T(t-h(t))Z_1x(t-h(t)) - 2 \int_{t-h(t)}^t x^T(s)Z_1\dot{x}(s)ds}_{0} \\ & + \underbrace{x^T(t-h(t))Z_2x(t-h(t)) - x^T(t-h_M)Z_2x(t-h_M) - 2 \int_{t-h_M}^{t-h(t)} x^T(s)Z_2\dot{x}(s)ds}_{0}. \end{aligned} \quad (27)$$

Adding (27) to \dot{V}_7 can be obtained as

$$\begin{aligned} \dot{V}_7 + \Xi_{ZE} = & h_M \begin{bmatrix} x(t) \\ \dot{x}(t) \end{bmatrix}^T \mathcal{R}_4 \begin{bmatrix} x(t) \\ \dot{x}(t) \end{bmatrix} \\ & + \begin{bmatrix} x(t) \\ x(t-h(t)) \\ x(t-h_M) \end{bmatrix}^T \text{diag}\{Z_1, Z_2 - Z_1, -Z_2\} \\ & \times \begin{bmatrix} x(t) \\ x(t-h(t)) \\ x(t-h_M) \end{bmatrix} \\ & - \int_{t-h(t)}^t \begin{bmatrix} x(s) \\ \dot{x}(s) \end{bmatrix}^T \left(\mathcal{R}_4 + \begin{bmatrix} 0 & Z_1 \\ Z_1 & 0 \end{bmatrix} \right) \begin{bmatrix} x(s) \\ \dot{x}(s) \end{bmatrix} ds \\ & - \int_{t-h_M}^{t-h(t)} \begin{bmatrix} x(s) \\ \dot{x}(s) \end{bmatrix}^T \left(\mathcal{R}_4 + \begin{bmatrix} 0 & Z_2 \\ Z_2 & 0 \end{bmatrix} \right) \begin{bmatrix} x(s) \\ \dot{x}(s) \end{bmatrix} ds \\ \leq & h_M \begin{bmatrix} x(t) \\ \dot{x}(t) \end{bmatrix}^T \mathcal{R}_4 \begin{bmatrix} x(t) \\ \dot{x}(t) \end{bmatrix} \\ & + \begin{bmatrix} x(t) \\ x(t-h(t)) \\ x(t-h_M) \end{bmatrix}^T \text{diag}\{Z_1, Z_2 - Z_1, -Z_2\} \\ & \times \begin{bmatrix} x(t) \\ x(t-h(t)) \\ x(t-h_M) \end{bmatrix} \\ = & \zeta^T(t) \Xi_7 \zeta(t). \end{aligned} \quad (28)$$

Here, the bound of \dot{V}_7 presented in (28) is valid when $\Psi_i > 0$ ($i = 4, 5$) hold.

By utilizing the authors' work [26], from (7), choosing $[u, v]$ as $[x(t), x(t-h(t))]$ and $[x(t-h(t)), x(t-h_M)]$ leads to

$$\begin{aligned} 0 \leq & -2[f(x(t)) - f(x(t-h(t)))] \\ & -K^-(x(t) - x(t-h(t)))^T H_1 \\ & \times [f(x(t)) - f(x(t-h(t)))] \\ & -K^+(x(t) - x(t-h(t))) \\ & -2[f(x(t-h(t))) - f(x(t-h_M))] \end{aligned}$$

$$\begin{aligned} & -K^-(x(t-h(t)) - x(t-h_M))^T H_2 \\ & \times [f(x(t-h(t))) - f(x(t-h_M))] \\ & -K^+(x(t-h(t)) - x(t-h_M)) \\ = & \zeta^T(t) \Omega_1 \zeta(t), \end{aligned} \quad (29)$$

where H_1 and H_2 are positive diagonal matrices.

Also, from (8), the following inequality holds

$$\begin{aligned} 0 \leq & -2[f(x(t)) - K_m x(t)]^T H_3 [f(x(t)) - K_p x(t)] \\ & -2[f(x(t-h(t))) - K_m x(t-h(t))]^T \\ & \times H_4 [f(x(t-h(t))) - K_p x(t-h(t))] \\ & -2[f(x(t-h_M)) - K_m x(t-h_M)]^T \\ & \times H_5 [f(x(t-h_M)) - K_p x(t-h_M)] \\ = & \zeta^T(t) \Omega_2 \zeta(t), \end{aligned} \quad (30)$$

where H_3 , H_4 , and H_5 are positive diagonal matrices.

Lastly, in succession, with the relational expression between $p(t)$ and $q(t)$, $p^T(t)p(t) \leq q^T(t)q(t)$, from the system (9), there exists any scalar $\epsilon > 0$ satisfying the following inequality:

$$\begin{aligned} 0 \leq & \epsilon \{q^T(t)q(t) - p^T(t)p(t)\} \\ = & \epsilon(-E_a x(t) + E_0 f(x(t)) + E_1 f(x(t-h(t))))^T \\ & \times (-E_a x(t) + E_0 f(x(t)) + E_1 f(x(t-h(t)))) \\ & - \epsilon p^T(t)p(t) \\ = & \zeta^T(t) \Theta \zeta(t). \end{aligned} \quad (31)$$

From (19)–(31) and by applying S-procedure [27], an upper bound of $\dot{V} - 2y^T(t)u(t) - \gamma u^T(t)u(t)$ can be

$$\begin{aligned} & \underbrace{\dot{V} - 2y^T(t)u(t) - \gamma u^T(t)u(t)}_{\zeta^T(t)\Gamma\zeta(t)} \\ \leq & \zeta^T(t) (\Xi_{[h(t)]} + \Omega_1 + \Omega_2 + \Gamma + \Theta) \zeta(t). \end{aligned} \quad (32)$$

By applying (i) and (iii) of Lemma 5, $\zeta^T(t)(\Xi_{[h(t)]} + \Omega_1 + \Omega_2 + \Gamma + \Theta)\zeta(t) < 0$ with $\Upsilon\zeta(t) = 0_{n-1}$ is equivalent to

$$(\Xi_{[h(t)]} + \Omega_1 + \Omega_2 + \Gamma + \Theta) + \text{sym}\{XY\} < 0 \quad (33)$$

for any free matrix X with appropriate dimension.

Lastly, by utilizing (ii) and (iii) of Lemma 5, one can confirm that the inequality (33) is equivalent to

$$(\Upsilon^\perp)^T (\Xi_{[h(t)]} + \Omega_1 + \Omega_2 + \Gamma + \Theta) \Upsilon^\perp < 0. \quad (34)$$

Therefore, if LMIs (14), (15), and (16) hold, then (34) holds, which means

$$\dot{V} - 2y^T(t)u(t) - \gamma u^T(t)u(t) < 0. \quad (35)$$

By integrating (35) with respect to t over the time period from 0 to t_p , we have

$$\begin{aligned} V(x(t_p)) - V(x(0)) - \gamma \int_0^{t_p} u^T(s)u(s)ds \\ \leq 2 \int_0^{t_p} y^T(s)u(s)ds, \end{aligned} \quad (36)$$

for $x(0) = 0$. Since $V(x(0)) = 0$, the inequality (10) in Definition 2 holds. This implies that the neural networks (1) are passive in the sense of Definition 2. This completes our proof. \square

In the second place, an improved passivity criterion for the system (9) will be derived in Theorem 7 by utilizing modified V_3 . The notations of several matrices are defined for simplicity:

$$\begin{aligned} \hat{\Xi}_{3[h(t)]} &= [e_1, e_8] \begin{bmatrix} Q_{2,11} & Q_{2,12} \\ Q_{2,12} & Q_{2,22} \end{bmatrix} [e_1, e_8]^T \\ &\quad - (1 - h_D) [e_2, e_9, e_1 - e_2] \mathcal{Q}_2 [e_2, e_9, e_1 - e_2]^T \\ &\quad + \text{sym} \{ h(t) e_6 Q_{2,13} e_4^T + e_{11} Q_{2,23} e_4^T \\ &\quad \quad + h(t) (e_1 - e_6) Q_{2,33} e_4^T \} \end{aligned} \quad (37)$$

and other notations will be used in Theorem 7.

Theorem 7. For given positive scalars h_M , h_D and diagonal matrices $K^- = \text{diag}\{k_1^-, \dots, k_n^-\}$ and $K^+ = \text{diag}\{k_1^+, \dots, k_n^+\}$, the system (9) is passive for $0 \leq h(t) \leq h_M$ and $\dot{h}(t) \leq h_D$, if there exist positive scalars ϵ and γ , positive diagonal matrices $\Lambda \in \mathbb{R}^{n \times n}$, $\Delta \in \mathbb{R}^{n \times n}$, $H_i = \text{diag}\{h_{1i}, \dots, h_{ni}\}$ ($i = 1, 2, \dots, 5$), positive definite matrices $\mathcal{P} \in \mathbb{R}^{4n \times 4n}$, $\mathcal{Q}_1 \in \mathbb{R}^{3n \times 3n}$, $\mathcal{Q}_2 = [Q_{2,ij}]_{3 \times 3} \in \mathbb{R}^{3n \times 3n}$, $R_i \in \mathbb{R}^{n \times n}$ ($i = 1, 2, 3$), $\mathcal{R}_4 \in \mathbb{R}^{2n \times 2n}$, any symmetric matrices $Z_i \in \mathbb{R}^{n \times n}$ ($i = 1, 2$), and any matrices $\mathcal{S}_1 \in \mathbb{R}^{2n \times 2n}$, $\mathcal{S}_2 \in \mathbb{R}^{n \times n}$ satisfying the LMIs (16) and

$$\begin{aligned} (\Upsilon^\perp)^T (\hat{\Xi}_{[0]} + \Omega_1 + \Omega_2 + \Gamma + \Theta) \Upsilon^\perp &< 0, \\ (\Upsilon^\perp)^T (\hat{\Xi}_{[h_M]} + \Omega_1 + \Omega_2 + \Gamma + \Theta) \Upsilon^\perp &< 0, \\ \Psi_i &> 0 \quad (i = 2, 3, 4, 5), \end{aligned} \quad (38)$$

where $\hat{\Xi}_{[h(t)]} = \Xi_{1[h(t)]} + \Xi_2 + \hat{\Xi}_{3[h(t)]} + \Xi_4 + \Xi_5 + \Xi_{6[h(t)]} + \Xi_7$.

Proof. By choosing V_3 as

$$\hat{V}_3 = \int_{t-h(t)}^t \begin{bmatrix} x(s) \\ f(x(s)) \\ \int_s^t \dot{x}(u) du \end{bmatrix}^T \mathcal{Q}_2 \begin{bmatrix} x(s) \\ f(x(s)) \\ \int_s^t \dot{x}(u) du \end{bmatrix} ds, \quad (39)$$

a newly Lyapunov-Krasovskii functional is given by

$$\hat{V} = V_1 + V_2 + \hat{V}_3 + V_4 + V_5 + V_6 + V_7. \quad (40)$$

Its new upper bound can be calculated as

$$\begin{aligned} \dot{\hat{V}} - 2y^T(t)u(t) - \gamma u^T(t)u(t) \\ \leq \zeta^T(t) (\hat{\Xi}_{[h(t)]} + \Omega_1 + \Omega_2 + \Gamma + \Theta) \zeta(t), \end{aligned} \quad (41)$$

where the following inequality

$$\begin{aligned} \dot{\hat{V}}_3 &= \begin{bmatrix} x(t) \\ f(x(t)) \\ 0_n \end{bmatrix}^T \mathcal{Q}_2 \begin{bmatrix} x(t) \\ f(x(t)) \\ 0_n \end{bmatrix} \\ &\quad - (1 - \dot{h}(t)) \begin{bmatrix} x(t-h(t)) \\ f(x(t-h(t))) \\ \int_{t-h(t)}^t \dot{x}(s) ds \end{bmatrix}^T \\ &\quad \times \mathcal{Q}_2 \begin{bmatrix} x(t-h(t)) \\ f(x(t-h(t))) \\ \int_{t-h(t)}^t \dot{x}(s) ds \end{bmatrix} \\ &\quad + 2 \int_{t-h(t)}^t \begin{bmatrix} x(s) \\ f(x(s)) \\ \int_s^t \dot{x}(u) du \end{bmatrix}^T \mathcal{Q}_2 \begin{bmatrix} 0_n \\ 0_n \\ \dot{x}(t) \end{bmatrix} ds \\ &\leq \begin{bmatrix} x(t) \\ f(x(t)) \\ 0_n \end{bmatrix}^T \mathcal{Q}_2 \begin{bmatrix} x(t) \\ f(x(t)) \\ 0_n \end{bmatrix} \\ &\quad - (1 - h_D) \begin{bmatrix} x(t-h(t)) \\ f(x(t-h(t))) \\ x(t) - x(t-h(t)) \end{bmatrix}^T \\ &\quad \times \mathcal{Q}_2 \begin{bmatrix} x(t-h(t)) \\ f(x(t-h(t))) \\ x(t) - x(t-h(t)) \end{bmatrix} \end{aligned}$$

$$\begin{aligned}
& + 2 \begin{bmatrix} \int_{t-h(t)}^t x(s) ds \\ \int_{t-h(t)}^t f(x(s)) ds \\ h(t)x(t) - \int_{t-h(t)}^t x(s) ds \end{bmatrix}^T \mathcal{Q}_2 \begin{bmatrix} 0_n \\ 0_n \\ \dot{x}(t) \end{bmatrix} \\
& = \zeta^T(t) \left([e_1, e_8] \begin{bmatrix} Q_{2,11} & Q_{2,12} \\ Q_{2,12} & Q_{2,22} \end{bmatrix} [e_1, e_8]^T \right. \\
& \quad \left. - (1 - h_D) [e_2, e_9, e_1 - e_2] \right. \\
& \quad \left. \times \mathcal{Q}_2 [e_2, e_9, e_1 - e_2]^T \right) \zeta(t) \\
& + 2 \left(\frac{1}{h(t)} \int_{t-h(t)}^t x(s) ds \right)^T (h(t) Q_{2,13}) \dot{x}(t) \\
& + 2 \left(\int_{t-h(t)}^t f(x(s)) ds \right)^T Q_{2,23} \dot{x}(t) \\
& + 2 \left(x(t) - \frac{1}{h(t)} \int_{t-h(t)}^t x(s) ds \right)^T (h(t) Q_{2,33}) \dot{x}(t) \\
& = \zeta^T(t) \widehat{\Xi}_{3[h(t)]} \zeta(t)
\end{aligned} \tag{42}$$

is used in (41). Here, other terms are very similar to the proof of Theorem 6, so it is omitted \square

Remark 8. In Theorem 6, Lemma 3 (Wirtinger-based integral inequality) was applied to only the integral term $-h_M \int_{t-h_M}^t \dot{x}^T(s) R_1 \dot{x}(s) ds$ obtained by calculating the time derivative of V_4 . The other integral terms such as $-h_M \int_{t-h_M}^t f^T(x(s)) R_1 f(x(s)) ds$ and $-h_M \int_{t-h_M}^t x^T(s) R_3 x(s) ds$ were estimated by using Jensen's inequality. In the authors' future work, further improved stability or passivity criteria for neural networks with time-varying delays will be proposed by utilizing Lemma 3 in estimating other integral terms.

Remark 9. Unlike Theorem 6, by utilizing \widehat{V}_3 as one of the terms of Lyapunov-Krasovskii functional, some new cross terms such as

$$\begin{aligned}
& - (1 - h_D) \begin{bmatrix} 0_n \\ 0_n \\ x(t) - x(t - h(t)) \end{bmatrix}^T \mathcal{Q}_2 \begin{bmatrix} 0_n \\ 0_n \\ x(t) - x(t - h(t)) \end{bmatrix}, \\
& 2 \left(\frac{1}{h(t)} \int_{t-h(t)}^t x(s) ds \right)^T (h(t) Q_{2,13}) \dot{x}(t), \\
& 2 \left(\int_{t-h(t)}^t f(x(s)) ds \right)^T Q_{2,23} \dot{x}(t), \\
& 2 \left(x(t) - \frac{1}{h(t)} \int_{t-h(t)}^t x(s) ds \right)^T (h(t) Q_{2,33}) \dot{x}(t)
\end{aligned} \tag{43}$$

are included, which may reduce the passivity criterion of Theorem 6. In the next section, the effectiveness of the proposed Lyapunov-Krasovskii functional will be shown by comparing maximum delay bounds which guarantee the passivity of the numerical examples.

Remark 10. When the information of $\dot{h}(t)$ is unknown, then, Theorems 6 and 7 can provide passivity criteria for the system (9) by choosing $\mathcal{Q}_2 = 0$.

4. Numerical Examples

In this section, two numerical examples are introduced to show the improvements of the proposed theorems. In examples, MATLAB, YALMIP, and SeDuMi 1.3 are used to solve LMI problems.

Example 11. Consider the neural networks (1) where

$$A = \begin{bmatrix} 2.2 & 0 \\ 0 & 1.5 \end{bmatrix}, \quad W_0 = \begin{bmatrix} 1 & 0.6 \\ 0.1 & 0.3 \end{bmatrix},$$

$$W_1 = \begin{bmatrix} 1 & -0.1 \\ 0.1 & 0.2 \end{bmatrix}, \quad C_1 = I_2,$$

$$C_2 = 0_2, \quad D = 0.1I_2,$$

$$E_a = 0.1I_2, \quad E_0 = 0.2I_2, \quad E_1 = 0.3I_2,$$

$$K^- = 0_2, \quad K^+ = I_2 \quad \text{with } f(x) = \frac{1}{2}(|x+1| - |x-1|).$$

(44)

The results of the maximum delay bounds for guaranteeing the passivity of the above neural networks with different h_D obtained by Theorems 6 and 7 are listed in Table 1. One can see that Theorem 6 for this example gives larger maximum delay bounds than those of [13–15, 19]. This indicates that the presented sufficient conditions relieve the conservativeness of the passivity caused by time-delay and parameter uncertainties. Furthermore, Theorem 7 provides larger delay bound than that of Theorem 6. This means that the newly constructed Lyapunov-Krasovskii functional plays an important role to reduce the conservatism of Theorem 6.

Example 12. Consider the neural networks (1) where

$$A = \begin{bmatrix} 2.2 & 0 \\ 0 & 1.8 \end{bmatrix}, \quad W_0 = \begin{bmatrix} 1.2 & 1 \\ -0.2 & 0.3 \end{bmatrix},$$

$$W_1 = \begin{bmatrix} 0.8 & 0.4 \\ -0.2 & 0.1 \end{bmatrix}, \quad C_1 = I_2,$$

$$C_2 = 0_2, \quad D = E_a = E_1 = E_2 = 0_2,$$

$$K^- = 0_2, \quad K^+ = I_2 \quad \text{with } f(x) = \frac{1}{2}(|x+1| - |x-1|).$$

(45)

In Table 2, the results of the maximum allowable delay bound for guaranteeing passivity are compared with the existing works. From Table 2, it can be seen that the maximum

TABLE 1: Maximum delay bounds h_M with different h_D (Example 1).

h_D	0.3	0.5	0.7	0.9	Unknown
[13]	0.4197	0.4145	0.4117	0.4082	0.3994
[14]	0.5624	0.5580	0.5565	0.5523	0.5420
[15]	0.5763	0.5679	0.5566	0.5273	0.5129
[19]	1.1921	1.1590	1.1297	1.1081	1.1008
Theorem 6	2.2044	2.1798	2.1504	2.1262	2.1209
Theorem 7	2.3290	2.2442	2.1718	2.1335	2.1209

TABLE 2: Maximum delay bounds h_M with different h_D (Example 2).

h_D	0.5	0.9	Unknown
[16]	0.5227	0.4613	0.4613
[17]	1.3752	1.3027	1.3027
[18] ($m = 2$)*	1.4693	1.4243	1.4240
Theorem 6	3.3289	3.0700	3.0534
Theorem 7	3.4305	3.0770	3.0534

* m is a delay-partitioning number.

delay bounds for guaranteeing the passivity of the above neural networks are significantly larger than those of [16–18].

5. Conclusions

In this paper, the two passivity criteria for neural networks with time-varying delays and parameter uncertainties have been proposed by the use of Lyapunov method and LMI framework. In Theorem 6, by constructing the suitable Lyapunov-Krasovskii functional and utilizing Wirtinger-based inequality, the sufficient condition for passivity of the concerned networks was derived. Based on the result of Theorem 6, the improved criterion for the networks was proposed in Theorem 7 by introducing the newly augmented Lyapunov-Krasovskii functional. Via two numerical examples that dealt with previous works, the improvements of the proposed passivity criteria have been successfully verified. Based on the proposed methods, future works will focus on solving various problems such as state estimation [28, 29], passivity analysis for neural networks [30], stabilization for BAM neural networks [31], synchronization for complex networks [32], stability analysis, and filtering for dynamic systems with time delays [33–37]. Moreover, in [38], to reduce the conservatism of stability sufficient conditions, the triple integral forms of Lyapunov-Krasovskii functional was proposed and its effectiveness was shown. Thus, by grafting such approach onto the proposed idea of this paper, further improved results will be investigated in the near future.

Conflict of Interests

The authors declare that there is no conflict of interests regarding the publication of this paper.

Acknowledgments

This research was supported by the Basic Science Research Program through the National Research Foundation of Korea (NRF) funded by the Ministry of Education, Science and Technology (2008-0062611) and by a grant of the Korea Healthcare Technology R & D Project, Ministry of Health & Welfare, Republic of Korea (A100054).

References

- [1] L. O. Chua and L. Yang, "Cellular neural networks: applications," *IEEE Transactions on Circuits and Systems*, vol. 35, no. 10, pp. 1273–1290, 1988.
- [2] A. Cichocki and R. Unbehauen, *Neural Networks for Optimization and Signal Processing*, John Wiley & Sons, Hoboken, NJ, USA, 1993.
- [3] G. Joya, M. A. Atencia, and F. Sandoval, "Hopfield neural networks for optimization: study of the different dynamics," *Neurocomputing*, vol. 43, pp. 219–237, 2002.
- [4] W.-J. Li and T. Lee, "Hopfield neural networks for affine invariant matching," *IEEE Transactions on Neural Networks*, vol. 12, no. 6, pp. 1400–1410, 2001.
- [5] F. Beaufays, Y. Abdel-Magid, and B. Widrow, "Application of neural networks to load-frequency control in power systems," *Neural Networks*, vol. 7, no. 1, pp. 183–194, 1994.
- [6] M. Galicki, H. Witte, J. Dörschel, M. Eiselt, and G. Griessbach, "Common optimization of adaptive preprocessing units and a neural network during the learning period. Application in EEG pattern recognition," *Neural Networks*, vol. 10, no. 6, pp. 1153–1163, 1997.
- [7] M. Zhenjiang and Y. Baozong, "Analysis and optimal design of continuous neural networks with applications to associative memory," *Neural Networks*, vol. 12, no. 2, pp. 259–271, 1999.
- [8] Z. Waszczyszyn and L. Ziemiański, "Neural networks in mechanics of structures and materials—new results and prospects of applications," *Computers and Structures*, vol. 79, no. 22–25, pp. 2261–2276, 2001.
- [9] A. Rawat, R. N. Yadav, and S. C. Shrivastava, "Neural network applications in smart antenna arrays: a review," *International Journal of Electronics and Communications*, vol. 66, no. 11, pp. 903–912, 2012.
- [10] O. Faydasicok and S. Arik, "Equilibrium and stability analysis of delayed neural networks under parameter uncertainties," *Applied Mathematics and Computation*, vol. 218, no. 12, pp. 6716–6726, 2012.
- [11] J. H. Park, "Further results on passivity analysis of delayed cellular neural networks," *Chaos, Solitons and Fractals*, vol. 34, no. 5, pp. 1546–1551, 2007.
- [12] J. C. Willems, "Dissipative dynamical systems. I. General theory," *Archive for Rational Mechanics and Analysis*, vol. 45, pp. 321–351, 1972.
- [13] B. Chen, H. Li, C. Lin, and Q. Zhou, "Passivity analysis for uncertain neural networks with discrete and distributed time-varying delays," *Physics Letters A: General, Atomic and Solid State Physics*, vol. 373, no. 14, pp. 1242–1248, 2009.
- [14] Y. Chen, W. Li, and W. Bi, "Improved results on passivity analysis of uncertain neural networks with time-varying discrete and distributed delays," *Neural Processing Letters*, vol. 30, no. 2, pp. 155–169, 2009.

- [15] J. Fu, H. Zhang, T. Ma, and Q. Zhang, "On passivity analysis for stochastic neural networks with interval time-varying delay," *Neurocomputing*, vol. 73, no. 4–6, pp. 795–801, 2010.
- [16] S. Xu, W. X. Zheng, and Y. Zou, "Passivity analysis of neural networks with time-varying delays," *IEEE Transactions on Circuits and Systems II: Express Briefs*, vol. 56, no. 4, pp. 325–329, 2009.
- [17] H.-B. Zeng, Y. He, M. Wu, and S.-P. Xiao, "Passivity analysis for neural networks with a time-varying delay," *Neurocomputing*, vol. 74, no. 5, pp. 730–734, 2011.
- [18] H. B. Zeng, Y. He, M. Wu, and H. Q. Xiao, "Improved conditions for passivity of neural networks with a time-varying delay," *IEEE Transactions on Cybernetics*, vol. 44, no. 6, pp. 785–792, 2014.
- [19] O. M. Kwon, M. J. Park, J. H. Park, S. M. Lee, and E. J. Cha, "Passivity analysis of uncertain neural networks with mixed time-varying delays," *Nonlinear Dynamics*, vol. 73, no. 4, pp. 2175–2189, 2013.
- [20] Y. Chen and W. X. Zheng, "Stability analysis of time-delay neural networks subject to stochastic perturbations," *IEEE Transactions on Cybernetics*, vol. 43, pp. 2122–2133, 2013.
- [21] A. Seuret and F. Gouaisbaud, "Wirtinger-based integral inequality: application to time-delay systems," *Automatica*, vol. 49, no. 9, pp. 2860–2866, 2013.
- [22] P. G. Park, J. W. Ko, and C. Jeong, "Reciprocally convex approach to stability of systems with time-varying delays," *Automatica*, vol. 47, no. 1, pp. 235–238, 2011.
- [23] S. H. Kim, P. Park, and C. K. Jeong, "Robust H_∞ stabilisation of networked control systems with packet analyser," *IET Control Theory and Applications*, vol. 4, no. 9, pp. 1828–1837, 2010.
- [24] M. C. de Oliveira and R. E. Skelton, "Stability tests for constrained linear systems," in *Perspectives in Robust Control*, pp. 241–257, Springer, Berlin, Germany, 2001.
- [25] K. Gu, "A further refinement of discretized Lyapunov functional method for the stability of time-delay systems," *International Journal of Control*, vol. 74, no. 10, pp. 967–976, 2001.
- [26] O. M. Kwon, J. H. Park, S. M. Lee, and E. J. Cha, "Analysis on delay-dependent stability for neural networks with time-varying delays," *Neurocomputing*, vol. 103, pp. 114–120, 2013.
- [27] S. Boyd, L. El Ghaoui, E. Feron, and V. Balakrishnan, *Linear Matrix Inequalities in System and Control Theory*, vol. 15 of *SIAM Studies in Applied Mathematics*, SIAM, Philadelphia, Pa, USA, 1994.
- [28] X. Liu and J. Cao, "Robust state estimation for neural networks with discontinuous activations," *IEEE Transactions on Systems, Man, and Cybernetics B, Cybernetics*, vol. 40, no. 6, pp. 1425–1437, 2010.
- [29] X. Liu and J. Cao, "On periodic solutions of neural networks via differential inclusions," *Neural Networks*, vol. 22, no. 4, pp. 329–334, 2009.
- [30] X. Liu, T. Chen, J. Cao, and W. Lu, "Dissipativity and quasi-synchronization for neural networks with discontinuous activations and parameter mismatches," *Neural Networks*, vol. 24, no. 10, pp. 1013–1021, 2011.
- [31] X. Liu, N. Jiang, J. Cao, S. Wang, and Z. Wang, "Finite-time stochastic stabilization for BAM neural networks with uncertainties," *Journal of the Franklin Institute*, vol. 350, no. 8, pp. 2109–2123, 2013.
- [32] X. Liu, J. Cao, and W. Yu, "Filippov systems and quasi-synchronization control for switched networks," *Chaos*, vol. 22, no. 3, Article ID 033110, 2012.
- [33] R. Lu, Y. Xu, and A. Xue, " H_∞ filtering for singular systems with communication delays," *Signal Processing*, vol. 90, no. 4, pp. 1240–1248, 2010.
- [34] R. Lu, H. Li, and Y. Zhu, "Quantized H_∞ filtering for singular time-varying delay systems with unreliable communication channel," *Circuits, Systems, and Signal Processing*, vol. 31, no. 2, pp. 521–538, 2012.
- [35] R. Lu, H. Wu, and J. Bai, "New delay-dependent robust stability criteria for uncertain neutral systems with mixed delays," *Journal of the Franklin Institute*, vol. 351, no. 3, pp. 1386–1399, 2014.
- [36] R. Lu, H. Su, J. Chu, and A. Xue, "A simple approach to robust d-stability analysis for uncertain singular delay systems," *Asian Journal of Control*, vol. 11, no. 4, pp. 411–419, 2009.
- [37] R. Lu, X. Dai, H. Su, J. Chu, and A. Xue, "Delay-dependant robust stability and stabilization conditions for a class of Lur'e singular time-delay systems," *Asian Journal of Control*, vol. 10, no. 4, pp. 462–469, 2008.
- [38] J. Sun, G. P. Liu, and J. Chen, "Delay-dependent stability and stabilization of neutral time-delay systems," *International Journal of Robust and Nonlinear Control*, vol. 19, no. 10, pp. 1364–1375, 2009.

Research Article

A Hybrid Intelligent Algorithm for Optimal Birandom Portfolio Selection Problems

Qi Li, Guo-Hua Cao, and Dan Shan

School of Economics and Business Administration, Chongqing University, Chongqing 400030, China

Correspondence should be addressed to Guo-Hua Cao; caoguohua@cqu.edu.cn

Received 4 May 2014; Accepted 31 May 2014; Published 16 June 2014

Academic Editor: He Huang

Copyright © 2014 Qi Li et al. This is an open access article distributed under the Creative Commons Attribution License, which permits unrestricted use, distribution, and reproduction in any medium, provided the original work is properly cited.

Birandom portfolio selection problems have been well developed and widely applied in recent years. To solve these problems better, this paper designs a new hybrid intelligent algorithm which combines the improved LGMS-FOA algorithm with birandom simulation. Since all the existing algorithms solving these problems are based on genetic algorithm and birandom simulation, some comparisons between the new hybrid intelligent algorithm and the existing algorithms are given in terms of numerical experiments, which demonstrate that the new hybrid intelligent algorithm is more effective and precise when the numbers of the objective function computations are the same.

1. Introduction

Portfolio theory was initially put forward by Markowitz [1] and has received great development since then. The main content of it is to study how to allocate one's capital to a large number of securities and the study mainly focuses on three aspects: the first is how to estimate the security return; the second is how to build portfolio models; the third is how to design efficient algorithms to solve these models. Many scholars have made great contributions in this field.

In the early literatures, security return was assumed to obey normal distribution. However, the following researches manifested that the assumption of normal distribution did not accord with the facts. Therefore, a lot of new distributions were used to describe the security return [2–9]. Among them, birandom distribution received great attention and development by some scholars [7–9] and literature [9] demonstrated that birandom distribution could reflect the features of securities' technical patterns and the investors' heterogeneity.

When the security return followed birandom distribution, the existing literatures established several birandom portfolio models and designed the corresponding hybrid intelligent algorithms [7–9]. However, all these algorithms were based on genetic algorithm (GA) and existed some

common shortcomings, such as low accuracy and inferior local search ability. To solve these birandom portfolio models effectively, this paper designs a new hybrid intelligent algorithm which integrates the improved LGMS-FOA algorithm and birandom simulation. The experimental results show that the new algorithm is more efficient.

The rest of this paper is organized as follows: Section 2 recalls some basic concepts about birandom theory; Section 3 provides an overview of birandom portfolio models; Section 4 presents a new hybrid intelligent algorithm which integrates the improved LGMS-FOA algorithm and birandom simulation; Section 5 provides numerical examples to test the effectiveness of the new hybrid intelligent algorithm; finally, a brief summary about this paper is given.

2. Birandom Theory

Definition 1. A birandom variable ε is a mapping from a probability space (Ω, A, \Pr) to a collection of random variables such that, for any Borel subset B of the real line R , the induced function $\Pr(\varepsilon(w) \in B)$ is a measurable function with respect to w [7].

Example 2. Let $\Omega = (\omega_1, \omega_2)$ (ω_1 represents security rising and ω_2 represents security falling) and $\Pr(\omega_1) = a$ and

$\Pr(\omega_2) = b$. Assume that ε is a function on (Ω, A, \Pr) as follows:

$$\varepsilon(\omega) = \begin{cases} \varepsilon_1 & \text{if } \omega = \omega_1 \\ \varepsilon_2 & \text{if } \omega = \omega_2, \end{cases} \quad (1)$$

where ε_1 and ε_2 follow uniform distribution; then ε is a birandom variable according to Definition 1.

Definition 3. Let $\varepsilon = (\varepsilon_1, \varepsilon_2, \dots, \varepsilon_n)$ be a birandom vector on (Ω, A, \Pr) , and let $f : R^n \rightarrow R^m$ be a vector-valued Borel measurable function. Then the primitive chance of birandom event characterized by $f(\varepsilon) \leq 0$ is a function from $(0, 1]$ to $[0, 1]$, defined as [8]

$$\begin{aligned} & \text{Ch} \{f(\varepsilon) \leq 0\}(\alpha) \\ &= \sup \{\beta \mid \Pr \{\omega \in \Omega \mid \Pr \{f(\varepsilon(\omega)) \leq 0\} \geq \beta\} \geq \alpha\}. \end{aligned} \quad (2)$$

Definition 4. Let ε be a birandom variable defined on the probability space (Ω, A, \Pr) . Then the expected value of birandom variable ε is defined as

$$\begin{aligned} E(\varepsilon) &= \int_0^\infty \Pr \{\omega \in \Omega \mid E[\varepsilon(\omega)] \geq t\} dt \\ &\quad - \int_{-\infty}^0 \Pr \{\omega \in \Omega \mid E[\varepsilon(\omega)] \leq t\} dt, \end{aligned} \quad (3)$$

provided that at least one of the above two integrals is finite [8].

3. Birandom Portfolio Models

In this section, we provide an overview of birandom portfolio models. Let x_i represent the investment proportion in security i and let k_i denote the return of the i th security for $i = 1, 2, \dots, n$, respectively. In particular, k_i follows birandom distribution for $i = 1, 2, \dots, n$. Depending on different measures of investment profit and risk, birandom portfolio models are divided into different types.

3.1. Birandom Safety-First Model. For each portfolio $x = (x_1, x_2, \dots, x_n)$, the chance that return of total asset (RTA) is no less than a disaster level is used to represent investment risk, which is given by

$$\text{Ch} \{x_1 k_1 + x_2 k_2 + \dots + x_n k_n \geq m\}(\beta_1) \geq a. \quad (4)$$

The chance that RTA is no less than some value is regarded to measure investment profit, which is represented by

$$\text{Ch} \{x_1 k_1 + x_2 k_2 + \dots + x_n k_n \geq t\}(\beta_2), \quad (5)$$

where m and t represent the disaster level and profit, respectively. β_1 , β_2 , and a represent the corresponding confidence level.

Using (4) and (5), we obtained the following Birandom safety-first model, which was proposed in [9]:

$$\begin{aligned} & \max \quad \text{Ch} \{x_1 k_1 + x_2 k_2 + \dots + x_n k_n \geq t\}(\beta_2) \\ & \text{s.t.} \quad \text{Ch} \{x_1 k_1 + x_2 k_2 + \dots + x_n k_n \geq m\}(\beta_1) \geq a \\ & \quad \sum_{i=1}^n x_i = 1 \\ & \quad x_i \geq 0 \quad i = 1, 2, \dots, n. \end{aligned} \quad (6)$$

3.2. Birandom Expected Value Model. In this model, investment risk was represented by (4) and the expect value of RTA was used to measure investment profit which was given by

$$E[x_1 k_1 + x_2 k_2 + \dots + x_n k_n]. \quad (7)$$

Based on (4) and (7), Birandom expect value model was proposed in [8], which was formulated as follows:

$$\begin{aligned} & \max \quad E[x_1 k_1 + x_2 k_2 + \dots + x_n k_n] \\ & \text{s.t.} \quad \text{Ch} \{x_1 k_1 + x_2 k_2 + \dots + x_n k_n \geq m\}(\beta_1) \geq a \\ & \quad \sum_{i=1}^n x_i = 1 \\ & \quad x_i \geq 0 \quad i = 1, 2, \dots, n. \end{aligned} \quad (8)$$

3.3. Birandom Chance-Constrained Model. Literature [7] proposed birandom chance-constrained model, which was listed as below:

$$\begin{aligned} & \max \quad \text{Ch} \{x_1 k_1 + x_2 k_2 + \dots + x_n k_n \geq t\}(\beta_2) \\ & \text{s.t.} \quad \sum_{i=1}^n x_i = 1 \\ & \quad x_i \geq 0 \quad i = 1, 2, \dots, n. \end{aligned} \quad (9)$$

Remark 5. The parameters of models (6), (8), and (9) have the same economic meaning.

Remark 6. For more details on these models, please refer to the corresponding literatures.

4. Hybrid Intelligent Algorithm

In this section, a new hybrid intelligent algorithm is designed to solve models (6), (8), and (9), where the improved LGMS-FOA algorithm and birandom simulation are used.

4.1. Birandom Simulation. Because of the uncertainty of birandom variable, we should use birandom simulation [10] to solve equations (4), (5), and (7).

Algorithm 1 (birandom simulation for (4)).

Step 1. Set $l = 1$.

Step 2. Generate w_1, w_2, \dots, w_N from Ω according to the probability Pr. Consider

$$w_i = \{y_1, y_2, \dots, y_n\}, \quad i = 1, 2, \dots, N. \quad (10)$$

Step 3. Compute the probability

$$\delta_i = \Pr \{x_1 k_1(y_1) + x_2 k_2(y_2) + \dots + x_n k_n(y_n) \geq m\},$$

$$i = 1, 2, \dots, N, \quad (11)$$

by stochastic simulation.

Step 4. Set N^* as the integer part of $\beta_1 N$.

Step 5. Return the N^* th largest element δ^* in $\{\delta_1, \delta_2, \dots, \delta_N\}$.

Step 6. If $\delta^* \geq a$, then $l = l + 1$; else $l = l + 0$.

Step 7. $l = 1$ means that the solution is feasible; $l = 0$ means that the solution is infeasible.

Algorithm 2 (birandom simulation for (5)).

Step 1. Generate w_1, w_2, \dots, w_N from Ω according to the probability Pr. Consider

$$w_i = \{y_1, y_2, \dots, y_n\}, \quad i = 1, 2, \dots, N. \quad (12)$$

Step 2. Compute the probability

$$\delta_i = \Pr \{x_1 k_1(y_1) + x_2 k_2(y_2) + \dots + x_n k_n(y_n) \geq t\},$$

$$i = 1, 2, \dots, N, \quad (13)$$

by stochastic simulation.

Step 3. Set N^* as the integer part of $\beta_2 N$.

Step 4. Return the N^* th largest element δ^* in $\{\delta_1, \delta_2, \dots, \delta_N\}$.

Algorithm 3 (birandom simulation for (7)).

Step 1. Set $e = 0$.

Step 2. Generate w_1, w_2, \dots, w_N from Ω according to the probability Pr. Consider

$$w_i = \{y_1, y_2, \dots, y_n\}, \quad i = 1, 2, \dots, N. \quad (14)$$

Step 3. Compute the probability

$$\delta_i = E [x_1 k_1(y_1) + x_2 k_2(y_2) + \dots + x_n k_n(y_n)],$$

$$i = 1, 2, \dots, N, \quad (15)$$

by stochastic simulation.

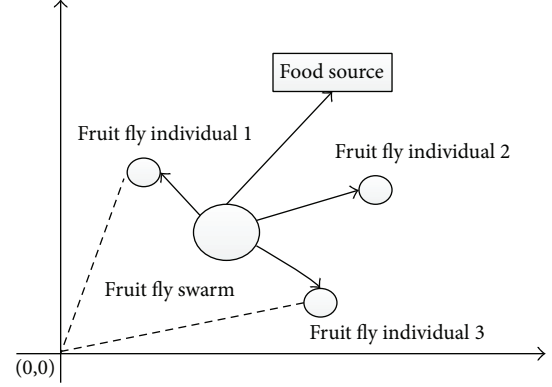


FIGURE 1: Food finding process of fruit fly swarm.

Step 4. Consider

$$e \leftarrow e + E [x_1 k_1(y_1) + x_2 k_2(y_2) + \dots + x_n k_n(y_n)]. \quad (16)$$

Step 5. Repeat the second to the fourth steps for N times.

Step 6. Consider

$$E [x_1 k_1 + x_2 k_2 + \dots + x_n k_n] = \frac{e}{N}. \quad (17)$$

4.2. The Improved LGMS-FOA. Recently, optimization algorithms are widely used in many fields [11–14]. Fruit fly optimization algorithm (FOA) is a new stochastic optimization technique proposed in 2012 [11] and has received rapid developments in recent years. The principle of FOA is based on the food finding behavior of fruit fly swarm. The food finding process was shown in Figure 1 and has two steps: first, it smells food and flies to that direction; then, it uses vision to find food.

To enhance the search ability of FOA, LGMS-FOA was proposed and had been proved to be an effective algorithm by numerical testing [12]. However, LMGS-FOA in the literature [12] is only applied to solve unconstrained optimization problems. To solve birandom portfolio models, the improved LGMS-FOA is proposed by means of combination of LGMS-FOA with penalty function method. Without loss of generality, we take model (6), for example, to introduce the improved LGMS-FOA. The steps of it are listed as follows.

Algorithm 4 (the improved LGMS-FOA).

Step 1. Parameters initialization.

The parameters include the number of iteration (maxgen), the population number (sizepop), the searching scope (r), the searching coefficient (d), the primary weight (w_0), and the weight adjustment coefficient (ρ).

Step 2. Initial fruit fly swarm location.

The fruit fly swarm location $x = (x_1, x_2, \dots, x_n)$ is randomly generated in the interval $[-r, r]$ and the searching scope becomes bigger with the increase of r .

Step 3. Give the random direction and distance for food finding of an individual fruit fly. Consider

$$\begin{aligned} x_p &= x + w \times d \times (2 \times \text{rand}(1, n) - 1), \\ P &= 1, 2, \dots, \text{sizepop}; \\ w &= w_0 \times \rho^{\text{gen}}. \end{aligned} \quad (18)$$

Step 4. Generate fruit fly swarm that fits the constraint $\sum_{i=1}^n y_i = 1$.

Step 4.1. A solution $y_p = (y_1, y_2, \dots, y_n)$ is represented by the individual fruit fly $x_p = (x_1, x_2, \dots, x_n)$, where the relation between y_p and x_p is formulated as follows:

$$y_i = \frac{x_i}{x_1 + x_2 + \dots + x_n}, \quad i = 1, 2, \dots, n, \quad (19)$$

which ensures that $\sum_{i=1}^n y_i = 1$.

Step 4.2. If the element of y_p is less than zero, repeat Step 4.1 until the number of individuals is *sizepop*.

Step 5. Calculate the smell concentration by inputting y_p into objective function.

Step 5.1. If $y_p = (y_1, y_2, \dots, y_n)$ satisfies

$$\text{Ch} \{y_1 k_1 + y_2 k_2 + \dots + y_n k_n \geq m\} (\beta_1) \geq a, \quad (20)$$

then let

$$\text{Smell}_i = \text{Ch} \{y_1 k_1 + y_2 k_2 + \dots + y_n k_n \geq t\} (\beta_2). \quad (21)$$

Step 5.2. If $y_p = (y_1, y_2, \dots, y_n)$ does not satisfy

$$\text{Ch} \{y_1 k_1 + y_2 k_2 + \dots + y_n k_n \geq m\} (\beta_1) \geq a, \quad (22)$$

then use penalty function method [13] and let

$$\text{Smell}_i = \text{Ch} \{y_1 k_1 + y_2 k_2 + \dots + y_n k_n \geq t\} (\beta_2) - b, \quad (23)$$

where b is a given positive integer.

Step 6. Find out the optimal individual among fruit fly swarm. Consider

$$[\text{best smell} \quad \text{best index}] = \max (\text{Smell}). \quad (24)$$

Step 7. Keep the optimal objective function value and the corresponding x coordinate; then the fruit fly swarm flies towards that location:

$$\begin{aligned} \text{Smell best} &= \text{best smell} \\ x &= x(\text{best index}). \end{aligned} \quad (25)$$

Step 8. Repeat Step 2 to Step 7 until termination condition is satisfied.

4.3. Hybrid Intelligent Algorithm. Through integrating the improved LGMS-FOA algorithm and birandom simulation, a new hybrid intelligent algorithm is built and the steps are listed as below.

Algorithm 5 (hybrid intelligent algorithm).

Step 1. Initialize N fruit fly individuals that satisfy the constraints.

Step 2. Calculate the objective function values for all fruit fly individuals by birandom simulation.

Step 3. Find out the optimal objective value.

Step 4. Keep the optimal objective value and the corresponding location of fruit fly individual.

Step 5. Repeat Step 2 to Step 5, until termination condition is satisfied.

5. Numerical Experiments

To test the effectiveness of the new hybrid intelligent algorithm, we compared it with the existing algorithm [7–9] through numerical examples.

5.1. Experimental Setup. Assume that the investor selects three securities represented by k_1 , k_2 , and k_3 . The security return follows the birandom distribution in Example 2 and the corresponding parameters of each security are shown in Table 1. Besides, the investor takes $t = 0.04$, $m = -0.06$, $\beta_1 = 0.7$, $\beta_2 = 0.5$, and $a = 0.6$; then, models (6), (8), and (9) satisfying the above parameters are changed into

$$\begin{aligned} \max \quad & \text{Ch} \{x_1 k_1 + x_2 k_2 + x_3 k_3 \geq 0.04\} (0.5) \\ \text{s.t.} \quad & \text{Ch} \{x_1 k_1 + x_2 k_2 + x_3 k_3 \geq -0.06\} (0.7) \geq 0.6 \\ & x_1 + x_2 + x_3 = 1 \\ & x_i \geq 0 \quad i = 1, 2, 3, \\ \max \quad & E[x_1 k_1 + x_2 k_2 + x_3 k_3] \\ \text{s.t.} \quad & \text{Ch} \{x_1 k_1 + x_2 k_2 + x_3 k_3 \geq -0.06\} (0.7) \geq 0.6 \\ & \sum_{i=1}^3 x_i = 1 \\ & x_i \geq 0 \quad i = 1, 2, 3, \end{aligned} \quad (26)$$

(27)

TABLE 1: The distributions of securities k_1 , k_2 , and k_3 .

Parameters	k_1	k_2	k_3
a_i ($i = 1, 2, 3$)	3/4	1/2	1/3
b_i ($i = 1, 2, 3$)	1/4	1/2	2/3
ε_{i1} ($i = 1, 2, 3$)	$U [0, 7\%]$	$U [0, 9\%]$	$U [0, 11\%]$
ε_{i2} ($i = 1, 2, 3$)	$U [-9\%, 0]$	$U [-11\%, 0]$	$U [-13\%, 0]$

TABLE 2: The optimal results of model (26).

Model	Algorithm	Optimal solution			Objective function
		x_1	x_2	x_3	
Model (26)	Algorithm 5	0.9996	0.0003	0.0001	0.4230
Model (26)	Algorithm 6	0.6854	0.2304	0.0842	0.0425
Model (26)	Algorithm 7	0.1562	0.6832	0.1606	0.0805

$$\begin{aligned}
& \max \quad \text{Ch} \{x_1 k_1 + x_2 k_2 + x_3 k_3 \geq 0.04\} (0.5) \\
& \text{s.t.} \quad \sum_{i=1}^3 x_i = 1 \\
& \quad \quad x_i \geq 0 \quad i = 1, 2, 3.
\end{aligned} \tag{28}$$

The parameters of Algorithm 5 are set up as follows.

- (1) The parameter of birandom simulation is $N = 2000$.
- (2) The parameters of the improved LGMS-FOA are $\text{maxgen} = 40$, $\text{sizepop} = 30$, $r = 40$, $d = 20$, $w_0 = 1$, and $\rho = 0.8$.

To show the efficiency of Algorithm 5, we choose two sets of parameters and the corresponding hybrid intelligent algorithms in [7, 8] which are named as Algorithms 6 and 7.

The parameters of Algorithm 6 are listed as below.

- (1) The parameter of birandom simulation is $N = 2000$.
- (2) The parameters of GA are as follows: the iteration number is 40, the population is 30, the mutation probability is 0.6, and the crossover probability is 0.1.

The parameters of Algorithm 7 are given as follows.

- (1) The parameter of birandom simulation is $N = 2000$.
- (2) The parameters of GA are as follows: the iteration number is 40, the population is 30, the mutation probability is 0.8, and the crossover probability is 0.05.

Remark 5. For Algorithms 5 to 7, the numbers of objective function computations are the same and this can ensure the fairness of comparisons.

5.2. Experimental Results. Compute models from (26) to (28) by using Algorithms from 5 to 7, respectively, and repeat the experiments for 20 times. The average values of the optimal results are shown in Tables 2, 3, and 4.

From Tables 2 to 4, it can be found that the final searching quality of Algorithm 5 is better than Algorithms 6 and 7. So it can be concluded that the new hybrid intelligent algorithm is more efficient and precise than the existing algorithms when the numbers of objective function computations are the same.

TABLE 3: The optimal results of model (27).

Model	Algorithm	Optimal solution			Objective function
		x_1	x_2	x_3	
Model (27)	Algorithm 5	0.9832	0.0043	0.0125	0.0159
Model (27)	Algorithm 6	0.6818	0.2948	0.0234	0.0071
Model (27)	Algorithm 7	0.6057	0.2634	0.1309	0.0062

TABLE 4: The optimal results of model (28).

Model	Algorithm	Optimal solution			Objective function
		x_1	x_2	x_3	
Model (28)	Algorithm 5	0.0005	0.9987	0.0008	0.5367
Model (28)	Algorithm 6	0.0908	0.8339	0.0753	0.3382
Model (28)	Algorithm 7	0.1221	0.8703	0.0076	0.4052

6. Conclusion

To solve birandom portfolio selection problems better, this paper designs a new hybrid intelligent algorithm which integrates the improved LGMS-FOA algorithm and birandom simulation. Comparisons between the new hybrid intelligent algorithm and the existing algorithms show that the new hybrid intelligent algorithm is more effective and precise when the numbers of the objective function computations are the same.

Conflict of Interests

The authors declare that there is no conflict of interests regarding the publication of this paper.

Acknowledgment

This paper is supported by the National Natural Science Foundation of China (Grant no. 71232004).

References

- [1] H. Markowitz, "Portfolio selection," *The Journal of Finance*, vol. 7, no. 1, pp. 77–91, 1952.
- [2] B. Gray and B. Hollified, "When will mean-variance efficient portfolio be well diversified?" *The Journal of Finance*, vol. 47, no. 5, pp. 1785–1809, 1992.
- [3] M. Linden, "A model for stock return distribution," *International Journal of Finance & Economics*, vol. 6, no. 2, pp. 159–169, 2001.
- [4] A. B. Romanovsky, "On version state recovery and adjudication in class diversity," *Computer Systems Science and Engineering*, vol. 17, no. 3, pp. 159–168, 2002.
- [5] F. Jian-Qiang and W. Fu-Xin, "A research on return distribution function of chinese stock-market," *Chinese Journal of Management Science*, vol. 11, pp. 82–90, 2007.
- [6] D. Da-Yong and J. Wei-Dong, "A subjective model of the distribution of returns and empirical analysis," *Chinese Journal of Management Science*, vol. 15, pp. 112–120, 2007.

- [7] L. Mei-Yan, "Chance-constrained portfolio selection with birandom returns," *Modern Applied Science*, vol. 3, no. 4, pp. 161–165, 2009.
- [8] L. Mei-Yan, "One type of optimal portfolio selection in birandom environments," *Modern Applied Science*, vol. 3, no. 6, pp. 121–126, 2009.
- [9] G.-H. Cao and D. Shan, "The effect of exit strategy on optimal portfolio selection with birandom returns," *Journal of Applied Mathematics*, vol. 2013, Article ID 236579, 6 pages, 2013.
- [10] J. Peng and B.-D. Liu, "Birandom variables and birandom programming," *Computers and Industrial Engineering*, vol. 53, no. 3, pp. 433–453, 2007.
- [11] W. T. Pan, "A new fruit fly optimization algorithm: taking the financial distress model as an example," *Knowledge-Based Systems*, vol. 26, pp. 69–74, 2012.
- [12] D. Shan, G.-H. Cao, and H.-J. Dong, "LGMS-FOA: an improved fruit fly optimization algorithm for solving optimization problems," *Mathematical Problems in Engineering*, vol. 2013, Article ID 108768, 9 pages, 2013.
- [13] X. He, C. Li, T. Huang, C. J. Li, and J. Huang, "A recurrent neural network for solving bilevel linear programming problem," *IEEE Transactions on Neural Networks and Learning Systems*, vol. 25, no. 4, pp. 824–830, 2014.
- [14] X. He, C. Li, T. Huang, and C. J. Li, "Neural network for solving convex quadratic bilevel programming," *Neural Networks*, vol. 51, pp. 17–25, 2014.

Research Article

Energy Efficient Multiresource Allocation of Virtual Machine Based on PSO in Cloud Data Center

An-ping Xiong^{1,2} and Chun-xiang Xu¹

¹ Department of Computer Science and Engineering, University of Electronic Science and Technology, Chengdu 610054, China

² Department of Computer Science and Technology, Chongqing University of Posts and Telecommunications, Chongqing 400065, China

Correspondence should be addressed to An-ping Xiong; xiongap@cqupt.edu.cn

Received 3 March 2014; Accepted 26 May 2014; Published 12 June 2014

Academic Editor: Qinggang Meng

Copyright © 2014 A.-p. Xiong and C.-x. Xu. This is an open access article distributed under the Creative Commons Attribution License, which permits unrestricted use, distribution, and reproduction in any medium, provided the original work is properly cited.

Presently, massive energy consumption in cloud data center tends to be an escalating threat to the environment. To reduce energy consumption in cloud data center, an energy efficient virtual machine allocation algorithm is proposed in this paper based on a proposed energy efficient multiresource allocation model and the particle swarm optimization (PSO) method. In this algorithm, the fitness function of PSO is defined as the total Euclidean distance to determine the optimal point between resource utilization and energy consumption. This algorithm can avoid falling into local optima which is common in traditional heuristic algorithms. Compared to traditional heuristic algorithms MBFD and MBFH, our algorithm shows significantly energy savings in cloud data center and also makes the utilization of system resources reasonable at the same time.

1. Introduction

With the fast development of cloud computing [1, 2], energy consumption is significantly increasing along with the explosive growth of cloud data center. Many reports have shown that computers consume more than 8% of the total energy produced [3], which becomes an escalating threat to the environment. In this situation, high-level energy efficiency in cloud data center is widely studied to reduce energy consumption by researchers all over the world.

There are two reasons which resulted in high energy consumption in cloud data center: one is rapid increasing of computers as well as the number of cloud users, which results in a significant amount of energy consumed by cloud data center due to their massive sizes [4, 5]; another reason is that resources allocation is not reasonable in cloud computing. Resources (such as CPU, disk, memory, and bandwidth) allocation becomes a key problem which needs to be resolved, as unreasonable resources allocation can cause more energy consumption in cloud data center [6–12]. Because resources allocation algorithm with high energy efficiency can greatly reduce the energy consumption, it has been widely studied in the field of cloud computing.

There are three broad goals in the problem of energy efficient resources studies [3]: (1) reduce in quality of service reasonable and minimize energy consumption; (2) given a total energy, maximize the performance; (3) make the performance and energy objectives simultaneously met. To be of practical importance, resources allocation in cloud data center is not only to reduce energy consumption but also to satisfy Quality of Service requirements or Service Level Agreements [12]. In cloud data center, virtualization technology plays an important role to satisfy the requirements of both energy and Quality of Service. Several servers are allowed to be consolidated to one physical node as virtual machine (VMs) by virtualization. This technology can greatly enhance the utilization of resources in applications [13, 14]. VMs allocation in cloud data center is generally viewed as a multidimensional bin packing problem with variable bin sizes and prices. The problem of determining optimal VMs allocations is NP-complete [15], and getting optimal resolution of VMs allocations is often computationally infeasible when the cloud computing has multiple hosts and customers [16].

A lot of researches have been done in energy efficient VMs allocations in cloud data center [7–12, 17, 18]. Many

heuristics policies such as Best Fit [12, 17], Best Fit Decrease (BFD) [7–10], and Modified Best Fit Decreasing (MBFD) [11] have been studied to find the approximate resolution for VMs allocations. Beloglazov et al. modified the Best Fit Decrease (BFD) algorithm and suggested a Modified Best Fit Decreasing (MBFD) algorithms [12, 19]. The solution which produces the least increase of energy consumption was found after VMs were sorted in decreasing order of their current CPU utilizations. This algorithm is implemented at heterogeneous hosts and VMs. However, the algorithms above only consider the energy efficiency of the CPU, rather than other resources such as disk, memory, and bandwidth. Once multiple resources in cloud data center are considered, the multidimensional bin packing problem tends to be more complicated. When resource requirements of VMs increase quickly, it is necessary to preserve free resources for hosts for preventing SLA violation. To satisfy the Quality of Service, some researchers set an upper utilization threshold for hosts and keep the total utilization of CPU below this threshold [12, 19]. Srikantaiah et al. study the relationship between energy consumption and resource utilization which focuses on two kinds of resource: CPU and disk, while a modified best fit heuristic algorithm [20, 21] (hereafter referred to as MBFH) is utilized for allocation. Note that here VMs are not sorted in decreasing order of current utilization in this MBFH. While keeping performance requirements satisfied, the authors analyse the utilizations of CPU and storage to minimize energy consumption in heterogeneous data center. As a result, the authors find the optimal balance between resource utilization and energy metrics reside around 50% on the CPU and 70% storage usage [20]. Inspired by the experimental results, the goal of energy conservation can be achieved via keeping the utilization of resource in an optimal utilization level. To minimize the total energy consumption, the number of active nodes should be reduced and the idle nodes should be turned off.

Although the traditional heuristic algorithms may find a solution for VMs allocations for energy efficiency, they are easy to fall into local optimal solutions [7–12]. Other choices to solve the multidimensional bin packing problem include genetic algorithm (GA) and particle swarm optimization (PSO) algorithm. GA is adaptive heuristic search algorithm premised on the evolutionary ideas of natural selection and genetic [22, 23], while particle swarm optimization (PSO) is a population based stochastic optimization technique developed by Eberhart and Kennedy in 1995, inspired by social behaviour of bird flocking or fish schooling [22–24]. However, many studies illustrated that PSO algorithm is able to get the better solution than GA in distributed system and grid computing [25, 26]. The PSO algorithm also converges faster than GA [25]. So particle swarm optimization is a feasible algorithm to optimize the multiresources energy efficient allocations in cloud data center.

In this paper, we focus on the virtual machine (VM) with multiresources allocation in cloud data center. A multiresource energy efficiency VMs allocation model is proposed. Based on the model and the particle swarm optimization (PSO), a multiresource energy efficiency based on particle swarm optimization (MREE-PSO) algorithm is designed and

applied to VMs allocation for energy efficiency in cloud data center. This algorithm can be divided into three parts: (1) particles are generated by FF (First Fit) algorithm; (2) the trust function of individual optimal solution and the global optimal solution of particles were defined to guide particle evolution; (3) the fitness function of PSO is defined as the total Euclidean distance which represents the optimal balance between resource utilization and energy consumption. This algorithm can deal with multiresources energy efficient allocations in cloud data center. It avoids falling into local optimal solution which is the disadvantage of traditional heuristic algorithm simulation. Compared to two important traditional heuristic algorithms MBFD [11, 12, 19] and MBFH [20, 21], the MREE-PSO algorithm shows closer to the optimal solution for the efficiency of system, and it also makes the utilization of system resources reasonable in cloud data center. The main contribution of this study: (1) PSO is introduced in VM allocation algorithms; (2) a multiresource energy efficiency VMs allocation model is proposed; (3) competitive analysis of dynamic VM allocation algorithms is shown.

The remainder of this paper is structured as follows. In Section 2, we review the related works about energy efficient VMs allocation. In Section 3, we provide a multiresource energy efficiency model. In Section 4, an energy efficient VMs allocation algorithm is designed based on particle swarm optimization (PSO). Section 5 provides the experimental simulation and evaluation with software tools CloudSim. Section 5 concludes the paper.

2. Related Works

Energy efficiency which is addressed by several researchers recently is one of the most important research issues. Such as the work of Ahmad about energy efficiency, system performance and energy consumption were firstly simultaneously optimized by game theoretical methodologies in large scale computing systems [3]. Then, a lot of researches have been done in energy efficiency models [4–8]. Energy efficiency is a mix of research issues related to large scale computing systems especially cloud computing.

In cloud data center, one of the most crucial research problems is the energy efficiency of cloud computing [6–10]. Some hardware and software technologies have been developed to reduce energy consumption to a certain degree in cloud data center, for example, energy efficient computer monitors, low-power CPUs, scheduling and resource allocation, task consolidation, and so on.

Virtualization technologies are a key component within task consolidation approach [13, 14]. Virtualization, in cloud computing, refers to the act of creating a virtual machine (VM). The main objection of virtualization technologies is improving the utilization of resources. In cloud data center, several servers are allowed to be consolidated to one physical node as virtual machine (VMs) by virtualization; several virtual machines (VMs) are also run on a single physical node.

Many works have been developed in energy efficient VMs allocations recently. among these works, the researches of Srikantaiah et al. [20] and Beloglazov et al. [11, 12, 19] focus on traditional heuristic algorithms in energy efficient virtual machines (VMs) allocations.

Srikantaiah et al. have studied the relationship between energy consumption and resource utilization which focuses on CPU and disk to minimize energy consumption. In this work, the authors explored the impact of workload consolidation on the energy-per-transaction depending on both the CPU and disk utilization. A modified best fit heuristic algorithm (MBFH) [20] was been proposed to achieve energy efficient virtual machines (VMs) allocation. The algorithm contains two steps: (1) find the optimal balance between resource utilization and energy metrics residing around 50% on the CPU and 70% storage usage; (2) the Euclidean distance between the current selection and the optimal point within each server was been used in the energy efficient resource allocation [20].

Beloglazov et al. modified the Best Fit Decrease (BFD) algorithm and suggested a Modified Best Fit Decreasing (MBFD) algorithm [11, 12, 19]. In this work, the authors sort all virtual machines (VMs) in decreasing order of their current CPU utilizations and allocate each virtual machine (VM) to a physical node which provides the least increase of energy consumption. The Flowchart for the algorithm is shown in Figure 1. In MBFD algorithm, all VMs are sorted in decreasing order of current utilization. Then each VM is allocated to a host that provides the least increase of power consumption due to this allocation. The complexity of MBFD algorithm is $n * m$, where n is the number of VMs and m is the number of hosts.

3. Multiresources Energy Efficient Allocation Model

In cloud data center, multiresources allocation problem can be described as a multidimensional bin packing problem with variable bin sizes and prices. Suppose that N is the number of VMs that should be allocated, M is the number of hosts in cloud data center, the search space of heuristic algorithm is M^N , and the problem of computing optimal VMs allocations is NP-complete [15].

The aim of allocation is to find the optimal energy efficient solution. Inspired by the study of Srikantaiah et al. [20], the consolidation status of multiresources significantly impacts the energy efficiency of the whole data center. Keeping the utilization of each resource in an optimal utilization level can achieve optimal energy conservation. Here, we define a total Euclidean distance δ as follows:

$$\delta = \sum_{i=1}^n \sqrt{\sum_{j=1}^d (u_j^i - ubest_i)^2}, \quad (1)$$

where d is the dimension which denotes kinds of resources, such as CPU, disk, memory, and bandwidth and n denotes the number of hosts in cloud data center. u_j^i is the utilization for host j and the resource i , $ubest_i$ is the best utilization

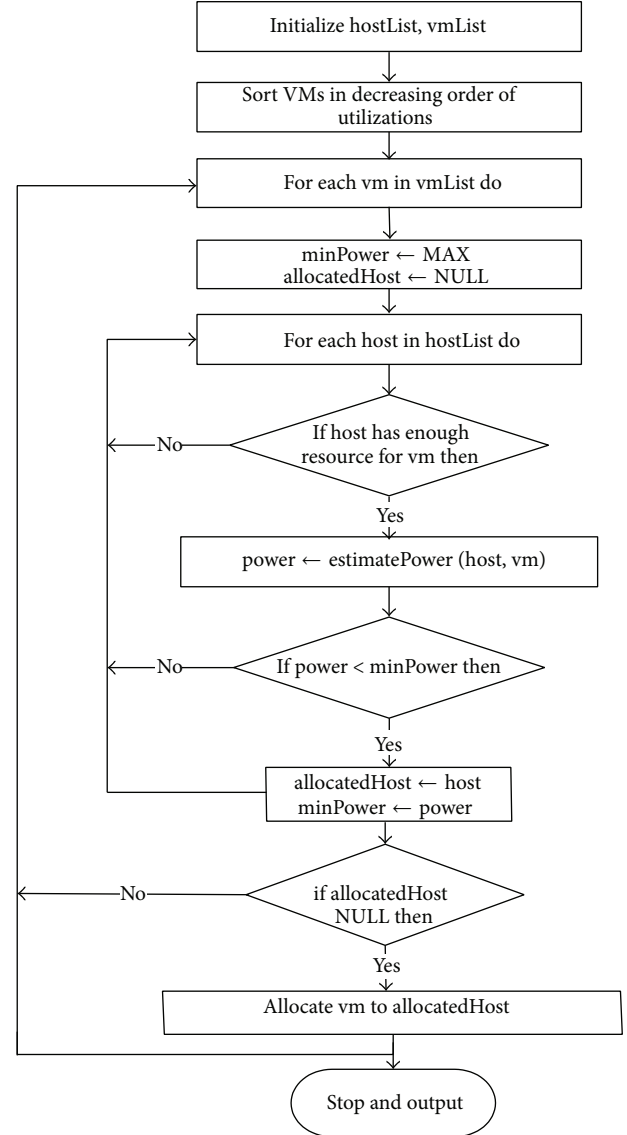


FIGURE 1: Flowchart of modified Best Fit Decreasing (MBFD) algorithm.

for u_j^i energy efficient, and each kind of resource has its best value of utilization, such as 50% CPU and 70% storage usage, which is an important experimental result from the study of Beloglazov et al. [11, 12, 19].

The total Euclidean distance δ denotes the optimal balance between multiresources utilization and energy consumption. Minimizing the total Euclidean distance δ will get optimal energy efficiency in the whole system. In this situation, the multiresources energy efficiency model is described as follows:

$$\text{objection: } \min \delta \quad (2)$$

$$\text{constraints: } x_h^j = 0$$

$$\sum_h x_h^j = 1, \quad \forall j, \quad (3)$$

where $x_h^j = 1$ denotes virtual machine VM j allocated to node h ; $x_h^j = 0$ denotes VM j not allocated to node h . And the expression (3) denotes that each VM can be allocated to only one node.

In order to satisfy the limitations, each resource must satisfy the following inequality constraints as follows:

$$\begin{aligned} \sum_j r_j^{\text{CPU}} * x_h^j &\leq c_h^{\text{CPU}}, & \sum_j r_j^{\text{RAM}} * x_h^j &\leq c_h^{\text{RAM}} \\ \sum_j r_j^{\text{BW}} * x_h^j &\leq c_h^{\text{BW}}, & \sum_j r_j^{\text{DISK}} * x_h^j &\leq c_h^{\text{DISK}}. \end{aligned} \quad (4)$$

In expression (4), $r_j^{\text{CPU}}, r_j^{\text{RAM}}, r_j^{\text{BW}}, r_j^{\text{DISK}}$ denotes the demand of CPU, memory, bandwidth, and disk for VM j , respectively; likewise, $c_h^{\text{CPU}}, c_h^{\text{RAM}}, c_h^{\text{BW}}, c_h^{\text{DISK}}$, respectively, denotes the capacity of these resources for VM j . If there are multiple VMs allocated on node h , the total resources demand of VMs should be smaller than the capacity of node h .

4. Allocation Algorithm Design and Implement Based on PSO

It has been successful to apply PSO in many applications and research areas [22, 24–26]. The particles of PSO constitute a swarm moving around in the search space looking for the best solution.

In this section, we design and implement a MREE-PSO algorithm to reduce energy consumption for virtual machine allocation, and this algorithm can deal with multiple resources in cloud data center.

4.1. Particle Swarm Optimization (PSO) Algorithm. Particle swarm optimization (PSO) is a population developed by Eberhart and Kennedy in 1995 based on stochastic optimization technique [22–24]. Social behavior of organisms motivated them to look into the effect of collaboration of species onto achieving their goals as a group, such as fish schooling and bird flocking. PSO has been widely applied in many applications and research areas in past several years. Compared with other methods such as GA, it is proved that PSO gets better results in a cheaper and faster way.

In PSO, the potential solutions are called particles which fly through the solution space by following the current optimum particles. Particles keep part of their previous state because they have memory. All particles preserve their individuality in any case, although they share the same point in belief space with no restriction. PSO algorithm evolves the position of each particle in problem space using (5). Each particle has an initial random velocity, and particle's movement is influenced by two randomly weighted factors: individuality and sociality. Individuality is defined as the tendency to return to the particle's best previous position and sociality is defined as the tendency to move towards the neighborhood's best previous position. At each time step, the particle swarm optimization changes the velocity of each particle toward its $pbest$ and $gbest$ locations. Acceleration is

TABLE 1: Parameters and the mean of parameters.

Parameters	Mean of parameters
v_i^t	Velocity of particle i at iteration t
x_i^t	Position of particle i at iteration t
w	Inertia weight
c_1, c_2	Acceleration coefficients
ψ_1, ψ_2	Random number between 0 and 1
$pbest_i$	Best position of particle i
$gbest$	Best position of entire particles in a population

weighted by a random term, with separate random numbers being generated for acceleration toward $pbest$ and $gbest$ locations. Additionally, particle swarm optimization is an approach which can be used for specific applications focused on a specific requirement. Particle swarm optimization is widely used because there are few parameters to adjust. The parameters and their mean of parameters are shown in Table 1.

Consider

$$\begin{aligned} v_i^{t+1} &= w \cdot v_i^t + c_1 \cdot \psi_1 \cdot (pbest_i - x_i^t) + c_2 \cdot \psi_2 \cdot (gbest - x_i^t) \\ x_i^{t+1} &= x_i^t + v_i^t. \end{aligned} \quad (5)$$

4.2. Particles Definition. Suppose that n is the number of VMs that should be allocated and m is the number of hosts in cloud data center. The position vector of particles is defined as $X_i^t = (x_{i1}^t, x_{i2}^t, \dots, x_{ij}^t, \dots, x_{im}^t)$, where t is the iteration number, i denotes the i th possible solution, and j is the serial number of VM. For example, if $X_i^t = (x_{i1}^t, x_{i2}^t, x_{i3}^t) = (1, 2, 1)$, it means that VM 1,2,3 is, respectively, allocated to node 1,2,1. While particles are updating, the position vector of particles X_i^t will transfer to a $m \times n$ (0,1)-matrix XX_i^t :

$$XX_i^t = \begin{bmatrix} s_{11}^t & s_{12}^t & \dots & s_{1h}^t & \dots & s_{1n}^t \\ s_{21}^t & s_{22}^t & \dots & s_{2h}^t & \dots & s_{2n}^t \\ \vdots & \vdots & & \vdots & & \vdots \\ s_{j1}^t & s_{j2}^t & \dots & s_{jh}^t & \dots & s_{jn}^t \\ \vdots & \vdots & & \vdots & & \vdots \\ s_{m1}^t & s_{m2}^t & \dots & s_{mh}^t & \dots & s_{mn}^t \end{bmatrix}. \quad (6)$$

If VM j is allocated to node h at iteration t , $s_{jh}^t = 1$; if not, $s_{jh}^t = 0$. One VM can be allocated to only one node, so there is a limitation for s_{jh}^t as below:

$$\sum_{h=1}^n s_{jh}^t = 1, \quad \forall j \in \{1, 2, \dots, m\}. \quad (7)$$

4.3. Position Update. At iteration t of our MREE-PSO algorithm, $Pbest_l^t = (pbest_{l1}^t, pbest_{l2}^t, \dots, pbest_{lj}^t, \dots, pbest_{lm}^t)$ is the personal best of particle l . Each particle keeps track of its coordinates in the solution space which are associated with the best solution (fitness) that has achieved so far by that

particle. And $Gbest^t = (gbest_1^t, gbest_2^t, \dots, gbest_j^t, \dots, gbest_m^t)$ is the best value obtained so far by any particle.

Suppose that the probability that VM j is allocated to node h is 0.5 at iteration $t + 1$; then $P(s_{jh}^{t+1} = 1) = P(s_{jh}^{t+1} = 0) = 0.5$. p_p and p_g , respectively, represents the fitness of personal and global best. That means the probability of finding the best solution. For easy description, we can introduce two parameters k_1 and k_2 . According to the Bayesian formula, we can get the following:

$$\begin{aligned}
 P(s_{jh}^{t+1} = 1 \mid pbest_{jh}^t = 1, gbest_{jh}^t = 1) &= \frac{p_p * p_g}{p_p * p_g + (1 - p_p)(1 - p_g)} = k_1 \\
 P(s_{jh}^{t+1} = 0 \mid pbest_{jh}^t = 1, gbest_{jh}^t = 1) &= \frac{(1 - p_p) * (1 - p_g)}{p_p * p_g + (1 - p_p)(1 - p_g)} = 1 - k_1 \\
 P(s_{jh}^{t+1} = 1 \mid pbest_{jh}^t = 1, gbest_{jh}^t = 0) &= \frac{p_p * (1 - p_g)}{p_p * (1 - p_g) + p_p * (1 - p_g)} = k_2 \\
 P(s_{jh}^{t+1} = 0 \mid pbest_{jh}^t = 1, gbest_{jh}^t = 0) &= \frac{p_g * (1 - p_p)}{p_p * (1 - p_g) + p_g * (1 - p_p)} = 1 - k_2.
 \end{aligned} \tag{8}$$

In (8), the probabilities of personal and global best should be better than average probability, so $0.5 < p_p < 1$, $0.5 < p_g < 1$. To avoid falling into local optimal solution, let $p_g < p_p$; then $0.5 < p_g < p_p < 1$. In our paper, we set the parameters as $p_p = 0.8$, $p_g = 0.7$, and $k_1 = 0.9$, $k_2 = 0.7$.

The positions of particles are updated as follows:

```

r = rand ();
if (pbestjht = 1 and gbestjht = 1) then
    if (r < k1) sjht+1 = 1 else sjht+1 = 0;
else if (pbestjht = 0 and gbestjht = 0) then
    if (r < 1 - k1) sjht+1 = 0 else sjht+1 = 1;
else if (pbestjht = 1 and gbestjht = 0) then
    if (r < k2) sjht+1 = 1 else sjht+1 = 0;
else
    if (r < 1 - k2) sjht+1 = 1 else sjht+1 = 0;

```

According the objective of VMs allocation, the fitness function is defined as a total Euclidean distance δ as seen in formula (1).

4.4. Algorithm Description. A flowchart of the energy efficient allocation algorithm based on PSO is shown in Figure 2. In this algorithm, there are four main steps which are explained as follows.

- (1) Initialize particles: generate N sequences of VMs at random. For each sequence, the VM is allocated to the node by First Fit algorithm which can supply the resources at the first time. Get N particles constituted a swarm.
- (2) Evaluate fitness for each particle: initialize the particle's $pbest$ and $gbest$ position to its initial position.
- (3) Update velocities and positions of particles: if all particles meet the constrains along with formulas (4) and (7), then update the particles. Otherwise, all particles cannot be updated. For VM j , while $\sum_{h=1}^n s_{jh}^t > 1$, it has been allocated to more than one node; while $\sum_{h=1}^n s_{jh}^t = 0$, it has not been allocated to any node.
- (4) If the iteration number is larger than the maximum, stop; otherwise, go to the second step.

5. Simulation and Performance Tests

5.1. Environment and Setting. The energy efficient multi-resources virtual machine allocation algorithm (MREE-PSO) has been evaluated by simulation using CloudSim toolkit [27] which supports user-defined policies for allocation of hosts to virtual machine and policies for allocation of host resources to virtual machine. CloudSim [27] is a framework for modeling and simulation of cloud computing infrastructures and services. It has been widely used to evaluate algorithms, applications, and policies before actual development of cloud products.

The following steps are required in the process of this experiment: parameters setting, programming in CloudSim, and performance evaluating. We evaluated the performance of our MREE-PSO with two important traditional heuristic algorithms: MBFD [11, 12, 19] and MBFH [20, 21] method in the same data center.

We simulate a data center that comprises 100 heterogeneous physical nodes. Half of these physical nodes are HP ProLiant ML110 G4 servers, and the others are HP ProLiant ML110 G5 servers. Each node is characterized by the CPU performance defined in Millions Instructions Per Second (MIPS), the MIPS of the HP ProLiant ML110 G4 and G5 server is 1860 and 2260, respectively. The storages of two kinds of servers are 640 GB and 1000 GB. The number of VMs ranges from 10 to 100. As seen in formula (1), let $d = 2$, $ubest_1 = 0.5$, and $ubest_2 = 0.7$ in our simulations.

In order to test the energy efficiency of the proposed algorithm in complicated environment, the simulated data center comprises different number of physical nodes. The nodes are modeled to have four classes of parameters as shown in Table 2.

Each parameter of virtual machine is initialized at random within a certain range according to the reference [20]: CPU (60~150), DISK (100~200), RAM (40~200), and BW

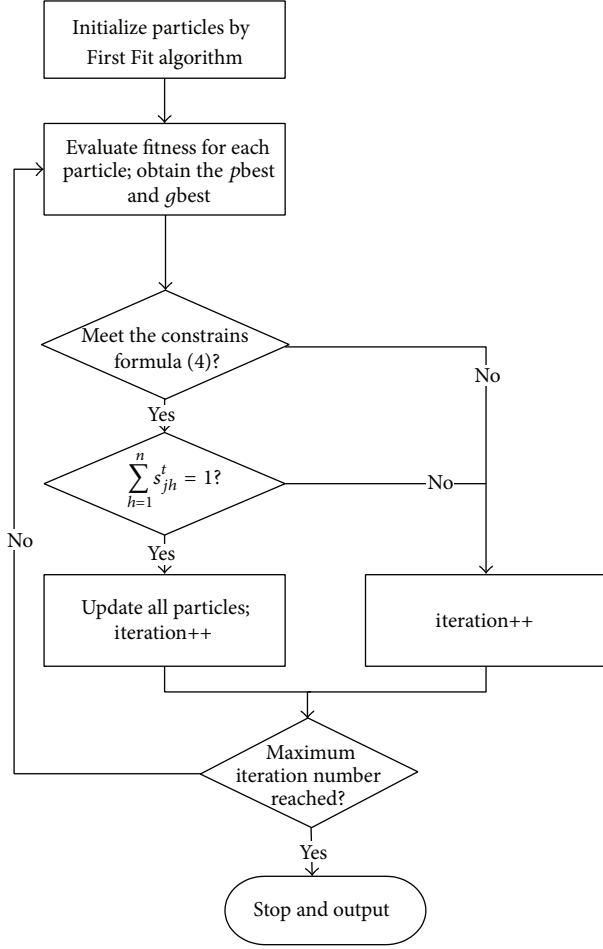


FIGURE 2: Flowchart of the energy efficient allocation algorithm based on PSO.

TABLE 2: Parameters for physical nodes.

Serial number	CPU (MIPS)	RAM (MB)	BW (MBPS)	DISK (GB)
1	600	2048	1000	1000
2	600	2048	2000	250
3	600	4096	1000	250
4	800	4096	1000	250

(30~100). We assume that the size of the group of particle is 20 and the maximum iteration number is 30. Repeat each simulation 10 times and get the average values.

5.2. Analysis of the Total Euclidean Distance. In this simulation, the total Euclidean distance is calculated by formula (1). To achieve an optimal energy conservation in cloud data center, the best value of utilization of each kind of resource should be set. Srikantaiah et al. [20] found the optimal balance between resource utilization and energy metrics residing around 50% on the CPU and 70% storage usage [10]. Based on this important result, we focus on the kinds of resource: CPU and disk. Our MREE-PSO algorithm

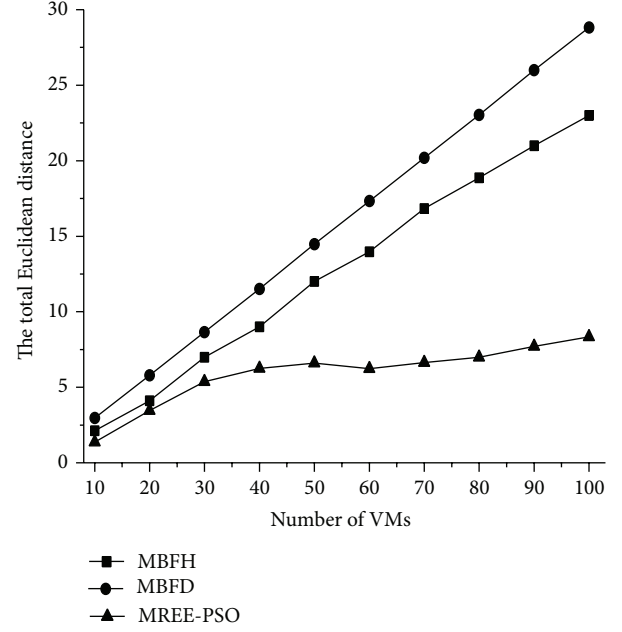


FIGURE 3: Comparison of the total Euclidean distance.

was performed using two important traditional heuristic algorithms MBFD [11, 12, 19] and MBFH [20, 21] method for comparison.

As shown in Figure 3, the total Euclidean distance increases with the number of virtual machines. However, the total Euclidean distance is lower for MREE-PSO; it also increases more slowly with increasing the number of virtual machines. Especially, while the number of virtual machines increases from 50 to 100, the total Euclidean distance of MREE-PSO does not increase too much. It is seen that the total Euclidean distance varies almost linearly for the traditional heuristic algorithms: MBFD [11, 12, 19] and MBFH [20, 21] method. The total Euclidean distance denotes the energy consumption, so the energy efficiency of MREE-PSO is always higher than MBFD [11, 12, 19] and MBFH [20, 21] with the same number of virtual machines.

5.3. Analysis of Resources Utilization. The resources utilizations are plotted in Figures 4 and 5. In each case, the resources utilizations of MREE-PSO are better than MBFD [11, 12, 19] and MBFH [20, 21] method. While the number of virtual machines increases from 10 to 40, the utilizations of CPU and disk are kept in a low level. But from 40 to 100, the resources utilizations of our method increase a lot with increasing number of virtual machines. When the number of virtual machines arrives at 100, the utilizations of CPU and disk, respectively, can increase to 45% and 65%. They are closed to the best value of utilization which is the optimal balance between resource utilization and energy consumption found by Srikantaiah et al. [20]. This will be helpful to enhance the energy efficiency of cloud data center.

The usage of the physical nodes was also investigated with these three algorithms. The results are shown in Figure 6. It is seen that usage of the physical nodes increases more

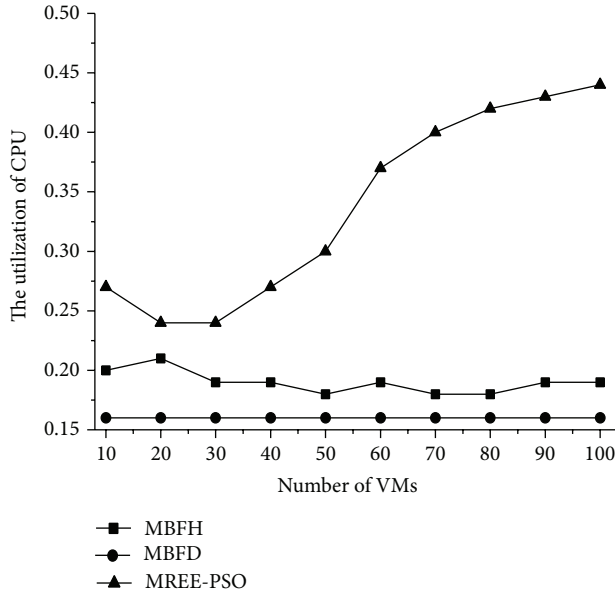


FIGURE 4: Comparison of CPU utilization.

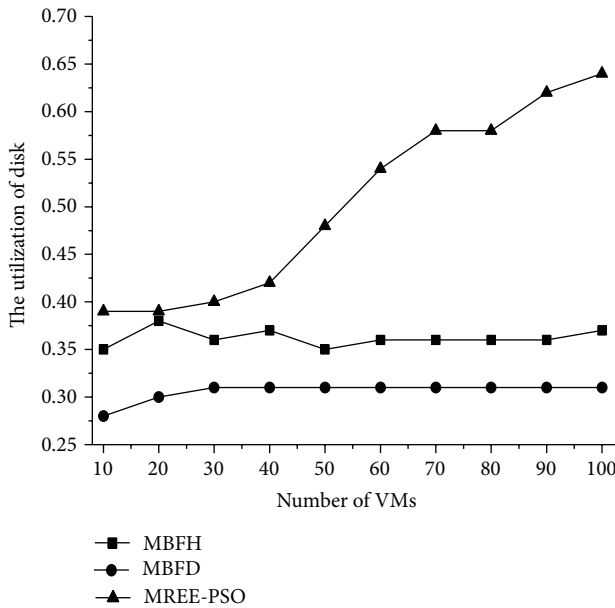


FIGURE 5: Comparison of disk utilization.

slowly for MREE-PSO than for MBFD [11, 12, 19] and MBFH [20, 21]. The usage of the physical nodes of MREE-PSO is always less than MBFD [11, 12, 19] and MBFH [20, 21] with the same number of virtual machines. Even the number of virtual machines arrives at 100; only 18 physical nodes are allocated for virtual machines. Thus, our method has a better energy efficiency than MBFD and MBFH which is important for cloud data center.

6. Conclusion

In cloud data center, the allocation of virtual machines with multiple resources plays an important role in improving the

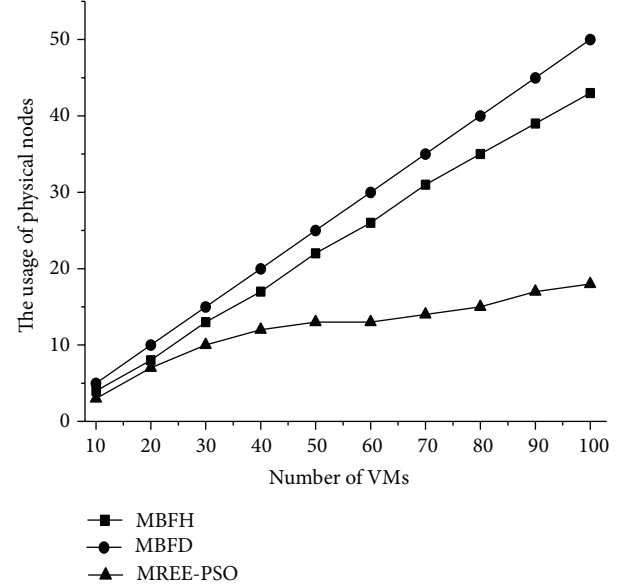


FIGURE 6: Comparison of usage of the physical nodes.

energy efficiency and performance of cloud computing. It will reduce the energy consumption of the cloud data center. The virtual machine allocation algorithm with multiple resources based on PSO described in this paper effectively improves energy efficiency. But the methods discussed here only considered the CPU and disk resources. Other resources such as network and memory should also be considered in the future research. The migration algorithm of virtual machines with multiple resources also should be introduced into the management of cloud data center in the future research.

Conflict of Interests

The authors declare that there is no conflict of interests regarding the publication of this paper.

Acknowledgments

This work was supported by the National Natural Science Foundation of China (no. 61370203) and the Scientific and Technological Research Program of Chongqing Municipal Education Commission (KJ120513, KJ120504).

References

- [1] B. Chang, H. Tsai, and C. Chen, "Empirical analysis of server consolidation and desktop virtualization in cloud computing," *Mathematical Problems in Engineering*, vol. 2013, Article ID 947234, 11 pages, 2013.
- [2] X. Wang, X. Liu, L. Fan, and X. Jia, "A decentralized virtual machine migration approach of data centers for cloud computing," *Mathematical Problems in Engineering*, vol. 2013, Article ID 878542, 10 pages, 2013.
- [3] H. F. Sheikh, H. Tan, I. Ahmad, S. Ranka, and P. By, "Energy- and performance-aware scheduling of tasks on parallel and

- distributed systems,” *ACM Journal on Emerging Technologies in Computing Systems*, vol. 8, no. 4, article 32, 2012.
- [4] M. Armbrust, A. Fox, R. Griffith et al., “A view of cloud computing,” *Communications of the ACM*, vol. 53, no. 4, pp. 50–58, 2010.
 - [5] R. Buyya, C. S. Yeo, S. Venugopal, J. Broberg, and I. Brandic, “Cloud computing and emerging IT platforms: vision, hype, and reality for delivering computing as the 5th utility,” *Future Generation Computer Systems*, vol. 25, no. 6, pp. 599–616, 2009.
 - [6] X. Zhu, D. Young, B. J. Watson et al., “1000 islands: an integrated approach to resource management for virtualized data centers,” *Cluster Computing*, vol. 12, no. 1, pp. 45–57, 2009.
 - [7] Y. Ajiro and A. Tanaka, “Improving packing algorithms for server consolidation,” in *Proceedings of the 33rd International Computer Measurement Group Conference*, pp. 399–406, CMG Press, San Diego, Calif, USA, December 2007.
 - [8] R. Gupta, S. K. Bose, S. Sundarrajan, M. Chebiyam, and A. Chakrabarti, “A two stage heuristic algorithm for solving the server consolidation problem with item-item and bin-item incompatibility constraints,” in *Proceedings of the IEEE International Conference on Services Computing (SCC '08)*, pp. 39–46, IEEE Computer Society Press, Honolulu, Hawaii, USA, July 2008.
 - [9] S. Agrawal, S. K. Bose, and S. Sundarrajan, “Grouping genetic algorithm for solving the server consolidation problem with conflicts,” in *Proceedings of the World Summit on Genetic and Evolutionary Computation*, pp. 1–8, ACM Press, June 2009.
 - [10] T. Wood, P. J. Shenoy, and A. Venkataramani, “Black-box and gray-box strategies for virtual machine migration,” in *Proceedings of the USENIX Symposium on Networked Systems Design and Implemetation*, pp. 229–242, GBR, Cambridge, UK, 2007.
 - [11] A. Beloglazov and R. Buyya, “Energy efficient allocation of virtual machines in cloud data centers,” in *Proceedings of the 10th IEEE/ACM International Symposium on Cluster, Cloud, and Grid Computing*, pp. 577–578, IEEE Computer Society Press, Melbourne, Australia, May 2010.
 - [12] A. Beloglazov, J. Abawajy, and R. Buyya, “Energy-aware resource allocation heuristics for efficient management of data centers for cloud computing,” *Future Generation Computer Systems*, vol. 28, no. 5, pp. 755–768, 2012.
 - [13] R. Nathuji and K. Schwan, “VirtualPower: coordinated power management in virtualized enterprise systems,” in *Proceedings of the 21st ACM Symposium on Operating Systems Principles (SOSP '07)*, vol. 41, no. 6, pp. 265–278, ACM Press, October 2007.
 - [14] R. Raghavendra, P. Ranganathan, V. Talwar, Z. Wang, and X. Zhu, “No “power” struggles: coordinated multi-level power management for the data center,” in *Proceedings of the 13th International Conference Architectural Support for Programming Languages and Operating Systems (ASPLOS '08)*, vol. 36, no. 1, pp. 48–59, ACM Press, 2008.
 - [15] V. M. Lo, *Task assignment in distributed systems [Ph.D. thesis]*, Department of Computer Science, University of Illinois, 1983.
 - [16] T. Widmer, M. Premmand, and P. Karaenke, “Energy-aware service allocation for cloud computing,” in *Proceedings of the International Conference on Wirtschaftsinformatik*, pp. 1147–1161, Leipzig, Germany, 2013.
 - [17] D. Kusic, J. O. Kephart, J. E. Hanson, N. Kandasamy, and G. Jiang, “Power and performance management of virtualized computing environments via lookahead control,” *Cluster Computing*, vol. 12, no. 1, pp. 1–15, 2009.
 - [18] X. Xu and H. Yu, “A game theory approach to fair and efficient resource allocation in cloud computing,” *Mathematical Problems in Engineering*, vol. 2014, Article ID 915878, 14 pages, 2014.
 - [19] A. Beloglazov and R. Buyya, “Managing overloaded hosts for dynamic consolidation of virtual machines in cloud data centers under quality of service constraints,” *IEEE Transactions on Parallel and Distributed Systems*, vol. 24, no. 7, pp. 1366–1379, 2013.
 - [20] S. Srikantaiah, A. Kansal, and F. Zhao, “Energy aware consolidation for cloud computing,” in *Proceedings of the IEEE Conference on Power Aware Computing and Systems*, pp. 577–578, IEEE Computer Society Press, San Diego, Calif, USA, 2010.
 - [21] P. Xiao, Z. Hu, and Y. Zhang, “An energy-aware heuristic scheduling for data-intensive workflows in virtualized datacenters,” *Journal of Computer Science and Technology*, vol. 28, no. 6, pp. 948–961, 2013.
 - [22] Y. del Valle, G. K. Venayagamoorthy, S. Mohagheghi, J.-C. Hernandez, and R. G. Harley, “Particle swarm optimization: basic concepts, variants and applications in power systems,” *IEEE Transactions on Evolutionary Computation*, vol. 12, no. 2, pp. 171–195, 2008.
 - [23] X. Wang, Y. Wang, and H. Zhu, “Energy-efficient multi-job scheduling model for cloud computing and its genetic algorithm,” *Mathematical Problems in Engineering*, vol. 2012, Article ID 589243, 16 pages, 2012.
 - [24] J. Kennedy and R. Eberhart, “Particle swarm optimization,” in *Proceedings of the IEEE International Conference on Neural Networks*, pp. 1942–1948, IEEE Computer Society Press, Perth, Australia, December 1995.
 - [25] A. Salman, I. Ahmad, and S. Al-Madani, “Particle swarm optimization for task assignment problem,” *Microprocessors and Microsystems*, vol. 26, no. 8, pp. 363–371, 2002.
 - [26] L. Zhang, Y. H. Chen, R. Y. Sun, S. Jing, and B. Yang, “A task scheduling algorithm based on PSO for grid computing,” *International Journal of Computational Intelligence Research*, vol. 4, no. 1, pp. 37–43, 2008.
 - [27] R. N. Calheiros, R. Ranjan, A. Beloglazov, C. A. F. De Rose, and R. Buyya, “CloudSim: a toolkit for modeling and simulation of cloud computing environments and evaluation of resource provisioning algorithms,” *Software: Practice and Experience*, vol. 41, no. 1, pp. 23–50, 2011.

Research Article

Stability and Bifurcation Analysis of a Modified Epidemic Model for Computer Viruses

Chuandong Li,¹ Wenfeng Hu,² and Tingwen Huang³

¹ College of Electronic and Information Engineering, Southwest University, Chongqing 400715, China

² Department of Mechanical and Biomedical Engineering, City University of Hong Kong, Hong Kong

³ Department of Mathematics, Texas A&M University at Qatar, P.O. Box 23874, Doha, Qatar

Correspondence should be addressed to Chuandong Li; licd@cqu.edu.cn

Received 8 January 2014; Accepted 10 May 2014; Published 5 June 2014

Academic Editor: He Huang

Copyright © 2014 Chuandong Li et al. This is an open access article distributed under the Creative Commons Attribution License, which permits unrestricted use, distribution, and reproduction in any medium, provided the original work is properly cited.

We extend the three-dimensional SIR model to four-dimensional case and then analyze its dynamical behavior including stability and bifurcation. It is shown that the new model makes a significant improvement to the epidemic model for computer viruses, which is more reasonable than the most existing SIR models. Furthermore, we investigate the stability of the possible equilibrium point and the existence of the Hopf bifurcation with respect to the delay. By analyzing the associated characteristic equation, it is found that Hopf bifurcation occurs when the delay passes through a sequence of critical values. An analytical condition for determining the direction, stability, and other properties of bifurcating periodic solutions is obtained by using the normal form theory and center manifold argument. The obtained results may provide a theoretical foundation to understand the spread of computer viruses and then to minimize virus risks.

1. Introduction

Computer viruses arose in the 1980s with the widespread use of Internet in a variety of fields, such as communication, Internet business, and commercial system [1, 2]. With the development of hardware and software technology, computer viruses started to be a major threat to the information security. Usually, computer viruses can cause severe damage to the individuals and the corporations by different ways, including acquiring confidential data from network users, attacking the whole system, and even causing fatal damage to the hardware [3]. So the behaviors of computer viruses have attracted much attention from the fundamental researchers to the network security professional.

It is well-known that computer virus is a malicious mobile code including virus, worm, Trojan horses, and logic bomb [4, 5]. Though different computer viruses vary in many respects, they all have many similar characteristics including infectivity, invisibility, latent, destructibility, and unpredictability [6]. The word “latent” means that the viruses

hide themselves in the computers and spread them in the Internet through a period of time. Thus, in the construction of the system, the latent period should not be ignored [7–9].

Because of a lot of similarities between the computer viruses and the infectious diseases, many researchers choose the epidemic models to find out the rule in the computer viruses [10, 11] and much attention is now paid to the effect of topological structure of the network on the spread of the viruses. Among the epidemic models, the SIR, SEI, and SEIR epidemic models are some of the most famous ones. Inspired by these epidemic models, the models of the computer virus have been proposed in recent years [12, 13].

However, some shortcomings of such models arose due to the inevitable difference between computer viruses and infectious diseases. Consequently, the results obtained from the infectious diseases models cannot be carried over to computer viruses completely. As a result, we need to make some modifications in order to model the computer viruses.

From the discussion above, we will propose a modified epidemic model for computer viruses and make some dynamic analysis on it. Specifically, we will extend the three-dimensional SIR model to four-dimensional SIRA model. However, because of the increased dimension, the complexity of the proposed model increases highly. We will present several theoretical results for its stability property and bifurcation dynamics by the rigorous mathematical analysis.

2. Model Description and Preliminaries

The present model is a modification of the original compartmental model [14]. Here, we assume that each node is denoted as one computer and the total population T can be divided into the following four groups by the state of each node:

- (1) $S(t)$ is the number of noninfected computers subjected to possible infection;
- (2) $I(t)$ is the number of infected computers;
- (3) $R(t)$ is the number of removed ones due to infection or not;
- (4) $A(t)$ is the antidotal population representing computers equipped with fully effective antivirus programs [15].

In the present paper, we use the antivirus distribution strategy; namely, we convert the susceptible into antidotal, which is proportional to the product SI and with a controlled parameter a_{SA} . In addition, the infected computers can be fixed by using antivirus programs, by which the infected computers can be converted into antidotal ones with a rate proportional to AI and a proportion factor given by a_{IA} , or we let the infected ones become useless and be removed with a rate controlled by δ because of the antivirus cost. Usually, the removed computers can be restored and converted into susceptible with a proportional factor σ . It is noticed that all the compartments have the mortality rate not due to the viruses. Here we assume all of them are the same and are denoted by the proportion coefficient μ . We further suppose that the influx rate N represents the incorporation of new computers to the network.

It should be pointed out that the rate of the conversion from susceptible into infected ones is called incidence rate. It has been suggested by several authors that the viruses' transmission process may have a nonlinear incidence rate. This allows one to include behavioral changes and prevent unbounded contact rates (e.g., [16]). In many epidemic models, the bilinear incidence rate βSI and the standard incidence rate $\beta SI/N$ are frequently used. The bilinear incidence rate is based on the law of mass action. This contact law is more appropriate for communicable diseases such as influenza but not for point-to-point computer viruses. In the paper,

we introduce the following saturated incidence rate $g(I)S$ into models, where $g(I)$ tends to a saturation level when I becomes large:

$$g(I) = \frac{\beta I(t - \tau)}{1 + \alpha I(t - \tau)}, \quad (1)$$

where $\beta I(t - \tau)$ measures the infection force of the viruses and $1/(1 + \alpha I(t - \tau))$ measures the inhibition effect from the behavioral change of the susceptible ones when their number increases or from the crowding effect of the infected ones. It is noticed that τ represents the latent period; it means a fixed time during which some viruses develop in a susceptible computer and it is only after that time the susceptible one is converted to an infected one.

Considering all these facts above, we can propose a new model with an economical use of the antivirus programs:

$$\begin{aligned} \dot{S} &= N - a_{SA}SA - \frac{\beta S(t - \tau)I(t - \tau)}{1 + \alpha I(t - \tau)} - \mu S + \sigma R, \\ \dot{I} &= \frac{\beta S(t - \tau)I(t - \tau)}{1 + \alpha I(t - \tau)} - a_{IA}AI - \delta I - \mu I, \end{aligned} \quad (2)$$

$$\dot{R} = \delta I - \sigma R - \mu R,$$

$$\dot{A} = a_{SA}SA + a_{IA}AI - \mu A.$$

For simplicity, let $a_{SA} = a_1$, $a_{IA} = a_2$, and $a_{SA} + a_{IA} = a_A$.

3. Mathematical Analysis

3.1. Virus-Free Equilibrium Point. Under the condition of virus-free, namely, we assume $I = 0$, there is no need to equip the computers with the antivirus programs, which means $A = 0$. Then, bringing the equilibrium point $E^* = [S^*, I^*, R^*, A^*]$ into (2), we get

$$\begin{aligned} N - a_1 S^* A^* - \frac{\beta S^* I^*}{1 + \alpha I^*} - \mu S^* + \sigma R^* &= 0, \\ \frac{\beta S^* I^*}{1 + \alpha I^*} - a_2 A^* I^* - \delta I^* - \mu I^* &= 0, \\ \delta I^* - \sigma R^* - \mu R^* &= 0, \\ a_1 S^* A^* + a_2 A^* I^* - \mu A^* &= 0. \end{aligned} \quad (3)$$

Based on (3), the virus-free equilibrium point can be calculated:

$$E_1 = (S_1, I_1, R_1, A_1) = \left(\frac{N}{\mu}, 0, 0, 0 \right). \quad (4)$$

The characteristic equation of (2) at E_1 is given by the following:

$$\det \begin{pmatrix} \lambda + \mu & \frac{N}{\mu} \beta e^{-\lambda \tau} & -\sigma & a_1 \frac{N}{\mu} \\ 0 & \lambda - \frac{N}{\mu} \beta e^{-\lambda \tau} + (\delta + \mu) & 0 & 0 \\ 0 & -\delta & \lambda + \sigma + \mu & 0 \\ 0 & 0 & 0 & \lambda - \frac{N}{\mu} a_1 + \mu \end{pmatrix} = 0, \quad (5)$$

which equals

$$\begin{aligned} & (\lambda + \mu) \left(\lambda - \frac{N}{\mu} \beta e^{-\lambda \tau} + (\delta + \mu) \right) \\ & \times (\lambda + \sigma + \mu) \left(\lambda - \frac{N}{\mu} a_1 + \mu \right) \\ & = (\lambda + \mu) (\lambda + \sigma + \mu) \left(\lambda - \frac{N}{\mu} a_1 + \mu \right) \quad (6) \\ & \times [\lambda + (\delta + \mu) (1 - K_0 e^{-\lambda \tau})] \\ & = 0, \end{aligned}$$

where $K_0 = \beta N / \mu (\delta + \mu)$.

Clearly, (6) always has two negative eigenvalues $\lambda_1 = -\mu$, $\lambda_2 = -\sigma - \mu$ and two indefinite eigenvalues $\lambda_3 = (N/\mu) a_1 - \mu$ and $\lambda_4 = -(\delta + \mu) (1 - K_0 e^{-\lambda \tau})$. We let $K_1 = a_1 N / \mu^2$.

It is clear to see that if $K_1 < 1$ and $K_0 < 1$, the other two eigenvalues must be negative too. So, the following theorem can be acquired.

Theorem 1. For the system (2), if $K_0 = \beta N / \mu (\delta + \mu) < 1$ and $K_1 = a_1 N / \mu^2 < 1$ are satisfied, then the virus-free equilibrium point $E_1 = (N/\mu, 0, 0, 0)$ is locally asymptotically stable. Besides, if $K_1 > 1$, the equilibrium point E_1 is unstable.

Remark 2. Theorem 1 investigates the local stability of the virus-free equilibrium point by analyzing the eigenvalues of the corresponding characteristic equation. We can see that when viruses do not appear, all computers in the network are subjected to possible infection.

3.2. Endemic Equilibrium Points. Endemic equilibrium points are characterized by the existence of infected ones in the network; that is, $I \neq 0$. First, we consider the case when the network has no antidotal node; namely, $A = 0$. Then, it is not difficult to solve (3) when $A = 0$, $I \neq 0$ and the solution is

$$E_2 = S_2, I_2, R_2, A_2 = S_2, I_2, R_2, 0, \quad (7)$$

where

$$I_2 = \frac{(\sigma + \mu) [\beta N - \mu (\delta + \mu)]}{(\sigma + \mu) (\delta + \mu) (\beta + \mu \alpha) - \beta \sigma \delta},$$

$$S_2 = \frac{(\delta + \mu) (1 + \alpha I_2)}{\beta},$$

$$R_2 = \frac{\delta I_2}{\sigma + \mu}. \quad (8)$$

It indicates that when $K_0 < 1$, $I_2 < 0$. Consequently, the condition $K_0 < 1$ can avoid the existence of the equilibrium point E_2 .

Another more important case is $A \neq 0$ when $I \neq 0$. Again, calculating (3) and the endemic point is given by

$$\begin{aligned} E_3 &= (S_3, I_3, R_3, A_3) \\ &= \left(\frac{\mu - a_2 I_3}{a_1}, I_3, \frac{\delta I_3}{\sigma + \mu}, \frac{\beta (\mu - a_2 I_3)}{a_1 a_2 (1 + \alpha I_3)} - \frac{\delta + \mu}{a_2} \right). \quad (9) \end{aligned}$$

Bringing the E_3 point into the first equation of (3), this leads to

$$\begin{aligned} & N - a_1 S_3 A_3 - \frac{\beta S_3 I_3}{1 + \alpha I_3} - \mu S_3 + \sigma R_3 \\ &= N - a_1 \frac{\mu - a_2 I_3}{a_1} \left(\frac{\beta (\mu - a_2 I_3)}{a_1 a_2 (1 + \alpha I_3)} - \frac{\delta + \mu}{a_2} \right) \\ & \quad - \frac{\beta I_3}{1 + \alpha I_3} \cdot \frac{\mu - a_2 I_3}{a_1} - \mu \frac{\mu - a_2 I_3}{a_1} + \sigma \frac{\delta I_3}{\sigma + \mu} \\ &= 0. \end{aligned} \quad (10)$$

Then, we expand (10) and merge the similar terms; we let $I = I_3$ without confusion:

$$\begin{aligned} & p_1 (1 + \alpha I) + p_2 I (1 + \alpha I) + p_3 (\mu - a_2 I) \\ & + p_4 (\mu - a_2 I) (1 + \alpha I) = 0, \end{aligned} \quad (11)$$

where

$$\begin{aligned} p_1 &= a_1 a_2 N (\sigma + \mu), & p_2 &= a_1 a_2 \sigma \delta, \\ p_3 &= -\mu \beta (\sigma + \mu), & p_4 &= (\sigma + \mu) (\mu a_1 + \delta a_1 - \mu a_2). \end{aligned} \quad (12)$$

Furthermore, a quadratic equation of the variable I is obtained:

$$b_1 I^2 + b_2 I + b_3 = 0, \quad (13)$$

where

$$\begin{aligned} b_1 &= p_2 \alpha - p_4 \alpha a_2, \\ b_2 &= p_1 \alpha + p_2 - p_3 a_2 + p_4 \alpha \mu - p_4 a_2, \\ b_3 &= p_1 + p_3 \mu + p_4 \mu. \end{aligned} \quad (14)$$

From (13), we have the following result.

Theorem 3. Suppose that S, I, R, A are all positive, and $K_2 > 1$, $K_3 > 1$. Then

- (1) if $b_1 = 0$ and $b_3/b_2 < 0$ hold, there exists unique positive solution (9) for (3), and $I_3 = -b_3/b_2$;

- (2) when $\Delta > 0$ always holds, then if $b_2/b_1 < 0$ and $b_3/b_1 > 0$, there exist two positive solutions, where $I_3^{(1)} = I_+$ and $I_3^{(2)} = I_-$; if $b_3/b_1 < 0$, there is only one positive solution $I_3 = I_+$ with $b_1 > 0$ or $I_3 = I_-$ with $b_1 < 0$; if $b_3 = 0$ and $b_2/b_1 < 0$, there is only one positive solution $I_3 = -b_2/b_1$;

- (3) if $\Delta = 0$ and $b_2/b_1 < 0$, there is only one positive solution $I_3 = -b_2/2b_1$,

where $K_2 = (\beta(\mu - a_2 I))/(a_1(1 + \alpha I)(\delta + \mu))$, $K_3 = \mu/a_2 I$, $\Delta = b_2^2 - 4b_1 b_3$, $I_+ = (-b_2 + \sqrt{b_2^2 - 4b_1 b_3})/2b_1$, and $I_- = (-b_2 - \sqrt{b_2^2 - 4b_1 b_3})/2b_1$.

Remark 4. Theorem 3 mainly focuses on the existence of the positive equilibrium point of the system. We can see that all conditions in the theorem are easily verified.

When the equilibrium point E_3 exists, the characteristic equation of (2) at the point is

$$\det \begin{pmatrix} \lambda + a_1 A_3 + \frac{\beta I_3 e^{-\lambda \tau}}{1 + \alpha I_3} + \mu & \frac{\beta S_3 e^{-\lambda \tau}}{(1 + \alpha I_3)^2} & -\sigma & a_1 S_3 \\ -\frac{\beta I_3 e^{-\lambda \tau}}{1 + \alpha I_3} & \lambda - \frac{\beta S_3 e^{-\lambda \tau}}{(1 + \alpha I_3)^2} + a_2 A_3 + \delta + \mu & 0 & a_2 I_3 \\ 0 & -\delta & \lambda + \sigma + \mu & 0 \\ -a_1 A_3 & -a_2 A_3 & 0 & \lambda \end{pmatrix} = 0. \quad (15)$$

We set $c_1 = \beta I_3/(1 + \alpha I_3)$, $c_2 = \beta S_3/(1 + \alpha I_3)^2$, $c_3 = a_1 A_3 + \mu$, and $c_4 = a_2 A_3 + \delta + \mu$. For notational simplicity, we use the (S, I, R, A) in place of E_3 . Then, the following four-degree exponential polynomial equation is obtained:

$$\begin{aligned} &\lambda^4 + d_1 \lambda^3 + d_2 \lambda^2 + d_3 \lambda + d_4 \\ &+ e^{-\lambda \tau} (d_5 \lambda^3 + d_6 \lambda^2 + d_7 \lambda + d_8) = 0, \end{aligned} \quad (16)$$

where

$$\begin{aligned} d_1 &= c_3 + c_4 + \sigma + \mu, \\ d_2 &= a_1^2 AS + a_2^2 AI + c_3 c_4 + (\sigma + \mu)(c_3 + c_4), \\ d_3 &= a_1^2 AS(c_4 + \sigma + \mu) + a_2^2 AI(c_3 + \sigma + \mu) + c_3 c_4(\sigma + \mu), \\ d_4 &= (\sigma + \mu)(a_1^2 c_4 AS + a_2^2 c_3 AI) + a_1 a_2 \sigma \delta AI, \\ d_5 &= c_1 - c_2, \\ d_6 &= c_1(c_4 + \sigma + \mu) - c_2(c_3 + \sigma + \mu), \\ d_7 &= A(a_2 I + a_1 S)(c_1 a_2 - c_2 a_1) \\ &\quad - c_1 \sigma \delta + (c_1 c_4 - c_2 c_3)(\sigma + \mu), \\ d_8 &= A(a_2 I + a_1 S)(c_1 a_2 - c_2 a_1)(\sigma + \mu). \end{aligned} \quad (17)$$

Multiplying $e^{\lambda \tau}$ on both sides of (16), it is obvious to get

$$\begin{aligned} J &= (\lambda^4 + d_1 \lambda^3 + d_2 \lambda^2 + d_3 \lambda + d_4) e^{\lambda \tau} \\ &+ (d_5 \lambda^3 + d_6 \lambda^2 + d_7 \lambda + d_8) = 0. \end{aligned} \quad (18)$$

Let $\lambda = i\omega_0$, $\tau = \tau_0$, and substituting this into (18), for the sake of simplicity, denote ω_0 and τ_0 by ω , τ , respectively; then (18) becomes

$$\begin{aligned} &(\omega^4 - id_1 \omega^3 - d_2 \omega^2 + id_3 \omega + d_4)(\cos \omega \tau + i \sin \omega \tau) \\ &+ (-id_5 \omega^3 - d_6 \omega^2 + id_7 \omega + d_8) = 0. \end{aligned} \quad (19)$$

Separating the real and imaginary parts, we have

$$\begin{aligned} &(\omega^4 - d_2 \omega^2 + d_4) \cos \omega \tau \\ &+ (d_1 \omega^3 - d_3 \omega) \sin \omega \tau = d_6 \omega^2 - d_8, \\ &(-d_1 \omega^3 + d_3 \omega) \cos \omega \tau \\ &+ (\omega^4 - d_2 \omega^2 + d_4) \sin \omega \tau = d_5 \omega^3 - d_7 \omega. \end{aligned} \quad (20)$$

By simple calculation, the following equations are obtained:

$$\cos \omega \tau = \frac{e_5 \omega^6 + e_6 \omega^4 + e_7 \omega^2 + e_8}{\omega^8 + e_1 \omega^6 + e_2 \omega^4 + e_3 \omega^2 + e_4}, \quad (21)$$

$$\sin \omega \tau = \frac{e_9 \omega^7 + e_{10} \omega^5 + e_{11} \omega^3 + e_{12} \omega}{\omega^8 + e_1 \omega^6 + e_2 \omega^4 + e_3 \omega^2 + e_4}, \quad (22)$$

where

$$\begin{aligned} e_1 &= d_1^2 - 2d_2, & e_2 &= -2d_1 d_3 + d_2^2 + 2d_4, \\ e_3 &= -2d_2 d_4 + d_3^2, & e_4 &= d_4^2, \\ e_5 &= d_6 - d_1 d_5, & e_6 &= d_1 d_7 - d_2 d_6 + d_3 d_5 - d_8, \\ e_7 &= d_2 d_8 - d_3 d_7 + d_4 d_6, & e_8 &= -d_4 d_8, \\ e_9 &= d_5, & e_{10} &= d_1 d_6 - d_2 d_5 - d_7, \\ e_{11} &= -d_1 d_8 + d_2 d_7 - d_3 d_6 + d_4 d_5, \\ e_{12} &= d_3 d_8 - d_4 d_7. \end{aligned} \quad (23)$$

As is known to all that $\sin^2 \omega \tau + \cos^2 \omega \tau = 1$, we get

$$\begin{aligned} \omega^{16} + f_7 \omega^{14} + f_6 \omega^{12} + f_5 \omega^{10} + f_4 \omega^8 + f_3 \omega^6 \\ + f_2 \omega^4 + f_1 \omega^2 + f_0 = 0, \end{aligned} \quad (24)$$

where

$$\begin{aligned} f_7 &= 2e_1 - e_9^2, & f_6 &= e_1^2 + 2e_2 - e_5^2 - 2e_9 e_{10}, \\ f_5 &= 2e_1 e_2 + 2e_3 - 2e_5 e_6 - 2e_9 e_{11} - e_{10}^2, \\ f_4 &= 2e_1 e_3 + e_2^2 + 2e_4 - 2e_5 e_7 - e_6^2 - 2e_9 e_{12} - 2e_{10} e_{11}, \\ f_3 &= 2e_1 e_4 + 2e_2 e_3 - 2e_5 e_8 - 2e_6 e_7 - 2e_{10} e_{12} - e_{11}^2, \\ f_2 &= 2e_2 e_4 + e_3^2 - 2e_6 e_8 - e_7^2 - 2e_{11} e_{12}, \\ f_1 &= 2e_3 e_4 - 2e_7 e_8 - e_{12}^2, \\ f_0 &= e_4^2 - e_8^2. \end{aligned} \quad (25)$$

Denote $z = \omega^2$; (24) can be rewritten as

$$\begin{aligned} z^8 + f_7 z^7 + f_6 z^6 + f_5 z^5 + f_4 z^4 \\ + f_3 z^3 + f_2 z^2 + f_1 z + f_0 = 0. \end{aligned} \quad (26)$$

We suppose that

(H₁) (26) has at least one positive real root.

Without loss of generality, we can assume the equation has l ($1 \leq l \leq 8$) positive real roots, which are represented as z_i ($1 \leq i \leq l$); then $\omega_i = \sqrt{z_i}$.

By (21), we get

$$\begin{aligned} \tau_k^j = \frac{1}{\omega_k} \left\{ \arccos \left(\frac{e_5 \omega_k^6 + e_6 \omega_k^4 + e_7 \omega_k^2 + e_8}{\omega_k^8 + e_1 \omega_k^6 + e_2 \omega_k^4 + e_3 \omega_k^2 + e_4} \right) + 2j\pi \right\}, \\ j = 0, 1, \dots \end{aligned} \quad (27)$$

From the early discussions, we know that the $\pm i\omega_k$ are a pair of purely imaginary roots of (16) with τ_k^j . Define

$$\tau_0 = \tau_{k_0}^0 = \min_{k \in \{1, \dots, l\}} \{\tau_k^0\}, \quad \omega_0 = \omega_{k_0}. \quad (28)$$

It is noted that when $\tau = 0$, (16) becomes

$$\begin{aligned} \lambda^4 + d_1 \lambda^3 + d_2 \lambda^2 + d_3 \lambda + d_4 + (d_5 \lambda^3 + d_6 \lambda^2 + d_7 \lambda + d_8) \\ = \lambda^4 + (d_1 + d_5) \lambda^3 + (d_2 + d_6) \lambda^2 \\ + (d_3 + d_7) \lambda + (d_4 + d_8) = 0. \end{aligned} \quad (29)$$

By virtue of the well-known Routh-Hurwitz criteria, a set of necessary and sufficient conditions for all roots of (29) to have the negative real part is given in the following form:

$$D_1 = d_1 + d_5 > 0, \quad (30)$$

$$\begin{aligned} D_2 = \begin{vmatrix} d_1 + d_5 & d_3 + d_7 \\ 1 & d_2 + d_6 \end{vmatrix} \\ = (d_1 + d_5)(d_2 + d_6) - (d_3 + d_7) > 0, \end{aligned} \quad (31)$$

$$\begin{aligned} D_3 = \begin{vmatrix} d_1 + d_5 & d_3 + d_7 & 0 \\ 1 & d_2 + d_6 & d_4 + d_8 \\ 0 & d_1 + d_5 & d_3 + d_7 \end{vmatrix} \\ = (d_1 + d_5)[(d_2 + d_6)(d_3 + d_7) - (d_1 + d_5)(d_4 + d_8)] \\ - (d_3 + d_7)^2 > 0, \end{aligned} \quad (32)$$

$$\begin{aligned} D_4 = \begin{vmatrix} d_1 + d_5 & d_3 + d_7 & 0 & 0 \\ 1 & d_2 + d_6 & d_4 + d_8 & 0 \\ 0 & d_1 + d_5 & d_3 + d_7 & 0 \\ 0 & 1 & d_2 + d_6 & d_4 + d_8 \end{vmatrix} \\ = (d_4 + d_8) D_3 > 0. \end{aligned} \quad (33)$$

If (30)–(33) hold, (29) has four roots with negative real parts, and therefore when $\tau = 0$, system (2) is stable near the equilibrium point E_3 .

In order to give the main results, it is necessary to make the following assumption:

$$(H_2) \quad \text{Re} \left(\frac{d\lambda}{d\tau} \right) \Big|_{\tau=\tau_0} \neq 0.$$

In order to calculate the derivative of λ with respect to τ in (18), it is followed by

$$\begin{aligned} \frac{d\lambda}{d\tau} &= -\frac{\partial J / \partial \tau}{\partial J / \partial \lambda} \\ &= -\left(\lambda \left(\lambda^4 + d_1 \lambda^3 + d_2 \lambda^2 + d_3 \lambda + d_4 \right) e^{\lambda \tau} \right. \\ &\quad \times \left(\left(4\lambda^3 + 3d_1 \lambda^2 + 2d_2 \lambda + d_3 \right) e^{\lambda \tau} + \tau e^{\lambda \tau} \right. \\ &\quad \times \left(\lambda^4 + d_1 \lambda^3 + d_2 \lambda^2 + d_3 \lambda + d_4 \right) \\ &\quad \left. \left. + \left(3d_5 \lambda^2 + 2d_6 \lambda + d_7 \right) \right)^{-1} \right) \end{aligned} \quad (34)$$

thus

$$\begin{aligned}
 & \left(\frac{d\lambda}{d\tau} \right)^{-1} \\
 &= \left((4\lambda^3 + 3d_1\lambda^2 + 2d_2\lambda + d_3) e^{\lambda\tau} + (3d_5\lambda^2 + 2d_6\lambda + d_7) \right) \\
 & \quad \times \left(-\lambda e^{\lambda\tau} (\lambda^4 + d_1\lambda^3 + d_2\lambda^2 + d_3\lambda + d_4) \right)^{-1} - \frac{\tau}{\lambda} \\
 &= \left((4\lambda^3 + 3d_1\lambda^2 + 2d_2\lambda + d_3) e^{\lambda\tau} \right. \\
 & \quad \left. + (3d_5\lambda^2 + 2d_6\lambda + d_7) \right) \\
 & \quad \times \left(d_5\lambda^4 + d_6\lambda^3 + d_7\lambda^2 + d_8\lambda \right)^{-1} - \frac{\tau}{\lambda}.
 \end{aligned} \tag{35}$$

When $\tau = \tau_0$, $\pm i\omega_0$ are a pair of purely imaginary roots of (16). Substituting the $\tau_0, i\omega_0$ into (35) and denoting τ_0 and ω_0 by τ, ω for simplicity, then

$$\begin{aligned}
 & \left(\frac{d\lambda}{d\tau} \right)^{-1} \Big|_{\lambda=i\omega_0, \tau=\tau_0} \\
 &= \left((-3d_1\omega^2 + d_3) \cos \omega\tau \right. \\
 & \quad \left. + (4\omega^3 - 2d_2\omega) \sin \omega\tau - 3d_5\omega^2 + d_7 \right) \\
 & \quad \times \left((d_5\omega^4 - d_7\omega^2) + i(-d_6\omega^3 + d_8\omega) \right)^{-1} \\
 & \quad + i \left((-4\omega^3 + 2d_2\omega) \cos \omega\tau \right. \\
 & \quad \left. + (-3d_1\omega^2 + d_3) \sin \omega\tau + 2d_6\omega \right) \\
 & \quad \times \left((d_5\omega^4 - d_7\omega^2) + i(-d_6\omega^3 + d_8\omega) \right)^{-1} \\
 & \quad - \frac{\tau}{i\omega}.
 \end{aligned} \tag{36}$$

We set $Q = (d_5\omega^4 - d_7\omega^2)^2 + (-d_6\omega^3 + d_8\omega)^2$,

$$\begin{aligned}
 & Q \cdot \operatorname{Re} \left(\frac{d\lambda}{d\tau} \right)^{-1} \Big|_{\tau=\tau_0} \\
 &= \left[(-3d_1\omega^2 + d_3) \cos \omega\tau \right. \\
 & \quad \left. + (4\omega^3 - 2d_2\omega) \sin \omega\tau - 3d_5\omega^2 + d_7 \right] \\
 & \quad \times (d_5\omega^4 - d_7\omega^2) \\
 & \quad + \left[(-4\omega^3 + 2d_2\omega) \cos \omega\tau \right. \\
 & \quad \left. + (-3d_1\omega^2 + d_3) \sin \omega\tau + 2d_6\omega \right] \\
 & \quad \times (-d_6\omega^3 + d_8\omega), \\
 & \operatorname{sgn} \left\{ \operatorname{Re} \left(\frac{d\lambda}{d\tau} \right) \Big|_{\tau=\tau_0} \right\} = \operatorname{sgn} \left\{ Q \cdot \operatorname{Re} \left(\frac{d\lambda}{d\tau} \right)^{-1} \Big|_{\tau=\tau_0} \right\}.
 \end{aligned} \tag{37}$$

On the basis of (H_2) , we can know that the roots of characteristic equation (16) cross the imaginary axis as τ continuously varies from a number less than τ_0 to one greater than τ_0 by Rouché's theorem [17]. Therefore, the transversality condition holds and the conditions for Hopf bifurcation are then satisfied at $\tau = \tau_0$.

Lemma 5 (see [18]). *Consider the exponential polynomial*

$$\begin{aligned}
 & P(\lambda, e^{-\lambda\tau_1}, \dots, e^{-\lambda\tau_m}) \\
 &= \lambda^n + p_1^{(0)} \lambda^{n-1} + \dots + p_{n-1}^{(0)} \lambda + p_n^{(0)} \\
 & \quad + [p_1^{(1)} \lambda^{n-1} + \dots + p_{n-1}^{(1)} \lambda + p_n^{(1)}] e^{-\lambda\tau_1} \\
 & \quad + \dots + [p_1^{(m)} \lambda^{n-1} + \dots + p_{n-1}^{(m)} \lambda + p_n^{(m)}] e^{-\lambda\tau_m},
 \end{aligned} \tag{38}$$

where $\tau_i \geq 0$ ($i = 1, 2, \dots, m$) and $p_j^{(i)}$ ($i = 0, 1, \dots, m; j = 1, 2, \dots, n$) are constants. As $(\tau_1, \tau_2, \dots, \tau_m)$ vary, the sum of the order of the zeros of $P(\lambda, e^{-\lambda\tau_1}, \dots, e^{-\lambda\tau_m})$ on the open right plane can change only if a zero appears on or crosses the imaginary axis.

From Lemma 5, it is easy to get the theorem.

Theorem 6. *Suppose that (H_1) and (H_2) hold; then*

- (1) *for system (2), the equilibrium point E_3 is asymptotically stable for $\tau \in [0, \tau_0)$;*
- (2) *system (2) undergoes a Hopf bifurcation at the E_3 when $\tau = \tau_0$. That is to say, it has a branch of periodic solutions bifurcating from the E_3 near $\tau = \tau_0$, where τ_0 can be calculated by (28).*

Furthermore, we can investigate the stability and direction of bifurcating periodic solutions by analyzing higher order terms according to Hassard et al. [19].

Remark 7. The analyses above study the existence of the Hopf bifurcation and obtain the critical value of the parameter τ . We can apply the theorem into the system; thus, through changing some parameters, some bad performances of the model can be avoided.

Remark 8. When we set $N = 0$, $\mu = 0$, $\alpha = 0$, and $\tau = 0$, the present model can be transformed to the model in [14]. However, [14] only calculated the disease-free/endemic equilibrium points and analyzed the stability. This paper expands the model and makes a detailed analysis about the bifurcations.

Remark 9. In this paper, we propose a new group called antidotal population, that is, $A(t)$, which is more reasonable when we study the computer viruses. It is well known that when dealing with Hopf bifurcation, the complexity of computation increases significantly as the dimension of system increases. Sometimes, it even cannot be calculated, especially when nonlinear terms $\beta S(t - \tau)I(t - \tau)/(1 + \alpha I(t - \tau))$ exist in our system. Partly because of this, the majority of the literatures published use the traditional SIR three-dimensional model to study the epidemic model or virus [7, 10, 20], which has some limitations.

3.3. Stability and Direction of the Hopf Bifurcation. We have obtained the conditions under which a family of periodic solutions bifurcate from the positive equilibrium E_3 at the critical value of τ_0 . In this subsection, the formulae for determining the direction of Hopf bifurcation and stability of bifurcating periodic solutions of system at τ_0 will be presented by employing the normal form theory and the center manifold reduction [19, 21–24].

For convenience, let $x_1 = S - S_3$, $x_2 = I - I_3$, $x_3 = R - R_3$, $x_4 = A - A_3$, $\bar{x}_i(t) = x_i(\tau t)$, and $\tau = \tau_0 + u$; we drop the bars for simplification of notations. In the light of multivariate Taylor expansion, system (2) can be transformed into an FDE in $C = C([-1, 0], R^3)$ as

$$\dot{x}(t) = L_u(x_t) + f(u, x_t), \quad (39)$$

where $x(t) = (x_1(t), x_2(t), x_3(t), x_4(t))^T \in R^4$, and $L_u : C \rightarrow R$, $f : R \times C \rightarrow R$ are given, respectively, by

$$\begin{aligned} L_u(\phi) &= (\tau_0 + u) \begin{pmatrix} -c_3 & 0 & \sigma & -a_1 S \\ 0 & -c_4 & 0 & -a_2 I \\ 0 & \delta & -\sigma - \mu & 0 \\ a_1 A & a_2 A & 0 & 0 \end{pmatrix} \begin{pmatrix} \phi_1(0) \\ \phi_2(0) \\ \phi_3(0) \\ \phi_4(0) \end{pmatrix} \\ &\quad + (\tau_0 + u) \begin{pmatrix} -c_1 & -c_2 & 0 & 0 \\ c_1 & c_2 & 0 & 0 \\ 0 & 0 & 0 & 0 \\ 0 & 0 & 0 & 0 \end{pmatrix} \begin{pmatrix} \phi_1(-1) \\ \phi_2(-1) \\ \phi_3(-1) \\ \phi_4(-1) \end{pmatrix} \\ &= (\tau_0 + u) B_1 \phi(0) + (\tau_0 + u) B_2 \phi(-1), \\ f(u, \phi) &= (\tau_0 + u) \\ &\quad \times \begin{pmatrix} l_1 \phi_2^2(-1) - l_2 \phi_1(-1) \phi_2(-1) - a_1 \phi_1(0) \phi_4(0) + h.o.t \\ -l_1 \phi_2^2(-1) + l_2 \phi_1(-1) \phi_2(-1) - a_2 \phi_2(0) \phi_4(0) + h.o.t \\ 0 \\ a_1 \phi_1(0) \phi_4(0) + a_2 \phi_2(0) \phi_4(0) \end{pmatrix}, \end{aligned} \quad (40)$$

where $l_1 = \alpha c_2 / (1 + \alpha I)$, $l_2 = c_2 / S$, and L_u is a one-parameter family of bounded linear operators in $C[-1, 0] \rightarrow R^4$.

By the Riesz representation theorem, there exists a function $\eta(\theta, u)$ of bounded variation for $\theta \in [-1, 0]$, such that

$$L_u \phi = \int_{-1}^0 d\eta(\theta, u) \phi(\theta) \quad \text{for } \phi \in C^1([-1, 0], R^4). \quad (41)$$

In fact, we can choose

$$\eta(\theta, u) = (\tau_0 + u) B_1 \delta(\theta) - (\tau_0 + u) B_2 \delta(\theta + 1), \quad (42)$$

where $\delta(\theta)$ is the Dirac delta function.

For $\phi \in C^1([-1, 0], R^4)$, define

$$A(u)\phi = \begin{cases} \frac{d\phi(\theta)}{d\theta}, & -1 \leq \theta < 0, \\ \int_{-1}^0 d\eta(\theta, u) \phi(\theta), & \theta = 0, \end{cases} \quad (43)$$

$$R(u)\phi = \begin{cases} 0, & \theta \in [-1, 0), \\ f(u, \phi), & \theta = 0. \end{cases}$$

Then, system (39) is equivalent to

$$\dot{x}_t = A(u)x_t + R(u)x_t, \quad (44)$$

where $x_t(\theta) = x(t + \theta)$, for $\theta \in [-1, 0)$, and $x = (x_1, x_2, x_3, x_4)^T$.

For $\psi \in C^1([0, 1], (R^4)^*)$, define

$$A^*(u)\psi = \begin{cases} -\frac{d\psi(s)}{ds}, & 0 < s \leq 1, \\ \int_{-1}^0 d\eta^T(t, u) \phi(-t), & s = 0. \end{cases} \quad (45)$$

In order to normalize the eigenvectors of operator A and adjoint operator A^* , the following bilinear inner product is needed to introduce

$$\begin{aligned} \langle \psi(s), \phi(\theta) \rangle &= \bar{\psi}(0) \phi(0) - \int_{-1}^0 \int_{\xi=0}^{\theta} \bar{\psi}(\xi - \theta) d\eta(\theta) \phi(\xi) d\xi, \end{aligned} \quad (46)$$

where $\eta(\theta) = \eta(\theta, 0)$.

From the early discussions, we know that $\pm i\tau_0\omega_0$ are eigenvalues of $A(0)$ and other eigenvalues have strictly negative real parts; thus, they are also eigenvalues of A^* . Define that

$$q(\theta) = (1, q_2, q_3, q_4)^T e^{i\tau_0\omega_0\theta}, \quad -1 < \theta \leq 0, \quad (47)$$

which is the eigenvector of $A(0)$ belonging to the eigenvalue $i\tau_0\omega_0$; namely, $A(0)q(\theta) = i\tau_0\omega_0 q(\theta)$. Then, we can easily obtain

$$\begin{aligned} \tau_0 \begin{pmatrix} i\omega_0 + c_3 + c_1 e^{-i\tau_0\omega_0} & c_2 e^{-i\tau_0\omega_0} & -\sigma & a_1 S \\ -c_1 e^{-i\tau_0\omega_0} & i\omega_0 + c_4 - c_2 e^{-i\tau_0\omega_0} & 0 & a_2 I \\ 0 & -\delta & i\omega_0 + \sigma + \mu & 0 \\ -a_1 A & -a_2 A & 0 & i\omega_0 \end{pmatrix} \\ \times q(0) = \begin{pmatrix} 0 \\ 0 \\ 0 \\ 0 \end{pmatrix}. \end{aligned} \quad (48)$$

Hence, we obtain

$$\begin{aligned} q_2 &= \frac{i\omega_0 c_1 e^{-i\tau_0\omega_0} - a_1 a_2 I A}{i\omega_0 (i\omega_0 + c_4 - c_2 e^{-i\tau_0\omega_0}) + a_2^2 I A}, \\ q_3 &= \frac{\delta (i\omega_0 c_1 e^{-i\tau_0\omega_0} - a_1 a_2 I A)}{(i\omega_0 + \sigma + \mu) [i\omega_0 (i\omega_0 + c_4 - c_2 e^{-i\tau_0\omega_0}) + a_2^2 I A]}, \\ q_4 &= \frac{a_1 A}{i\omega_0} + \frac{a_2 A (i\omega_0 c_1 e^{-i\tau_0\omega_0} - a_1 a_2 I A)}{-\omega_0^2 (i\omega_0 + c_4 - c_2 e^{-i\tau_0\omega_0}) + i\omega_0 a_2^2 I A}. \end{aligned} \quad (49)$$

Suppose that the eigenvector q^* of A^* belonging to the eigenvalue $-i\tau_0\omega_0$ is

$$q^*(s) = \frac{1}{\rho} (1, q_2^*, q_3^*, q_4^*) e^{i\tau_0\omega_0 s}, \quad 0 \leq s < 1. \quad (50)$$

Similar to the calculation of (49), we can get

$$\begin{aligned} q_2^* &= \frac{i\omega_0 (i\omega_0 - c_3 - c_1 e^{i\tau_0\omega_0}) + a_1^2 AS}{-i\omega_0 c_1 e^{i\tau_0\omega_0} - a_1 a_2 IA}, \\ q_3^* &= \frac{\sigma}{-i\omega_0 + \sigma + \mu}, \\ q_4^* &= \frac{a_1 S}{i\omega_0} + \frac{a_2 I i \omega_0 (i\omega_0 - c_3 - c_1 e^{i\tau_0\omega_0}) + a_1^2 a_2 IAS}{\omega_0^2 c_1 e^{i\tau_0\omega_0} - i\omega_0 a_1 a_2 IA}. \end{aligned} \quad (51)$$

Let $\langle q^*, q \rangle = 1$; then

$$\begin{aligned} \langle q^*(s), q(\theta) \rangle &= \frac{1}{\rho} (1 + q_2 q_2^* + q_3 q_3^* + q_4 q_4^*) \\ &\quad - \int_{\theta=-1}^0 \int_{\xi=0}^{\theta} \frac{1}{\rho} (1, \bar{q}_2^*, \bar{q}_3^*, \bar{q}_4^*) e^{-i\tau_0\omega_0(\xi-\theta)} d\eta(\theta) \\ &\quad \times \begin{pmatrix} 1 \\ q_2 \\ q_3 \\ q_4 \end{pmatrix} e^{i\tau_0\omega_0 \xi} d\xi \\ &= \frac{1}{\rho} (1 + q_2 q_2^* + q_3 q_3^* + q_4 q_4^*) \\ &\quad - \int_{-1}^0 \frac{1}{\rho} (1, \bar{q}_2^*, \bar{q}_3^*, \bar{q}_4^*) \theta e^{i\tau_0\omega_0 \theta} d\eta(\theta) \begin{pmatrix} 1 \\ q_2 \\ q_3 \\ q_4 \end{pmatrix} \\ &= \frac{1}{\rho} \left\{ (1 + q_2 q_2^* + q_3 q_3^* + q_4 q_4^*) \right. \\ &\quad \left. + \tau_0 e^{-i\tau_0\omega_0} [(\bar{q}_2^* - 1)(c_1 + \alpha c_2)] \right\}, \end{aligned} \quad (52)$$

which leads to

$$\begin{aligned} \bar{\rho} &= (1 + q_2 q_2^* + q_3 q_3^* + q_4 q_4^*) \\ &\quad + \tau_0 e^{-i\tau_0\omega_0} [(\bar{q}_2^* - 1)(c_1 + \alpha c_2)]. \end{aligned} \quad (53)$$

In the following, we apply the method in [19] to compute the coordinates describing the center manifold Ω_0 near $u = 0$. Let x_t be the solution of (39) when $u = 0$. We define

$$z(t) = \langle q^*, x_t \rangle, \quad W(t, \theta) = x_t(\theta) - 2 \operatorname{Re} [z(t) q(\theta)]. \quad (54)$$

On the center manifold Ω_0 , we have $W(t, \theta) = W(z(t), \bar{z}(t), \theta)$, where

$$\begin{aligned} W(z(t), \bar{z}(t), \theta) &= W_{20}(\theta) \frac{z^2}{2} + W_{11}(\theta) z \bar{z} + W_{02}(\theta) \frac{\bar{z}^2}{2} + W_{30}(\theta) \frac{z^3}{6} + \dots \end{aligned} \quad (55)$$

In fact, z and \bar{z} are local coordinates of center manifold Ω_0 in the direction of q and q^* , respectively. For solution $x_t \in \Omega_0$ of (44), since $u = 0$, we get

$$\begin{aligned} \dot{z}(t) &= \langle q^*, \dot{x}_t \rangle \\ &= i\tau_0\omega_0 z(t) + \bar{q}^*(0) \\ &\quad \times f(0, W(t, 0) + 2 \operatorname{Re} [z(t) q(0)]) \\ &= i\tau_0\omega_0 z(t) + \bar{q}^*(0) f_0(z, \bar{z}) \\ &\triangleq i\tau_0\omega_0 z(t) + g(z, \bar{z}). \end{aligned} \quad (56)$$

It is noted that

$$\begin{aligned} g(z, \bar{z}) &= \bar{q}^*(0) f_0(z, \bar{z}) \\ &= g_{20} \frac{z^2}{2} + g_{11} z \bar{z} + g_{02} \frac{\bar{z}^2}{2} + g_{21} \frac{z^2 \bar{z}}{2} + \dots \end{aligned} \quad (57)$$

By (54), we know that

$$\begin{aligned} x_t(\theta) &= (x_{1t}(\theta), x_{2t}(\theta), x_{3t}(\theta), x_{4t}(\theta)) \\ &= W(t, \theta) + z q(\theta) + \bar{z} \cdot \bar{q}(\theta). \end{aligned} \quad (58)$$

Considering (47) and (55), we have

$$\begin{aligned} x_{1t}(0) &= z + \bar{z} + W_{20}^{(1)}(0) \frac{z^2}{2} \\ &\quad + W_{11}^{(1)}(0) z \bar{z} + W_{02}^{(1)}(0) \frac{\bar{z}^2}{2} + o(|(z, \bar{z})|^3), \\ x_{2t}(0) &= q_2 z + \bar{q}_2 \bar{z} + W_{20}^{(2)}(0) \frac{z^2}{2} \\ &\quad + W_{11}^{(2)}(0) z \bar{z} + W_{02}^{(2)}(0) \frac{\bar{z}^2}{2} + o(|(z, \bar{z})|^3), \\ x_{4t}(0) &= q_4 z + \bar{q}_4 \bar{z} + W_{20}^{(4)}(0) \frac{z^2}{2} \\ &\quad + W_{11}^{(4)}(0) z \bar{z} + W_{02}^{(4)}(0) \frac{\bar{z}^2}{2} + o(|(z, \bar{z})|^3), \\ x_{1t}(-1) &= z e^{-i\tau_0\omega_0} + \bar{z} e^{i\tau_0\omega_0} + W_{20}^{(1)}(-1) \frac{z^2}{2} \\ &\quad + W_{11}^{(1)}(-1) z \bar{z} + W_{02}^{(1)}(-1) \frac{\bar{z}^2}{2} + o(|(z, \bar{z})|^3), \end{aligned}$$

$$\begin{aligned}
x_{2t}(-1) &= zq_2 e^{-i\tau_0\omega_0} + \bar{z} \cdot \bar{q}_2 e^{i\tau_0\omega_0} + W_{20}^{(2)}(-1) \frac{z^2}{2} \\
&\quad + W_{11}^{(2)}(-1) z\bar{z} + W_{02}^{(2)}(-1) \frac{\bar{z}^2}{2} + o(|(z, \bar{z})|^3).
\end{aligned} \tag{59}$$

It follows that

$$\begin{aligned}
g(z, \bar{z}) &= \bar{q}^*(0) f_0(z, \bar{z}) \\
&= \frac{\tau_0}{\rho} (1, \bar{q}_2^*, \bar{q}_3^*, \bar{q}_4^*) \\
&\quad \times \begin{pmatrix} l_1 x_{2t}^2(-1) - l_2 x_{1t}(-1) x_{2t}(-1) - a_1 x_{1t}(0) x_{4t}(0) + h.o.t \\ -l_1 x_{2t}^2(-1) + l_2 x_{1t}(-1) x_{2t}(-1) - a_2 x_{2t}(0) x_{4t}(0) + h.o.t \\ 0 \\ a_1 x_{1t}(0) x_{4t}(0) + a_2 x_{2t}(0) x_{4t}(0) \end{pmatrix} \\
&= \frac{\tau_0}{\rho} \left\{ [l_1 (1 - \bar{q}_2^*) q_2^2 e^{-2i\tau_0\omega_0} + l_2 (\bar{q}_2^* - 1) q_2 e^{-2i\tau_0\omega_0} \right. \\
&\quad \left. + a_1 (\bar{q}_4^* - 1) q_4 + a_2 (\bar{q}_4^* - \bar{q}_2^*) q_2 q_4] z^2 \right. \\
&\quad \left. + [l_1 (1 - \bar{q}_2^*) \bar{q}_2^2 e^{2i\tau_0\omega_0} + l_2 (\bar{q}_2^* - 1) \bar{q}_2 e^{2i\tau_0\omega_0} \right. \\
&\quad \left. + a_1 (\bar{q}_4^* - 1) \bar{q}_4 + a_2 (\bar{q}_4^* - \bar{q}_2^*) \bar{q}_2 \bar{q}_4] \bar{z}^2 \right. \\
&\quad \left. + [l_1 (1 - \bar{q}_2^*) 2q_2 \bar{q}_2 + l_2 (\bar{q}_2^* - 1) (q_2 + \bar{q}_2) \right. \\
&\quad \left. + a_1 (\bar{q}_4^* - 1) (q_4 + \bar{q}_4) \right. \\
&\quad \left. + a_2 (\bar{q}_4^* - \bar{q}_2^*) (q_2 \bar{q}_4 + \bar{q}_2 q_4)] z\bar{z} \right. \\
&\quad \left. + [l_1 (1 - \bar{q}_2^*) \right. \\
&\quad \left. \times (2q_2 W_{11}^{(2)}(-1) e^{-i\tau_0\omega_0} + \bar{q}_2 W_{20}^{(2)}(-1) e^{i\tau_0\omega_0}) \right. \\
&\quad \left. + l_2 (\bar{q}_2^* - 1) \right. \\
&\quad \left. \times (W_{11}^{(2)}(-1) e^{-i\tau_0\omega_0} + \frac{1}{2} W_{20}^{(2)}(-1) e^{i\tau_0\omega_0} \right. \\
&\quad \left. + \frac{1}{2} \bar{q}_2 W_{20}^{(1)}(-1) e^{i\tau_0\omega_0} \right. \\
&\quad \left. + q_2 W_{11}^{(1)}(-1) e^{-i\tau_0\omega_0}) \right. \\
&\quad \left. + a_1 (\bar{q}_4^* - 1) \right. \\
&\quad \left. \times (W_{11}^{(4)}(0) + \frac{1}{2} W_{20}^{(4)}(0) \right. \\
&\quad \left. + \frac{1}{2} \bar{q}_4 W_{20}^{(1)}(0) + q_4 W_{11}^{(1)}(0)) \right. \\
&\quad \left. + a_2 (\bar{q}_4^* - \bar{q}_2^*) \right. \\
&\quad \left. \times (q_2 W_{11}^{(4)}(0) + \frac{1}{2} \bar{q}_2 W_{20}^{(4)}(0) \right. \\
&\quad \left. + \frac{1}{2} \bar{q}_4 W_{20}^{(2)}(0) + q_4 W_{11}^{(2)}(0)) \right] \\
&\quad \times z^2 \bar{z} + \dots \Big\}.
\end{aligned} \tag{60}$$

Comparing the coefficients in (57) with those in (60), it follows that

$$\begin{aligned}
g_{20} &= \frac{2\tau_0}{\rho} [l_1 (1 - \bar{q}_2^*) q_2^2 e^{-2i\tau_0\omega_0} \\
&\quad + l_2 (\bar{q}_2^* - 1) q_2 e^{-2i\tau_0\omega_0} + a_1 (\bar{q}_4^* - 1) q_4 \\
&\quad + a_2 (\bar{q}_4^* - \bar{q}_2^*) q_2 q_4], \\
g_{02} &= \frac{2\tau_0}{\rho} [l_1 (1 - \bar{q}_2^*) \bar{q}_2^2 e^{2i\tau_0\omega_0} \\
&\quad + l_2 (\bar{q}_2^* - 1) \bar{q}_2 e^{2i\tau_0\omega_0} \\
&\quad + a_1 (\bar{q}_4^* - 1) \bar{q}_4 + a_2 (\bar{q}_4^* - \bar{q}_2^*) \bar{q}_2 \bar{q}_4], \\
g_{11} &= \frac{\tau_0}{\rho} [l_1 (1 - \bar{q}_2^*) 2q_2 \bar{q}_2 + l_2 (\bar{q}_2^* - 1) (q_2 + \bar{q}_2) \\
&\quad + a_1 (\bar{q}_4^* - 1) (q_4 + \bar{q}_4) \\
&\quad + a_2 (\bar{q}_4^* - \bar{q}_2^*) (q_2 \bar{q}_4 + \bar{q}_2 q_4)], \\
g_{21} &= \frac{2\tau_0}{\rho} [l_1 (1 - \bar{q}_2^*) \\
&\quad \times (2q_2 W_{11}^{(2)}(-1) e^{-i\tau_0\omega_0} + \bar{q}_2 W_{20}^{(2)}(-1) e^{i\tau_0\omega_0}) \\
&\quad + l_2 (\bar{q}_2^* - 1) \\
&\quad \times (W_{11}^{(2)}(-1) e^{-i\tau_0\omega_0} + \frac{1}{2} W_{20}^{(2)}(-1) e^{i\tau_0\omega_0} \\
&\quad + \frac{1}{2} \bar{q}_2 W_{20}^{(1)}(-1) e^{i\tau_0\omega_0} + q_2 W_{11}^{(1)}(-1) e^{-i\tau_0\omega_0}) \\
&\quad + a_1 (\bar{q}_4^* - 1) \\
&\quad \times (W_{11}^{(4)}(0) + \frac{1}{2} W_{20}^{(4)}(0) \\
&\quad + \frac{1}{2} \bar{q}_4 W_{20}^{(1)}(0) + q_4 W_{11}^{(1)}(0)) \\
&\quad + a_2 (\bar{q}_4^* - \bar{q}_2^*) \\
&\quad \times (q_2 W_{11}^{(4)}(0) + \frac{1}{2} \bar{q}_2 W_{20}^{(4)}(0) \\
&\quad + \frac{1}{2} \bar{q}_4 W_{20}^{(2)}(0) + q_4 W_{11}^{(2)}(0))].
\end{aligned} \tag{61}$$

Since the $W_{20}(\theta)$ and $W_{11}(\theta)$ exist in (61), we need to compute them. From (44) and (54), we have

$$\begin{aligned}
\dot{W} &= \dot{x}_t - \dot{z}q - \dot{\bar{z}} \cdot \bar{q} \\
&= Ax_t + Rx_t - [i\tau_0\omega_0 z + \bar{q}^*(0) f_0(z, \bar{z})] q \\
&\quad - [-i\tau_0\omega_0 \bar{z} + q^*(0) \bar{f}_0(z, \bar{z})] \bar{q}
\end{aligned}$$

$$\begin{aligned}
&= A (W + 2 \operatorname{Re} (zq)) + Rx_t \\
&\quad - 2 \operatorname{Re} [\bar{q}^* (0) f_0 (z, \bar{z}) q] - 2 \operatorname{Re} [i\tau_0 \omega_0 zq] \\
&= \begin{cases} AW - 2 \operatorname{Re} [\bar{q}^* (0) f_0 (z, \bar{z}) q (\theta)], & -1 \leq \theta < 0, \\ AW - 2 \operatorname{Re} [\bar{q}^* (0) f_0 (z, \bar{z}) q (\theta)] + f, & \theta = 0, \end{cases} \\
&\triangleq AW + H (z, \bar{z}, \theta),
\end{aligned} \tag{62}$$

where

$$H (z, \bar{z}, \theta) = H_{20} (\theta) \frac{z^2}{2} + H_{11} (\theta) z\bar{z} + H_{02} (\theta) \frac{\bar{z}^2}{2} + \dots \tag{63}$$

Substituting (55) and (63) into (62), we get

$$\begin{aligned}
\dot{W} &= (AW_{20} + H_{20}) \frac{z^2}{2} \\
&\quad + (AW_{11} + H_{11}) z\bar{z} + (AW_{02} + H_{02}) \frac{\bar{z}^2}{2} + \dots
\end{aligned} \tag{64}$$

Taking the derivate of W with respect to t in (55), we have

$$\begin{aligned}
\dot{W} &= W_z \dot{z} + W_{\bar{z}} \dot{\bar{z}} \\
&= \left(W_{20} z + W_{11} \bar{z} + W_{30} \frac{z^2}{2} + \dots \right) (i\tau_0 \omega_0 z + g) \\
&\quad + (W_{11} z + W_{02} \bar{z} + \dots) (-i\tau_0 \omega_0 \bar{z} + \bar{g}) \\
&= i\tau_0 \omega_0 W_{20} z^2 + z\bar{z} (i\tau_0 \omega_0 W_{11} - i\tau_0 \omega_0 W_{11}) \\
&\quad - i\tau_0 \omega_0 W_{02} \bar{z}^2 + \dots
\end{aligned} \tag{65}$$

Then, together with the two above equations, we obtain

$$AW_{20} + H_{20} = 2i\tau_0 \omega_0 W_{20}, \quad AW_{11} + H_{11} = 0. \tag{66}$$

By (62), we know that

$$\begin{aligned}
H (z, \bar{z}, \theta) &= -gq (\theta) - \bar{g} \cdot \bar{q} (\theta) + Rx_t \\
&= -\left(g_{20} \frac{z^2}{2} + g_{11} z\bar{z} + g_{02} \frac{\bar{z}^2}{2} + \dots \right) q (\theta) \\
&\quad - \left(\bar{g}_{20} \frac{\bar{z}^2}{2} + \bar{g}_{11} z\bar{z} + \bar{g}_{02} \frac{z^2}{2} + \dots \right) \bar{q} (\theta) + Rx_t.
\end{aligned} \tag{67}$$

We know that when $-1 \leq \theta < 0$ $Rx_t = 0$, comparing the coefficients of the z^2 , $z\bar{z}$ in (63) and (67), respectively, we can find

$$\begin{aligned}
H_{20} (\theta) &= -g_{20} q (\theta) - \bar{g}_{02} \bar{q} (\theta), \\
H_{11} (\theta) &= -g_{11} q (\theta) - \bar{g}_{11} \bar{q} (\theta).
\end{aligned} \tag{68}$$

Combining (66) with (68), it follows that

$$\begin{aligned}
\dot{W}_{20} (\theta) &= 2i\tau_0 \omega_0 W_{20} (\theta) + g_{20} q (\theta) + \bar{g}_{02} \bar{q} (\theta), \\
\dot{W}_{11} (\theta) &= g_{11} q (\theta) + \bar{g}_{11} \bar{q} (\theta), \\
&\quad -1 \leq \theta < 0.
\end{aligned} \tag{69}$$

We solve (69) and get the solutions in the following form:

$$\begin{aligned}
W_{20} (\theta) &= \frac{ig_{20}}{\tau_0 \omega_0} q (0) e^{i\tau_0 \omega_0 \theta} \\
&\quad - \frac{\bar{g}_{02}}{3i\tau_0 \omega_0} \bar{q} (0) e^{-i\tau_0 \omega_0 \theta} + E_1 e^{2i\tau_0 \omega_0 \theta}, \\
W_{11} (\theta) &= \frac{g_{11}}{i\tau_0 \omega_0} q (0) e^{i\tau_0 \omega_0 \theta} \\
&\quad - \frac{\bar{g}_{11}}{i\tau_0 \omega_0} \bar{q} (0) e^{-i\tau_0 \omega_0 \theta} + E_2.
\end{aligned} \tag{70}$$

Next, we consider (66) again when $\theta = 0$; we can see that

$$\begin{aligned}
AW_{20} (0) &= \int_{-1}^0 d\eta (\theta) W_{20} (\theta) = 2i\tau_0 \omega_0 W_{20} (0) - H_{20} (0), \\
AW_{11} (0) &= \int_{-1}^0 d\eta (\theta) W_{11} (\theta) = -H_{11} (0).
\end{aligned} \tag{71}$$

Furthermore, from (62) and (63), we have

$$\begin{aligned}
H_{20} (0) &= -g_{20} q (0) - \bar{g}_{02} \bar{q} (0) \\
&\quad + 2\tau_0 \begin{pmatrix} l_1 q_2^2 e^{-2i\tau_0 \omega_0} - l_2 q_2 e^{-2i\tau_0 \omega_0} - a_1 q_4 \\ -l_1 q_2^2 e^{-2i\tau_0 \omega_0} + l_2 q_2 e^{-2i\tau_0 \omega_0} - a_2 q_2 q_4 \\ 0 \\ a_1 q_4 + a_2 q_2 q_4 \end{pmatrix},
\end{aligned} \tag{72}$$

$$\begin{aligned}
H_{11} (0) &= -g_{11} q (0) - \bar{g}_{11} \bar{q} (0) \\
&\quad + \tau_0 \begin{pmatrix} 2l_1 |q_2|^2 - l_2 (q_2 + \bar{q}_2) - a_1 (q_4 + \bar{q}_4) \\ -2l_1 |q_2|^2 + l_2 (q_2 + \bar{q}_2) - a_2 (q_2 \bar{q}_4 + \bar{q}_2 q_4) \\ 0 \\ a_1 (q_4 + \bar{q}_4) + a_2 (q_2 \bar{q}_4 + \bar{q}_2 q_4) \end{pmatrix}.
\end{aligned} \tag{73}$$

Substitute (70) and (72) into (71) and notice that

$$\begin{aligned} \left(i\tau_0\omega_0 I - \int_{-1}^0 e^{i\tau_0\omega_0\theta} d\eta(\theta) \right) q(0) &= 0, \\ \left(-i\tau_0\omega_0 I - \int_{-1}^0 e^{-i\tau_0\omega_0\theta} d\eta(\theta) \right) \bar{q}(0) &= 0. \end{aligned} \quad (74)$$

It is easy to yield

$$\int_{-1}^0 d\eta(\theta) E_1 e^{2i\tau_0\omega_0\theta}$$

which leads to

$$\begin{aligned} E_1 &= 2 \begin{pmatrix} 2i\omega_0 + c_3 + c_1 e^{-2i\tau_0\omega_0} & c_2 e^{-2i\tau_0\omega_0} & -\sigma & a_1 S \\ -c_1 e^{-2i\tau_0\omega_0} & 2i\omega_0 + c_4 - c_2 e^{-2i\tau_0\omega_0} & 0 & a_2 I \\ 0 & -\delta & 2i\omega_0 + \sigma + \mu & 0 \\ -a_1 A & -a_2 A & 0 & 2i\omega_0 \end{pmatrix}^{-1} \\ &\cdot \begin{pmatrix} l_1 q_2^2 e^{-2i\tau_0\omega_0} - l_2 q_2 e^{-2i\tau_0\omega_0} - a_1 q_4 \\ -l_1 q_2^2 e^{-2i\tau_0\omega_0} + l_2 q_2 e^{-2i\tau_0\omega_0} - a_2 q_2 q_4 \\ 0 \\ a_1 q_4 + a_2 q_2 q_4 \end{pmatrix} \triangleq 2M_1^{-1}M_2. \end{aligned} \quad (75)$$

By the similar way we can get the E_2 as in the following:

$$\begin{aligned} E_2 &= \begin{pmatrix} c_3 + c_1 & c_2 & -\sigma & a_1 S \\ -c_1 & c_4 - c_2 & 0 & a_2 I \\ 0 & -\delta & \sigma + \mu & 0 \\ -a_1 A & -a_2 A & 0 & 0 \end{pmatrix}^{-1} \\ &\times \begin{pmatrix} 2l_1 |q_2|^2 - l_2 (q_2 + \bar{q}_2) - a_1 (q_4 + \bar{q}_4) \\ -2l_1 |q_2|^2 + l_2 (q_2 + \bar{q}_2) - a_2 (q_2 \bar{q}_4 + \bar{q}_2 q_4) \\ 0 \\ a_1 (q_4 + \bar{q}_4) + a_2 (q_2 \bar{q}_4 + \bar{q}_2 q_4) \end{pmatrix}. \end{aligned} \quad (77)$$

Thus, we can calculate the $W_{20}(\theta)$ and $W_{11}(\theta)$ from (70). Consequently, g_{21} in (61) can be received. Then, we need to compute the following parameters [19]:

$$C_1(0) = \frac{i}{2\tau_0\omega_0} \left(g_{20}g_{11} - 2|g_{11}|^2 - \frac{|g_{02}|^2}{3} \right) + \frac{g_{21}}{2}, \quad (78)$$

$$\begin{aligned} \mu_2 &= -\frac{\operatorname{Re}\{C_1(0)\}}{\operatorname{Re}\{\lambda'(\tau_0)\}}, & \beta_2 &= 2\operatorname{Re}\{C_1(0)\}, \\ T_2 &= -\frac{\operatorname{Im}\{C_1(0)\} + \mu_2 \operatorname{Im}\{\lambda'(\tau_0)\}}{\tau_0\omega_0}, \end{aligned} \quad (79)$$

which determine the characteristic of bifurcating periodic solutions in the center manifold at the critical value τ_0 . More details are given in the following theorem.

Theorem 10. *Under the conditions of Theorem 6 one has the following.*

- (1) $u = 0$ is Hopf bifurcation value of system (39).

$$\begin{aligned} &= 2i\tau_0\omega_0 E_1 \\ &- 2\tau_0 \begin{pmatrix} l_1 q_2^2 e^{-2i\tau_0\omega_0} - l_2 q_2 e^{-2i\tau_0\omega_0} - a_1 q_4 \\ -l_1 q_2^2 e^{-2i\tau_0\omega_0} + l_2 q_2 e^{-2i\tau_0\omega_0} - a_2 q_2 q_4 \\ 0 \\ a_1 q_4 + a_2 q_2 q_4 \end{pmatrix}, \end{aligned} \quad (75)$$

- (2) The direction of Hopf bifurcation is determined by the sign of μ_2 : if $\mu_2 > 0$, the Hopf bifurcation is supercritical; if $\mu_2 < 0$, the Hopf bifurcation is subcritical.
- (3) The stability of bifurcating periodic solutions is determined by β_2 : if $\beta_2 < 0$, the periodic solutions are stable; if $\beta_2 > 0$, they are unstable.
- (4) The sign of T_2 determines the period of the bifurcating periodic solutions: if $T_2 > 0$, the period increases; if $T_2 < 0$, the period decreases.

4. Numerical Example

In this section, we will present some numerical simulations for verifying our theoretical analysis. Our example involves 9 parameters, including the delay τ .

Case 1. Consider $a_1 = 0.025$, $a_2 = 0.25$, $\sigma = 0.8$, $\alpha = 0.5$, $\beta = 0.5$, $\delta = 0.4$, $\mu = 0.2$, and $N = 0.2$. In this example, according to Theorems 1 and 3, the system in Case 1 only has one reasonable equilibrium point $[1, 0, 0, 0]$ and this equilibrium is locally asymptotically stable with arbitrarily τ , because $K_0 = 0.8333 < 1$, $K_1 = 0.1250 < 1$, $K_2 = 0.6009 < 1$, and $K_3 = 0.5621 < 1$. When we let $\tau = 0.5$, with the randomly chosen initial value $[0.6145 \ 0.5077 \ 1.6924 \ 0.5913]$, the time response curves are shown in Figures 1 and 2.

Case 2. Consider $a_1 = 0.025$, $a_2 = 0.25$, $\sigma = 0.8$, $\alpha = 1$, $\beta = 4$, $\delta = 0.3$, $\mu = 0.1$, and $N = 0.2$. We can calculate that $K_2 = 1.7838 > 1$, $K_3 = 1.0653 > 1$, $D_1 = 2.3180 > 0$, $D_2 = 4.3667 > 0$, $D_3 = 2.1135 > 0$, $D_4 = 0.0711 > 0$, and $\tau_0 = 2.3581$; we can see that all conditions of Theorem 6 are satisfied; thus, it is easy to obtain the following results.

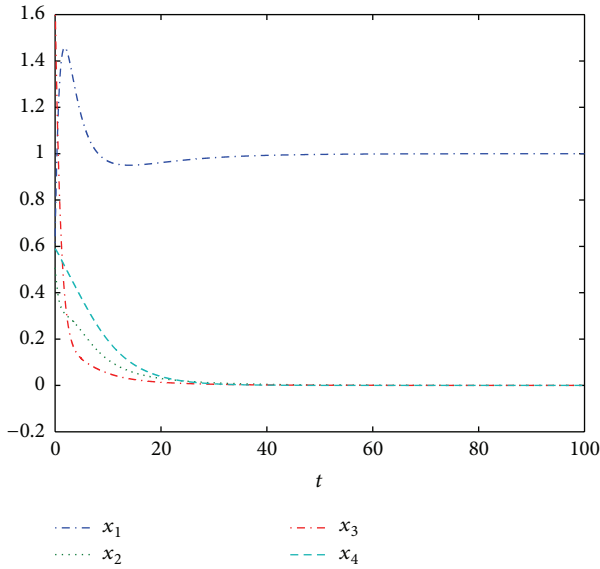


FIGURE 1: All components of the system converge to the equilibrium.

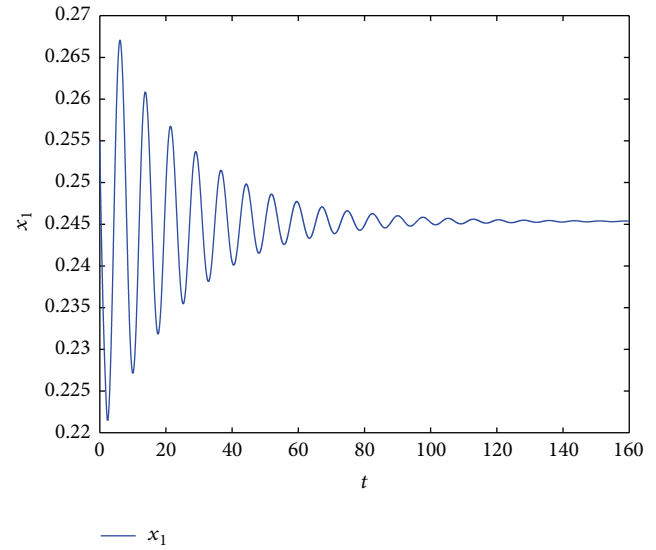


FIGURE 3: The first component of the system converges to 0.2454.

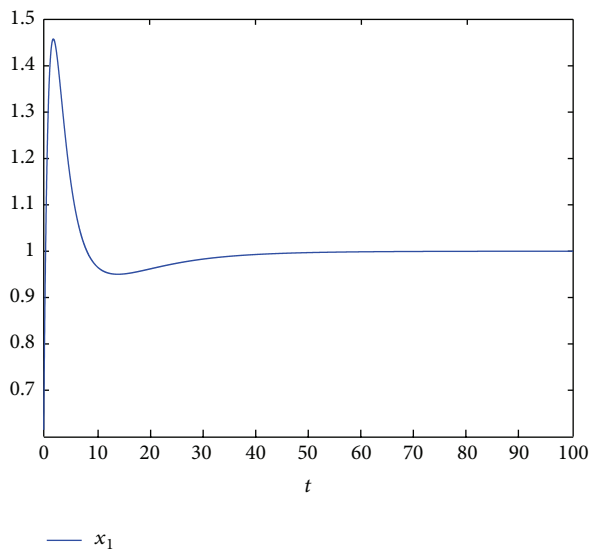
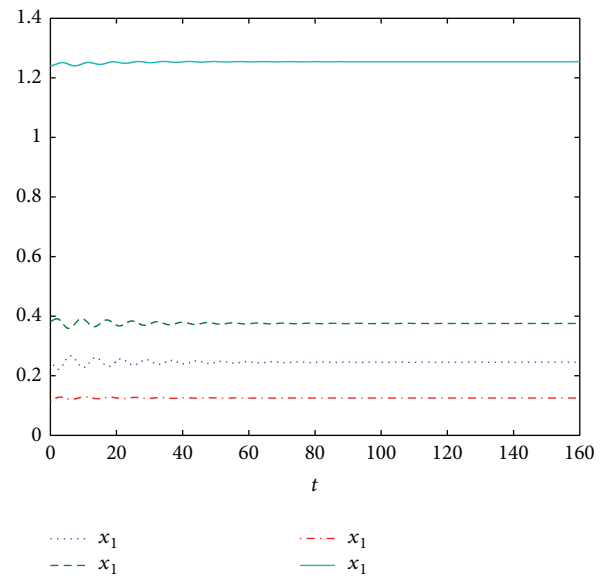


FIGURE 2: The first component of the system converges to 1.

FIGURE 4: Other three components of the system converge to $[0.3755 \ 0.1252 \ 1.2540]$.

When $\tau \in [0, \tau_0)$, there is only one positive equilibrium point $[0.2454 \ 0.3755 \ 0.1252 \ 1.2540]$, which is asymptotically stable. In simulation, we choose $[0.255 \ 0.38 \ 0.11 \ 1.24]$ as initial values; when $\tau = 2 < \tau_0$, the simulation results are Figures 3 and 4; the system in Case 2 undergoes a Hopf bifurcation at the equilibrium point when $\tau = 2.3581 = \tau_0$, as shown in Figures 5 and 6.

Furthermore, when adopting Theorem 10, it is easy to acquire more details about the bifurcating periodic solutions. By (79), we can compute that $C_1(0) = -4.1125 - 4.2861i$, $\mu_2 = 43.8461 > 0$, $\beta_2 = -8.2251 < 0$, and $T_2 = 7.8990 > 0$. Hence, by Theorem 10, we know that the bifurcating point is supercritical, the periodic solutions are stable, and the period increases.

5. Conclusions

In this paper, a modified SIRA model with time delay and nonlinear terms has been proposed, and sufficient conditions on the existence of the virus-free and endemic equilibrium points have been derived. We also obtained several results guaranteeing the stability of the equilibrium and the occurrence of the Hopf bifurcation at the critical value. By using normal form and center manifold theory, the explicit formulae which determine the stability, direction, and other properties of bifurcating periodic solutions have been established. Numerical simulations have been presented to verify the accuracy of our results. The present model

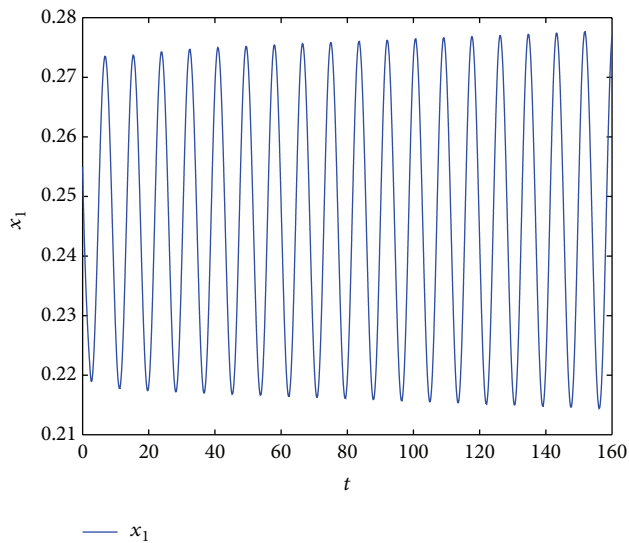


FIGURE 5: The first component oscillates as a periodic solution.

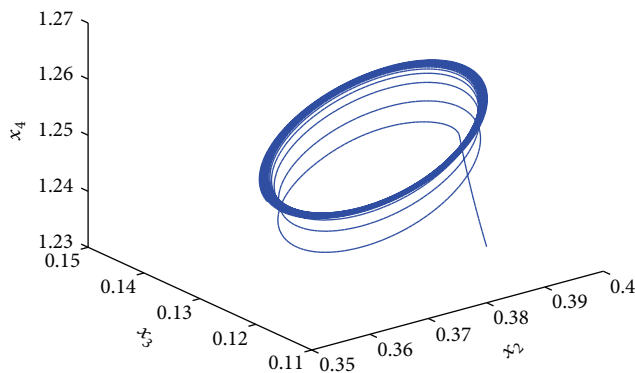


FIGURE 6: The system undergoes a Hopf bifurcation.

can be extended to formulate the more general network for computer virus spread.

Conflict of Interests

The authors declare that there is no conflict of interests regarding the publication of this paper.

Acknowledgments

This publication was made possible by NPRP Grant no. NPRP 4-1162-1-181 from the Qatar National Research Fund (a member of Qatar Foundation). The statements made herein are solely the responsibility of the authors. This work was also supported by Natural Science Foundation of China (Grant no. 61374078).

References

- [1] P. J. Denning, *Computers under Attack: Intruders, Worms, and Viruses*, Addison-Wesley, Reading, Mass, USA, 1990.

- [2] F. Cohen, "A short course on computer viruses," *Computers and Security*, vol. 8, pp. 149–160, 1990.
- [3] L. Billings, W. M. Spears, and I. B. Schwartz, "A unified prediction of computer virus spread in connected networks," *Physics Letters A*, vol. 297, no. 3–4, pp. 261–266, 2002.
- [4] J. O. Kephart and S. R. White, "Measuring and modeling computer virus prevalence," in *Proceedings of the IEEE Computer Society Symposium on Research in Security and Privacy*, pp. 2–15, Oakland, Calif, USA, May 1993.
- [5] R. Perdisci, A. Lanzi, and W. Lee, "Classification of packed executables for accurate computer virus detection," *Pattern Recognition Letters*, vol. 29, no. 14, pp. 1941–1946, 2008.
- [6] Y. B. Kafai, "Understanding virtual epidemics: children's folk conceptions of a computer virus," *Journal of Science Education and Technology*, vol. 17, no. 6, pp. 523–529, 2008.
- [7] X. Han and Q. L. Tan, "Dynamical behavior of computer virus on Internet," *Applied Mathematics and Computation*, vol. 217, no. 6, pp. 2520–2526, 2010.
- [8] R. Xu and Z. E. Ma, "Stability of a delayed SIRS epidemic model with a nonlinear incidence rate," *Chaos, Solitons and Fractals*, vol. 41, no. 5, pp. 2319–2325, 2009.
- [9] W. Ma, M. Song, and Y. Takeuchi, "Global stability of an SIR epidemic model with time delay," *Applied Mathematics Letters*, vol. 17, no. 10, pp. 1141–1145, 2004.
- [10] C. J. Sun, Y. P. Lin, and M. A. Han, "Stability and Hopf bifurcation for an epidemic disease model with delay," *Chaos, Solitons and Fractals*, vol. 30, no. 1, pp. 204–216, 2006.
- [11] R. Xu, Z. E. Ma, and Z. P. Wang, "Global stability of a delayed SIRS epidemic model with saturation incidence and temporary immunity," *Computers and Mathematics with Applications*, vol. 59, no. 9, pp. 3211–3221, 2010.
- [12] S. J. Wang, Q. M. Liu, X. F. Yu, and Y. Ma, "Bifurcation analysis of a model for network worm propagation with time delay," *Mathematical and Computer Modelling*, vol. 52, no. 3–4, pp. 435–447, 2010.
- [13] X. Y. Shi, J. G. Cui, and X. Y. Zhou, "Stability and Hopf bifurcation analysis of an eco-epidemic model with a stage structure," *Nonlinear Analysis*, vol. 74, no. 4, pp. 1088–1106, 2011.
- [14] J. R. C. Piqueira and V. O. Araujo, "A modified epidemiological model for computer viruses," *Applied Mathematics and Computation*, vol. 213, no. 2, pp. 355–360, 2009.
- [15] J. R. C. Piqueira, B. F. Navarro, and L. H. A. Monteiro, "Epidemiological models applied to viruses in computer networks," *Journal of Computer Science*, vol. 1, no. 1, pp. 31–34, 2005.
- [16] W. M. Liu, H. W. Hethcote, and S. A. Levin, "Dynamical behavior of epidemiological models with nonlinear incidence rates," *Journal of Mathematical Biology*, vol. 25, no. 4, pp. 359–380, 1987.
- [17] J. Dieudonné, *Foundations of Modern Analysis*, Academic Press, New York, NY, USA, 1960.
- [18] S. Ruan and J. Wei, "On the zeros of transcendental functions with applications to stability of delay differential equations with two delays," *Dynamics of Continuous, Discrete and Impulsive Systems A: Mathematical Analysis*, vol. 10, no. 6, pp. 863–874, 2003.
- [19] B. Hassard, D. Kazarino, and Y. Wan, *Theory and Applications of Hopf Bifurcations*, Cambridge University Press, Cambridge, UK, 1981.
- [20] Z. C. Jiang and J. J. Wei, "Stability and bifurcation analysis in a delayed SIR model," *Chaos, Solitons and Fractals*, vol. 35, no. 3, pp. 609–619, 2008.

- [21] W. W. Yu and J. D. Cao, "Stability and Hopf bifurcation analysis on a four-neuron BAM neural network with time delays," *Physics Letters A*, vol. 351, no. 1-2, pp. 64–78, 2006.
- [22] J. D. Cao and M. Xiao, "Stability and Hopf bifurcation in a simplified BAM neural network with two time delays," *IEEE Transactions on Neural Networks*, vol. 18, no. 2, pp. 416–430, 2007.
- [23] J. Q. Lu, J. He, J. D. Cao, and Z. Q. Gao, "Topology influences performance in the associative memory neural networks," *Physics Letters Section A*, vol. 354, no. 5-6, pp. 335–343, 2006.
- [24] J. Q. Lu, Z. D. Wang, J. D. Cao, D. C. Ho, and J. Kurths, "Pinning impulsive stabilization of nonlinear dynamical networks with time-varying delay," *International Journal of Bifurcation and Chaos*, vol. 22, no. 7, Article ID 1250176, 2012.

Research Article

The Kirchhoff Index of Toroidal Meshes and Variant Networks

Jia-Bao Liu,^{1,2,3} Xiang-Feng Pan,¹ Jinde Cao,^{2,4} and Xia Huang⁵

¹ School of Mathematical Sciences, Anhui University, Hefei 230601, China

² Department of Mathematics, Southeast University, Nanjing 210096, China

³ Department of Public Courses, Anhui Xinhua University, Hefei 230088, China

⁴ Department of Mathematics, Faculty of Science, King Abdulaziz University, Jeddah 21589, Saudi Arabia

⁵ College of Electrical Engineering and Automation, Shandong University of Science and Technology, Qingdao 266590, China

Correspondence should be addressed to Jinde Cao; jdcao@seu.edu.cn

Received 14 March 2014; Accepted 20 May 2014; Published 3 June 2014

Academic Editor: He Huang

Copyright © 2014 Jia-Bao Liu et al. This is an open access article distributed under the Creative Commons Attribution License, which permits unrestricted use, distribution, and reproduction in any medium, provided the original work is properly cited.

The resistance distance is a novel distance function on electrical network theory proposed by Klein and Randić. The Kirchhoff index $Kf(G)$ is the sum of resistance distances between all pairs of vertices in G . In this paper, we established the relationships between the toroidal meshes network $T_{m \times n}$ and its variant networks in terms of the Kirchhoff index via spectral graph theory. Moreover, the explicit formulae for the Kirchhoff indexes of $L(T_{m \times n})$, $S(T_{m \times n})$, $T(T_{m \times n})$, and $C(T_{m \times n})$ were proposed, respectively. Finally, the asymptotic behavior of Kirchhoff indexes in those networks is obtained by utilizing the applications of analysis approach.

1. Introduction

Throughout this paper we are concerned with finite undirected connected simple graphs (networks). Let $G = (V, E)$ be a graph with vertices labelled $1, 2, \dots, n$. The adjacency matrix $A(G)$ of G is an $n \times n$ matrix with the (i, j) -entry equal to 1 if vertices i and j are adjacent and 0 otherwise. Suppose $D(G) = \text{diag}(d_1(G), d_2(G), \dots, d_n(G))$ is the degree diagonal matrix of G , where $d_i(G)$ is the degree of the vertex i , $i = 1, 2, \dots, n$. Let $L(G) = D(G) - A(G)$ be called the Laplacian matrix of G . Then, the eigenvalues of $A(G)$ and $L(G)$ are called eigenvalues and Laplacian eigenvalues of G , respectively.

Given graphs G and H with vertex sets U and V , the Cartesian product $G \square H$ of graphs G and H is a graph such that the vertex set of $G \square H$ is the Cartesian product $U \times V$; and any two vertices (u, u') and (v, v') are adjacent in $G \square H$ if and only if either $u = v$ and u' is adjacent with v' in H or $u' = v'$ and u is adjacent with v in G [1]. It is well known that many of the graphs (networks) operations can produce a great deal of novel types of graphs (networks), for example, Cartesian product of graphs, line graph, subdivision graph, and so on. The clique-inserted graph, denoted by $C(G)$, is defined as a line graph of the subdivision graph $S(G)$

[2, 3]. The subdivision graph of an r -regular graph is $(r, 2)$ -semiregular graph. Consequently, the clique-inserted graph of an r -regular graph is the line graph of an $(r, 2)$ -semiregular graph.

The resistance distances between vertices i and j , denoted by r_{ij} , are defined as the effective electrical resistance between them if each edge of G is replaced by a unit resistor [4]. A famous distance-based topological index, the Kirchhoff index $Kf(G)$, is defined as the sum of resistance distances between all pairs of vertices in G ; that is, $Kf(G) = (1/2) \sum_{i=1}^n \sum_{j=1}^n r_{ij}(G)$, known as the Kirchhoff index of G [4]; recently, this classical index has also been interpreted as a measure of vulnerability of complex networks [5].

The Kirchhoff index attracted extensive attention due to its wide applications in physics, chemistry, graph theory, and so forth [6–13]. Besides, the Kirchhoff index also is a structure descriptor [14]. Unfortunately, it is rather hard to directly design some algorithms [15–17] to calculate resistance distances and the Kirchhoff indexes of graphs. So, many researchers investigated some special classes of graphs [18–21]. In addition, many efforts were also made to obtain the Kirchhoff index bounds for some graphs [17, 22]. Details on

its theory can be found in recent papers [17, 22] and the references cited therein.

Motivated by the above results, we present the corresponding calculating formulae for the Kirchhoff index of $L(T_{m \times n})$, $S(T_{m \times n})$, $T(T_{m \times n})$, and $C(T_{m \times n})$ in this paper. The rest of this paper is organized as follows. Section 2 presents some underlying notations and preliminaries in our discussion. The proofs of our main results and some asymptotic behavior of Kirchhoff index are proposed in Sections 3 and 4, respectively.

2. Notations and Some Preliminaries

In this section, we introduced some basic properties which we need to use in the proofs of our main results. Suppose that $T_{m \times n}$ stands for the graphs $C_m \square C_n$ for the convenience of description. It is trivial for m, n are 1, 2, without loss of generality, we discuss the situations for any positive integer $m, n \geq 3$.

Zhu et al. [15] and Gutman and Mohar [8] proved the relations between Kirchhoff index of a graph and Laplacian eigenvalues of the graph as follows.

Lemma 1 (see [8, 15]). *Let G be a connected graph with $n \geq 2$ vertices and let $\mu_1 \geq \mu_2 \geq \dots \geq \mu_n = 0$ be the Laplacian eigenvalues of graph G ; then*

$$Kf(G) = n \sum_{i=1}^{n-1} \frac{1}{\mu_i}. \quad (1)$$

The line graph of a graph G , denoted by $L(G)$, is the graph whose vertices correspond to the edges of G with two vertices of $L(G)$ being adjacent if and only if the corresponding edges in G share a common vertex. The subdivision graph of a graph G , denoted by $S(G)$, is the graph obtained by replacing every edge in G with a copy of P_2 (path of length two). The total graph of a graph G , denoted by $T(G)$, is the graph whose vertices correspond to the union of the set of vertices and edges of G , with two vertices of $T(G)$ being adjacent if and only if the corresponding elements are adjacent or incident in G . Let $P_G(x)$ be the characteristic polynomial of the Laplacian matrix of a graph G ; the following results were shown in [23].

Lemma 2 (see [23]). *Let G be an r -regular connected graph with n vertices and m edges; then*

$$P_{L(G)}(x) = (x - 2r)^{m-n} P_G(x),$$

$$P_{S(G)}(x) = (-1)^m (2 - x)^{m-n} P_G(x(r + 2 - x)),$$

$$P_{T(G)}(x)$$

$$= (-1)^m (r + 1 - x)^n (2r + 2 - x)^{m-n} P_G\left(\frac{x(r + 2 - x)}{r - x + 1}\right), \quad (2)$$

where $P_{L(G)}(x)$, $P_{S(G)}(x)$, and $P_{T(G)}(x)$ are the characteristic polynomials for the Laplacian matrix of graphs $L(G)$, $S(G)$, and $T(G)$, respectively.

A bipartite graph G with a bipartition $V(G) = (U, V)$ is called an (r, s) -semiregular graph if all vertices in U have degree r and all vertices in V have degree s . Apparently, the subdivision graph of an r -regular-graph G is $(r, 2)$ -semiregular graph.

Lemma 3 (see [24]). *Let G be an (r, s) -semiregular connected graph with n vertices. Then*

$$P_{L(G)}(x) = (-1)^n (x - (r + s))^{m-n} P_G(r + s - x), \quad (3)$$

where $P_{L(G)}(x)$ is the Laplacian characteristic polynomial of the line graph $L(G)$ and m is the number of edges of G .

Lemma 4 (see [23]). *Let G be a connected simple r -regular graph with n vertices and m edges and let $L(G)$ be the line graph of G . Then*

$$Kf(L(G)) = \frac{r}{2} Kf(G) + \frac{1}{4} n(m - n). \quad (4)$$

Lemma 5 (see [23]). *Let G be a connected simple r -regular graph with $n \geq 2$ vertices; then*

$$Kf(S(G)) = \frac{(r + 2)^2}{2} Kf(G) + \frac{(r^2 - 4)n^2 + 4n}{8}. \quad (5)$$

The following lemma gives an expression on $Kf(T(G))$ and $Kf(G)$ of a regular graph G .

Lemma 6 (see [25]). *Let G be a r -regular connected graph with n vertices and m edges, and $r \geq 2$; then*

$$Kf(T(G)) = \frac{n(r + 2)(r + 4)}{2(r + 3)} \sum_{i=1}^{n-1} \frac{1}{\mu_i + 3 + r} + \frac{(r + 2)^2}{2(r + 3)} Kf(G) + \frac{n^2(r^2 - 4)}{8(r + 1)} + \frac{n}{2}. \quad (6)$$

Lemma 7 presents the formula for calculating Kirchhoff index of $T_{m \times n}$; in the following proof, some techniques in [26] are referred to.

Lemma 7 (see [26]). *For the toroidal networks $T_{m \times n}$ with any positive integer $m, n \geq 3$,*

$$Kf(T_{m \times n}) = mn \sum_{i=1}^{m-1} \sum_{j=1}^{n-1} \frac{1}{4\sin^2(i\pi/m) + 4\sin^2(j\pi/n)} + n \frac{m^3 - m}{12} + m \frac{n^3 - n}{12}. \quad (7)$$

Proof. Suppose the Laplacian eigenvalues of C_m and C_n are $4\sin^2(i\pi/m)$ and $4\sin^2(j\pi/n)$, $i = 0, 1, \dots, m - 1$; $j = 0, 1, \dots, n - 1$; then the Cartesian product $G \square H$ and the Laplacian eigenvalues of $L_{(C_m \square C_n)}$ are

$$4\sin^2 \frac{i\pi}{m} + 4\sin^2 \frac{j\pi}{n}, \quad i = 0, 1, \dots, m - 1; \quad j = 0, 1, \dots, n - 1. \quad (8)$$

According to Lemma 1, the Kirchhoff index of the toroidal networks $Kf(T_{m \times n})$ is

$$\begin{aligned}
 Kf(T_{m \times n}) &= mn \sum_{(i,j) \in A \times B \setminus \{(0,0)\}} \frac{1}{4\sin^2(i\pi/m) + 4\sin^2(j\pi/n)}, \\
 A &= \{0, 1, \dots, m-1\}, \quad B = \{0, 1, \dots, n-1\} \\
 &= mn \sum_{i=0}^{m-1} \sum_{j=0}^{n-1} \frac{1}{4\sin^2(i\pi/m) + 4\sin^2(j\pi/n)}, \\
 &\quad (i, j) \neq (0, 0) \\
 &\quad (9) \\
 &= mn \left(\sum_{i=1}^{m-1} \frac{1}{4\sin^2(i\pi/m)} + \sum_{j=1}^{n-1} \frac{1}{4\sin^2(j\pi/n)} \right. \\
 &\quad \left. + \sum_{i=1}^{m-1} \sum_{j=1}^{n-1} \frac{1}{4\sin^2(i\pi/m) + 4\sin^2(j\pi/n)} \right) \\
 &= n \left(m \sum_{i=1}^{m-1} \frac{1}{4\sin^2(i\pi/m)} \right) \\
 &\quad + m \left(n \sum_{j=1}^{n-1} \frac{1}{4\sin^2(j\pi/n)} \right) \\
 &\quad + mn \sum_{i=1}^{m-1} \sum_{j=1}^{n-1} \frac{1}{4\sin^2(i\pi/m) + 4\sin^2(j\pi/n)} \\
 &= n Kf(C_m) + m Kf(C_n) \\
 &\quad + mn \sum_{i=1}^{m-1} \sum_{j=1}^{n-1} \frac{1}{4\sin^2(i\pi/m) + 4\sin^2(j\pi/n)} \\
 &= mn \sum_{i=1}^{m-1} \sum_{j=1}^{n-1} \frac{1}{4\sin^2(i\pi/m) + 4\sin^2(j\pi/n)} \\
 &\quad + n \frac{m^3 - m}{12} + m \frac{n^3 - n}{12}.
 \end{aligned} \tag{10}$$

Since $Kf(C_n) = (n^3 - n)/12$, (10) in the last line holds.

The following consequence was presented in [26]. Here we give a short proof. \square

Lemma 8 (see [26]). *For the toroidal networks $T_{m \times n}$ with any positive integer $m, n \geq 3$,*

$$\lim_{m \rightarrow \infty} \lim_{n \rightarrow \infty} \frac{Kf(T_{m \times n})}{m^2 n^2} \approx 1.905. \tag{11}$$

Proof. By virtue of (9), one can derive that

$$\begin{aligned}
 \frac{Kf(T_{m \times n})}{mn} &= \sum_{i=0}^{m-1} \sum_{j=0}^{n-1} \frac{1}{4\sin^2(i\pi/m) + 4\sin^2(j\pi/n)}, \\
 &\quad (i, j) \neq (0, 0).
 \end{aligned} \tag{12}$$

Hence,

$$\begin{aligned}
 &\lim_{m \rightarrow \infty} \lim_{n \rightarrow \infty} \frac{Kf(T_{m \times n})}{m^2 n^2} \\
 &= \lim_{m \rightarrow \infty} \lim_{n \rightarrow \infty} \frac{1}{mn} \sum_{i=0}^{m-1} \sum_{j=0}^{n-1} \frac{1}{4 - 2\cos(2\pi i/m) - 2\cos(2\pi j/n)}, \\
 &\quad (i, j) \neq (0, 0) \\
 &= \frac{1}{2\pi} \frac{1}{2\pi} \int_0^{2\pi} \int_0^{2\pi} \frac{d_x d_y}{4 - 2\cos x - 2\cos y} \\
 &\approx 1.905.
 \end{aligned}$$

(13)
 \square

3. Main Results

3.1. The Kirchhoff Index of $L(T_{m \times n})$. In the following theorem, we proposed the formula for calculating the Kirchhoff index of the line graph of $T_{m \times n}$, denoted by $Kf(L(T_{m \times n}))$.

Theorem 9. *Let $L(T_{m \times n})$ be line graphs of $T_{m \times n}$ with any positive integer $m, n \geq 3$; then*

$$\begin{aligned}
 Kf(L(T_{m \times n})) &= 2mn \sum_{i=1}^{m-1} \sum_{j=1}^{n-1} \frac{1}{4\sin^2(i\pi/m) + 4\sin^2(j\pi/n)} \\
 &\quad + n \frac{m^3 - m}{6} + m \frac{n^3 - n}{6} + \frac{m^2 n^2}{4}.
 \end{aligned} \tag{14}$$

Proof. Apparently the toroidal networks $T_{m \times n}$ are 4-regular graphs which have mn vertices and $2mn$ edges, respectively.

We clearly obtained the following relationship $Kf(L(T_{m \times n}))$ and $Kf(T_{m \times n})$ from Lemma 4:

$$\begin{aligned}
 Kf(L(T_{m \times n})) &= \frac{r}{2} Kf(T_{m \times n}) + \frac{(r-2)m^2 n^2}{8} \\
 &= 2 Kf(T_{m \times n}) + \frac{m^2 n^2}{4}.
 \end{aligned} \tag{15}$$

Substituting the results of Lemma 7 into (15), we can get the formula for the Kirchhoff index of $Kf(L(T_{m \times n}))$,

$$\begin{aligned}
 Kf(L(T_{m \times n})) &= 2mn \sum_{i=1}^{m-1} \sum_{j=1}^{n-1} \frac{1}{4\sin^2(i\pi/m) + 4\sin^2(j\pi/n)} \\
 &\quad + n \frac{m^3 - m}{6} + m \frac{n^3 - n}{6} + \frac{m^2 n^2}{4},
 \end{aligned} \tag{16}$$

which completes the proof. \square

3.2. The Kirchhoff Index of $S(T_{m \times n})$. In an almost identical way as Theorem 9, we derived the formula for the Kirchhoff index on the subdivision graph of $T_{m \times n}$, denoted by $Kf(S(T_{m \times n}))$.

Theorem 10. Let $S(T_{m \times n})$ be subdivision graphs of $T_{m \times n}$ with any positive integer $m, n \geq 3$; then

$$\begin{aligned} \text{Kf}(S(T_{m \times n})) &= 18mn \sum_{i=1}^{m-1} \sum_{j=1}^{n-1} \frac{1}{4\sin^2(i\pi/m) + 4\sin^2(j\pi/n)} \\ &\quad + 3n \frac{m^3 - m}{2} + 3m \frac{n^3 - n}{2} + \frac{3m^2n^2 + mn}{2}. \end{aligned} \quad (17)$$

Proof. Noting that $T_{m \times n}$ are 4-regular graphs which have mn vertices, we clearly obtained from Lemma 5

$$\begin{aligned} \text{Kf}(S(T_{m \times n})) &= \frac{(r+2)^2}{2} \text{Kf}(T_{m \times n}) + \frac{(r^2 - 4)m^2n^2 + 4mn}{8} \\ &= 18 \text{Kf}(T_{m \times n}) + \frac{3m^2n^2 + mn}{2}. \end{aligned} \quad (18)$$

Together with the results of Lemma 7 and (18), we can get the formula for the Kirchhoff index on the subdivision graph of $T_{m \times n}$:

$$\begin{aligned} \text{Kf}(S(T_{m \times n})) &= 18mn \sum_{i=1}^{m-1} \sum_{j=1}^{n-1} \frac{1}{4\sin^2(i\pi/m) + 4\sin^2(j\pi/n)} \\ &\quad + 3n \frac{m^3 - m}{2} + 3m \frac{n^3 - n}{2} + \frac{3m^2n^2 + mn}{2}. \end{aligned} \quad (19)$$

The proof is completed. \square

3.3. The Kirchhoff Index of $T(T_{m \times n})$. Now we proved the formula for estimating the Kirchhoff index in the total graph of $T_{m \times n}$, denoted by $\text{Kf}(T(T_{m \times n}))$.

Theorem 11. Let $T(T_{m \times n})$ be total graphs of $T_{m \times n}$ with any positive integer $m, n \geq 3$; then

$$\begin{aligned} \text{Kf}(T(T_{m \times n})) &= \frac{18}{7}mn \sum_{i=1}^{m-1} \sum_{j=1}^{n-1} \frac{1}{4\sin^2(i\pi/m) + 4\sin^2(j\pi/n)} \\ &\quad + \frac{24mn}{7} \sum_{i=0}^{m-1} \sum_{j=0}^{n-1} \frac{1}{7 + 4\sin^2(i\pi/m) + 4\sin^2(j\pi/n)} \\ &\quad + \frac{3}{14}n(m^3 - m) + \frac{3}{14}m(n^3 - n) + \frac{3m^2n^2}{10} + \frac{mn}{2}, \\ &\quad (i, j) \neq (0, 0). \end{aligned} \quad (20)$$

Proof. Supposing that the Laplacian eigenvalues of $L_{(C_m \square C_n)}$ are μ_{ij} , one can readily see that

$$\mu_{ij} = 4\sin^2 \frac{i\pi}{m} + 4\sin^2 \frac{j\pi}{n}, \quad (21)$$

$$i = 0, 1, \dots, m-1; \quad j = 0, 1, \dots, n-1.$$

Applying Lemma 6, the following result is straightforward:

$$\begin{aligned} \text{Kf}(T(T_{m \times n})) &= \frac{18}{7} \text{Kf}(T_{m \times n}) + \frac{3m^2n^2}{10} + \frac{mn}{2} \\ &\quad + \frac{24mn}{7} \sum_{(i,j) \neq (0,0)} \frac{1}{7 + \mu_{ij}}. \end{aligned} \quad (22)$$

Notice that $L_{(C_m \square C_n)}$ have $mn - 1$ nonzero Laplacian eigenvalues, and

$$\sum_{(i,j) \neq (0,0)} \frac{1}{7 + \mu_{ij}} = \sum_{i=0}^{m-1} \sum_{j=0}^{n-1} \frac{1}{7 + 4\sin^2(i\pi/m) + 4\sin^2(j\pi/n)}, \quad (i, j) \neq (0, 0), \quad (23)$$

where $i = 0, 1, \dots, m-1$ and $j = 0, 1, \dots, n-1$.

Consequently, the relationships between $T_{m \times n}$ and its variant networks $T(T_{m \times n})$ for Kirchhoff index are as follows:

$$\begin{aligned} \text{Kf}(T(T_{m \times n})) &= \frac{18}{7} \text{Kf}(T_{m \times n}) \\ &\quad + \frac{24mn}{7} \sum_{i=0}^{m-1} \sum_{j=0}^{n-1} \frac{1}{7 + 4\sin^2(i\pi/m) + 4\sin^2(j\pi/n)} \\ &\quad + \frac{3m^2n^2}{10} + \frac{mn}{2}, \quad (i, j) \neq (0, 0). \end{aligned} \quad (24)$$

According to the results of Lemma 7, we can verify the formula for the Kirchhoff index of the total graph of $\text{Kf}(T(T_{m \times n}))$ from (24). Consider

$$\begin{aligned} \text{Kf}(T(T_{m \times n})) &= \frac{18}{7}mn \sum_{i=1}^{m-1} \sum_{j=1}^{n-1} \frac{1}{4\sin^2(i\pi/m) + 4\sin^2(j\pi/n)} \\ &\quad + \frac{24mn}{7} \sum_{i=0}^{m-1} \sum_{j=0}^{n-1} \frac{1}{7 + 4\sin^2(i\pi/m) + 4\sin^2(j\pi/n)} \\ &\quad + \frac{3}{14}n(m^3 - m) + \frac{3}{14}m(n^3 - n) \\ &\quad + \frac{3m^2n^2}{10} + \frac{mn}{2}, \quad (i, j) \neq (0, 0). \end{aligned} \quad (25)$$

This completes the proof of Theorem 11. \square

3.4. The Kirchhoff Index of $C(T_{m \times n})$. We will explore the formula for estimating the Kirchhoff index in the clique-inserted graph of $T_{m \times n}$, denoted by $\text{Kf}(C(T_{m \times n}))$.

Theorem 12. Let $C(T_{m \times n})$ be clique-inserted graphs of $T_{m \times n}$ with any positive integer $m, n \geq 3$; then

$$\begin{aligned} \text{Kf}(C(T_{m \times n})) &= 4mn \sum_{i=0}^{m-1} \sum_{j=0}^{n-1} \frac{1}{3 - \sqrt{5 + 2 \cos(2\pi i/m) + 2 \cos(2\pi j/n)}} \\ &\quad + 4mn \sum_{i=0}^{m-1} \sum_{j=0}^{n-1} \frac{1}{3 + \sqrt{5 + 2 \cos(2\pi i/m) + 2 \cos(2\pi j/n)}} \\ &\quad + \frac{5}{3} m^2 n^2, \end{aligned} \quad (26)$$

where the first summation $i = 0, 1, \dots, m-1$; $j = 0, 1, \dots, n-1$, and $(i, j) \neq (0, 0)$.

Proof. Noting that $S(T_{m \times n})$ is $(r, 2)$ -semiregular graphs and supposing that $S(T_{m \times n})$ has p vertices and q edges, then obviously $p = 3mn$, $q = 4mn$, and $r = 4$, respectively.

By virtue of Lemma 3,

$$P_{L(G)}(x) = (-1)^n (x - (r + s))^{m-n} P_G(r + s - x). \quad (27)$$

Let G be the graph $S(T_{m \times n})$; that is,

$$P_{L(S(T_{m \times n}))}(x) = (-1)^p (x - (r + s))^{q-p} P_{S(T_{m \times n})}(r + s - x). \quad (28)$$

From the definition of clique-inserted graph, one can immediately obtain that

$$\begin{aligned} P_{C(T_{m \times n})}(x) &= (-1)^p (x - (r + 2))^{q-p} P_{S(T_{m \times n})}(6 - x) \\ &= (-1)^{3mn} (x - 6)^{mn} P_{S(T_{m \times n})}(6 - x). \end{aligned} \quad (29)$$

Obviously, it follows from Lemma 2,

$$P_{S(G)}(x) = (-1)^m (2 - x)^{m-n} P_G(x(r + 2 - x)). \quad (30)$$

Replace x with $6 - x$ in (30); moreover, $T_{m \times n}$ have mn vertices and $2mn$ edges; we have that

$$P_{S(T_{m \times n})}(6 - x) = (-1)^{mn} (x - 4)^{mn} P_{T_{m \times n}}(x(6 - x)). \quad (31)$$

Based on (29) and (31),

$$P_{C(T_{m \times n})}(x) = (-1)^{4mn} ((x - 4)(x - 6))^{mn} P_{T_{m \times n}}(x(6 - x)). \quad (32)$$

Since the roots of $x(6 - x) = \mu_{ij}$ are

$$3 \pm \sqrt{9 - \mu_{ij}}, \quad (33)$$

where μ_{ij} are the Laplacian eigenvalues of $T_{m \times n}$ and $\mu_{ij} = 4\sin^2(i\pi/m) + 4\sin^2(j\pi/n)$, $i = 0, 1, \dots, m-1$; $j = 0, 1, \dots, n-1$.

It follows from (32) that the Laplacian spectrum of $C(T_{m \times n})$ is

$$\begin{aligned} \text{Spec}_L(C(T_{m \times n})) &= \begin{pmatrix} 4 & 6 & \mu_{ij}(C(T_{m \times n})) & \mu'_{ij}(C(T_{m \times n})) \\ mn & mn & 1 & 1 \end{pmatrix}, \end{aligned} \quad (34)$$

where $\mu_{ij}(C(T_{m \times n})) = 3 - \sqrt{9 - \mu_{ij}}$, $\mu'_{ij}(C(T_{m \times n})) = 3 + \sqrt{9 - \mu_{ij}}$, $i = 0, 1, \dots, m-1$, and $j = 0, 1, \dots, n-1$.

Employing Lemma 1, (33), and the Laplacian spectrum of $C(T_{m \times n})$, the following result is straightforward:

$$\begin{aligned} \text{Kf}(C(T_{m \times n})) &= 4mn \left(\frac{mn}{4} + \frac{mn}{6} + \sum_{(i,j) \neq (0,0)} \frac{1}{\mu_{ij}(C(G))} + \sum \frac{1}{\mu'_{ij}(C(G))} \right) \\ &= \frac{5}{3} m^2 n^2 + 4mn \left(\sum_{(i,j) \neq (0,0)} \frac{1}{3 - \sqrt{9 - \mu_{ij}}} \right. \\ &\quad \left. + \sum \frac{1}{3 + \sqrt{9 - \mu_{ij}}} \right) \\ &= 4mn \sum_{i=0}^{m-1} \sum_{j=0}^{n-1} \frac{1}{3 - \sqrt{5 + 2 \cos(2\pi i/m) + 2 \cos(2\pi j/n)}}, \\ &\quad (i, j) \neq (0, 0), \\ &\quad + 4mn \sum_{i=0}^{m-1} \sum_{j=0}^{n-1} \frac{1}{3 + \sqrt{5 + 2 \cos(2\pi i/m) + 2 \cos(2\pi j/n)}} \\ &\quad + \frac{5}{3} m^2 n^2. \end{aligned} \quad (35)$$

Hence Theorem 12 holds. \square

Remark 13. The consequences of Lemma 7 and Theorems 9–12 above present closed-form formulae for immediately obtaining its Kirchhoff indexes in terms of finite various networks; however, the quantities are rather difficult to calculate directly.

4. The Asymptotic Behavior of Related Kirchhoff Index

We explore the asymptotic behavior of Kirchhoff index for the investigated networks above as m, n tend to infinity. It is interesting and surprising that the quantity tends to a constant even though $\text{Kf}(G) \rightarrow \infty$, as m, n tend to infinity; that is,

$$\lim_{m \rightarrow \infty} \lim_{n \rightarrow \infty} \frac{\text{Kf}(G)}{m^2 n^2} = C, \quad m, n \rightarrow \infty. \quad (36)$$

Moreover, one can employ the applications of analysis approach to obtain the explicit approximate values of Kirchhoff index for the related networks.

Theorem 14. Let $L(T_{m \times n})$ be line graphs of $T_{m \times n}$ with any positive integer m, n ; then

$$\lim_{m \rightarrow \infty} \lim_{n \rightarrow \infty} \frac{Kf(L(T_{m \times n}))}{m^2 n^2} \approx 4.060. \quad (37)$$

Proof. According to (15) and the result of Lemma 8, we can derive that

$$\begin{aligned} Kf(L(T_{m \times n})) &= 2 Kf(T_{m \times n}) + \frac{m^2 n^2}{4} \\ &= 4.060 m^2 n^2. \end{aligned} \quad (38)$$

Consequently,

$$\lim_{m \rightarrow \infty} \lim_{n \rightarrow \infty} \frac{Kf(L(T_{m \times n}))}{m^2 n^2} \approx 4.060. \quad (39)$$

The result is equivalent to $L(T_{m \times n})$ having asymptotic Kirchhoff index,

$$Kf(L(T_{m \times n})) \approx 4.060 m^2 n^2, \quad m, n \rightarrow \infty. \quad (40)$$

□

Theorem 15. Let $S(T_{m \times n})$ be subdivision graph of $T_{m \times n}$ with any positive integer m, n ; then

$$\lim_{m \rightarrow \infty} \lim_{n \rightarrow \infty} \frac{Kf(S(T_{m \times n}))}{m^2 n^2} \approx 35.790. \quad (41)$$

Proof. Similarly, according to (18), we can easily verify that

$$\begin{aligned} Kf(S(T_{m \times n})) &= 18 Kf(T_{m \times n}) + \frac{3m^2 n^2 + mn}{2} \\ &= 35.790 m^2 n^2. \end{aligned} \quad (42)$$

Hence,

$$\lim_{m \rightarrow \infty} \lim_{n \rightarrow \infty} \frac{Kf(S(T_{m \times n}))}{m^2 n^2} \approx 35.790. \quad (43)$$

□

Theorem 16. Let $T(T_{m \times n})$ be total graph of $T_{m \times n}$ with any positive integer $m, n \geq 3$; then

$$\lim_{m \rightarrow \infty} \lim_{n \rightarrow \infty} \frac{Kf(T(T_{m \times n}))}{m^2 n^2} \approx 5.521. \quad (44)$$

Proof. Consider the summation term $\sum_{i=0}^{m-1} \sum_{j=0}^{n-1} (1/(7 + 4\sin^2(i\pi/m) + 4\sin^2(j\pi/n)))$.

Since

$$\begin{aligned} &\lim_{m \rightarrow \infty} \lim_{n \rightarrow \infty} \frac{1}{m} \frac{1}{n} \sum_{i=0}^{m-1} \sum_{j=0}^{n-1} \frac{1}{7 + 4\sin^2(i\pi/m) + 4\sin^2(j\pi/n)} \\ &= \lim_{m \rightarrow \infty} \lim_{n \rightarrow \infty} \frac{1}{m} \frac{1}{n} \sum_{i=0}^{m-1} \sum_{j=0}^{n-1} \frac{1}{11 - 2\cos(2\pi i/m) - 2\cos(2\pi j/n)} \\ &= \frac{1}{4\pi^2} \int_0^{2\pi} \int_0^{2\pi} \frac{d_x d_y}{11 - 2\cos x - 2\cos y} \approx 0.094. \end{aligned} \quad (45)$$

The value in last line via the mathematic software MATLAB, which can obtain the result above.

Combining with (22), we can obtain that

$$\begin{aligned} &Kf(T(T_{m \times n})) \\ &= \frac{18}{7} Kf(T_{m \times n}) \\ &\quad + \frac{24mn}{7} \sum_{i=0}^{m-1} \sum_{j=0}^{n-1} \frac{1}{7 + 4\sin^2(i\pi/m) + 4\sin^2(j\pi/n)} \\ &\quad + \frac{3m^2 n^2}{10} + \frac{mn}{2}, \quad (i, j) \neq (0, 0) \\ &\approx 5.521 m^2 n^2. \end{aligned} \quad (46)$$

So

$$\lim_{m \rightarrow \infty} \lim_{n \rightarrow \infty} \frac{Kf(T(T_{m \times n}))}{m^2 n^2} \approx 5.521. \quad (47)$$

□

Theorem 17. Let $C(T_{m \times n})$ be clique-inserted graph of $T_{m \times n}$ with any positive integer $m, n \geq 3$; then

$$\lim_{m \rightarrow \infty} \lim_{n \rightarrow \infty} \frac{Kf(C(T_{m \times n}))}{m^2 n^2} \approx 38.591. \quad (48)$$

Proof. From the proof of Theorem 12, we know that

$$\begin{aligned} &Kf(C(T_{m \times n})) \\ &= 4mn \sum_{i=0}^{m-1} \sum_{j=0}^{n-1} \frac{1}{3 - \sqrt{5 + 2\cos(2\pi i/m) + 2\cos(2\pi j/n)}} \\ &\quad + 4mn \sum_{i=0}^{m-1} \sum_{j=0}^{n-1} \frac{1}{3 + \sqrt{5 + 2\cos(2\pi i/m) + 2\cos(2\pi j/n)}} \\ &\quad + \frac{5}{3} m^2 n^2, \end{aligned} \quad (49)$$

where the first summation $i = 0, 1, \dots, m-1$; $j = 0, 1, \dots, n-1$, and $(i, j) \neq (0, 0)$.

As m, n tend to infinity, it follows from the first summation term:

$$\begin{aligned} \lim_{m \rightarrow \infty} \lim_{n \rightarrow \infty} \frac{1}{m} \frac{1}{n} \sum_{i=0}^{m-1} \sum_{j=0}^{n-1} \frac{1}{\sqrt{5 + 2 \cos(2\pi i/m) + 2 \cos(2\pi j/n)}} \\ = \frac{1}{4\pi^2} \int_0^{2\pi} \int_0^{2\pi} \frac{d_x d_y}{3 - \sqrt{5 + 2 \cos x + 2 \cos y}} \approx 9.037. \end{aligned} \quad (50)$$

Similarly, it holds from the second summation term when m, n tend to infinity,

$$\begin{aligned} \lim_{m \rightarrow \infty} \lim_{n \rightarrow \infty} \frac{1}{m} \frac{1}{n} \sum_{i=0}^{m-1} \sum_{j=0}^{n-1} \frac{1}{\sqrt{5 + 2 \cos(2\pi i/m) + 2 \cos(2\pi j/n)}} \\ = \frac{1}{4\pi^2} \int_0^{2\pi} \int_0^{2\pi} \frac{d_x d_y}{3 + \sqrt{5 + 2 \cos x + 2 \cos y}} \approx 0.195. \end{aligned} \quad (51)$$

Combining with the consequences of Theorem 12 and (50) and (51), it follows that

$$\lim_{m \rightarrow \infty} \lim_{n \rightarrow \infty} \frac{\text{Kf}(C(T_{m \times n}))}{m^2 n^2} \approx 38.591. \quad (52)$$

Summing up, we complete the proof. \square

5. Conclusions

Resistance distance was introduced by Klein and Randić as a generalization of the classical distance. In this paper, we have deduced the relationships between the toroidal meshes network $T_{m \times n}$ and its variant networks in terms of the Kirchhoff index via spectral graph theory. The explicit formulae for calculating the Kirchhoff indexes of $L(T_{m \times n})$, $S(T_{m \times n})$, $T(T_{m \times n})$, and $C(T_{m \times n})$ were proposed for any positive integer $m, n \geq 3$, respectively.

The asymptotic behavior of Kirchhoff indexes has been investigated with the applications of analysis approach, and the explicit approximate values are obtained by calculations for the related networks. The values of Kirchhoff indexes with respect to various networks can be immediately obtained via this approach; however, the quantities are rather difficult to calculate directly.

Conflict of Interests

The authors declare that there is no conflict of interests regarding the publication of this paper.

Acknowledgments

The work of Jia-Bao Liu is partly supported by the Natural Science Foundation of Anhui Province of China under Grant no. KJ2013B105. The work of Xiang-Feng Pan is partly supported by the National Science Foundation of China under Grant nos. 10901001, 11171097, and 11371028.

References

- [1] J. M. Xu, *Topological Structure and Analysis of Interconnection Networks*, Kluwer Academic, London, UK, 2001.
- [2] T. Shirai, "The spectrum of infinite regular line graphs," *Transactions of the American Mathematical Society*, vol. 352, no. 1, pp. 115–132, 2000.
- [3] F. Zhang, Y.-C. Chen, and Z. Chen, "Clique-inserted-graphs and spectral dynamics of clique-inserting," *Journal of Mathematical Analysis and Applications*, vol. 349, no. 1, pp. 211–225, 2009.
- [4] D. J. Klein and M. Randić, "Resistance distance," *Journal of Mathematical Chemistry*, vol. 12, no. 1–4, pp. 81–95, 1993.
- [5] E. Estrada and N. Hatano, "A vibrational approach to node centrality and vulnerability in complex networks," *Physica A: Statistical Mechanics and Its Applications*, vol. 389, no. 17, pp. 3648–3660, 2010.
- [6] X. Y. Liu and W. G. Yan, "The triangular kagomé lattices revisited," *Physica A: Statistical Mechanics and Its Applications*, vol. 392, no. 22, pp. 5615–5621, 2013.
- [7] B. Zhou and N. Trinajstić, "A note on Kirchhoff index," *Chemical Physics Letters*, vol. 455, no. 1–3, pp. 120–123, 2008.
- [8] I. Gutman and B. Mohar, "The quasi-Wiener and the Kirchhoff indices coincide," *Journal of Chemical Information and Computer Sciences*, vol. 36, no. 5, pp. 982–985, 1996.
- [9] E. Estrada and N. Hatano, "Topological atomic displacements, Kirchhoff and Wiener indices of molecules," *Chemical Physics Letters*, vol. 486, no. 4–6, pp. 166–170, 2010.
- [10] A. D. Maden, A. S. Cevik, I. N. Cangul, and K. C. Das, "On the Kirchhoff matrix, a new Kirchhoff index and the Kirchhoff energy," *Journal of Inequalities and Applications*, vol. 2013, article 337, 2013.
- [11] J. B. Liu, J. Cao, X.-F. Pan, and A. Elaiw, "The Kirchhoff index of hypercubes and related complex networks," *Discrete Dynamics in Nature and Society*, vol. 2013, Article ID 543189, 7 pages, 2013.
- [12] J. Liu, X.-F. Pan, Y. Wang, and J. Cao, "The Kirchhoff index of folded hypercubes and some variant networks," *Mathematical Problems in Engineering*, vol. 2014, Article ID 380874, 9 pages, 2014.
- [13] J. B. Liu, X. F. Pan, J. Cao, and F. F. Hu, "A note on some physical and chemical indices of clique-inserted lattices," *Journal of Statistical Mechanics: Theory and Experiment*. In press.
- [14] W. J. Xiao and I. Gutman, "Resistance distance and Laplacian spectrum," *Theoretical Chemistry Accounts*, vol. 110, no. 4, pp. 284–289, 2003.
- [15] H.-Y. Zhu, D. J. Klein, and I. Lukovits, "Extensions of the Wiener number," *Journal of Chemical Information and Computer Sciences*, vol. 36, no. 3, pp. 420–428, 1996.
- [16] D. Babić, D. J. Klein, I. Lukovits, S. Nikolić, and N. Trinajstić, "Resistance-distance matrix: a computational algorithm and its applications," *International Journal of Quantum Chemistry*, vol. 90, no. 1, pp. 166–176, 2002.
- [17] J. L. Palacios and J. M. Renom, "Bounds for the Kirchhoff index of regular graphs via the spectra of their random walks," *International Journal of Quantum Chemistry*, vol. 110, no. 9, pp. 1637–1641, 2010.
- [18] J. L. Palacios, "Closed-form formulas for Kirchhoff index," *International Journal of Quantum Chemistry*, vol. 81, no. 2, pp. 135–140, 2001.
- [19] I. Lukovits, S. Nikolić, and N. Trinajstić, "Resistance distance in regular graphs," *International Journal of Quantum Chemistry*, vol. 71, no. 3, pp. 217–225, 1999.

- [20] H. P. Zhang, Y. J. Yang, and C. Li, "Kirchhoff index of composite graphs," *Discrete Applied Mathematics*, vol. 157, no. 13, pp. 2918–2927, 2009.
- [21] C. Arauz, "The Kirchhoff indexes of some composite networks," *Discrete Applied Mathematics*, vol. 160, no. 10-11, pp. 1429–1440, 2012.
- [22] M. Bianchi, A. Cornaro, J. L. Palacios, and A. Torriero, "Bounds for the Kirchhoff index via majorization techniques," *Journal of Mathematical Chemistry*, vol. 51, no. 2, pp. 569–587, 2013.
- [23] X. Gao, Y. F. Luo, and W. W. Liu, "Kirchhoff index in line, subdivision and total graphs of a regular graph," *Discrete Applied Mathematics*, vol. 160, no. 4-5, pp. 560–565, 2012.
- [24] B. Mohar and Y. Alavi, "The Laplacian spectrum of graphs," in *Graph Theory, Combinatorics, and Applications*, vol. 2, pp. 871–898, 1991.
- [25] Z. You, L. You, and W. Hong, "Comment on 'Kirchhoff index in line, subdivision and total graphs of a regular graph,'" *Discrete Applied Mathematics*, vol. 161, no. 18, pp. 3100–3103, 2013.
- [26] L. Ye, "On the Kirchhoff index of some toroidal lattices," *Linear and Multilinear Algebra*, vol. 59, no. 6, pp. 645–650, 2011.

Research Article

A Study of How the Watts-Strogatz Model Relates to an Economic System's Utility

Lunhan Luo and Jianan Fang

School of Information Science and Technology, Donghua University, Shanghai 201620, China

Correspondence should be addressed to Jianan Fang; jafang@dhu.edu.cn

Received 7 February 2014; Revised 8 May 2014; Accepted 8 May 2014; Published 1 June 2014

Academic Editor: He Huang

Copyright © 2014 L. Luo and J. Fang. This is an open access article distributed under the Creative Commons Attribution License, which permits unrestricted use, distribution, and reproduction in any medium, provided the original work is properly cited.

Watts-Strogatz model is a main mechanism to construct the small-world networks. It is widely used in the simulations of small-world featured systems including economic system. Formally, the model contains a parameters set including three variables representing group size, number of neighbors, and rewiring probability. This paper discusses how the parameters set relates to the economic system performance which is utility growth rate. In conclusion, it is found that, regardless of the group size and rewiring probability, 2 to 18 neighbors can help the economic system reach the highest utility growth rate. Furthermore, given the range of neighbors and group size of a Watts-Strogatz model based system, the range of its edges can be calculated too. By examining the containment relationship between that range and the edge number of an actual equal-size economic system, we could know whether the system structure has redundant edges or can achieve the highest utility growth ratio.

1. Introduction

In the 1990s, Watts and Strogatz [1] have shown that the connection topology of biological, technological, and social networks is neither completely regular [2] nor completely random [3] but stays somehow in between these two extreme cases [4]. To get the small-world network, they have proposed the Watts-Strogatz model (WS model) to interpolate between regular and random networks. Since then, a rapid surge of interest for small-world networks throughout natural and social sciences has witnessed the diffusion of new concepts.

Alexander-Bloch et al. [5] systematically explored relationships between functional connectivity, small-world featured complex network topology, and anatomical (Euclidean) distance between connected brain regions. Céline and Guy [6] developed new classification and clustering schemes based on the relative local density of subgraphs on geography and described how the notions and methods contribute on a conceptual level, in terms of measures, delineations, explanatory analyses, and visualization of geographical phenomena. Using the small-world approach Corso et al. [7] suggested a network model for economy. Based on evolving network model, the wealth distribution of a society was constructed qualitatively. Sparked by an increasing need in science and

technology for understanding complex interwoven systems as diverse as the world wide web [8, 9], cellular metabolism, and human social interactions [10, 11], there has been an explosion of interest in network dynamics, the computational analysis of the structure, and function of large physical and virtual networks. Besides, some researchers focused on researching the mechanism of the WS model. Kleinberg [12] explained why arbitrary pairs of strangers should be able to find short chains of acquaintances that link them together.

Generally, the abovementioned researchers utilize the WS model as a modeling tool through which they construct the systems with their expertise. Their research looks at the system's "small-world" characteristics such as the average shortest path length [13], clustering coefficient [14], and degree distribution [15]. With the same route, we have built a small-world featured economic system and analyzed the correlation between the system structure and utility growth rate (UGR). A brief review of the works focused on utility is listed as follows. John et al. [16] discussed the economic utility function in the supply chain management covering logistics and marketing scheme. Ben and Mark [17] studied the relationship between net worth and economic performance measured by utility variation. Due to

the broad implication of “utility,” some researchers from entities other than economic system are drawn into the topic. Torrance [18] provided a new utility measurement and cost-utility analysis method in healthcare. Birati and Tziner [19] introduced the concept of economic utility into the training program usually representing major outlay for many corporations.

During our research we found out that the removal of edges (at least one in five) in the system would not raise any impact on the value of utility function. It can be deduced that there are redundant edges in this small-world featured economic system. Many studies on the network stability [20, 21] also revealed that some edges missing caused by the intentionally attack would not reduce the network connectivity and reliability, despite being considered the advantage of small-world network. However, in an economic system, the useless edges, bringing costs but no profits, are not expected.

The result inspires us to trace back the origins of these redundant edges, that is, the WS model. Since no modification to the group size and the connections among the nodes after the modeling process has been taken, we hypothesize that the system structure is the product of WS model. Equivalently, the WS model would surely exert influence on UGR, because of the proven fact that the system structure has impact on the economic system’s performance [22, 23]. Normally, the WS model is expressed as a function with three parameters (group size, number of neighbors, and rewiring probability) controlling the modeling process. The fact is that, during the modeling process, “group size” is fixed and “rewiring probability” has nothing to do with the total amount of edges, and the only variable that may cause redundant edges is “number of neighbors.” In this paper, our purpose is to find out how many neighbors and what rewiring probability can help the given size economic system reach the highest UGR and keep the redundant edges as little as possible. Once found, a benchmark network can be generated in accordance with these parameters, compared with which the amount of redundant edges can be detected.

The structure of the paper is designed as follows. Section 2 introduces the WS model and economy model. Based on the model and theory, Section 3 designs the experiment plans. Section 4 is the collection of experimental results. In Section 5, the main contributions of this research are summarized.

2. Literature Review

In this section, we will conduct a literature review on relevant studies. The review includes the description of WS model and economy model.

2.1. WS Model. The WS model is a random graph generation model that produces graphs with small-world properties, including short average path lengths and high clustering. It was proposed by Watts and Strogatz in their joint Nature paper [1].

The mechanism of the model is as follows.

- (1) Create a ring over n nodes.
- (2) Each node in the ring is connected with its k nearest neighbors ($k-1$ neighbors if k is odd).
- (3) For each edge in the “ n -ring with k nearest neighbors,” shortcuts are created by replacing the original edges $u-v$ with a new edge $u-w$ with uniformly random choice of existing node w at rewiring probability p .

The WS model is included in software package normally expressed as a function. The model contains three forms, including `watts_strogatz_graph()`, `newman_watts_strogatz_graph()` [24], and `connected_watts_strogatz_graph()` [25]. These three models have the approximately same mechanism described above but still there are differences. The `watts_strogatz_graph()` is in strict accordance with the mechanism. The `newman_watts_strogatz_graph()` differs in the third step, which is the rewiring probability substituted by the probability of adding a new edge for each node. The `connected_watts_strogatz_graph()` will repeat the steps in the mechanism till a *connected watts-strogatz graph* is constructed. In contrast with `newman_watts_strogatz_graph()`, the random rewiring does not increase the number of edges and is not guaranteed to be connected as in `connected_watts_strogatz_graph()`.

In NetworkX [26], a Python language software package [27] for the creation, manipulation, and study of the structure, dynamics, and functions of complex network, there is a random WS small-world graph generator:

$$\text{watts_strogatz_graph}(n, k, p), \quad (1)$$

where n is the number of nodes in the graph, k is the number of neighbors each node connected to, and p is the probability of rewiring each edge in the graph.

2.2. Economy Model. This economy model derives from the one proposed by Wilhite [28] and is designed according to the definition of utility [29]. Utility is a means of accurately measuring the desirability of various types of goods and services and the degree of well-being those products provide for consumers. This measure is normally presented in the form of a mathematical expression utility function [30] and can be utilized with just about any type of goods or service that is secured and used by a consumer.

In this model, a certain amount of independent agents is created. Two types of goods, one of which must be traded in whole units and the other is infinitely divisible, are assigned to each agent as the existing wealth to circulate in the market. The portion of the goods is randomly assigned at the beginning of the experiment. There is no production and no imports; thus the aggregate stock of goods at the beginning of the experiment is the stock at the end.

Each agent’s objective is to improve its own Cobb-Douglas utility function [31] in each period by engaging in voluntary trade. Formally, U^i depends on the individual’s existing wealth of g_1 and g_2 :

$$U^i = g_1^i g_2^i, \quad i \in \{1, \dots, n\}, \quad (2)$$

where n is the amount of agents.

The entire economic society is composed of every transaction. A transaction is a process in which two nodes exchange the goods since one node's questing for a negotiating price chance is being responded. An opportunity for mutually beneficial transaction exists if the marginal rate of substitution (MRS) of two agents differs. MRS reflects the agent's willing to give up g_2 for a unit of g_1 . With the utility function in (1), the MRS of agent i is

$$\text{MRS}^i = \frac{U' (g_1^i)}{U' (g_2^i)} = \frac{g_2^i}{g_1^i}, \quad i \in \{1, \dots, n\}, \quad (3)$$

where $U'(\cdot)$ is the first derivative of U .

The model assumes that each agent reveals its MRS. In the experiment, agents search for beneficial trade opportunities according to the MRS and then establish a price to initiate a transaction. Any agent can either trade g_2 for g_1 or trade g_1 for g_2 at the expense of price. Throughout these experiments, the trading price $p_{i,j}$ between agent i and agent j is set according to the following rule:

$$p_{i,j} = \frac{g_2^i + g_2^j}{g_1^i + g_1^j}, \quad i, j \in \{1, \dots, n\}. \quad (4)$$

The questing node would pay $p_{i,j}$ by g_2 to exchange one unit of g_1 . Meanwhile, the responding node would add $p_{i,j}$ to its stock of g_2 and sell one unit of g_1 to the questing node. The transaction proceeds as long as the trade benefits each node's U^i , and stops when one of the nodes is in lack of g_1 or cannot afford the price $p_{i,j}$. Each transaction is atomic in the experiments; namely, it would not suspend till the whole process is fulfilled. In the experiments, every active transaction will be considered as one time trade with two portions of trade volumes, since the income and outcome string are both taken into account.

Once a transaction stops, the questing node will search again for a new opportunity according to the trade rules until no node responds to it and so on. Another node is selected as questing node to engage in a transaction. The economy society evolves like this and stops at the network's equilibrium. The utility growth rate (UGR) is

$$\text{UGR} = \frac{\sum_{i=1}^n U_e^i - \sum_{i=1}^n U^i}{\sum_{i=1}^n U^i}, \quad i \in \{1, \dots, n\}, \quad (5)$$

where U_e^i is the posttrade economic utility of node i .

Equilibrium is a point when agents cannot find trading opportunities that benefit any individuals. Feldman [32] studied the equilibrium characteristics of welfare-improving bilateral trade and showed that as long as all agents possess some nonzero amount of one of the commodities (all agents have some g_1 or all agents have some g_2), then the pairwise optimal allocation is also a Pareto optimal allocation. In this experiment, all agents are initially endowed with a positive amount of both goods; thus the equilibrium is Pareto optimal [33].

3. Experimental Design

A series of experiments are designed to run in the environment of Python program, aiming at finding out how many neighbors and what rewiring probability can help the given size economic system reach the highest UGR.

At the beginning of the experiments, artificial economy society is abstracted to a network composed of nodes and edges to conduct the analysis by the network theory. According to the economy model in Section 2.2, each society has agents (represented by nodes), trading rules (represented by edges), and goods g_1 and g_2 (represented by the endowment of each node).

The design can discuss any market with nodes in multiple of 10. We list the economic system at the group size from 10 to 200 in this paper. After the generation of nodes, a portion of the society wealth is assigned to each node and so does the same Cobb-Douglas utility it intends to maximize. Network structure defines the edges among the nodes, constraining the extent of trade partners each node can reach. Then the systems undertake the trading process keeping to the one defined in the economy model. Once the economic system reaches the equilibrium, the UGR of the system can be computed and bonded to the parameters set as the correspondence.

The network structures are generated by the random WS model complying with the mechanism in Section 2.1. This is the key process of the experiments. Different parameter sets (PS), including the group size (gs), the number of neighbors (nn), and the rewiring probability (rp), represented as PS = (gs, nn, rp) would be endowed to the WS model. The initial parameter set is PS = (10, 2, 0.01) and each variable would increase progressively. To enhance the operability, the parameters would increase linearly at different step size as follows.

- (1) The group size starts at 10 and grows with a step size of 10.
- (2) The number of neighbors starts at 2 and grows with a step size of 2. The WS model constraints that the number of neighbor each node attach to cannot exceed half of the group size and must be integer.
- (3) The rewiring probability starts at 0.01 and grows with step size of 0.01.

The forming of a new parameter set would trigger the modeling and trading process.

A hierarchical nested loop is designed for fulfilling the incrementing as follows.

- (1) *Fixing gs and rp.* After the succeeding modeling and trading process, increase nn by its step size. To generate sufficient experimental data, simulations are taken repeatedly under the same parameter set.
- (2) Once nn reaches its upper bound, increase rp by its step size and go to (1).
- (3) Once rp reaches its upper bound, the experiments stop.

Figure 1 describes the design of the experiment.

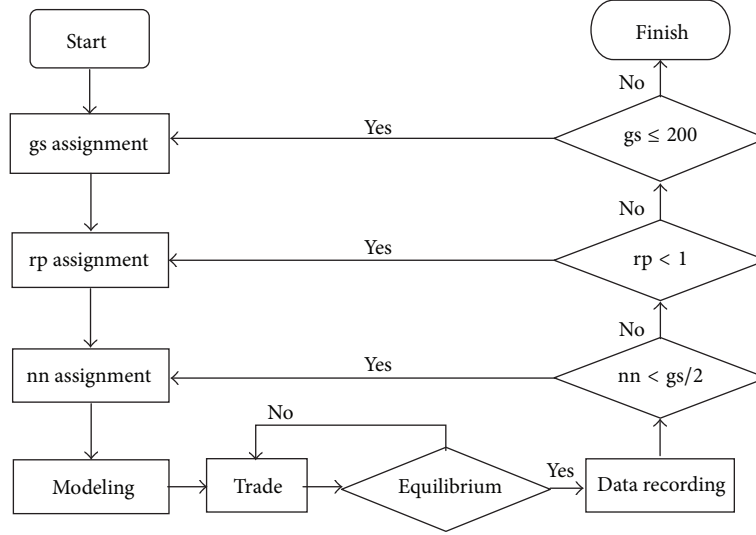


FIGURE 1: Experimental design.

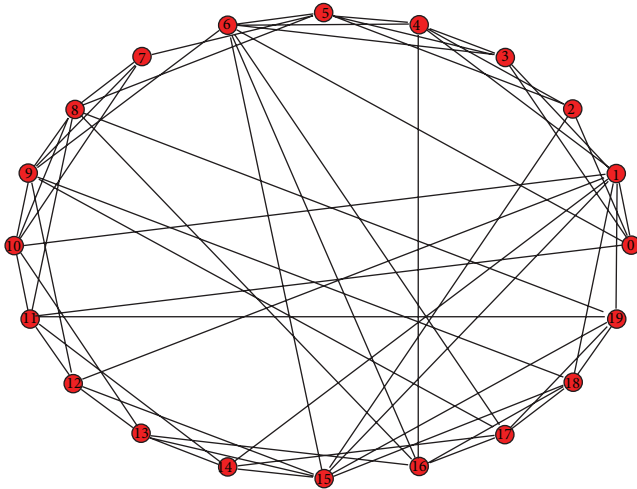


FIGURE 2: An instance of a small-world network.

Figure 2 is an instance of a network assigned by the parameter set (20, 6, 0.02).

4. Experimental Result

In this section, we collected the results of the experiments. Figure 3 illustrates, under the same rp , the probability when nn takes a defined value so that the economic system generated by the WS model reaches the highest UGR. The x axis represents the number of neighbors each node can have, and y axis in unit of percent (%) shows the probability that the corresponding nn achieves the highest UGR, represented as hp . Each subgraph is an average record of 100-time repeated simulations. 6 different sized systems are showed as examples. Through the observation, it is found that, regardless of

TABLE 1: A comparison of NE among different group size systems.

Group size	Uttermost neighbors	the upper end of hp	E_{hp}
50	600	450	300
100	2400	900	600
150	5550	1350	900
200	9800	1800	1200

the group size, 2 to 18 neighbors can achieve the highest UGR of an economic system; that is,

$$hp \in [2, 18]. \quad (6)$$

Moreover, Figure 3 also reveals the rising tendency of hp when the group size grows.

This conclusion is reconfirmed in Figure 4(a), which describes the total sum of hp in the group size from 10 to 200. Lining up the points in Figure 4(a) and getting Figure 4(b), the pattern of the probability approximates the Poisson distribution [34] and the mathematical expectation $E_{hp} = 12$.

Since the extent of hp has been found, bonding with gs , the extent of edges can be calculated also. It can be deduced that once the value of nn goes beyond the extent, the WS model would surely generate redundant edges in the economic system. Table 1 compares the number of edges (NE) when each node has the uttermost neighbors, upper end of hp , and E_{hp} neighbors. Under the same group size, uttermost neighbors generate the maximum edges the WS model can; the upper end of hp generates the upper bound number of edges, indexing that beyond this bound the system definitely has redundant edges; E_{hp} generates the mathematical expectation number of edges.

In Table 1, compared to the systems generated under the upper end of hp and E_{hp} , the one under uttermost neighbors has multiple edges and the gap would exaggerate along with the enlargement of group size. Due to the guiding

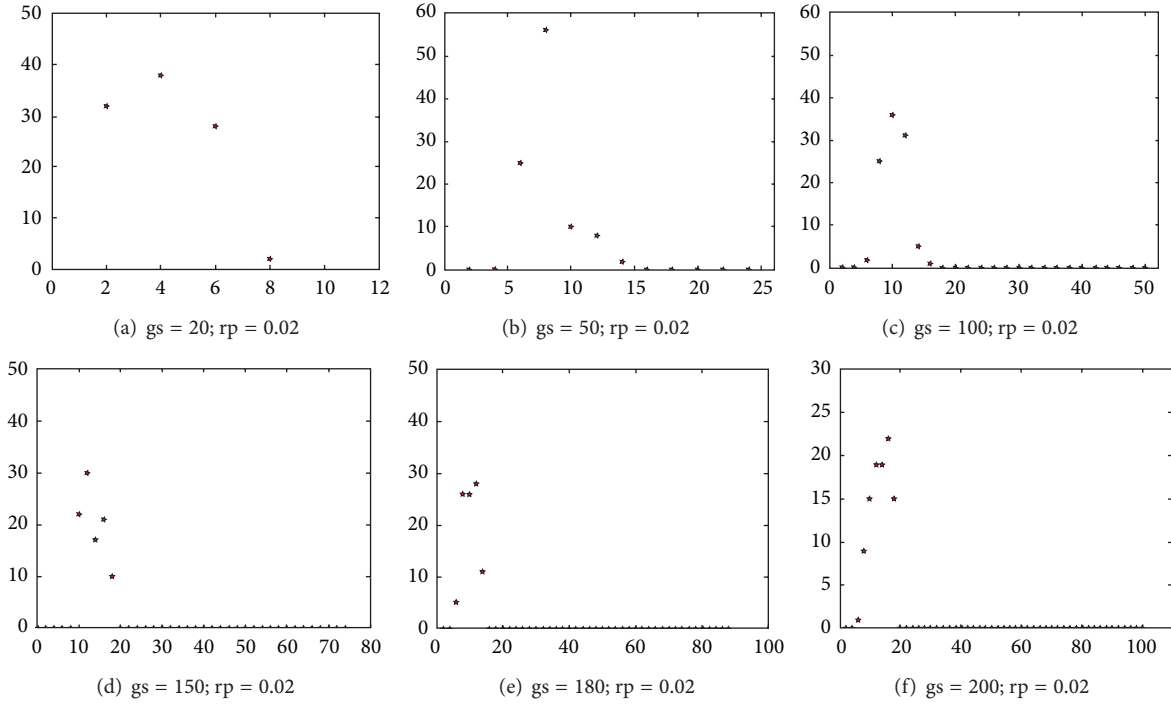


FIGURE 3: The probability when nn takes a defined value so that the economic system reaches the highest UGR.

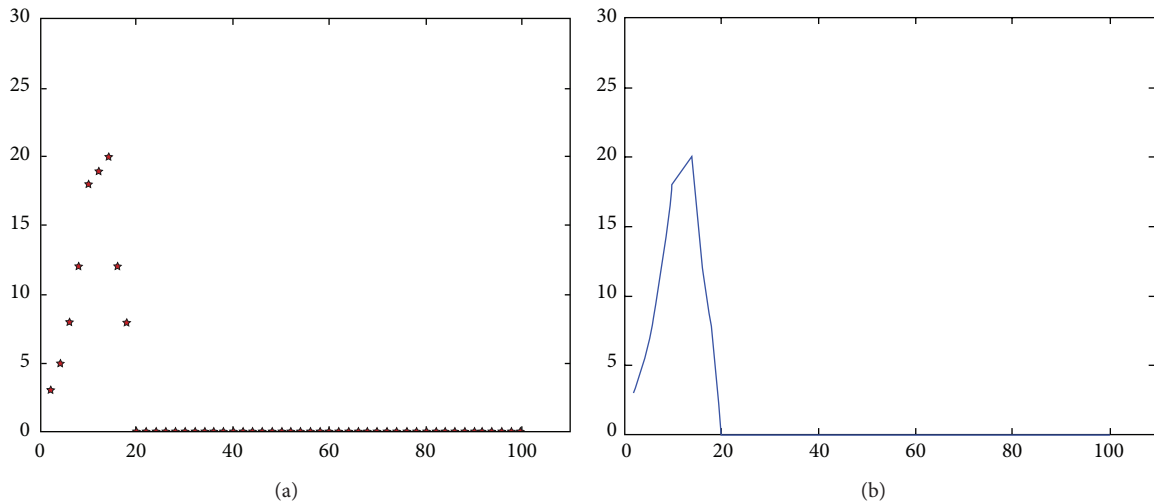


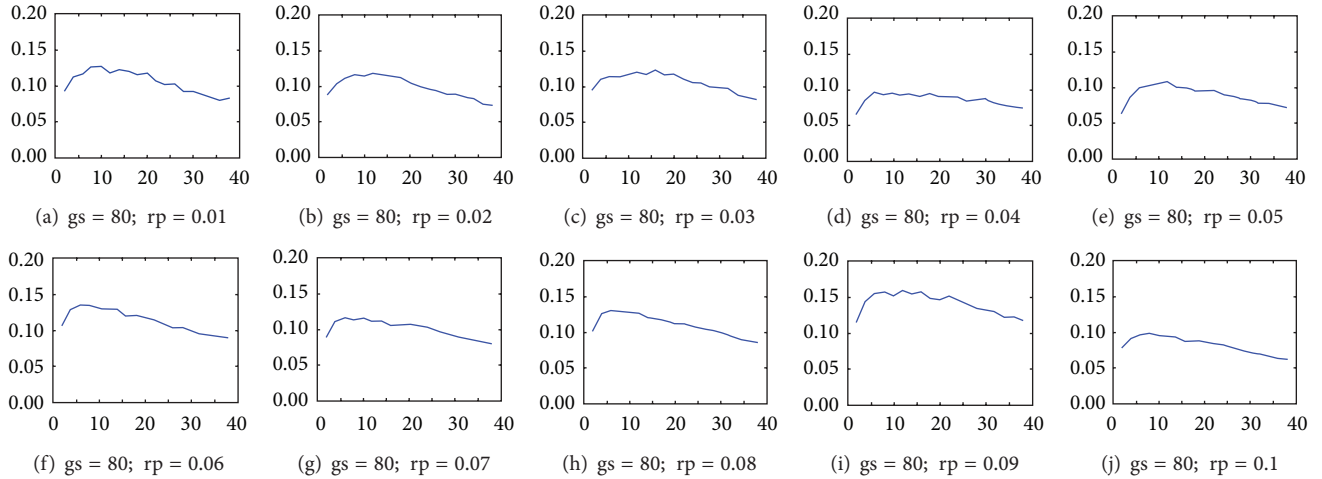
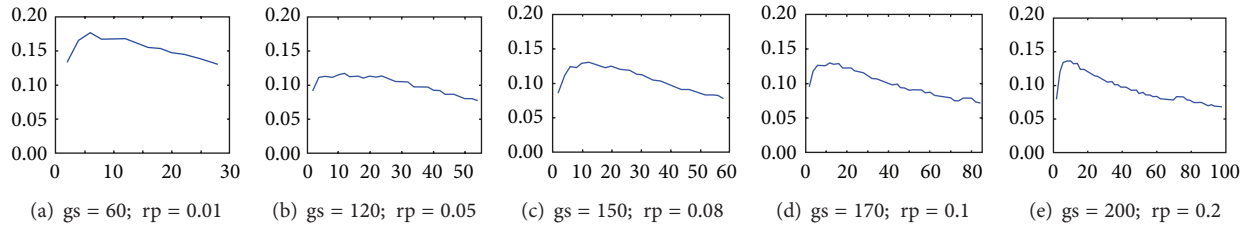
FIGURE 4: The total sum of hp in the group size from 10 to 200.

significance of the bound generated by the upper end of hp , any system with NE beyond the bound has costly redundant edges. However, the redundant edges have advantages as shields when the economic system confronts the random or deliberate attacks. Thus the complete removal of redundant edges is unnecessary.

In the random WS model, variable rp cannot bring changes in NE but can reform the network structure. Figure 5 combines a group of graphs describing the correlation between nn (x axis) and UGR (y axis) when $gs = 80$. It reveals that, under the same group size, UGR differs if the network

structure and endowment changes are reflected in the pattern of each subgraph varying. However, the pattern of each graph conforms to the range $hp \in [2, 18]$ and has similar curvature.

Despite the observation on Figure 5, we suppose that the pattern of UGR would decrease gradually when nn is beyond 18, which is the upper end of hp . To verify the conjecture, gs , rp , and nn in the parameter set would increase linearly as defined in Section 3 and after repeated simulations the UGR of systems generated by WS model is collected in Figure 6. It is confirmed that independent of group size and rewiring probability, if $nn > 18$, the UGR would decrease

FIGURE 5: The pattern of UGR when $gs = 80$ and rp increases linearly.FIGURE 6: The pattern of UGR when gs , rp , and nn increase linearly.

gradually. Although it may not be a monotonic decreasing, the decreasing tendency would be kept.

When constructing the systems in Figures 5 and 6, we also consider that the possible effect on hp and UGR may be exerted by the endowments to goods g_1 and g_2 . The fixed group size systems in Figure 5 are endowed with randomly generated g_1 and g_2 and, in Figure 5, different group size systems are discussed, which means that their endowments cannot keep consistent with each other. The result shows that the UGR varies on account of the endowments and network structure, but the range of hp cannot be influenced.

5. Conclusion

This research combines economic theory, network theory, and computer simulations to examine the parameters set assigned to the WS model relating to an economic system's UGR. We discovered that, regardless of the group size and rewiring probability, (1) 2 to 18 neighbors and the corresponding computable number of edges can help an economic system reach the highest UGR; (2) if the node has more than 18 neighbors, the UGR would decrease gradually and the pattern is not monotonic but would keep the decreasing tendency; (3) different endowments to goods g_1 and g_2 would not impact the range of neighbors which can help the system achieve the highest UGR. In the practical application, it can be construed that (1) acting as a measurement judges whether a system can reach the highest UGR based on its

current structure; (2) when the resource is in the hands of a fraction of people, the resource can derive the highest value for the owners and the rest of people; (3) once keeping the superiority of minority owners, the value of resource would not decrease or increase according to its quantity.

Conflict of Interests

The authors declare that there is no conflict of interests regarding the publication of this paper.

References

- [1] D. J. Watts and S. H. Strogatz, "Collective dynamics of "small-world" networks," *Nature*, vol. 393, no. 6684, pp. 440–442, 1998.
- [2] W.-K. Chen, *Graph Theory and Its Engineering Applications*, World Scientific, Singapore, 1997.
- [3] P. Erdős and A. Rényi, "On random graphs. I," *Publicationes Mathematicae*, vol. 6, pp. 290–297, 1959.
- [4] D. J. Watts, "Networks, dynamics, and the small-world phenomenon," *The American Journal of Sociology*, vol. 105, no. 2, pp. 493–527, 1999.
- [5] A. F. Alexander-Bloch, P. E. Vértes, R. Stidd et al., "The anatomical distance of functional connections predicts brain network topology in health and schizophrenia," *Cerebral Cortex*, vol. 23, no. 1, pp. 127–138, 2013.
- [6] R. Céline and M. Guy, "A small world perspective on urban systems," in *Methods for Multilevel Analysis and Visualisation of Geographical Networks*, vol. 11, pp. 19–32, 2013.

- [7] G. Corso, L. S. Lucena, and Z. D. Thomé, "The small-world of economy: a speculative proposal," *Physica A: Statistical Mechanics and Its Applications*, vol. 324, no. 1-2, pp. 430–436, 2003.
- [8] K. Musiał and P. Kazienko, "Social networks on the internet," *World Wide Web*, vol. 16, no. 1, pp. 31–72, 2013.
- [9] X. Cheng, J. Liu, and C. Dale, "Understanding the characteristics of internet short video sharing: a youtube-based measurement study," *IEEE Transactions on Multimedia*, vol. 15, no. 5, pp. 1184–1194, 2013.
- [10] D. Eppstein, M. T. Goodrich, M. Löffler, D. Strash, and L. Trott, "Category-based routing in social networks: membership dimension and the small-world phenomenon," *Theoretical Computer Science*, vol. 514, pp. 96–104, 2013.
- [11] D. César and L. Igor, "Structure and dynamics of transportation networks: models, methods and applications," in *The SAGE Handbook of Transport Studies*, pp. 347–364, 2013.
- [12] J. Kleinberg, "The small-world phenomenon: an algorithm perspective," in *Proceedings of the 32nd Annual ACM Symposium on Theory of Computing*, pp. 163–170, 2000.
- [13] S. Milgram, "The small-world problem," *Psychology Today*, vol. 2, pp. 60–67, 1967.
- [14] A. Kemper, *Valuation of Network Effects in Software Markets: A Complex Networks Approach*, Springer, Heidelberg, Germany, 2010.
- [15] R. Albert and A.-L. Barabási, "Statistical mechanics of complex networks," *Reviews of Modern Physics*, vol. 74, no. 1, pp. 47–97, 2002.
- [16] T. John, P. Theodore, and L. Terry, "Supply chain management and its relationship to logistics, marketing, production, and operations management," *Journal of Business Logistics*, vol. 29, no. 1, pp. 31–46, 2008.
- [17] B. Ben and G. Mark, "Financial fragility and economic performance," *The Quarterly Journal of Economics*, vol. 105, no. 1, pp. 87–114, 1990.
- [18] G. W. Torrance, "Utility measurement in healthcare: the things I never got to," *PharmacoEconomics*, vol. 24, no. 11, pp. 1069–1078, 2006.
- [19] A. Birati and A. Tziner, "Economic utility of training programs," *Journal of Business and Psychology*, vol. 14, no. 1, pp. 155–164, 1999.
- [20] C. Li and G. Chen, "Stability of a neural network model with small-world connections," *Physical Review E—Statistical, Nonlinear, and Soft Matter Physics*, vol. 68, no. 5, Article ID 052901, 2003.
- [21] X. Li and X. Wang, "Controlling the spreading in small-world evolving networks: stability, oscillation, and topology," *IEEE Transactions on Automatic Control*, vol. 51, no. 3, pp. 534–540, 2006.
- [22] M. O. Jackson and A. Wolinsky, "A strategic model of social and economic networks," *Journal of Economic Theory*, vol. 71, no. 1, pp. 44–74, 1996.
- [23] Y. A. Ioannides, "Evolution of trading structures," in *The Economy as an Evolving Complex System II*, W. B. Arthur, S. Durlauf, and D. Lane, Eds., pp. 129–168, 1997.
- [24] M. E. J. Newman and D. J. Watts, "Renormalization group analysis of the small-world network model," *Physics Letters A: General, Atomic and Solid State Physics*, vol. 263, no. 4–6, pp. 341–346, 1999.
- [25] <http://networkx.github.io/documentation/latest/>.
- [26] A. Hagberg and D. Conway, "Hacking social networks using the Python programming language (module II—why do SNA in NetworkX)," in *Proceedings of the International Network for Social Network Analysis Sunbelt Conference*, 2010.
- [27] "Python 3.4.0 beta 3," Python Software Foundation, 2014.
- [28] A. Wilhite, "Bilateral trade and "small-world" networks," *Computational Economics*, vol. 18, no. 1, pp. 49–64, 2001.
- [29] A. Marshall, *Principles of Economics: An Introductory Volume*, Macmillan, London, UK, 8th edition.
- [30] J. E. Ingersoll Jr., *Theory of Financial Decision Making*, Rowman and Littlefield, Totowa, NJ, USA, 1987.
- [31] D. W. Caves and L. R. Christensen, "Global properties of flexible functional forms," *The American Economic Review*, vol. 70, no. 3, pp. 422–432, 1980.
- [32] A. Feldman, "Bilateral trading processes, pairwise optimality, and Pareto optimality," *Review of Economic Studies*, vol. 40, no. 4, pp. 463–473, 1973.
- [33] A. Sen, "Markets and freedoms: achievements and limitations of the market mechanism in promoting individual freedoms," *Oxford Economic Papers*, vol. 45, no. 4, pp. 519–541, 1993.
- [34] J. H. Ahrens and U. Dieter, "Computer methods for sampling from gamma, beta, poisson and binomial distributions," *Computing*, vol. 12, no. 3, pp. 223–246, 1974.

Research Article

Combination-Combination Hyperchaos Synchronization of Complex Memristor Oscillator System

Zhang Jin-E

School of Mathematics and Statistics, Hubei Normal University, Huangshi, Hubei, China

Correspondence should be addressed to Zhang Jin-E; zhang86021205@163.com

Received 30 March 2014; Accepted 3 May 2014; Published 29 May 2014

Academic Editor: He Huang

Copyright © 2014 Zhang Jin-E. This is an open access article distributed under the Creative Commons Attribution License, which permits unrestricted use, distribution, and reproduction in any medium, provided the original work is properly cited.

The combination-combination synchronization scheme is based on combination of multidrive systems and combination of multiresponse systems. In this paper, we investigate combination-combination synchronization of hyperchaotic complex memristor oscillator system. Several sufficient conditions are provided to ascertain the combination of two drive hyperchaotic complex memristor oscillator systems to synchronize the combination of two response hyperchaotic complex memristor oscillator systems. These new conditions improve and extend the existing synchronization results for memristive systems. A numerical example is given to show the feasibility of theoretical results.

1. Introduction

Since the characteristics of passive two-terminal memristor are reviewed, lots of emulators and macromodels have been proposed. One remarkable use for memristor is in complex memristor oscillator systems, where nonlinear oscillators from Chua's oscillators are replaced by using memristors [1–10]. The complex behaviors for such systems were analyzed in [1–5, 8–10]. When nonlinear memristor is applied to electronic device, the behavior of the new-type device becomes complicated and difficult to predict due to the unique nonlinear mechanism of memristor [11–14]. However, to apply to the practical engineering, its electrical characteristics must be able to be fully understood. So it is vital to understand the characteristics and behaviors of memristive devices. In [1], the transient chaos was studied for a smooth flux-controlled complex memristor oscillator system. In [2], the local and global behavior of the basic oscillator on complex memristor oscillator system was investigated. Itoh and Chua [3] discussed some interesting oscillation properties and rich nonlinear dynamics of several complex memristor oscillator systems from Chua's oscillators. Talukdar et al. [7] reported the nonlinear dynamics of three memristor-based phase shift oscillators. As we all know, the electrical characteristics of complex memristor oscillator system can vary depending

upon its circuit structure. The internal behavior of high order (fifth-order or more) complex memristor oscillator system still is not being analyzed [9, 10]. In high order complex memristor oscillator system, there are still many unknown fields waiting for us to exploit them. Specifically, the current studies about complex memristor oscillator system have mostly remained at the basic chaotic dynamic theory. Compared with common chaos with only one positive Lyapunov exponent, hyperchaos with more than one positive Lyapunov exponents can exhibit multidirectional expansion and extremely complex behaviors. Can we design high order complex memristor oscillator system to achieve the hyperchaotic effect? If this is really so, many different applications might be proposed, such as ultradense nonvolatile memory and high-performance secure communication [9, 10].

The topic of chaos synchronization of oscillator systems is extensively investigated because of possible relevance to information encryption [8–11, 15–28]. Various kinds of synchronization laws have been obtained, for example, complete synchronization [8, 11, 15–18], compound synchronization [10], antisynchronization [19–21], phase synchronization [22, 23], lag synchronization [24–26], projective synchronization [10, 27], and combination synchronization [9, 28]. However, in the existing literature, most of synchronization laws are based on one drive system and one response system. In

this way, when chaos synchronization is applied to secure communication, the information signal is transmitted by only one chaotic system, which is not suitable for very high-performance secure communication. Can the information signal be transmitted by the combination of multiple chaotic systems? If we can successfully provide some ways to do this, then the transmitted signals will be more complex and unpredictable, and thereby the security of communication can be effectively enhanced. Thus, a theoretical question is whether we can design a synchronization scheme on the combination of multidrive systems and combination of multiresponse systems. Such a combination design may help to improve the secrecy in communications [9, 28].

Motivated by the above discussions, in this paper, firstly, a new hyperchaotic complex memristor oscillator system is introduced and studied. Secondly, we bring in the scheme of combination-combination synchronization and establish some synchronization criteria. Roughly stated, the main advantages of this paper include the following three points.

- (1) Hyperchaotic complex memristor oscillator system is systematically investigated. Hyperchaos is often considered better than common chaos in many engineering fields. Theoretically, hyperchaotic complex memristor oscillator system might improve the security of chaotic communication system.
- (2) The synchronization control between combination of two drive hyperchaotic complex memristor oscillator systems and combination of two response hyperchaotic complex memristor oscillator systems in drive-response coupled system is investigated. The generalization of synchronization scheme will provide a wider scope for the designs and applications of memristive system.
- (3) The proposed scheme of combination-combination synchronization in this paper can be applied to the general nonlinear systems.

The rest of this paper is arranged as follows. Section 2 describes some preliminaries and problem formulation. Section 3 derives some sufficient conditions on combination-combination synchronization for hyperchaotic complex memristor oscillator system and then presents a numerical example to demonstrate the validity of the theoretical results. Section 4 concludes the paper with some remarks.

2. Preliminaries

Consider a fifth-order complex memristor oscillator system with its dynamics described by the following ordinary differential equations:

$$\begin{aligned}\dot{v}_1(t) &= \frac{1}{C_1} \ell_1(t) - \frac{1}{C_1} W_1(\varphi(t)) v_1(t), \\ \dot{v}_2(t) &= -\frac{1}{C_2} \ell_1(t) + \frac{1}{C_2} \ell_2(t),\end{aligned}$$

$$\begin{aligned}\dot{\ell}_1(t) &= \frac{1}{L_1} v_2(t) - \frac{1}{L_1} v_1(t) - \frac{R}{L_1} \ell_1(t), \\ \dot{\ell}_2(t) &= -\frac{1}{L_2} v_2(t), \\ \dot{\varphi}(t) &= v_1(t),\end{aligned}\tag{1}$$

where $v_1(t)$ and $v_2(t)$ denote voltages, $\ell_1(t)$ and $\ell_2(t)$ represent currents, C_1 and C_2 denote capacitors, L_1 and L_2 represent inductors, $W(\varphi(t))$ is memductance function, and $\varphi(t)$ and R are magnetic flux and resistor, respectively.

Similarly as in [1, 9, 10], a cubic memristor is chosen; then

$$W(\varphi(t)) = a + 3b\varphi(t)^2,\tag{2}$$

where a and b are parameters.

From (1) and (2),

$$\begin{aligned}\dot{v}_1(t) &= \frac{1}{C_1} \ell_1(t) - \frac{a}{C_1} v_1(t) - \frac{3b}{C_1} v_1(t) \varphi(t)^2, \\ \dot{v}_2(t) &= -\frac{1}{C_2} \ell_1(t) + \frac{1}{C_2} \ell_2(t), \\ \dot{\ell}_1(t) &= \frac{1}{L_1} v_2(t) - \frac{1}{L_1} v_1(t) - \frac{R}{L_1} \ell_1(t), \\ \dot{\ell}_2(t) &= -\frac{1}{L_2} v_2(t), \\ \dot{\varphi}(t) &= v_1(t).\end{aligned}\tag{3}$$

Let $x_{11}(t) = v_1(t)$, $x_{12}(t) = v_2(t)$, $x_{13}(t) = \ell_1(t)$, $x_{14}(t) = \ell_2(t)$, $x_{15}(t) = \varphi(t)$, $\alpha_1 = 1/C_1$, $\alpha_2 = a/C_1$, $\alpha_3 = 3b/C_1$, $\alpha_4 = 1/C_2$, $\alpha_5 = 1/L_1$, $\alpha_6 = R/L_1$, $\alpha_7 = 1/L_2$; then (3) can be rewritten as

$$\begin{aligned}\dot{x}_{11} &= \alpha_1 x_{13} - \alpha_2 x_{11} - \alpha_3 x_{11} x_{15}^2, \\ \dot{x}_{12} &= -\alpha_4 x_{13} + \alpha_4 x_{14}, \\ \dot{x}_{13} &= \alpha_5 x_{12} - \alpha_5 x_{11} - \alpha_6 x_{13}, \\ \dot{x}_{14} &= -\alpha_7 x_{12}, \\ \dot{x}_{15} &= x_{11}.\end{aligned}\tag{4}$$

Let parameters $\alpha_1 = 9$, $\alpha_2 = -10.8$, $\alpha_3 = 10.8$, $\alpha_4 = 1$, $\alpha_5 = 30$, $\alpha_6 = 30$, $\alpha_7 = 15$, the initial state $x_{11}(0) = 0.01$, $x_{12}(0) = 0.01$, $x_{13}(0) = 0.01$, $x_{14}(0) = 0.01$, $x_{15}(0) = 0.01$, by mean of computer program with MATLAB, the corresponding Lyapunov exponents of system (4) are 0.279403, 0.023752, -0.038779, -7.391447, -16.291929. The numerical result is shown in Figure 1, where the first two Lyapunov exponents are positive. Clearly, it implies that memristor oscillator system (4) is hyperchaotic. Figure 2 describes the hyperchaotic attractors.

Many efforts have been paid in recent years to develop efficient circuit implementation for the generation of hyperchaotic memristor oscillator system. However, to the best of our knowledge, up to now, the hyperchaotic memristor

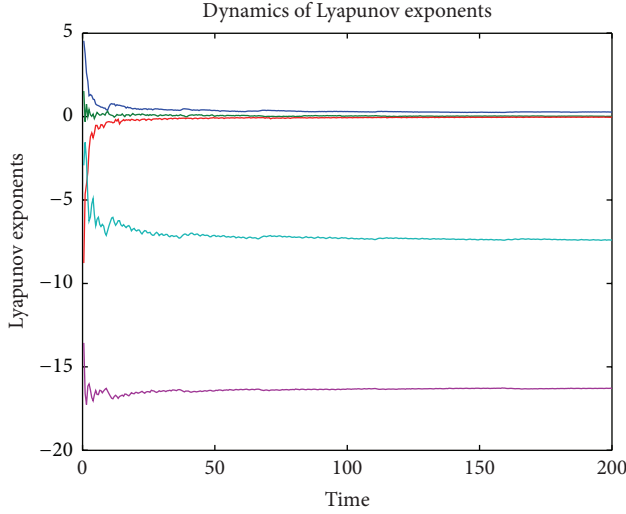


FIGURE 1: Dynamics of Lyapunov exponents from memristor oscillator system (4).

oscillator system is still very unusual. Thus, hyperchaotic memristor oscillator system (4) is important for our understanding of hyperchaotic memristive devices.

In the following, we end this section with the scheme of combination-combination synchronization, which will be used in subsequent section.

In engineering field, generally, combination-combination synchronization is based on multiple drive systems and multiple response systems. In many engineering applications and hardware implementations, combination-combination synchronization constituting of two drive systems and two response systems is usually considered. Figure 3 describes a schematic diagram of combination-combination synchronization scheme. In fact, combination-combination synchronization has its unique physical interpretation. For example, in Figure 3, the combination of two drive systems generates the resultant signal; then the combination of two response systems tracks the resultant signal.

Next, we give specific mathematical descriptions of combination-combination synchronization scheme.

Consider the drive system:

$$\dot{\chi}_1 = f_1(\chi_1). \quad (5)$$

The other drive system is given by

$$\dot{\chi}_2 = f_2(\chi_2), \quad (6)$$

and two response systems are described by

$$\begin{aligned} \dot{\chi}_3 &= f_3(\chi_3) + u, \\ \dot{\chi}_4 &= f_4(\chi_4) + u^*, \end{aligned} \quad (7)$$

where state vectors $\chi_1 = (\chi_{11}, \chi_{12}, \dots, \chi_{1n})^T$, $\chi_2 = (\chi_{21}, \chi_{22}, \dots, \chi_{2n})^T$, $\chi_3 = (\chi_{31}, \chi_{32}, \dots, \chi_{3n})^T$, and $\chi_4 = (\chi_{41}, \chi_{42}, \dots, \chi_{4n})^T$ and vector functions $f_1(\cdot), f_2(\cdot), f_3(\cdot), f_4(\cdot) : \mathcal{R}^n \rightarrow \mathcal{R}^n$, $u = (u_1, u_2, \dots, u_n)^T$, $u^* = (u_1^*, u_2^*, \dots, u_n^*)^T$:

$\mathcal{R}^n \times \mathcal{R}^n \times \dots \times \mathcal{R}^n \rightarrow \mathcal{R}^n$ are the appropriate control inputs that will be designed in order to obtain a certain control objective.

Definition 1. The drive systems (5) and (6) are realized combination-combination synchronization with the response systems (7) if there exist n -dimensional constant diagonal matrices $A_1, A_2, A_3 \neq 0$, and $A_4 \neq 0$ such that

$$\lim_{t \rightarrow +\infty} \|e\| = \lim_{t \rightarrow +\infty} \|A_1 X_1 + A_2 X_2 - A_3 X_3 - A_4 X_4\| = 0, \quad (8)$$

where $\|\cdot\|$ is vector norm, $e = (e_1, e_2, \dots, e_n)^T$ is the synchronization error vector, $X_1 = \text{diag}(\chi_{11}, \chi_{12}, \dots, \chi_{1n})$, $X_2 = \text{diag}(\chi_{21}, \chi_{22}, \dots, \chi_{2n})$, $X_3 = \text{diag}(\chi_{31}, \chi_{32}, \dots, \chi_{3n})$, and $X_4 = \text{diag}(\chi_{41}, \chi_{42}, \dots, \chi_{4n})$.

Remark 2. As stated earlier, according to Definition 1, the physical implication of combination-combination synchronization is rather intuitionistic. The resultant signal of the combination of two drive systems (5) and (6) is tracked by the synthetic signal of the combination of two response systems (7).

Remark 3. In [28], Sun et al. apply combination-combination design to study the synchronization control of some classical chaotic systems. Generally speaking, this synchronization method for chaotic system is quite novel.

Remark 4. In Definition 1, matrices A_1, A_2, A_3 , and A_4 are often called the scaling matrices. It is not hard to find that the scheme of combination-combination synchronization in Definition 1 contains the combination of two drive systems and the combination of two response systems. Moreover, one advantage of combination-combination synchronization is that the drive systems or the response systems can be completely identical or different.

Remark 5. The scheme of combination-combination synchronization improves and generalizes some existing synchronization schemes. When scaling matrices $A_3 = 0$ or $A_4 = 0$, the combination-combination synchronization will degrade into combination synchronization. When scaling matrices $A_1 = A_3 = 0$ or $A_1 = A_4 = 0$ or $A_2 = A_3 = 0$ or $A_2 = A_4 = 0$, the combination-combination synchronization will be reduced to complete synchronization. When scaling matrices $A_1 = A_2 = A_3 = 0$ or $A_1 = A_2 = A_4 = 0$, the combination-combination synchronization will change into chaos control.

3. Synchronization Criteria

In this section, we will devote to investigate combination-combination synchronization of hyperchaotic complex memristor oscillator system.

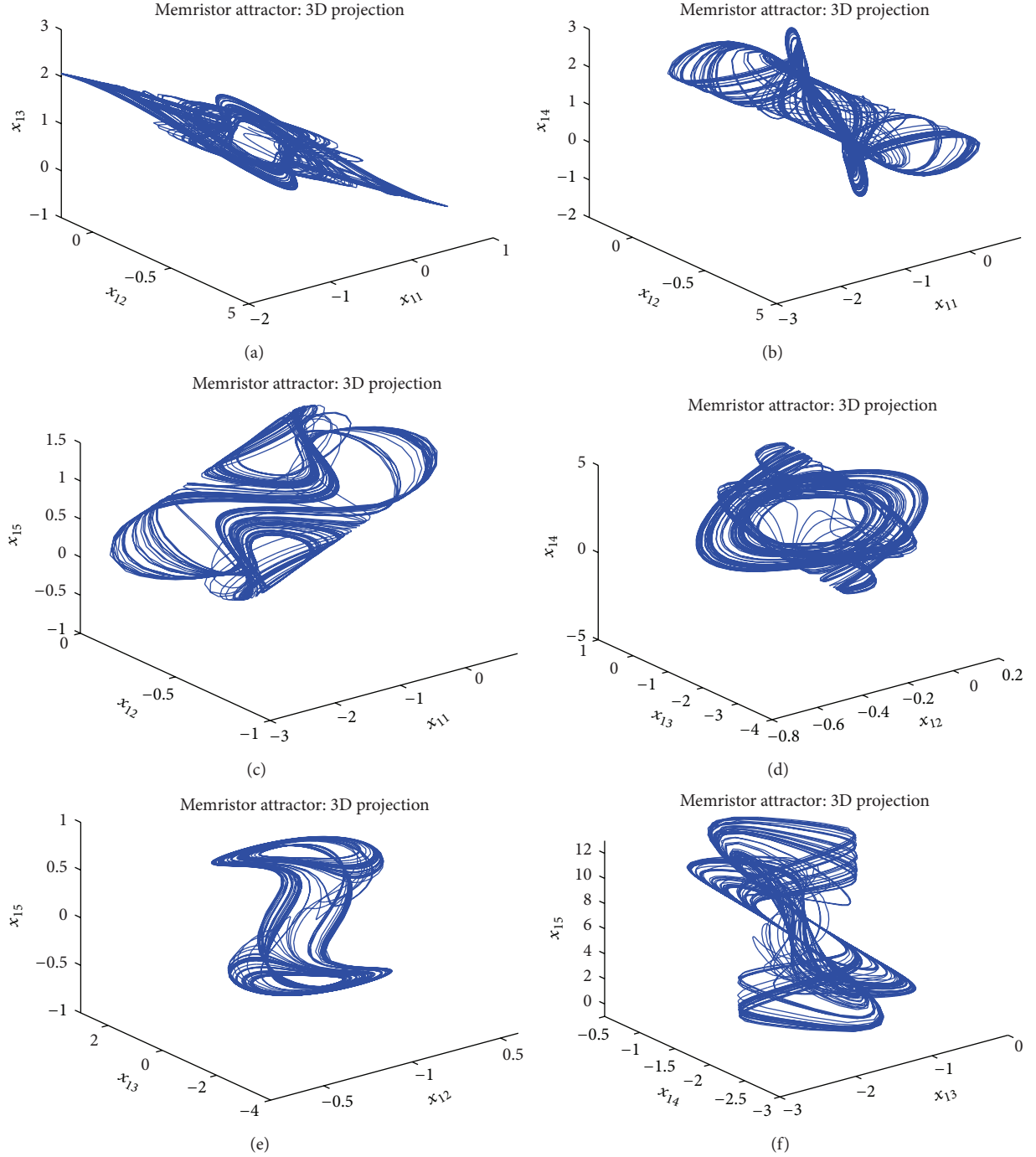


FIGURE 2: 3D projections of the hyperchaotic attractor from memristor oscillator system (4).

Corresponding to (4), the other drive system is given as

$$\begin{aligned}
 \dot{x}_{21} &= \beta_1 x_{23} - \beta_2 x_{21} - \beta_3 x_{21} x_{25}^2, \\
 \dot{x}_{22} &= -\beta_4 x_{23} + \beta_4 x_{24}, \\
 \dot{x}_{23} &= \beta_5 x_{22} - \beta_5 x_{21} - \beta_6 x_{23}, \\
 \dot{x}_{24} &= -\beta_7 x_{22}, \\
 \dot{x}_{25} &= x_{21},
 \end{aligned} \tag{9}$$

and two response systems are described as follows:

$$\begin{aligned}
 \dot{x}_{31} &= \gamma_1 x_{33} - \gamma_2 x_{31} - \gamma_3 x_{31} x_{35}^2 + u_1, \\
 \dot{x}_{32} &= -\gamma_4 x_{33} + \gamma_4 x_{34} + u_2, \\
 \dot{x}_{33} &= \gamma_5 x_{32} - \gamma_5 x_{31} - \gamma_6 x_{33} + u_3, \\
 \dot{x}_{34} &= -\gamma_7 x_{32} + u_4, \\
 \dot{x}_{35} &= x_{31} + u_5,
 \end{aligned} \tag{10}$$

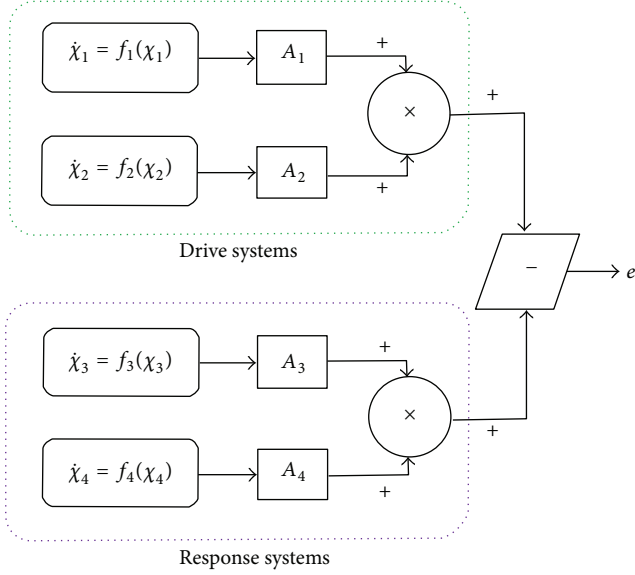


FIGURE 3: The physical realization of combination-combination synchronization scheme.

$$\begin{aligned}
 \dot{x}_{41} &= \eta_1 x_{43} - \eta_2 x_{41} - \eta_3 x_{41} x_{45}^2 + u_1^*, \\
 \dot{x}_{42} &= -\eta_4 x_{43} + \eta_4 x_{44} + u_2^*, \\
 \dot{x}_{43} &= \eta_5 x_{42} - \eta_5 x_{41} - \eta_6 x_{43} + u_3^*, \\
 \dot{x}_{44} &= -\eta_7 x_{42} + u_4^*, \\
 \dot{x}_{45} &= x_{41} + u_5^*,
 \end{aligned} \tag{11}$$

where $\beta_1, \beta_2, \beta_3, \beta_4, \beta_5, \beta_6, \beta_7, \gamma_1, \gamma_2, \gamma_3, \gamma_4, \gamma_5, \gamma_6, \gamma_7, \eta_1, \eta_2, \eta_3, \eta_4, \eta_5, \eta_6$, and η_7 are parameters and $u_1, u_2, u_3, u_4, u_5, u_1^*, u_2^*, u_3^*, u_4^*$, and u_5^* are the control inputs to be designed.

In our synchronization scheme, let

$$\begin{aligned}
 A_1 &= \text{diag}(a_{11}, a_{12}, a_{13}, a_{14}, a_{15}), \\
 A_2 &= \text{diag}(a_{21}, a_{22}, a_{23}, a_{24}, a_{25}), \\
 A_3 &= \text{diag}(a_{31}, a_{32}, a_{33}, a_{34}, a_{35}), \\
 A_4 &= \text{diag}(a_{41}, a_{42}, a_{43}, a_{44}, a_{45}).
 \end{aligned} \tag{12}$$

Thus,

$$\begin{aligned}
 e_1 &= a_{11}x_{11} + a_{21}x_{21} - a_{31}x_{31} - a_{41}x_{41}, \\
 e_2 &= a_{12}x_{12} + a_{22}x_{22} - a_{32}x_{32} - a_{42}x_{42}, \\
 e_3 &= a_{13}x_{13} + a_{23}x_{23} - a_{33}x_{33} - a_{43}x_{43}, \\
 e_4 &= a_{14}x_{14} + a_{24}x_{24} - a_{34}x_{34} - a_{44}x_{44}, \\
 e_5 &= a_{15}x_{15} + a_{25}x_{25} - a_{35}x_{35} - a_{45}x_{45}.
 \end{aligned} \tag{13}$$

Obviously, we have

$$\begin{aligned}
 \dot{e}_1 &= a_{11}\dot{x}_{11} + a_{21}\dot{x}_{21} - a_{31}\dot{x}_{31} - a_{41}\dot{x}_{41}, \\
 \dot{e}_2 &= a_{12}\dot{x}_{12} + a_{22}\dot{x}_{22} - a_{32}\dot{x}_{32} - a_{42}\dot{x}_{42}, \\
 \dot{e}_3 &= a_{13}\dot{x}_{13} + a_{23}\dot{x}_{23} - a_{33}\dot{x}_{33} - a_{43}\dot{x}_{43}, \\
 \dot{e}_4 &= a_{14}\dot{x}_{14} + a_{24}\dot{x}_{24} - a_{34}\dot{x}_{34} - a_{44}\dot{x}_{44}, \\
 \dot{e}_5 &= a_{15}\dot{x}_{15} + a_{25}\dot{x}_{25} - a_{35}\dot{x}_{35} - a_{45}\dot{x}_{45}.
 \end{aligned} \tag{14}$$

Combining with (4) and (9)–(11), then the synchronization error system (14) can be transformed into the following form:

$$\begin{aligned}
 \dot{e}_1 &= a_{11}(\alpha_1 x_{13} - \alpha_2 x_{11} - \alpha_3 x_{11} x_{15}^2) \\
 &\quad + a_{21}(\beta_1 x_{23} - \beta_2 x_{21} - \beta_3 x_{21} x_{25}^2) \\
 &\quad - a_{31}(\gamma_1 x_{33} - \gamma_2 x_{31} - \gamma_3 x_{31} x_{35}^2 + u_1) \\
 &\quad - a_{41}(\eta_1 x_{43} - \eta_2 x_{41} - \eta_3 x_{41} x_{45}^2 + u_1^*), \\
 \dot{e}_2 &= a_{12}(-\alpha_4 x_{13} + \alpha_4 x_{14}) + a_{22}(-\beta_4 x_{23} + \beta_4 x_{24}) \\
 &\quad - a_{32}(-\gamma_4 x_{33} + \gamma_4 x_{34} + u_2) \\
 &\quad - a_{42}(-\eta_4 x_{43} + \eta_4 x_{44} + u_2^*), \\
 \dot{e}_3 &= a_{13}(\alpha_5 x_{12} - \alpha_5 x_{11} - \alpha_6 x_{13}) \\
 &\quad + a_{23}(\beta_5 x_{22} - \beta_5 x_{21} - \beta_6 x_{23}) \\
 &\quad - a_{33}(\gamma_5 x_{32} - \gamma_5 x_{31} - \gamma_6 x_{33} + u_3) \\
 &\quad - a_{43}(\eta_5 x_{42} - \eta_5 x_{41} - \eta_6 x_{43} + u_3^*), \\
 \dot{e}_4 &= a_{14}(-\alpha_7 x_{12}) + a_{24}(-\beta_7 x_{22}) - a_{34}(-\gamma_7 x_{32} + u_4) \\
 &\quad - a_{44}(-\eta_7 x_{42} + u_4^*), \\
 \dot{e}_5 &= a_{15}x_{11} + a_{25}x_{21} - a_{35}(x_{31} + u_5) - a_{45}(x_{41} + u_5^*).
 \end{aligned} \tag{15}$$

Denote

$$\begin{aligned}
 U_1 &= a_{31}u_1 + a_{41}u_1^*, \\
 U_2 &= a_{32}u_2 + a_{42}u_2^*, \\
 U_3 &= a_{33}u_3 + a_{43}u_3^*, \\
 U_4 &= a_{34}u_4 + a_{44}u_4^*, \\
 U_5 &= a_{35}u_5 + a_{45}u_5^*.
 \end{aligned} \tag{16}$$

Then (15) can be rewritten as

$$\begin{aligned}
 \dot{e}_1 &= a_{11} (\alpha_1 x_{13} - \alpha_2 x_{11} - \alpha_3 x_{11} x_{15}^2) \\
 &\quad + a_{21} (\beta_1 x_{23} - \beta_2 x_{21} - \beta_3 x_{21} x_{25}^2) \\
 &\quad - a_{31} (\gamma_1 x_{33} - \gamma_2 x_{31} - \gamma_3 x_{31} x_{35}^2) \\
 &\quad - a_{41} (\eta_1 x_{43} - \eta_2 x_{41} - \eta_3 x_{41} x_{45}^2) - U_1, \\
 \dot{e}_2 &= a_{12} (-\alpha_4 x_{13} + \alpha_4 x_{14}) + a_{22} (-\beta_4 x_{23} + \beta_4 x_{24}) \\
 &\quad - a_{32} (-\gamma_4 x_{33} + \gamma_4 x_{34}) \\
 &\quad - a_{42} (-\eta_4 x_{43} + \eta_4 x_{44}) - U_2, \\
 \dot{e}_3 &= a_{13} (\alpha_5 x_{12} - \alpha_5 x_{11} - \alpha_6 x_{13}) \\
 &\quad + a_{23} (\beta_5 x_{22} - \beta_5 x_{21} - \beta_6 x_{23}) \\
 &\quad - a_{33} (\gamma_5 x_{32} - \gamma_5 x_{31} - \gamma_6 x_{33}) \\
 &\quad - a_{43} (\eta_5 x_{42} - \eta_5 x_{41} - \eta_6 x_{43}) - U_3, \\
 \dot{e}_4 &= -a_{14} \alpha_7 x_{12} - a_{24} \beta_7 x_{22} + a_{34} \gamma_7 x_{32} + a_{44} \eta_7 x_{42} - U_4, \\
 \dot{e}_5 &= a_{15} x_{11} + a_{25} x_{21} - a_{35} x_{31} - a_{45} x_{41} - U_5.
 \end{aligned} \tag{17}$$

In fact, (16) is called the controller to be designed.

Theorem 6. *If the control law is chosen as follows:*

$$\begin{aligned}
 U_1 &= a_{11} [\alpha_1 x_{13} + (1 - \alpha_2) x_{11} - \alpha_3 x_{11} x_{15}^2] \\
 &\quad + a_{21} [\beta_1 x_{23} + (1 - \beta_2) x_{21} - \beta_3 x_{21} x_{25}^2] \\
 &\quad - a_{31} [\gamma_1 x_{33} + (1 - \gamma_2) x_{31} - \gamma_3 x_{31} x_{35}^2] \\
 &\quad - a_{41} [\eta_1 x_{43} + (1 - \eta_2) x_{41} - \eta_3 x_{41} x_{45}^2] \\
 &\quad + (a_{12} x_{12} + a_{22} x_{22} - a_{32} x_{32} - a_{42} x_{42}), \\
 U_2 &= a_{12} (x_{12} - \alpha_4 x_{13} + \alpha_4 x_{14}) \\
 &\quad + a_{22} (x_{22} - \beta_4 x_{23} + \beta_4 x_{24}) \\
 &\quad - a_{32} (x_{32} - \gamma_4 x_{33} + \gamma_4 x_{34}) \\
 &\quad - a_{42} (x_{42} - \eta_4 x_{43} + \eta_4 x_{44}) \\
 &\quad - (a_{11} x_{11} + a_{21} x_{21} - a_{31} x_{31} - a_{41} x_{41}) \\
 &\quad + (a_{13} x_{13} + a_{23} x_{23} - a_{33} x_{33} - a_{43} x_{43}), \\
 U_3 &= a_{13} [\alpha_5 x_{12} - \alpha_5 x_{11} + (1 - \alpha_6) x_{13}] \\
 &\quad + a_{23} [\beta_5 x_{22} - \beta_5 x_{21} + (1 - \beta_6) x_{23}] \\
 &\quad - a_{33} [\gamma_5 x_{32} - \gamma_5 x_{31} + (1 - \gamma_6) x_{33}]
 \end{aligned}$$

$$\begin{aligned}
 &- a_{43} [\eta_5 x_{42} - \eta_5 x_{41} + (1 - \eta_6) x_{43}] \\
 &- (a_{12} x_{12} + a_{22} x_{22} - a_{32} x_{32} - a_{42} x_{42}) \\
 &+ (a_{14} x_{14} + a_{24} x_{24} - a_{34} x_{34} - a_{44} x_{44}), \\
 U_4 &= - (a_{13} x_{13} + a_{23} x_{23} - a_{33} x_{33} - a_{43} x_{43}) \\
 &+ a_{14} (x_{14} - \alpha_7 x_{12}) + a_{24} (x_{24} - \beta_7 x_{22}) \\
 &- a_{34} (x_{34} - \gamma_7 x_{32}) - a_{44} (x_{44} - \eta_7 x_{42}) \\
 &+ (a_{15} x_{15} + a_{25} x_{25} - a_{35} x_{35} - a_{45} x_{45}), \\
 U_5 &= a_{15} (x_{11} + x_{15}) + a_{25} (x_{21} + x_{25}) \\
 &- a_{35} (x_{31} + x_{35}) - a_{45} (x_{41} + x_{45}) \\
 &- (a_{14} x_{14} + a_{24} x_{24} - a_{34} x_{34} - a_{44} x_{44}),
 \end{aligned} \tag{18}$$

then the drive systems (4) and (9) will achieve combination-combination synchronization with the response systems (10) and (11).

Proof. Consider the following Lyapunov function:

$$\begin{aligned}
 V(e(t)) &= V(e_1, e_2, e_3, e_4, e_5) \\
 &= \frac{1}{2} (e_1^2 + e_2^2 + e_3^2 + e_4^2 + e_5^2).
 \end{aligned} \tag{19}$$

Calculating the upper right Dini derivative of V along the trajectory of (17), then

$$\begin{aligned}
 D^+V &= e_1 \dot{e}_1 + e_2 \dot{e}_2 + e_3 \dot{e}_3 + e_4 \dot{e}_4 + e_5 \dot{e}_5 \\
 &= e_1 [a_{11} (\alpha_1 x_{13} - \alpha_2 x_{11} - \alpha_3 x_{11} x_{15}^2) \\
 &\quad + a_{21} (\beta_1 x_{23} - \beta_2 x_{21} - \beta_3 x_{21} x_{25}^2) \\
 &\quad - a_{31} (\gamma_1 x_{33} - \gamma_2 x_{31} - \gamma_3 x_{31} x_{35}^2) \\
 &\quad - a_{41} (\eta_1 x_{43} - \eta_2 x_{41} - \eta_3 x_{41} x_{45}^2) - U_1] \\
 &+ e_2 [a_{12} (-\alpha_4 x_{13} + \alpha_4 x_{14}) + a_{22} (-\beta_4 x_{23} + \beta_4 x_{24}) \\
 &\quad - a_{32} (-\gamma_4 x_{33} + \gamma_4 x_{34}) \\
 &\quad - a_{42} (-\eta_4 x_{43} + \eta_4 x_{44}) - U_2] \\
 &+ e_3 [a_{13} (\alpha_5 x_{12} - \alpha_5 x_{11} - \alpha_6 x_{13}) \\
 &\quad + a_{23} (\beta_5 x_{22} - \beta_5 x_{21} - \beta_6 x_{23}) \\
 &\quad - a_{33} (\gamma_5 x_{32} - \gamma_5 x_{31} - \gamma_6 x_{33}) \\
 &\quad - a_{43} (\eta_5 x_{42} - \eta_5 x_{41} - \eta_6 x_{43}) - U_3] \\
 &+ e_4 [-a_{14} \alpha_7 x_{12} - a_{24} \beta_7 x_{22} \\
 &\quad + a_{34} \gamma_7 x_{32} + a_{44} \eta_7 x_{42} - U_4]
 \end{aligned}$$

$$\begin{aligned}
& + e_5 [a_{15}x_{11} + a_{25}x_{21} - a_{35}x_{31} - a_{45}x_{41} - U_5] \\
= & e_1 [\Delta_1 - U_1] + e_2 [\Delta_2 - U_2] + e_3 [\Delta_3 - U_3] \\
& + e_4 [\Delta_4 - U_4] + e_5 [\Delta_5 - U_5],
\end{aligned} \tag{20}$$

where

$$\begin{aligned}
\Delta_1 &= a_{11} (\alpha_1 x_{13} - \alpha_2 x_{11} - \alpha_3 x_{11} x_{15}^2) \\
&+ a_{21} (\beta_1 x_{23} - \beta_2 x_{21} - \beta_3 x_{21} x_{25}^2) \\
&- a_{31} (\gamma_1 x_{33} - \gamma_2 x_{31} - \gamma_3 x_{31} x_{35}^2) \\
&- a_{41} (\eta_1 x_{43} - \eta_2 x_{41} - \eta_3 x_{41} x_{45}^2), \\
\Delta_2 &= a_{12} (-\alpha_4 x_{13} + \alpha_4 x_{14}) + a_{22} (-\beta_4 x_{23} + \beta_4 x_{24}) \\
&- a_{32} (-\gamma_4 x_{33} + \gamma_4 x_{34}) - a_{42} (-\eta_4 x_{43} + \eta_4 x_{44}), \tag{21} \\
\Delta_3 &= a_{13} (\alpha_5 x_{12} - \alpha_5 x_{11} - \alpha_6 x_{13}) \\
&+ a_{23} (\beta_5 x_{22} - \beta_5 x_{21} - \beta_6 x_{23}) \\
&- a_{33} (\gamma_5 x_{32} - \gamma_5 x_{31} - \gamma_6 x_{33}) \\
&- a_{43} (\eta_5 x_{42} - \eta_5 x_{41} - \eta_6 x_{43}), \\
\Delta_4 &= -a_{14} \alpha_7 x_{12} - a_{24} \beta_7 x_{22} + a_{34} \gamma_7 x_{32} + a_{44} \eta_7 x_{42}, \\
\Delta_5 &= a_{15} x_{11} + a_{25} x_{21} - a_{35} x_{31} - a_{45} x_{41}.
\end{aligned}$$

On the basis of (18), we have

$$\begin{aligned}
\Delta_1 - U_1 &= -(a_{11}x_{11} + a_{21}x_{21} - a_{31}x_{31} - a_{41}x_{41}) \\
&- (a_{12}x_{12} + a_{22}x_{22} - a_{32}x_{32} - a_{42}x_{42}), \\
\Delta_2 - U_2 &= (a_{11}x_{11} + a_{21}x_{21} - a_{31}x_{31} - a_{41}x_{41}) \\
&- (a_{12}x_{12} + a_{22}x_{22} - a_{32}x_{32} - a_{42}x_{42}) \\
&- (a_{13}x_{13} + a_{23}x_{23} - a_{33}x_{33} - a_{43}x_{43}), \\
\Delta_3 - U_3 &= (a_{12}x_{12} + a_{22}x_{22} - a_{32}x_{32} - a_{42}x_{42}) \\
&- (a_{13}x_{13} + a_{23}x_{23} - a_{33}x_{33} - a_{43}x_{43}) \tag{22} \\
&- (a_{14}x_{14} + a_{24}x_{24} - a_{34}x_{34} - a_{44}x_{44}), \\
\Delta_4 - U_4 &= (a_{13}x_{13} + a_{23}x_{23} - a_{33}x_{33} - a_{43}x_{43}) \\
&- (a_{14}x_{14} + a_{24}x_{24} - a_{34}x_{34} - a_{44}x_{44}) \\
&- (a_{15}x_{15} + a_{25}x_{25} - a_{35}x_{35} - a_{45}x_{45}), \\
\Delta_5 - U_5 &= (a_{14}x_{14} + a_{24}x_{24} - a_{34}x_{34} - a_{44}x_{44}) \\
&- (a_{15}x_{15} + a_{25}x_{25} - a_{35}x_{35} - a_{45}x_{45}).
\end{aligned}$$

That is,

$$\begin{aligned}
\Delta_1 - U_1 &= -e_1 - e_2, \\
\Delta_2 - U_2 &= e_1 - e_2 - e_3, \\
\Delta_3 - U_3 &= e_2 - e_3 - e_4, \\
\Delta_4 - U_4 &= e_3 - e_4 - e_5, \\
\Delta_5 - U_5 &= e_4 - e_5.
\end{aligned} \tag{23}$$

Together with (20) and (23), then

$$\begin{aligned}
D^+V &= e_1 (-e_1 - e_2) + e_2 (e_1 - e_2 - e_3) \\
&+ e_3 (e_2 - e_3 - e_4) + e_4 (e_3 - e_4 - e_5) \\
&+ e_5 (e_4 - e_5) \\
&= -e_1^2 - e_2^2 - e_3^2 - e_4^2 - e_5^2 = -e^T e,
\end{aligned} \tag{24}$$

where $e = (e_1, e_2, e_3, e_4, e_5)^T$.

Let $t > 0$ be arbitrarily given; integrating the above Equation (24) from 0 to t , then

$$\int_0^t \|e(s)\|^2 ds = \int_0^t -\dot{V} ds = V(e(0)) - V(e(t)) \leq V(e(0)), \tag{25}$$

where $\|\cdot\|$ is the Euclidean vector norm.

According to Barbalat's lemma, we have $\|e(t)\|^2 \rightarrow 0$ as $t \rightarrow +\infty$. Hence, $(e_1, e_2, e_3, e_4, e_5) \rightarrow (0, 0, 0, 0, 0)$ as $t \rightarrow +\infty$. It implies that the drive systems (4) and (9) can achieve combination-combination synchronization with the response systems (10) and (11). The proof is completed. \square

Remark 7. The nonlinear degree of control input in (18) is somewhat high. In the sense of control theory, the control input in (18) may not be the best. However, in many applications, firstly one often needs to understand whether the control system designed has the desired properties such as the combination-combination synchronization behavior. In fact, as the works in [9, 28], because of the unique construction about combination design, the control input in synchronization scheme via combination design is usually a bit more complicated. How to design easy and efficient synchronization criteria will be the topic of future research.

Remark 8. For the controller design of combination-combination synchronization, once we get proper controller (16), then the u_i and u_i^* ($i = 1, 2, 3, 4, 5$) in the response systems (10) and (11) can be obtained via $a_{3i}u_i + a_{4i}u_i^* = U_i$ ($i = 1, 2, 3, 4, 5$). Obviously, these u_i and u_i^* ($i = 1, 2, 3, 4, 5$) have wide choices, which can provide the designer with the richness of flexibility. Of course, for the whole controller design of combination-combination synchronization, we merely concern the controller (16).

Next we extend Theorem 6 to other possible cases.

Corollary 9. *If the control law is chosen as follows:*

$$\begin{aligned}
 \bar{U}_1 &:= a_{31}u_1 \\
 &= a_{11} [\alpha_1 x_{13} + (1 - \alpha_2) x_{11} - \alpha_3 x_{11} x_{15}^2] \\
 &\quad + a_{21} [\beta_1 x_{23} + (1 - \beta_2) x_{21} - \beta_3 x_{21} x_{25}^2] \\
 &\quad - a_{31} [\gamma_1 x_{33} + (1 - \gamma_2) x_{31} - \gamma_3 x_{31} x_{35}^2] \\
 &\quad + (a_{12} x_{12} + a_{22} x_{22} - a_{32} x_{32}), \\
 \bar{U}_2 &:= a_{32}u_2 \\
 &= a_{12} (x_{12} - \alpha_4 x_{13} + \alpha_4 x_{14}) \\
 &\quad + a_{22} (x_{22} - \beta_4 x_{23} + \beta_4 x_{24}) \\
 &\quad - a_{32} (x_{32} - \gamma_4 x_{33} + \gamma_4 x_{34}) \\
 &\quad - (a_{11} x_{11} + a_{21} x_{21} - a_{31} x_{31}) \\
 &\quad + (a_{13} x_{13} + a_{23} x_{23} - a_{33} x_{33}), \\
 \bar{U}_3 &:= a_{33}u_3 \\
 &= a_{13} [\alpha_5 x_{12} - \alpha_5 x_{11} + (1 - \alpha_6) x_{13}] \\
 &\quad + a_{23} [\beta_5 x_{22} - \beta_5 x_{21} + (1 - \beta_6) x_{23}] \\
 &\quad - a_{33} [\gamma_5 x_{32} - \gamma_5 x_{31} + (1 - \gamma_6) x_{33}] \\
 &\quad - (a_{12} x_{12} + a_{22} x_{22} - a_{32} x_{32}) \\
 &\quad + (a_{14} x_{14} + a_{24} x_{24} - a_{34} x_{34}), \\
 \bar{U}_4 &:= a_{34}u_4 \\
 &= -(a_{13} x_{13} + a_{23} x_{23} - a_{33} x_{33}) \\
 &\quad + (a_{15} x_{15} + a_{25} x_{25} - a_{35} x_{35}) \\
 &\quad + a_{14} (x_{14} - \alpha_7 x_{12}) + a_{24} (x_{24} - \beta_7 x_{22}) \\
 &\quad - a_{34} (x_{34} - \gamma_7 x_{32}), \\
 \bar{U}_5 &:= a_{35}u_5 \\
 &= a_{15} (x_{11} + x_{15}) + a_{25} (x_{21} + x_{25}) \\
 &\quad - a_{35} (x_{31} + x_{35}) - (a_{14} x_{14} + a_{24} x_{24} - a_{34} x_{34}),
 \end{aligned} \tag{26}$$

then the drive systems (4) and (9) will achieve combination synchronization with the response system (10).

Corollary 10. *If the control law is chosen as follows:*

$$\begin{aligned}
 \bar{U}_1 &:= a_{41}u_1^* \\
 &= a_{11} [\alpha_1 x_{13} + (1 - \alpha_2) x_{11} - \alpha_3 x_{11} x_{15}^2] \\
 &\quad + a_{21} [\beta_1 x_{23} + (1 - \beta_2) x_{21} - \beta_3 x_{21} x_{25}^2]
 \end{aligned}$$

$$\begin{aligned}
 &- a_{41} [\eta_1 x_{43} + (1 - \eta_2) x_{41} - \eta_3 x_{41} x_{45}^2] \\
 &\quad + (a_{12} x_{12} + a_{22} x_{22} - a_{42} x_{42}),
 \end{aligned}$$

$$\begin{aligned}
 \bar{U}_2 &:= a_{42}u_2^* \\
 &= a_{12} (x_{12} - \alpha_4 x_{13} + \alpha_4 x_{14}) \\
 &\quad + a_{22} (x_{22} - \beta_4 x_{23} + \beta_4 x_{24}) \\
 &\quad - a_{42} (x_{42} - \eta_4 x_{43} + \eta_4 x_{44}) \\
 &\quad - (a_{11} x_{11} + a_{21} x_{21} - a_{41} x_{41}) \\
 &\quad + (a_{13} x_{13} + a_{23} x_{23} - a_{43} x_{43}),
 \end{aligned}$$

$$\begin{aligned}
 \bar{U}_3 &:= a_{43}u_3^* \\
 &= a_{13} [\alpha_5 x_{12} - \alpha_5 x_{11} + (1 - \alpha_6) x_{13}] \\
 &\quad + a_{23} [\beta_5 x_{22} - \beta_5 x_{21} + (1 - \beta_6) x_{23}] \\
 &\quad - a_{43} [\eta_5 x_{42} - \eta_5 x_{41} + (1 - \eta_6) x_{43}] \\
 &\quad - (a_{12} x_{12} + a_{22} x_{22} - a_{42} x_{42}) \\
 &\quad + (a_{14} x_{14} + a_{24} x_{24} - a_{44} x_{44}),
 \end{aligned}$$

$$\begin{aligned}
 \bar{U}_4 &:= a_{44}u_4^* \\
 &= -(a_{13} x_{13} + a_{23} x_{23} - a_{43} x_{43}) \\
 &\quad + (a_{15} x_{15} + a_{25} x_{25} - a_{45} x_{45}) \\
 &\quad + a_{14} (x_{14} - \alpha_7 x_{12}) + a_{24} (x_{24} - \beta_7 x_{22}) \\
 &\quad - a_{44} (x_{44} - \eta_7 x_{42}),
 \end{aligned}$$

$$\begin{aligned}
 \bar{U}_5 &:= a_{45}u_5^* \\
 &= a_{15} (x_{11} + x_{15}) + a_{25} (x_{21} + x_{25}) \\
 &\quad - a_{45} (x_{41} + x_{45}) - (a_{14} x_{14} + a_{24} x_{24} - a_{44} x_{44}),
 \end{aligned} \tag{27}$$

then the drive systems (4) and (9) will achieve combination synchronization with the response system (11).

Corollary 11. *If the control law is chosen as follows:*

$$\begin{aligned}
 \bar{U}_1 &:= a_{31}u_1 \\
 &= a_{11} [\alpha_1 x_{13} + (1 - \alpha_2) x_{11} - \alpha_3 x_{11} x_{15}^2] \\
 &\quad - a_{31} [\gamma_1 x_{33} + (1 - \gamma_2) x_{31} - \gamma_3 x_{31} x_{35}^2] \\
 &\quad + (a_{12} x_{12} - a_{32} x_{32}), \\
 \bar{U}_2 &:= a_{32}u_2 \\
 &= a_{12} (x_{12} - \alpha_4 x_{13} + \alpha_4 x_{14})
 \end{aligned}$$

$$\begin{aligned}
& -a_{32}(x_{32} - \gamma_4 x_{33} + \gamma_4 x_{34}) \\
& - (a_{11}x_{11} - a_{31}x_{31}) + (a_{13}x_{13} - a_{33}x_{33}), \\
\tilde{U}_3 &:= a_{33}u_3 \\
&= a_{13}[\alpha_5 x_{12} - \alpha_5 x_{11} + (1 - \alpha_6)x_{13}] \\
& - a_{33}[\gamma_5 x_{32} - \gamma_5 x_{31} + (1 - \gamma_6)x_{33}] \\
& - (a_{12}x_{12} - a_{32}x_{32}) + (a_{14}x_{14} - a_{34}x_{34}), \\
\tilde{U}_4 &:= a_{34}u_4 \\
&= - (a_{13}x_{13} - a_{33}x_{33}) + a_{14}(x_{14} - \alpha_7 x_{12}) \\
& - a_{34}(x_{34} - \gamma_7 x_{32}) + (a_{15}x_{15} - a_{35}x_{35}), \\
\tilde{U}_5 &:= a_{35}u_5 \\
&= a_{15}(x_{11} + x_{15}) - a_{35}(x_{31} + x_{35}) \\
& - (a_{14}x_{14} - a_{34}x_{34}), \tag{28}
\end{aligned}$$

then the drive system (4) will achieve complete synchronization with the response system (10).

According to Corollary 11, on the complete synchronization criteria between (4) and (11), or (9) and (10), or (9) and (11), one can make some parallel promotions. So we will not repeat all of those corollaries here.

Corollary 12. *If the control law is chosen as follows:*

$$\begin{aligned}
\tilde{U}_1 &:= a_{31}u_1 \\
&= -a_{31}[\gamma_1 x_{33} + (1 - \gamma_2)x_{31} - \gamma_3 x_{31}x_{35}^2] \\
& - a_{32}x_{32}, \\
\tilde{U}_2 &:= a_{32}u_2 \\
&= -a_{32}(x_{32} - \gamma_4 x_{33} + \gamma_4 x_{34}) \\
& + a_{31}x_{31} - a_{33}x_{33}, \\
\tilde{U}_3 &:= a_{33}u_3 \\
&= -a_{33}[\gamma_5 x_{32} - \gamma_5 x_{31} + (1 - \gamma_6)x_{33}] \\
& + a_{32}x_{32} - a_{34}x_{34}, \\
\tilde{U}_4 &:= a_{34}u_4 \\
&= a_{33}x_{33} - a_{34}(x_{34} - \gamma_7 x_{32}) \\
& - a_{35}x_{35}, \\
\tilde{U}_5 &:= a_{35}u_5 \\
&= -a_{35}(x_{31} + x_{35}) + a_{34}x_{34}, \tag{29}
\end{aligned}$$

then system (10) is asymptotically stabilizable.

Corollary 13. *If the control law is chosen as follows:*

$$\begin{aligned}
\tilde{U}_1 &:= a_{41}u_1^* \\
&= -a_{41}[\eta_1 x_{43} + (1 - \eta_2)x_{41} - \eta_3 x_{41}x_{45}^2] \\
& - a_{42}x_{42}, \\
\tilde{U}_2 &:= a_{42}u_2^* \\
&= -a_{42}(x_{42} - \eta_4 x_{43} + \eta_4 x_{44}) \\
& + a_{41}x_{41} - a_{43}x_{43}, \\
\tilde{U}_3 &:= a_{43}u_3^* \\
&= -a_{43}[\eta_5 x_{42} - \eta_5 x_{41} + (1 - \eta_6)x_{43}] \\
& + a_{42}x_{42} - a_{44}x_{44}, \\
\tilde{U}_4 &:= a_{44}u_4^* \\
&= a_{43}x_{43} - a_{44}(x_{44} - \eta_7 x_{42}) \\
& - a_{45}x_{45}, \\
\tilde{U}_5 &:= a_{45}u_5^* \\
&= -a_{45}(x_{41} + x_{45}) + a_{44}x_{44}, \tag{30}
\end{aligned}$$

then system (11) is asymptotically stabilizable.

Remark 14. Just like Remark 7, the nonlinear degree of control input in the above corollaries is somewhat high. How to design some less conservative criteria, this issue, will be the topic of future research.

Remark 15. In many existing works, the combination of multiple drive systems may induce the combination states to be asymptotically stable or emanative. And theoretically, a direct consequence of such combination of multiple drive systems is the information signal extraction which is extremely difficult or completely useless. In this paper, the combination of two drive systems can be always hyperchaotic; thus, the dynamic behavior is more abundant and complex (see the subsequent numerical example). In theory, when it is used to chaotic communication, this would greatly enhance the security and reliability for high-performance communication.

Remark 16. Theoretically, in the past chaotic communication via drive-response model, the transmitted signal only depends on one drive system. However, in theory, when designing secure communication via combination-combination synchronization, the transmitted signal and received signal can both be split into multiple different chaotic systems. Compared to some conventional design methods, this design approach maybe have stronger antiattack ability.

In the following, we give a numerical example to illustrate the superiority of theoretical results via computer simulations.

Assume $\alpha_1 = \beta_1 = \gamma_1 = \eta_1 = 9$, $\alpha_2 = \beta_2 = \gamma_2 = \eta_2 = -10.8$, $\alpha_3 = \beta_3 = \gamma_3 = \eta_3 = 10.8$, $\alpha_4 = \beta_4 = \gamma_4 = \eta_4 = 1$, $\alpha_5 = \beta_5 = \gamma_5 = \eta_5 = 30$, $\alpha_6 = \beta_6 = \gamma_6 = \eta_6 = 30$, $\alpha_7 = \beta_7 = \gamma_7 = \eta_7 = 15$. Let $A_1 = \text{diag}(a_{11}, a_{12}, a_{13}, a_{14}, a_{15}) = \text{diag}(1, 1, 1, 1, 1)$, $A_2 = \text{diag}(a_{21}, a_{22}, a_{23}, a_{24}, a_{25}) = \text{diag}(1, 1, 1, 1, 1)$, $A_3 = \text{diag}(a_{31}, a_{32}, a_{33}, a_{34}, a_{35}) = \text{diag}(1, 1, 1, 1, 1)$, $A_4 = \text{diag}(a_{41}, a_{42}, a_{43}, a_{44}, a_{45}) = \text{diag}(1, 1, 1, 1, 1)$, according to Theorem 6; then the control law can be designed as

$$\begin{aligned}
 U_1 &= \begin{bmatrix} 9x_{13} + 11.8x_{11} - 10.8x_{11}x_{15}^2 \\ 9x_{23} + 11.8x_{21} - 10.8x_{21}x_{25}^2 \\ 9x_{33} + 11.8x_{31} - 10.8x_{31}x_{35}^2 \\ 9x_{43} + 11.8x_{41} - 10.8x_{41}x_{45}^2 \end{bmatrix} \\
 &\quad + (x_{12} + x_{22} - x_{32} - x_{42}), \\
 U_2 &= (x_{12} - x_{13} + x_{14}) + (x_{22} - x_{23} + x_{24}) \\
 &\quad - (x_{32} - x_{33} + x_{34}) - (x_{42} - x_{43} + x_{44}) \\
 &\quad - (x_{11} + x_{21} - x_{31} - x_{41}) \\
 &\quad + (x_{13} + x_{23} - x_{33} - x_{43}), \\
 U_3 &= \begin{bmatrix} 30x_{12} - 30x_{11} - 29x_{13} \\ 30x_{22} - 30x_{21} - 29x_{23} \\ 30x_{32} - 30x_{31} - 29x_{33} \\ 30x_{42} - 30x_{41} - 29x_{43} \end{bmatrix} \\
 &\quad - (x_{12} + x_{22} - x_{32} - x_{42}) \\
 &\quad + (x_{14} + x_{24} - x_{34} - x_{44}), \\
 U_4 &= -(x_{13} + x_{23} - x_{33} - x_{43}) \\
 &\quad + (x_{14} - 15x_{12}) + (x_{24} - 15x_{22}) \\
 &\quad - (x_{34} - 15x_{32}) - (x_{44} - 15x_{42}) \\
 &\quad + (x_{15} + x_{25} - x_{35} - x_{45}), \\
 U_5 &= x_{11} + x_{15} + x_{21} + x_{25} \\
 &\quad - (x_{31} + x_{35}) - (x_{41} + x_{45}) \\
 &\quad - (x_{14} + x_{24} - x_{34} - x_{44}).
 \end{aligned} \tag{31}$$

By (16), it follows that

$$\begin{aligned}
 U_1 &= u_1 + u_1^*, \\
 U_2 &= u_2 + u_2^*, \\
 U_3 &= u_3 + u_3^*,
 \end{aligned}$$

$$U_4 = u_4 + u_4^*,$$

$$U_5 = u_5 + u_5^*.$$

(32)

then u_i and u_i^* ($i = 1, 2, 3, 4, 5$) can be chosen according to different requirements. For example, it allows

$$\begin{aligned}
 u_1 &= \begin{bmatrix} 9x_{13} + 11.8x_{11} - 10.8x_{11}x_{15}^2 \\ 9x_{23} + 11.8x_{21} - 10.8x_{21}x_{25}^2 \\ 9x_{33} + 11.8x_{31} - 10.8x_{31}x_{35}^2 \\ 9x_{43} + 11.8x_{41} - 10.8x_{41}x_{45}^2 \end{bmatrix}, \\
 u_1^* &= x_{12} + x_{22} - x_{32} - x_{42}, \\
 u_2 &= (x_{12} - x_{13} + x_{14}) + (x_{22} - x_{23} + x_{24}) \\
 &\quad - (x_{32} - x_{33} + x_{34}) - (x_{42} - x_{43} + x_{44}), \\
 u_2^* &= -(x_{11} + x_{21} - x_{31} - x_{41}) \\
 &\quad + (x_{13} + x_{23} - x_{33} - x_{43}), \\
 u_3 &= \begin{bmatrix} 30x_{12} - 30x_{11} - 29x_{13} \\ 30x_{22} - 30x_{21} - 29x_{23} \\ 30x_{32} - 30x_{31} - 29x_{33} \\ 30x_{42} - 30x_{41} - 29x_{43} \end{bmatrix}, \\
 u_3^* &= -(x_{12} + x_{22} - x_{32} - x_{42}) \\
 &\quad + (x_{14} + x_{24} - x_{34} - x_{44}), \\
 u_4 &= -(x_{13} + x_{23} - x_{33} - x_{43}) \\
 &\quad + (x_{14} - 15x_{12}) + (x_{24} - 15x_{22}) \\
 &\quad - (x_{34} - 15x_{32}) - (x_{44} - 15x_{42}), \\
 u_4^* &= x_{15} + x_{25} - x_{35} - x_{45}, \\
 u_5 &= x_{11} + x_{15} + x_{21} + x_{25} \\
 &\quad - (x_{31} + x_{35}) - (x_{41} + x_{45}), \\
 u_5^* &= -x_{14} + x_{24} - x_{34} - x_{44}.
 \end{aligned} \tag{33}$$

Of course, the u_i and u_i^* ($i = 1, 2, 3, 4, 5$) in (33) are just one case rather than the norm. The designers can choose what they need via the combination-combination controller (31).

Simulation result of the combination of two drive systems (4) and (9) is depicted in Figure 4. The computer simulation suggests that the combination of two drive systems (4) and (9) has a hyperchaotic attractor, as shown in Figure 4, which has verified that the combination of drive systems (4) and (9) remains hyperchaotic. Meanwhile, according to Theorem 6, the combination of two drive systems (4) and (9) can achieve

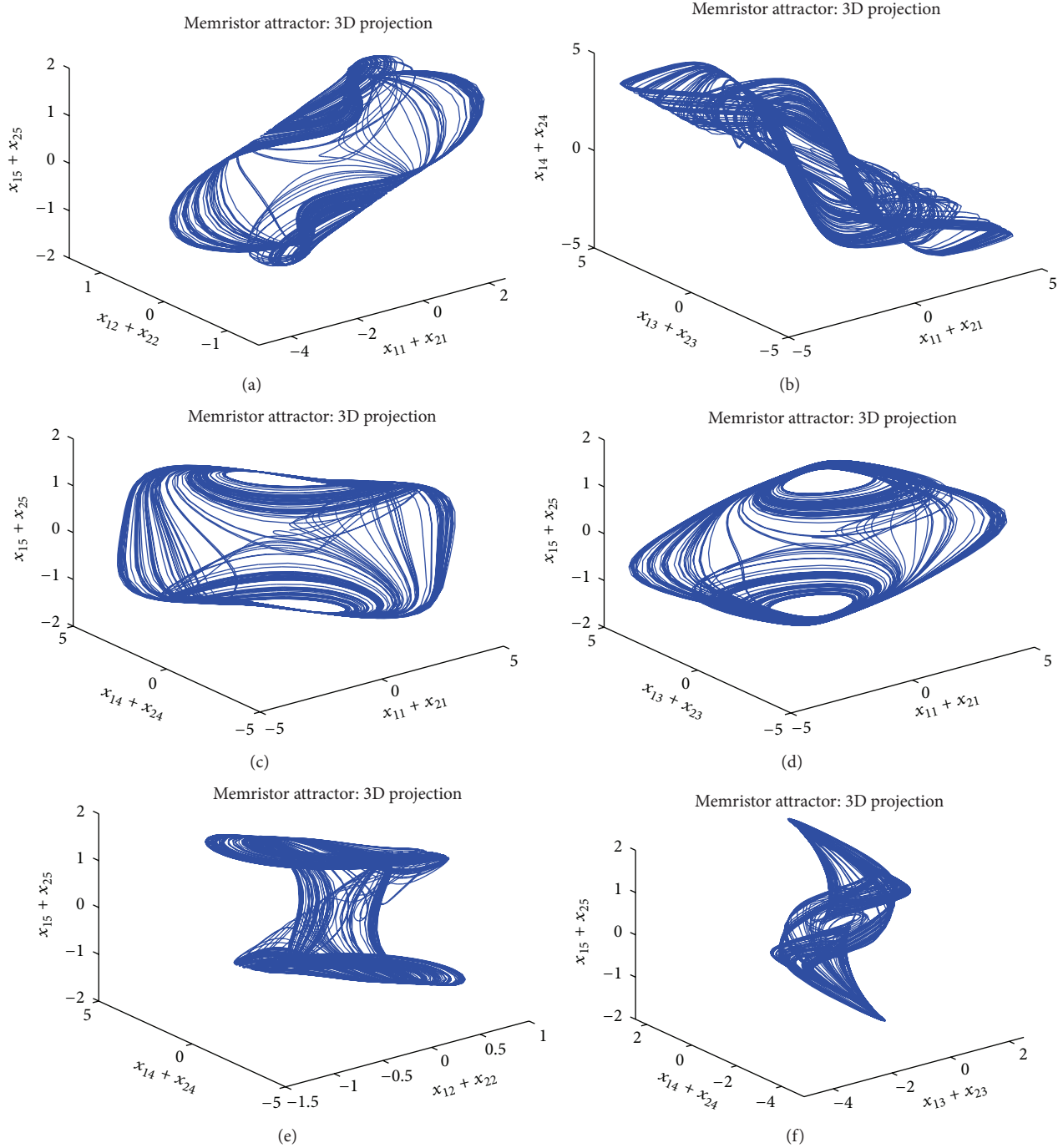


FIGURE 4: 3D projections of the hyperchaotic attractor from combination of two drive systems.

synchronization with the combination of two response systems (10) and (11). Figure 5 depicts the time response of the synchronization error $e(t) = (e_1(t), e_2(t), e_3(t), e_4(t), e_5(t))^T$.

4. Concluding Remarks

A fifth-order complex memristor oscillator system with hyperchaotic effect is presented in this paper. Some sufficient

conditions are derived to guarantee the hyperchaotic complex memristor oscillator system for realizing combination-combination synchronization. The hyperchaotic complex memristor oscillator system is useful in secure communication systems with enhanced security features that protect against deciphering. Also, the scheme of combination-combination synchronization might overcome some design issues associated with previous schemes for using chaos in communications. Application of new intelligent control

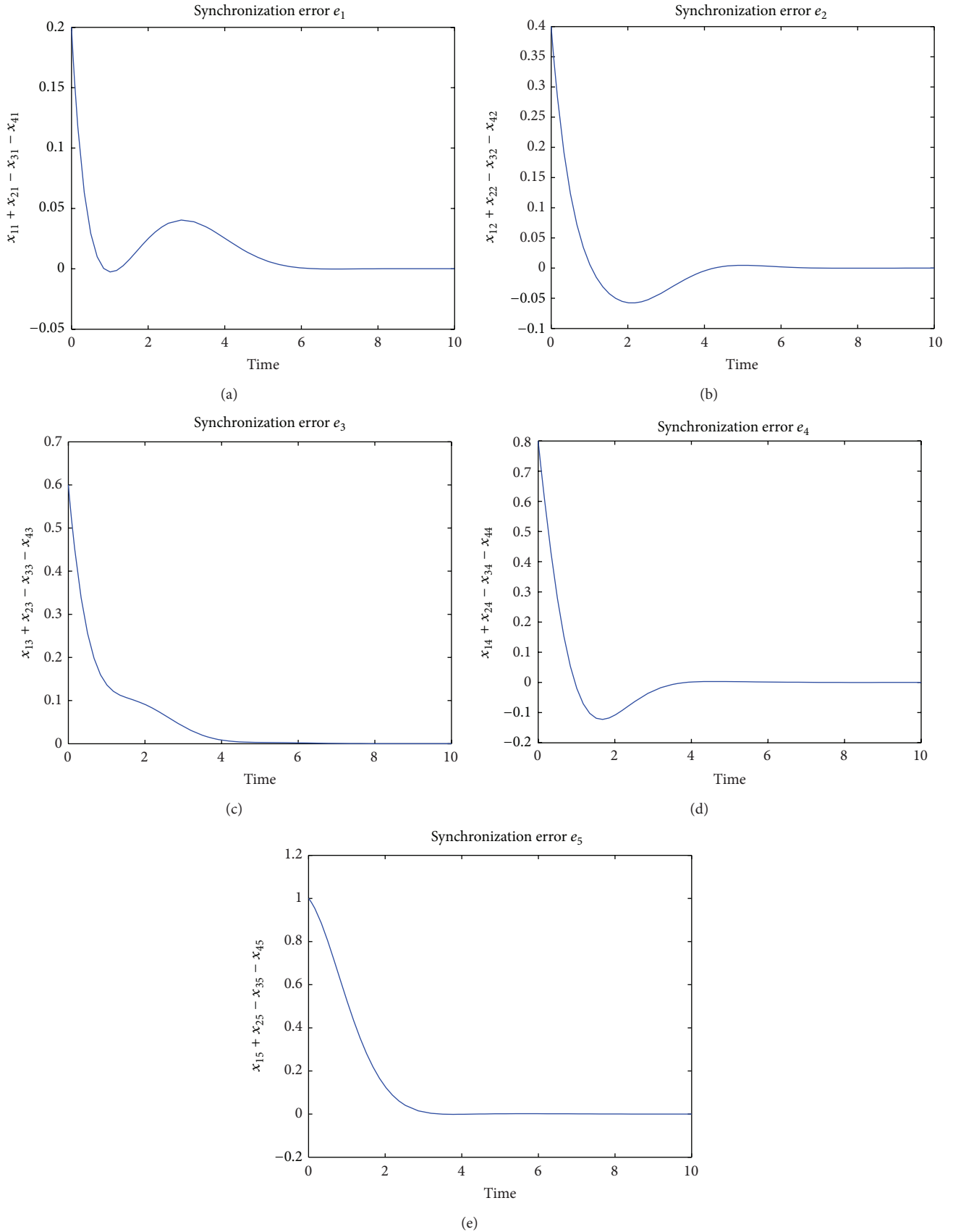


FIGURE 5: Time response curve for synchronization error $e(t) = (e_1(t), e_2(t), e_3(t), e_4(t), e_5(t))^T$.

methods to complex memristor oscillator model yields a deep insight into the behaviors under investigation.

Conflict of Interests

The author declares that there is no conflict of interests regarding the publication of this paper.

Acknowledgment

The work is supported by the Research Project of Hubei Provincial Department of Education of China under Grant T201412.

References

- [1] B. C. Bao, Z. Liu, and J. P. Xu, "Steady periodic Memristor oscillator with transient chaotic behaviours," *Electronics Letters*, vol. 46, no. 3, pp. 237–238, 2010.
- [2] F. Corinto, A. Ascoli, and M. Gilli, "Nonlinear dynamics of Memristor oscillators," *IEEE Transactions on Circuits and Systems I: Regular Papers*, vol. 58, no. 6, pp. 1323–1336, 2011.
- [3] M. Itoh and L. O. Chua, "Memristor oscillators," *International Journal of Bifurcation and Chaos*, vol. 18, no. 11, pp. 3183–3206, 2008.
- [4] B. Muthuswamy and P. P. Kokate, "Memristor-based chaotic circuits," *IETE Technical Review*, vol. 26, no. 6, pp. 417–429, 2009.
- [5] R. Riaza, "First order mem-circuits: modeling, nonlinear oscillations and bifurcations," *IEEE Transactions on Circuits and Systems I: Regular Papers*, vol. 60, no. 6, pp. 1570–1583, 2013.
- [6] A. Talukdar, A. G. Radwan, and K. N. Salama, "Generalized model for Memristor-based Wien family oscillators," *Microelectronics Journal*, vol. 42, no. 9, pp. 1032–1038, 2011.
- [7] A. Talukdar, A. G. Radwan, and K. N. Salama, "Non linear dynamics of memristor based 3rd order oscillatory system," *Microelectronics Journal*, vol. 43, no. 3, pp. 169–175, 2012.
- [8] S. P. Wen, G. Bao, Z. G. Zeng, Y. R. Chen, and T. W. Huang, "Global exponential synchronization of Memristor-based recurrent neural networks with time-varying delays," *Neural Networks*, vol. 48, pp. 195–203, 2013.
- [9] A. L. Wu, "Hyperchaos synchronization of Memristor oscillator system via combination scheme," *Advances in Difference Equations*, vol. 2014, article 86, pp. 1–11, 2014.
- [10] A. L. Wu and J. Zhang, "Compound synchronization of fourth-order Memristor oscillator," *Advances in Difference Equations*, vol. 2014, article 100, pp. 1–16, 2014.
- [11] A. L. Wu, S. P. Wen, and Z. G. Zeng, "Synchronization control of a class of Memristor-based recurrent neural networks," *Information Sciences*, vol. 183, no. 1, pp. 106–116, 2012.
- [12] A. L. Wu and Z. G. Zeng, "Dynamic behaviors of Memristor-based recurrent neural networks with time-varying delays," *Neural Networks*, vol. 36, pp. 1–10, 2012.
- [13] A. L. Wu and Z. G. Zeng, "Exponential stabilization of memristive neural networks with time delays," *IEEE Transactions on Neural Networks and Learning Systems*, vol. 23, no. 12, pp. 1919–1929, 2012.
- [14] A. L. Wu, Z. G. Zeng, and J. Xiao, "Dynamic evolution evoked by external inputs in Memristor-based wavelet neural networks with different memductance functions," *Advances in Difference Equations*, vol. 2013, article 258, pp. 1–14, 2013.
- [15] T. W. Huang, C. D. Li, W. W. Yu, and G. R. Chen, "Synchronization of delayed chaotic systems with parameter mismatches by using intermittent linear state feedback," *Nonlinearity*, vol. 22, no. 3, pp. 569–584, 2009.
- [16] T. W. Huang and C. D. Li, "Chaotic synchronization by the intermittent feedback method," *Journal of Computational and Applied Mathematics*, vol. 234, no. 4, pp. 1097–1104, 2010.
- [17] T. W. Huang, G. R. Chen, and J. Kurths, "Synchronization of chaotic systems with time-varying coupling delays," *Discrete and Continuous Dynamical Systems B*, vol. 16, no. 4, pp. 1071–1082, 2011.
- [18] T. W. Huang, D. Gao, C. D. Li, and M. Q. Xiao, "Anticipating synchronization through optimal feedback control," *Journal of Global Optimization*, vol. 52, no. 2, pp. 281–290, 2012.
- [19] C. D. Li and X. F. Liao, "Anti-synchronization of a class of coupled chaotic systems via linear feedback control," *International Journal of Bifurcation and Chaos*, vol. 16, no. 4, pp. 1041–1047, 2006.
- [20] A. L. Wu and Z. G. Zeng, "Anti-synchronization control of a class of memristive recurrent neural networks," *Communications in Nonlinear Science and Numerical Simulation*, vol. 18, no. 2, pp. 373–385, 2013.
- [21] G. D. Zhang, Y. Shen, and L. M. Wang, "Global anti-synchronization of a class of chaotic memristive neural networks with time-varying delays," *Neural Networks*, vol. 46, pp. 1–8, 2013.
- [22] D. Li, X. L. Li, D. Cui, and Z. H. Li, "Phase synchronization with harmonic wavelet transform with application to neuronal populations," *Neurocomputing*, vol. 74, no. 17, pp. 3389–3403, 2011.
- [23] Z. Odibat, "A note on phase synchronization in coupled chaotic fractional order systems," *Nonlinear Analysis: Real World Applications*, vol. 13, no. 2, pp. 779–789, 2012.
- [24] C. D. Li, X. F. Liao, and K.-W. Wong, "Chaotic lag synchronization of coupled time-delayed systems and its applications in secure communication," *Physica D: Nonlinear Phenomena*, vol. 194, no. 3–4, pp. 187–202, 2004.
- [25] X. S. Yang, Q. X. Zhu, and C. X. Huang, "Generalized lag-synchronization of chaotic mix-delayed systems with uncertain parameters and unknown perturbations," *Nonlinear Analysis: Real World Applications*, vol. 12, no. 1, pp. 93–105, 2011.
- [26] J. Yu, C. Hu, H. J. Jiang, and Z. D. Teng, "Exponential lag synchronization for delayed fuzzy cellular neural networks via periodically intermittent control," *Mathematics and Computers in Simulation*, vol. 82, no. 5, pp. 895–908, 2012.
- [27] J.-W. Xiao, Z.-W. Wang, W.-T. Miao, and Y.-W. Wang, "Adaptive pinning control for the projective synchronization of drive-response dynamical networks," *Applied Mathematics and Computation*, vol. 219, no. 5, pp. 2780–2788, 2012.
- [28] J. W. Sun, Y. Shen, G. D. Zhang, C. J. Xu, and G. Z. Cui, "Combination-combination synchronization among four identical or different chaotic systems," *Nonlinear Dynamics*, vol. 73, no. 3, pp. 1211–1222, 2013.

Research Article

Study on Evolutionary Path of University Students' Entrepreneurship Training

Daojian Yang and Xicang Zhao

School of Management, Jiangsu University, Zhenjiang, Jiangsu Province 212013, China

Correspondence should be addressed to Daojian Yang; 15785907@qq.com

Received 15 February 2014; Accepted 21 April 2014; Published 22 May 2014

Academic Editor: Jianguo Du

Copyright © 2014 D. Yang and X. Zhao. This is an open access article distributed under the Creative Commons Attribution License, which permits unrestricted use, distribution, and reproduction in any medium, provided the original work is properly cited.

Aiming at studying the evolution pattern of cultivating the ability of university students' entrepreneurship, this paper established the payoff matrix between the university and students agent with the evolutionary economics method. The analysis of the evolution of the communication process model reveals how the choice strategy of individuals influences that of groups. Numerical simulation also demonstrates the influences of different values of decision-making parameters and the change of initial conditions on the result of evolution. It is found that the evolution path system of university students' entrepreneurial ability has two kinds of modes: one is the ideal state; and the other one is the bad "lock" state. By adjusting parameters, we can jump out of the bad "lock" state, thus optimizing cultivation path.

1. Introduction

It has become a necessity for universities to cultivate students' entrepreneurial ability to adapt to the economic transformation and upgrading, as well as to the construction and development of entrepreneurial economy. It is also important to improve the education system in colleges and universities, strengthening the innovation training of entrepreneurial talent. With this progress, promoting the overall development of people and cultivating entrepreneurial qualities of a new generation can be achieved. Gorman et al. analyzed the literature about entrepreneurship education in the 10 years from 1985 to 1994 and point out that the cultivation of entrepreneurship for college students plays the function of entrepreneurship preparation and can enhance the individual's self-efficacy. During this process, universities should focus on the improvement of students' entrepreneurial qualities and skills [1]. Fayolle discussed the concept of entrepreneurial education and its theoretical framework, the pioneering education paradigm, entrepreneurship education mode, education assessment, target, function, interdisciplinary approach, and so forth, putting forward the innovative teaching mode to enhance the level of entrepreneurship [2]. O'Connor believes that entrepreneurial talent training is an effective mean of promoting economic development [3].

Research on college students' entrepreneurial ability training was mainly concentrated on the content of entrepreneurship education and entrepreneurial ability training mode. For entrepreneurship education content, Harrison and Leitch's research "Entrepreneurship and Leadership: education and enlightenment" has paved the way for the research on entrepreneurship education content [4]. Jack and Anderson find that entrepreneurship education activity involves the areas of science and art, which need to research entrepreneurship education theory to connect the gap between science and art [5]. Fiet studied the theoretical dimension of teaching entrepreneurship, emphasizing that more attention should be paid to the teaching of entrepreneurship theory [6]. Kent and Anderson argue that the spirit of cooperation, social ability, and pioneering consciousness should be put into the training content of entrepreneurship education [7]; some other scholars suggest "business failure" as one part of entrepreneurial education [8]. Sudharson et al. tried to wake up all engineering students' entrepreneurial ideas and inspire their entrepreneurial spirit, so in the original curriculum system, they design to added a few additional modules about entrepreneurship [9]. For entrepreneurial ability training mode, Johannisson et al. make an analysis of Kolb's learning mode. Through the test of entrepreneurial action, they found that different groups (engineering students,

TABLE 1: Payoff matrix of universities and students' strategy.

Universities	Students	
	Participation N_Y	No participation N_N
Positive training M_Y	$\alpha(\gamma_{S1} - 1)C_S - C_C, (\gamma_{S1} - 1)C_S$	$-C_C, (\gamma_{S2} - 1)C_S$
Negative training M_N	$\alpha(\gamma_{S3} - 1)C_S, (\gamma_{S3} - 1)C_S$	$0, (\gamma_{S2} - 1)C_S$

business school students, and the business operators) have different study effects [10]. Fiet explored the teaching dimension of entrepreneurship theory, finding that there exist some challenges for the research and education of entrepreneurship. When entrepreneurship teaching becomes predictable, teaching cannot achieve good results. He holds that entrepreneurship education should be based on the theory of entrepreneurship [6]. Above all, the existing studies are mainly carried out from the perspective of education part—schools—to cultivate the ability of entrepreneurship, but they ignore the entrepreneurial ability training process, which is the mutual process of university and college students.

Evolutionary game theory combines the game theory with dynamic evolution process. It is the result of biological evolutionary theory. The analysis of the system of social habits, specification, or spontaneous formation and influence factors has made remarkable achievements. In fact, due to the insufficient understanding of entrepreneurial ability, too much attention has been focused on the theory, less on cultivating the ability of entrepreneurship; thus, problems exist. In this case, this paper is intended to discuss how to make both universities and students evolve in an expected way (inspiring and guiding students' entrepreneurial ability) so as to improve the training effectiveness of students' entrepreneurial ability.

2. Model Building

In constructing an evolutionary game model, we must make some basic assumptions of behavior interaction between university and college students, up to the present status of the management of universities. The two sides are the university and students, respectively, with both sides having limited rationality. The group-colleges and universities have two strategies: one is to actively develop the students' ability of entrepreneurship through various channels, hereinafter referred to as "positive training," remembered as M_Y and the other strategy is negative cultivation of college students' entrepreneurial ability, which means universities do not even do anything, which is referred to as "negative training," remembered as M_N . Strategy community of university is set as S_C {positive training, M_Y ; negative training, M_N }. The group-students also have two strategies: one is actively participating in activities to develop their entrepreneurial skills, hereinafter referred to as "participation," remembered as N_Y , while the second strategy is not involved in their activities that develop their entrepreneurial skills, hereinafter referred to as "no participation," noted as N_N . The strategy of

university student group is set as S_S {participation, N_Y and no participation, N_N }.

If universities actively cultivate their students' entrepreneurial ability, they will improve the system of entrepreneurship education management and entrepreneurship education system and create entrepreneurship training base and so on. The cost of these activities is set as C_C .

If students are actively involved in developing their entrepreneurial ability, they need to spend the costs of time and energy, set as C_S .

When universities are active in entrepreneurial ability training and students are also active in developing their business ability, students will increase their human capital value, and their costs will have higher returns γ_{S1} , $\gamma_{S1} \geq 1$. At this point, the net income for the students is $(\gamma_{S1} - 1)C_S$. The net income of colleges and universities is $\alpha(\gamma_{S1} - 1)C_S - C_C$, where α is the reputation and alumni support through cultivating high level students for colleges and universities, and $0 \leq \alpha \leq 1$. If students do not participate in developing the ability of business, they can spare the time and energy in other activities, so at this time, the investment rate of return is γ_{S2} , and $\gamma_{S2} \leq \gamma_{S1}$. At this point, the net income for the students is $(\gamma_{S2} - 1)C_S$ and the net income of universities is $-C_C$.

When universities are negative in cultivating the students' entrepreneurial ability, students can promote entrepreneurship ability through self-study or internship. Without the help, support, and guidance of universities, the rate of return on its investment is lower, set as γ_{S3} , $\gamma_{S3} \leq \gamma_{S2}$. At this point, the net income for the students is $(\gamma_{S3} - 1)C_S$ and the net income of universities is $\alpha(\gamma_{S3} - 1)C_S$. If students themselves do not actively promote entrepreneurship ability but spend the time and energy in other activities, the net income for the students would be $(\gamma_{S2} - 1)C_S$, and the net income of universities is 0.

Based on the above assumptions, we constructed the strategy payoff matrix between the universities and students, as shown in Table 1.

3. The Evolution of the Model and Its Equilibrium Analysis

3.1. The Evolution of the Model. Assume that, in the initial state, the proportion of universities choosing M_Y is p and that the proportion of universities choosing strategy M_N is $1 - p$; the proportion of students choosing strategy N_Y is q ; then, the proportion of students choosing N_N is $1 - q$. Here we calculate the corresponding expected revenue and average income.

TABLE 2: Local stability analysis results.

Equilibrium point	DetJ		Tr		Result
$p = 0, q = 0$	$-C_C(\gamma_{S3} - \gamma_{S2})C_S$	+	$-C_C + (\gamma_{S3} - \gamma_{S2})C_S$	-	ESS
$p = 0, q = 1$	$-\alpha(\gamma_{S1} - \gamma_{S3})C_S - C_C(\gamma_{S3} - \gamma_{S2})C_S$	+	$\alpha(\gamma_{S1} - \gamma_{S3})C_S - C_C - (\gamma_{S3} - \gamma_{S2})C_S$	+	Not stable
$p = 1, q = 0$	$C_C(\gamma_{S1} - \gamma_{S2})C_S$	+	$C_C + (\gamma_{S1} - \gamma_{S2})C_S$	+	Not stable
$p = 1, q = 1$	$[\alpha(\gamma_{S1} - \gamma_{S3})C_S - C_C](\gamma_{S1} - \gamma_{S2})C_S$	+	$-\alpha(\gamma_{S1} - \gamma_{S3})C_S - C_C - (\gamma_{S1} - \gamma_{S2})C_S$	-	ESS
$p = p^*, q = q^*$	$-p^*q^*(1 - p^*)(1 - q^*)\alpha(\gamma_{S1} - \gamma_{S3})^2C_S^2$	-	0		saddle point

U_1 is the expected return of the selection of universities to M_Y strategy; U_2 is the expected return of universities choosing M_N strategy; \bar{U} is the average income of universities. Consider the following:

$$\begin{aligned} U_1 &= q[\alpha(\gamma_{S1} - 1)C_S - C_C] + (1 - q)(-C_C) \\ &= q\alpha(\gamma_{S1} - 1)C_S - C_C, \\ U_2 &= q\alpha(\gamma_{S3} - 1)C_S, \\ \bar{U} &= pU_1 + (1 - p)U_2. \end{aligned} \quad (1)$$

Similarly, V_1 is the expected return of students choosing N_Y strategy; V_2 is the expected return for students choosing N_N strategy; \bar{V} is the average income for students. Consider the following:

$$\begin{aligned} V_1 &= p(\gamma_{S1} - 1)C_S + (1 - p)(\gamma_{S3} - 1)C_S \\ &= p(\gamma_{S1} - \gamma_{S3})C_S + (\gamma_{S3} - 1)C_S, \\ V_2 &= (\gamma_{S2} - 1)C_S, \\ \bar{V} &= qV_1 + (1 - q)V_2. \end{aligned} \quad (2)$$

According to the Malthusian dynamic equation, the growth rate of the strategy is equal to its corresponding fitness [11, 12]; hence, we can draw dynamics equations of the interaction strategy that evolved over time between universities and students:

$$\begin{aligned} F(p) &= \frac{dp}{dt} = p(U_1 - \bar{U}) \\ &= p(1 - p)[q\alpha(\gamma_{S1} - \gamma_{S3})C_S - C_C], \\ F(q) &= \frac{dq}{dt} = q(V - \bar{V}) \\ &= q(1 - q)[p(\gamma_{S1} - \gamma_{S3})C_S + (\gamma_{S3} - \gamma_{S2})C_S]. \end{aligned} \quad (3)$$

Through (3), we can study the evolution of the interaction behavior between universities and students. Mark the Jacobian matrix of (3) as J which is expressed by

$$\begin{aligned} J &= \begin{bmatrix} \frac{dF(p)}{dp} & \frac{dF(p)}{dq} \\ \frac{dF(q)}{dp} & \frac{dF(q)}{dq} \end{bmatrix} \\ &= \begin{bmatrix} (1 - 2p)[q\alpha(\gamma_{S1} - \gamma_{S3})C_S - C_C] & p(1 - p)\alpha(\gamma_{S1} - \gamma_{S3})C_S \\ q(1 - q)(\gamma_{S1} - \gamma_{S3})C_S & (1 - 2q)[p(\gamma_{S1} - \gamma_{S3})C_S + (\gamma_{S3} - \gamma_{S2})C_S] \end{bmatrix}. \end{aligned} \quad (4)$$

The determinant of the Jacobian matrix is marked as Det J , and the trace of the Jacobian matrix is marked as Tr. Consider

$$\begin{aligned} \text{Det } J &= (1 - 2p)(1 - 2q)[q\alpha(\gamma_{S1} - \gamma_{S3})C_S - C_C] \\ &\quad \times [p(\gamma_{S1} - \gamma_{S3})C_S + (\gamma_{S3} - \gamma_{S2})C_S] \\ &\quad - pq(1 - p)(1 - q)\alpha(\gamma_{S1} - \gamma_{S3})^2C_S^2, \end{aligned} \quad (5)$$

$$\begin{aligned} \text{Tr} &= (1 - 2p)[q\alpha(\gamma_{S1} - \gamma_{S3})C_S - C_C] \\ &\quad + (1 - 2q)[p(\gamma_{S1} - \gamma_{S3})C_S + (\gamma_{S3} - \gamma_{S2})C_S]. \end{aligned} \quad (6)$$

3.2. Equilibrium and Its Stability Analysis. Since p and q , respectively, represent the proportion of universities' and students' choices of the strategies above, it is drawn that $0 \leq p \leq 1, 0 \leq q \leq 1$. On a plane $M^* = \{(p, q) \mid 0 \leq p, q \leq 1\}$, the system has 5 equilibrium points: $(0, 0)$, $(0, 1)$, $(1, 0)$, $(1, 1)$, and (p^*, q^*) . Among them, $p^* = (\gamma_{S2} - \gamma_{S3})/(\gamma_{S1} - \gamma_{S3})$ and $q^* = C_C/\alpha(\gamma_{S1} - \gamma_{S3})C_S$. According to the Jacobian matrix, we can have the local buckling analysis results in Table 2.

According to Table 2, (p^*, q^*) is the saddle point, and $(0, 1)$ and $(1, 0)$ are the instability points. $(0, 0)$ and $(1, 1)$ are the evolutionary stable strategy, corresponding to the modes (M_N, N_N) and (M_Y, N_Y) . Here, (M_N, N_N) means the university and students both choose negative action, which

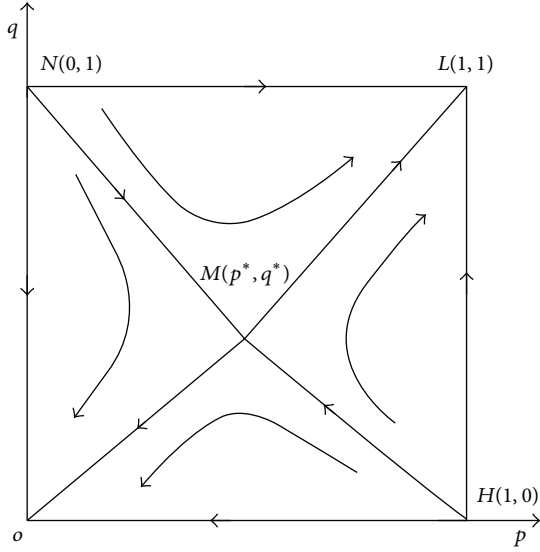


FIGURE 1: Systematic dynamic evolution.

is badly locked; (M_Y, N_Y) means the university and students choose positive action, which is an ideal condition. Figure 1 shows the strategy communication process of university and students groups.

4. The Influence of Parameter Change on the Convergence System

(1) The impact of C_C , α and C_S on the system convergence

In the saddle point, $\partial p / \partial C_C = 0$, $\partial q / \partial C_C = 1 / \alpha (\gamma_{S1} - \gamma_{S3}) C_S > 0$. When other parameters remain constant, C_C increases, α or C_S decreases, and saddle point goes upward vertically. The probability of converging to mode (M_N, N_N) increases, and the probability of convergence to (M_Y, N_Y) decreases; on the contrary, the probability of converging to mode (M_N, N_N) is reduced, and the probability of convergence to (M_Y, N_Y) increases, which is shown in Figure 2.

(2) The impact of γ_{S1} on the system convergence

In the saddle point, $\partial p / \partial \gamma_{S1} = -(\gamma_{S2} - \gamma_{S3}) / (\gamma_{S1} - \gamma_{S2})^2 < 0$, $\partial q / \partial \gamma_{S1} = -C_C / \alpha (\gamma_{S1} - \gamma_{S3})^2 C_S < 0$. When the other parameters remain constant, γ_{S1} increases, and saddle point moves to the lower left corner, so the probability of converging to mode (M_N, N_N) is reduced, and the probability of convergence in (M_Y, N_Y) increases; on the contrary, the probability of converging to mode (M_N, N_N) increases, and the probability of convergence in (M_Y, N_Y) is reduced, which is shown in Figure 3.

(3) The impact of γ_{S2} on the system convergence

In the saddle point, $\partial p / \partial \gamma_{S2} = 1 / (\gamma_{S1} - \gamma_{S2}) > 0$, $\partial q / \partial \gamma_{S2} = 0$. When the other parameters remain constant, γ_{S2} increases, and saddle point moves to the right corner, so the probability of converging to mode (M_N, N_N) increases, and the probability of convergence in (M_Y, N_Y) decreases; on the contrary, the probability of converging to mode (M_N, N_N) reduces, and the probability of convergence in (M_Y, N_Y) increases, which is shown in Figure 4.

(4) The impact of γ_{S3} on the system convergence

In the saddle point, $\partial p / \partial \gamma_{S3} = -1 / (\gamma_{S1} - \gamma_{S2}) < 0$, $\partial q / \partial \gamma_{S3} = C_C / \alpha (\gamma_{S3} - \gamma_{S1})^2 C_S > 0$. When the other parameters remain constant, γ_{S3} increases, and the saddle point moves to the top left; on the contrary, the saddle point moves to the lower right, as is shown in Figure 5. The impact of γ_{S3} on the results of the convergence system is not clear, which needs further numerical analysis.

5. The Result Analysis of Numerical Experiments

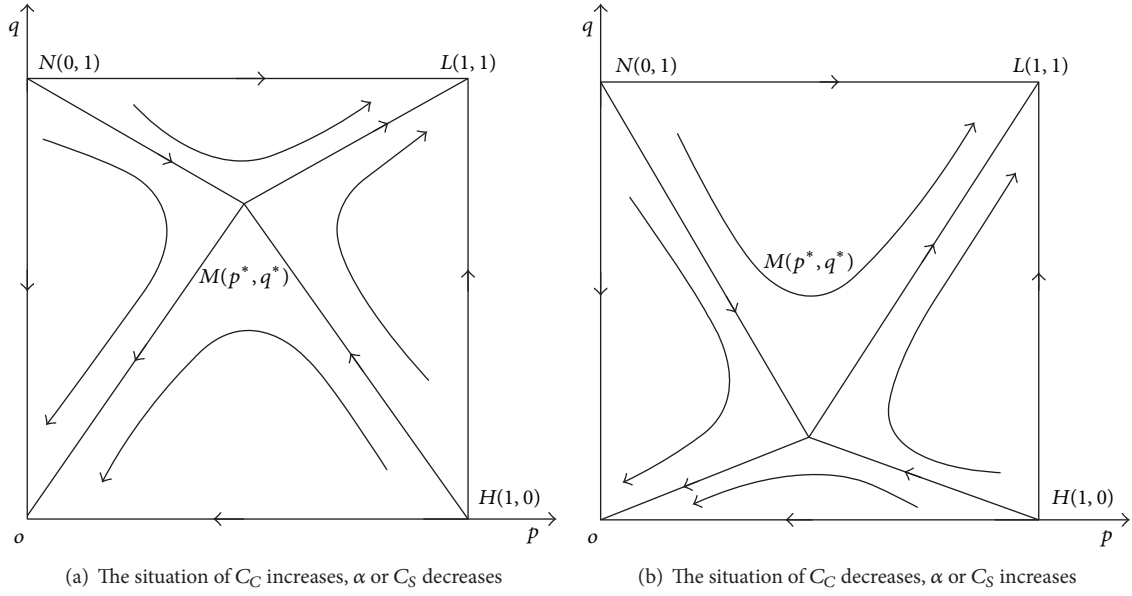
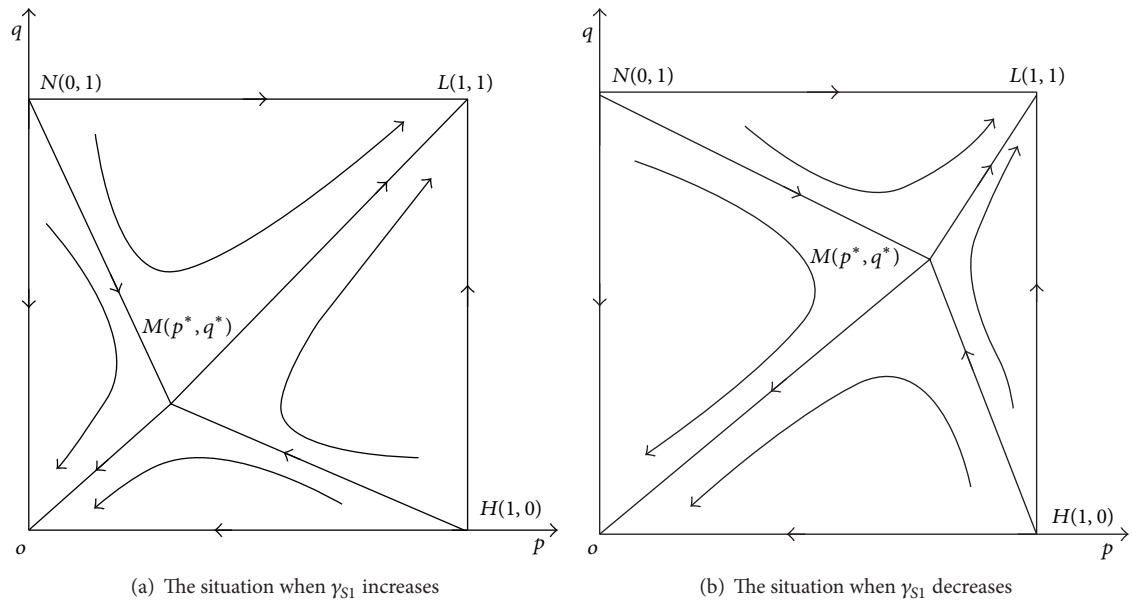
In behavior strategy communication system between university and students, some parameters are involved: the proportion of initial population p and q , the respective cost of college and students C_C and C_S , the rate of reward γ_{S1} , γ_{S2} , and γ_{S3} of students under different situations, and reward coefficient α of universities. These parameters will influence the earnings of university and students, which will further influence the evolution of the system.

(1) The impact of the changes of p_0 and q_0 on the result of system evolution

According to the numerical experiment shown in Figure 6, p_0 and q_0 , respectively, represent the proportion of the initial population that university chooses M_Y and students who choose N_Y . Parameter values are $C_C = 1$, $C_S = 10$, $\alpha = 0.2$, $\gamma_{S1} = 2$, $\gamma_{S2} = 1.5$, and $\gamma_{S3} = 1.2$. It can be seen from Figure 6 the dependence of the path when university and students are in the process of behavior strategy interaction. With different initial ratio the convergence curves do not overlap before reaching their equilibrium. Convergence speed is influenced not only by the initial proportion students choosing to have entrepreneurial ability training, but also by the initial proportion that students have related actions to improve their entrepreneurial abilities at the same time. The closer the proportion gets to the equilibrium, the faster the convergence speed is. As long as the proportion of initial M_Y strategy use is very low (e.g., $p_0 = 0.1$), the system will eventually be locked in a “bad” state; if this proportion is very high (e.g., $p_0 = 0.9$), the system can eventually evolve to the ideal mode (M_Y, N_Y) . In general circumstances, as the proportion of students choosing to have positive action increases, it will also help the system evolve toward the ideal mode; therefore, universities must first enhance the entrepreneurship education actively, arousing the students’ enthusiasm.

(2) The impact of the change of C_C on the result of system evolution

Numerical test results of the impact are shown in Figure 7. The reason that we set the proportion of students taking part in the entrepreneurship activities as 0.4 is that as the impact of the change of the initial population on the evolution is analyzed above, it is clear that when the initial choice ratio of universities’ cultivating students’ entrepreneurship is high, the system will converge to (M_Y, N_Y) mode; if the initial choice ratio of universities’ cultivating students’ entrepreneurship is lower, the system will converge to mode (M_N, N_N) . So $q = 0.4$ is a typical situation. At the same time, combining

FIGURE 2: The impact of C_C , α , C_S on the system convergence.FIGURE 3: The impact of γ_{S1} on the system convergence.

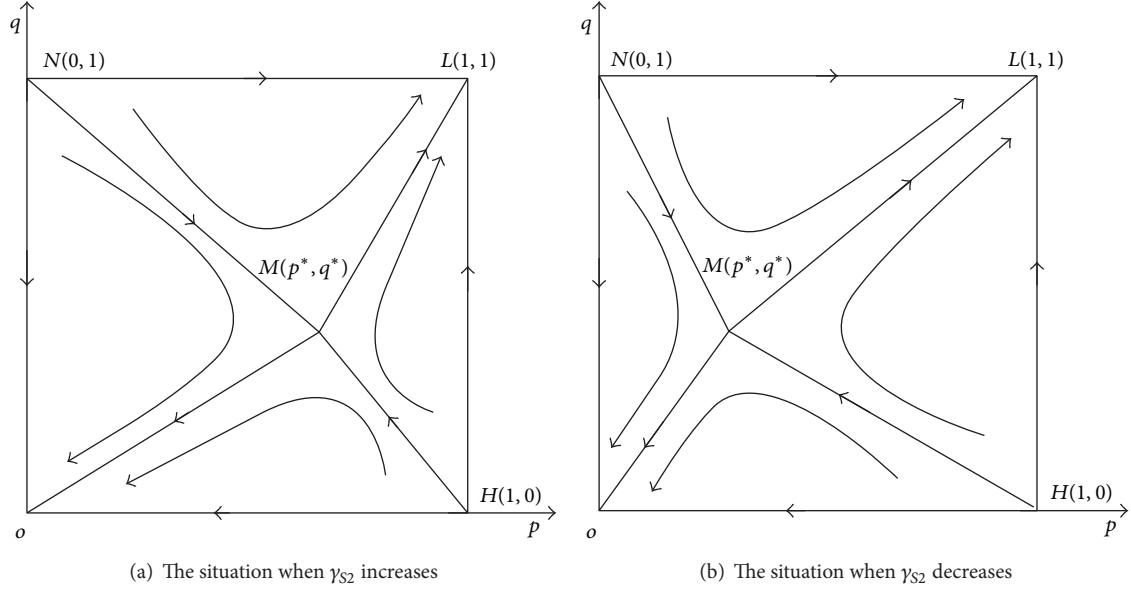
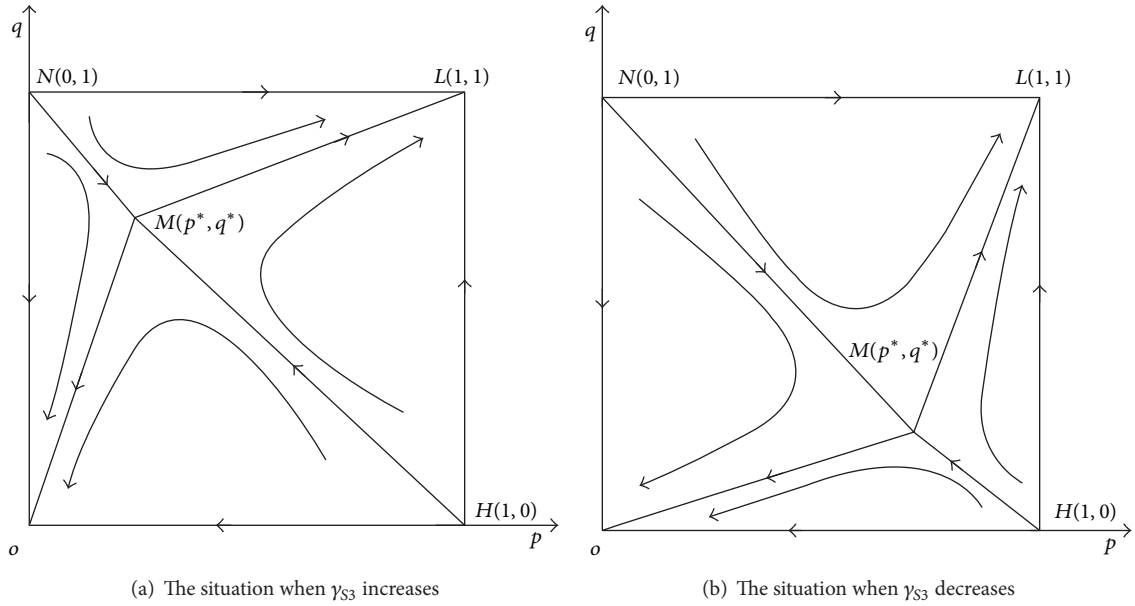
the fact that the overall university students are in high enthusiasm but with lower ability in entrepreneurial activities (national college students entrepreneurship research report shows that 14% of students participated in a training program or entrepreneurship competition and that 48.8% of college students hope to be provided with business related professional training) and choosing $q = 0.4$, which is more in line with the actual situation, other parameter values are as follows: $C_S = 10$, $\alpha = 0.2$, $\gamma_{S1} = 2$, $\gamma_{S2} = 1.5$, and $\gamma_{S3} = 1.2$.

As Figure 7 shows, with the increase of university's training cost C_C , the convergence speed of the system slows down and the time of convergence to equilibrium mode

increases, and the system's evolutionary direction converts from mode (M_Y, N_Y) to a bad lock mode (M_N, N_N) . Universities' training cost represents the burden of entrepreneurship training of universities. Under the certain level of total cost of entrepreneurship training, universities' burden should be eased by broadening the financing channels. This can not only guarantee the training level, but also arouse universities' training enthusiasm.

(3) The impact of the change of C_S on the result of system evolution

The impact is shown in Figure 8. The parameter values are as follows: $q = 0.4$, $C_C = 1$, $\alpha = 0.2$, $\gamma_{S1} =$

FIGURE 4: The impact of γ_{S2} on the system convergence.FIGURE 5: The impact of γ_{S3} on system convergence.

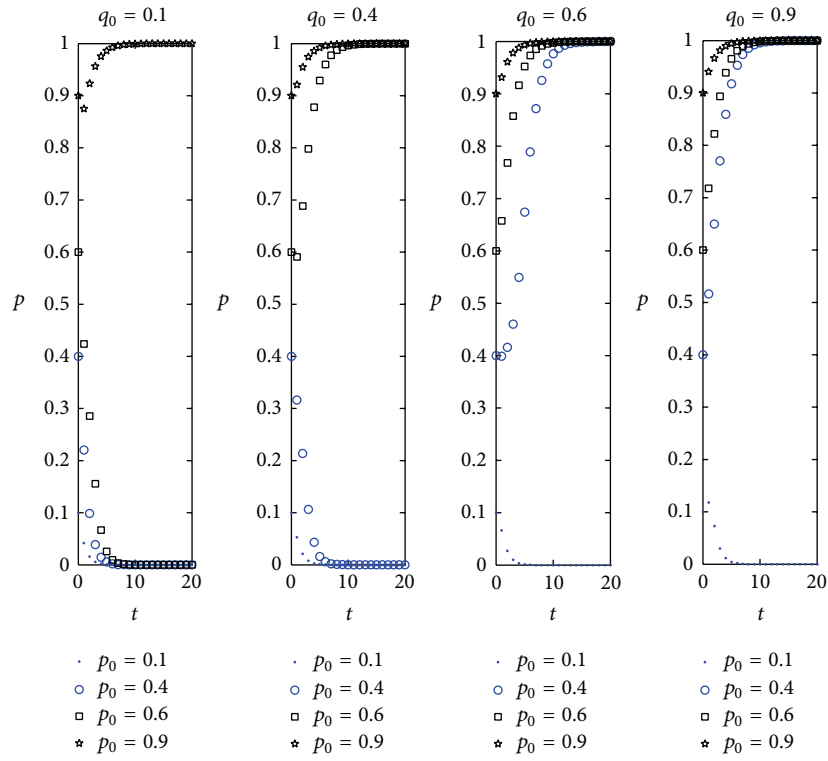
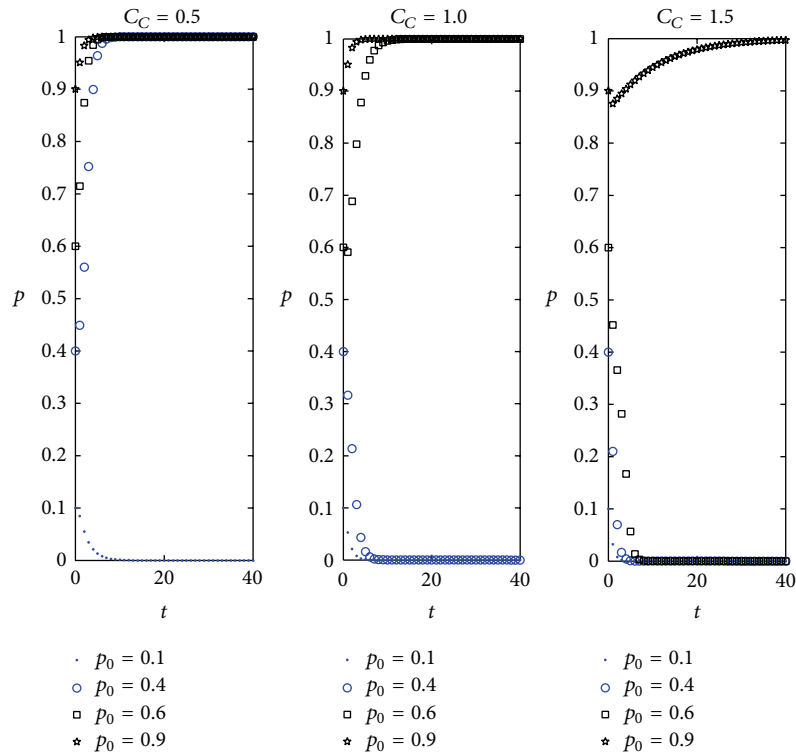
2, $\gamma_{S2} = 1.5$, and $\gamma_{S3} = 1.2$. It can be seen from Figure 8 that with the increase of students' entrepreneurial activity costs C_S , system convergence speeds up, and the time of converging to equilibrium mode reduces. The evolution direction of the system will also change from bad lock mode (M_N, N_N) to the ideal mode (M_Y, N_Y). The cost C_S reflects the difficulty level of promoting entrepreneurship skills. We can see that more college students tend to participate in the school's entrepreneurial ability training program, rather than to choose self-study to gain their entrepreneurial skills. Therefore, in the process of entrepreneurship education, universities should pay more attention to the core and important

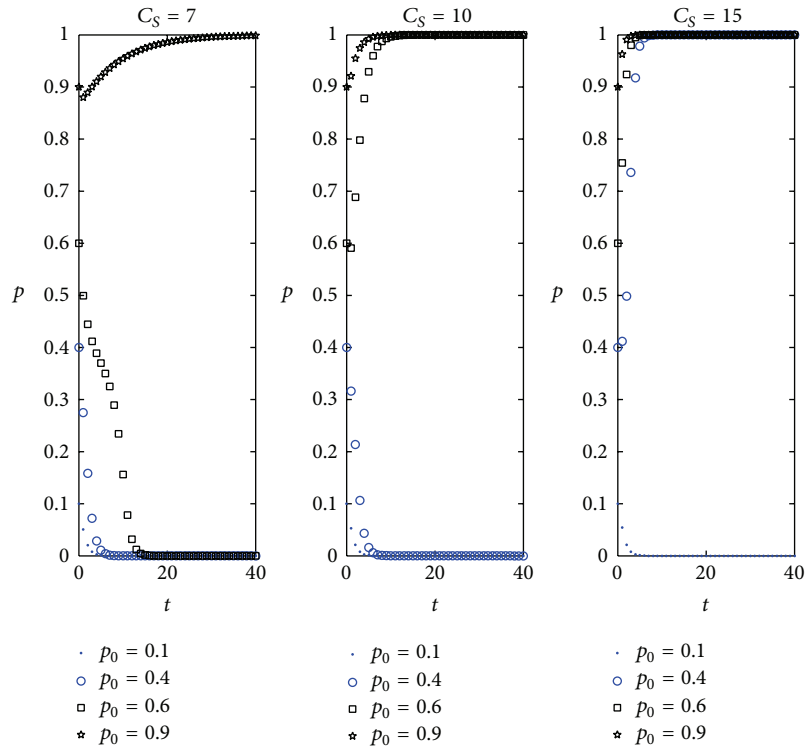
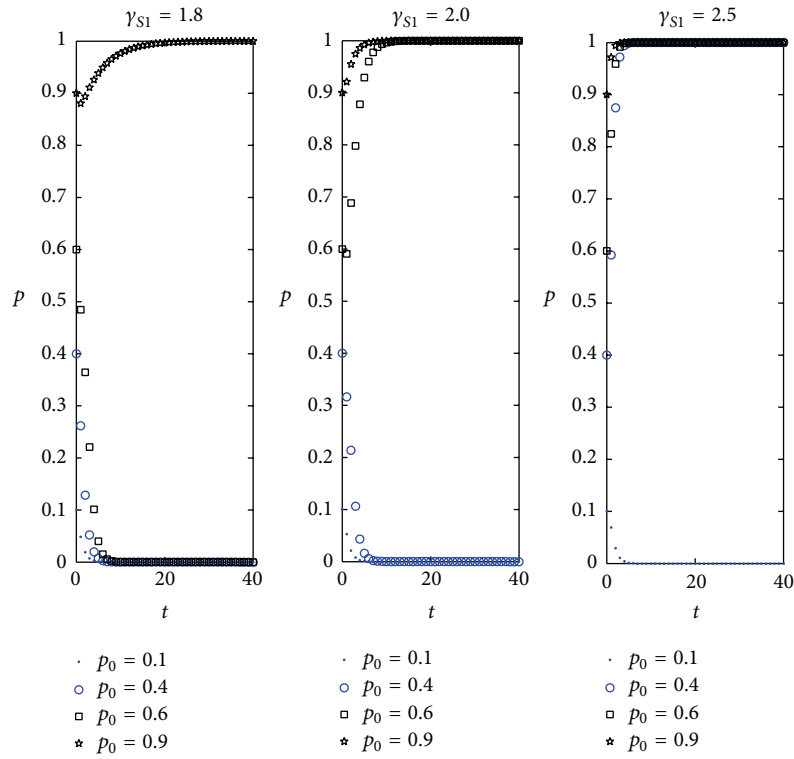
business knowledge, while the simple and easy knowledge can be learned by students themselves. Universities need to distinguish between the focus of entrepreneurship education and the investment of education resources.

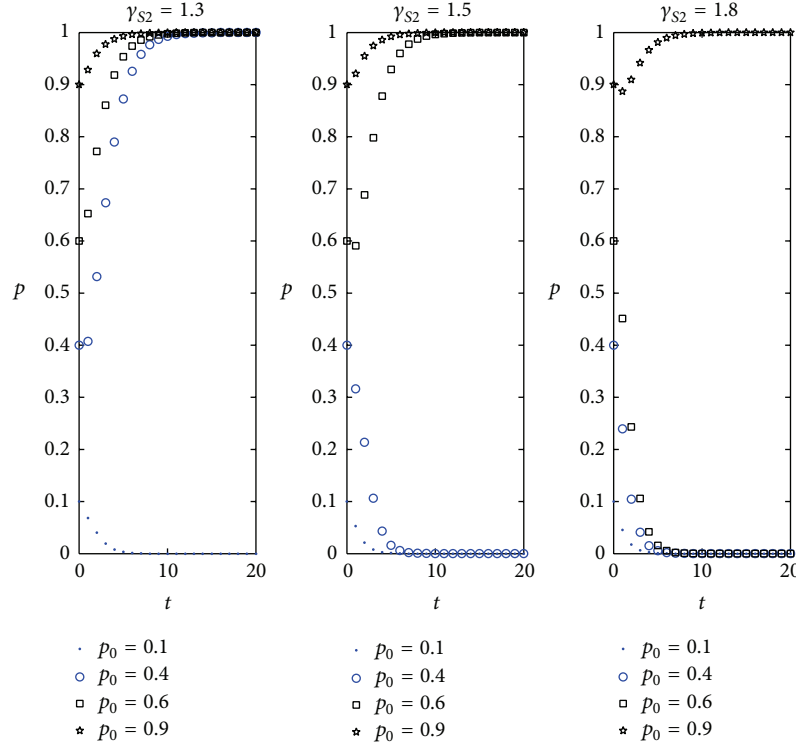
(4) The impact of the change of γ_{S1} on the result of system evolution

The impact is shown in Figure 9, and the parameter value selections are as follows: $q = 0.4$, $C_C = 1$, $C_S = 10$, $\alpha = 0.2$, $\gamma_{S2} = 1.5$, $\gamma_{S3} = 1.2$.

As can be seen from Figure 9, with the increase of the investment return ratio γ_{S1} of students' entrepreneurial ability improvement, the system convergence speeds up, and the

FIGURE 6: Impact of the change of p_0 and q_0 on the result of the system evolution.FIGURE 7: Impact of the changes of C_C on the result of the system evolution.

FIGURE 8: Impact of the changes of C_S on the result of the system evolution.FIGURE 9: Impact of the change of γ_{S1} on the result of the system evolution.

FIGURE 10: Impact of the change of γ_{S2} on the result of the system evolution.

evolution direction of the system will be changed from (M_N, N_N) into the ideal mode (M_Y, N_Y) . Increasing γ_{S1} means that more entrepreneurial investment can lead to ability improvement and significant increase of their own human capital value. At the same time universities can also get high school reputation. In the condition of a higher γ_{S1} , both universities and students tend to take positive action. Only when the investment return ratio is high enough, the enthusiasm of university students' participation will be high. Therefore, universities need to improve training effectiveness further to increase the investment return ratio of university students' entrepreneurial ability improvement.

(5) The impact of the change of γ_{S2} on the result of system evolution

The impact is shown in Figure 10, and the parameter value selections are as follows: $q = 0.4$, $C_C = 1$, $C_S = 10$, $\alpha = 0.2$, $\gamma_{S1} = 2$, and $\gamma_{S3} = 1.2$.

Figure 10 indicates that the rate of system convergence increases with the growth of γ_{S2} , with systematic evolution transforming from mode (M_Y, N_Y) to mode (M_N, N_N) . So, when making decision on participating in entrepreneurship training or not, university students consider not only the investment return ratio, but also the opportunity costs of participation. It again showed that improvement training effectiveness further to increase the gains of university students' participation is the key to improve the students' enthusiasm to participate in the entrepreneurial ability training.

(6) The impact of the change of γ_{S3} on the result of system evolution

Figure 11 shows the influence of return rate γ_{S3} of enhancement of college students' entrepreneurial ability on

system convergence. The parameters are listed as follows: $q = 0.4$, $C_C = 1$, $C_S = 10$, $\alpha = 0.2$, $\gamma_{S1} = 2$, and $\gamma_{S2} = 1.5$.

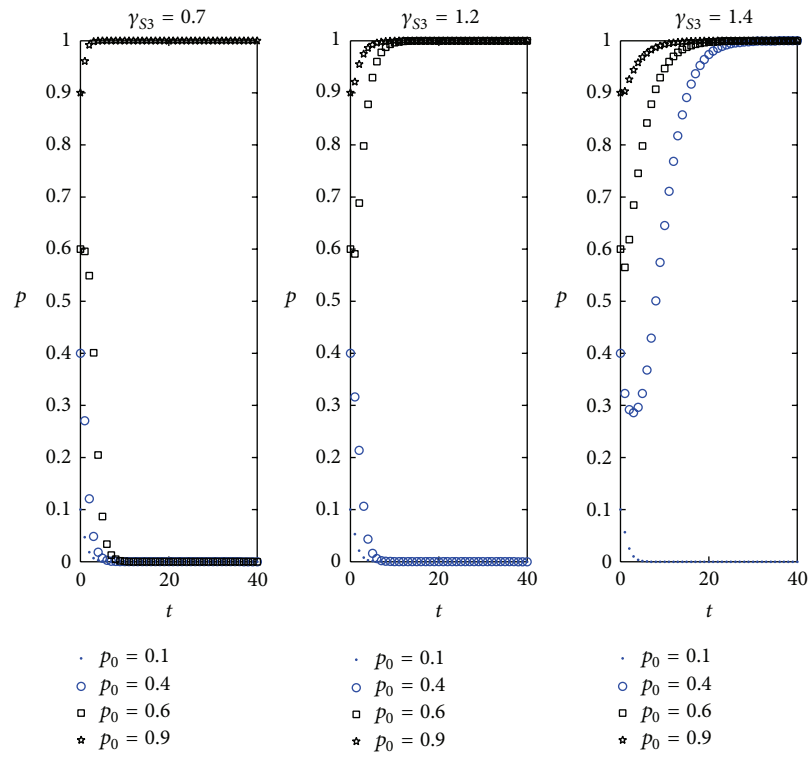
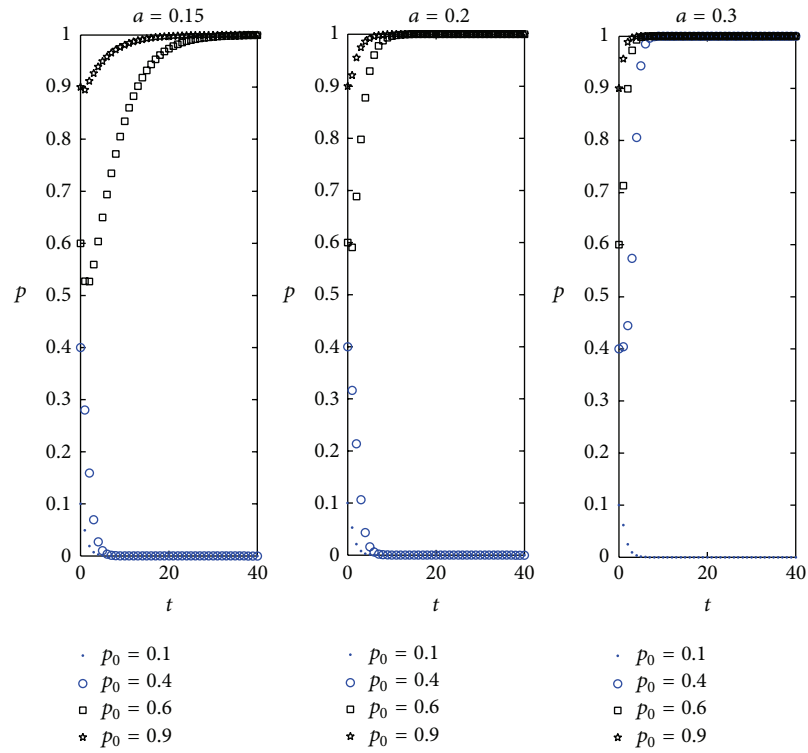
We may find that, in Figure 11, the impact of γ_{S3} on systematic evolution direction is similar to that of γ_{S1} on the system; the impact of γ_{S3} on system convergence rate, however, is more obvious. It becomes slow with the increase of γ_{S3} . $p_0 = 0.4$ and $p_0 = 0.6$ evolve in the direction towards (M_N, N_N) in the early periods and then in a short time they change towards (M_Y, N_Y) and converge at (M_Y, N_Y) .

Further analysis finds that γ_{S1} , γ_{S2} , and γ_{S3} are decided by the values of $\gamma_{S1} - \gamma_{S3}$ and $\gamma_{S2} - \gamma_{S3}$, which are further decided by the balance of return rate and return rate of time and energy used in other field, with or without assistance by universities. A larger balance between γ_{S1} and γ_{S2} brings the evolution to (M_Y, N_Y) in the ideal stage. But a larger balance between γ_{S2} and γ_{S3} brings (M_Y, N_Y) more to a bad lock mode. Anyway, higher investment of entrepreneurship training leads to easier involvement to ideal mode. Hence, higher education institutions should take more efforts to enhance the efficiency in talent education so as to increase the reward rate of students' participation in the education.

(7) The impact of α on the result of system evolution

Figure 12 shows the influence of return coefficient α of university entrepreneurship training on system convergence. Parameters are listed as follows: $q = 0.4$, $C_C = 1$, $C_S = 10$, $\gamma_{S1} = 2$, $\gamma_{S2} = 1.5$, and $\gamma_{S3} = 1.2$.

Figure 12 shows that, with the increase of return coefficient α , system converges faster to the ideal mode (M_Y, N_Y) and the system will change toward the ideal mode. In colleges and universities, the purpose of entrepreneurship education and entrepreneurial ability is mainly to relieve employment

FIGURE 11: The influence of the change of γ_{S3} on the result of the system evolution.FIGURE 12: The influence of return coefficient α of university entrepreneurship training on system convergence.

pressure, and by conducting entrepreneurial education and training, to inspire students' entrepreneurial enthusiasm and encourage students' entrepreneurship. The purpose of cultivating the ability of entrepreneurship is not only to encourage students to take part in the entrepreneurial activities during their stay in school or after graduation, but also to focus on the implementation of the students' entrepreneurial potential and help students accumulate human capitals and entrepreneurial energy stored for appropriate time for future.

6. Conclusion

Entrepreneurial talent training needs students' positive participation. The purpose of this research is to investigate the interaction between universities and students in the process of students' entrepreneurial ability training and the system evolution law, in order to find effective strategies for promoting the enthusiasm and initiative of university students' entrepreneurial ability.

Through the construction of payoff matrix of students' behavior, the evolution of behavior interaction system, its equilibrium, and the influence of different parameters on the system convergence are analyzed. The MatLab software is used for the results of numerical experiments under different parameters of the evolution system. We found that modes (M_Y, N_Y) and (M_N, N_N) are two evolutionary stable strategies by the interaction between universities and students, and the mode (M_N, N_N) is badly locked.

At present, students' understanding of entrepreneurial ability is insufficient. There exist some negative attitudes toward entrepreneurship education activity, which is not conducive to the improvement of students' entrepreneurial ability. Model analysis and numerical experiment show that the system can evolve towards ideal pattern through improving the initial proportion of the positive involvement of group selection of entrepreneurial talent training in universities, reducing investment cost of universities' entrepreneurship, increasing the rate of return of universities' entrepreneurship education, stressing the investment on higher knowledge and ability, or increasing the efficiency of the entrepreneurial ability training to promote the reward rate of both universities and students.

Conflict of Interests

The authors declare that there is no conflict of interests regarding the publication of this paper.

Acknowledgments

This work was supported in part by the National Natural Science Foundation of China under Grants 71373104 and 71171099, the Jiangsu Philosophy and Societal Science Research Project under Grants 2012SJB630010 and 2012SJB880021, the Soft Science Research Project of Zhenjiang City under Grant YJ2012005, and the College Students' Ideological and Political Education Project of Jiangsu University under Grant JDXGCB201305.

References

- [1] G. Gorman, D. Hanlon, and W. King, "Some research perspectives on entrepreneurship education, enterprise education and education for small management: a ten year literature review," *International Small Business Journal*, vol. 15, no. 3, pp. 56–77, 1997.
- [2] A. Fayolle, *Handbook of Research in Entrepreneurship Education*, Edward Elgar, Northampton, Mass, USA, 2007.
- [3] A. O'Connor, "A conceptual framework for entrepreneurship education policy: meeting government and economic purposes," *Journal of Business Venturing*, vol. 28, no. 4, pp. 546–563, 2013.
- [4] R. T. Harrison and C. M. Leitch, "Entrepreneurship and leadership: the implication for education and development," *Entrepreneurship and Regional Development*, vol. 6, no. 2, pp. 111–125, 1994.
- [5] S. L. Jack and A. R. Anderson, "Entrepreneurship education within the enterprise culture: producing reflective practitioner," *International Journal of Entrepreneurial Behavior and Research*, vol. 5, no. 3, pp. 110–125, 1999.
- [6] J. O. Fiet, "The theoretical side of teaching entrepreneurship," *Journal of Business Venturing*, vol. 16, no. 1, pp. 1–24, 2001.
- [7] C. A. Kent and L. P. Anderson, "Social capital, social entrepreneurship and entrepreneurship education," *International Journal of Entrepreneurship Education*, vol. 2, no. 1, pp. 41–59, 2004.
- [8] D. A. Shepherd, "Educating entrepreneurship students about emotion and learning from failure," *Academy of Management Learning and Education*, vol. 3, no. 3, pp. 274–287, 2004.
- [9] K. Sudharson, A. M. Ali, and A. M. Sermakani, "An organizational perspective of knowledge communication in developing entrepreneurship education for engineering students," *Procedia: Social and Behavioral Sciences*, vol. 73, no. 27, pp. 590–597, 2013.
- [10] B. Johannisson, H. Landstrom, and J. Rosenberg, "University training for entrepreneurship-an action frame of reference," *European Journal of Engineering Education*, vol. 23, no. 4, pp. 477–496, 1998.
- [11] D. Friedman, "Evolutionary games in economics," *Economica*, vol. 59, no. 3, pp. 637–666, 1991.
- [12] Z.-H. Sheng and D.-P. Jiang, *Evolutionary Economics*, Shanghai Joint, Shanghai, China, 2002.

Research Article

Sampled-Data Synchronization for Complex Dynamical Networks with Time-Varying Coupling Delay and Random Coupling Strengths

Jian-An Wang and Xin-Yu Wen

School of Electronics Information Engineering, Taiyuan University of Science and Technology, Taiyuan, Shanxi 030024, China

Correspondence should be addressed to Jian-An Wang; wangjianan588@163.com

Received 14 January 2014; Revised 31 March 2014; Accepted 14 April 2014; Published 6 May 2014

Academic Editor: He Huang

Copyright © 2014 J.-A. Wang and X.-Y. Wen. This is an open access article distributed under the Creative Commons Attribution License, which permits unrestricted use, distribution, and reproduction in any medium, provided the original work is properly cited.

This paper is concerned with the problem of sampled-data synchronization for complex dynamical networks (CDNs) with time-varying coupling delay and random coupling strengths. The random coupling strengths are described by normal distribution. The sampling period considered here is assumed to be less than a given bound. By taking the characteristic of sampled-data system into account, a discontinuous Lyapunov functional is constructed, and a delay-dependent mean square synchronization criterion is derived. Based on the proposed condition, a set of desired sampled-data controllers are designed in terms of linear matrix inequalities (LMIs) that can be solved effectively by using MATLAB LMI Toolbox. Numerical examples are given to demonstrate the effectiveness of the proposed scheme.

1. Introduction

In the real world, many practical and natural systems can be described by models of complex networks such as internet, food webs, electric power grids, scientific citation networks, and social networks. Therefore, a dynamical network can be regarded as a dynamical system with a special structure. In the last few years, complex dynamical networks (CDNs) have received extensive attention and increasing interest across many fields of science and engineering [1–3]. CDNs are a large set of interconnected nodes, in which each node represents an element with certain dynamical system and edge represents the relationship between them. With the important discovery of the “small-world” and “scale-free” properties, complex dynamical networks have become a focal research topic in the area of complexity science.

It is very common that many natural systems often exhibit collective cooperative behaviors among their constituents. Synchronization, as a kind of typical collective behavior, is one of key issues in the study of complex dynamical networks. The main reason is that network synchronization not only can explain many natural phenomena but also has wide

applications in many fields including secure communications, synchronous information exchange in the internet, genetic regulatory process, the synchronous transfer of digital signals in communication networks, and so on. Over the past several decades, the synchronization in CDNs has been intensively investigated from various fields such as sociology, biology, and physics [4–16]. The authors in [5] focused the synchronization stability of general CDNs with coupling delay. In [6], the authors investigated the locally and globally adaptive synchronization of an uncertain complex dynamical network. The problem of globally exponential synchronization of impulsive dynamical networks was investigated in [7]. The pinning synchronization problems in CDNs have been analyzed in [8, 9]. In [10], the authors studied the global exponential synchronization and synchronizability for general dynamical networks. In [11], some sufficient conditions for CDNs with and without coupling delays in the state to be passive were presented. Recently, the guaranteed cost synchronization of a CDN via dynamic feedback control was addressed in [15].

It is well known that the coupling strength of complex dynamical network plays an important role in the realizing

synchronization. In general, the coupling strength of the considered CDNs is deterministic [4–16]. If the deterministic coupling strength is large enough, a complex network can realize synchronization by itself. However, according to the discussion in [17, 18], because of the effects of environment and artificial factor, the coupling strength of complex dynamical networks may randomly vary around some constants. If the upper or lower bound of the random coupling strength is only considered, some conservative result will be derived. That is to say, random phenomena in coupling strength should be taken into account when dealing with the synchronization of CDNs. Furthermore, the normal distribution characteristic of random variables can be easily obtained by statistical methods. Therefore, it is interesting to investigate the synchronization of CDNs with random coupling strengths described by normal distribution.

On the other hand, the sampled-data control system, whose control signals are allowed to change only at discrete sampling instants, can drastically reduce the amount of information transmitted and increase the efficiency of bandwidth usage. Therefore, sampled-data control has received notable attention [19–22]. The input delay approach proposed in [19] is very popular in the study of sampled control system, where the system is modeled as a continuous-time system with a time-varying sawtooth delay in the control input induced by sample-and-hold. In [20], by constructing the time-dependent Lyapunov functional, a refined input delay approach was presented. Later, the chaos synchronization problems are investigated by using sampled-data control [23–26]. Recently, in the framework of the input delay approach, the sampled-data synchronization problem has been investigated for a class of general complex networks with time-varying coupling delays in [27]. Furthermore, some improved sampled-data synchronization criterion has been derived to ensure the exponential stability of the closed-loop error system and corresponding sampled-data feedback controllers are designed in [28]. By combining the time-dependent Lyapunov functional approach and convex combination technique, the exponential sampled-data synchronization of CDNs with time-varying coupling delay and uncertain sampling was studied in [29]. However, the Lyapunov functional proposed in [27, 28] ignored the substitutive characteristic of sampled-data system, which leads to some conservatism inevitably. In addition, the results obtained in [29] are sufficient conditions, which imply that there is still room for further improvement. To the best of our knowledge, the sampled-data synchronization problem of complex dynamical networks with time-varying coupling delays and random coupling strengths has not been studied in the literature.

Motivated by the aforementioned discussions, in this paper, the problem of sampled-data synchronization of CDNs with time-varying coupling delay and random coupling strengths is investigated. The sampling period is assumed to be time varying but less than a given bound. The random coupling strengths are described by normal distribution. By capturing the characteristic of sampled-data control system, a new discontinuous Lyapunov functional is constructed. By using the low bound lemma and convex combination

approach, a mean square synchronization condition is formulated in terms of LMIs. The corresponding sampled-data controllers are designed that can achieve the synchronization of the considered CDNs. The proposed method can lead to a less conservative result than the existing ones. Finally, numerical examples are given to illustrate the effectiveness and less conservatism of the presented sampled-data control scheme.

Notation. The notations used throughout this paper are fairly standard. R^n and $R^{m \times n}$ denote the n -dimensional Euclidean space and the set of all $m \times n$ real matrix, respectively. $P > 0$ or $P < 0$ means that P is symmetric and positive or negative definite. The superscript “ T ” represents the transpose, and “ I ” and “ 0 ” denote the identity and zero matrix with appropriate dimensions. $\text{diag}\{l_1, l_2, \dots, l_n\}$ stands for a block diagonal matrix. The symmetric terms in a symmetric matrix are denoted by $*$.

2. Preliminaries and Model Description

Consider a class of linearly coupled complex dynamical networks consisting of N identical coupled nodes, in which each node is an n -dimensional subsystem

$$\begin{aligned} \dot{x}_i(t) = & f(x_i(t)) + c_1(t) \sum_{j=1}^N G_{ij} D x_j(t) \\ & + c_2(t) \sum_{j=1}^N G_{ij} A x_j(t - \tau(t)) + u_i(t), \end{aligned} \quad (1)$$

$$i = 1, 2, \dots, N,$$

where $x_i = (x_{i1}, x_{i2}, \dots, x_{in}) \in R^n$ and $u_i(t) \in R^n$ are, respectively, the state variable and the control input of the node i . $f : R^n \rightarrow R^n$ is a continuous vector-valued function. $c_1(t)$ and $c_2(t)$ are mutually independent random variables, which denote the random coupling strengths of nondelayed coupling and time-delayed couplings, respectively. $\tau(t)$ denotes the time-varying coupling delay satisfying $0 \leq \tau(t) \leq h$, $\dot{\tau}(t) \leq \mu$, where $h > 0$ and μ are known constants. $D = (d_{ij})_{n \times n} \in R^{n \times n}$ is the constant inner-coupling matrix and $A = (a_{ij})_{n \times n} \in R^{n \times n}$ is the time-delay inner-coupling matrix. $G = (g_{ij}) \in R^{N \times N}$ is the coupling configuration matrix, where g_{ij} is defined as follows: if there is a connection between node i and node j ($i \neq j$), then $g_{ij} > 0$; otherwise, $g_{ij} = 0$, and the diagonal elements of matrix G are defined by $g_{ii} = -\sum_{j=1, j \neq i}^N G_{ij}$, $i = 1, 2, \dots, N$.

Remark 1. The coupling configuration matrix G represents the topological structure of network (1). In this paper, the matrix G is not assumed to be symmetric or irreducible. In [27, 28], the coupling configuration matrix is assumed to be symmetric, which is quite restrictive in practice. In this regards, the network model considered here is more general.

In this paper, similar to [17, 18], we assume that almost all the values of $c_i(t)$, $i = 1, 2$, are taken on some nonnegative intervals, that is, $c_i(t) \in (\sigma_i, \rho_i)$, where σ_i, ρ_i ($i = 1, 2$) are nonnegative constants with $\sigma_i < \rho_i$. Almost all the values of $c_i(t)$ satisfying $c_i(t) \in (\sigma_i, \rho_i)$ imply that $\text{Prob}\{c_i(t) \in (\sigma_i, \rho_i)\} = 1$. It should be noted that the actual minimum and maximum allowable coupling strength bounds are not σ_i and ρ_i , respectively. It just means that $\text{Prob}\{c_i(t) < \sigma_i\} = 0$ and $\text{Prob}\{c_i(t) > \rho_i\} = 0$. The actual lower bounds of $c_i(t)$ may be very small and the actual upper bounds of them may be very large. This is very different from synchronization results obtained by traditional method, in which constant coupling strength is always preassumed or deterministic.

Remark 2. We assume the coupling strengths satisfy the normal distribution, which can randomly vary around some given intervals. This is very different from the considered network models in [27–29], in which constant coupling strengths are always preassumed or deterministic. Therefore, for the random coupling strength, most of existing results with constant coupling strength may not be applicable anymore. In addition, it is worth pointing out that when $c_1(t) = c_{10}$ and $c_2(t) = c_{20}$ or $\delta_1 = \delta_2 = 0$, system (1) includes the models in [27–29] as a special case.

Assumption 3. There nonlinear function f satisfies

$$\begin{aligned} & [f(x) - f(y) - U(x - y)]^T [f(x) - f(y) - V(x - y)] \\ & \leq 0, \quad \forall x, y \in R^n, \end{aligned} \quad (2)$$

where U and V are constant matrices of appropriate dimensions.

Assumption 4. The mathematical expectation and variance of $c_i(t)$ are $E\{c_i(t)\} = c_{i0}$ and $E\{(c_i(t) - c_{i0})^2\} = \delta_i^2$, respectively, where c_{i0} and δ_i are nonnegative constants.

On the basis of the property of variables $c_i(t)$, system (1) can be rewritten in the following form:

$$\begin{aligned} \dot{x}_i(t) = & f(x_i(t)) + c_{10} \sum_{j=1}^N G_{ij} D x_j(t) \\ & + (c_1(t) - c_{10}) \sum_{j=1}^N G_{ij} D x_j(t) \\ & + c_{20} \sum_{j=1}^N G_{ij} A x_j(t - \tau(t)) \\ & + (c_2(t) - c_{20}) \sum_{j=1}^N G_{ij} A x_j(t - \tau(t)) + u_i(t), \\ & i = 1, 2, \dots, N. \end{aligned} \quad (3)$$

Let $e_i(t) = x_i(t) - s(t)$ be the synchronization error, where $s(t) \in R^n$ is the state trajectory of the unforced isolate node $\dot{s}(t) = f(s(t))$. Then, the error dynamics is given by

$$\begin{aligned} \dot{e}_i(t) = & g(e_i(t)) + c_{10} \sum_{j=1}^N G_{ij} D e_j(t) \\ & + (c_1(t) - c_{10}) \sum_{j=1}^N G_{ij} D e_j(t) \\ & + c_{20} \sum_{j=1}^N G_{ij} A e_j(t - \tau(t)) \\ & + (c_2(t) - c_{20}) \sum_{j=1}^N G_{ij} A e_j(t - \tau(t)) + u_i(t), \\ & i = 1, 2, \dots, N, \end{aligned} \quad (4)$$

where $g(e_i(t)) = f(x_i(t)) - f(s(t)) = [f_1(e_{i1}(t)) \ f_2(e_{i2}(t)) \ \dots \ f_n(e_{in}(t))]^T$.

The control signal is assumed to be generalized by using a zero-order-hold (ZOH) function with a sequence of hold times $0 = t_0 < t_1 < \dots < t_k < \dots$. Therefore, the state feedback controller takes the following form:

$$\begin{aligned} u_i = & K_i e_i(t_k) = K_i (x_i(t_k) - s(t_k)), \quad t_k \leq t < t_{k+1}, \\ & i = 1, 2, \dots, N, \end{aligned} \quad (5)$$

where K_i is the feedback gain matrix to be determined and $e_i(t_k)$ is the discrete measurement of $e_i(t)$ at sampling instant t_k . In this paper, the sampling is not required to be periodic, and the only assumption is that the distance between any two consecutive sampling instants is less than a given bound. It is assumed that $t_{k+1} - t_k = h_k \leq p$ for any integer $k \geq 0$, where $p > 0$ represents the largest sampling interval.

By substituting (5) into (4), we obtain

$$\begin{aligned} \dot{e}_i(t) = & g(e_i(t)) + c_{10} \sum_{j=1}^N G_{ij} D e_j(t) \\ & + (c_1(t) - c_{10}) \sum_{j=1}^N G_{ij} D e_j(t) \\ & + c_{20} \sum_{j=1}^N G_{ij} A e_j(t - \tau(t)) \\ & + (c_2(t) - c_{20}) \sum_{j=1}^N G_{ij} A e_j(t - \tau(t)) + K_i e_i(t_k), \\ & i = 1, 2, \dots, N. \end{aligned} \quad (6)$$

Furthermore, by using the Kronecker product, system (6) can be rewritten as

$$\begin{aligned}\dot{e}(t) = & \bar{g}(e(t)) + c_{10}(G \otimes D)e(t) \\ & + (c_1(t) - c_{10})(G \otimes D)e(t) \\ & + c_{20}(G \otimes A)e(t - \tau(t)) \\ & + (c_2(t) - c_{20})(G \otimes A)e(t - \tau(t)) \\ & + Ke(t_k), \quad i = 1, 2, \dots, N,\end{aligned}\quad (7)$$

where $e(t) = [e_1^T(t) \ e_2^T(t) \ \dots \ e_N^T(t)]^T$, $\bar{g}(e(t)) = [g^T(e_1(t)) \ g^T(e_2(t)) \ \dots \ g^T(e_N(t))]^T$, and $K = \text{diag}\{K_1, K_2, \dots, K_N\}$.

To proceed further, the following definition and useful lemmas are needed.

Definition 5. The coupled complex dynamical network (1) is said to be globally synchronized in mean square sense if $\lim_{t \rightarrow \infty} E\{\|e_i(t)\|^2\} = 0, i = 1, 2, \dots, N$, holds for any initial values.

Lemma 6 (extended Wirtinger inequality [22]). Let $z(t) \in W[a, b]$ and $z(a) = 0$. Then for any matrix $R > 0$, the following inequality holds:

$$\int_a^b z^T(\alpha) R z(\alpha) d\alpha \leq \frac{4(b-a)^2}{\pi^2} \int_a^b \dot{z}^T(\alpha) R \dot{z}(\alpha) d\alpha. \quad (8)$$

Lemma 7 (reciprocally convex approach [30]). Let $f_1, f_2, \dots, f_N : R^m \mapsto R$ have positive values in an open subset D of R^m . Then, the reciprocally convex combination of f_i over D satisfies

$$\min_{\{\alpha_i | \alpha_i > 0, \sum_i \alpha_i = 1\}} \sum_i \alpha_i f_i(t) = \sum_i \alpha_i f_i(t) + \max_{g_{i,j}(t)} \sum_{i \neq j} g_{i,j}(t) \quad (9)$$

subject to

$$\left\{ g_{i,j} : R^m \mapsto R, g_{j,i}(t) \triangleq g_{i,j}(t), \begin{bmatrix} f_i(t) & g_{i,j}(t) \\ g_{j,i}(t) & f_j(t) \end{bmatrix} \geq 0 \right\}. \quad (10)$$

The aim of this paper is to design a set of sampled-data controllers (5) with sampling period as big as possible to ensure synchronizing the complex network (1) in mean square sense. By some transformation, the synchronization problem of the delayed complex network (1) can be equivalently converted into the mean square asymptotical stability problem of error system (7). Therefore, we are interested in two main issues in our paper, one is to find some stability conditions for error system (7) in mean square for given K_i , and the other is to derive the design method of sampled-data controllers.

3. Main Results

In this section, by considering the characteristic of sampled-data system, we first give a delay-dependent condition to

ensure error system (7) to be globally stable in mean square sense. Then, based on the derived condition, the design method of the sampled-data controllers is proposed. Before presenting the main results, for the sake of presentation simplicity, we denote

$$\begin{aligned}\bar{U} &= \frac{(I_N \otimes U)^T (I_N \otimes V)}{2} + \frac{(I_N \otimes V)^T (I_N \otimes U)}{2}, \\ \bar{V} &= -\frac{(I_N \otimes U)^T + (I_N \otimes V)^T}{2}.\end{aligned}\quad (11)$$

Theorem 8. Under Assumptions 3-4, for given controller gain matrices K_i , the error system (7) is globally asymptotically stable in mean square sense if there exist matrices $P > 0$, $Q_1 > 0$, $Q_2 > 0$, $Q_3 > 0$, $Z_1 > 0$, $Z_2 > 0$, $U > 0$, $R > 0$, $W > 0$, S_1 , S_2 , N , and a scalar $\varepsilon > 0$ such that the following LMIs are satisfied:

$$\begin{bmatrix} \Sigma - p\bar{R} & \Gamma_1 & pN \\ * & -X_1 & 0 \\ * & * & -pU \end{bmatrix} < 0, \quad (12)$$

$$\begin{bmatrix} \Sigma + p\bar{R} & \Gamma_2 \\ * & -X_2 \end{bmatrix} < 0, \quad (13)$$

$$\begin{bmatrix} Z_i & S_i \\ * & Z_i \end{bmatrix} \geq 0, \quad i = 1, 2, \quad (14)$$

where

$$\Sigma = \begin{bmatrix} \Sigma_{11} & \Sigma_{12} & \Sigma_{13} & \Sigma_{14} & \Sigma_{15} & \Sigma_{16} \\ * & \Sigma_{22} & \Sigma_{23} & -N_4 & -N_5 & -N_6 \\ * & * & \Sigma_{33} & 0 & 0 & 0 \\ * & * & * & \Sigma_{44} & \Sigma_{45} & 0 \\ * & * & * & * & \Sigma_{55} & 0 \\ * & * & * & * & * & -\varepsilon I \end{bmatrix},$$

$$\Sigma_{11} = c_{10}P(G \otimes D) + c_{10}(G \otimes D)^T P$$

$$+ Q_1 + Q_2 + Q_3 - \frac{1}{4}\pi^2 W - \varepsilon \bar{U}$$

$$- Z_1 - Z_2 + N_1 + N_1^T,$$

$$\Sigma_{12} = PK + \frac{1}{4}\pi^2 W + Z_1 - S_1 - N_1^T + N_2,$$

$$\Sigma_{13} = S_1 + N_3,$$

$$\Sigma_{14} = P(G \otimes A) + Z_2 - S_2 + N_4,$$

$$\Sigma_{15} = S_2 + N_5,$$

$$\Sigma_{16} = P - \varepsilon \bar{V} + N_6,$$

$$\Sigma_{22} = -2Z_1 - \frac{1}{4}\pi^2 W + S_1 + S_1^T - N_2 - N_2^T,$$

$$\Sigma_{23} = Z_1 - S_1 - N_3,$$

$$\Sigma_{33} = -Q_1 - Z_1,$$

$$\begin{aligned}
\Sigma_{44} &= -(1-\mu)Q_3 - 2Z_2 + S_2 + S_2^T, \\
\Sigma_{45} &= Z_2 - S_2, \\
\Sigma_{55} &= -Q_2 - Z_2, \\
\Gamma_1 &= [\Omega_1^T \quad \delta_1 \Omega_2^T \quad \delta_2 \Omega_3^T], \\
\Gamma_2 &= [\widehat{\Omega}_1^T \quad \delta_1 \widehat{\Omega}_2^T \quad \delta_2 \widehat{\Omega}_3^T], \\
\Omega_1 &= [c_{10}Z(G \otimes D) \quad ZK \quad 0 \quad c_{20}Z(G \otimes A) \quad 0 \quad Z], \\
\Omega_2 &= [Z(G \otimes D) \quad 0 \quad 0 \quad 0 \quad 0 \quad 0], \\
\Omega_3 &= [0 \quad 0 \quad 0 \quad Z(G \otimes A) \quad 0 \quad 0], \\
\widehat{\Omega}_1 &= [c_{10}(Z + pU)(G \otimes D) \quad (Z + pU)K \quad 0 \\
&\quad \times c_{20}(Z + pU)(G \otimes A) \quad 0 \quad (Z + pU)], \\
\widehat{\Omega}_2 &= [(Z + pU)(G \otimes D) \quad 0 \quad 0 \quad 0 \quad 0 \quad 0], \\
\widehat{\Omega}_3 &= [0 \quad 0 \quad 0 \quad (Z + pU)(G \otimes A) \quad 0 \quad 0], \\
X_1 &= \text{diag}\{-Z, -Z, -Z\}, \\
X_2 &= \text{diag}\{-Z - pU, -Z - pU, -Z - pU\}, \\
Z &= p^2 Z_1 + h^2 Z_2 + p^2 W, \\
\overline{R} &= \text{diag}\{0, R, 0, 0, 0, 0\}.
\end{aligned} \tag{15}$$

Proof. Consider the following Lyapunov functional:

$$V(t) = V_1(t) + V_2(t) + V_3(t) + V_4(t), \tag{16}$$

where $t \in [t_k, t_{k+1})$ and

$$\begin{aligned}
V_1(t) &= e^T(t) P e(t) + \int_{t-p}^t e^T(s) Q_1 e(s) ds \\
&\quad + \int_{t-h}^t e^T(s) Q_2 e(s) ds \\
&\quad + \int_{t-\tau(t)}^t e^T(s) Q_3 e(s) ds, \\
V_2(t) &= \int_{-p}^0 \int_{t+\theta}^t \dot{e}^T(s) Z_1 \dot{e}(s) ds d\theta \\
&\quad + h \int_{-h}^0 \int_{t+\theta}^t \dot{e}^T(s) Z_2 \dot{e}(s) ds d\theta, \\
V_3(t) &= (p - (t - t_k)) \int_{t_k}^t \dot{e}^T(s) U \dot{e}(s) ds \\
&\quad + (p - (t - t_k)) (t - t_k) e^T(t_k) R e(t_k),
\end{aligned}$$

$$\begin{aligned}
V_4(t) &= p^2 \int_{t_k}^t \dot{e}^T(s) W \dot{e}(s) ds \\
&\quad - \frac{\pi^2}{4} \int_{t_k}^t [x(s) - x(t_k)]^T W [x(s) - x(t_k)] ds.
\end{aligned} \tag{17}$$

It is clear that at any $t > 0$ except the sampling instants t_k , $V_3(t)$ is continuous and nonnegative, and right after the jump instants t_k , $V_3(t)$ becomes zero; that is, $V_3(t_k^-) \geq 0$, $V_3(t_k^+) = 0$. According to Lemma 7, we can easily find that $V_4(t) \geq 0$ and $V_4(t)$ vanishes at $t = t_k$. Thus, we have $V(t_k^-) \geq V(t_k^+)$.

Define the infinitesimal operator L of $V(t)$ as follows:

$$LV(t) = \lim_{\Delta \rightarrow 0^+} \Delta^{-1} [E\{V(t + \Delta) | e(t)\} - V(t)]. \tag{18}$$

Taking the derivative of (16) along the solution of system (7) for $\forall t \in [t_k, t_{k+1})$, it yields

$$\begin{aligned}
LV_1(t) &\leq 2e^T(t) \\
&\quad \times P(\overline{g}(e(t)) + c_{10}(G \otimes D)e(t) \\
&\quad + c_{20}(G \otimes A)e(t - \tau(t)) \\
&\quad + Ke(t_k)) + e^T(t) Q_1 e(t) \\
&\quad - e^T(t - p) Q_1 e(t - p) \\
&\quad + e^T(t) Q_2 e(t) - e^T(t - h) Q_2 e(t - h) \\
&\quad + e^T(t) Q_3 e(t) \\
&\quad - (1 - \mu) e^T(t - \tau(t)) Q_3 e(t - \tau(t)), \\
LV_2(t) &= \dot{e}^T(t) Z \dot{e}(t) - \int_{t-p}^t \dot{e}^T(s) Z_1 \dot{e}(s) ds \\
&\quad - h \int_{t-h}^t \dot{e}^T(s) Z_2 \dot{e}(s) ds, \\
LV_3(t) &= (p - (t - t_k)) \dot{e}^T(t) U \dot{e}(t) \\
&\quad - \int_{t_k}^t \dot{e}^T(s) U \dot{e}(s) ds \\
&\quad + (p - (t - t_k)) e^T(t_k) R e(t_k) \\
&\quad - (t - t_k) e^T(t_k) R e(t_k), \\
LV_4(t) &= p^2 \dot{e}^T(t) W \dot{e}(t) \\
&\quad - \frac{\pi^2}{4} [x(t) - x(t_k)]^T W [x(t) - x(t_k)].
\end{aligned} \tag{19}$$

If (14) is satisfied, then by utilizing Lemma 6, we have

$$\begin{aligned}
& -p \int_{t-p}^t \dot{e}^T(s) Z_1 \dot{e}(s) ds \\
& \leq - \begin{bmatrix} e(t) - e(t_k) \\ e(t_k) - e(t-p) \end{bmatrix}^T \begin{bmatrix} Z_1 & S_1 \\ * & Z_1 \end{bmatrix} \\
& \quad \times \begin{bmatrix} e(t) - e(t_k) \\ e(t_k) - e(t-p) \end{bmatrix}, \\
& -h \int_{t-h}^t \dot{e}^T(s) Z_2 \dot{e}(s) ds \\
& \leq - \begin{bmatrix} e(t) - e(t-\tau(t)) \\ e(t-\tau(t)) - e(t-h) \end{bmatrix}^T \begin{bmatrix} Z_2 & S_2 \\ * & Z_2 \end{bmatrix} \\
& \quad \times \begin{bmatrix} e(t) - e(t-\tau(t)) \\ e(t-\tau(t)) - e(t-h) \end{bmatrix}.
\end{aligned} \tag{20}$$

On the other hand, the following inequality is true for any matrix N with appropriate dimensions:

$$\begin{aligned}
& - \int_{t_k}^t \dot{e}^T(s) U \dot{e}(s) ds \\
& \leq (t - t_k) \xi^T(t) N U^{-1} N^T \xi(t) \\
& \quad + 2 \xi^T(t) N (e(t) - e(t_k)),
\end{aligned} \tag{21}$$

where

$$\begin{aligned}
& \xi(t) \\
& = \begin{bmatrix} (t) & e^T(t_k) & e^T(t-p) & e^T(t-\tau(t)) & e^T(t-h) & \bar{g}^T(e(t)) \end{bmatrix}^T.
\end{aligned} \tag{22}$$

Let $\Omega = \Omega_1 + (c_1(t) - c_{10})\Omega_2 + (c_2(t) - c_{20})\Omega_3$. Because $c_1(t)$ and $c_2(t)$ are mutually independent random variables, it can be obtained from (7) that

$$\begin{aligned}
& E \{ \dot{e}^T(t) Z \dot{e}(t) \} = E \{ \xi^T(t) \Omega^T Z \Omega \xi(t) \} = \xi^T(t) \bar{\Omega}_1 \xi(t), \\
& E \{ \dot{e}^T(t) U \dot{e}(t) \} = E \{ \xi^T(t) \Omega^T U \Omega \xi(t) \} = \xi^T(t) \bar{\Omega}_2 \xi(t),
\end{aligned} \tag{23}$$

where $\bar{\Omega}_1 = \Omega_1^T Z \Omega_1 + \delta_1^2 \Omega_2^T Z \Omega_2 + \delta_2^2 \Omega_3^T Z \Omega_3$, $\bar{\Omega}_2 = \Omega_1^T Z_3 \Omega_1 + \delta_1^2 \Omega_2^T Z_3 \Omega_2 + \delta_2^2 \Omega_3^T Z_3 \Omega_3$.

In addition, based on Assumption 3, for any $\varepsilon > 0$, we have

$$y(t) = \varepsilon \begin{bmatrix} e(t) \\ \bar{g}(e(t)) \end{bmatrix}^T \begin{bmatrix} \bar{U} & \bar{V} \\ * & I \end{bmatrix} \begin{bmatrix} e(t) \\ \bar{g}(e(t)) \end{bmatrix} \leq 0. \tag{24}$$

Combining (18)–(24) and taking mathematical exceptions on both sides of (16) give that

$$E \{ LV(t) \} \leq \xi^T(t) \Phi \xi(t), \tag{25}$$

where $\Phi = \Sigma + \bar{\Omega}_1 + (p - (t - t_k))(\bar{\Omega}_2 + \bar{R}) + (t - t_k)(NU^{-1}N^T - \bar{R})$.

Noting that Φ is a convex combination of $t - t_k$ and $p - (t - t_k)$, so $\Phi < 0$ if and only if

$$\begin{aligned}
& \Sigma + \bar{\Omega}_1 + pNU^{-1}N^T - p\bar{R} < 0, \\
& \Sigma + \bar{\Omega}_1 + p(\bar{\Omega}_2 + \bar{R}) < 0.
\end{aligned} \tag{26}$$

From the Schur complement, (12) and (13) can ensure $\Phi < 0$. This means that $E\{LV(t)\} \leq -\rho\|e(t)\|^2$ for a sufficiently small $\rho > 0$. We can conclude that system (7) is asymptotically stable in the mean square sense. This completes the proof. \square

Remark 9. Inspired by [20, 22], the characteristic of sampling instants has been considered in the construction of the Lyapunov functional. The discontinuous terms $V_3(t)$ and $V_4(t)$ can make full use of the sawtooth structure characteristic of sampling instants and play the key role in the reduction of conservatism. In the process of taking the derivative of $V(t)$, reciprocally convex approach and convex combination technique were employed, which were beneficial to lead less conservativeness. Moreover, the derived synchronization criterion is formulated in terms of LMIs that can be easily verified by using available software.

Next, we will consider how to design the desired sampled-data controllers. Based on Theorem 8, a set of sampled-data controllers are presented as follows.

Theorem 10. Under Assumptions 3-4, the complex dynamical networks (1) with random coupling strength is globally asymptotically synchronized in mean square by the sampled-data controllers (5) if there exist matrices $P = \text{diag}\{P_1, P_2, \dots, P_N\} > 0$, $Q_1 > 0$, $Q_2 > 0$, $Q_3 > 0$, $Z_1 > 0$, $Z_2 > 0$, $U > 0$, $R > 0$, $W > 0$, S_1 , S_2 , N , $X = \text{diag}\{X_1, X_2, \dots, X_N\}$, and a scalar $\varepsilon > 0$ such that (14) and the following LMIs are satisfied:

$$\begin{aligned}
& \begin{bmatrix} \hat{\Sigma} - p\bar{R} & Y & pN \\ * & -\hat{X}_1 & 0 \\ * & * & -pU \end{bmatrix} < 0, \\
& \begin{bmatrix} \hat{\Sigma} + p\bar{R} & Y \\ * & -\hat{X}_2 \end{bmatrix} < 0,
\end{aligned} \tag{27}$$

where

$$\hat{X}_1 = \text{diag} \{-2P + Z, -2P + Z, -2P + Z\},$$

$$\begin{aligned}
\hat{X}_2 = & \text{diag} \{-2P + Z + pU, -2P \\
& + Z + pU, -2P + Z + pU\},
\end{aligned}$$

$$Y = \begin{bmatrix} Y_1^T & \delta_1 Y_2^T & \delta_2 Y_3^T \end{bmatrix},$$

$$Y_1 = \begin{bmatrix} c_{10}P(G \otimes D) & X & 0 & c_{20}P(G \otimes A) & 0 & P \end{bmatrix},$$

$$Y_2 = \begin{bmatrix} P(G \otimes D) & 0 & 0 & 0 & 0 & 0 \end{bmatrix},$$

$$Y_3 = [0 \ 0 \ 0 \ P(G \otimes A) \ 0 \ 0],$$

$$\widehat{\Sigma} = \begin{bmatrix} \Sigma_{11} & \widehat{\Sigma}_{12} & \Sigma_{13} & \Sigma_{14} & \Sigma_{15} & \Sigma_{16} \\ * & \Sigma_{22} & \Sigma_{23} & -N_4 & -N_5 & -N_6 \\ * & * & \Sigma_{33} & 0 & 0 & 0 \\ * & * & * & \Sigma_{44} & \Sigma_{45} & 0 \\ * & * & * & * & \Sigma_{55} & 0 \\ * & * & * & * & * & -\varepsilon I \end{bmatrix},$$

$$\widehat{\Sigma}_{12} = X + \frac{1}{4}\pi^2 W + Z_1 - S_1 - N_1^T + N_2, \quad (28)$$

and the other terms follow the same definitions as those in Theorem 8. Moreover, the desired controllers gain matrices are given by

$$K_i = P_i^{-1} X_i, \quad i = 1, 2, \dots, N. \quad (29)$$

Proof. Define matrices $X = PK$, $J_1 = \text{diag}\{I, I, I, I, I, I, PZ^{-1}, PZ^{-1}, PZ^{-1}\}$, and $J_2 = \text{diag}\{I, I, I, I, I, I, P(Z + pU)^{-1}, P(Z + pU)^{-1}, P(Z + pU)^{-1}\}$. Note that $-PZ^{-1}P \leq -2P + Z$ and $-P(Z + pU)^{-1}P \leq -2P + Z + pU$ are true for $Z > 0$ and $U > 0$. Then, performing a congruence transformation of J_1 to (12) and performing a congruence transformation of J_2 to (13), respectively, and considering the relation $X = PK$, we can obtain that if (27) holds, then (12) and (13) hold. This completes the proof. \square

If $c_1(t) = c_{10}$ and $c_2(t) = c_{20}$, the random coupling strengths reduce to constant, and the error system (7) can be rewritten as following simple form:

$$\begin{aligned} \dot{e}(t) &= \bar{g}(e(t)) + c_{10}(G \otimes D)e(t) \\ &+ c_{20}(G \otimes A)e(t - \tau(t)) + Ke(t_k), \quad (30) \\ i &= 1, 2, \dots, N. \end{aligned}$$

Based on Theorems 8 and 10, by eliminating δ_1 and δ_2 , we can easily get the following results.

Corollary 11. Under Assumption 3, for given controller gain matrices K_i , the error system (30) with sampled-data controllers K_i can achieve synchronization, if there exist matrices $P > 0$, $Q_1 > 0$, $Q_2 > 0$, $Q_3 > 0$, $Z_1 > 0$, $Z_2 > 0$, $U > 0$, $R > 0$, $W > 0$, S_1 , S_2 , N , and a scalar $\varepsilon > 0$ such that (10) and the following LMIs are satisfied:

$$\begin{aligned} \begin{bmatrix} \Sigma - p\bar{R} & \Omega_1^T & pN \\ * & -Z & 0 \\ * & * & -pU \end{bmatrix} &< 0, \\ \begin{bmatrix} \Sigma + p\bar{R} & \widehat{\Omega}_1^T \\ * & -Z - pU \end{bmatrix} &< 0, \end{aligned} \quad (31)$$

where the other terms follow the same definitions as those in Theorem 8.

Corollary 12. Under the Assumption 3, the complex dynamical network (1) with random coupling strengths is globally asymptotically synchronized in mean square by the

sampled-data controllers (5) if there exist matrices $P = \text{diag}\{P_1, P_2, \dots, P_N\} > 0$, $Q_1 > 0$, $Q_2 > 0$, $Q_3 > 0$, $Z_1 > 0$, $Z_2 > 0$, $U > 0$, $R > 0$, $W > 0$, S_1 , S_2 , N , $X = \text{diag}\{X_1, X_2, \dots, X_N\}$, and a scalar $\varepsilon > 0$ such that (10) and the following LMIs are satisfied:

$$\begin{aligned} \begin{bmatrix} \widehat{\Sigma} - p\bar{R} & Y_1^T & pN \\ * & -2P + Z & 0 \\ * & * & -pU \end{bmatrix} &< 0, \\ \begin{bmatrix} \widehat{\Sigma} + p\bar{R} & Y_1 \\ * & -2P + Z + pU \end{bmatrix} &< 0, \end{aligned} \quad (32)$$

where the other terms follow the same definitions as those in Theorem 10.

Remark 13. Since the characteristic of sampled-data control system is fully considered, the conservatism of Corollary 12 is much less than those not taking delay characteristic into account [27, 28], which will be verified by numerical example in next section.

Remark 14. It is worth pointing out that the main result here can be extended to some more general complex dynamical networks with probabilistic time-varying coupling delay [18] or distributed coupling delay. Owing to the space limit, it is omitted here.

4. Numerical Examples

In this section, two numerical examples are given to show the validity of the proposed results.

Example 1. Consider complex network model (1) with three nodes. The out-coupling matrix is assumed to be $G = (G_{ij})_{N \times N}$ with

$$G = \begin{bmatrix} -1 & 0 & 1 \\ 0 & -1 & 1 \\ 1 & 1 & -2 \end{bmatrix}. \quad (33)$$

The time-varying coupling delay is chosen as $\tau(t) = 0.2 + 0.05 \sin(10t)$. A straight-forward calculation gives $h = 0.25$ and $\mu = 0.5$. The nonlinear function f is taken as

$$f(x_i(t)) = \begin{bmatrix} -0.5x_{i1} + \tanh(0.2x_{i2}) + 0.2x_{i2} \\ 0.95x_{i2} - \tanh(0.75x_{i2}) \end{bmatrix}. \quad (34)$$

It can be found that f satisfies (2) with

$$U = \begin{bmatrix} -0.5 & 0.2 \\ 0 & 0.95 \end{bmatrix}, \quad V = \begin{bmatrix} -0.3 & 0.2 \\ 0 & 0.2 \end{bmatrix}. \quad (35)$$

The inner-coupling matrices are given as $D = 0$ and

$$A = \begin{bmatrix} 1 & 0 \\ 0 & 1 \end{bmatrix}. \quad (36)$$

Let the coupling strength $c_2(t)$ be a constant; that is, $c_2(t) = c$. For different c , Table 1 lists the maximum sampling interval

TABLE 1: Maximum sampling interval p for different coupling strength c .

	c	
	0.5	0.75
[27]	0.5409	0.1653
[28]	0.5573	0.2277
[29]	0.9016	0.8957
Corollary 12	0.9795	0.9121

p obtained by Corollary 12 and [27–29]. From this table, we can see that our result has less conservatism than the existing ones.

Furthermore, choosing $c = 0.5$ and applying MATLAB LMI toolbox to solve the LMIs in Corollary 12, the gain matrices of the desired controllers can be obtained as follows:

$$\begin{aligned} K_1 &= \begin{bmatrix} -0.6578 & -0.0978 \\ -0.0172 & -1.2316 \end{bmatrix}, \\ K_2 &= \begin{bmatrix} -0.6578 & -0.0978 \\ -0.0172 & -1.2316 \end{bmatrix}, \\ K_3 &= \begin{bmatrix} -0.4543 & -0.1223 \\ -0.0185 & -1.1988 \end{bmatrix}. \end{aligned} \quad (37)$$

In the numerical simulation, assume that the initial values are $x_1(0) = [3 \ 5]^T$, $x_2(0) = [-2 \ -1]^T$, $x_3(0) = [2 \ 1]^T$, and $s(0) = [-5 \ 3]^T$. The state trajectories of the synchronization error and the control inputs $u_i(t)$ are given in Figures 1 and 2, respectively. Clearly, the synchronization errors are globally asymptotically stable in mean square under the proposed sampled-data scheme.

Example 2. The isolated node of the dynamical networks and the coupling delay are the same as Example 1. The inner-coupling matrices are given as

$$D = A = \begin{bmatrix} 0.1 & 0 \\ 0 & 0.1 \end{bmatrix}, \quad (38)$$

and the outer-coupling matrix

$$G = \begin{bmatrix} -3 & 1 & 0 & 2 & 0 & 0 \\ 0 & -2 & 0 & 1 & 1 & 0 \\ 1 & 0 & -3 & 1 & 0 & 1 \\ 0 & 2 & 0 & -2 & 0 & 0 \\ 1 & 1 & 1 & 1 & -4 & 0 \\ 1 & 1 & 0 & 0 & 1 & -3 \end{bmatrix}. \quad (39)$$

We assume that $c_1(t)$ and $c_2(t)$ are two mutually independent random variables satisfying normal distribution with $c_{10} = 5$, $c_{20} = 1$, $\delta_1 = 0.5$, and $\delta_2 = 0.15$. According to the property of normal distribution, almost all the values of $c_i(t)$ satisfy $c_i(t) \in (c_{i0} - 3\delta_i, c_{i0} + 3\delta_i)$; that is $c_1(t) \in (3.5, 6.5)$ and $c_2(t) \in (1.55, 2.45)$. Figures 3 and 4 depict the random coupling strengths $c_1(t)$ and $c_2(t)$, respectively.

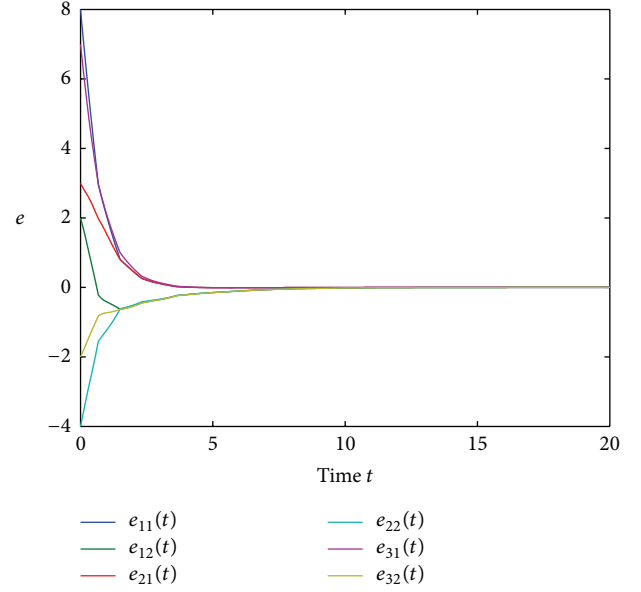


FIGURE 1: Synchronization error states.

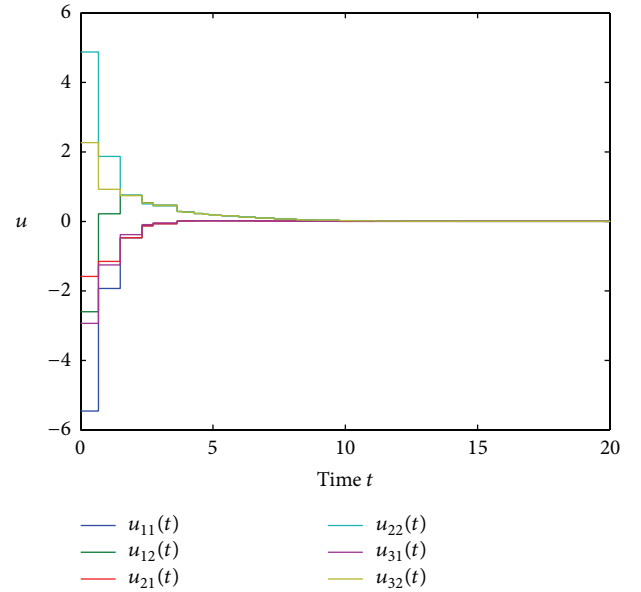


FIGURE 2: Sampled-data control inputs.

Let $p = 0.05$; based on Theorem 10, we can get the corresponding sampled-data controller gain matrices

$$\begin{aligned} K_1 &= \begin{bmatrix} -0.1314 & -0.1212 \\ -0.0709 & -1.1841 \end{bmatrix}, \\ K_2 &= \begin{bmatrix} -0.4319 & -0.1243 \\ -0.0753 & -1.3982 \end{bmatrix}, \\ K_3 &= \begin{bmatrix} 0.1045 & -0.1144 \\ -0.0747 & -0.9176 \end{bmatrix}, \end{aligned}$$

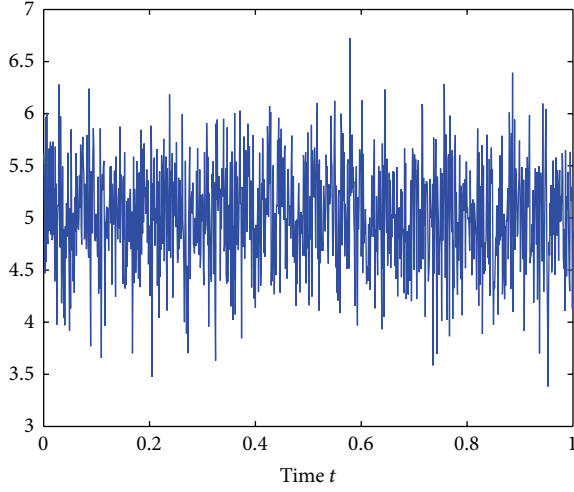
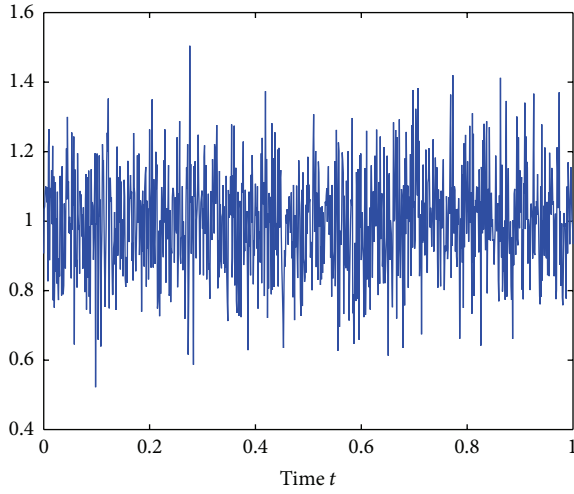
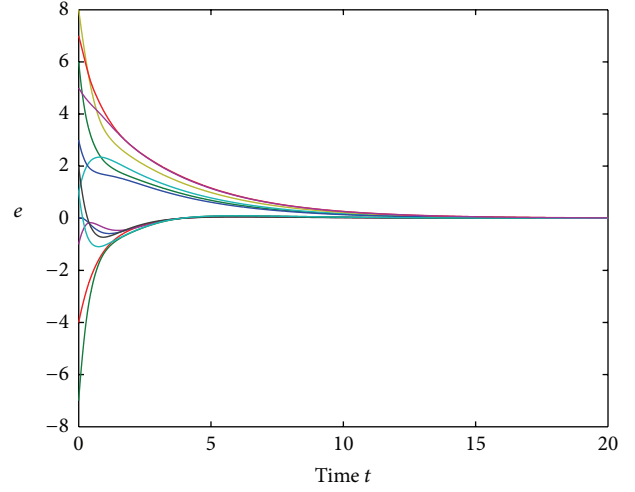
FIGURE 3: Random coupling strength $c_1(t)$.FIGURE 4: Random coupling strength $c_2(t)$.

FIGURE 5: Synchronization error states.

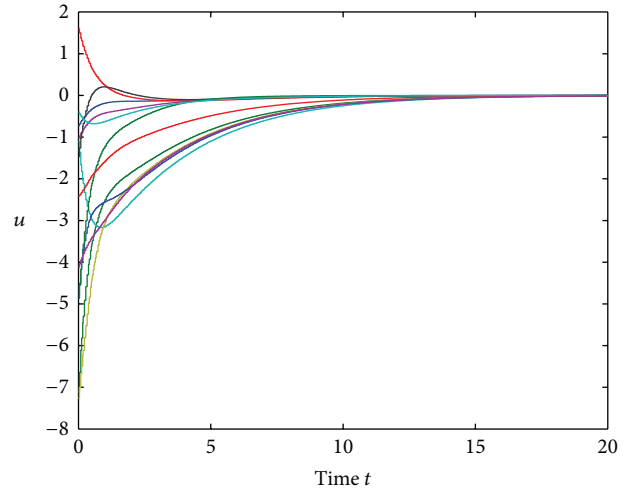


FIGURE 6: Sampled-data control inputs.

$$\begin{aligned}
 K_4 &= \begin{bmatrix} -0.5565 & -0.1190 \\ -0.0665 & -1.5593 \end{bmatrix}, \\
 K_5 &= \begin{bmatrix} 0.5769 & -0.1184 \\ -0.0688 & -0.4136 \end{bmatrix}, \\
 K_6 &= \begin{bmatrix} 0.1801 & -0.1154 \\ -0.0846 & -0.8069 \end{bmatrix}.
 \end{aligned} \tag{40}$$

In the numerical simulation, assume that the initial values are $x_1(0) = [3 \ 2]^T$, $x_2(0) = [-1 \ -3]^T$, $x_3(0) = [2 \ 4]^T$, $x_4(0) = [5 \ -1]^T$, $x_5(0) = [-4 \ 3]^T$, $x_6(0) = [4 \ 1]^T$, and $s(0) = [3 \ -4]^T$. The state trajectories of the synchronization error and the control inputs $u_i(t)$ are given in Figures 5 and 6, respectively.

5. Conclusions

In this paper, the sampled-data synchronization problem has been considered for a kind of complex dynamical networks with time-varying coupling delay and random coupling strengths. The sampling period and random coupling strengths considered here are assumed to be time varying but bounded and to obey normal distribution, respectively. By capturing the characteristic of sampled-data system, a novel discontinuous Lyapunov functional is defined. By using reciprocally convex approach and convex combination technique, a mean square synchronization criterion is proposed based on LMIs. The corresponding desired sampled-data controllers are designed. Numerical examples show the effectiveness of the proposed result.

Conflict of Interests

The authors declare that there is no conflict of interests regarding the publication of this paper.

Acknowledgments

The work is Supported by the National Natural Science Foundation of China (Grant nos. 61203049 and 61303020), the Doctoral Startup Foundation of Taiyuan University of Science and Technology (Grant no. 20112010), and Shanxi Education Department Foundation (Grant no. 20121068).

References

- [1] S. H. Strogatz, "Exploring complex networks," *Nature*, vol. 410, no. 6825, pp. 268–276, 2001.
- [2] R. Albert and A.-L. Barabási, "Statistical mechanics of complex networks," *Reviews of Modern Physics*, vol. 74, no. 1, pp. 47–97, 2002.
- [3] X. F. Wang and G. R. Chen, "Complex networks: small-world, scale-free and beyond," *IEEE Circuits and Systems Magazine*, vol. 3, no. 1, pp. 6–20, 2003.
- [4] X. F. Wang and G. R. Chen, "Synchronization in scale-free dynamical networks: robustness and fragility," *IEEE Transactions on Circuits and Systems. I. Fundamental Theory and Applications*, vol. 49, no. 1, pp. 54–62, 2002.
- [5] Y. Wang, Z. D. Wang, and J. L. Liang, "A delay fractioning approach to global synchronization of delayed complex networks with stochastic disturbances," *Physics Letters A: General, Atomic and Solid State Physics*, vol. 372, no. 39, pp. 6066–6073, 2008.
- [6] J. Zhou, J.-A. Lu, and J. Lü, "Adaptive synchronization of an uncertain complex dynamical network," *Institute of Electrical and Electronics Engineers. Transactions on Automatic Control*, vol. 51, no. 4, pp. 652–656, 2006.
- [7] J. Q. Lu, W. D. C. Ho, and J. D. Cao, "A unified synchronization criterion for impulsive dynamical networks," *Automatica*, vol. 46, no. 7, pp. 1215–1221, 2010.
- [8] W. W. Yu, G. R. Chen, and J. H. Lü, "On pinning synchronization of complex dynamical networks," *Automatica*, vol. 45, no. 2, pp. 429–435, 2009.
- [9] Q. Song and J. D. Cao, "On pinning synchronization of directed and undirected complex dynamical networks," *IEEE Transactions on Circuits and Systems. I. Regular Papers*, vol. 57, no. 3, pp. 672–680, 2010.
- [10] J. Lu and W. D. C. Ho, "Globally exponential synchronization and synchronizability for general dynamical networks," *IEEE Transactions on Systems, Man, and Cybernetics B: Cybernetics*, vol. 40, no. 2, pp. 350–361, 2010.
- [11] J. Yao, Z.-H. Guan, and D. J. Hill, "Passivity-based control and synchronization of general complex dynamical networks," *Automatica*, vol. 45, no. 9, pp. 2107–2113, 2009.
- [12] M. J. Park, O. M. Kwon, J. H. Park, S. M. Lee, and E. J. Cha, "Synchronization criteria for coupled stochastic neural networks with time-varying delays and leakage delay," *Journal of the Franklin Institute. Engineering and Applied Mathematics*, vol. 349, no. 5, pp. 1699–1720, 2012.
- [13] Y. H. Xu, W. N. Zhou, J. A. Fang, W. Sun, and L. Pan, "Topology identification and adaptive synchronization of uncertain complex networks with non-derivative and derivative coupling," *Journal of the Franklin Institute. Engineering and Applied Mathematics*, vol. 347, no. 8, pp. 1566–1576, 2010.
- [14] C. W. Wu, "Synchronization and convergence of linear dynamics in random directed networks," *Institute of Electrical and Electronics Engineers. Transactions on Automatic Control*, vol. 51, no. 7, pp. 1207–1210, 2006.
- [15] T. H. Lee, J. H. Park, D. H. Ji, O. M. Kwon, and S. M. Lee, "Guaranteed cost synchronization of a complex dynamical network via dynamic feedback control," *Applied Mathematics and Computation*, vol. 218, no. 11, pp. 6469–6481, 2012.
- [16] J.-L. Wang and H.-N. Wu, "Local and global exponential output synchronization of complex delayed dynamical networks," *Nonlinear Dynamics. An International Journal of Nonlinear Dynamics and Chaos in Engineering Systems*, vol. 67, no. 1, pp. 497–504, 2012.
- [17] X. S. Yang, J. D. Cao, and J. Q. Lu, "Synchronization of Markovian coupled neural networks with nonidentical mode-delays and random coupling strengths," *IEEE Transactions on Neural Networks and Learning Systems*, vol. 23, no. 1, pp. 60–71, 2012.
- [18] X. S. Yang, J. D. Cao, and J. Q. Lu, "Synchronization of coupled neural networks with random coupling strengths and mixed probabilistic time-varying delays," *International Journal of Robust and Nonlinear Control*, vol. 23, no. 18, pp. 2060–2081, 2013.
- [19] E. Fridman, A. Seuret, and J.-P. Richard, "Robust sampled-data stabilization of linear systems: an input delay approach," *Automatica*, vol. 40, no. 8, pp. 1441–1446, 2004.
- [20] E. Fridman, "A refined input delay approach to sampled-data control," *Automatica*, vol. 46, no. 2, pp. 421–427, 2010.
- [21] B. H. K. Lam, "Output-feedback sampled-data polynomial controller for nonlinear systems," *Automatica*, vol. 47, no. 11, pp. 2457–2461, 2011.
- [22] K. Liu and E. Fridman, "Wirtinger's inequality and Lyapunov-based sampled-data stabilization," *Automatica*, vol. 48, no. 1, pp. 102–108, 2012.
- [23] J. G. Lu and D. J. Hill, "Global asymptotical synchronization of chaotic Lur'e systems using sampled data: a linear matrix inequality approach," *IEEE Transactions on Circuits and Systems II: Express Briefs*, vol. 55, no. 6, pp. 586–590, 2008.
- [24] Z. G. Wu, P. Shi, H. Y. Su, and J. Chu, "Exponential synchronization of neural networks with discrete and distributed delays under time-varying sampling," *IEEE Transactions on Neural Networks and Learning Systems*, vol. 23, no. 9, pp. 1368–1376, 2012.
- [25] Z. G. Wu, P. Shi, H. Y. Su, and J. Chu, "Stochastic synchronization of Markovian jump neural networks with time-varying delay using sampled-data," *IEEE Transactions on Cybernetics*, vol. 43, no. 6, pp. 1796–1806, 2013.
- [26] C. K. Zhang, Y. He, and M. Wu, "Exponential synchronization of neural networks with time-varying mixed delays and sampled-data," *Neurocomputing*, vol. 74, no. 1–3, pp. 265–273, 2010.
- [27] N. Li, Y. L. Zhang, J. W. Hu, and Z. Y. Nie, "Synchronization for general complex dynamical networks with sampled-data," *Neurocomputing*, vol. 74, no. 5, pp. 805–811, 2011.
- [28] Z.-G. Wu, J. H. Park, H. Su, B. Song, and J. Chu, "Exponential synchronization for complex dynamical networks with sampled-data," *Journal of the Franklin Institute. Engineering and Applied Mathematics*, vol. 349, no. 9, pp. 2735–2749, 2012.

- [29] Z. G. Wu, P. Shi, H. Y. Su, and J. Chu, "Sampled-data exponential synchronization of complex dynamical networks with time-varying coupling," *IEEE Transactions on Neural Networks and Learning Systems*, vol. 24, pp. 1177–1187, 2013.
- [30] P. Park, J. W. Ko, and C. Jeong, "Reciprocally convex approach to stability of systems with time-varying delays," *Automatica*, vol. 47, no. 1, pp. 235–238, 2011.

Research Article

Investigating Nonlinear Shoreline Multiperiod Change from Orthophoto Map Information by Using a Neural Network Model

Tienfuan Kerh,¹ Hsienchang Lu,¹ and Rob Saunders²

¹ Department of Civil Engineering, National Pingtung University of Science and Technology, Pingtung 91207, Taiwan

² Faculty of Architecture, Design and Planning, University of Sydney, NSW 2006, Australia

Correspondence should be addressed to Tienfuan Kerh; tfkerh@gmail.com

Received 3 February 2014; Revised 31 March 2014; Accepted 31 March 2014; Published 27 April 2014

Academic Editor: Zhichun Yang

Copyright © 2014 Tienfuan Kerh et al. This is an open access article distributed under the Creative Commons Attribution License, which permits unrestricted use, distribution, and reproduction in any medium, provided the original work is properly cited.

The effects of extreme weather and overdevelopment may cause some coastal areas to exhibit erosion problems, which in turn may contribute to creating disasters of varying scale, particularly in regions comprising islands. This study used aerial survey information from three periods (1990, 2001, and 2010) and used graphical software to establish the spatial data of six beaches surrounding the island of Taiwan. An overlaying technique was then implemented to compare the sandy area of each beach in the aforementioned study periods. In addition, an artificial neural network model was developed based on available digitised coordinates for predicting coastline variation for 2015 and 2020. An onsite investigation was performed using a global positioning system for comparing the beaches. The results revealed that two beaches from this study may have experienced significant changes in total sandy areas under a statistical 95% confidence interval. The proposed method and the result of this study may provide a valuable reference in follow-up research and applications.

1. Introduction

Problems related to global warming and rising sea levels have been the focus of related research in recent years, because such problems may cause various types of disaster, depending on the affected area's geographical location and land characteristics [1–3]. Furthermore, the melting of icebergs in the polar region as a result of the “greenhouse effect” may cause the gradual rising of sea levels and that may result in a loss of land area. In severe cases, this phenomenon can destroy an island country if no action is taken for preventing this type of gradually formed disaster. Other factors, such as extreme weather, tidal current, drifting sand, land subsidence, the estuarine effect, and industrial development, may also cause a complex process to affect a shoreline area [4, 5]. Therefore, examining shoreline changes during various periods is worthwhile for understanding how to protect the environment and manage land.

Investigation of the shoreline change along populated coastal region usually involved problems with a very large scale, which will rely on a suitable model for increasing prediction accuracy. An early proposed schematic erosion

prediction method by Bruun [6], showed that beach profile may be predicted from an empirical model. Following the same concept and by considering many factors such as wave motion, sediment transport, and sea bed conditions, various models are reported for studying different type of shoreline erosion problems [7, 8]. Other aspects of these studies entailed focusing on the development of a numerical model with the aid of hydraulic modelling experiments for a specified coastal region, to simulate and predict the possibility of shoreline variation [9–12]. Relevant research has provided useful references for evaluating the suitability of designing or planning construction projects along shorelines.

The development of modern geographic information system (GIS) and aerial survey photographs at coastal zones can provide greater reliability and accuracy for analyzing and visualization. Thus, these methods are also frequently adopted recently for monitoring the shoreline [13–18]. However, this image based method may be costly and time consuming for collecting, rectifying, and transferring the information from photographs to digitalized map. Besides, some errors may be generated during the transferring process of the geometric complexity and fragmented patterns of

coastlines. Nevertheless, this method does provide a possible solution for evaluating the shoreline change in different periods.

To avoid complicating model process, simple forecast methods such as end rate, linear regression, and robust parameter estimation, are widely used recently [19–21]. These methods are in general need to assume that the determination of future shorelines is based on modelling points on past shorelines, and a function form may be obtained for predicting shoreline change. In contrast, the recently developed neural network approach offers a good way for linking different types of data sets by learning, and the trained and verified model can then be used for prediction.

The neural network approach is extensively employed in various engineering fields including the application in coastal engineering due to its simplicity, flexibility, and effectiveness [22–25]. However, it can be seen that most of previous studies are focussed on forecasting tidal level and land use evolution patterns. There was a paper dealing with beach profile and shoreline features by using neural network and survey image [26], but the technique is used to delineate the shoreline. The application of this approach directly to predict shoreline variation in future years based on the model developed from available multiperiod orthophoto images is relatively difficult to find up to the present time [27]. Therefore, without going for shoreline complicated evolution process, the combination of using neural network with digitized spatial information from orthophoto images may be considered as a new way for nonlinear shoreline prediction and sand-beach area calculation.

The first stage of this study involved examining orthophoto survey maps, obtained from the Aerial Office of Taiwan's Forestry Bureau, produced in three years (1990, 2001, and 2010). Based on available information, nine major beaches around the island of Taiwan were examined for evaluating the sand-line variation during these periods by using AutoCAD, a computer software package used in many professions for drafting, designing, and modelling. The second stage entailed employing an artificial neural network from known sand-line coordinates (1990 and 2001) to develop a model for targeting the known sand-line coordinates (2010). After the capability of the model was verified, a new neural network model was developed based on data interpolated from coordinates for forecasting possible shoreline changes in 2015 and 2020. Calculations were performed on the total sandy areas for each of the beaches to confirm the significance of variation during these periods. The third and final stage involved an onsite investigation using a global positioning system (GPS) receiver to compare the beach data. Image treatment, model development, and result analysis regarding the research area are presented and discussed in detail in the following sections.

2. Research Beaches and Treatment of Shoreline Survey Images

The island of Taiwan is located at 120° – 122° in longitude and 22° – 25° in latitude, approximately 377 km north south and

approximately 142 km east west. In addition, the length of shoreline is approximately 1,200 km in circumference. On the east side of Taiwan, because of mountains and cliffs situated near the coastal region, the slope of the sea bottom is steep, and sand beaches are relatively small in scale. Conversely, the slope of sand beaches along the west shoreline is not as substantial, because the mountains are farther away from the shoreline. In addition, because most of the rivers on the island of Taiwan flow west into the Taiwan Strait, a large amount of sand has accumulated in the estuarine region, extending the scale of sand beaches on this side. Some manmade factors, such as overdevelopment of land, overpumping of groundwater, and various economic activities in the coastal region, have caused acute shoreline erosion problems in recent years.

Figure 1 displays the locations of initially chosen nine major beaches (BH1–BH9) around the island of Taiwan. These nine beaches required a preliminary on-site investigation before digitising the beach survey images. By examining the aerial survey images over these periods, it was established that BH7 and BH8 exhibit extreme changes in the sand-beach regions. The causes may be attributed to typhoons, tidal effects, floating wood, garbage, contamination, or manmade structures. Regardless of the causes, the process of sand erosion and accretion has been disturbed in these two beaches, making them unsuitable for prediction by using a neural network model. Similarly, as a result of harbour engineering construction at BH9 during the study periods, the survey images demonstrate a sizeable difference in sand area for the three years. Therefore, the three beaches that exhibit extreme changes are omitted for further analysis in this study.

This study sought to obtain the earliest and highest-quality images for each aerial survey map, representing the same year of investigation for the examined beaches. However, the quality of some of the images was not as reliable as desired, and the length of investigation time for each beach was not consistent. In considering the development of survey techniques, two types of images, aerial survey maps and orthophoto maps, were obtained for the three examined years (1990, 2001, and 2010). The aerial survey map does not have a standard proportion, whereas the orthophoto map is an aerial photograph geometrically corrected so that the scale is uniform [28], having a fixed proportion of 1:5,000. Thus, these images required adjustment by using geographic information system (GIS) software to ensure that all images appear in the same proportion and at the same position during comparisons.

In applying the corrected images, the computer's graphical software package, AutoCAD, was used to digitise the survey maps and draw the sand line for each beach. Note that the coordinate system TWD67 was employed for the 1990 maps, whereas the coordinate system TWD97 was employed for the 2001 and 2010 maps [29]. Therefore, a conversion procedure was required for applying the global coordinate system to the surveying technique of the GPS. After unifying all of the images to the same coordinate system, the output

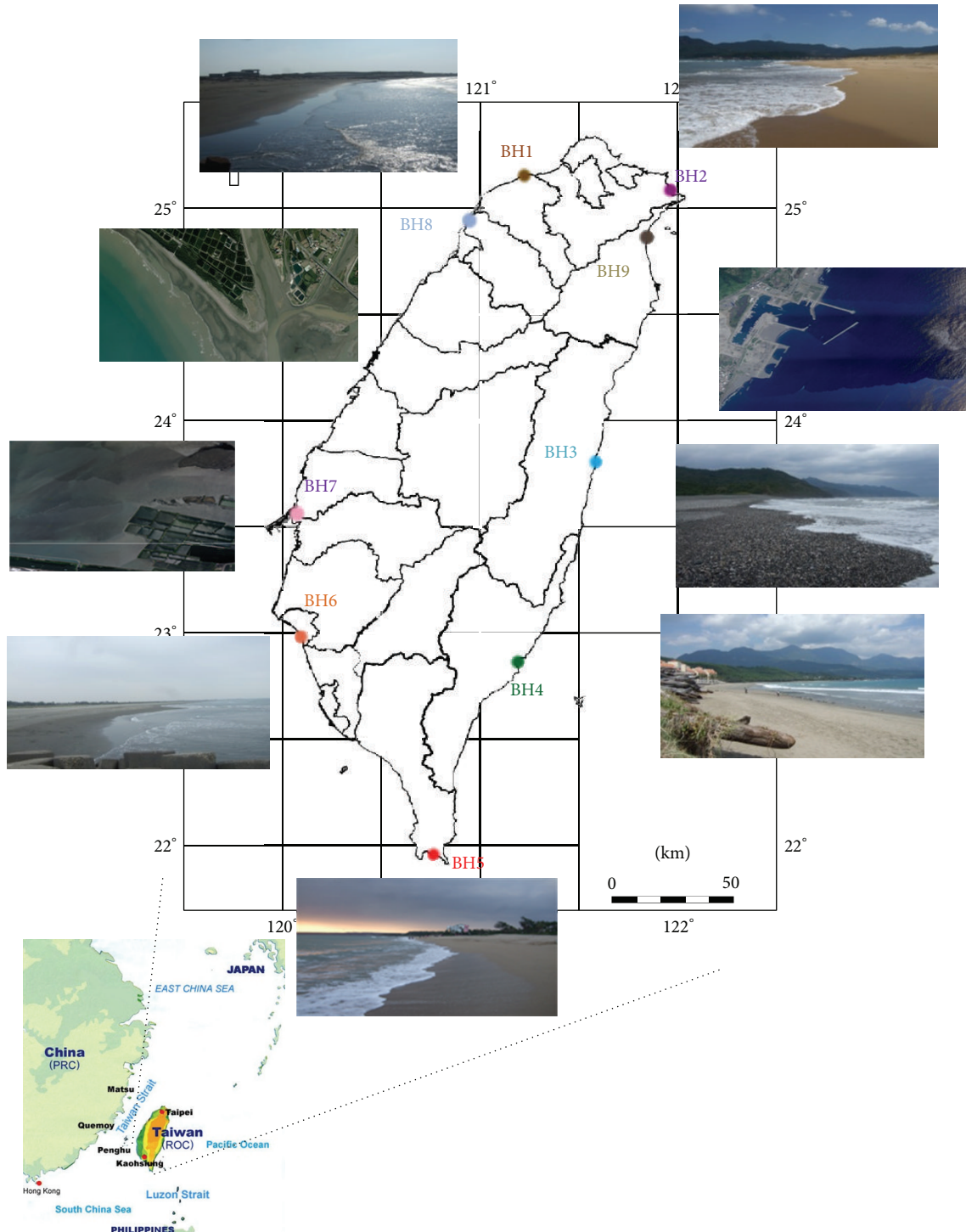


FIGURE 1: Location of research area and the chosen nine major beaches in the island of Taiwan (map source <http://www.unc.edu/depts/diplomat/item/2010/0912/comm/norris.quemoymatsu.html>).

coordinates of each beach were then ready for analysis by using the spread sheet software Excel.

By loading the image into AutoCAD, the range of the sand line could be drawn for each beach for each given year. The set-fold function was then used to determine the shoreline variation of each beach. The set-fold function is

not a mathematical equation but a computer technique for overlaying shorelines transparently. This method provides an easy way to compare the change of shorelines and to calculate the sandy areas in different years. Figure 2 shows an example (BH1) of six beaches that were investigated; the change of the sand region can be observed in the overlapping lines in

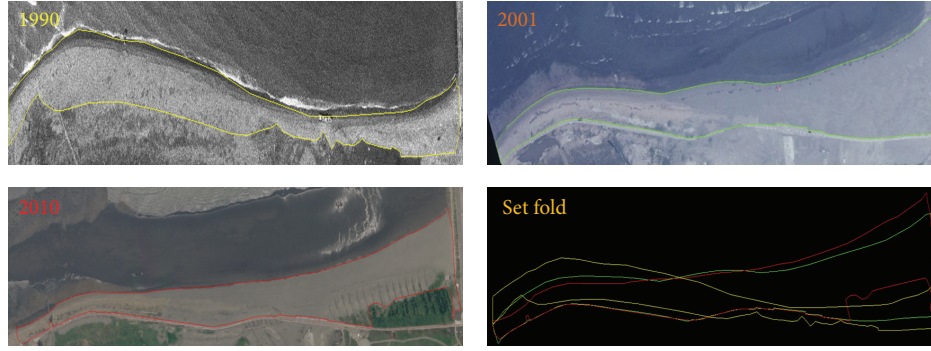
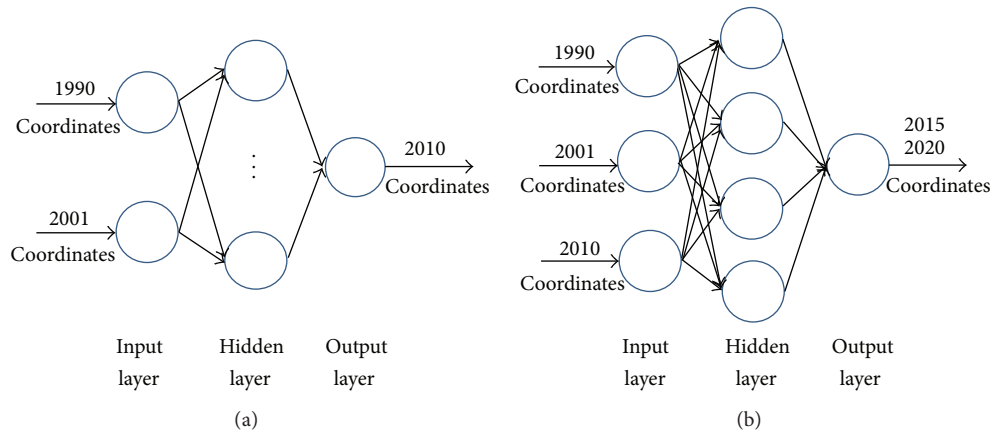


FIGURE 2: Variation of shoreline and sandy region for beach BH1 in multiperiod.

FIGURE 3: Structure of neural network models $I_2H_nO_1$ (left) and $I_3H_4O_1$ (right).

the figures. Based on this figure, the sandy areas of all of the beaches can also be calculated and compared with each other for the 3 given years.

3. Comparison of Neural Network Models

A neural network approach can be applied to solve various engineering problems, and a wide range of relevant literature [30–32] on the topic can be found. According to the theory of neural networks, the basic equation and evaluation index are briefly discussed in this paper. Regarding the multilayered neural network, the equation for each layer may be written as

$$Y_j = F\left(\sum W_{ij}X_i - \theta_j\right), \quad (1)$$

where Y_j is the output of neuron j , W_{ij} represents the connection weight from neuron i to neuron j , X_i is the input signal generated for neuron i , θ_j is the bias term associated with neuron j , and $F(x) = 1/(1 + e^{-x})$ is the commonly used nonlinear activation function.

The performance of a neural network model can generally be evaluated using the following two equations:

$$CC = \frac{\sum_{i=1}^m (x_i - \bar{x})(y_i - \bar{y})}{\sqrt{\sum_{i=1}^m (x_i - \bar{x})^2 \sum_{i=1}^m (y_i - \bar{y})^2}}, \quad (2)$$

$$RMSE = \sqrt{\sum_{n=1}^N \frac{(T_n - Y_n)^2}{N}},$$

where CC is the coefficient of correlation, x_i and \bar{x} are the recorded value and its average value, respectively, y_i and \bar{y} are the estimated value and its average value, respectively, and m denotes the number of data points in the analysis. In addition, RMSE is the root-mean-square error, N is the number of learning cases, T_n is the target value for case n , and Y_n is the output value for case n .

Figure 3 shows a diagram of the neural network models used in this study. The model on the left side uses coordinated information of the years 1990 and 2001 as the inputs and the coordinates of the year 2010 as the target values. Different numbers of neurons in the hidden layer are used to verify the performance of the neural network model based on the coefficient of correlation and root-mean-square error. Because these inputs and outputs are all known coordinates from survey maps, the test result may verify the ability of

TABLE 1: Performance (CC^2) of neural network models under different data arrangements.

NN model	$I_2H_2O_1$ (Type 1)			$I_2H_3O_1$ (Type 1)			$I_2H_4O_1$ (Type 1)		
	TN	VF	TS	TN	VF	TS	TN	VF	TS
Averaged CC^2	0.9786	0.9728	0.9723	0.9861	0.9771	0.9764	0.9864	0.9806	0.9803
NN model	$I_2H_2O_1$ (Type 2)			$I_2H_3O_1$ (Type 2)			$I_2H_4O_1$ (Type 2)		
	TN	VF	TS	TN	VF	TS	TN	VF	TS
Averaged CC^2	0.9760	0.9767	0.9750	0.9861	0.9901	0.9878	0.9873	0.9927	0.9831

TABLE 2: Calculated root-mean-square errors for each beach with the use of different models.

NN model (Type 1)	RMSE						Averaged RMSE
	BH1	BH2	BH3	BH4	BH5	BH6	
$I_2H_2O_1$	0.0101	0.0101	0.0867	0.0195	0.0163	0.0090	0.0253
$I_2H_3O_1$	0.0067	0.0039	0.0717	0.0155	0.0146	0.0056	0.0197
$I_2H_4O_1$	0.0062	0.0024	0.0703	0.0152	0.0108	0.0056	0.0184
NN model (Type 2)	RMSE						Averaged RMSE
	BH1	BH2	BH3	BH4	BH5	BH6	
$I_2H_2O_1$	0.0098	0.0097	0.0878	0.0215	0.0158	0.0060	0.0251
$I_2H_3O_1$	0.0065	0.0038	0.0678	0.0169	0.0145	0.0056	0.0192
$I_2H_4O_1$	0.0069	0.0023	0.0656	0.0159	0.0106	0.0056	0.0178

TABLE 3: Comparison of actual sandy area and estimated sandy area in the year of 2010.

2010 Beach	Actual sandy area (m^2)	$I_2H_4O_1$ (Type 1) Estimated area (m^2)	Type 1 error (%)	$I_2H_4O_1$ (Type 2) Estimated area (m^2)	Type 2 error (%)
BH1	31589	31471	0.373	31539	0.159
BH2	218476	218162	0.144	218118	0.163
BH3	99883	96311	3.577	99308	0.576
BH4	95079	96867	1.881	98657	3.763
BH5	69844	70855	1.447	69908	0.092
BH6	408235	407557	0.166	408042	0.047

the developed model, and a relatively more favourable result may be obtained for the beaches. The model on the right side, with four neurons in the hidden layer, is then observed for analysis, and an extension for including three input parameters is performed to predict the sand line of each beach in 2015 and 2020. The performance of neural network models and the prediction results are illustrated as in the following tables and figures.

For each beach, the original coordinates along the shoreline have 1,000 points, where 100 evenly distributed points were used for developing the neural network model. Two types of data sets—Type 1: 60%-30%-10% and Type 2: 70%-20%-10%, with coordinate data randomly divided into three groups—were used for training (TN), verification (VF), and testing (TS) the model, respectively. Table 1 displays the averaged square value of the correlation coefficient at different stages of calculation for the two types of data arrangement. It was found that all of the models can obtain a satisfactory performance because all CC^2 values are over 0.9, indicating a high relationship between actual data and neural network estimation. Note that the model with four neurons in the hidden layer, in the type of data arrangement where 70% is used for training, 20% for verification, and 10% for testing, achieves a relatively improved performance (slightly higher

CC^2 values) over that of the other models. Furthermore, based on the calculated root-mean-square errors shown in Table 2, the same model exhibits the smallest averaged RMSE, calculated at 0.0178. Therefore, this neural network model is preferable for the shoreline cases studied herein.

Table 3 shows a comparison of the performance of neural network models in the sandy areas of each beach. The numerical result indicated that the aforementioned, preferable model $I_2H_4O_1$ (Type 2) can obtain a more accurate result in most of the beach cases. The average percentage error for the six beaches is 0.800% for using data arrangement, 70% for training, 20% for verification, and 10% for testing the model (Type 2), which is an improvement over that of the percentage error of 1.265% for model $I_2H_4O_1$, which uses 60% for training, 30% for verification, and 10% for testing the Type 1 model. Therefore, this preferred neural network model was used for the shoreline prediction of each beach.

4. Prediction of Shoreline Variation and Onsite Investigation

The data in the previous section prove that using previous shoreline information (1990, 2001) in the neural network

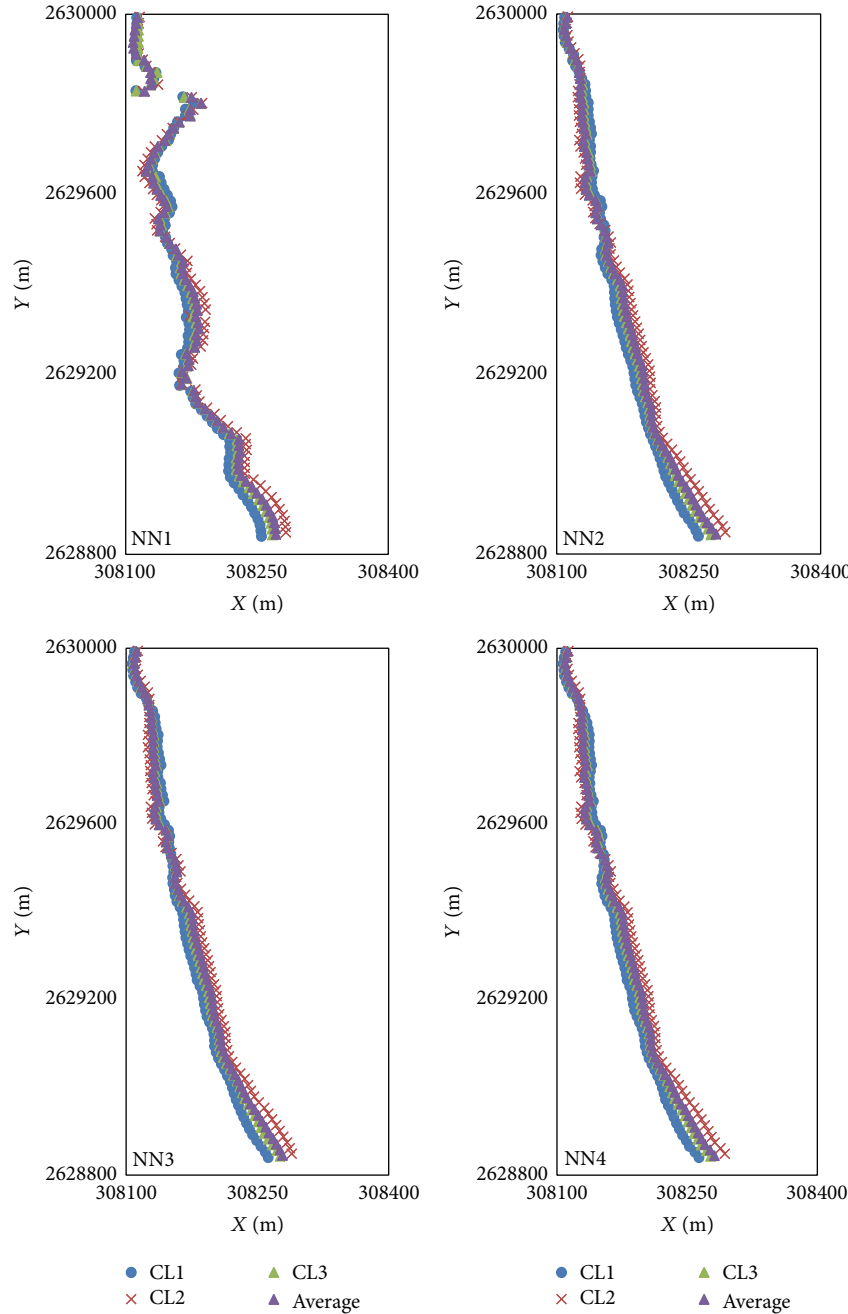


FIGURE 4: Comparison of neural network models for predicting beach BH3 in 2015.

model can accurately predict a future shoreline change (2010). For forecasting shoreline variation in the given future years (2015 and 2020), basic reference shoreline coordinates were required for developing a neural network model, by interpolating shoreline coordinates from previous years for the four models: NN1 (1990 and 2001); NN2 (2001 and 2010); NN3 (1990 and 2010); and NN4 (1990, 2001, and 2010). The coordinated differences (CL1, CL2, CL3, and the average) in shoreline of each beach from these years can help to yield reference data as well as developing a new neural network model for forecasting work.

To verify the newly developed neural network model, the model exhibiting the lowest performance, at BH3, is used as an example, and the comparative result is shown in Figure 4. The prediction results show that model NN1 demonstrated the worst performance, exhibiting a discontinuity at some points, whereas all of the other models exhibit a smooth prediction result. Model NN4 ($I_3H_4O_1$, see structure diagram in Figure 4), which uses information from 3 previous years, demonstrated slightly improved performance and more stability than the other models did. Therefore, this model was used for other beaches and for additional comparisons.

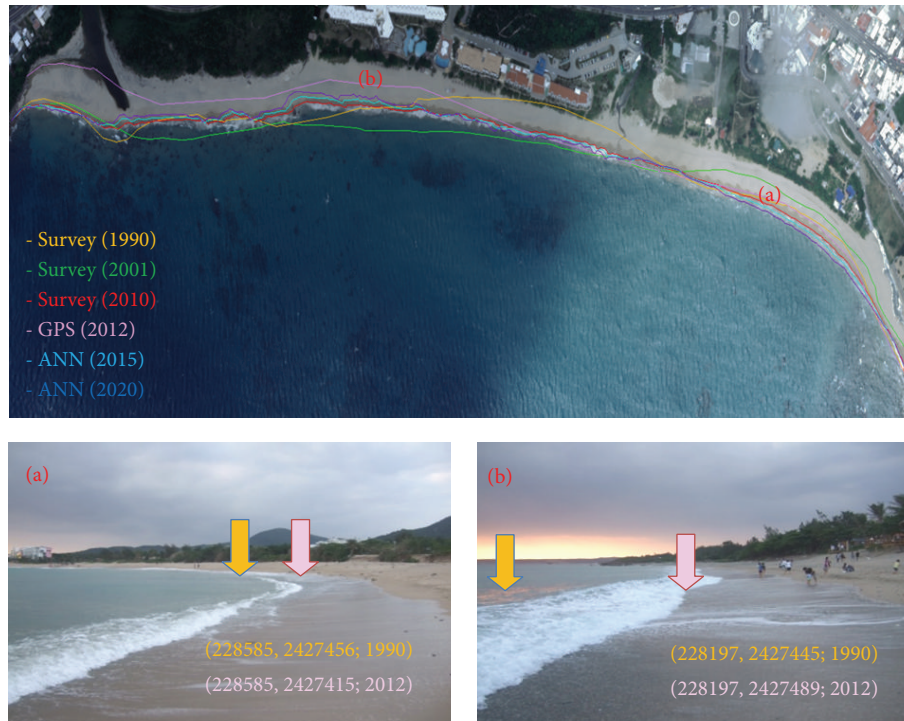


FIGURE 5: Shoreline change in different years and onsite beach condition for beach BH5.

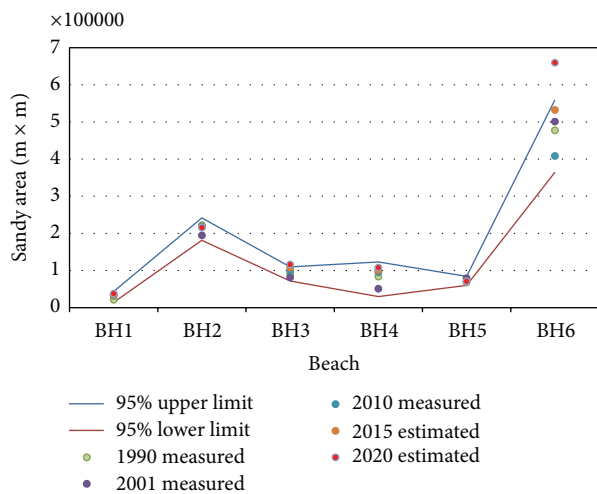


FIGURE 6: Total sandy area for each beach in different years.

For this study, observing the current shoreline condition for each beach was essential. An onsite assessment using a GPS receiver (GPSmap 60CSx manufactured by Garmin Corp.) was performed in 2012. An example of shoreline change according to year for each beach is shown in Figure 6. Based on the results for all six beaches, an accretion phenomenon is found in BH1; both erosion and accretion phenomena occurred in BH2, BH4, BH5, and BH6, whereas BH3 has a serious erosion problem during the studied period.

The shoreline for each beach may experience erosion or accretion at different local regions. Therefore, calculating the

total sandy area is essential for examining the change of the nonlinear coastline. Figure 6 shows that the total sandy area for the six beaches in each year is below a 95% confidence interval. All of the survey data (1990, 2001, and 2010) show that the total sandy areas are situated within the upper and lower limits; that is, there is no statistically significant change in sandy area for any beach (see Figure 5). However, including the future-predicted data (2015 and 2020) in the calculation involving neural network models reveals that at two beaches, BH3 and BH6, the total sandy area for the former may slightly exceed the limit, whereas the latter may significantly exceed the upper limit in 2020.

The results presented in this study may indicate that the erosion problem under current conditions is not acute in the beaches studied herein. However, the investigation period from 1990 to 2020 covers only 30 years. Presently, the effects of global warming and rising sea levels may still have influenced shoreline change in the Taiwan region; the shoreline must be monitored as often as possible to prevent negative impacts.

5. Conclusion

Natural disasters near coastline regions can include earthquake-induced tsunamis, typhoons, and flooding. These disasters may cause instantaneous damage to structures and may inflict harm to humans. Conversely, shoreline erosion problems are gradual, which may cause loss of land area and may endanger the existence of a country that comprises mostly islands that do not rise much above sea level. Therefore, examining shoreline change is worthwhile when considering both global warming and local concerns.

Three methods were used in this study to examine shoreline change problems on the island of Taiwan: (1) comparing the difference in the shorelines by using multiperiod survey maps; (2) developing a neural network model according to digitised coordinates for predicting possible variations; and (3) performing an onsite investigation by using a GPS receiver. Based on the beaches studied, the results show that sand erosion and accretion exist in some local regions of each beach, but the total sandy area of each beach has not significantly changed under a 95% statistical confidence interval. However, the prediction results show that two beaches have the potential to experience an increase in their sand areas in future years.

By avoiding complex procedures, this study used the most basic method possible to examine shoreline change problems. Therefore, only the factor of time (i.e., multiperiod aerial survey maps) was considered in the comparison analysis and model development. The reliability of the results obtained might be questionable, but other influencing events on shoreline change, such as wave motion, sea current, tide rise and fall, and land use in watersheds, all occur over time and, hence, should be included in the time factor. Therefore, this study provides a valuable reference for the examined region and may be applicable to other coastlines of interest worldwide.

Conflict of Interests

The authors declare that there is no conflict of interests regarding the publication of this paper.

Acknowledgments

Support from the National Science Council under Project no. NSC102-2221-E-020-027 is greatly appreciated. The Aerial Office, Forestry Bureau of Taiwan, is also acknowledged for providing the orthophoto images and aerial survey maps. Additionally, the editing work to improve the usage of English by Bill Thornton is acknowledged.

References

- [1] A. E. Carlson and K. Winsor, "Northern hemisphere ice-sheet responses to past climate warming," *Nature Geoscience*, vol. 5, pp. 607–613, 2012.
- [2] C. A. Thatcher, J. C. Brock, and E. A. Pendleton, "Economic vulnerability to sea-level rise along the Northern U.S. gulf coast," *Journal of Coastal Research*, vol. 63, pp. 234–243, 2013.
- [3] P. N. DiNezio and J. E. Tierney, "The effect of sea level on glacial indo-pacific climate," *Nature Geoscience*, vol. 6, pp. 485–491, 2013.
- [4] Y. F. Chiu, "Coastal erosion and protection strategy in Taiwan," *Civil Technology*, vol. 3, no. 3, pp. 102–110, 1999.
- [5] M. Y. Hsu, "A study on the coastal erosion and backward at east side of Taiwan," *Civil Technology*, vol. 2, no. 3, pp. 64–89, 1999.
- [6] P. Bruun, "Sea level rise as a cause of shore erosion," *Journal of Waterways and Harbors Division*, vol. 88, pp. 117–133, 1962.
- [7] D. L. Kriebel, *Beach Erosion Model (EBEACH) Users Manual: Theory and Background*, vol. 2, Division of Beaches and Shores, Florida Department of Natural Resources, Tallahassee, Fla, USA, 1984.
- [8] G. Masselink and A. D. Short, "The effect of tide range on beach morphodynamics and morphology: a conceptual beach model," *Journal of Coastal Research*, vol. 9, no. 3, pp. 785–800, 1993.
- [9] Ó. Ferreira, T. Garcia, A. Matias, R. Taborda, and J. A. Dias, "An integrated method for the determination of set-back lines for coastal erosion hazards on sandy shores," *Continental Shelf Research*, vol. 26, no. 9, pp. 1030–1044, 2006.
- [10] A. Jadidi, M. A. Mostafavi, Y. Bédard, B. Long, and E. Grenier, "Using geospatial business intelligence paradigm to design a multidimensional conceptual model for efficient coastal erosion risk assessment," *Journal of Coastal Conservation*, vol. 17, pp. 527–543, 2013.
- [11] D. L. Millar, H. C. M. Smith, and D. E. Reeve, "Modelling analysis of the sensitivity of Shoreline change to a wave farm," *Ocean Engineering*, vol. 34, no. 5-6, pp. 884–901, 2007.
- [12] T. M. Ravens, B. M. Jones, J. Zhang, C. D. Arp, and J. A. Schmutz, "Process-based coastal erosion modeling for drew point, North Slope, Alaska," *Journal of Waterway, Port, Coastal and Ocean Engineering*, vol. 138, no. 2, pp. 122–130, 2012.
- [13] J. O. Adegoke, M. Fageja, James, G. Agbaje G, and T. E. Ologunorisa, "An assessment of recent changes in the niger delta coastline using satellite imagery," *Journal of Sustainable Development*, vol. 3, no. 4, pp. 277–296, 2010.
- [14] A. A. Alesheikh, A. Ghorbanali, and N. Nouri, "Coastline change detection using remote sensing," *International Journal of Environmental Science and Technology*, vol. 4, no. 1, pp. 61–66, 2007.
- [15] F. A. Armah, "GIS-based assessment of short term Shoreline changes in the coastal erosion-sensitive zone of Accra, Ghana," *Journal of Environmental Sciences*, vol. 5, no. 7, pp. 643–654, 2011.
- [16] C. Fletcher, J. Rooney, M. Barbee, S.-C. Lim, and B. Richmond, "Mapping Shoreline change using digital orthophotogrammetry on Maui, Hawaii," *Journal of Coastal Research*, no. 38, pp. 106–124, 2003.
- [17] A. Guariglia, A. Buonamassa, A. Losurdo et al., "A multisource approach for coastline mapping and identification of Shoreline changes," *Annals of Geophysics*, vol. 49, no. 1, pp. 295–304, 2006.
- [18] H. W. Wang, C. T. Wang, K. S. Chen, and Y. L. Lin, "Analysis change detection waterline in West Taiwan using satellite SAR imagery," *Journal of Photogrammetry and Remote Sensing*, vol. 12, no. 2, pp. 107–119, 2007.
- [19] B. C. Douglas and M. Crowell, "Long-term Shoreline position prediction and error propagation," *Journal of Coastal Research*, vol. 16, no. 1, pp. 145–152, 2000.
- [20] M. S. Fenster, R. Dolan, and J. F. Elder, "A new method for predicting Shoreline positions from historical data," *Journal of Coastal Research*, vol. 9, no. 1, pp. 147–171, 1993.
- [21] R. M. Goncalves, J. L. Awange, C. P. Krueger, B. Heck, and L. S. Coelho, "A comparison between three short-term Shoreline prediction models," *Ocean and Coastal Management*, vol. 69, pp. 102–110, 2012.
- [22] H.-K. Chang and L.-C. Lin, "Multi-point tidal prediction using artificial neural network with tide-generating forces," *Coastal Engineering*, vol. 53, no. 10, pp. 857–864, 2006.
- [23] S. Karimi, O. Kisi, J. Shiri, and O. Makarynsky, "Neuro-fuzzy and neural network techniques for forecasting sea level in Darwin Harbor, Australia," *Computers and Geosciences*, vol. 52, pp. 50–59, 2013.

- [24] J. O. Pierini, M. Lovallo, L. Telesca, and A. Gómez, “Investigating prediction performance of an artificial neural network and a numerical model of the tidal signal at Puerto Belgrano, Bahia Blanca Estuary (Argentina),” *Acta Geophysica*, vol. 61, no. 6, pp. 1522–1537, 2013.
- [25] J. Rocha, J. C. Ferreira, J. Simões, and J. A. Tenedório, “Modelling coastal and land use evolution patterns through neural network and cellular automata integration,” *Journal of Coastal Research*, no. 50, pp. 827–831, 2007.
- [26] T. W. Ryan, P. J. Sementilli, P. Yuen, and B. R. Hunt, “Extraction of Shoreline features by neural nets and image processing,” *Photogrammetric Engineering & Remote Sensing*, vol. 57, no. 7, pp. 947–955, 1991.
- [27] T. Kerh, G. S. Hsu, and D. Gunaratnam, “Forecasting of nonlinear Shoreline variation based on aerial survey map by neural network approach,” *International Journal of Nonlinear Sciences and Numerical Simulation*, vol. 10, no. 9, pp. 1211–1221, 2009.
- [28] Wikipedia, “Orthophoto,” Wikimedia Foundation, 2013, <https://en.wikipedia.org/wiki/Orthophoto>.
- [29] L. F. Chen, L. G. Chen, and F. Yuen, *Transformation Design and Application of TWD97 Coordinate System*, Aerial Office, Forestry Bureau, 2002.
- [30] A. I. Galushkin, *Neural Networks Theory*, Springer, Berlin, Germany, 2007.
- [31] M. Y. Rafiq, G. Bugmann, and D. J. Easterbrook, “Neural network design for engineering applications,” *Computers and Structures*, vol. 79, no. 17, pp. 1541–1552, 2001.
- [32] Y. C. Yeh, *Application and Practice of Neural Networks*, Rulin Publishing Company, 2009.

Research Article

Stability Analysis of Pulse-Width-Modulated Feedback Systems with Time-Varying Delays

Zhong Zhang, Huahui Han, Qiling Zhao, and Lixia Ye

College of Mathematics and Statistics, Chongqing University, Chongqing 400044, China

Correspondence should be addressed to Zhong Zhang; zhanguicqu@gmail.com

Received 3 January 2014; Revised 26 March 2014; Accepted 7 April 2014; Published 27 April 2014

Academic Editor: Chuandong Li

Copyright © 2014 Zhong Zhang et al. This is an open access article distributed under the Creative Commons Attribution License, which permits unrestricted use, distribution, and reproduction in any medium, provided the original work is properly cited.

The stability problem of pulse-width-modulated feedback systems with time-varying delays and stochastic perturbations is studied. With the help of an improved functional construction method, we establish a new Lyapunov-Krasovskii functional and derive several stability criteria about p th moment exponential stability.

1. Introduction

PWM has been widely used in many fields, such as attitude control systems, adaptive control systems, signal processing, and modeling of neuron behavior [1–3]. In actual progress, it has always operated in all kinds of disturbances. At the same time, time-varying delays inevitably occur owing to the unavoidable finite switching speed of amplifiers. For some systems, the effect of time-varying delays can be ignored. How to keep the scheduled operation or work of the state running well, especially in engineering applications, is becoming more and more significant.

A growing number of scholars are devoting time to the PWM feedback systems; meanwhile a set of stability results has been established by a variety of methods [4–12]. Also, lots of scholars have researched some systems with delays [7, 13–19]. In [15], the authors investigated robust exponential stability and delayed-state-feedback stabilization of uncertain impulsive stochastic systems with time-varying delays. Sun and Cao [16] gave some definitions on the p th moment exponential stability in mean and established several p th moment globally stability criteria in mean. By using the Lyapunov technique and Razumikhin method, the authors in [17] investigated impulsive effects on stability analysis of high-order BAM neural networks with time delays. And in [18], they established the global exponential stability of the neural networks with its estimated exponential convergence

rate. The authors in [19] gave a time-varying delay-dependent criterion for impulsive synchronization to ensure the delayed discrete complex networks switching topology tending to a synchronous state.

To the best of the author's knowledge, there are a few (if any) results for the stability analysis of the critical case of PWM systems with time-varying delays and stochastic perturbations, most of the existing work only considers one condition [7, 8, 15]. In the present paper, we try to make a contribution to this issue. It is noted that the linear plant in this paper has one and only one pole at origin, and the rest of the poles are in the left side of the complex plane, which is more representative and more universal. Based on the references [7, 13], the present paper will further study the stability of PWM feedback systems with time-varying delays and establish several new stability criteria. In Section 2, we give some definitions and lemmas. In Section 3, firstly, a criterion on mean square exponential stability of stochastic feedback systems with time-varying delays is given. Secondly, by introducing new variables, we will establish a new Lyapunov-Krasovskii functional with the help of an improved functional construction method. Then, associating with linear matrix inequalities, we will establish criteria for the p th moment exponential stability and the p th moment exponential asymptotic stability. Finally, we demonstrate the applicability of our results by means of an example.

2. Notations and Definitions

A pulse-width modulator is described by

$$u(t) = m(e(t)) = \begin{cases} M \operatorname{sgn}(e(kT)), & t \in [kT, kT + T_k), \\ 0, & t \in [kT + T_k, kT + T), \end{cases} \quad (1)$$

with

$$T_k = \begin{cases} \beta |e(kT)|, & |e(kT)| \leq \frac{T}{\beta}, \\ 0, & |e(kT)| > \frac{T}{\beta}, \end{cases} \quad (2)$$

where $e(t) = r(t) - f(t)$, $r(t)$ is the external input and $f(t)$ is the system output and T_k is the pulse-width for $k = 0, 1, 2, \dots$. The sampling period T , the amplitude of the pulse M , and β are all assumed to be constants.

Consider the following stochastic PWM feedback system with time-varying delays:

$$\begin{aligned} dx(t) &= Ax(t)dt + A_d x(t-d)dt + Hu(t)dt \\ &\quad + D\vartheta(t, x(t), x(t-d))dW_t, \\ z(t) &= C_1 x(t) + C_2 x(t-d), \end{aligned} \quad (3)$$

where $x \in R^n$, $u, \vartheta \in R$, u is the output of the pulse-width modulator, ϑ is the nonlinear stochastic perturbations, A, A_d, H, D are the matrices of appropriate dimensions, H is the pulse-width control matrix, $0 < d \leq T_k$, and W_t is a scalar wiener process which is defined on the probability space (Ω, F, P) .

Note that $x_e = 0$ is an equilibrium point of stochastic PWM feedback systems.

Definition 1. Let (X, d) be a metric space, $X \subset R^n$, $A \subset X$, and $T \subset R^+$. For any fixed $a \in A$ (a is called the initial state), $t_0 \in T$, a stochastic process $\{x(t, \omega, a, t_0), t \in T_{a, t_0}\}$ with domain X is called a stochastic motion if $x(t_0, \omega, a, t_0) = a$ for all $\omega \in \Omega$, where $T_{a, t_0} = [t_0, t_1) \cap T$, $t_1 > t_0$, and t_1 is finite or infinite.

Definition 2. Let S be a family of stochastic motions with domain X given by

$$S \subset \{x(\cdot, \cdot, a, t_0) : x(t_0, \omega, a, t_0) = a, \omega \in \Omega, a \in A, t_0 \in T\}. \quad (4)$$

We call the four-tuple $\{T, X, A, S\}$ a stochastic dynamical system.

Definition 3 (see [20, 21]). For any fixed functional V , the infinitesimal generation operator $\mathcal{L}V(x(t), t)$ is

$$\begin{aligned} \mathcal{L}V(x(t), t) \\ = \lim_{\Delta \rightarrow 0^+} \frac{1}{\Delta} [E(V(x(t+\Delta), t+\Delta) - V(x(t), t))] \end{aligned} \quad (5)$$

Definition 4 (see [20, 21]). A stochastic system is p th moment exponential stability. If for any fixed initial condition, there exist $\alpha > 0$ and $\beta \geq 1$, then

$$E\|x(t)\|^p \leq \beta \exp(-\alpha t) \sup_{-d \leq \theta \leq 0} E\|\xi(\theta)\|^p, \quad \forall t \geq 0. \quad (6)$$

Especially, when $p = 2$, we called the system mean square exponential stability.

Definition 5 (see [20, 21]). A stochastic system is p th moment exponential asymptotic stability. If for any fixed initial condition, then

$$\lim_{t \rightarrow \infty} E\|x(t)\|^p = 0. \quad (7)$$

Especially, when $p = 2$, we called the system mean square exponential asymptotic stability.

Lemma 6 (see [20, 21]). A stochastic system $u(t) = Fy(t)$ is mean square stability if there exists a Lyapunov-Krasovskii functional $V(x(t), t) > 0$ and its infinitesimal generation operator satisfies $\mathcal{L}V(x(t), t) < 0$.

Lemma 7 (see [14]). For any constant matrix $M \in R^{m \times m}$, $M = M^T > 0$, scalar $\gamma > 0$, and vector function $\omega : [0, \gamma] \rightarrow R^m$, the integrations in the following are well defined; then

$$\gamma \int_0^\gamma \omega^T(\beta) M \omega(\beta) d\beta \geq \left(\int_0^\gamma \omega(\beta) d\beta \right)^T M \left(\int_0^\gamma \omega(\beta) d\beta \right). \quad (8)$$

Lemma 8(a) (see [22] (Schur complement 1)). Given the Hermite matrix $S = \begin{pmatrix} S_{11} & S_{12} \\ S_{12}^T & S_{22} \end{pmatrix}$, then $S < 0$ is equivalent to any one of the following conditions:

- (1) $S_{11} < 0, S_{22} - S_{12}^T S_{11}^{-1} S_{12} < 0$,
- (2) $S_{22} < 0, S_{11} - S_{12} S_{22}^{-1} S_{12}^T < 0$.

Lemma 8(b) (see [23, 24] (Schur complement 2)). Assuming that $A = \begin{pmatrix} A_{11} & A_{12} \\ A_{12}^T & A_{22} \end{pmatrix}$ is a Hermite matrix, then

- (1) $A > 0 \Leftrightarrow A_{11} > 0, A_{22} - A_{12}^T A_{11}^{-1} A_{12} > 0$,
- (2) If $A_{11} > 0$, then $A \geq 0 \Leftrightarrow A_{22} - A_{12}^T A_{11}^{-1} A_{12} \geq 0$.

Lemma 9 (see [25] (Gronwall inequality)). If $x(t) \leq h(t) + \int_{t_0}^t k(s)x(s)ds$, $t \in [t_0, T)$, where all the functions involved are continuous on $[t_0, T)$, $T \leq +\infty$, and $k(t) \geq 0$, then $x(t)$ satisfies

$$x(t) \leq h(t) + \int_{t_0}^t h(s) k(s) \exp \left[\int_s^t k(u) du \right] ds \quad (9)$$

$$t \in [t_0, T).$$

If, in addition, $h(t)$ is nondecreasing, then

$$x(t) \leq h(t) \exp \left(\int_{t_0}^t k(s) ds \right), \quad t \in [t_0, T). \quad (10)$$

3. Stability Analysis

The block diagram of the PWM feedback system (3) is shown in Figure 1.

Now, consider the following stochastic feedback system with time-varying delays:

$$\begin{aligned} dx(t) = & Ax(t)dt + A_d x(t-d)dt + Bp(t)dt \\ & + g(t, x(t), x(t-d))dW_t, \end{aligned} \quad (11)$$

where $x \in \mathbb{R}^n$, $p(t)$ is a function of $x(t), x(t-d)$, g is the nonlinear stochastic perturbations, A, A_d, B are matrices of appropriate dimensions, $0 < d \leq T_k$, and W_t is a scalar wiener process which is defined on the probability space (Ω, F, P) .

For system (11), we let

$$g(t) \triangleq g(t, x(t), x(t-d)), \quad (12)$$

which satisfies that

$$\text{tr} [g^T(t)g(t)] \leq \|G_1(x(t))\|^2 + \|G_2(x(t-d))\|^2, \quad (13)$$

where G_1, G_2 are constant matrices of appropriate dimensions.

We construct the Lyapunov-Krasovskii functional as follows:

$$V(x(t), t) = \sum_{i=1}^5 V_i(x(t), t), \quad (14)$$

with

$$\begin{aligned} V_1(x(t), t) &= x^T(t)Px(t), \\ V_2(x(t), t) &= \int_{t-d}^t x^T(s)R_1x(s)ds, \\ V_3(x(t), t) &= \int_{t-d}^t \int_s^t x^T(\gamma)R_2x(\gamma)d\gamma ds, \\ V_4(x(t), t) &= 2x^T(t)Z \int_{t-d}^t x(s)ds, \\ V_5(x(t), t) &= \int_{-d}^0 \int_{-d}^0 x^T(t)Qx(t+\zeta)d\zeta ds. \end{aligned} \quad (15)$$

Denoting the parameter set as $\Phi := \{P, R_1, R_2, Z, Q\}$, P, R_1, R_2, Z, Q are Hermite matrices of appropriate dimensions.

Proposition 10 (see [13]). *Lyapunov-Krasovskii functional (14) is positive definite if the parameter set Φ satisfies*

$$R_1 > 0, \quad R_2 > 0, \quad \begin{bmatrix} P & Z \\ Z^T & d^{-1}R_1 + Q \end{bmatrix} > 0. \quad (16)$$

Theorem 11 (see [13]). *For a fixed scalar $d > 0$, the stochastic system (11) with time-varying delays is mean square exponential stability if there exist scalars $\rho > 0, \varepsilon > 0$, and*

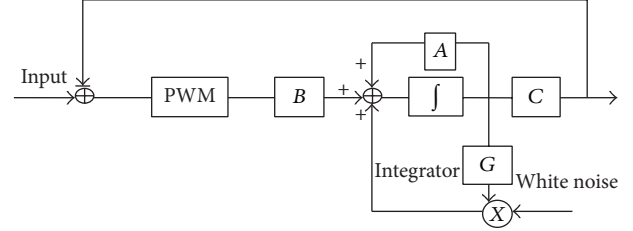


FIGURE 1: Block diagram of PWM feedback systems subjected to multiplicative disturbances.

the parameter set Φ satisfies Proposition 10, then there exists a linear matrix inequality

$$\Theta = \begin{bmatrix} \Theta_{11} & PA_d - Z + \varepsilon E_1^T E_2 & dA^T Z + dQ & PB \\ * & -R_1 + \rho G_2^T G_2 + \varepsilon E_2^T E_2 & dA_d^T Z - dQ & 0 \\ * & * & -h^{-1}R_2 & dZ^T B \\ * & * & * & -\varepsilon I \end{bmatrix} < 0, \quad (17)$$

where $P \leq \rho I$:

$$\begin{aligned} \Theta_{11} = & PA + A^T P + R_1 + dR_2 + Z + Z^T \\ & + \varepsilon E_1^T E_1 + \rho G_1^T G_1. \end{aligned} \quad (18)$$

From [13], one obtains that, for $t > 0$,

$$E\|x(t)\|^2 \leq \frac{\lambda_{\max}(P) + \Delta}{\lambda_{\min}(P)} \sup_{-d \leq \theta \leq 0} E\|\xi(\theta)\|^2 \exp\left(-\frac{\mu t}{\lambda_{\min}(P)}\right), \quad (19)$$

where $\Delta = \lambda_{\max}(Z^T Z) + d + \lambda_{\max}(R_1) + d\lambda_{\max}(R_2) + d\lambda_{\max}(Q)$.

Now, let us consider the stochastic PWM feedback system (3) with time-varying delays (Figure 2). After variable substitution, system (3) can be represented as

$$\begin{aligned} dx(t) &= Ax(t)dt + A_d x(t-d)dt + u'(t)dt + g'(t)dW_t, \\ u'(t) &= Hu(t), \\ g'(t) &= G\vartheta(t, x(t), x(t-d)), \\ z(t) &= C_1 x(t) + C_2 x(t-d). \end{aligned} \quad (20)$$

Note that in system (20),

$$\|u'(t)\| \leq \left\| MH \sum_{k=1}^n \text{sgn}(e(kt)) \right\| \leq M \|\lambda H\|, \quad (21)$$

$$-n \leq \lambda \leq n,$$

where n is the amount of the PWM period.

By choosing appropriate PWM, we can get $0 \leq \lambda \leq \varepsilon$. Then

$$\|u'(t)\| \leq \lambda M \|H\|. \quad (22)$$

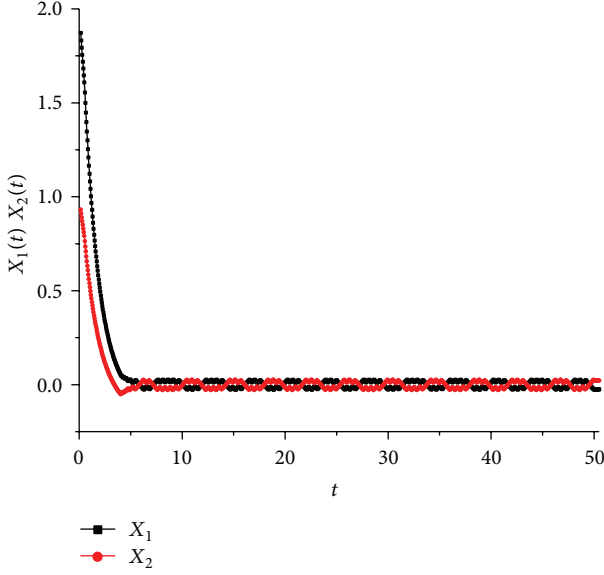


FIGURE 2: Sample response of system (3) with time-varying delays in Example 1 when $M = 0.3$.

Associating with (13), we also assume that the stochastic perturbations $g'(t)$ satisfy

$$\text{tr} [g'^T(t) g'(t)] \leq \|DG_1(x(t))\|^2 + \|DG_2(x(t-d))\|^2. \quad (23)$$

where $P \leq \rho I$, $\Psi_{11} = PA + A^T P + R + Z + Z^T + \lambda^2 \varepsilon M^2 H^T H + \rho D^T G_1^T G_1 D$.

Proof. Using the Itô isometry, we get infinitesimal generation operators of functional (20). Consider

$$\begin{aligned} \mathcal{L}V_1(y(t), t) &= \lim_{\Delta \rightarrow 0^+} \frac{1}{\Delta} [E(V_1(y(t+\Delta), t+\Delta) - V_1(y(t), t))] \\ &= 2y^T(t) P [Ay(t) + A_d y(t-d) + u'(t)] \\ &\quad + \text{Trace} [G^T W^T(t) P W(t) G] \\ &\leq 2y^T(t) P [Ay(t) + A_d y(t-d) + u'(t)] \\ &\quad + \|GW_1(y(t))\|^2 + \|GW_2(y(t))\|^2, \\ \mathcal{L}V_2(y(t), t) &= y^T(t) Ry(t) - y^T(t-d) Ry(t-d), \end{aligned}$$

By simplifying functional (14), we get a new Lyapunov-Krasovskii functional

$$V(y(t), t) = \sum_{i=1}^4 V_i(y(t), t), \quad (24)$$

with

$$\begin{aligned} V_1(y(t), t) &= y^T(t) P y(t), \\ V_2(y(t), t) &= \int_{t-d}^t y^T(s) R y(s) ds, \\ V_3(y(t), t) &= 2y^T(t) Z \int_{t-d}^t y(s) ds, \\ V_4(y(t), t) &= \int_{-d}^0 \int_{-d}^0 y^T(t) Q y(t+\zeta) d\zeta ds. \end{aligned} \quad (25)$$

Denoting the parameter set as $\Phi_1 := \{P, R, Z, Q\}$, $R > 0$, $y(t) = x^{p/2}(t)$, $p \in N_+$, P, R, Z, Q are Hermite matrices of appropriate dimensions.

Let functional (24) satisfy Proposition 10, then it is positive definite.

Theorem 12. For time-varying delay $d > 0$, the stochastic PWM feedback system (3) with time-varying delays is p th moment exponential stability if there exist scalars $\rho > 0$, $\varepsilon > 0$, and the parameter set Φ_1 and if the following linear matrix inequality holds:

$$\Psi = \begin{bmatrix} \Psi_{11} & PA_d - Z & dA^T Z + dQ & P \\ * & -R + \rho D^T G_2^T G_2 D + \lambda^2 \varepsilon M^2 H^T H & dA_d^T Z - dQ & 0 \\ * & * & 0 & dZ^T \\ * & * & * & -\varepsilon I \end{bmatrix} < 0, \quad (26)$$

$$\mathcal{L}V_3(y(t), t) = 2[Ay(t) + A_d y(t-d) + u'(t)]^T$$

$$\begin{aligned} &\times Z \int_{t-d}^t y(s) ds \\ &+ 2y^T(t) Z [y(t) - y(t-d)], \end{aligned}$$

$$\begin{aligned} \mathcal{L}V_4(y(t), t) &= 2y^T(t) Q \int_{t-d}^t y(s) ds \\ &+ 2y^T(t-d) Q \int_{t-d}^t y(s) ds. \end{aligned} \quad (27)$$

Based on (22), we can get $\lambda^2 \varepsilon M^2 H^T H - \varepsilon u'^T u' \geq 0$. Then

$$\begin{aligned} \mathcal{L}V(y(t), t) &= \sum_{i=1}^4 \mathcal{L}V_i(y(t), t) \\ &\leq \frac{1}{d} \int_{t-d}^t \eta^T(t, s) \Psi \eta(t, s) ds, \end{aligned} \quad (28)$$

where $\eta^T(t, s) = [y^T(t) \ y^T(t-d) \ y^T(s) \ u^T(t)]$. Consider

$$\mathcal{L}V(y(t), t) < 0 \quad \text{if } \Psi \text{ satisfies } \Psi < 0. \quad (29)$$

By Schur complement 1, there exists a scalar $\mu > 0$, which makes

$$\mathcal{L}V(y(t), t) \leq -\mu \|y(t)\|^2. \quad (30)$$

Then, by Dynkin formula, one observes that

$$\begin{aligned} EV(y(t), t) &= EV(y(0), 0) + E \int_0^t \mathcal{L}V(y(s), s) ds, \\ V_2(y(t), t) &\leq \lambda_{\max}(R) \int_{-d}^0 \|y(t+\theta)\|^2 d\theta, \\ V_3(y(t), t) &\leq \lambda_{\max}(Z^T Z) \|y(t)\|^2 + d \int_{-d}^0 \|y(t+\theta)\|^2 d\theta, \\ V_4(y(t), t) &\leq d \lambda_{\max}(Q) \int_{-d}^0 \|y(t+\theta)\|^2 d\theta. \end{aligned} \quad (31)$$

Then

$$\begin{aligned} EV(y(0), 0) &\leq (\lambda_{\max}(P) + \nabla) \sup_{-d \leq \theta \leq 0} E\|\xi(\theta)\|^2, \\ EV(y(t), t) &\geq \lambda_{\min}(P) E\|y(t)\|^2, \\ \nabla &= \lambda_{\max}(Z^T Z) + d + \lambda_{\max}(R) + d \lambda_{\max}(Q). \end{aligned} \quad (32)$$

Thus, by Lemma 9 (Gronwall inequality), we have that

$$\begin{aligned} E\|y(t)\|^2 &= E\|x(t)^{p/2}\|^2 \\ &= E\|x(t)\|^p \leq \frac{\lambda_{\max}(P) + \nabla}{\lambda_{\min}(P)} \\ &\quad \times \sup_{-d \leq \theta \leq 0} E\|\xi(\theta)\|^2 \exp\left(-\frac{\mu t}{\lambda_{\min}(P)}\right), \\ E\|x(t)\|^p &\leq \frac{\lambda_{\max}(P) + \nabla}{\lambda_{\min}(P)} \\ &\quad \times \sup_{-d \leq \theta \leq 0} E\|\zeta(\theta)\|^p \exp\left(-\frac{\mu t}{\lambda_{\min}(P)}\right), \\ \zeta(\theta) &= (\xi(\theta))^{p/2}. \end{aligned} \quad (33)$$

Associating with Definition 4, we know that the system (3) is p th moment exponential stability. \square

Corollary 13. A stochastic PWM feedback system with time-varying delays which satisfies the conditions of Theorem 12 is p th moment exponential asymptotic stability.

Proof. From the above proof, we obtain

$$E\|x(t)\|^p \leq \frac{\lambda_{\max}(P) + \nabla}{\lambda_{\min}(P)} \sup_{-d \leq \theta \leq 0} E\|\zeta(\theta)\|^p \exp\left(-\frac{\mu t}{\lambda_{\min}(P)}\right), \quad (34)$$

where $\lambda_{\max}(p)$, $\lambda_{\min}(p)$, ∇ , $\sup E\|\zeta(\theta)\|^p$, μ are all constants.

Similarly,

$$\begin{aligned} E\|x(t)\|^p &\leq K_1 K_2 \exp(-K_3 t), \\ \text{where } K_1, K_2, K_3 &\text{ are constants.} \end{aligned} \quad (35)$$

Then, we have

$$\lim_{t \rightarrow \infty} E\|x(t)\|^p \leq \lim_{t \rightarrow \infty} K_1 K_2 \exp(-K_3 t) = 0. \quad (36)$$

By Definition 5, the system (3) is p th moment exponential asymptotic stability.

Then, we discuss the functional (24) based on its parameter set.

As the parameter set satisfies $R > 0$, $\begin{bmatrix} P & Z \\ Z^T & d^{-1}R + Q \end{bmatrix} > 0$, by Schur complement 2, we observe that

$$P > 0, \quad d^{-1}R + Q - Z^T P^{-1} Z > 0. \quad (37)$$

Then we can obtain an estimate about matrix P , such that

$$P > 0 \cap P < (Z^T)^{-1} (d^{-1}R + Q) Z^{-1}. \quad (38)$$

\square

Remark 14. For system (3), only H can be controlled easily in reality. So we may let $P = H$ and H satisfies formula (38). Then we get another corollary which can be applied in reality.

Corollary 15. For time-varying delay $d > 0$, the system (3) is p th moment exponential stability and p th moment exponential asymptotic stability if there exist scalars $\rho > 0$, $\varepsilon > 0$, and the parameter set Φ_1 such that the following linear matrix inequality holds:

$$\Psi = \begin{bmatrix} \Psi_{11} & HA_d - Z & dA^T Z + dQ & H \\ * & -R + \rho D^T G_2^T G_2 D + \lambda^2 \varepsilon M^2 H^T H & dA_d^T Z - dQ & 0 \\ * & * & 0 & dZ^T \\ * & * & * & -\varepsilon I \end{bmatrix} < 0, \quad (39)$$

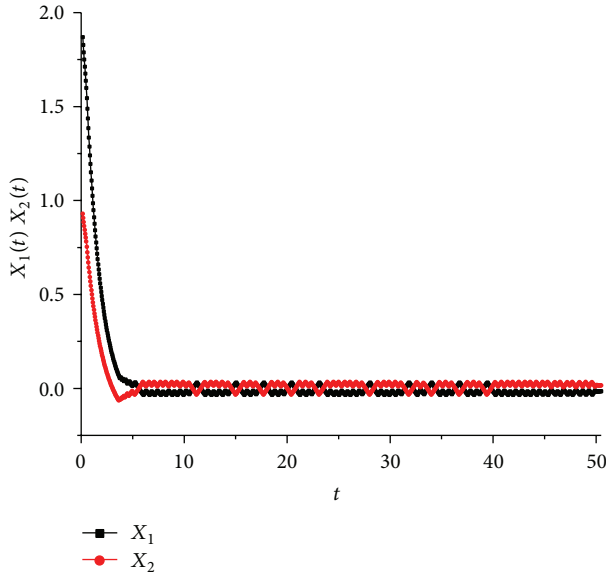


FIGURE 3: Sample response of system (3) with time-varying delays in Example 1 when $M = 0.4$.

where $H \leq \rho I$, $\Psi_{11} = HA + A^T H + R + Z + Z^T + \lambda^2 \varepsilon M^2 H^T H + \rho D^T G_1^T G_1 D$ (Figure 3).

4. Example

Example 1. Consider the system (3). Letting $A = \begin{bmatrix} -2 & 0 \\ 0 & -1 \end{bmatrix}$, $A_d = \begin{bmatrix} -1 & 0 \\ 0 & -1 \end{bmatrix}$, $H = I$, the amplitude of the PWM $M = 0.3$, the sampling period $T = 1$, and the constant $\beta = 1$, the perturbations satisfy $g'(t) = \begin{bmatrix} 0.02 & 0 \\ 0 & 0.01 \end{bmatrix}$.

We assume the time accuracy is 0.01 seconds and the system has a tenfold lag; that is, $d = 0.1$. And also at the system initial, there is no 0.1 second lag, while it has a 0.1 second lag at system shutdown. The perturbations function on the whole process. For initial-value $x(0) = (2, 1)^T$, we observe that the system (3) is stable.

By modulating the pulse-width control matrix H , we set $M = 0.4$. Then, we can get better result of the system (3).

5. Conclusions

In this paper, we studied the stochastic PWM feedback systems with time-varying delays and stochastic perturbations. Then, several criteria are established by employing the linear matrix inequality (LMI). Based on the result, an example is presented, which illustrates the effectiveness of the new criteria.

Conflict of Interests

The authors declare that there is no conflict of interests regarding the publication of this paper.

Acknowledgment

This paper is supported by the National Natural Science Foundation of China (Grant no. 11202249).

References

- [1] I. Takahashi and H. Mochikawa, "A new control of PWM inverter wave form for minimum loss operation of an induction motor drive," *IEEE Transactions on Industry Applications*, vol. 21, no. 3, pp. 580–587, 1985.
- [2] G. Heinle, "The structure of optimized pulse patterns," in *Proceedings of the 5th European Conference on power Electronics and Applications (EPE '93)*, pp. 378–383, Brighton, UK, 1993.
- [3] J. Holtz, "Pulsewidth modulation—a survey," *IEEE Transactions on Industrial Electronics*, vol. 39, no. 5, pp. 410–420, 1992.
- [4] A. Halanai, "Positive definite kernels and the stability of automatic systems," *Revue Roumaine de Mathématiques Pures et Appliquées*, vol. 9, pp. 751–765, 1964 (Russian).
- [5] R. A. Skoog, "on the stability of pulse width modulated feedback systems," *IEEE Transactions on Automatic Control*, vol. 13, no. 5, pp. 532–538, 1968.
- [6] V. M. Kuntsevich and Y. N. Chekhovoi, *Nonlinear Systems with Pulse Frequency and Pulse Width Modulation*, Tekhnika, Kiev, Ukraine, 1970.
- [7] Z. Zhang and L. Ye, "pth moment exponential stability of stochastic PWM feedback systems with time-varying delays," *Abstract and Applied Analysis*, vol. 2012, Article ID 796104, 19 pages, 2012.
- [8] Z. Zhang and L. Ye, "Moment stability of the critical case of PWM feedback systems with stochastic perturbations," *Abstract and Applied Analysis*, vol. 2012, Article ID 736408, 19 pages, 2012.
- [9] J.-C. Bor and C.-Y. Wu, "Realization of the CMOS pulsewidth-modulation (PWM) neural network with on-chip learning," *IEEE Transactions on Circuits and Systems II: Analog and Digital Signal Processing*, vol. 45, no. 1, pp. 96–107, 1998.
- [10] L. Hou and A. N. Michel, "Stability analysis of pulse-width-modulated feedback systems," *Automatica*, vol. 37, no. 9, pp. 1335–1349, 2001.
- [11] L. Hou, *Qualitative analysis of discontinuous deterministic and stochastic dynamical systems [Ph.D. thesis]*, University of Notre Dame, 2000.
- [12] L. Liu, Y. Shen, and F. Jiang, "The almost sure asymptotic stability and pth moment asymptotic stability of nonlinear stochastic differential systems with polynomial growth," *IEEE Transactions on Automatic Control*, vol. 56, no. 8, pp. 1985–1990, 2011.
- [13] W. Qian, *Some issues of systems with time-varying delays [Ph.D. thesis]*, Zhejiang University, 2009.
- [14] K. Gu, "An integral inequality in the stability problem of time-delay systems," in *Proceedings of the IEEE Conference on Decision and Control*, pp. 2805–2810, Sydney, Australia, 2000.
- [15] P. Cheng, F. Deng, and Y. Peng, "Robust exponential stability and delayed-state-feedback stabilization of uncertain impulsive stochastic systems with time-varying delay," *Communications in Nonlinear Science and Numerical Simulation*, vol. 17, no. 12, pp. 4740–4752, 2012.
- [16] Y. Sun and J. Cao, "pth moment exponential stability of stochastic recurrent neural networks with time-varying delays," *Nonlinear Analysis: Real World Applications*, vol. 8, no. 4, pp. 1171–1185, 2007.

- [17] C. Li, C. Li, X. Liao, and T. Huang, "Impulsive effects on stability of high-order BAM neural networks with time delays," *Neurocomputing*, vol. 74, no. 10, pp. 1541–1550, 2011.
- [18] C. Li, C. Li, and T. Huang, "Exponential stability of impulsive high-order Hopfield-type neural networks with delays and reaction-diffusion," *International Journal of Computer Mathematics*, vol. 88, no. 15, pp. 3150–3162, 2011.
- [19] C. Li, D. Y. Gao, C. Liu, and C. Guo, "Impulsive control for synchronizing delayed discrete complex networks with switching topology," *Neural Computing and Applications*, vol. 24, no. 1, pp. 59–68, 2014.
- [20] X. Mao, *Stochastic Differential Equations and Their Applications*, Horwood Publishing, Chichester, UK, 1997.
- [21] B. Øksendal, *Stochastic Differential Equations: An Introduction with Applications*, Springer, New York, NY, USA, 2003.
- [22] W. Huang, *Schur complement's properties and its application [Ph.D. thesis]*, Nanjing University of Information Engineering.
- [23] S. Wang and Z. Yang, *Generalized Inverse Matrix and Its Application*, Beijing Industrial University Press, Beijing, China, 1996.
- [24] S. Boyd, L. El Ghaoui, E. Feron, and V. Balakrishnan, *Linear Matrix Inequalities in System and Control Theory*, vol. 15, Society for Industrial and Applied Mathematics, 1994.
- [25] H. Ye, J. Gao, and Y. Ding, "A generalized Gronwall inequality and its application to a fractional differential equation," *Journal of Mathematical Analysis and Applications*, vol. 328, no. 2, pp. 1075–1081, 2007.

Research Article

Modeling and Characteristic Study of Thin Film Based Biosensor Based on COMSOL

Yang Su

Faculty of Information Engineering, Southeast University, Nanjing, Jiangsu 211109, China

Correspondence should be addressed to Yang Su; suyang620@163.com

Received 9 January 2014; Accepted 6 March 2014; Published 7 April 2014

Academic Editor: Jianguo Du

Copyright © 2014 Yang Su. This is an open access article distributed under the Creative Commons Attribution License, which permits unrestricted use, distribution, and reproduction in any medium, provided the original work is properly cited.

The model of thin film based biosensor is built based on COMSOL in order to simulate and optimize the electronic characteristic of dipolar electrodes system and tetrapolar electrodes system. Zones of negative sensitivity exist between current carrying electrodes and voltage measuring electrodes while the polarization occurs at the edges of electrodes. By changing the parameters embracing distance between electrodes, thickness of electrodes, and the width of inner electrodes (for tetrapolar electrodes system only), the polarization and zones of negative sensitivity can be receded to some extent, which improves the system's performance. Tetrapolar electrodes system has less polarization but more negative-sensitivity zones compared to dipolar electrodes system and different setups response differently to these changing parameters.

1. Introduction

Biological detection techniques exist in multitudes of aspects of human's daily life, especially in the area of chemistry and biology. Numerous devices have already been demonstrated using CMOS technology, such as DNA detection [1, 2] and ion sensitive field effect transistor arrays [3]. However, there are postprocessing problems associated with CMOS, for example, circuit passivation [4] and biocompatible electrode deposition, which increase cost and manufacturing complexity. Thin film transistor based devices have the potential to solve some of these issues. For salient instance, they are low cost and use low temperature fabrication processes [5] using glass, flexible plastic, and eventually paper substrates, with no addition processing required. Large TFT arrays have already been demonstrated for flat panel displays so could easily be translated into sensor pixels for massively parallel measurement.

Thin film based biosensor is a kind of cutting-edge technology which can be applied in electronic system for biological sensing. The chip used electrochemical impedance spectroscopy (EIS) as a sensing technique [6–10]. EIS has shown potential to be a sensitive method for label-free sensing. Here, direct electrochemistry of the target analyses is

used, with no immobilised enzymes or mediators. At present, bipolar setup with two electrodes which both carry current and measure voltage is widely used. However, this setup can lead to unwanted phenomenon embracing polarization and zones of negative sensitivity [11] which affect the accuracy to some extent. It is essential to design an appropriate thin film sensor in order to reduce the polarization and zones of negative sensitivity as greatly as possible.

This paper concentrates on how three factors embracing geometry, dimension, and configuration for electrodes will affect those two parameters which are mentioned above. At the end of this paper, a better setup of electrodes together with several solutions to improving the performance pertinent to thin-film sensor will be worked out.

2. Modeling and Experimental Design

The model of electrodes is based on COMSOL Multiphysics [12] which is a finite element analysis, solver and simulation software package for various physics and engineering applications. In the model, the substrate is made of silica glass while the material of electrodes is gold. The system is studied in NaCl solution, which is the standard solution for the calibration of electrochemical system. The domain

frequency is chosen to be 10000 Hz and the concentration relevant to the solution is 1.76 S/m which are bilateral typical values in biosensor test. Three typical types of geometry with regard to electrodes are included in this paper, which are horizontal rectangle, vertical rectangle, and horizontal ring. On the other hand, three factors are taken with reference to dimension, embracing electrode-wise thickness, the distance between electrodes, and the condition where the pair for carrying current and the other for measuring voltage have different size (for tetrapolar electrode system) into consideration, which share affect the polarization and zones of negative sensitivity to some extent. In addition, it is substantial to find out how a tetrapolar electrode system improves the performance compared to the corresponding dipolar one.

In accordance to the simulation results, the strongest polarization appears at the edges of electrodes. As a result, the highest degree is extracted in the case of polarization at edges to access its degree. The sensitivity is a measure of how different component in the measured biomaterial contributes to the total measure impedance, provided that resistivity is uniform throughout the material. The sensitivity S is derived as

$$S = \frac{J_1 \cdot J_2}{I^2}, \quad (1)$$

where J_1 is the current density measure when a current is injected I between the electrodes for carrying current while J_2 is the current density measure when the current is injected between the voltage measuring electrodes. A positive value for the sensitivity means that if the resistivity of this volume element is increased, a higher total resistance will be measured. A negative value for the sensitivity, on the other hand, means that increased resistivity in that volume gives a lower total measured resistance, which will lead to errors of measurement. The research on sensitivity is on the basis of the 2D picture in the light of the distribution of sensitivity. For two-electrode system the sensitivity is always positive in that the two electrodes carry the current and measure the voltage at the same time. For tetrapolar electrode system, the current carrying electrode pair and the voltage measuring pair should be arranged as shown in Figure 1; otherwise sensitivity of most volumes will be negative which is unacceptable [13].

3. Experimental Tests

3.1. Electrode Polarization. Polarization is a kind of phenomenon which widely exists in biosensor system. The existence of polarization will lead to additional impedance which will affect the accuracy to some extent. The strongest polarization exists at different position for diversity setups. For dipolar electrode system, the edge of terminal electrode always has the highest degree of polarization while the situation becomes complicated for tetrapolar electrode system. To be more precise, the point polarized mostly of tetrapolar horizontal rectangle electrode system is the edge of inner terminal one while the point changes to the edge of outer terminal electrode when it turns to tetrapolar vertical rectangle one. Additionally, the edge of electrode 1 has the strongest polarization for tetrapolar horizontal

ring electrode system. In this paper strongest polarization is called "leading polarization." Virtually, electrode polarization cannot be overcome completely but some measures can be done to minimize it. Three factors of dimension are taken into consideration here, embracing thickness, distance between electrodes, and width of inner electrode pair (for tetrapolar electrode system). According to the simulation, diverse setups of electrode system respond differently to those parameters.

For horizontal rectangle electrode system, the variation of polarization is not regular, which means it is not effective to improve the performance by changing those two factors. It is a bit different when it turns to vertical rectangle electrode system. The degree of leading polarization almost keeps steady as the distance increases while it decreases gradually as the electrodes get thicker. As to horizontal ring electrode system, it is the other way round. In accordance with experiments, it is certain that the increase of distance and thickness make the degree of polarization go down. What is identical in those pictures is that the employment of tetrapolar electrode relieves the effects of polarization greatly. That is to say, using four-electrode system instead of two-electrode system is a brilliant alternative to minimize the effects of polarization.

There are some special results in the condition where the inner electrode pair has a different size from the outer pair. In accordance to Figure 2, the leading polarization pertaining to horizontal rectangle tetrapolar electrode system drops remarkably as the width of inner electrode pair increases. Meanwhile, the leading polarization with regard to vertical rectangle tetrapolar electrode system drops dramatically once the inner pair's height exceeds the outer pair's.

3.2. Zones of Negative Sensitivity and Uniformity of Sensitivity. It is nevertheless a fact that tetrapolar systems are more vulnerable to errors than bipolar system [14]. A four-electrode system will typically have small volumes with negative sensitivity between current carrying electrodes and voltage measuring ones. As demonstrated in Figure 3, it can be seen explicitly how the zones of negative sensitivity distribute among the space. There are two main negative-sensitivity zones for horizontal and vertical rectangle four-electrode systems while there are four of them. Besides, another factor which is the lowest value of sensitivity is taken into consideration to assess the uniformity of sensitivity. Figure 4 demonstrates how the lowest values relevant to sensitivity of three systems response to the change of distance between electrodes and the width of inner electrode pair. Thickness is not included here in that it nearly has no effect on sensitivity. It can be seen clearly that the lowest values of sensitivity are raised by increasing the distance or the width of inner electrode pair, which means the uniformity is improved to some extent. However, the area of negative-sensitivity zones increases when the distance between electrodes gets larger. The area of negative-sensitive zones mainly depends on the lateral area of current carrying electrode and voltage measuring electrode together with the distance between them. As a result, those two factors can be reduced in order to minimize the volumes of negative sensitivity. On the other

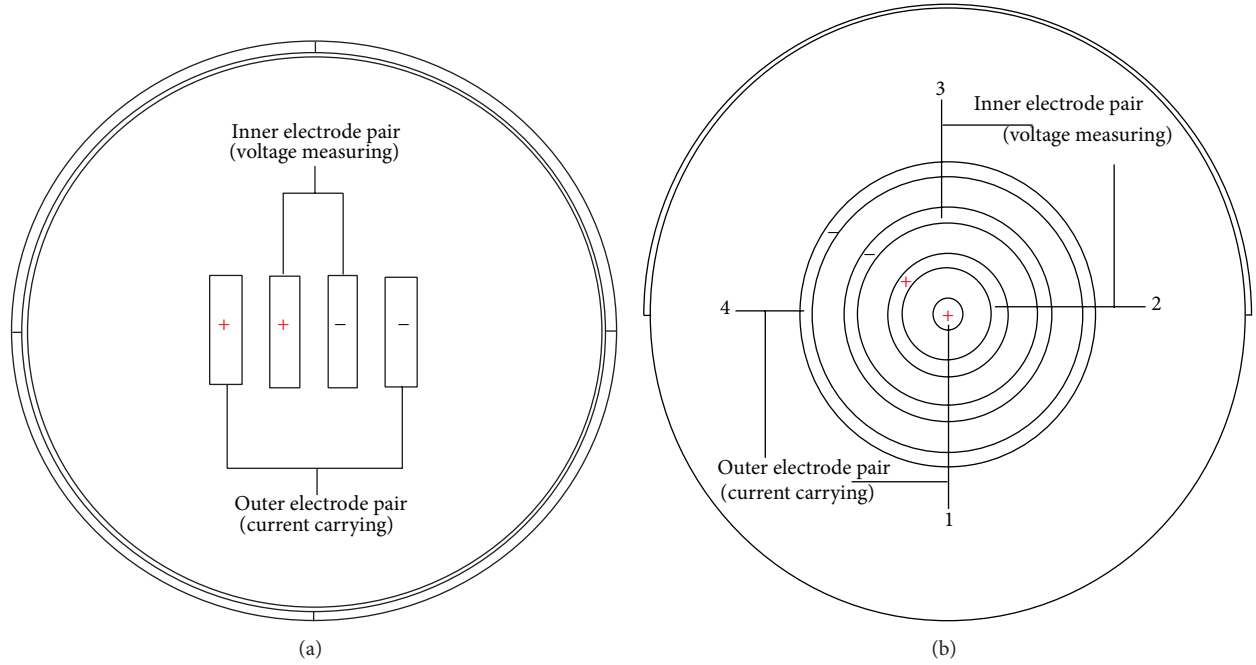


FIGURE 1: Arrangement for electrodes of (a) tetrapolar horizontal or vertical rectangle electrode system and (b) tetrapolar horizontal ring electrode system.

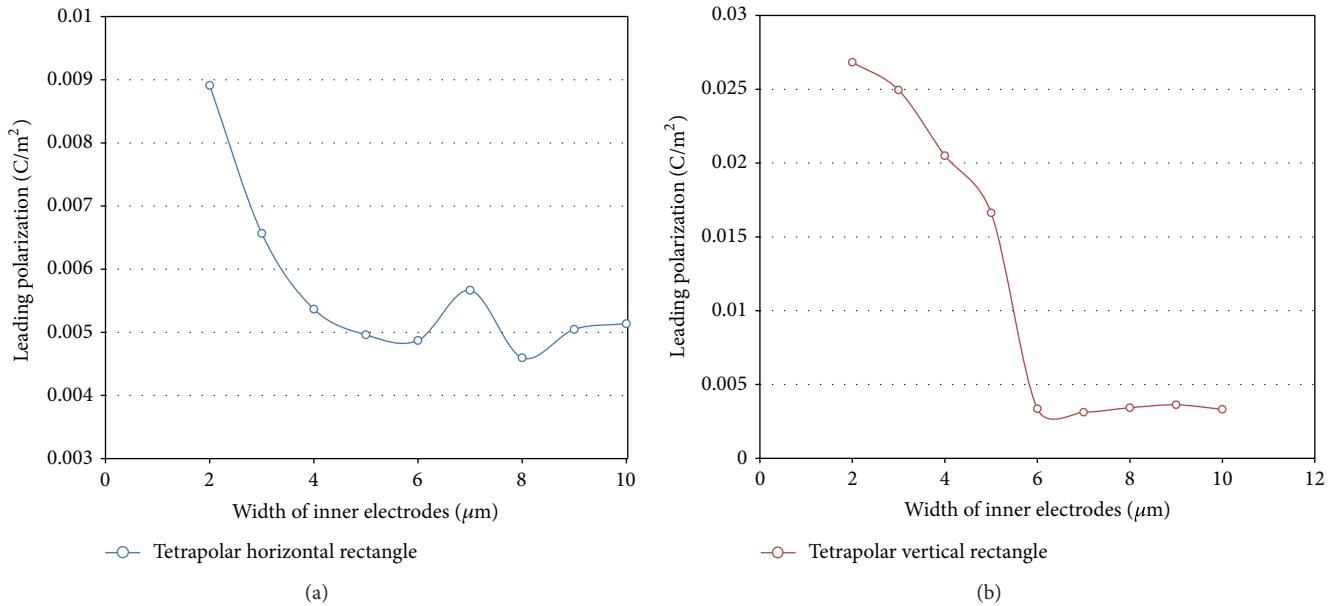


FIGURE 2: The response of leading polarization pertinent to (a) tetrapolar horizontal rectangle electrode system and (b) tetrapolar vertical rectangle electrode system to the change of width of inner electrode pair (width of outer electrodes: 5 μm; thickness of electrodes: 100 nm; length of electrodes: 20 μm; distance between electrodes: 10 μm).

hand, although horizontal ring tetrapolar electrode system has more zones of negative sensitivity than the other two kinds, its degree of uniformity is the highest among them.

4. Comparison and Analysis

In order to find out the best setup of electrode system, it is essential to make comparison on polarization and sensitivity

between diversity types of electrode system. It can be seen explicitly from what has been mentioned above that the employment of tetrapolar electrode system instead of dipolar electrode system can relieve the phenomenon of polarization to a large extent, which means if the device mainly focuses on lowering the degree of polarization, four-electrode system will be the better alternative. Unfortunately, two-electrode electrode system does have its advantage in sensitivity. There are no zones of negative sensitivity for dipolar electrode

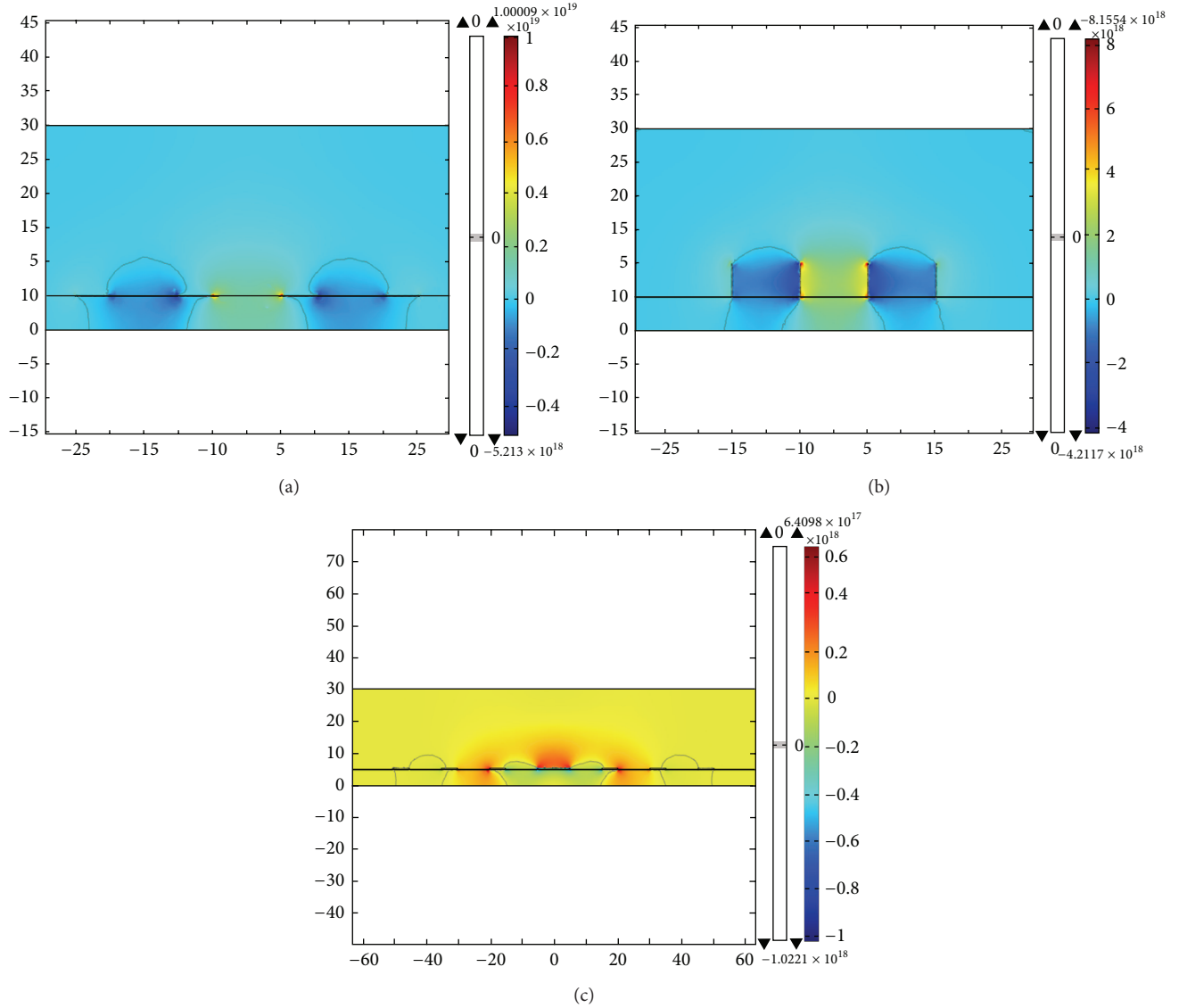


FIGURE 3: Sensitivity distribution of (a) tetrapolar horizontal rectangle electrode system, (b) tetrapolar vertical rectangle electrode system, and (c) tetrapolar horizontal ring electrode system.

system in that its electrodes function as current carrying electrodes and voltage measuring electrodes at the same time, which makes the product of J_1 and J_2 always positive. As for the factor of geometry, it can be seen clearly from Figure 5 that vertical rectangle electrode system has the highest degree of polarization at the case of two-electrode systems and four-electrode systems. For dipolar electrode system, the degree of polarization pertaining to horizontal ring electrode system is second to that of vertical rectangle electrode system while horizontal rectangle electrode system has the weakest electrode polarization. But the polarization degree in the case of horizontal rectangle and horizontal ring electrode system keeps at the same level. Diversity systems respond differently to the change of dimension and the simulation results relevant to polarization are listed in Table 1. As a result, horizontal rectangle electrode system is much likely to be

the best option for two-electrode system. It is substantial to take the factor of sensitivity when trying to work out the best setup of electrode system when it turns to four-electrode systems. Meanwhile, the electrode of polarization can be relieved by increasing the distance between electrodes, which will optimize its performance to some extent. From what has been mentioned previously, tetrapolar horizontal rectangle electrode system has the smallest area of negative-sensitivity zones although its uniformity of sensitivity is not as good as tetrapolar horizontal ring electrode system. That is to say, horizontal rectangle electrode system may be the best option, of which performance can be improved by increasing the width of inner electrode pair and reducing the distance between current carrying electrode and voltage measuring electrode.

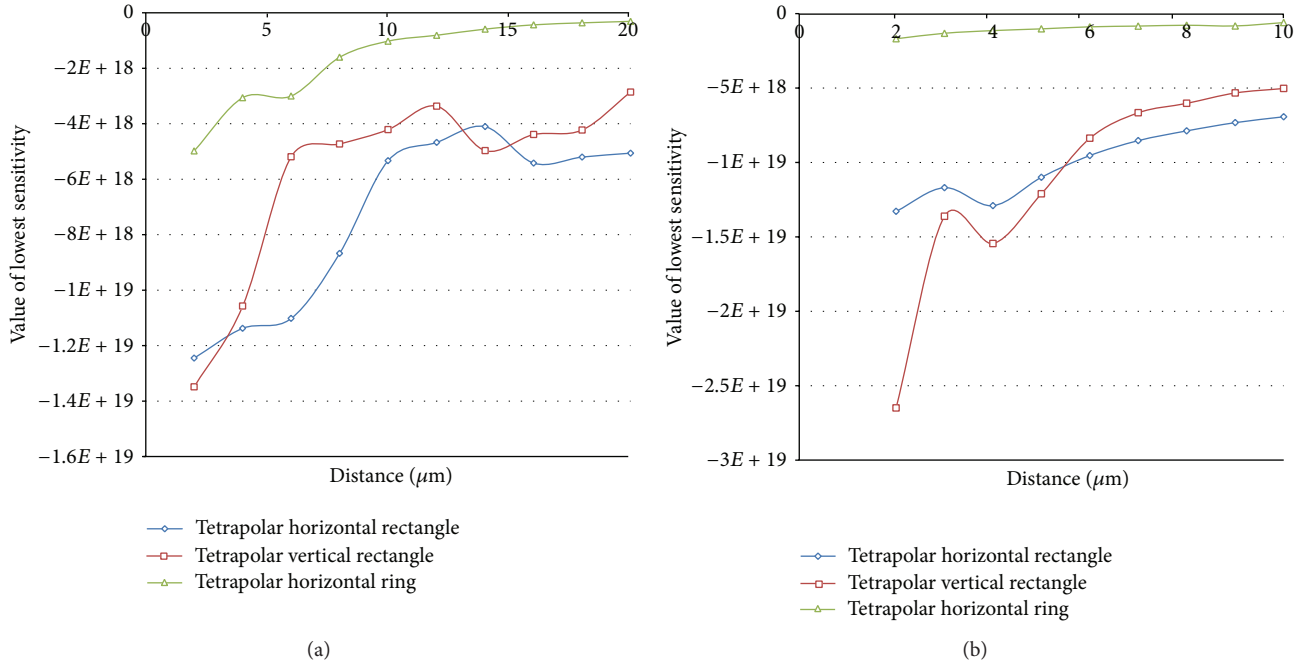


FIGURE 4: The response of lowest sensitivity pertinent to tetrapolar electrode system to the change of (a) distance between electrodes (width of electrodes: $5\ \mu\text{m}$; length of electrodes: $20\ \mu\text{m}$; thickness of electrodes: $100\ \text{nm}$) and (b) width of inner electrodes (width of outer electrodes: $5\ \mu\text{m}$; thickness of electrodes: $100\ \text{nm}$; length of electrodes: $20\ \mu\text{m}$; distance between electrodes: $10\ \mu\text{m}$).

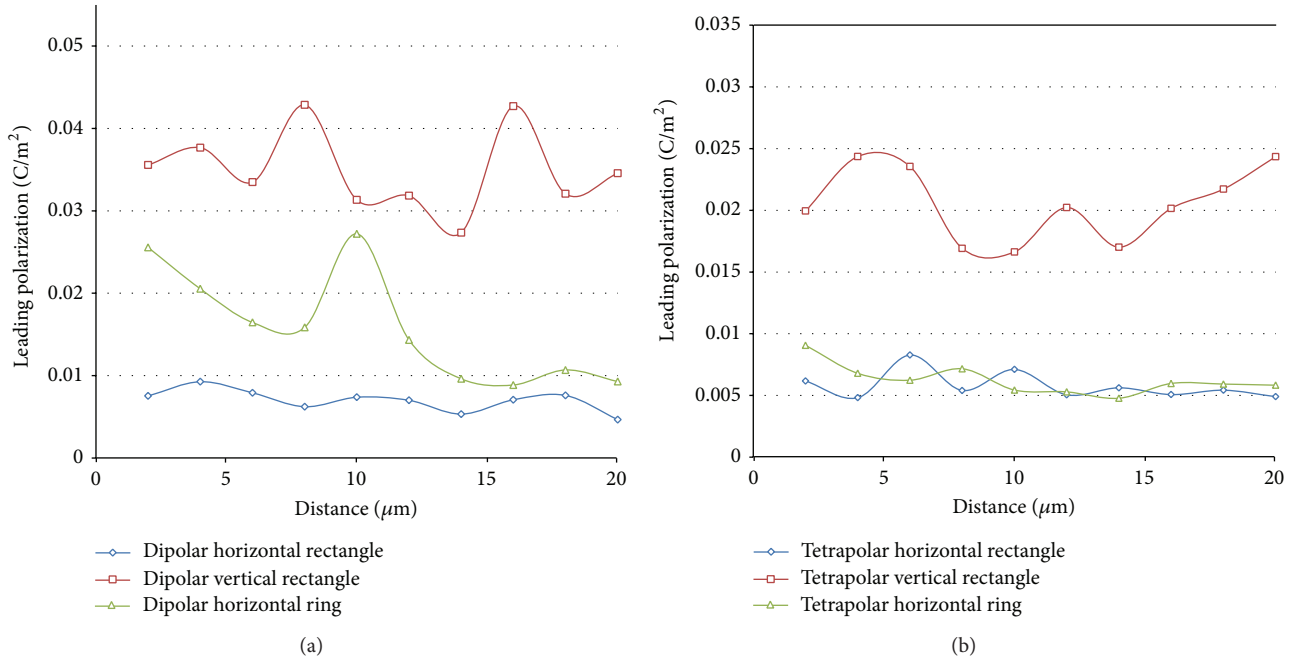


FIGURE 5: The response of leading polarization pertinent to (a) dipolar and (b) tetrapolar electrode system to the change of distance between electrodes (width of electrodes: $5\ \mu\text{m}$; length of electrodes: $20\ \mu\text{m}$; thickness of electrodes: $100\ \text{nm}$).

5. Conclusion

- (1) Terapolar electrodes system has less polarization than dipolar electrodes system.
- (2) For tetrapolar electrodes system, zones of negative sensitivity exist between current carrying electrodes and voltage measuring electrodes.
- (3) For tetrapolar vertical electrodes system, the degree of leading polarization drops remarkably when the width of inner electrodes is larger than the outer ones.
- (4) With respect to the polarization of dipolar electrodes system, horizontal rectangle system has the lowest degree.

TABLE 1: Relief of polarization due to cncreasing parameters.

Increasing parameters	Dipolar horizontal rectangle	Dipolar vertical rectangle	Dipolar horizontal ring	Tetrapolar horizontal rectangle	Tetrapolar vertical rectangle	Tetrapolar horizontal rectangle
Distance	√		√			√
Thickness		√			√	√
Width of inner electrodes	—	—	—	√	√	

- (5) As to the polarization of tetrapolar electrodes system, horizontal electrodes systems are better than vertical one.
- (6) For tetrapolar electrodes system, the degree of negative-sensitivity zones regarding horizontal ring electrodes system is the lowest among the three setups.
- (7) By increasing the corresponding parameters listed in Table 1, the performance of the biosensor can be improved to some extent.

Conflict of Interests

The author declares that there is no conflict of interests regarding the publication of this paper.

References

- [1] H. Mazhab-Jafari, L. Soleymani, and R. Genov, "16-channel CMOS impedance spectroscopy DNA analyzer with dual-slope multiplying ADCs," *IEEE Transactions on Biomedical Circuits and Systems*, vol. 6, no. 5, pp. 468–478, 2012.
- [2] D. M. Garner, H. Bai, P. Georgiou et al., "A multichannel DNA SoC for rapid point-of-care gene detection," in *Proceedings of the IEEE International Solid-State Circuits Conference (ISSCC '10)*, pp. 492–493, February 2010.
- [3] J. M. Rothberg, W. Hinz, T. M. Rearick et al., "An integrated semiconductor device enabling non-optical genome sequencing," *Nature*, vol. 475, no. 7356, pp. 348–352, 2011.
- [4] M. Schindler, S. K. Kim, C. S. Hwang, C. Schindler, A. Offenhäusser, and S. Ingebrandt, "Novel post-process for the passivation of a CMOS biosensor," *Physica Status Solidi—Rapid Research Letters*, vol. 2, no. 1, pp. 4–6, 2008.
- [5] D. Gonçalves, D. M. F. Prazeres, V. Chu, and J. P. Conde, "Detection of DNA and proteins using amorphous silicon ion-sensitive thin-film field effect transistors," *Biosensors and Bioelectronics*, vol. 24, no. 4, pp. 545–551, 2008.
- [6] F. Lisdat and D. Schäfer, "The use of electrochemical impedance spectroscopy for biosensing," *Analytical and Bioanalytical Chemistry*, vol. 391, no. 5, pp. 1555–1567, 2008.
- [7] L. Añorga, A. Rebollo, J. Herrán, S. Arana, E. Bandrés, and J. García-Foncillas, "Development of a DNA microelectrochemical biosensor for CEACAM5 detection," *IEEE Sensors Journal*, vol. 10, no. 8, pp. 1368–1374, 2010.
- [8] H. Liu, R. Malhotra, M. W. Peczu, and J. F. Rusling, "Electrochemical immunosensors for antibodies to peanut allergen Ara h2 using gold nanoparticle-peptide films," *Analytical Chemistry*, vol. 82, no. 13, pp. 5865–5871, 2010.
- [9] O. Pänke, W. Weigel, S. Schmidt, A. Steude, and A. A. Robitzki, "A cell-based impedance assay for monitoring transient receptor potential (TRP) ion channel activity," *Biosensors and Bioelectronics*, vol. 26, no. 5, pp. 2376–2382, 2011.
- [10] A. Manickam, C. A. Johnson, S. Kavusi, and A. Hassibi, "Interface design for CMOS-integrated electrochemical impedance spectroscopy (EIS) biosensors," *Sensors*, vol. 12, no. 11, pp. 14446–14488, 2012.
- [11] S. Grimnes and Ø. G. Martinsen, "Sources of error in tetrapolar impedance measurements on biomaterials and other ionic conductors," *Journal of Physics D: Applied Physics*, vol. 40, no. 1, pp. 9–14, 2007.
- [12] COMSOL, "Product Suite[DB/OL]," 2013, <http://www.comsol.com/products>.
- [13] B.V. Metrohm Autolab, "Fuel cells part 3—characterization using EIS," Autolab Application Note FC03, http://www.ecochemie.nl/download/Applicationnotes/Autolab_Application_Note_FC03.pdf.
- [14] S. Grimnes and Ø. G. Martinsen, "Positive phase bioimpedance and system inductive properties," in *Proceedings of the World Congress in Medical Physics and Biomedical Engineering*, Sydney, Australia, 2003.